CONF-780649--

Nineteenth Annual Logging Symposium Transactions

June 13-16, 1978

El Paso, Texas

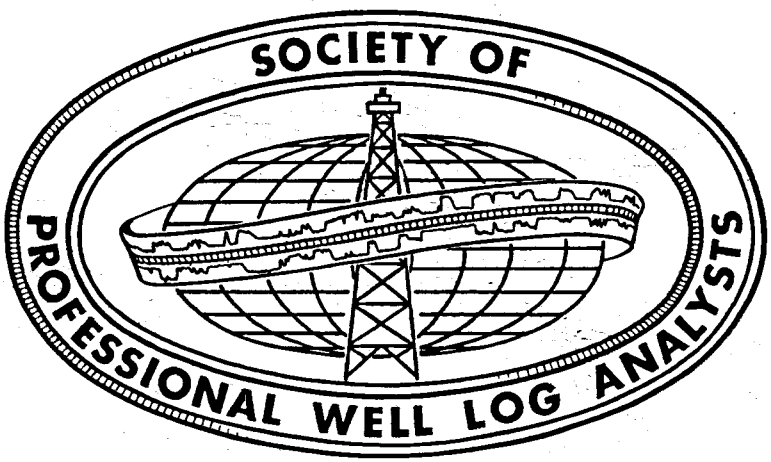

S P W L A

DISCLAIMER

TRANSACTIONS

OF THE

SPWLA
NINETEENTH
ANNUAL LOGGING SYMPOSIUM

Sponsored by

THE SOCIETY OF PROFESSIONAL WELL LOG ANALYSTS, INC.
806 Main Street, Suite B-1
Houston, Texas 77002 USA

Presented at

El Paso Civic Center

El Paso, Texas

June 13 - 16, 1978

SPWLA OFFICIALS 1977-1978

President:	Beaumont B. Cooley, Chevron Oil Co. of Spain, Madrid, Spain
V-P Technological:	Walter H. Fertl, Dresser Atlas, Houston, Texas
V-P Membership:	Don Ross, Mobil Oil Corp., Houston, Texas
V-P Public Relations:	Erwin E. King, Atlantic Richfield Co., Tulsa, Oklahoma
V-P Publications:	Lewis Raymer, Schlumberger-Doll Research Center, Ridgefield, Connecticut
Secretary-Treasurer:	Elbert B. Davis, Continental Oil Co., Corpus Christi, Texas
Director-at-Large:	Glenda C. Harris, Champlin Petroleum Co., Englewood, Colorado
Director-at-Large:	Thomas L. Caskey, Texas Pacific Oil Co., Oklahoma City, Okla.
Past President:	W. A. Grieves, Exxon Co., U.S.A., Houston, Texas

Executive Secretary: Paul A. Wichmann
Publications Manager: C. Richard Glanville

SPWLA TECHNOLOGICAL COMMITTEE 1977-1978

Chairman:	Walter H. Fertl, Dresser Atlas, Houston, Texas
Members:	Roberto Aguilera, SOQUIP, Sainte-Foy, Quebec, Canada
	James C. Albright, Conoco R. & D., Ponca City, Oklahoma
	Zoltan Barlai, Univ. of Tripoli, Tripoli, Libyan Arab Republic
	Raymond L. Campbell, Schlumberger Well Services, Houston, Texas
	Thomas C. Caskey, Texas Pacific Oil Co., Oklahoma City, Okla.
	Myron H. Dorfman, University of Texas, Austin, Texas
	Lyman M. Edwards, Dresser Industries, Houston, Texas
	Marvin Gearhart, GO International, Ft. Worth, Texas
	David L. Greenwood, Pan Canadian Petroleum, Calgary, Alta., Can.
	James K. Hallenburg, Century Geophysical Corp., Tulsa, Okla.
	Wilmer A. Hoyer, Exxon Production Research Co., Houston, Texas
	Bill A. Kithas, Welex, Midland, Texas
	Charles E. Konen, Amoco International Oil Co., Chicago, Ill.
	Robert A. Lane, Shell Oil Co., New Orleans, Louisiana
	David W. Mann, UK Dept. of Energy, London, England
	Bernardo J. Martell, Petroleos Mexicanos, Mexico City, Mexico
	A. V. Messineo, Atlantic Richfield Co., Dallas, Texas
	J. S. Milligan, Amoco Production Co., Denver, Colorado
	Donald M. Pert, U. S. Geological Survey, Metairie, Louisiana
	James M. Price, Gulf R. & D., Houston, Texas
	Jean R. Raiga-Clemenceau, BEICIP, Paris, France

SPWLA SYMPOSIUM ARRANGEMENTS COMMITTEE, 1978

General Chairman:	Elton Rodgers, Getty Oil Co., Midland, Texas
Asst. Gen. Chairman and Publicity:	Bill Kithas, Welex, Midland, Texas
Entertainment:	Art Schmidt, Consultant, Midland, Texas
Exhibits:	Jack Flynn, Dresser Atlas, Odessa, Texas
Housing:	Wayne Gibson, Texaco, Midland, Texas
Registration:	George Horst, Schlumberger, Midland, Texas
Technical Equipment:	C. D. Stenberg, Gulf Oil Co., Midland, Texas
Treasurer:	Bill Markgraf, Union Texas Petroleum Co., Midland, Texas
Ladies Activities:	Mrs. Bill Kithas, Mrs. Art Schmidt, and Mrs. Bernardo Martell

LIST OF TRANSACTIONS

A. "The Uncertainty of Evaluating Original Oil-in-Place in Naturally Fractured Reservoirs", Roberto Aguilera (SOQUIP, Quebec, Canada).

B. "The Determination of Prior Depth of Burial (Uplift and Erosion) Using Interval Transit Time", William H. Lang, Jr. (Union Oil Co. of California).

C. "Some Practical Applications to Improve Formation Evaluation of Sandstones in the Mackenzie Delta", W. L. Johnson and W. A. Linke (Chevron Standard Ltd., Calgary, Alta., Canada).

D. "The F-ϕ-m Cross Plot - A New Approach for Detecting Natural Fractures in Complex Reservoir Rocks by Well Log Analysis", Orlando Gomez-Rivero (Petroleos Mexicanos, Mexico City, Mexico).

E. "Determination of Logging Parameters in Shaly Sand", Makoto Miyairi and Toshinobu Itoh (Japan Petroleum Exploration Co., Tokyo, Japan).

F. "Log Analysis in a Rocky Mountain Heavy Oil Reservoir", D. A. Chesnut and D. O. Cox (Energy Consulting Associates, Inc.)

G. "Dipmeter Log Analysis - An Essay", M. H. Rider (Compagnie Francaise des Petroles, Bordeaux, France).

H. "The Use and Validity of Pulsed Neutron Surveys in Currently Drilling Tests", Shelby W. Smith (Texaco, Inc.)

I. "A Study of the Relationship Between Two Intrinsic Reservoir Parameters, the Lithologic Influence Factor and the Pore Geometrical Factor", Z. Barlai, Reda A. Mawla, and Faleh T. Al-Saadoon (Al-Fateh University, Tripoli, Libya).

J. "Normalization Techniques and Interpretive Practices of Relative Permeability Curves of Reservoir Rocks", Reda A. Mawla and Faleh T. Al-Saadoon (Al-Feteh University, Tripoli, Libya).

K. "The Detection of Water Leakage from Dams Using Streaming Potentials", Brent M. Haines (Queensland Institute of Technology, Brisbane, Australia)

L. "Analisis de Registros Geofisicos en Arenas Arcillosas, Metodo de Fertl Modificado", Miguel Linares Flores and Ramiro Garza de la Garza (Petroleos Mexicanos, Reynosa, Tams., Mexico)(IN SPANISH).

M. "Mineral Composition, an Aid in Classical Log Analysis Used in Jurassic Sandstones of the Northern North Sea", ϕ. Nyberg, K. Lien, P. A. Lindberg, and J. K. Smistad (Statoil, Stavanger, Norway).

N. "Relationship Between the Conductivities of Tertiary Water-Bearing Sands and Nearby Shales, Offshore Louisiana", H. J. Ritch and E. S. Pennebaker (Shell Oil Co.)

O. "A New Approach to Carbonate Analysis", W. H. Nugent, G. R. Coates, and R. P. Peebler (Schlumberger Well Services).

P. "Some Aspects of the Calculation of Gypsum-Free Porosity", Elton Frost, Jr. (Dresser Atlas).

Q. "Logging Tests in Porous Media to Evaluate the Influence of their Permeability on Acoustic Waveforms", F. Lebreton and J. P. Sarda (Institut Francais du Petrole), F. Trocqueme (Societe Nationale Elf-Aquitaine (Production)), and P. Molier (Laboratoire de Mechanique des Roches de l'Ecole Polytechnique).

R. "The Laterolog Groningen Phantom Can Cost You Money", R. Woodhouse (The British Petroleum Co., Ltd., London, England).

S. "The Compu-Log Concept and Practice", R. Kinkade, J. West, and J. Hallenburg (Century Geophysical Corp.).

T. "Uranium Ore Body Analysis Using the DFN Technique", J. West and J. Hallenburg (Century Geophysical Corp.).

U. "Use of the Spontaneous Potential Curve in a Mineral Mapping Technique", James K. Hallenburg (Century Geophysical Corp.).

V. "Estimation of Formation Pressures in Clean Gas Sands from the Dual-Spacing TDT Log", J. S. Blackburn (Schlumberger Well Services) and R. C. Brimage (Schlumberger Offshore Services).

W. "Evaluation of Very Low-Porosity Carbonates (Malossa, Italy)", J. Suau and C. Boyeldieu (Schlumberger Inland Services, London, England), R. Roccabianca and M. Cigni (AGIP, Milano, Italy), and M. Spila (Schlumberger Italiana S. p. A., Milano, Italy).

X. "Well Log Interpretation of Shaly Sands with the Programmable Calculator", Kenneth D. Thompson (Schlumberger Well Services).

Y. "The Method of Autocalibration and its Computer Applications /SAIK System/ ", Janusz Frydecki (Warsaw University), Zdzislaw Debski (Municipal Information and Computer Centre of Warsaw), and Stefan Basista (Enterprise of Geophysical Prospecting, Warsaw).

Z. "A Computer-Processed Wellsite Log Computation", D. L. Best, J. S. Gardner, and J. L. Dumanoir (Schlumberger Well Services).

AA. "The Spider in the Web of the Role of the Petrophysicist in the World's Quest for Petroleum", G. E. Dawson-Grove (Petrophysical Consultants International Ltd., Calgary, Alta., Canada).

BB. "The Prediction of Water Saturation and Recoverable Hydrocarbon Volumes in Shaly Sand Reservoirs", Daniel A. Krygowski (Cities Service Co.) and G. R. Pickett (Colorado School of Mines).

CC. "Log Interpretation of Shaly Formations Using the Velocity Ratio Plot", Richard Leeth (Welex) and Michael Holmes (Independent Geological Consultant).

DD. "Permeability Determination in Liquid Dominated Geothermal Reservoirs Using the Dual Induction Laterolog", I. Ershaghi, E. L. Dougherty, D. Herzberg, and H. Ucok (University of Southern California).

EE. "Evaluation of Oil Wells by Logging Methods in the USSR", V. Laptev (All-Union Research Institute of Oil Field Geophysicists, Moscow, USSR).

FF. "Formation Evaluation Concepts for Geothermal Resources", T. W. Ehring, L. A. Lusk, and J. M. Grubb (Aminoil USA), and R. B. Johnson, M. R. DeVries, and W. H. Fertl (Dresser Atlas).

GG. "A Practical Shale Compensated Chlorine Log", J. W. Fletcher and J. Walter (NL McCullough/NL Industries, Inc.).

HH. "Carbon/Oxygen Log Applications to Shaly Sand Formations Contaminated with Tuffite Minerals", E. L. Sacco (Dresser Atlas, Buenos Aires, Argentina).

II. "Coal Exploration in West Germany by Well Logging", K. Otto (Dresser Atlas, Bremen, Germany) ABSTRACT ONLY.

A

THE UNCERTAINTY OF EVALUATING ORIGINAL OIL-IN-PLACE IN NATURALLY FRACTURED RESERVOIRS

Roberto Aguilera
SOQUIP
Quebec, Canada

ABSTRACT

Calculation of original oil-in-place by volumetric means in naturally fractured reservoirs requires previous knowledge of area, net pay, oil formation volume factor, matrix and fracture porosities, and matrix and fracture water saturations.

To establish exact values for the previous parameters is essentially impossible. This is specially true for fracture porosity and fracture water saturation. Fracture reservoirs may produce at very high initial oil rates which might lead to very optimistic forecasts. These initial high rates are due to the original oil-in-place within the fractures. Upon depletion of the fracture system the oil production may decline drastically usually with strong increases in gas-oil ratios. From there on production depends on the facility with which the oil bleeds-off from the matrix into the fractures. Consequently, the importance of having reasonable estimates of original oil-in-place within the fracture network cannot be overemphasized.

The object of this paper is to illustrate procedures to obtain estimates of original oil-in-place in naturally fractured reservoirs. The Montecarlo Simulation approach has been used to calculate ranges and probability distributions of total porosity ($\emptyset$), double-porosity exponent (m), total water saturation (S_w), fracture porosity ($\emptyset_f$), water saturation within the fractures (S_{wf}), original oil-in-place within the fractures (N_f), and total original oil-in-place (N) in a hypotetical double-porosity reservoir.

It is concluded that better decisions can be made regarding naturally fractured reservoirs if the uncertainty of calculating oil-in-place is quantitatively measured.

INTRODUCTION

Experience indicates that development of naturally fractured reservoirs has led to many economic fiascos. This has occurred because high initial oil rates have led engineers to overestimate the production forecasts of the wells. Reservoir engineers usually make the assumption that (1) the fractures have a negligible storage capacity and are only channels of very high permeability that allow the fluids to flow, and (2) the matrix has an

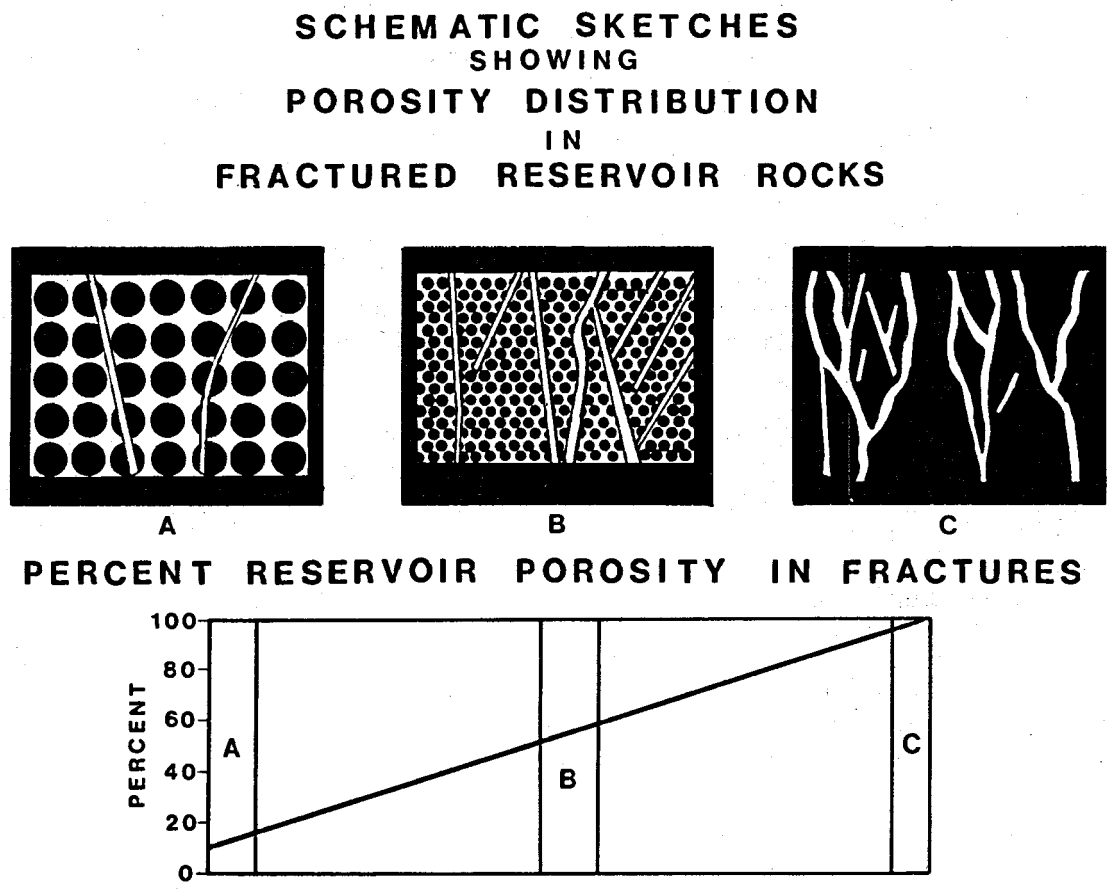

Fig. 1- Sketch A - Reservoir with high storage capacity in rock matrix (primary pore spaces) and very low storage capacity in fractures. Sketch B - Sediment having approximately equal storage capacities in matrix and fractures. Sketch C - Rock having all of its storage capacity in fractures. (After McNaughton and Garb[1]).

A

important storage capacity but a very small permeability.

Assumption 1 is believed to be quite weak. This assumption has led to many fiascos in the development of naturally fractured reservoirs. In fact, many reservoirs that produce at initial rates decline very drastically in short periods of time. This occurs because all the producible oil has been stored in the fracture system. Consequently it is important to be able to make reasonable estimates of oil-in-place within the fracture system.

Assumption 2 above has to be considered carefully. If the permeability of the matrix is very low, then the bleed-off of oil from the matrix into the fractures will be very slow and only the oil originally within the fractures will be produced in a reasonable span of time. If the matrix has a reasonable permeability, then the storage capacity of the matrix becomes of paramount importance.

It is important to visualize that the storage capacity of naturally fractured reservoirs varies intensively depending on the degree of fracturing of the formation and the value of primary porosity. The greater the value of primary porosity, the greater the success possibilities of naturally fractured reservoirs. The storage capacity in the matrix porosity of Figure 1-A is large compared with the storage capacity in the fractures. For the schematic of Figure 1-A, 10% of the total porosity is made out of fractures. In this case the fractures may be an evil rather than a bless, because they may help to create problems during drilling operations such as mud losses, blowouts, fires, etc... The schematic of Figure 1-B shows a rock with about the same storage capacity in fracture and matrix porosities. In this case, the reservoir matrix is rather tight and the fractures provide avenues of nearly infinite permeability. This is an ideal combination of porosities that have permitted to produce over 100 million STBO in individual wells of Iran[1].

Figure 1-C shows the schematic of a rock where the matrix porosity is zero. In this case all the storage capacity is due to fractures. In general reservoirs of this type are characterized by producing at very high initial rates that decline to uneconomic limits in rather short times. There are, however, exceptions reported in the literature. For example, the Edison[2] and Mountain View Fields in the San Joaquin Valley of California and the El Segundo[3], Wilminton and Playa de Rey fields in the Los Angeles Basin produced above 15000 BOPD from fractured pre-cretaceous basement schist. The storage in the basement rock of the La Paz-Mara[4] oil fields in Western Venezuela is in the fracture system. This field produced over 80000 BOPD from the basement reservoir. Matrix porosity contributes very little if at all to the over-all reservoir capacity of the Osage and Meramec limestones in the Eastern Anadarko basin[5]. In these limestones essentially all the oil is within the fracture system.

Summarizing, it is believed that there is enough evidence to banish the generalized assumption that the storage capacity of a fractured system is negligible as compared with the storage capacity of the matrix.

It is the objective of this paper to describe a procedure to e-

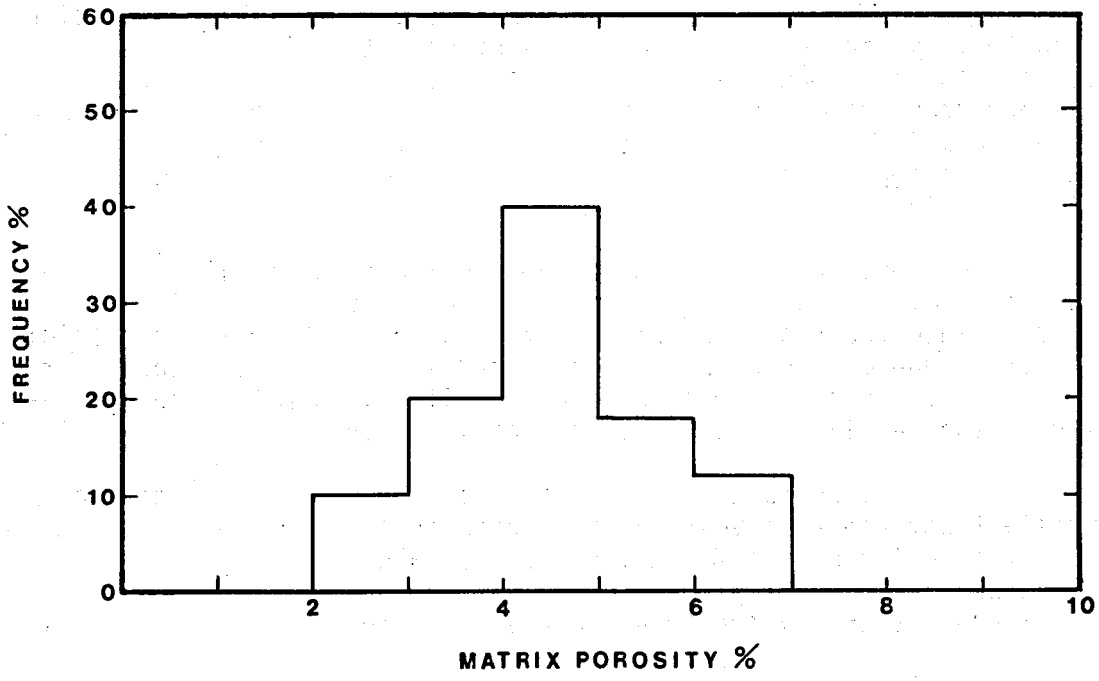

Fig. 2- Distribution of matrix porosity for example problem.

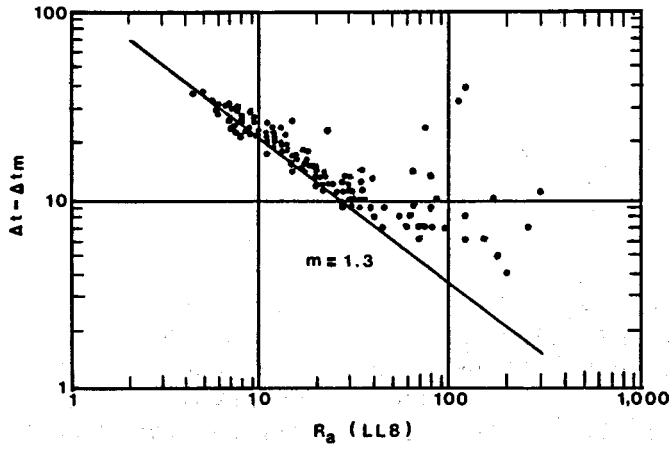

Fig. 3- R_a - Porosity response cross-plot permits evaluation of the double-porosity exponent, m. (After Aguilera [8,9]).

A

valuate the uncertianty of calculating original oil-in-place in naturally fractured reservoirs. This procedure is not claimed to be perfect. However, it has provided the author with an additional tool in the huge problem of evaluating fractured media.

ORIGINAL OIL-IN-PLACE

Total original oil-in-place in a naturally fractured reservoir can be calculated volumetrically from the relationship:

$$N = \frac{7758\ Ah\ \phi\ (1 - S_w)}{B_o} \qquad (1)$$

where
- N = original oil-in-place, STBO
- A = area, acres
- h = net pay, feet
- ϕ = total porosity, fraction
- S_w = total water saturation, fraction
- B_o = initial oil formation volume factor, bbl/STBO

The original oil-in-place within the fractures can be approximated from:

$$N_f = \frac{7758\ Ah\ \phi_f\ (1 - S_{wf})}{B_o} \qquad (2)$$

where
- N_f = original oil-in-place within the fractures, STBO
- ϕ_f = fracture porosity, fraction
- S_{wf} = water saturation within the fractures, fraction.

The following sections will present procedures to estimate the parameters that go into equations 1 and 2.

Total Porosity

The total porosity can be calculated as a function of the matrix porosity and the partitioning coefficient from the equation:[6]

$$\phi = \frac{\phi_b}{1 - v\ (1 - \phi_b)} \qquad (3)$$

where
- ϕ_b = matrix porosity, fraction
- v = partitioning coefficient, fraction.

The partitioning coefficient represents the fraction of total pore volume made up of fractures. Its value can be estimated using the method of Locke and Bliss[7] or pressure analysis.[6] The matrix porosity can be obtained from analysis of intergranular cores in the laboratory. It must be noted that experience indicates that matrix porosity has usually a normal distribution (Figure 2).

Double-Porosity Exponent

The double-porosity exponent, m, for naturally fractured reservoirs has been found previously to be smaller[8,9] than the porosity exponent of intergranular systems. Sometimes, it is possible to estimate the value of m from logs alone when a statiscally significant number of zones is available as shown in Figure 3. If this is not the case it is still possible to estimate the value of the double-porosity system from the relationship:[9]

$$m = -\log\left[\frac{1}{v\phi - (1 - v)/\phi_b^{-m_b}}\right] \Big/ \log \phi \qquad (4)$$

where m = double-porosity exponent
m_b = matrix porosity exponent

The matrix porosity exponent is obtained in the laboratory from the analysis of intergranular cores. Other parameters that go into equation 4 are obtained as described previously.

Total Water Saturation

Total water saturation can be calculated from the relationship:[10]

$$S_w = \left[\frac{R_w}{\phi^m R_t}\right]^{1/n} \qquad (5)$$

where S_w = total water saturation, fraction
R_t = true formation resistivity, -m
n = water saturation exponent

Values of R_w can be otbained from the SP log, water analysis, or

regional water resistivity tables. The total porosity and the double-porosity exponent, m, can be obtained as discussed previously. The true formation resistivity is obtained from resistivity logs. In this paper it is assumed that the water saturation exponent, n, is equal to the double-porosity exponent, m. This assumption does not appear unreasonable based on previous experience in intergranular and fractured reservoirs. [9,11]

Fracture Porosity

An estimate of fracture porosity is necessary to calculate the original oil-in-place within the fracture system. The fracture porosity is approximated by the difference between the total porosity as determined from equation 3 and the matrix porosity as determined from core analysis, or

$$\phi_f = \phi - \phi_b \qquad (6)$$

As discussed in the introduction of this paper, the importance of a quantitative estimate of fracture porosity cannot be overemphasized. It is strongly recommended to avoid the generalized assumption that the fracture porosity contribution to storage capacity is negligible.

Water Saturation in the Fractures

The possibility of estimating water saturation in the fractures has been usually overlooked in the petroleum engineering literature. However, it is possible to make such an estimate by considering the fractures as a bundle of tubes as recommended by Hilchie and Pirson. [12] Figure 4 shows the relative permeability curves for a bundle of tubes as presented by Fatt. [13] These curves indicate that the relative permeability to water is equal to the water saturation in the fractures. The problem then is to calculate the value of k_{rw} as a function of oil and water viscosities, initial water oil ratio, and initial oil formation volume factor. This can be accomplished with the use of the equation:

$$S_{wf} = k_{rw} = \frac{\mu_w \, WOR}{B_o \mu_o - \mu_w \, WOR} \qquad (7)$$

where k_{rw} = relative permeability to water, fraction
μ_w = water viscosity, cp
μ_o = oil viscosity, cp
WOR = initial water-oil ratio

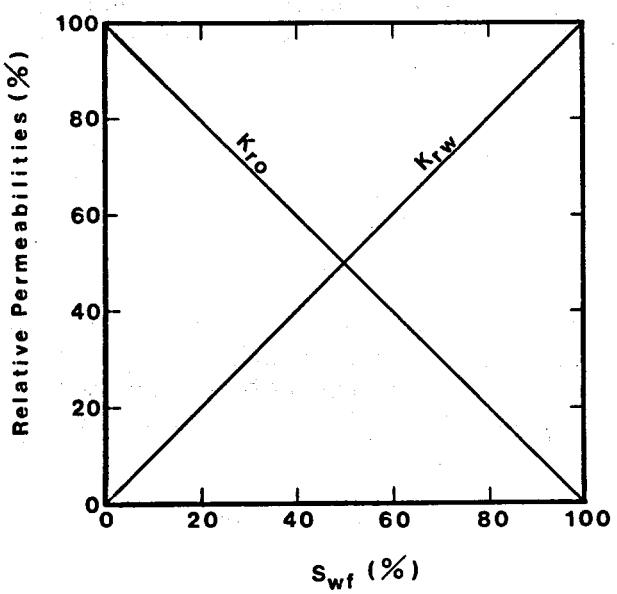

Fig. 4- Relative permeability curves for a bundle of tubes (After Fatt[13]).

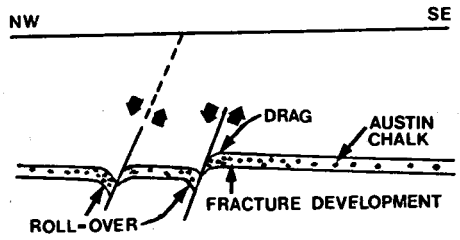

Fig. 5- Luling - Mexia type fault (After Pirson[14]).

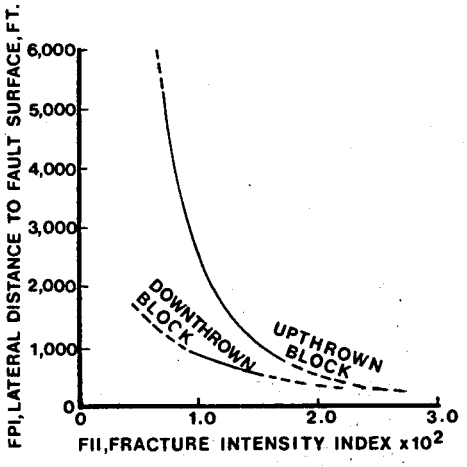

Fig. 6- Fault proximity index (FPI) as a function of fracture intensity index (FII) in chalk. (After Pirson[14]).

Equation 7 has been used to forecast initial water-oil ratios with sound results. [12] This enforces the possibility of using it to calculate initial water saturation in the fractures.

Reservoir Area

Aerial photography has been used successfully in some areas to map fracture trends. Alpay [14] has reported a field application of aerial photography in eight reservoirs of west Texas. He found that, in general, a good match was obtained between predominant fractured trends determined from aerial photography and subsurface trends derived from reservoir performance. The mapping of fractured trends from aerial photography must be carried out by experts, as man-made features such as fences, power lines, roads, pipelines, etc., may be mistaken for natural fractured trends. To avoid the previous possible mistakes, it is better to resort, whenever possible, to areas that have not been man-touched.

Other method [15] to map fracture trends makes use of a fracture intensity index derived from conventional well logs. This index has provided valuable information for estimating distance to faults in the Austin chalk of Texas and appears as a very promissory tool in the Saint Lawrence lowlands of Quebec. The fracture intensity index (FII) is defined by:

$$FII = \frac{\phi - \phi_b}{1 - \phi_b} \qquad (8)$$

The value of FII increases as a fault is approached as shown in Figure 5. From the calculated value of FII it is possible to estimate the lateral distance to a fault from a plot similar to the one show in Figure 6 for the Austin chalk. Mapping of the fractured trend permits order-of-magnitude estimates of the reservoir area.

Another promissory approach for delineation of fracture trends makes use of optical processing of remote sensor imagery. [16]

Net Pay

Conventional methods to determine net pays can be used sometimes if there is evidence that vertical fractures extend all over the section of interest. Other potential tools that may prove useful for determining fracture pay include variable intensity logs, [17] Dual Induction-Laterolog 8, [18] sonic and neutron or density logs, [18] core porosity and neutron logs, [19] borehole televiewer, [20] comparison of matrix porosity, m_b, with the double-porosity exponent, m, [9] cycle skipping, [21] SP curves, [22]

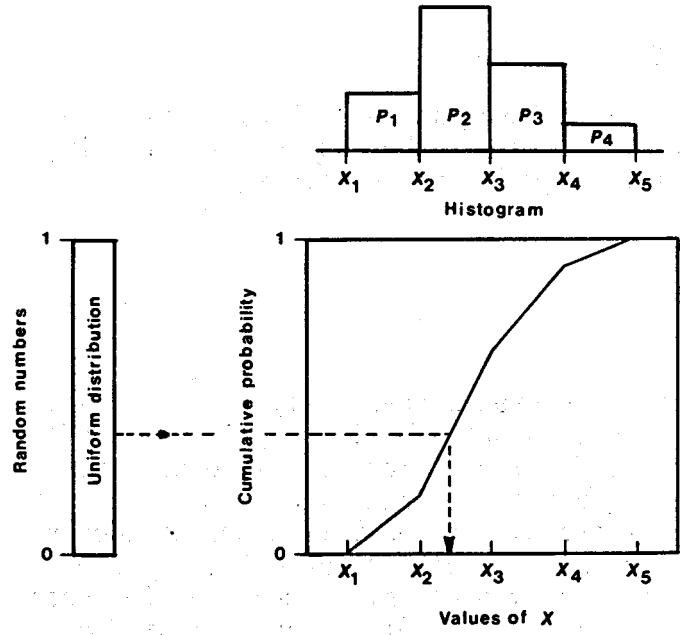

Fig. 7- Schematic of Random Selection from a Histogram Distribution.

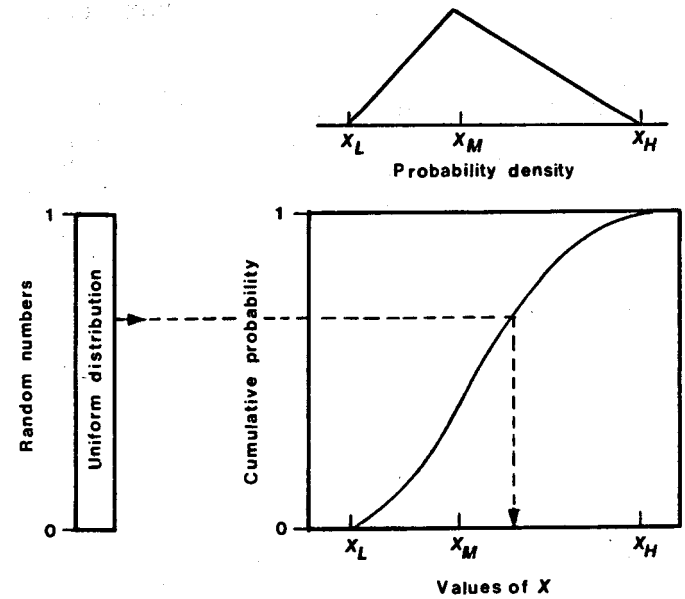

Fig. 8- Schematic of Random Selection from a Triangular Distribution.

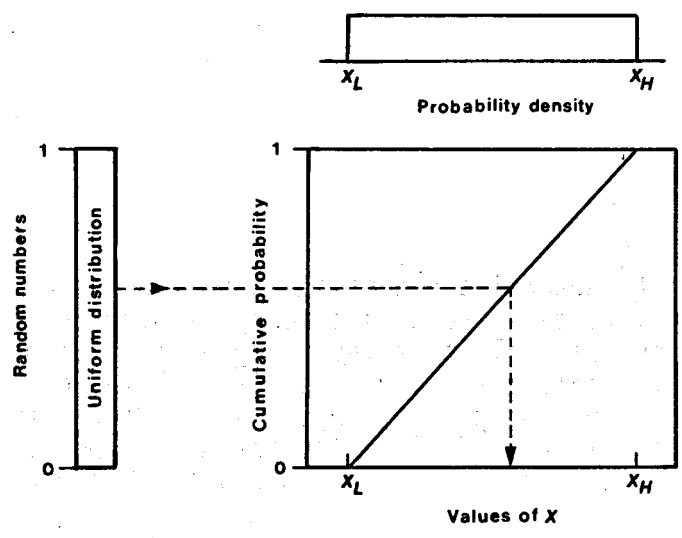

Fig. 9- Schematic of Random Selection from a Uniform Distribution (After Mc Cray[26]).

A

correction curve on the compensated density log, [23] comparison of shale volume to uranium index, [22] lithoporosity cross-plot, [24] comparison of long and short normal curves, [15] production index, [25] and temperature and sibilation logs. [25]

MEASURE OF UNCERTAINTY

The log analyst is painfully aware that the previous equations or any other set of equations to evaluate fracture reservoirs are not exact. These equations can provide meaningful information, however, if the analyst places reasonable ranges in the parameters that go into the solution of each equation. The choice of range must reflect as close as possible the present knowledge of the basic data. The analyst must also choose the best probability distribution for the data at hand. This information permits a probabilistic analysis with the use of the Montecarlo simulation technique. Essentially, a Montecarlo simulation takes the probability distributions of the input data and generates random values within the pre-established minimum and maximum values of the data. By repeating a calculation many times (for instance 100, 200 or maybe 1000 or more times) the analyst ends up with enough information to generate a plot of the various answers (for instance oil-in-place) versus probability of occurrence. The generated data permit analysts and managers to decide whether or not they like the odds.

[26,27]

Several distributions have been discussed in the literature. This paper will consider histogram, triangular and rectangle distributions.

Histogram Distribution

Experience indicates that most intergranular porosity distributions are symmetrical.[28] Consequently the histogram distribution appears as a good choice to input primary porosity when dealing with naturally fractured reservoirs. Random values from a histogram are selected as indicated in Figure 7.

Triangular Distribution

It can be used upon knowledge of the lower, most likely, and upper values of the data. The selection of random values from a triangular distribution is illustrated in Figure 8.

Rectangular Distribution

It is also referred to as uniform distribution. This type of

Fig. 10- Probability of occurrence of calculated values in example problem.

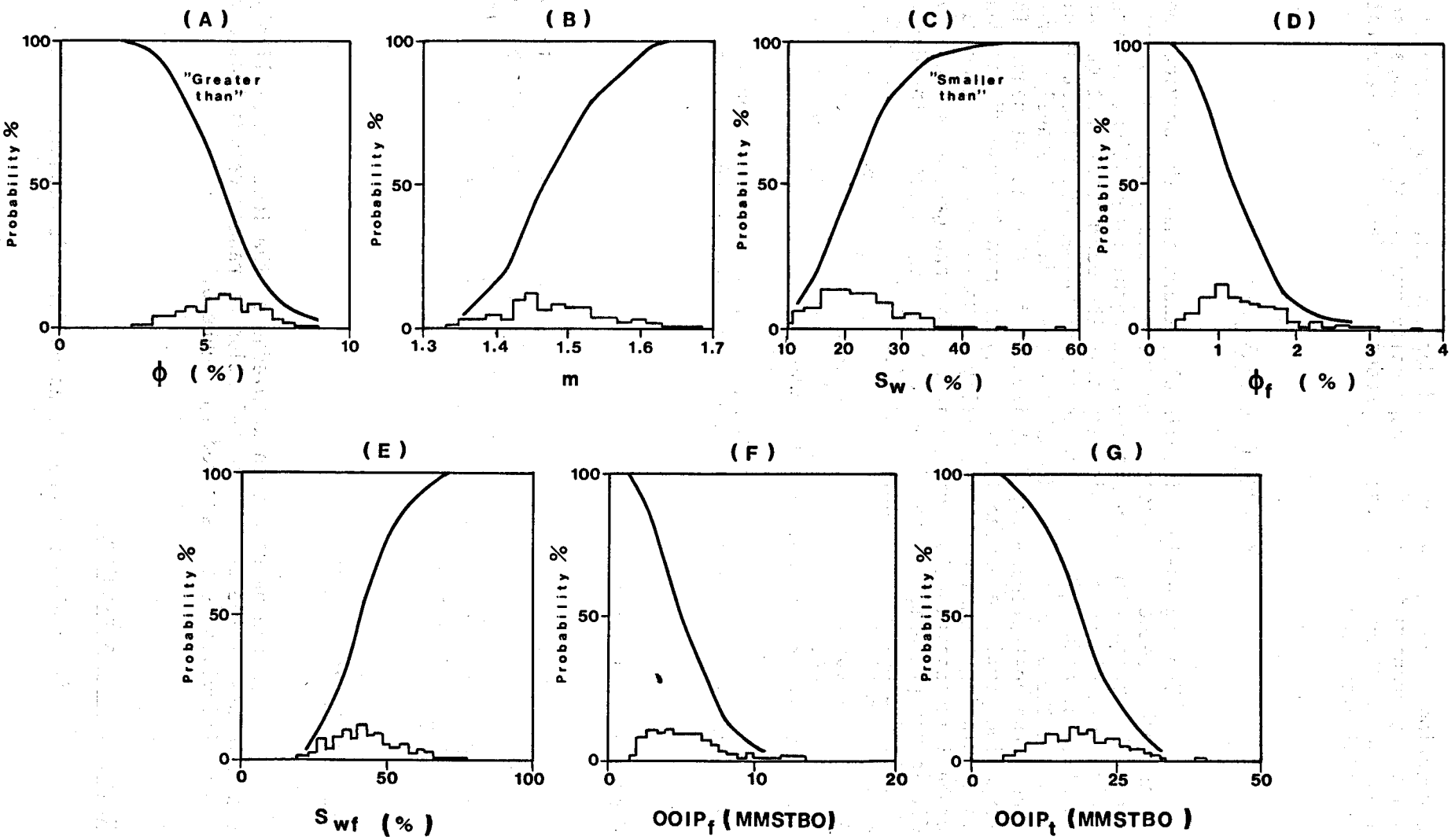

distribution is used when there is a high degree of uncertainty in the input data and only the lower and upper limits of the range are known. The selection of random values from a uniform distribution is depicted in Figure 9.

EXAMPLE

This example is designed to provide a working knowledge of how to quantify uncertainty in the evaluation of a naturally fractured reservoir. The data available for the analysis are presented below:

Parameter	Distribution	VALUES Lower	Most Likely	Higher	Sources of Data
v	Triangular	0.10	0.20	0.40	Core[7] and pressure[6] analysis
m_b	Rectangular	1.90	--	2.10	Analysis of intergranular cores
R_t	Triangular	30.00	35.00	50.00	Logs
R_w	Rectangular	0.05	--	0.07	SP Log, water analysis, R_w tables, Ø-R cross plots.
B_o	Rectangular	1.30	--	1.45	PVT analysis, empirical charts.
h	Triangular	90.00	110.00	150.00	Logs, core analysis

In addition a histogram of matrix porosity ($Ø_b$) has been constructed (Figure 2) using core data with the following results:

Matrix Porosity Interval	Frequency
.02 to .03	.10
.03 to .04	.20
.04 to .05	.40
.05 to .06	.18
.06 to .07	.12
	1.00

Values of total porosity, Ø, were calculated with the use of equation 3 and the Montecarlo simulation approach. The results are presented in Figure 10-A. The calculated total porosities range between a minimum of 2.6% and a maximum of 9.9%. Figure 10-A also indicates that there is a

50% probability that the total porosity will be 5.6% or greater, and an 80% probability that it will be greater than 4.3%.

The calculated values of the double porosity exponent, m, are presented in Figure 10-B. Note that the calculated values of m range between 1.321 and 1.678 as compared with the input m_b values which range between 1.9 and 2.1.

Figure 10-C shows that the total water saturation, S_w, varies between 9.7 and 57%. It also shows that there is a 50% chance that the water saturation is 22% or less, and an 80% probability that it will be 27% or less.

Notice that in Figure 10-A the probability of occurrence is plotted in such a form as to indicate values of porosity "greater than" a certain value. In Figure 10-C, the probability of occurrence is plotted in such a form as to indicate values of water saturation "smaller than" a certain value. This is plotted in this fashion because we are looking for the largest possible porosities and the smallest possible water saturations.

Fracture porosity is found to range between 0.47 and 3.70% as shown in Figure 10-D, and there is a 50% probability that fracture porosity is equal to or greater than 1.8%.

Values of water saturation in the fractures are calculated to range between 21 and 77% with a most likely value of 41% as shown in Figure 10-E.

The main objective of this study, i.e., the quantification of oil-in-place in the fracture system is illustrated in Figure 10-F. The variation is striking as the oil-in-place within the fractures ranges between 1.85 and 13.46 MMSTBO. There is a 50% probability that the oil-in-place will be 5.1 MMSTBO or greater. There is an 80% probability that the oil-in-place will be 3.5 MMSTBO or greater.

Finally, the total oil-in-place (matrix plus fractures) ranges between 3.6 and 40.9 MMSTBO with a 50% probability that it will be 18 MMSTBO or greater.

SUMMARY AND CONCLUSIONS

Log analysts are painfully aware that their results are not always correct. Moreover they are aware that their results are not exact, as the log analysis science and art is based upon empirical relationships. Strong uncertainty arises specially when dealing with naturally fractured reservoirs. This uncertainty can be quantitatively measured using the Montecarlo simulation approach. The set of equations presented in this paper has provided reasonable results in the author's experience. However, this or any other set of equations is imperfect and as such must be treated. It is important to quantify the amount of oil-in-place within the fracture system to make sound projections of reservoir life.

High initial oil rates in naturally fractured reservoirs are the result of oil stored within the fractures. Strong production declines may arise when the fracture network is depleted, depending on the rate with which oil bleeds-off from the matrix into the fractures.

It is concluded that better decisions can be made regarding naturally fractured reservoirs if the uncertainty of calculating oil-in-place is quantitatively measured.

REFERENCES

1. McNaughton, D.A., and Garb, F.A.: "Finding and Evaluating Petroleum Accumulations in Fractured Reservoir Rock," Proceedings of the Southwestern Legal Foundation, Exploration and Economics of the Petroleum Industry, volume 13, Copyright 1975 by Matthew Bender & Company, Inc., New York, New York.

2. Beach, J.H.: "Geology of Edison Oil Field, Kern County, California," in Structure of Typical American Oil Fields, Amer. Assoc. Pet. Geol., Tulsa, Oklahoma (1948) 3, 58-85.

3. Porter, L.E.: "El Segundo Oil Field, California," Trans. AIME (1943) 127, 451.

4. Smith, J.E.: "Basement Reservoir of La Paz-Mara Oil Fields, Western Venezuela," Bull. Am. Assoc. Pet. Geol. (February, 1956) 40, 380-385.

5. Harp, L.J.: "Do not Overlook Fractured Zones," World Oil (April, 1966) 119-123.

6. Pirson, S.J.: "Petrophysical Interpretation of Formation Tester Pressure Build-Up Records," Trans. SPWLA (May 17-18, 1962).

7. Locke, L.C., and Bliss, J.E.: "Core Analysis Technique for Limestone and Dolomite," World Oil (Sept., 1950) 204.

8. Aguilera, Roberto: "Analysis of Naturally Fractured Reservoirs from Sonic and Resistivity Logs," J. Pet. Tech. (Nov., 1974) 1233-1238.

9. Aguilera, Roberto "Analysis of Naturally Fractured Reservoirs From Conventional Well Logs," J. Pet. Tech. (July, 1976) 764-772.

10. Archie, G.E.: "The Electrical Resistivity Log as an Aid in Determining Some Reservoir Characteristics," Trans., AIME (1942) 146, 54-67.

11. Coates, G.R., and Dumanoir, J.L.: "A New Approach to Improve Log-Derived Permeability," Trans. SPWLA, Lafayette-Lousiana (May 6-9, 1973).

12. Hilchie, D.W., and Pirson, S.J.: "Water Cut Determination from Well Logs in Fractured and Vuggy Formations," Trans. SPWLA, Dallas, Texas (May 18-19, 1961)

13. Fatt, I.: "The Network Model of Porous Media, II, Dynamic Properties of a Single Size Tube Network," Trans., AIME (1956) 207, 160-163.

14. Alpay, O.A.: "Application of Aerial Photographic Interpretation to the Study of Reservoir Natural Fracture Systems," Paper SPE 2567 presented at the 44th Annual Meeting of the SPE of AIME, Denver, Colorado (Sept. 28 - Oct. 1, 1969).

15. Pirson, S.J.: "How to Map Fracture Development from Well Logs," World Oil (March, 1967) 106-114.

16. Rabshevsky, G.A.: "Optical processing of Remote Sensor imagery," Proceeding of the Seventh Appalachian Petroleum Geology Symposium held at Morgantown, W. Va. (March 1-4, 1976) 100.

17. Walker, Terry: "Progress Report on Acoustic Amplitude Logging for Formation Evaluation," paper SPE 451 presented at the 37th Annual Fall Meeting of the SPE of AIME in Los Angeles, California (Oct., 1962).

18. Log Interpretation Principles - Schlumberger - Chapter 18, p. 105 (1973).

19. Pickett, G.R. and Reynolds, E.B.: "Evaluation of Fractured Reservoirs," Soc. Pet. Eng. J. (March, 1969) 28.

20. Zemanek, J., Caldwell, R.L., Glenn, E.E., Holcomb, S.V., Norton, L.J., and Strauss, A.J.D.: "The Borehole Televiewer - A New Logging Concept for Fracture Location and Other types of Borehole Inspection," J. Pet. Tech. (June, 1969) 762-774.

21. Pickett, G.R.: "Acoustic character Logs and Their Applications in Formation Evaluation," Trans. AIME (1963) 228, 659-667.

22. Heflin, J.D., Neill, B.E., and DeVries, M.R.: "Log Evaluation in the California Miocene Formations," paper SPE 6160 presented at the 51th Annual Meeting of SPE of AIME held in New Orleans (Oct., 1976).

23. Beck, J., Schultz, A., and Fitzgerald, D.: "Reservoir Evaluation of Fractured Cretaceous Carbonates in South Texas," Trans. SPWLA (1977) paper M.

24. Burke, J.A., Campbell, R.L., and Schmidt, A.W.: "The Litho-Porosity Cross-Plot," Trans. SPWLA (1969).

25. Myung, J.I.: "Fracture Investigation of the Devonian Shale Using Geophysical Well Logging Techniques," Proceeding of the 7th Appalachian Petroleum Geology Symposium held at Morgantown, W. Va. (March 1-4, 1976).

26. McGray, A.W.: Petroleum Evaluations and Economic Decisions, Prentice-Hall, Inc. Englewood Cliffs, New Jersey (1975) 201.

27. Walstron, J.E., Mueller, T.D., and Mc Farlane, R.C.: "Evaluating Un-

certainty in Engineering Calculations," J. Pet. Tech. (Dec. 1967) 1595.

28. Amyx, J.W., Bass, D.M., and Whiting, R.L.: Petroleum Reservoir Engineering - Physical Properties, McGraw-Hill Book Company, New York, Toronto, London (1960) 538.

ACKNOWLEDGEMENT

The author thanks the management of SOQUIP for permission to publish this paper.

ABOUT THE AUTHOR

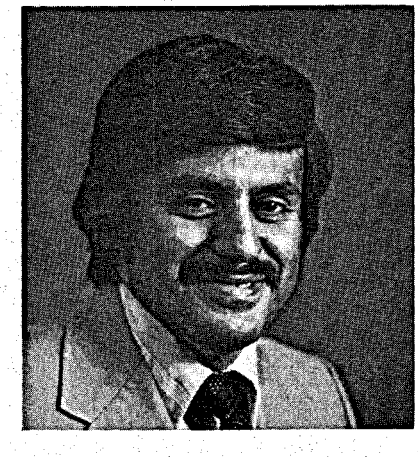

Roberto Aguilera is Chief of Production and Reservoir Engineering of Société Québécoise d'Initiatives Pétrolières (SOQUIP) in Quebec, Canada. He is a Petroleum Engineer graduate of the Universidad de America at Bogota, Colombia, and holds Master's and Ph.D. degrees in petroleum engineering from the Colorado School of Mines. Previously he worked for various international petroleum companies in Colombia, the United States and Argentina. He is a member of SPWLA, SPE of AIME and the Colombian Society of Petroleum Engineers (ACIPET). Presently he is serving on the Publications Committee of The Log Analyst and the Technological Committee of SPWLA.

THE DETERMINATION OF PRIOR DEPTH OF BURIAL (UPLIFT AND EROSION) USING INTERVAL TRANSIT TIME

B

By William H. Lang, Jr.
Union Oil Company of California

ABSTRACT

In 1930 a relationship was suggested between the observed compaction of shale sediments and the depth of burial. It was suggested that in disturbed areas this would be useful for the determination of the maximum depth of burial.

Various researchers have directly and indirectly used this concept in relating interval transit time-porosity-depth of burial. The author describes a method to construct a transit time-depth plot (TDP) for a given well, taking a number of wells and assembling a type compaction gradient for a given sedimentary basin.

The compaction gradient on the TDP on each well within the basin is compared to the type gradient for the basin, and the relative amount of uplift (prior depth of burial) is determined. It then becomes possible to better recreate the paleo-basin and the probable sequence of geologic events.

INTRODUCTION

In 1930 Athy stated: "If a definite relation were established between compaction and depth of burial, it would be possible to determine the maximum depth to which shales in any undisturbed area had once been buried." Athy physically measured the density of over 2,200 shale samples in Northeastern Oklahoma and parts of Texas and established a compaction (density or porosity) - depth relation. One of his most important conclusions was: "By applying the compaction - depth data derived...it is estimated that the eroded overburden is 4,000 - 4,500 feet." Athy was able to determine prior depth of burial and subsequent uplift and erosion from shale density data.

This concept should be extremely useful to exploration geologists in recreating the geologic events in many sedimentary basins. It may possibly answer the question: Is a particular stratigraphic unit missing because of nondeposition or is it absent because of uplift and erosion? Athy is remembered more for indicating that porosity decreases with depth rather than these aspects of his work.

Open hole resistivity well logs were being introduced to the industry in 1930, and Athy's technique depended upon the physical recovery of rock

samples and the measurement of parameters beyond the capability of the logging service companies. It was later recognized by Faust (1951) that seismic velocity was apparently a function of depth and geologic time. Figure 1 (Faust) indicates the relation of interval velocity plotted against depth for geologic age groupings.

In 1953 Faust included a lithologic factor in his velocity function. He minimized geologic time as an important consideration in his reference to Heiland's (1940) statement: "An increased age merely increases the probability that it (the strata) has undergone a greater degree of dynamometamorphism." Hedberg, 1936, had covered that by repeating, "...the porosity of the well-known Cambrian clays of Finland and Russia is relatively high."

The reciprocal of interval velocity, i.e., interval transit time was found to be useful for disciplines other than seismology. Wyllie, et al., determined a relationship between interval transit time and porosity through the time-average equation. This relation is now used by the various service companies in the determination of porosity from elastic wave-type well logs. Porosity computations from the time-average equation are reasonably accurate under certain circumstances. Sarmiento (1961) described some of the geological factors which should be considered for a precise porosity-transit time relationship. These are: "Age, composition, tectonic history (compaction), shaliness, and type of fluid in its pores."

The reference in Sarmiento's paper to tectonic history and compaction is the first intimation that interval transit time is modified by "...the degree of tectonism." Allied to this line of thought, the effect of depth was considered to be an important factor. Figure 2 shows Tertiary and Cretaceous sandstones in Wyoming and Alberta and the transit time-depth relation. Thirty years prior to the above paper, Athy had demonstrated the relationship between density, porosity, and depth of burial. Sarmiento did not cite Athy in his work and may not have been aware of the parallelism of their effort regarding tectonic implication.

In 1962 Jankowsky used interval transit time-porosity and related them to the reconstruction of the structural history of a basin. He wrote, "...customary methods fail when the reference planes have been eroded by uplifting. It is fortunate that diagenesis imparted to the sediments primarily physical changes..." "Considerable research has brought about the knowledge of the theoretical and practically irreversible decrease of rock porosity with increasing depths as the result of the increase in overlying pressure." Apparently, Jankowsky also was not aware of Athy's work. He used the same procedure, but derived the data from transit time measurements rather than core samples. The porosity of clay and claystone was used because they "...most easily permit the exclusion of other complicating factors." Jankowsky used the porosity-burial-uplift relationship to construct maps showing "residual lifting". In other words, the amount of uplift not reversed by subsequent subsidence.

Philip, et al., (1963) used the transit time-porosity-depth relationship

to aid in the reconstruction of the geological history of the Gifhorn Trough. Maximum depth of burial was determined using a transit-time-porosity relation in shales. Pennebaker (1968) showed a family of normal compaction lines, Figure 3, that was related to the age of Gulf Coast sediments. He noted a "shift from inland, older sediments to more recent, less compacted sediments..." If this is taken a step further in a conformable sedimentary sequence, a stair step compaction profile might be expected such as Figure 4. A stair step decrease in transit time, however, has not been seen in any of the Tertiary basins along the West Coast and Circum-Pacific Area.

Interval transit time in a California Basin at the top of the Pliocene, Miocene, and Oligocene from forty-nine horizons was plotted versus depth on log paper, Figure 5. There is very little difference in the Pliocene and Miocene, but the Oligocene points show a scatter apart from the trend. It is difficult to infer families of curves for different age rock, although the Oligocene, as mentioned, does show significantly lower transit times but in a shot gun pattern.

Where the sedimentary sequence is conformable and has not been greatly disturbed by tectonics no stair step velocity change has been noted in the field. A fairly large change in transit time or velocity frequently may be seen at major unconformity surfaces. Figure 6 shows a well in the Ventura Basin that penetrated a conformable section from recent sediments through the lower Miocene. The only step that can be inferred is the one at the base of the Monterey Formation where a change of 10 microseconds may be seen. This change is more due to the complex lithology encountered in the Monterey.

Interval transit time has been used by Magara (1976) in several different ways. His paper outlined a process to determine the thickness of removed sedimentary rocks in Canada. In previous work Magara worked with porosity derived from transit time logs--but uses transit time directly in this latest paper. This is an improvement in technique due to the geological factors described by Sarmiento in relating transit time to porosity.

A transit time-depth plot (TDP) may be constructed in several different ways. Basically, values of transit time in shales are plotted logarithmically against linear depth. A computer program has been written to automatically make this plot. The Denson Program (Serra, et al., 1975) using shale indicators from well logs, records a high density of transit time from shale sections semi-logarithmically.

Although Magara (1976) is not specific, an inspection of the figures in his paper indicates that he is taking between ten and twenty values per 1,000 feet. The author constructs a TDP by taking two or more values in shales at 50-foot intervals. All of the shale discriminators are used but frequently only the SP and resistivity curves are available. This plot can be made manually or by the computer if the logs have been digitized. Shales are used for compaction studies rather than sands to eliminate possible

porosity and gas effects. (In many of the "relatively" quartz deficient sandstones in the West Coast the sandstones "compact" at the same rate as do the shales.)

CONSTRUCTION OF THE TYPE COMPACTION GRADIENT

In a tectonically active sedimentary basin, wells will frequently encounter low transit time (high interval velocity) at an abnormally shallow depth. Figure 7 shows transit time depth plots on wells in a California Tertiary Basin. The arrows show the intersection of the transit time in the shales at 100 microseconds with depth. Plotting the log of transit time versus linear depth produces a straight line fit of the shale points on all of the wells. This line then becomes the compaction gradient for that particular well. Projecting the fit to the surface on Wells A and E gives a value of approximately 189 microseconds or an interval velocity of 5,300 feet per second. This is fluid velocity and probably close to the velocity of a clay slurry which has not been subjected to burial.

With burial the clay sediments are subjected to the mechanical, thermal, and chemical changes associated with increasing depth of burial. Wells A and E show gradually decreasing transit times from the approximate value of fluid velocity at the surface. This decrease is considered to be "normal" in Wells A and E with the possible exception of slight overpressure which may be encountered at 12,000 feet in Well A. "Normal" in this context means that only subsidence and deposition has taken place with no subsequent uplift and erosion.

Arrows denote the depth of 100 microseconds on Wells A through E. On the "normal" wells this depth is at 10,000 feet, while the depth to 100 microseconds in Wells B, C, and D is at 9,000, 5,000, and 2,000 feet respectively. It is possible to take segments of the TDP on each well and composite them to produce a type compaction gradient. In much the same manner as a type geologic section is compiled from measured outcrop sections around a basin, a type compaction gradient may be constructed from transit time logs run on wells drilled in a tectonically active basin, as shown by Figure 8. Followed to the logical conclusion it can be inferred that there has been 2,000 feet of uplift and erosion in Well B, 7,000 feet in Well C, and 9,500 feet in Well D.

Usually in most sedimentary basins no well ever penetrates the entire section in the center of the basin, so that it is necessary to construct a type gradient as in Figure 8. A geologic section of over 19,000 feet was put together in this basin. The deepest well available is Well E and when superimposed on the type gradient, as in Figure 9, an excellent agreement may be noted.

INTERPRETATION OF THE TDP

An application of this concept is illustrated by Figures 10 and 11. In the same California basin where the type compaction gradient was constructed, two

wells were drilled approximately four miles apart. The TDP on each well is shown by Figure 8. Paleontological control indicates a correlative marker at about 13,500 feet in Well K and at 1,500 feet in Well J for a 12,000 foot structural difference. The paleo data indicates that the marker in both wells was deposited in an environment with a water depth of at least 6,000 feet (now found at a depth of 1,500 feet in Well J).

Compaction gradients were drawn on the TDP of Wells K and J and it was found that the transit time at the II-5 marker was 86 microseconds in Well K and 122 microseconds in Well J. Comparing these transit times to the type gradient for the basin, Figure 8, it can be determined that the correlative marker in Well K has experienced no discernible uplfit. On the other hand 122 microseconds at 1,500 feet in Well J occurs at 6,200 feet on the compaction gradient. Figure 11 shows both of these wells at their maximum depth of burial. At the maximum depth of burial Well J is 7,300 feet higher than Well K rather than the present 12,000 foot structural difference.

A reconstruction of the geologic history of these wells would be as follows:

> The II-5 marker was deposited in 6,000 feet of water. Paleo data indicates a gradual shallowing of the depositional environment in the sediments above the II-5 marker. Well J received 6,200 feet of sediments deposited above the II-5 marker.
>
> Well K continued subsiding and receiving deposition, while Well J was uplifted 4,700 feet with that amount of sediment eroded.

The preceding example indicates that a structural difference of 12,000 feet was caused by a combination of subsidence in the one well and uplift in the other. Interval transit time and the use of type compaction gradient allowed that interpretation to be made.

A further example from another West Coast Basin shows an entirely different burial-uplift relationship. Well P and Well Q are ten miles apart. The TDP on these wells is shown on Figure 12. Paleontological control indicates that Well P is 1,700 feet structurally higher than Well Q.

A compaction gradient was fitted to each well and iso-transit times were connected. It may be seen that the iso-transit time lines parallel the paleo control points. A reconstruction of the geologic history is as follows:

> The "F-marker" and "F-2" zones were deposited and buried to an equivalent depth. After burial and compaction, Well P was uplifted 1,700 feet more than Well Q. The structural difference in this example is due entirely to uplift rather than uplift and subsidence as shown in the preceding example.

It is interesting to note that paleontological data indicates several unconformities that are present in these wells. The unconformities show up clearly

in Well P at the breaks in the compaction gradient. The unconformities are not to apparent, however, on the Well Q TDP. Another use of the TDP is the overpressure indication at 5,700 feet in Well P.

EFFECT OF CHEMICAL AND TEMPERATURE DIFFERENCES

Depth of burial provides the necessary factors or environment for the metamorphism of sand and shale sediments. There is evidence that high heat flow is of maximum importance in the depth of burial-compaction regime. Muffler and White (1969) describe the transformation of sedimentary rocks in two areas in the Salton Trough. Rocks of the same age and type in these areas in the trough are undergoing similar low-grade metamorphism. In the Salton Sea Geothermal Field, there is an extremely high heat flow. The sediments show a higher degree of metamorphism at a shallower depth than the sediments in the well in the lower heat flow area. Figure 13, a TDP on a well within the field (high heat flow), illustrates the heat effect. From 1,600 - 3,900 feet a great decrease in transit time may be noted, with relatively little change below that point. The temperature gradient in the field is on the order of 12°F/100'.

Bradley (1975) holds that the loss of porosity with depth appears to be a chemical process rather than a mechanical compression. It does appear as mentioned, that there is a greater decrease in interval transit time per foot of depth in basins with a high temperature gradient in comparison to a basin with lower temperature gradients. Care must be exercised in determining prior depth of burial by insuring that the temperature gradient is relatively the same within the area studied. Higher heat flow tends to accelerate the "compaction" process and can cause erroneous assumptions.

CONCLUSION

The reconstruction of past geologic events is frequently hampered by missing section. It is of importance to determine whether the section is missing due to nondeposition or missing due to uplift and erosion. Structures may be formed by crestal uplift, synclinal subsidence, or a combination. Present day structural position may not reflect the past structure. The concept presented herein, should allow the geologist to more accurately reconstruct the paleo basin.

B

REFERENCES

Athy, L.F., 1930, Density, porosity, and compaction of sedimentary rocks: AAPG Bull., v. 14, No. 1, pp. 1-24.

Bradley, J.S., 1975, Abnormal formation pressure: AAPG Bull., v. 59, pp. 957-973.

Faust, L.Y., 1951, Seismic velocity as a function of depth and geologic time: Geophysics, v. XVI, No. 2, pp. 192-206.

_____, 1953, A velocity function including lithologic variation: Geophysics v. XVIII, No. 2, pp. 271-288.

Hedberg, H.D., 1936, Gravitational compaction of clays and shales: Am. Jor. of Science, v. 31, No. 184, pp. 241-287

Heiland, C.A., 1940, Geophysical Exploration: Prentice-Hall, 475 p.

Jankowsky, W., 1962, Diagenesis and oil accumulation as aids in the analysis of the structural history of the Northwestern German Basin: Zeitschrift der Deutschen Geologischen Gesellschaft, v. 114, pp. 452-460.

Magara, K., 1976, Thickness of removed sedimentary rocks, paleopore pressure, and paleotemperature, southwestern part of Western Canada basin: AAPG Bull., v. 60, No. 4, pp. 554-565.

Muffler, L.J.P. and White, D.E., 1969, Active metamorphism of upper Cenozoic sediments in the Salton Sea Geothermal Field and the Salton Trough, Southeastern California: GSA Bull., v. 80, pp. 157-182.

Pennebaker, E.S., 1968, The use of geophysics in abnormal pressure applications: SPE, September 29-October 2.

Philip, W., et al., 1963, The history of migration in the Gifhorn Trough (NW-German): Frankfurt, Germany, Sixth WPC.

Sarmiento, R., 1961, Geological factors influencing porosity estimates from velocity logs: AAPG Bull., v. 45, No. 5, pp. 633-644.

Serra, O., et al., 1975, Automatic study of clay compaction: The Denson program: The Log Analyst, July-August.

Wyllie, M.R.J., et al., 1956, Elastic wave velocities in heterogeneous and porous media: Geophysics, v. 21, No. 1, pp. 41-70.

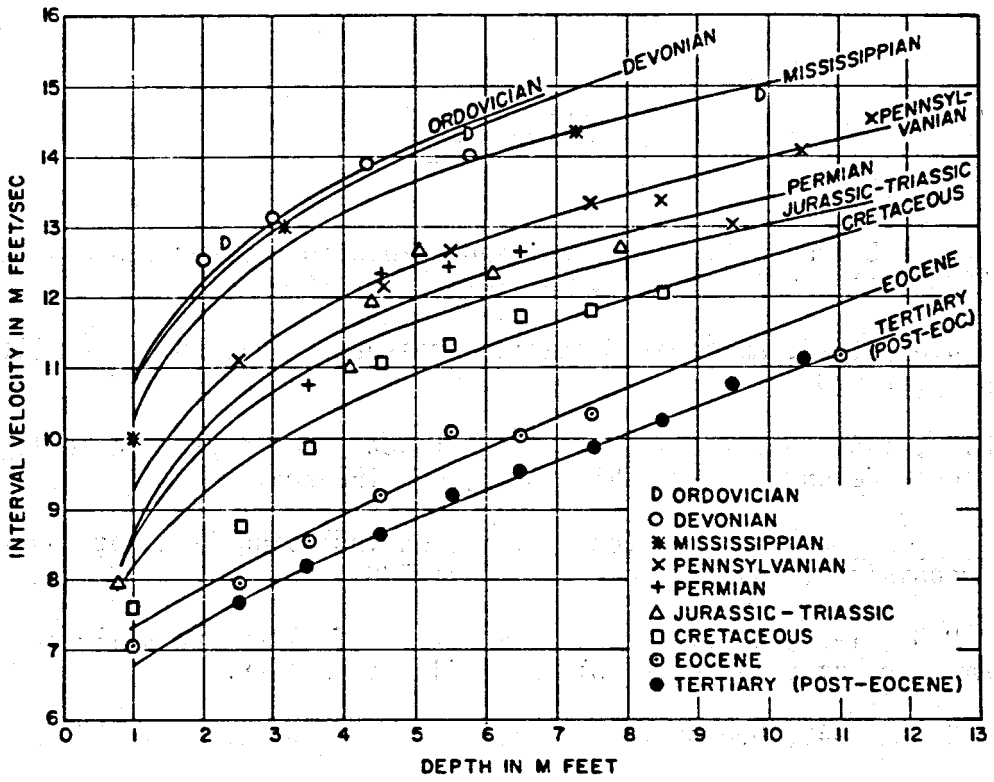

Figure 1 - after Faust

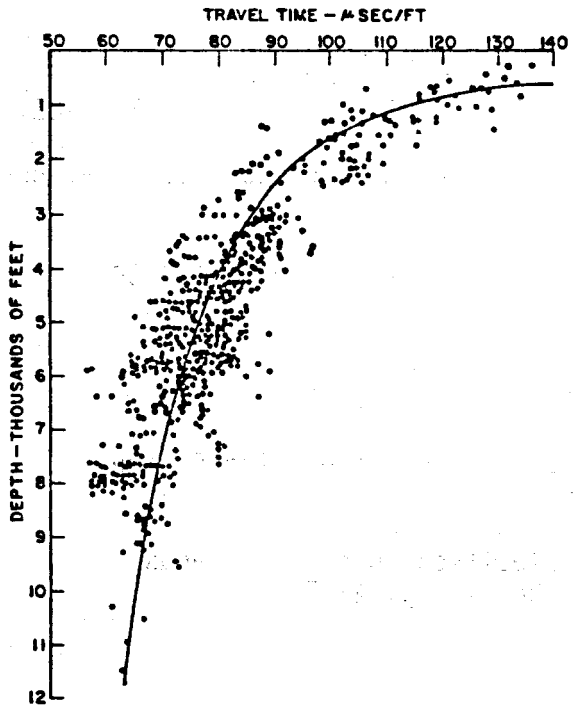

Figure 2 - after Sarmiento

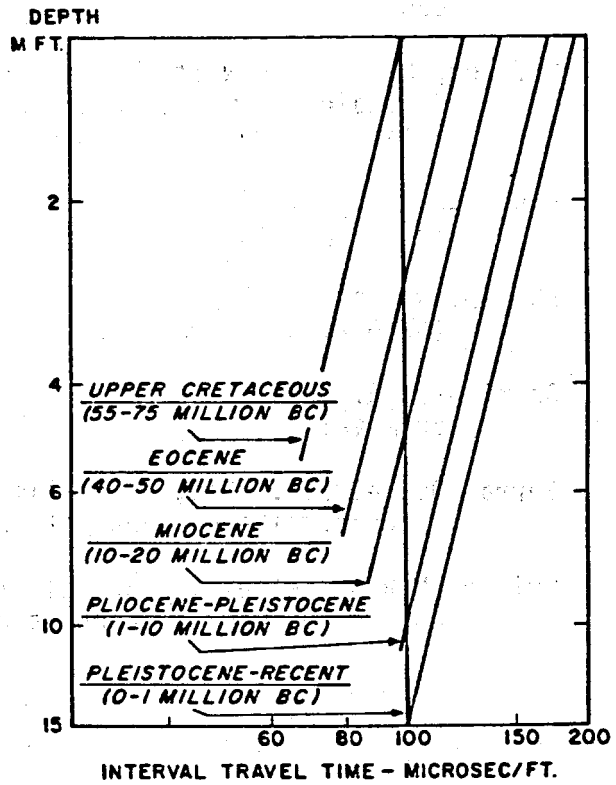

Figure 3 - after Pennebaker

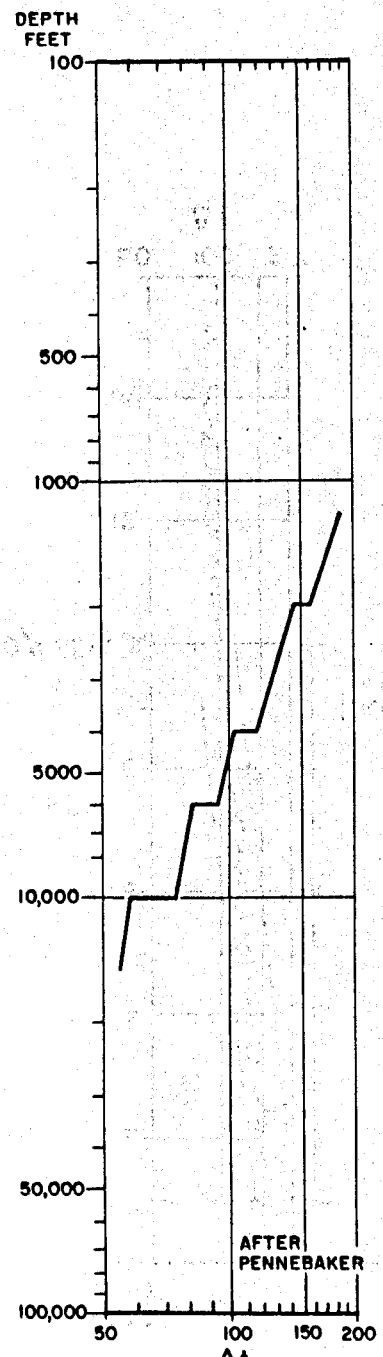

Figure 4

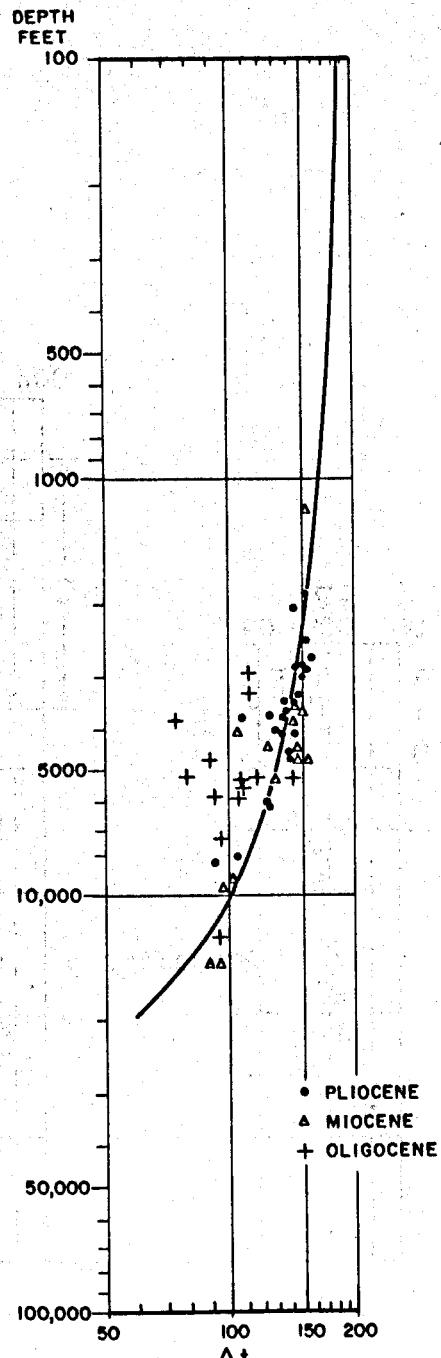

Figure 5

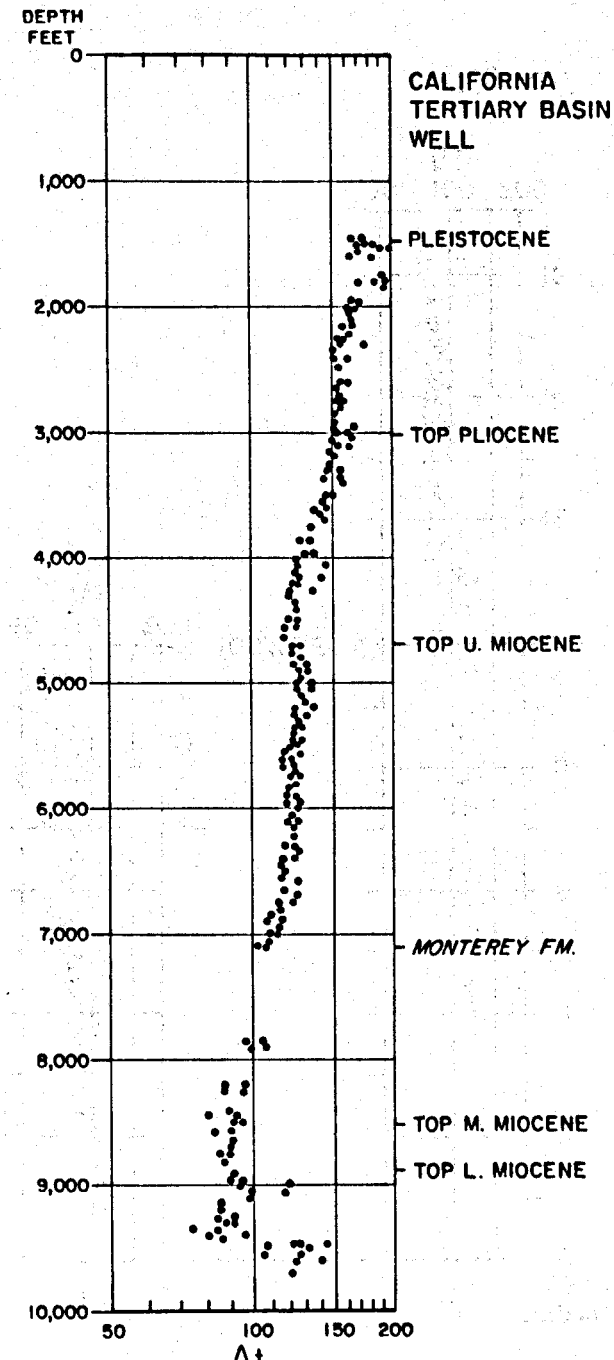

Figure 6

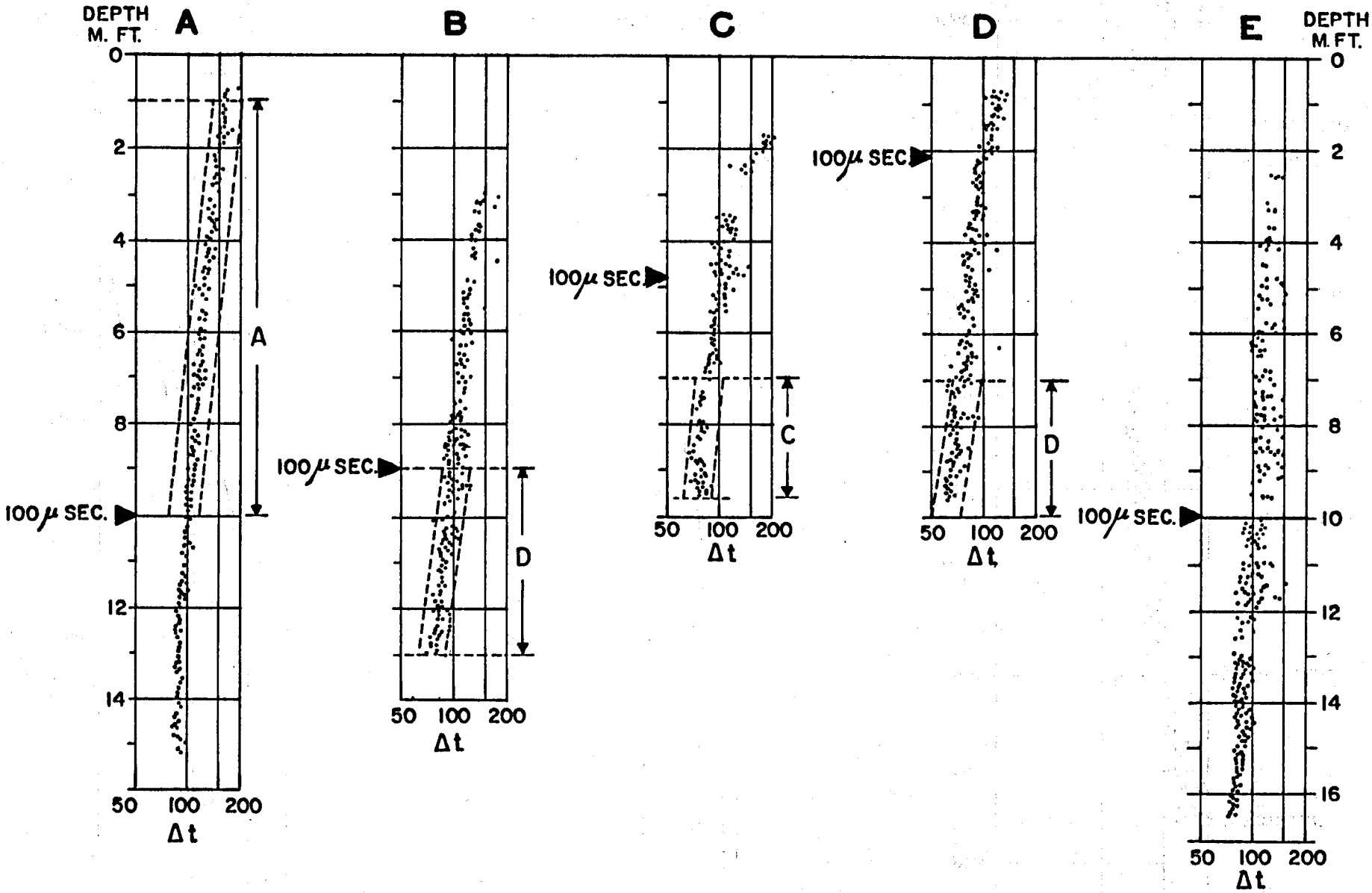
DEPTH M. FT.
A
B
C
D
E
DEPTH M. FT.
0
2
4
6
8
10
12
14
16
100μ SEC.
A
D
C
D
50 100 200
Δt

Figure 7

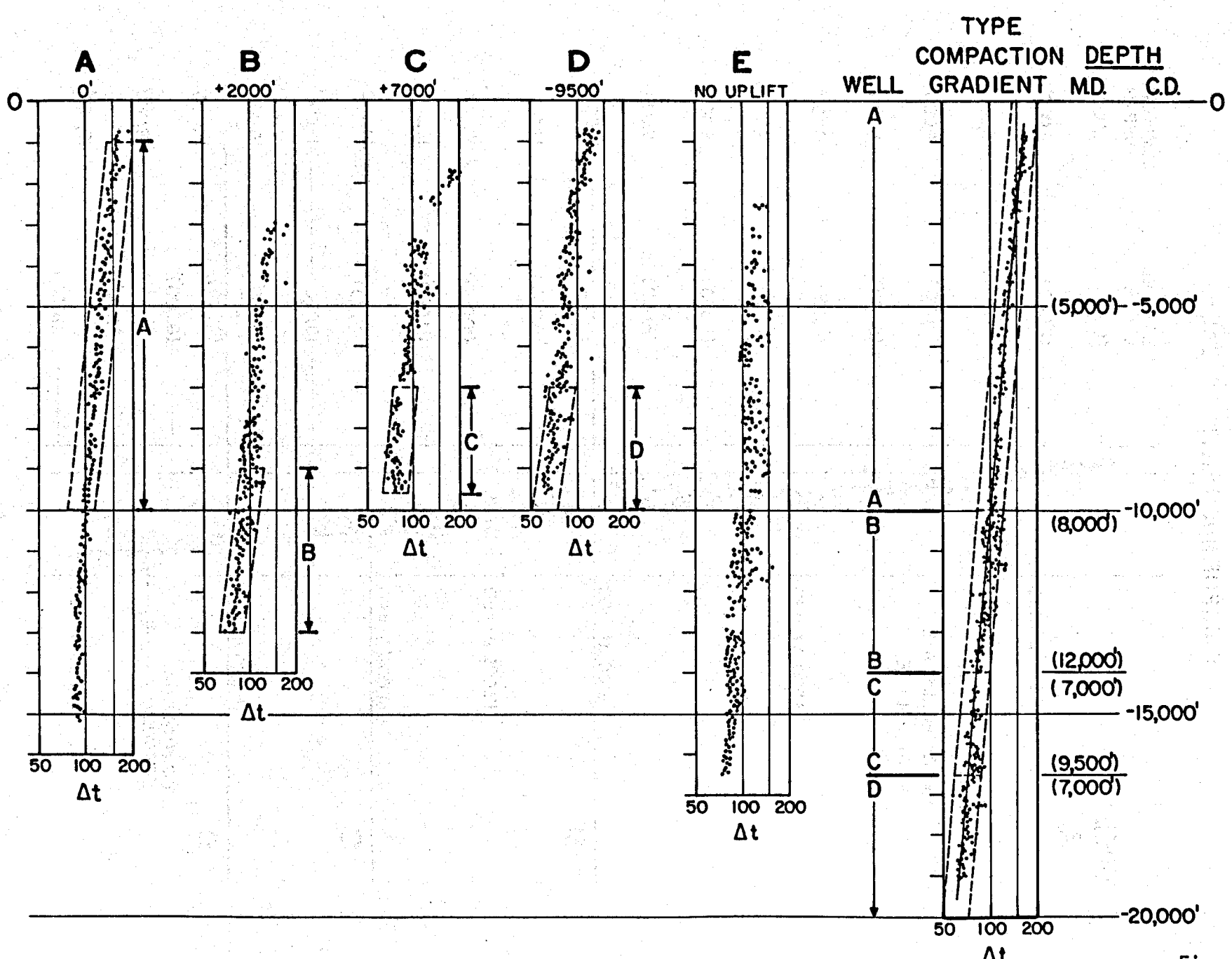
A
0'
B
+2000'
C
+7000'
D
-9500'
E
NO UPLIFT
TYPE
COMPACTION DEPTH
WELL GRADIENT M.D. C.D.
0
A
B
C
D
50 100 200
Δt
(5,000')
-5,000'
(8,000')
-10,000'
(12,000')
(7,000')
-15,000'
(9,500')
(7,000')
-20,000'

Figure 8

TYPICAL COMPACTION GRADIENT
CALIFORNIA TERTIARY BASIN

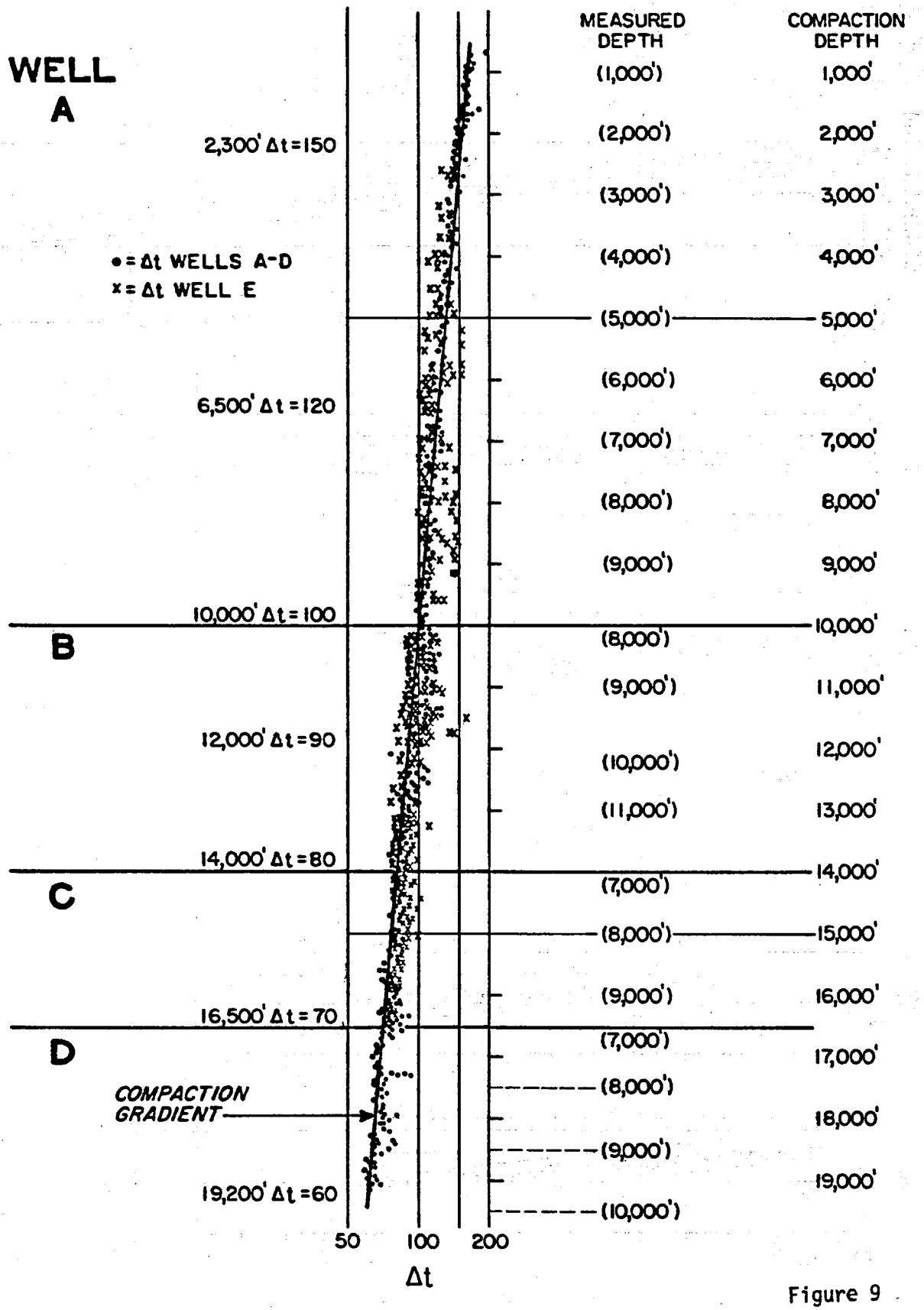

Figure 9

B

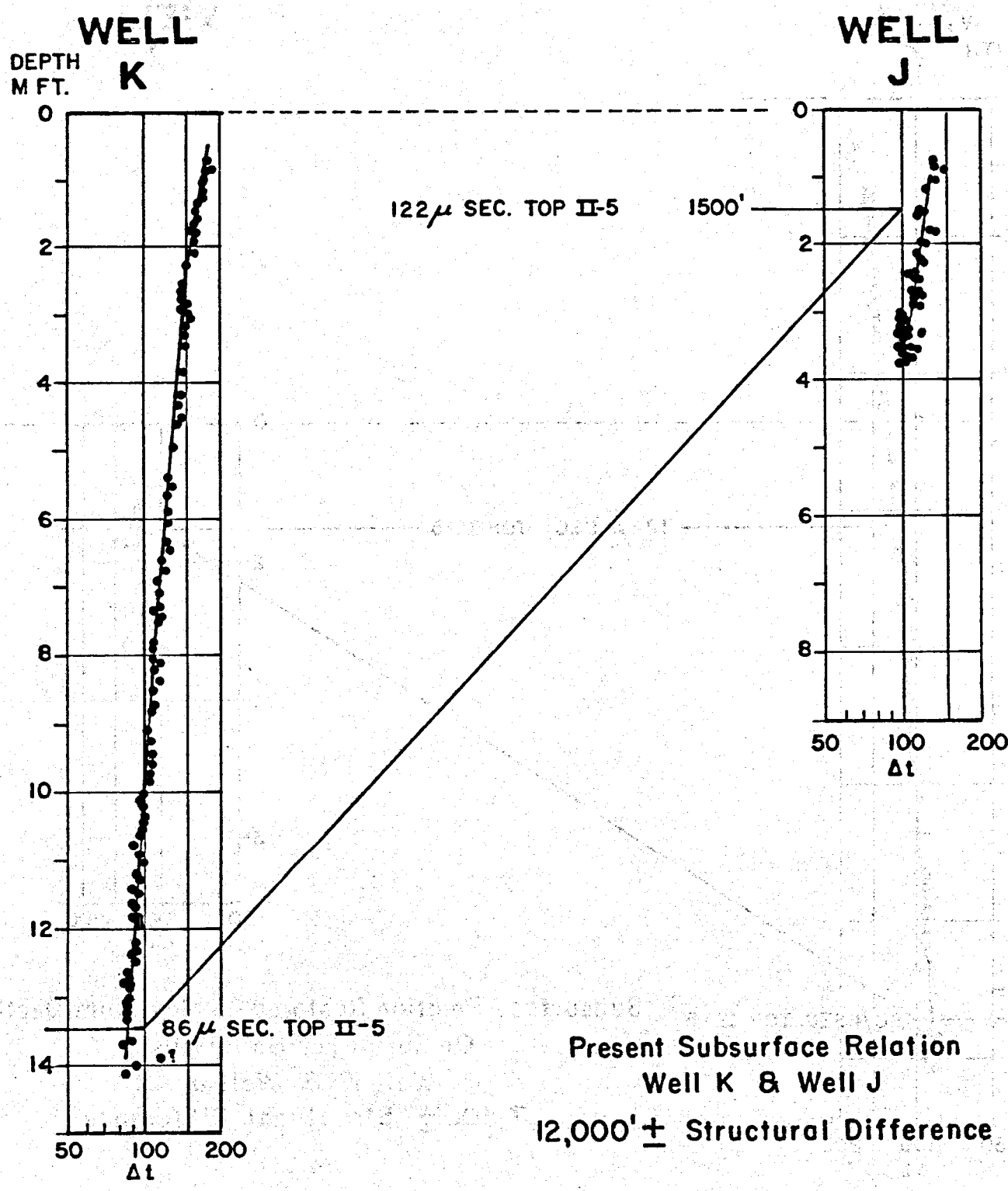
WELL
K
DEPTH
M FT.
0
2
4
6
8
10
12
14
50
100
200
Δt
122μ SEC. TOP II-5
86μ SEC. TOP II-5
WELL
J
1500'
0
2
4
6
8
50
100
200
Δt
Present Subsurface Relation
Well K & Well J
12,000'± Structural Difference

Figure 10

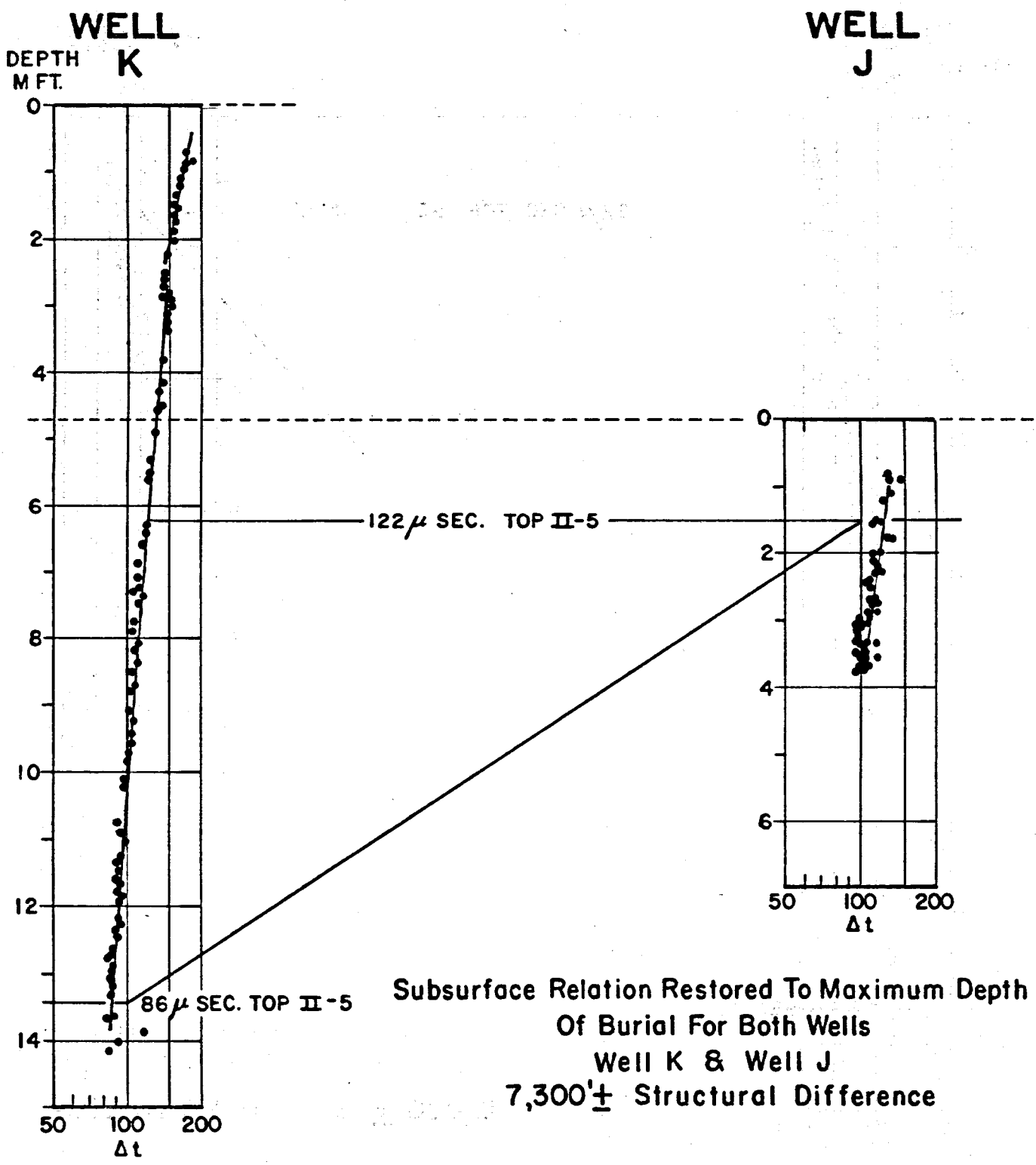
WELL
K
DEPTH
M FT.
0
2
4
6
8
10
12
14
50
100
200
Δt
WELL
J
0
2
4
6
50
100
200
Δt
122μ SEC. TOP II-5
86μ SEC. TOP II-5
Subsurface Relation Restored To Maximum Depth
Of Burial For Both Wells
Well K & Well J
7,300'± Structural Difference

Figure 11

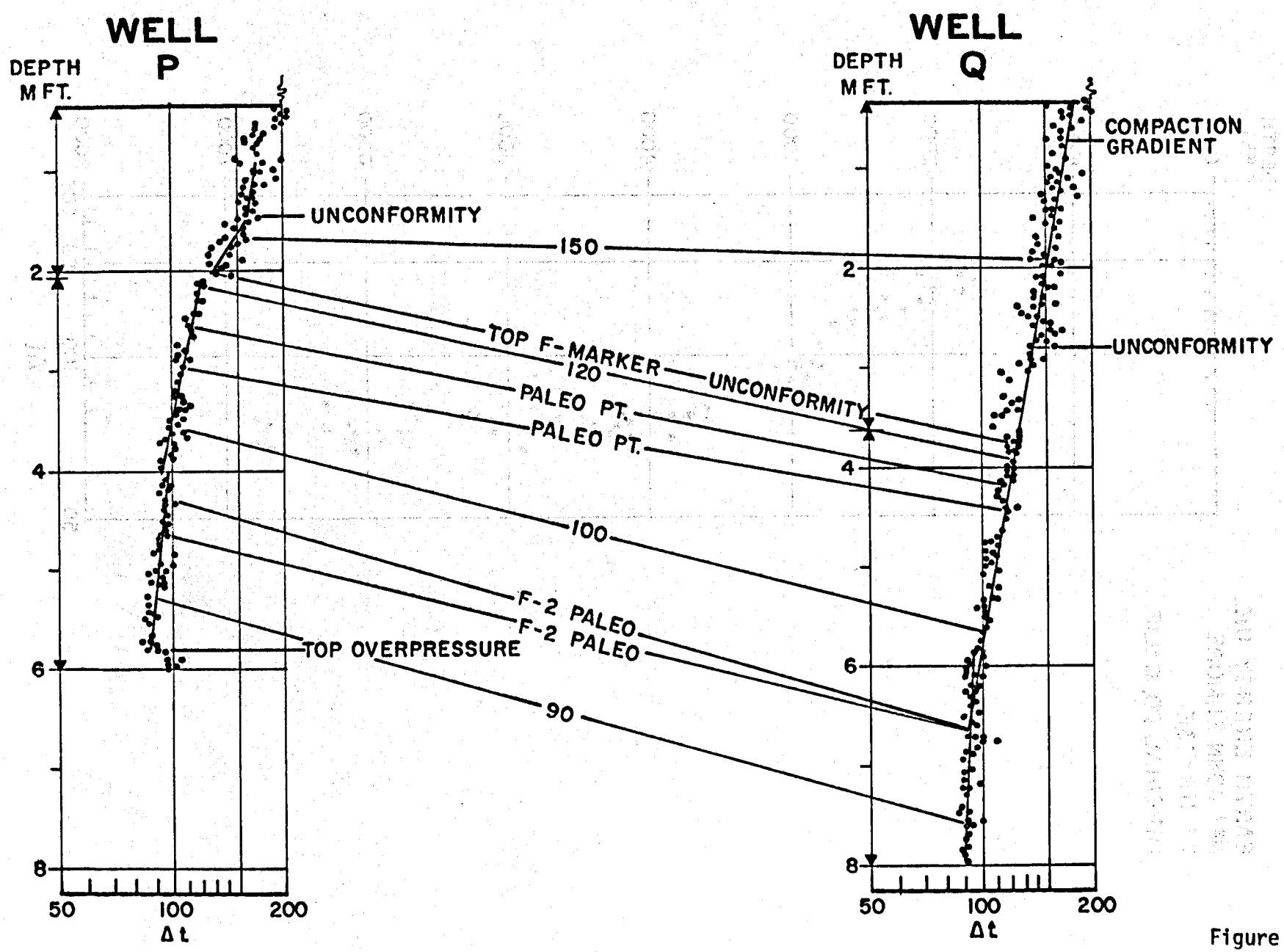
WELL
P
DEPTH
M FT.
UNCONFORMITY
150
TOP F-MARKER
120
PALEO PT.
PALEO PT.
100
F-2 PALEO
F-2 PALEO
TOP OVERPRESSURE
90
2
4
6
8
50
100
200
Δt
WELL
Q
DEPTH
M FT.
COMPACTION
GRADIENT
UNCONFORMITY
UNCONFORMITY
2
4
6
8
50
100
200
Δt

Figure 12

EARTH ENERGY INC.
Nº 1 JOHN ELMORE
27-11S-13E
IMPERIAL CO, CALIF.

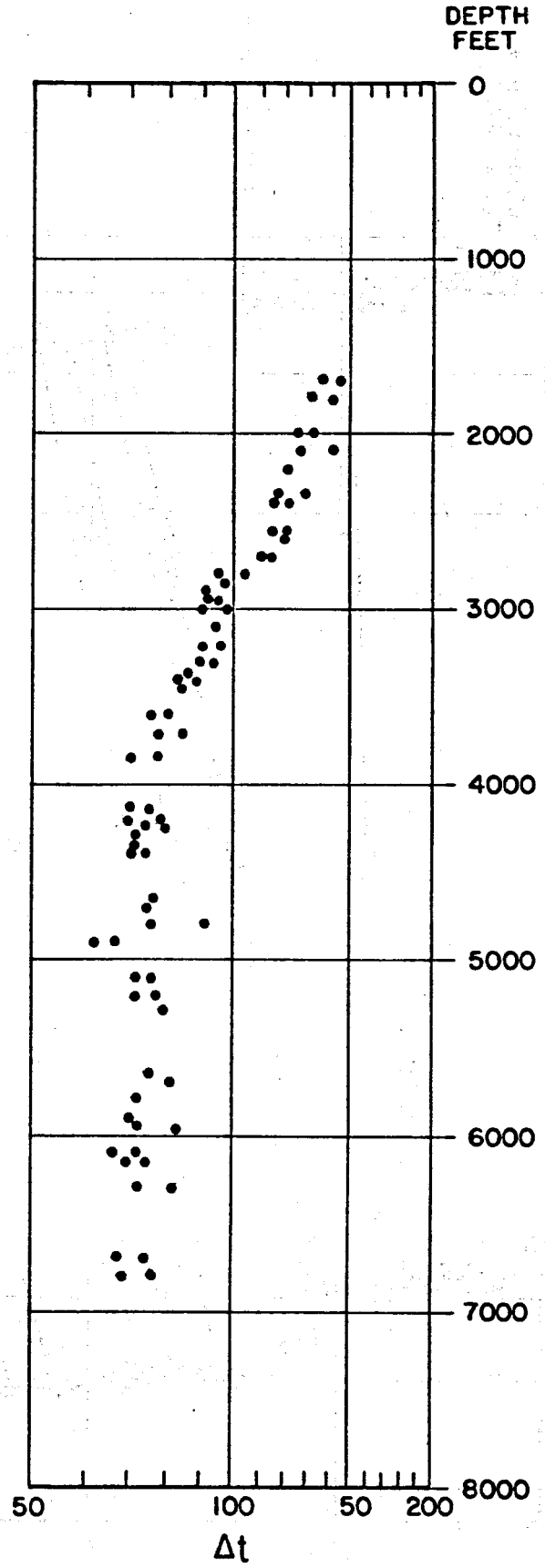

Figure 13

B

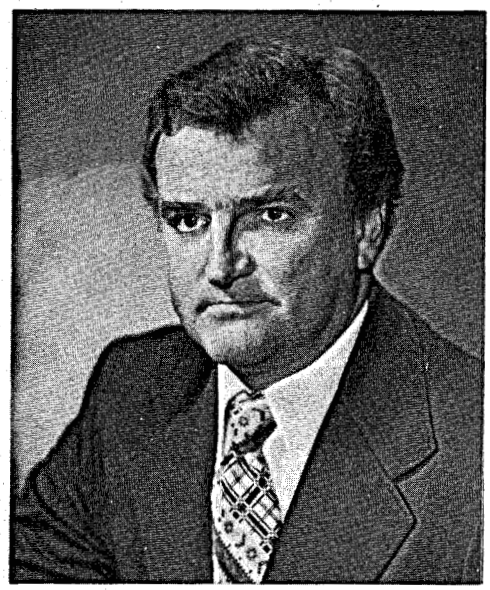

William H. Lang, Jr., is the Western Region Well Log Supervisor for the Union Oil Company of California. After receiving his Geological Engineering degree from the Colorado School of Mines in 1954 he spent two years in the U.S. Army. He joined Cities Service Oil Company in 1956 and was assigned to the Well Logging Department in 1958. In 1964 he was hired by Belco Petroleum Corporation in New York City as Area Geologist and Log Analyst. Lang joined Union Oil Company in his present position in 1969.

In addition to his present duties he taught Formation Evaluation on the graduate level from 1969-1977 at USC. He is a member of SPWLA, serving as Vice President Membership (1976-1977). He is a past President of the Southern California Well Logging Society and a member of AAPG. At the 13th Annual Logging Symposium (1972) he presented "Porosity-Resistivity Cross-Plotting".

SOME PRACTICAL APPLICATIONS TO IMPROVE FORMATION EVALUATION OF SANDSTONES IN THE MACKENZIE DELTA

By

W. L. Johnson
W. A. Linke
Chevron Standard Limited
Calgary - Alberta

ABSTRACT

A large volume of well log and other formation evaluation data has become available from more than seventy wells drilled in the Mackenzie Delta. In order to effectively evaluate and document this data, much of the analytical work has to be handled through a computer. In some instances, the well logs have been difficult to interpret as to reservoir content and often difficult in determining accurate values of water saturation needed for reserve calculations. The interpretational problems are believed largely attributable to the combined effects of generally low salinity formation waters and the type and amount of clays present in the reservoir sands. As will be shown there are some clays which can have a pronounced effect on the resistivity logs and those which have little or no effect. The existing interpretation technique whereby effective porosity and shale volumes are derived from cross plots of neutron and density data is believed to overstate the amount of clay present and render effective porosities which are too low. An alternative method, related to CEC measurements is offered which it is believed can, more simply and accurately, derive effective porosities and effective clay volumes from well logs. Some additional formation evaluation parameters such as formation factors versus porosity are also offered.

INTRODUCTION

Over the past two years, a considerable amount of well log and other formation evaluation data has become available from more than seventy wells drilled in the Mackenzie Delta (see Figure 1). Most of the well log data has either been recorded digitally in the field and/or digitized since by various companies in-house for their own use. In order to adequately evaluate and document this large amount of data, much of the analytical work has to be handled through a computer. In some instances, the well logs have been difficult to interpret in terms of defining reservoir content, producibility, and often difficult in determining accurate values of water saturation. These interpretational problems are believed largely attributable to the combined effects of low salinity formation waters and the type and amount of clays present in the reservoir sands. As will be shown, there are some clays which have a pronounced effect on the resistivity logs and some which have little or no effect.

Initial interpretational procedures involved the use of cross plots of neutron and density data combined with a gamma ray to determine a volume of clay present and the effective porosity. With various degrees of manipulation, the cross plots could be made to produce reasonable answers. However, it is our contention that the cross plot method overstates the volume of clay which has

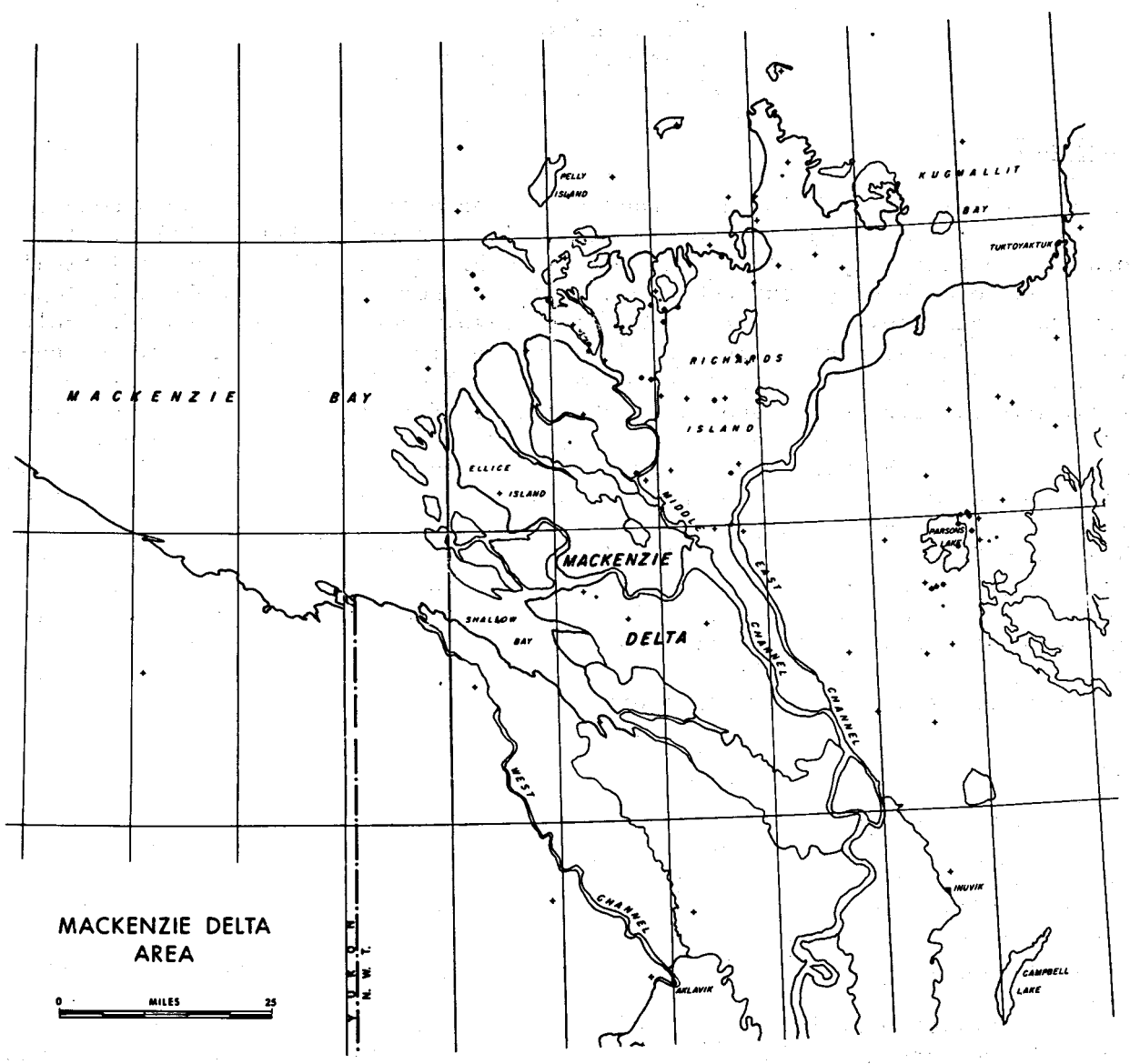
MACKENZIE BAY
PELLY ISLAND
KUGMALLIT BAY
TUKTOYAKTUK
RICHARDS ISLAND
ELLICE ISLAND
MACKENZIE DELTA
SHALLOW BAY
PARSONS LAKE
EAST CHANNEL
CHANNEL
WEST CHANNEL
INUVIK
CAMPBELL LAKE
ARLAVIK
MACKENZIE DELTA AREA
0 MILES 25
Y.T. N.W.T.

FIG. 1

an effect on the resistivity logs. It also renders effective porosity values which are too low. Effective porosity as used here for sandstones implies that the density or neutron/density log derived porosity minus any effects for clay and/or hydrocarbons will be the effective porosity ($\emptyset_e$). Alternate shaly sand models have been examined and used but with only limited success. With the advent of locally available commercial laboratory measured values of cation exchange capacity (CEC*) a set of empirically derived equations has been developed which can utilize well logs to determine volume of clay and reservoir water saturations. Comparisons of density porosities with core analysis indicates that the density log is accurate in defining reservoir porosity. In addition, special core analysis data released by several operators in the Mackenzie Delta is presented to illustrate the reduction in laboratory measured porosities and permeabilities which occurs when the same samples are subjected to increasing net overburden pressures. These data appear to fit very well with similar determinations made in such diverse areas as the North Sea and the US Gulf Coast.

C

STANDARDIZATION OF LOG DATA

As with any project involving the handling of a large volume of well logs, some attempt has to be made to standardize these data for such factors as tool miscalibrations, borehole effects, changes in mud properties, etc. The problems of standardizing well logs is a separate topic in itself and hence will not be discussed in any detail here. Reference is made to a paper by E. T. Connoly[1] (1968) in which he discusses problems encountered with the standardization of log data in the Rainbow area of northwest Alberta. The problem is more difficult in the Mackenzie Delta as there are no well-defined lithologies such as dense limestones and/or anhydrites to use as downhole calibration checks. Useful approaches to standardization have been to generate histograms, cross plots and depth plots of shale transit time, density, neutron response and resistivity. The latter has been most successfully applied when standardizing multiple log runs obtained in the same borehole. These attempts to standardize still have some uncertainty when used over a large area as regional changes in log responses may occur.

SHALY SAND LOG EVALUATION

Researchers[7] dealing with shaly sands noted that a plot of laboratory derived Ro versus Rw did not always equal a constant as predicted by Archie[2] in his classical paper of 1942 (refer to Figure 2). This divergence was especially prominent where the saturating fluid has a high resistivity. In these low salinity, highly resistive formation waters, the values of Ro are much lower than would be anticipated by the Archie relationship. This apparent decrease in Ro is attributed to the fact that the clay in the pore space of the shaly sand and the saturating fluid both contribute ions which together define the total conductivity of the rock. To put it another way, the Archie equation assumes that the matrix is inert, when in actual fact some clays can contribute ions which significantly change the electrical properties of the rock.

---

*A characteristic that describes the number of active points on a clay surface at which cations can be exchanged. The higher the CEC, the greater is the ability of the solid surface to conduct an electric current.

FIG. 2

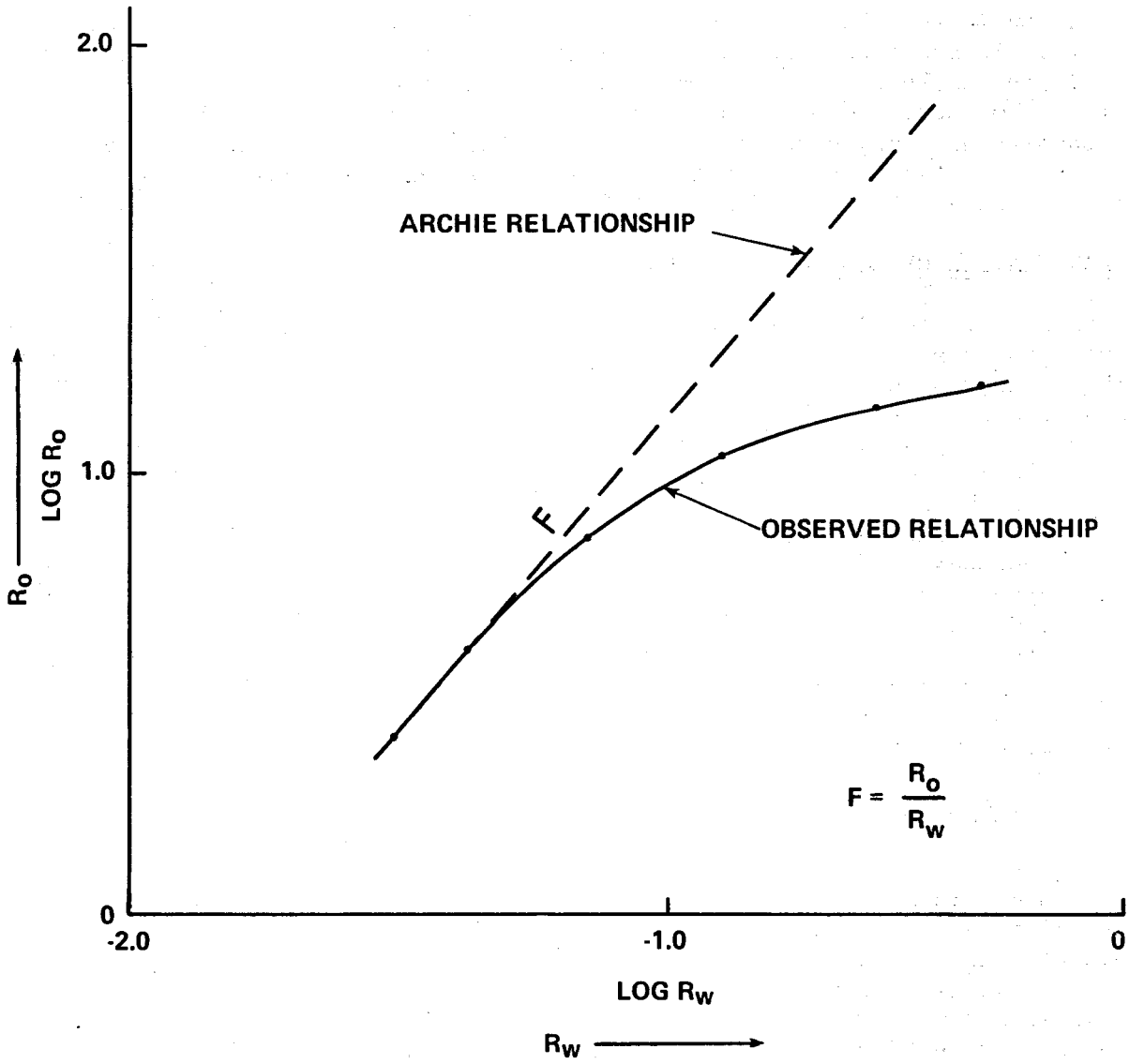
2.0
1.0
0
-2.0
-1.0
0
LOG R_o
R_o
ARCHIE RELATIONSHIP
OBSERVED RELATIONSHIP
F
$F = \frac{R_o}{R_w}$
LOG R_w
R_w

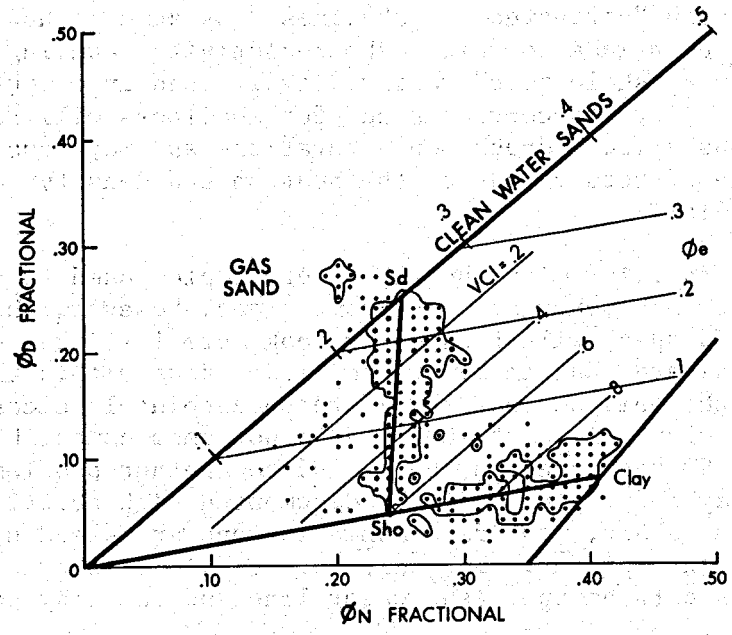

FIG. 3a

NEUTRON - DENSITY CROSSPLOT SHOWING TYPICAL GROUPING OF POINTS FOR A SAND - SHALE SEQUENCE

(AFTER POUPON et al, 1970)

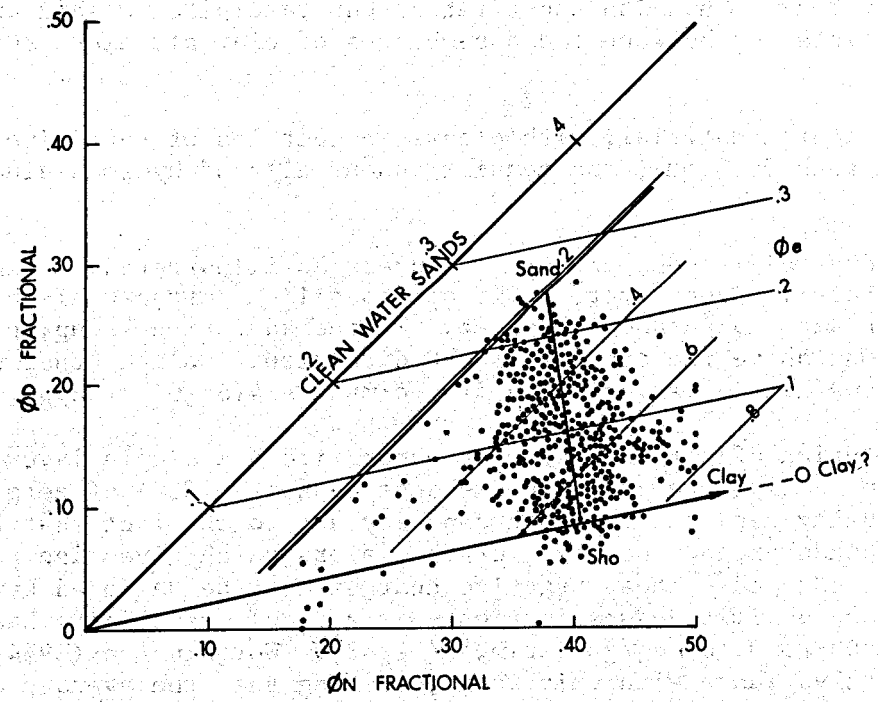

FIG. 3b

COMMON NEUTRON - DENSITY CROSSPLOT FOR THE MACKENZIE DELTA AREA

(WATER BEARING SANDS)

When a reservoir has been "corrected for shaliness" by some method, it implies that some attempt has been made to remove the resistivity reducing effect of the clay, so that only a "shale free" resistivity is used in computing hydrocarbon saturations. Failure to correct sands for shaliness will result in the derivation of erroneously low hydrocarbon saturations and may cause pay zones to be overlooked. The effects of gas on the neutron and density logs must also be removed (see Appendix 1).

Most log analysts are familiar with the ϕ_N, ϕ_D cross plot used to derive Vcl and ϕ_e (Figure 3a after Schlumberger). In some areas, however, when ϕ_N and ϕ_D data are plotted, the display will frequently look more like that of Figure 3b. This would seem to indicate that there are no clean sands within the interval being plotted. It might well be that there are no absolutely clean sands but the indicated minimum clay volume of 20-25% does not seem compatible with the good gamma ray and/or SP responses in these sands. Another problem with this method is that the clay point can seldom be documented with actual log data (see Figure 3b). As a result, many data manipulations are based upon subjective decisions of the interpreter. In addition, as will be shown later, the division of Vcl values between the clean water line and the clay point is not linear.

GENERAL ASPECTS OF CLAY MINERALOGY

Mention has been made of laboratory measurements of cation exchange capacity (CEC) of various clay minerals. Cation exchange capacity, as used here, is defined as the amount of positive ion substitution that takes place per unit weight of dry rock. This ion substitution can take place within an assembly of clay platelets, or between two assemblages of clay platelets separated by pore water.

Clays are a natural material, with plastic properties of very fine size grades (less than 0.03 mm), and consist essentially of hydrous aluminum silicates.

A kaolinite crystal is composed of two layers as illustrated in Figure 4 (after Core Labs). Each layer, comprising a silica tetrahedral sheet combined with an alumina octahedral sheet. In the kaolinite group, crystals are stacked one above the other in the C direction. Unlike other clays, kaolinite shows little variation in its formula $Al4(Si_4O_{10})(OH)_8$.

Since substitution of cations does not occur within a single layer, kaolinite should theoretically have a cation exchange capacity (CEC) of zero. In nature, kaolinite usually has some exchange capacity due to the fact that there are some broken bonds around the edges of the layers which give rise to unsatisfied negative charges. These negative charges must be balanced by cations which can undergo limited substitution. As a result, kaolinite has a very low CEC of 0.03 to 0.10 meq/gm (Grim,[3] 1968). Worthington (1974, unpublished) is somewhat at variance with this range, stating that the average CEC is 0.03 meq/gm. In any event, the CEC of kaolinite can be considered to be a low value.

Clays which have a high cation exchange capacity play a leading role in the resistivity reduction observed in shaly sands. Because kaolinite has a very low CEC, it functions largely as a nearly inert pore filler, with only minor

FIG. 4

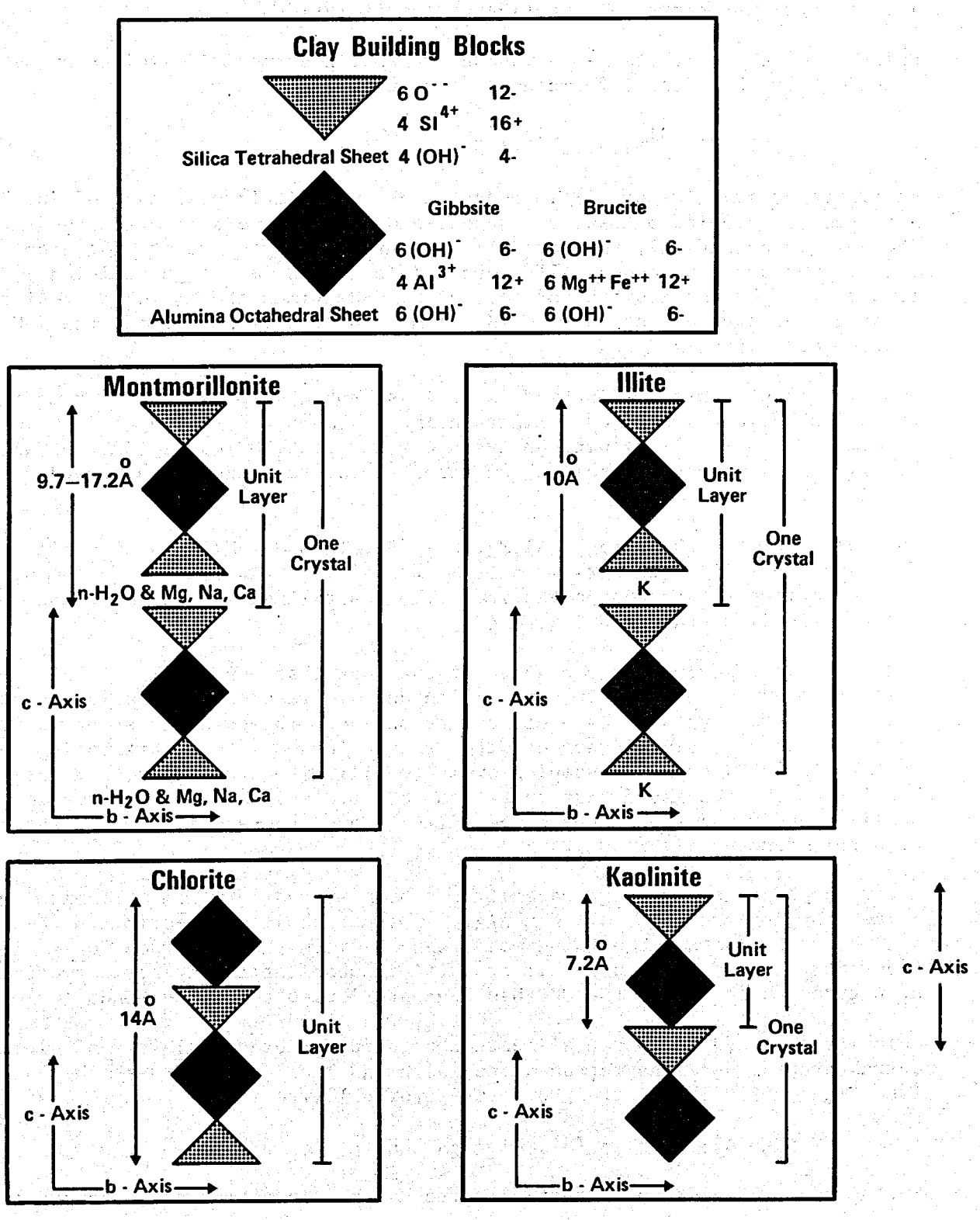

Schematic of Clay Crystal Structures

(AFTER CORE LABORATORIES INC.)

resistivity reducing properties. Failure to recognize that kaolinite does not play an important part in reducing the resistivity of the shaly sand, could lead to serious errors in computing water saturations.

Unlike kaolinite, illite has a variable chemical composition which can be described by the general formula

$$K_{1-1.5}Al_4(Si_{6.5-7.0}Al_{1-1.5}O_{20})(OH)_4$$

An illite crystal (Figure 4) is composed of two unit layers, each of which consists of one alumina octrahedron sandwiched between two silica tetrahedrons. The unit is essentially the same as for montmorillonite except that about 1/6 of the Si^{+4} are replaced by Al^{+3} ions. This creates a charge deficiency which is satisfied by the addition of potassium. Sometimes the K^{+} ion is replaced by other cations such as Ca^{+2}, Mg^{+2}, or H^{+}. However, in general, the K_2O content of illite is 8-10%.

Substitutions within the lattice as well as broken bonds account for most of the CEC observed in illites. Illite commonly has a CEC ranging from 0.10 to 0.40 meq/gm (Grim, 1968) with an average value of 0.20 meq/gm (Deer et al, 1974).[4] This is approximately seven times the average CEC value recorded for kaolinite.

Montmorillonite $(1/2Ca,Na)_{0.7}(Al,Mg,Fe)_4(Si,Al)_8O_{20}(OH)_4$ though similar in structure to illite, differs in that Mg^{+2}, Na^{+1} or Ca^{+2} tend to be the substituting cations rather than potassium. The generalized structure of montmorillonite is illustrated in Figure 4.

Probably, most geologists are aware of the fact that montmorillonite is a swelling clay which takes in variable amounts of water. Frequently, montmorillonite containing Na^{+1} as a cation has only one molecular layer of water but contains two molecular layers of water when calcium is the substituting ion. Foster[5] (1953) examined samples of montmorillonite from twelve separate localities and concluded that there was no correlation between the degree of swelling and the cation exchange capacity. Core Laboratories Inc. disagrees with this finding (in press).

A very high cation exchange capacity can be measured on montmorillonites with values ranging from 0.8 to 1.5 meq/gm. Worthington (1974) estimates the average CEC to be 1 meq/gm, a value more than 33 times that recorded for kaolinite. About 80% of the CEC is a result of lattice substitution in the montmorillonite structure, while 20% of the CEC has been attributed to broken bonds (Grim, 1968).

Chlorite is a hydrous green silicate consisting of ordered layers of alumina octrahedrons and silica tetrahedrons, with basal cleavage between the layers (see Figure 6). The general composition of chlorite is

$$(Mg, Al, Fe^{+2})_{12}(Si, Al)_8O_{20}(OH)_{16}$$

Worthington (1974) reports that chlorite has a zero cation exchange capacity.

In summary then, montmorillonite and illite have generally high CEC values while kaolinite and chlorite show very low to 0 CEC values.

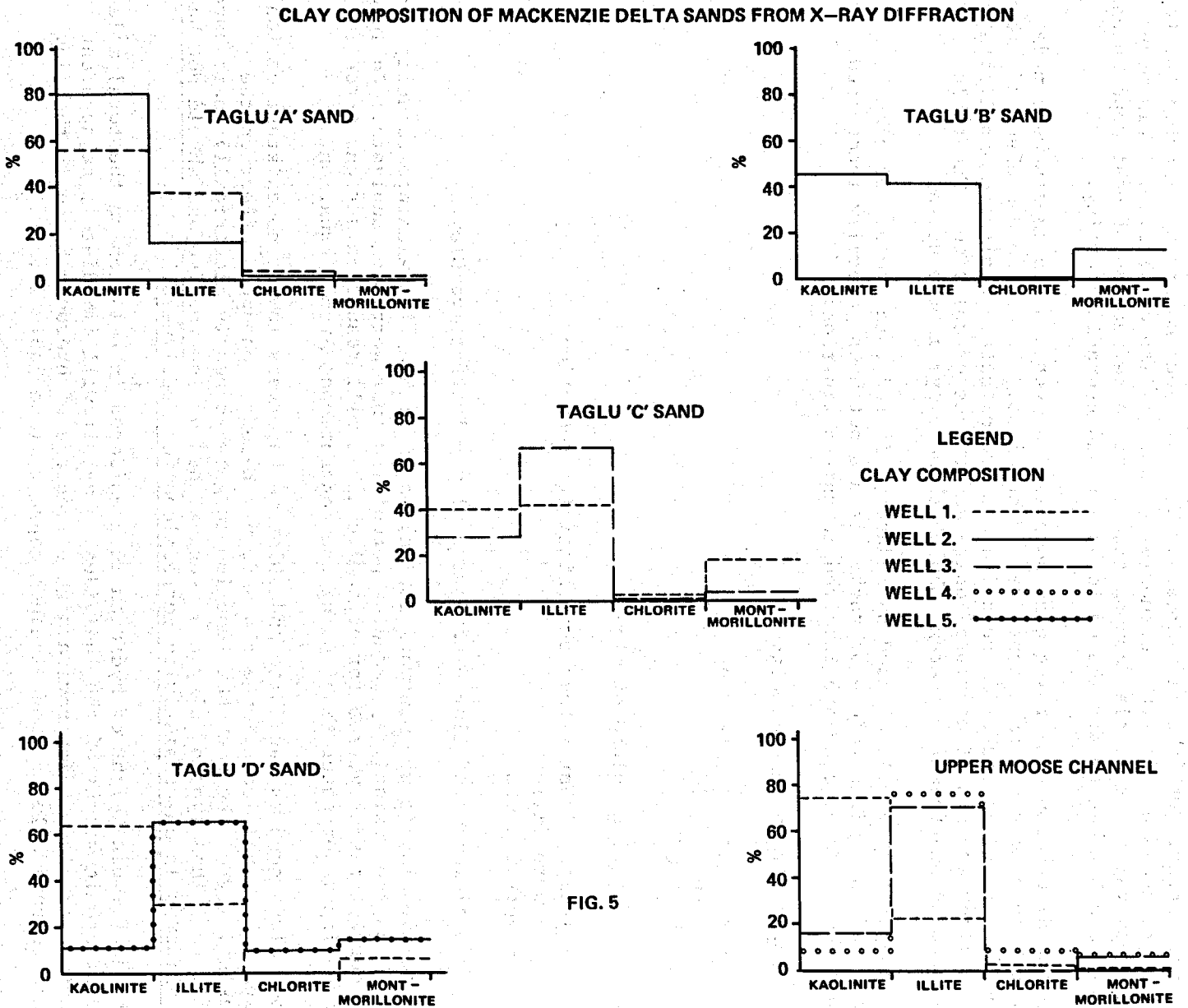
CLAY COMPOSITION OF MACKENZIE DELTA SANDS FROM X–RAY DIFFRACTION
TAGLU 'A' SAND
TAGLU 'B' SAND
TAGLU 'C' SAND
TAGLU 'D' SAND
UPPER MOOSE CHANNEL
%
100
80
60
40
20
0
KAOLINITE
ILLITE
CHLORITE
MONT – MORILLONITE
LEGEND
CLAY COMPOSITION
WELL 1.
WELL 2.
WELL 3.
WELL 4.
WELL 5.

FIG. 5

Figure 5 is a bar graph illustrating the clay composition from X-ray diffraction of the Taglu A to D and Moose Channel sands. Depth of the sands is in order of listing with the A sand being the shallowest sand and the Moose Channel being the deepest sand. A Lower Eocene age has been attached to the Taglu sands, while a Paleocene-Maestrichtian age has been assigned to the Moose Channel sands. Other data indicates that this section has not reached the temperature necessary for the montmorillonite to illite conversion. This means that any variation in clay composition is not a reflection of post depositional processes but can be attributed to source and hydraulic sorting.

In the discussion concerning clay composition, various statements were made about the cation exchange capacity of the clays. Reference was also made to the fact that the clays in the delta are predominately kaolinite and illite, with minor amounts of montmorillonite and traces of chlorite. The table attached summarizes the average CEC of these clays in the delta.

Volume of clay (Vcl), as used by industry, is the total volume of clay measured in a given volume of rock. It has not been generally recognized that two types of clay are involved in this definition:

1. Effective volume of clay

   - a resistivity reducer
   - a pore filler
   - high CEC

2. Ineffective volume of clay

   - insignificant effect on resistivity reduction
   - a pore filler
   - very low CEC

Total Volume of Clay = Effective Clay + Ineffective Clay

Effective clay (e.g., montmorillonite) has a high cation exchange capacity and contains the resistivity reducing porosities that worry log analysts. Failure to correct resistivities for effective clays will result in serious error in computing water saturations using the conventional Archie equation.

Some clays such as kaolinite and chlorite have very low to nonexistent cation exchange capacities. These clays do not have a pronounced effect on the resistivity of the rock but function largely as nearly electrically inert pore fillers. This type of clay has been defined as ineffective and should not be considered in any resistivity corrections for "shaliness."

If the formula weight of hydrogen is considered in relation to the total molecular atomic weight of the individual clay, it will immediately be apparent that delta clays which have a high percentage of hydrogen bound in the clay tend to have a low cation exchange capacity (see Table 1).

How does this affect the logs? Both the neutron and the density logs will see the free water in the pore space as porosity. However, the neutron log will exhibit a higher porosity reading in a shaly sand than the density log because it recognizes hydroxyl ions bound in the crystal lattice in addition to the hydrogen of the pore water.

TABLE 1

Clay Name	Formula	Pma	% Hydrogen	Average CEC
Kaolinite	$Al_4(Si_4O_{10})(OH)_8$	2.69	1.5	0.03 meq/gm
Illite	$K_{1-1.5}Al_4(Si_{6.5-7.0}Al_{1.0-1.5}O_{20})(OH)_4$	2.76	0.5	0.20 meq/gm
Montmorillonite	$(1/2Ca,Na)_{0.7}(Al,Mg,Fe)_4(Si,Al_8O_{20})(OH)_4$	2.33	0.5	1.0 meq/gm
Chlorite	$(Mg,Al,Fe)_{12}(Si,Al)_8O_{20}(OH)_{16}$	2.77	1.2	0.0 meq/gm

FIG. 6
MACKENZIE DELTA WELL
TAGLU B SAND 4696 to 4722

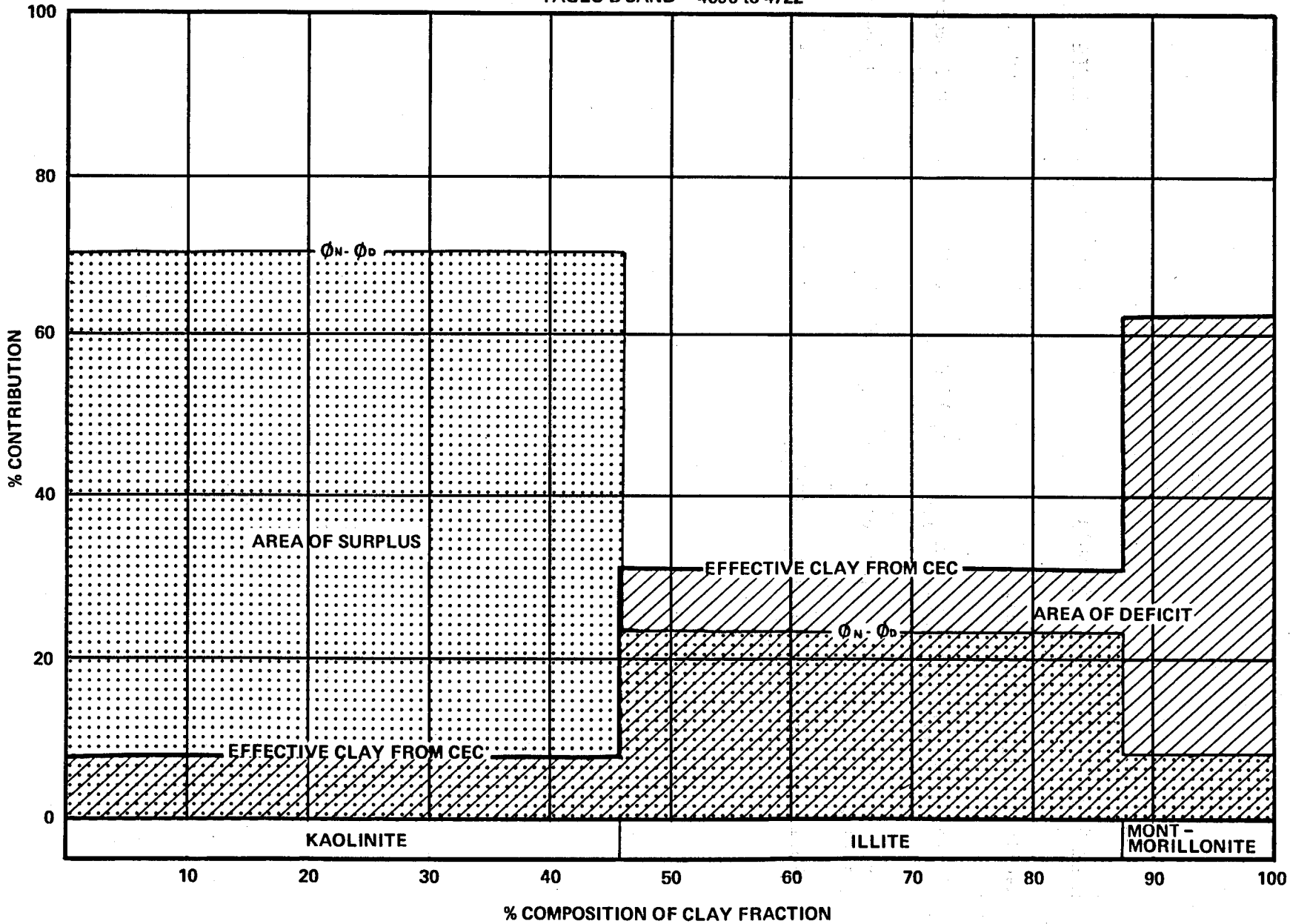

Worthington (1974) of COFRC developed a method to compute the approximate theoretical response a neutron log would give in a shaly sand of given porosity. Using his formulas and the clay composition from X-ray diffraction (see Figure 6), the percent each of the clay constituents makes towards the total (ϕ_N-ϕ_D) response on the log was calculated. Examination of Figure 6 indicates that while kaolinite constitutes about 45% of the total clay composition in this particular Taglu B sand, it contributes 70% towards the total (ϕ_N-ϕD) response observed on the log. Illite, which constitutes 42% of the clay present, contributes only 23% to the (ϕ_N-ϕ_D) response. The remaining clay volume of 13% is montmorillonite and it contributes only 8% to the total (ϕ_N-ϕ_D) response.

From the above data it would seem that the amount of separation occurring between the ϕ_N and ϕ_D curves throughout a shaly sand is not only a function of the volume of clay present, but is also dependent on the type of clay present.

By knowing the average CEC of the constituents, the clay composition, and the total CEC measured in the lab, the percent contribution each of the clay constituents makes towards the total CEC reading can roughly be determined. In a general way, (ϕ_N-ϕ_D) values suggest an inverse relationship to cation exchange capacity, i.e., clays which have a high amount of hydrogen tend to have a low CEC (refer to Figure 7). The ϕ_N, ϕ_D cross plot technique attempts to relate the amount of (ϕ_N-ϕ_D) separation to the total volume of clay. Log analysts calculating Sw using shale corrected resistivities require the effective volume of clay.

At first glance, it might appear that even if an inverse relationship does exist between CEC and (ϕ_N-ϕ_D), the problem of determining effective volume of clay could simply be done by calibrating the (ϕ_N-ϕ_D) with laboratory derived CEC values. However, as Figure 7 illustrates, thermal absorbers and erratic compositional changes in the clay mineralogy result in a CEC versus (ϕ_N-ϕ_D) relationship which is rather unpredictable. Compare the reliability of this data with the identical CEC values in Figure 8a plotted versus gamma ray. It is obvious that the gamma ray is much more correlatable with cation exchange capacity, and should be used in preference to the (ϕ_N-ϕ_D) as a clay indicator. Based on data from two wells, CEC can be calculated from the gamma ray using the equation:

$$CEC = 0.00197 \text{ gamma} - 0.0949$$
(correlation coefficient 0.95)

To overcome problems of gamma ray miscalibration, the same CEC values measured in the laboratory have also been correlated with relative gamma ray deflection (refer to Figure 8b). The intercept in Figure 8a implies that in this well, a sand with zero cation exchange capacity has a gamma ray value of 48 API. This closely agrees with the laboratory measurement which determined that a sand with a radioactivity of 55 API had a very low cation exchange capacity of only 0.009 meq/gm.

The gamma ray log does not respond to kaolinite and chlorite because they lack any natural radioactivity. By coincidence, these two clays are nearly electrically inert in that they do not possess any significant ability to lower the resistivity of a shaly sand. Illite contains radioactive potassium which is recognized by the gamma ray log. Montmorillonite rich beds in the delta tend

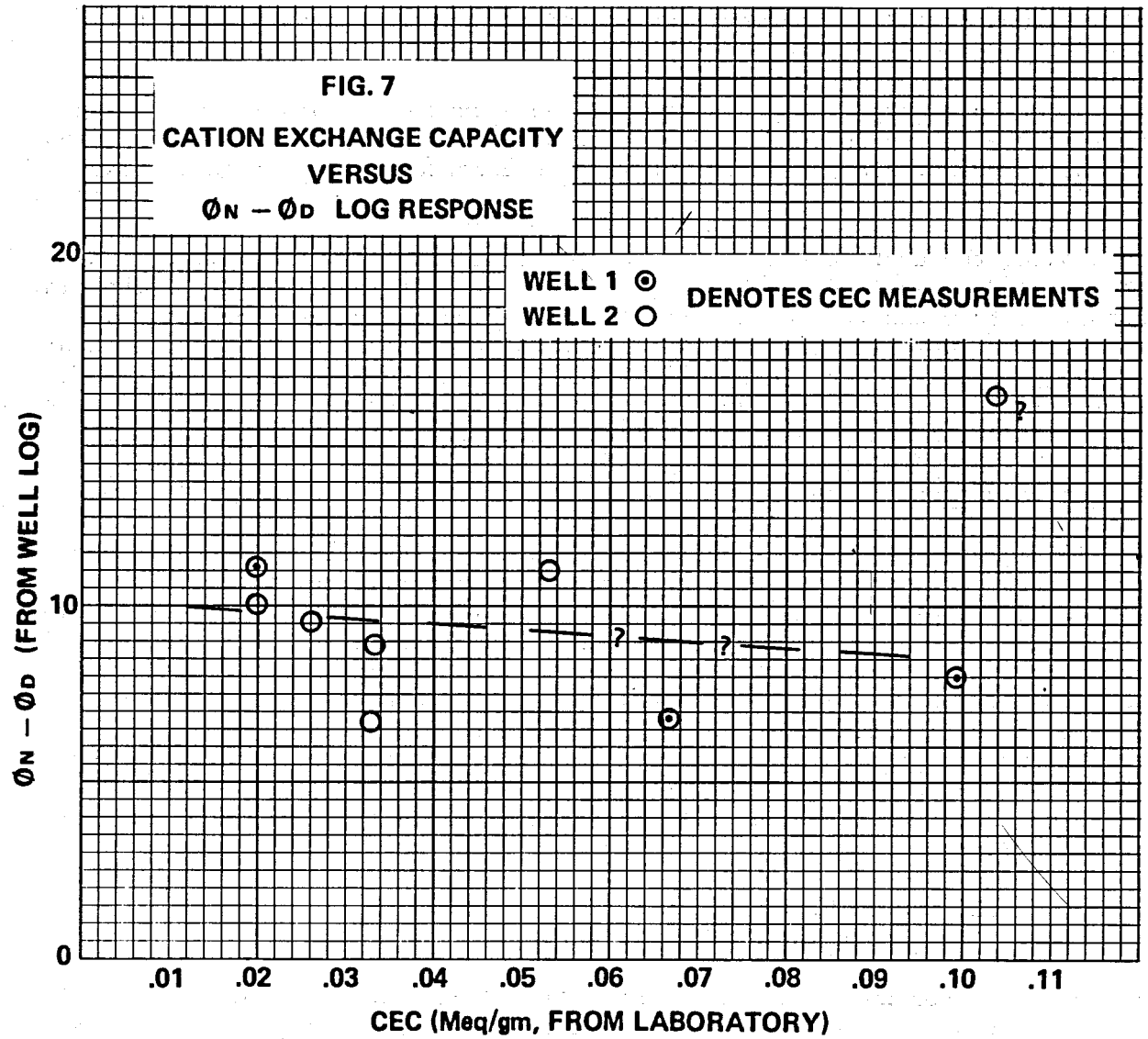
FIG. 7
CATION EXCHANGE CAPACITY
VERSUS
ØN – ØD LOG RESPONSE
WELL 1 ⊙
WELL 2 ○
DENOTES CEC MEASUREMENTS
20
10
0
ØN – ØD (FROM WELL LOG)
.01
.02
.03
.04
.05
.06
.07
.08
.09
.10
.11
CEC (Meq/gm, FROM LABORATORY)

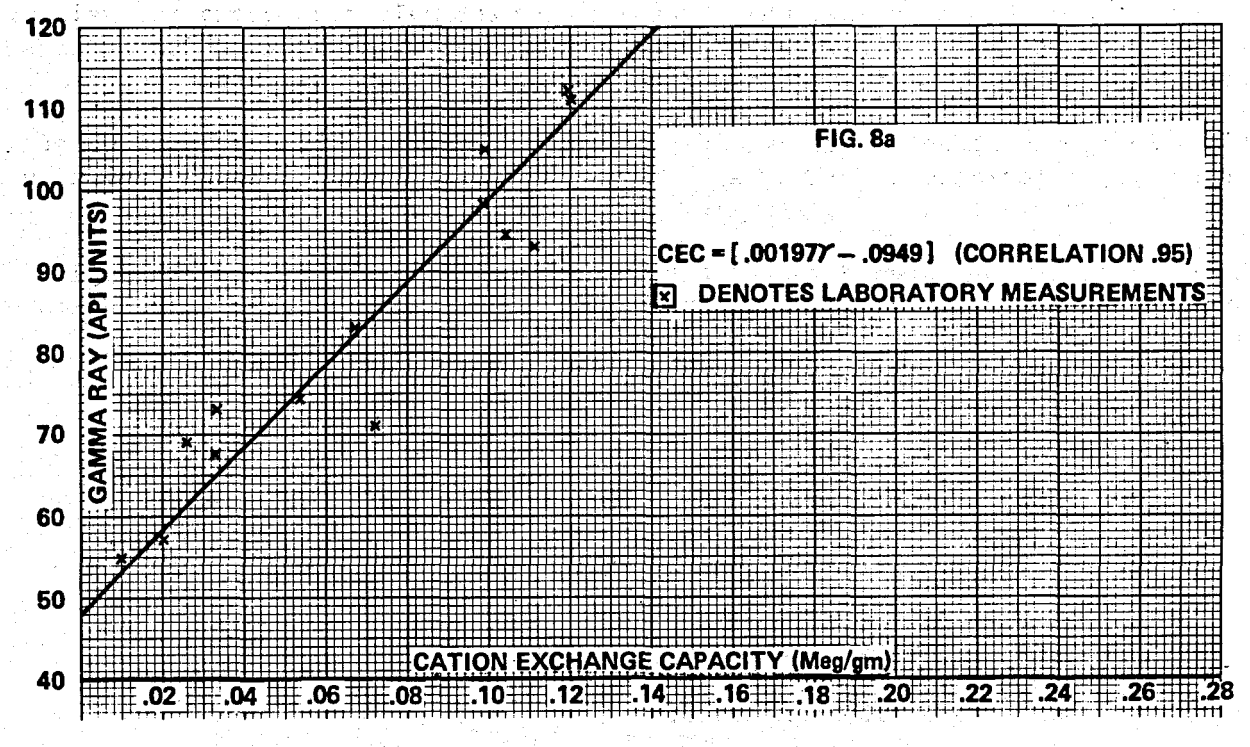
120
110
100
90
80
70
60
50
40
GAMMA RAY (API UNITS)
CATION EXCHANGE CAPACITY (Meg/gm)
.02
.04
.06
.08
.10
.12
.14
.16
.18
.20
.22
.24
.26
.28
FIG. 8a
CEC = [.00197γ – .0949] (CORRELATION .95)
⊠ DENOTES LABORATORY MEASUREMENTS

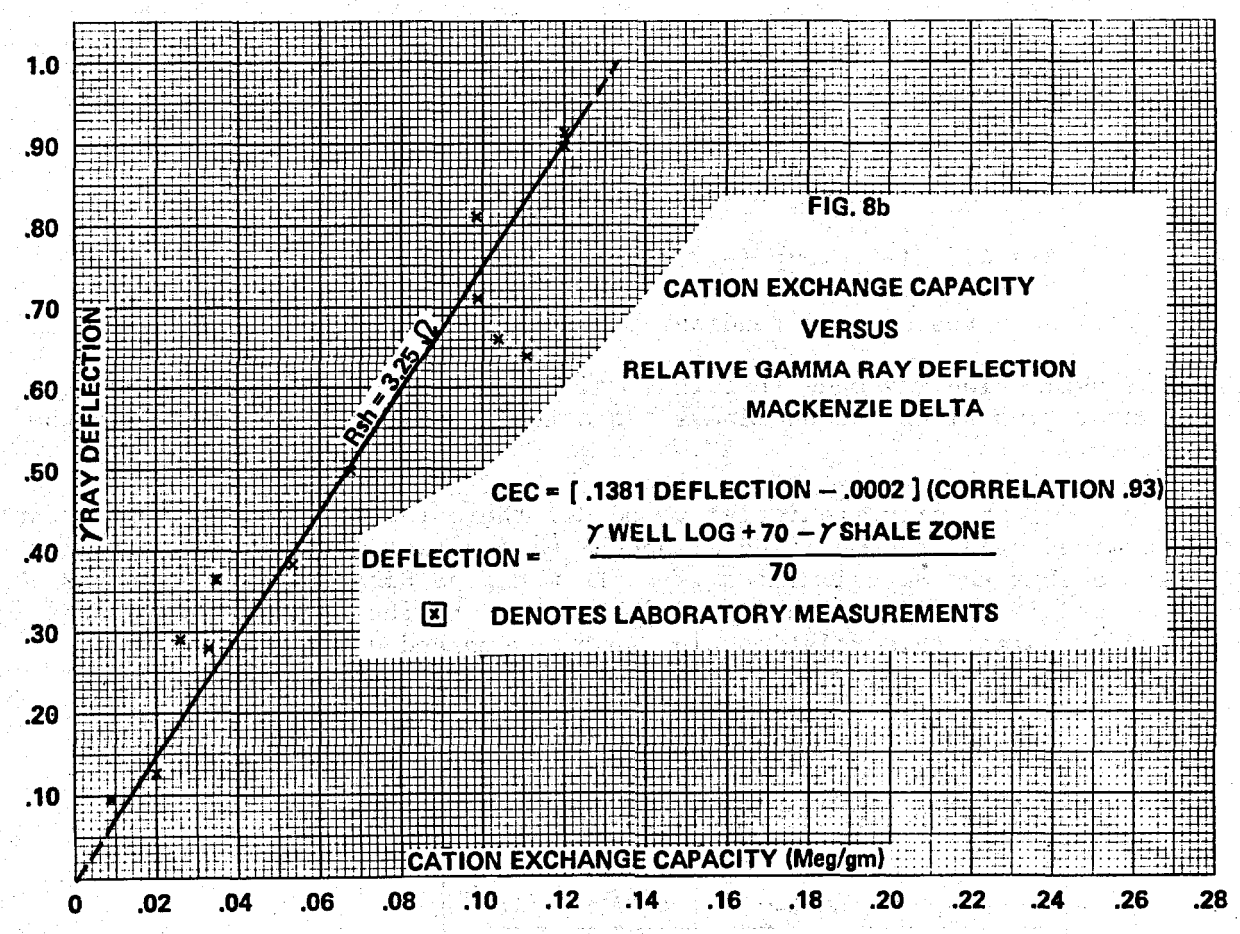
1.0
.90
.80
.70
.60
.50
.40
.30
.20
.10
γRAY DEFLECTION
Rsh = 3.25 Ω
CATION EXCHANGE CAPACITY (Meg/gm)
0
.02
.04
.06
.08
.10
.12
.14
.16
.18
.20
.22
.24
.26
.28
FIG. 8b
CATION EXCHANGE CAPACITY
VERSUS
RELATIVE GAMMA RAY DEFLECTION
MACKENZIE DELTA
CEC = [.1381 DEFLECTION – .0002] (CORRELATION .93)
DEFLECTION = (γ WELL LOG + 70 – γ SHALE ZONE) / 70
⊠ DENOTES LABORATORY MEASUREMENTS

to have a high U_3O_8 content, which results in extremely high gamma ray values. Both illite and montmorillonite are characterized by a high CEC which reduces the resistivity of the reservoir. Since the delta sands are largely composed of kaolinite and illite, the gamma ray log should be reasonably accurate in determining the effective volume of clay to be used in shale corrected water saturation calculations. This is a result of its ability to ignore kaolinite (ineffective clay), while responding to illite (effective clay).

From laboratory measurements, the cation exchange capacity of a rock sample was determined and water saturation was calculated using a form of the Waxman-Smits[6] equation:

$$Sw = \frac{-(BQvRw_2) + \left((BQvRw_2)^2 + 4(F^*Rw_1)/Rt\right)^{\frac{1}{2}}}{2}$$

Where:

Qv = Quantity of cation exchangeable clay present - meq/ml of pore space expressed here as $CEC\frac{(1-\phi)}{\phi}\ Pg$

$\overline{Pg}$ = grain density of rock solids, gms/cm^3

Rw_1 = Rw a formation temperature

Rw_2 = Rw at 77°F

F^* = Formation resistivity factor where formation or formation sample is saturated with a very low resistivity brine, expressed here as $0.79\phi^{-2.09}$

B = Specific counterion inductance. This is expressed as

$$B = 4.6\ \ 1\text{-}0.6 \exp(-.77/Rw_2)$$

Rt = deep resistivity reading.

Then the assumption was made that this value of Sw should represent the true water saturation since the shaliness was actually physically measured in the laboratory.

Using the same porosity, resistivity and Rw, the effective volume of clay can be determined using the modified Simandoux[8] equation. To do this, it must be assumed that the Sw calculated from the modified Simandoux equation has validity and is therefore equal to Sw calculated by the above method. In terms of formulas, this relationship can be expressed as:

$$\left[\frac{F^*Rw_1\ (1\text{-}Vcl)}{Rt} + \frac{0.79\ (1\text{-}Vcl)(Vcl)\ Rw_1}{2\phi^{2.09}\ Rsh}\right]^{\frac{1}{2}} - \left[\frac{0.79\ Rw_1\ (1\text{-}Vcl)Vcl}{2\phi^{2.09}Rsh}\right] \text{ is equal to } -\left[\frac{(BQvRw_2) + \left((BQvRw_2)^2 + 4(F^*Rw_1)/Rt\right)^{\frac{1}{2}}}{2}\right]$$

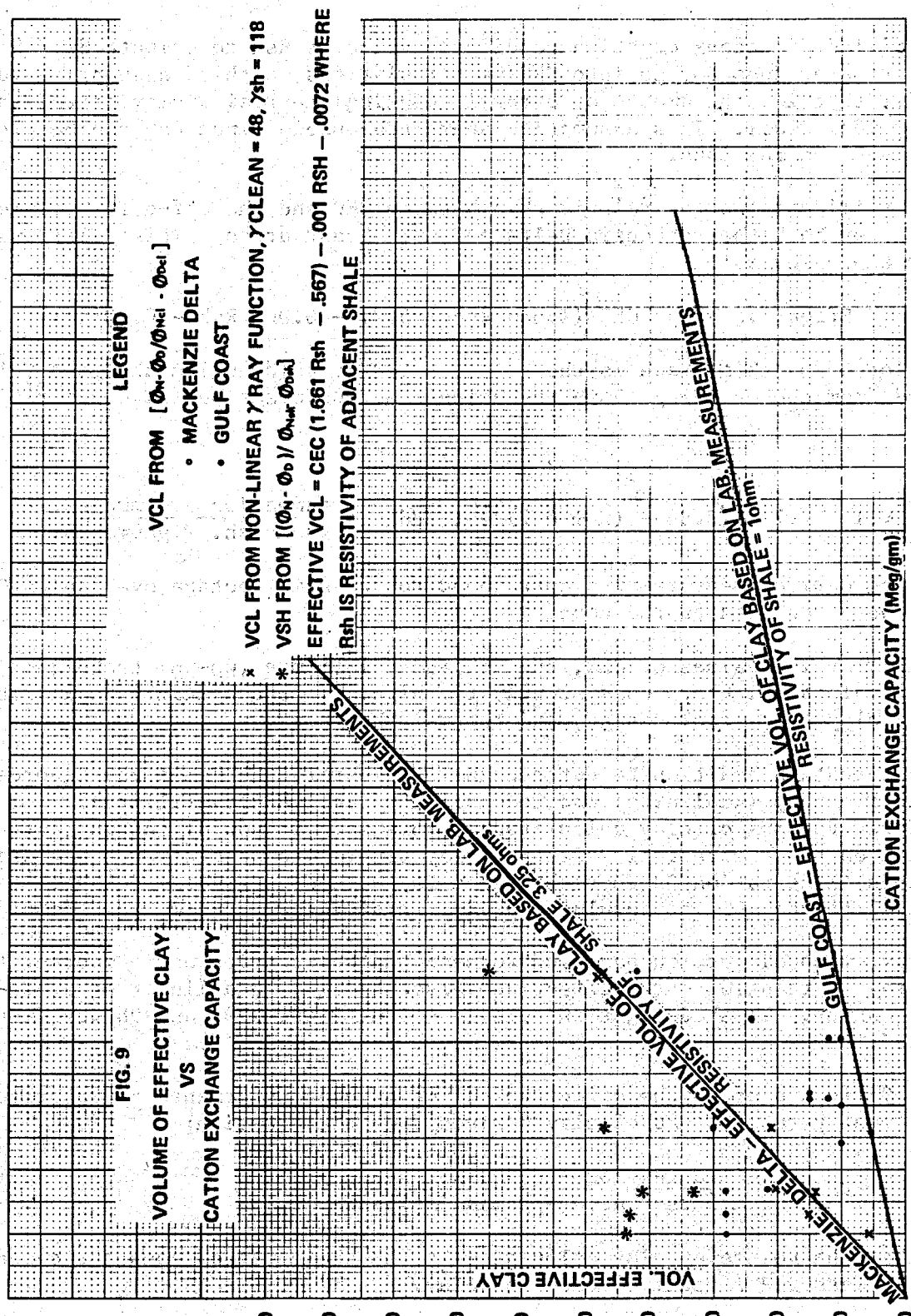

FIG. 9
VOLUME OF EFFECTIVE CLAY
VS
CATION EXCHANGE CAPACITY

or

$$Sw \text{ (modified Simandoux)} = Sw \text{ (modified Waxman-Smits)}$$

The modified Simandoux equation requires a value of Rsh to compute Sw. Since this parameter does not go into CEC/Sw calculations, a third assumption must be made; that is, the amount of error in picking the resistivity of the shale zone is very small. This assumption seems reasonable since Rsh can be picked with ease from the logs.

Figure 9 illustrates the relationship between CEC and the effective volume of clay for both the Mackenzie Delta and Gulf Coast areas. This relationship can be expressed as:

$$\text{Effective Vcl} = \text{CEC } (1.661\ \text{Rsh} - 0.567) - 0.001\ \text{Rsh} - 0.0072$$

Also plotted on this graph is the Vcl computed by a $(\phi_N - \phi_D)$ method and Vcl derived from the well log gamma ray using a method described by Clavier[9] (1971),

where:

$$Vcl = 1.7 - \left(3.38 - (x + 0.7)^2\right)^{\frac{1}{2}}, \text{ and } x = \frac{\text{gamma log - gamma ss.}}{\text{gamma sh. - gamma ss.}}$$

These log derived measurements correspond to the same footage over which CEC values were recorded on the core.

Note that at low values of CEC, the Vsh and Vcl from a $(\phi_N - \phi_D)$ technique exhibit values which are consistently too high. This can mainly be attributed to clay type, tool design, and thermal absorbers.

Remember that in addition to not recognizing quartz, the gamma ray ignores ineffective clay (kaolinite) and recognizes effective clay (illite). Therefore, volumes of clay calculated by this method should, and in fact do, fall on the theoretical effective clay line. The conclusion to be drawn from this illustration is that the gamma ray method of finding Vcl relates very well to the CEC and should be used in preference to a $(\phi_N - \phi_D)$ technique.

Recently, much discussion has been focused on the question as to whether the gamma ray is related to the effective volume of clay in a linear or a non-linear manner. To shed light on this question, Figures 9a and 9b were constructed.

Figure 9a is a plot of the effective volume of clay determined by laboratory measurement versus volume of clay derived from the equation:

$$Vcl = \frac{\text{gamma ray log - gamma ray sand}}{\text{gamma ray shale - gamma ray sand}}$$

Note that the volume of clay calculated by the above method does not agree with the measured effective volume of clay.

The absorption equation can be written as:

$$\text{gamma ray detected} = \text{gamma ray clay } e^{(-\text{distance x Pb x mass abs. coefficient})}$$

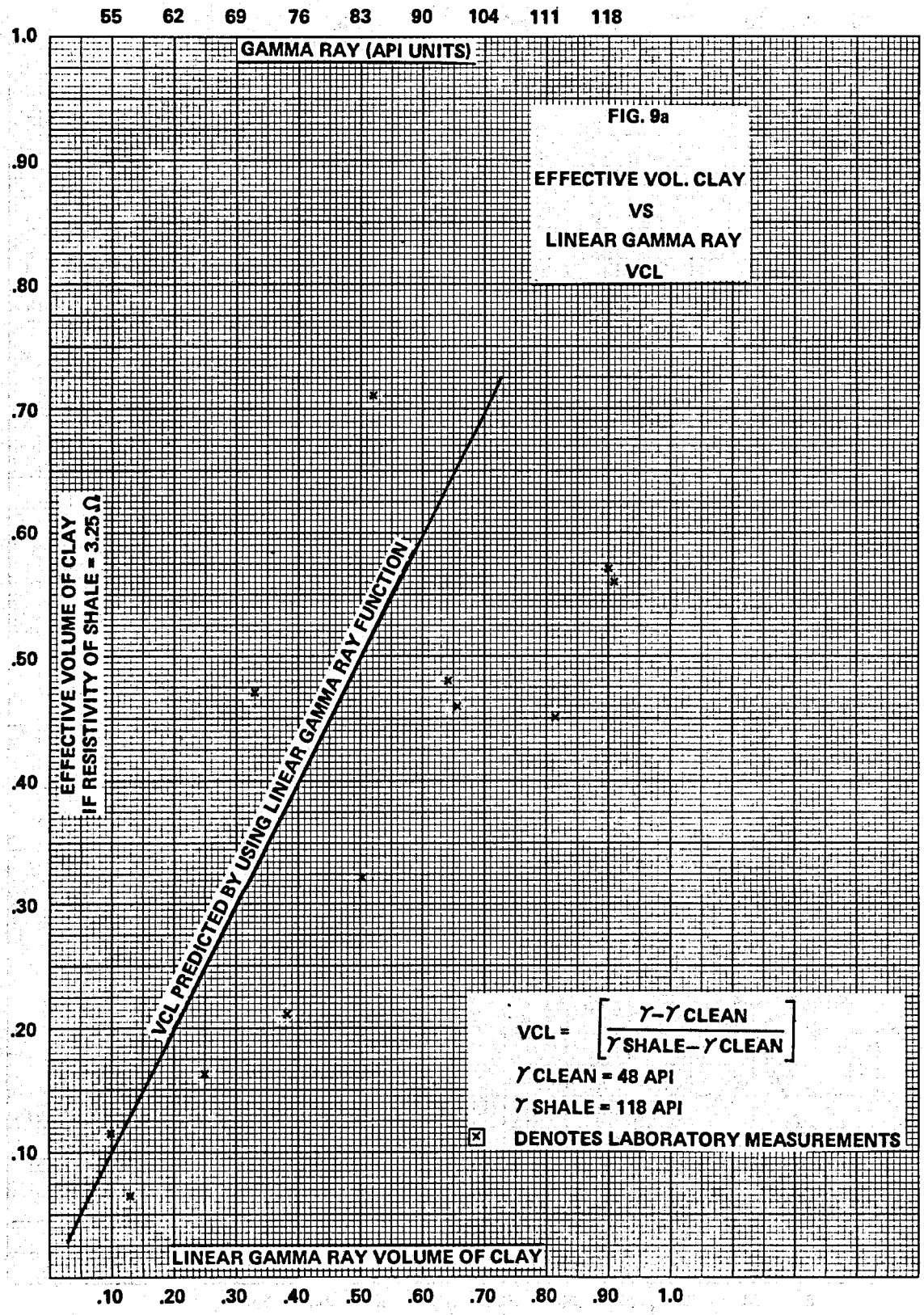
55 62 69 76 83 90 104 111 118
GAMMA RAY (API UNITS)
1.0
.90
.80
.70
.60
.50
.40
.30
.20
.10
EFFECTIVE VOLUME OF CLAY
IF RESISTIVITY OF SHALE = 3.25 Ω
VCL PREDICTED BY USING LINEAR GAMMA RAY FUNCTION
LINEAR GAMMA RAY VOLUME OF CLAY
.10 .20 .30 .40 .50 .60 .70 .80 .90 1.0
FIG. 9a
EFFECTIVE VOL. CLAY
VS
LINEAR GAMMA RAY
VCL
VCL = [(γ − γ CLEAN) / (γ SHALE − γ CLEAN)]
γ CLEAN = 48 API
γ SHALE = 118 API
DENOTES LABORATORY MEASUREMENTS

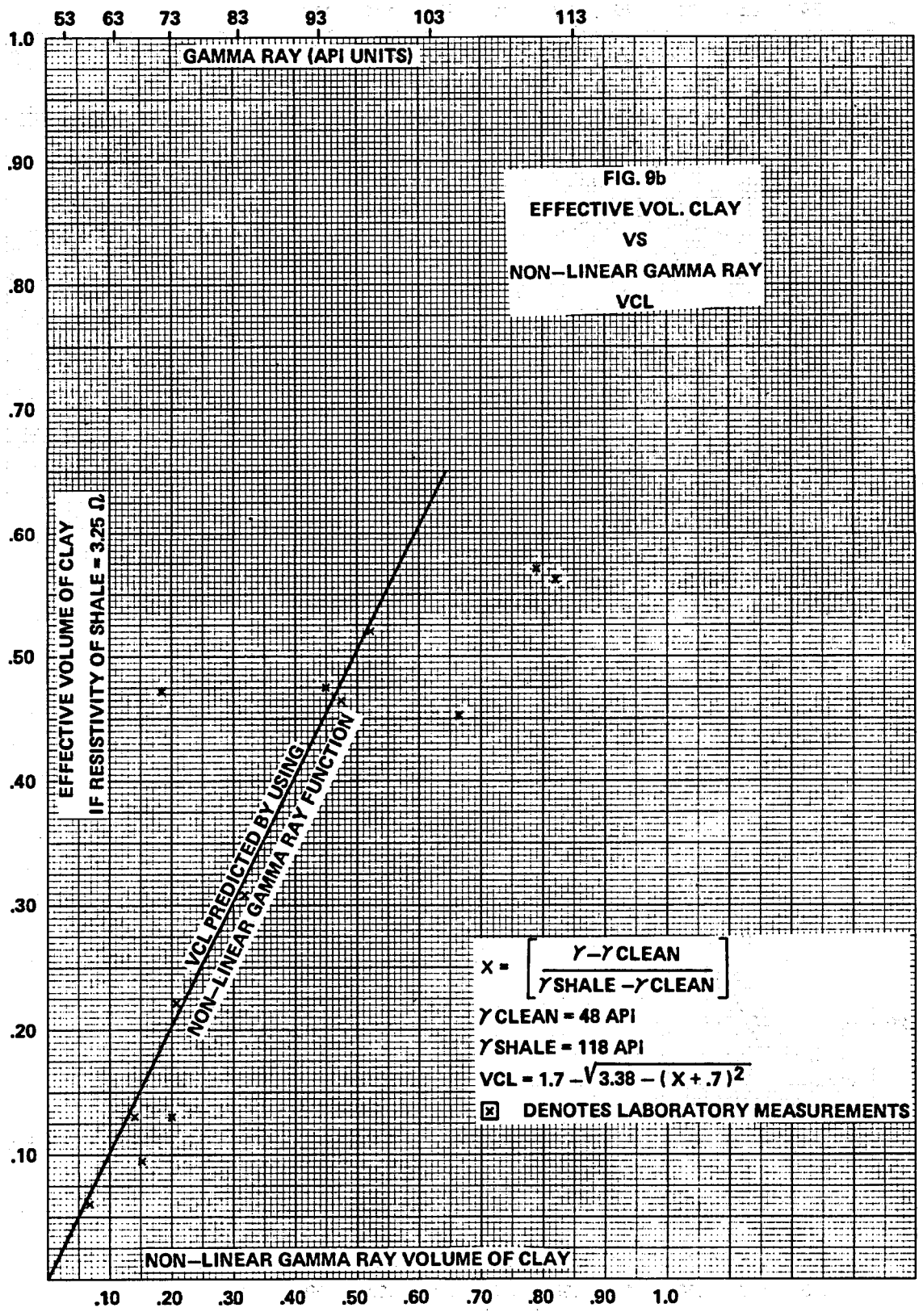
53 63 73 83 93 103 113
GAMMA RAY (API UNITS)
1.0 .90 .80 .70 .60 .50 .40 .30 .20 .10
EFFECTIVE VOLUME OF CLAY
IF RESISTIVITY OF SHALE = 3.25 Ω.
VCL PREDICTED BY USING NON-LINEAR GAMMA RAY FUNCTION
NON-LINEAR GAMMA RAY VOLUME OF CLAY
.10 .20 .30 .40 .50 .60 .70 .80 .90 1.0
FIG. 9b
EFFECTIVE VOL. CLAY
VS
NON-LINEAR GAMMA RAY
VCL
X = [γ − γ CLEAN / γ SHALE − γ CLEAN]
γ CLEAN = 48 API
γ SHALE = 118 API
VCL = 1.7 − √(3.38 − (X + .7)²)
⊠ DENOTES LABORATORY MEASUREMENTS

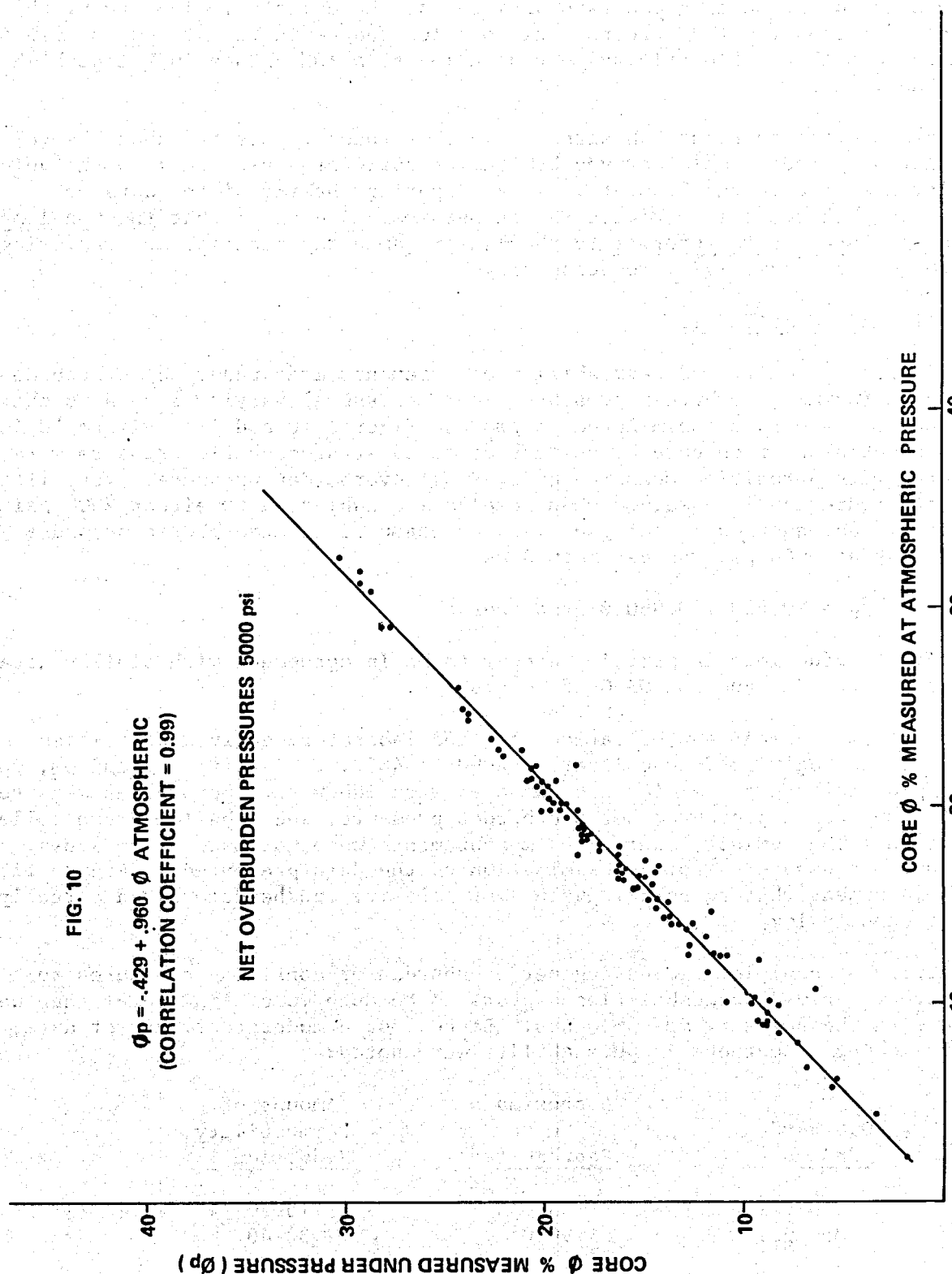
CORE Ø % MEASURED UNDER PRESSURE (Øp)
CORE Ø % MEASURED AT ATMOSPHERIC PRESSURE
10
20
30
40
NET OVERBURDEN PRESSURES 5000 psi
Øp = -.429 + .960 Ø ATMOSPHERIC
(CORRELATION COEFFICIENT = 0.99)

FIG. 10

This relationship implies that in a theoretical sense that the gamma ray cannot be related to a shaly sand in a linear manner. As sand becomes more shaly, the bulk density of the sand will increase in value. This will result in an exponential decrease in gamma rays arriving at the detector. Therefore, the amount of radioactivity corresponding to a 10% change in Vcl at low Pb values is much less than radioactivity corresponding to a 10% change in Vcl at high Pb values.

The data plotted in Figure 9b agrees with this theory. Observe that the Vcl calculated by the formula derived by Clavier correlates very well to the volume of clay measured in the laboratory. In comparing the fit of the data in Figure 9b with the fit in Figure 9a, it becomes quite clear that the non-linear gamma ray function is superior to the linear gamma ray function in predicting the volumes of resistivity reducing clays.

POROSITY AND PERMEABILITY

Core derived porosity and permeability measurements made under net overburden pressures (normal overburden pressure - pore pressure) varying from atmospheric to 5000 psi have been assimilated to produce Figures 10 and 11. Figure 10 is the plot obtained when core porosities measured at atmospheric pressure were compared with porosities measured under a net overburden pressure. Very little porosity reduction is observed when samples are subjected to either 2000 psi or 5000 psi. An equation relating porosities measured at atmospheric pressure with those at 5000 psi was determined as

$$\phi_p = -0.429 + 0.960\ \phi \text{ atmospheric}$$

The slight reductions in porosity appear to be in agreement with similar data from the North Sea and the US Gulf Coasts.

Figure 11 is a comparison of various log and laboratory derived porosities from a cored Taglu sandstone interval 4090 to 4697.7. Density log and ϕ_N, ϕ_D cross plot derived porosities are compared with laboratory porosities measured under atmospheric pressure, net overburden pressure, and a humidity controlled condition. The humidity controlled measurements were not made using a net overburden pressure. From an examination of the data presented in Figure 11, it would appear that acceptable values of porosity can be determined directly from a density log.

The effect of applying increasing net overburden or confining pressures to laboratory derived permeabilities appears to be much more significant than was noted with the porosity measurements. Based upon a moderate amount of data, the following reductions in permeability were noted:

Net Overburden Pressure	Approximate Depth Represented	Amount of Permeability Reduction %
2000 psi	3500'	15-20
5000 psi	9000'	33-40

Based on permeability measurements from 24 samples subjected to 300 psi and 5000 psi net overburden pressure respectively, the following equation was derived:

$$K_{5000\ psi} = 5.03 + 0.64\ K_{300\ psi}$$

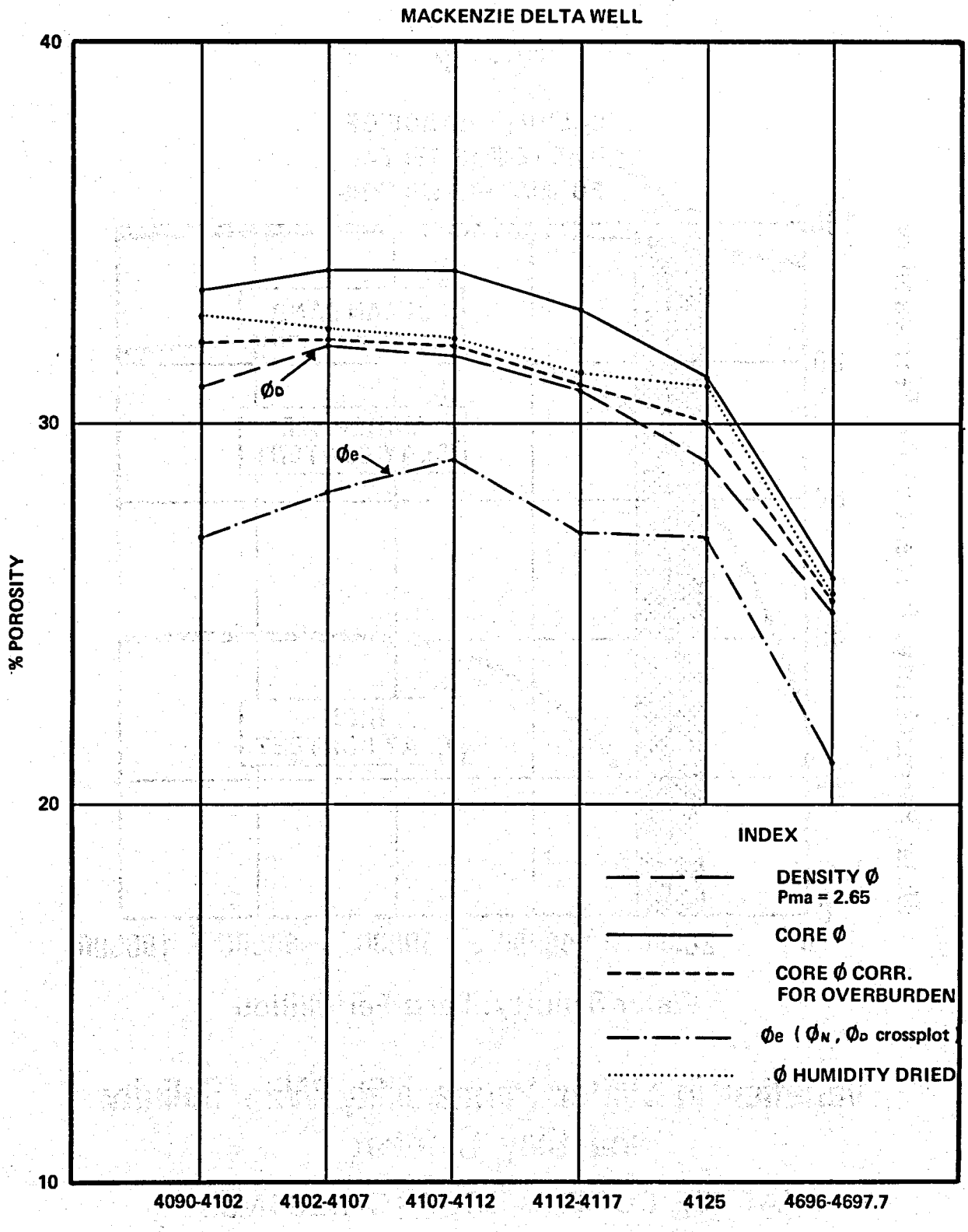
MACKENZIE DELTA WELL
40
30
20
10
% POROSITY
ØD
Øe
INDEX
DENSITY Ø
Pma = 2.65
CORE Ø
CORE Ø CORR.
FOR OVERBURDEN
Øe (ØN , ØD crossplot)
Ø HUMIDITY DRIED
4090-4102
4102-4107
4107-4112
4112-4117
4125
4696-4697.7
CORED INTERVALS (POROSITY AVERAGED FOR INTERVAL)

FIG. 11

FIG. 12

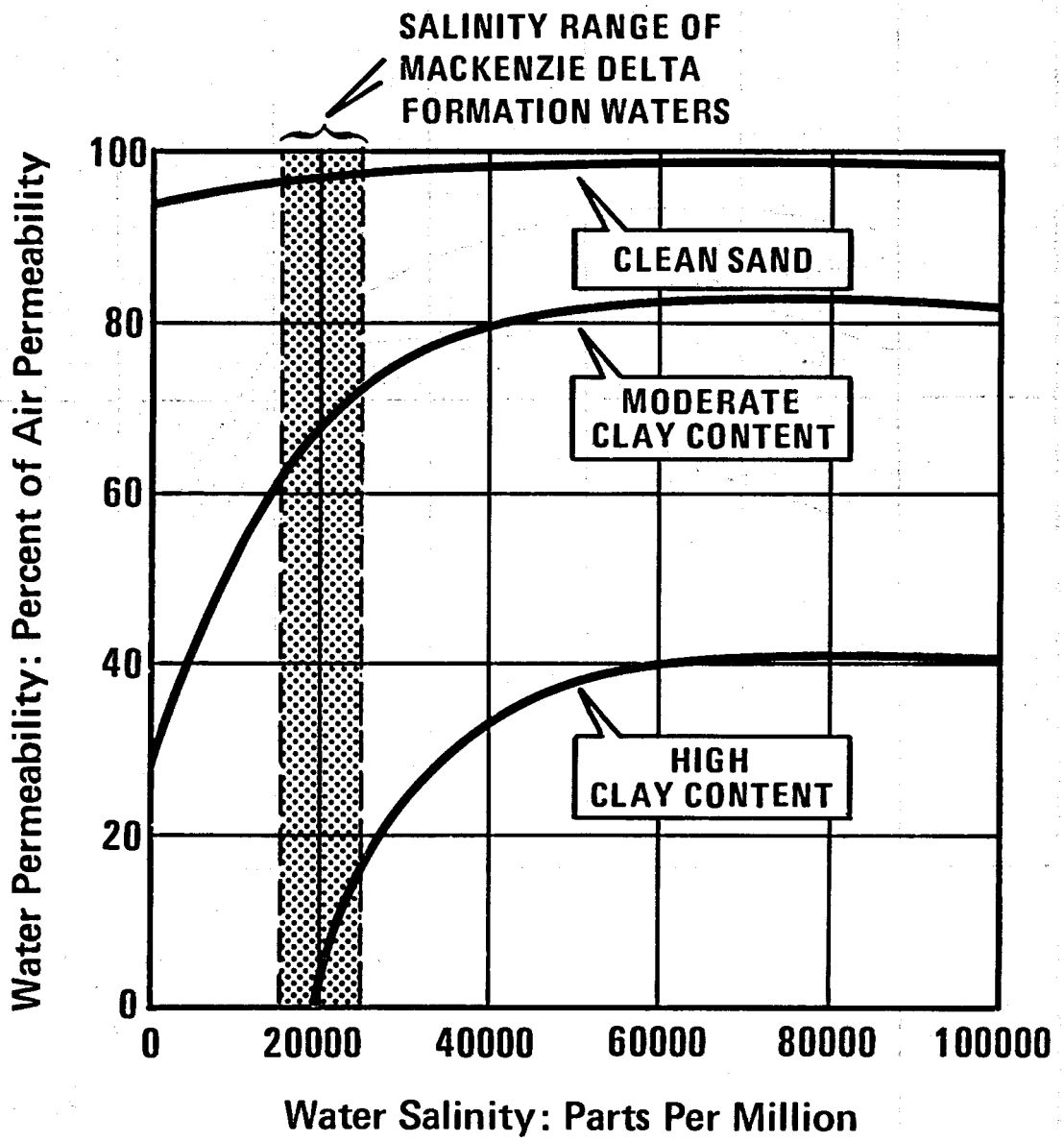

Variation in Water Permeability With Salinity and Clay Content

(AFTER CORE LABORATORIES INC.)

The reduction in permeability observed above probably represents a maximum since all measurements were made on cleaned and dried core samples. The problem with this is that the confining pressure used in the laboratory cannot be transmitted to a pore fluid as would normally occur in the subsurface environment.

A further consideration when assessing the potential productivity of liquid bearing reservoirs in the Mackenzie Delta is illustrated in Figure 12. The comparison being made is between permeability to air of a cleaned and dried sample versus permeability to water in the presence of varying amounts of clay and changing formation water salinity. The salinity range of Mackenzie Delta formation waters is illustrated by the two dashed vertical lines. Note that in this range even moderate amounts of clay present in the matrix will significantly lower the permeability to water. The reduction in permeability in the case where the fluid is oil may not be as significant.

FORMATION FACTOR VERSUS POROSITY

The following equation relating formation factor to porosity has been used with success in the Mackenzie Delta.

$$F = 0.79\phi^{-2.09}$$

This equation was derived from laboratory measurements made on core samples subjected to a net overburden pressure of 5000 psi. It is essentially the same as the "Humble Formula."

RESULTS AND CONCLUSIONS

In judging the results of the shaly sand analysis technique discussed in this paper, reference is first made to Figure 13 which is a ϕ_N, ϕ_D cross plot similar to that shown in Figure 3b. Superimposed on Figure 13 are the volumes of clay as determined from the conventional ϕ_N, ϕ_D cross plot (dashed lines) and the effective clay volumes as determined through relationships, CEC-Effective Vcl, CEC-gamma ray, and gamma ray vs. $(\phi_N-\phi_D)$. Note that the latter method results in considerably lower Vcl percentages. The data points which appear closest to the clean water sand line, now have Vcl values of 5% to 10% rather than the 30% as determined from the conventional ϕ_N, ϕ_D cross plot. Note also that the subdivision of Vcl between 0 (clean sand line) and 100% is not linear as is assumed in the ϕ_N, ϕ_D cross plot method. The reduced clay volume is more compatible with the other log data for the plotted interval. Some variance between the two methods is probably reflecting the difference between effective and total clay volumes.

Figures 14 and 15 are computer plots from two wells in the Mackenzie Delta. These wells were selected because of the difficulty in determining hydrocarbon presence from conventional log analysis. Porosities are from density logs. Of main interest is the difference in water saturation values as determined from the Waxman-Smits equation and that from the standard Archie equation. Where the sands are relatively clean such as approximately 4,350 feet in Figure 14, the two Sw values are quite similar and show without any problem the presence of hydrocarbons. In the shalier portions, the shaly sand corrected Sw data is clearly more compatible with the DST data shown in the centre columns.

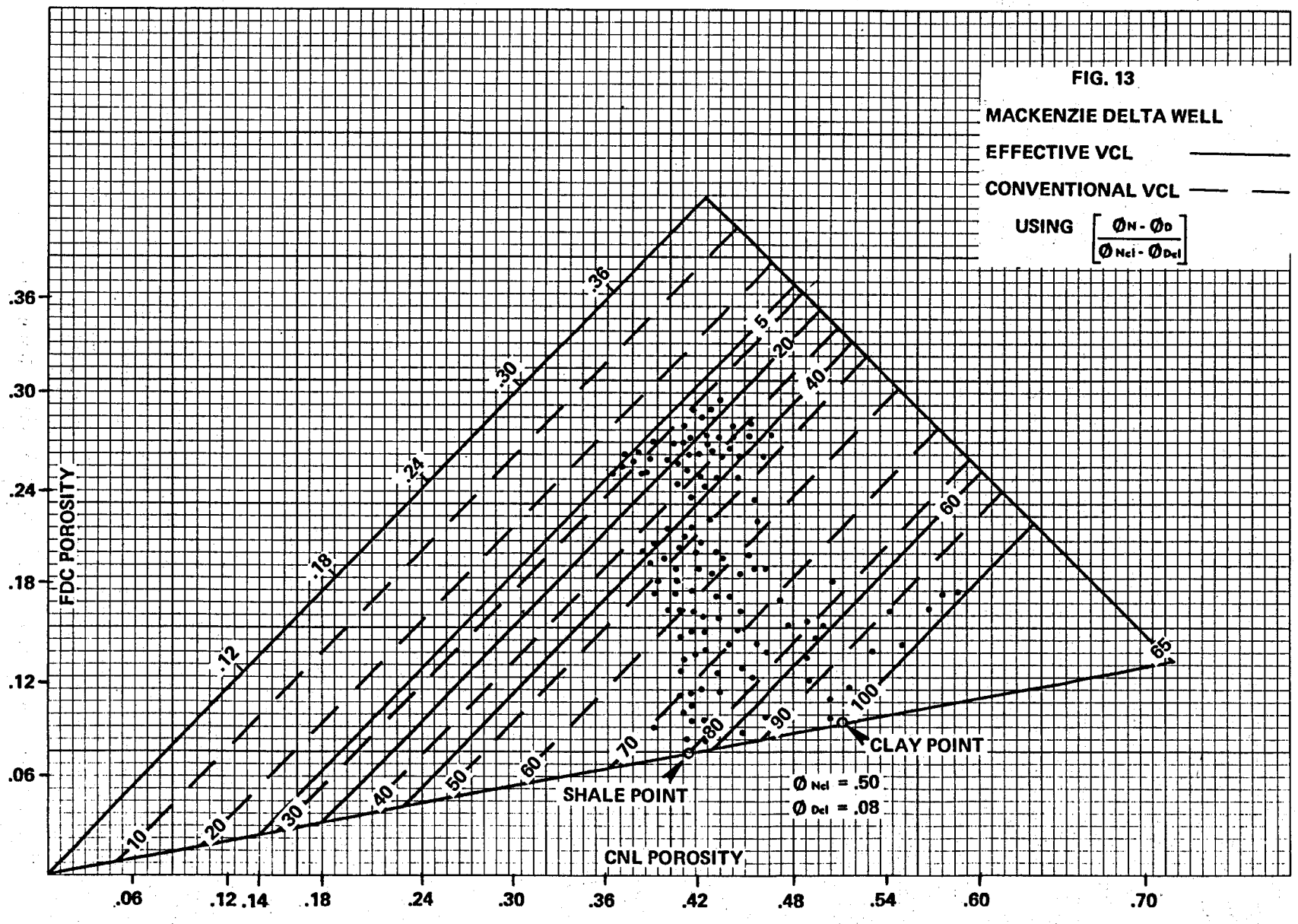
FIG. 13
MACKENZIE DELTA WELL
EFFECTIVE VCL
CONVENTIONAL VCL
USING $\left[\frac{\phi_N - \phi_D}{\phi_{Ncl} - \phi_{Dcl}}\right]$
FDC POROSITY
CNL POROSITY
.36
.30
.24
.18
.12
.06
.06
.12
.14
.18
.24
.30
.36
.42
.48
.54
.60
.70
.36
.30
.24
.18
.12
5
20
40
60
65
100
90
80
70
60
50
40
30
20
10
CLAY POINT
SHALE POINT
ϕ_{Ncl} = .50
ϕ_{Dcl} = .08

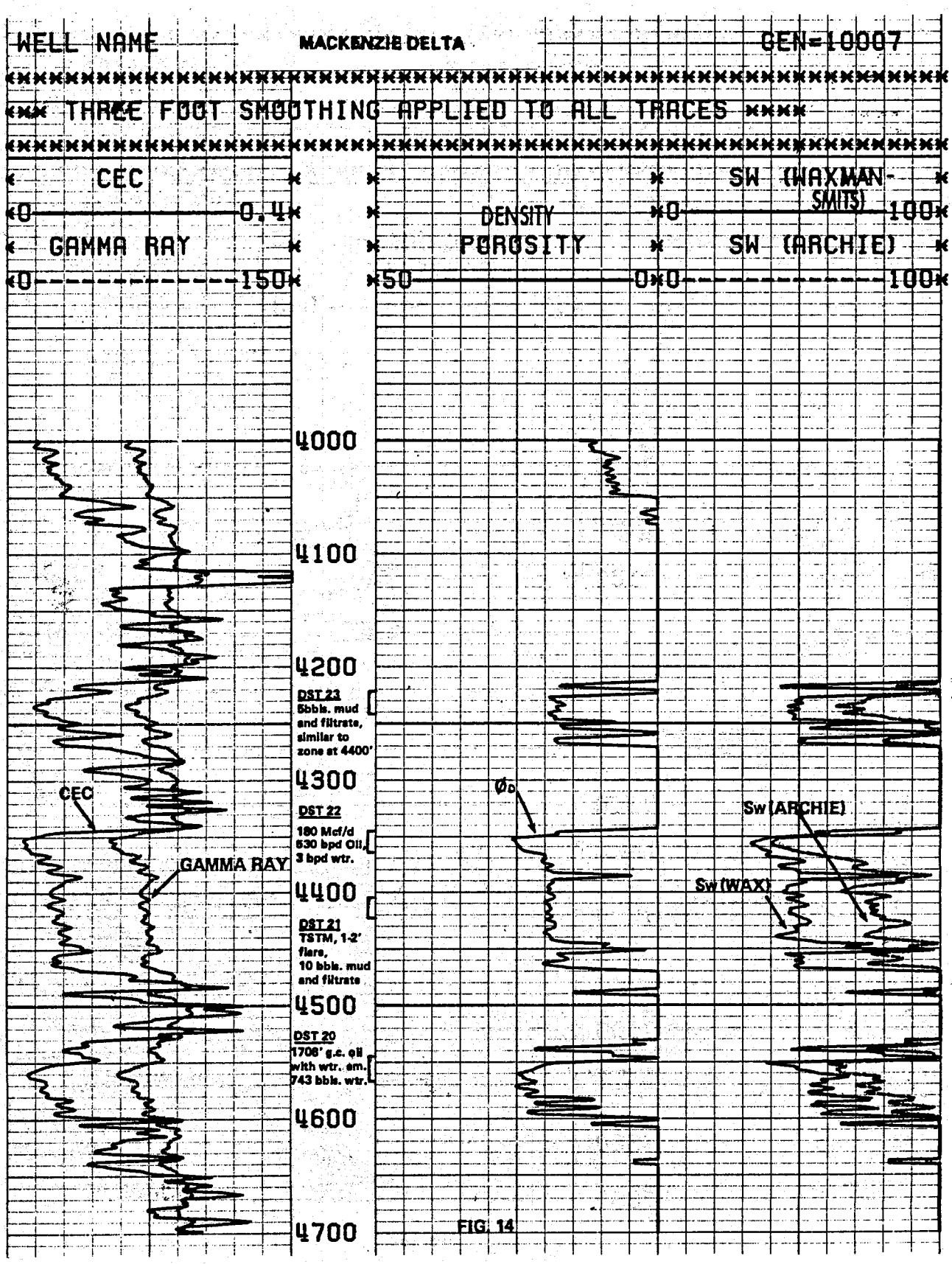
WELL NAME
MACKENZIE DELTA
GEN=10007
THREE FOOT SMOOTHING APPLIED TO ALL TRACES
CEC
0
0.4
GAMMA RAY
0
150
DENSITY
POROSITY
50
0
SW (WAXMAN-SMITS)
0
100
SW (ARCHIE)
0
100
4000
4100
4200
4300
4400
4500
4600
4700
DST 23
5bbls. mud and filtrate, similar to zone at 4400'
DST 22
180 Mcf/d
630 bpd Oil,
3 bpd wtr.
DST 21
TSTM, 1-2' flare,
10 bbls. mud and filtrate
DST 20
1708' g.c. oil with wtr. em.
743 bbls. wtr.
CEC
GAMMA RAY
ϕ_D
Sw (ARCHIE)
Sw (WAX)

FIG. 14

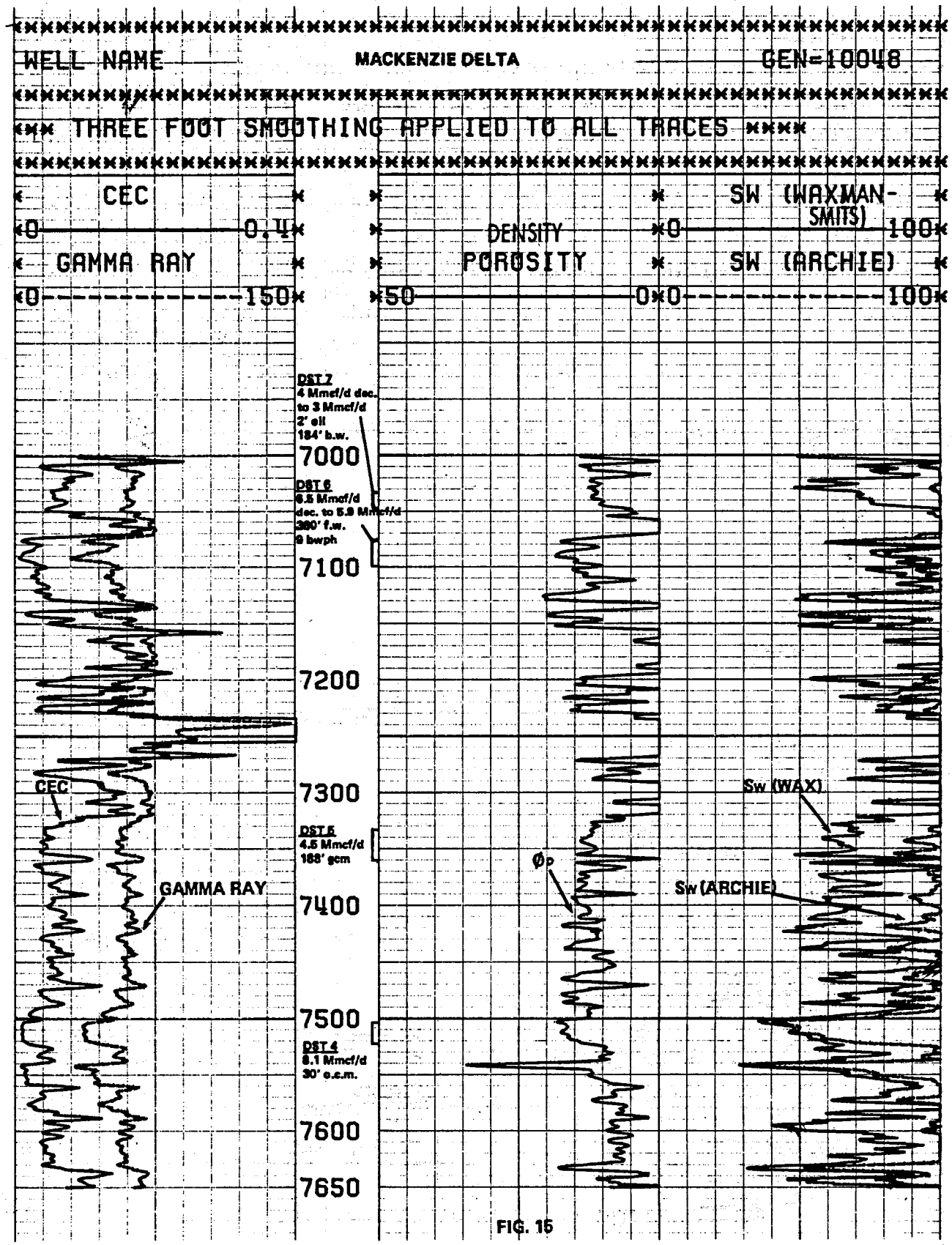
WELL NAME
MACKENZIE DELTA
GEN=10048
THREE FOOT SMOOTHING APPLIED TO ALL TRACES
CEC
0
0.4
GAMMA RAY
0
150
DENSITY POROSITY
50
0
SW (WAXMAN-SMITS)
100
SW (ARCHIE)
0
100
DST 7
4 Mmcf/d dec. to 3 Mmcf/d
2' oil
184' b.w.
DST 6
6.5 Mmcf/d
dec. to 5.9 Mmcf/d
380' f.w.
9 bwph
DST 5
4.5 Mmcf/d
188' gcm
DST 4
6.1 Mmcf/d
30' o.c.m.
7000
7100
7200
7300
7400
7500
7600
7650
CEC
GAMMA RAY
Sw (WAX)
Sw (ARCHIE)

FIG. 15

In conclusion, it is our contention that density logs alone can be effective porosity values of acceptable accuracy and that the gamma ray curve can determine effective volumes of clay, i.e., the clays which have a reducing effect on resistivity logs. Further CEC work is necessary in other areas in order to establish a set of interrelationships between CEC, gamma ray, Rsh and Vcl.

ACKNOWLEDGEMENT

The authors wish to thank the management of Chevron Standard for their permission to publish this paper. They also express gratitude to Mr. P.A.T. Haines for reviewing the paper prior to publication, and to Chevron Geophysical for its promptness in handling computer analysis requests.

REFERENCES

1. CONNOLLY, E. T., 1968: Standardization of Large Volumes of Log Data for Computer Analysis; Trans. CWLS Symposium.

2. ARCHIE, G. E., 1942: The Electrical Resistivity Log as an Aid in Determining Some Reservoir Characteristics; AIME T. P. 1942, Petroleum Tech.; also in AIME Trans. 146, Petroleum Div., p. 54-62.

3. GRIM, R. E., 1968: Clay Mineralogy; McGraw Hill, p. 51-124, 188-225.

4. DEER et al, 1974: An Introduction to the Rock Forming Minerals; Longmans, p. 250-275.

5. FOSTER, Margaret, 1953: Geochemical Studies of Clay Minerals II - Relation Between Ionic Substitution and Swelling in Montmorillonite; American Mineralogist, v. 38, p. 994-1006.

6. WAXMAN, M. H. and SMITS, L.J.M., 1968: Electrical Conductivities in Oil-Bearing Shaly Sands; Trans. AIME (SPE), v. 243, p. 107-122.

7. _____ and THOMAS, E. C., 1972: Electrical Conductivities in Shaly Sands; Annual Meeting AIME (SPE, Paper 4094).

8. SIMANDOUX, P., in Schlumberger Log Interpretation, v. 1, p. 93.

9. CLAVIER, C., 1971: Quantitative Interpretation of Thermal Neutron Decay Time Logs; J.P.T., v. 23, p. 751.

10. STEFFENSEN, J., 1976: Unpublished Memo - Formerly Chev. Std., now Petro-Canada.

APPENDIX I

NEUTRON/DENSITY DRY GAS CORRECTION

Density logs in gas zones typically exhibit too high a porosity with the reverse being true for neutron logs. In order to calculate the clay content and/or water saturation of a gas zone, the porosity from the density and/or neutron logs must be corrected for the gas effect.

A common method is to plot (ϕ_N-ϕ_D) versus gamma ray in a manner depicted in Figure A for the widest possible array of API values. Since the composition of clays can be erratic both laterally and with depth, it is recommended that plots be broken up into intervals of about 500'. This should allow for a fairly linear correlation of gamma ray with (ϕ_N-ϕ_D) in the water saturated zone(s). This linear correlation has been referred to as the "liquid line." Where the profile takes on a banana-shaped character, as is quite often the the case, the clay composition has probably changed or more likely the correlation between (ϕ_N-ϕ_D) and gamma ray has ceased to be linear beyond a certain value of increasing clay content. Fortunately, the correlation is usually sufficient linear over the range where a gas correction is most significant (see Figure B).

Gas filling the pore spaces of the sand will cause the points to drop below the liquid line. This distance is measured and entered along with the slope and intercept of the liquid line into the following equations (Steffensen[10] 1977).

$$\phi DC \text{ gas corrected} = \phi D1 - Z\left((K\gamma + P) - (\phi N1 - \phi D1)\right)$$

$$\phi NC \text{ gas corrected} = \phi N1 + Y\left((K\gamma + P) - (\phi N1 - \phi D1)\right)$$

Where:

P = Intercept
K = Slope
γ = gamma ray API
$\phi N1$, $\phi D1$ = log porosity values
Z = 0.366 if ϕh = 0
Z = 0.403 if ϕh = 0.1
Z = 0.491 if ϕh = 0.3
Z = 0.579 if ϕh = 0.5
Z = 0.877 if ϕh = 0.7
Let $\phi DC = \phi D1$ if $\phi h \geq 0.7$
Y = 0.634 if ϕh = 0
Y = 0.597 if ϕh = 0.1
Y = 0.509 if ϕh = 0.3
Y = 0.421 if ϕh = 0.5
Y = 0.123 if ϕh = 0.7
Let $\phi NC = \phi N1$ if $\phi h \geq 0.7$

Example: Refer to Figure A

FIG. A

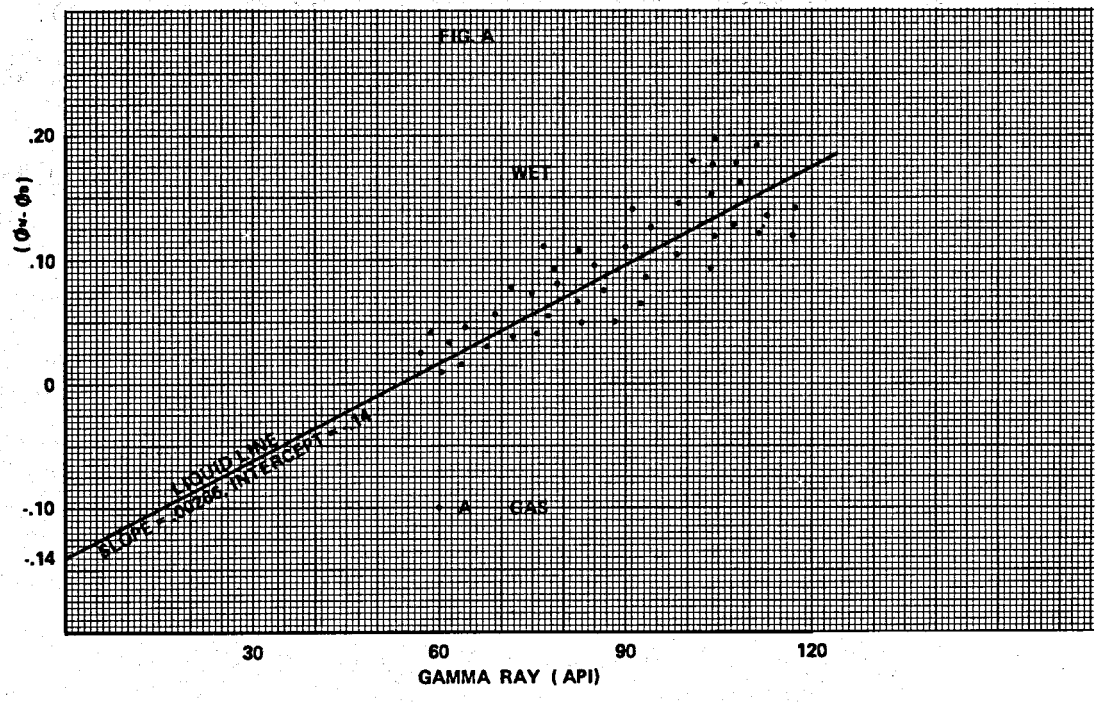
.20
.10
0
-.10
-.14
(Øn-Øa)
WET
GAS
30
60
90
120
GAMMA RAY (API)

FIG. B

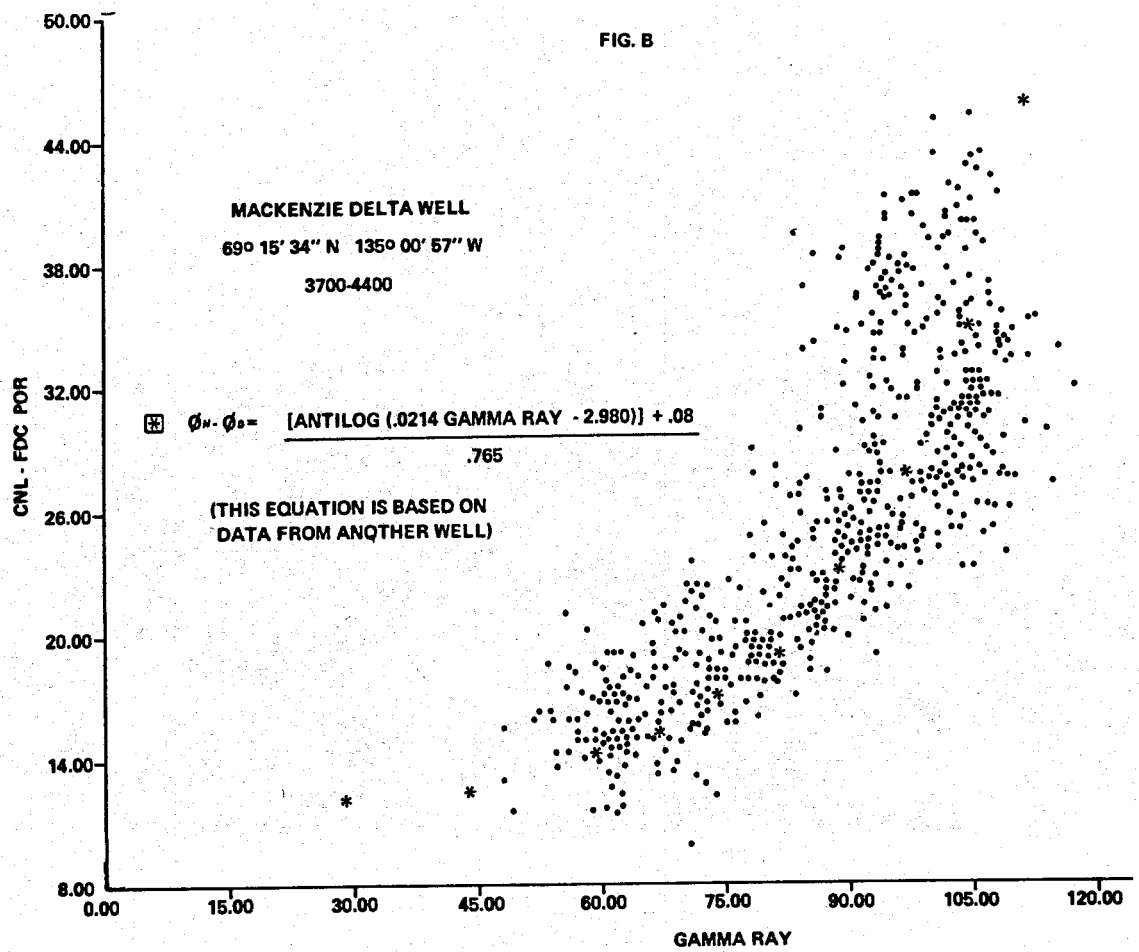
50.00
44.00
38.00
32.00
26.00
20.00
14.00
8.00
CNL - FDC POR
MACKENZIE DELTA WELL
69° 15' 34" N 135° 00' 57" W
3700-4400
Øn-Øa= [ANTILOG (.0214 GAMMA RAY - 2.980)] + .08
.765
(THIS EQUATION IS BASED ON DATA FROM ANQTHER WELL)
0.00
15.00
30.00
45.00
60.00
75.00
90.00
105.00
120.00
GAMMA RAY

Point A has a $\phi N = 0.25$, $\phi D = 0.35$, $\rho h = 0$ and a $\gamma ray = 60$ API. The slope of the liquid line is 0.0026 and the intercept is -0.14 (see Figure A).

$$\phi DC \text{ gas corrected} = 0.35 - 0.366\left(0.00266(60) + (-0.14) - (.25 - .35)\right)$$

$$\phi DC \text{ gas corrected} = 0.306$$

$$\phi NC \text{ gas corrected} = 0.25 + 0.634\left(0.00266(60) + (-0.14) - (0.25-0.35)\right)$$

$$\phi NC \text{ gas corrected} = 0.326$$

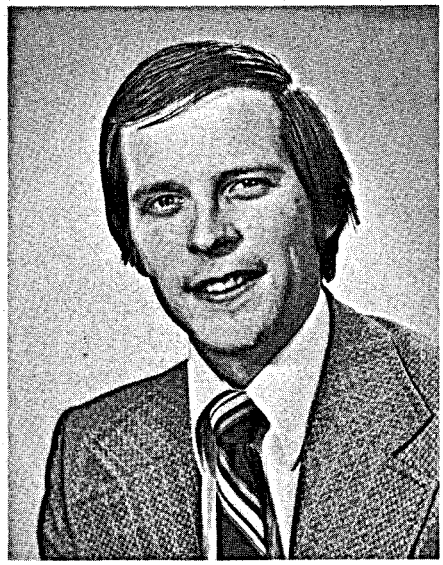

WALTER JOHNSON

BILL LINKE

ABOUT THE AUTHORS

WALTER L. JOHNSON is a formation evaluation geologist at Chevron Standard Limited in Canada. He received his BSc with distinction in Geology from the University of Calgary, Calgary, Alberta, in 1973. For several years, he has been involved with shaly sand analysis in the Mackenzie Delta and the Alberta Plains. Currently, he is engaged in a computer shaly sand analysis project for the parent corporation. He is a member of the APEGGA, CSPG, CWLS and the AAPG.

WILLIAM A. LINKE is a staff geologist, formation evaluation with Chevron Standard Limited in Calgary, Alberta, Canada. He received his BSc in Geology from the University of Alberta in 1951. For the past twenty-five years, he has worked as a formation evaluation geologist in Canada and Trinidad WI. In addition to conducting numerous well logging courses for Chevron Standard, he has conducted courses for the University of Calgary and the Southern Alberta Institute of Technology. Bill is a member of the CWLS, SPWLA, CSPG and the AAPG.

THE F-Ø-m CROSS PLOT — A NEW APPROACH FOR DETECTING NATURAL FRACTURES IN COMPLEX RESERVOIR ROCKS BY WELL LOG ANALYSIS

By

Orlando Gómez-Rivero

Petroleos Mexicanos, Mexico City, Mexico

I. ABSTRACT

A computer oriented method is presented for detecting the presence of natural fractures in complex reservoir rocks with very low matrix porosity using only conventional well logs. Vugs, complicate still more the problem of fractured reservoir rocks. The method also allows for the determination of probable existence of vugs. This novel approach is characterized mainly by a new practical use of the formation resistivity factor, F, together with porosity and all other parameters normally employed in well log analysis. It is necessary the use of nuclear porosity logs, such as neutron and density gamma-gamma, but it can be applied even in cases with limited logging program. Minimum well logging program, however, normally requires deep and shallow suitable resistivity logs and at least one nuclear porosity log; a gamma-ray curve is desirable. As a matter of fact, the method is a general approach; therefore, it can be applied also, with advantage, to non fractured, non complex reservoirs, for computing connate water saturation and a permeability indicator.

The application of this method may permit a better selection of intervals for testing wells in reservoir rocks with complex porosity system, which can save considerable rig time during completion operations. The method is illustrated with example wells which include fractured reservoirs from the recently discovered fields of Southeast Mexico.

II. INTRODUCTION

Naturally fractured reservoirs have always been a very difficult task for their study and operation. A recent publication[1] shows the importance of the problem, as testified by the 214 references it contains on literature about this special subject. This world-wide problem has been approached in different ways, which vary from core analysis through reservoir performance studies; well logging tchniques and well log analysis have been one of the most important ways for a more comprehensive understanding of this problem. Vugs, frequently present together with fractures, and lithology changes, complicates more the problem.

Fracturing may occur in any kind of reservoir rock, but more typically they are present in carbonate rocks. Their characteristics may range from massive, vuggy and fractured reservoirs to the highly stratified reservoirs, depending upon the position of the reservoir rock with respect to the original depositional environment and the influence of further diagenetic processes modifying their original textures. Even though the amount of primary porosity in initial carbonate sediments is higher than in initial sandstone sediments, the final porosity in carbonate rocks is smaller than in sandstone rocks. In carbonate rocks, primary intergranular porosity is more variable than in sands, because of its wide variety in grain size and shape; besides, these carbonate rock original pore systems can be modified because of the post-depositional diagenetic effects.

There are five main natural processes of porosity and permeability alteration that commonly occur in carbonate rocks[2]. Some of them can increase these reservoir parameters, some can decrease them and some others can produce either of these effects. Such processes are: leaching, dolomitization, fracturing, recristalization and cementation.

Leaching, generally improve porosity and enhance permeability. Dolomitization, on the other hand, may increase the pore size or may destroy permeability. But, main effect of dolomitization seems to be permeability increase, as observed in practice [2], by better development of solution vugs in dolomites; as a consequence of dolomitization, natural fracturing may be produced more easily because of the brittle nature of dolomites.

Fracturing may become productive very low porosity rocks, which otherwise would be non productive. Generally, fractures increase porosity very little but notably increases permeability. They are more common in tectonically active areas, such as the area where the recently discovered fields in SE Mexico[3] are located.

Recristalization, can produce higher porosities in carbonate rocks but the associated permeability is very low and difficult to determine. Certain cements can destroy porosity even in small amounts.

The method here presented is intended to identify complex porous fractured rocks, such as those briefly outlined above, by using only well logs. It makes use of a computer program that may throw numerical listed results of Sw, $\emptyset$, m, a and F which can also be displayed as computed curves. Nevertheless, one of the most efficient presentations of data for getting the most out of the method is as F-$\emptyset$-m cross-plots. The different presentation of data serves different purposes. Listed numerical values are used for selecting the intervals for testing the well and evaluating the importance of the well oil and gas reserve. The F-$\emptyset$-m cross-plot gives an overall view of the well as a prospect for obtaining

production from naturally fractured zones, from non fractured zones or if an artificial fracturing will be necessary for making the well productive or more productive.

III. BASIS OF THE METHOD

III. 1 Theoretical and Practical Background

Main theoretical and practical basis of this new approach are contained in two previous publications [4,5], and will be briefly reviewed here upon. The more general F-Ø relationship is considered to be:

$$F = a / \emptyset^m \qquad \ldots \qquad (1)$$

On the other hand, the following relationship has been found to exist between parameters a and m of the above equation[4]:

$$m = A - B \log a \qquad \ldots \qquad (2)$$

Various practical applications have been derived from the basic relation (2). The scope of this study is the development of a method for detecting natural fractures by an approach which basically involves the use of Eq. (2). New abundant additional data of a and m, for sands and carbonate rocks, have verified this relationship and supports its validity; the statistical correlation coefficient is above 0.9. When Eq. (2) is combined with Eq. (1), the following expression is obtained [4]:

$$\log a = \frac{A \log \emptyset + \log F}{1 + B \log \emptyset} \qquad \ldots \qquad (3)$$

Equations (2) and (3) show that a and m can be computed by only using well logs; i. e, no assumptions are necessary for these parameters. A method have been established for computing a and m with reasonable accuracy, even in hydrocarbon bearing formations. [4,5] For making more easy in some cases the computation of m, charts of Figs. 1, 2, and 3 were developed, which are solutions of Eqs. (2) and (3). These charts are widely used in this method and have the following characteristics.

—Numerical values of constans A and B are as listed below.

Table I. Numerical Values of Constants A and B

Rock Type	Constant	
	A	B
Sand	1.8	1.29
Carbonate	2.03	0.9

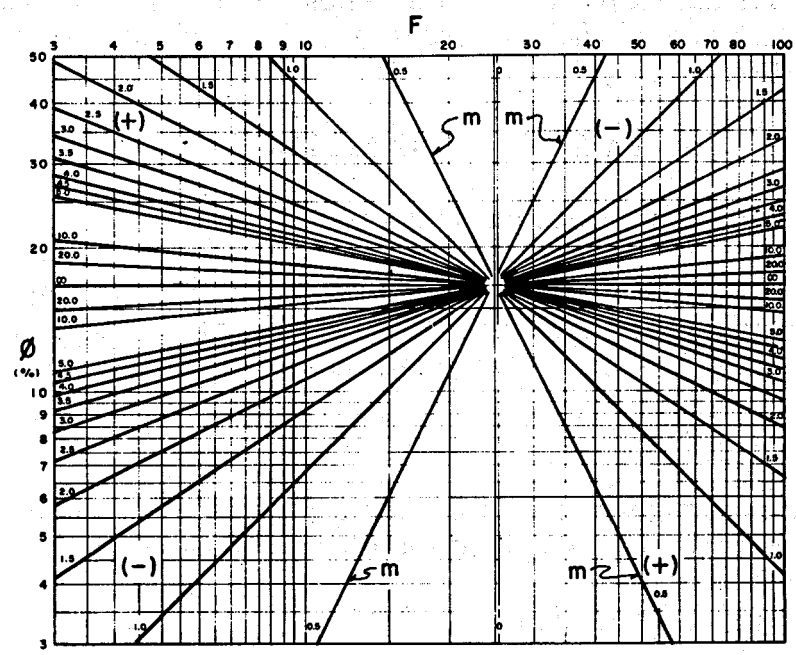

Fig. 1.- Chart for determining Ø, F, or m for sands.[4]

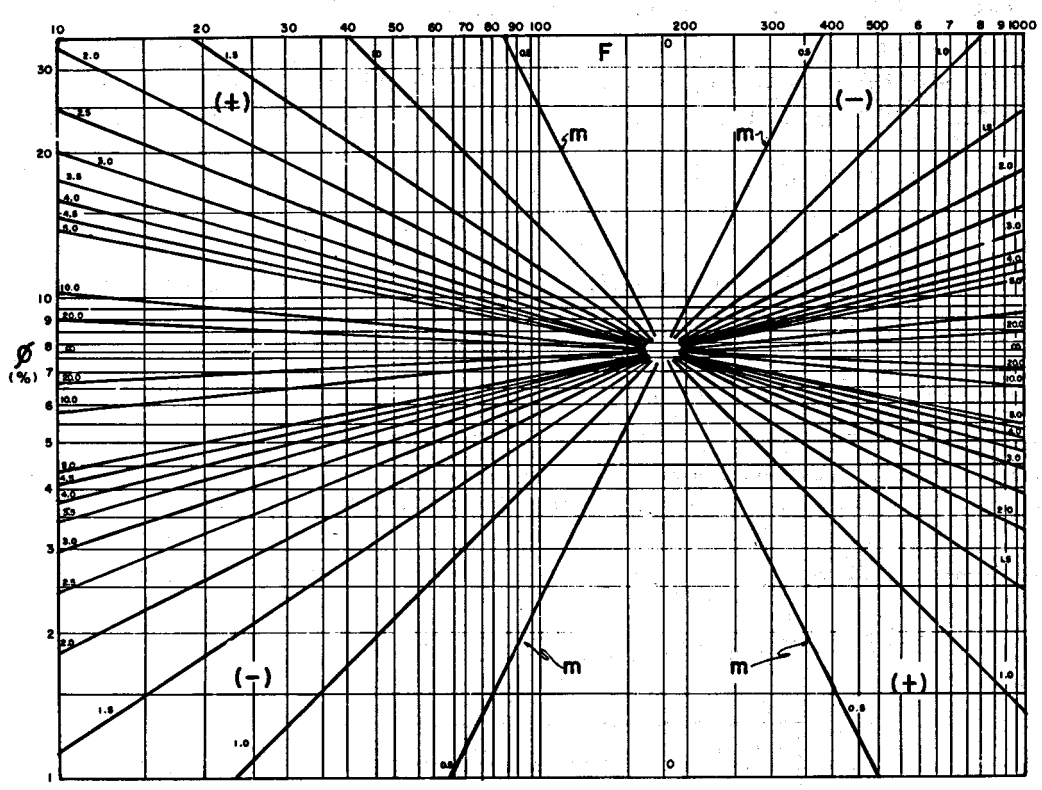

Fig. 2.- Chart for determining Ø, F or m for carbonate rocks.[4]

As A and B are statistical constants, their value may vary according to the amount and nature of a and m data available. Nevertheless, it has been found in practice that this variation is just small and

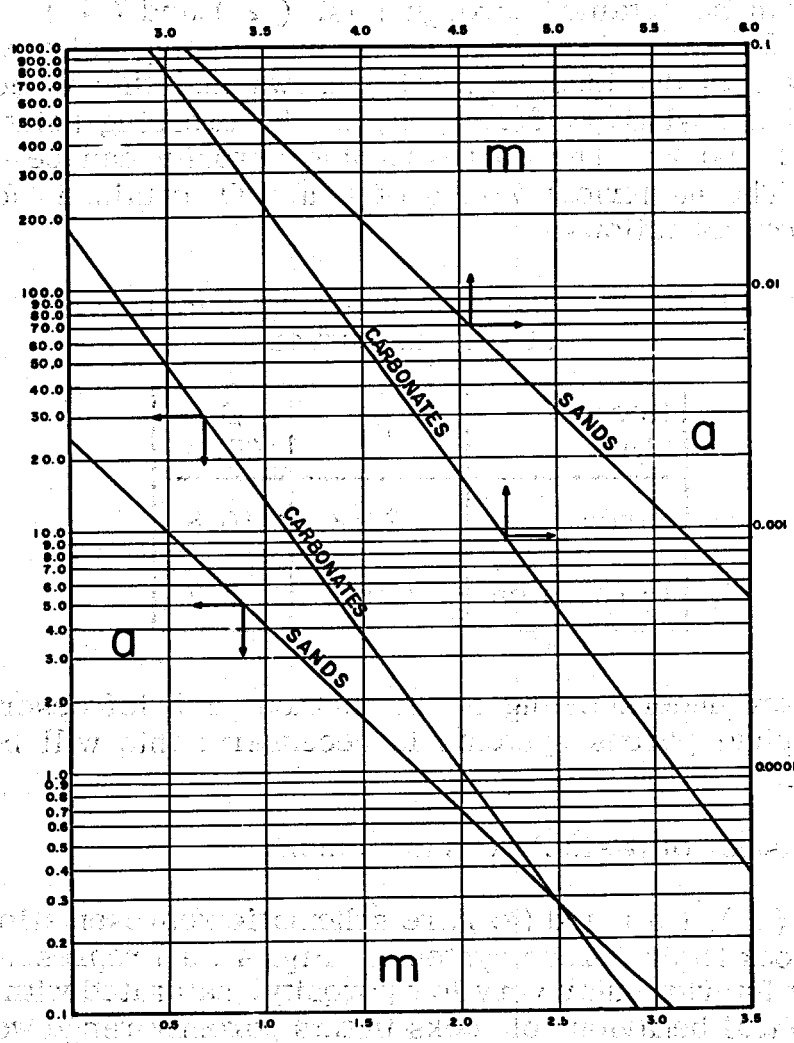

Fig. 3.- Chart for determing a or m.[4]

unimportant for practical quantitative and qualitative interpretation purposes.

– Porosity $\emptyset$, is total shale or clay free porosity; therefore, it includes intergranular primary porosity and any other kind of porosity such as fractures and vugs, effective or not effective.

– Formation factor, F, is effective formation factor; accordingly, isolated, non interconnected porosity will behave, electrically, as non porous permeable matrix rock.

As can be observed in Figs. 1 and 2, every m curve crosses each

other at a common point. This is a very important and basic information. The relative position of this point in the charts depends upon the values of constants A and B. Unique values of F and $\emptyset$ characterizes this point for each of both charts. The coordinates, F and $\emptyset$, of these crossing points can be obtained through Eqs. (2) and (1). By making $m = 0$ in Eq. (2) the value of $\bar{a}$ at the intersecting point with the $\bar{a}$ axis in Fig. 3 is obtained; Eq. (1) shows that this value also equals the formation resistivity factor, F, at the crossing point of all m curves of Figs. 1 and 2. The corresponding porosity can be obtained from Eq. (1). The numerical values of F and $\emptyset$ obtained for the crossing points are as follows:

Table 2. - Common crossing points of the m curves.

Rock Type	F	$\emptyset$ (%)
Sands	24.8	16.8
Carbonates	180	7.7

For a better understanding of the method, a brief description of some complex typical porous systems is necessary; this will be accomplished in the next section.

III. 2 Characteristics of Basic Porous Systems.

Figures 4 (a), (b) and (c) are schematic representations of three carbonate rock basic porous systems. Fig. 4 (a) represents a rock with only primary intergranular very low porosity, saturated with only brine. The normal electrical behaviour of rocks in this porosity range would follow the illustrated trend in the companion figure at the right.

Now, let us assume that the same porous system as above exists, but with effective fractures (Fig. 4 b). Even when fractures, generally, do not increase porosity very much, it do increase permeability; of course, cases are where fractures constitutes almost the total porosity. Fractures, are also very efficient channels for electricity flow; accordingly, formation resistivity factor for this second porous system would be lower than in case (a) and the position of the F, $\emptyset$, point would be very different; the more intensive and effective the fracturing, the lower the resistivity factor.

Finally, a third typical case may exist, as shown in Fig. 4 (c). The same rock as in the first case but with solution channels and inter-

connected vugs. Even though leaching does not increases porosity very much, permeability is notably increased; as conductivity is also increased very much, resistivity factor decreases. Total porosity is higher than - in the two preceding cases and frequently is in the medium to low range; then the position of the F, $\emptyset$, point would be quite different, as indicated in the companion diagram.

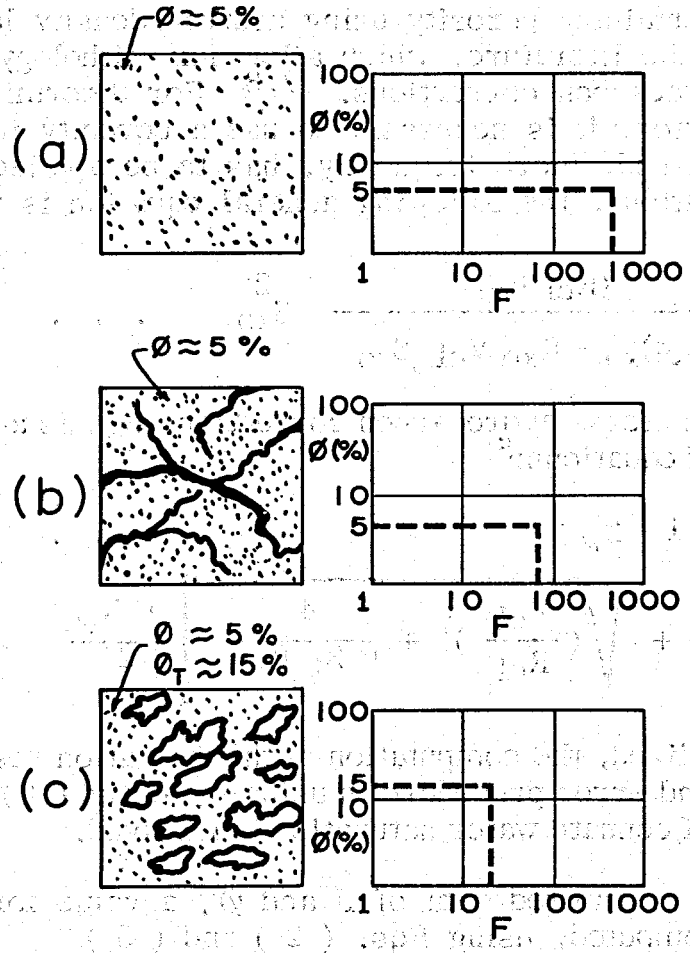

Fig. 4. - Basic porous systems and their electrical behaviour.

The relative position of the F, $\emptyset$, point in the F, $\emptyset$, m cross-plot is one of the basic interpretation points of departure of the method here presented for detecting fractures. There are well logging techni-- ques from which reasonable accurate porosity values can be obtained, - but resistivity factor determination still can rely on computations - - through equations. The approach here presented is characterized mainly by the computation of formation resistivity factors by only well logs; but in practice this has to be performed principally in hydrocarbon bearing intervals, and the more accurate this determination the more dependable the method. The mechanism to arrive at computed F values will

be described in what follows immediately.

IV. DESCRIPTION OF THE METHOD

The method here presented for detecting fractures, essentially consists in determining the total porosity and the formation resistivity factor in each analyzed level. Porosity must be obtained from nuclear logs. Equations for obtaining porosity using neutron-density logs combinations are given in the literature, which allow for lithology, shale or clay content and hydrocarbon corrections.[6,7,8] For determining the formation resistivity factor, it is necessary to use a porosity independent equation. As the method, more frequently, has to be applied to hydrocarbon bearing formations, the following general equation is used:[5]

$$F = \frac{R_{xo}}{R_{mf}} \quad \frac{(R_{cl})_{xo}}{(R_{cl})_{xo} - R_{xo}\, V_{cl}\, S_{xo}} \quad S_{xo}^2 \qquad \ldots \qquad (4)$$

in terms of clay parameters; hydrocarbon correction S_{xo}, is accomplished by the following set of equations:[5]

$$S_{xo} = 1 - f_{hr}\,(1 - S_w) \qquad \ldots \qquad (5)$$

$$S_w = \left[- \frac{V_{cl}}{R_{cl}} + \sqrt{\left(\frac{V_{cl}}{R_{cl}}\right)^2 + \frac{4}{F\, R_t\, R_w}} \right] \frac{F\, R_w}{2} \qquad \ldots \qquad (6)$$

As may be realized, the computation of the formation resistivity factor, implies a trial and error procedure in using equations (4) through (6), and the computation of connate water saturation is involved.

With the final computed data of F and ϕ, a value for parameters a and m is also computed, using Eqs. (2) and (3).

Each point, defined by the F, ϕ, computed data as above, is plotted on charts of figures 1 and 2. The relative position of any point with respect to F, ϕ and m in the cross-plot will help to determine whether or not the analyzed level is within a fractured zone, has predominantly vugular porosity or is a normal reservoir rock with almost only primary intergranular porosity.

In applying Eqs. (4) through (6) in fractured rocks, several assumptions have to be made.

— Oil may be accumulated in primary porosity, fractures and vugs. Microfractures, provide the necessary means for draining hydrocarbons from the low porosity small blocks to the main fracture system.

— Mud filtrate flushing occurs in the low primary porosity system - as well as in fractures and effective vugs.

— The electrical deep and shallow devices measure, respectively, - average values of R_t and R_{xo} of the composite porous system of primary - porosity, vugs and fractures.

— Computed water saturations are average values of the total effective porous system.

V. INTERPRETATION PRINCIPLES OF THE METHOD

V. 1 Detection of Fractures

Wyllie and Gregory [9], conducted laboratory experiments in order to ascertain the effect of increasing the amount of cement on the formation resistivity factor of initially unconsolidated porous medium. The - result was a rapid increase in resistivity factor, ensuing as porosity is decreased by the presence of cement material. This was true for all the different artificial porous systems used by the authors, every one of which had its own F-Ø relationship, i.e., its particular parameters a and m. A similar cementation process like this is supposed to have - taken place in natural original sediments. As was mentioned in other - section, original porosity of sediments is high and, during the geologic time, several factors can modify it, one of which is the cementation - - process. But these excellent experiments of Wyllie and Gregory do not reveal what will happen when porosity reduction is carried out to the - lowest range of porosity found in practice. This is what will be tried on below.

Figure 5, is a crossplotting of laboratory F, Ø, data reported by Keller [10], of modern reef sediments (dots). For comparison, F, Ø, laboratory data of basalt rock reported by Keller et al [11] are also crossplotted in the same figure (squares). They include unlithified and partially lithified - sediments, leached and recristalized limestone and dolomite. In general, the higher porosities and their corresponding lower formation resistivity - factors of the carbonate group belonging to the unlithified and partially lithified sediments, are what more resemble the initial F - Ø characteristics - of primary sediments before any diagenetic and diastrophic process may - - have ocurred. The rest of the sediments have suffered some alteration ei- - ther by diagenesis and/or moderate diastrophism.

It can be observed that the carbonate sediment plotted points follow the general m curves trend; most of them are located in the cross plot NW region and only just a few in the SW. It can also be realized that the m values for each plotted point are consistently high. All this sediments petrophysical behaviour recall the results of the Wyllie and - Gardner experiments cited at the begining of this section; i.e., the - -

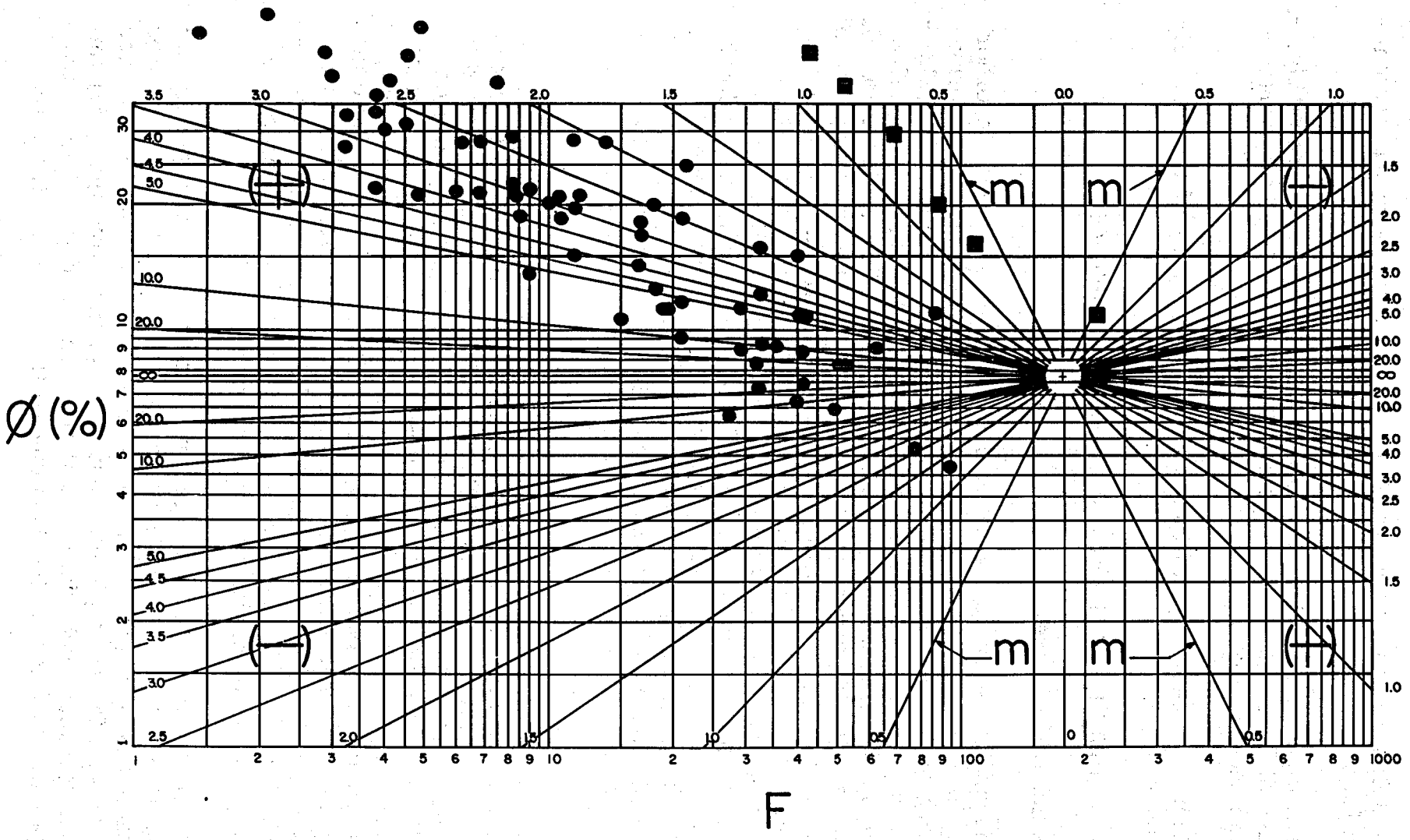

Fig. 5 . Crossplotting of F, Ø , laboratory data reported by Keller [10] and Keller et al. [11] of modern reef sediments (dots) and basalt rock (squares).

more the reduction of initial porosity, the higher the resistivity factor. But all these observable facts deserve some further analysis and will be reviewed with more detail below.

Figure 6 is designed to represent the general petrophysical behaviour of initially unconsolidated sediments, when subject to increased cementation. Let us assume we have a very high porosity, very high permeability porous carbonate sediment, with an initial resistivity factor and primary porosity of about 2 and 40%, respectively. As soon as the cementing natural process starts, porosity reduction begins to occur; consequently, resistivity factor increases. If no other geological modifying factor is present, this cementation process would continue to the lowest porosity ranges in the highest resistivity factor region, following the same m curves trend. But this rarely happens in nature as an isolated process, during the geologic time. Compaction, a process necessarily present, also reduces porosity. Diastrophism, may be present in a variable degree and is one of the processes which most favorably modify the characteristics of some rocks. A high porosity, moderatly cemented rock can support more efficiently all kind of deformations without fracturing, but a very low porosity, very cemented rock is more susceptible to fracturing. It seems to exist a porosity critical point for a rock, below which chances for fracturing increase. It is postulated that this porosity is given by the common intersecting point of all the m curves in Figs. 1 and 2, as appears in Table 2. Suppose a rock continuously being cemented has reached a low primary porosity value of about 5% with a resistivity factor around 700, as schematically indicated in Fig. 6. Let us postulate also that this same rock is fractured and porosity remains about the same order of magnitud; resistivity factor, however, will decrease considerably, as shown also in same figure at left, and the point may change its relative position from SE to SW; the more intensive the fracturing the more the shifting of the point to the left.

During the cementation process, pore interconnection may be destroyed and constitute isolated important porous volume. No matter the nature of their fluid content, these voids will behave, electrically, as they were non porous material; this means high resistivity factors for the total pore system; nevertheless, nuclear logs will give total porosity. The combination of highly non interconnected or poorly interconnected porosities, above the crossing point of the m curves, and high resistivity factors will locate the F, $\emptyset$, points in the NE cross-plot area.

V. 2 Detection of Probable Vugs.

Return now to the cross-plots NW region of Figs. 5 and 6. When leaching creates effective vuggy porous systems, permeability is very high. High permeability often is also a characteristic of reefal systems. Nevertheless, porosity is not necessarily high for these porous models,

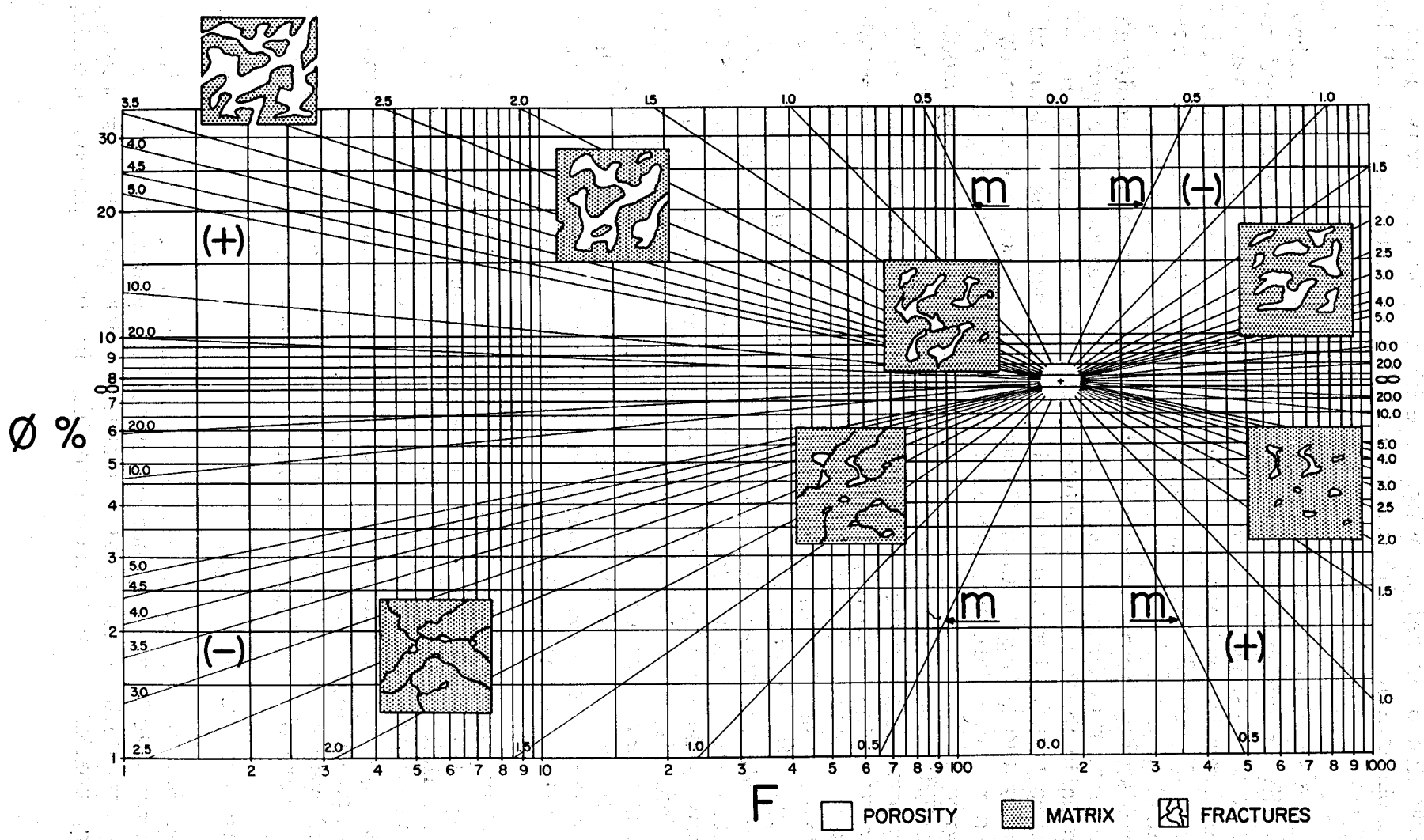

Fig. 6 .- Sketch showing the behaviour of a rock being continuously cemented and then fractured, and a rock with isolated porosity.

and frequently is in the medium to low range, as mentioned before. These conditions all together may produce another porous system model of economic importance of low to very low formation resistivity factor. Representative F, ϕ, points of effective vugular conditions will fall in the cross-plots NW area with high m computed values.

V.3 Primary Porosity.

If only primary porosity exists, the plotted points will fall in the NW and SE areas with moderate to low m values. The higher the value of m, the higher the permeability.[5] Some points may fall also in the NE region, when not interconnected primary porosity exists.

V.4 Ambiguous Cross-Plot Regions.

As it normally happens in statistical studies, almost always there will be doubtful F, ϕ, points which may belong to one of two cross-plot regions. For example, in the case of fractured systems, some plotted points will fall in the limit area of SW and SE regions. Criteria must be exerted in these cases in order to interpret the results of computations. Some points in the SE region may be considered as fractured rock conditions, favorable for production; probably, limiting values are in the range of m = 0.5.

Other important ambiguous cross-plot regions are located in the limit between the NW and SW areas. The F,ϕ, plotted points, close to the limiting line, may belong to rocks with petrophysical characteristics of both contiguous areas; i.e., vugs and fractures. But this case is not a critical one, because these two conditions are favorable for production.

By following a similar reasoning as above, alike conclusions can be derived for the NW-NE and NE-SE areas. But these are the less favorable limits between areas, for production.

VI. FIELD EXAMPLES

Well 1

This case is presented for comparison and reference conditions. Fig. 7 is the F-ϕ-m computer cross-plot of a well drilled in a Jurassic oölitic limestone. As can be realized, most of the F,ϕ, plotted points fall within the NW area, and the computed m values are within the range found in the laboratory for this particular field. Few points are scattered in all the remaining areas. Computed values of F are considered to be moderate. Initial production of this well was about 700 Bls/day.

The interpretation of this cross-plot indicates the well production

is from primary porosity and permeability because the values of the computed parameters mostly belongs to these particular conditions.

Well 2

Fig. 8 is the F-ϕ-m cross-plot of the producing interval of a well of the new Southeast Mexico Cretaceous area. The reservoir rock is known to be a low porosity fractured complex carbonate. Unlike the preceding example, almost all the plotted points fall within the SW area, which confirms the well is producing from a fractured rock. Initial production of this well was 3,500 Bls/day of oil.

VII. CONCLUSIONS

A method has been presented for detecting natural fractures in complex reservoir rocks by well log analysis. First results show that the method can be applied principally for differentiating potentially productive from non productive low porosity reservoir rocks. It can also be applied for detecting probable vuggy porosity when this is a predominant characteristic.

The application of the method requires the use of porosity nuclear logs and suitable electrical resistivity logs.

Numerical values of F, ϕ, S_w, a and m, are obtained through a computer program, which can also be displayed as computed logs. By a special crossplotting of the F, ϕ, computed data, the main probable characteristics of the porous systems can be predicted; i.e., whether fractured, vuggy or with only primary porosity.

First results of the application of the method indicate that highly productive low porosity fractured reservoir rocks are characterized mainly by relatively low computed formation resistivity factors and negative computed values of m. Very low resistivity factors, medium to high porosities, and high positive m computed values, characterize probable vuggy zones.

Equations for computing F and S_w, are general expressiones, used whatsoever the porosity system be; therefore, the validity of computations remains for any case. If the rock has only primary porosity, the computed values of a and m can be used as permeability indicators.

ACKNOWLEDGEMENT

The author would like to express his appreciation to the Pemex's management for permission to present and publish this paper. Appreciation is also indebted to Mr. Roberto Torres Navarro from the Mexican Petroleum Institute who directed the necessary computations for the example wells.

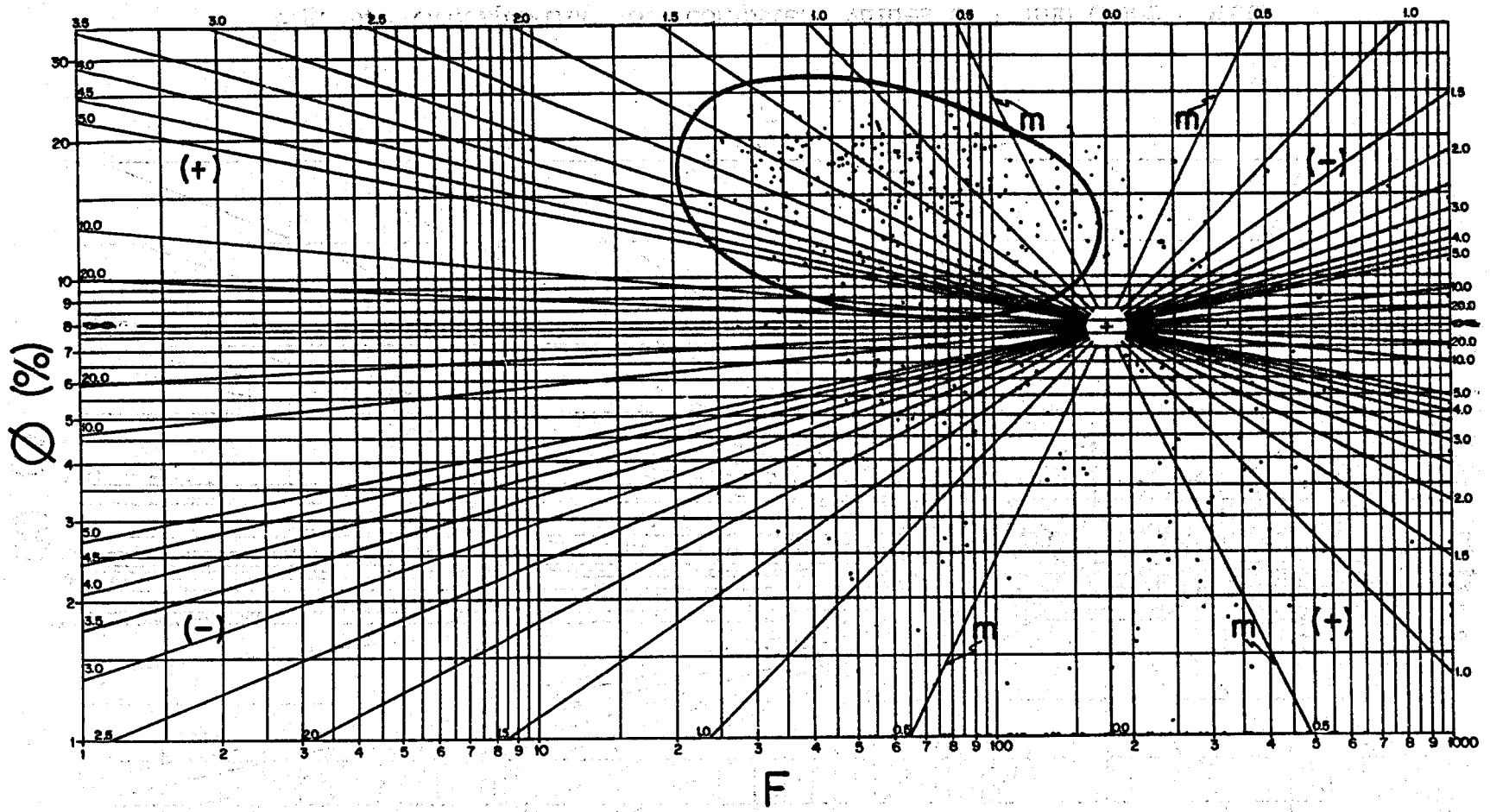

Fig. 7. Crossplotting of computed values of F and Ø for a well producing from a carbonate rock characterized mainly by primary porosity.

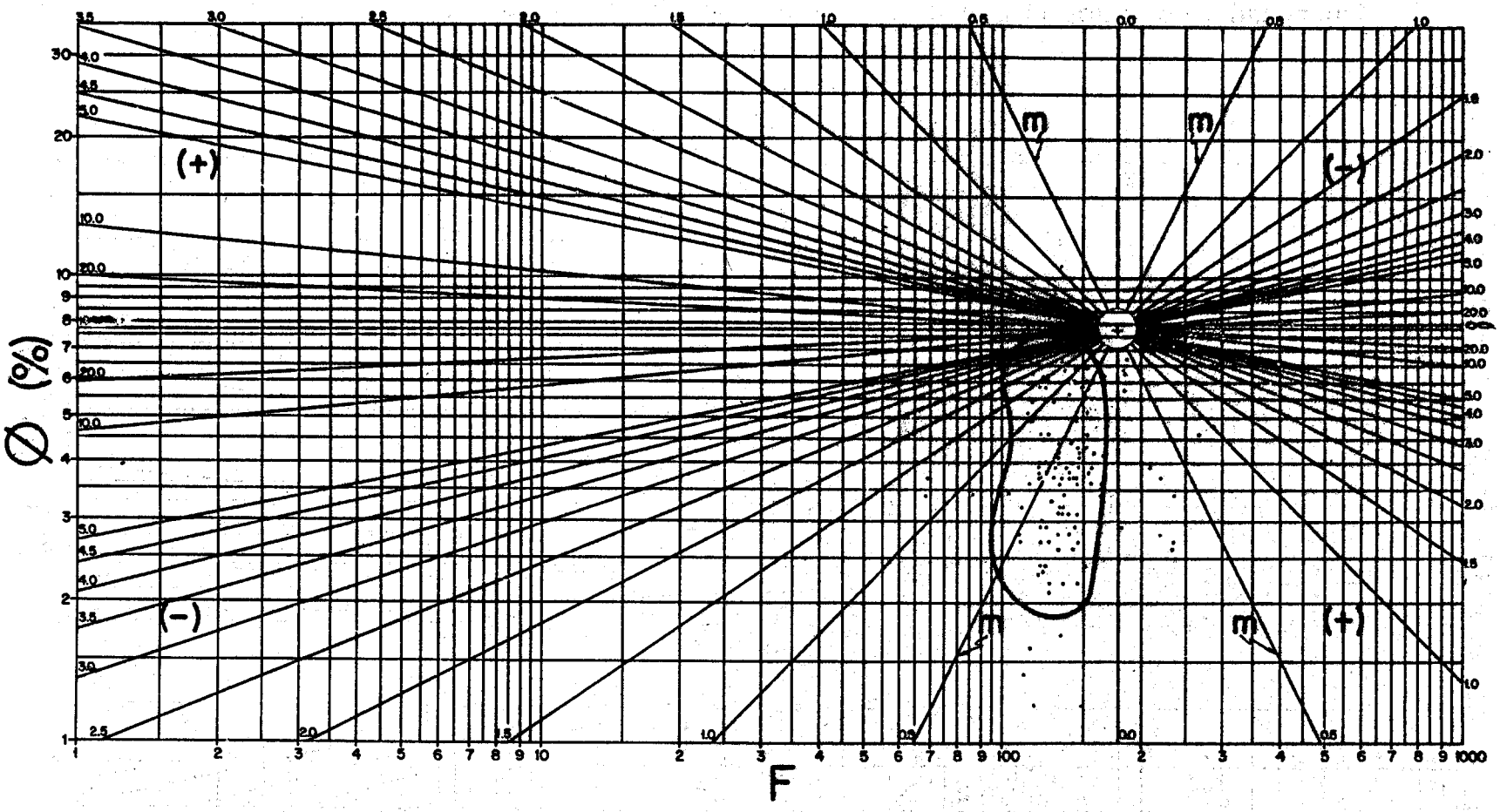

Fig. 8. - Crossplotting of computed values of F and Ø for a well producing from a low porosity fractured carbonate rock.

List of Symbols

F : Formation resistivity factor

Ø : Porosity

Sw : Connate water saturation

Sxo : Mud filtrate water saturation

R_t : Formation true resistivity

Rxo : Formation true resistivity in the flushed zone

Rw : Formation water resistivity

Rmf : Mud filtrate resistivity

Rcl : Clay resistivity

Vcl : Clay fraction in the rock.

m : Cementation exponent

a : Coefficient of F-Ø relation

A and B: Statistical constants of the a-m relation

f_{hr} : Residual hydrocarbon correction factor

REFERENCES

1. - Aguilera, R.; Van Poolen, H.K.: "Current Status on the Study of naturally Fractured Reservoirs". The Log Analyst May-June, 1977.

2. - Jordine, D.; Andrews, D.F.; Wishart, J.W.; Young, J.W.:"Distribution and Continuity of Carbonate Reservoirs". Jour. Pet. Tech. July, 1977.

3. - Franco, Alvaro:"Giant New Trend Balloons SE Mexico's Oil Potential". The Oil & Gas Jour. Sept. 19, 1977.

4. - Gómez-Rivero, O.: "A Practical Method for Determining Cementation - Exponents and Some Other Parameters as an Aid in Well Log Analysis". The Log Analyst, Sept.-Oct., 1976.

5. - Gómez-Rivero, O.: "Some Considerations About the Possible Use of the Parameters a and m as a Formation Evaluation Tool Through - Well Logs." SPWLA 18th Annual Logging Symposium, June 5-8, 1977 Houston, Texas.

6. - Burke, J.A.; Campbell, R.L. Jr.; "Schmidt, A.W.: The Litho-Porosity Crossplot ", The Log Analyst (SPWLA), Nov.-Dec. 1969.

7. - Poupon, A.; Clavier, C.; Dumanoir, J.; Gaymard, R.; Misk, A.: "Log Analysis of Sand-Shale Sequences — A Systematic Approach ", -- Jour. Pet. Tech, July 1970.

8. - Poupon, A.; Hoyle, W.R.; Schmidt, A.W.: "Log Analysis in For-- mations with Complex Lithologies" SPE Paper 2925, 45th SPE AIME Fall Meeting, 1970.

9. - Wyllie, M.R.J.; Gregory, A.R.: "Formation Factors of Unconsolidated Porous Media: Influence of Particle Shape and Effect of Cementation". Pet. Trans. AIME, 1953.

10. - Keller, George V.: "Electrical Resistivity of Modern Reef Sediments from Midway Atoll, Hawaii". SPWLA 10th Annual Logging Symposium, May 25-28, 1969. Houston, Texas.

11. -Keller, G.V.; Murray, J.C.; Towle, G.H.: "Geophysical Well Logs from the Kilauea Geothermal Research Drill Hole". SPWLA Trans. - 1974.

ABOUT THE AUTHOR

ORLANDO GOMEZ RIVERO, is presently - at the head of the Reserves General Department of Petroleos Mexicanos(PEMEX) at Mexico City, which has the responsibility for reserves estimates and well log analysis. After graduating from the Instituto Politécnico Nacional, Mexico City, with a petroleum engineering degree in 1953, - he has been always working for Pemex; - first in Coatzacoalcos, Veracruz, where he was in charge of the South Zone Reservoir Engineering Department from 1957 to 1966. After this latter date he was promoted to Mexico City Reservoir Engineering General Offices. He has taught well logs at the Instituto Politécnico Nacional and is the author of the book: "REGISTROS DE POZOS- PARTE I - TEORIA E INTERPRETACION" (1975). Also he has authored and coauthored sixteen articles. He received the 1967 "JUAN HEFFERAN" medal prize of the Asociación de Ingenieros Petroleros de México (AIPM) for best article published. He is a member of SPE of AIME, SPWLA, AIPM, Colegio de Ingenieros Petroleros de México and Asociación Mexicana de Geólogos Petroleros. His name is listed in Who's Who in the South and Southwest of U. S. A.

DETERMINATION OF LOGGING PARAMETERS IN SHALY SAND

MAKOTO MIYAIRI
TOSHINOBU ITOH
Central Technical Laboratory
Japan Petroleum Exploration Co., Ltd.

ABSTRACT

At the well log interpretation in shaly sand, the most reasonable values of logging parameters are found out by the use of several kinds of computer crossplot methods with a help of data from core analysis and data from well production test.

The formation interpreted in this case study consists of an alternation of shaly sand and clay having a very thin bed thickness. Because an average formation resistivity at the production zone is less than 2 ohm-m, a water saturation (S_w) calculated by the use of the standard values of $m = n = 2$, $b = 2 - V_{sh}$ and $a = 0.8$ on Poupon's equation (1971) shows always over 70% even the formation producing gas without any water. Therefore, those logging parameters must be arranged to be a suitable value for fitting with the result of production test.

The parameters of a and m on Porosity term can be determined from $R_t - \phi$ crossplot, the parameter of n on Water Saturation term can be determined from $Z - \phi$ crossplot basing on a formula modified of the standard equation as $\log Z = n \log \phi - \log (S_w \phi)^n$, when $S_w \phi =$ constant is satisfied at an irreducible water saturated zone, and the parameter of b on V_{sh} term can also be determined from $X - V_{sh}$ crossplot basing on a formula modified of the standard equation as $\log X = b \log V_{sh} - \log R_{sh}$. Where, X and Z are expressed as X, $Z = f(V_{sh}, R_t, R_{sh}, \phi, aR_w)$.

The logging parameters driven from those crossplot methods are $m = 2$, $a = 0.85$, $n = 1.4$, $b = 2$ at $0 \leq V_{sh} < 0.26$ and $b = 1.8$ at $0.26 \leq V_{sh} \leq 1$ and those values were well coincided with the data given by the core analysis.

I. Introduction

At the fundamental equation in shaly sand intorduced with Poupon et al., [1] as shown in the following,

$$\frac{1}{\sqrt{R_t}} = \left(\frac{V_{sh}^{b/2}}{\sqrt{R_{sh}}} + \frac{\phi^{m/2}}{\sqrt{a R_w}} \right) S_w^{n/2} \qquad \cdots\cdots\cdots\cdots\cdots\cdots \quad (1)$$

parameters, a, m, n, b, etc., have an important weight on the calculation of S_w. Authors have been engaged to the log interpretation of oil and gas field having a very low resistivity.

Fig. 1 is a typical well log of the oil field adopted in this case study.

Fig. 1

Although the formation at the depth from 8,050 ft to 8,430 ft is a gas producing zone on this well, an average formation resistivity at this zone is about 2 ohm-m, and the calculated S_w value shows over 70% when the standard values of parameters, such as $m = n = 2$, $a = 0.8$ and $b = 2 - V_{sh}$, are used at the equation (1). However, this zone is placing at the upper level from the main oil producing zone at the depth from 8,500 ft to 8,600 ft, and produced a pure gas without any water at the production test.

A cause of such inconsistency between the result of log interpretation and the result of production test was discussed with a help of the data given by the core analysis of which cores were taken at this well. On such discussion, it is cleared that, at the formation which is composed with an alternation of very shaly uncompacted sand and clay having a very thin bed thickness as shown in Fig. 2, the values of log parameters may differ from the standard one.

Fig. 2

Therefore, a method for determination of the reasonable values of those parameters has been studied with a help of the various crossplot methods basing on the log data and $F - \phi$, $\phi - S_w$ crossplots basing on the core data.

The results on this case studies are as follows;

1) The values of a and m are $m = 2.01$ and $a = 0.85$, and those are nearly same as the standard values of $m = 2$ and $a = 0.8$.
2) The value of n is $n = 1.4$, and this is quite different from the standard value of $n = 2$.
3) The value of b is $b = 2$ for $0 \leq V_{sh} < 0.26$ and $b = 1.8$ for $0.26 \leq V_{sh} \leq 1$.

The method for determining the log parameters tried in this case study can also be applied to other fields, the paper describes the detail of this method including the flow sheet for the computer processing of the method.

II. Determination of a and m

1. Clean Sand

A modified formula of Archie's equation is as follows.

$$-\log R_t = m \log \phi - \log aR_w + n \log S_w \quad \ldots\ldots\ldots\ldots\ldots\ldots \quad (2)$$

When $R_t - \phi$ crossplot is taken in a log-log scaled graph, it is well known that the points which are corresponding to the one on water bearing zone will drop at the linear line which is so called as Clean Water Line.

At the hydrocarbon bearing formation, the points will drop at the specific side of such clean water line because the third term on the equation (2) is not zero. Therefore,

when $R_t - \phi$ crossplot is taken with all points including the one on hydrocarbon bearing zone, the line crossing the points which are placing at the critical position will be coincident with the clean water line. When R_t-ϕ crossplot is taken at the log-log graph of which R_t is in an ordinate and ϕ is in an abscissa, the line crossing the most north west side points is in correspondence with the clean water line, and then, the value of m can be driven from the gradient of the line and the value of a can be given by the crosspoint between this line and the vertical line at $\phi = 1$.

2. Shaly Sand

When the equation (1) is modified as a logarithmic formula, the relationship between R_t and ϕ is expressed as follows.

$$- \log R_t = m \log \phi - \log aR_w + n \log S_w + 2 \log \left(1 + \sqrt{\frac{aR_w}{\phi^m} \cdot \frac{V_{sh}{}^b}{R_{sh}}} \right) \quad \cdots\cdots\cdots\cdots\cdots \quad (3)$$

At the water bearing zone, the equation (3) can be rewritten as follows.

$$- \log R_o = m \log \phi - \log aR_w + 2 \log \left(1 + \sqrt{\frac{aR_w}{\phi^m} \cdot \frac{V_{sh}{}^b}{R_{sh}}} \right) \quad \cdots\cdots \quad (4)$$

Where, R_o is a resistivity of water bearing formation. Since the third term of the right side of the equation (4) is always bigger than 1, the points of crossplot corresponding to the one on shaly sand will drop at the more northern west side of the clean water line. Therefore, the critical line crossing the most north west side points is no more coincided with the clean water line. When the relation of $\phi_x = \phi + V_{sh}\phi_{xsh}$ is used instead of ϕ conveniently, the equation (4) can be rewritten as follows.

$$- \log R_o^* = m \log \phi_x - \log aR_w + 2 \log \left(1 + \sqrt{\frac{aR_w}{\phi_x^m} \cdot \frac{V_{sh}{}^b}{R_{sh}}} \right) \quad \cdots\cdots\cdots \quad (5)$$

Where, ϕ_x and ϕ_{xsh} are corresponding to ϕ_N and ϕ_{Nsh} for Neutron Log Porosity, ϕ_D and ϕ_{Dsh} for Density Log Porosity, and ϕ_S and ϕ_{Ssh} for Sonic Log Porosity respectively, and R_o^* is a pseudo resistivity regulated by the equation (5).

When R_o given from Resistivity Tools is used at the equation (5) instead of R_o^* conveniently, the points of R_o-ϕ_x crossplot will move to the clean water line regulated by the equation of $- \log R_o = m \log \phi - \log aR_w$. Moreover, when the points of R_o-ϕ_x crossplot satisfies the following condition.

$$m \log \phi_x > m \log \phi + 2 \log \left(1 + \sqrt{\frac{aR_w}{\phi^m} \cdot \frac{V_{sh}{}^b}{R_{sh}}} \right)$$

All the points will drop at the southern east side of the clean water line. Since ϕ_x is expressed as $\phi_x = \phi + V_{sh}\phi_{xsh}$, the above equation can be rewritten as follows.

$$(\phi + V_{sh}\phi_{xsh})^{m/2} > \sqrt{\frac{aR_w}{R_{sh}}} \cdot V_{sh}^{b/2} + \phi^{m/2}$$

When the values of m and b are taken as m = b = 2 conveniently, the above equation

becomes as $\phi + V_{sh}\phi_{xsh} > \sqrt{\frac{aR_w}{R_{sh}}} \cdot V_{sh} + \phi$, and then,

$$\phi_{xsh} > \sqrt{\frac{aR_w}{R_{sh}}} \quad \text{..... (6)}$$

When $\phi_{xsh} \geqslant \sqrt{\frac{aR_w}{R_{sh}}}$ is satisfied, the points of R_t-ϕ_x crossplot will move to the more southern east side from the clean water line, and the critical points placing at the most north west side of the graph will mainly be corresponding to the one on clean water bearing sand. Therefore, among those three ϕ_x-R_t crossplots (ϕ_N-R_t, ϕ_D-R_t and ϕ_S-R_t crossplots), the line placing at the most southern east side in the graph will be the most reasonable line to be used as the clean water line.

Fig. 3 is a schematic explanation of the principle mentioned above.

Fig. 3

a) Determination of m

Fig. 4a is F-ϕ crossplot based on the data from the core analysis of which cores were taken at the well shown in Fig. 1, and the salinity of formation water is 20,000 ppm of NaCl in this example.

Fig. 4

The core samples were separated into several groups in accordance with the block of the formation at first, and then, two or three samples at each group were selected for the purpose of getting the representative V_{sh} value of groups. The shaly-ness of the core was estimated by the measurement of deviation ratio of F values when the formation salinity was 20,000 ppm, 10,000 ppm and 5,000 ppm respectively.

The points marked ◔ and ◕ are corresponding to the sample of $V_{sh} < 15\%$, especially, the points marked◉ are corresponding to the one on clean formation of $V_{sh} < 5\%$. Since the all points corresponding to the samples of $V_{sh} < 15\%$ are placing at the inside of broken lines, the points marked ● at the inside of broken lines may also be corresponding to the one on clean sand, because those were represented by the other sample at same group whose V_{sh} value was less than 15%. The points at the northern west side crossing over the broken line of A may be corresponding to the one on very shaly formation as explained at equation (4).

The solid line is an average line given by means of a least square method basing on the total points inside the broken lines, and then, $m = 1.614$ and $a = 1.368$ can be driven from this line. However, because the crossplot points disperse rather widely in the graph and the sample number of 60 is not enough to determine a reasonable line on such point distributions, this average line may not be representative of F - ϕ relationship of the actual formation.

Fig. 4b is a frequency plot of those points shown in Fig. 4a, the window width of F and ϕ is 0.063 on log F scale and 0.02 on log ϕ scale respectively, and the broken lines shown at Fig. 4a are also projected into this graph. The chained line is an average line given by means of a least square method basing on the points at the each window level on log F scale, and then, the values of m and a are given as $m = 1.999$

± 0.14 and a = 0.795 from this line.

When such average line is re-projected into Fig. 4a, marked chained line, the position of this line is not well fitting with the density of the points inside the broken lines.

Since a mid-weight point of all the points inside the broken lines will represent the density of those points, the chained line must be replaced to be crossing such mid-weight point, $\phi_{AV} = 0.258$, $F_{AV} = 12.37$ in this example. A relationship of m and a of the lines passing through this point is given as follows.

$$m = -1.70 \log a + 1.858 \quad \ldots\ldots\ldots\ldots\ldots\ldots\ldots\ldots \quad (7)$$

Therefore, the value of a can be driven as a = 0.83 from this equation by putting the value of m = 1.999 into equation.

The dotted line in Fig. 4a is a final line driven from the equation (7), and which crosses with the average line taken at the first step at this mid-weight point. Because of those reasons mentioned above, this line may be the most reasonable average line which regulates the relationship of $F = \frac{a}{\phi^m}$ for those points.

According to this case study, it is cleared that the gradient of critical line may represent the one of the average line, but the value of a given by this critical line is not representative of the density of clean points. Therefore, a reasonable value of a must be driven by means of mid-weight average method.

On the next step, this method was applied into the well log interpretation. Fig. 5a, 5b and 5c are R_t-ϕ_N, R_t-ϕ_D and R_t-ϕ_S crossplots by the use of logging data respectively.

Fig. 5

Since the values of m and a are not cleared at this step, ϕ_x and R_t have been taken the one given by log readings automatically. At R_t-ϕ_N crossplot, the critical line crossing the most north-west side points gives the m and a values as m = 2.01 and a = 0.69. The solid lines at R_t-ϕ_D and R_t-ϕ_S crossplots are a projected line given at R_t-ϕ_N crossplot. Such projected line at R_t-ϕ_S crossplot is well coincided with the critical line crossing the most north-west side points in the graph. However, at R_t-ϕ_D crossplot, the plenty of points drop at the northern west side from such line. Therefore, with the parameters of $\phi_{Dsh} = 0.25$ determined from M-N or ϕ_D-ϕ_N crossplot, $R_{sh} = 1$ ohm-m determined from R_t-GR crossplot and $aR_w = 0.097$ ohm-m determined from aR_w-GR crossplot, the criteria regulated with the equation (6) was checked out for R_t-ϕ_D crossplot. Then, it is cleared that the criteria of $\phi_{Dsh} > \sqrt{\frac{aR_w}{R_{sh}}}$ was not satisfied in this crossplot.

The first values of m and a were taken as m = 2.01 and a = 0.69 on R_t-ϕ_N crossplot as a rule of this method.

b) Determination of a

To determine a reasonable value of a, the points which are corresponding to the one on clean water sand must be pointed out. Therefore, the following three steps of the selection have been done for taking the clean water points.

i) Determination of aR_W on clean water bearing sand

With the values of m and a given by R_t-ϕ_N crossplot, the value of aR_W at the level by level of depth is calculated at first, and then, a crossplot of aR_W-GR will be taken with such aR_W and GR readings. Since the clean sand shows normally a low GR readings, the lowest value of aR_W corresponding to the minimum GR reading will represent the one on clean sand.[2] On this example, such aR_W value on clean sand can be determined as $aR_W = 0.097$ ohm-m from aRw-GR crossplot.

ii) Selection of water bearing sand

The points of which aR_W value shows as $aR_W \leqq 0.097$ ohm-m may be corresponding to the one on water bearing sand (including the shaly sand). Fig. 6a and 6b are F-ϕ_N and F-ϕ_D crossplots of which points are satisfying the criteria of $aR_W \leqq 0.097$ ohm-m.

Fig. 6

iii) Selection of clean water bearing sand

According to the results of core analysis, it is cleared that the core sample having the V_{sh} value less than 15% can be treated as clean sand. Such criteria of $V_{sh} < 15\%$ on the core data are corresponding to the criteria of $|\phi_N - \phi_D| < 0.01$ on the log data of which criteria were checked out by the level by level calculation. The points marked ● in the graph are satisfying the criteria of $|\phi_N - \phi_D| < 0.01$. The chained lines at the upper north west side of the graphs are the projected lines given at R_t-ϕ_N crossplot (Fig. 5a).

At those figures, it is cleared that the clean water points can also be discriminated from the other points at F-ϕ_D crossplot, while those points were not discriminated at R_t-ϕ_D crossplot. On the clean water bearing formation, the porosities given by Neutron Log and Density Log must be coincided with each other theoretically. However, some deviations of the position of points are seen between F-ϕ_N and F-ϕ_D crossplots. Then, F-ϕ crossplot of which porosity is an average between ϕ_N and ϕ_D has been taken as shown in Fig. 6c, and the mid-weight point of all points inside the critical lines was marked as ▲.

A relationship of a and m of the lines passing through this mid-weight point is given as $m = -1.745 \log a + 1.893$. Therefore, the value of a can be driven as $a = 0.85$ by putting the value of $m = 2.01$ into the equation.

The values of $m = 2.01$ and $a = 0.85$ given by log data are well coincided with the one given by core data ($m = 2.00$ and $a = 0.83$).

III. Determination of n and b

1. Determination of n[3]

The fundamental equation for determining the value of n is as follows by multiplying of $\phi^{m/2}$ to the both sides of equation (1).

$$\frac{\phi^n}{(S_w\phi)^n} = \left(V_{sh}^{b/2}\sqrt{\frac{R_t}{R_{sh}}} + \phi^{m/2}\sqrt{\frac{R_t}{aR_w}}\right)^2$$

A logarithmic formula of this equation is as follows, when the right side of equation is replaced as $Z = \left(V_{sh}^{b/2}\sqrt{\frac{R_t}{R_{sh}}} + \phi^{m/2}\sqrt{\frac{R_t}{aR_w}}\right)^2$.

$$\log Z = n \log \phi - \log (S_w\phi)^n \quad \ldots\ldots\ldots\ldots\ldots\ldots\ldots\ldots \quad (8)$$

When Z-ϕ crossplot is taken at the log-log scaled graph, the points which are corresponding to the specific $S_w\phi$ will drop at the linear line, and then, the value of n can be driven by the gradient of that line. However, the formation lithology and water saturation will vary at the level by level of the depth, and the points of Z-ϕ crossplot will widely disperse in the graph in accordance with the physical conditions of the formation. The usual method which determines the value of n is a direct measurement of n exponent by the use of the core sample basing on the following equation.[4]

$$n = \frac{\log R_{t1}/R_{to}}{\log S_{wo}/S_{w1}} \quad \ldots\ldots\ldots\ldots\ldots\ldots\ldots\ldots \quad (9)$$

Where, R_{to} and R_{t1} is a resistivity of the sample at the water saturation of S_{wo} and S_{w1} respectively. However, this method is not convenient to the practical usage for getting an average value with the large number of samples, because many difficulties are existing to measure an accurate S_w value at the lower range of it, and a rather long time will be required to get the final data.[5] Since a condition of $S_w\phi$ = constant is oftenly seen at the irreducible water saturated zone in the oil field, Z-ϕ crossplot can be used as a determination of the n value on such irreducible water saturated zone.

Fig. 7a is S_w-ϕ crossplot basing on the core data of which core samples were taken at the depth from 8,500 ft to 8,600 ft on the well shown in Fig. 1, and Fig. 7b is the one basing on the production test achieved at this zone.[6]

Fig. 7

Fig. 7a shows that, when the formation is in the condition of irreducible water saturated, the value of $S_w\phi$ = constant will be as $S_w\phi = 0.08$ for the coarse sand and as $S_w\phi = 0.1$ for the medium sand. S_w-ϕ crossplot basing on the production test data is also well coincided with the one of core data, and shows that this zone is in the condition of irreducible water saturated.

Fig. 8a is Z-ϕ crossplot basing on the log data at this zone.

Fig. 8

The points at the most north west side in the graph may be corresponding to the one of minimum value of $S_w\phi$ = constant. The gradient of the critical line crossing those points gives the n value as $n = 1.4$.

Fig. 8b is R_t-S_w crossplot basing on the equation (9) by the use of typical core sample at this well[7], and the n value is also given as $n = 1.4$ from the gradient of this curve.

2. Determination of b and R_{sh}

A modified formula of the equation (1) as follows.

$$\frac{V_{sh}^{b}}{R_{sh}} = \left(\frac{1}{\sqrt{R_t S_w^n}} - \frac{\phi^{m/2}}{\sqrt{aR_w}} \right)^2$$

A logarithmic formula of above equation is as follows, when the right side of equation is replaced as $X' = \left(\frac{1}{\sqrt{R_t S_w^n}} - \frac{\phi^{m/2}}{\sqrt{aR_w}} \right)^2$,

$$\log X' = b \log V_{sh} - \log R_{sh} \qquad \text{.....} \qquad (10)$$

However, the value of X' can not be calculated as long as the value of S_w is not cleared. When X is taken as $X = \left(\frac{1}{\sqrt{R_t}} - \frac{\phi^{m/2}}{\sqrt{aR_w}} \right)^2$ instead of X' conveniently, X at $S_w = 1$ will be expressed as follows.

$$X_o = \left(\frac{1}{\sqrt{R_o}} - \frac{\phi^{m/2}}{\sqrt{aR_w}} \right)^2$$

Since the condition of $R_t > R_o$ is satisfied at the hydrocarbon bearing zone, $X < X_o$ is also satisfied in accordance with the equations written above. Therefore, when X-V_{sh} crossplot is taken at the log-log scaled graph, the most north west side points are mainly corresponding to the one on water bearing formation, and the points which are corresponding to the one on hydrocarbon bearing zone will drop at the south east side under such critical line.

Fig. 9 is X-V_{sh} crossplot basing on the log data, and then, the values of b and R_{sh} are given as $b = 2$ for $0 \leq V_{sh} < 0.26$ and $b = 1.8$ for $0.26 \leq V_{sh} \leq 1$ and $R_{sh} =$ 1 ohm-m.

Fig. 9

IV. Conclusion and Discussion

Fig. 10 shows a flow sheet for computer processing based on this method.

Fig. 10

Since the values of ϕ and V_{sh} must be cleared at the step of Z-ϕ and X-V_{sh} crossplots. Therefore, the process of those crossplots will be done after the level by level calculation of ϕ and V_{sh} values.

The final check of all parameters can be achieved by the following equation which is a modified formula of equation (1).

$$\frac{\phi^m}{a} = \left(\sqrt{\frac{R_w}{R_t S_w^n}} - V_{sh}^{b/2} \sqrt{\frac{R_w}{R_{sh}}} \right)^2$$

A logarithmic formula of above equation is as follows, when the right side of equation is replaced as $Y' = 1/(\sqrt{\frac{R_w}{R_t S_w^n}} - V_{sh}^{b/2}\sqrt{\frac{R_w}{R_{sh}}})^2$.

$$-\log Y' = m \log \phi - \log a \quad \ldots\ldots\ldots\ldots\ldots\ldots\ldots\ldots \quad (11)$$

However, the value of Y' can not be calculated as long as the value of S_w is not cleared. When Y is taken as $Y = 1/(\sqrt{\frac{R_w}{R_t}} - V_{sh}^{b/2}\sqrt{\frac{R_w}{R_{sh}}})^2$ instead of Y' conveniently, Y at $S_w = 1$ will be expressed as follows.

$$Y_o = 1/(\sqrt{\frac{R_w}{R_o}} - V_{sh}^{b/2}\sqrt{\frac{R_w}{R_{sh}}})^2$$

Since a condition of $R_t > R_o$ is satisfied at the hydrocarbon bearing formation, $Y > Y_o$ is also satisfied in accordance with the equations written above. Therefore, when Y-ϕ crossplot is taken at the log-log scaled graph, the points at the most north west side are mainly corresponding to the one on water bearing formation, and points which correspond to the one on hydrocarbon bearing zone will drop at the south east side under the such critical line.

Fig. 11 is Y-ϕ crossplot basing on the log data, the solid line is a critical line calculated from the equation (11) with the parameters of $m = 2.01$ and $a = 0.85$.

Fig. 11

Because, all the points drop at the south east side of the critical line, the parameters determined by this method might be in the reasonable values.

When the plenty of points drop at the north west side crossing over the critical line, it may be said that the fundamental equation is not suitable for the formation being in the interpretation. Therefore, another equations introduced by de Witte[8], etc. must be tried.

Fig. 12 is a computer log basing on this log interpretation.

Fig. 12

ACKNOWLEDGMENT

We wish to express our appreciations to Japan Petroleum Exploration Co., Ltd. who allowed us to achieve this case studies of computer processing of well log interpretation, and also to express our appreciations to Mr. Masami Murakami and Fumio Okabe, Technical Laboratory and Exploration Section of Japan Petroleum Exploration Co., Ltd. who gave us the valuable data of core analysis and production test of the oil field. Many thanks for Mr. Takeshi Ando, Technology Center of Japan Petroleum Development Corp., who gave us a kind help and technical advice at the computer processing stage.

REFERENCES

1. Poupon, A. and Leveaux, J.: "Evaluation of Water Saturation in Shaly Formations," Trans., SPWLA 12th Logging Symposium, May 1971.

2. Ratliff, J. R. et al.: "Applications of the SARABAND Sand-Shale Technique in North America," Trans., SPWLA 12th Logging Symposium, May 1971.

3. Miyairi, M., Itoh, T. and Okabe, F.: "Water Saturation in Shaly Sands; Logging Parameters from Log-Derived Values," Trans., 17th Logging Symposium, June 9-12, 1976.

4. Hossin, A.: "Calcul des Saturations en Eau par la Methode du Ciment Argileux (Formule d'Archie Generalisee), Bulletin, AFTP, March 1960.

5. ARTEP: "IIIe Colloque ARTFP, Jun. 10-14, 1968, Conductivite en Milieux Poreux Argileux Interpretation de Diagraphies."

6. Scala, C. and Raymer, L.: "Determination of the Archie Exponent m and n in an Unconsolidated Volcanic Core from JAPEX Aga-Oki SI - A3," Schlumberger Research Memorandum, Sep. 23rd, 1976.

7. Okabe, F. and Inoma, A.: "Aga-Oki Field, The History, Geology and Formation Evaluation," Offshore South East Asia Conference, Feb. 21-24, 1978, South Asia Petroleum Exploration Society Session.

8. de Witte, L.: "Relation between Resistivities and Fluid Contents of Porous Rocks," Oil and Gas Journal, Aug. 24, 1950.

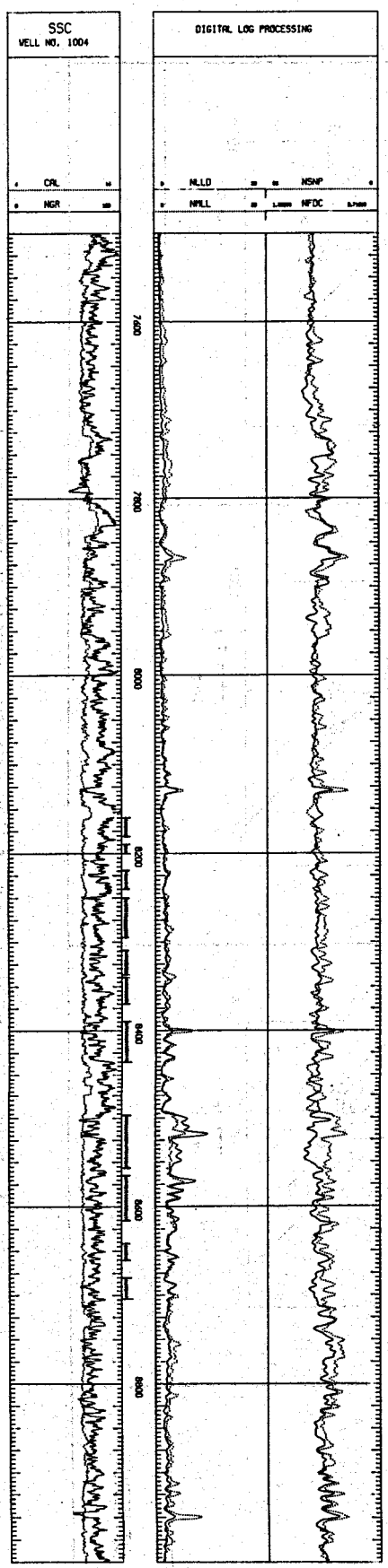

Fig. 1 Example of logs used in this case study

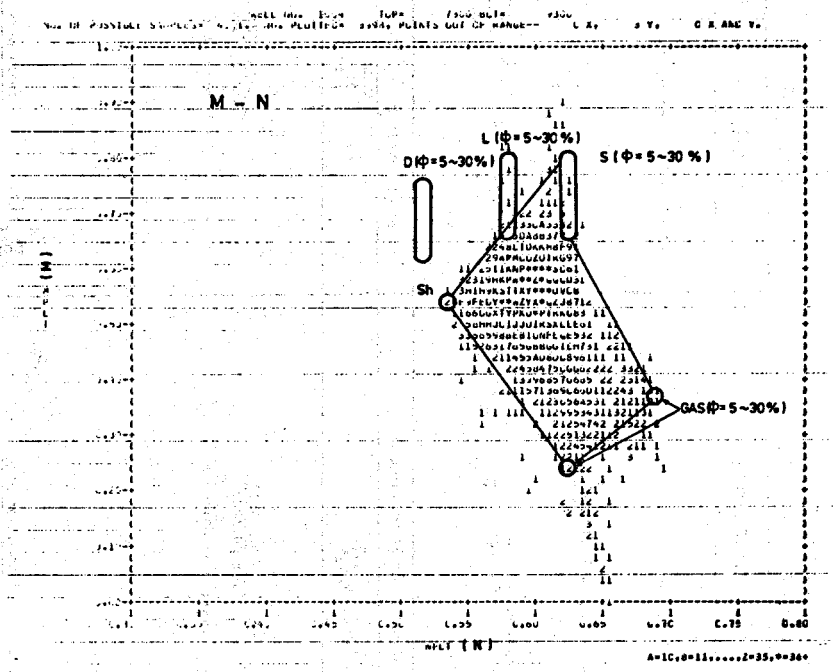

Fig. 2 M-N crossplot from example of Fig. 1 which shows uncompacted shaly sand with gas

TYPES	Rt - ϕD	Rt - ϕN	Rt - ϕS^*
USES	m , aRw , Quick look	m , aRw , Quick look	m , aRw , Quick look
EQUATIONS			
Clean water bearing	$-\log Rt = m\log\phi D - \log aRw$	$-\log Rt = m\log\phi N - \log aRw$	$-\log Rt = m\log\phi S - \log aRw$
Clean hydrocarbon bearing	$-\log Rt = m\log\phi D - \log aRw + \log \frac{Sw^n}{(1+Shr\phi Dh)^m}$	$-\log Rt = m\log\phi N - \log aRw + \log \frac{Sw^n}{(1-Shr\phi Nh)^m}$	
Shaly water bearing	$-\log Rt = m\log\phi D - \log aRw + 2\log \frac{(\phi D - Vsh\phi Dsh)^{m/2} + Vsh^{b/2}(aRw/Rsh)^{1/2}}{\phi D^{m/2}}$	$-\log Rt = m\log\phi N - \log aRw + 2\log \frac{(\phi N - Vsh\phi Nsh)^{m/2} + Vsh^{b/2}(aRw/Rsh)^{1/2}}{\phi N^{m/2}}$	$-\log Rt = m\log\phi S - \log aRw + 2\log \frac{(\phi S - Vsh\phi Ssh)^{m/2} + Vsh^{b/2}(aRw/Rsh)^{1/2}}{\phi S^{m/2}}$
ASSUMED TERMS	Single mineral & known lithology	Single mineral & known lithology	Single mineral & known lithology
CRITERIA	$\phi Dsh > \sqrt{\frac{aRw}{Rsh}}$	$\phi Nsh > \sqrt{\frac{aRw}{Rsh}}$	$\phi Ssh > \sqrt{\frac{aRw}{Rsh}}$
PRESENTATION & EFFECT of SHALE and HYDROCARBON	m : Slop $m = \frac{\log(Rt2/Rt1)}{\log(\phi D1/\phi D2)}$ aRw=Rt when ϕD=100 %	m : Slop $m = \frac{\log(Rt2/Rt1)}{\log(\phi N1/\phi N2)}$ aRw=Rt when ϕN=100 %	m : Slop $m = \frac{\log(Rt2/Rt1)}{\log(\phi S1^*/\phi S2^*)}$ aRw=Rt when ϕS =100 %
OTHERS			

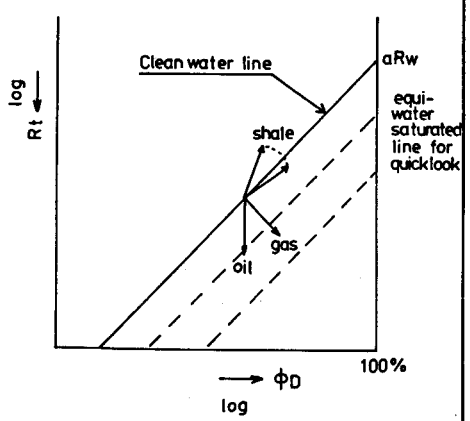

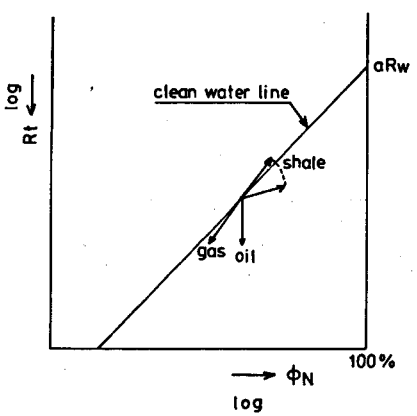

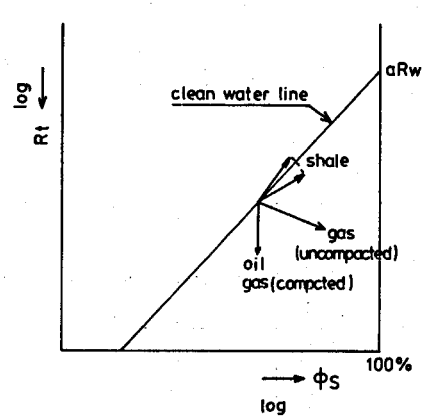

Fig. 3 Schematic explanation of Resistivity - Porosity crossplots

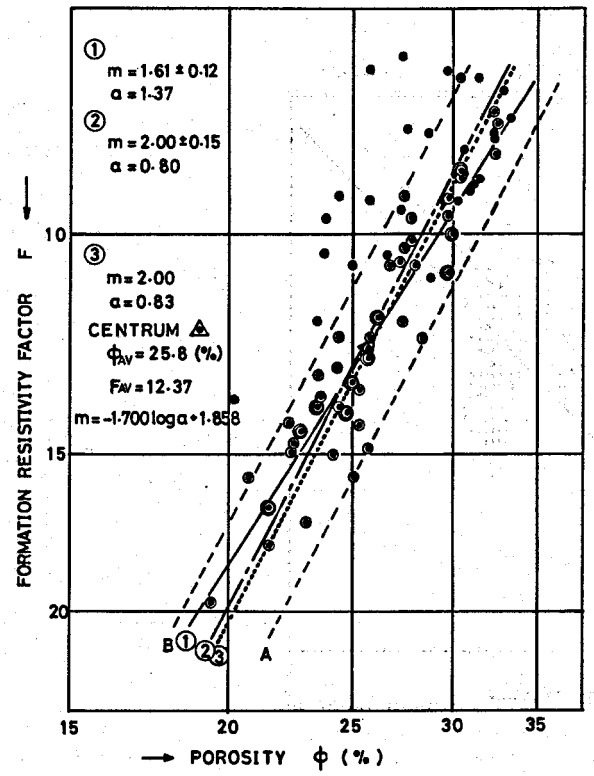

Fig. 4-a F-Ø crossplot from core

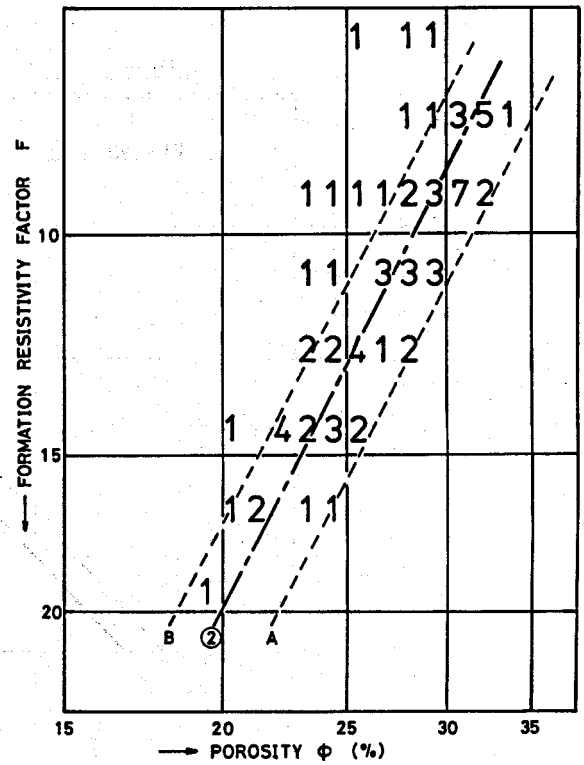

Fig. 4-b Frequency crossplot of the points shown in Fig. 4-a

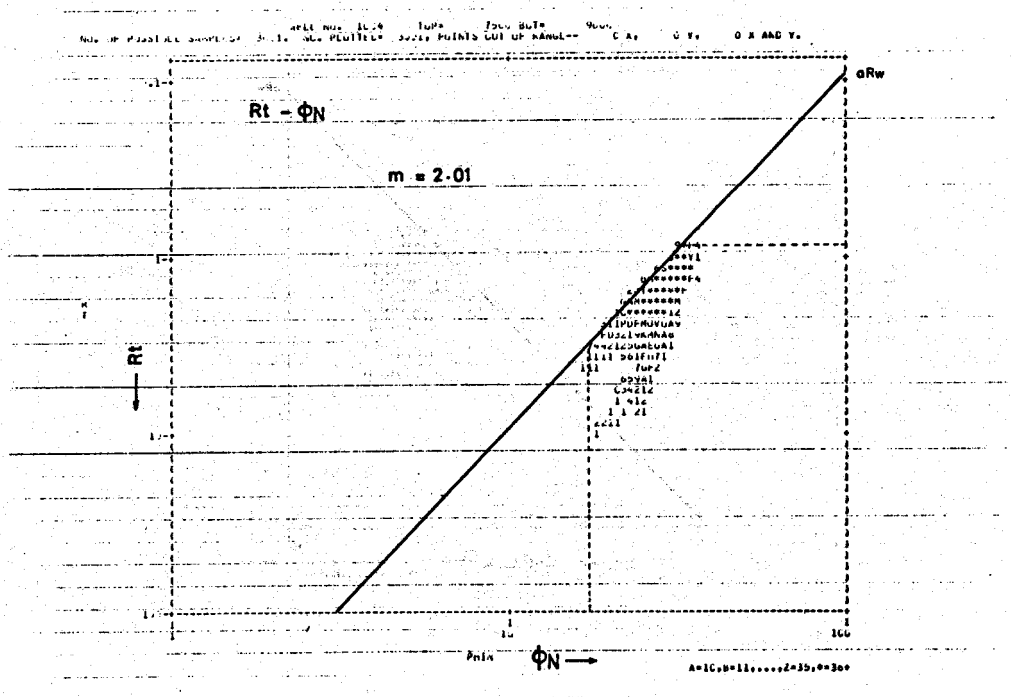

Fig. 5-a R_t-$Ø_N$ frequency crossplots from example of Fig. 1

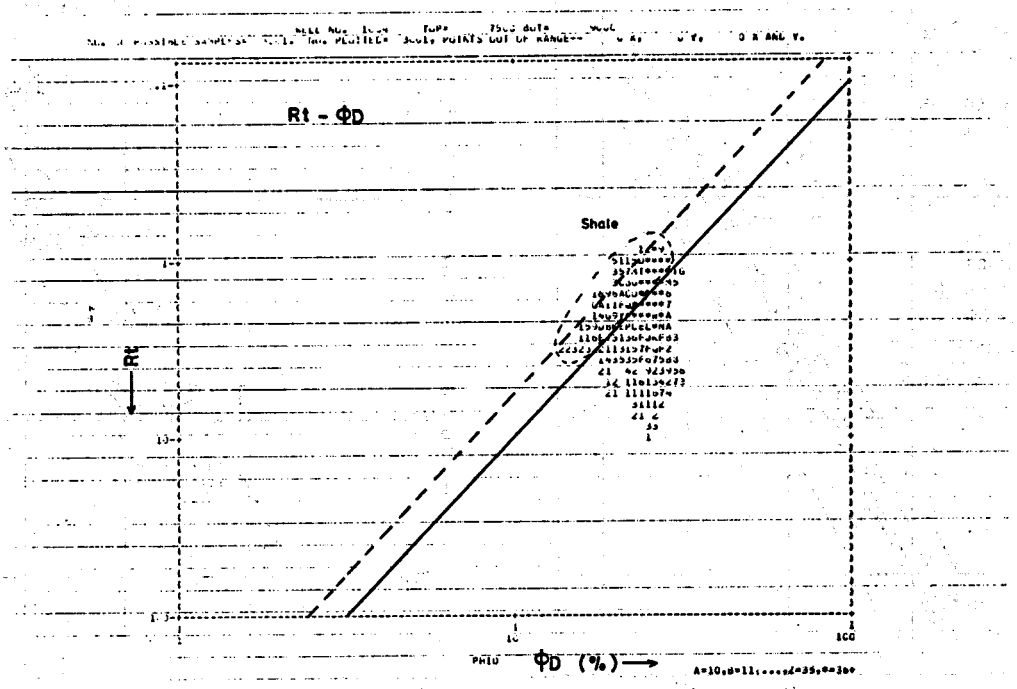

Fig. 5-b R_t-$\emptyset_D$ frequency crossplots from example of Fig. 1

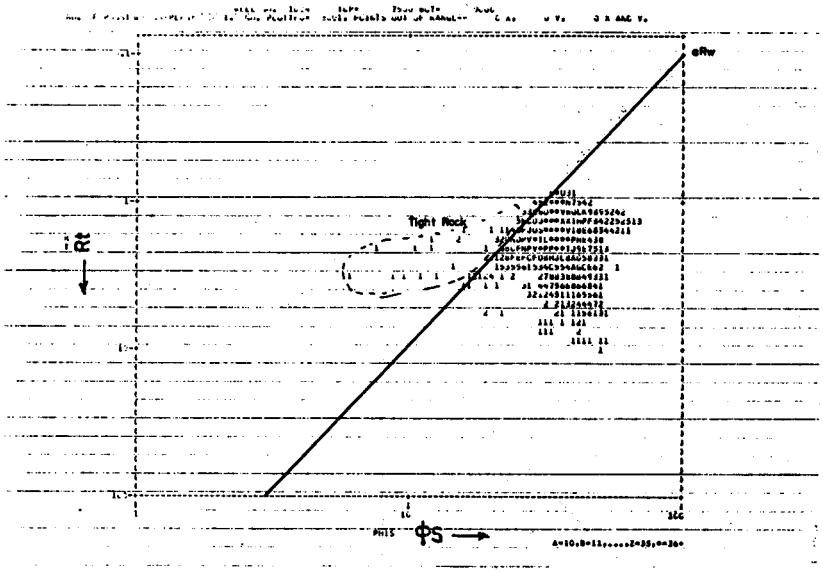

Fig. 5-c R_t-$\emptyset_S$ frequency crossplots from example of Fig. 1

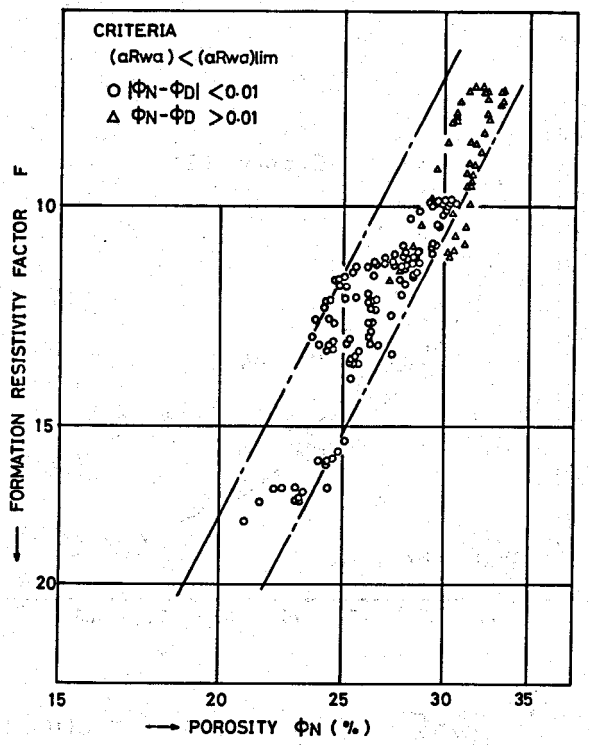

Fig. 6-a F-$\emptyset_N$ crossplot by selected points from Fig. 5

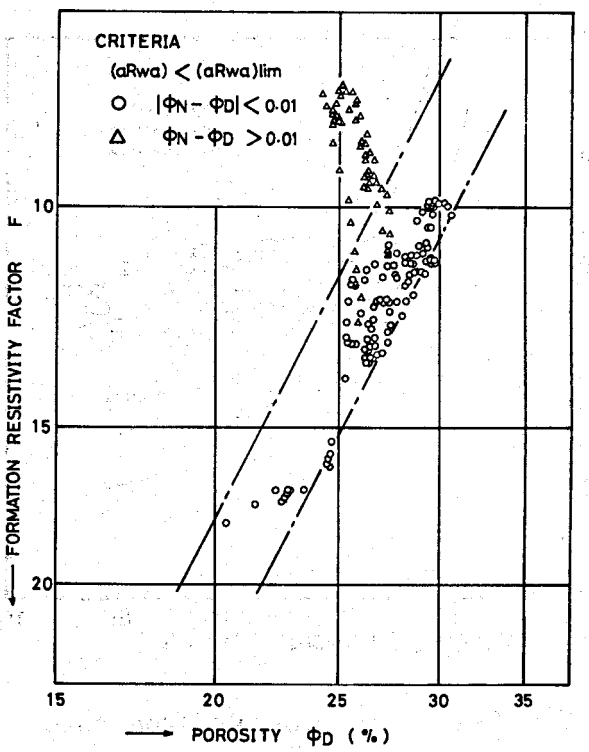

Fig. 6-b F-$\emptyset_D$ crossplot by selected points from Fig. 5

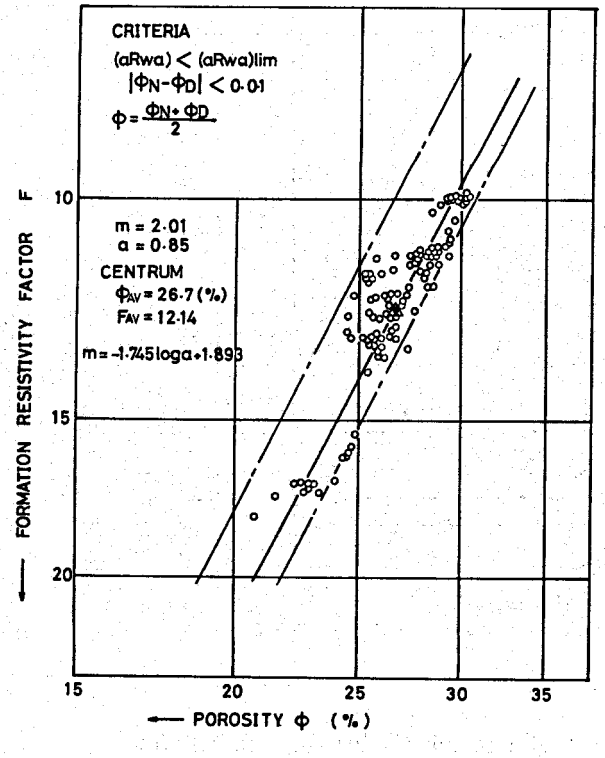

Fig. 6-c F-$\emptyset$ crossplot by selected point

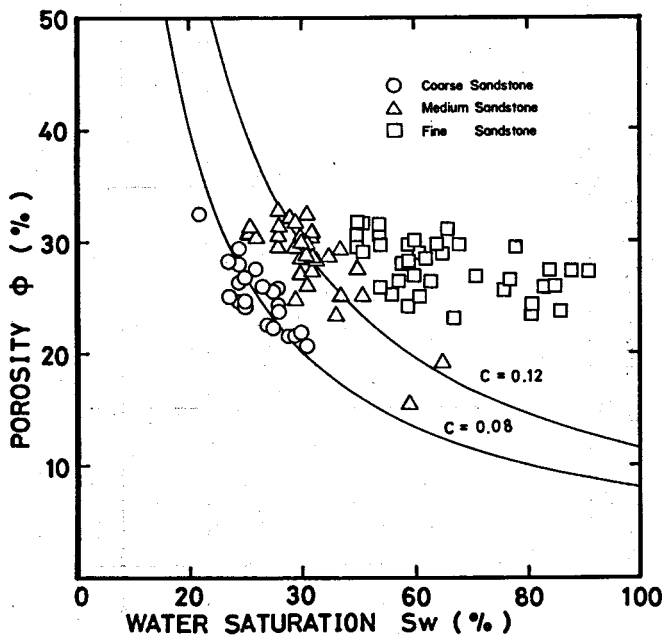

Fig. 7-a S_W-Ø crossplot from core

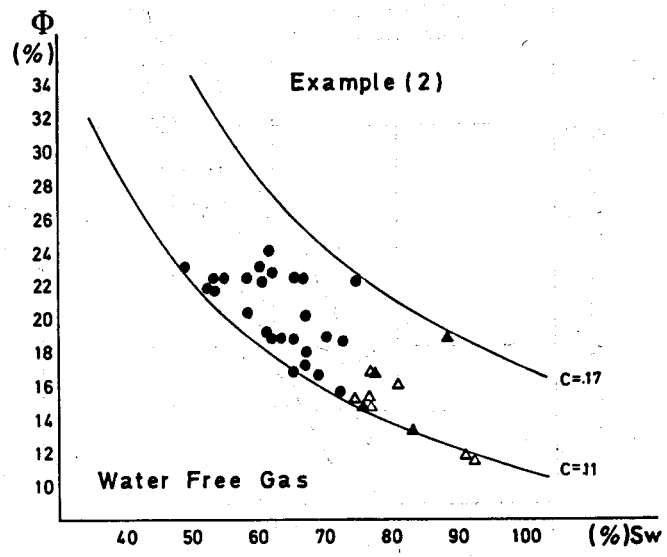

Fig. 7-b S_W-Ø crossplot from production test[7)]

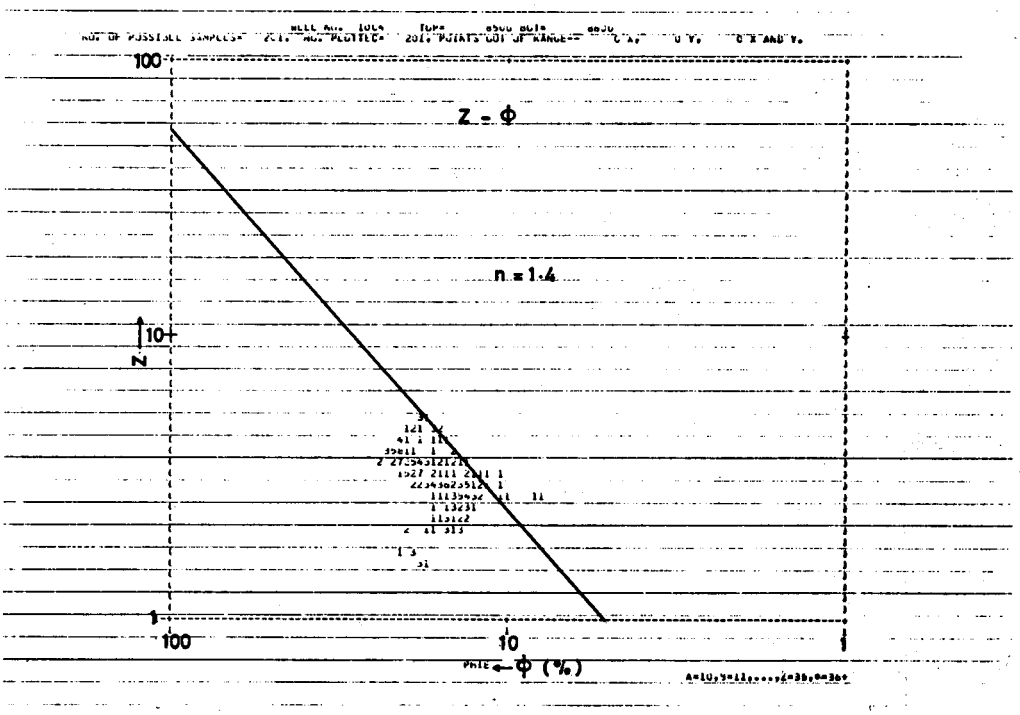

Fig. 8-a Z-Ø crossplot from example of Fig. 1 (8,500 ft - 8,600 ft)

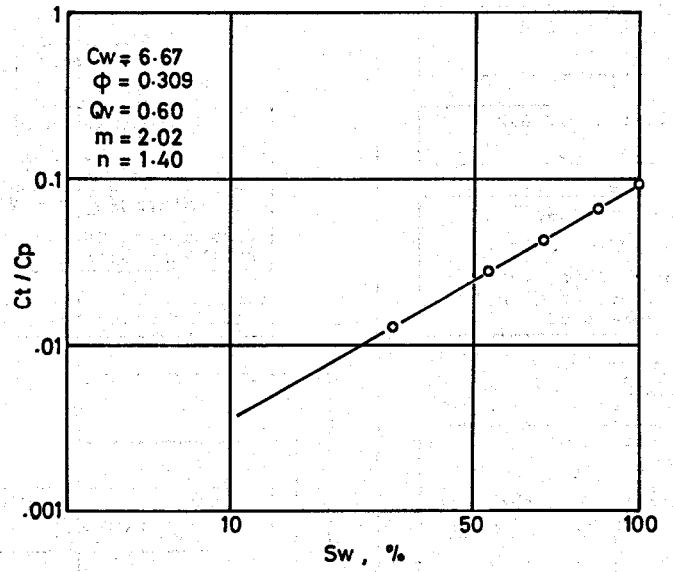

Fig. 8-b Saturation exponent from core[6)]

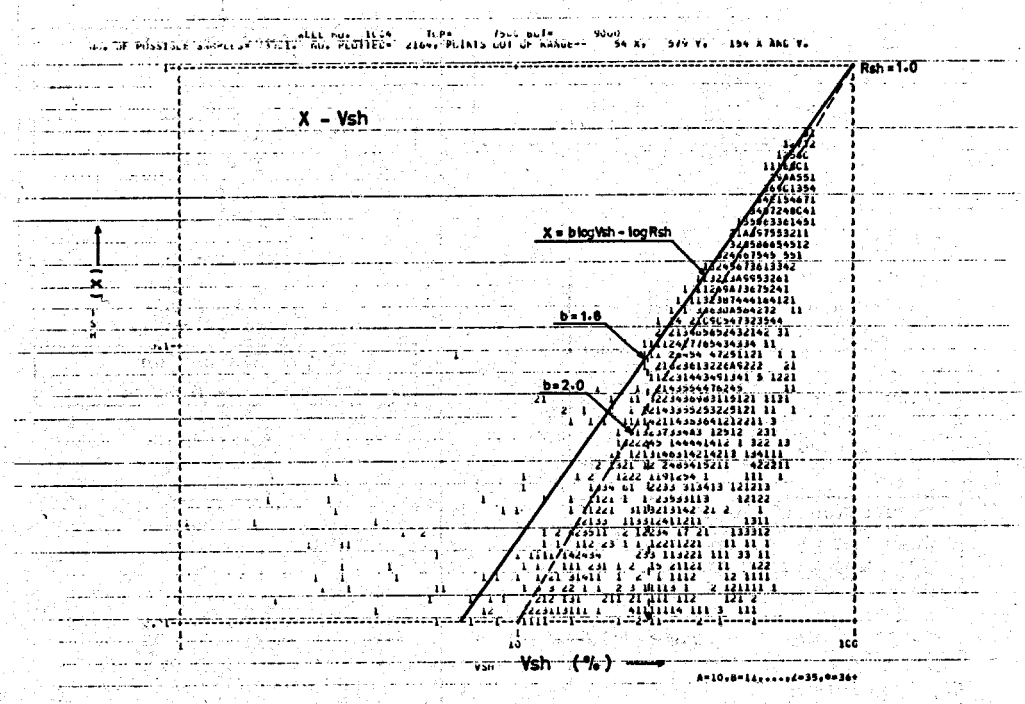

Fig. 9 X-V_{sh} crossplot from example of Fig. 1

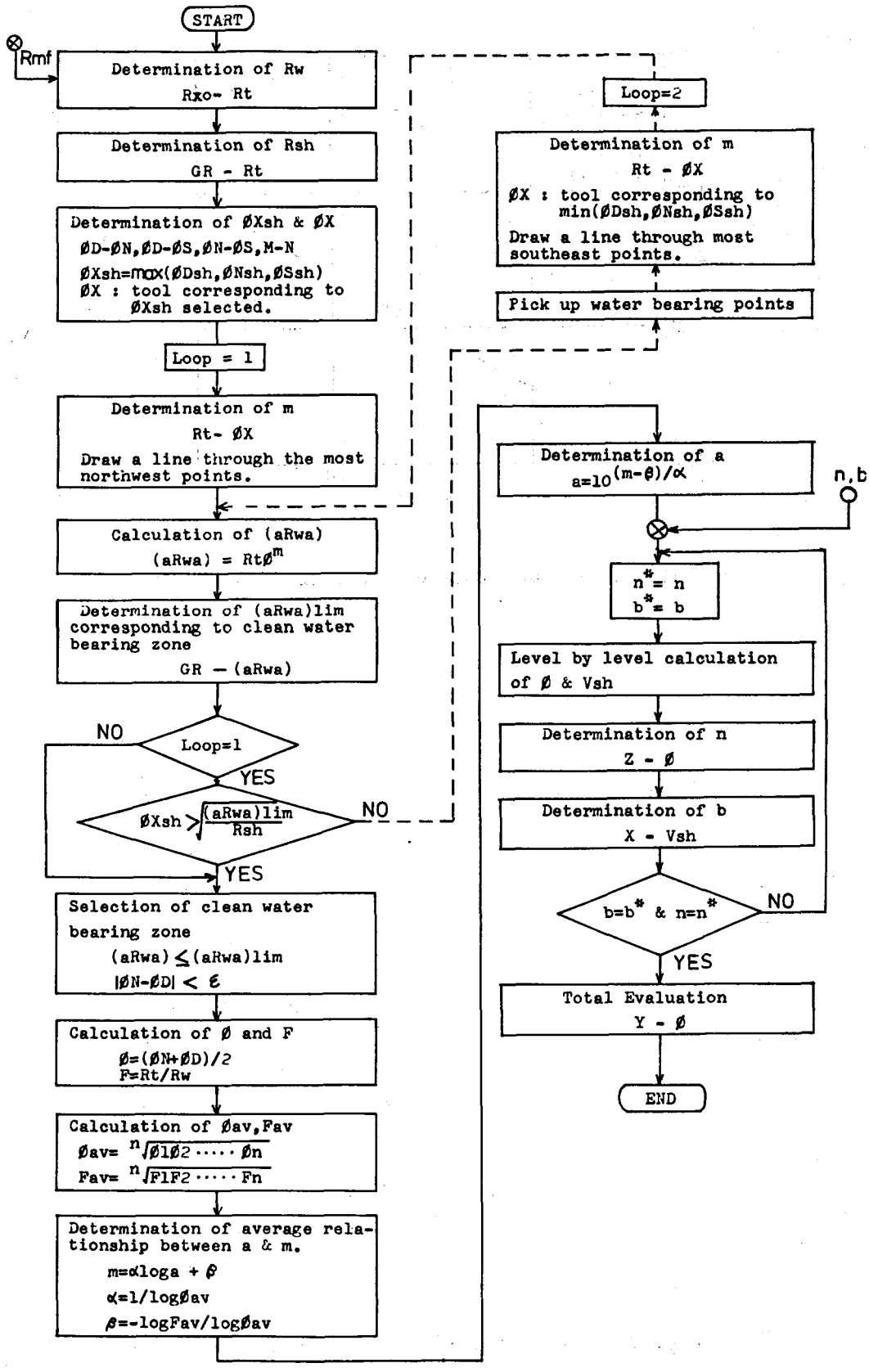

Fig. 10 Flow chart for determining parameters; a, m, n, b; in computer processing of log interpretation

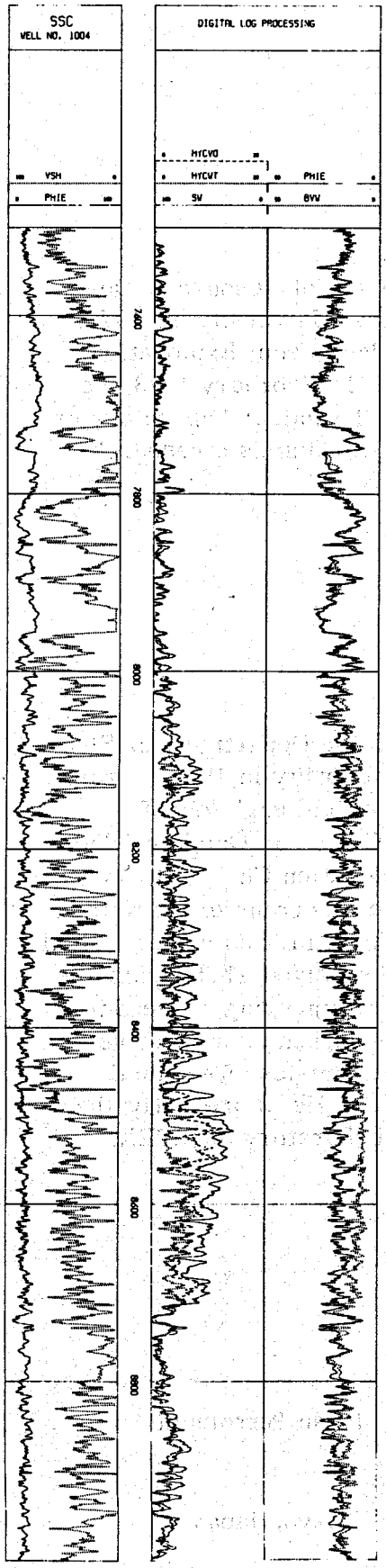

Fig. 12 Computed logs from example of Fig. 1

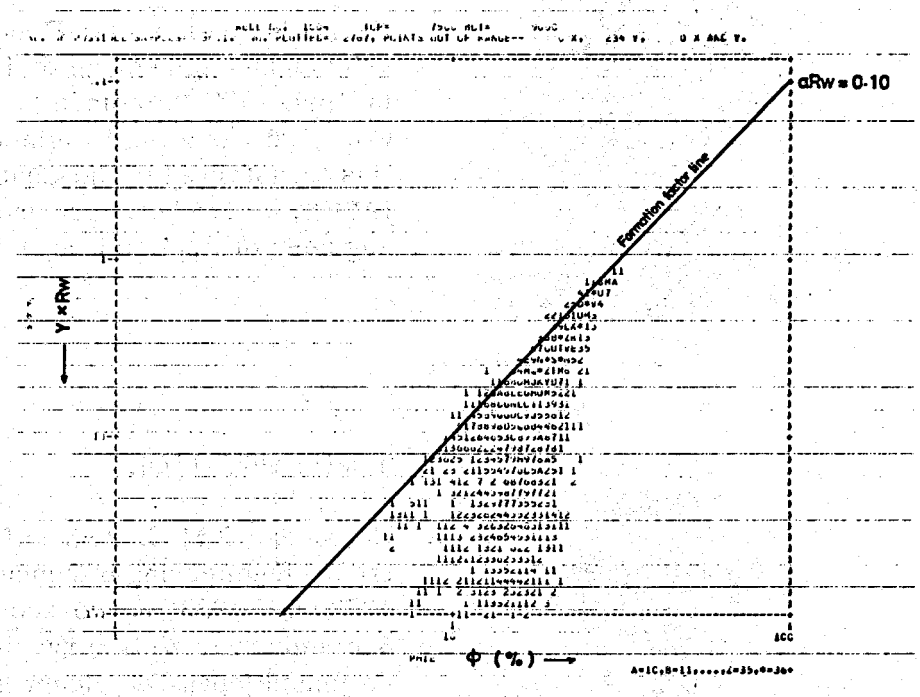

Fig. 11 Y-Ø crossplot from example of Fig. 1

ABOUT THE AUTHORS

MAKOTO MIYAIRI

He graduated from the Department of Resources Development Engineering of Tohoku University in 1972. In April 1972, he joined Japan Petroleum Exploration Co., Ltd. as a field engineer. In February 1973, he was transferred to the Central Technical Laboratory of JAPEX, where he is presently working as a research engineer of Applied Geophsics.

TOSHINOBU ITOH

He received M.S. degree from the Department of Electronic Engineering of Nihon University in 1958. From 1958 until 1960, he worked as a field engineer of Schlumberger Well Surveying Corp. In October 1960, he joined Japan Petroleum Exploration Co., Ltd. as a log analyst. In April 1965, he was transferred to the Central Technical Laboratory of JAPEX as a geophysical engineer. In March 1973, he received Ph.D from the Department of Atomic Energy Engineering of the University of Tokyo. In 1975, he worked as a guest researcher for the Institute of Geophysics, Technical University of Clausthal, F.R.G. He is presently the vice-president of the Central Laboratory of JAPEX.

Company: Central Technical Laboratory, Japan Petroleum Exploration Co., Ltd.

Mailing Address: 3190-1, Hane, Hamura-Machi, Tokyo, Japan

Log Analysis in a Rocky Mountain Heavy Oil Reservoir

by

D.A. Chesnut and D.O. Cox

Energy Consulting Associates, Inc.

ABSTRACT

In evaluating a heavy oil accumulation in Wyoming for an enhanced recovery pilot, log analysis with conventional "clean sand" evaluation techniques was found to yield computed oil saturations much less than core saturations. The formation involved was the Tensleep, which is generally considered to be a clean sand.

Formation water, however, is fresh, containing less than 800 parts per million total dissolved solids, predominantly calcium bicarbonate. Measured water resistivity is 9.4 ohm-meters at 68F. Because of the high water resistivity, any clays which are present would decrease the resistivity recorded by the logs, compared to the resistivity that would be observed with the same pore geometry and fluid content in the absence of surface conductivity.

To evaluate the possiblity of clay conductance affecting the log resistivities, the cation exchange capacity (CEC) was measured on several core samples. Measure CEC's averaged 1.04 meq/100 gr. which indicates a small clay conductance--CEC's for shaly sands may be as high as 6 meq/100 gr. X-ray diffraction measurements were also obtained on much of the core; in general, the indicated clay content was less than 10% by weight of the total rock. The X-ray diffraction data were also used to estimate CEC, using average CEC's for the different types of clay minerals present. For the same samples on which CEC's were measured, estimated average CEC was 1.27 meq/100 gr., indicating that X-ray diffraction data may be used to estimate cation exchange capacity with fair accuracy. For the entire Tensleep interval, estimated average CEC was 1.39 meq/100 gr.

The Waxman-Smits equation[1] was then used to compute oil saturation, taking into account the clay conductance term. It was found that computed oil saturations averaged almost 50 oil saturation percent higher than comparable "clean sand" calculations. The clay conductance in this instance contributes about three-fourths of the total conductance of the formation. These results indicate that the effects of clays on computed oil saturations must be considered when high resistivity formation water is encountered, even for sands which are considered to be clean.

In this instance, the use of "shaly sand" instead of "clean sand" methods of log analysis showed that there was enough oil content to justify considerable field testing to attempt to develop a profitable recovery method.

Introduction

Log analysis, combined with other data, is often used to determine whether or not a conventional oil or gas well should be completed. The amount of money resting on the decision to complete a single well may range from a few tens of thousands of dollars to several hundred thousand dollars. The decision must be made quickly, and ambiguities can normally be resolved by well testing, if justified by the overall magnitude of the program. Under these conditions, simple methods of log interpretation are generally adequate, or can be corrected empirically as experience is gained in a given province.

More sophisticated methods of analysis are needed when large expenditures of time and money are required to demonstrate conclusively either the success or failure of a venture. This is the case in enhanced recovery projects, particularly when little or no primary oil can be produced. It then becomes more critical to analyze and interpret correctly all the available data to develop a consistent description of the reservoir and its fluids. Ideally, the description will be sufficiently accurate to help select the most promising enhanced recovery method for pilot testing. Subsequently, this reservoir description is used to design and evaluate a pilot test. Ultimately, after some modification based on pilot performance, the reservoir description becomes part of an economic analysis to decide whether to terminate the project or to expand it to a commercial scale.

Total oil in place is one of the most important numbers to estimate accurately for enhanced recovery projects. With enough well control, the gross reservoir volume can be accurately determined, and, with modern log suites, so can porosity. Hence, reservoir pore volume can be considered to be a relatively precise quantity, and most of the uncertainty in total oil in place results from uncertainties in estimating oil saturation. The following paper illustrates the use of "shaly sand" log interpretation techniques to improve the precision of oil saturation estimates in a "clean sand" reservoir containing heavy oil and fresh water.

General Description of Evaluation Program

A multi-well evaluation program was completed a few years ago to investigate the feasibility of enhanced recovery from an apparently large oil accumulation in the Tensleep sandstone in Wyoming. Objectives of the program included:

1. Obtaining well control for defining the limits of the oil accumulation.
2. Establishing the average oil content per unit volume within the accumulation. Some enhanced recovery methods require a minimum specific oil content to be economic, even with perfect efficiency; hence, this parameter was needed for process screening.

3. Providing accurate estimates for rock and fluid properties to allow proper ranking of different recovery methods, to use in design of a pilot test, and to assist in the interpretation of behavior observed in pilot testing.

Three of the evaluation wells are shown on the schematic crosssection of Fig. 1. The Tensleep formation is divided into members I - IV by dolomite streaks, which can be observed on cores and on logs. Well A lies entirely in the oil column, well B penetrates the oil-water contact, and well C is water saturated. Table I summarizes the coring and logging program for these wells.

Preliminary Interpretation of Data from the Evaluation Program

In Fig. 2, data from routine core analyses are plotted for wells A and B, along with qualitative indications of the amounts of odor and oil bleeding taken from the well-site geologist's reports. More frequent and profuse bleeding was observed from the core taken in well A than that taken in well B. This is consistent with the structural positions (relative to the oil/water contact) shown in Fig. 1.

Average core analysis oil saturation is 26.3% for well A and 13.8% for well B. Average core porosity is 17.1% for well A and 17.0% for well B. Average core permeability is 140 md.

Because of the low porosities, bleeding losses of 20 cc of oil per foot of core represent a decrease in measured oil content of almost 10 saturation percent. For this reason alone, core analysis oil saturations are low by an unknown but probably significant amount where bleeding was reported. Also, some flushing losses were suspected, since the reservoir is underpressured. Even though the oil viscosity is over 2000 cp at the reservoir temperature of 70F, the overbalance (estimated at several hundred psi) during coring would cause high pressure gradients and flush out an unknown amount of oil when the core was cut. Mud filtrate invasion was shown by the log responses. For these reasons, log analysis became the primary tool to determine oil saturation.

In one attempt to obtain quantitative saturation estimates from the logs, Schlumberger's CORIBAND® analysis was run on well A. Table 2 summarizes the results obtained from using R_w = 1.5 ohm-m, R_{mf} = 0.2 ohm-m, and m=n=2. Although the oil saturation values shown in Table 2 are high enough to indicate a large enhanced recovery target, the water resistivity and mud filtrate resistivity were much too low. Actual R_{mf} was about 2.2 ohm-m at reservoir temperatures, and formation water resistivity is 9.4 ohm-m at 68F. An analysis of formation water is shown as Table 3.

Clay Conductance Effects

We suspected that the use of artificially low resistivities for mud filtrate and formation water in the CORIBAND® analysis was an ad

hoc correction for shaliness. Although the Tensleep is regarded as a "clean" sand, in that it contains only a small fraction of clays, clay conductance makes a significant contribution to total conductivity when porosity is low and water resistivity is high.

Five core samples, with a wide range of porosities and gamma ray responses, were selected for laboratory determination of cation exchange capacities (CEC). The results are shown in Table 4, along with core analysis porosities and oil saturations, proximity log resistivities and invaded zone water saturations computed from an Archie equation[2]:

$$R_{xo} = (\phi S_{xo})^{-2} R_{mf} \qquad (1)$$

In using Eq. 1, we assumed that the proximity log recorded essentially the invaded zone resistivity and used the observed value for mud filtrate resistivity. Note that only one of the calculated invaded zone water saturations is less than one, even though all of the core samples contained significant amounts of oil.

In order to determine the magnitude of the clay conductance effect, the Waxman-Smits equations were used. These equations are[1]

$$F^* = \phi^{-m^*} \qquad (2)$$

$$R_o = F^* R_w / (1 + R_w B Q_v) \qquad (3)$$

$$S_w^{-n^*} = \frac{R_t}{R_o}\left(\frac{1 + R_w B Q_v / S_w}{1 + R_w B Q_v}\right) \qquad (4)$$

Note that if $Q_v = 0$, Eq. 3 reduces to $R_o = F^* R_w$, the usual Archie equation. Equations 2, 3 and 4 may be combined to derive

$$R_t = \frac{S_w^{-n^*} \phi^{-m^*} R_w}{1 + R_w B Q_{vb} / S_w} \qquad (5)$$

Data presented by Waxman and Thomas[3] and by Koerperich[4] show that $n^* = m^*$ within normal experimental scatter. For computation purposes, it is convenient to use $m^* = n^* = \nu$, and set $Q_v = Q_{vb}/\phi$, where Q_{vb} is the cation exchange capacity per cm^3 of bulk volume, rather than per cm^3 of pore volume. With these simplifications, the general resistivity equation based on the Waxman-Smits conductivity model becomes

$$R_t = \frac{(\phi S_w)^{-\nu} R_w}{1 + R_w B Q_{vb} (\phi S_w)^{-1}} \qquad (6)$$

In this form, porosity and water saturation appear only as the product of ϕS_w.

Using Eq. 6, the ratio S/C of surface (clay) conductance to total conductance may be evaluated as

$$S/C = \left(1 + \frac{\phi S_w}{R_w B Q_{vb}}\right)^{-1} \qquad (7)$$

When S/C is close to zero, the surface conductance may correctly be ignored. S/C takes on minimum values for S_w equal to 1.0. By inserting average values of ϕ = .15, R_w = 2.2 ohm-m, Q_{vb} = .02, and B = 1.2, the minimum S/C ratio in the invaded zone is found to be 0.26--that is, surface conductance in the invaded zone contributes at least 26% of the total conductance in the invaded zone. In the undisturbed zone (R_w = 9.4, B = 0.77), surface conductance contributes at least 50% of the total conductance.

With the above results in hand, we felt that a more complete determination of the CEC's of the formation was necessary to determine values of oil saturation. To avoid the expense of laboratory measurements on many samples, two other methods of CEC determination were tried.

First, X-ray diffraction measurements had been performed on the Tensleep core of well A, to determine clay content of the rock. The approximate weight percentage of different clay minerals was obtained. Using the average values of CEC for each clay mineral given in Table 5, the CEC of each foot of core was estimated. Table 6 shows a comparison between estimated CEC's from X-ray diffraction measurements and the CEC's actually measured in the lab. As shown by Table 6, fairly good agreement was obtained between the two methods. For the entire Tensleep interval, the average CEC estimated from X-ray diffraction data was 1.39 meq/100 gr. Figure 3 shows the X-ray diffraction results and the computed Q_{vb} for well A.

A second method for estimating CEC was devised using Eq. 6 and the log response at well C. Well C lies below the oil-water contact and is water saturated. With porosity known from a neutron-density crossplot (no cores were taken in well C), water resistivity known from the analysis of Table 3, formation resistivity obtained from logs, B estimated with the relation of Waxman and Smits[1], ν equal to 2 and water saturation equal to 1, Eq. 6 was rearranged to evaluate the CEC. The results of this computation are presented in Figure 4. Good qualitative agreement is seen between Figs. 3 and 4. The average CEC obtained from this analysis is 1.39 meq/100 gr., the same as the result obtained from X-ray diffraction data.

Oil Saturation Calculations

Using the average value of CEC of 1.39 meq/100 gr., the oil saturation was computed for each foot in each well. Although it is not strictly correct to use the average CEC,[4] computed average oil saturation for

each zone differed little from that computed using the CEC's estimated for each foot. For example, the average oil saturation for well A was 49.7% computed with the average CEC, and 48.9% computed with the continuous estimates of CEC.

Table 7 illustrates the magnitude of the error which is incurred by using "clean sand" techniques instead of Eq. 6. As seen on Table 7, clean sand methods underestimate oil content by more than 40 saturation percent for wells A and B. The surface conductance for these wells accounts for about 70 percent of the total conductance. For all wells in the evaluation program, the error in oil saturation arising from "clean sand" log analysis averages 50 saturation percent and the average ratio of surface conductance to total conductance is 75 percent.

Discussion

It might be argued that the above comparison between "clean sand" and "shaly sand" evaluation techniques is spurious. Commonly, an "apparent water resistivity" is used rather than the observed formation water resistivity. Although the use of R_{wa} improves the estimates of saturation, it still leaves considerable error, because the correct R_{wa} varies with ϕS_w.

To illustrate this point, R_{wa} was computed for well C, using the Archie equation, giving an average value of R_{wa} of 3.45 ohm-m. Using this R_{wa} for the structurally higher wells leads to computed oil saturations which are still 10 to 24 saturation percent less than those obtained with the Waxman-Smits equation.

Another approach to correcting for clay effects is to use true water resistivity with an "apparent" exponent in the Archie equation; as shown by Koerperich,[4] however, this method is useful only when the range of saturations encountered is limited--i.e., it has the same limitations as the use of an apparent water resistivity.

Throughout this discussion and in the remainder of this paper, we have implicitly assumed that saturation estimates based on the Waxman-Smits "shaly sand" equations are the "true" values and that other estimates are in error. Of course, this is not strictly correct, since the actual saturations are never known exactly. However, estimates based on the "shaly sand" techniques are more compatible with the observations of oil bleeding from most of the cores, with capillary pressure measurements, and with well behavior during subsequent pilot testing, than are either the core analysis results or log analyses based on lean sand" methods. Hence, we believe the former estimates to be the most nearly correct.

Conclusions

1. Clay conductance has an important effect, even in clean sands, on the saturation-resistivity behavior of rocks with relatively low porosity when water resistivity is high.

2. The Waxman-Smits model provides an apparently reliable method for estimating saturation from resistivity. However, it should be mentioned that all reported lab work verifying this model has been with sodium chloride solutions, rather than with the calcium-magnesium-bicarbonate waters encountered in many Rocky Mountain reservoirs.

3. Cation exchange capacities can be estimated with sufficient accuracy for most purposes from X-ray diffraction data and by calculation from logs taken in the same formation below the oil water contact.

4. Techniques using an apparent water resistivity tend to seriously underestimate oil saturation.

References

1. Waxman, M.J. and Smita, L.J.M.: "Electrical Conductivities in Oil-Bearing Shaly Sands," Soc. Pet. Eng. J. (June 1978) 107-122; Trans., AIME, 254.

2. Archie, G.E.: "Electrical Resistivity Log as an Aid in Determining Some Reservoir Characteristics," Trans., AIME (1942) 146, 54-67.

3. Waxman, M.H. and Thomas, E.C.: "Electrical Conductivities in Shaly Sands - I. The Relation Between Hydrocarbon Saturation and Resistivity Index; II. The Temperature Coefficient of Electrical Conductivity," J. Pet. Tech. (Feb. 1974) 213-225; Trans., AIME, 257.

4. Koerperich, E.A.: "Utilization of Waxman-Smits Equations for Determining Oil Saturation in a Low-Salinity, Shaly Sand Reservoir," J. Pet. Tech. (Oct. 1975) 1204-1208.

Acknowledgement

We would like to thank the companies for which this study was performed for permission to publish this paper.

Nomenclature

- B - equivalent conductance of clay exchange cations (cm^3/meq-ohm-m)
- CEC - cation exchange capacity of rock (meq/100 gr. dry rock)
- F^* - formation resistivity factor for shaly sands (ohm-m/ohm-m)
- m^* - porosity exponent for shaly sands (Eq. 2)
- n^* - saturation exponent for shaly sands (Eq. 4)
- Q_v - cation exchange capacity of rock (meq/cm^3 pore volume)
- Q_{vb} - cation exchange capacity of rock (meq/cm^3 bulk volume)
- R_{mf} - mud filtrate resistivity (ohm-m)
- R_o - formation resistivity when 100% saturated with formation water (ohm-m)
- R_t - true formation resistivity (ohm-m)
- R_w - formation water resistivity (ohm-m)
- R_{xo} - invaded zone resistivity (ohm-m)
- S_w - water saturation in undisturbed formation
- S_{xo} - water saturation in invaded zone
- S/C - ratio of surface (clay) conductance to total conductance (mho-m^{-1}/mho-m^{-1})
- ϕ - porosity
- ν - exponent in Eq. 6

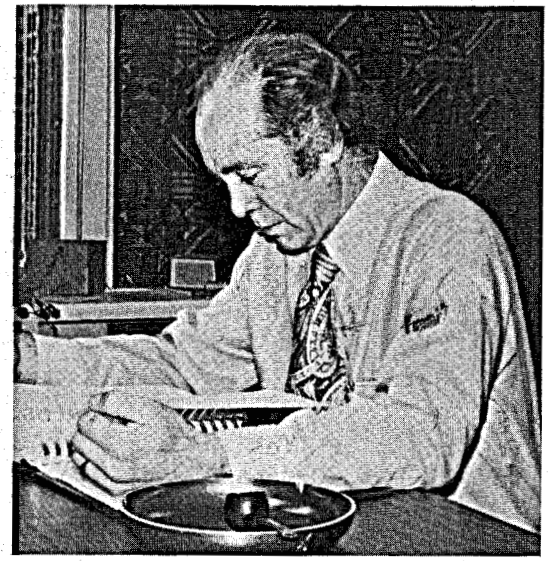

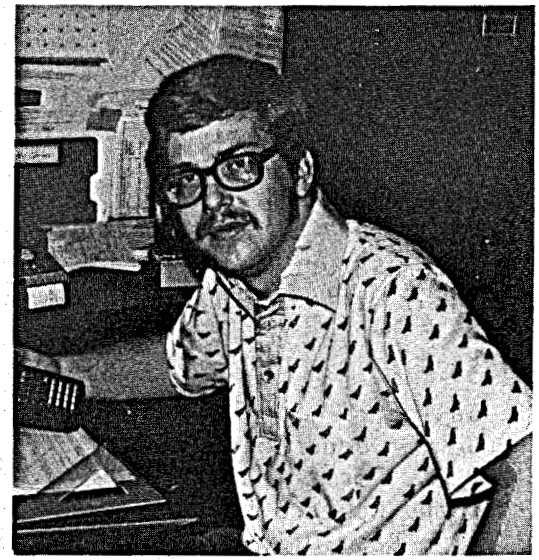

About the Authors

Dwayne A. Chesnut is president of Energy Consulting Associates, Inc. He has a Bachelor of Science degree in Chemical Engineering and a Ph.D. in Physical Chemistry, both from Rice University. He has worked in the areas of research chemistry, formation evaluation, reservoir modelling and evaluation, and enhanced recovery, and is a member of SPE of AIME and various other technical organizations.

Dave O. Cox is an engineer for Energy Consulting Associates, Inc., in Denver, Colorado. He has worked in the areas of formation evaluation, reservoir evaluation, and enhanced oil recovery. He has Bachelor and Master of Science degrees in Petroleum Engineering from the Colorado School of Mines and is a member of SPWLA and SPE of AIME.

Table 1: Summary of Coring and Logging Programs

	Well A	Well B	Well C
Feet of Core	269	180	0
Core Description	Yes	Yes	N.A.*
Core Analysis			
Capillary Pressures	Yes†	Yes†	N.A.
CEC Measurements	Yes†	No	N.A.
Grain Density	Yes	Yes	N.A.
Oil Saturation	Yes	Yes	N.A.
Permeability	Yes	Yes	N.A.
Porosity	Yes	Yes	N.A.
Water Saturation	Yes	Yes	N.A.
X-Ray Diffraction	Yes	No	N.A.
Well Logs			
Caliper	Yes	Yes	Yes
Cement Bond Log	Yes	Yes	Yes
Comp. Formation Density Log	Yes	Yes	Yes
Comp. Neutron Log	Yes	Yes	Yes
High Resolution Dipmeter	Yes	Yes	No
Dual Laterolog	No	No	Yes
Gamma Ray	Yes	Yes	Yes
Laterolog	Yes	Yes	No
Microlog	Yes	Yes	No
Proximity Log	Yes	Yes	No

* N.A. = Not Applicable

† Measurements performed on selected samples

Table 2: Summary of CORIBAND® Analysis, Well A

Zone	Thickness, ft.	Average Porosity	Average Oil Saturation
I	56	.191	.424
II	44	.173	.538
III	138	.161	.571
IV	58	.127	.591
Overall	296	.155	.559

Table 3: Formation Water Analysis, Well C

Ion	Concentration, mg/l	Activity, meq/l
Sodium	29	1.26
Potassium	16	0.41
Calcium	179	8.93
Magnesium	31	2.55
Sulfate	230	4.78
Chloride	20	0.56
Bicarbonate	476	7.81

Total Dissolved Solids: 739 mg/l

Measured Resistivity: 9.4 ohm-m at 68F

Table 4: Cation Exchange Capacity and Other Data, Well A

Sample	Measured CEC, meq/100 gr	Core Oil Saturation	Core Porosity	Proximity Log Resistivity (ohm-m)	Calculated Invaded Zone Water Saturation
a	0.95	0.312	0.167	69.2	1.07
b	1.09	0.286	0.013	832	3.96
c	1.02	0.317	0.079	236	1.22
d	1.00	0.338	0.162	76.6	1.05
e	1.14	0.115	0.113	194	0.94

Table 5: Average CEC of Clay Minerals[4]

Type of Clay	CEC (meq/100 gr)
Kaolinite	5
Illite	25
Montmorillonite	85
Mixed Layer	35

Table 6: Comparison Between Calculated and Measured CEC, Well A

Sample	Measured CEC/meq/100 gr)	CEC Computed from X-Ray Diffraction (meq/100 gr)	Clay Types Present
a	0.95	0.73	K, I, M
b	1.09	1.42	K, M
c	1.02	1.55	K, M, ML
d	1.00	0.93	K, M
e	1.14	1.73	K, I, M, ML
Average	1.04	1.27	

Figure 1: Schematic Cross Section of Tensleep Reservoir

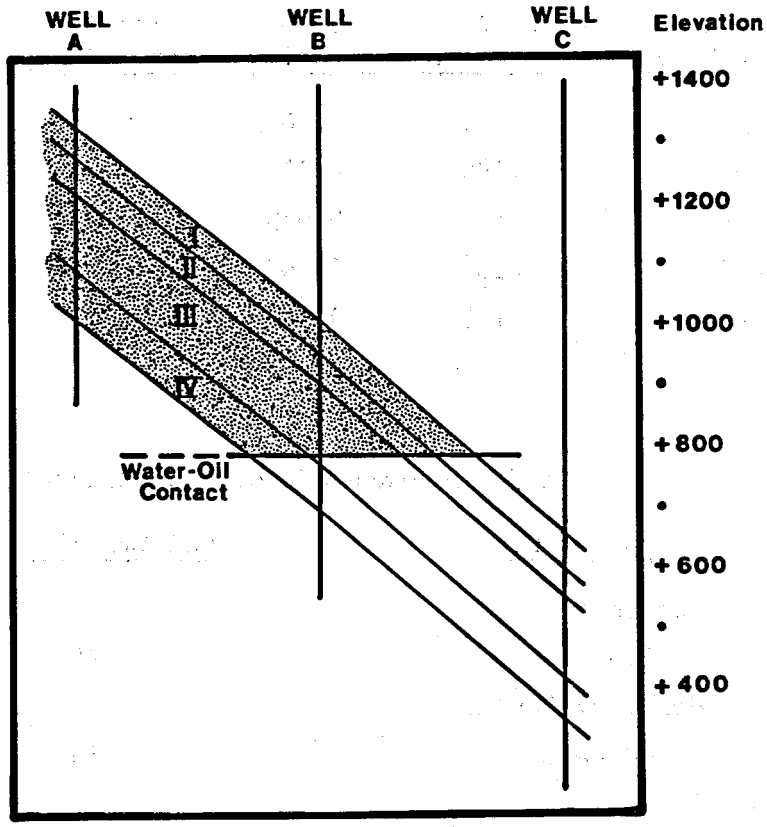

Table 7: Oil Saturation Calculations, Wells A and B

Well A

Elevation	Porosity	Formation Resistivity	Core Oil Saturation	Clean Sand Computation of Oil Saturation	Shaly Sand Computation of Oil Saturation	S/C Ratio
1325	.18	326	NA	.057	.485	.702
1300	.19	236	.180	-.050	.374	.645
1275	.15	463	.352	.050	.542	.767
1250	.20	217	.142	-.041	.364	.626
1225	.15	410	.382	-.009	.495	.749
1200	.20	317	.428	.139	.520	.690
1175	.19	340	.360	.125	.525	.705
1150	.16	309	.217	-.090	.404	.701
1125	.17	252	.220	-.136	.342	.664
1100	.17	233	.156	-.182	.302	.651
1075	.16	622	.291	.232	.661	.805
1050	.16	1129	.211	.430	.797	.873
		Average	.267	.044	.484	.715

Well B

1000	.22	273	NA	.157	.506	.529
975	.19	237	.11	-.048	.376	.646
950	.19	380	.09	.172	.564	.723
925	.22	288	.028	.179	.525	.666
900	.19	368	.079	.159	.553	.718
875	.18	313	.016	.037	.469	.696
850	.19	414	.107	.207	.593	.736
825	.21	329	.199	.195	.553	.692
800	.21	219	NA	.013	.395	.624
775	.14	268	NA	-.338	.250	.686
750	.15	232	NA	-.342	.215	.658
		Average	.091	.036	.454	.670

Figure 2: Core Analysis Results

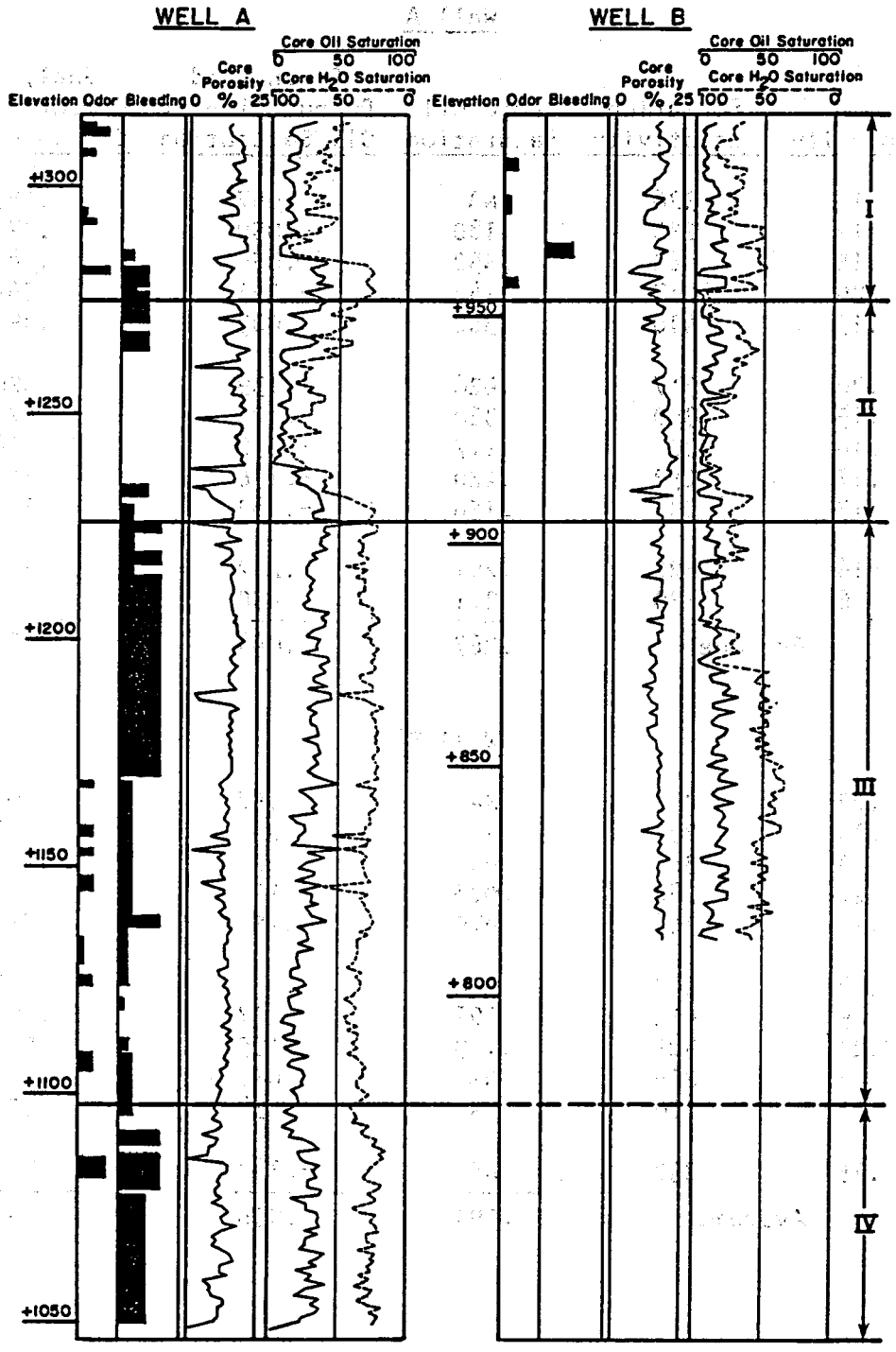

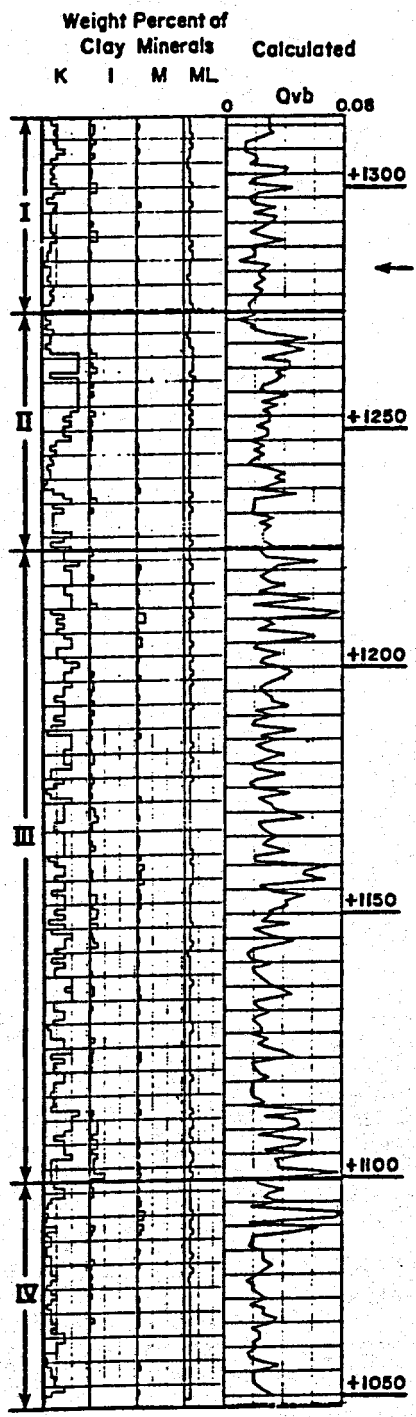

Figure 3: X-Ray Diffraction Measurements of Clay Content and Estimated Qvb, Well A
K = Kaolinite
I = Illite
M = Montmorillonite
ML = Mixed Layer
Scale for each clay mineral is 0-15 weight percent

Figure 4: Estimated Qvb from Log Analysis, Well C

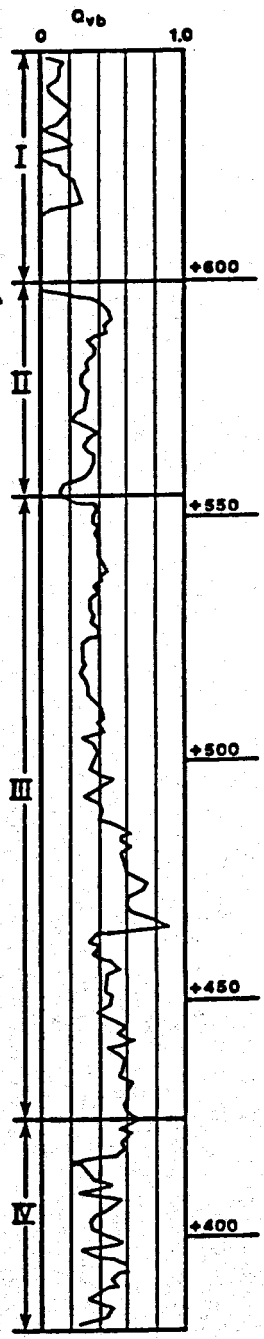

DIPMETER LOG ANALYSIS

AN ESSAY

by

M. H. Rider

Compagnie Française des Pétroles

Bordeaux, France

ABSTRACT

The greatest difficulty with the dipmeter seems to be a lack of consumer confidence. This is not necessarily in the tool itself but of the manner in which it is interpreted. It is in the existing systems of analysis that the doubt lies.

Quite a number of articles have been written in which comprehensive systems for dipmeter interpretation have been proposed. This paper does not have similar ambitions : it is only an essay.

The first object is to compare dipmeter results with measurements and observations on cores and, where possible, to draw conclusions. A second object is to use a quasi-statistical approach to dipmeter analysis (rather than pattern analysis). This approach is used both in the comparisons with core data and in the example of interpretation which is given.

INTRODUCTION

One fundamental problem in dipmeter analysis is to know what the tool is measuring. Can we put confidence in the dips we see on the log ?

When a geologist takes a dip in the field he measures it on a surface of discontinuity : a change in lithology, a bed junction or a lamination. The dipmeter tries to do the same by comparing four micro-resistivity curves from four quadrants of the borehole : the comparisons are made by computer (ALLAUD et al. 1969).

To what extend do these dips resemble those taken by eye ? In recent years a number of possible programmes and variations of treatment for comparing the curves have become available, which is the best ?

To reply to these questions dipmeter log results have been compared to measurements made directly on cores. Various methods of computer curve analysys are used and contrasted (Schlumberger geodip, HDT conventional correlation

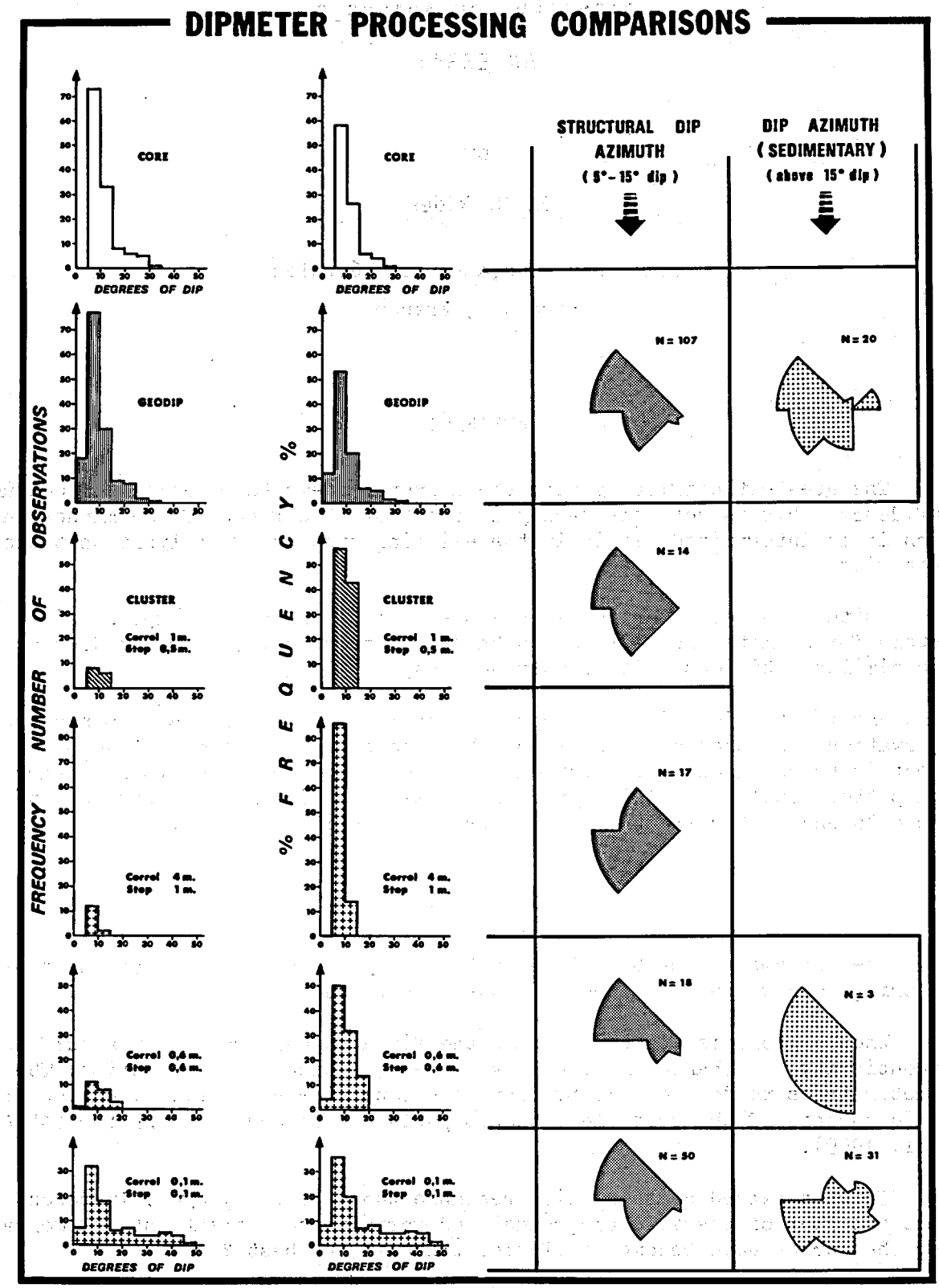

Fig. 1 : Comparative dipmeter processings from a 14 m (46 feet) interval of interbedded sands & shales.

and Cluster : Exploration Computing correlations).

In order to compare the dipmeter results with un-oriented cores, rather than make point by point comparisons, dips were pooled by increments of degrees of dip and plotted in histograms. That is, the histogram is a plot of frequency (number or in percentage) against degrees of dip (counted in 5° increments) (Fig. 1). Directions of dip have been largely ignored. In this way the artificiel orientation of a core is unnecessary. Moreover, the pooled dips can be used in comparisons with examples in the literature.

The comparisons with cores are treated under three headings ; correlation scale and "noise", lithology and facies and sedimentary structures.

CORRELATION SCALE AND "NOISE"

With the advent of very detailed dipmeter surveys (small correlation intervals for the HDT) the number of dip measurements per interval have increased phenomenally. The problem is to know if quality is impaired in these fine correlations. Put in a more scientific way, to what extent do artefacts produced by the computer programme (or "noise") increase as the number of dips increase ? As has been noted already "error does occur, but so does truth" (HEPP et al. 1975). But in what proportions are truth and error mixed and where is error likely to occur ?

The following comparisons are made in a series of interbedded sands and shales 14 meters (46 feet) thick (sand beds between 1 cm and 35 cm thick [1/2"-10"]). The interval was cored. The dipmeter log was subject to five variations of computer processing (Table 1).

TABLE 1 INTERVAL 5°-15° DIP

Correlation Int.	Step	N° of dips	% (of all dips)
+ 4.0 m	1.0 m	14	100
+ 0.6 m	0.6 m	18	82
+ 0.1 m	0.1 m	50	57
C O R E		106	84
G E O D I P		107	73
⁂ 1.0 m	0.5 m	14	100

+ EXPLORATION COMPUTING ⁂ CLUSTER

A comparison has been made using histograms of the degrees of dip as explained previously (Fig. 1). As can be seen, basically the same form is reproduced from one histogram to the next. (The borehole drift was nearly 5° in a direction exactly opposed to the structural dip. For this reason 5° was added to all core dips to reconstitute the true values. There are therefore

no dips between 0 and 5° and a slightly exaggerated number between 5° and 10° : the original 0-5 ° dips having been tilted to this increment).

The 5 to 15 degrees class obviously contains the structural dip. Comparing, therefore, this class (Table 1) we see the differences between the various computer programmes and treatments (see also Fig. 2).

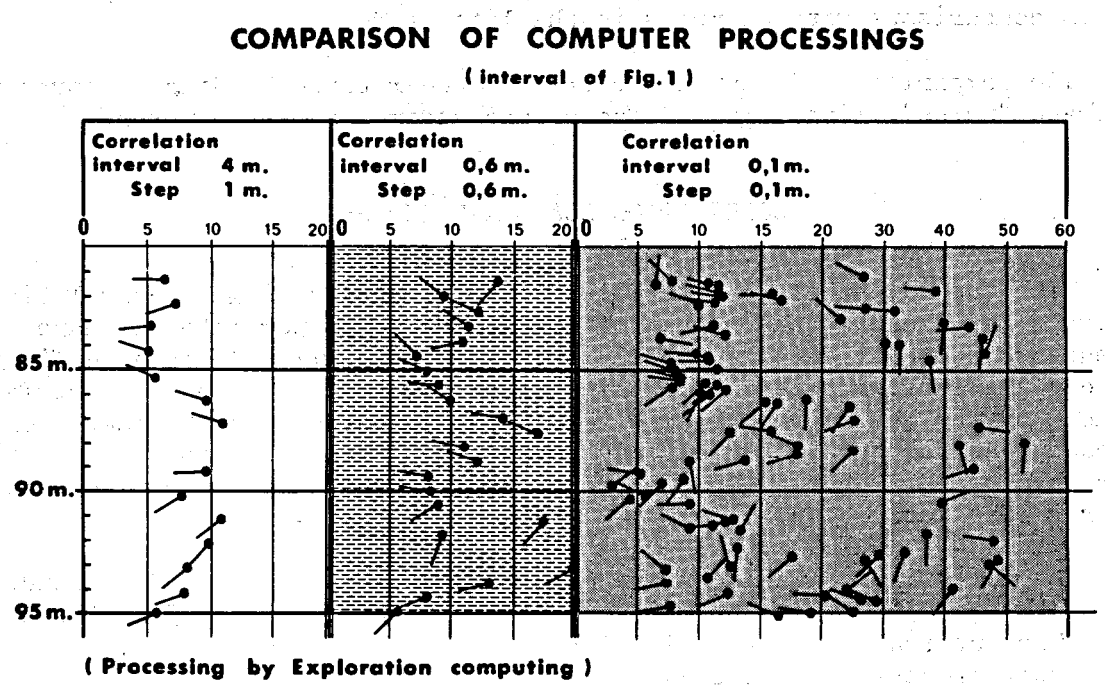

Fig. 2 : Arrow plots of three different computer processings. The interval is that used in Fig. 1

With the same programme (Exploration Computing) but decreasing correlation interval (the distance along which the resistivity curves are compared) we see the number of dip points increased considerably from 14 to 50 but the relative percentage decreased from 100 % to 57 % (Table 1). The cluster programme gave results similar to the large correlation small step programme (4.0 m x 1.0 m). The eye measured 106 dips (84 %) and geodip 107 dips (73 %).

The first point of note is the number, or density of dips. Geodip approaches the eye in detail (the density of measurements on the core was in fact made to resemble that of geodip : the eye could have added more). The fine correlation (0.1 m x 0.1 m) sees only one half this number and the other programmes less than one sixth. There is thus great variation in detail, especially between geodip and the other programmes.

But of these dips, how much is "noise" ?

In this context it is interesting to compare the number of dips above 15 degrees for the various programmes and treatments. (Table 2).

TABLE 2 DIPS ABOVE 15 °

Correlation Int.	Step	N° of dips	% (of all dips)
1.0 m	1.0 m	0	0
0.6 m	0.6 m	3	13.5
0.1 m	0.1 m	31	35
C O R E		12	9.5
G E O D I P		20	14
1.0 m	0.5 m	0	0

The fine correlation 0.1 m x 0.1 m) shows 31 dips (35 %) above 15 ° while the core shows only 12 dips (9.5 %). If, from these figures, we consider that only 10 % of the dips should be above 15 degrees, 25 % of the dips of the fine correlation (35 % above 15 degrees) are "noise". That is there is a 3 % to 4 % "noise" level in each of the 5 degree increments, probably over the scale from 0-45 degrees. The histogram, in fact, shows this very well, there being an overall platform around 4 % in each increment between 15 and 45 degrees of dip. The overall error will be an alarming 35 % (approximately). The other treatments do not show this.

The degree of "noise" is difficult to discern in the remaining treatments using this method. It is interesting, however, to add the azimuths to the histograms to see if differences which can be attributed to noise exist (Fig. 1). Two azimuths are given, that of dips with the structural dip of between 5 and 15 degrees (Fig. 1 column 3) and that of dips over 15 degrees (Fig. 1 col. 4) (Dips are grouped into 45 ° segments for these plots).

The structural dip azimuths are all remarkably similar except that the 4 m x 1 m processing shows a slight variation, probably because of the few points contributing to the statistics. This indicates that grouping the points in this manner no "noise" is visible, even in the fine treatment (0.1 m x 0.1 m) shown above to be "noisy".

The azimuths of dips above 15 degrees, where they exist, show more variation. The fine treatment (0.1 m x 0.1 m) shows only a slightly prefered orientation due to the "noise" already discussed. The 4 m x 1 m treatment shows a reasonable orientation but with spread and is based on very little data : it is not reliable. The geodip shows a strong prefered orientation (similar to the structural) and does not appear to show "noise".

Conclusion.

The different methods of computer curve correlation give a density (number of dips) which varies considerably (to the order of 10 times in this example).

With a classical treatment, a fine correlation interval (in this case

.1 m x .1 m) engenders "noise" but also increases true dips at the same time. Coarse correlations appear to lack"noise"but lack reliability because of the few dip points available (in this case Cluster 1 m x 0.5 m and Exploration Computing 4 m x 1 m). Geodip gives considerable detail with apparently little "noise".

If results are pooled, as in the present example, "noise" appears to be eliminated and the various treatments give very similar results. Fine correlation gives more data, usable if results are pooled : coarser treatments lack data at higher dip angles.

LITHOLOGY AND FACIES

Facies most certainly has a strong influence on the quality of dipmeter logs. Otherwise stated, lithology and facies have a strong influence on the type of micro-resistivity curve. A lack of resistivity contrast will give poor quality correlation, good resistivity contrast, good correlation.

The following comparisons show some examples of this.

Interlaminated sand and shale facies.

The first comparison is between core data, geodip and an original HDT processing (correlation interval 1 m step 1 m) over a 5 m (16 feet) interval of finely interlaminated sands and shales (Fig. 3a). A second example compares core data from 5 m (16 feet) also of finely interlaminated sands and shales to a geodip treatment (Fig. 3b).

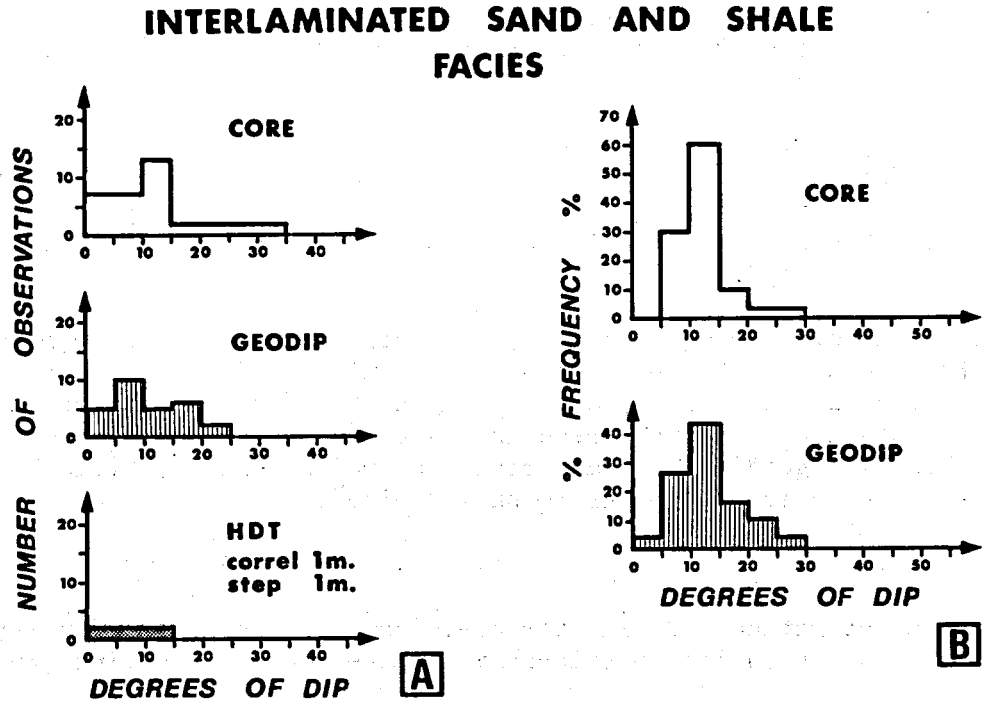

Fig. 3 : Dip frequency histograms of two examples from a finely interlaminated sand and shale facies.

In the first example the correspondence between geodip and what the eye sees is reasonable. The original HDT programme gives reasonable but sparse data. In the second example the correspondence is excellent.

Obviously this is a facies favourable to dipmeter measurements in general regardless of processing. The reason, presumably, is because the fine interbedding of sand and shale gives good, small scale, resistivity contrasts. In fact it is found that any finely laminated deposit with resistivity contrast (shale in sand, evaporites in limestone etc) gives similar results.

Bioturbated sandstone facies.

The core, in this comparison is in a bioturbated, fine grained, shaly sandstone. The lithologies are terribly mixed and secondary, bioturbation structures, dominate. The eye read dips come mainly from very irregular laminations. The original HDT processing (correlation interval 1 m step 1 m) and geodip are used (Fig. 4).

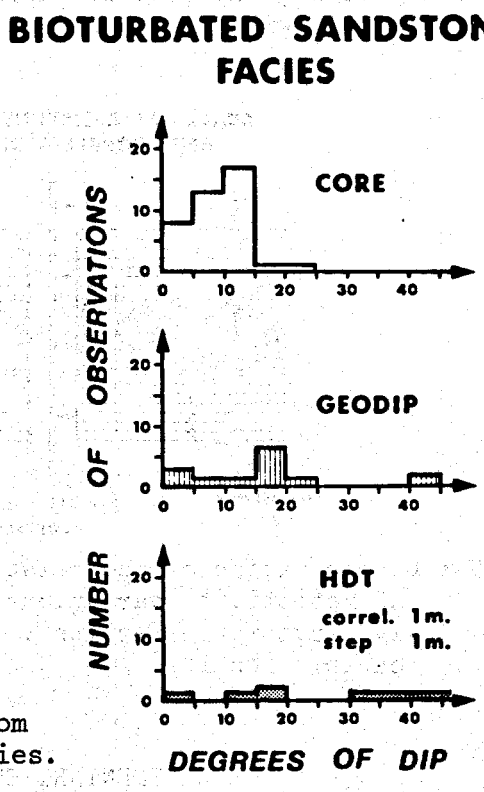

Fig. 4 : Dip frequency histograms from a bioturbated sandstone facies.

The correspondence between the core and the logs is null. This seems to be a case where "mathematical dips" or "noise" dips are almost the only ones recorded. The irregular laminations seen by the eye are probably not recorded on the logs since they do not cross the entire borehole (in this case 12 1/4") intact. That is, few, if any of the laminations are seen on all four curves of the dipmeter.

Evidently this facies is inhospitable to dip measurements. Nevertheless dips are given. They can be recognised as "noise" by being spread more or less evenly over the interval of dip values and having no definite azimuth, as was discussed previously.

Discussion-conclusions

The lesson from these comparisons between facies and dipmeter (regrettably too few) is that when conditions (facies) are favourable the dipmeter works well : when conditions (facies) are unfavourable dip readings are still given but are spurious. Favourable facies are those in which regular resistivity variations exist. Unfavourable facies are those in which there are no resistivity contrasts.

The concepts of favourable and unfavourable are not absolute : it depends to some extent on the scale of correlations (correlation interval) for the conventional computer process. The example (Fig. 2) shows how dips spread as the correlation interval is decreased (This is the same interval used in the discussion on "noise"). With small (thin) correlation intervals the facies is unfavourable (lots of "noise"), with a large (thick) correlation interval the facies is favourable. This simply indicates the level at which the resistivity contrasts take place. A correlation interval finer than the resistivity variations will give a great deal of "noise" (Fig. 5), but larger than the resistivity variations will give good dips.

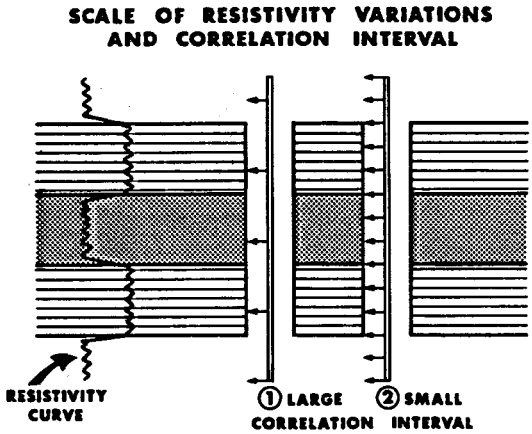

Fig. 5 : Demonstration of the relationship between correlation interval and resistivity variations. The correlation interval ① will give favourable results : the small correlation interval ② unfavourable results.

SEDIMENTARY STRUCTURES.

It is often supposed that the dipmeter is able to "see" sedimentary structures. In this context the comparison cited below raises interesting problems.

The example is of a 13 m (43 foot) foreset sandstone interval (of which 10 m - 33 feet) were cored with a Processing by Exploration Computing. The illustration (Fig. 6) shows the core lithology, lamination characteristics and corresponding dipmeter results. The processing used a correlation interval of 60 cms (2 feet) with a step of 30 cms (1 foot).

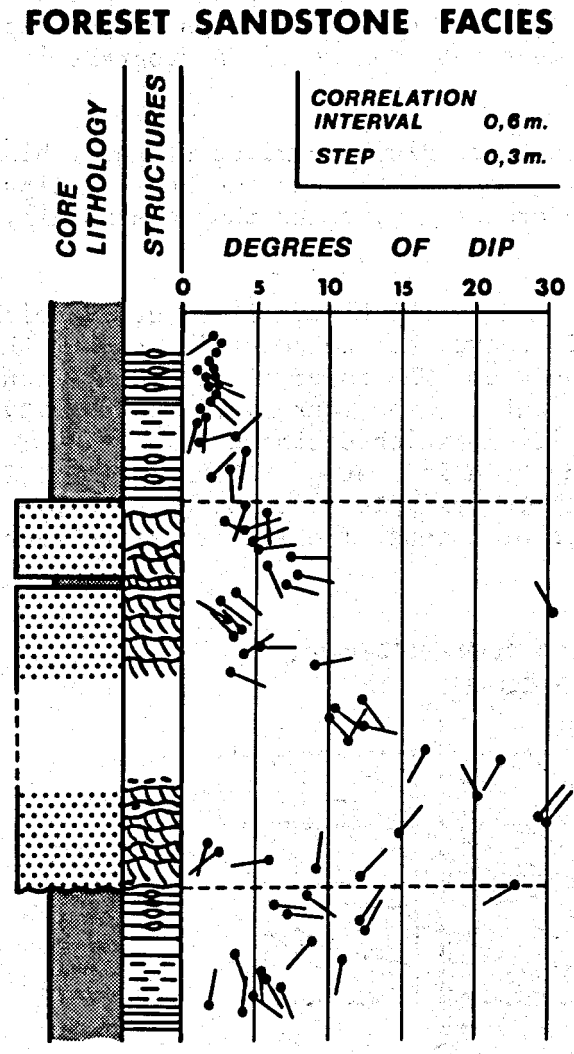

Fig. 6 : Core log and arrow plot of a foreset sandstone facies.

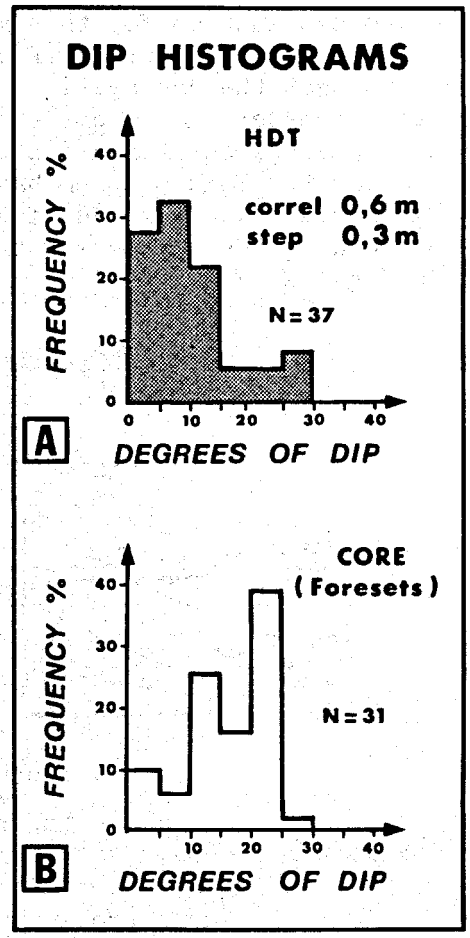

Fig. 7 : Dip frequency histograms of the foreset sandstone facies of figure 6.

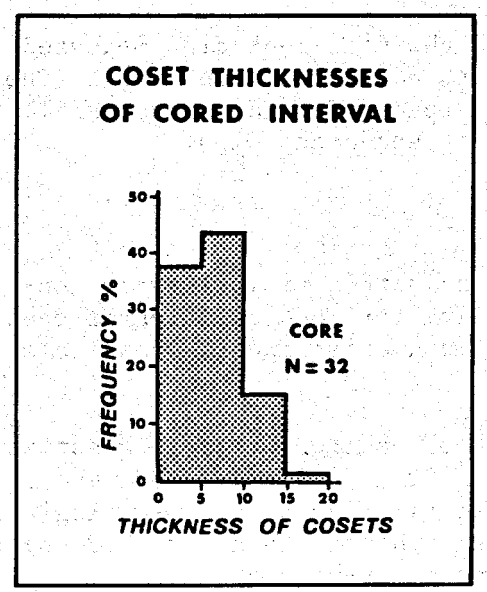

Fig. 8 : Coset thickness histogram as measured in the foreset sandstone interval of figure 6.

The histograms resume the interval in degrees of dip first (Fig. 7a) from the log and secondly (Fig. 7b) from the core. The core dips are those that correspond only to foreset dips (that is ignoring the dips of junctions between cosets). The lack of correspondence between the two histograms is evident.

The dipmeter log (Fig. 6) shows that the dipmeter gives slightly higher dips in the sands than in the surrounding shales. However the lack of dips between 20-25 degrees, the predominant foreset dip, shows that essentially the foresets are not seen.

The explanation for this may be found in the histogram of coset thickness for the cored interval (Fig. 8). It shows that no coset is thicker than 20 cm and that the average is between 5-10 cm. The interval of correlation for this dipmeter was 60 cm. (2 feet). That is, the four micro-resistivity curves are compared over a distance of 60 cm, which distance will cover four or more cosets. This problem has already been indicated (Schlumberger 1970, p. 50) though in a different fashion. In the example cited here the dipmeter is not reading the foresets but the dips of cosets. The latter are between 0 and 10 degrees (Fig. 9).

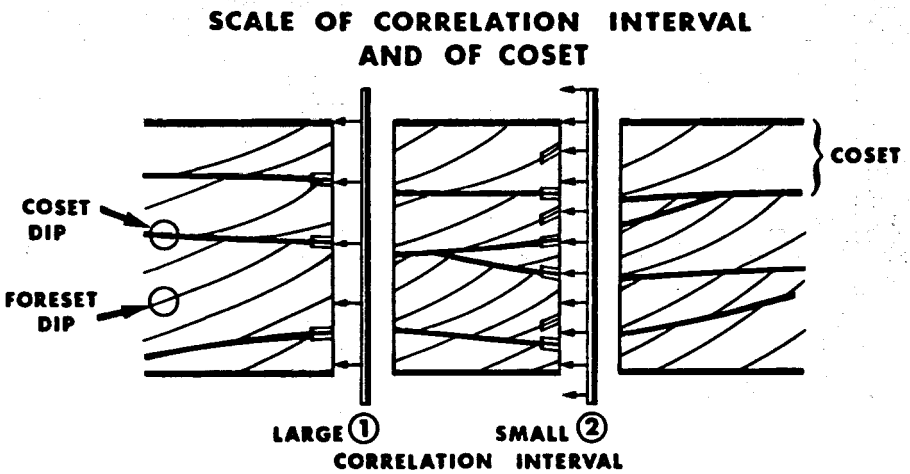

Fig. 9 : Diagrammatic representation of the different dips measured in foreset sands using different correlation intervals. The large correlation interval ① reads coset dips, the small correlation interval ② foreset and coset dips.

Discussion-Conclusions.

The suggestion from the above comparison is that visibility or non-visibility of sedimentary structures by the dipmeter is a question of scale (geodip excluded). At what scale do the phenomena exist and at what scale can we expect results?

The size of cross-beds varies from that of small ripples to giant waves and eolian dunes, from 1-2 cm (inches) to over 30 m. (100 feet). However, examples shown here indicate the order of size familiar to sedimentologists (Figs 10, 11). The greater number of cosets are thinner than 1 m (3 feet) : the number thicker than this varying with type of structure.

This means that a 1 metre (3 feet) correlation interval will "see" very few cross-strata, a 60 cms (2 feet) correlation will "see", in favourable cases one quater of the structures and a 30 cm (1 foot) correlation perhaps one third (geodip excluded). If we compare the histograms and log given as examples (Figs 10, 11) there will be considerable variation from one region to another.

COSET THICKNESS AND FORESET DIP VARIATIONS

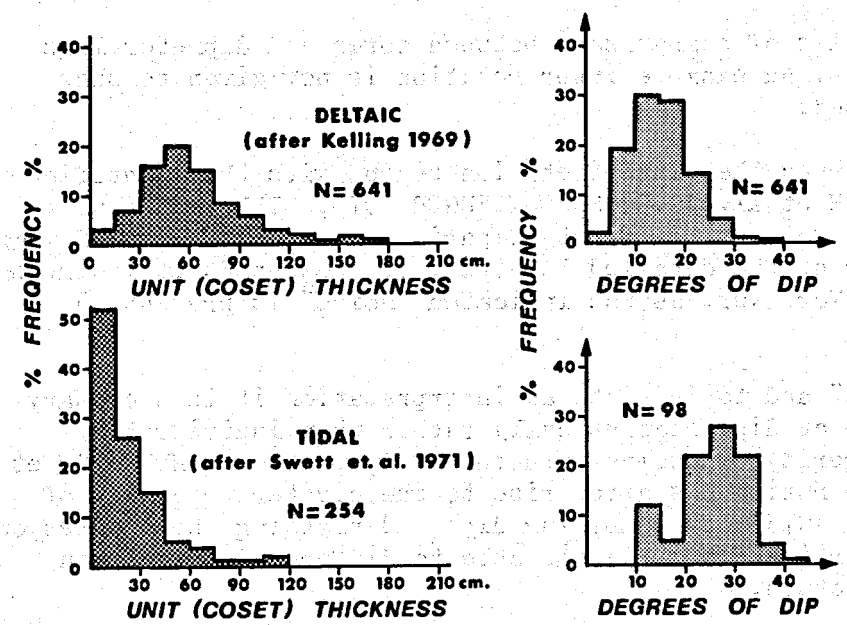

Fig. 10 : Examples of coset thickness and dip angles. A. Upper Carboniferous, deltaic facies (after Kelling 1969) B. Cambrian tidal facies (after Swett et al 1971).

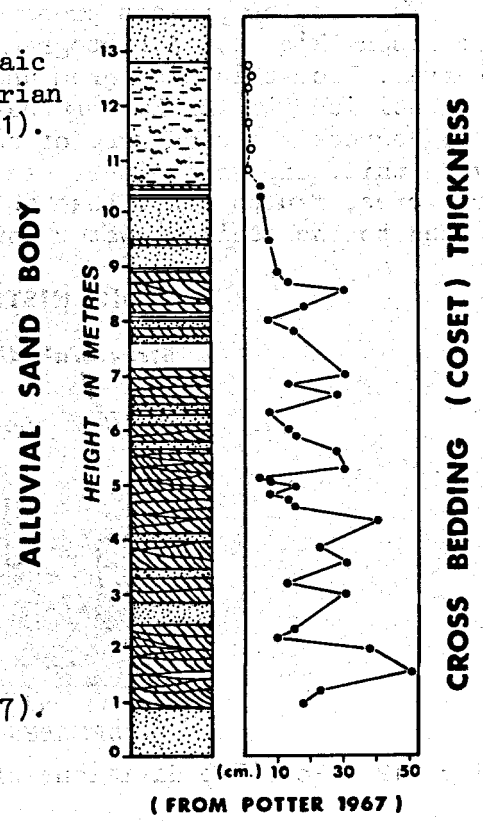

Fig. 11 : Example of coset thickness from an alluvial sand body (from Potter 1967).

The conclusion, therefore, is that it is possible to see sedimentary foreset structures but most, even with short correlation distances, will be missed. The most frequently read dips will be those of cosets or beds.

More data are needed in this domaine. The behaviour of geodip has not been documented.

INTERPRETATION

The foregoing examples of comparisons between cores and dipmeter logs gave rise to various ideas. An example interpretation is now given to show how these ideas can be used.

It is generally assumed that interpretation begins with the identification of patterns (GILREATH et al. 1969, SCHLUMBERGER 1970, GILREATH et al. 1971, GOETZ et al. 1977). However the first comparison gave an example of very detailed logs. One glance at the detailed log (Fig. 2) shows that it is impossible to trace patterns. Moreover, as was indicated "noise" is present in these detailed logs.

To eliminate "noise" and to initiate an interpretation it is necessary to pool results : to look at dips statistically rather than individually. This idea was used in Nigeria to resolve structural dip problems (NEDERLOF et al 1971) and recently the notion has given rise to the cluster programme of Schlumberger (HEPP et al. 1975). By combining dips and plotting their poles on a stereonet, another author (PERRIN 1975) was able to differentiate between types of sedimentary structure.

The pooling process proposed here is that used in the first example of comparison (Fig. 1). A histogram is made of the degrees of dip over a chosen interval. From this histogram and other data if necessary the structural dip is identified (Fig. 12). Knowing that the ordinary maximum angle of sedimentary dip is 35 degrees a second zone of possible sedimentary dips can be delineated. Beyond this, dips are either secondary (slumps, bioturbations etc) or tectonic (fractures, faults etc), that is formed in the interior of the sediment (as opposed to the sediment-water interface).

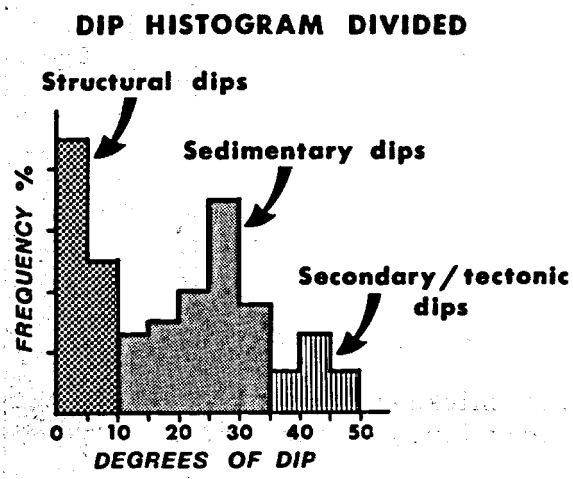

Fig. 12 : Possible divisions of the dip frequency histogram.

Azimuth plots are then made of the various slices of degrees of dip identified (Fig. 1). It is probable that false dips are included in the statistics but their influence is outweighed by the true dips.

The example (Fig. 13) shows a single sand reservoir (identified by correlation) which was penetrated by 25 wells. The dipmeter was run in all the wells but was not processed in the same way in each (programmes include 1 m x 1 m, 0.9 m x 0.6 m and 0.6 m x 0.3 m). The results are often a confusing mass of dips. The sand body and its equivalent interval are shown by a gamma-ray curve with lithology added (Fig. 13). The histogram is of the degrees of dip for the interval concerned and has been divided into a structural element and a sedimentary element as described above.

The azimuths of the structural element are plotted on an isobath map (Fig. 14). Correspondence between the isobaths and the dips indicates that the structural element has been identified.

The azimuths of the sedimentary element are plotted on the isopachite map of the sand body (Fig. 15). It is known from other data that the sand body represents a north-south trending channel derived from the north. A southerly element in the azimuths for the central part of the sand body is evident. However a westerly dipping element is present along the entire western edge.

As was previously discussed, the dipmeter in sands seldom sees the dip of foresets. It is probably the case in this example where core data suggests that cosets are generally not thicker than 20 cm. and correlation intervals varied from 1 m. to 0.60 cm. Therefore, as suggested, the dips registered are those of cosets and beds which are consequently only slightly superior to the structural dip. The southerly component in the centre of the sand body is thus a downstream coset dip. The westerly dips at the border of the body are probably due to distortion during compaction. Since the coset dips are not strong they are easily re-oriented by the warping which takes place during compaction.

The one anomalous northerly sedimentary dip in the north-eastern quadrant demands comment. A study of the gamma ray profile shows a high shale content and the dipmeter shows extremely regular and good quality dips. The facies is certainly conducive to dip measurement and, drawing on the examples quoted above, will consist of a regular, fine interlamination of sand an shale. This is the sort of facies found in channel fills. The northerly element of dip is therefore the result of the deposition of the laminae of the channel fill.

Conclusion.

The technique of pooling dips enables the separation of three dip elements, structural, sedimentary and secondary and also diminishes the effects of "noise". The example shows that a reliable structural dip and azimuth can be extracted from intervals of apparently confused dips. The sedimentary dip is best exploited when pooling is made by sedimentary interval. However, since the actual sedimentary feature being measured is not always evident the interpretation of sedimentary dips should be given with reserve.

More experience is needed in the application and interpretation of the system both to outcrops and wells.

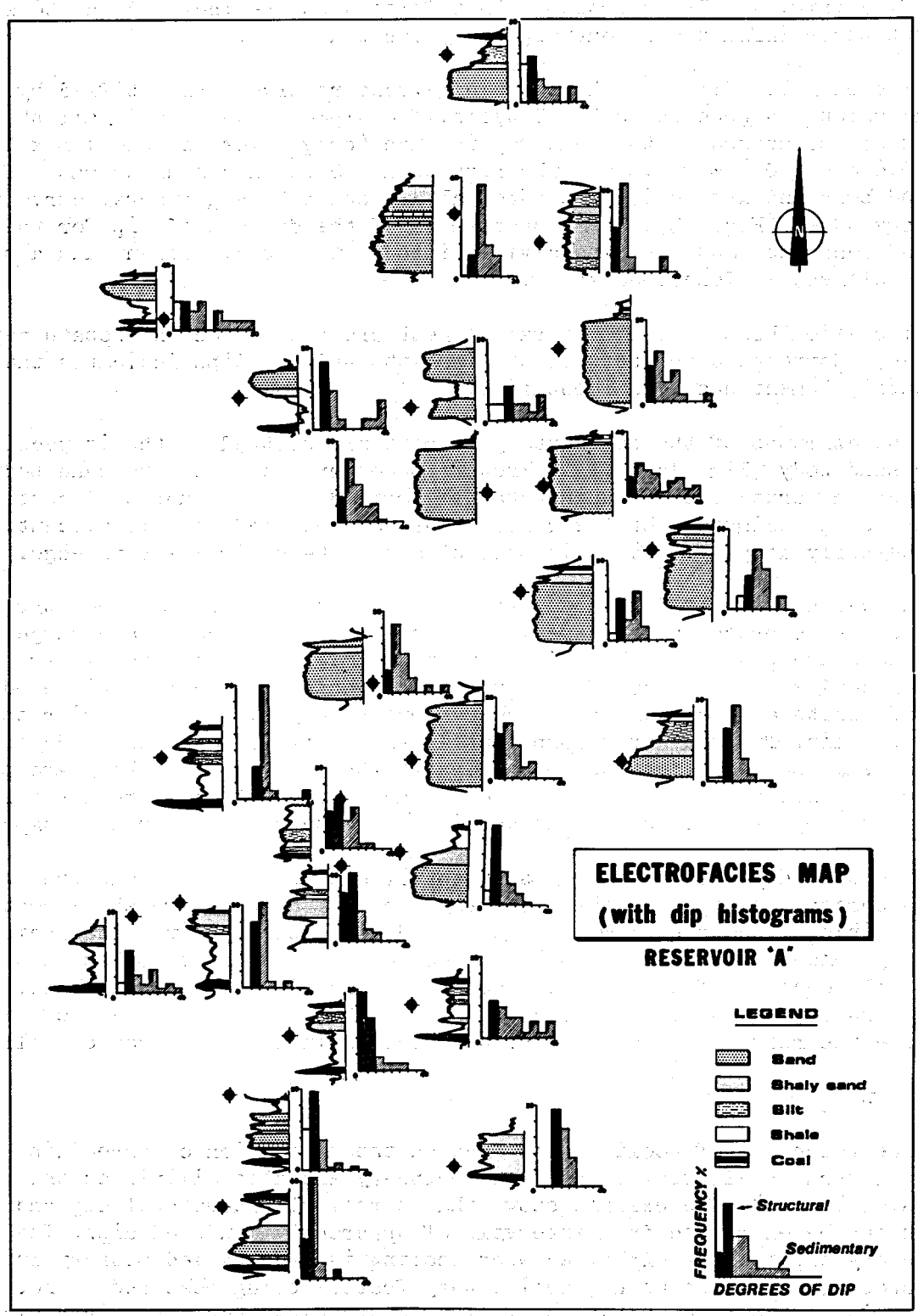

Fig. 13 : Electrofacies map of Reservoir "A" with gamma ray profile, lithology and dip frequency histogram.

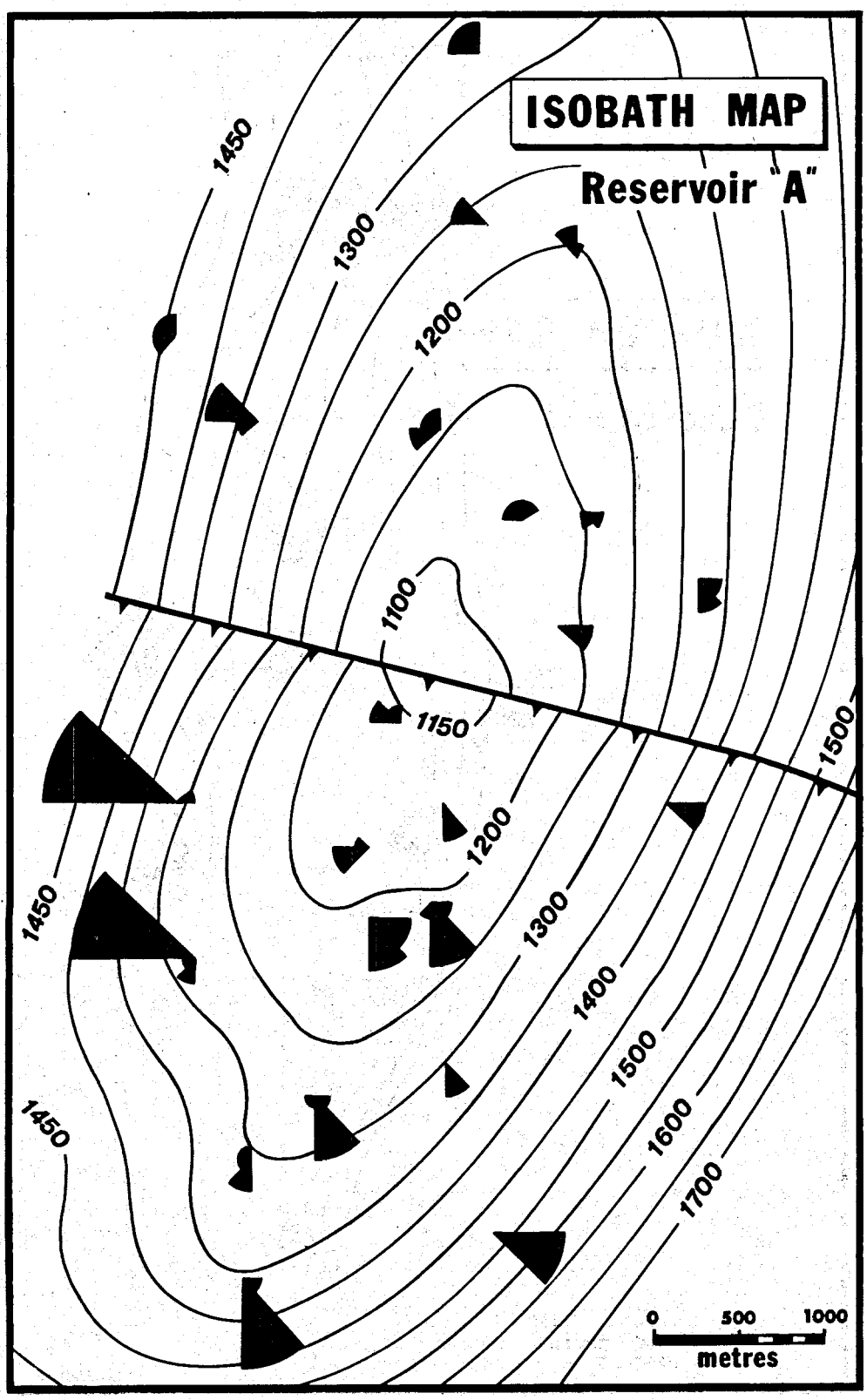

Fig. 14 : Isobath map of Reservoir "A" with structural dip azimuths. Depths in metres.

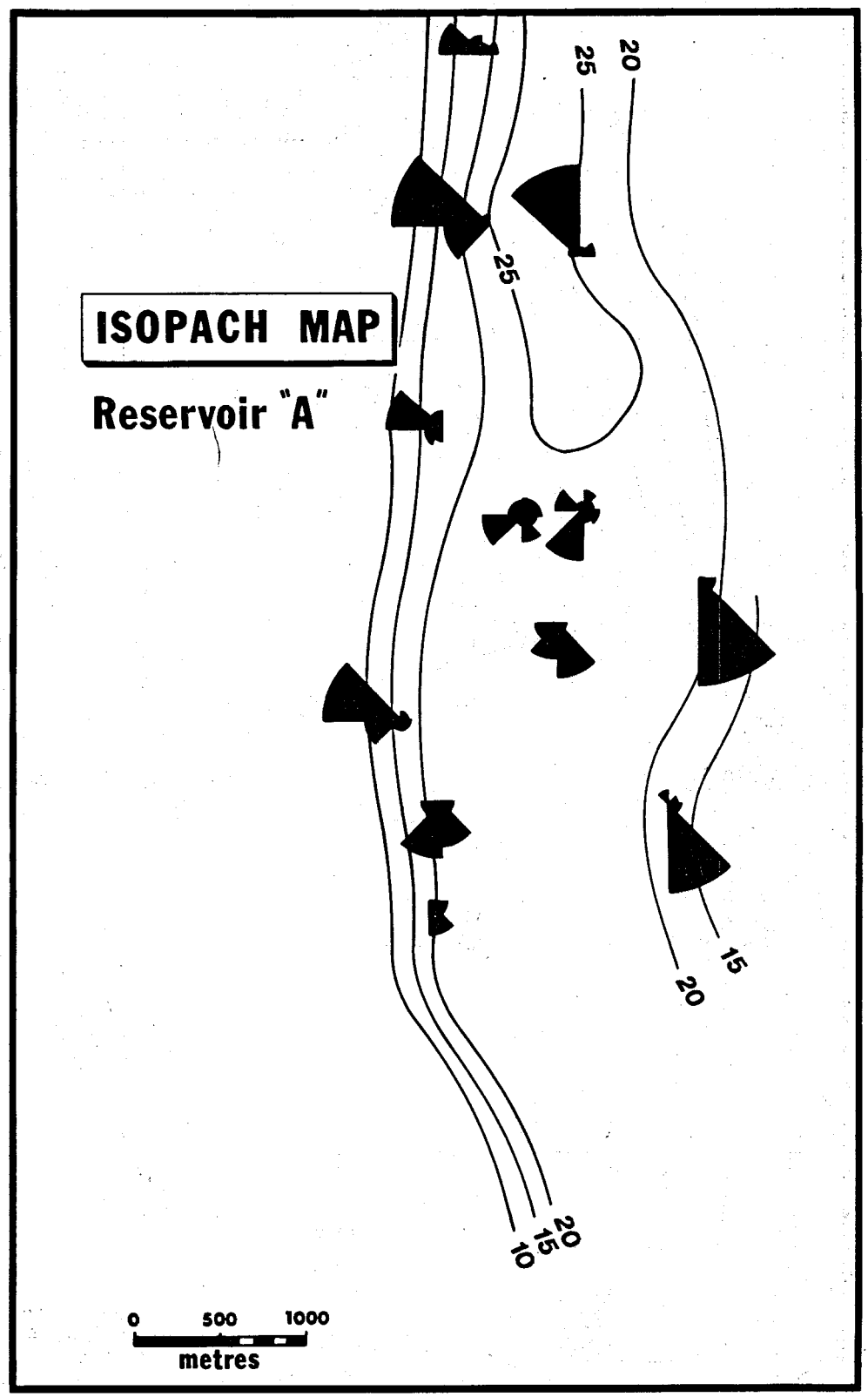

Fig. 15 : Isopach map of Reservoir "A" with sedimentary dip azimuths. Thickness in metres.

ACKNOWLEDGEMENTS

Thanks are due to the Company Française des Pétroles for permission to publish. The author was considerably helped in his work by P. BAXERES, H. BOSDEDORE and D. LAURIER, to whom thanks are given.

REFERENCE

ALLAUD, L.A. and RINGOT, J., 1969, The High Resolution Dipmeter Tool. The Log Analyst, vol. 10, pt. 3, p. 3-11.

CAMPBELL, R.L., 1968, Stratigraphic Applications of Dipmeter Data in Mid Continent. A.A.P.G. vol. 52, N° 9, p. 1700-1719.

GILREATH, J.A., HEALY, J.S. and YELVERTON, J.N., 1969, Depositional Environments defined by Dipmeter Interpretation. GCAGS, Vol. 19, p. 101-111.

GILREATH, J.A. and STEPHENS, R.W., 1971. Distributary Front Deposits Interpreted from Dipmeter Patterns. GCAGS. Vol. 21.

GOETZ, J.F., PRINS, W.J. and LOGAR, J.F., 1977, Reservoir Delination by Wireline Techniques. Log Analyst, Vol. 18, N° 5, p. 12-40.

HEPP, V. and DUMESTRE, A.C., 1975, Cluster- A method for Selecting the most Probable dip results from Dipmeter Surveys. SPE of AIME 50 Annual Fall Meeting, Dallas, Paper SPE 5543.

KELLING G., 1969, The Environmental Significance of Cross Stratification Parameters in an Upper Carboniferous Fluvial Basin. Journ. Sed. Pet., Vol. 39, N° 3, p. 857-875.

LEBLANC, M., 1976, Projet de Recherche "Pendagemétrie". Interprétation de la Pendagemétrie Schlumberger. Rpt Inst. Fr. des Pet. 24649.

MARSHALL, A.G.B., 1976, The "Cluster" programme applied to Dipmeter Interpretation in South East Asia. SEAPEX Proc. Vol. 3, p. 50-72.

NEDERLOF, M.H. and WEBER, K.J., 1971, A three Dimensional vector method as an Aid to Continuous-Dipmeter Interpretation. Geol. en Mijn. Vol. 50 N° 6, p. 725-732.

PERRIN, G., 1975, Comparaison entre des Structures Sédimentaires à l'affleurement et les Pendagemétries de sondage. Bull. Centre Rech. Pau- S.N.P.A. Vol. 9, n° 7, p. 147-181.

POTTER, P.E., 1967, Sand Bodies and Sedimentary Environments : a Review. AAPG Vol. 51 n° 3, p. 337-365.

SCHLUMBERGER (Ltd), 1970, Fundamentals of Dipmeter Interpretation. Schlumberger, New-York, 145 p.

SHIELDS, C. and GAHAN, M.J., 1974, The Dipmeter used to Recognise Depositional Environment. A.P.E.A. Journal, p. 181-188.

SWETT, K., KLEIN, G.D. and SMIT, D.E., 1971, A Cambrian Tidal Sand Body - the Eriboll Sandstone of North West Scotland : An Ancient Recent Analog. Journ. Geol. Vol. 79, p. 400-415.

VINCENT, Ph., GARTNER, J.E. and ATTALI, G., 1977, Geodip, an Approach to detailed Dip Determination using correlation by Pattern Recognition. SPE of AIME 52 Annual Fall meeting, Denver, paper SPE 6823.

ABOUT THE AUTHOR

Malcolm Rider was educated at Oxford, where he gained an M.A. degree and London, where he completed a Ph.D. in Sedimentology. He is at present in the research section of the Compagnie Française des Pétroles.

THE USE AND VALIDITY OF PULSED NEUTRON SURVEYS IN CURRENTLY DRILLING TESTS

SHELBY W. SMITH

TEXACO INC., OFFSHORE DIVISION, NEW ORLEANS, LOUISIANA

ABSTRACT

The pulsed neutron tool with its multiple uses is possibly developing into the most significant evaluation tool since the introduction of the SP and resistivity logs in 1931. The "Thermal Decay Time" or "Nuclear Lifetime Log" is the only tool ever developed or even suggested that can essentially reproduce the same log prior to and subsequent to setting casing. This paper offers examples and recommended uses of the tool not originally anticipated by the service companies, i.e., logging of very high angle holes (45^{o}-80^{o}) through drill pipe prior to pulling the last bit, logging a test with stuck drill pipe or a test which is shut in under pressure and cannot sustain higher mud weights.

The tool response may be affected by mud filtrates or where there is deep invasion and there has been insufficient time for the filtrates to dissipate. However, in high porosity sands, there are often many unusual and adverse hole conditions where this tool will give a satisfactory qualitative response that is sufficient to make the final operational decision to either run additional logs, set final casing for completion, or pull out and abandon the hole immediately after cessation of drilling, or even while the bit is still on the bottom.

A pulsed neutron survey may offer significant opportunities in the initial logging program of many non-normal wells.

It is seriously doubted that participants in the experimental radioactive logging program of Golden Meadow Field, Louisiana, in 1965 would believe that the tool would develop into what is probably the most significant well evaluation device since the Schlumbergers developed the SP and Resistivity log in 1931. The current tool called the "Neutron Lifetime Log" (NLL) by Dresser Atlas and "Thermal Neutron Decay Time Log" (TDT) by Schlumberger is the only tool ever developed that can reproduce essentially the same log prior to and subsequent to setting casing.

This paper is not a recommendation to replace resistivity surveys with pulsed neutron logs, which may be seriously affected by mud filtrates in currently drilling tests except under the unusual and adverse hole conditions which are being encountered more and more frequently in the Offshore area of the Southeast United States.

Multiple references state "TDT logs in open holes are usually too strongly influenced by invasion to permit a quantitative evaluation of saturation."[1] The key word is quantitative. For our purpose, it is necessary that a qualitative analysis, including stratigraphic, structural and correlative

characteristics, enables Management to make a decision to complete or abandon the test with a minimum of, or no additional surveys. An IES tool run initially is normally the best choice. However, Offshore operations are trending towards deeper water, smaller reservoirs or small, updip, undrained reservoir segments, all of which lead to longer, higher angle, directionally controlled holes.

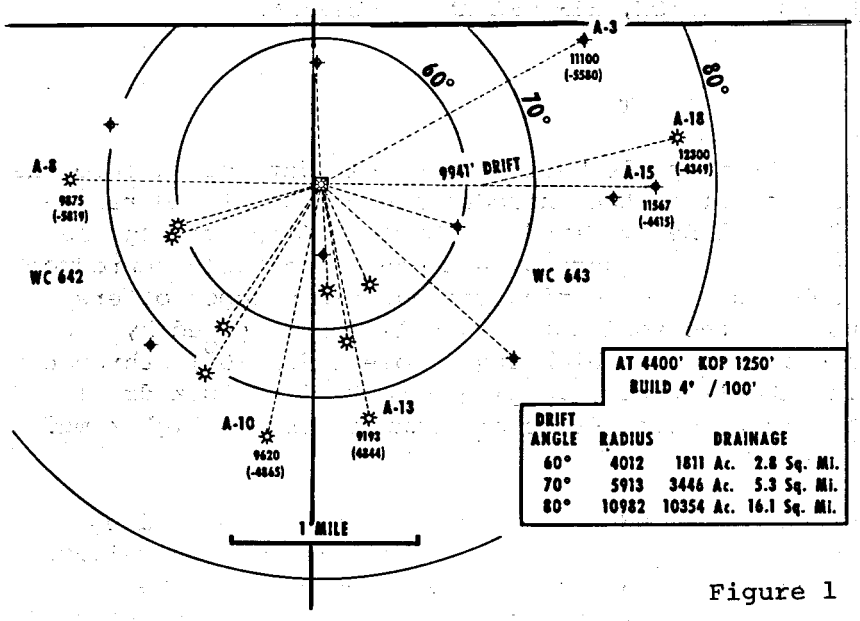

Figure 1

Figure 1 illustrates one area with the above problems. It is a jointly owned Texaco-Tenneco operated facility located in the Gulf of Mexico, West Cameron Area, Blocks 642-643, water depth 375', 124 miles from shore. There are eight wells which have been deflected more than 6200' from point of origin at the platform. In order to have a sufficient number of drainage wells for the primary gas sands, which averages approximately -4400' deep, four wells were drilled with drift angles of 70°±. Two have drift angles in excess of 78° and 82° with individual portions having angles of 86° from vertical. The maximum drift was 9941'. Figure 2 illustrates the objective of Well #A-18, a gas reservoir defined by an expendable exploratory well but with insufficient reserves to justify an additional $13MM platform.

Texaco's Offshore Division has been closely associated with the highest achievable angles to the greatest distance in the Gulf of Mexico, but not without periods of considerable trepidations, particularly in how to achieve a

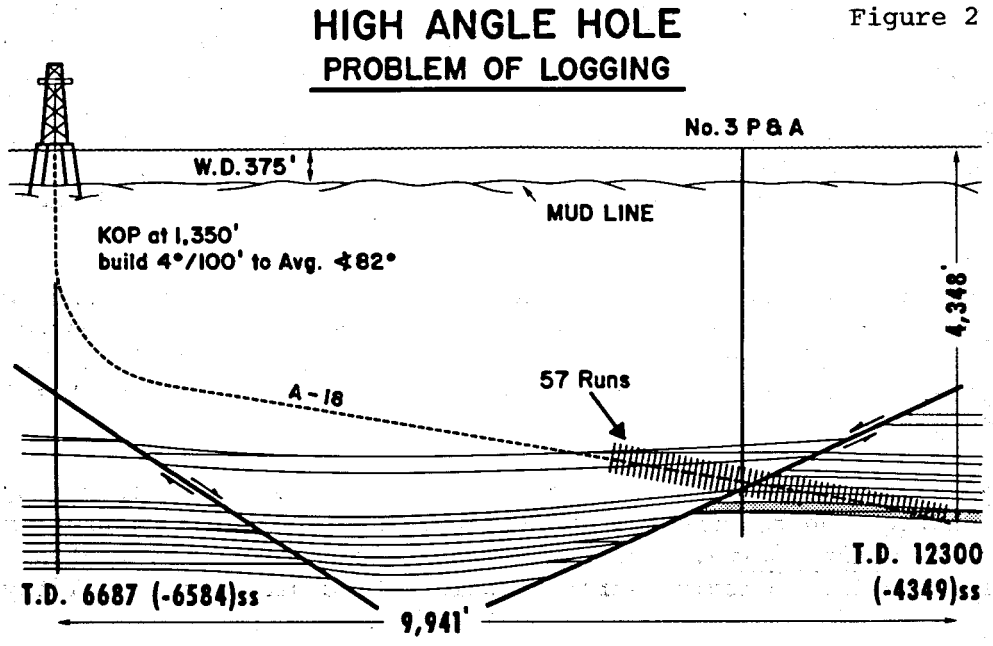

Figure 2

satisfactory log with drift angles of 76°, which were achieved in some of our first efforts in South Pass 54 in 1970. In such high angle holes, the sondes will not descend by gravity alone and must be pumped down and out of drill pipe.

A review of the highlights of the theory and interpretation of this logging system is desirable in order to understand the problems and advantages it offers.

The embryo, Pulsed Neutron Log, was initially called a chlorine log as this common element is by far the strongest thermal neutron absorber of the common earth elements. The log responds largely to the amount of capturing NaCL present in the formation water. When lithology and porosity data are known, a log of neutron absorption properties permits the determination of formation fluid saturations, oil-water contacts, and direct detection of gas behind casing or drill pipe, even better, in some cases, than the older open hole logs.

As the two names imply, Neutron Lifetime - Thermal Neutron Decay Time, the pulsed neutron log is primarily a device that measures the life time of fast epithermal neutrons after emission into a formation.

Neutron lifetimes are shortest in shale, longer in oil than in saline water, and longer still in gas. Thus, if the measurement of neutron lifetime is displayed in an analog curve format, the lifetime curve will look very much like a resistivity curve.

Data are obtained by activating a neutron generator in the sonde which bombards the formation for about 20-100 microseconds. After sufficient time has elapsed to allow borehole effects to dissipate, counting is begun. These epithermal neutrons have a life of from six microseconds in halite to 900 microseconds in quartzite. In porous formations, it is essentially a direct relationship to the amount of chlorine present. Determination of these lifetimes then allows, under most conditions, identification of several formation characteristics (e.g., lithology, porosity and fluid saturations).

It is the intent of this timing procedure to measure the time required for the neutron population to decline by a predetermined percentage, 63% for Schlumberger and 50% for Dresser Atlas. This may be done by either counting the neutrons themselves, which may evaluate only 2" - 3" about the tool, or by counting the gamma rays emitted as each fast neutron is slowed to thermal neutron velocity and then captured by a nucleus (most often chlorine, in sands). The gamma rays may travel 2-3 feet back to the detector from their point of emission in the formation. It is estimated that the emitted fast neutrons collide elastically 100± times with hydrogen atoms before being captured. This may be only one inch in 100% water.[2]

With normal borehole conditions, the log is independent of borehole size, fluid content and instrument position in the borehole. Severe borehole environment would be considered to be a large borehole filled with oil, fresh water or air. A normal depth of investigation is considered to be 14"-16", with a bed resolution of 3' at a logging speed of 1200'/hour.

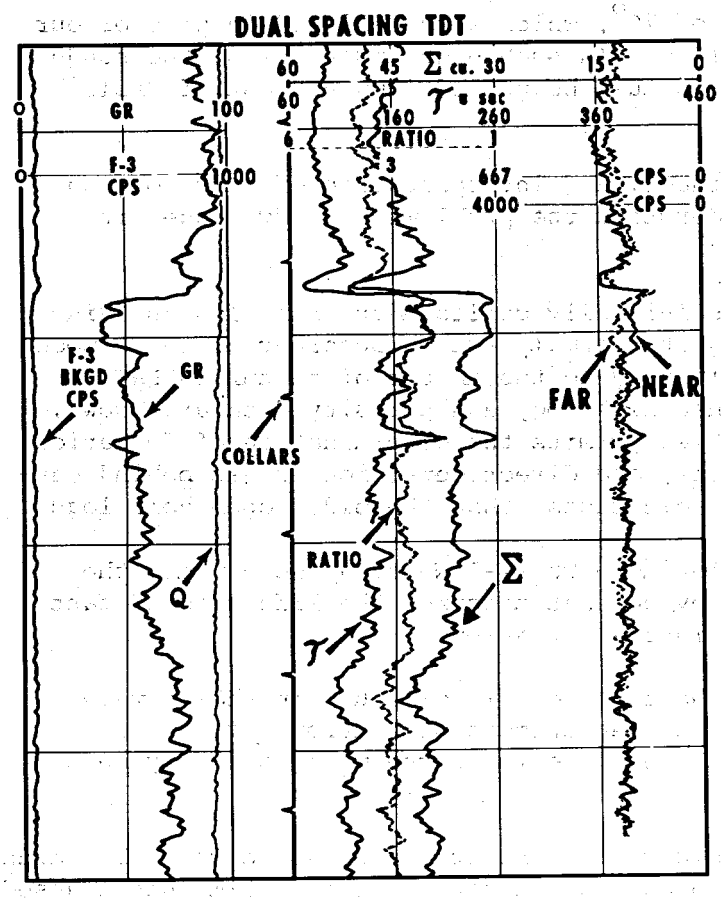

Figure 3

The following examples will illustrate the results of data derived both in the laboratory and empirically utilizing pulsed neutron logs and show how qualitative interpretation can then be applied.

Figure 3 illustrates the common presentation of a Schlumberger TDT survey. Nine galvanometers are available for the thirteen channels of information gathered and/or calculated for full evaluation. Data not presented on the log are recorded on digital tape.

In the left track, four curves are frequently plotted:

1. The F_3 curve which is a "low sensitivity gamma ray curve", scaled 0-1000± API units;

2. A standard gamma ray curve scaled 0-100± API units;

3. Pulse rate quality monitor curve (Q), frequently omitted;

4. Casing collars uncorrected for depth.

In the right track, the remaining five curves can be recorded:

5. N_1 - the near detector, count rates, solid;

6. F_1 - the far detector, count rates, dotted;

7. TAU - formation time constant in microseconds;

8. Σ - the calculated neutron capture cross section ($10^{-3} cm^2/cm^3$);

9. The calculated ratio curve; = near count/far count; (-background).

Figure 4 illustrates the Dresser Atlas presentation of the "Nuclear Lifetime Log". "TAU" (Schlumberger) or "L" (as it is called by Dresser Atlas) is the elapsed time in microseconds for a percentage of the high energy neutrons to be slowed enough to be captured. Sigma is calculated as:

Schlumberger $= \frac{4550}{TAU}$ Dresser $= \frac{3150}{L}$

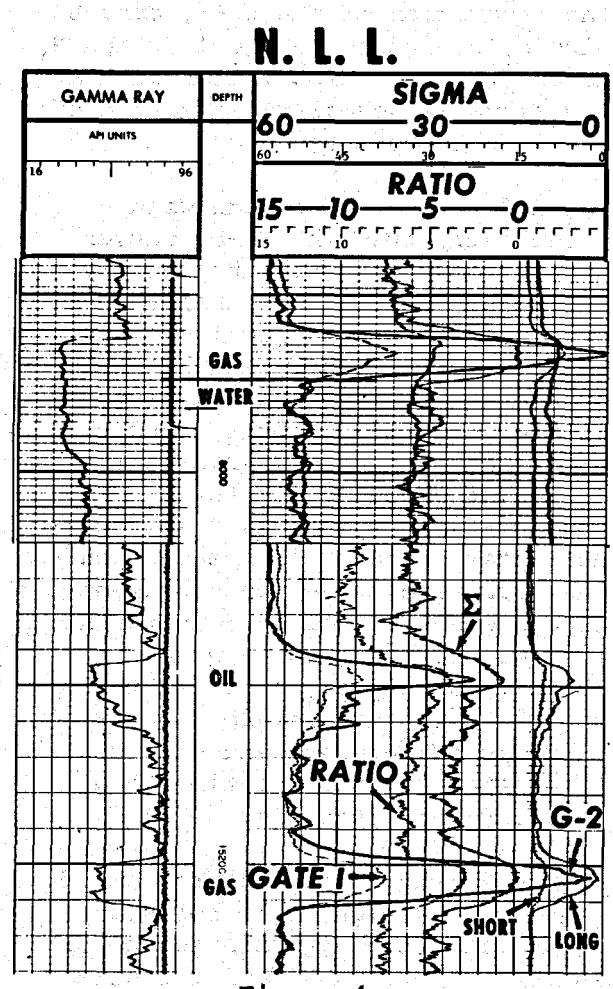

Figure 4

The Sigma value is relatively the most important of all the derived data for interpretation and represents the summation of "capture cross sections" of a specific interval of the formation, or its ability to slow down and capture high speed neutrons.

The near-far detector count rate sensitivities have been designed to normally track in water and oil sands in order that their frequent divergence in gas sands is recognizable.

Behind the basic principle of interpretation is the fact that all elements have a natural, constant, thermal neutron decay time and a calculated sigma or neutron capture cross section.

Some common sigma values are shown here as tabulated by Schlumberger:

	SIGMA	TAU (MICRO-SECONDS)
Methane @ 1500 PSI-100°F	3.8	1200
Quartz	4.3	1060
Dolomite - Pure	4.7	980
Limestone - Pure	7.1	635
Granite	22	206
Basalt	33	138
Gulf Coast Oil	22	207
Fresh Water	22	207
Water 250k ppm	120	38
Chlorine	570	8
Halite	770	6
Cadmium	18,000	.253
Boron	45,000	0.10

Shale Σ's are commonly 33-55 as observed in well logs.

Even though natural sediment mixtures make elemental identification very complex, there is normally enough distinction between hydrocarbon and salt water log signatures to allow identification in a sand.

Most of the figures included are of Schlumberger's TDT but this is not intended to indicate a partiality or preference. Figure 5 illustrates a field example of water-oil and gas observed in a sand. It should be noted that water is listed first. It is highly desirable that one or more wet, clean sands be logged for comparison, as it is appreciably more difficult to recognize the zones prospective for hydrocarbons without these base values. Many times the difference between wet and productive sands may be quite subtle, ½-1 division on some curves, particularly if the zones are shaly or invaded.

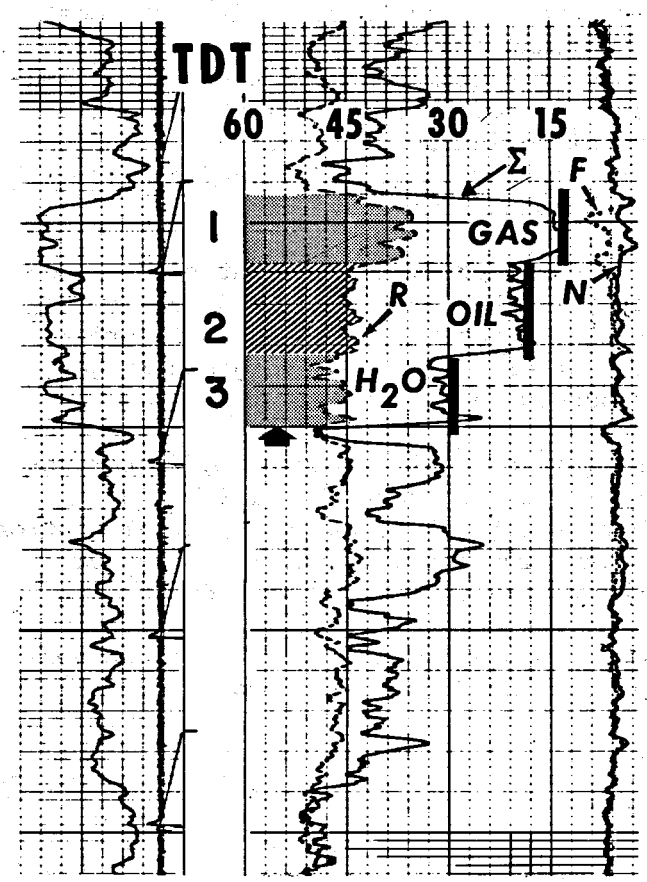

Figure 5

The separation of the N_1-F_1 curves with F_1 deflecting to the left and N_1 to the right in association with a low sigma is normally diagnostic of the presence of free gas.

The underlying oil column with essentially tracking N_1-F_1 curves and a sigma less than the underlying water, but greater than the overlying gas, is typical. If the sand is not too shaly and has greater than 2 ohms resistivity, greater than 15% porosity, and no significant invasion, practically an instantaneous check for a neutron-type porosity and an apparent water salinity can be made on the departure curves by crossplotting sigma vs. ratio. Henceforth then we shall use the "rule of thumb" that any sigma lower, to the right, than in obvious water sands is of interest and strong F_1 left divergence relative to N_1 normally indicates gas.

Figure 2 returns to the problem of logging very high angle holes and illustrates the approximate number of runs (57) that could be required to evaluate the bottom half of the hole without a "through drill pipe log". It is the way all initial high angle holes were logged and is still the method of obtaining required supplemental resistivity surveys. Open ended drill pipe is run to total depth. A small diameter IES tool is pumped down and out, the pipe raised out of the hole one stand, ninety feet± of hole logged, the sonde retrieved, one stand of drill pipe is taken off and the process repeated until sufficient hole is surveyed to evaluate all objectives and necessary correlation points. It may be a problem to find the objective sand unless it is structurally well-defined.

Further, in a 75° hole, only 23.3' of vertical hole is logged per 90' stand and only 15.6' for an 80° drift angle (17.3'/100'). Correlation is not impossible, but at 3:00 A.M., it may appear so.

Receipt of this log, A-18, Figure 6, made through drill pipe in an 82° angle hole, was most encouraging. No IES was attempted and all of the elements desired for interpretation are present; low sigma, low ratio, positive left divergence of the F_1 vs. N_1 curve (indicated by shading) and a fairly clean sand by gamma ray. There are positive separations showing in the lower sand but the ratio and sigma comparisons indicate no hydrocarbon accumulation. It is further confirmed by the base survey made in casing two months later. Although this well did not penetrate the original reservoir as proposed, a pump-down IES was not considered necessary for a well completion decision.

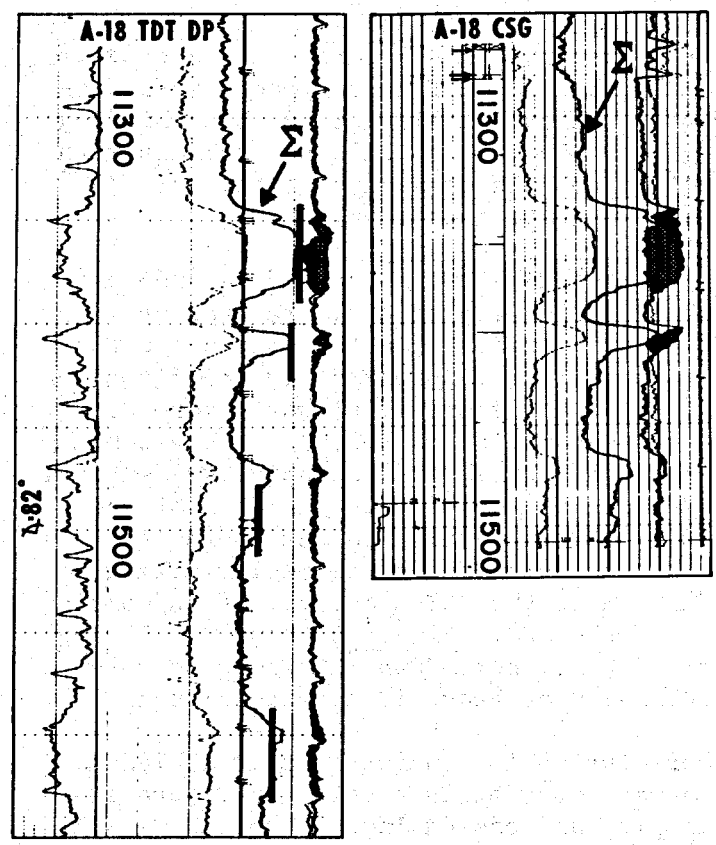

Figure 6

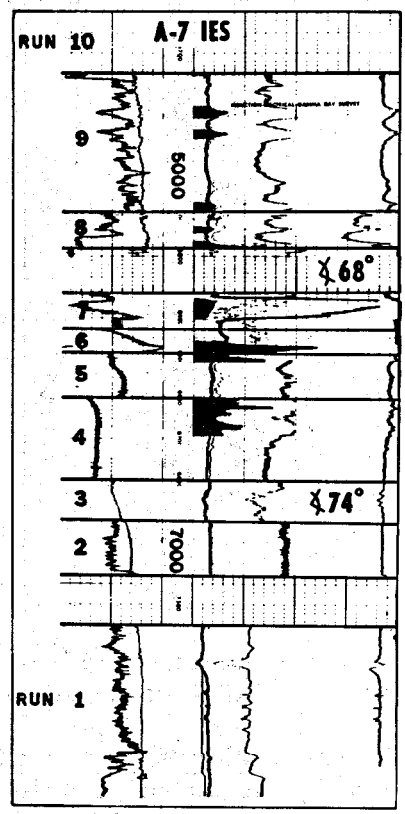

Figure 8

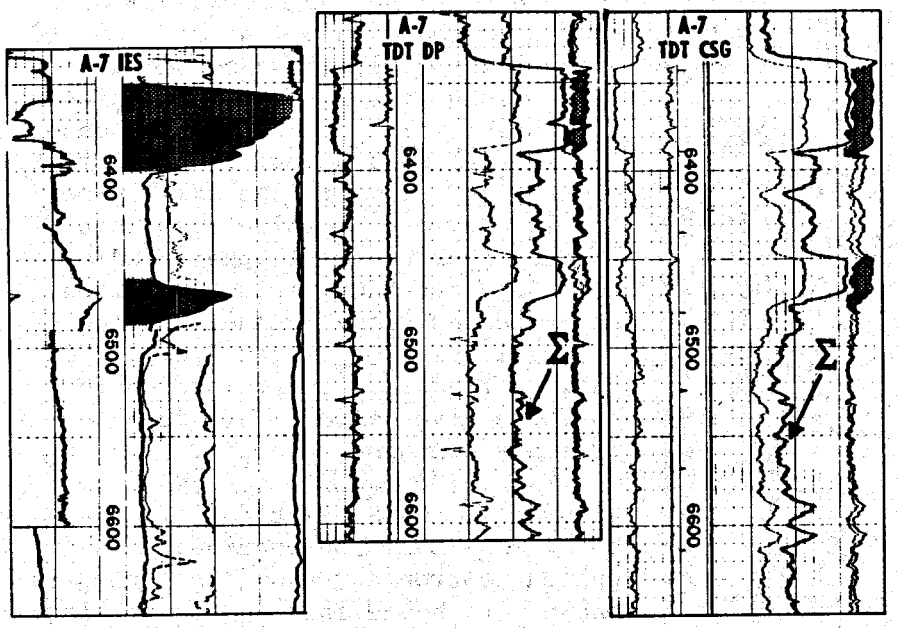

Figure 7

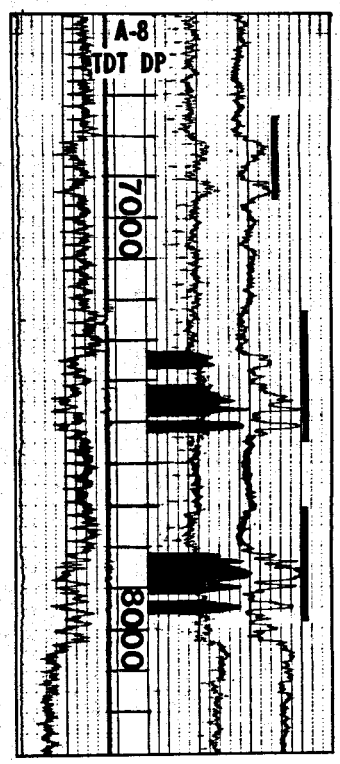

Figure 9

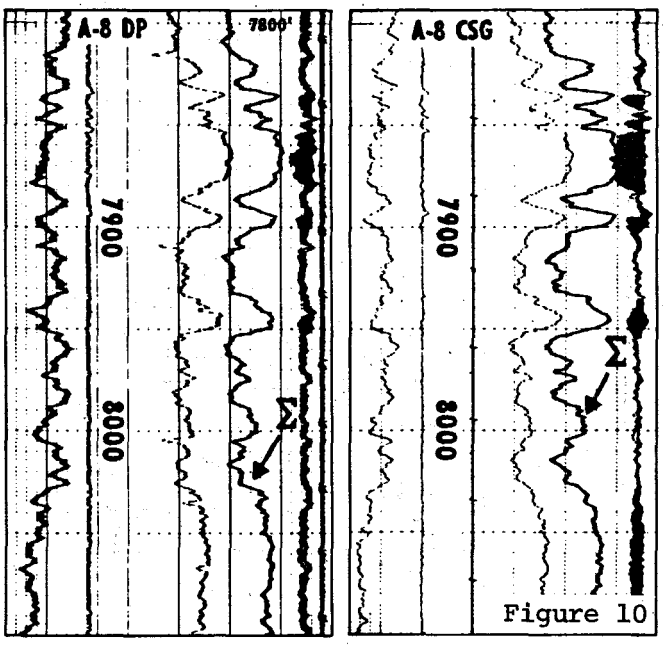

Figure 10

Geological interpretations are not always infallable! A TDT, Figure 7, was run on A-7 early in the program, it did not fit everyone's interpretation but all agreed that this log indicated at least six members with probable gas and possibly more (2 members are shown).

An IES, TDT in drill pipe, and a casing log of A-7, are presented for comparison. In the casing log the ratio is approximately one division lower, there is slightly more gas separation on the N_1 F_1 curves but the sigmas are essentially identical. The SP on various portions of the IES is unreliable but there is no question about the resistivities. Here the TDT-gamma ray is supporting the IES. Figure 8 shows the 1" log. With the hole angle of 68°-74°, ten more, short, pump-down IES log runs were required for full evaluation but the TDT saved at least 19 additional runs.

In Well #A-8, Figure 9, the one inch correlation log indicates that at least two major sands in the middle portion have sigmas of interest. In Figure 10 are the five inch portions of the drill pipe and casing logs. From the drill pipe log it was obviously a well capable of completion in the upper sand at 7850'MD.

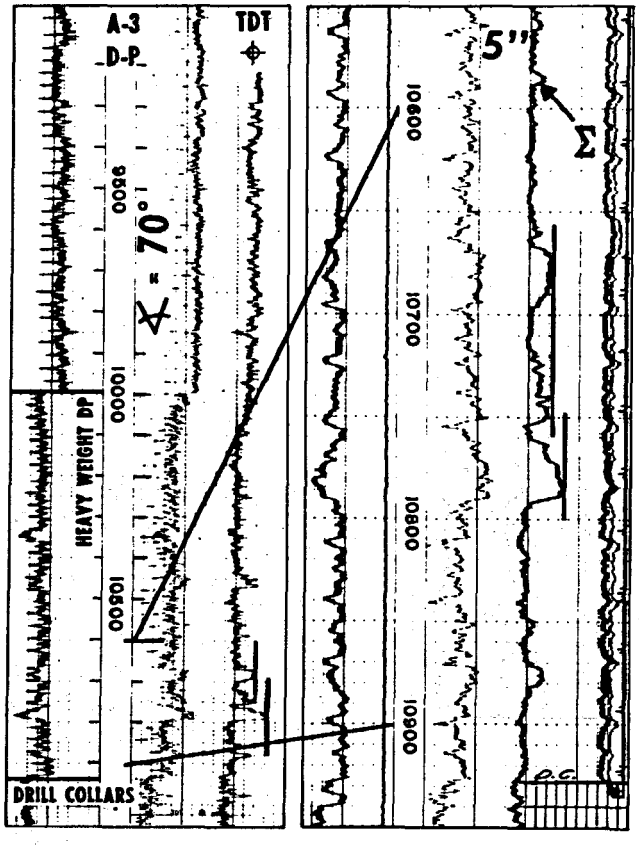

Figure 11

On the base log, Sigma is essentially identical in the three upper members on both logs and the divergence of N_1 F_1 has improved on all sands. A visual examination of the sand at 8050' would give a first impression of possible oil. There is some possible N_1 F_1 separation, the sand is cleaner and sigma on the drill pipe log is only one division less than in the upper sand. In the cased hole log, the time period has given an increased sigma (wetness) value of +½ division, a slight decrease in ratio but a definitely discernable positive divergence. This zone probably contains some gas.

Figure 11. Management decisions are being made based on confidence in pulsed neutron surveys. Well #A-3 is shown with a one inch and detail log. From the one inch correlation log, only two zones appear to be of interest. In this known gas area, there

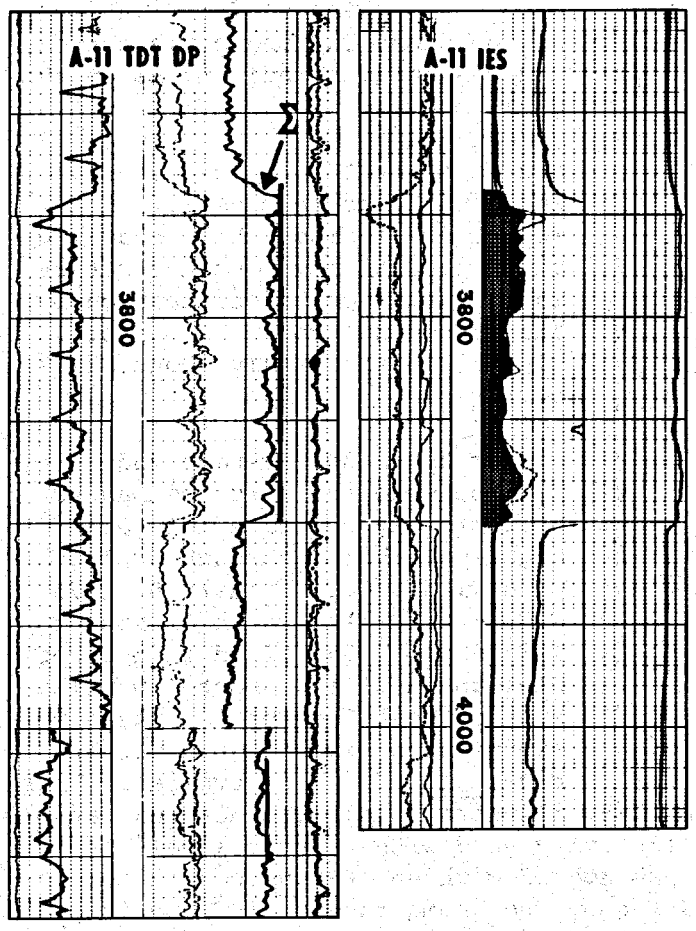

Figure 12

is no positive divergence exhibited by the N_1 F_1 curves, sigma on the upper member is no less than all the other sands up the hole (not shown) and the lower member exhibits no gas effect on either the N_1 F_1 or ratio values. The well is considered dry and was plugged and abandoned. No resistivity survey was made.

Figure 12. The "classic rule" of "near-far" separation, expected in gas, does not always take place dramatically. In the drill pipe TDT of Eugene Island 367, A-11, there is very little separation, in fact, the curves track across most of the gas sand which may be considered shaly and relatively low resistive (4 ohms). Upon close evaluation of the log, it may be noted that above and below the gas sand there is a negative, right, separation of approximately one division of the F_1 curve instead of tracking. Projecting this into the sand, it may be assumed that there is, therefore, an implied separation. The sigma value for this sand averages, however, 3/4 division lower than a wet, cleaner sand 4000' deeper where the N_1 F_1 curves also track.

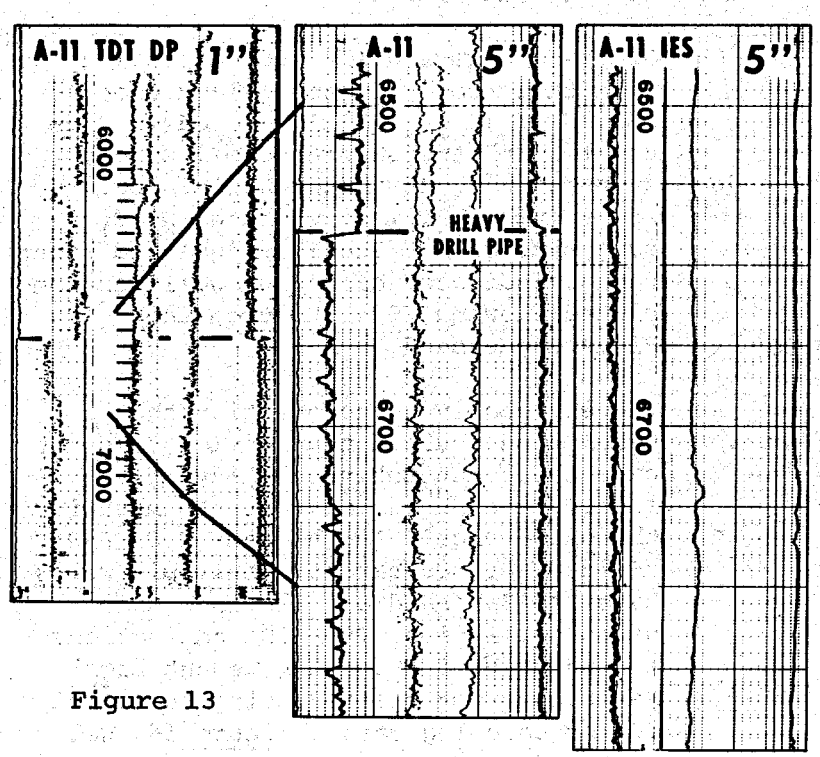

Figure 13

Figure 13. This same test presented an interesting evaluation of the TDT tool through heavy weight drill pipe. An initial attempt to log with an IES failed to descend below approximately 6300'. Drill pipe was run in the deviated hole and a TDT survey made. In this case, one of the objective sands was anticipated to be encountered in the portion of the well logged through heavy weight drill pipe. There was great concern as to whether the heavy

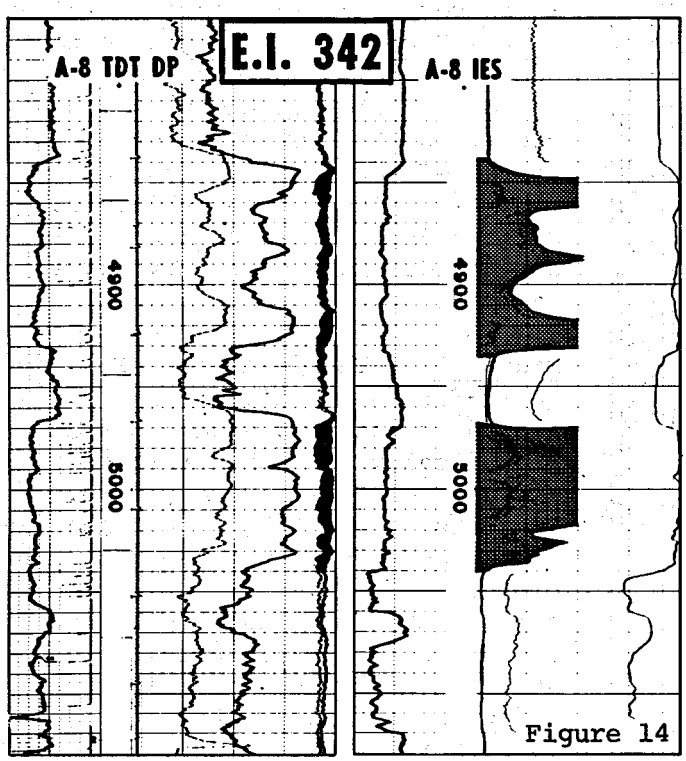

Figure 14

pipe was masking sand indications on the gamma ray and sigma curves, and masking gas indications on the N_1 F_1 curves.

A subsequent IES indicates only sandy shale to be present. Heavy weight drill pipe, while reducing curve sensitivity does not materially influence the evaluation by the pulsed neutron. We cannot say this definitively about drill collars.

To our knowledge, Texaco and Tenneco were the first companies to routinely evaluate all very high angle holes through drill pipe with a TDT (January 5, 1975, W.C. 642 #A-1). Texaco's Eugene Island Block 342 Field is another Pleistocene field about 100 miles east of West Cameron 642 where we experienced similar good results. Figure 14 of A-8 is typical. This drill pipe log, shown with a subsequent IES, illustrates all the desired parameters in a relatively clean, higher resistivity sand with a water level. All of the objective sands in this field were logged with an IES subsequent to running the TDT with major rig time savings. The gamma ray and TDT specifically located the exact depth of the sands and few non-diagnostic IES surveys were made. Under present conditions and with our past experiences, many of these wells would now probably be completed without an IES.

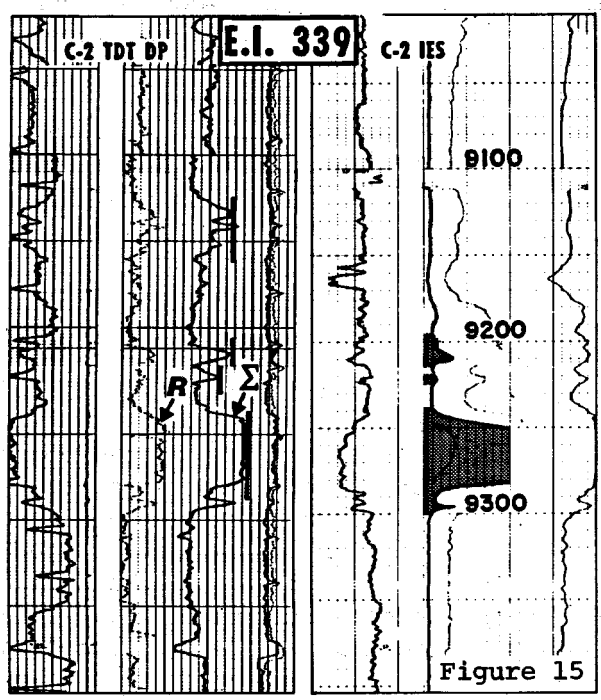

Figure 15

Oil sands are equally subject to logging with this tool. Eugene Island Block 339, Well #C-2, is illustrated in Figure 15 with two saturated oil sands, compared with a subsequent IES log. The initial TDT log, with the N_1 F_1 curves tracking, the low sigma and lower ratio, indicated oil. The well was completed flowing 208 BOPD from the Pleistocene sand.

There probably is no question that a drill pipe, pulsed neutron log does not have the quantitative ability of a later, cased hole log, but how much is the difference? In the same W.C. 643 field discussed earlier, multiple wells have had Saraband calculations made using drill pipe, TDT-IES combinations and then (Production Management Logs) Sarabands recalculated using the cased TDT or base log data. Figure 16, Well

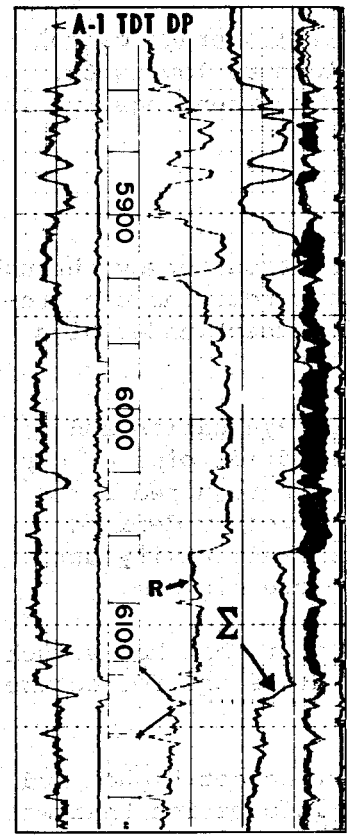

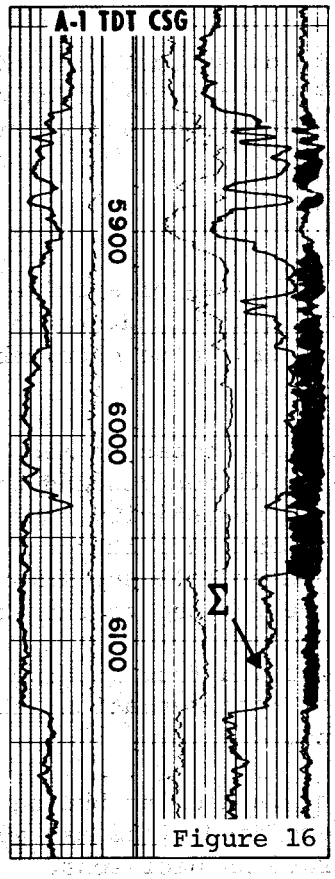

Figure 16

#A-1 is typical of the group. The sand illustrated here is the primary reservoir and the water level is readily apparent on this log. Note the reduced porosity effect due to gas on the ratio curve. With the base log alongside, there are small, detectable differences between the two logs run 60 days apart in this clean sand. There is about ½ to 1 division difference in the N_1 F_1 separation, which results in approximately ½ to 1 division difference in ratio. Sigmas vary even less.

The IES in Figure 17 brings into perspective the sand's characteristics as seen by our common denominator evaluation survey.

Figure 18 is a comparison of original TDT gas and cased hole gas. As the laboratory experts in pulsed neutron logs have predicted, the base TDT shows increased amounts of movable gas over that calculated from the drill pipe log. The additions, cross-hatched, range from 2 to 9 porosity units and as expected the largest changes are seen in the shalier zones where a greater

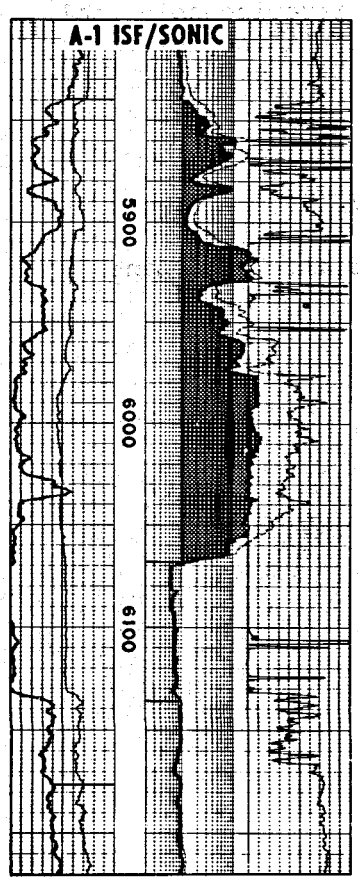

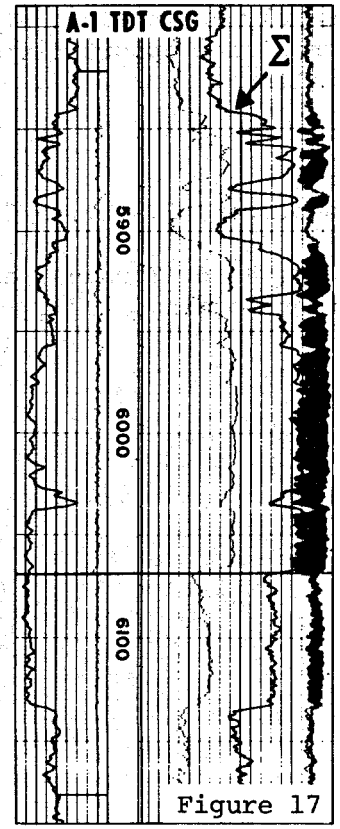

Figure 17

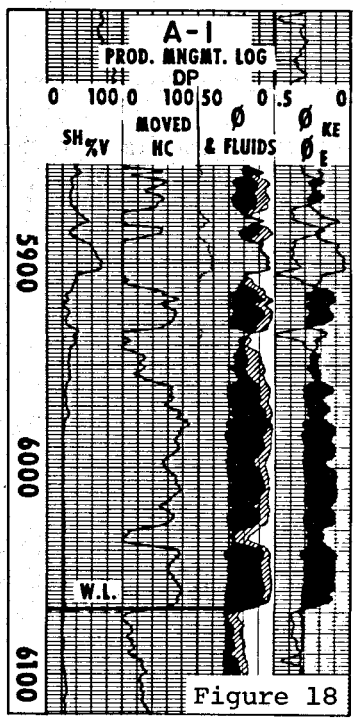

Figure 18

time was required for the filtrate to dissipate. The overall average calculated porosity of the gas sand is 25%. Water saturations calculate as low as 6%. The average calculated difference in observed gas reserves between logs run in drill pipe and casing is 27.9%.

CONCLUSIONS:

Empirically, we have determined that the use of a Pulsed Neutron survey through drill pipe in a currently drilling test under adverse hole conditions can provide qualitative data that may not otherwise be obtainable except under high risk conditions, i.e.:

1. A complete log of very high angle holes can be made for evaluation and correlation where resistivity sondes will not descend below drill pipe or casing. This procedure can save multiple resistivity runs, when required for additional evaluation, or look for a sand in a structurally poorly defined area. In shaly or low resistive sections, all supplemental resistivity surveys may not be eliminated but will be reduced to the absolute minimum.

2. Significant information may be derived from logging a test that has struck drill pipe. It may materially affect recommendations and decisions for future well operations under such conditions.

3. Conditions can exist where a test is kicking but cannot accept higher mud weights. Use of this tool under these conditions may add information that will simplify and/or aid in drilling operations decisions.

Although this tool is considered primarily an invaluable, irreplaceable tool in workover operations, it offers significant opportunities in the initial logging programs of many non-normal wells.

REFERENCES:

1. Interpretation of TDT Logs, Schlumberger, J.M.H., 5/17/74.

2. Neutron Lifetime, A New Nuclear Log, A. H. Youmans, et al, 1963, Lane Wells, SPWLA reprint, Pulsed Neutron Logging, 1974.

ABOUT THE AUTHOR

SHELBY W. SMITH is presently the Senior Development Geologist, Log Analyst and Geological Training Coordinator for the Offshore Division of Texaco Inc., New Orleans, Louisiana. He is a former Naval Aviator and is a Commander, U.S.N.R.-Retired (Air Intelligence). He received a B.A. Degree in Geology in 1950 from Texas Christian University, Ft. Worth, Texas, did graduate work at Texas University, and was awarded an M.S. Degree from Texas Technological College, Lubbock, Texas, in 1951.

Shelby's initial employment was with Texaco in Jackson, Mississippi, in 1951. However, since his transfer to New Orleans in 1954, he has been employed in the Gulf Coast area with temporary assignments in Europe and West Africa. His experience has been as a Geologist, District Development Geologist and Senior Development Geologist. He has held various positions in the New Orleans Geological Society, is presently a Director of N.O.G.S. and its immediate Past President. Shelby is a member of the SPWLA, a past Delegate of the AAPG and a past State President of the American Institute of Professional Geologists.

A STUDY OF THE RELATIONSHIP BETWEEN TWO INTRINSIC RESERVOIR PARAMETERS, THE LITHOLOGIC INFLUENCE FACTOR AND THE PORE GEOMETRICAL FACTOR

Barlai, Z., Reda A. Mawla, and Faleh T. Al-Saadoon
Petroleum Engineering Dep., Faculty of Petroleum and Mining Engineering
Al-Fateh University, Tripoli, Libya

ABSTRACT

For a better characterization of a porous medium and for a better understanding of some complicating effects in quantitative interpretation of reservoir parameters, two compounded intrinsic petrophysical factors are utilized. These two factors are, namely; the lithologic influence factor and the pore geometrical factor.

Theoretical studies and experimental investigations have been carried out in order to relate the pore geometrical factor to the lithologic influence factor. It has been concluded that a close and direct relationship exists between those two factors.

Those two factors are favorably used for characterizing microscopically the complexity of the pore structure of the reservoir.

The lithologic influence factor, which is a well logging parameter, can be obtained as a continuous record along the borehole axis. The pore geometrical factor, which is a special core analysis parameter, can be evaluated for individual core samples. Thus, a quantitative relationship between the two factors will make the pore geometrical factor available in a continuous form.

Thus, this paper deals with the correlation of a well logging parameter, namely; the lithologic influence factor, with a special core analysis parameter, namely; the pore geometrical factor.

INTRODUCTION

In estimating reserves and in analyzing and controlling recovery processes, formation evaluation methods are always faced with the complexity of the reservoir caused by drastic changes in mineralogical composition and pore geometry of the sandstones. The pore geometry is usually affected by grain

size, grain shape, grain sorting, grain packing, cementation, and clay or shale.

During recent years practical application of two intrinsic reservoir parameters, the lithologic (influence) factor, C, and the pore (geometrical) factor, G, have been made [1,2,3,4] . These two compounded parameters are capable of indicating the complexity of the pore structure of reservoirs composed of sandstones and shales. By determining the lithologic factor, C, and the pore factor, G, any appreciable changes of mineralogical composition, grain size, and pore size distribution can be detected and described quantitatively.

Lithologic factor, C, is a well logging parameter, whereas the pore factor is a core analysis parameter. Both parameters, however, describe the intrinsic microphysics of the sandstones pore structure. Thus through the linkage of those two factors, a direct correlation between well logging and core analysis can be established. In addition, the pore factor, G, is usually determined in the laboratory on cores extracted from distinct intervals of the reservoir, whereas the lithologic factor, C, is a continuous record along the borehole axis. Thus, by establishing a correlation between G and C, a continuous record of G can also be determined along the borehole axis.

A better understanding and evaluation of the complexity of the pore structure and heterogeneity of the reservoir can be arrived at through the joint application of both parameters. By the joint use of both parameters any appreciable changes in the following parameters can be detected: the absolute permeability, k, the irreducible water saturation, S_{wi}, the internal surface area of the interconnected pores per unit pore volume, S_p, the displacement pressure, P_d, mineralogical composition, and pore size distribution.

While C and G can be used in describing the reservoir along the borehole axis, they can be utilized effectively in determining proper representitive average characteristics (in relation to rather homogeneous sections of the reservoir), thereby distributing the total complex hydraulic unit (reservoir) into homogeneous units. This can be done through proper statistical analysis of C and G.

THE LITHOLOGIC INFLUENCE FACTOR, C

The lithologic factor, C, was derived and introduced as early as 1969 [5] in a microphysical mathematical model of oil- and gas-bearing sandstones. It is a dimensionless quotient of two electric conductances, the conductance, σ_{ga}, of adsorption water (and electrically charged ion) shells covering the solid mineral grains in the rocks over the conductance of interconnected pores, σ_{ϕ}, completely saturated with interstitial water of resistivity R_w:

$$C = \frac{\sigma_{ga}}{\sigma_{\phi}} \tag{1}$$

where σ_{ϕ} is given by the simple formula:

$$\sigma_{\phi} = \frac{\phi}{R_w} \tag{2}$$

and σ_{ga} was described in the mathematical model referred to previously [1,2,3,5]. In the model, the sandstone is considered to be composed of n different types of solid minerals, and each component is taken into account by its particular grain size distribution, $v_i(d)$, where:

i, refers to the i^{th} component and

$v_i(d)$ refers to the relative volume of component i at a grain size d, related to a unit grain size interval around d, i.e., $v_i(d)$ is a probability density function of the relative volume component i in the rock.

Some further probability variables were also defined in the model, as follows

$\varepsilon_i(d)$: relative volume of adsorption water of component i, related to the volume $v_i(d)$. Thus this variable is also a probability density function of grain size d;

$\frac{1}{r_i(d)}$: electrical conductivity of adsorption water of component i.

Electrical conductance, σ_{ga}, of adsorption water in the rock was described as a sum of definite integrals of $\frac{v_i(d) * \varepsilon_i(d)}{r_i(d)}$ with respect to variable

d, between integration limits $d_{i,min}$ and $d_{i,max}$

where:

$d_{i,min}$: minimum grain size of component i,

$d_{i,max}$: maximum grain size of component i.

Thus

$$\sigma_{ga} = \sum_{i=1}^{n} \int_{d_{i,min}}^{d_{i,max}} \frac{v_i(d) * \varepsilon_i(d)}{r_i(d)} \, dd \qquad (3)$$

By substituting equations (2) and (3) into (1), the lithologic factor becomes equal to

$$C = \frac{\sum_{i=1}^{n} \int_{d_{i,min}}^{d_{i,max}} \frac{v_i(d) * \varepsilon_i(d)}{r_i(d)} \, dd}{\frac{\phi}{R_w}} \qquad (4)$$

It appears from Eq. (4) that C describes the relative surface electric conductance of the solid minerals exerted by their ionic adsorption shells, related to the conductance of the effective pores when completely saturated with water. Therefore, the lithologic factor, C, increases with increasing volume of sheet silicates, especially clay minerals, and with decreasing grain sizes. Thus the lithologic influence factor, C, is a measure of the deterioration of the reservoir properties as affected by the sheet silicates of minor grain sizes.

It can be expected as well that with the deterioration of the reservoir properties, a systematic increase in the specific surface area of the interconnected pores, S_p, will occur. This relationship can be derived mathematically as follows.

The specific surface area of the solid grains, S_{ga}, per unit bulk volume can be described by the following equation:

$$S_{ga} = \sum_{i=1}^{n} \int_{d_{i,min}}^{d_{i,max}} \frac{v_i(d) * \varepsilon_i(d)}{\Delta t_i(d)} \, dd \qquad (5)$$

where

$\Delta t_i(d)$ is the thickness of the adsorption water shells in component i, as a probability variable.

In order to express σ_{ga} in terms of S_{ga}, Eq. (3) is rewritten in another form so that the thickness of the adsorption water is included. Thus

$$\sigma_{ga} = \sum_{i=1}^{n} \int_{d_{i,min}}^{d_{i,max}} \left[\frac{v_i(d) * \varepsilon_i(d)}{\Delta t_i(d)} \right] \cdot \Delta t_i(d) \cdot \frac{1}{r_i(d)} \cdot dd \qquad (6)$$

The same is described by macroscopic expression:

$$\sigma_{ga} = S_{ga} \cdot \overline{\Delta t} \cdot \frac{1}{\bar{r}} \qquad (7)$$

where

S_{ga} is the bulk surface area of the grains as described in Eq.(5),

$\overline{\Delta t}$ is the average thickness of adsorption water shells, i.e., the most probable value,

$\frac{1}{\bar{r}}$ is the average conductivity of adsorption water shells, i.e., the most probable value.

By substituting equations (7) and (2) into equation (1), one gets

$$C = \frac{S_{ga}}{\phi} \cdot \overline{\Delta t} \cdot \frac{R_w}{\bar{r}} = (S_{ga})_p \cdot \overline{\Delta t} \cdot \frac{R_w}{\bar{r}} \qquad (8)$$

In equation (8), $(S_{ga})_p$ is the specific surface area of the grains as related to unit pore volume. Equation (8) may be solved for the specific surface area as shown in equation (9):

$$(S_{ga})_p = C \cdot \frac{\bar{r}}{R_w} \cdot \frac{1}{\overline{\Delta t}} \tag{9}$$

or

$$S_p = C \cdot \frac{\bar{r}}{R_w} \cdot \frac{\gamma}{\overline{\Delta t}} \tag{10}$$

where S_p is the specific surface area of the interconnected pores as related to unit pore volume. γ is a coefficient relating the specific surface area of the grains to the specific surface area of the interconnected pores. It usually approaches one for unconsolidated sandstones.

If R_w, $\bar{r}$, $\overline{\Delta t}$, and γ are considered as constants for a homogeneous unit of a reservoir, eguation (10) may be reduced into the following simple linear form

$$S_p = A \cdot C \tag{11}$$

where A is a proportionality constant that can be determined experimentally.

Thus equation (11) serves for determining the specific surface area of the interconnected pores, S_p, as related to unit pore volume from the lithologic factor, C.

Another very important reservoir parameter, namely; the absolute permeability, k, can also be determined from the lithologic factor, C, by means of the Kozeny-Carman equation:

$$k = \frac{\phi}{k_z S_p^2} \tag{12}$$

where k_z is the Kozeny constant. Carman reported that the value of k_z lies in

the range from 4.5 to 5.5 for unconsolidated sands.

By substituting equation (10) into (12), equation (13) may be obtained

$$k = \frac{\phi}{k_z \left(\frac{\bar{r}}{R_w} \cdot \frac{2}{\overline{\Delta t}} \right)^2} \cdot \frac{1}{C^2} = B \frac{\phi}{C^2} \qquad (13)$$

or

$$C = \frac{\sqrt{B}}{\sqrt{\frac{k}{\phi}}} \qquad (14)$$

The constant B can be experimentally determined and is fairly constant for a homogeneous unit of a reservoir.

Thus the permeability can be determined from C and ϕ by means of equation (13). This value of permeability is equal to that determined when the core is completely saturated with water. It can be also seen that with increasing deterioration of reservoir characteristics, i.e. as C increases, the permeability will decrease. It can be also noted that a plot of C vs $\sqrt{\frac{k}{\phi}}$ will yield a straight line.

Since capillary pressure curves are, in general, considered to reflect some of the fundamental characteristics of porous media, a relation between the lithologic factor and capillary pressure curve is sought. To meet this objective, a well accepted formula is used [6] as shown in equation (15)

$$k = \frac{\phi \alpha^2 * 10^8}{k_z} \int_{S_w = S_{wi}}^{S_{w=1.0}} \frac{d S_w}{P_c^2} \qquad (15)$$

where

α is the interfacial tension between the wetting and non-wetting fluid phases in the interconnected pores, in dynes/cm,

k is the absolute permeability, in darcys,

P_c is the capillary pressure in dynes/cm^2 which is a function of

wetting-fluid saturation, S_w.

By substituting equation (15) into equation (13), the following equation is obtained.

$$\int_{S_{wi}}^{1.00} \frac{d S_w}{P_c^2} = \frac{10^{-8}}{\gamma^2} \left(\frac{R_w}{\bar{r}} \cdot \frac{\overline{\Delta t}}{\alpha} \right)^2 \cdot \frac{1}{C^2} = D \cdot \frac{1}{C^2} \qquad (16)$$

where D is an experimental coefficient, which is considered as a constant for a homogeneous unit of a reservoir.

The importance of the integral, $\int_{S_{wi}}^{1.00} \frac{dS_w}{P_c^2}$, need not to be emphasized in any reservoir studies. By means of well logs and through the utilization of the lithologic influence factor, C, the integral can be determined. Any deterioration in the reservoir characteristics is sharply indicated by a reduction in the value of the integral as suggested by equation (16).

THE PORE GEOMETRICAL FACTOR, G

The pore geometrical factor was introduced as early as 1960 [7]. However, it was used very widely by a recent paper published several years ago [4] based on a study of capillary behavior of sandstone reservoirs.

As it is well known, the capillary pressure curve reflects some basic properties regarding the pore geometry of the sample under consideration. The location of the curve with respect to the S_w-P_c axes is a measure of the irreducible wetting-fluid saturation, S_{wi}, and of the minimum pressure required to start desaturation, P_d, respectively. The shape of the curve itself depends on the interconnection of the pores and the pore-size distribution.

It is postulated that when the measured values of P_c and S_w of a sample are plotted on natural log-log scale, a smooth best fitting curve approximating a

hyperbola is obtained. Assuming that deviations from a smooth curve are not of interest for the purpose of this investigation, and that these smooth curves represent true hyperbolas, then the relation between P_c and S_w can be expressed as follows:

$$Ln \frac{P_c}{P_d} * Ln \frac{S_w}{S_{wi}} = G \qquad (17)$$

where

P_d is the displacement pressure
S_{wi} is the irreducible wetting-fluid saturation
G is the pore geometrical factor.

The pore geometrical factor, G, is a constant for a particular sample. The location and shape of capillary pressure curve can be defined by the parameters appearing in equation (17), namely; the displacement pressure, the irreducible wetting-fluid saturation, and the pore geometrical factor.

It can be shown mathematically that G is a special value of $Ln \frac{P_c}{P_d}$ at a distinct position of P_c-S_w curve when $Ln \frac{S_w}{S_{wi}} = 1$, or when $S_w = e*S_{wi} = 2.718\ S_{wi}$.

This is shown in equation (18):

$$G = \left(Ln \frac{P_c}{P_d} \right)_{S_w = 2.718\ S_{wi}} \qquad (18)$$

It can be concluded from equation (18) that at a constant value of irreducible wetting-fluid saturation, S_{wi}, higher values of G indicate higher degree of complexity in the pore structure of the sample under consideration.

Thus, the pore geometrical factor associated with the value of irreducible wetting-fluid saturation will characterize the complexity of the geometry of the interconnected pores in oil- and gas-bearing sandstones.

It is worth mentioning here that a study is being considered by the authors for a further improvement of G by introducing a generalized logarithmic hyperbolic form of 2-degree of mathematical freedom, as follows:

$$Ln\left(\frac{P_c}{P_d}\right) * \left(Ln\frac{S_w}{S_{wi}}\right)^a = G \qquad (19)$$

where (a) is a power which, besides G, presents a 2-degrees of freedom for statistically better fitting.

Some further forms of the pore geometrical factor are also being considered by the authors, e.g.,

$$Ln\left(\frac{P_c}{P_d}\right) * \left(Ln\frac{1-S_{wi}}{1-S_w}\right)^a = G \qquad (20)$$

The study [4] has shown that the pore geometrical factor, G, is related very strongly to $\sqrt{\frac{k}{\phi}}$. As a matter of fact, a plot of G vs $\sqrt{\frac{k}{\phi}}$ on a log-log scale yielded a straight line for the formation under study. It was also shown that the pore geometrical factor is directly related to the wettability of the sample under consideration. In other words G is related to n, the saturation exponent, which is believed to be characterization factor of reservoir wettability. A plot of G vs n on a log-log scale yielded a straight line as well for the particular formation under study.

THE RELATIONSHIP BETWEEN C AND G

The intrinsic relationship between the lithologic influence factor, C, and the pore geometrical factor, G, has been revealed from basic concepts and from observation. To establish a mathematical correlation between them, the integral, $\int_{S_{wi}}^{1.00} \frac{d\,S_w}{P_c^2}$, is used as a starting point,

since $$\int_{S_{wi}}^{1.00} \frac{d\,S_w}{P_c^2} = f(G) \qquad (21)$$

P_c can be expressed from Eq. (17) in the following form

$$P_c = Exp\left[Ln\ P_d + \frac{G}{Ln\ \frac{S_w}{S_{wi}}}\right] \tag{22}$$

Thus Eq. (21) can be written as

$$\text{Integral} = I = \int_{S_{wi}}^{1.00} \frac{dS_w}{Exp\left[2 \cdot Ln\ P_d + \frac{2G}{Ln\ \frac{S_w}{S_{wi}}}\right]} \tag{23}$$

By transforming the independent variable S_w into S (where $S = \frac{S_w}{S_{wi}}$), the integral becomes

$$I = S_{wi} \int_{1.00}^{\frac{1}{S_{wi}}} \frac{dS}{Exp\left[2 \cdot Ln\ P_d + \frac{2G}{Ln S}\right]} = S_{wi} \int_{1.00}^{\frac{1}{S_{wi}}} f(s)\ dS \tag{24}$$

where the integrandus, f(s), is a function of S and can be represented by the following equation

$$f(s) = e^{-\left[2 \cdot Ln\ P_d + \frac{2G}{Ln S}\right]} \tag{25}$$

For carrying out an approximative integration, the Taylor development of f(s) is established at the particular value $S = \frac{1}{S_{wi}}$. That is

$$f(s) \cong f\left(\frac{1}{S_{wi}}\right) + f'\left(\frac{1}{S_{wi}}\right) * \left(S - \frac{1}{S_{wi}}\right) + \\ + \frac{1}{2} f''\left(\frac{1}{S_{wi}}\right) * \left(S - \frac{1}{S_{wi}}\right)^2 + \cdots \tag{26}$$

After deriving the first and second derivaties, f'(s) and f"(s), and replacing S by $\frac{1}{S_{wi}}$, and then substituting into Eq. (26), the Taylor development of the function f(s) is obtained in the following form:

$$f(s) \cong \frac{1}{P_d^2} \cdot Exp\left[-\frac{2}{|Ln\, S_{wi}|} \cdot G\right] \cdot \left\{1 + \frac{2G\, S_{wi}}{(Ln\, S_{wi})^2}\left(S - \frac{1}{S_{wi}}\right) + \right.$$

$$+ \frac{4G^2 S_{wi}^2 - 2G S_{wi}^2 (Ln\, S_{wi})^2 + 4G S_{wi}^2\, Ln\, S_{wi}}{2(Ln\, S_{wi})^4}\left(S - \frac{1}{S_{wi}}\right)^2 +$$

$$\left. + \cdots \right\} \qquad (27)$$

The integrandus, f(s), according to Eq. (27) is introduced into the integral, I, and by carrying out the integration between the limits, the following result is obtained

$$I \cong \frac{1}{P_d^2} \cdot Exp\left[-\frac{2}{|Ln\, S_{wi}|} \cdot G\right]\left\{(1 - S_{wi}) - GA + G^2 B\right\} \qquad (28)$$

where the compound coefficients, A and B, are as follows:

$$A = \frac{4 - 9S_{wi} + 6S_{wi}^2 - S_{wi}^3 + \dfrac{2 - 6S_{wi} + 6S_{wi}^2 - 2S_{wi}^3}{|Ln\, S_{wi}|}}{3(Ln\, S_{wi})^2} \quad \ldots \qquad (29)$$

$$B = \frac{2 - 6S_{wi} + 6S_{wi}^2 - 2S_{wi}^3}{3(Ln\, S_{wi})^4} \qquad \ldots \qquad (30)$$

Equation (28) shows that the integral, $\int_{S_{wi}}^{1.00} \frac{d\, S_w}{P_c^2}$, can be described

as the product of an exponential and a second degree power function of the pore geometrical factor, G. The coefficients, A and B, are functions of the irreducible wetting-fluid saturation, S_{wi}, only. One coefficient of Eq. (28) is determined by the displacement pressure, P_d. Thus, it is shown mathematically that the integral, I, is a function of G, S_{wi}, and P_d.

Table 1. shows the magnitudes of the coefficients A and B for $0.1 \leq S_{wi} \leq 0.5$. It is noted that both increase with S_{wi}.

Table 1. Some Tabulated Values of the Coefficients Appearing in Eq. (28) as a Function of Wetting-Fluid Saturation

S_{wi}	$1 - S_{wi}$	$-\frac{2}{\text{Ln } S_{wi}}$	A	B
0.10	0.90	0.8686	0.2384	0.0173
0.15	0.85	1.0542	0.3176	0.0316
0.20	0.80	1.2427	0.3949	0.0509
0.25	0.75	1.4427	0.4714	0.0761
0.30	0.70	1.6611	0.5479	0.1088
0.35	0.65	1.9051	0.6249	0.1507
0.40	0.60	2.1827	0.7016	0.2043
0.45	0.55	2.5047	0.7791	0.2728
0.50	0.50	2.8856	0.8569	0.3611

The determination of the pore geometrical factor, G, from the lithologic factor, C, is a task of utmost importance. It is with this procedure that the pore geometrical factor, G, can be evaluated from the well logging parameter, C, i.e. from well logs. By combining equations (16) and (28),

one obtains

$$\frac{1}{P_d^2}\,Exp\left[-\frac{2}{|Ln\,S_{wi}|}\cdot G\right]\left\{(1-S_{wi})-AG+BG^2\right\}=$$

$$=\frac{10^{-8}}{\zeta^2}\left(\frac{R_w}{\bar{r}}\cdot\frac{\overline{\Delta t}}{\alpha}\right)^2\cdot\frac{1}{C^2}\quad=$$

$$=D\,\frac{1}{C^2} \qquad (31)$$

where the compound quantities A and B have been defined by equations (29) and (30) and whose values are tabulated in Table 1.

By solving equation (31), the pore geometrical factor, G, can be evaluated from well logs, since C is a well logging parameter. C can be evaluated from a combination of the Gamma Ray and the SP curves, as it was shown in Fig.5. of reference [2] . C can also be evaluated by other techniques.

For the solution of Eq. (31) for G, also S_{wi} and P_d ought to be known in advance. For this purpose S_{wi} is determined also from the well logs, and some reasonable estimation should be done for the value of P_d. An investigation is in progress concerning the relationship between P_d and C. It is expected that C increases with increasing value of P_d.

By rearranging equation (31), equation (32) may be obtained which shows the joint effect of C and P_d, $\left(\frac{P_d}{C}\right)^2$, on G:

$$Exp\left[-\frac{2}{|Ln\,S_{wi}|}\cdot G\right]\left\{(1-S_{wi})-AG+BG^2\right\}=D\left(\frac{P_d}{C}\right)^2 \qquad (32)$$

CONCLUSIONS AND COMMENTS

The lithologic influence factor and the pore geometrical factor are two intrinsic reservoir parameters which characterize the complexity of the microphysical pore structure of sandstones. Any marked changes in the mineralogical composition, grain size, and pore size distribution will be reflected by those two factors. Thus those two factors can be utilized jointly in detailed reservoir studies.

The lithologic influence factor, which can be evaluated from Gamma-Ray - SP curves, is a well logging parameter that can be obtained as a continuous record along the borehole axis. The pore geometrical factor, which can be evaluated from capillary pressure curve, is a core analysis parameter that can be obtained on individual core samples. Thus a quantitative correlation between the two factors will make it possible to obtain the pore geometrical factor in a continuous form.

A mathematical correlation is obtained between the lithologic influence factor and the pore geometric factor.

A comprehensive research work is in progress at the Petroleum Engineering Department, Faculty of Petroleum and Mining Engineering, Al-Fateh University, Tripoli, Libya for the full utilization of the possibilities involved in the suggested theory.

REFERENCES

1. Barlai, Z.:"A New Theory of the Well Logging Characteristics of Hydrocarbon Bearing Sandstones", SPWLA 13:th Annual Logging Symposium, Paper J, p. 1-61, Tulsa, Oklahoma, (1972)

2. Barlai, Z.:"Effects of Fine Grains and Shale Laminae on Well Log Evaluation of the Hydrocarbon-Bearing Neogene Sandstones in Hungary", 3:d European Formation Evaluation Symposium of the SPWLA, Paper I, p. 1-46, London, UK, (1974)

3. Barlai, Z.:"Determination of Permeability and Specific Surface Area of the Pore Channels from Well Logs in Fine Grained Sandstones", SPWLA 17:th Annual Logging Symposium, Paper C, p. 1-46, Denver, Colorado, (1976)

4. Taher A. Hadidi, A. Reda Abdel Mawla, Essam M. Abdallah:"Pore Geometrical Factor as Defined from Capillary Pressure Curves and its Influence on W/O Relative Permeability", Cairo University, Bulletin of the Faculty of Engineering, 1973-1974, Petroleum Engineering, Paper 2, p. 1-16, (1974)

5. Barlai, Z.:"Well Logging Parameters of Hydrocarbon-Bearing Sandstones Composed of Sands, Silt and Shale; Evaluation of Water Saturation, Porosity and Grain-Size Distribution", SPWLA 10:th Annual Logging Symposium, Paper X., p. 1-42, Houston, Texas, (1969)

6. Wyllie, M.R.J., Spangler, M.B.:"Application of Electrical Resistivity Measurements to Problem of Fluid Flow in Porous Media", Bulletin of AAPG, Vol. 36, p. 359, (1952)

7. Thomeer, J.H.M.:"Introduction of a Pore Geometrical Factor Defined by the Capillary Pressure Curve", Tran. AIME, Vol. 219, (1960)

ABOUT THE AUTHORS

BARLAI

ABDEL MAWLA

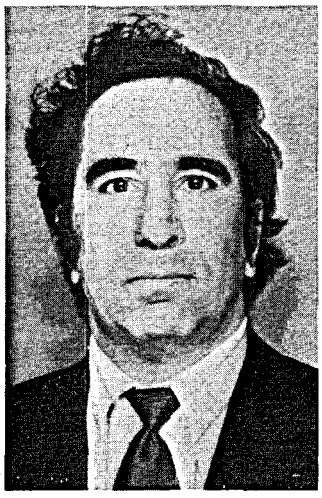

AL-SAADOON

DR ZOLTAN BARLAI is currently the professor of Formation Evaluation with Al-Fateh University, Petroleum Engineering Department, Tripoli, Libya. He graduated from the Technical University of Budapest in mechanical and electrical engineering in 1950 (B.S.) and from the Technical University of Sopron, Hungary, in oil engineering, in 1952 (B.S.) He holds a Ph.D. in geophysics at the Hungarian Academy of Sciences, Budapest since 1966. In 1974 he achieved the highest Hungarian scientific degree, Doctor of Technical Sciences, at the Hungarian Academy of Sciences in Budapest. He has been employed since 1952 in the Hungarian Oil and Gas Industry, where

he has dealt continuously with well logging and formation evaluation. He is a directory member of the Association of Hungarian Geophysicists since 1964, where he is the Chairman of the Well Logging Section. He has been a member of the Geophysical Scientific Committee of the Hungarian Academy of Sciences since 1967. In 1976 he has been elected the Chairman of the Committee for a 3-year period. He moved from Budapest to Tripoli in December of 1976 with a state contract.

DR REDA ABDEL MAWLA received his B.S degree in Petroleum Engineering from Cairo University in 1960. He worked for the Egyptian Industrial Organization (Petroleum Engineering Sector) as a junior engineer, and as a teaching assistant at the Petroleum Engineering Department, Cairo University until 1963. In 1969 he received his Ph.D. in reservoir engineering from Moscow Petroleum Institute. Upon receiving his Ph.D., he joined the Petroleum Eng. Dept. of Cairo University as an assistant professor. In 1973 he joined the Petroleum Eng. Dept. of the Faculty of Petroleum and Mining Eng., Al-Fateh University, Tripoli, Libya. He became in 1975 the chairman of the Pet. Eng. Dept. Dr R.A. Mawla is the author of many publications in the fields of Petrophysics and reservoir engineering, and the co-author of three Arabic petroleum engineering textbooks. He was a member of the Consulting Technical Committee of the Egyptian General Petroleum Corporation and has done some consulting work for local and foreign companies.

DR FALEH T. AL-SAADOON holds a B.S. and an M.S. degrees in Petroleum Engineering, and a Ph.D. degree in Chemical Engineering. He received his B.S. and M.S. from West Virginia University in 1965 and 1966 respectively, and his Ph.D. from University of Pittsburgh in 1970. He worked in the United States as a junior engineer with IGT, as a research assistant with the Coal Research Bureau, and as a teaching assistant with the University of Pittsburgh. In 1970, he joined the University of Baghdad, College of Engineering as an assistant professor. In 1971 he became the head of the Petroleum Engineering Department. He held that position until 1975 when he joined Al-Fateh University of Tripoli, Libya. Dr Al-Saadoon is the author of many technical publications and the co-author of three Arabic Petroleum Engineering text books. He has done some consulting work for local and foreign firms. He is a member of many scientific and honorary societies and he has served in the board of directors of some technical journals.

NORMALIZATION TECHNIQUES AND INTERPRETIVE PRACTICES OF RELATIVE PERMEABILITY CURVES OF RESERVOIR ROCKS

Reda Abdel Mawla and Faleh T. Al-Saadoon
Petroleum Engineering Department
Faculty of Petroleum and Mining Engineering
Al-Fateh University, Tripoli, Libya

ABSTRACT

This paper deals with normalization techniques currently used for adjusting laboratory relative permeability curves. It reviews the current state of the art with examples based on actual data. It was shown that different techniques may lead to different curves for the same set under study. Hence the intention of this paper was to establish some criteria so that the denormalized curves reflect actual reservoir characteristics.

The most critical part in the normalization is the proper selection of the end points. The end points selected are those which may correlate best with parameters such as $\sqrt{\frac{k}{\phi}}$ or k.

The best normalization technique to be used is the one that retains the general flow characteristics of the reservoir rock.

The present work suggests that a better selection of end points may be accomplished by using the pore geometrical factor, as deduced from capillary pressure curve, as a correlation parameter. Other tools of formation evaluation may assist in the final selection.

INTRODUCTION

Accurate knowledge of reservoir rock properties; namely, lithology, porosity, permeability, water saturation, capillary pressure, relative permeability, and wettability is very important to the reservoir engineer in order to properly characterize the reservoir under study and to evaluate its performance. Hewitt (1) and other authors (2,3) have demonstrated that lithologic characteristics control reservoir properties.

Capillary pressure curves are, in general, believed to reflect some of the fundamental characteristics of porous media (4,5). Capillary pressure--saturation relationship is dependent on many factors; namely, pore geometry, fluids and solids involved, and the history of the saturation process. It is well known that pore size distribution and capillary pressure are directly related. This is the basis for a recent paper (6) correlating the pore geometrical factor with the lithologic influence factor using a hyperbolic capillaric model as a foundation for the analytical approach. This approach may be used for a better understanding of multiple saturation fluid flow behavior.

The great practical importance of relative permeability measurements to reservoir mechanics has been outlined by Osoba (7), Branson (8), and others. Several investigations have also pointed out that relative permeability is a function of prevailing fluid saturation, the rock-wetting characteristics, the geometry of the pores of the rock, and the history of the saturation process. Morgan and Gordon (9) have studied the influence of the pore geometry on some water-oil relative permeability curves using photomicrographs of thin sections taken from the ends of relative permeability measured sandstone plugs. Microscopic examination reveals that rocks with large well interconnected pores have relative permeability curves with the following characteristics:

a - initial k_{ro} is a high fraction of k_{air},

b - irreducible water saturation (Sw_r) is low,
c - final k_{rw} is relatively high but is a small fraction of, k_{air} when compared to k_{ro} and
d - the two-phase flow region occurs over a wide range.

The general characteristics of sandstone core with smaller pores, as compared to those with large pores, are

a - initial k_{ro} and final k_{rw} are smaller fractions of k_{air},
b - irreducible water saturation is higher, and
c - the two-phase region occurs over a narrower region.

Since relative permeability measurements are often carried on few core samples taken from a number of wells in the reservoir under study, different curves are obtained. Thus, the reservoir engineer is faced with two problems; namely, the selection of samples to properly characterize the reservoir and the adjustment of laboratory data to reflect actual reservoir conditions.

The samples selected for laboratory testing should cover the permeability and porosity ranges found in the reservoir.

The most generally accepted adjusting (normalization) methods use prescribed end values (Sw_e, So_r, Sg_r, k_{ro} @ Sw_e, k_{ro} @ So_r or Sg_r, k_{rw} @ Sw_e, k_{rw} @ So_r, k_{rg} @ Sw_e, and k_{rg} @ Sg_r) to determine an average adjusted (normalized) curve, and finally constructs an average (denormalized) curve to reflect reservoir conditions. It should be emphasized that the proper determination of the end points is the most critical part in those normalization techniques. These end points are usually determined from an average of the core data, or log analysis, or correlation, or any combination.

The purpose of this paper is to explain some of the practical aspects of the normalization techniques and its application. It is a part of a project undertaken to evaluate the susceptibility of a particular sandstone structure (hereafter referred to as the X-structure) to a natural water drive and/or water flooding. Thus this paper is based on an actual study.

Two sets of relative permeability curves to oil and to water were obtained, hereby designated as set # 1 and set # 2, respectively. The first set consists of ten tests and the second set consists of four tests. The samples selected for laboratory testing covered permeability and porosity ranges found in the reservoir.

Steady-state relative permeability tests were used in both cases, and for the correct direction of saturation change, namely; increasing wetting phase saturation or imbibition.

The laboratory data were developed from flooding refined oil sandstone cores containing an irreducible water phase. Simulated formation brine was used as the displacing phase during the tests.

A summary of the results obtained for set # 1 is given in Table 1. Figs (1) and (2) represent the experimental relative permeability curves obtained for set # 1.

NORMALIZATION TECHNIQUES

Normalization is a valuable tool in evaluating the average relative permeability curve of a statistically homogeneous rock zone, based on a limited number of relative permeability curves determined on cores cut from said zone. It can be used for both imbibition and drainage permeability curves (10).

In this study, three normalization techniques are used in adjusting the laboratory data so that they reflect actual reservoir conditions. The discussion in this section will be limited set # 1 only.

In the first case, the following normalized quantities are employed (11):

Table 1. Basic Lab. Data for Set # 1

Sample No.	Permeability, md.			Porosity %	Irreducible water saturation, Sw_r, % pore space	Oil in place, % pore space	Residual oil saturation So_r, % pore space	Oil recovered % pore space
	To air	To oil @ Sw_r	To water @ So_r					
14	724	616	96	17.1	7.7	92.3	35.8	56.6
4	634	457	172	15.2	9.8	90.2	45.7	35.5
17	557	236	43	16.9	9.2	90.8	60.9	29.9
7	446	387	103	15.1	5.4	94.6	43.5	51.1
3	406	299	108	13.2	5.6	94.4	61.6	32.8
8	279	275	72	16.4	9.0	91.0	46.5	44.5
6	194	148	30.5	13.4	9.1	90.9	40.6	50.3
19	179	147	13.8	12.7	5.8	94.2	56.2	38.0
10	106	80	23.0	10.8	6.8	93.2	53.1	40.1
2	12	8.9	-	7.6	21.1	78.9	Sample fractured during analysis	

$$S_w^* = \frac{Sw - Sw_e}{(1 - So_r) - Sw_e} \tag{1}$$

$$S_o^* = 1 - S_w^* = \frac{So - So_r}{(1 - So_r) - Sw_e} \tag{2}$$

$$K_{rw}^* = \frac{K_{rw} @ Sw}{K_{rw} @ So_r} \tag{3}$$

$$K_{ro}^* = \frac{K_{ro} @ Sw}{K_{ro} @ Sw_e} \tag{4}$$

Thus for a water-oil system, $K_{rw}^* = 1.00 @ S_w^* = 1.00$ and $K_{ro}^* = 1.00 @ S_w^* = 0$.

The terms S_w^* and S_o^* are called the effective water and oil saturations, respectively. They represent normalized liquid saturations in the range where both water and oil are mobile.

To perform the normalization, the following step-by-step procedure is followed:

a - Calculate S_w^*, K_{rw}^*, and K_{ro}^* at different values of Sw.

b - Plot K_{ro}^* and K_{rw}^* versus Sw on a semi-log scale for all samples under study as shown in Fig. (3). Fig. (3) represents the normalized curve for set # 1.

c - Regenerate an average k_{ro} and k_{rw} curve for each group of samples. Arithmetic averages of Sw_e, So_r, $k_{rw} @ So_r$, and $k_{ro} @ Sw_e$ are used in this method. The resulting graph of the average denormalized relative permeability curves of set # 1 is shown in Fig (4).

In the second case, the following normalized quantities are employed

$$S_w^* = \frac{Sw - Sw_r}{1 - Sw_r} \tag{5}$$

$$S_o^* = \frac{So - So_r}{1 - Sw_r} \tag{6}$$

It should be noted that the sum of S_w^* and S_o^* does not add up to one. S^* represents the fraction of the fluid phase saturation which is mobile.

Another normalized quantity for oil saturation is employed and is given by equation (7).

$$S_o^{**} = 1 - S_w^* = \frac{S_o}{1 - S_{w_r}} \tag{7}$$

The values of S_{o_r} and S_{w_r} are taken directly from the data reported in Table (1).

To perform the normalization, the following step-by-step procedure is followed:

(a) Correlate k_{rw} with S_w^* and k_{ro} with S_o^* and with S_o^{**} for each test sample. Then deduce a general correlation for k_{rw} with S_w^* and k_{ro} with S_o^* and with S_o^{**} for the whole set. The least square method was used in this study. The following three equations were obtained for set # 1.

$$k_{rw} = 0.806\ S_w^{*\,1.677} \tag{8}$$

$$k_{ro} = 1.635\ S_o^{*\,1.883} \tag{9}$$

and

$$k_{ro} = 7.586\ S_o^{**\,15.742} \tag{10}$$

(b) Denormalize S_w^*, S_o^*, and S_o^{**} by rearranging equations (5), (6), and (7), respectively.

(c) Plot k_{ro} and k_{rw} versus Sw on a semi-log scale. The resulting graph of the average denormalized relative permeability curves for set # 1 is shown in Fig. (4).

In the third normalization technique, the following modified forms of Corey Equations (to account for actual nonhomogeneous samples) are used (11).

$$Sw^{*} = \frac{Sw - Sw_r}{(1 - So_r) - Sw_r} \tag{11}$$

$$So^{*} = 1 - Sw^{*} = \frac{So - So_r}{(1 - So_r) - Sw_r} \tag{12}$$

$$k_{rw} = \left[f'_w(s)\right]^4 = \left[\frac{m(Sw - Sw_r)}{(1 - So_r) - Sw_r}\right]^4 \tag{13}$$

$$k_{ro} = \left[f'_o(s)\right]^4 = \left[\frac{m(1 - So_r - Sw)}{(1 - So_r) - Sw_r}\right]^4 \tag{14}$$

where k_{rw} and k_{ro} are the experimentally determined parameters, and m represents a stratification factor.

To perform the normalization, the following step-by-step procedure is followed:

(a) Calculate $f'_w(s)$ and $f'_o(s)$ at different values of Sw. $f'_w(s)$ and $f'_o(s)$ are calculated from $(k_{rw})^{0.25}$ and $(k_{ro})^{0.25}$, respectively.

(b) Plot $f'_w(s)$ and $f'_o(s)$ versus Sw - the resulting graphs should be straight lines. Any deviation from a straight line is a measure of the validity of the test sample under consideration. Determine So_r, Sw_r, and m by using the following criteria:

when $f'_w(s) = 0$, $Sw = Sw_r$

when $f'_o(s) = 0$, $Sw = 1 - So_r$ or $So_r = 1 - Sw$

when $Sw = Sw_r$, $m = f'_o(s)$

(c) Determine a representative average value for So_r for the whole set by plotting So_r/Sw_r versus Sw_r. The usual graphical relationship between So_r/Sw_r versus Sw_r should be as that shown in Fig. (7). By using a representative average value for Sw_r and entering Fig. (7), a representative value for So_r is determined.

(d) Determine an arithmetic average value for the stratification factor, m.

(e) Solve Equations (13) and (14) for k_{rw} and k_{ro} respectively in terms of Sw by substituting the predetermined average values of m, Sw_r, and So_r, namely; 0.851, 0.150, and 0.488, respectively.

The following two equations were obtained for k_{rw} and k_{ro}, respectively.

$$k_{rw} = \left[2.351\ (Sw - 0.150)\right]^4 \qquad (15)$$

$$k_{ro} = \left[2.351\ (0.512 - Sw)\right]^4 \qquad (16)$$

(f) Plot k_{rw} and k_{ro} versus Sw on a semi-log scale. The resulting graph of the average denormalized relative permeability curves of set # 1 is shown in Fig. (4).

DISCUSSION OF DATA AND RESULTS

Discussion of Data

Detailed core analysis (conventional and special) were performed on set # 1 and set # 2. These include porosity, permeability, water-oil saturations, water-oil relative permeability, and capillary pressure. In view of the heterogenity of the structure due to the presence of tight sections in its upper part and shales distributed within, each one of the cored interval was treated as a statistically homogeneous unit.

The weighted and geometric averages were used to process porosity and permeability data, respectively. The average values for porosity and permeability were calculated as 13.37 % and 276.3 millidarcys (md) respectively for set # 1, and 17.18 % and 425.2 md. respectively for set # 2. The overall average porosity and permeability (as obtained from all sets) for the whole structure is 14.94 % and 206 md. respectively.

The capillary pressure curves were determined by the use of the restored state method for an air-water system. An air drive of 35 psig was used for set # 1

and 45 psig was used for set # 2 in order to establish capillary equilibrium at the irreducible brine saturation. The average irreducible brine saturation for the whole structure as obtained from the resulting average capillary pressure curve is 10.2 %.

The weighted average porosity as obtained by well logging is 13.7 % for set # 1 and 13.5 % for the whole structure. Those results compare favorably with those obtained by core analysis.

Thus, it can be stated that set # 1 is a good representative set for the structure as a whole. It is definitely better than set # 2 for two reasons. First, set # 1, consists of ten test samples whereas set # 2 consists of only four test samples. Second, the average porosity and permeability values of set # 1, are closer to those of the whole structure than those of set # 2.

Hence it can be stated that set # 1 is a good representative sample of the structure as a whole and that it covers the permeability and porosity ranges found in the reservoir(13).

Relative permeability data were developed from flooding oil filled sandstone cores containing an irreducible brine phase.

A summary of relative permeability data for set # 1 is presented in Table (1), and the relative permeability curves are shown in Figs. (1) and (2). By comparing k_{rw} at different values of Sw with the corresponding value of k_{rw} @ So_r which can be calculated from Table (1), a big discrepancy appears. The relative permeability to water at the residual oil saturation (k_{rw} @ So_r) should attain the highest value for any test sample. This is not, however, the case in this study. Thus, k_{rw} @ So_r and K_{ro} @ Sw_e are not used as end points in the preceding normalization techniques.

Discussion of Results

Figure (4) represents the denormalized relative permeability curves for set # 1 as obtained by the three preceding normalization techniques. It appears from

the graph that great differences exist in the final denormalized curves for the same set of samples under study. That is, different normalization methods may lead to different results. Thus the selection of improper normalization technique may lead to serious erroneous results during application.

Likewise, the same normalization technique may lead to different results (as shown by Fig. 4 for the 2^{nd} technique) depending upon the end values fed into the procedure. This means proper normalization requires the proper selection of end points and technique. Thus, it is very necessary to keep in mind that normalization should not be considered as a routine work. Calculations may be performed by a machine, but the programming and the final selection should be done with caution. The selection of the proper end points and technique are of utmost importance in performance calculations.

It is unlikely that different end points and different techniques will yield the same results. It is very possible, though, that none of them will yield satisfactory results.

It may be asked then what end points and what technique need to be used? It is a matter of judgement and then the trial of many combinations. For instance, if you have any doubt about some end points, ignore them (as was done in this study). The number of trials can be reduced, however, by correlating the end points with some well accepted parameters. k and/or $\sqrt{\frac{k}{\phi}}$ are used very widely as correlating parameters for the characteristic (or "end") points of relative permeability curves measured on each sample. It is also believed that $\sqrt{\frac{k}{\phi}}$ is better than k as a correlation parameter (10, 12).

It is well accepted that the pore geometry of a reservoir rock affects the behavior of multiphase flow very strongly. It can be utilized very effectively in explaining the influence of many factors; namely, relative dispersion of one phase in the other, wettability, and other surface effects on the general characteristics of the relative permeability curve. Hence, it

is believed that the pore geometrical factor could serve as a correlation parameter and it may give a better correlation than $\sqrt{\frac{k}{\phi}}$. This belief stems from the fact that a plot of $\sqrt{\frac{K}{\phi}}$ versus the pore geometrical factor gave a straight line on a log-log scale (12). In addition the pore geometric factor is a dynamic parameter, whereas $\sqrt{\frac{k}{\phi}}$ is a parameter characterizing the pore size distribution only. Thus, it is believed that using the concept of pore geometrical factor may help to insure the validity of laboratory relative permeability curves (12). The authors are investigating that possibility.

In this study, end points saturations and relative permeabilities were plotted versus $\sqrt{\frac{k}{\phi}}$ on regular coordinate paper as shown in Figs. (6) and (7), respectively. It is shown in Fig. (6) that all end point saturations used gave good correlations. It is noted that all end point oil saturations gave a single correlation, whereas the end point water saturations gave three correlations. Sw_e (the experimentally determined end point) is higher than Sw_r (the irreducible end point) as expected. Corey's method gave an intermediate value.

Fig. 7 indicates that the first technique gave the best correlation for the end points relative permeabilities. As often observed (10), the correlation line is curved rather, than straight, and a trend of increasing k_{ro} with increasing $\sqrt{\frac{k}{\phi}}$ and of decreasing k_{rw} with increasing $\sqrt{\frac{k}{\phi}}$. This trend is probably an indication that the set is preferentially oil wet. This indication is justified by the high residual oil saturations and the low irreducible water saturations occuring in this set.

It is very important to note that the end points are not the only criteria in characterizing relative permeability curves. Thus it is necessary to consider the shapes of the curves, i.e. oil and water relative permeabilities at intermediate saturations between the end (terminal) values. The shape of the curves will reflect the general characteristics of the reservoir under study. Those general characteristics (and hence the shape) are governed by the pore geometry, fluid-rock wetting characteristics, and the direction of saturation change. Improper selection will make the denormalized curve not valid over a portion of the curve or over the whole range, except the

terminal points. As mentioned before, the pore geometrical factor will account for both the end points and the shape in between.

Keeping in mind the preceding remarks about proper normalization and the importance of generating a denormalized relative permeability curve that retains the physical characteristics of the reservoir rock under study, the reservoir engineer can proceed in making the final selection.

It is believed that the first technique gave the best denormalized curves for the set under study. The 2nd technique gave denormalized curves comparable in quality to that of the first technique.

A similar procedure employed for set # 2 and the final selected denormalized curves are shown in Fig. (8). No attempt was made to regenerate an average relative permeability curve for the whole structure based on those two sets of samples for the following reasons:

1. The large discrepancy in the residual oil saturations obtained, i.e. 49.32 % for set # 1 and 18.63 % for set # 2.
2. The two wells are located very close to each other in the structure, and thus the appearing discrepancy may indicate lithologic heterogeneity.

CONCLUSIONS

Normalization techniques, which allow the evaluation of average relative permeability curves reflecting actual reservoir conditions, were reviewed. Actual field data were used for illustrative purposes.

It was emphasized that the most important aspect to be considered in applying these techniques is the proper selection of end points. Different approaches were used in defining the end points of the sets of curves presented and consequently different denormalized curves were obtained. It was suggested that the pore geometrical factor could serve as a correlation parameter

better than k and/or $\sqrt{\frac{k}{\phi}}$. It is believed that this parameter will help insure the validity of the denormalized relative permeability curves.

The following rules of thumb ought to be observed whenever possible:

1. Samples selected for laboratory test should cover permeability and porosity ranges and rock types found in the reservoir.

2. The validity of the set chosen to represent the reservoir rock should be established by core analysis, well logging, and any other means.

3. Normalization is not to be considered as a simple analytical process. It requires the taking of many decisions on the part of the analyst with respect to the selection of end points and the final selection of the curves.

4. End points may be chosen by correlating them with the pore geometrical factor, or $\sqrt{\frac{k}{\phi}}$, or k and in that order.

5. The final curves to be selected should retain the same general characteristics of the reservoir under study.

NOMENCLATURE

Sw = water saturation, per cent pore space

Sw_e = end point water saturation as obtained from experimentally determined relative permeability curve to water, per cent pore space

Sw_r = irreducible water saturation, per cent pore space

So_r = residual oil saturation, per cent pore space

Sg_r = residual gas saturation, per cent pore space

k_{rw} = relative permeability to water, fraction

k_{ro} = relative permeability to oil, fraction

k_{rg} = relative permeability to gas, fraction

Sw^* = normalized or dimensionless water saturation

So^* or So^{**} = normalized or dimensionless oil saturation

K^*_{rw} = normalized or dimensionless relative permeability to the water phase

K^*_{ro} = normalized or dimensionless relative permeability to the oil phase

$f'_w(s) = (k_{rw})^{0.25}$

$f'_o(s) = (k_{ro})^{0.25}$

m = stratification factor.

REFERENCES

1. Hewitt, C.H.: "How Geology Can Help Engineer Your Reservoirs", Oil and Gas Jour., Nov. 14, 1966, p. 171-178.

2. Hewitt, C.H. and Morgan, J.T.:" The Fry In Situ Combustion Test-Reservoir Characteristics", J.P.T., March, 1965.

3. Wayhan, D.A. and McCaleb, J.A.:" Elk Basin Madison Heterogenity - Its Influence on Performance", J.P.T., Feb., 1969.

4. Tixier, M.P.:"Evaluation of Permeability From Electric-Log Resistivity Gradients", Oil and Gas Jour., June, 1949.

5. Purcell, W.R.:"Capillary Pressures- Their Measurement Using Mercury and

The Calculation of Permeability Therefrom", Trans. AIME, V. 186, Feb., 1949, p. 39-48.

6. Barlai, Z., Mawla, R.A., and Al-Saadoon, F.T.:"A Study of the Relationship Between Two Intrinsic Reservoir Parameters, the Lithologic Influence Factor and the Pore Geometrical Factor", to be published in the Transactions of the 19:th Annual Symposium of SPWLA.

7. Osoba, J.S.:"Relative Permeability - what It Is, and How to Put It to Use in the Field"., Oil and Gas Jour., V. 52, July 27, 1953, p. 326-333.

8. Branson, U.S.Jr.:"Measurement and Use of Relative Permeability Data. World Oil.", V. 133, No.1, July 1, 1951, p. 184-193.

9. Morgan, J.T., and Gordon, D.T.:"Influence of Pore Geometry on Water-Oil Relative Permeability", Soc. Pet.Eng. J., Oct., 1970, p.1179.

10. Chierci, G.L.:"On the Normalization of Relative Permeability Curves", Communication to JPT Forum Paper SPE 5962 Presented at 49:th Annual Fall Meeting of AIME in Houston, Texas, Oct 6-9, 1974.

11. Reference Unknown.

12. Hadidi, T.A.,Abdel Mawla, A.R., and Abdallah, E.M.: " Pore Geometrical Factor As Defined From Capillary Curves and Its Influence on W/O Relative Permeability", Bulletin of the Faculty of Engineering, Cairo University, paper 2, 1973-1974.

13..Keelan, D.K.: "A Practical Approach to Determination of Imbibition Gas--Water Relative Permeability", SPE 4988, 49:th Annual Fall Meeting of the Society of Petroleum Engineers of AIME, Houston, Texas, Oct. 6-9, 1974.

(Editor's note: Biographical sketches for Drs. Mawla and Al-Saadoon appear with Paper I.)

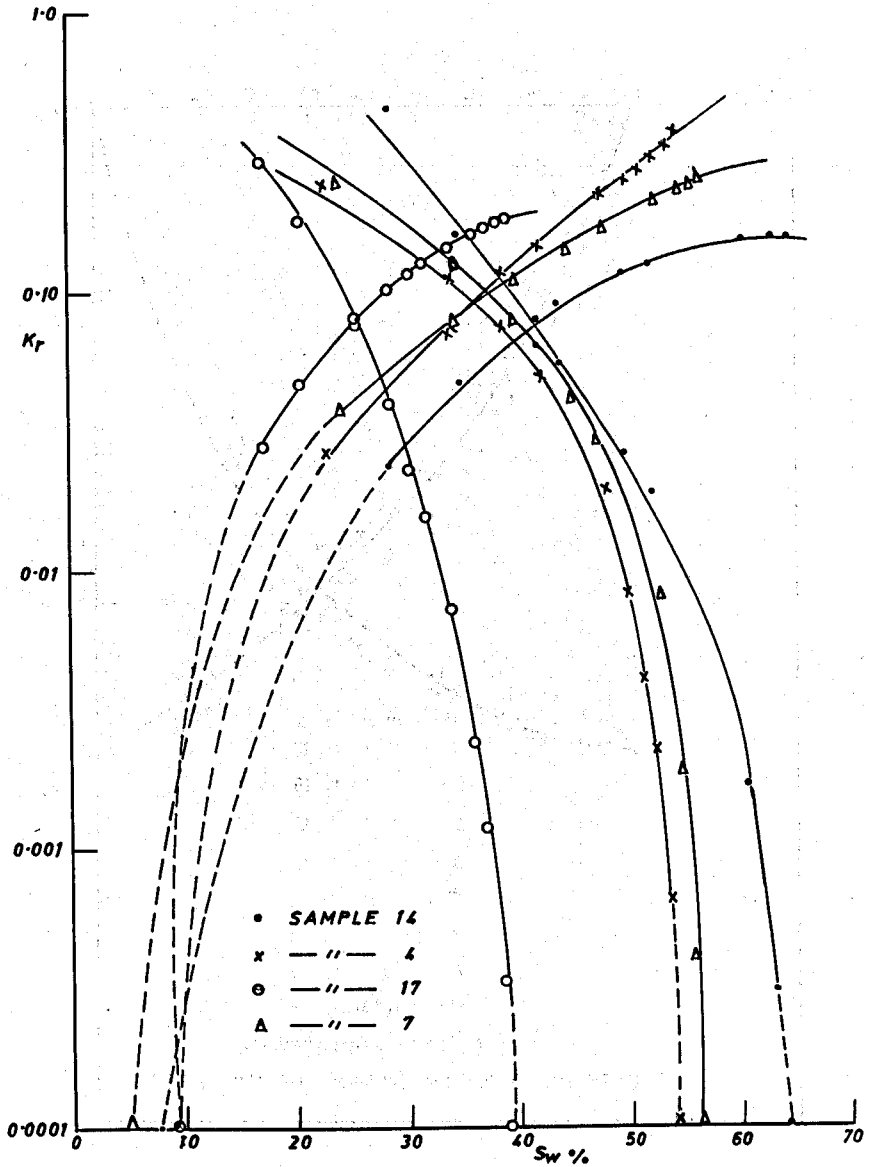

Fig 1 – Relative permeability curves (Set#1)

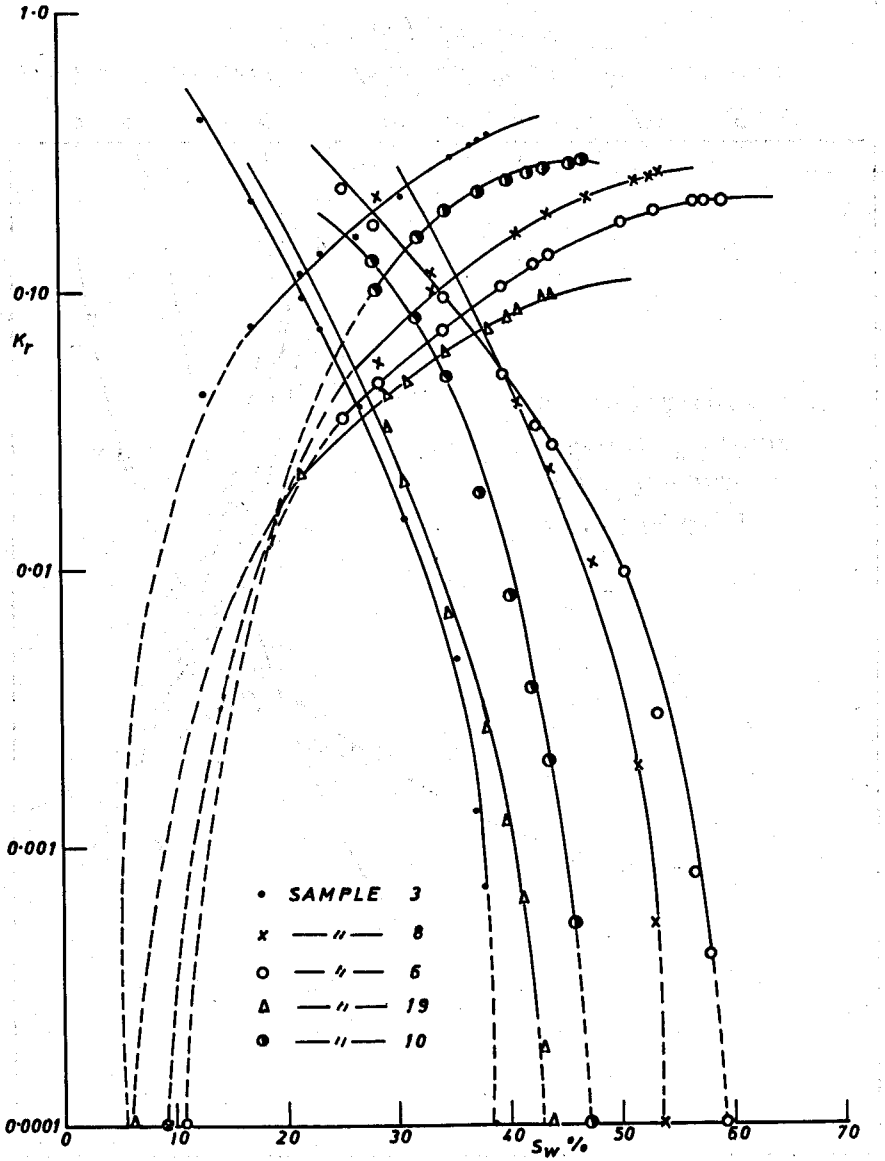

Fig 2 – Relative permeability curves (Set#1)

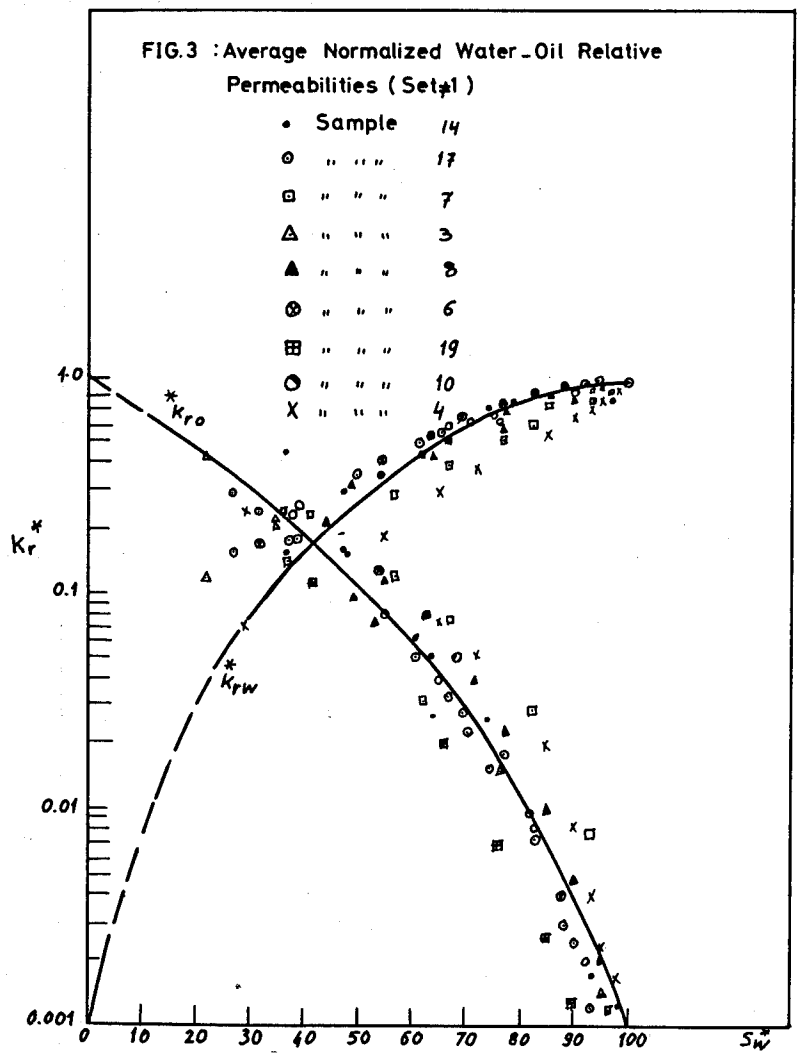

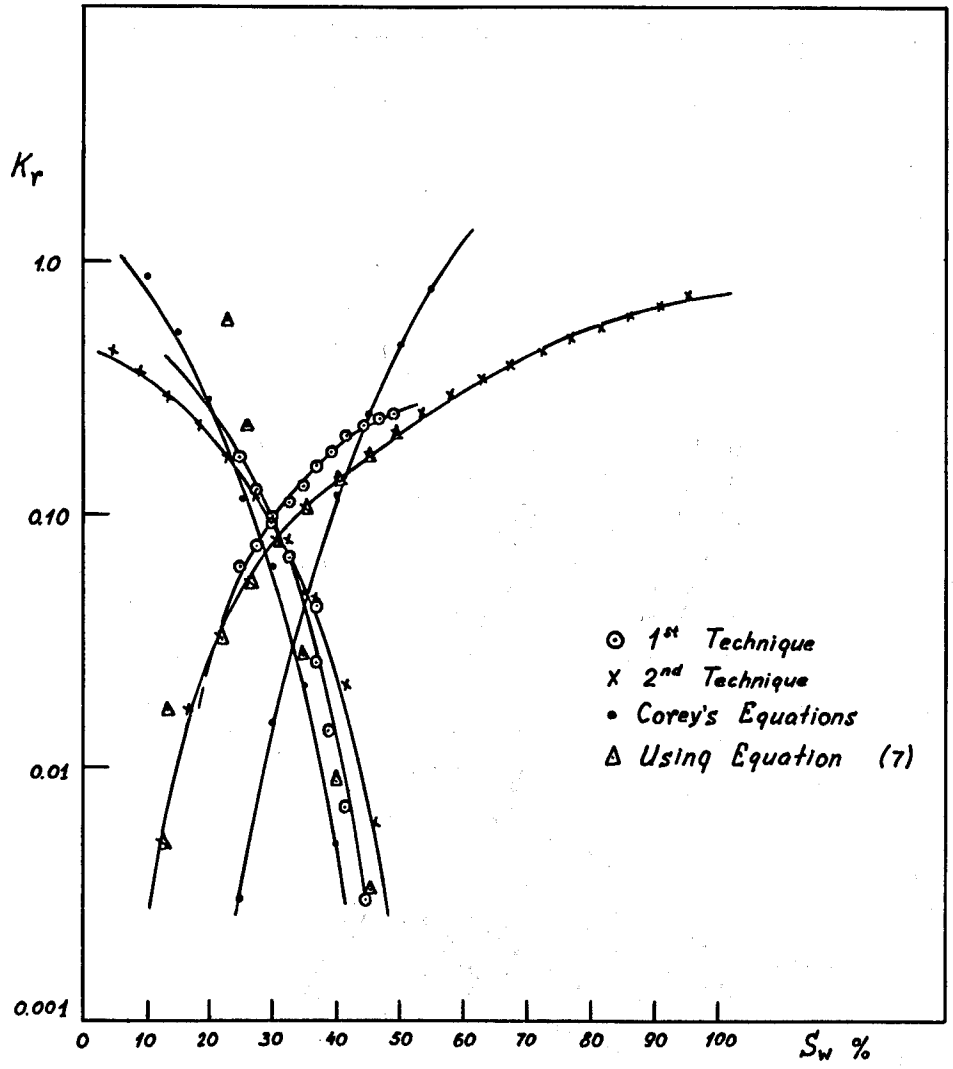

Fig. 4 — Denormalized Water-Oil Relative Permeabilities (Set #1) Using Different Techniques.

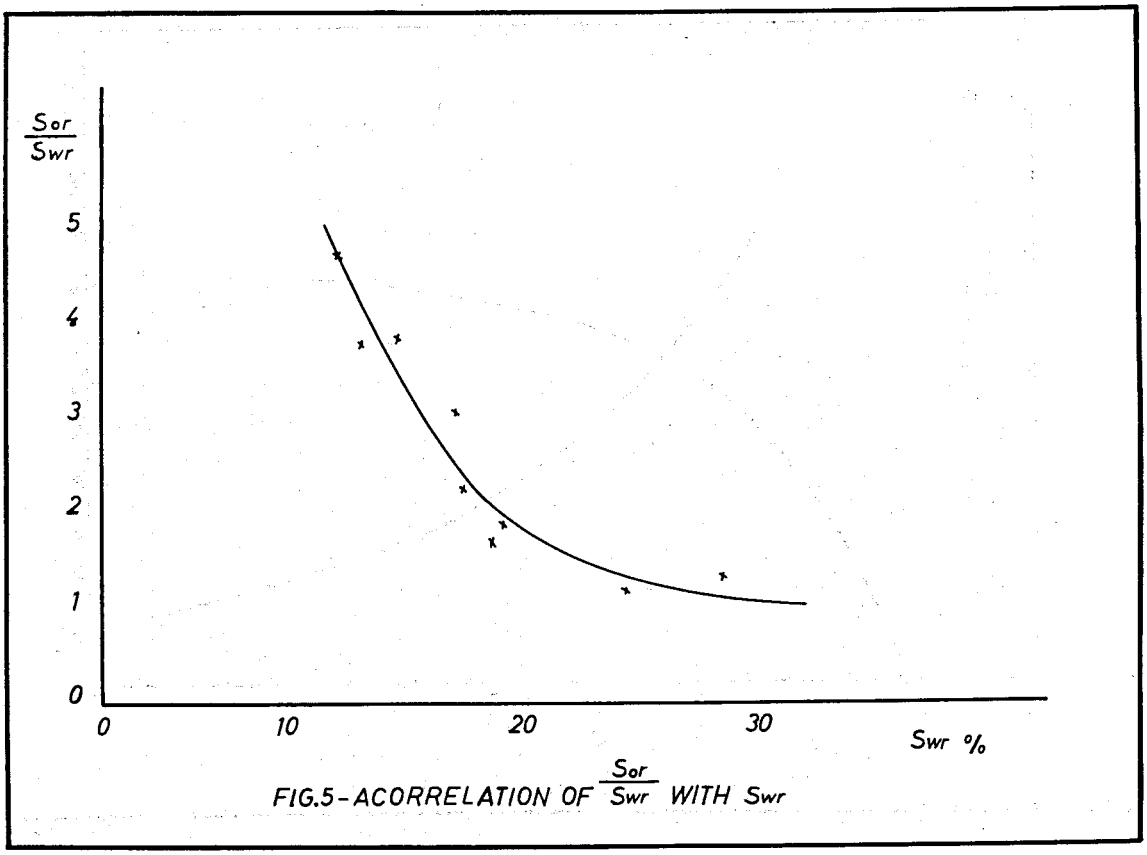

FIG.5-ACORRELATION OF $\frac{S_{or}}{S_{wr}}$ WITH S_{wr}

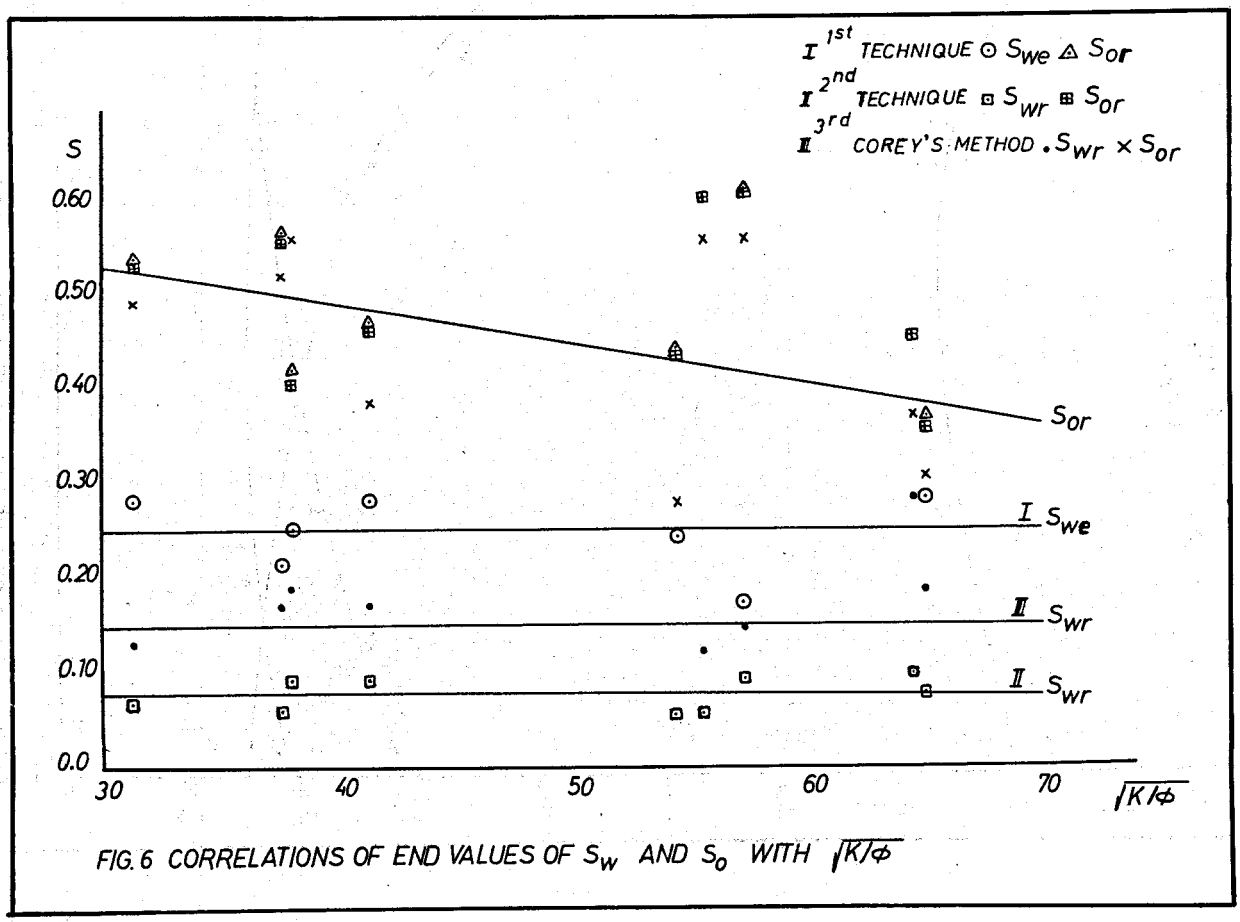

FIG. 6 CORRELATIONS OF END VALUES OF S_w AND S_o WITH $\sqrt{K/\phi}$

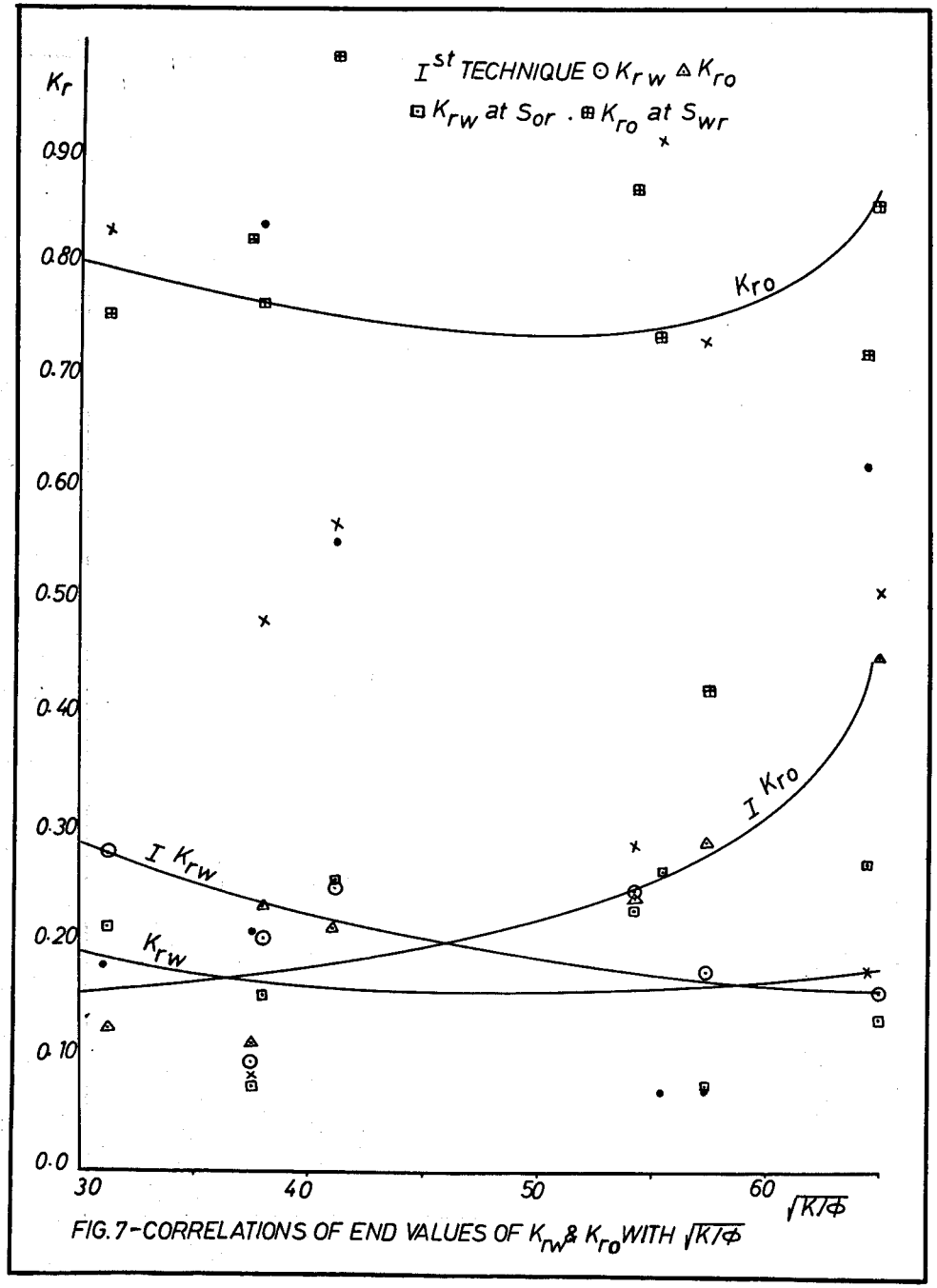

FIG. 7 - CORRELATIONS OF END VALUES OF K_{rw} & K_{ro} WITH $\sqrt{K/\phi}$

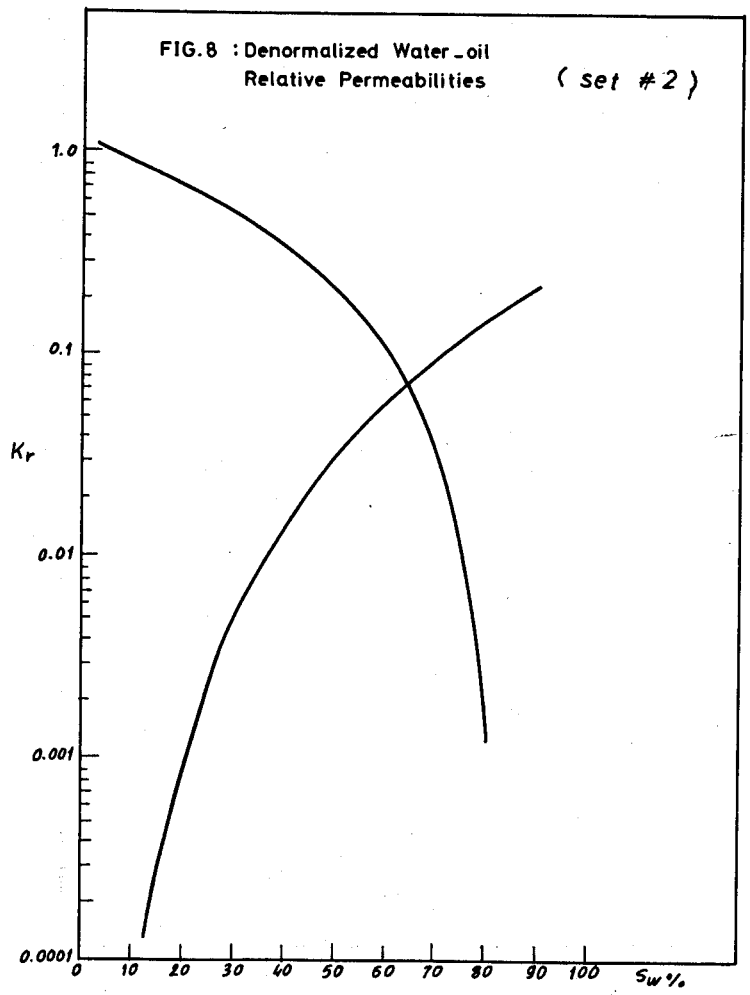

THE DETECTION OF WATER LEAKAGE FROM DAMS USING STREAMING POTENTIALS

by

Brent M. Haines
Lecturer - Dept. of Applied Geology,
Queensland Institute of Technology
Brisbane, Australia.

ABSTRACT

Streaming potentials have long been recognised as one of the group of electrokinetic phenomena. Geophysically, these potentials are encountered as components of down-hole S.P., surface S.P., and "noise" associated with D.C. surface electrical measurements.

Quantitatively the magnitude of the streaming potential may be related to various properties of the fluid and the rock matrix, and to the velocity of the fluid. It is this last relationship which is of primary interest in the work described herein.

An initial survey has been conducted over Gold Creek Reservoir, one of the water supply storages for the city of Brisbane. This dam has exhibited leakage through the wall for several years. Field data collected using quite unsophisticated equipment has indicated the efficacy of the method - there is a streaming potential effect which correlates readily with the known leakage zones.

This work will be extended to test dams of much greater capacity, also with known leakage problems. Ultimately it is envisaged that a routinely applicable technique will be developed to detect and evaluate water losses from dams and other water-retaining structures.

INTRODUCTION

Electrokinetics have been studied for many years, by such researchers as Lorenz (1952) and Street (1961), who recognise three distinct phenomena belonging to the group:-

Electro-osmosis: the displacement produced by an applied e.m.f., of a liquid with respect to the surface of a solid;

Electrophoresis: the movement of suspended solid or liquid particles in an electric field; and

Streaming potential: the production of an electric field by the movement of a liquid containing suspended solid or liquid particles.

The theoretical basis for the development of this streaming potential is found in the Helmholtz equation (Street, op.cit.):-

$$E_s = \frac{P \lambda \partial}{K \eta}$$

where E_s is the streaming potential;
P is the pressure drop;
λ is the double-layer thickness;
∂ is the surface charge density;
K is the conductivity of the liquid;
and η is the viscosity of the liquid.

While this equation was developed for the case of flow in a capillary tube, several aspects of practical import derive from it:-
(a) the magnitude of the streaming potential is inversely proportional to the liquid conductivity. In the context of fresh water storages, this magnitude should be relatively large. Such is borne out by the work of Abaza & Clyde, (1969);
(b) there is a direct proportionality between E_S and such parameters of the medium as charge density and double-layer thickness. This would suggest that E_S will be smaller in finer grained media, and will decrease in the presence of clay (see, for example, Ghosh, Rakshit and Chattoraj, 1953);
(c) other factors equal, streaming potential is directly dependent on pressure drop. Since this will also determine the rate of fluid flow, it is evident that E_S will depend strongly on velocity. Workers such as Ogilvy, Ayed and Bogoslovsky (1969) and Schriever and Bleil (1957) frequently regard the ratio E_S/P as a constant for a particular medium and fluid. A further relationship obtaining from the work of these authors is that the streaming potential is inversely dependent on grain size - in accord with (b) above.

STREAMING POTENTIALS IN EXPLORATION GEOPHYSICS

There are three situations pertaining to different fields of exploration geophysics, where streaming potentials are encountered.

(i) S.P. logging. The fact that streaming potentials contribute to the S.P. curve, along with liquid-junction, membrane and electrode potentials, has long been recognised. Such has been high-lighted by workers such as Pirson and Wong (1972).

In general the existence of this component of the S.P. curve has been either assumed to be negligible, or ignored. Largely this has been due to a lack of understanding of the mechanism of streaming potential generation, or a lack of adequate basic data which would permit quantitative evaluation. In those cases where Rw is low and reservoir pore-spaces are small, the magnitude of the streaming potential is probably insignificant.
(ii) Surface S.P. surveys. In these, geophysicists often recognise a "topographic" effect, that is, areas of higher altitude tend to be relatively negative compared to areas of lower altitude. This effect is a combination of at least two factors: one a membrane potential, due to the downslope movement of soil moisture in a typically clayey medium; the other a streaming potential, still essentially related to the downslope motion of soil moisture and

shallow groundwater. An excellent treatment of this effect is provided by Poldini (1938-9).

(iii) Surface D.C. electrical methods. Here, it is imperative to use non-polarising electrodes, to overcome the serious problem of electrode potentials. Despite their use, resort must still be had to an "S.P. bucking" device, to remove further unwanted potentials present before current is applied. Such potentials are probably the resultant of several effects, such as tellurics, membrane and liquid-junction potentials, evaporation potential and streaming potential.

FIELD EQUIPMENT

Equipment suitable for gathering streaming potential data on water storages is quite unsophisticated, rather similar to that employed in surface S.P. surveys. Essentially there are two facets: equipment for collecting S.P. data, and a position-fixing system. The former comprises non-polarising electrodes, cables, and a 10 Meg-ohm millivoltmeter. For the latter, a system of floating polyethylene rope marked at ten metre intervals and located by steel posts on shore, in combination with a small aluminium punt, has proven entirely satisfactory.

Development has been necessary only in the case of the electrodes. Non-polarising silver/silver chloride types were chosen because of their stability, and because they comprise only solid, insoluble components. However, such electrodes are relatively fragile, and care had to be exercised to ensure they were adequately protected during field usage.

A cross-section through the mobile electrode is illustrated in figure 1. The following notes are pertinent:-

(a) the two electrodes - mobile and fixed - are essentially identical, the difference being in overall length because of the greater lead mass used in the mobile electrode so that it will sink readily;
(b) the silver electrode itself is composed of 26 square centimetres (about four square inches) of pure silver mesh, rolled into a cylinder and electrodeposited with solid silver chloride. It is imperative that the surface area of such electrodes be as large as possible to minimise contact resistance. Even so, with these electrodes in fresh water, contact resistances of the order of 200,000 ohms are observed - hence it is essential that the millivoltmeter in series has an input impedance of at least 10 Megohms;
(c) apart from the silver/silver chloride electrode itself, care was taken to ensure that no metallic components of the electrodes are exposed, to avoid spurious electrode polarisation effects;
(d) the mobile electrode is lowered to the bottom of the water storage by means of the winch from an S.I.E. T100 minilogger. This is used for reasons of convenience, plus the utility of its depth-measuring odometer.

SURVEY METHOD

The survey method consisted of firstly, laying the floating ropes across the ponded area at a convenient line spacing - as shown in figure 2. At a chosen point, the fixed electrode was emplaced at the water's edge. Electrode imbalance was checked by placing the mobile electrode in close proximity to the fixed electrode, and confirming a zero reading on the millivoltmeter.

FIGURE 1

NON-POLARISING ELECTRODE

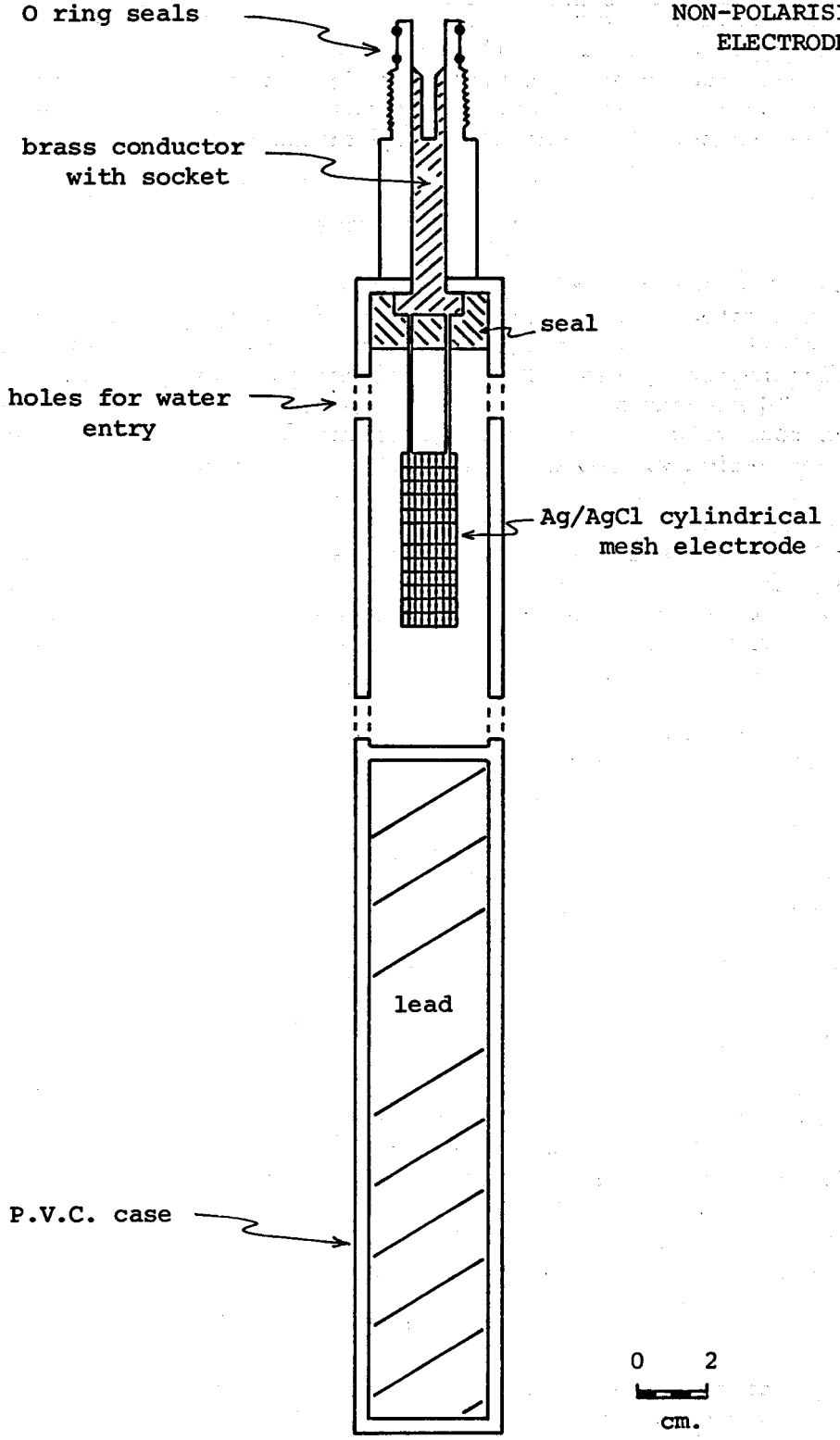

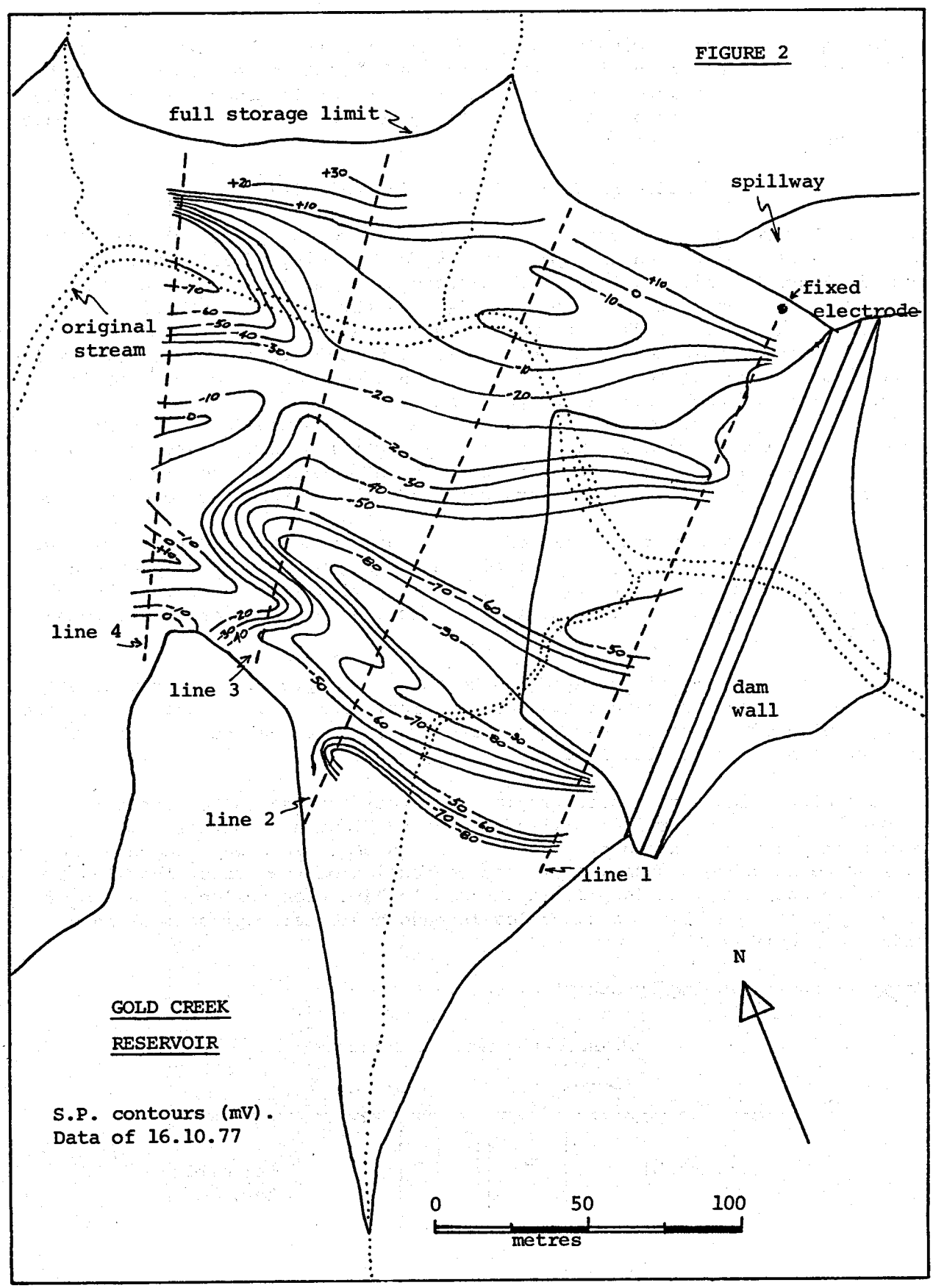
FIGURE 2
full storage limit
spillway
fixed electrode
original stream
line 4
line 3
line 2
line 1
dam wall
GOLD CREEK RESERVOIR
S.P. contours (mV).
Data of 16.10.77
N
0
50
100
metres

Following this, a cable was laid through the water from the fixed electrode to the commencement of the line to be measured. Stations at ten metre intervals along this line were occupied, with the mobile electrode lowered to the water bottom by the winch. At each station, note was taken of position, water depth and measured potential.

FIELD RESULTS: GOLD CREEK RESERVOIR

Gold Creek Reservoir is a small water storage operated by the Brisbane City Council as part of the water supply system for the city of Brisbane. Country rock is Bunya Phyllite, a low-grade Palaeozoic metamorphic, often heavily jointed. This reservoir has exhibited leakage through the earth-filled dam wall itself (Johnson, 1977), in two distinct areas:-
(i) approximately in the centre of the wall, on the downstream side, a small collection system has indicated leakage in this central region at a maximum observed rate of about 5.7 litres per minute;
and (ii) on the southern end of the wall, a slump on the downstream side occurred several years ago. This slump was rectified using heavy earthmoving machinery, and ever since a moist zone has been evident in the vicinity. Possibly the seal between impervious core and country-rock has been impaired.

Data were collected over a small portion of the ponded area in the region adjacent to the wall. Surveys were conducted during October 1977, when the water level was high (about 0.7 metres below spillway) and during early 1978 by which time the water level had fallen a further 5 metres or so due to an unusually dry summer.

Based on the work of Ogilvy, Ayed and Bogoslovsky (op.cit.), an initial attempt was made to recognise leakage zones on an areal basis - as illustrated in the contour plan of figure 2. Data contoured are raw S.P. values from the 1977 survey, when the water level was relatively high.

These contours indicate a broad region of large negative values extending across the southern portions of lines 1, 2 and 3, with a further similar region on the northern end of line 4. While such regions may indicate zones of leakage in a broad sense, it is the contention of the author that leakage zones are best examined in profile where data have been collected in two or more separate periods where water levels (and hydrostatic pressures) have differed significantly.

Consider the following hypothetical case:-

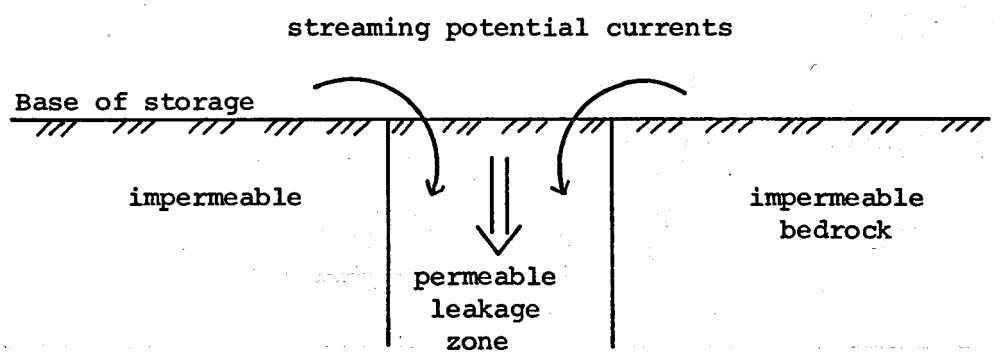

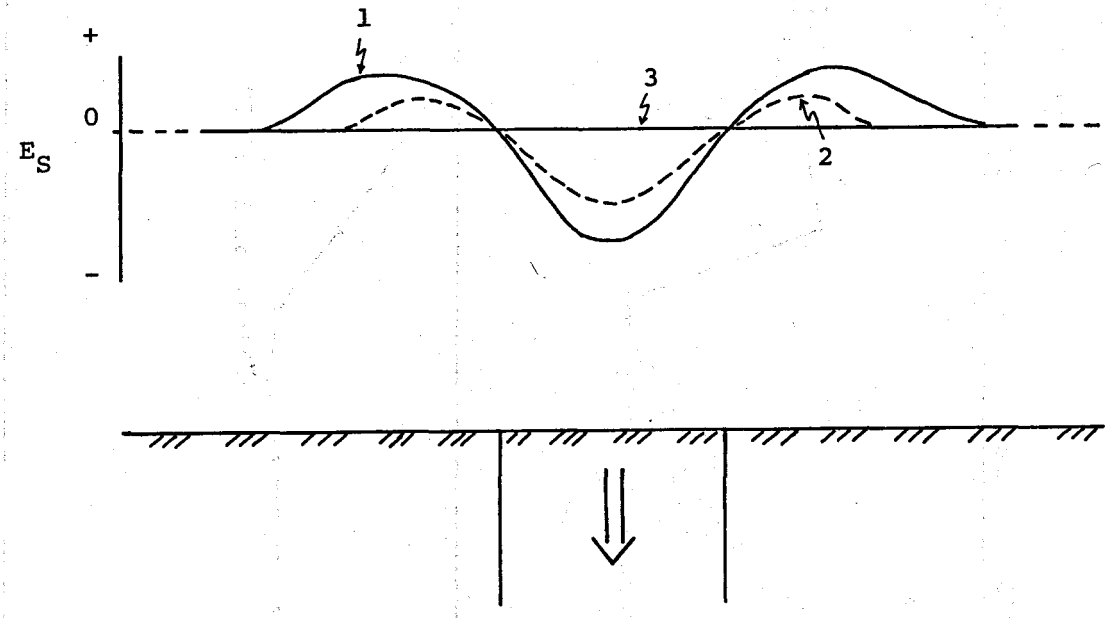

In this figure, a permeable zone is bounded by impermeable bedrock. When water levels are high, leakage through the permeable zone is promoted by the increased hydrostatic pressure, and an S.P. profile such as (1) is measured (note the adjacent positive peaks). At a lower water level, as in profile (2), the amplitudes are reduced. When the water level has fallen to zero, a zero profile is recorded (as in (3)).

Examining the Gold Creek Reservoir data in this fashion, results are most promising, and are illustrated in figures 3 to 6. Data of line 1, closest to the dam wall, are plotted in figure 3. During the survey in October 1977, the water depth averaged about 4.7 metres. For the second survey in February 1978, the water level had fallen to such an extent that the line of survey at that stage was along the water's edge.

The following points may be made concerning figure 3:-
(a) both sets of data are of readily measured magnitude. The fixed electrode position for the 1978 data was located 28 metres along the line from the northern end, because of the changed position of the water's edge at that time;
(b) the 1977 data show no correlation with the water depth profile. It had been anticipated that there would be a correlation, since laboratory experiments had indicated the consistency of E_S/P. There is however a marked gradient from north to south (similar to lines 2 and 3, and opposite to line 4) possibly due to a telluric field;
(c) spurious potentials are evident at the ends of the line - similar to that shown on other lines. These are ascribed to a combination of biochemical potentials (dense water lillies with stems often 5 metres long) and a steep water temperature gradient in the upper levels (in October 1977, temperatures of 14°C at the bottom and 22°C at the top were reported by F. Johnson). However, on

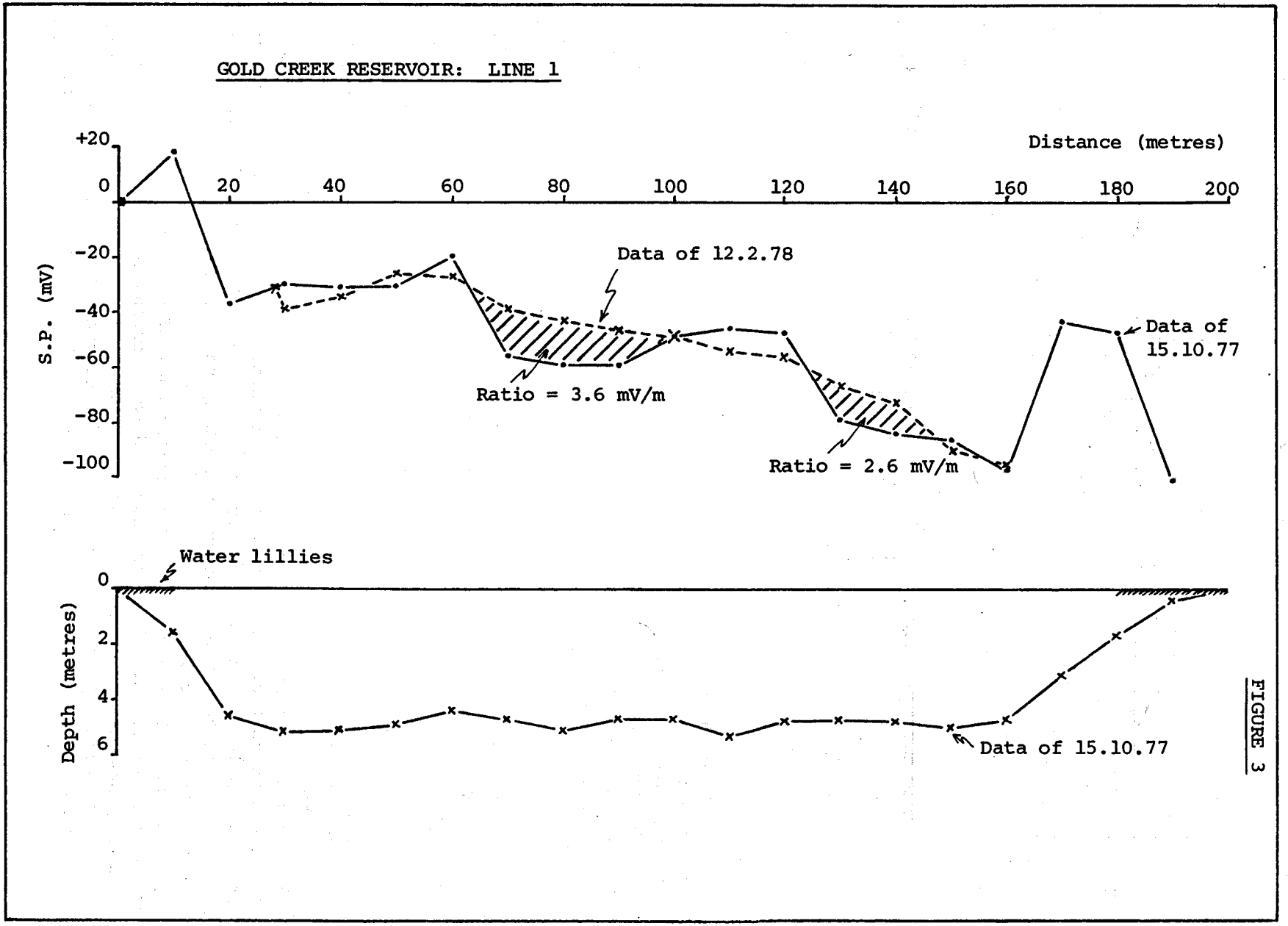
GOLD CREEK RESERVOIR: LINE 1
+20
0
-20
-40
-60
-80
-100
S.P. (mV)
20
40
60
80
100
120
140
160
180
200
Distance (metres)
Data of 12.2.78
Ratio = 3.6 mV/m
Ratio = 2.6 mV/m
Data of 15.10.77
Water lillies
0
2
4
6
Depth (metres)
Data of 15.10.77

FIGURE 3

this latter topic, Abaza and Clyde (op.cit.) have experimentally determined a small dependence of streaming potential on water temperature.
(d) zones of leakage are clearly evident in those regions - shown hachured - where the deeper water 1977 data are negative with respect to the zero water depth 1978 data. The two zones are between 65 and 100 metres, and between 125 and 150 metres, in excellent correlation with the positions of observed leakage on the downstream face of the wall.

Note that the ratio of potential variation to water level change is about 3.6 mV/m or about 2.5 mV/psi in the central zone, and about 2.6 mV/m or about 1.8 mV/psi in the southern zone. This is possibly an indication of a greater rate of water loss in the central zone. Further field and experimental work may show that such ratios are quantifiable in terms of velocity of flow and/or rock permeability.

Data of line 2 are displayed in figure 4. Here again there is no correlation between measured potentials and water depth. No zones of leakage as evidenced in figure 3, are apparent in the data. However, given scope for experimental and instrumental errors, it is possible that a zone of leakage is present at about 150 metres.

Figure 5 illustrates the data of line 3. Here, a leakage zone is evident between 120 and 135 metres, with a ratio of 2.2 mV change per metre of water depth change (i.e. about 1.6 mV/psi). Line 4 as depicted in figure 6 was not repeated during early 1978. Nonetheless, a potential leakage zone exists between perhaps 20 and 50 metres, as suggested by the magnitude of the observed potentials.

CONCLUSIONS

Based on the limited number of field data collected to date, the method appears to offer a means for the investigation of water losses from water storage dams and other water retaining structures. Concerning the interpretation of the data, it is suggested that delineation of leakage zones is facilitated by the comparison of two or more data sets, collected at times when water levels are markedly different. Leakage zones appear as S.P. troughs bounded by small positive peaks, when high water level data are compared with lower water level data. In other words, zones of leakage will become more negative as water levels increase. Impervious zones will suffer little or no variation on the S.P. profile, with the exception of the appearance of relatively positive peaks adjacent to leakage zones when leakage is active.

Intuitively, it would appear that the ratio of S.P. variation to water level change offers the prospect of quantifying these qualitative indications, in terms of rate of flow and/or rock permeability. Such an approach may also have potential for evaluating streaming potentials as a component of the S.P. curve.

ACKNOWLEDGEMENTS

The author gratefully acknowledges the encouragement and assistance of his Ph.D. supervisor, Dr. S.H. Hall - Dept. of Geology and Mineralogy, University of Queensland. He is further indebted to the Dept. of Geology and Mineralogy, University of Queensland, and to the Dept. of Applied Geology, Queensland

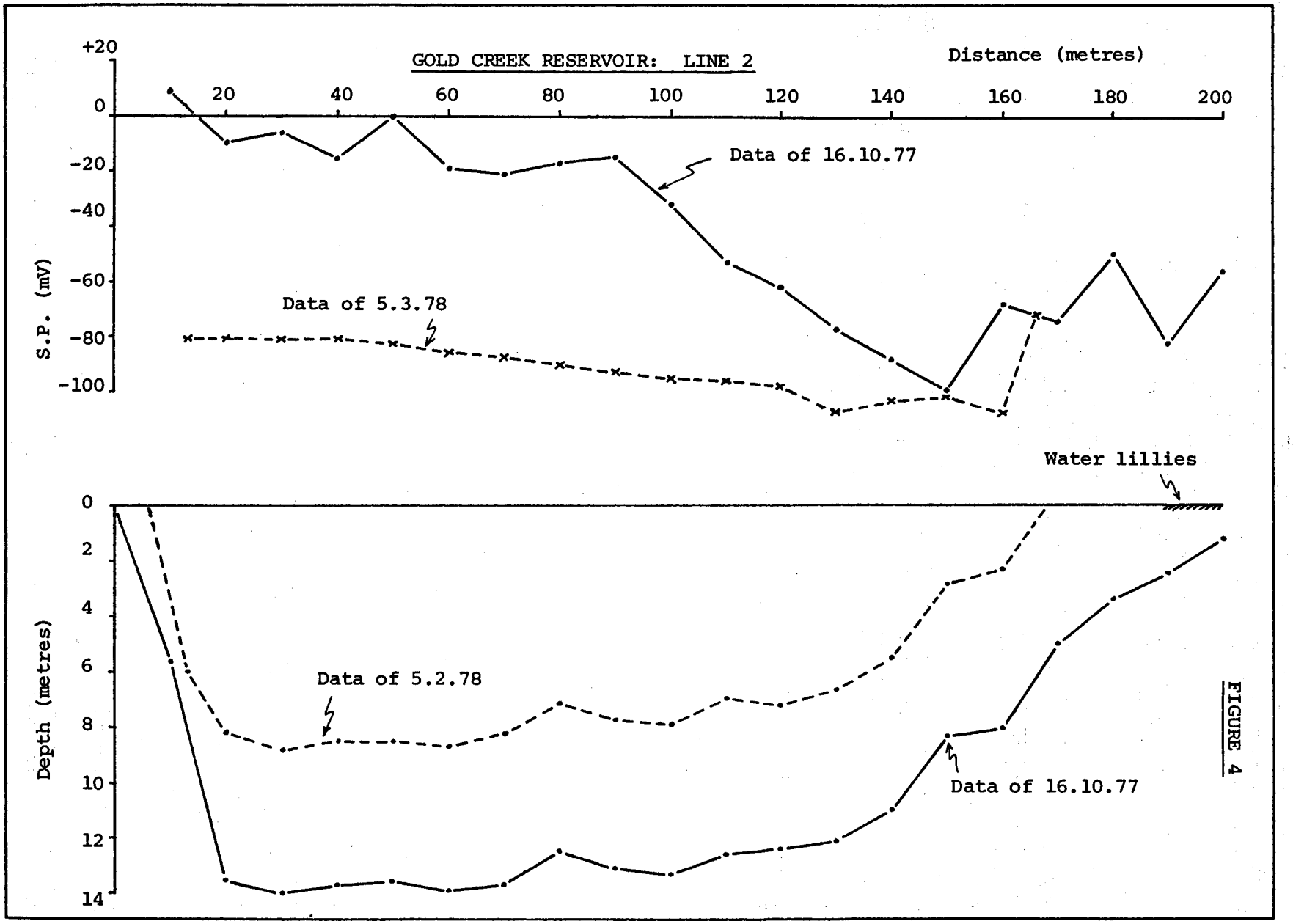
GOLD CREEK RESERVOIR: LINE 2
Distance (metres)
+20
0
-20
-40
-60
-80
-100
S.P. (mV)
20
40
60
80
100
120
140
160
180
200
Data of 16.10.77
Data of 5.3.78
Water lillies
0
2
4
6
8
10
12
14
Depth (metres)
Data of 5.2.78
Data of 16.10.77

FIGURE 4

FIGURE 5

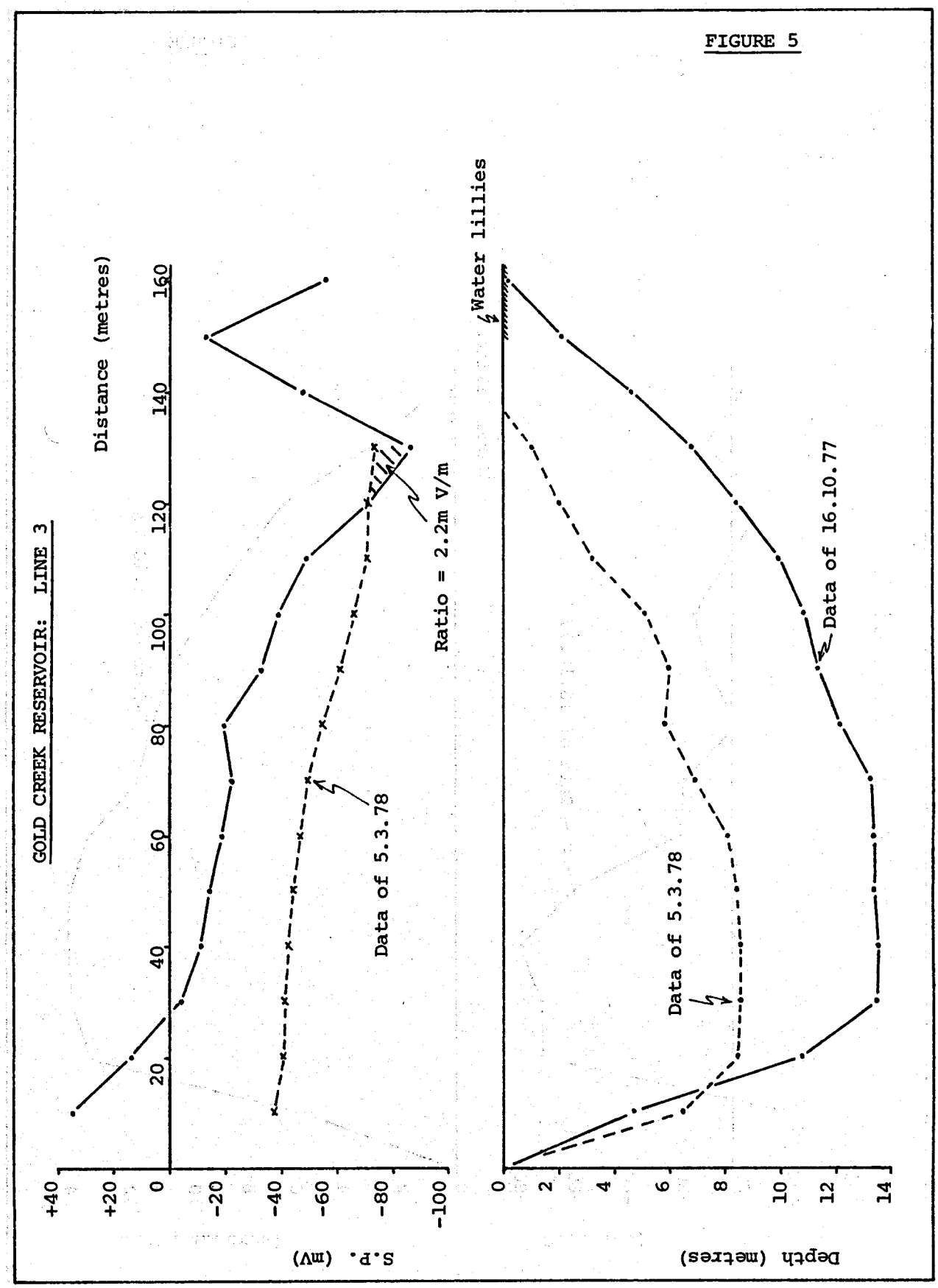
GOLD CREEK RESERVOIR: LINE 3
Distance (metres)
20
40
60
80
100
120
140
160
+40
+20
0
-20
-40
-60
-80
-100
S.P. (mV)
Ratio = 2.2m V/m
Data of 5.3.78
Water lillies
0
2
4
6
8
10
12
14
Depth (metres)
Data of 5.3.78
Data of 16.10.77

FIGURE 6

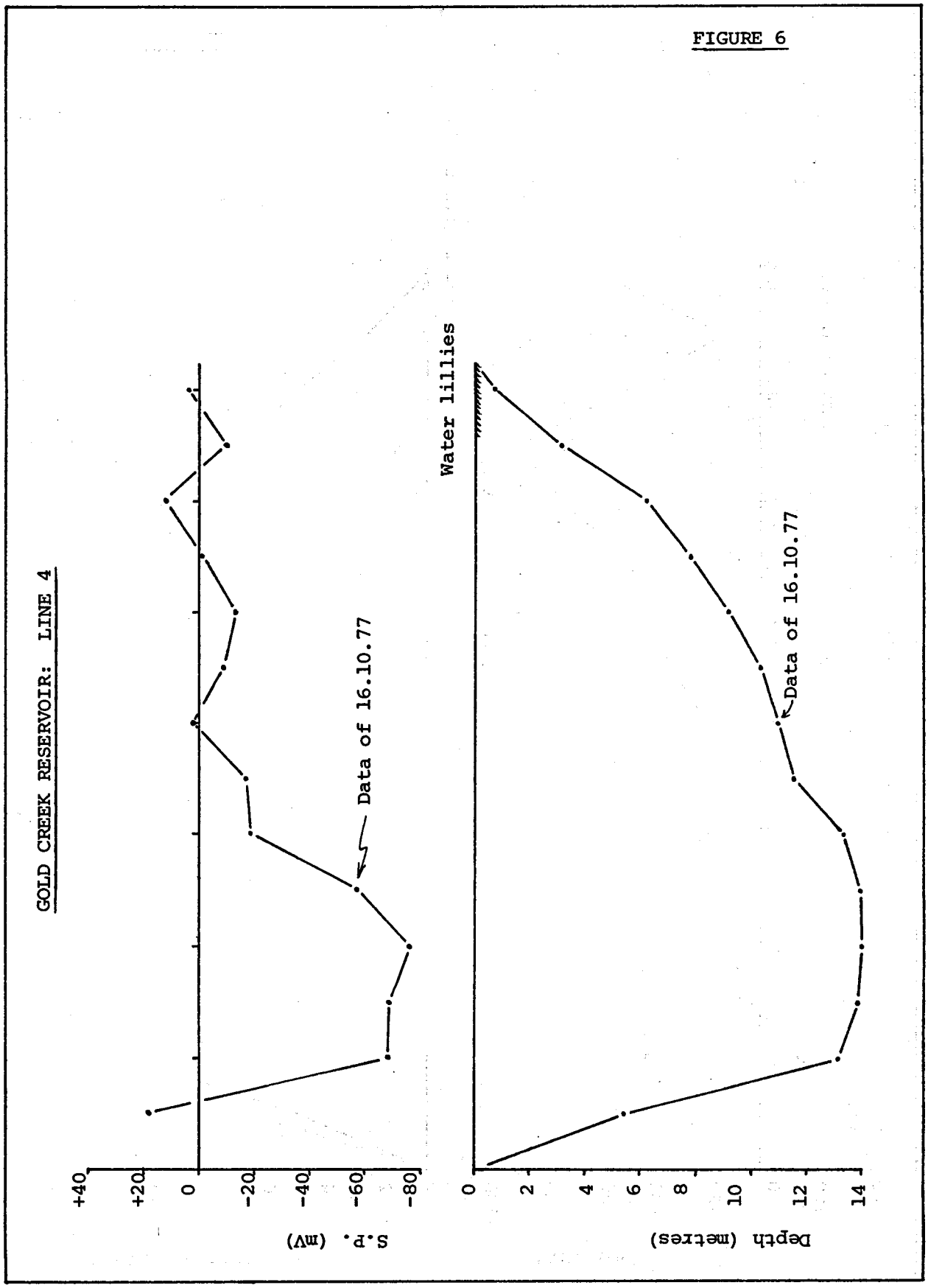
GOLD CREEK RESERVOIR: LINE 4
S.P. (mV)
+40
+20
0
-20
-40
-60
-80
Data of 16.10.77
Water lillies
Depth (metres)
0
2
4
6
8
10
12
14
Data of 16.10.77

Institute of Technology, for their support. Finally, gratitude is expressed to the Brisbane City Council for permission to collect data on Gold Creek Reservoir.

REFERENCES

ABAZA, M.M.I. and CLYDE, C.G., 1969: "Evaluation of the Rate of Flow through Porous Media using Electrokinetic Phenomena". Water Resources Research. Vol. 5 No. 2, p. 470-483.

JOHNSON, F., 1977 - personal communication: Caretaker, Gold Creek Reservoir.

GHOSH, B.N., RAKSHIT, S.C. and CHATTORAJ, D.K., 1953: "The Evaluation of True Zeta - Potentials of Quartz Particles of Different Size from Measurements of Streaming Potential". Jour. Indian Chem. Soc. Vol. 30 No. 9, p. 601-606.

LORENZ, P.B., 1952: "The Phenomenology of Electro-Osmosis and Streaming Potential". Jour. Phys. Chem. Vol. 56 p. 775-778.

OGILVY, A.A., AYED, M.A., and BOGOSLOVSKY, V.A., 1969: "Geophysical Studies of Water Leakages from Reservoirs". Geophysical Prospecting Vol. 17 p. 36-62.

PIRSON, S.J., and WONG, F.S., 1972: "The Neglected S.P. Curve". S.P.W.L.A. 13th Ann. Log. Symp., Trans., paper C.

POLDINI, E., 1938-9: "Geophysical Exploration by Spontaneous Polarisation Methods". The Mining Magazine. Nov. and Dec. 1938, Jan and Feb. 1939.

SCHRIEVER W., and BLEIL, C.E., 1957: "Streaming Potential in Spherical-grain Sands". Jour. Electrochem. Soc., p. 170-176.

STREET, N., 1961: "Electrokinetic Effects in Laboratory Permeability Measurement". Producers Monthly Vol. 25, p. 12-14.

K

Brent M. Haines has been a lecturer in geophysics and hydrogeology in the Dept. of Applied Geology, Queensland Institute of Technology since 1973. He graduated from the University of Sydney with a B.Sc. in geology and geophysics (1967) and an M.Sc. on water well logging (1971). He has worked as a field geophysicist with Pickands Mather & Co. International (Tasmania, 1966-7), and with the N.S.W. Water Resources Commission (1968 and 1972-3).

During 1969-71 he was employed by the University of Sydney, firstly as a demonstrator in exploration geophysics, then as Project Officer for an Australian Water Resources Council project on the interpretation of well logs in water-wells in unconsolidated sediments. He has published several papers on groundwater geophysics and water-well logging, and is presently working towards a Ph.D. at the University of Queensland. He is interim secretary, Australian Society of Exploration Geophysicists (Queensland Branch) and a member of S.P.W.L.A., S.E.G., E.A.E.G. and Australasian I.M.M.

ANALISIS DE REGISTROS GEOFISICOS EN ARENAS ARCILLOSAS METODO DE FERTL MODIFICADO

Miguel Linares Flores
Ramiro Garza de la Garza
Petróleos Mexicanos
Reynosa, Tams., México.

R E S U M E N

Se presenta el método de análisis de Registros Geofísicos para arenas arcillosas, basado en el trabajo publicado por Walter H. Fertl, en el que se considera que las resistividades de - agua de formación (Rw) no son de alta salinidad como para despreciarlas con respecto a la resistividad de la arcilla diseminada (Rc). Se incluyen ciertas modificaciones para la determinación de la saturación de agua (Sw) cuando no se conoce la constante "a" función de la tortuosidad y el factor de cementación — "m".

También se incluye, la variación de la saturación de agua, al variar el exponente de saturación de la zona lavada (n') cuando se toma en cuenta la resistividad del filtrado de lodo (Rmf), permeabilidad (K) y salinidad de agua (P) y se considera variable la resistividad de la arcilla diseminada.

I N T R O D U C C I O N

En la actualidad, las computadoras electrónicas han -- venido a solucionar el problema de resolver modelos muy laboriosos que con anterioridad se hacían manualmente y con la consiguiente pérdida de tiempo, debido al número de ecuaciones que intervienen en el modelo y de las combinaciones que son necesarias efectuar.

Con la ayuda de las computadoras ha sido posible someter a variaciones los parámetros petrofísicos que intervienen en las ecuaciones de los análisis de registros geofísicos, de modoque se observen comportamientos. Esto es debido a que los datos necesarios para resolver las ecuaciones están relacionadosdirectamente con las propiedades de las rocas almacenadoras y de los fluidos que contienen, que para conocerlos se necesitan muestras representativas, de las cuales por lo general no se dispone.

El método se basa en trabajos presentados en la literatura y requiere de la combinación de un registro de resistividad y uno de porosidad, además de la presencia de una arena invadida de agua, aunque no se disponga de todos los datos para su apli-- cación.

CONSIDERACIONES TEORICAS

Este estudio es un método de análisis de arenas arcillosas basado en el artículo de Walter H. Fertl[1].

El artículo original, toma como referencia el trabajo de Alger[2] donde presenta la ecuación de saturación de agua, basada en el modelo de arcilla dispersa.

$$Sw = \sqrt{\frac{\frac{Fz\ Rw}{Rt} + \left[q\frac{(Rc-Rw)}{2\ Rc}\right]^2 - q\frac{(Rc+Rw)}{2\ Rc}}{1-q}} \qquad (1)$$

donde:

Sw - Saturación de agua

Fz - Factor de formación correspondiente a la porosidad total.

Rw - Resistividad del agua de la formación

Rt - Resistividad verdadera de la formación

q - Fracción de la porosidad total ocupada por arcilla

Rc - Resistividad de la arcilla dispersa

En ese mismo trabajo, se propuso que la arcilla dispersa, debe ser considerada como una mezcla dentro de los fluidos de la formación y que la fracción del volumen poroso de arena ocupado por arcilla queda descrita - - - por la ecuación:

$$q = \frac{\phi_s - \phi_D}{\phi_s} \qquad (2)$$

donde:

ϕ_s y ϕ_D - Porosidad obtenida de los registros sónico y densidad.

En el trabajo de Fertl se hacen las siguientes consideraciones:

Las respuestas de los registros de densidad y sónico en arenas arcillosas-invadidas de agua pueden ser expresadas como:

$$\phi_D = \phi_e + x_1 . \ Vsh \qquad (3)$$

$$\phi_s = \phi_e + x_2 . \ Vsh \qquad (4)$$

donde:

ϕ_e – Porosidad efectiva de la formación

Vsh – Volumen de lutita, obtenida de algún indicador de lutita como resistividad, potencial espontáneo (SP), rayos gamma y porosidad neutrón.

$x_1 = \frac{\rho ma - \rho sh}{\rho ma - \rho f}$ – factor de corrección por lutita a la respuesta del registro de densidad, como una función de la densidad de la matriz de la arena (ρma), de la densidad de la lutita (ρsh) y de la densidad del filtrado del lodo (ρf).

$x_2 = \frac{\Delta tsh - \Delta tma}{\Delta tf - \Delta tma}$ - factor de corrección por lutita a la respuesta del registro sónico, como una función del tiempo de tránsito de la matriz de la arena (Δtma), de la lutita (Δtsh) y del filtrado del lodo. (Δtf)

Restando la ecuación (3) de la (4) se obtiene:

$$\phi_s - \phi_D = a_1 \, Vsh \qquad (5)$$

entonces

$$\phi_s = \phi_D + a_1 \, Vsh \qquad (6) \text{ y}$$

$$\phi_D = \phi_s - a_1 \, Vsh \qquad (6A) \text{ siendo}$$

$$a_1 = x_2 - x_1$$

Donde x_2 por lo general varía entre 0.2 y 0.4, x_1 es comunmente muy-pequeño (0.05 a 0.10), a_1 se na encontrado entre 0.15 y 0.36. En tres-pozos del D.F.N.E. x_2 estuvo entre 0.26 y 0.42, x_1 entre 0.06 y 0.12 y a_1 entre 0.19 y 0.29.

Substituyendo las ecuaciones (5) y (6) en (2) se tiene:

$$\eta = \frac{a_1 . \, Vsh}{\phi_D + a_1 . Vsh} \qquad (7)$$

Esta ecuación (7) se substituye en la (1) y queda:

$$Sw = \frac{\sqrt{\frac{Fz \, Rw}{Rt} + \left[\frac{a_1 \, Vsh}{\phi_D + a_1 Vsh} \cdot \frac{Rc - Rw}{2 \, Rc}\right]^2} - \frac{a_1 \, Vsh}{\phi_D + a_1 \, Vsh} \cdot \frac{Rc + Rw}{2 \, Rc}}{1 - \frac{a_1 \, Vsh}{\phi_D + a_1 \, Vsh}} \qquad (8)$$

En la actualidad, en los pozos de desarrollo se cuenta con un juego li-- mitado de registros, en esos casos, la ecuación (8) puede ser aplicada tomando la forma correspondiente de acuerdo con los datos con que se cuente.

1. RESISTIVIDAD - DENSIDAD

Se tienen dos opciones:

1.1 Cuando no se dispone de la constante "a" función de la tor— tuosidad y del factor de cementación (m), la ecuación (8), se puede simplificar como sigue:

$$Sw = \frac{\sqrt{\frac{Fz\,Rw}{Rt}(\phi_D + a_1 Vsh)^2 + \left[\frac{a_1 Vsh\,(Rc-Rw)}{2Rc}\right]^2} - \frac{a_1 Vsh\,(Rc+Rw)}{2Rc}}{\phi_D} \qquad (9)$$

Los parámetros que intervienen en la ecuación anterior, se- obtienen de:

Fz - El factor de formación, se puede determinar de su valor aparente corrigiendo la saturación de agua en la zona lavada (S_{xo}), por hidrocarburos residuales:

$$Fz = \frac{R_{xo}}{Rmf}(S_{xo})^{n'} \qquad (10)$$

donde:

R_{xo} - Lectura de resistividad de la zona lavada deter— minada del micro-registro, micro-laterolog o de la normal corta.

Rmf- Resistividad del filtrado de lodo.

S_{xo} - Saturación de agua en la zona lavada.

n' - Exponente que es función de la resistividad del — filtrado de lodo, permeabilidad y salinidad del - agua de la formación (P).

Para determinar la S_{xo} se utiliza la expresión[3].

$$S_{xo} = 1 - fhr\,(1-Sw_1) \qquad (11)$$

donde:

fhr - factor de corrección por hidrocarburos residuales, - que estadísticamente se toma igual a 0.5.

n' - El exponente de saturación de la zona lavada[4], ha - sido definido por cualquiera de las siguientes tres ex presiones, según los datos con que se cuente.

$$n' = 0.904 - 0.515 \log Rmf_1 + 0.325 \log K \qquad (12)$$

$$n' = 1.347 - 0.519 \log Rmf_1 \qquad (13)$$

$$n' = 1.095 + 0.442 \log P \qquad (14)$$

donde:

Rmf_1 - Resistividad del filtrado del lodo a 24°C

K - Permeabilidad de la formación

P - Salinidad del agua de formación en 10^3ppm. de - cloruro de sodio.

Rw - La salinidad del agua de formación en el D.F.N.E. en arenas varía entre 10×10^3 y 60×10^3 ppm. de - NaCl como para considerar la resistividad de la mis ma como despreciable y poder simplificar aún más- la ecuación (9), como sucede en otros trabajos.

Rt - La resistividad verdadera de la formación, obtenida del registro de inducción.

ϕ_D - La porosidad determinada de la lectura del registro de densidad de acuerdo con:

$$\phi_D = \frac{\rho_{ma} - \rho_b}{\rho_{ma} - \rho_{fl}} \qquad (15)$$

donde:

ρ_b - Densidad de la formación.

a_1 - Al coeficiente se le puede asignar el valor promedio de la estadística de los E.E. U.U. en caso de no dis poner de un valor fijo, por considerar a las forma-- ciones semejantes a las del D.F.N.E.

Vsh - El valor de Vsh[5], se determina de los indicadores de arcilla siguientes:

1. Resistividad $Vsh = \sqrt{\frac{Rsh}{Rt}}$ (16)

Rsh - Resistividad de la lutita vecina a la arena en análisis .

2. Potencial espontáneo. $Vsh = 1 - \frac{PSP}{SSP}$ (17)

PSP - Potencial espontáneo del punto analizado.

SSP - Potencial espontáneo de una arena 100% invadida de agua.

3. Rayos Gamma. $Vsh = \frac{GR - GR_1}{GR_2 - GR_1}$ (18)

GR - Lectura de rayos gamma del punto en análisis

GR_1 - Lectura de rayos gamma en arenas limpias

GR_2 - Lectura de rayos gamma en las lutitas vecinas al punto en análisis.

4. Neutrón $Vsh = \frac{\phi N}{\phi N_{sh}}$ (19)

ϕ_N - Porosidad del registro neutrón de la arena en estudio

$\phi_{N_{sh}}$ - Porosidad del registro neutrón en una lutita vecina a la arena analizada.

Rc - La resistividad de la arcilla dispersa en los espacios porosos de un yacimiento, se supone que es menor que el de las lutitas adyacentes, para lo cual, se han reportado en la literatura los valores siguientes:

$Rc = 0.5\ Rsh$[6] (20)

$Rc = 0.4\ Rsh$[7] (21)

$Rc = 10\ Rw$[8] (22)

1.2 Cuando se tienen la constante "a" función de la tortuosidad y el factor de cementación, se substituye el factor de formación por:

$Fz = \frac{a}{\phi_s^m}$ (23), donde además por la ecuación (6) queda :

$$Fz = \frac{a}{(\phi_D + a_1\ Vsh)^m} \quad (24)$$

finalmente: (25)

$$Sw = \frac{\sqrt{\frac{a}{(\phi_D + a_1 Vsh)}\, m\, \frac{Rw}{Rt}\,(\phi_D + a_1 Vsh)^2 + \left[\frac{a_1 Vsh(Rc-Rw)}{2\,Rc}\right]^2} - \frac{a_1 Vsh(Rc+Rw)}{2\,Rc}}{\phi_D}$$

Las ecuaciones (9) y (25) son las ecuaciones de saturación de agua para la combinación de registros Resistividad-Densidad.

La ecuación (8), toma otras formas cuando se tiene la combinación:

2. RESISTIVIDAD - SONICO.

Como en el caso de la combinación Resistividad-Densidad, aquí también se tienen dos ecuaciones de saturación de agua. Al substituir las ecuaciones (6) y (6A) en (9) queda:

$$Sw = \frac{\sqrt{\frac{Fz\,Rw}{Rt}(\phi_s)^2 + \left[\frac{a_1 Vsh(Rc-Rw)}{2\,Rc}\right]^2} - \frac{a_1 Vsh\,(Rc+Rw)}{2\,Rc}}{\phi_s - a_1 Vsh} \qquad (26)$$

y substituyendo (6) y (6A) en (25) dá:

$$Sw = \frac{\sqrt{\frac{a}{\phi_s m}\,\frac{Rw}{Rt}\,\phi_s^2 + \left[\frac{a_1 Vsh(Rc-Rw)}{2\,Rc}\right]^2} - \frac{a_1 Vsh(Rc+Rw)}{2\,Rc}}{\phi_s - a_1 Vsh} \qquad (27)$$

en las que:

$$\phi_s = \frac{\Delta t - \Delta tma}{\Delta t_f - \Delta tma} \cdot \frac{1}{Cp} \cdot fhcs. \qquad (28)$$

en donde:

Δt - Tiempo de tránsito de el punto en análisis.

Cp - Factor de corrección por falta de compactación.

fhcs - Factor de corrección por hidrocarburos[9], 0.7 para gas y 0.9 para aceite.

SECUELA DE CALCULO

Las ecuaciones (9) y (26) se resuelven por medio de ensaye y error siguiendo la siguiente secuela:

a) Se inicia por resolver la ecuación (11), suponiendo un valor de Sw_1, el cual estará de acuerdo con la Sw media en el área.

b) Se resuelven las ecuaciones (12), (13) ó (14), según los datos con que se cuente y se substituye el valor de Sxo en la ecuación (10).

c) Se obtiene la Vsh con los indicadores de arcilla, eligiéndose el mínimo. Con este último y los demás factores, se calcula Sw.

d) Se compara la Sw_1 supuesta con la Sw calculada, tomando en cuenta una tolerancia, en caso de que no se cumpla, la Sw calculada se supone como la nueva Sw_1, repitiendo la secuela hasta satisfacer la tolerancia, la cual se toma igual a 0.001 en este caso.

e) Al concluir los cálculos de Sw, el siguiente paso es determinar la constante "a" función de tortuosidad y el factor de cementación "m". En la combinación Resistividad-Densidad se tiene:

$$\log a = \frac{A \log (\phi_D + a_1 Vsh) + \log Fz}{1 + B \log (\phi_D + a_1 Vsh)} \qquad (29)$$

$$m = \frac{\log \frac{a}{Fz}}{\log (\phi_D + a_1 Vsh)} \qquad (30)$$

En la combinación Resistividad-Sónico es:

$$\log a = \frac{A \log \phi_s + \log Fz}{1 + B \log \phi_s} \qquad (31)$$

$$m = \frac{\log \frac{a}{Fz}}{\log \phi_s} \qquad (32)$$

Los valores de las constantes A y B corresponden a la estadística llevada a cabo con datos de todo el sistema[4] obteniéndose los siguientes datos:

	Arenas	Carbonatos
A	1.8	2.03
B	1.29	0.9

En caso de que se conozcan la constante "a" función de la tor-

tuosidad y el factor de cementación, la saturación de agua se - puede calcular con las ecuaciones (25) y (27), de acuerdo con la combinación de registros geofísicos disponibles. Cuando solo - se conoce el exponente decementación, antes de determinar la - Sw, se obtiene el valor de "a" con:

$$a = 10^{\frac{A - m}{B}} \qquad (33)$$

donde A y B, son las constantes mencionadas previamente.

f) Después de calcular la Sw, se puede determinar la porosidad -- efectiva ϕ_e, según la combinación de registros que se haya usado,con:

$$\phi_e = \phi_D - x_1 \, Vsh \qquad (3')$$

$$\phi_e = \phi_s - x_2 \, Vsh \qquad (4')$$

También se puede calcular el factor de formación con:

$$F = \frac{a}{\phi_e^{\,m}} \qquad (23')$$

g) Con base en lo anterior se puede calcular el volumen de hidrocarburos movibles de acuerdo a:

$$Vhc_{mov.} = \phi_e \, (Sxo - Sw) \qquad (34)$$

h) Además, de acuerdo con las gráficas[4] de F vs Ø, cuyos orígenes son:

	Ø	F
Arenas	17.0	25
Carbonatos	7. 8	182

se puede localizar el cuadrante al cual corresponde el factor de - cementación "m".

E J E M P L O S :

Se presenta como ejemplo, el cálculo de la saturación de agua de la arena - P-12 A en el pozo Oasis No. 9D, en la Fig. No. 5 se presenta la sección de los registros donde aparece esta arena y los resultados en la Tabla No. 1. El formato de la Tabla No. 1 es el siguiente:

Profundidad en metros — Como consecuencia de usar la computadora, la - lectura de profundidad puede hacerse a intervalos tan pequeños como se desee (0.20, 0.50 m. etc.).

Porosidad efectiva (FIE) en fracción. En esta columna además del valor de ϕ_e aparece el símbolo S ó D según se haya usado registro sónico o densidad respectivamente.

Factor de formación F. — Como resultado de las constantes "a" y "m" y la porosidad efectiva.

Exponente de cementación (M). — Este factor se calcula para cada una de las profundidades incluídas. Cuando se dá como dato, aparece un solo valor.

Cuadrante de M. — El significado de esta columna es el de dar una idea de la situación de M en la gráfica de F vs Ø estando M como parámetro, su ubicación normal es NW ó SE.

Tortuosidad A — Este valor también se calcula para cada una de las profundidades. En caso de darse como dato, se registra un solo valor.

Volumen de arcilla Vsh. — En esta columna aunado al valor de Vsh, se encuentra el símbolo de RT y GR lo que significa que en ese punto el indicador de arcilla utilizado fué resistividad y rayos gamma. También tiene-

la opción de poner N y SP en el caso de utilizar - registro neutrón y potencial espontáneo.

Saturación de agua (Sw) Corregida por el contenido y resistividad de la - arcilla.

Volumen de hidrocarburos movibles. Refleja la fracción de los hidrocarburos totales que van a ser movibles.

CONCLUSIONES

Por este método de Fertl modificado, se puede determinar:

- El valor de la constante de tortuosidad "a" y el factor de cementación "m" que intervienen en la evaluación del Factor de Formación.
- La porosidad efectiva se obtiene como consecuencia de corregir la porosidad aparente por contenido de arcilla.
- La cantidad de hidrocarburos movibles.

REFERENCIAS:

1. Shaly sands analysis in development wells.
   Walter H. Fertl. SPWLA Logging Symposium
   Transactions 1975.

2. Formation density log application in liquid filled holes.
   Alger R. P. et al J. Petroleum Technology. March 1963.

3. Log analysis of sand-shale sequences-A systematic approach.
   A. Poupon et al. Journal Petroleum Technology. July 1970.

4. Un método práctico para determinar exponentes de cementación y otros parámetros como ayuda en el análisis de registros de pozos.
   Gómez Rivero O. Petróleos Mexicanos.
   Suptcia. Gral. de Ingría. de Yacimientos, México, D.F. Agosto de 1972

5. The evaluation of clay content from logs.
   Poupon A. and Gaymond R. Transactions SPWLA 1970.

6. A contribution to electric log interpretation in shaly sands.
   A. Poupon et al Journal Petroleum Technology. August 1954.

7. Conductive en miliev poreus argileux. Interpretation des Diagraphies. Atlan et al. Colloque de 1'ARTFP.
   Pau, Sept. 23 - 26, 1968.

8. Log evaluation of low resistivity pay sands in the Gulf Coast.
   Tixier M.P. Transactions of SPWLA. June 1968.

9. Log interpretation charts, Schlumberger well surveying Corporation, Houston, Tex. 1966.

10. Programa de cómputo: Compresión Escalonada. S.G.I.Y. México, D.F.

TABLA Nº 1

P E T R O L E O S M E X I C A N O S
DEPTO. DE INGENIERIA DE YACIMIENTOS

ANALISIS DE REGISTROS GEOFISICOS POR EL METODO DE FERTL -MODIFICADO-

DISTRITO FRONTERA NORESTE, Z.N. OASIS NO 9-C

ARENA P-12 A

PROFUNDIDAD MTS.	POROSIDAD FIE	FACTOR DE FORMACION, F	EXPONENTE DE CEMENTACION, M	CUADRANTE DE M	TORTUOSIDAD -A-	VOLUMEN DE ARCILLA, VSH	SATURACION DE AGUA, SW	VOL. HIDROCARB. MOVIBLES
1805.00	0.11	116.37	3.37	SE	0.06	0.63 RT	0.20	0.04
1805.50	0.11	87.64	3.33	SE	0.06	0.60 RT	0.19	0.05
1806.00	0.22	10.04	3.30	NW	0.07	0.25 GR	0.28	0.06
1806.50	0.25	6.86	3.26	NW	0.07	0.16 GR	0.29	0.09
1807.00	0.25	6.29	3.41	NW	0.06	0.13 GR	0.29	0.09
1807.50	0.30	3.91	3.12	NW	0.09	0.00 GR	0.30	0.11
1808.00	0.29	4.26	3.30	NW	0.07	0.03 GR	0.28	0.10
1808.50	0.30	3.83	3.30	NW	0.07	0.00 GR	0.31	0.10
1809.00	0.28	3.83	3.63	NW	0.04	0.00 GR	0.33	0.09
1809.50	0.31	3.13	3.36	NW	0.06	0.00 GR	0.33	0.10
1810.00	0.28	4.58	3.42	NW	0.06	0.09 GR	0.33	0.09
1810.50	0.26	6.97	2.95	NW	0.13	0.25 GR	0.31	0.09
1811.00	0.27	6.23	2.84	NW	0.16	0.25 GR	0.29	0.10
1811.50	0.29	5.26	2.80	NW	0.17	0.19 GR	0.30	0.10
1812.00	0.32	4.59	2.61	NW	0.23	0.09 GR	0.34	0.11
1812.50	0.32	5.00	2.53	NW	0.27	0.16 GR	0.32	0.11
1813.00	0.26	7.80	2.60	NW	0.24	0.31 GR	0.29	0.09
1813.50	0.22	11.38	2.65	NW	0.15	0.38 GR	0.30	0.08
1814.00	0.19	17.22	2.85	NW	0.15	0.50 GR	0.33	0.06
1814.50	0.11	66.01	2.61	SE	0.24	0.76 RT	0.35	0.04
1815.00	0.13	44.23	2.17	SE	0.51	0.71 RT	0.43	0.04
1815.50	0.16	27.17	4.74	SE	0.01	0.31 GR	0.25	0.06
1816.00	0.16	29.63	4.19	SE	0.01	0.38 GR	0.29	0.06
1816.50	0.22	11.30	2.78	NW	0.17	0.34 GR	0.36	0.07
1817.00	0.24	9.23	2.78	NW	0.17	0.31 GR	0.35	0.08
1817.50	0.23	9.78	2.88	NW	0.15	0.31 GR	0.35	0.08
1818.00	0.24	8.10	3.08	NW	0.10	0.28 GR	0.32	0.08
1818.50	0.24	7.99	3.12	NW	0.10	0.28 GR	0.32	0.08
1819.00	0.22	10.28	3.12	NW	0.10	0.34 GR	0.31	0.08
1819.50	0.22	10.39	3.08	NW	0.10	0.34 GR	0.31	0.08
1820.00	0.24	8.73	2.87	NW	0.15	0.28 GR	0.36	0.08

DATOS FIJOS EN LOS CALCULOS
RSH? 2.0 SW1?0.05 SSP? 0 GR1? 24 GR2? 56 FINSH?0.00 PT? 2029.5 TF? 79.0 TS? 23.0
Nº FIMA? 0.0 RMF1? 2.71 K? 5.30 P? 0.0 RW1?0.37 RC?0.80 CP?1.00 FHC?1.00 FHR? 0.5 A? 0.00 M? 0.00 A1?0.24 X1?0.06 X2?0.30

LOS DATOS FUERON TOMADOS DEL REGISTRO SONIC

JUNIO 29 DE 1976 AMADO MARINA P.

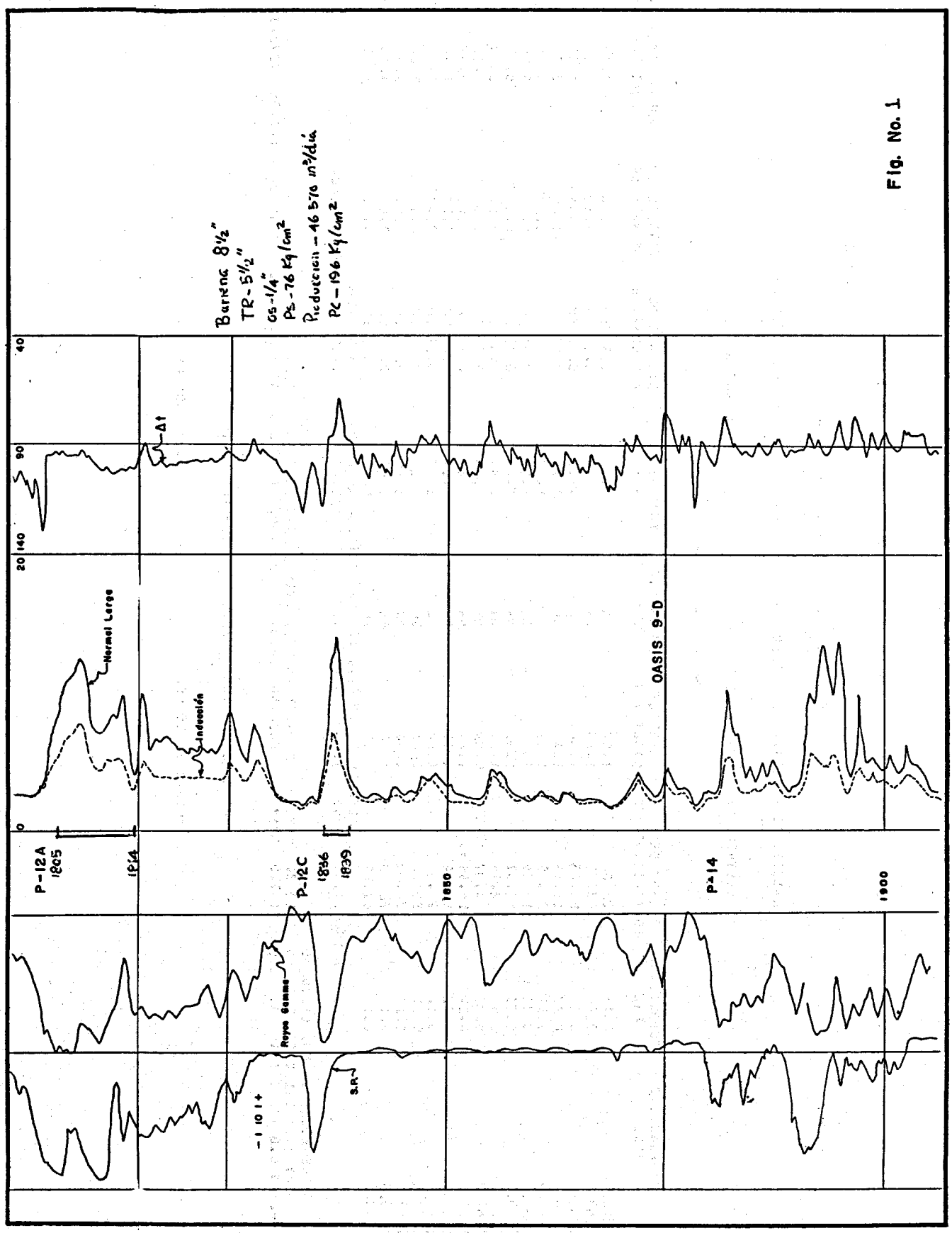
Barena 8½"
TR-5½"
GS-1/4"
Ps-76 Kg/cm²
Reduccion -46 570 m³/día
Pc-196 Kg/cm²
Fig. No. 1
40
90
140
20
0
Normal Large
Induccion
OASIS 9-D
P-12A
1805
1814
P-12C
1836
1839
1850
P-14
1900
Rayos Gamma
-1101+
S.P.

TABLA Nº 2

P E T R O L E O S M E X I C A N O S
DEPTO. DE INGENIERIA DE YACIMIENTOS

ANALISIS DE REGISTROS GEOFISICOS POR EL METODO DE FERTL -MODIFICADO-

DISTRITO FRONTERA NORESTE, Z.N. POZO CANTINA NO 1

CPO. A 1483.0 M

PROFUNDIDAD MTS.	POROSIDAD FIE	FACTOR DE FORMACION, F	EXPONENTE DE CEMENTACION, M	CUADRANTE DE M	TORTUOSIDAD -A-	VOLUMEN DE ARCILLA, VSH	SATURACION DE AGUA, SW	VOL. HIDROCARB. MOVIBLES
1483.0	0.18	22.64	1.57	NW	1.50	0.69 SP	0.46	0.05
1483.5	0.27	13.85	1.23	NW	2.79	0.38 SP	0.53	0.06
1484.0	0.24	15.23	1.37	NW	2.15	0.46 SP	0.49	0.06
1484.5	0.23	15.45	1.48	NW	1.76	0.42 SP	0.46	0.06
1485.0	0.19	20.09	1.42	NW	1.97	0.46 SP	0.50	0.05
1485.5	0.22	16.29	1.44	NW	1.89	0.46 SP	0.48	0.06
1486.0	0.30	11.57	1.31	NW	2.40	0.31 SP	0.57	0.06
1486.5	0.42	8.15	1.20	NW	2.89	0.00 SP	0.56	0.09
1487.0	0.32	14.37	0.83	NW	5.63	0.23 SP	0.65	0.06
1487.5	0.24	14.95	1.44	NW	1.89	0.42 SP	0.45	0.07
1488.0	0.22	17.74	1.15	NW	3.17	0.46 SP	0.51	0.06
1488.5	0.17	24.06	1.62	NW	1.37	0.62 SP	0.41	0.05
1489.0	0.14	33.38	1.67	SE	1.26	0.69 SP	0.43	0.04
1489.5	0.17	24.32	1.08	NW	3.60	0.62 SP	0.57	0.04
1490.0	0.18	22.43	1.42	NW	1.98	0.58 SP	0.46	0.05
1490.5	0.13	41.60	1.75	SE	1.08	0.57 SP	0.42	0.04

EL VALOR DE SW NO ESTA EN LOS LIMITES IND.-SON. SIN AY?0 M

H?1540.00 FIS? 0.2 SXO? 0.8 FZ? 20.42 SH? 1.11 ITERACION NO. 0

DATOS FIJOS EN LOS CALCULOS

RSH? 2.0 SW1?0.50 SSP? 65 GR1? 27 GR2? 75 FINSH?0.45 PT? 1915.0 TF? 95.0 TS? 22.0

Nº RIMA? 0.0 RMF1? 1.15 K? 1.00 P? 0.0 RW1?0.07 RC?0.80 CP?1.00 FHC?1.00 FHR? 0.5 A? 0.00 M? 0.00 A1?0.24 X1?0.06 X2?0.30

LOS DATOS FUERON TOMADOS DEL REGISTRO SONICO

AGOSTO 24 DE 1976 J. M. MORALES S.

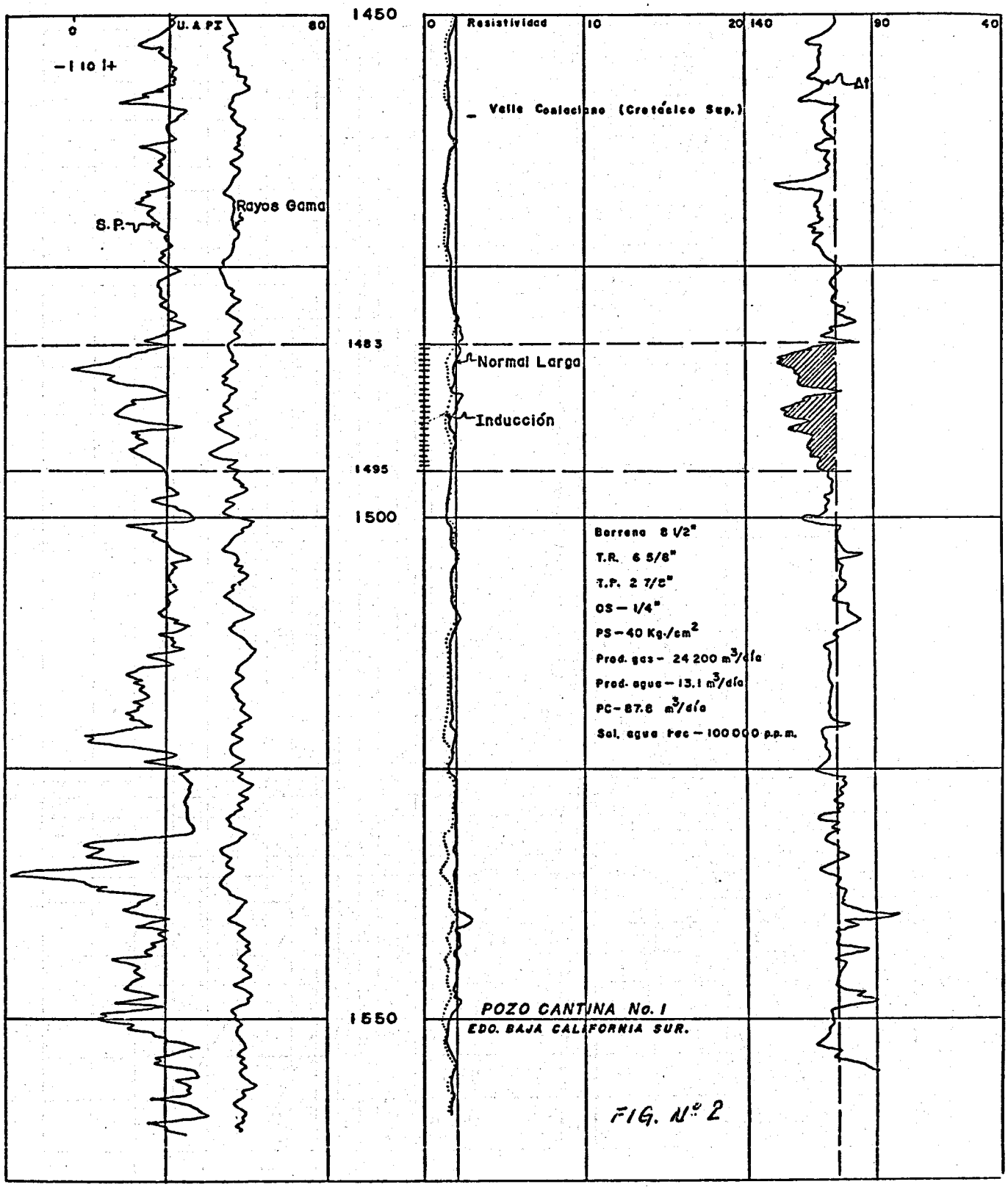
0
U. A PI
80
-1 10 1+
S.P.
Rayos Gama
1450
0
Resistividad
10
20
140
90
40
Δt
Valle Coniaciano (Cretácico Sup.)
1483
Normal Larga
Inducción
1495
1500
Barrena 8 1/2"
T.R. 6 5/8"
T.P. 2 7/8"
OS — 1/4"
PS — 40 Kg./cm²
Prod. gas - 24 200 m³/día
Prod. agua — 13.1 m³/día
PC — 87.6 m³/día
Sal. agua frc — 100 000 p.p.m.
1550
POZO CANTINA No. 1
EDO. BAJA CALIFORNIA SUR.

FIG. Nº 2

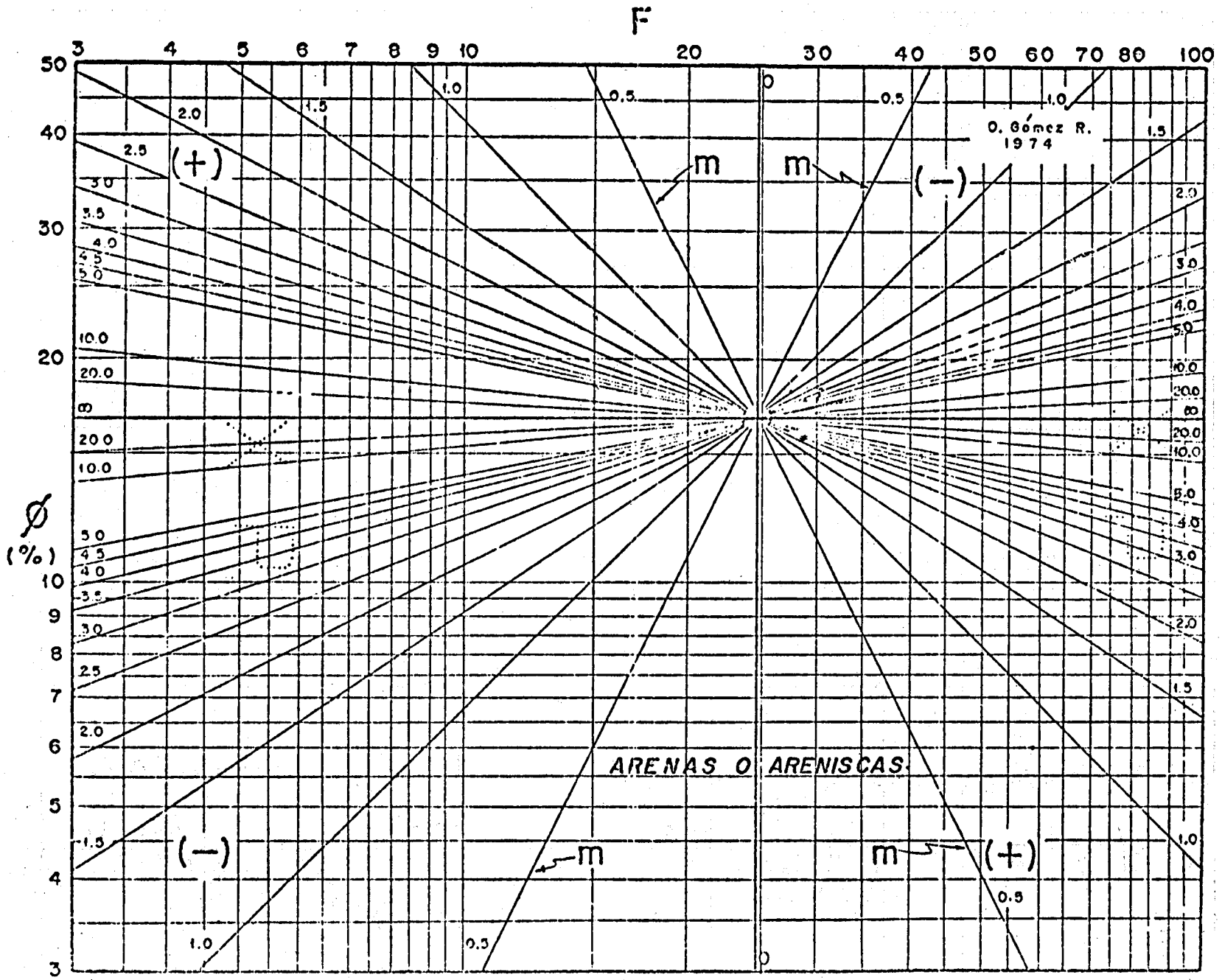
F
3 4 5 6 7 8 9 10 20 30 40 50 60 70 80 100
50 40 30 20 10 9 8 7 6 5 4 3
Ø (%)
O. Gómez R. 1974
(+)
(−)
m
m
(−)
m
m
(+)
ARENAS O ARENISCAS.

FIG. Nº 3

MINERAL COMPOSITION, AN AID IN CLASSICAL LOG ANALYSIS USED IN JURASSIC SANDSTONES OF THE NORTHERN NORTH SEA.

Ø. Nyberg
K. Lien
P.A. Lindberg
J.K. Smistad

Den norske stats oljeselskap a/s
Statoil, Stavanger, Norway

ABSTRACT

The complex mineralogy of the Jurassic sandstones of the Northern North Sea have made the porosity evaluation from logs difficult. To illustrate the problems involved, two typical wells have been used in this paper.

Mineralogical and chemical analysis were performed on 15 samples in well A, by thin section study and x-ray flourescence. The samples contain considerable amounts of potassium feldspar, mica and a variable amount of siderite. The chemical composition shows an appreciable amount of K_2O in accordance with the content of potassium feldspar and mica.

As the characteristics of these minerals affect the logs and are significant contributors to the radioactive measurements, the quantified results of the mineral study give an important contribution to the porosity evaluation.

The data from the mineral analysis together with core and logs were compiled into a computerized model for calculation of porosity. The calculated results were then compared to previous evaluations based on logs alone. The values of porosity show a significant difference where the "shaly sand approach" gives too low a porosity, even to the extent that it neglected productive zones.

Based on aquired information it can be said that by introduction of quantified mineral analysis to the porosity evaluation, the confidence level of the calculated values has increased in zones where the standard petrophysical measurements do not measure the rock properties in enough detail.

INTRODUCTION

The Northern North Sea basin consists of thick Mesozoic and Tertiary sediments. The oil fields of the basin are situated along a north-south rift whose bounding faults lie on either side of the median line separating the British and Norwegian part of the continental shelf. Many of the Jurassic oil reservoirs are trapped on the crest of faulted and tilted blocks. The main Jurassic reservoir occur in the Middle Jurassic stratigraphic horizons and represent parts of regressive cycles of complex delta systems built out across the northern North Sea region. Phases of tectonic movement in the Jurassic period resulted in erosion of Caledonian basement blocks. The igneous and the metamorphic rocks of the basement are one of the sources of the sediments and yielded mineralogical immature arkosic sands with abundant feldspar and mica. These minerals are of great significance when considering the evaluation and development of the reservoirs.

The zones studied are interpreted to represent the prograding marine part of a delta-environment, and are found to be mainly of one single upward fining sequence. The beds consist of planar cross-laminated, very fine to fine grained and well sorted sandstones. The mica percentage fluctuates but tend to increase when the grain size of the sandstone decreases. Carbonate cemented streaks and well defined carbonate horizons with no visible porosity are irregularly distributed within the sandstones.

The micaceous part of the Jurassic sandstones has been a challenge to the log analyst for the last years. Since the "mica" has been so clearly visible in the core material, the problem has typically enough been characterized as the "mica problem". To fully understand the effect of the mica on petrophysical measurements, several approaches have been tried, although none is fully acceptable.

This paper will indicate that not only the micaceous minerals have to be considered, but that all radioactive and heavy minerals have to be taken into account in the porosity calculation. This makes the evaluation rather complex and can cause productive zones to be overlooked by use of only classical log interpretation.

The model calculates porosity values well within the tolerances against core porosities and in addition gives a reasonable mineral distribution compared to the mineralogical and geochemical results. This of course gives a much higher confidence level to the total results.

From the complex procedures a more simplified log interpretation was developed which also seems to offer satisfactory results.

For the remaining part of the study the discussion will be limited to Well A and B which are typical examples from the "micaceous Jurassic sandstone".

For plots and figures, see appendix.

CONVENTIONAL LOG ANALYSIS

The following logs are used in the evaluation:

- Density/Neutron - Gamma Ray
- Induction/Acoustic - Gamma Ray
- Dual Laterolog
- Shallow Focused Resistivity Survey

Unfortunately no Gamma Ray Spectroscopy/Spectralog is available, which could improve the total shale and porosity evaluation.

For both well A and B, core material was available with core porosity, permeability, and grain density. At this stage the mineralogical and geochemical analysis was not available.

Figure 1 and 2 in the appendix (well A and B) show typical log sequences in the lower part of the Jurassic sandstone from the northern North Sea. The sharp transition between the upper sand and the lower "mica" sand is clearly defineable. This can easily be proven by comparison of the core material with the log. The logs also indicate a clear trend of increasing fine materials towards the massive shale at the bottom of the sand. The change of grain size is also defineable. However, the caliper in well A reads considerable mudcake thickness in the bottom part of this zone, which indicates permeability and virtually no calculated porosity.

Well A interpretation discussion.

A classical log interpretation of this sequence is shown on fig. 3. The gamma-ray curve has been used as shale indicator in this example. The porosity is computed from the density/neutron crossplot, and the water saturation is calculated from the Nigeria equation with standard values for cementation and saturation exponents. The interpretation gives a shaly zone with moderate porosity, see figure 3.

Below 414 feet, the model calculates relative low porosities.

A perforated interval of 16' in this zone produced 2000 BOPD, which suggest good reservoir charcteristics.

Figure 4 shows a similar interpretation with the difference that in this case several shale indicators have been used. Porosity and water saturation are computed after the same method as example 3.

The shale indicators which have been utilized are shown in an analog form in figure 5. VSHGR is the shale volume estimated from the gamma-ray curve. VSHDN is the shale volume computed from the Density/Neutron crossplot in figure 6. VSHRT is shale volume from the R_t curve (Deep laterolog). VSHDS is the computed shale volume from the Density/Sonic crossplot in figure 7.

The final volume shale is estimated as the minimum value of all shale indicators. As can be seen in fig. 5, VSHRT is the indicator which gives minimum values of VSH over the zone of interest. VSHDN gives slightly lower values in some small intervals.

This interpretation gives a considerably higher porosity than the first example and corresponds with helium porosity (PORHE) measured on core plugs.

One of the problems encountered by using the Rt-curve as shale indicator is that it is valid only under conditions where irreducible water saturation (Swirr) exists. It can therefore not be applied in transition zones and water zones. Well A and B are both at "in situ" irreducible water saturation in the zones of interest.

Comparison of log-derived porosity to core porosity.

Figure 8 shows a plot of core porosity (PORHE) versus log derived porosity from the interpretation done in the example in figure 3.

The conclusion is that the log-derived porosity is too low, caused by too high a shale volume calculation. The difference between core porosity and log-derived porosity is in the order of 7 - 10 porosity percent. This clearly shows that in classical log interpretation the gamma ray is not usable as a quantitative shale indicator in this type of formation.

Figure 9 shows a similar plot of core porosity versus log derived porosity for the example in figure 4. The correlation between core data and log data is much better in this case. This example shows that the volume of shale estimated from the Rt-curve could be valid under irreducible water saturation conditions.

Table I shows a comparison of log-derived porosities and core porosities for the two interpretations.

The approach using VSHGR correlates poorly with core data because the shale volume estimates are too high. Using VSHRT gives a good correlation with average core and log data. Cored interval at 202' - 240' gives a correction factor of 0,990 on core porosity, while the bottom cored interval gives a correction factor of 0,951. A correction factor for core porosities less than unity might be expected on North Sea Jurassic sandstones.

MINERAL STUDY

Description of procedures.

A. Thin section preparation.
The thin sections were prepared from samples impregnated with epoxy. This was done to preserve the samples during preparation.

In order to identify the feldspars, the thin section were etched by concentrated hydro-fluoric acid, (HF) for a minute, washed, and exposed to a concentrated solution of sodium cobalt nitrite. The potash feldspars - orthoclase, perthites and microcline - assume a yellow color from the formation of potassium cobalt nitrite. The quartz is unaffected by the HF, and only minor etching of other components occurs.

B. Thin section analysis.
The optical microscopic images of the thin sections were quantitative examined by use of the Lietz-ASM image analysis system. The system is designed for the analysis of manually drawn outlines. In measuring, the components of interest are traced with an electronic pen. The measuring and data processing are then automatically solved, and computation of stereological parameters is performed.

The yellow stained K-feldspar and the different types of mica were easily recognized and quantitatively determined by this method.

C. Chemical analysis.
The major elements Si, Ti,Al, Fe^{3+},Fe^{2+}, Mg,Ca,K and Na were determined by X-ray fluorescence spectrography employing a Phillips Sequence x-Ray spectrometer at the Geological Institute of Bergen University, Norway. To achieve homogeneous samples, material dried at 110°C was mixed with lithium-tetraborate in the ratio 1:4 and melted into pellets. The content of $Fe^{2+}$was determined by a wet chemical titration method. The ignition loss was determined as the weight loss of material dried at 110°C after heating for 2 hours at 1050°C. The results are presented in the appendix. (Table II).

D. X-ray diffraction analysis
The silt and clay fraction (<32μ) was studied. Qualitative determinations of the clay mineralogy were performed by using a Siemens diffractometer at Geological Institute of Oslo. The samples studied were prepared by pipetting suspended material on to glass slides. The mineral identification criteria were taken from "The X-ray identification and crystal structures of clay minerals" edited by Brown (1961).

Determination of clay - and mafic mineral component.

The main mineral components were estimated by a combined method based on the result of the chemical and the thin section analysis. The major components are:
Quartz, feldspar (microcline, orthoclase, albite, perthite), heavies (muscovite, biotite, pyrite, siderite and clastic Fe/Ti - minerals) and clay minerals. (Kaolinite and illite determined by x-ray analysis)

A. Clay mineral components.
The amounts of Al_2O_3 and K_2O forming the minerals is calculated. Based on the modal values in table III (actual mineral composition expressed in volume percentages) of K-feldspar and mica and the chemical composition of these minerals is listed in the table. The differences give the content of Al_2O_3 and K_2O forming the clay components of the samples. Knowing the Al_2O_3 and K_2O of the clay minerals (kaolinite and illite) and their chemical composition the content of these clay minerals can be calculated.

The calculations assume: 1) All the sodium is bound up with the Na-feldspar.

2) All the potassium is present in three minerals only: feldspar, muscovite and illite.

3) The aluminum is distributed in the feldspar, the muscovite, the illite and the kaolinite only.

The calculations determining the clay minerals, kaolinite and illite are shown in the appendix.

B. Mafic (Ferromagnesian) minerals.
In order to get simple calculations all the ferrous iron is assigned to siderite and pyrite in equal amounts. The ferric iron is calculated as haematite and the TiO_2 is reserved for rutile. The sum of these minerals is obtained by adding the amounts of Fe_2O_3, TiO_2 and FeOx1.64 given by the chemical analysis.

$$\frac{Mw(FeS_2+FeCO_3) \times 0.5}{Mw(FeO)} = 1.64 \qquad Mw = \text{Molar Weight}$$

Discussion of accuracy.

K-feldspar is the most accuratly determined component. The error in estimating K-feldspar by the use of the Leitz-ASM method is probably less than by the usual point counting methods.

The content of mica is slightly underestimated due to its platey form and parallel orientation. On the other hand, the content of the mafic minerals are calculated slightly too high because all the iron and titanium are assigned to the mafics.

By combining the mafic and the mica minerals into a heavy mineral group, the systematic errors of each of them are more or less cancelled out.

MODEL AND REINTERPRETATION DESCRIPTION

A general model for computerized applications was constructed. The mineral study emphasized the presence of the following radioactive and non-radioactive minerals:

Radioactive:
- Muscovite
- K-feldspar

Non-Radioactive:
- Quartz
- Siderite
- Na-feldspar
- Kaolinite
- Pyrite

Siderite occurs in considerable amounts, and as this has a very high grain density, it effects the density measurement and porosity calculations.

The non-radioactive feldspar is present in significant amounts, but is considered to cause approximately the same log responses as quartz.

The kaolinite appears in most cases as either I) "grains" i.e. part of the matrix or 2) dispersed in the pore volume. Consequently, both types have to be taken into account.

Heavy minerals other than muscovite and siderite play a less important role from the point of view of log porosity computations, perhaps with the exception of pyrite.

In many cases the micaceous minerals are partly solid and unaltered, and partly split up and squeezed out into the pore volume. These altered forms of the minerals have certain other physical properties than the unaltered mineral. These forms are often transformed into a dispersed type of kaolinite. This dispersed clay will influence the porosity calculation from well logs.

Taking this mineralogical information into account, a model for porosity calculations was established. (See figure 10). This model can be divided into matrix, clay and porosity where the problem of separately quantifying the matrix minerals and the clay arises.

The matrix components are: Quartz, feldspar, (microcline, albite), kaolinite and muscovite, siderite and other heavy minerals such as pyrite. The clay is considered to be of the dispersed type, composed mainly of kaolinite squeezed out into the pore volume, and minor amounts of other clay minerals.

For log interpretation purposes the following simplification was done:

Matrix : "Quartz" (actual quartz, Na-feldspar, Kaolinite grains)
"Feldspar" (K-feldspar)
"Heavy Minerals" (muscovite, siderite, others)
Clay : Dispersed clay.

K-feldspar and mica are separated because of their different density values. Their presence as part of the matrix and not as clay/shale is very important for the porosity calculations.

This mineral model was set into a computer application for solution of porosity and contents of the present minerals. The computer application assumes linear tool respones to the amount of minerals and porosity. In this case the following tools were taken into consideration: Density, Neutron, Sonic and the Gamma ray.

The basic linear tool equations used by the computer model are as follows:

$$\rho_b = \rho_{fl} * \Phi_T + \rho_{cl} * V_{cl} + \sum_{i=1}^{n} \rho_i * X_i$$

$$\Phi_N = \Phi_{NW} * \Phi_T + \Phi_{Ncl} * V_{cl} + \sum_{i=1}^{n} \Phi_{ni} * X_i$$

$$\Delta t = \Delta t_{fl} * \emptyset_T + \Delta t_{cl} * V_{cl} + \sum_{i=1}^{n} \Delta t_i * X_i$$

$$GR = GR_{cl} * V_{clD} + GR_{cl} * V_{clL} + GR_{cl} * V_{clS} + \sum_{i=1}^{n} GR_i * X_i$$

ρ_b : Bulk Density
ρ_{fl} : Density of fluid
Φ_N : Neutron Porosity
Φ_{NW} : Fluid Neutron Porosity
Δt : Sonic Transit time
Δtfl : Fluid Transit Time

$\rho_i * X_i$: Matrix Density * Volume of Mineral i
$\Phi_{Ni} * X_i$: Matrix Neutron * Volume of Mineral i
$\Delta_{ti} * X_i$: Transit Time * Volume of Mineral i

V_{cl} : Clay Volume
V_{clD} : Volume of Dispersed Clay
V_{clL} : Volume of Laminated Clay
V_{clS} : Volume of Structural Clay
$\emptyset_T$: Porosity

The program also makes corrections for hydrocarbons, and additional "material balance" conditions are considered when the equations are solved.

Several runs were performed before an acceptable fit was obtained with the quantified results of the mineralogical and geochemical study.

A second criteria for the computer application was to generate grain densities in agreement with measurements on core plugs and crushed samples. Table V shows grain density results from core plugs, crushed samples and the computer application from the final run of Well A. This run gives the best agreement with the mineralogical analysis.

The run is presented in figure 11. The matrix parameters used are listed in table VI. The computer application assumes the simplified model discussed above. The quantified mineral analysis and the computer application are compared in figure 12.

An alternative clay concept using clay properties from the massive shale below 430' was tried. The result from this run in well A is presented in figure 13. The clay content is much higher and consequently the porosity considerably lower. In addition, the mineral content from this run does not coincide with the results of the mineral study.

Figure 14 shows the computed porosity from the dispersed clay model plotted against helium porosity from cores. The agreement is fully acceptable. The applied matrix parameters used in the computer application listed in table VI are reasonable. The high value of the sonic is due to the sonic reading the clay as water filled porosity. The clay effects on the density and the neutron are less pronounced. An average value of

the matrix density parameters (not considering the clay) is about 2.67 - 2.68 gr/cc, and the average sonic matrix transit time is about 58 - 60 μsec/ft. Both are reasonable results, although the sonic matrix travel time of the heavy minerals might seem to be high. Figure 15 and figure 16 show sonic transit time for Well A and B plotted versus porosity calculated from the density log.

The sonic matrix travel time from these plots seems higher than 60 μsec/ft. However, considering a dispersed clay volume of 10 - 12%, which is in agreement with the computer result, this gives a matrix travel time of around 60 μsec/ft. The volume of dispersed clay, V_{dis}, equals $\phi_s - \phi_D$, where ϕ_s is the sonic porosity and ϕ_D is the density porosity.

A rather complex computer application is not prectical for standard log interpretations. Therefore, a simplified approximation was generated from the synthesis of mineral studies and computer applications.

Considering tne applied matrix parameters and the grain density measurements, average values of 2.68 gr/cc and 58 - 60 μsec/ft are reasonable.

The simplified log interpretation was based on the density log for porosity calculations, and a clay volume derived from $V_{dis} = \phi_s - \phi_D$. The agreement in porosity and clay volume between the more complex computer application and this simple approach is good. However, the dispersed clay model under-estimates the clay content in the lower part of the formation. The clay occupies more than 35-40% of the pore volume, and can no longer be of the dispersed type. The dispersed clay is considered where the "q-factor" with $q = (\phi_s - \phi_D)/\phi_s$, is less than 35-40%, and a laminated shale model is used where the clay is no longer dispersed.

The result of this simplified approximation is displayed in figure 17. The plotting of the log porosity versus the core porosity is presented in figure 18. The method was also applied in well B where the result is presented in figure 19. The porosity is crossplotted versus core porosity in figure 20.

The reason for the good correlation with core data is that the density tool recognizes the dispersed clay as solid particles. This indicates that the density - porosity relation $\phi = (\rho_{ma} - \rho_b)/(\rho_{ma} - \rho_{fl})$ will be valid as a very good approximation in cases where $\rho_{fl} \approx \rho_{ma}$. On the other hand the sonic and the neutron would be more difficult to interprete alone.

SUMMARY

The Jurassic sand model of the Northern North Sea applied in this paper indicates the importance of radioactive feldspar as an contributing factor to porosity and permeability. This fact changes the problem from being a "mica-problem"

to a more general mineral description exercise where the main problems are: 1) to estimate the types and amounts of minerals, radioactive or not, which are important contributors to porosity, and 2) to estimate the actual clay content.

In this model a dispersed clay approach has been used based on analysis of thin sections and a trial-and-error computer procedure. However, a more detailed investigation of the clay minerals would probably offer a better understanding of the clay effects on logs.

The multi-mineral computer application gives good results for porosities and correlates well with core data. It generates mineral percentages in close agreement with the mineralogical and geochemical analysis. Average values of grain density are similar to those found from core analysis of plugs or crushed samples.

The data basis for this study is somewhat limited to allow for general conclusions. An increased quantified description of the mineralogy would possibly improve the model. Although there is still work to be done in this area, the mineral model used in this paper has proven to give good results in porosity computations from well logs.

CONCLUSIONS.

The conclusions to be drawn from this example and similar experiences in the Jurassic sandstone in the Northern North Sea are:

1) A good knowledge of the mineral composition gives a sound base for improving the porosity calculation and increasing the confidence level in the total evaluation.

2) On not considering the mineral composition of the formation to some degree, productive zones can easily be overlooked because of log responses from unknown minerals. The order of magnitude in this case is 5 - 10 porosity percent difference using a classical log interpretation compared with the approach presented in this paper.

3) By performing detailed mineral studies in some wells, a simple evaluation procedure can be applied for accurate and less resource-demanding evaluations.

APPENDIX

DETERMINATION OF CLAY CONTENT

The Al_2O_3 material balance is given by:

I

$$a = b + c + d + e$$

where

a is the weight percentage of Al_2O_3 of the samples, table II

b is the weight percentage of Al_2O_3 forming the K-feldspars of the samples.

c is the weight percentage of Al_2O_3 forming the Na-feldspars of the samples.

d is the weight percentage of Al_2O_3 forming the muscovite of the samples.

e is the weight percentage of Al_2O_3 forming the clay of the samples.

II

From table IV

$$\left(\frac{Al_2O_3}{Na_2O+CaO}\right) \text{albite} = 1.75 \quad \text{and} \quad (CaO)\text{albite} = \frac{Na_2O}{11}$$

replacing CaO in Eq. II by its value, we obtain

$$\frac{Al_2O_3}{\left(Na_2O+\frac{Na_2O}{11}\right)\text{albite}} = 1.75$$

Rearranging, we have

III

$$(Al_2O_3)\ \text{albite} = 1.91\ Na_2O = c$$

IV

$$(Al_2O_3)\text{K-feldspar} = \frac{fxg}{100} = c$$

where f is the mode of K-feldspar in % by volume, table III
g is the weight % Al_2O_3 in K-feldspar, table IV

V

$$(Al_2O_3)\ \text{muscovite} = \frac{hxi}{100} = d$$

where h is the mode of muscovite in % by volume, table III
i is the weight % Al_2O_3 in muscovite, table IV

Replacing b, c and d in Eq. I by their values in III, IV and V, we obtain

$$a = 1.91\ Na_2O + \frac{f \times g}{100} + \frac{h \times i}{100} + e$$

Rearranging, we have

VI

$$e = a - \frac{1.91\ Na_2O + fxg+hxi}{100}$$

Inserting the values of a, f, g, h, i from the tables II, III and IV , gives e, the amount of Al_2O_3 forming the clay components.

The K_2O material balance is given by:

VII

$$j = k + l + m$$

where j = is the weight percentage of K_2O of the samples, table II
k = is the weight percentage of K_2O forming the K-feldspars of the samples.
l = is the weight percentage of K_2O forming the muscovite of the samples.
m = is the weight percentage of K_2O forming the clay of the samples.

VIII

$$(K_2O)\ \text{feldspar} = k = \frac{fxn}{100}$$

where n is the weight % K_2O in K-feldspar, table IV

IX

$$(K_2O)\ \text{muscovite} = l = \frac{hxp}{100}$$

where p is the weight % K_2O in muscovite, table IV

Replacing k and c in Eq. VII by their values in VIII and IX, we obtain

X

$$j = \frac{fxn}{100} + \frac{hxp}{100} + m$$

Rearranging, we have

XI

$$m = \frac{100j - (fxn+hxp)}{100}$$

where m is the amount of K_2O forming the clay components.

The weight % of illite, (il) is

$$(il) = \frac{m \times 100}{r}$$

where r is the weight % K_2O in illite, table IV,

XII

$$(il) = \frac{100j - (fxn+hxp)}{r}$$

XIII

$$e = s + t$$

where s is the content of Al_2O_3 forming the kaolinite
where t is the content of Al_2O_3 forming the illite

XIV

$$(Al_2O_3)\ \text{illite} = t = \frac{(il) \times u}{100}$$

where u is the weight % Al_2O_3 in illite, table IV

Replacing t in Eq. XIV by its value in XIII, we obtain

$$e = \frac{s + (il) \times u}{100}$$

Rearranging, we have

XV

$$s = \frac{100\ e - (il) \times u}{100}$$

The weight % of kaolinite, (ka)

$$(ka) = \frac{s \times 100}{v}$$

where v is the weight % Al_2O_3 in kaolinite, table IV
Replacing s by its value in XV, we obtain

XVI

$$(ka) = \frac{100\ e - (il) \times u}{v}$$

BIBLIOGRAPHY

Brown, G. (Ed.), 1961. "The X-ray identification and crystal structures of clay minerals". Mineral. Soc., London.

Deer, W.A., Howie, R.A. & Zussmann, J., Vol. 3, 1962, Vol.4 1963, "Rock-forming minerals". Longman Group Limited, London.

"Log Interpretation Charts", Schlumberger 1972

"Log Interpretation, Volume I", - Principles, Schlumberger 1972.

"Log Interpretation, Volume II", - Applications, Schlumberger 1974.

Savre, W.C., 1963, "Determination of a More Accurate Porosity and Mineral Composition in Complex Lithologies with the Use of the Sonic, Neutron and Density Surveys", Journal of Petroleum Technology, September 1963 (945 - 959).

Selley, R.C. 1976. "The habit of North Sea Oil". Geologists' Association, Vol. 87, Part 4, (359-388).

"The Essentials of log interpretation practice", Schlumberger 1972.

About the Authors

Øistein Nyberg is presently section manager of petrophysics with Statoil. He graduated from South Dakota School of Mines and Technology in 1967 with a B.S.C.E. From 1967 - 1969 he was employed as a design engineer with the Boeing Co in Seattle, Washington. After being employed by Schlumberger Overseas until 1974 he joined Statoil.

Per A. Lindberg is presently group leader in the petrophysics section. He received a "B.S" in geological engineering at the University of Upsala, Sweden in 1971, and worked as a ground water hydrologist in Algeria for a Swedish consultant co. In 1974 he joined the United Nations Development Projects and worked as an associated expert in ground water hydrology in Mali until he joined Statoil in 1975.

Klaus Lien is presently employed as a petrophysical engineer with Statoil. He received a "can.real" degree in geology in 1974 at the University of Oslo. Since joining Statoil in 1974 he has been employed as geologist in the exploration department and since 1977 as a "log analyst" specializing in mineralogy/sedimentalogy in the Production Dept. petrophysics section.

Jon K. Smistad is presently employed as a petrophysical engineer with Statoil. He graduated from the "Institute of Petroleum Engineering and Applied Geophysics at the University of Trondheim in 1975 holding a M.S. in Petroleum Engineering. He was employed by Statoil in 1976 upon receiving his degree.

FIGURE 1 LOGS WELL A

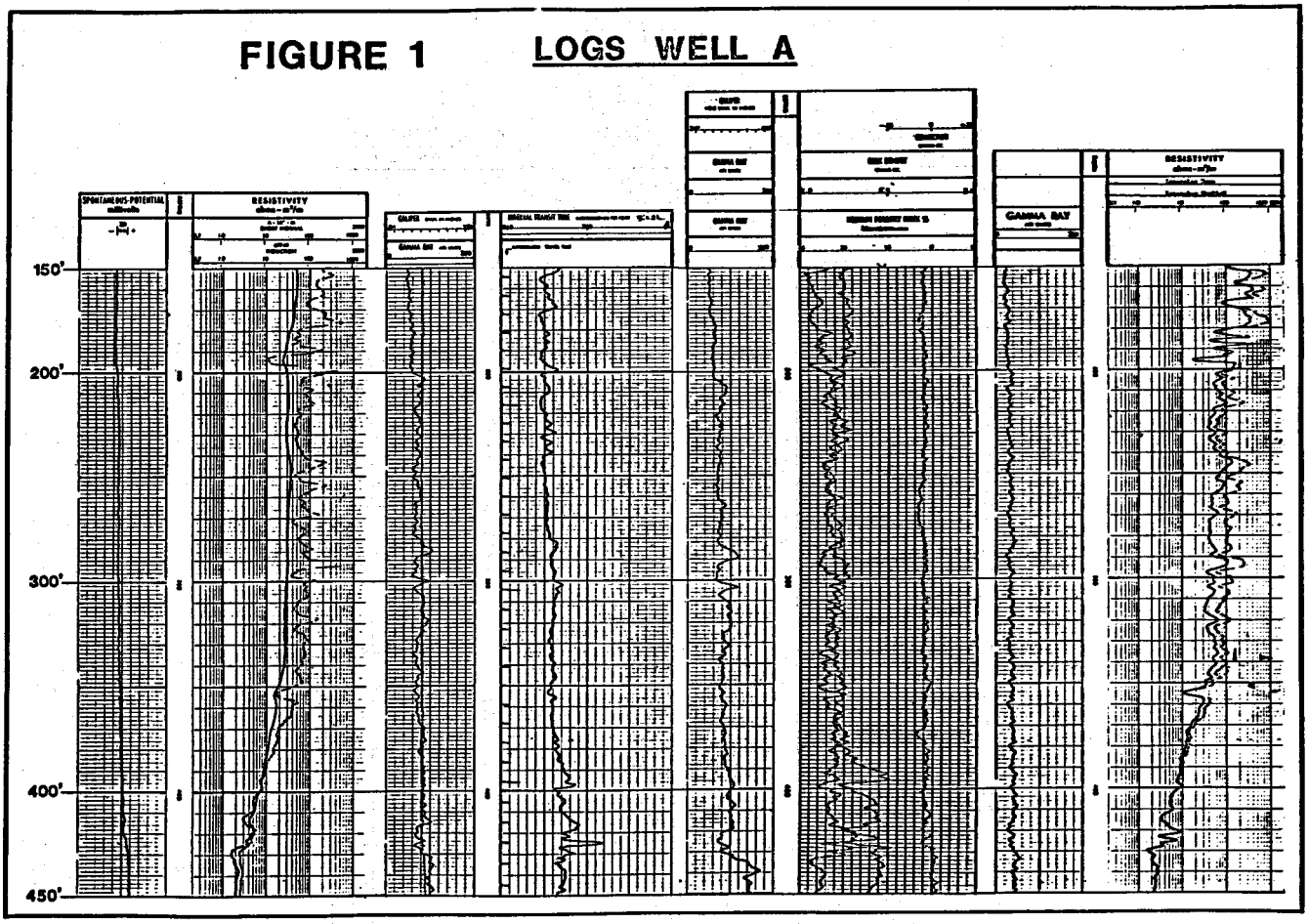

FIGURE 2 LOGS WELL B

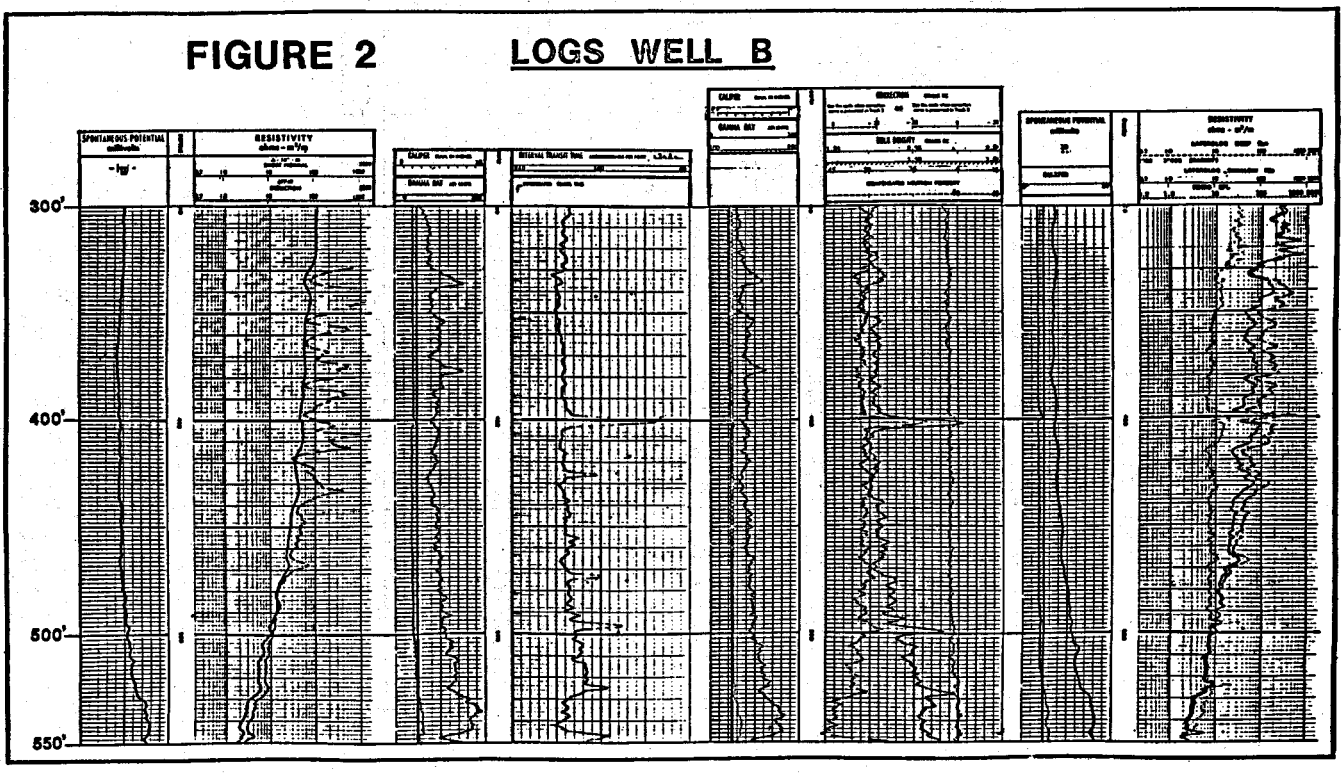

WELL A

FIGURE 3

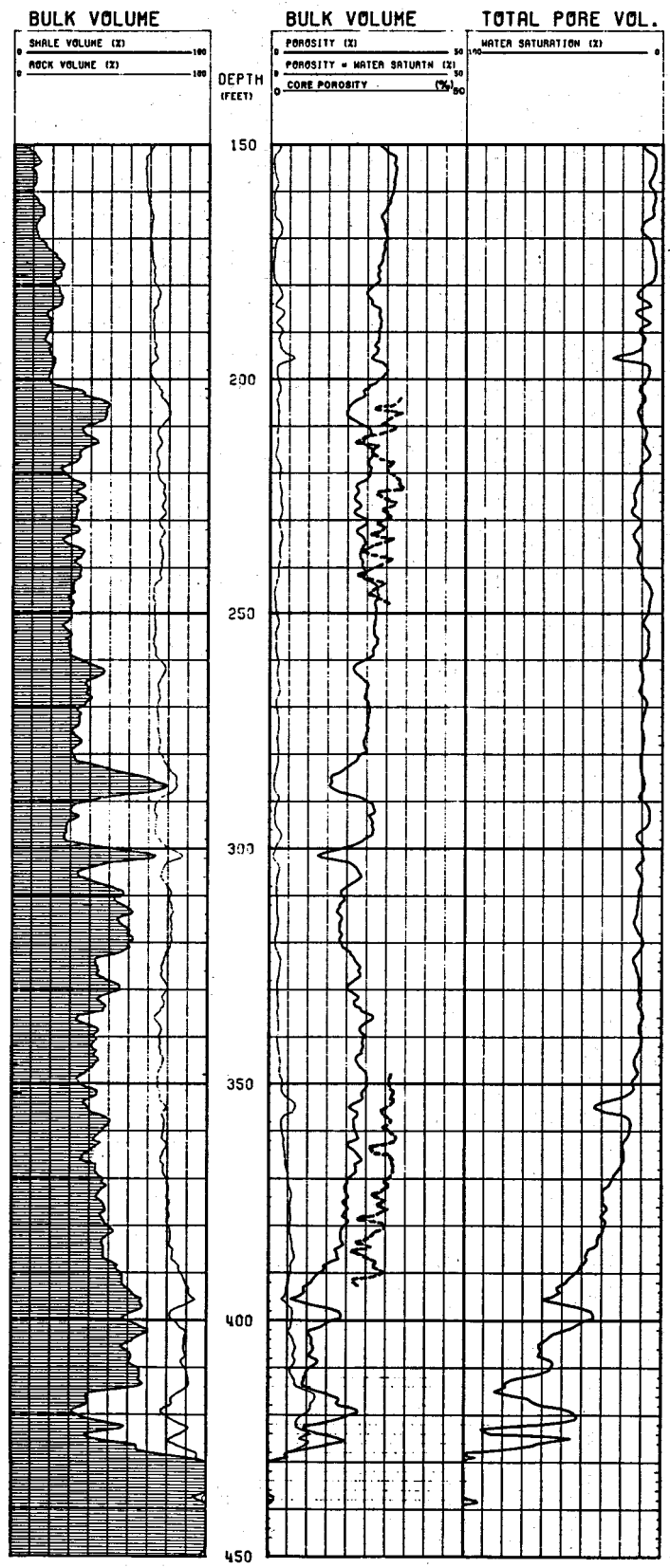

WELL A

FIGURE 4

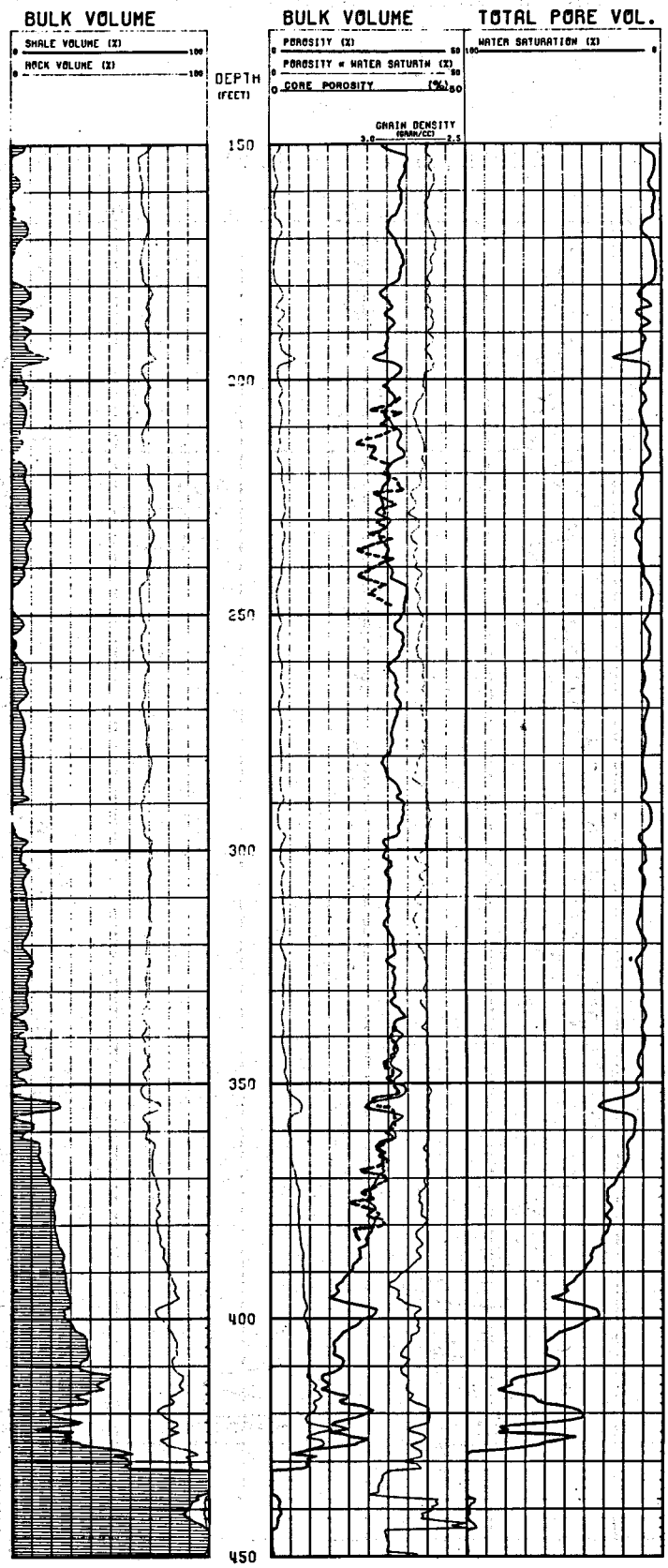

FIGURE 5

VOLUME SHALE INDICATORS

WELL A

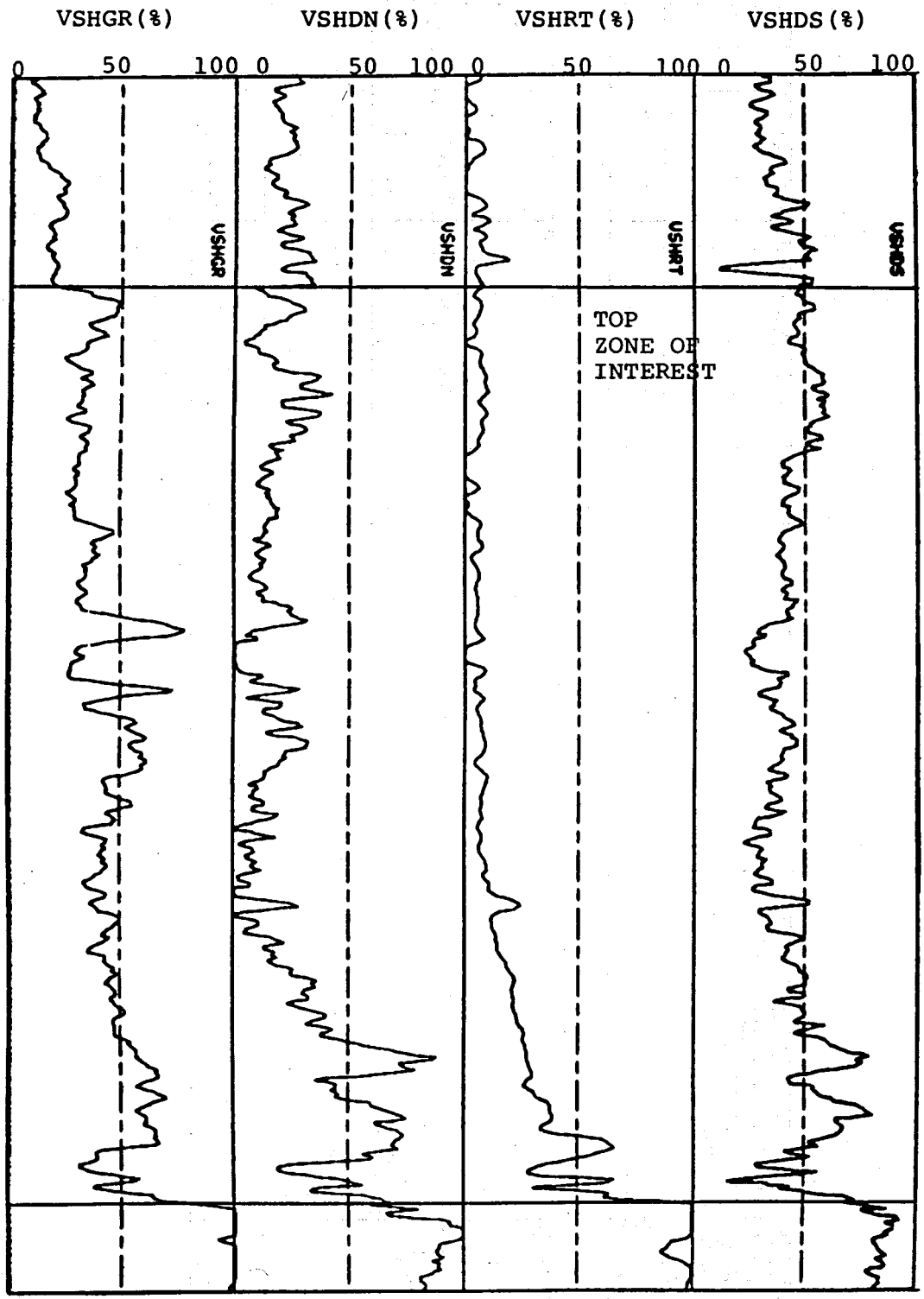

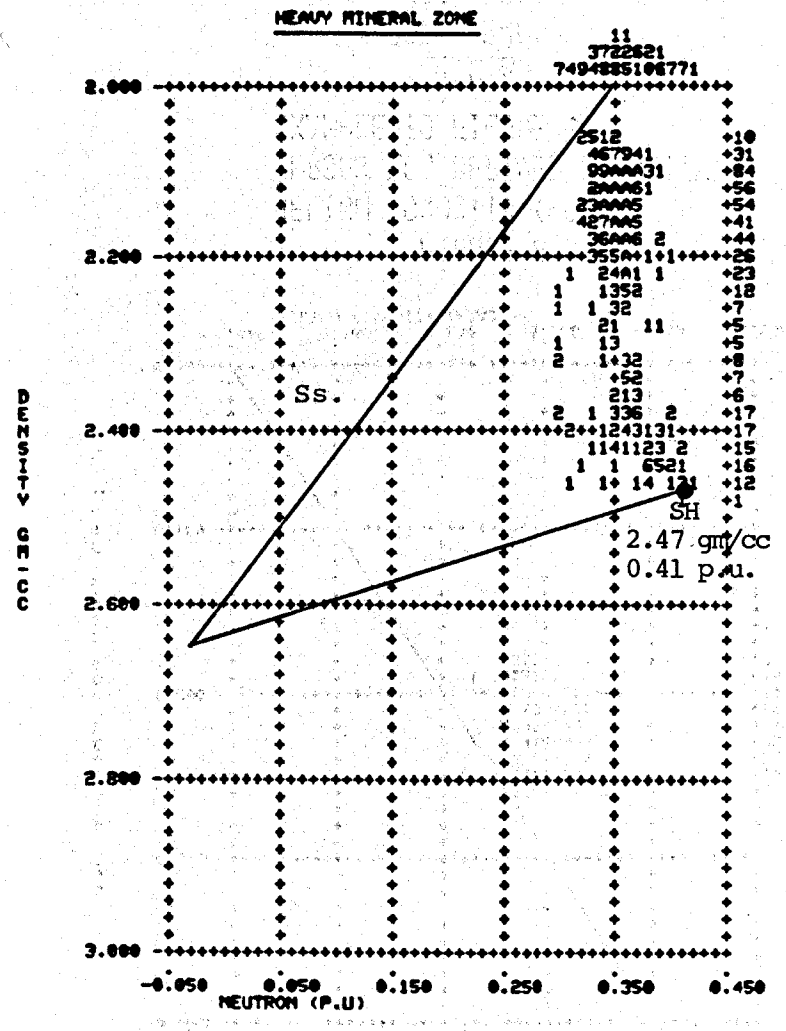

FIGURE 6
DENSITY/NEUTRON CROSSPLOT
WELL A

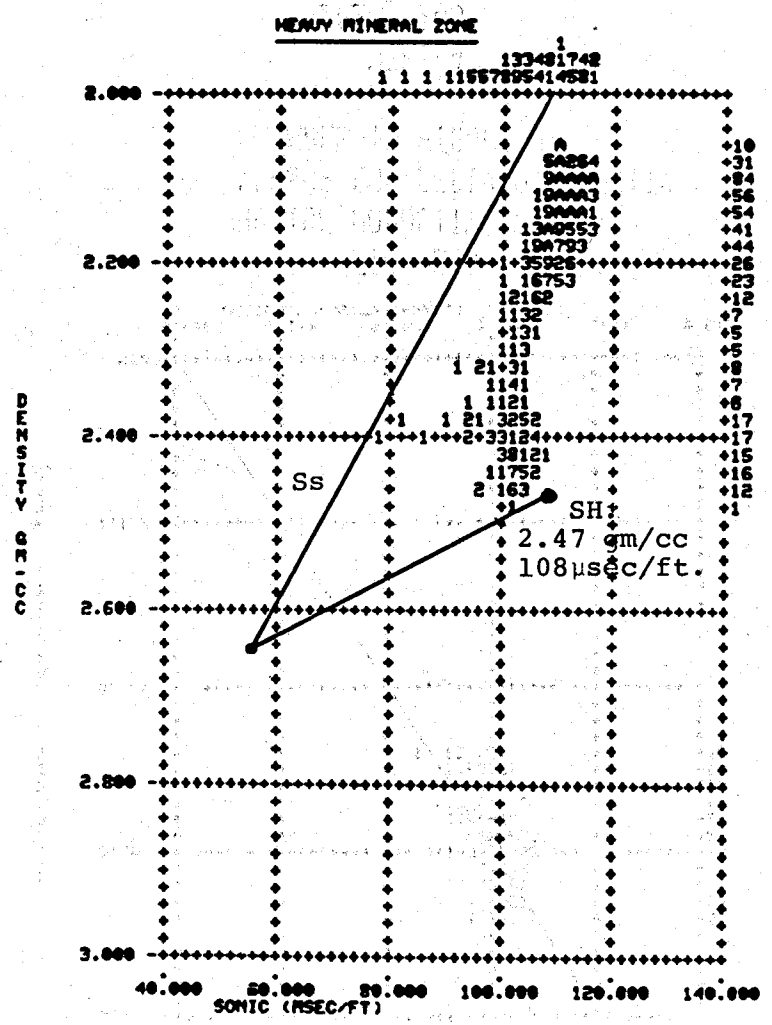

FIGURE 7
DENSITY/SONIC CROSSPLOT
WELL A

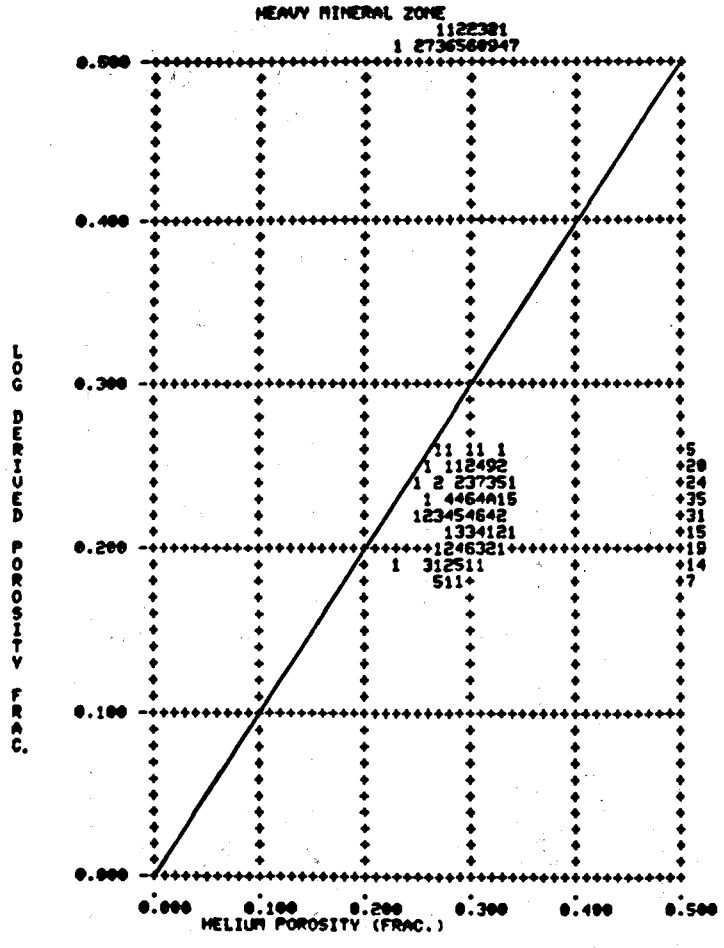

FIGURE 8
HELIUM POROSITY (PORHE)
VERSUS LOG DERIVED POROSITY
EXAMPLE TO FIGURE 3

WELL A
202'- 240'
338'- 384'

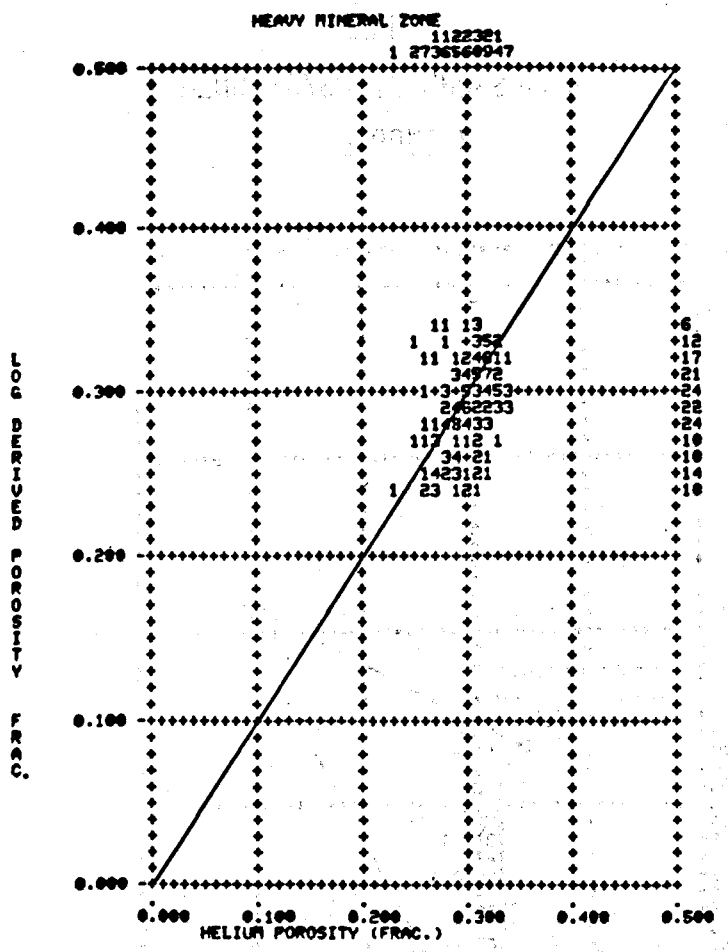

FIGURE 9
HELIUM POROSITY (PORHE)
VERSUS LOG DERIVED POROSITY
EXAMPLE TO FIGURE 4

WELL A
202'- 240'
338'- 384'

FIGURE 10

MINERAL MODEL

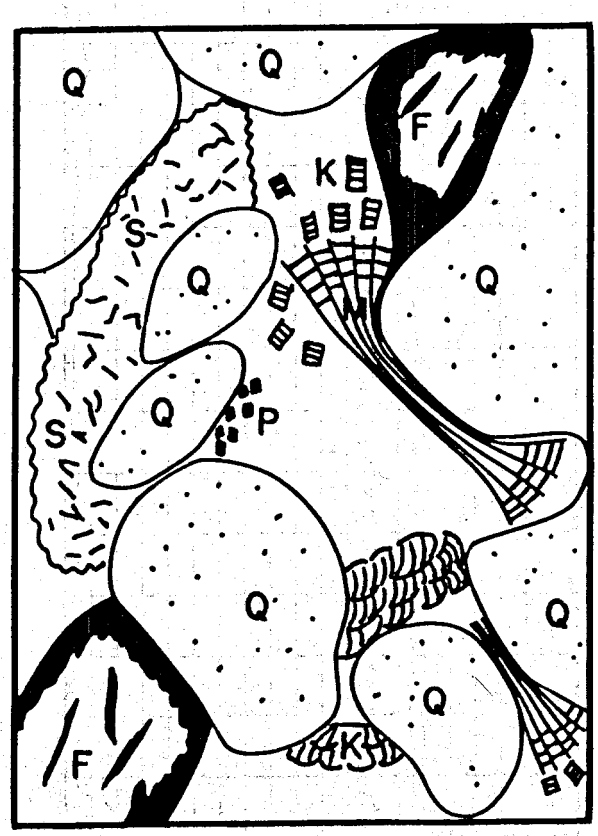

Q	Quartz
F	Feldspar.
M	Muscovite
S	Siderite
K	Kaolinite
P	Pyrite

FIGURE 11

WELL A

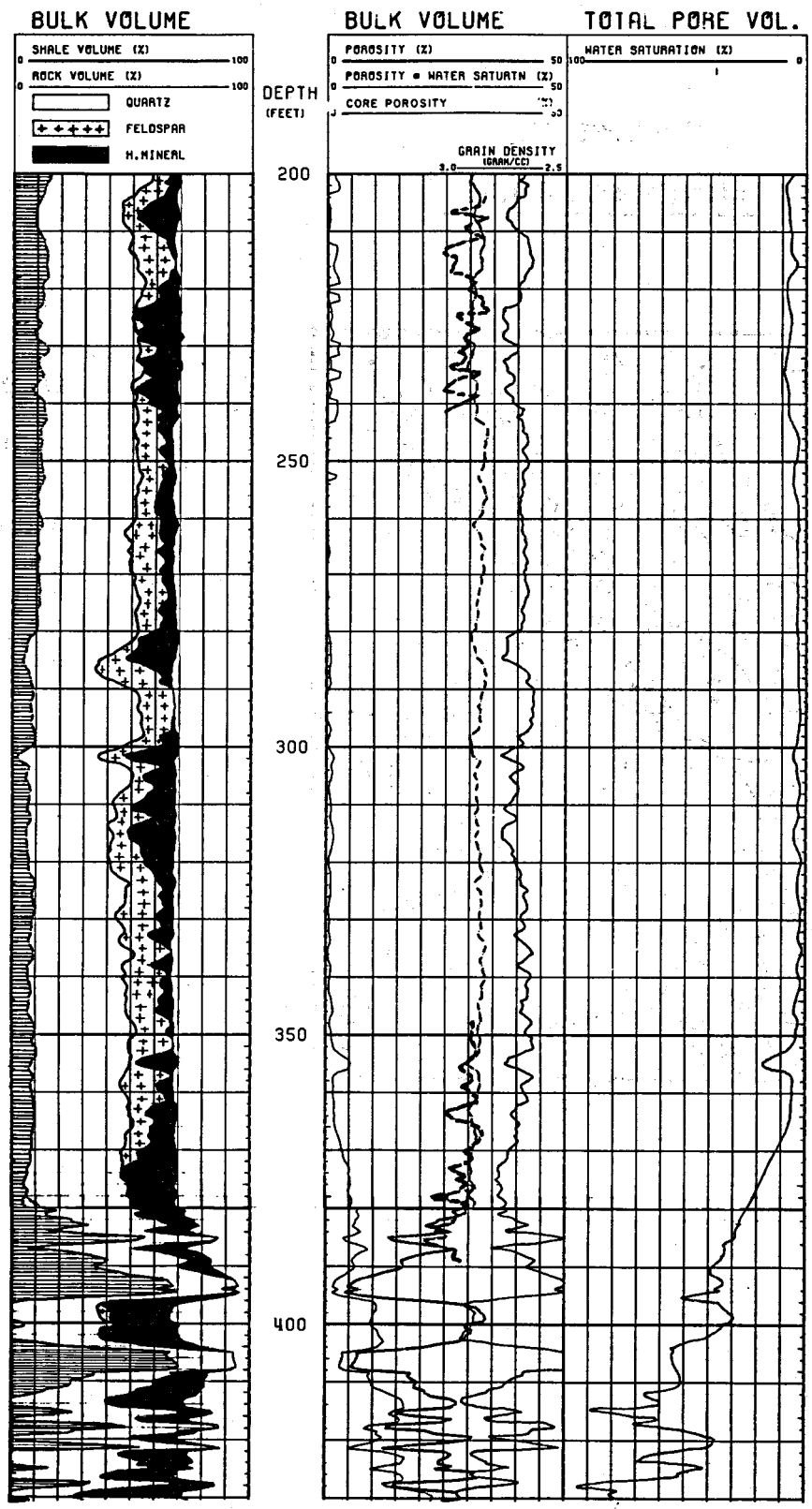

FIGURE 12

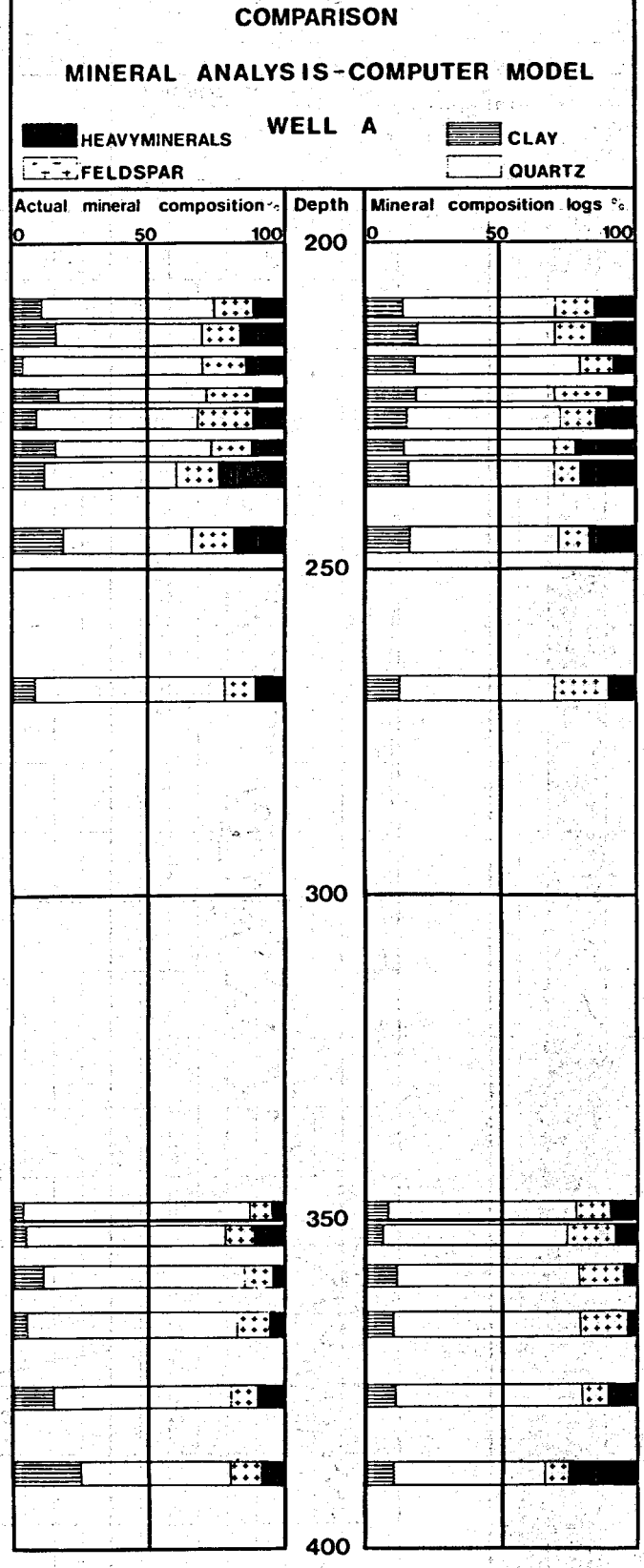
COMPARISON
MINERAL ANALYSIS-COMPUTER MODEL
WELL A
HEAVYMINERALS
CLAY
FELDSPAR
QUARTZ
Actual mineral composition %
Depth
Mineral composition logs %
0
50
100
200
250
300
350
400

FIGURE 13

WELL A

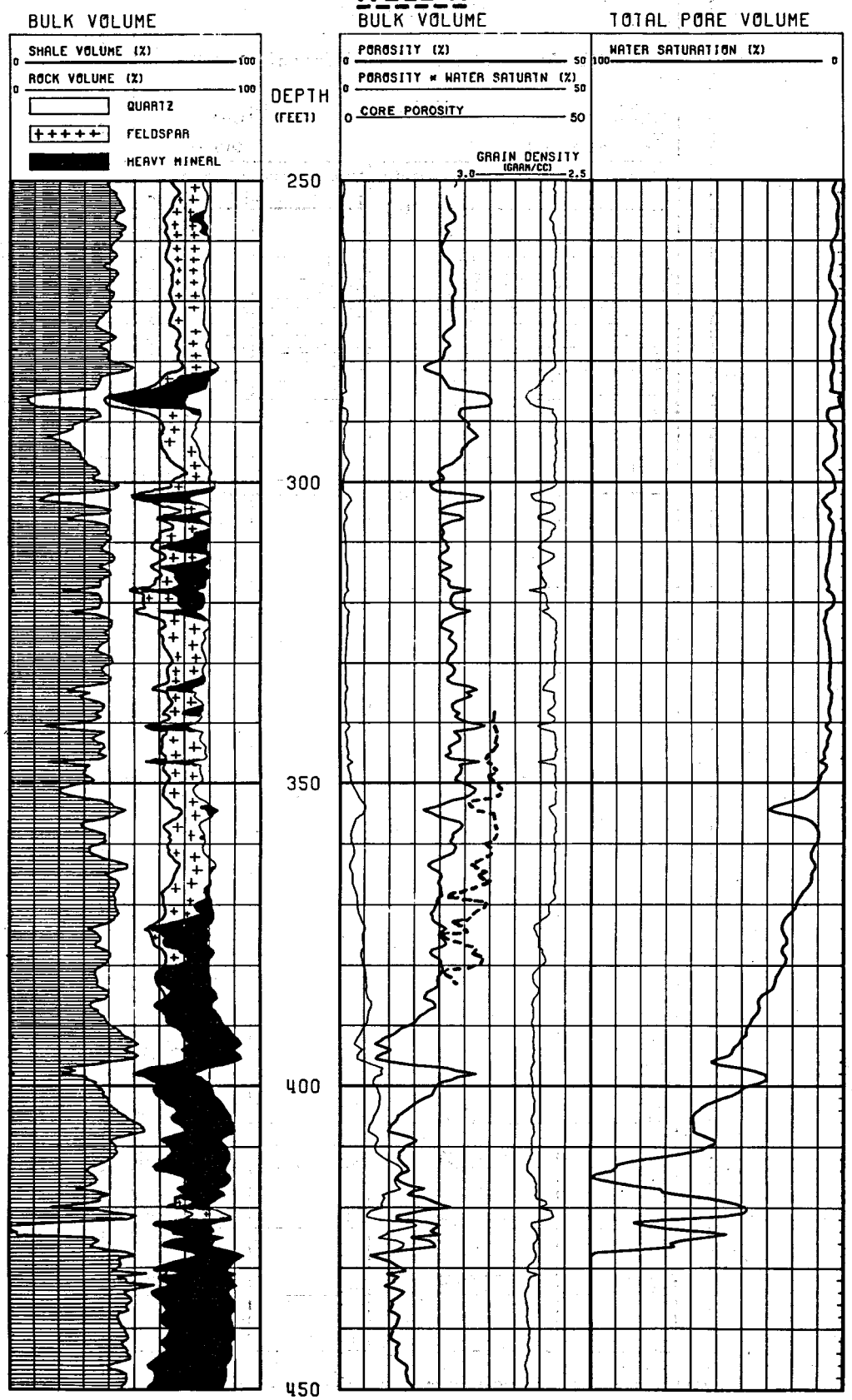

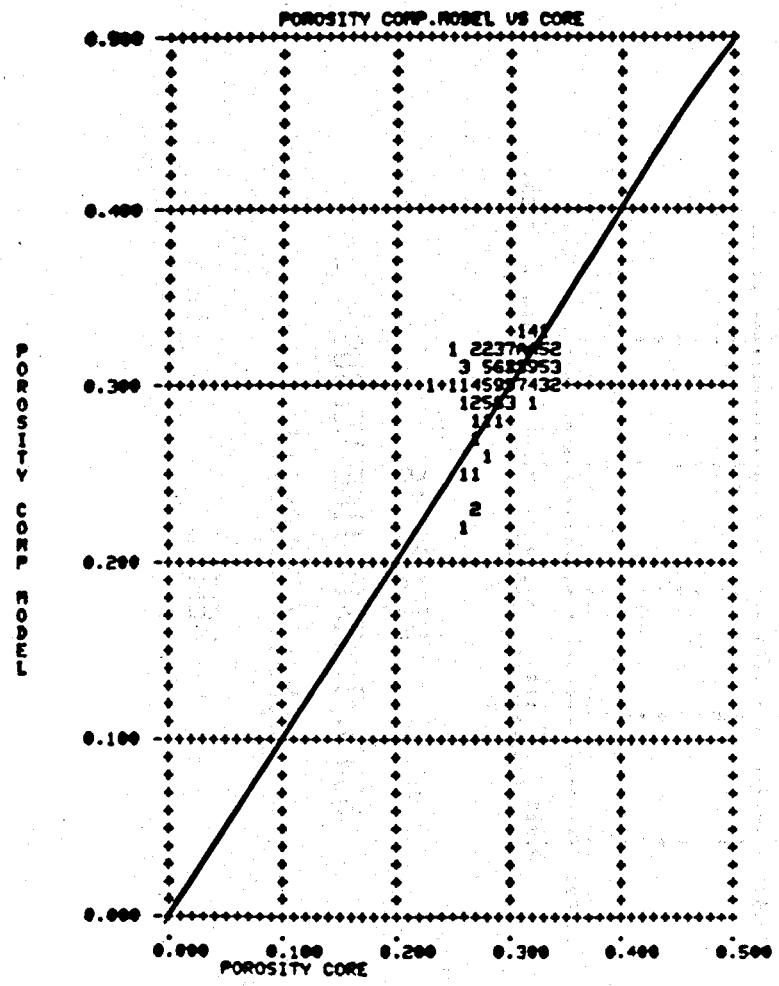

FIGURE 14

POROSITY COMPUTER MODEL VS CORE POROSITY

WELL A

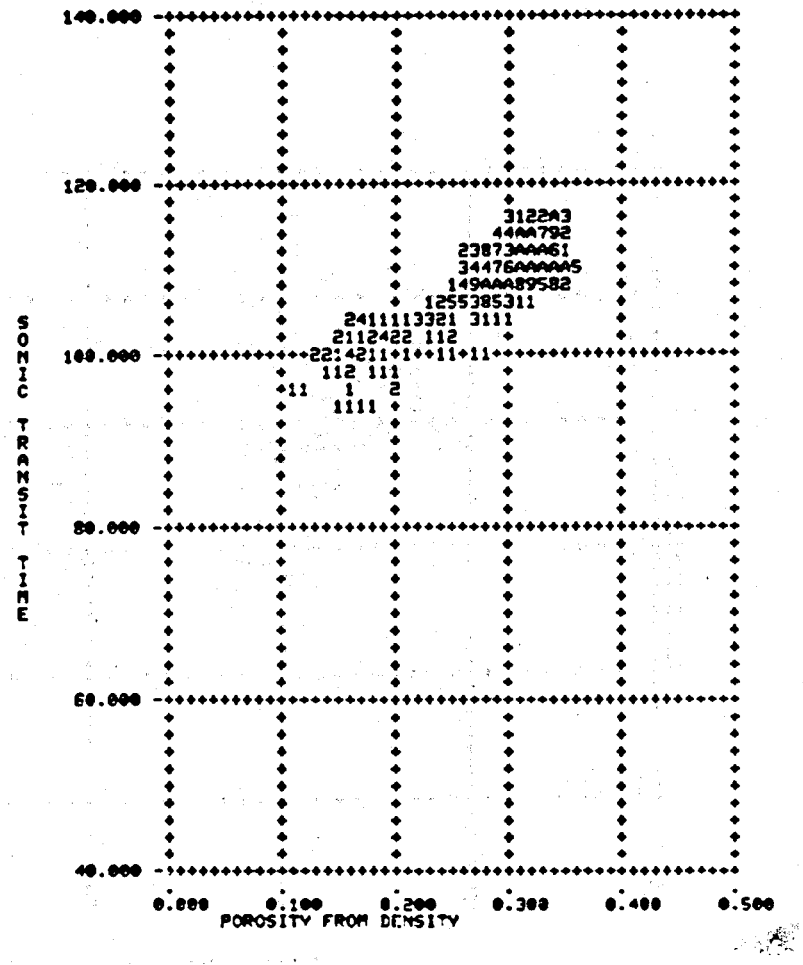

FIGURE 15

SONIC TRANSIT TIME VERSUS DENSITY POROSITY

WELL A

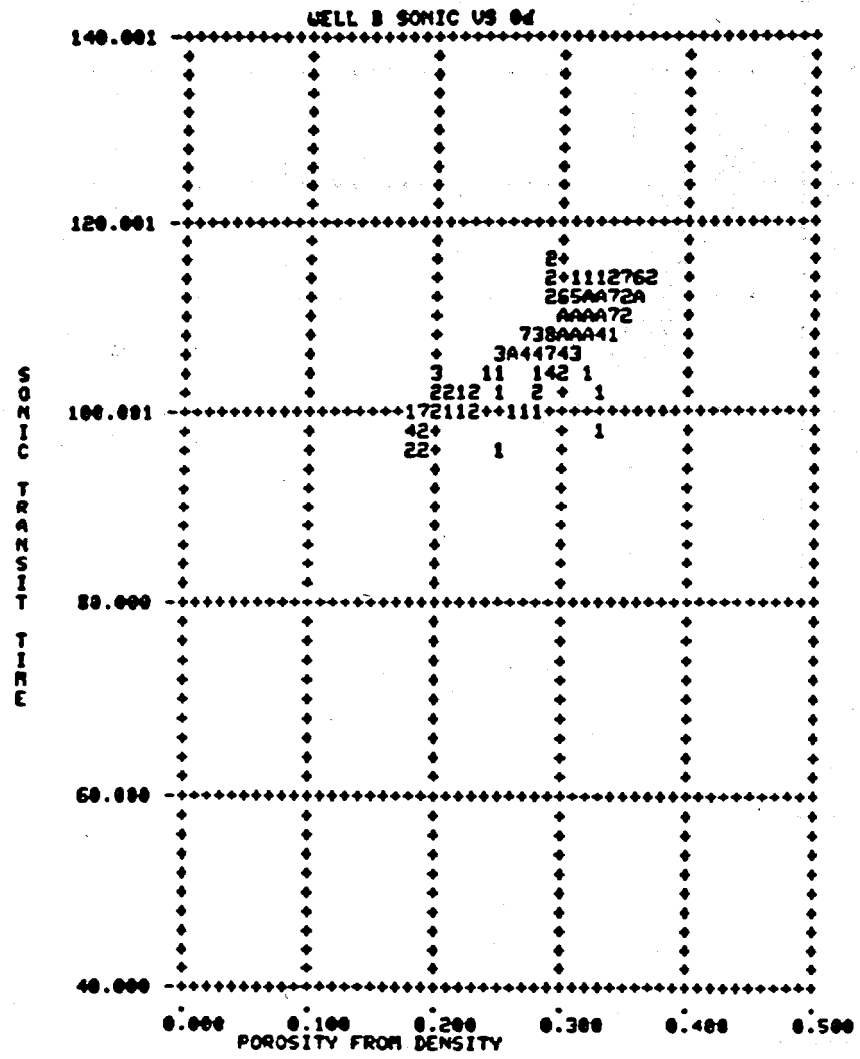

FIGURE 16

SONIC TRANSIT TIME VERSUS

DENSITY POROSITY

WELL B

FIGURE 17

WELL A

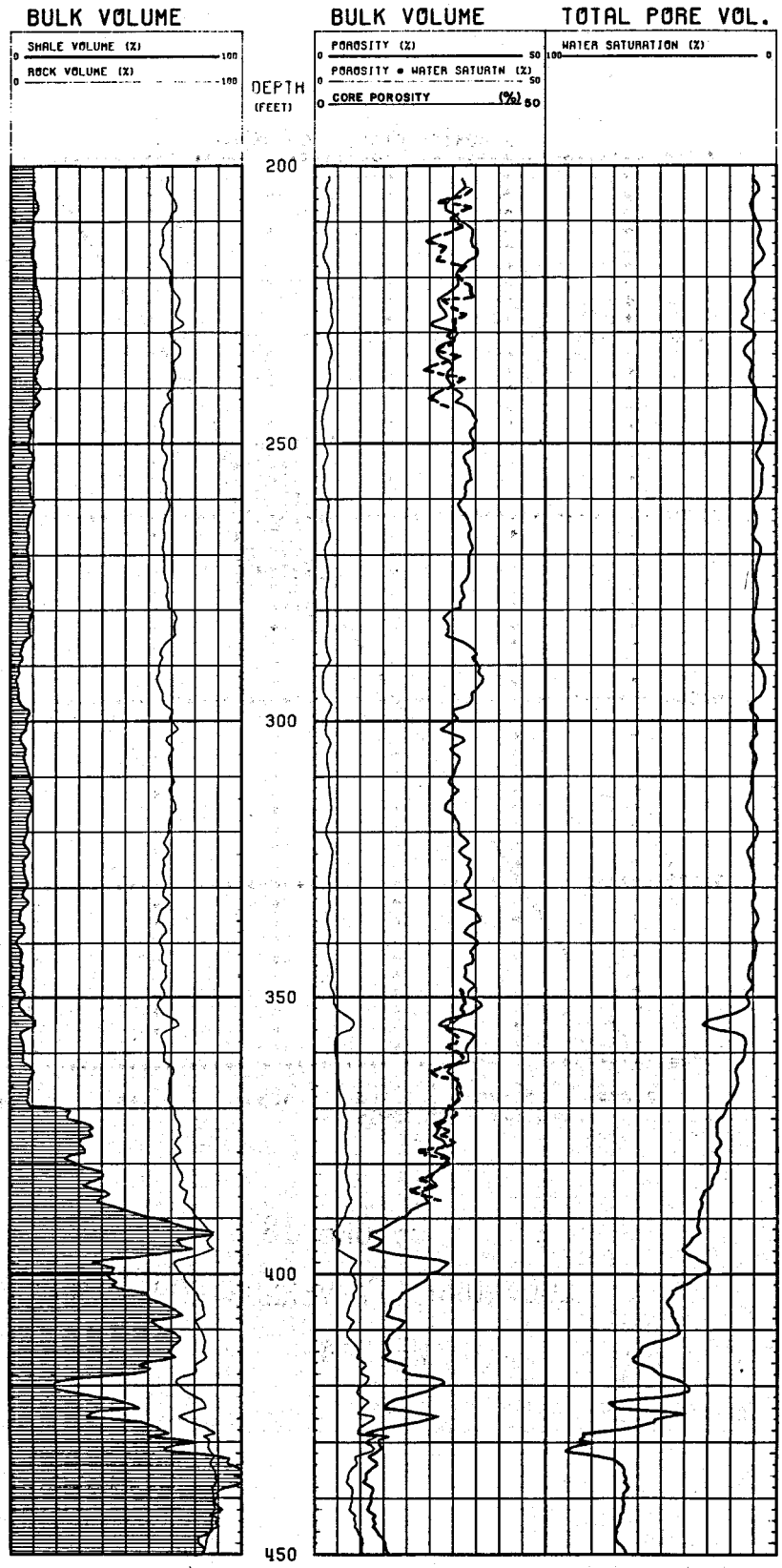

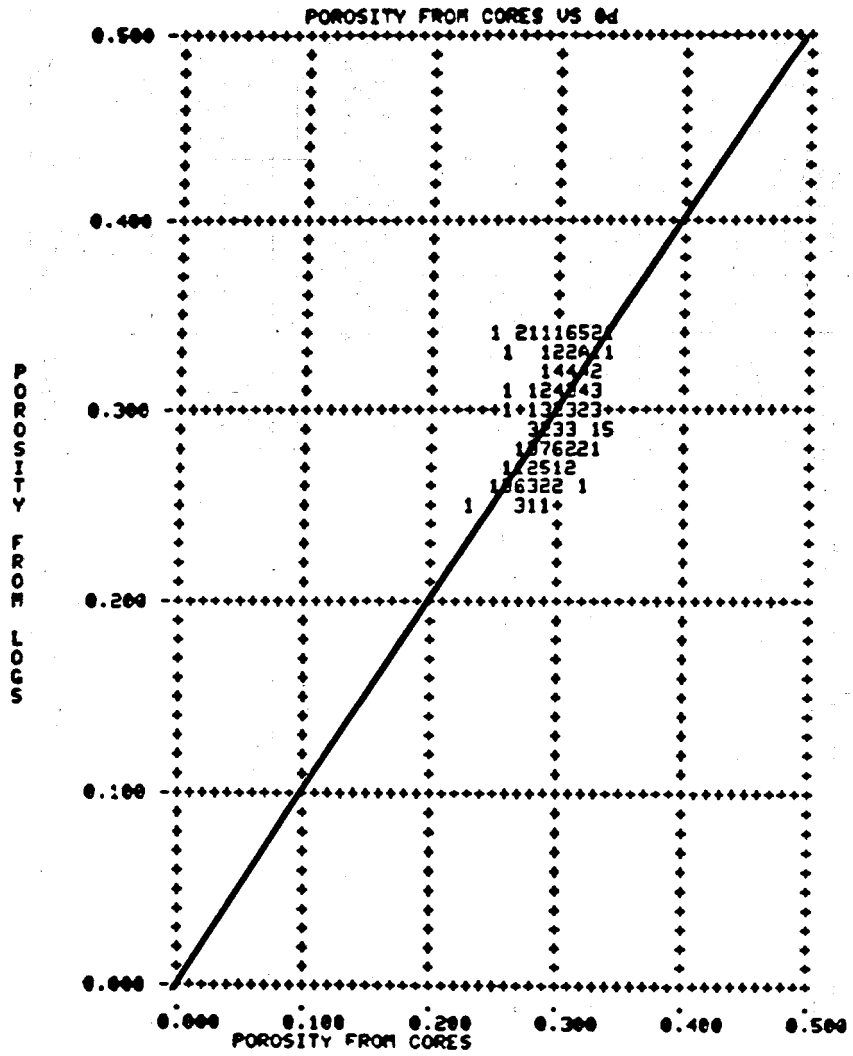

FIGURE 18

LOG POROSITY VERSUS CORE POROSITY

WELL A

FIGURE 19

WELL B

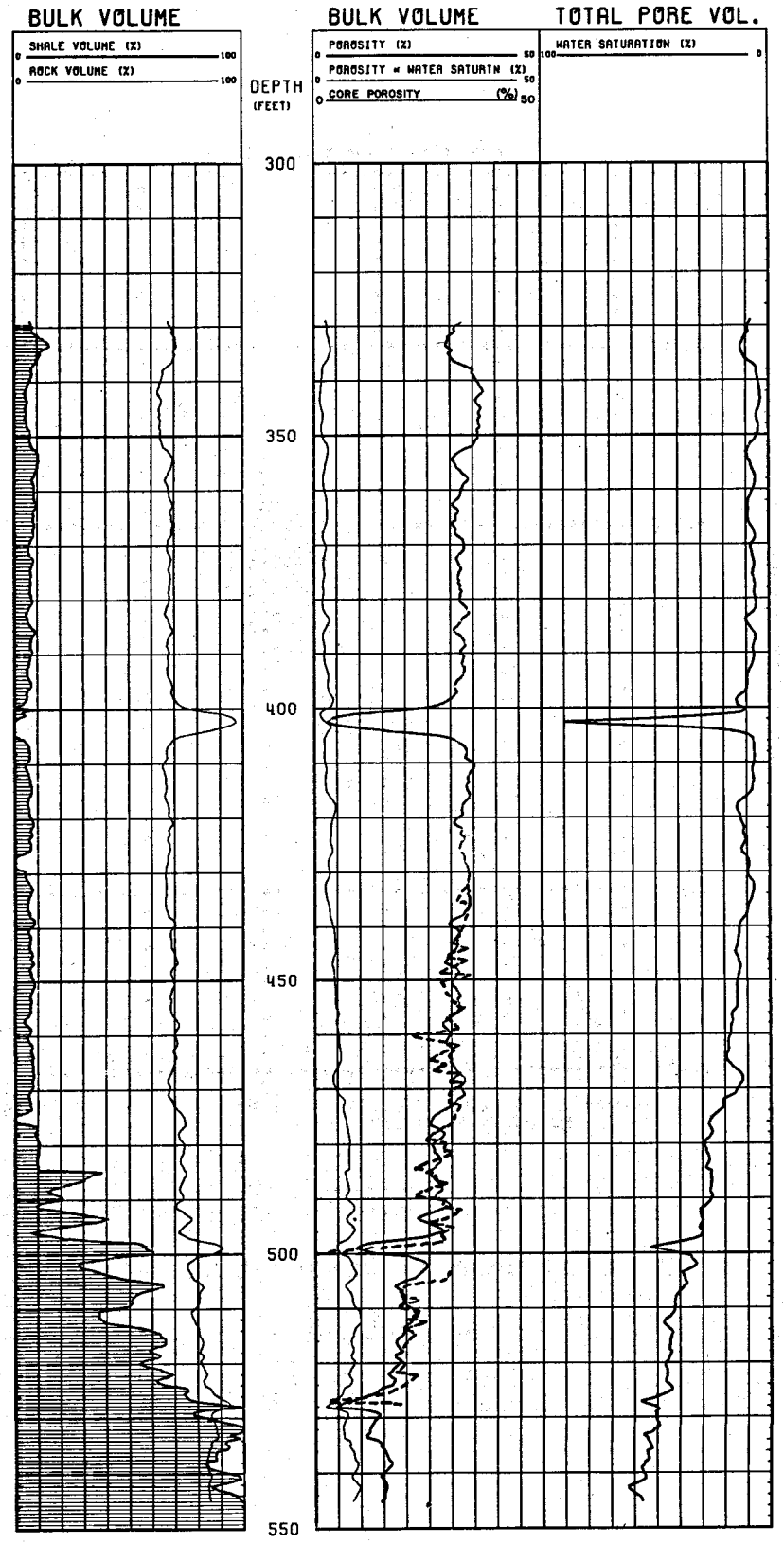

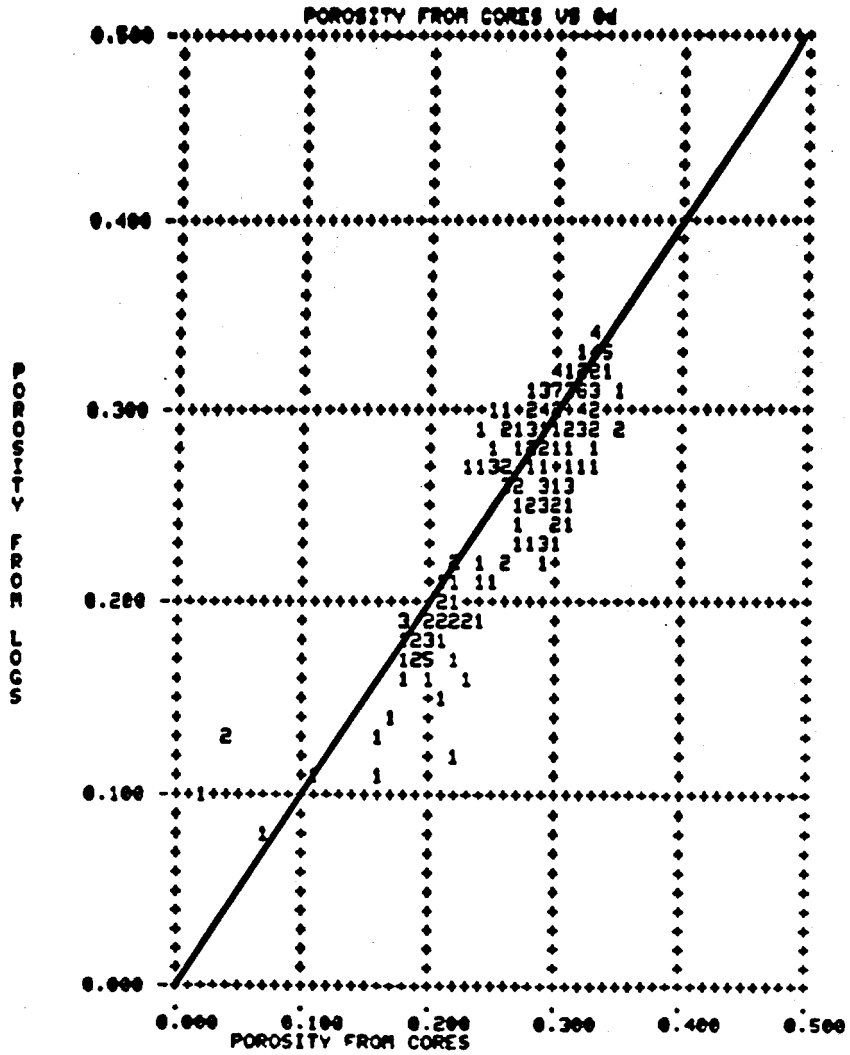

FIGURE 20

LOG POROSITY VERSUS CORE POROSITY

WELL B

TABLE I

INTERPRETATION EXAMPLE	INTERVAL 202'- 240'	INTERVAL 338'- 384'	INTERVAL 202'- 240'	INTERVAL 338'- 384'
	AVERAGE LOG POROSITY(%)	AVERAGE LOG POROSITY(%)	AVERAGE CORE POROSITY(%)	AVERAGE CORE POROSITY(%)
FIGURE 3	23,6	22,0	30,6	30,6
FIGURE 4	30,3	29,1		

TABLE II
CHEMICAL ANALYSIS, WEIGHT PERCENTAGES, SAMPLE NR. REFER TO DEPTH IN FEET

	208	212	217	222	225	231	233	243	266	347	351	357	364	375	387
SiO_2	77.2	67.6	78.3	72.1	73.7	74.4	66.2	65.6	79.0	80.5	77.6	82.0	81.0	76.0	71.5
TiO_2	1.9	0.7	0.6	0.7	0.8	0.6	0.7	0.6	1.3	1.3	0.8	0.7	0.9	0.9	0.8
Al_2O_3	11.6	11.7	10.5	12.7	12.1	12.2	15.0	14.3	9.4	6.0	7.0	8.2	7.0	10.4	13.3
Fe_2O_3	1.0	2.7	1.1	1.7	1.3	1.6	2.6	2.0	1.3	0.4	0.5	0.2	0.8	1.5	1.1
FeO	0.5	4.2	0.8	1.9	1.6	1.1	2.9	3.2	1.1	1.1	4.5	1.4	2.1	1.6	2.1
MgO	0.7	0.9	0.7	1.9	0.7	0.8	1.1	1.4	0.6	0.4	0.8	0.7	0.9	0.9	1.4
CaO	0.1	0.1	0.1	0.1	0.1	0.2	0.1	0.1	0.1	0.2	0.4	0.1	0.3	0.2	0.2
Na_2O	1.1	1.1	0.8	0.7	0.9	1.2	0.8	0.7	1.0	1.2	1.4	1.3	1.4	1.4	1.3
K_2O	2.9	3.3	3.1	3.5	3.5	3.6	3.9	4.1	2.4	1.6	1.9	2.2	2.1	2.7	3.2
Loss ignition	4.2	8.0	4.6	5.9	5.4	5.3	7.0	7.3	4.6	7.9	5.8	3.9	4.1	4.7	5.3
Total	101.2	100.3	100.6	100.2	100.1	101.0	100.3	99.3	100.8	100.6	100.7	100.7	100.6	100.3	100.3

TABLE III.
MINERALOGICAL COMPOSTIONS (MODUL VALUES), BASED ON THIN SECTION STUDY, AND CHEMICAL ANALYSIS

	208	212	217	222	225	231	233	243	266	347	351	357	364	375	387
Quartz	63.5	54.9	64.9	54.2	57.8	59.4	47.0	47.6	69.0	81.5	73.6	75.5	77.5	66.5	55.9
Feldspar	14.5	13.7	16.8	19.0	20.6	16.1	17.9	15.9	10.9	8.5	10.0	9.7	10.5	11.5	12.9
Clay	10.3	15.9	4.4	16.5	9.7	14.7	11.5	18.1	9.3	3.7	4.5	10.5	5.2	14.6	24.3
Mica	8.0	5.2	10.9	4.7	7.1	5.7	15.5	10.5	6.3	2.7	3.2	1.9	1.7	2.3	1.6
Mafic	3.7	10.3	3.0	5.6	4.8	4.1	8.1	7.9	4.5	3.6	8.7	2.4	5.1	5.1	5.3
Total	100.0	100.0	100.0	100.0	100.0	100.0	100.0	100.0	100.0	100.0	100.0	100.0	100.0	100.0	100.0

TABLE IV. ASSUMED CHEMICAL COMPOSITION OF SOME RECOGNIZED MINERALS IN THIS STUDY.

	K-feldspar	Na-feldspar	Muscovite	Illite	Kaolinite
SiO_2	64.5	67.0	49.5	51.5	45.5
Al_2O_3	19.5	21.0	35.0	30.0	39.0
Fe_2O_3				3.0	
CaO		1.0			
Na_2O	1.5	11.0	0.5	0.5	
K_2O	13.5		10.0	8.0	
Loss ignition			4.0	6.0	14.5
Total	99.0	100.0	99.0	99.0	99.0

TABLE V
WELL A
GRAIN DENSITIES FROM
CRUSHED CORES, PLUGS AND LOGS

Sample No.	Grain densities gr/cc		
	Chrused samples	From plugs	Calc.logs
1	2.68	2.75	2.70
2	2.71	2.71	2.72
3	2.67	2.64	2.70
4	2.65	2.66	2.65
5	2.64	2.64	2.64
6	2.65	2.68	2.64
7	2.67	2.67	2.69
8	2.66	2.66	2.68
9	2.65	2.68	2.68
10	2.68	-	2.68
11	2.67	2.66	2.67
12	2.65	2.66	2.65
13	-	2.67	2.69
14	-	2.67	2.69
15	-	2.68	2.74

TABLE VI

MATRIX PARAMETERS

FOR COMPUTER APPLICATION

WELL A

Mineral	Matrix density ρma	Matrix neutron ϕNma	Matrix sonic Δtma travel time	Matrix gamma GRma
Quartz	2.65 gr/cc	- 3.5 p.u.	55.5 μsec/ft	20 API
Feldspar	2.68 gr/cc	- 6.0 p.u.	65.0 μsec/ft	170 API
Heavy M.	3.05 gr/cc	25.0 p.u.	80.0 μsec/ft	140 API
Disp.clay	2.66 gr/cc	36.0 p.u.	187.0 μsec/ft	20 API

RELATIONSHIP BETWEEN THE CONDUCTIVITIES OF TERTIARY WATER-BEARING SANDS AND NEARBY SHALES, OFFSHORE LOUISIANA

By

H. J. Ritch
&
E. S. Pennebaker

Shell Oil Company
New Orleans, Louisiana

SUMMARY

A quantitative relationship between the conductivities of clean water-bearing sands and nearby shales has been established for the Tertiary formation of Offshore Louisiana. From this relationship, the connate water resistivity of the sands can be calculated using the conductivity of the nearby shales. The ability to independently calculate water resistivity is very important, especially where there are no clean water-bearing sands near or adjacent to hydrocarbon-bearing sands.

Although empirical, industry-accepted clean and shaly sand petrophysical relationships help explain why this method yields acceptable values.

An example is given for the South Marsh Island 130 Field where there is an unusually wide range of formation water resistivities over a depth interval of about 2000 feet (4000-6000 feet). This relationship appears statistically accurate for the prediction of sand water resistivities from the nearby shale conductivities.

INTRODUCTION

Accurate connate water resistivities are needed in order to calculate correct hydrocarbon volumes. Sometimes in wildcat wells and the early stages of field development, it is difficult to find enough nearby water-bearing sands from which to calculate water resistivity. Therefore, in these cases an independent means of determining water resistivity is desirable. We studied the relationship between the resistivities, or conductivities, of clean water-bearing Pleistocene sands and nearby shales to determine if shale resistivities could be used to accurately estimate sand water resistivities.

In general, there appeared to be a correlation between conductivities of the clean water-bearing sands and nearby shales. As the shale conductivity decreased between 3000 feet and 4000 feet, so did the sand conductivity as shown in Figure 1, for example, for the normal pressured Pleistocene in the South Marsh Island 130 Field area. Between 4000 feet and 6000 feet, the sand

conductivity showed a marked increase except for a small section around 5500 feet. However, the shale conductivity only slightly increased from 4000 feet to 5000 feet and then remained essentially constant to 6500 feet. These changes in sand conductivity are caused by connate water resistivity changes since sand porosities only decrease slightly over this depth range. Therefore, we concluded that the changes in shale conductivity were also caused by changes in the shale water resistivity. Between 3000 feet and 5000 feet, the shape of the shale conductivity curve compared with the shape of the sand conductivity curve supports this conclusion. Below 5000 feet, the relationship of shale conductivity to sand conductivity is more subtle. However, as will be shown later, due to the higher compaction rate of the shales resulting in larger porosity changes, the shale conductivity would have shown a constant decrease in conductivity from 5000 feet to 6500 feet if the shale water resistivity had remained constant (after correcting for temperature differences). Since the shale conductivity remained essentially constant over this depth range, we viewed this as evidence that the shale water resistivities were also changing (increasing).

One question remained: how to quantitatively relate the sand and shale conductivities and predict sand water resistivities from the shale conductivities.

METHOD

In order to better understand Pleistocene sand-shale relationships, we plotted and cross-plotted data from a large number of wells over the entire Offshore Louisiana Pleistocene. The most meaningful type of cross-plot resulting from this study is shown in Figure 2. At an average depth of 4000 feet (Figure 2) there is a suggested relationship as shown by the "eyeball" average line. (We observed that the shales closest to the sands were more silty than the shales farther removed from the sands. Therefore, we collected data from clean sands and the nearby silty shales.) Are there equations to describe this relationship? As long as the sands are clean, the Archie Equation adequately describes the relationship between porosity and water resistivity. Waxman[1] showed that the Waxman-Smits equations, normally applied to shaly sands, could be used to accurately describe salinity variations of shales if the shale porosity and cation exchange capacity were known. The Archie and Waxman-Smits equations are:

ARCHIE

$$Co_{sd} = \frac{1000}{Ro} = \frac{1000}{F\ Rw} = \frac{1000}{Rw\ \phi^{-m}} \qquad \text{Equation 1}$$

Where:

Co_{sd} = conductivity of 100% water-bearing clean sand, mmho/m

Ro = resistivity of 100% water-bearing clean sand, Ω-m

F = formation resistivity factor of clean sand, dimensionless

ϕ = porosity, dimensionless, fraction

m = lithological exponent, dimensionless

Rw = formation (sand) water resistivity, Ω-m

WAXMAN-SMITS

$$Co_{sh} = \frac{1000}{\phi_{sh}^{-m^*}} \left(BQ_v + \frac{1}{Rw_{sh}}\right) = \frac{1000}{F^*} \left(BQ_v + \frac{1}{Rw_{sh}}\right) \qquad \text{Equation 2}$$

Where:

Co_{sh} = conductivity of shale, mmho/m

F* = formation (shale) resistivity factor, dimensionless

B = equivalent cationic conductivity of the clay counterions,

$\frac{1}{\Omega\text{-m}}$/Eq./liter

Q_v = exchange capacity per unit pore volume, meq/ccPV

Rw_{sh} = shale water resistivity, Ω-m

m* = lithological exponent for shale, dimensionless

ϕ_{sh} = shale porosity, fraction

Therefore, if all the variables are known in the above equation, then the conductivity of both sand and shale can be calculated.

The data shown in Figure 2 are from the normal pressured Pleistocene for which we have constructed representative compaction curves for both clean sand and silty shale as shown in Figure 3. Based on measurements from Pleistocene cores, we found that the average cation exchange capacity (CEC) of silty shale was 15 meq/100 gms of dry shale. An average temperature for the Pleistocene can be calculated as a function of depth. The only remaining variable is water resistivity since the B factor is dependent on the water resistivity and temperature. Upon specifying water resistivity, the sand and shale conductivities can be calculated.

Shown in Figure 4 are the calculated sand versus shale conductivities over the full range of water resistivities at 4000 feet (from fresh to

saturated salt water) for one case with the water resistivity in the shales equal to that of the sand. Note that the calculated relationship is different from the average line drawn through the data points from Figure 2. In particular, the calculated shale conductivities are higher than the log observed values.

For the other case, we obtained reasonable agreement between observed sand-shale conductivities and calculated values using the Archie and Waxman-Smits equations when the water resistivity in the shales was about 2.86 times higher than the water resistivity in the sands (also shown in Figure 4). This difference in water resistivity represents a significantly lower salinity in the shales than the sands.

Is it reasonable to expect a large difference in salinity between the sands and shales if they are in chemical equilibrium? Many investigators have studied this problem using Donnan equilibrium theory and have agreed that large salinity differences can exist. According to Donnan equilibrium theory, a base exchanging clay (a shale) immersed in a salt solution will contain a lower internal salinity than the salinity of the solution surrounding the base exchanging clay. Hedberg[2] concluded, while studying compositions of shale interstitial water to determine their original depositional environment, that the average pore-water chlorinities within a shale sequence range from 40 to 50 percent of that of the underlying sand.[3] Based on cores from a Pliocene-Miocene well Offshore Louisiana, Russel[3] concluded that the salinities of formation waters in sands is significantly higher than those in nearby shales - sometimes by as much as a factor of 10-12. Baharloui[4] studied interstitial waters from Paleozoic shales and sandstones in Oklahoma and found that the total dissolved solids in the shale waters was about a third of the dissolved solids in the associated sandstone waters. Schmidt[5] found that shale pore waters in a Calcasieu Parish, Louisiana well had lower salinities than the waters in the adjacent normally pressured sandstones. Also, several investigators including Engelhardt and Gaida[6] conclude that the ratio of shale water salinity to sand water salinity increases as compaction increases. Therefore, based on theory and considerable research, there can be large differences in water salinities between sands and shales.

According to Waxman[7], our Pleistocene data (Figure 2) does not follow simple Donnan equilibrium or further, the Donnan compaction model described by Smith[8]. This suggests that a non-equilibrium condition exists for the Pleistocene sand-shale system. Also this probably implies that the system is in a quasi steady-state condition caused by salt being introduced from domes by diffusion and/or the expulsion of water from the shales by compaction. Furthermore, the ratio of RwSd/RwSh increases with depth (Figure 7) in spite of increasing Qv (exchange capacity per unit pore volume) of the shales. Since the influence of nearby shale is less effective, this is further evidence that the simple Donnan equilibrium theory is not being obeyed.

For sand water resistivity use, the "reasonable agreement" curve in Figure 4 can be replotted as shown in Figure 5 which is the shale conductivity versus sand water resistivity plot at 4000 feet for the normally pressured Pleistocene.

As shown in Figure 2, there was a considerable data scatter about the data average. Much of this scatter can be accounted for by the silty shales having different porosities and CEC values than the average shale properties presented in Figure 3. A change of ±20 percent in the CEC value (range from 12 to 18 meq/100 gms of dry shale) is reasonable based on our Pleistocene core data. Shown in Figure 6 is the range in the calculated shale conductivities due to this range of CEC values between 12 and 18. Note that this range in CEC encompasses most of the lower conductivity shale data points from Figure 2. The higher conductivity shale data points are probably due to even higher shale CEC values or maybe a different type shale.

Using the technique outlined in Figures 2, 3 and 4, sand and shale conductivity data were fitted between depths 2000 feet to 10,000 feet. The composite reasonable agreement curves are shown in Figure 7. Plots of shale conductivity versus sand water resistivity can then be made (similar to Figure 5) at every 1000 feet of depth or for the zone of interest.

APPLICATION

The first few wells drilled in the South Marsh Island (SMI) 130 Field penetrated several hydrocarbon pay sands from 4000 feet to 6000 feet. However, few wet sands were encountered from which to calculate water resistivity. Moreover, low resistivity mud systems and hydrocarbon effects prevented accurate water resistivity estimations from the SP curve.

We initially assumed the water salinity to remain essentially constant throughout this depth range, an assumption often made for the Offshore Louisiana area. However, after observing from shale resistivity pore pressure plots, such as the one shown in Figure 8, that the decrease in shale resistivity from 4000 feet to 6000 feet was not due to an increase in pore pressure, we assumed that the big change was due to shale water salinity differences. If so, the sand water salinities probably also varied greatly. Therefore, we applied the technique of determining sand water resistivity from nearby shale conductivity.

Sand and nearby shale conductivity data for a thick, clean, wet sand from 2950 feet to 3100 feet from several wells were cross-plotted as shown in Figure 9. The "best" fit trend line through the data was with using shale CEC = 18 meq/100 gms. Additional trend lines every 1000 feet between 3000 feet and 6000 feet were extrapolated based on Figure 7. These additional trend lines are shown in Figure 10. Finally, the sand water resistivity was then calculated every 1000 feet by using calculated temperature and the sand formation resistivity factor given in Figure 3.

The first few wells drilled provided enough data from which production platforms were justified and subsequently installed in the SMI 130 Field. Some 21 development wells in 16 sands have been drilled that penetrated water levels so that more conventionally derived water resistivities could be determined and compared to those computed by the nearby shale conductivity technique. Figure 11 shows a comparison of sand water resistivity obtained

by conventional and shale conductivity methods for 16 wet sand penetrations. There is some scatter but values from the shale conductivity method are within 0.010 ohm-meters (one standard deviation) of conventionally derived values for water resistivity between 0.016 and 0.053 ohm-meters. The correlation is increased considerably by averaging the shale conductivity method estimates for individual sands, as shown in Figure 12. The average estimates are within 0.003 ohm-meters (one standard deviation) of the conventionally derived values. Note that the scatter of data "tightens up" statistically, leaving no apparent anomalies between 0.016 and 0.050 ohm-meters. Above 0.060 ohm-meter, the shale conductivity method gives low estimates. These low estimate differences could probably be minimized if the "control sand" water resistivity had been in the high resistivity range rather than the low range (see Figures 9, 10 and 11).

By way of comparison, sand water resistivity estimates were made using the SP curve in these same 21 wells for 13 of the 16 previous sands. These SP derived water resistivity estimates, averaged by sand, are shown in Figure 13 compared to conventionally calculated values. Note that the SP derived values are considerably higher than the conventionally calculated water resistivities.

Up to now, all the data shown has been for normal pressured Pleistocene sediments. However, we have on occasion extended this technique to geopressured intervals on a well-by-well basis. Geopressures drastically affect the porosity compaction of shale and to some extent the sands. Porosity in turn governs the formation resistivity factor (see Figure 3). Therefore, no universal, or average, correlation curves can be constructed for geopressured intervals since hardly any two wells encounter the geopressure top at the same depth and have the same pressure profile below top of geopressures.

CONCLUSIONS

1. The conductivities of clean water-bearing sands and nearby silty shales have been empirically related for the normal pressured Pleistocene Offshore Louisiana.

2. The sand connate water resistivity can be determined from nearby shale conductivity. This relationship gave statistically accurate sand water resistivities for the interval 4000 feet to 6000 feet in the SMI 130 Field.

3. This relationship can be extended to geopressured measures but only on an individual well basis.

REFERENCES

1. Waxman, M. H. (1971), Inter-Company Report Regarding Anomalous Shale Resistivities, Shell E&P Research, Houston, Texas.

2. Hedberg, W. H. (1967), Pore-Water Chlorinities of Subsurface Shales, Ph.D. Thesis, Geology, The University of Wisconsin.

3. Russell, K. L. (1971), Fresher Interstitial Waters from Normal Marine Shales, Trans. Amer. Geophys. Union, V. 52, No. 11 P. 929, November

4. Baharloui, A. (1973), A Comparison of the Chemical Composition of Interstitial Waters of Shales and Associated Brines, Ph.D. Thesis, The University of Tulsa.

5. Schmidt, G. W. (1973), Interstitial Water Composition and Geochemistry of Deep Gulf Coast Shales and Sandstones, AAPG Bulletin, V. 57, No. 2, P. 321, February.

6. Engelhardt, W. V. and Gaida, K. H. (1963), Concentration Changes of Pore Solutions during the Compaction of Clay Sediments, Journal of Sedimentary Petrology, V. 33, No. 4, P. 919, December.

7. Waxman, M. H. (1978), Personal Communication, Shell E&P Research, Houston, Texas, March.

8. Smith, J. E. (1977). The Thermodynamics of Salinity Changes Accompanying Compaction of Shaly Rocks, Society of Petroleum Engineering Journal, P. 377-386.

ABOUT THE AUTHORS

HARLAN J. RITCH graduated from Texas A&M University in 1957 and 1958 with a B.S. and M.S. degree in Petroleum Engineering, respectively. After joining Shell in 1958, Ritch worked as a field engineer in East Texas before moving to Houston. After working in East Texas, South Texas, and along the Gulf Coast, Ritch currently has the position of Staff Petrophysical Engineer in the Onshore Division Production Department of Shell Oil Company in New Orleans.

STRODE PENNEBAKER graduated from the University of Texas at Austin in 1973 with a B.S. degree in Mechanical Engineering. After joining Shell in 1974, Pennebaker worked in Production Engineering until his current position of Petrophysical Engineer in the Offshore Division Production Department of Shell Oil in New Orleans.

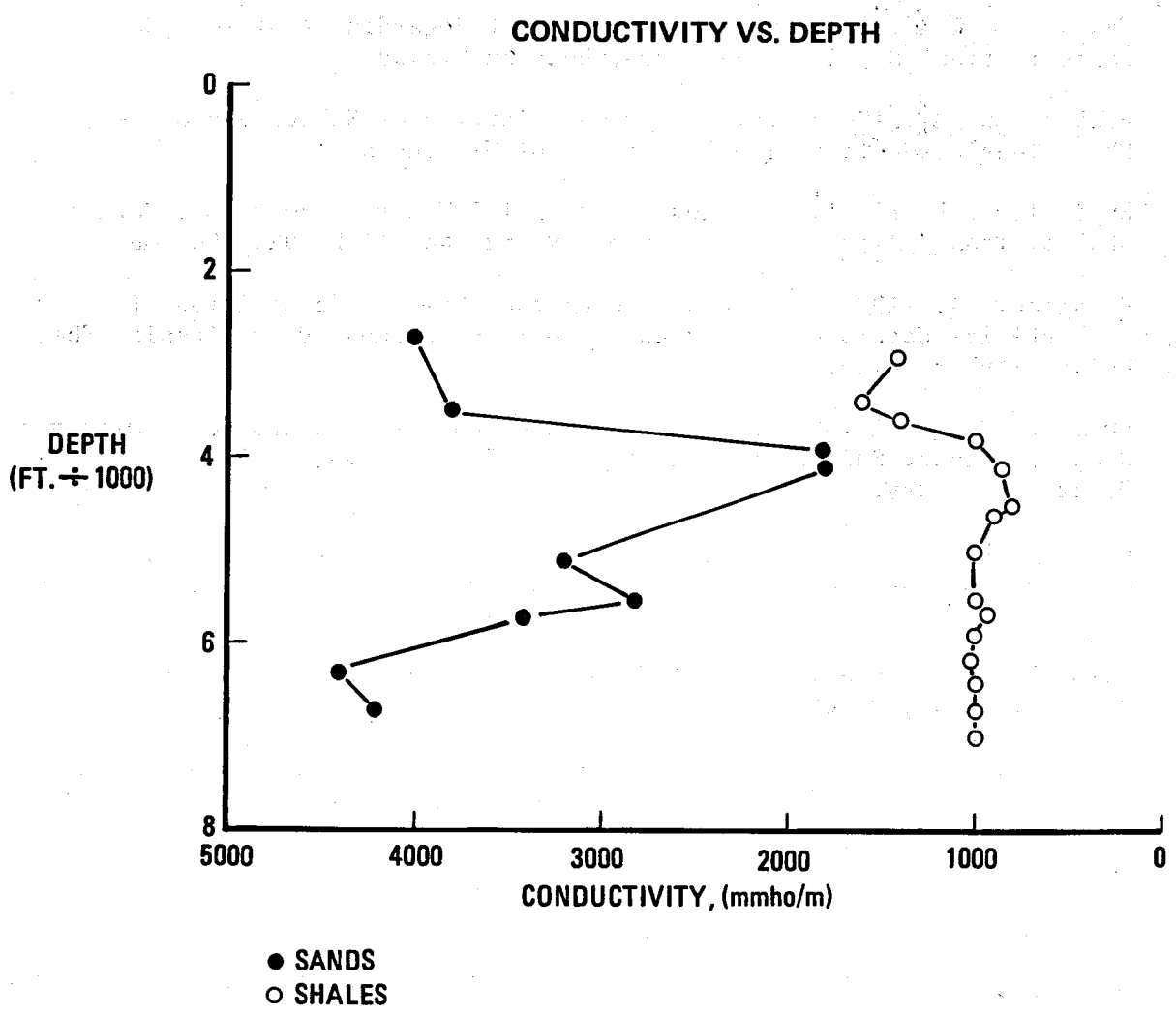

FIGURE 1 - VARIATIONS IN SAND AND SHALE CONDUCTIVITIES, SOUTH MARSH ISLAND 130 FIELD AREA

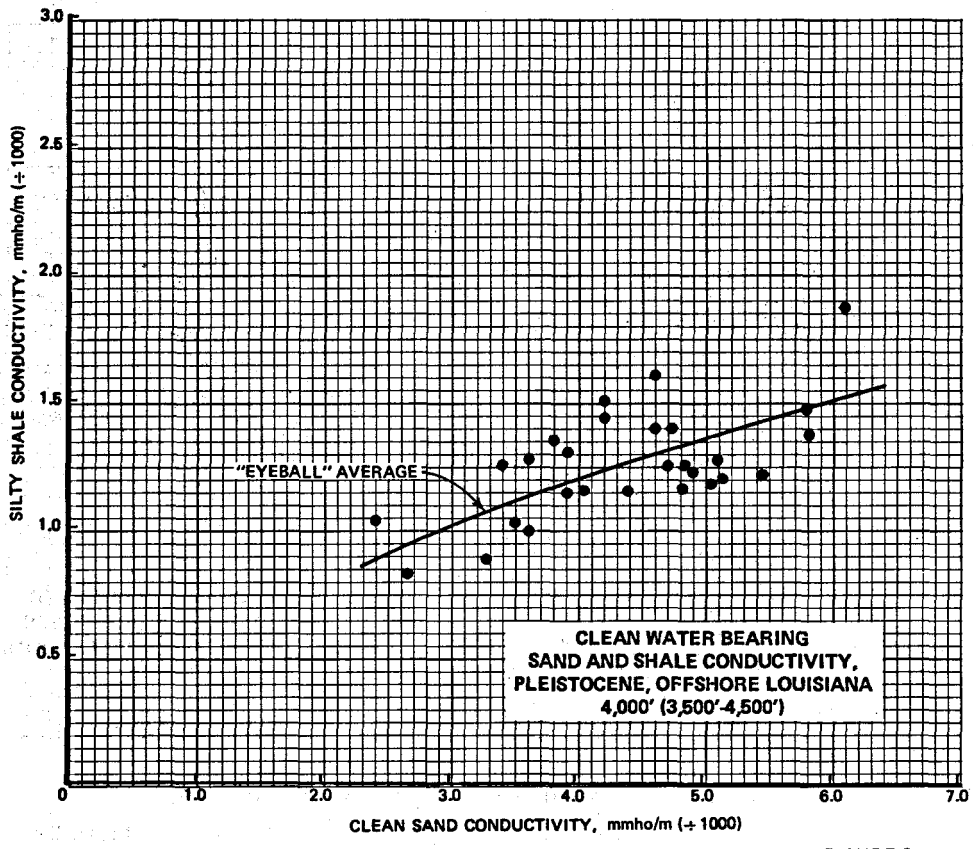

FIGURE 2

LITHOLOGY	GRAIN DENSITY	m	CEC meq/100 gms
CLEAN SAND	2.65	1.75	0
SILTY SHALE	2.69	2.10	15

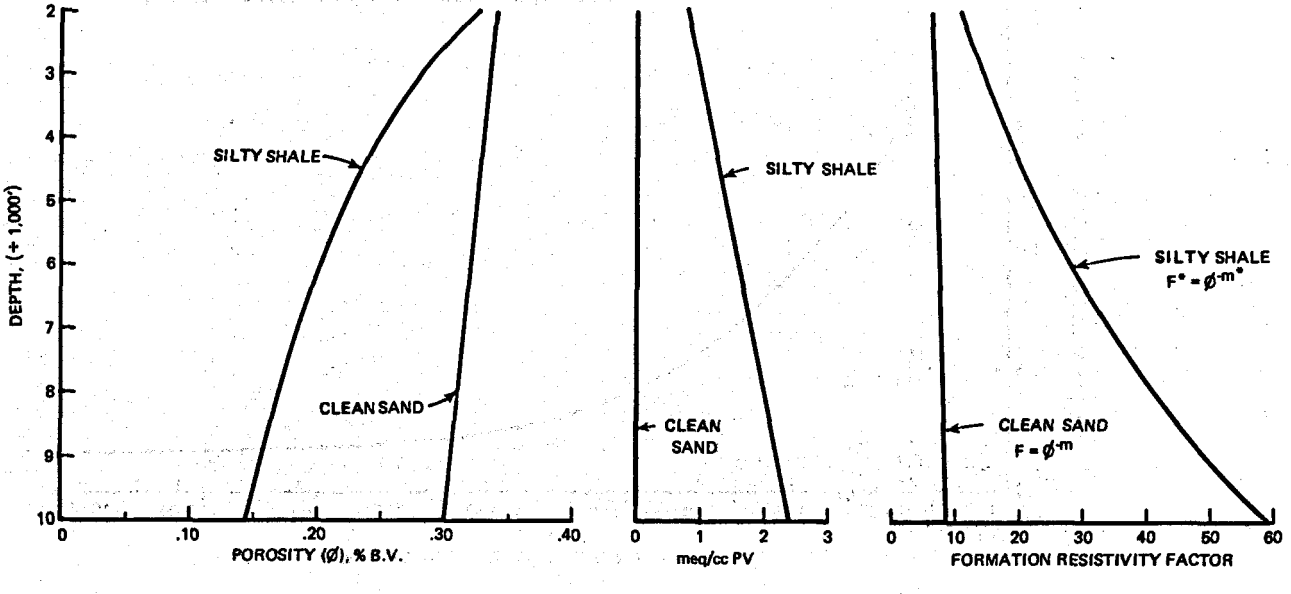

COMPACTION OF PLEISTOCENE SAND & SHALE
OFFSHORE LOUISIANA

FIGURE 3

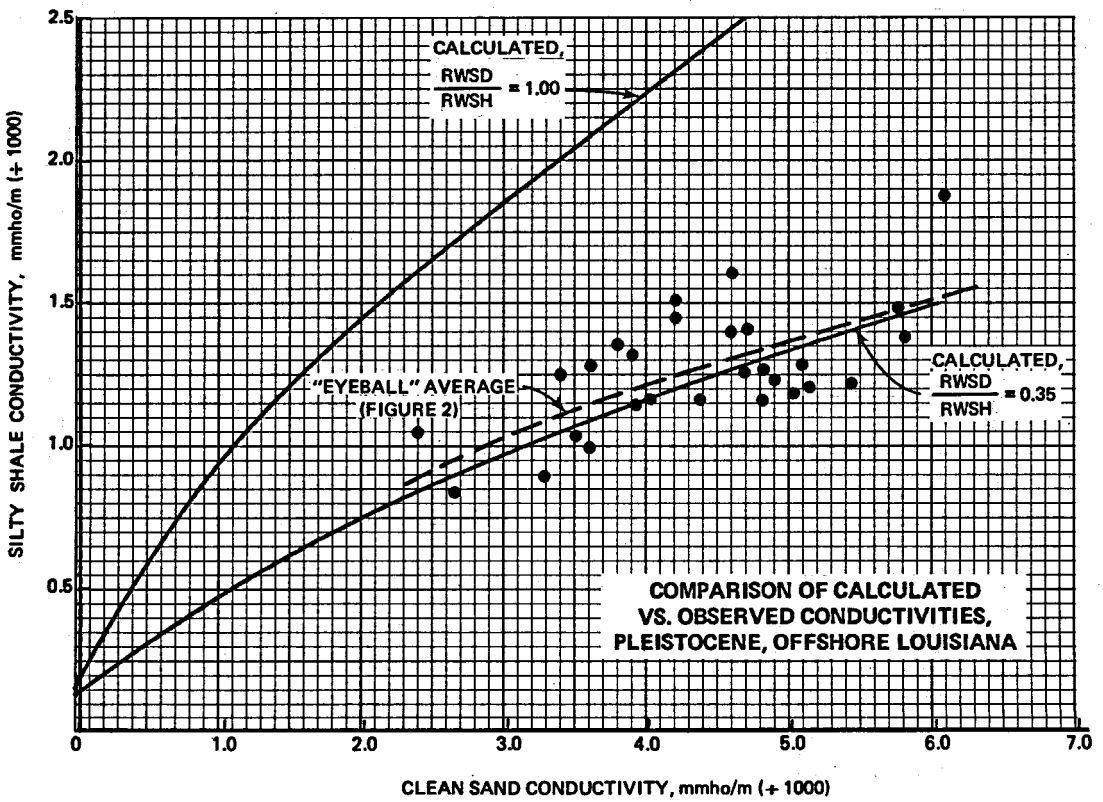

FIGURE 4

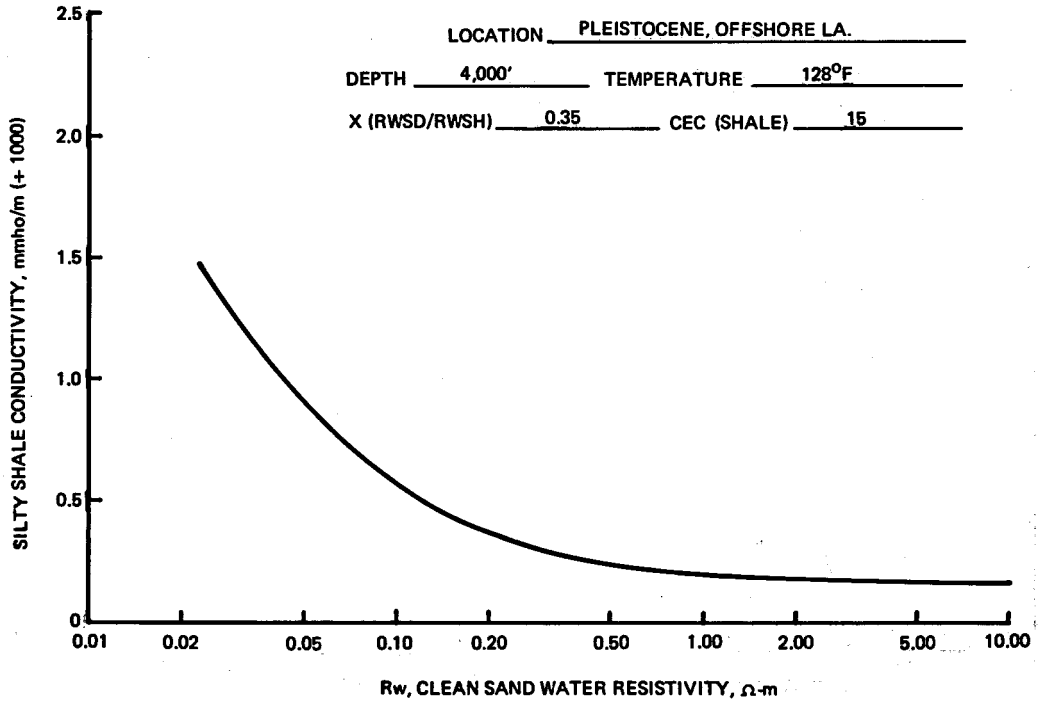

CLEAN SAND WATER RESISTIVITY VS. SILTY SHALE CONDUCTIVITY

FIGURE 5

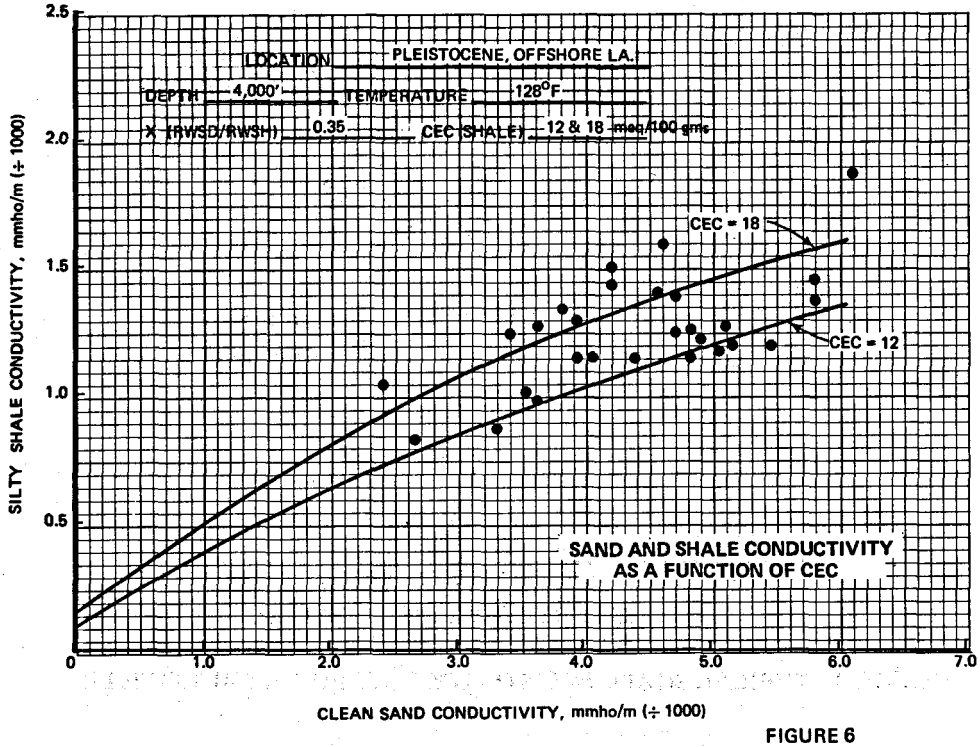

FIGURE 6

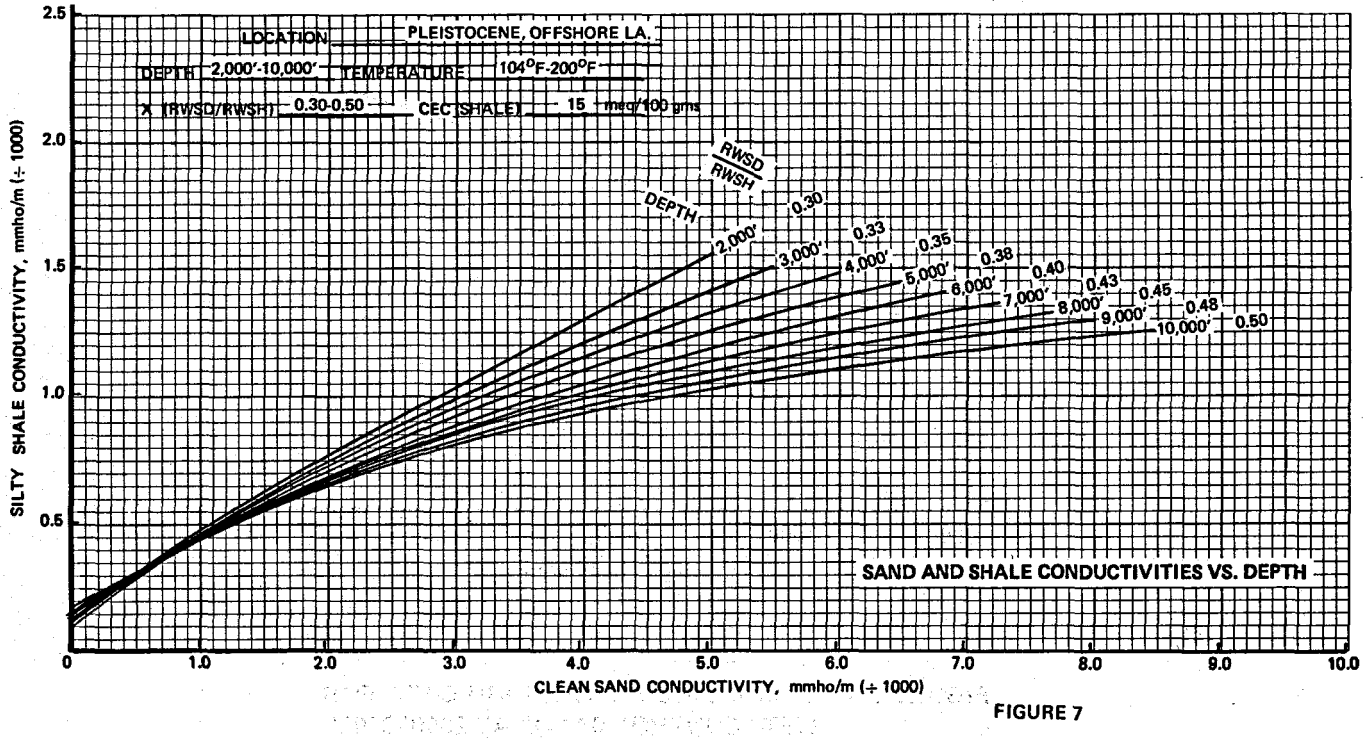

FIGURE 7

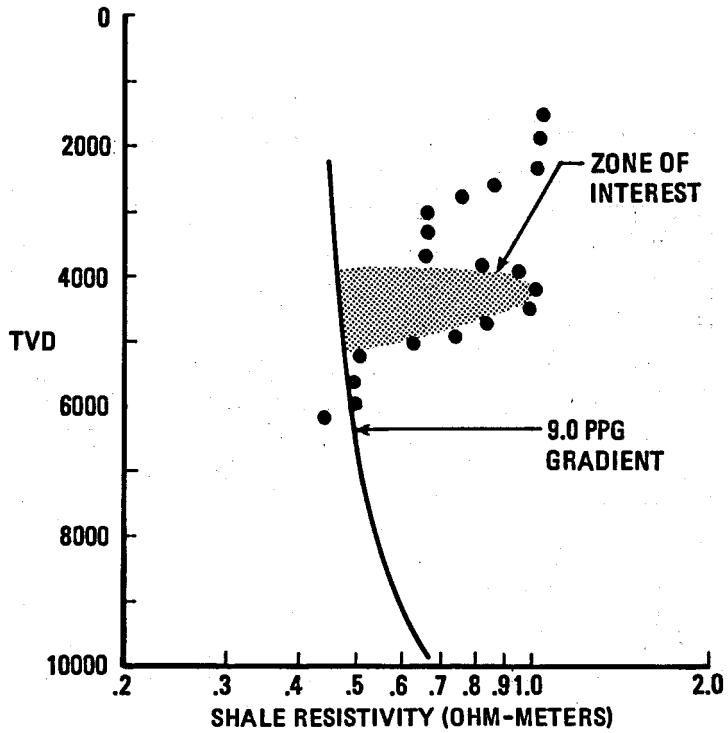

FIGURE 8 - TYPICAL SHALE RESISTIVITY PLOT FOR A SMI 130 WELL

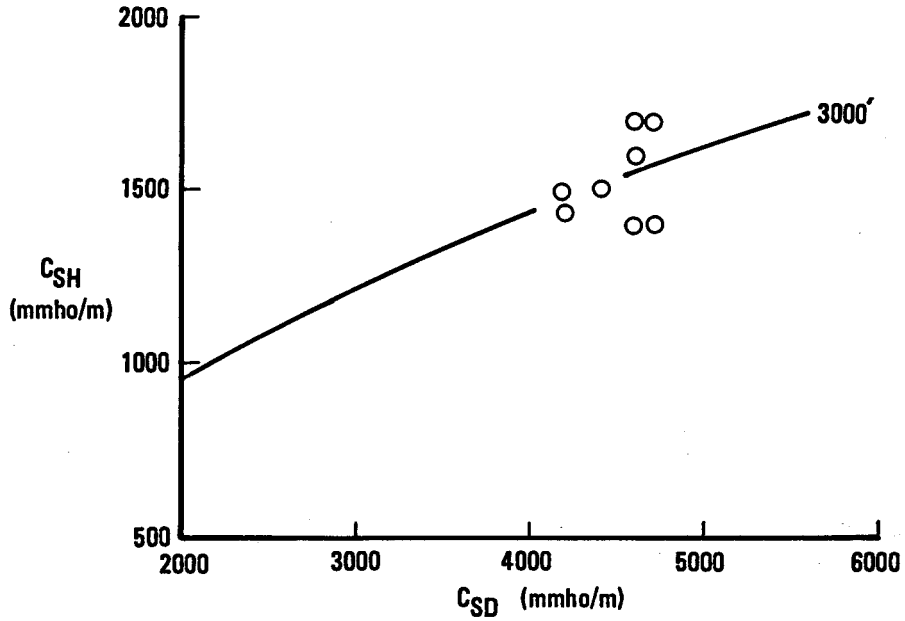

FIGURE 9 – TREND LINE FIT THROUGH DATA FOR WET "CONTROL SAND" AT 2950'-3100' USING CEC = 18 & RwSd/RwSh = 0.33

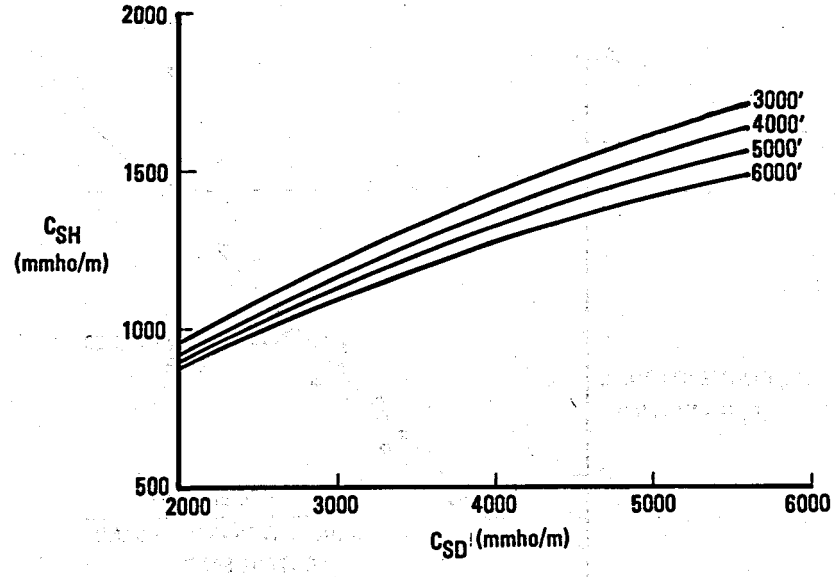

FIGURE 10 – EXTRAPOLATED TREND LINES 3,000' TO 6,000' BETWEEN SAND & SHALE CONDUCTIVITY

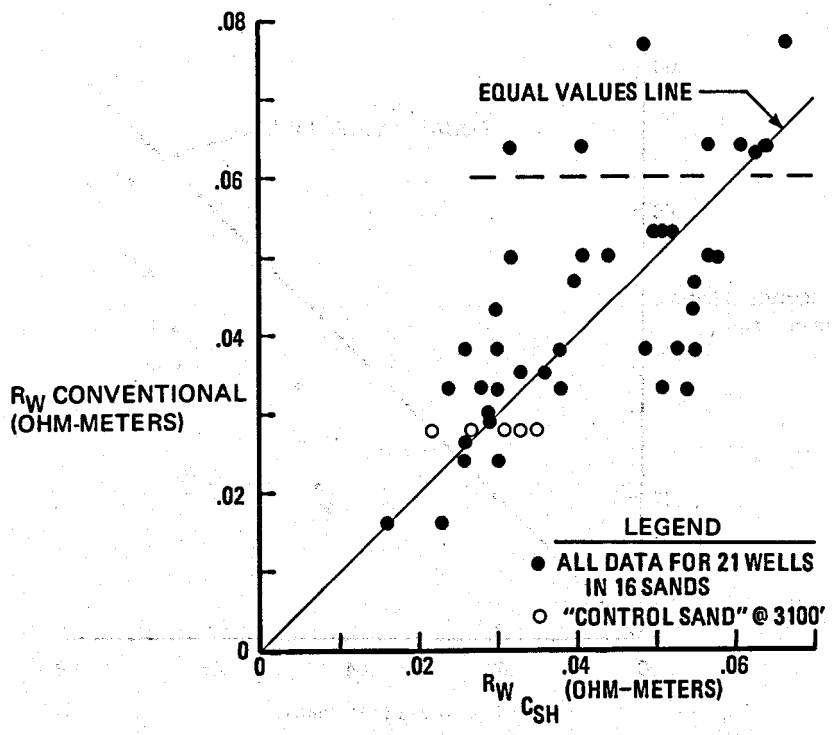

FIGURE 11 - COMPARISON OF R_W OBTAINED BY CONVENTIONAL METHOD AND SHALE CONDUCTIVITY TECHNIQUE

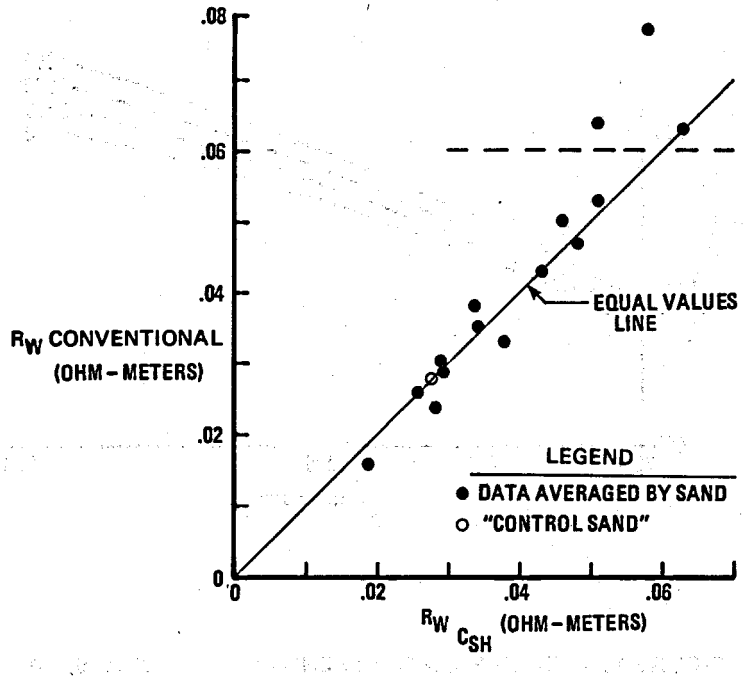

FIGURE 12 - AVERAGING R_W IMPROVES ACCURACY OF THE TECHNIQUE. (SEE FIGURE 11)

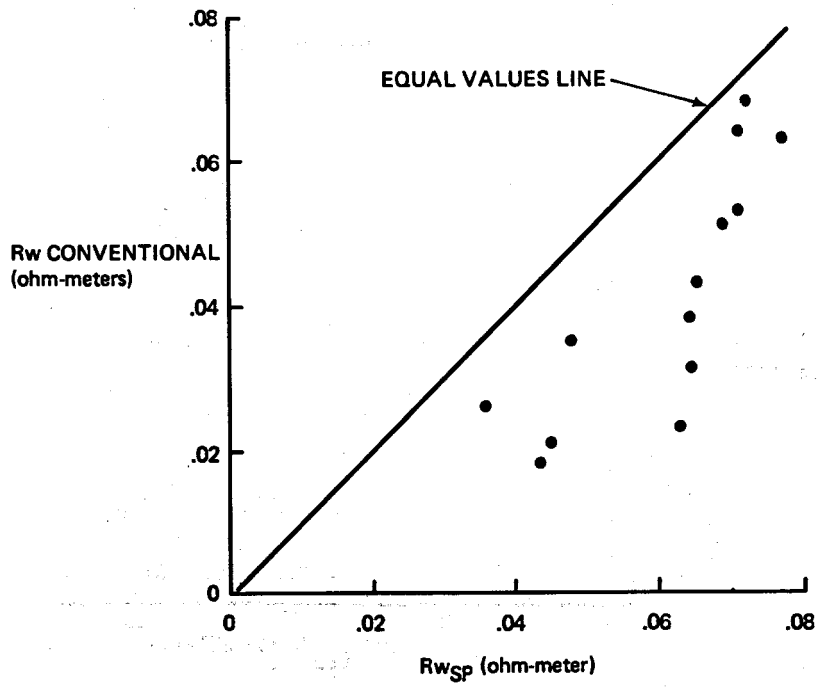

FIGURE 13 - COMPARISON OF Rw OBTAINED BY CONVENTIONAL METHOD AND SP CURVE TECHNIQUE

A NEW APPROACH TO CARBONATE ANALYSIS

by

W. H. Nugent, Schlumberger Well Services, Abilene, Texas
G. R. Coates, Schlumberger Well Services, Houston, Texas
R. P. Peebler, Schlumberger Well Services, Corpus Christi, Texas

ABSTRACT

Water saturations from vuggy or oolicastic carbonates are often over-optimistic. Here we present an empirical but well-established technique that permits confident evaluation of such formations. This method makes use of the fact that sonic logs respond differently to vugs and oolicasts than do the nuclear porosity logs.

INTRODUCTION

Log analysis in complex lithologies often depends upon the Formation Density (FDC*) and Neutron (CNL* or SNP*) logs to provide determinations of porosity and lithology. The neutron-density porosity, ϕ_{ND}, represents total liquid-filled porosity. If the pore space is entirely intergranular, ϕ_{ND} permits reliable Archie-type derivations of water saturation.[1] However, if the porosity distribution is non-uniform, as in vuggy or oolicastic rocks, the relationship between porosity and formation factor may change significantly. In such cases, S_w's based on neutron-density porosities are likely to be wrong.

The sonic log has been a useful means for identifying the presence of vugs or oolicasts. It is speculated that the sonic is blind to such secondary porosity because the acoustic energy bypasses the relatively large cavities. (A "Secondary Porosity Index" (SPI) has been defined as $\phi_{ND} - \phi_{SV}$.) This speculation seems to be borne out when the cavities are scattered and poorly connected; but in oolicastic or microvuggy rocks the sonic pulses can no longer follow direct paths through the matrix. Travel time and sonic porosity are increased, though ϕ_{SV} never reaches equality with ϕ_{ND} so long as secondary porosity is a factor.

---

* Mark of Schlumberger.

Interpretation

The variation in the formation factor/porosity relationship seems to indicate that the porosity added by vugs does not contribute significantly to the formation conductivity. Consequently, the controlling factor for resistivity tools is the matrix porosity, which is analogous to a series resistor network. Note that this behavior is more like that of the sonic than of the neutron-density tools.

From this, it would seem logical to use the resistivity and sonic logs together, and the density and neutron together. The problem consists of finding a way to do this that will provide reliable production forecasts in either intergranular, vuggy, or oolicastic porosity.

Technique

The method described here is an adaptation of the water saturation/porosity relationship of Morris and Biggs[2], which is based on a knowledge or assumption of the irreducible water saturation, S_{wi}. A hyperbolic relationship is proposed on the S_w-ϕ crossplot, the equation being:

$$S_{wi} = C/\phi \qquad (1)$$

where C is a constant of the rock, and also, since $C = S_{wi} \times \phi$, it represents the bulk volume fraction of water in the rock at irreducible saturation.

Our method proposes to assume irreducible water saturation in all formations, and compute an "apparent C" value from the log readings. To avoid confusion, we will call this value "PRI", for "Productivity Ratio Index", since its principal purpose is to predict the water-oil ratio to be expected.

The success of the method depends on using the logs in compatible combinations. Thus we use the resistivity and sonic readings to find S_w, and the neutron and density logs for ϕ.

It is also necessary to know or assume the water/hydrocarbon ratio in the vugs. Experience indicates that this is given with acceptable accuracy by the sonic-derived S_w values (S_{wSV}).

Thus we have:

$$PRI = \phi_{ND} \times S_{wSV} \qquad (2)$$

where

$$S_{wSV} = \sqrt{\frac{1}{\phi_{SV}^2} \times \frac{R_w}{R_t}}$$

Note that this method requires no manipulations of the Archie exponents m and n in the basic saturation equation: $S_w^n = 1/\phi^m \times R_w/R_t$. Both m and n are taken to be 2 throughout.

The significance of Eq. 1 is that, in conditions of irreducible saturation, PRI thus computed is analogous to C, and is reasonably well known in most carbonates. In our experience, the value PRI = 0.02 serves well in vuggy or oolicastic formations at irreducible water saturation. Hence, when PRI ≤ 0.02, clean hydrocarbon production is indicated. As PRI increases above 0.02, increasing watercut can be expected up to PRI ≈ 0.04, at which point the production will reach 100 percent water.

It is important, however, to discriminate between primary (intergranular) and secondary (vuggy, oolicastic) porosity. If the reservoir consists of primary porosity, PRI at irreducible saturation will be more nearly in the range of 0.04. For this reason, it is necessary for confident log analysis to have all three basic porosity logs, in addition to resistivity, whenever both primary and secondary reservoir porosity are possibilities.

Field Applications

Though empirical, this technique is well proved in West Texas and other carbonate-reservoir areas, under conditions which rendered other watercut-estimating methods unreliable. Examples 1-4 illustrate both hydrocarbon and water predictions by hand computations.

The PRI method has also been adapted for computer application, by a modification to the CORIBAND* processing technique. Examples 5, 6, and 7 illustrate the uses of this presentation.

Example 1 (Garza County, Texas, wildcat)

These logs (Fig. 1) indicate intergranular porosity ($\phi_{ND} \approx \phi_{SV}$) in the zone around 8,200 feet, with a PRI computed as follows:

---

* Mark of Schlumberger.

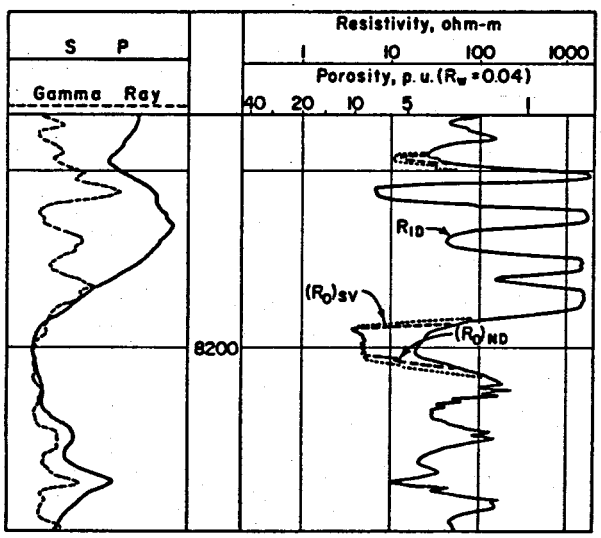

Fig. 1

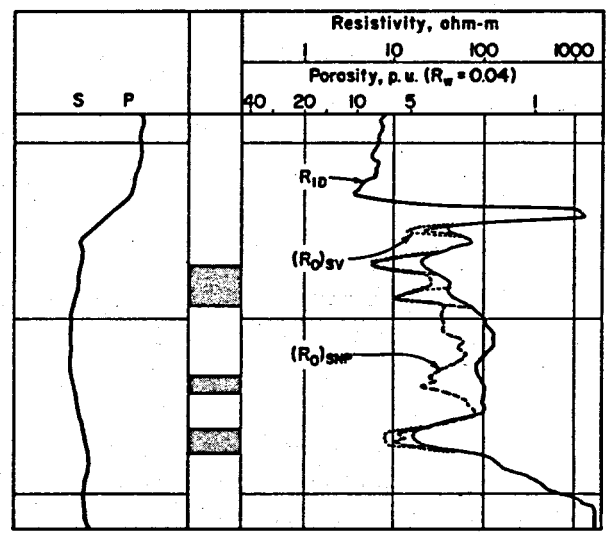

Fig. 2

$$R_w = 0.04$$

$$R_t = 25$$

$$\phi_{SV} = 9 \text{ p.u.}$$

$$S_w^2 = 1/0.09^2 \times 0.04/25 = 0.20$$

$$S_w = 0.04$$

$$PRI = \phi_{ND} S_{wSV} = 0.09 \times 0.44 = \underline{0.04}$$

Since 0.04 is a reasonable value for PRI in intergranular rocks, this formation should produce clean hydrocarbon. In fact, on a straddle-packer DST, it flowed oil at the rate of 1,400 B/D with no water.

Example 2 (Kent County, Texas, Strawn Limestone, wildcat)

This is another case of primary porosity ($\phi_N \approx \phi_{SV}$). The logs in Fig. 2 show several potentially productive zones. Local experience dictates limits of PRI between 0.03 and 0.05 for water-free production in intergranular porosity, as we have here.

The indicated zones were perforated and acidized. Each zone satisfies the PRI criterion: $0.03 \leq PRI \leq 0.05$. Well showed potential of 75 BOPD pumping, no water.

Example 3 (Kent County, Texas, Strawn Limestone, wildcat)

Here we have a vuggy formation, revealed by the separation between ϕ_{SV} and ϕ_{SNP}* (Fig. 3). PRI should be between 0.01 and 0.02 in this rock.

S_w calculations indicate possible oil production, but the PRI calculates as:

$$PRI = \phi_{SNP} \times S_{wSV}$$

$$= 0.11 \times \sqrt{\frac{1}{(0.07)^2}} \times \frac{0.04}{17}$$

$$= .07 +$$

which is well above the 100-percent water value of 0.04. And in fact, a straddle-packer test produced 560 feet of mud-cut salt water, with no show of oil or gas.

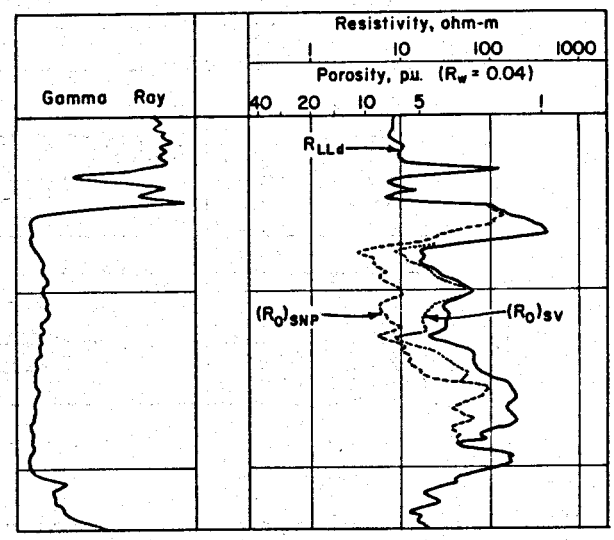

Fig. 3

* Mark of Schlumberger.

Example 4 (Borden County, Texas, Strawn Limestone, micro-vugs)

Again the PRI condemns zones which appear productive by conventional log analysis.

Fig. 4 shows the DIL* with R_0 overlays, and some results of log analysis. As you see, these zones must be considered potentially productive on the basis of these figures. However, vuggy porosity is indicated by the $(R_0)_N$ - $(R_0)_{SV}$ separation. And in the best zone at A, PRI computes as:

$$PRI = \phi_N \times S_{wSV}$$

$$= 0.07 \times 0.48$$

$$= 0.0336$$

which indicates over 50 percent water production.

This zone recovered 1,600 cc water and 50 cc oil on a DST.

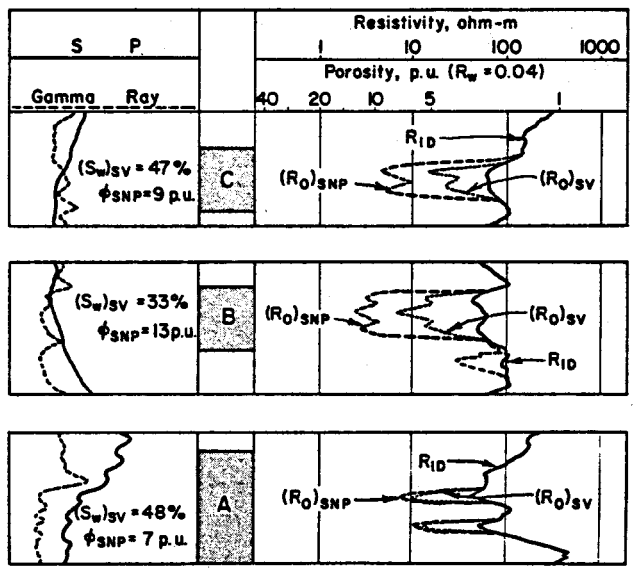

Fig. 4

Zone B shows PRI = 0.043, indicating 100 percent water production. The DST recovered 500 cc mud, 1,500 cc water, and no oil.

Zone C is also condemned by PRI, with a value of 0.042. The DST results: 2,150 cc salt water, no oil.

* Mark of Schlumberger.

Example 5 (Lea County, New Mexico)

Fig. 5 is a CORIBAND output with the PRI ($\phi_{ND} \times S_{wSV}$) values substituted for the conventional Bulk Volume Water curve in Track 4, with the area under the curve shaded. Secondary Porosity Index (SPI) is also plotted, left-to-right, area coded clear. In addition, a dotted curve representing S_w from sonic F values is added to CORIBAND S_w's (solid curve) in Track 2.

The zone of interest is at 6,500 ft. From the Productivity Log we see that S_w from CORIBAND is about 35 percent (Track 2), and bulk volume of water from the above S_w and ϕ_{ND} is 0.05 (Track 3). If the reservoir porosity is intergranular, this zone should be productive; but look at the SPI curve in Track 4. This says the zone has up to 5 percent secondary porosity, meaning it is vuggy or oolicastic. And the PRI curve reads above 0.06 (Track 4), which unequivocally condemns the zone.

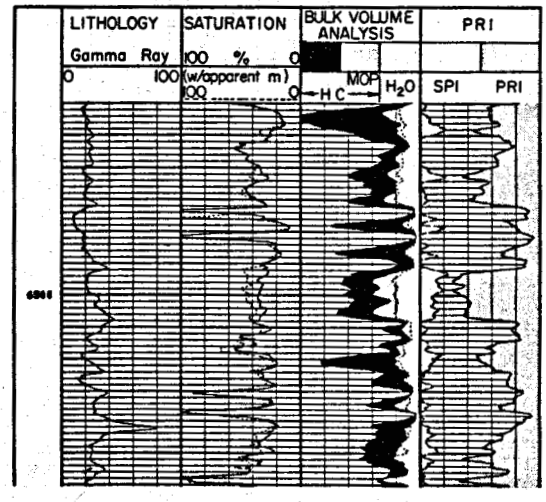

Fig. 5

This zone was tested at considerable length. The best test yielded 3 BO and 225 BW pumping in 24 hours.

Example 6 (Tom Green County, Texas, wildcat)

Again the CORIBAND looks good, but the SPI says it is vuggy, and the PRI condemns it. The zone at 5,310 (Fig. 6) shows $S_w \approx 30$ percent. However, the SPI curve indicates up to 5 percent ϕ_2, while PRI is over at 0.05 in most of the interval. Conclusion: vuggy or oolicastic rock, water productive.

A drillstem test across this interval was misleading, yielding 500 ft of gas, 112 ft of slightly oil and gas-cut mud, and no water. However, the production tests after acidizing gave up only salt water with a trace of oil.

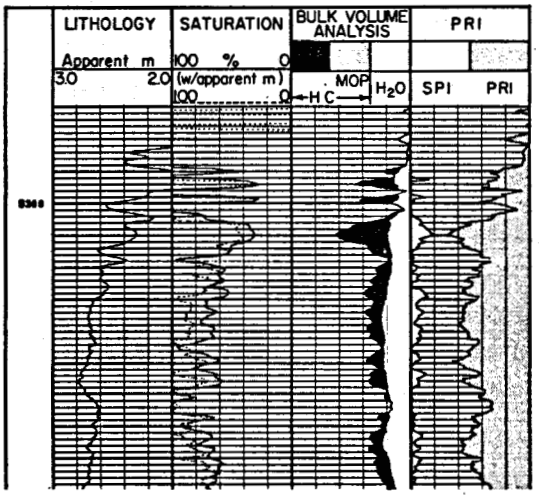

Fig. 6

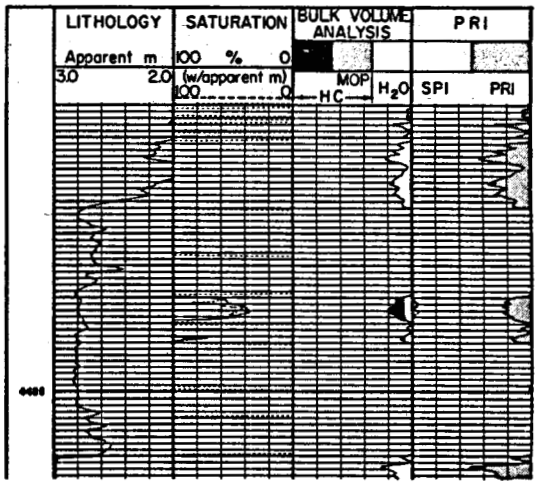

Fig. 7

Example 7 (Runnels County, Texas, Gardner Limestone)

This well illustrates the ability of the PRI technique to predict the approximate watercut to be expected. The zone at 4,370 feet doesn't look as good as those in Examples 5 and 6, but the PRI is only 0.022. Since this lies between our empirical limits, somewhat on the low side, we conclude that the zone will produce oil, but with a fairly low watercut. After acidizing and fracturing, the zone produced 100 BOPD pumping, plus 10 to 15 percent water. (Fig. 7)

SUMMARY

Experience shows that conventional log analysis is often erroneously optimistic in carbonate rocks, especially when the porosity distribution includes vugs or casts.

The addition of a sonic log to the usual suite of resistivity, neutron, and density logs offers a way to recognize these errors and to predict reliable water-oil ratios before the well is completed.

This technique consists of computing a Productivity Ratio Index (PRI) as follows:

$$PRI = S_{wSV} \times \phi_{ND}$$

and comparing this PRI value with known limits for production of clean oil and watercut oil. Though local experience is helpful in choosing these limits, the following values have proved widely applicable in vuggy or oolicastic carbonates:

Condition	Prediction
$PRI \leq 0.02$	Clean oil
$0.04 > PRI > 0.02$	Water plus oil
$PRI \geq 0.04$	Water, no oil

The sonic log will also verify the presence of rocks with intergranular porosity; in such cases $\phi_{SV} \approx \phi_{ND}$. When this happens, conventional interpretation methods can be used with confidence.

REFERENCES

1. Schlumberger Log Interpretation-Vol. 1: Principles, Schlumberger Limited, New York, 1972.

2. Morris, R. L. and Biggs, W. P.: "Using Log-Derived Values of Water Saturation and Porosity", Transactions, SPWLA Symposium, 1967.

ABOUT THE AUTHORS

W. HARRISON NUGENT

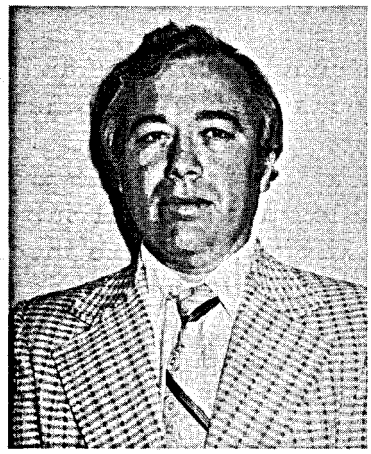

GEORGE R. COATES

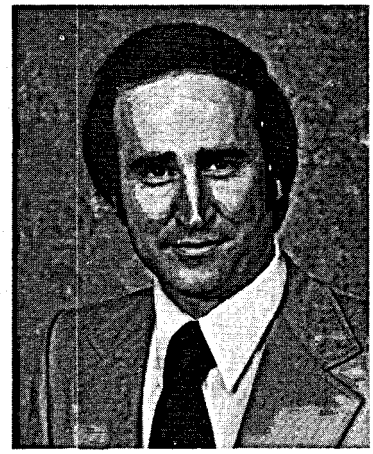

ROBERT P. PEEBLER

W. HARRISON NUGENT is a Senior Sales Engineer with Schlumberger, at Abilene, Texas. He has 30 years with the company, all in Texas.

Mr. Nugent is a graduate of Louisiana Polytechnic Institute, with a BS-ME degree. Prior to joining Schlumberger, he served with the U.S. Navy and the U.S. Maritime Service.

GEORGE R. COATES is a Senior Interpretation Engineer in the Operations/Marketing Department of Schlumberger in Houston. He holds a BS-ME degree from South Dakota State, graduating in 1961.

His affiliation with Schlumberger began in 1964, in the capacity of Field Engineer. Prior to his present assignment, he served for two years as head of the Log Interpretation Research section at Schlumberger-Doll Research Center, Ridgefield, Connecticut.

ROBERT P. PEEBLER is Division Manager of Schlumberger's South Texas Division. He began with Schlumberger as a Field Engineer at Woodward, Oklahoma, in 1970. Since then he has held various sales, staff, and management positions in Louisiana and Texas.

Bob graduated from the University of Kansas with a BS-EE degree.

ACKNOWLEDGMENT

The authors wish to thank the several oil companies who released logs and other data used in this paper.

SOME ASPECTS OF THE CALCULATION OF GYPSUM-FREE POROSITY

By

Elton Frost, Jr.
Dresser Atlas Division, Dresser Industries, Inc.
Houston, Texas

ABSTRACT

The techniques of using log-derived data in complex lithologies to derive reasonable pictures of the true lithologies are as numerous and varied as the possible combinations of the minerals encountered in the rock itself. This paper will review some of the methods available for identifying and coping with one of these minerals, gypsum, which is sometimes present in a potentially productive reservoir. Some of the more frequently used methods will be discussed in the hope that new insight will be gained into their use in bulk volume mineral calculation. A new method of considering the percent gypsum content and porosity will also be presented. Examples of the usefulness of this new method will be given.

INTRODUCTION

Within the last few years, a considerable work and effort has gone into establishing methods of identifying complex lithologies as to mineral and shale content. By determining these parameters, the techniques are now available to calculate a much more accurate value of formation porosity. These efforts have primarily dealt with the three most common reservoir minerals, along with shale and, in some cases, anhydrite. While these are all of primary concern, the presence of another mineral, gypsum, will at times present a problem to both manual and computer-processed interpretation of porosity, mineral type, and shale content in reservoir rocks.

The primary purpose of this paper is to discuss some of the methods now available for calculating the percent volumes of several minerals in a reservoir when gypsum is present. An effort will also be made to examine a new technique in mineral identification which may possibly lead to a more accurate field determination of the true mineral content when gypsum is present. This technique will employ a modified version of the standard "Litho-Porosity Crossplot."

SINGLE-POROSITY INTERPRETATION

In order to evaluate the effect of gypsum on a single porosity device, a comparision of the normal responses of the acoustic, neutron, and density instruments to the three primary reservoir minerals versus their response to the mineral gypsum should be made.

The presence of gypsum will be manifested on a Densilog® as a much lower bulk density than would occur if only the normal configuration of the possible combinations of sandstone, limestone, and dolomite were present. This is apparent since the normal matrix value contrast is from 2.65 gm/cm^3 for sandstone to 2.87 gm/cm^3 for dolomite versus a matrix value of 2.35 gm/cm^3 for gypsum. Gypsum is a basically low gamma ray value type of mineral and exhibits a very high apparent resistivity. With a Densilog-Gamma Ray Log combination, a formation where gypsum is present can easily be mistaken for a clean formation with an optimistic porosity and low water saturation value. This zone could then be considered a pay section without anyone being aware of the presence of gypsum within that zone.

The variation in the Neutron Log response on a limestone porosity scale varies from about -3.5 percent for sandstone to approximately +3.5 percent for dolomite, compared to an apparent Neutron Log response of approximately 49 percent for the mineral gypsum. It is apparent that the Neutron Log response will also show an optimistic porosity when gypsum is present. Here again, the presence of gypsum is not readily apparent when only one porosity device is available. The calculation of such an optimistic neutron porosity due to the presence of gypsum in a zone of interest could very easily lead to the perforation of that zone where there is no possibility of hydrocarbon production.

The Acoustilog® provides the only porosity measurement which is not extensively affected by the presence of gypsum. Due to the fact that gypsum has a transit time of 52 μsec, this value lies within the bounds of the three major reservoir minerals (55.5 μsec for sandstone to 43.5 μsec for dolomite). Even with the Acoustilog, gypsum could still cause a porosity error of from -3 percent to +6 percent in a zone, depending upon the actual reservoir matrix components and the amount of gypsum present.

The use of only one porosity device does not allow the calculation of the amount of gypsum present or even a positive determination that there is gypsum present within a zone of interest. In considering any of the porosity measuring devices discussed, if only one device is available, any indication of the presence of gypsum will have to come from a comparison of drill cuttings or core studies of the interval of interest to the actual recorded log response.

DUAL-POROSITY INTERPRETATION

The use of two porosity measuring devices means that a two-mineral reservoir model can be assumed for solving for the bulk volume percentages of each mineral and the porosity. This is usually done by solving the following system of equations:

$$\Delta t = \phi \Delta t_f + V_1 \Delta t_{ma_1} + V_2 \Delta t_{ma_2} \quad (1)$$

$$\phi_N = \phi (\phi_N)_f + V_1 (\phi_N)_{ma_2} + V_2 (\phi_N)_{ma_2} \quad (2)$$

$$\rho_b = \phi \rho_f + V_1 \rho_{ma_2} + V_2 \rho_{ma_2} \quad (3)$$

$$1.0 = \phi + V_1 + V_2 \quad (4)$$

where ϕ = fractional porosity

V_k, k = 1,2 = bulk volume fraction of the total matrix

Each of equations (1) through (3) represents the actual separation of the total logging instrument response into its respective fluid and matrix components.

Only two of the equations (1), (2), or (3) are required in addition to equation (4) to solve this system. Note that the solution of this system is based upon the assumption that the response of each porosity measuring device to the porosity and varying lithology is a linear function. Due to the non-linearity of the Neutron Log response in a dolomite, it is necessary to construct a set of linear straight-line functions for the neutron device when dolomite is involved in order to be able to use the foregoing equations. The graphical solution of this set of equations is illustrated in

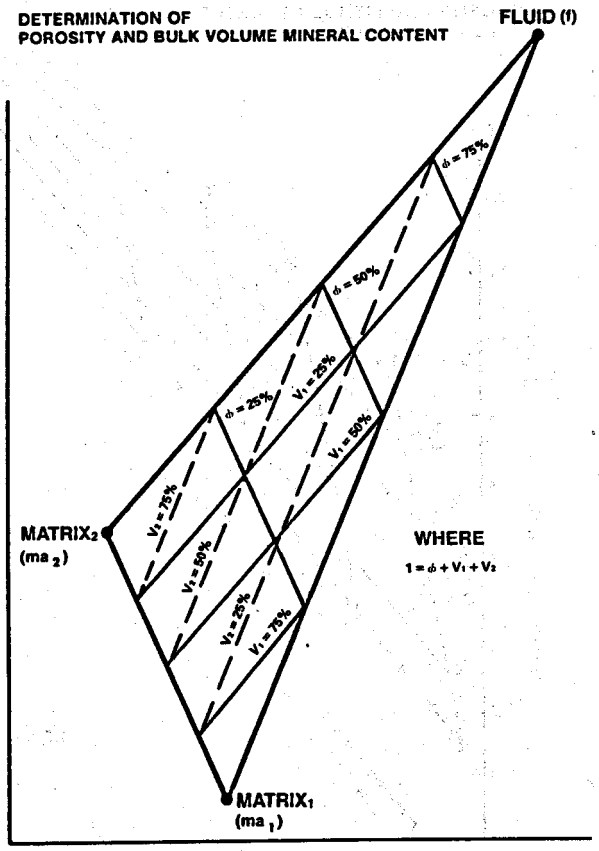

FIGURE 1

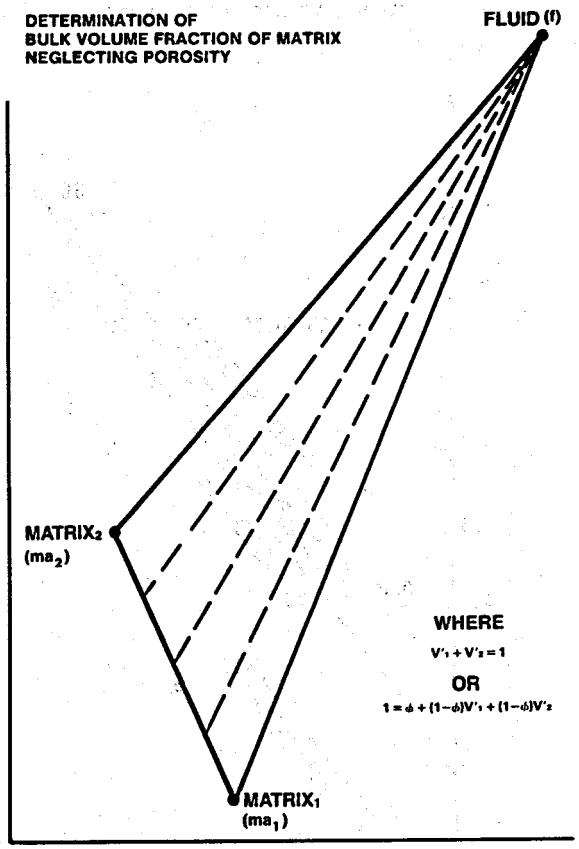

FIGURE 2

Figure 1. A solution is also possible for the bulk volume fraction of the matrix rock (neglecting porosity) as seen in Figure 2. In this case, the previous equations can still be used if it is considered that

$$V_1 = (1 - \phi)V'_1$$

$$V_2 = (1 - \phi)V'_2$$

$$\text{where } V'_1 + V'_2 = 1$$

Now consider the three possible combinations of two-porosity measuring devices when gypsum is present in the formation. With two-porosity devices, a much more accurate determination of the presence and quantity of gypsum is possible. In order to understand the gypsum effect more clearly, consider the dual-porosity crossplots.[2,3]

The gypsum point is prominent and isolated from the three primary matrix-to-fluid-point lines on the Densilog® vs. Acoustilog® crossplot (see Figure 3). This plot will show the presence of gypsum as a distinct shift of data points to the northwest in a clean formation. Also, note that shale causes a shift of the data points toward the east. Depending upon the shale and gypsum concentration, there is a possibility that the two will cancel out each other's effect and mask the presence of both shale and gypsum. Gas shifts the points toward the north-northwest in the same general direction as the gypsum matrix point. In a possible gas zone, gypsum will look like gas and gas will look like gypsum, if the formation contains gypsum. Secondary porosity can have

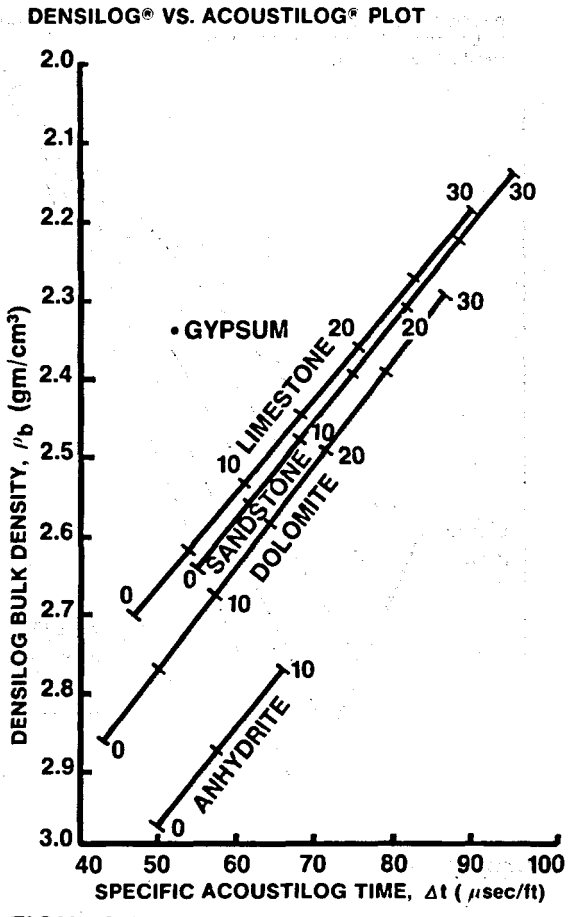

FIGURE 3

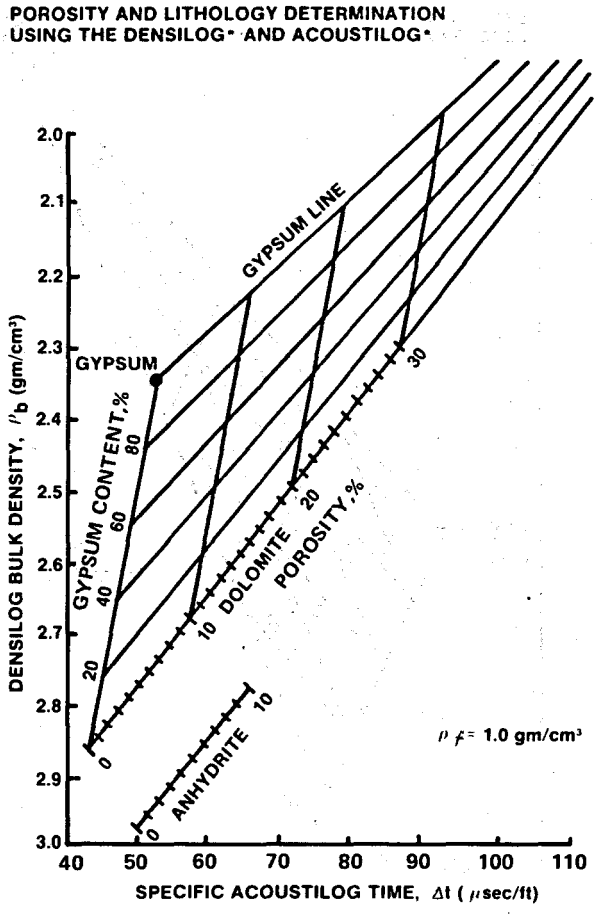

FIGURE 4

the same effect, since it causes a westerly shift into the gypsum area. Thus, if the zone is clean and non-gas-bearing, the presence of gypsum may be seen on the Densilog vs. Acoustilog crossplot. In fact, if an assumption is made that the reservoir is composed of only one mineral besides gypsum, the crossplot can be scaled in terms of porosity and the percentage of gypsum (see Figure 4).

In Figure 4, the assumption was made that only gypsum and dolomite were present in the reservoir. Note that the scaling in Figure 4 is a combination of the scaling techniques used in Figures 1 and 2. This is done in order to calculate both the porosity and the amount of gypsum versus the amount of dolomite in the formation. This technique can be used for any two mineral pairs, but no more than two minerals at a time can be considered, since only two porosity measuring devices were involved. If the actual primary reservoir rock is different from that which was assumed, there is the possibility that a large error can occur in the porosity value and gypsum content calculation.

The porosity uncertainty has always been inherent in the Densilog vs. Acoustilog crossplot due to the close proximity of the three primary matrix-to-fluid-point lines and the large relative displacements of the zero porosity matrix points of these lines. A small miscalculation as to the primary mineral present in the reservoir will cause a very large error in the porosity value determined from this crossplot. Since each of the matrix-to-fluid-point lines is unique for each of the primary minerals, an incorrect primary mineral choice will result in an incorrect lithology triangle being assumed, and hence, an error in the gypsum content calculated from this triangle.

EPITHERMAL NEUTRON VS. DENSILOG® PLOT

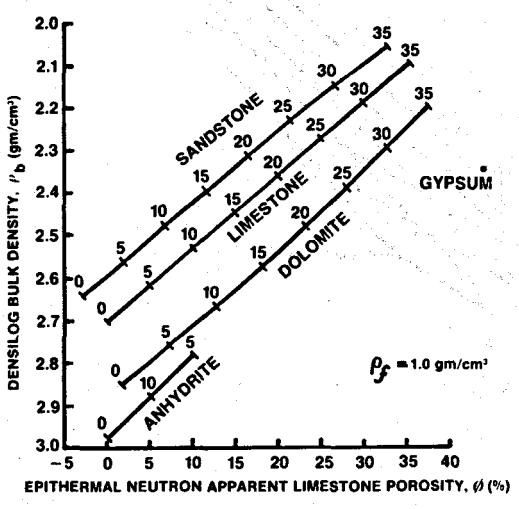

FIGURE 5

POROSITY AND LITHOLOGY DETERMINATION USING THE EPITHERMAL NEUTRON VS. DENSILOG®

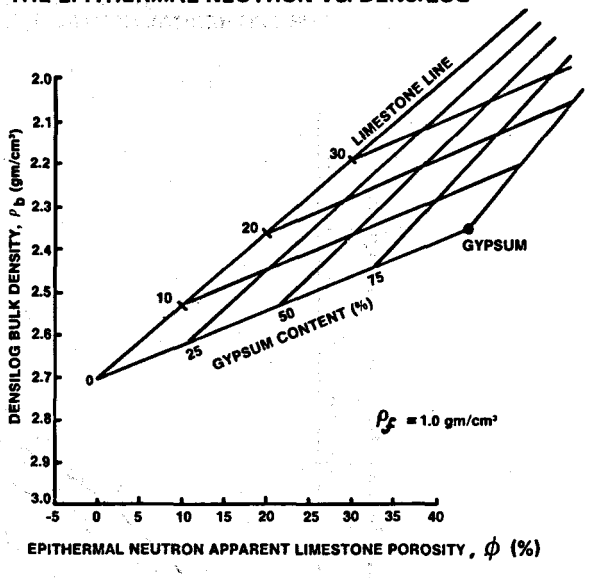

FIGURE 6

The Densilog vs. Neutron crossplot (Figure 5) is another two-porosity combination that must be considered. This is probably the most frequently used crossplot available today. The matrix porosity lines are well defined. A miscalculation in lithology will cause less than a two percent error in the calculated porosity value when the reservoir is composed of some combination of sandstone, limestone, and/or dolomite. Shale has the effect of pushing the data points in a primarily east-northeast direction. The presence of gas will cause a northwesterly shift of the data points. Since both the Neutron Log and the Densilog respond to the total porosity, secondary porosity does not present a problem. If the location of the gypsum matrix point is considered, it can be seen that it lies in a north-northeasterly direction from the matrix points of the sandstone, limestone, and dolomite porosity lines. Thus, in order to use this plot to determine gypsum content, only clean or shale-corrected zones must be considered. The presence of shale forces the data points out away from the main porosity lines in the same manner as would the gypsum. The presence of gas has an opposing influence when compared to the effect of gypsum; hence, gas and gypsum together will cancel out each other and mask each other's presence. Thus, in order to determine the true gypsum content, it is necessary to have a non-gas-bearing formation which is either clean, or is one in which the porosity values have been shale corrected. In this case a dual-mineral model of gypsum and one other mineral was assumed in setting up a triangle scaled to calculate gypsum content and porosity (Figure 6).

This scaling works satisfactorily for the sandstone and limestone lines. However, the dolomite porosity line is a non-linear function due to the Neutron Log response to the dolomite. This can be compensated for, as in Figure 7, by assuming a straight-line relationship between the fluid point and a pseudo dolomite matrix point. In Figure 7, the calculated porosities greater than 5.5 percent will be accurate, while those below 5.5 percent will not be as accurate. Two other pseudo-matrix points may be assumed to handle the range of porosities less than 5.5 percent. This process is acceptable if the actual matrix density of the mineral other than gypsum is known. If this matrix density is not correct, a large error in the calculated gypsum content and the calculated porosity value can occur. This can be readily seen by studying an overlay of Figures 6 and 7 as shown in Figure 8.

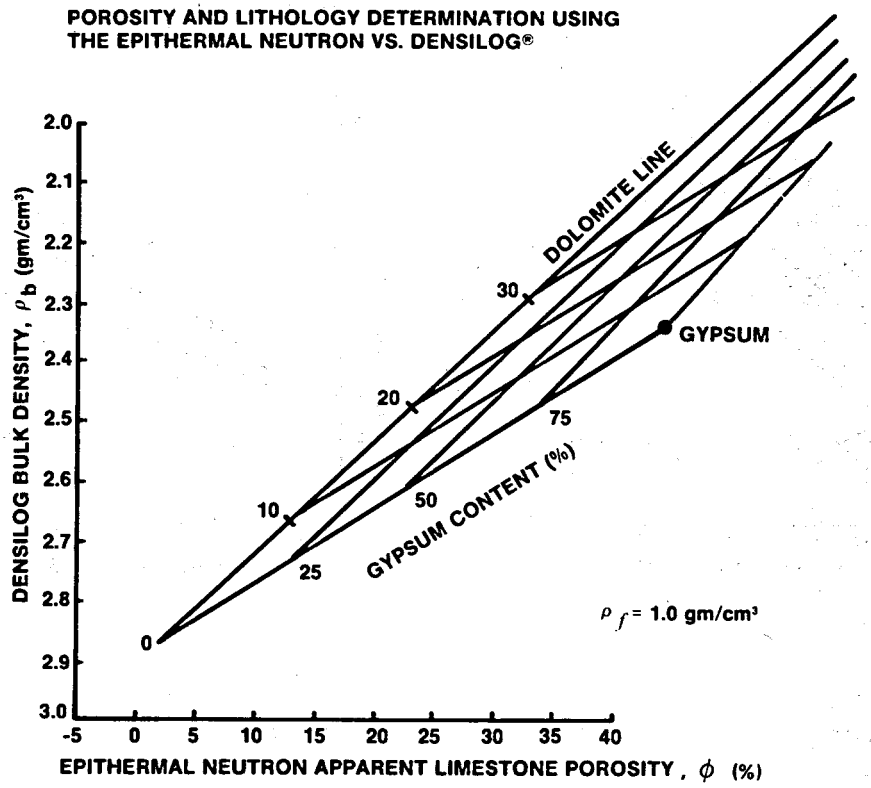

FIGURE 7

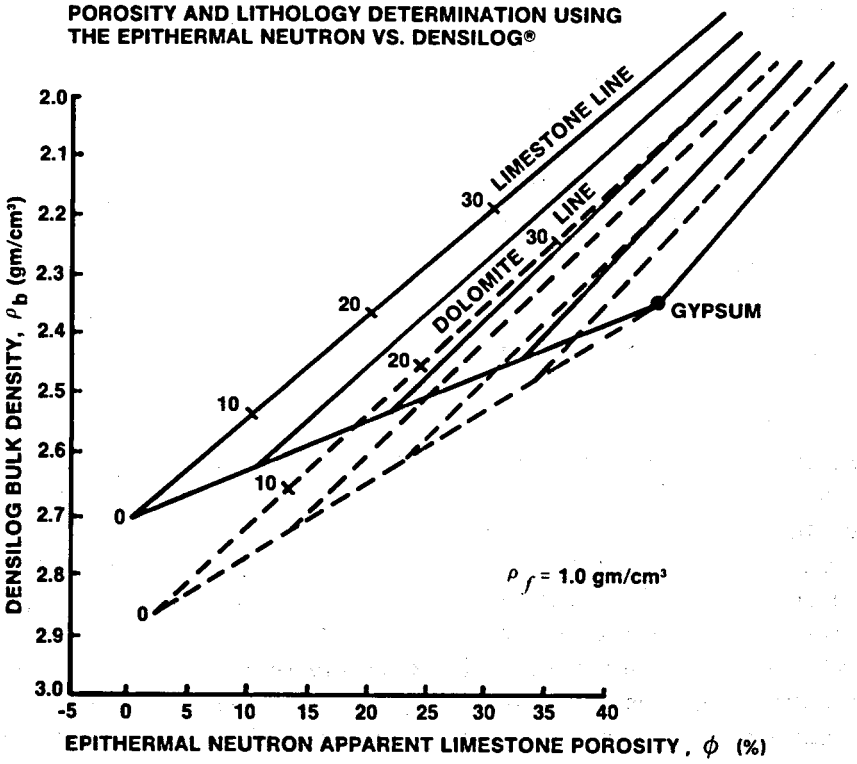

FIGURE 8

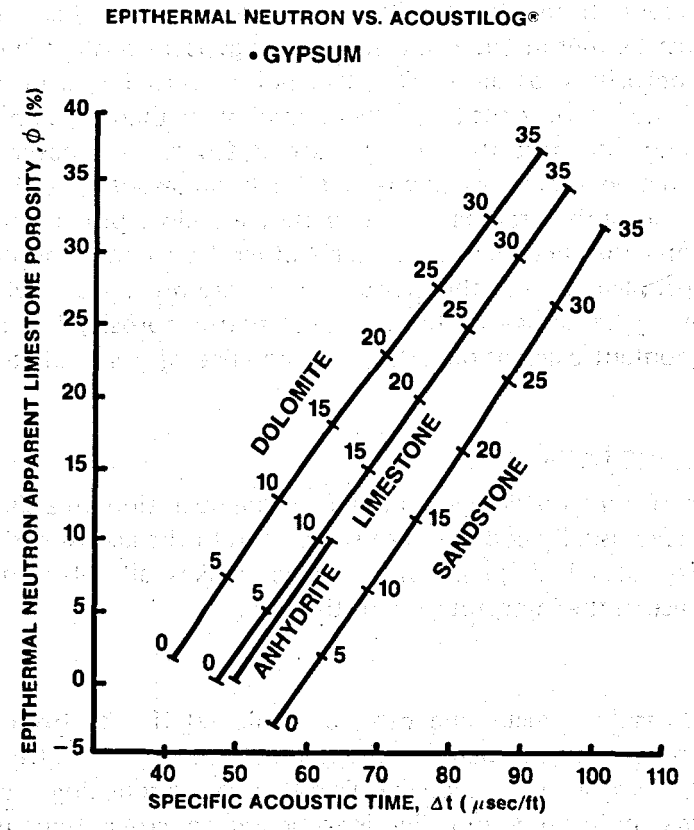

FIGURE 9

The remaining dual porosity crossplot combination is the Neutron Log vs. Acoustilog crossplot (see Figure 9). The gypsum matrix point is a prominent point on this crossplot and lies in a northwesterly direction from the sandstone, limestone, and dolomite lines. Shale affects both the neutron porosity and acoustic time values, and thus causes the points to move in a primarily northeasterly direction. The presence of gas moves the points toward the south, and secondary porosity causes a westerly movement of the data points. As in the previous two cases, the presence of both gas and gypsum have a canceling effect. The presence of both shale and gypsum have combined responses which can cause a point to plot as a clean point with optimistic porosity. Thus, in order to see the true presence of gypsum, the formation must be clean and non-gas-bearing.

If this is the case, the crossplot can be scaled in terms of the gypsum content and the percent porosity by assuming a single matrix-to-fluid-point line and a gypsum-to-fluid-point line in the same manner as was used for the other dual-porosity crossplots. The same problems of matrix choice, along with the problem of non-linearity of the dolomite-neutron response, are still present. The problem of secondary porosity also enters into the calculation. Since the Acoustilog sees very little of the secondary porosity, this causes a westward shift of the points away from the primary matrix-to-fluid-point line. If the plot has been scaled as mentioned, the westward shift will cause the calculated gypsum-free porosities to be too low. This can be compensated for by changing the fluid point to pivot the porosity line through these points. However, all of the points are not normally considered to have secondary porosity, much less secondary porosity which has a linear decrease in the total amount with decreasing total porosity. The same argument is also applicable to changing the matrix point to compensate for the secondary porosity which may be present while leaving the fluid point constant.

It becomes very apparent from the foregoing statements that there are some stringent requirements which must be met in order to calculate the gypsum content and the porosity from any of the three dual-porosity crossplots. The data points must be clean or have had a shale correction applied, and the matrix density of the mineral other than gypsum which was assumed must be accurate. Secondary porosity must be accounted for whenever an Acoustilog® is considered. These requirements manifest themselves for two reasons. The three primary mineral lines for the crossplots are either too far apart or they are close but the zero porosity matrix points are shifted a long distance relative to each other (as in the Densilog® vs. Acoustilog crossplot). The other problem is that the gypsum points are not far enough from the porosity lines, so that a change in the choice of the assumed matrix porosity line causes a fairly large change in the gypsum content calculation. Also, the presence of gas tends to mask the presence of gypsum.

TRI-POROSITY INTERPRETATION

The maximum number of porosity devices run in a logging operation on a single well is generally three. The three devices are usually composed of some form of the acoustic, density, and neutron devices. The availability of all three porosity devices makes all three of the dual-porosity crossplots available for use in the interpretation of the well.

M vs. N Crossplot

The "Litho-Porosity Crossplot" technique can be employed if data from the three porosity devices are available. This technique calculates the slope of each of the matrix-to-fluid-point lines on the Densilog vs. Neutron Log and the Densilog vs. Acoustilog crossplots with the assumption that each matrix-to-fluid-point line is to be a linear straight-line function (see Figure 10).

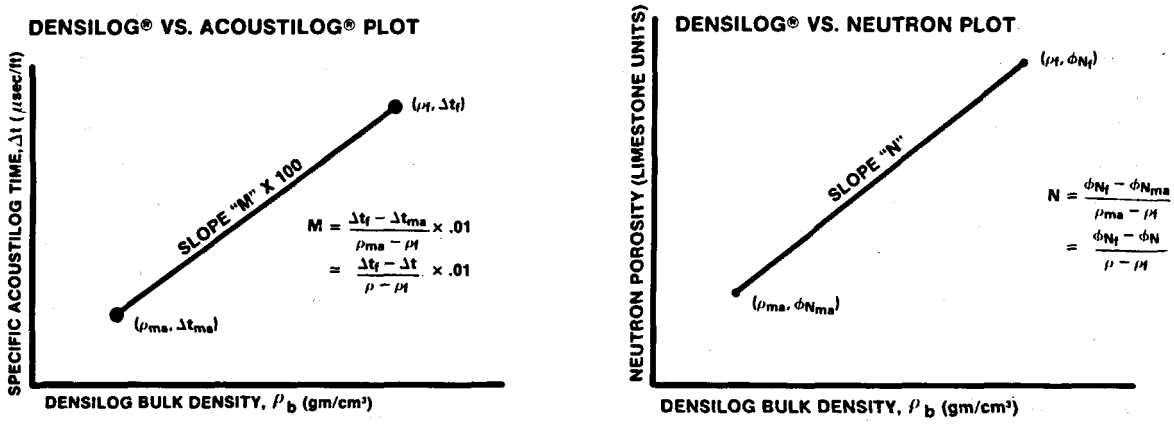

FIGURE 10

By definition,

$$M = \frac{\Delta t_f - \Delta t_{log}}{\rho_{log} - \rho_f} \times .01, \text{ and}$$

$$N = \frac{(\phi_N)_f - (\phi_N)_{log}}{\rho_{log} - \rho_f},$$ where the neutron response is in apparent limestone porosity units.

The M values are the slopes of the porosity lines in the Densilog® vs. Acoustilog® crossplot. The N values are the slopes of the porosity lines in the Densilog vs. Neutron Log crossplot. These slopes are independent of the porosity value and dependent only upon the fluid and matrix characteristics as long as a linear straight-line response between the matrix and fluid points is assumed. The non-linear neutron response is compensated for by assuming more than one matrix-to-fluid-point straight-line relation. Thus, each mineral has a unique set of M and N values (see Figure 11). The three points established for dolomite are to compensate for the non-linearity of the neutron response. The two points established for sandstone are due to the fact that the range of matrix travel times of sandstone varies from 51.2 μsec/ft to 55.5 μsec/ft.

The presence of gypsum will be very prominent on this plot. The gypsum point is of sufficient distance from the three primary matrix points to allow for an easy isolation of zones with gypsum content. Secondary porosity and gypsum content can mask each other's presence even in this crossplot. This can be seen from the north-northwest trend of gypsum and the northerly trend of points which contain secondary porosity. The presence of gas and the presence of gypsum show up as obvious differences in direction of movement, since points containing gas plot to the northeast and points containing gypsum have a trend to the north-northwest. The presence of shale pushes points to the south-southwest so that when both gypsum and shale are present, it is possible to see a point which has both shale and gypsum plot within the area where the clean minerals sandstone, limestone, and dolomite lie.

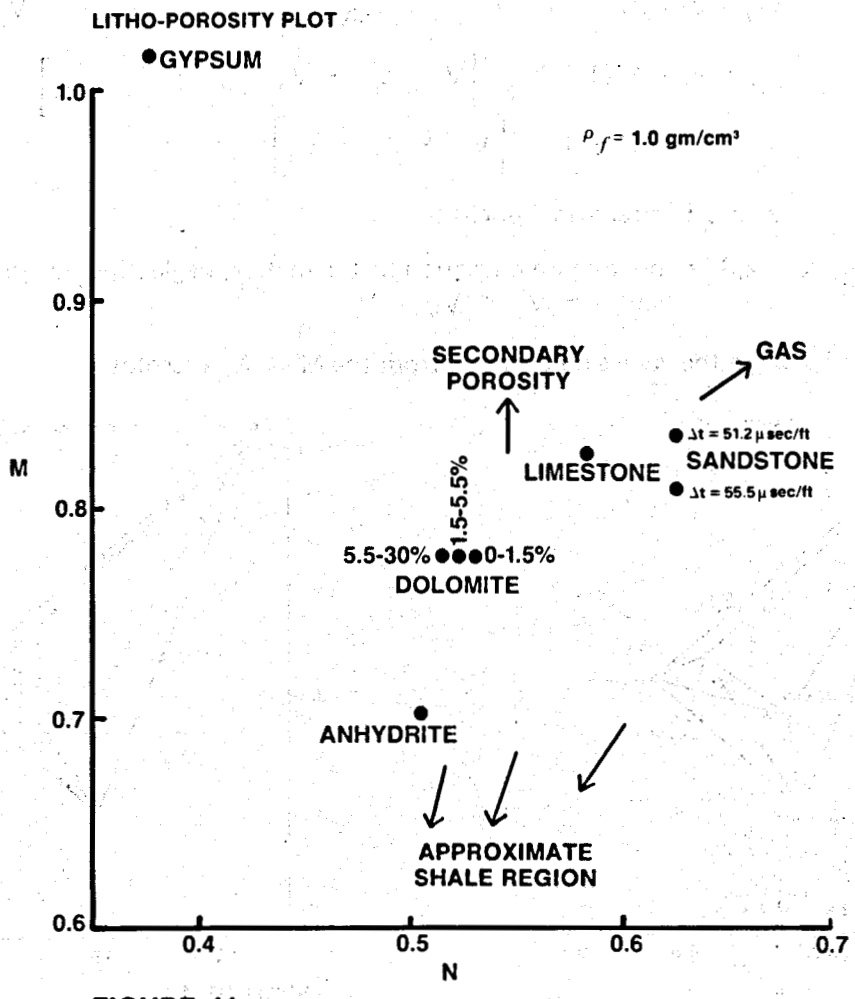

FIGURE 11

Even with these problems, the gypsum point remains fairly prominent. Normally, this makes it possible to see those zones which contain gypsum even though secondary porosity or shale may be present in small quantities. This plot can be scaled into tri-mineral triangles rather than into dual mineral-fluid point triangles as was the case for the dual-porosity crossplots (see Figure 12). Points which lie within a particular triangle are assumed to be composed of the three minerals which comprise the vertices of the enclosing triangle. The use of these enclosing triangles with three mineral points as the vertices is not as simple as it appears. Scaling the tri-mineral triangles in terms of the percent content of each mineral cannot be done as easily as with the dual-mineral crossplots. This is due to the fact that the M and N slope values are the tangents of the matrix-to-fluid-point lines. This is well illustrated in Figure 13 by the points plotted between the matrix points. The points designated by X are where one would assume that a 25-75, 50-50, and 75-25 mixture of each two-mineral pair would lie. The points designated by (•) are where these points actually lie. The difference in the assumed and actual location of these points is easily illustrated by calculating the M and N values for a 50-50 mixture of any two minerals, and comparing this value to the value of the M and N coordinates of the midpoint of the line on the M-N plot which connects these two minerals. Thus, if one properly scales the triangles, then the percent volumes of the three minerals involved can be derived and a corrected porosity value can be arrived at by solving the system of equations:

$$\Delta t = \phi\Delta_f + (1-\phi)\left[V_1\Delta t_{ma_1} + V_2\Delta t_{ma_2} + V_3\Delta t_{ma_3}\right]$$

$$\phi_N = \phi(\phi_N)_f + (1-\phi)\left[V_1(\phi_N)_{ma_1} + V_2(\phi_N)_{ma_2} + V_3(\phi_N)_{ma_3}\right]$$

$$\rho_b = \phi\rho_f + (1-\phi)\left[V_1\rho_{ma_1} + V_2\rho_{ma_2} + V_3\rho_{ma_3}\right]$$

$$1 = \phi + (1-\phi)\left[V_1 + V_2 + V_3\right]$$

where ϕ = fractional porosity

V_k, k=1,2,3 = bulk volume fraction of the matrix, neglecting porosity, and $1 = V_1 + V_2 + V_3$

NOTE: V_k, k=1,2,3 are the values determined from the M vs. N crossplot.

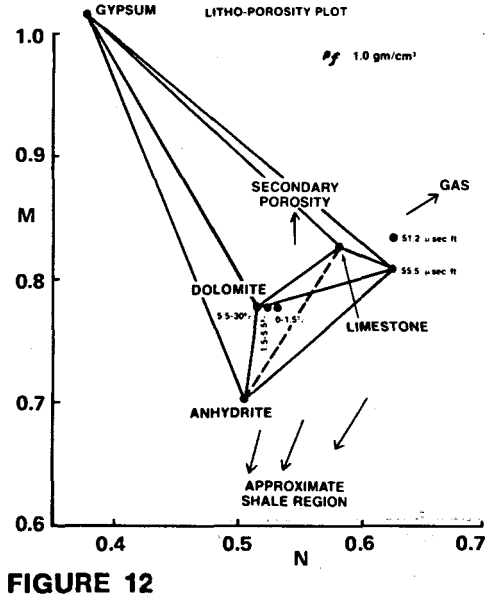

FIGURE 12

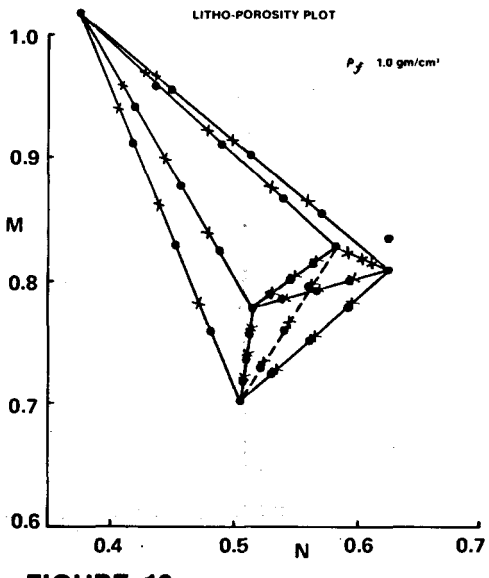

FIGURE 13

Thus, this tri-porosity crossplot is very useful in gypsum delineation if used properly. An accurate choice of the two minerals to be used with gypsum in the tri-mineral triangle will allow the determination of an accurate value of the true gypsum content and porosity value.

K vs. A Crossplot

M and N are not the only functions of slope which may be considered. Another tri-porosity crossplot technique which employs the use of the matrix-to-fluid-point slopes will now be examined.

Consider the following:

$$A = \frac{\rho_{log} - \rho_f}{(\phi_N)_f - (\phi_N)_{log}} \quad \text{and}$$

$$K = \frac{\Delta t_f - \Delta t_{log}}{(\phi_N)_f - (\phi_N)_{log}} \times .01, \quad \text{where the neutron response is in apparent limestone porosity units.}$$

The A values are obtained by considering each of the slopes of the matrix-to-fluid-point lines on the Neutron Log vs. Densilog® plot (see Figure 14A). The K values are obtained from the slopes of the matrix-to-fluid-point lines on the Neutron Log vs. Acoustilog® crossplot (see Figure 14B). Now consider the fact that

$$A = \frac{1}{N} \qquad (5)$$

and

$$K = \frac{M}{N} \qquad (6)$$

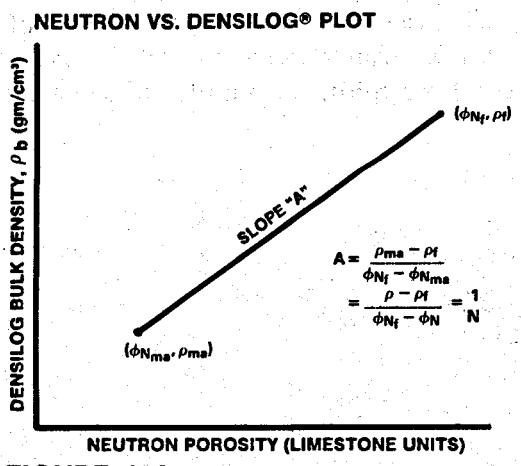

FIGURE 14A

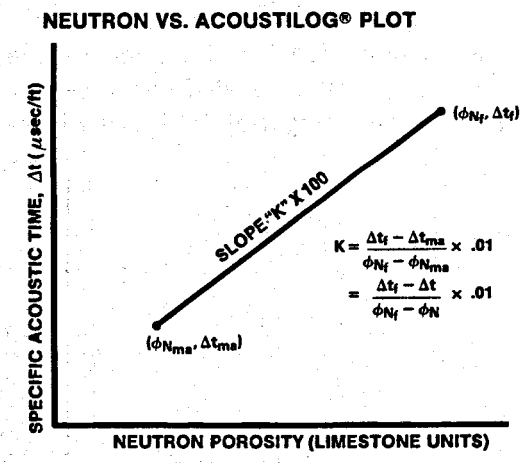

FIGURE 14B

Since M and N are constant and independent of porosity effects, then K and A are also porosity independent due to equations (5) and (6). Thus, there are two values, A and K, which, like M and N, seem to be dependent only on the fluid and matrix characteristics and are not dependent upon the effect of changes in porosity. The values of M and N and, consequently, for A and K, are true strictly for a linear log response. The non-linearity of the neutron-dolomite response will once more be compensated for by making more than one choice of matrix-to-fluid-point lines, and thus, by the choice of more than one set of A and K values.

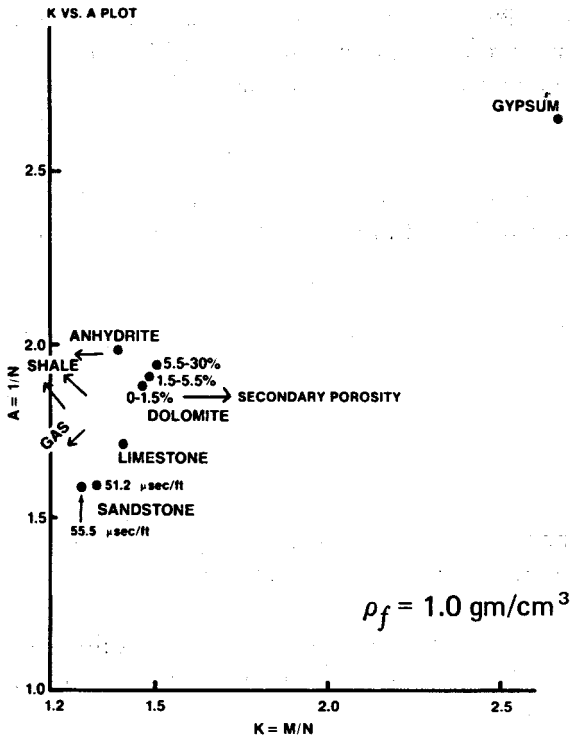

FIGURE 15

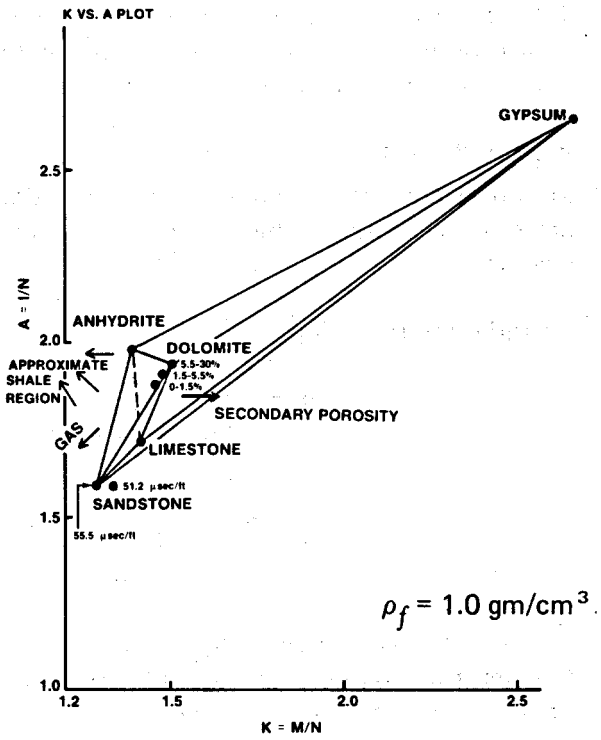

FIGURE 16

A plot of the values of K and A for each of the major reservoir minerals is shown in Figure 15. Construction of possible tri-mineral triangles produces Figure 16. On Figure 16, gypsum shows up as a point far to the northeast of the sandstone, limestone, and dolomite points. This is a larger relative displacement of the gypsum point from these three primary minerals when considered in relation to the relative size of the sandstone, limestone, dolomite triangle than that encountered on the M vs. N crossplot. This allows for much easier detection and calculation of the gypsum content if scaling of the tri-mineral triangles is again considered. The K vs. A crossplot must be scaled in the same manner as the M vs. N crossplot, since a plot of slope vs. slope is still being dealt with (see Figure 17).

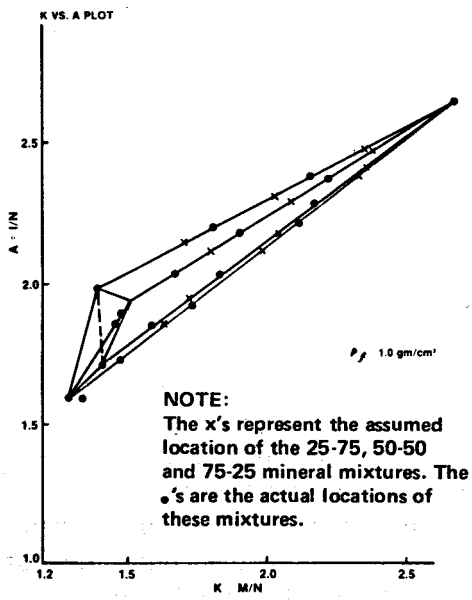

FIGURE 17

The presence of shale and gas present an opposing effect to the trend of the gypsum-bearing points. Also, secondary porosity and gypsum cannot be distinguished separately when both are present. It should be noted that an error in the selection of the two other minerals besides gypsum in a tri-mineral triangle does not necessarily mean that a large error will occur in calculation of the amount of gypsum. This is due to the relatively close spacing of the sandstone, limestone, and dolomite points when compared to their distance from the gypsum point.

Once the percent content of each mineral is determined from the K vs. A crossplot, the porosity can be determined by solving the following system of equations:

$$\Delta t = \phi \Delta t_f + (1 - \phi) \left[V_1 \Delta t_{ma_1} + V_2 \Delta t_{ma_2} + V_3 \Delta t_{ma_3} \right]$$

$$\phi_N = \phi (\phi_N)_f + (1 - \phi) \left[V_1 (\phi_N)_{ma_1} + V_2 (\phi_N)_{ma_2} + V_3 (\phi_N)_{ma_3} \right]$$

$$\rho_b = \phi \rho_f + (1 - \phi) \left[V_1 \rho_{ma_1} + V_2 \rho_{ma_2} + V_3 \rho_{ma_3} \right]$$

$$1 = \phi + (1 - \phi) \left[V_1 + V_2 + V_3 \right]$$

where ϕ = fractional porosity

V_k, k=1, 2, 3 = bulk volume fraction of the matrix, neglecting porosity, where $1 = V_1 + V_2 + V_3$

NOTE: V_k, k=1, 2, 3 is determined from the K vs. A plot.

In order to evaluate some of the other factors which make this plot useful, study the plot assuming that only two porosity tools are run.

This is of interest since in the majority of the cases where gypsum is present, either a Densilog®-Neutron Log combination or an Acoustilog®-Neutron Log combination is run. If A and K are considered, note that A involves the Densilog-Neutron Log combination, while K involves an Acoustilog-Neutron Log combination. This is not the case with the "Litho-Porosity Crossplot." If it is assumed that there is only a primary mineral and gypsum present, then there is no longer a triangle, i.e., there is a straight line from the gypsum point to a matrix point which can be accessed with either an A or K value to obtain a percent gypsum value (see Figure 18).

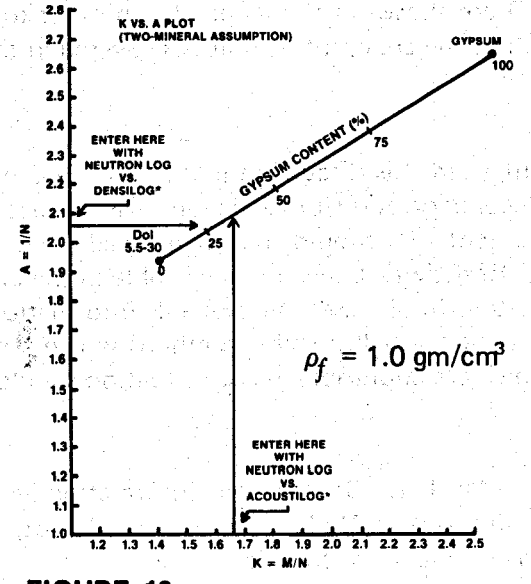

FIGURE 18

Then consider:

$$\Delta t_{ma_{corr}} = V_1 \Delta t_{ma_1} + V_2 \Delta t_{ma_2}$$

$$\rho_{ma_{corr}} = V_1 \rho_{ma_1} + V_2 \rho_{ma_2}$$

$$(\phi_N)_{ma_{corr}} = V_1 (\phi_N)_{ma_1} + V_2 (\phi_N)_{ma_2}$$

$$1 = V_1 + V_2$$

where the neutron response is in apparent limestone units.

Thus, a corrected total matrix value results, and for clean formations:

$$\phi_{corr} = \frac{\Delta t_{log} - \Delta t_{ma_{corr}}}{\Delta t_f - \Delta t_{ma_{corr}}}$$

$$\text{or} = \frac{\rho_{ma_{corr}} - \rho_{log}}{\rho_{ma_{corr}} - \rho_f}$$

$$\text{or} = \frac{(\phi_N)_{log} - (\phi_N)_{ma_{corr}}}{(\phi_N)_f - (\phi_N)_{ma_{corr}}}$$

Thus, there is a method to calculate both gypsum content and porosity from a single straight-line relationship. The vertex-to-vertex line has again been scaled in the actual terms of percent of mineral content. This plot possibly could prove useful in field interpretation where both ease and speed of use are necessities in order for a method to prove itself at the wellsite. An effort should always be made to use three porosity measuring instruments; however, with either two or three instruments, the described methods lends itself to the needs of a simple and quick method of wellsite interpretation.

EXAMPLES

Example wells A through D are shown in the Appendix in order to illustate some of the advantages and limitations of each of the crossplot techniques covered in this paper.

CONCLUSION

It quickly becomes apparent from this discussion that any single crossplot technique cannot give all the required answers. Secondary porosity, shale, and gas all present problems relative to the calculation of gypsum content. It should be mentioned that the Gamma Ray, Caliper, Spontaneous Potential, and Resistivity Logs are all valuable in the determination of the presence and percent content of gypsum. In all cases, all available information should be utilized in order to provide the best answer available. All possible methods which have been discussed should be considered, and all those which are applicable in each situation should be used.

ACKNOWLEDGEMENTS

Acknowledgement is made to Mr. Larry Schoonover, Information Services Section, Dresser Atlas, for pointing out that for both the M vs. N plot and the K vs. A plot, lines connecting each pair of minerals are not normal straight-line linear functions.

REFERENCES

1. Burke, J. A., Campbell, R. L., Jr., and Schmidt, A. W., "The Litho-Porosity Cross Plot," *The Log Analyst.* (Nov. - Dec., 1969), X, No. 6, 25-43.
2. Vercellino, W. C., and Hilchie, D. W., *Computer Crossplots for Well Evaluation of Complex Lithology,* Dresser Atlas Technical Memorandum, (July, 1975), Vol. 6, No. 2.
3. Dresser Atlas, *Log Interpretation* – Chart Book, 1974.

OTHER REFERENCES

1. McFadzean, T. B., "Cross-Plotting – A Neglected Technique in Log Analysis," SPWLA Fourteenth Annual Logging Symposium, (May 6-9, 1973).
2. Neinast, G. S., and Knox, C. C., Sun Oil Company, "Normalization of Well Log Data," SPWLA Fourteenth Annual Logging Symposium (May 6-9, 1973).
3. Raymer, L. L., and Biggs, W. P., "Matrix Characteristics Defined by Porosity Computations," *Trans., SPWLA Fourth Annual Logging Symposium,* (1963).
4. Wilson, D. A., and Hensel W. M., "Computer Log Analysis and Core Analysis = Improved Formation Evaluation in West Howard-Glassock Unit," Society of Petroleum Engineers of AIME, 51st Annual Fall Conference (Oct. 3-6, 1976). Paper No. SPE 6188.
5. Youmans, A. H., Lebreton, F., Wilson, B. F., and Oshry, H. I., *Nuclear Logs for Open Hole Porosity Measurement,* Lane Wells Publication, (January, 1965).

ABOUT THE AUTHOR

Elton Frost, Jr. received a B.S. degree in 1973 and an M.A. degree in 1975 from Southwest Texas State University.

He was employed with Schlumberger Well Services from 1975 to 1977, progressing from Junior Field Engineer to Senior Field Engineer.

Elton is currently a Computer Log Analyst for the Dresser Atlas Division of Dresser Industries, Inc.

APPENDIX

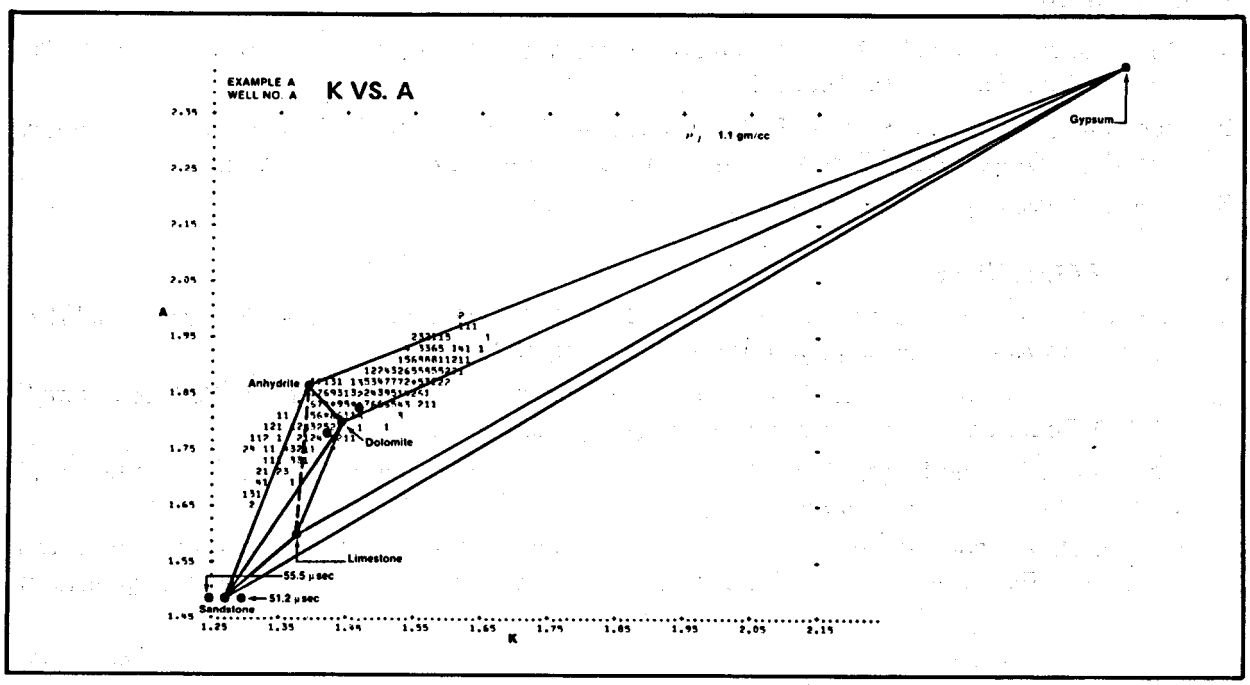

The K vs. A plot shows this reservoir is composed primarily of dolomite, anhydrite, quartz, and gypsum. This conclusion is supported by core data from this interval. Note the distinct trend of data points toward the gypsum point and the lack of secondary porosity.

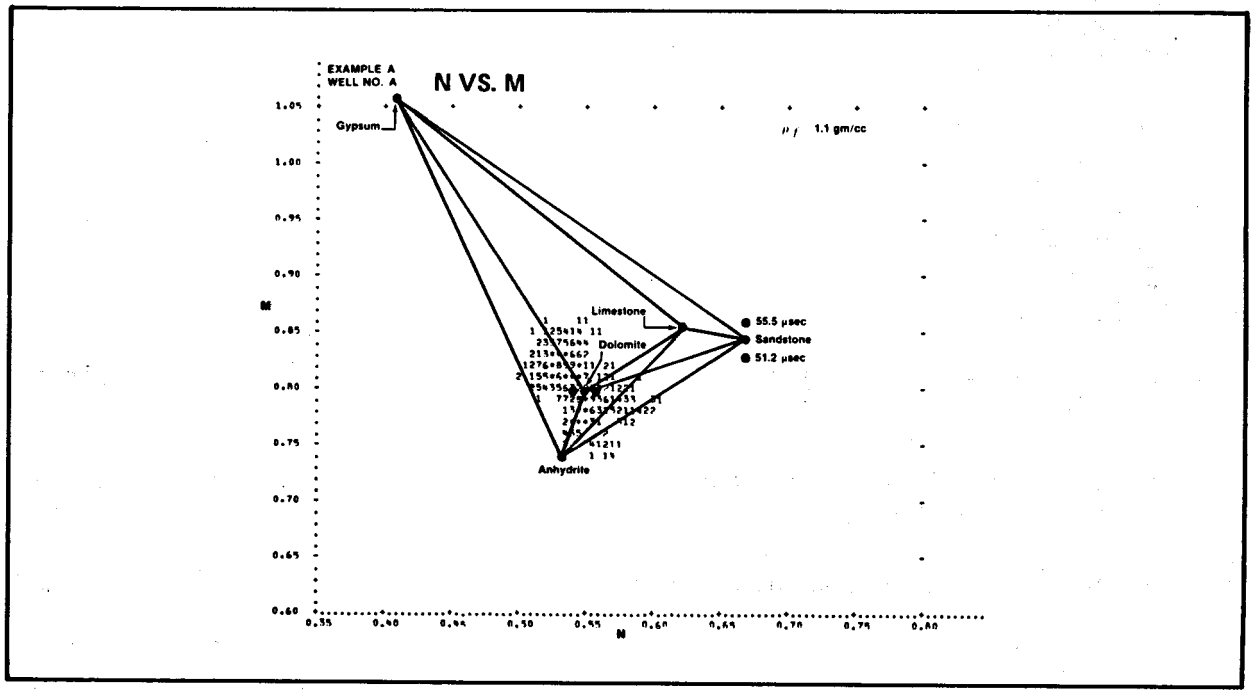

This plot shows the trend of data points toward the gypsum point. Although the lithology is well defined by this plot, the gypsum trend is not as pronounced as on the K vs. A plot.

From this plot, it is clear that there is anhydrite and dolomite, but the amount of gypsum present is not as obvious.

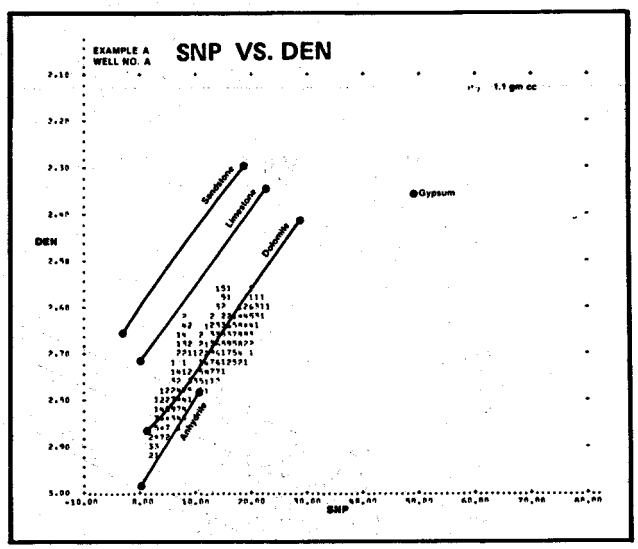

This plot shows a distinct trend of data points toward the gypsum point. Note the trend toward the sandstone line as the quartz percentage increases.

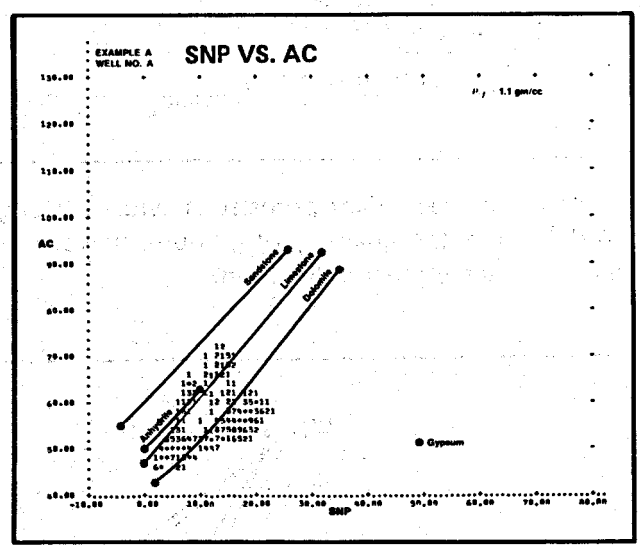

The presence of both anhydrite and dolomite is obvious from this plot. The amount of gypsum present, however, is not quite as clear.

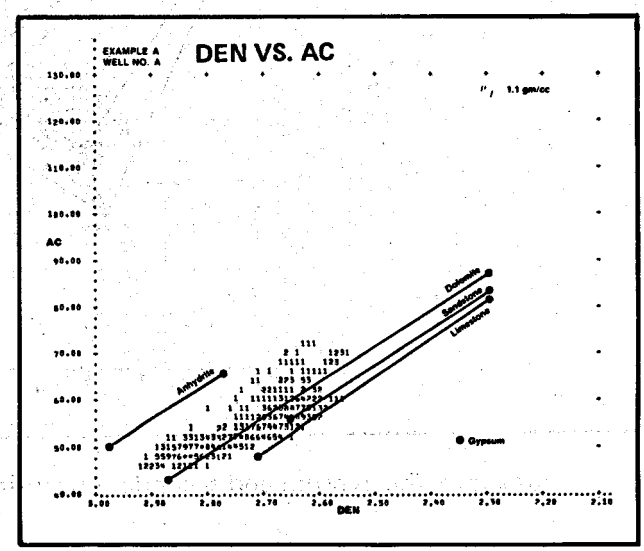

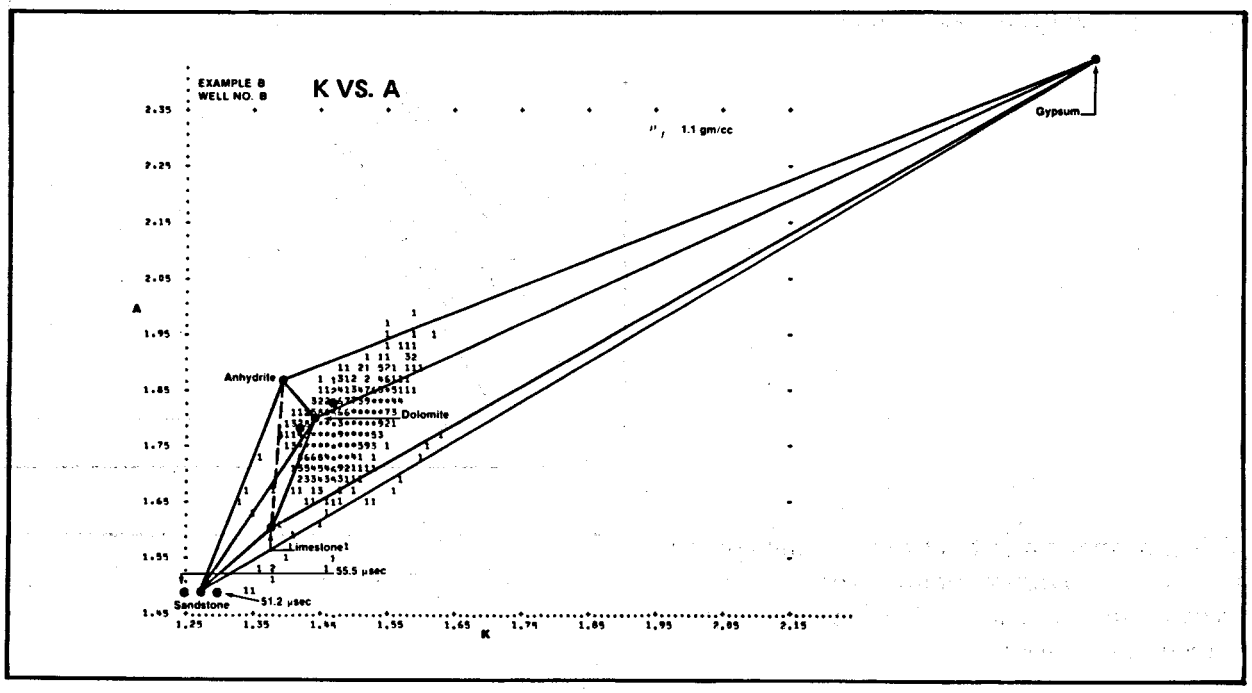

In this plot, secondary porosity is evident, along with the presence of gypsum. It is not possible to determine the quantity of gypsum, however, since the secondary porosity and gypsum trend are in the same general direction.

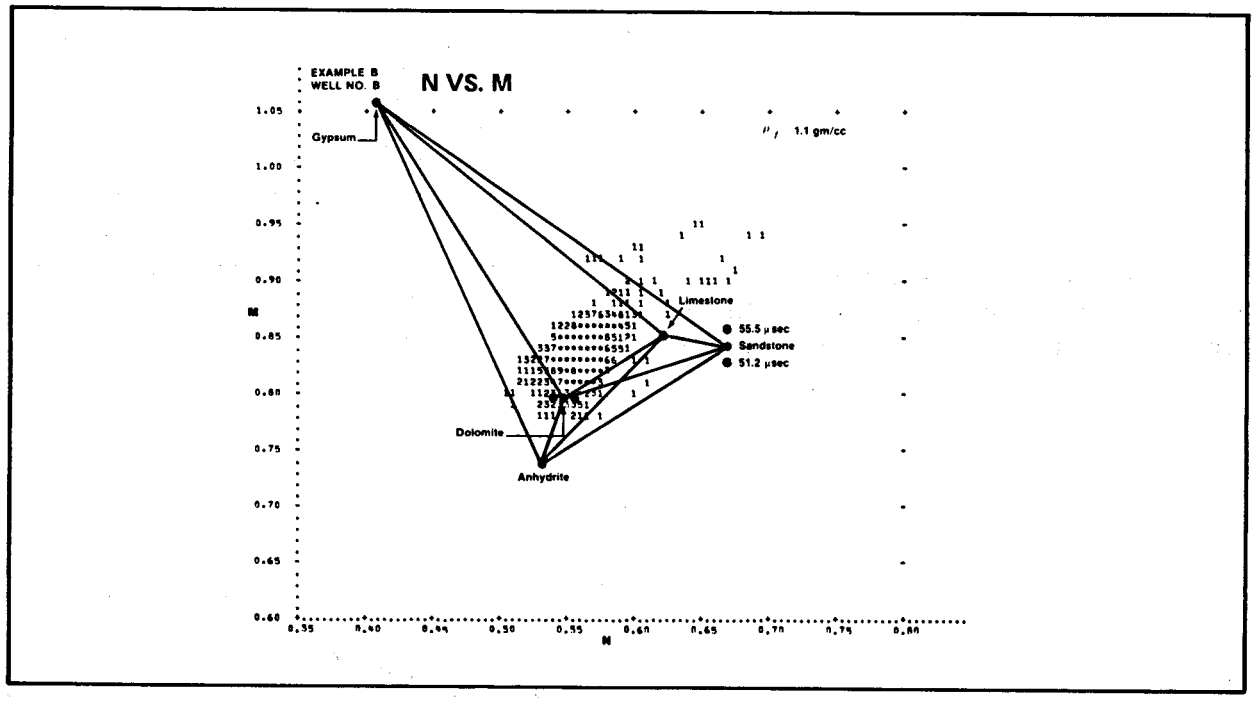

This plot shows the gypsum and secondary porosity trend in the same general direction.

In this plot, the presence of gypsum is detectable, but one must make an assumption as to the dolomite-limestone mixture in order to calculate the amount of gypsum present.

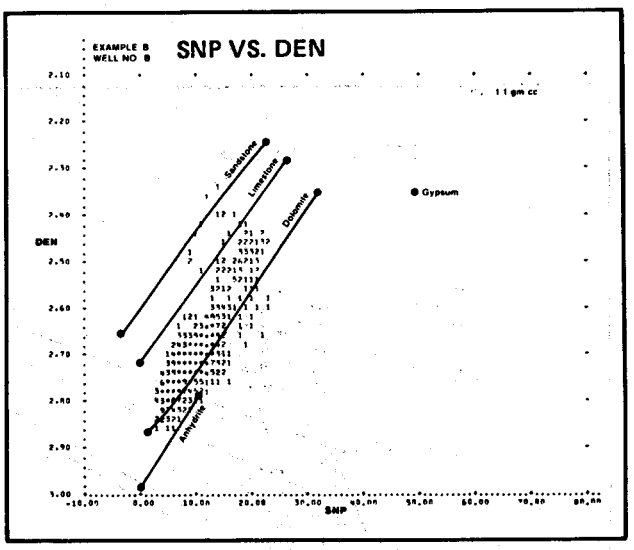

Here, also, the presence of gypsum is shown. The same problem with the limestone-dolomite mixture is encountered. The difference in the presence of secondary porosity and gypsum is not obvious.

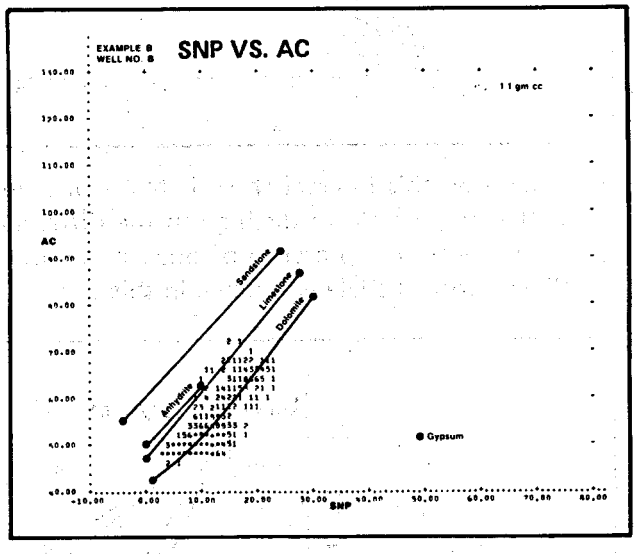

The presence of anhydrite is shown more readily in this plot than is the presence of gypsum. It is hard to differentiate the secondary porosity and gypsum.

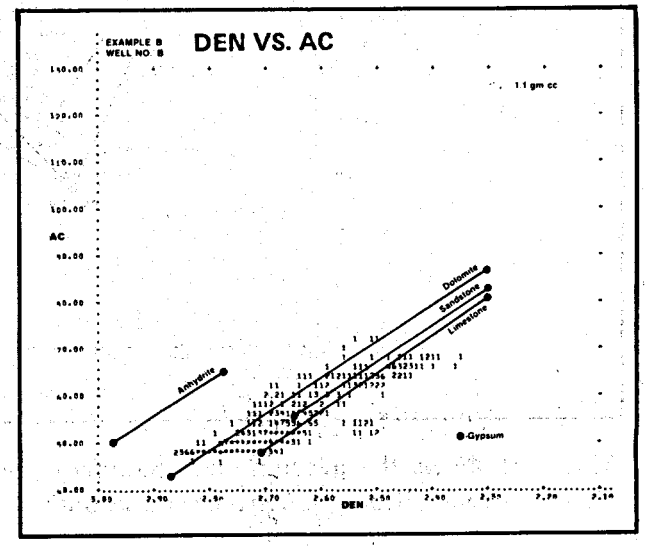

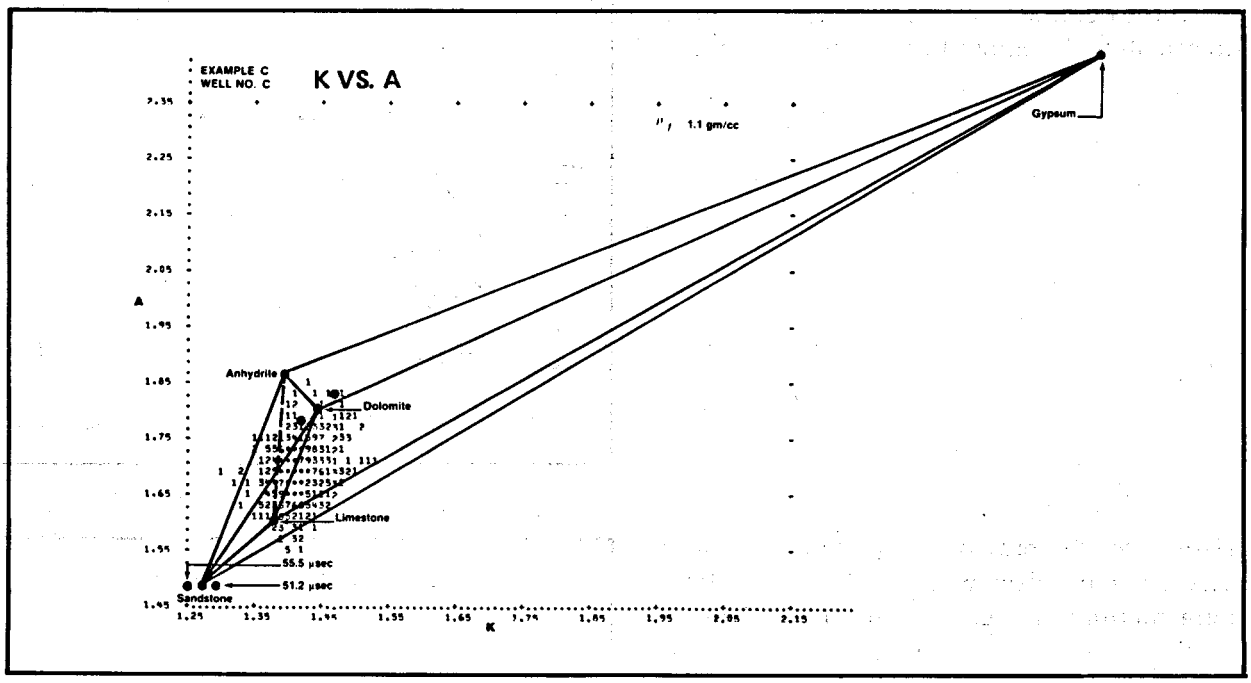

Core data on this interval show it to be of a vugular nature with small amounts of gypsum present. It is impossible to distinguish the difference in secondary porosity and gypsum within this plot. However, the presence of one or the other is shown on the plot. Notice the possibility of small amounts of shale also being in this zone.

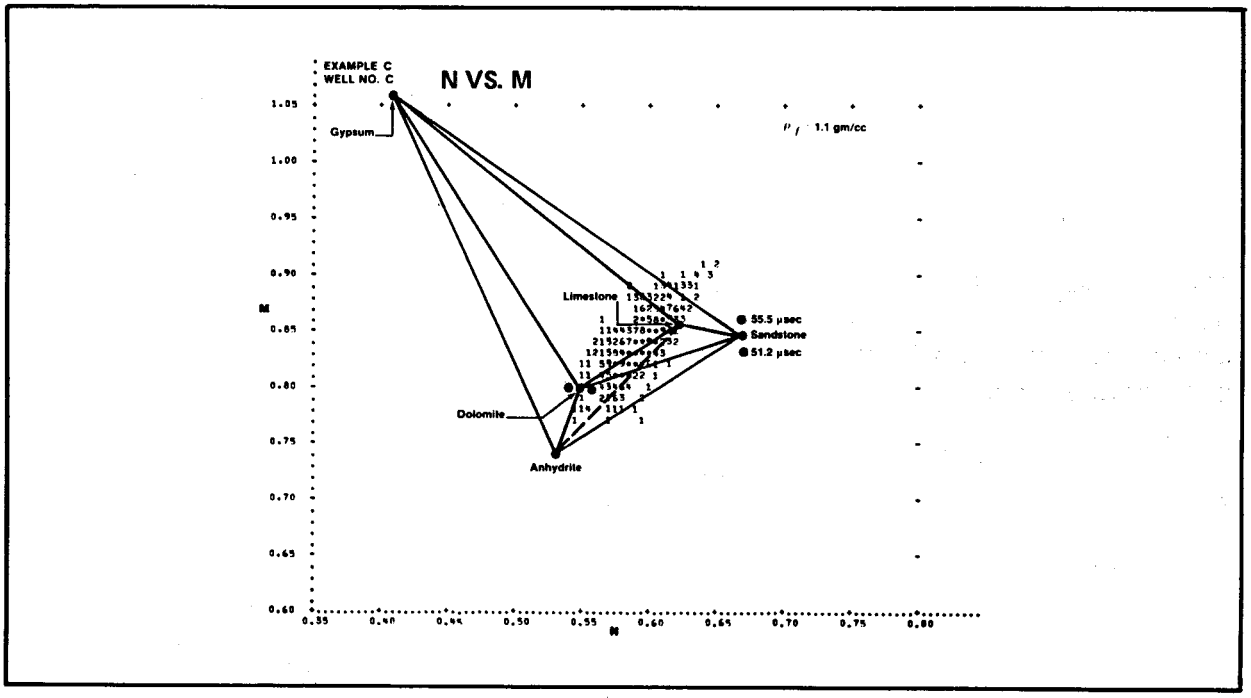

This plot shows the gypsum and secondary porosity along with some shale. It is impossible to distinguish the difference between the secondary porosity and gypsum.

This plot shows only a limestone-dolomite mixture. There is no indication of gypsum or shale content.

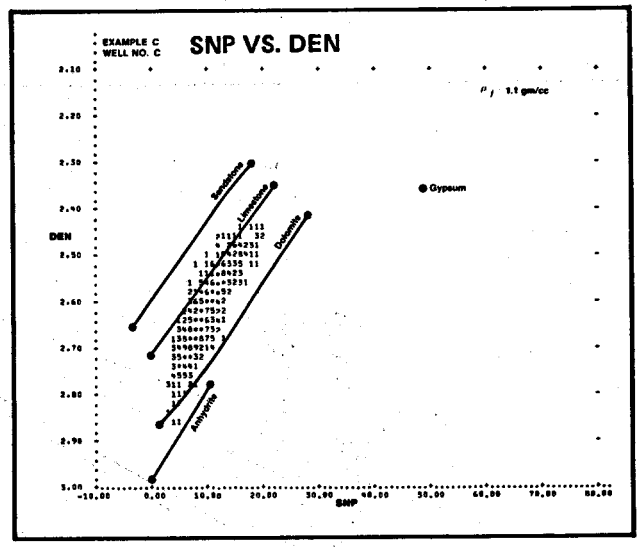

Neither the presence of gypsum nor of secondary porosity is apparent in this plot.

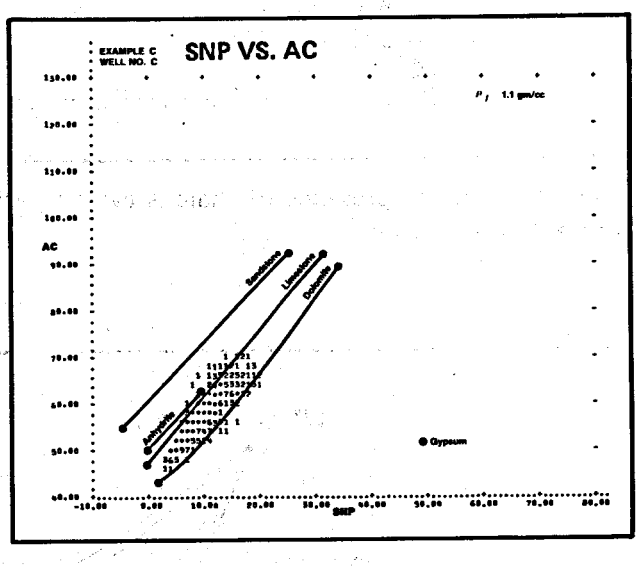

Secondary porosity and gypsum look alike in this plot. The lithology as to dolomite, sandstone, and limestone is also not obvious.

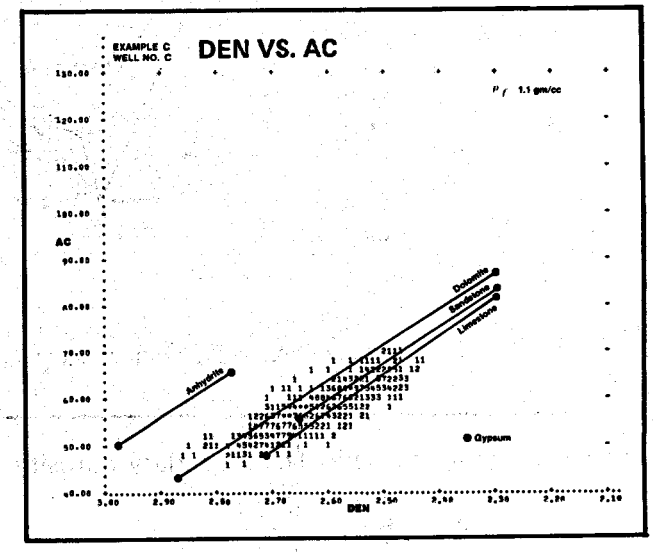

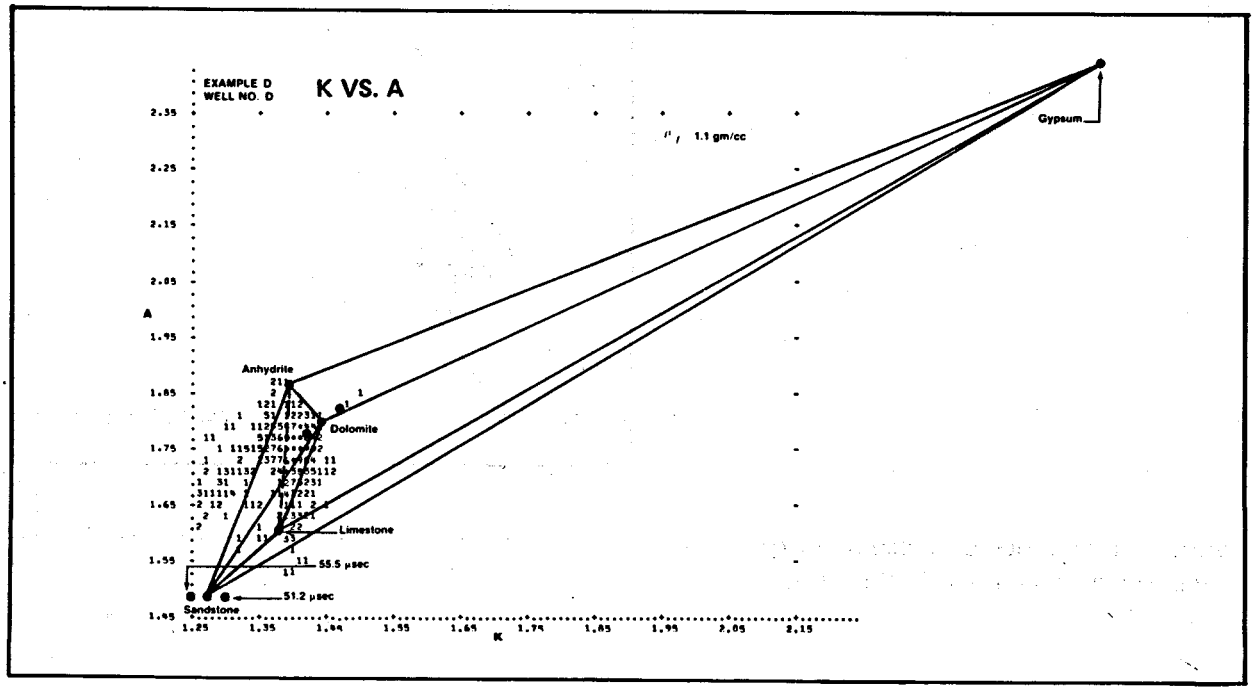

In this zone, the presence of shale is evident. Whether there is a secondary porosity or gypsum present is not obvious.

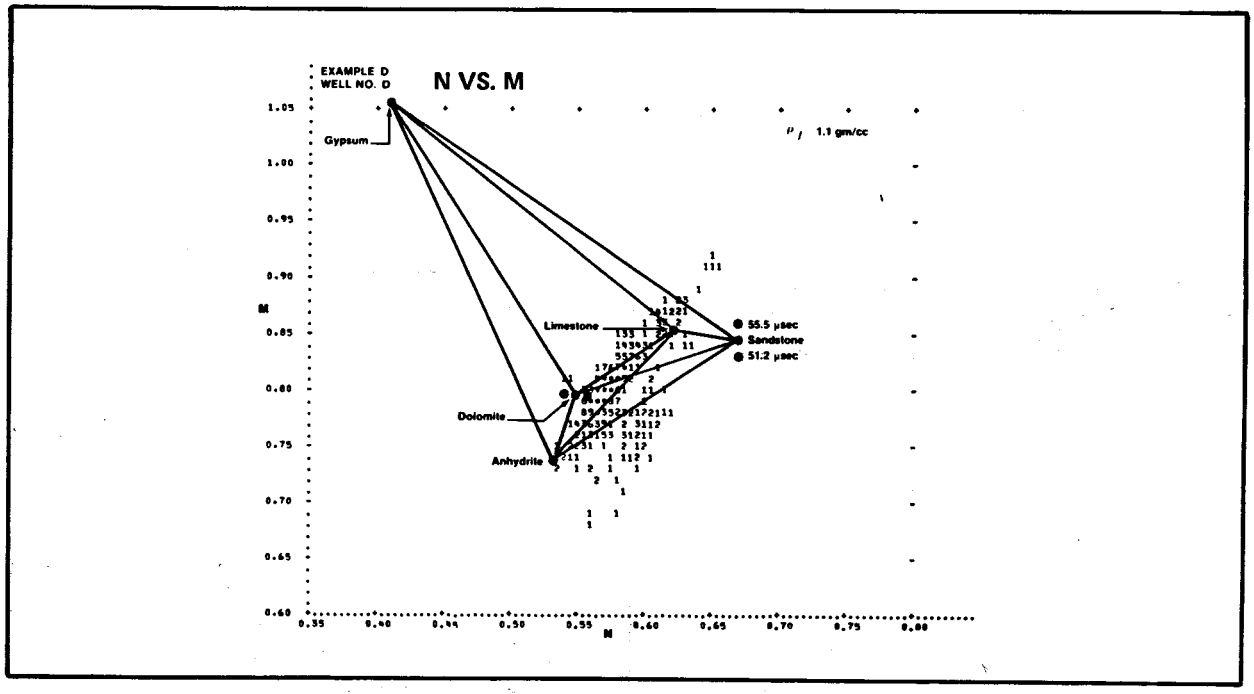

Shale is prominent here. The secondary porosity and gypsum are indistinguishable.

This plot shows a primarily clean mixture of limestone, dolomite, and anhydrite.

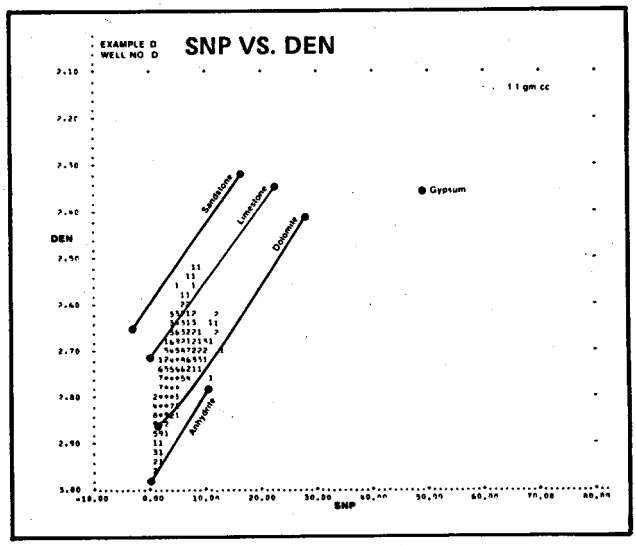

The shale makes this plot look as if there is some sandstone content in the interval. Gypsum is not seen at all in this case.

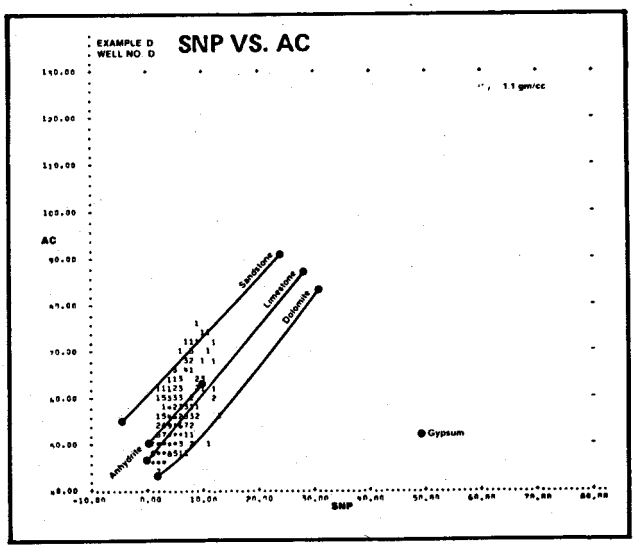

The presence of both anhydrite and shale can be seen in this plot. The presence of gypsum and secondary porosity is indistinguishable.

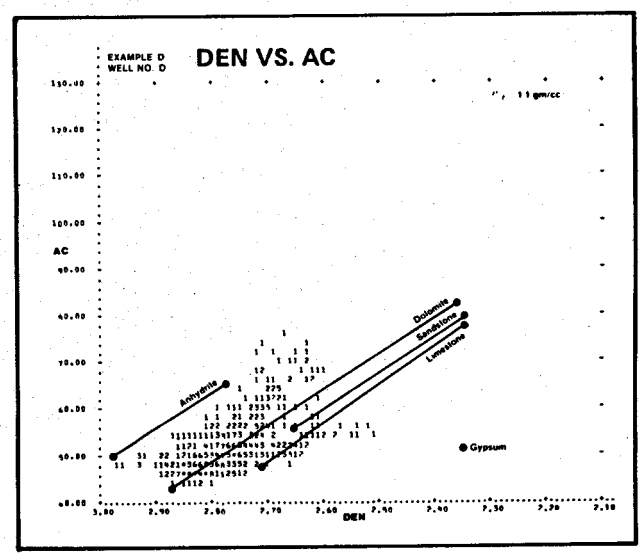

LOGGING TESTS IN POROUS MEDIA TO EVALUATE THE INFLUENCE OF THEIR PERMEABILITY ON ACOUSTIC WAVEFORMS

F. LEBRETON, Institut Français du Pétrole

J.P. SARDA, Institut Français du Pétrole

F. TROCQUEME, Societe Nationale Elf-Aquitaine (Production)

P. MORLIER, Laboratoire de Mécanique des Roches de l'Ecole Polytechnique*

ABSTRACT

A new acoustic parameter is proposed in view of building a permeability log.

First results of actuals trials performed in wells, are reported.

Then methods and results of experiments in artificial porous media are described.

This new acoustic parameter seems to be useful for evaluating rock permeability.

I - INTRODUCTION

I.1 - Advantages of Logging Permeability

In a well, the fluids saturating reservoir rocks are more easily detected and produced when the rock permeability value is known over the entire depth of the borehole. However, as of now, only porosity and water saturation can be logged continuously.

Although direct and continuous evaluation of rock permeability in a well is not yet possible, some permeability indications may be obtained by running :

- flowmeter log,
- temperature log,
- spontaneous potential log,
- combinations of several different resistivity logs, with filtrate invasion diameter estimation.

Of course rock permeability measurements can always be made :

- from analysis of recovered proper-size cores under restored bottom hole conditions,
- from pressure tests over intervals known to be productive.

* Now with INSTITUT UNIVERSITAIRE DE TECHNOLOGIE (Department Civil Engineering), Bordeaux.

Unfortunately both cored and tested intervals always have quite limited thickness.

The permeability evaluation of drilled rocks therefore seems to be an objective that must be attained as soon as possible.

I.2 - Previous Attempts in That Direction

During the 1960s, analysts tried to detect permeability from nuclear magnetic resonance, but specially from acoustical methods.

Each of these acoustic methods was based on interpreting the pseudo-sinewave impulse (12 to 30 kHz) already chosen by logging companies for measuring compressional wave velocity over short intervals.

The principal attempts were the following :

a) - Amplitude measurements (Morlet-Schwaetzer)

From actually recorded signals, these authors found relationships between amplitude and lithology, between pore saturating fluid, "matrix continuity", and permeability ; but they were more interested in studying the influence of transducer shape on various signal amplitudes.

b) - Attenuation log (Morlet-Schwaetzer)

The above mentioned work led its authors to propose a tool consisting of a transmitter and two receivers, together with special recording equipment.

Attenuation, but not permeability, can be derived from such a log when both receivers are situated in similar acoustic impedance media.

c) - Absolute amplitude interpretation (Morris et al.)

According to these investigators, fractures encountered by the path of an elastic wave weaken its amplitude. The influence of fracture orientation on amplitude seems to be defined, at least in the laboratory.

d) - Measurement of the first pseudo-period of the compressional wave and total energy of the acoustic signal, are linked by Fons (7) to the permeability value and to open fracturing in porous media. Indeed, empirical applications of these measurements have sometimes been useful.

e) - Continuous recording of the signal, known as "variable density display" (Christensen (8) and Walker (9)), suggests that the "Chevrons" on that display correspond to fractured intervals, whether or not these fractures are open.

f) - The "MICROSONIC" (Schlumberger (10)) was used to give a shear-wave ($\pm$ 300,000 Hz) amplitude log. This wave amplitude was normally weakened after passing through fissured or fractured media. But the "MICROSONIC" would not always select the shear-wave properly.

g) - The $\frac{s}{c}$ ratio of shear-wave maximum amplitude (s) to a compressional wave amplitude (c) having circulated in a rock volume was proposed by Zemanek (11) as a permability index of that volume. However, it does not discriminate between shaly, impervious and clean permeable intervals.

h) - In cemented-cased wells, measurement of the compressional wave first amplitude in the received signal (Thurber (12) and Grosmangin (13) makes up the "Cement Bond Log". Also the "Variable density dispaly" may indicate the cement bond to casing (Brown, Grijava, Raymer (14). But the special configuration of the medium is not then representative of normal open-hole conditions.

i) - Last but not least, in strictly intergranular porosities, a permeability estimate may be derived from a combination of logs (Coates, Dumanoir (15) and Raïga-Clemenceau (16)). But fissures, fractures and/or clay content disturb the quality of these estimates.

o

o o

The above references lead to the conclusion that, after an acoustic signal has circulated into a rock or any porous medium, its shape and amplitude are normally affected. The signal therefore represents a kind of "signature", implying certain physical properties of the porous medium.

However, up to now, only the relationship between wave velocity and rock porosity (Wyllie, 1955) has been firmly established.

II - CHOICE OF A NEW ACOUSTIC PARAMETER

In order to encourage research on acoustic parameters, logging companies have recorded a great number of signals in wells, and the choice of our new parameter came from an examination of these signals, an examination strengthened by :

a) - the model we had of saturated porous media in a transitory vibrating state,
b) - the comparison of this parameter with direct permeability measurements made on these media.

As a word of caution, we must remind the reader that emitted signal charateristics were then unkown to us. We knew only that the emission type was constant, and therefore the shape and amplitude had to be constant.

II.1 - Definition of the New Parameter

Commercial tool transmitter-receiver spacings are currently between three and six feet. Signals are recorded at the rate of one per foot or per two feet.

Figure (1) shows the shape of a signal as usually received, in that it comes on the scope while the sonde is going up the borehole.

The first cycles certainly belong to a compresional wave, followed by a wave whose velocity is that of a shear-wave having passed through in the same medium.

Several signal examinations show an interference later than compressional-wave arrival, but earlier than normal shear-wave arrival time.

The parameter chosen in the compressional wave is :

$$Ic = \frac{V_2 + V_3}{V_1}$$

V_1, V_2 and V_3, being the amplitudes of the first three half-cycles of that compressional wave. On signals recorded in several wells, we noticed that this parameter ranges from about 1.5 to about 20.

This variation range was later defined when we were able to study the emitted signal, transmitter and receiver characteristics from our own sonde ; these same characteristics being unavailable for commercial sondes.

II.2 - Physical Meaning of Ic

As a working hypothesis, we can today consider this parameter, representative of the shape of the wave, as a measurement of the attenuation influence of a frittering medium on a constant impulse (17).

Here the frittering medium is a saturated porous medium, and the impulse is an acoustic one.

The presumed source of loss is the relative solid-fluid motion, because in consolidated porous media, energy dissipation due to solid-solid friction or liquid-liquid friction is always smaller than that due to solid fluid friction.

We think that energy dissipation will alter the shape of a transitory signal : we propose to show this alteration by the Ic index.

In a medium of given porosity and saturation, energy dissipation will increase with permeability. A relationship between these factors and the Ic index could then be expected.

This relationship, as we shall see, appears to be single-valued, and opposite a given well interval the Ic index and permeability value indeed seem to vary in the same direction.

III - EARLY TRIALS IN 37 WELLS

Based on the conclusions of the above study and thanks to the help of ARTEP* and the kindness of logging companies, between 1963 and 1968 we studied acoustic signals recorded with industrial sondes, such as the "Sonic", for measuring wave velocities.

These signals came from open-hole intervals surveyed in 37 wells drilled into different oil provinces.Ic index logs were then compiled for these 37 wells, and we tried to compare their variations with those of permeability measurements evaluated directly on the drilled rocks.

III.1 - Direct Permeability Data in These Wells

Due to the scarcity of such measurements, we collected information on rock permeability from every possible source.

This information was of unequal value.

In a decreasing order of reliability we found :

- flow measurement on whole cores,
- flow measurement on sampled plugs,
- flowmeter logs,
- test results, but unfortunately without having available any recorded curves of built-up pressures.

III.2 - Comparison of "Ic" vs. Direct Permeability : "K"

This comparison is summed up in the following table made out in cooperation with the oil companies involved.

---

* ARTEP : A French Association for research in oil production techniques ; IFP, SNEA (P), CFP and GDF are its present members.

TABLE I

Number and origin of direct permeability data	Ic.vs.K agreement*	Ic.vs.K disagreement
8 (whole cores)	8	0
12 (sampled plugs)	9	3
14 (flowmeters)	10	4
16 (tests)	12	4

a) - An examination of this table shows that Ic vs K disagreements never occur when K was estimated on whole cores whose volumes may be considered really representative of the acoustically investigated volume.

b) - Divergences between flowmeter and test results on the one hand, and Ic indications on the other hand show that the new parameter Ic, the way it was then taken, may be blind to certain permeable intervals. However, it should be noted that the disagreements noted here were always obtained opposite gas reservoirs which were tested only after the casing had been set, cemented and perforated, whereas, of course, acoustic signals had been recorded in the open-hole.

III.3 - Function Linking Ic and Permeability

In the only wells where rock permeability was known on whole cores, flow measurements were always made along the core axis. Under these conditions the following relationship is suggested :

$$Ic = \alpha \log \frac{Kv}{\mu} + \beta$$

with Kv = vertical permeability
μ = rock wetting fluid viscosity
α, β = constants for a given equipment and a given well.

* There is agreement between Ic vs K :
either : when a correlation coefficient higher than 0.5 is found between both parameter series.
or : when every high Ic index interval corresponds to a productive interval, and every low Ic index interval corresponds to a 100 % shale interval.

III.4 - Repeatability of Ic Measurement in a Given Well

According to information given by logging companies a reasonably constant emitted signal could be expected. On the other hand, sonde excentering has a serious effect on the successive amplitudes of the signal received, and good centering is not easily obtained if only because the borehole section is not always circular.

Figure (2) explains how eccentering due to the hole and/or to the sonde may generate out-of-phase components between various acoustic paths into the rock around the borehole. This eccentering particularly affects amplitudes V_2 and V_3 and therefore $\frac{V2 + V3}{V1}$.

To these eccentering problems, disturbances already reported by Morlet (ref. 3) must be borne in mind, because the transducer's cylindrical shape can not be equated with that of a single point.

III.5 - In spite of some encouraging results, we could not go on with this type of experiment because they all had to be made with equipment which we were not able to control or modify, inside wells where rock permeability was known over intervals whose cumulative thickness was, and would always be, limited.

IV - EXPERIMENTS IN ARTIFICIAL POROUS MEDIA

Therefore we chose to start a new study in a large, specially built model where every geometric parameter could be controlled :

- transducer positions,
- sonde stand-off in the hole,
- mud-cake thickness,
- log investigation radius,

and, of course,

- direct porosity and permeability measurements.

In addition it was now possible to know transducer characteristics precisely, as well as the transfer function of the receiver and transmission cable.

V.1 - Objective

This new type of experiment was aimed at comparing the new acoustic index Ic with direct permeability measurements made on the porous model, whose petrophysical properties were verifiable at all times and at every point.

Indeed, along this model, we wanted permeability to be the only variable parameter : so its range of values had to be large, for instance 1 to 1000. Of course this target cannot be reached when every other factor such as :

- porosity,
- density,
- specific surface area,
- structure, etc....

remains constant, since all these petrophysical parameters are linked together ; but slight simultaneous alterations of these factors made it possible to modify the permeability level.

In order to simulate saturated porous rocks around a cylindrical borehole of usual size, this model first had to act as an infinite medium for acoustic logging ; it had also to be suitable for every type of measuring and sampling.

IV.2 - Building the Model

These conditions were respected by building the model from mortars (cement, sand, water, additive). These mortars were placed in a rectangular pit, buried in and flush with, the ground. Its dimensions were :

1.4 x 1.4 x 12 m i.e. 5' x 5' x 40'

The pit walls were made out of an impervious concrete without any iron. The pit ends were extended by troughs useful for dilling and emptying the pit.

Three different permeable media were placed in this pit. The least permeable was sandwhiched between the two more permeable ones.

The well was simulated by a semi-cylindrical hollow volume (Figure 3) extending across the three media of the model. This arrangement gave good access to any part of the well and of the sonde.

IV.3 - Petrophysical measurements

a) - Measurements made on samples taken from the mortars while casting them.

The model is made up of three different mortars (sand of given grain size, cement, water, additive, in given proportions) poured into the put simultaneously.

Their permeability and porosity data, as measured on the check-samples,are in agreement with the expected trends : see following table II.

TABLE II

Chek-Samples from Medium N° :	Porosity Ø %	Permeability taken with air mD	Structure estimated from thin-sections (see fig.4)
I. permeable	20 to 24	500 to 1800	channels sometimes cemented, t = 100 μ
II. impervious	21 to 24	1 to 6	Vuggy
III. intermediate	20 to 60	20 to 60	Intermediate

In view of the way these mortars were made, there was no reason to believe that their structure should be anisotropic ; however they might have been heterogeneous and measurements on check-samples are not sufficient to represent them. The permeability of the mortars therefore had to be evaluated in the very volume where the acoustic waves were actually travelling, all along the simulated well.

b) - Core Data of the Model North Side

After completion of all the acoustic logging, thirteen vertical cylinders (d = 10 cm, h = 30 cm) were cored 4 cm from the well surface all along the model's North side.

The distance between cores was about 80 cm.

The core sampling of the model's North side amounted to only 10 % of its total length. However, vertical and horizontal permeability data obtained on these cores were found to be scaled as expected (Figure 5).

c) - Water Build-up in North Side Voids

The cores having been removed the permeability of the mortars left in-situ could be tested.

To do this, we dried up the cylindrical volumes left empty after coring ; the well remained water-filled, and we measured the timing of the water build-up inside the voids. The results are noted in Figure 6. Once again permeabilities are scaled as expected.

The data in Figure 6 are considered the most representative of the model's North side permeability, since they cover 90 % of the model's North side.

d) - Direct Permeability Measurement on the Model's South Side

On this side we decided to measure the mortar permeability by injecting a water flow, i.e. by a non-destructive and repeatable method.

A piezometric tube (Figure 7) was attached to the flat vertical surface of the well and through it water was injected under low pressure (2 psi). The injection points were as near as possible to each other, i.e. every .25 m and .25 m below the water level in the model.

The results are reported on Figure 8. Water-flow data are proportional to the absolute values of permeability all along the model's South Side.

e) - Porosity Log Data

Relative porosity measurements of the mortars were made by running a gamma-gamma density log and a velocity ("Sonic") log all along the well in the model. Absolute porosity could be derived from both these logs if proper porosity calibrations had been made on similar mortars.

According to check-sample data, these mortar porosities range from 20 % to 24 %. This represents a slight relative variation for the model as a whole.

Thanks to these density and velocity logs, it is confirmed that, placed in the middle of the model, the most impervious mortar has a porosity of at least 15 % and an average porosity of more than 20 %.

As supplementary information Figure 9 gives the velocity log. The specific transit time ranges from 75 to 105 μsec/ft, and this suggests a porosity range of about 15 % to 35 %.

f) - Acoustic Data

The acoustic equipment used in our present experiments was initially made up of industrial tools that we progressively modified.

We tried above all to make a transmitter and a receiver in such a way that they would behave as if they were geometric points.

Eventually all the necessary prerequisites were merged into the design and manufacture of an experimental sonde whose performances will now be described.

With that sonde, we evaluated :

a) - Effect on the Ic index of a mud-cake deposited on the well bottom surface,

b) - Determination of the investigation volume of the Ic acoustic index.

c) - Determination of Ic index over a o.8 m spacing and this, every 0.2 m along the well.

IV.4 - Mud-cake Effect on Various Acoustic Measurements

Cake deposited over any section of the path of an elastic wave -(the compressional wave in the present case)- should attenuate its amplitudes.

In an actual well, cake is made up of clay, cuttings, mud, and additives ; cake thickness may range up to 3 cm.

In the present experiment pure sand, then bentonitic cakes of controlled and varied thicknesses were deposited along the well bottom, and we noted their effects on acoustic signals emitted by our sonde.

Each of the first three amplitudes, V1, V2 and V_3 was measured for each cake thickness.

Results are displayed in Figure 10. They show a strong amplitude reduction proportional to increase in cake thickness.

For example, when cake thickness increases from zero to 3 cm, we note an amplitude reduction by a factor of 9, while the Ic index remains constant at $\pm$ 20 % and part of this latter variation may be due to mistaken readings on V_1, V_2 and V_3.

This data leads to the conclusion that all further Ic-index measurements may be performed in a model-well filled with clear-water.

On the contrary, amplitude measurements, if any, should take cake-thickness and sonde stand-off into account. Conversely, attenuation data might provide information about cake characteristics.

IV.5 - Investigation Radius and Reading Point for the New Ic Parameter

In order that the petrophysical measurements made on the model may be compared with Ic values, we must define the shape of the zone investigated by the acoustic parameter.

In any medium and for an acoustic measurement, the depth of the investigated zone is affected, in particular by :

- Signal frequency,
- Wave propagation velocity,
- transmitter-to- receiver spacing,
- transducer geometry.

Normally the investigated zone will increase with the wavelength, i.e. when the frequency is low and the medium is "fast".

Taking for granted that our sonde reading level is at approximately the spacing mid-point, and in view of the present signal pseudo-frequency (about 15,000 Hz), we worked out an experiment for evaluating the sonde investigation radius at this mid-point and for this frequency.

Sixty centimeter and seventy-centimeter spacings were tested.

Two-centimeter wide cylindrical grooves were successively drilled into the mortar, starting from the pit-wall, then going nearer and nearer the central well.

Between each new groove drilling, acoustic measurements were performed and we noted an increase from 9 to 27 for the Ic-index when the groove discontinuity is situated between 3 cm and 16 cm from the well surface.

Discontinuities beyond 16 cm have no effect what-never on the Ic index, cf. figure (11).

From another experiment described later on in this paper, we knew that a core removed 8 cm from the well surface provokes in the model a discontinuity which increases the Ic index taken with an acoustic sonde of the same spacing.

Hence we conclude that in this case the average investigation depth measured from the well surface was about 12 cm. Since the compressional wavelength in this particular mortar is about 26 cm, the investigation depth seems to be equivalent to half a wavelength, which agrees with previously reported experiments.

IV.6 - Interpretation of Ic Index vs Permeability K

For the three porous media of the model, we found it convenient to distinguish between the North and the South sectors, i.e. the two sides of the horizontal well. Indeed the first acoustic logs run had shown differences between the mortars in the two sectors : the North side was more heterogeneous,and the South side more homogeneous.

Ic reference logs vs. K were therefore taken on each side.

North Side

Ic index : the log will be found in Figure 12.

Permeability K : The log of water-build up in core-holes will be found in Figure 7.

N.B. : After the thirteen cores had been taken from the North side mortar, a new Ic log was built, which will be found in the same Figure 12.

South Side

Ic index : the log will be found in Figure 14.
Permeability K : the injected flow log will be found in Figure 8 and 8 b.

IV.7 - Ic vs.K : North Side

Each of the Ic values found before coring was plotted versus the water height linearly interpolated between the two nearest values actually found.

This permeability evaluation encompasses a volume greater than does the acoustic reading. Therefore the above-mentioned plot does not yield a calibration of Ic as a function of K. However, true to forecasts, the Ic index increases qualitatively with permeability.

After the cores were removed, the model's North Side simulated highly broken rock with large open cavities. The change undergone by Ic is better displayed by superimposing both logs before and after coring (Figure 13).

When the compressional wave investigated zone includes one of the voids left by the cores, the Ic index should normally increase, and indeed it does.

On the contrary, when the compressional wave investigated zone includes no voids, the Ic index should keep its previous value, and in fact it does.

Examination of Figure 13 shows how advantageous it would be to resume these experiments in natural media whose permeability is partially generated by fractures.

IV.8 - Ic.vs.K, South Side

First let us remember that on this side the mortal is reasonably homogenous.

Moreover, along the well, permeability K (every .25 m)and the Ic index (every .20 m) were evaluated with good accuracy over equivalent volumes and with the precautions listed in IV.5.

The corresponding Ic vs.K semi-logarithmic plot is therefore the most representative of all our experiments.

Figure 16 shows that South Side permeability is evaluated by the Ic index with an error smaller than half a decade.

V - CONCLUSION

With the objective of logging rock permeability in wells, and following observations made on industrially recorded acoustic waves, we started studying an index some of whose properties are reviewed here.

Then this index was compared with permeability over rock intervals in a number of wells. The outcome warranted further study of this index in a large-size model simulating an actual drilled well, and in which permeability was the only petrophysical parameter showing large variations.

All the results, and most especially those obtained whith this model and with our own sonde, lead us to propose the logging of this index in order to evaluate in-situ rock permeability alongside the well bore.

o

o o

This work was performed with the help of ASSOCIATION DE RECHERCHE DES TECHNIQUES DE FORAGE ET PRODUCTION (ARTEP).

REFERENCES

(1) -	SEEVERS,D.O.	A Nuclear Magnetic Méthod for determining the permeability of sandstones	SPWLA, Symposium, 1966
(2) -	KUMAR, J., FATT, I.	A Nuclear Magnetic Resonance study of Porosity, Permeability and surface Area of Unconsolidated Porous Materials.	The Log Analyst 1970, vol. XI, n° 1, 13.
(3) -	MORLET et SCHWAETZER	Mesures d'amplitude des ondes soniques dans les sondages	Geophysical Prospecting, 1961, vol. 9, n° 4.
(4) -	MORLET et SCHWAETZER	Le log d'atténuation	22è réunion EAEG, Londres, 23 mai 1962
(5) -	COMPAGNIE D'EXPLORATION PETROLIERE	Brevets français n° 1.348.538 et n° 1.378.019	Bulletin de la propriété industrielle du 2-12-1963 du 5-10-1964
(6) -	MORRIS et al.	The use of compressional and shear acoustic amplitude for locations of fractures	Journal of Petroleum Technology, June 1964
(7) -	FONS, LLOYD C.	Acoustic Scope Pictures	SPE - Fall Meeting Oct. 1963
(8) -	CHRISTENSEN, D.T.	(About) 3 - D Velocity log.	SPWLA Meeting, May 1964
(9) -	WALKER, T.	Interpretation of the fracture finder microseismogram.	Transactions SPWLA Meeting, May 1964
(10) -	SOCIETE DE PROSPECTION ELECTRIQUE (SCHLUMBERGER)	Brevet français n° 1.401.258	Bulletin de la propriété industrielle 2-4-1964

(11) -	ZEMANEK, J.	U.S. Patent n° 3.362011	Granted Jan.2, 1968
(12) -	THURBER et al.	Acoustic log checks casing cement jobs	Petroleum Engineer Dec. 1960
(13) -	GROSMANGIN et al.	The Cement bond log	Journal of Petroleum Technology, Feb. 1961
(14) -	BROWN H.D. et al.	New developments in sonic wave train display and analysis in cased holes	The Log Analyst, Jan., Feb. 1971
(15) -	COASTES, G.R. et DUMANOIR, J.L.	A new approach to improved log-derived permeability	Log Analyst, 1974, vol. XV, n° 1, 17
(16) -	RAIGA-CLEMENCEAU, J.	L'exposant de cimentation dans la relation porosité-facteur de formation : l'effet de la perméabilité.	SPWLA Symposium, Houston, 1977
(17) -	DUPUY, M. LEBRETON, F., SARDA, J.P.	Numerical study of the influence of attenuation in rocks on the form of acoustic signals.	Actes du 2è colloque SAID, 15 octobre 1973, Paris.
(18) -	MORLIER, P. SARDA, J.P.	Atténuation des ondes élastiques dans les roches poreuses saturées.	Colloque de l'ARTEP, de juin 1971, Rueil-Malmaison, communication n° 6.

ABOUT THE AUTHORS

Francisque Lebreton graduated from the Ecole Centrale in Paris in 1946 and is currently a research scientist with the Institut Français du Pétrole. He previously worked for Société de Prospection Electrique and then for Lane-Wells Company.

Jean-Paul Sarda graduated from the Ecole des Mines in Paris in 1962 as a mining engineer. The first part of his carrier was spent working at the Laboratoire Central des Ponts et Chaussées in Paris from 1962 to 1964. Since 1966 he has been working as a research engineer at the Institut Français du Pétrole in the Rock Mechanics and Reservoir Stimulation Department. He has mainly worked on the problem of the absorption of elastic waves by saturated porous rocks as well as on various other problems linked to rock mechanics, in particular the origin and mechanical behavior of in-situ fissuring.

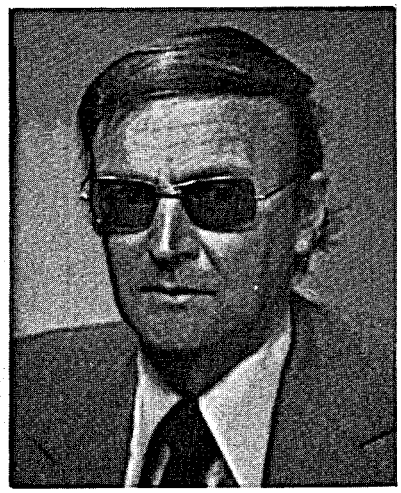

FIG. 1

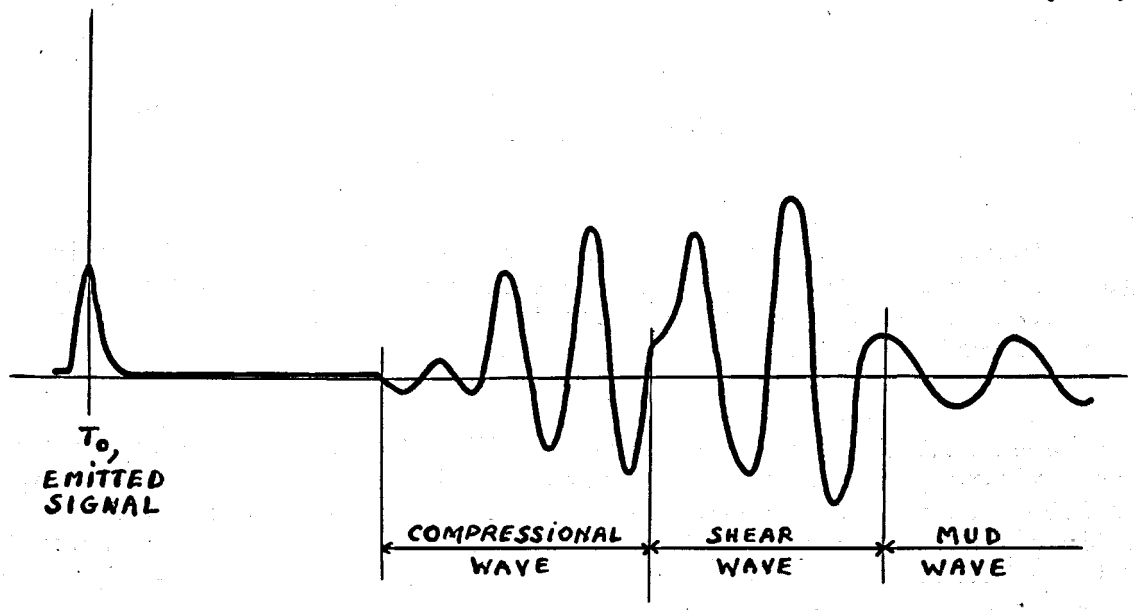

TYPICAL SHAPE OF AN ACOUSTIC SIGNAL WHEN RECEIVED IN A WELL FEW FEET ABOVE THE TRANSMITTER

FIG. 2

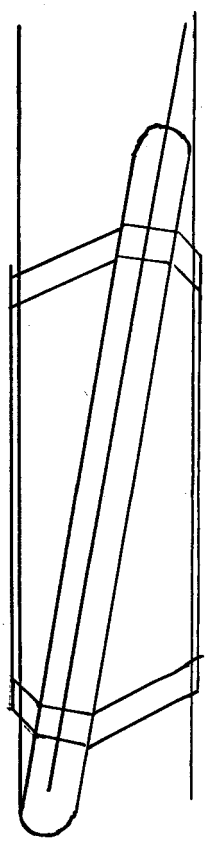

POSITION OF AN ACOUSTIC PROBE IN A BOREHOLE

VIEW OF THIN SECTIONS TAKEN FROM CHECK SAMPLES

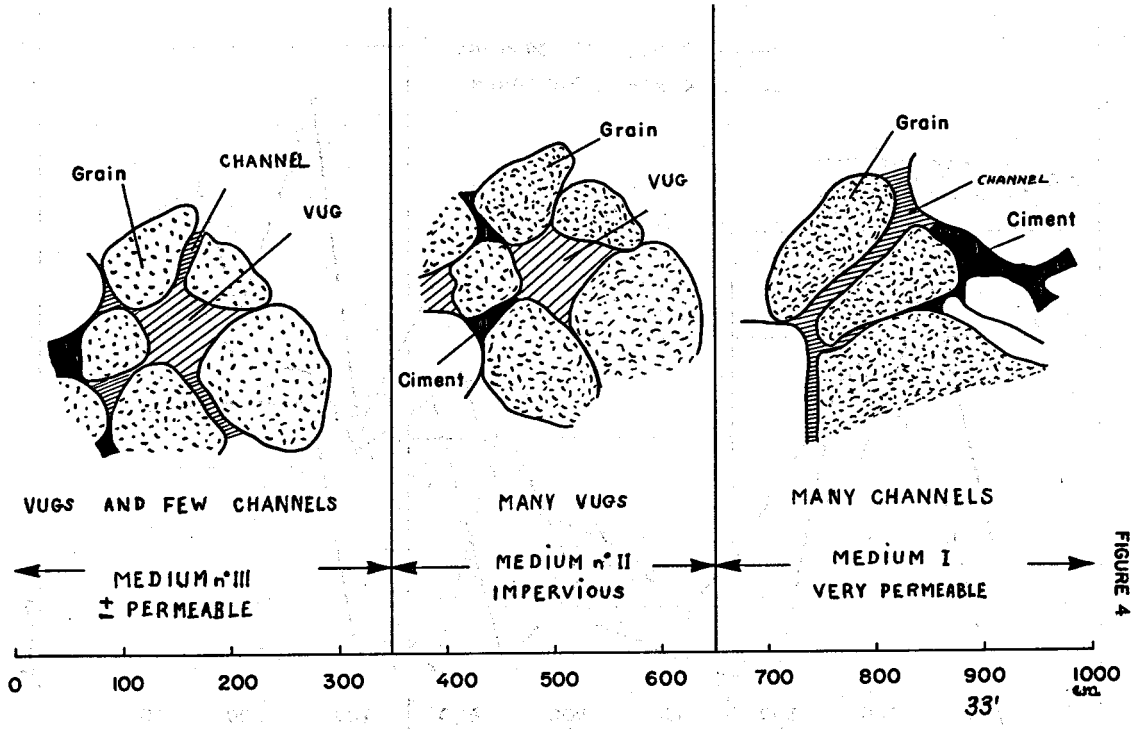

FIGURE 4

FIG.3

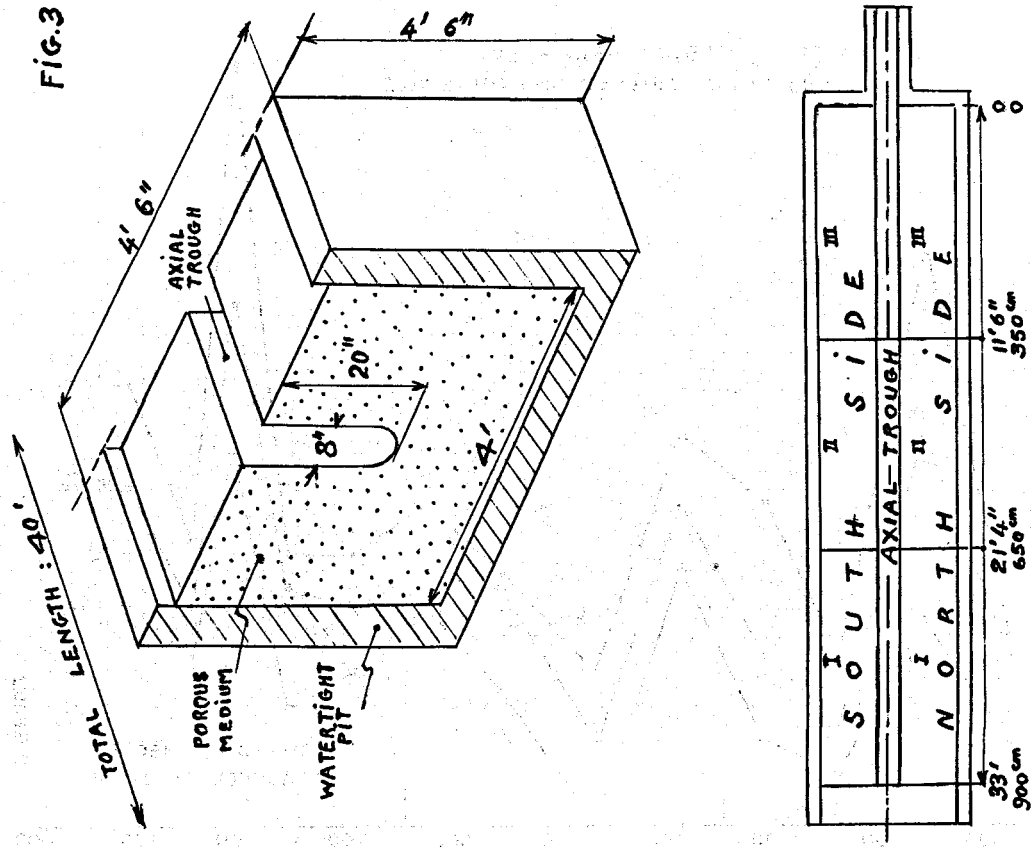

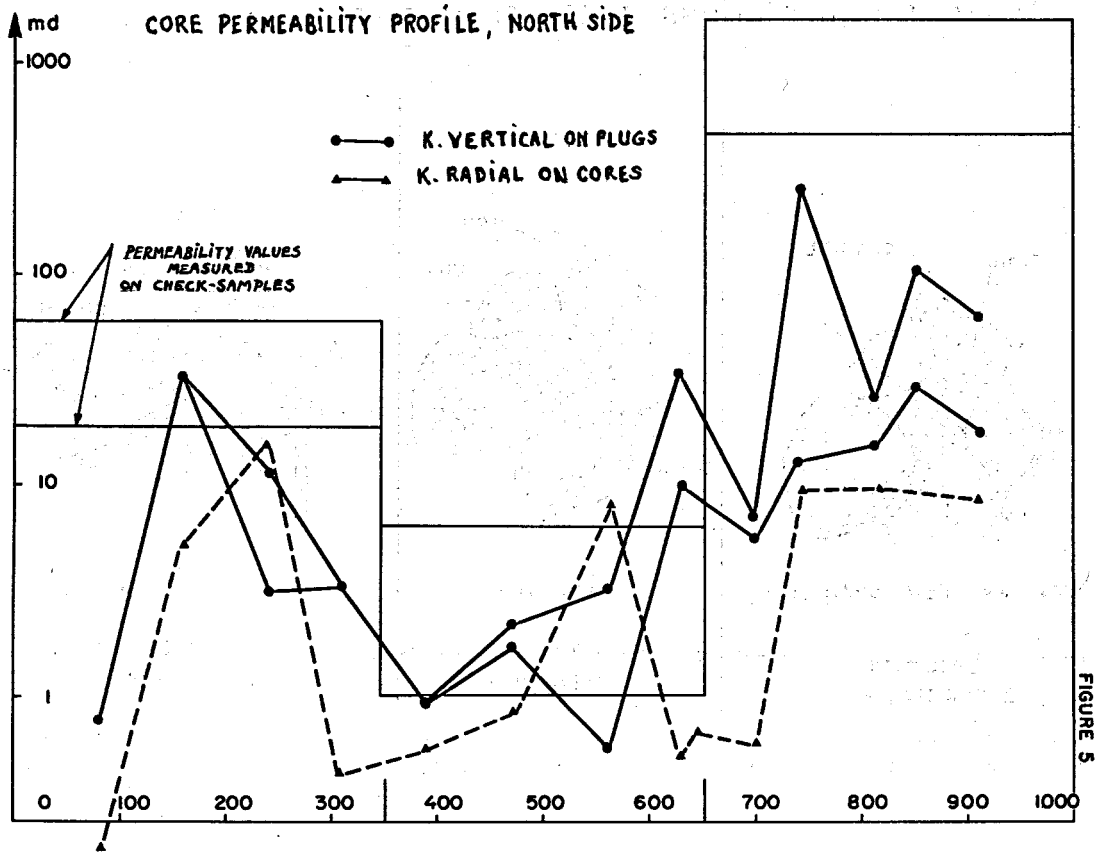

FIGURE 5

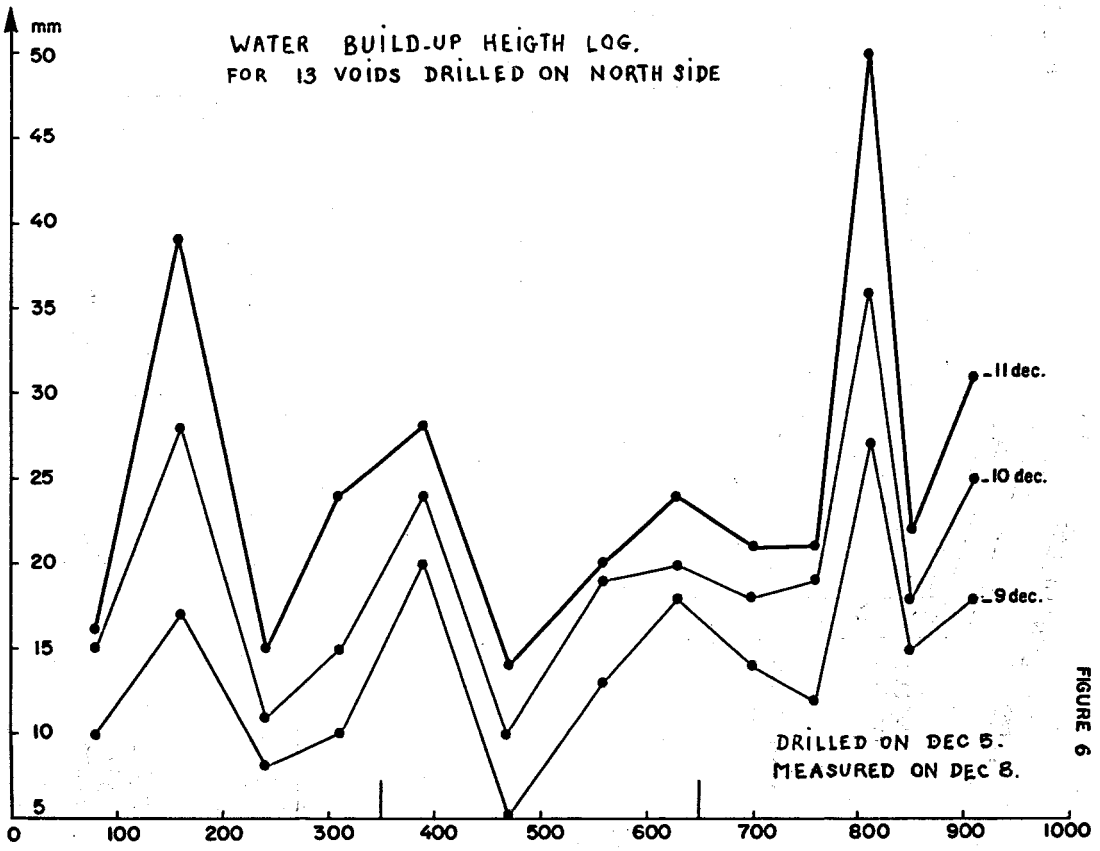

FIGURE 6

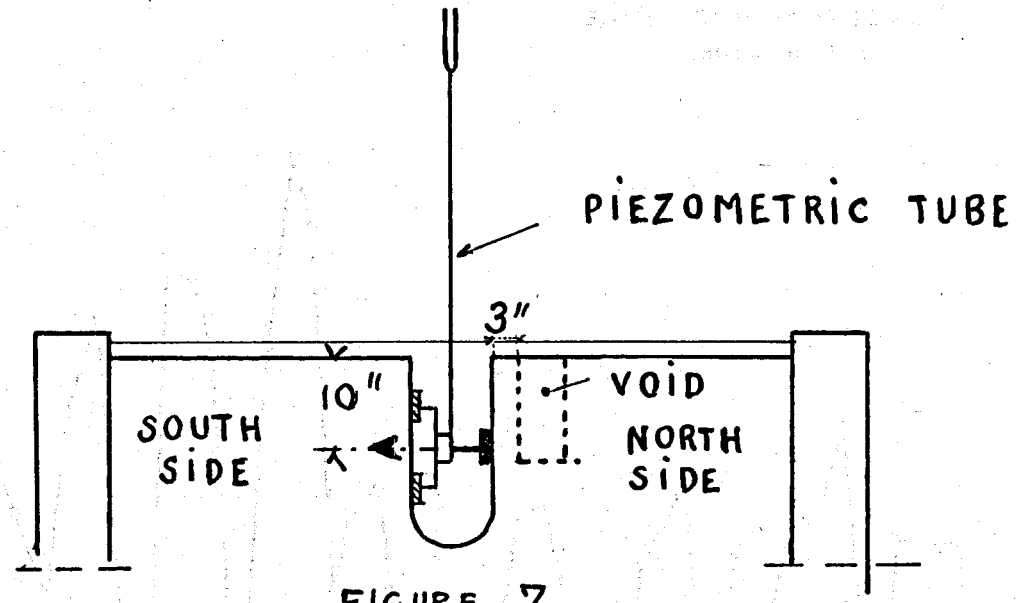

FIGURE 7

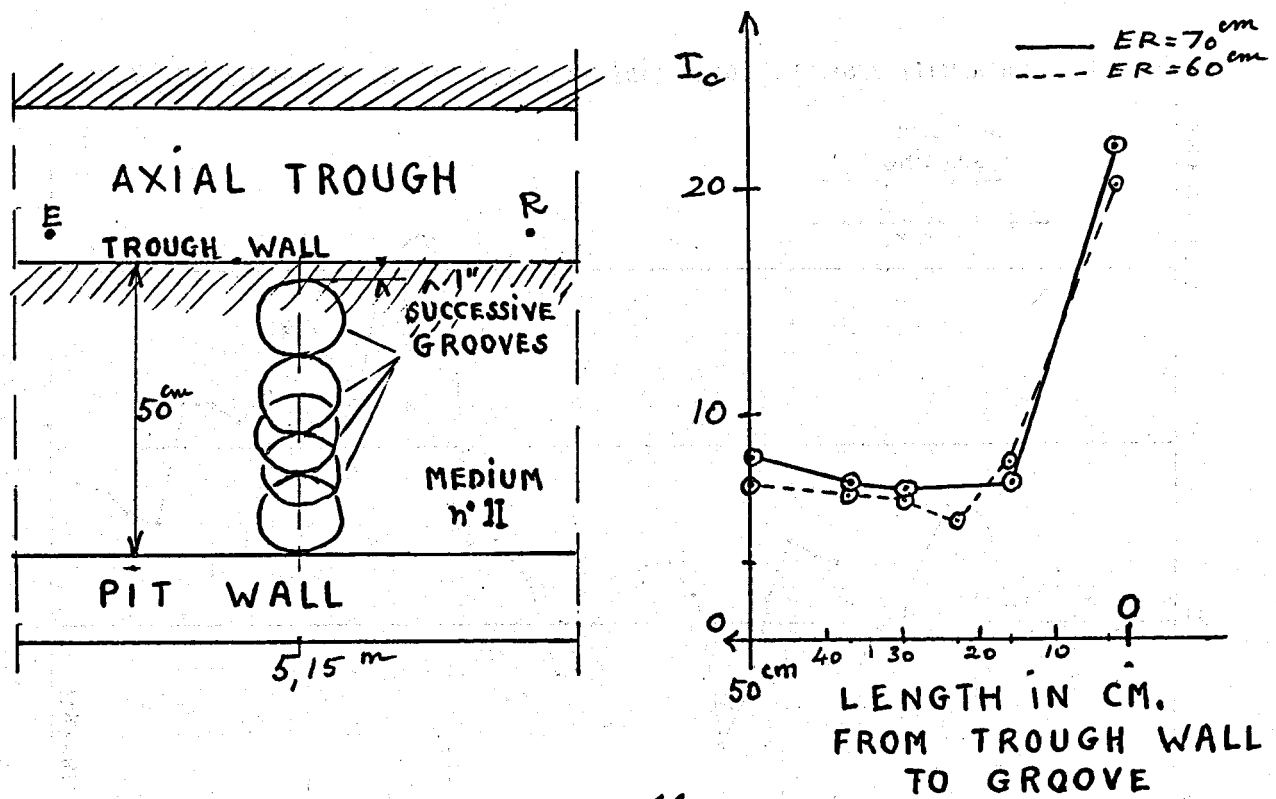

FIGURE 11

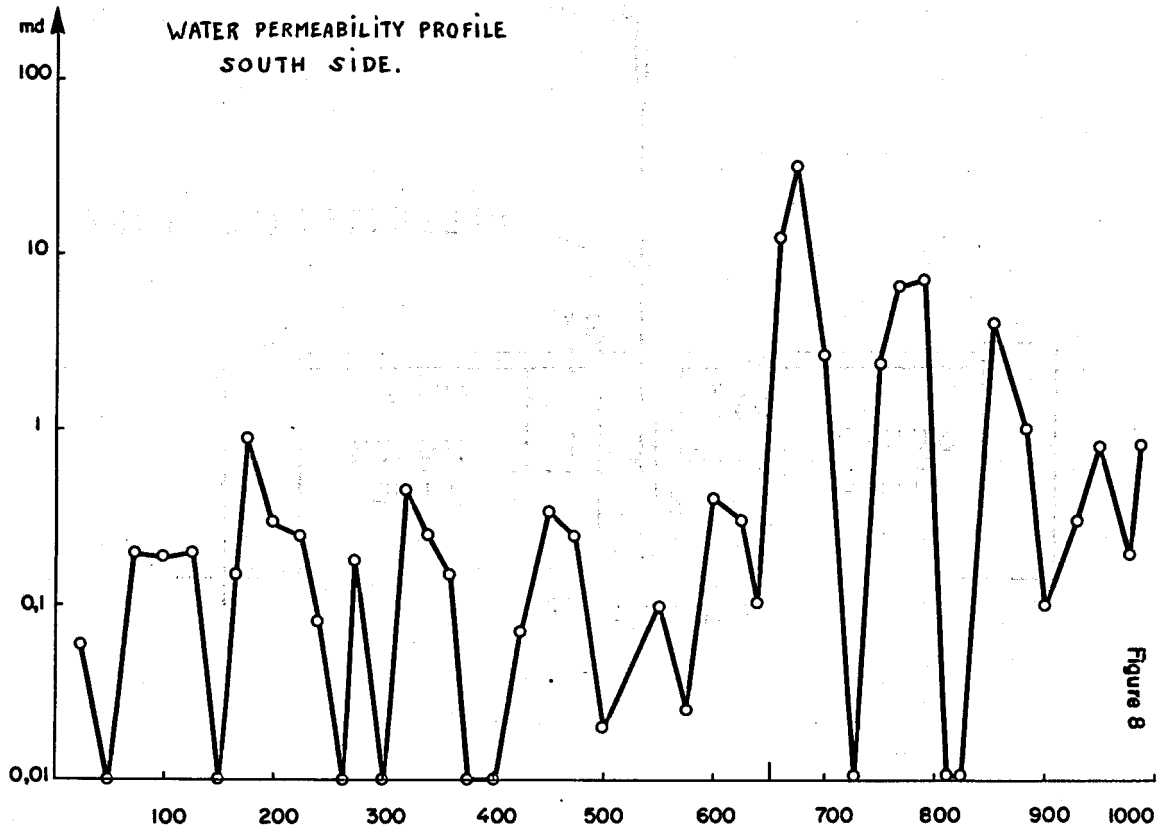

Figure 8

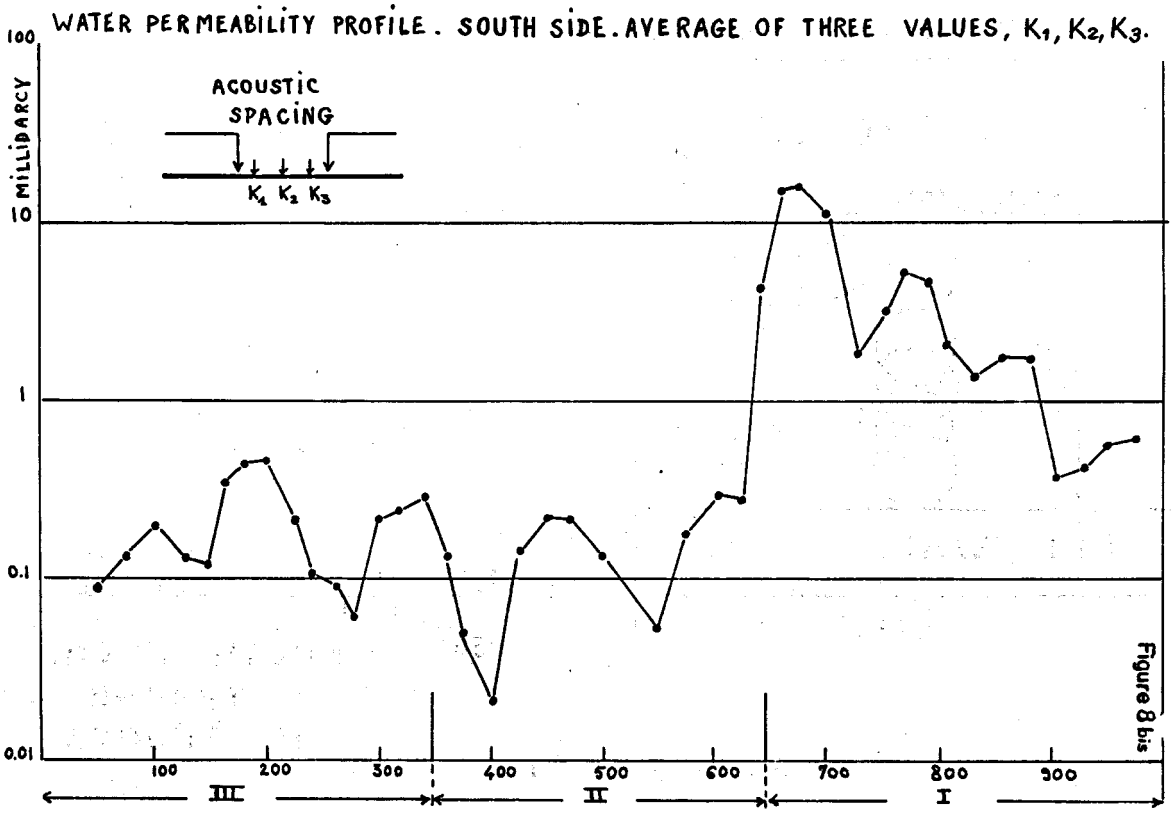

Figure 8 bis

COMPRESSIONAL WAWE VELOCITY LOG.
SOUTH SIDE

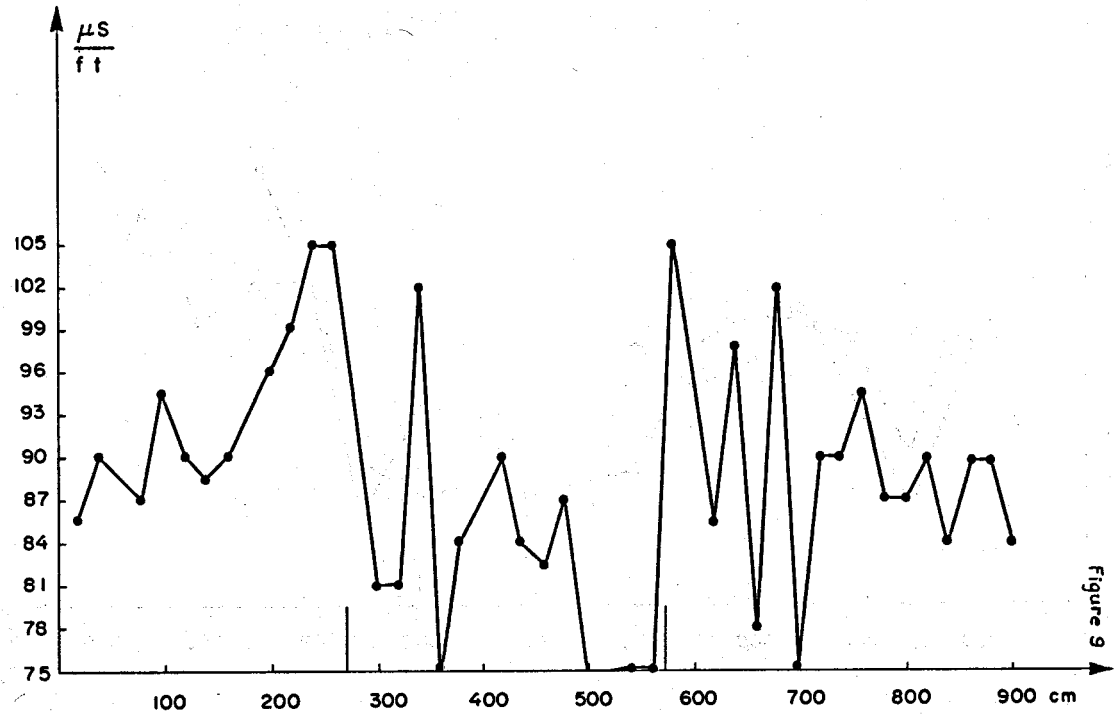

Figure 9

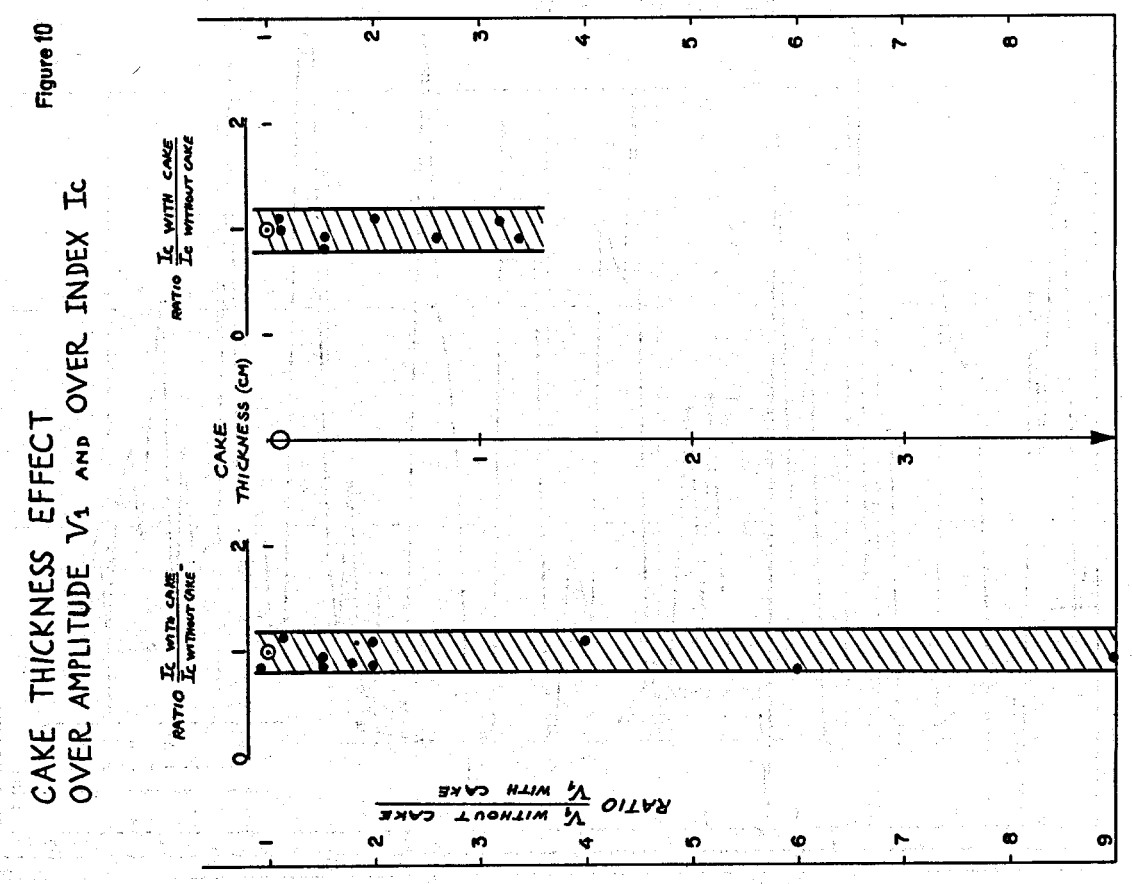

Figure 10

CAKE THICKNESS EFFECT
OVER AMPLITUDE V_1 AND OVER INDEX Ic

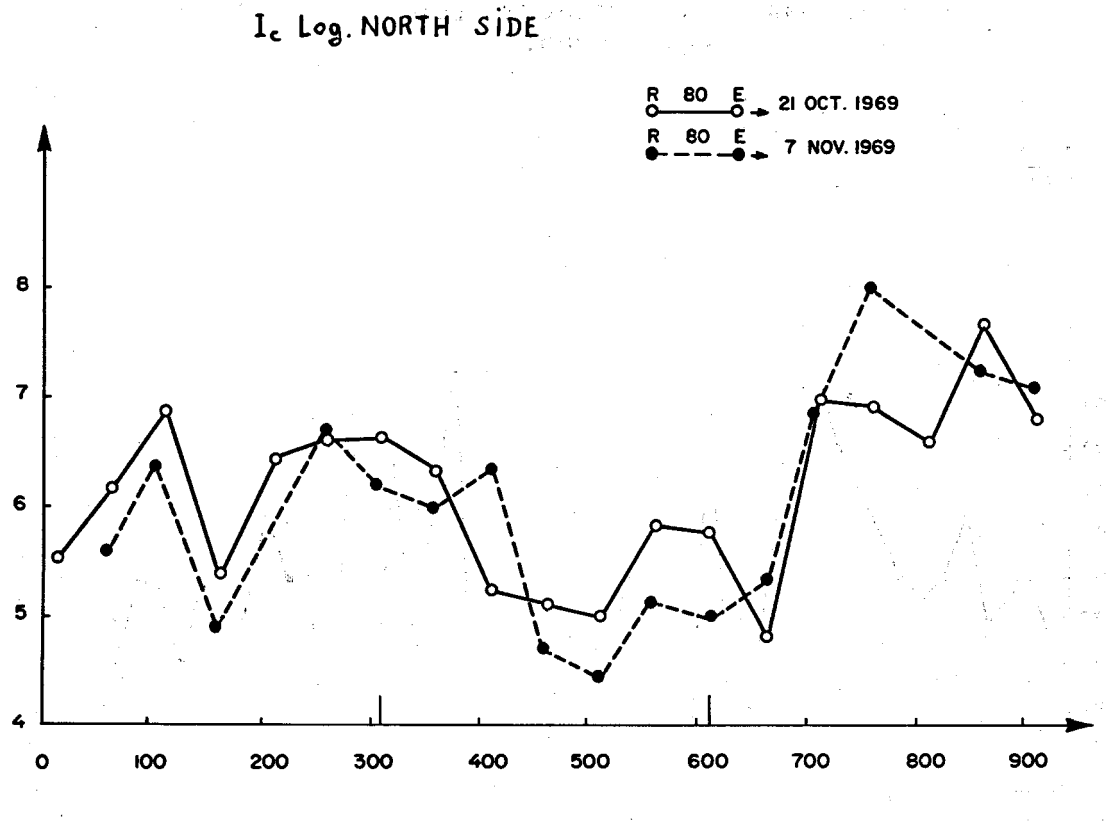

Figure 12

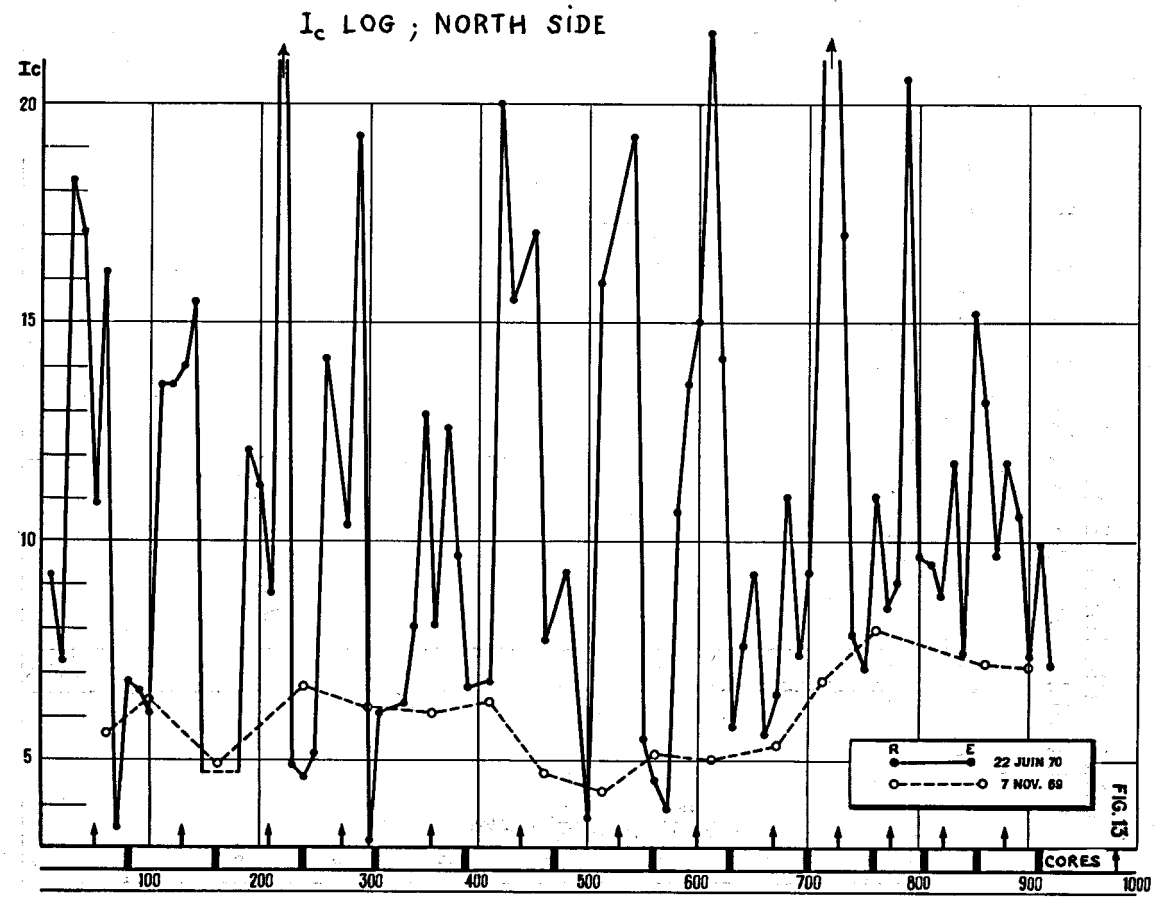

FIG. 13

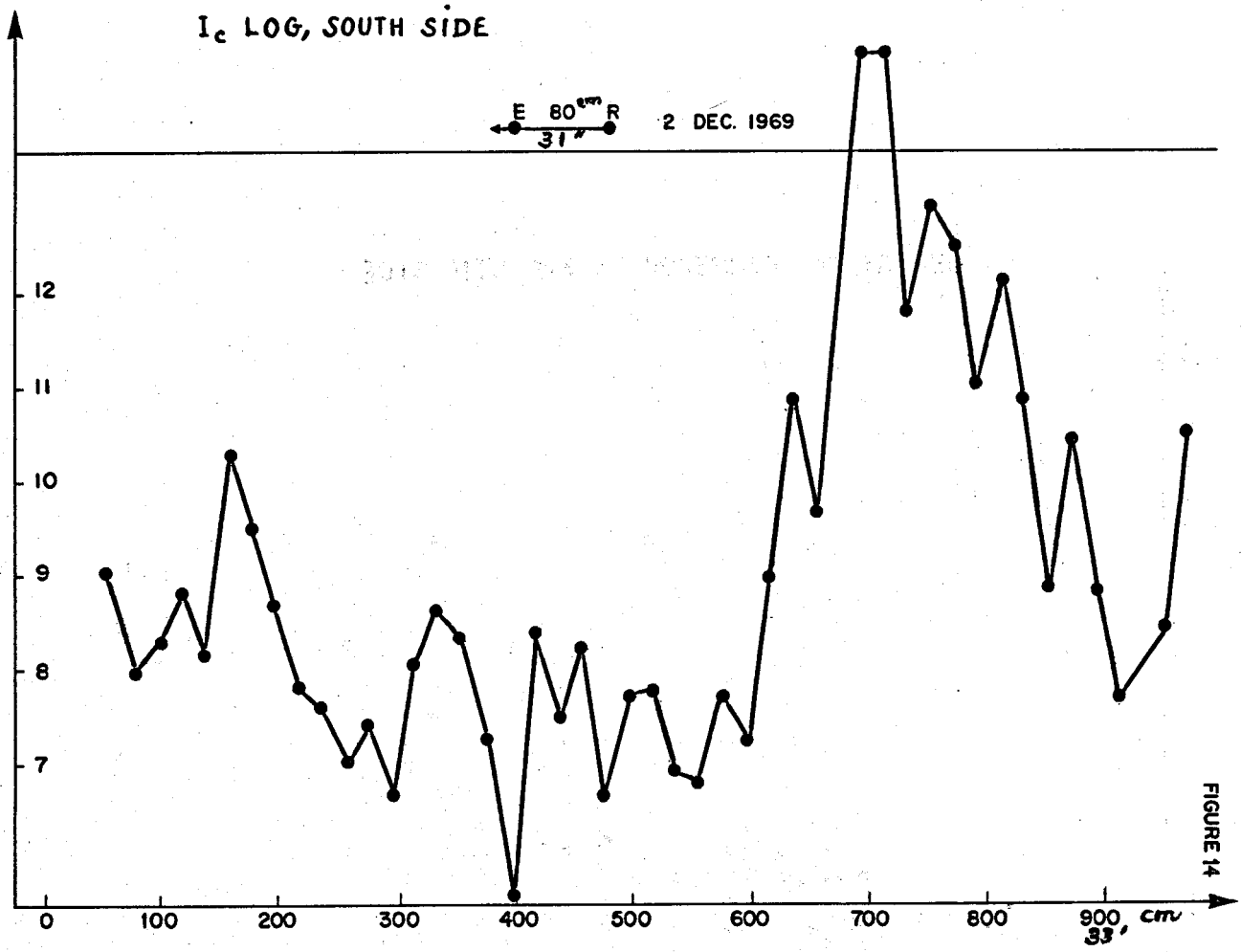

FIGURE 14

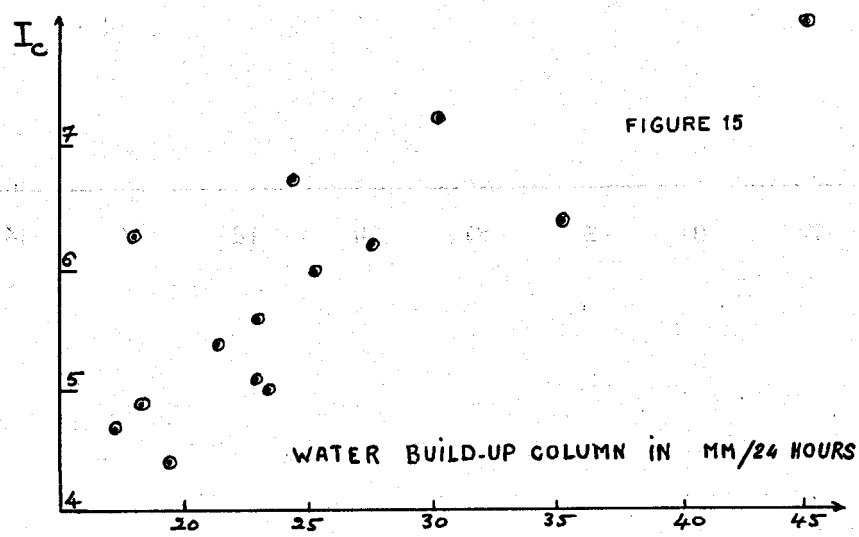

FIGURE 15

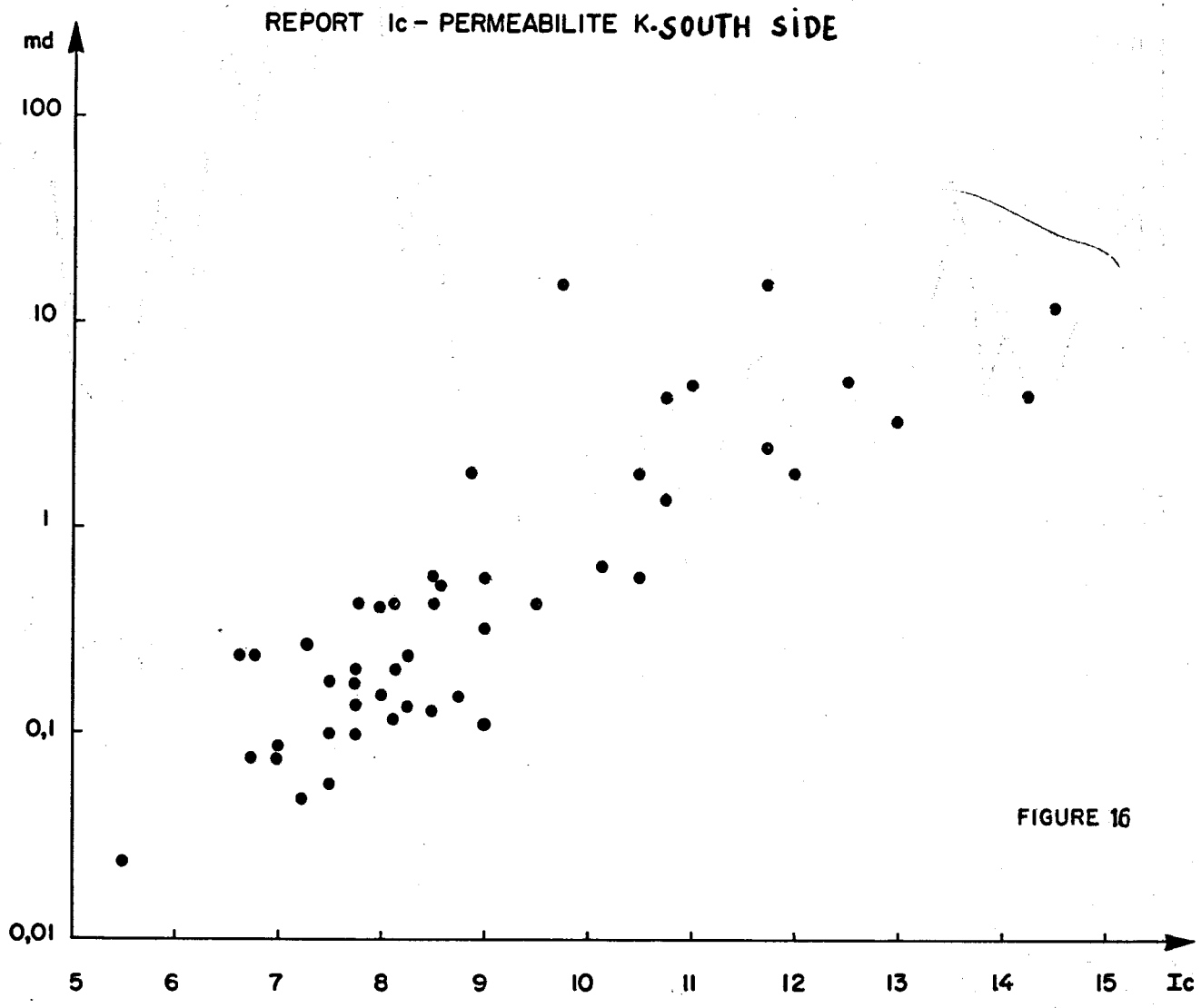
REPORT Ic - PERMEABILITE K. SOUTH SIDE
md
100
10
1
0,1
0,01
5
6
7
8
9
10
11
12
13
14
15
Ic

FIGURE 16

THE LATEROLOG GRONINGEN PHANTOM CAN COST YOU MONEY

R. Woodhouse : The British Petroleum Company Limited,
London, England.

ABSTRACT

Early Laterolog tools had erroneously high readings below high resistivity beds - this became known as the 'Delaware Effect'. Shifting the measure current return electrode to surface significantly reduced the problem.

The new generation of deep reading Laterolog tools is shown in this paper to be affected by the 'GRONINGEN PHANTOM' - a new manifestation of the old Delaware Effect. The Phantom has been observed to a maximum distance of 272 feet (83 metres) below high resistivity beds. The erroneously high resistivity reading of the Phantom is greatest when R_t is low. Log readings of three times the correct deep Laterolog reading are common.

Examples of the Phantom in shale beds, water and hydrocarbon bearing sandstones are presented together with observations in eleven wells.

The GRONINGEN PHANTOM costs you money when it leads to unjustified optimism - the setting of a liner and the flow testing of 'Phantom Hydrocarbon'. It is equally important that actual hydrocarbon bearing zones are not dismissed as Phantoms. Careful consideration must be given to all the evidence in a well and particularly the LLS, micro-resistivity and neutron/density logs.

GENERAL INTRODUCTION

Older configurations of the laterolog resistivity tool showed some unusual responses below high resistivity beds. The Guard, LL3 and seven electrode systems with the measure current return electrode in the borehole showed the Delaware Effect (Suau et al, 1972). Log resistivities up to 50 times the normally expected values were observed for 70 feet below infinite resistivity beds.

Removal of the measure current return electrode to surface reduced the problem. Selection of a reduced measure current frequency for the simultaneous nine electrode array was reported to have solved the Delaware Effect. The Anti-Delaware Effect, a reduced resistivity for about 15 feet below a high resistivity bed, was reported by Suau, 1972, to be solved by the nine electrode tool.

It has become clear that these modern tools still exhibit imperfect measurements in the same areas as the old Delaware Effect. It is understood that the problem was first recognised in the Groningen gas field in the Netherlands - hence the name the 'Groningen Phantom'. All deep reading laterologs with a measure current return at surface exhibit the 'Groningen Phantom' to some extent.

OBSERVATIONS OF THE PHANTOM

Well G (Figure 1)

The lithology is halite (salt) above 1995m with shale below. The halite has practically infinite resistivity. The shale below 2040m has a resistivity of about 2.5 ohm.m; here the micro SFL and the LLD are equal, and the LLS is a little greater at 3.0 ohm.m. Starting at about 2034m the LLD gradually increases until at 2002m it reads 6 ohm.m. The LLS and MSFL continue to read the same as previously.

Since the formation is shale and the hole is not badly caved the separation between the resistivities is not caused by hydrocarbon.

Well B (Figure 2)

Above 1774m the formation is anhydrite; below 1774m it is shale. Below 1850m the LLD shale is about 0.7 and the LLS is about 0.6 ohm.m. Above about 1833m the LLD and LLS diverge gradually until at 1805m the LLD is about 1.5 when the LLS remains at 0.6 ohm.m. Above 1799m there is a sudden jump in the LLD to about 4 ohm.m.

As with Well G this separation is not caused by hydrocarbon, caving, change in shale resistivity or operator error.

Well A (Figure 3)

The lithology above 1600m is halite followed by shale to 1610m and then a sandstone with interbeds of shale. Below 1640m the LLD and LLS are equal at about 0.4. The MSFL read 0.6 ohm.m (not shown on Figure 3).

Above 1640m the LLD and LLS diverge until at 1626m the LLS (and MSFL) are unchanged whereas the LLD reaches 0.55 ohm.m. This might be caused by hydrocarbon except that the LLS (and MSFL) both continue to indicate 100% water saturation values. Note also that the LLD in the shale reads higher than the LLS.

Patterns begin to emerge from these three examples. A further eight examples were investigated.

Data from Eleven Observations

Table 1 shows relevant data from eleven wells where there are modern nine electrode laterolog measurements below high resistivity beds. The code letters for the wells correspond with those of the example log suites.

DEDUCTIONS FROM THE OBSERVATIONS

Two parameters usefully describe the Phantom - the resistivity error and the Phantom height.

Resistivity Error

Figure 4 shows the values of actual log readings versus an estimate of the true log reading (taken usually from the LLS).

The maximum observed resistivity error is at low resistivity. A log reading of 1.5 ohm.m can occur in a formation of 0.5 ohm.m. The error decreases with increasing resistivity until above 30 ohm.m there is practically zero error.

If a water bearing sand resistivity is close to 0.5 ohm.m the S_w would be calculated at about $(0.5/1.5)^{\frac{1}{2}}$ or 55% and the zones would appear rather optimistic.

The two data points (B and G) with larger errors may have some other problem besides the Phantom so this data has not been used to estimate the maximum Phantom resistivity error. (These two responses are reminiscent of the Delaware Effect). The bold line drawn on Figure 4 is the MAXIMUM OBSERVED Phantom. There are many observations with a lower resistivity error. It would therefore appear that the chart is difficult to apply. In practice the Phantom would be diagnosed from the logs in an individual well and the chart would add confidence from previous observations.

Phantom Height

Figure 5 shows a plot of casing distance versus the height of the observed Phantom. The average resistivity of the formation with the Phantom is shown by each data point. In the examples, the casing is always shallower than the base of the high resistivity bed.

The maximum observed Phantom height is 83 metres (272 feet) and occurs when the casing is close to the base of the high resistivity bed. No Phantom is observed at high formation resistivity. There is a general trend of decreasing Phantom height with increasing formation resistivity and with distance to the casing shoe. It is understood that the Phantom exists even when the casing penetrates below the high resistivity bed.

It is again emphasised that the line on the plot is the MAXIMUM OBSERVED height. As with the resistivity error discussed above, the chart should be used to add confidence to a diagnosis arrived at using the individual well data.

EXPLANATION FOR THE PHANTOM

In a homogeneous formation the measure current flow spreads out over a very large volume of formation after the current leaves the focused current sheet. Therefore a potential very close to that of B, the measure current return electrode, will be created at the reference potential electrode N. The current spread over a large volume is a pre-condition to the use of N as a reference of the near zero potential.

Figure 6 shows schematically what happens to the LLD measure currents when an infinite resistivity bed is interposed between the tool and the surface. Since low frequency alternating current is used for the tool there is a finite skin-depth* of about 85 metres for a one ohm.m formation. The measure current "sees" the return path via the borehole mud and casing as a lower resistance path than the high resistivity bed. The current paths will tend towards the borehole as illustrated.

*Footnote: Skin Depth $\delta = (\pi f \mu \sigma)^{-\frac{1}{2}}$

where δ = Skin depth for 67% loss. μ = permeability of freespace.

f = frequency in cps.

σ = conductivity of medium (ohm/m)

R

Although the resistivity of the actual formation remains unchanged, the concentration of the current lines increases the resistance presented by the formation and more potential is lost than in the homogeneous case before they reach the reference electrode N. As far as the electrode array and electronics are concerned the measured resistivity is higher than it would have been in the absence of measure current flow-line concentration.

The factors influencing the magnitude of the Groningen Phantom can now be analysed. The Phantom is greater when there is a greater preference for the measure current to flow into the borehole. It will therefore increase in magnitude with increasing:

High resistivity bed resistivity.

High resistivity bed thickness.

High resistivity bed areal extent.

Proximity of the casing shoe.

Mud conductivity (and hole diameter?).

Frequency of measure current.

Formation conductivity.

Distance of faults and other casing strings through the high resistivity bed.

Presence of further high resistivity beds up-hole.

The Phantom has now been observed and explained in simple terms. The explanation in terms of electromagnetic theory we leave to others.

HOW DOES THE PHANTOM COST YOU MONEY?

Well H (Figure 7)

Well H shows an LLD with a long resistivity gradient. The interval 2622-2635m shows a substantial separation between the LLD and the LLS (1.8 and 0.6 ohm.m, respectively). The LLD suggests an S_w of 50-60%.

Optimism grows.

In the interval 2585-2605m the hole is badly caved but the GR and the sonic indicate a changed lithology with a porosity of about 8%. The salt saturated formation water has an R_w of about 0.02 ohm.m so the 100% water bearing formation would have a resistivity of 3 ohm.m. The LLD reads more than this.

Optimism grows again and leads to a DST. The DST produced water and not the expected hydrocarbon.

Closer inspection of the LLS shows that it remains close to R_o throughout. If hydrocarbon is present it can reasonably be expected that the LLS would be influenced by at least residual hydrocarbon saturation. In this particular area this formation is a gas prospect and if gas were present it should be seen as a separation on the neutron/density combination.

Previous observations summarised on Figure 4 and 5 show that in Well H, where the casing is only 12 metres above the base of a 165m thick high resistivity bed, a long (60-90m) Phantom can be expected. The LLD and LLS actually begin to separate at 2660m, 83 metres below the high resistivity bed. At 2630m the LLD reads 1.8 ohm.m. Figure 4 indicates a maximum correction down to about 0.6 ohm.m. At 2600m the LLD reads 7 ohm.m and the corrected value is about 4 ohm.m. Both these corrected resistivity values are almost equal to the LLS readings.

The "Phantom Hydrocarbon" disappears. Careful inspection of the individual well data and the previous observations in Figures 4 and 5 will lead to less optimistic evaluations and money can be saved by not testing the "Phantom Hydrocarbon".

WHAT HAPPENS WHEN HYDROCARBON IS PRESENT?

Well F (Figure 8) shows an LLD which can be expected to exhibit the Phantom because the reservoir lies under 442 metres of evaporites and the casing is 1150 metres above. The beginnings of a possible Phantom occur at about 6116 feet where the LLD and LLS separate.

However, the LLS and the neutron/density clearly indicate the presence of gas above 6090 feet. The well was tested over the interval 6017-6089 feet and produced 21 MMSCFD gas and water.

Closer inspection of the transition zone shows no gas indications on the LLS and neutron/density below 6090 feet. The LLS has the water bearing formation resistivity and the neutron/density separation is the same as in the water bearing sandstone below. The hydrocarbon suggested by the LLD below 6090 is "Phantom Hydrocarbon".

Because of the Phantom, the corrected LLD reads less than the log LLD in the whole of the gas bearing section. Invasion corrections would again boost R_t to some unknown higher value but this, of course, is an entirely separate problem to the Groningen Phantom.

A quick look at the LLD alone is dangerous. In this case the raised LLD might easily have been dismissed as a Phantom. The other logs such as an Induction, LLS or micro-resistivity tool MUST be carefully inspected. Indeed they become the PRIMARY resistivity logging tools.

EXPERIMENTS TO OVERCOME THE PHANTOM

It is understood that the resistivity bedding and current flow alteration have been successfully modelled. The appearance of the Phantom can be predicted. This gives some reason to hope that a solution can eventually be found. However, as far as the author is aware, no new tool has actually been designed - indeed such a tool may be too costly for the industry to justify new hardware. The present LLS and induction tools may be cheaper to run.

The Phantom can be detected now by repeating the LLD with a different frequency. This changes the formation impedance and therefore the magnitude of the Phantom.

CONCLUSIONS

1. On first inspection of any deep reading laterolog with measure current return at the surface, the readings below high resistivity beds should be reviewed. Long resistivity gradients that look like transition zones should be suspected as a "Groningen Phantom". The Phantom is not limited to the Groningen gas field, nor the European Permian Sandstones. It occurs anywhere - even on your logs! The high resistivity bed need not be of low porosity - the Phantom can occur below a hydrocarbon accumulation.

2. The Phantom has become more obvious since the introduction of the latest generation of laterolog tools because of the simultaneous recording of an unaffected shallower laterolog. The Phantom was always there but now it is easier to identify.

3. The magnitude of the Phantom is increased when the formation resistivity is low and the casing is near.

4. Two charts are presented which show observations of the Phantom. The maximum observed magnitudes are shown. Local conditions for an individual well may produce a lower (even a zero) Phantom.

5. Thorough examination of other resistivity logs will enable hydrocarbons to be properly identified even when the Groningen Phantom is present on the LLD. Indeed the other resistivity logs (e.g. the LLS) become the primary resistivity measurements.

6. Use of the principles described in this work can save money on unwarranted testing of water bearing formations which appear to contain "Phantom Hydrocarbon".

RECOMMENDATION

The logging contractors should, in the near future, add any further useful knowledge that they possess on the "Groningen Phantom".

ACKNOWLEDGEMENTS

I thank the several companies who generously gave their permission to publish the logs. I express my appreciation to Jean Suau of Schlumberger for his counsel.

I thank The British Petroleum Company Limited for their permission to publish the work.

BIBLIOGRAPHY

Doll, H.G.	1951	The Laterolog, JPT November
Schlumberger Limited.	1972	Log Interpretation Volume 1 - Principles.
Suau, J. et al	1972	The Dual Laterolog - R_{xo} SPE Paper No. 4018 SPE Fall Meeting, October.

ABOUT THE AUTHOR

RICHARD WOODHOUSE is a graduate of Bristol University, England, where he read physics and mathematics. He worked from 1964/67 as a field engineer for Schlumberger, mostly in Nigeria. From 1967 to 1969 he was with BPB Instruments, in Nottingham, England, where he developed the coal logging methods. He joined BP in 1970.

He is currently at BP's London Office working on all aspects of Formation Evaluation.

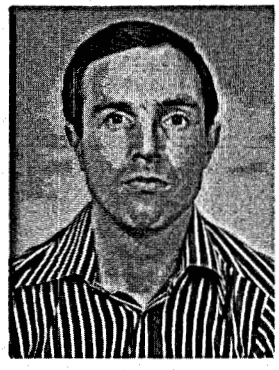

TABLE 1: ELEVEN OBSERVATIONS OF THE GRONINGEN PHANTOM (PART 1)

HOLE INFORMATION				PROPERTIES OF HIGH RESISTIVITY BED (HRB)				PROPERTIES OF BED UNDER THE HIGH RESISTIVITY BED				REMARKS
WELL CODE NAME	MUD SALINITY Kppm NaCl	HOLE DIAMETER inch	CASING SHOE DEPTH m.	THICKNESS HRB m.	APPROXIMATE RESISTIVITY OF HRB ohm.m	BASE OF HRB m.	DISTANCE OF CASING SHOE TO BASE OF HRB m.	BASE OF GRONINGEN PHANTOM m.	DISTANCE OF BASE OF PHANTOM BELOW HRB m.	APPARENT LLD RESISTIVITY OF PHANTOM ohm.m	ESTIMATED CORRECTED LLD RESISTIVITY ohm.m	
A	200	12¼	1505	75	halite ∞	1600	95	1640	40	0.55 2.7	0.30 2.0	Sandstone/Shale
B	250	12¼	1338	74	halite ∞	1774	436	1833	59	1.2 2.0 4.0 5.0 20.0	0.5 0.8 0.7 3.5 20.0	Shale
C	190	8½	2198	53	dolomite 500	2223	25	2290	67	3.0	2.0	Sandstone tested Water bearing
D	170	8½	2435	25*	dolomite 200	2448	13	2493	67	4.0	3.0	Sandstone tested Water bearing
E	300	12¼	1983	96	halite ∞	2896	913	2944	48	3.0	2.0	Shale
F	240	12¼	(2223 ft) 678m	(1450ft) 442m	anhydrite ∞	(5996 ft) 1828m	(3773 ft) 1150m	(6116 ft) 1864m	(120 ft) 37m	1.6 1.0 30.0	1.0? 0.7 25.0	Sandstone Flowed Gas and Water on test.

Continued on page 9 ...

...Continued from page 8

HOLE INFORMATION				PROPERTIES OF HIGH RESISTIVITY BED (HRB)				PROPERTIES OF BED UNDER THE HIGH RESISTIVITY BED				REMARKS
WELL CODE NAME	MUD SALINITY Kppm NaCl	HOLE DIAMETER inch	CASING SHOE DEPTH m.	THICKNESS HRB m.	APPROXIMATE RESISTIVITY OF HRB ohm.m	BASE OF HRB m.	DISTANCE OF CASING SHOE TO BASE OF HRB m.	BASE OF GRONINGEN PHANTOM m.	DISTANCE OF BASE OF PHANTOM BELOW HRB m.	APPARENT LLD RESISTIVITY OF PHANTOM ohm.m	ESTIMATED CORRECTED LLD RESISTIVITY ohm.m	
G	190	8½	850	110	halite ∞	1995	1145	2034	39	6.5	2.5	Shale
H	150	5⅞	2565	165	anh/dol > 1000	2577	12	2660	83	10.0 2.0 1.5	6.0 0.7 0.5	Sandstone Flowed water on test
J	220	8½	2180	50	anh/dol > 1000	700	700	NONE	0	25. 40.	25. 40.	Tight sst.
K	200	8½	830	27	anh/dol > 1000	1273	1273	NONE	0	10.	10.	Shale
L	180	8½	2093	300	anhydrite ∞	633	633	2765	40	17.	14.	Shale

* = Further high resistivity beds up the hole

TABLE 1: ELEVEN OBSERVATIONS OF THE GRONINGEN PHANTOM (PART 2)

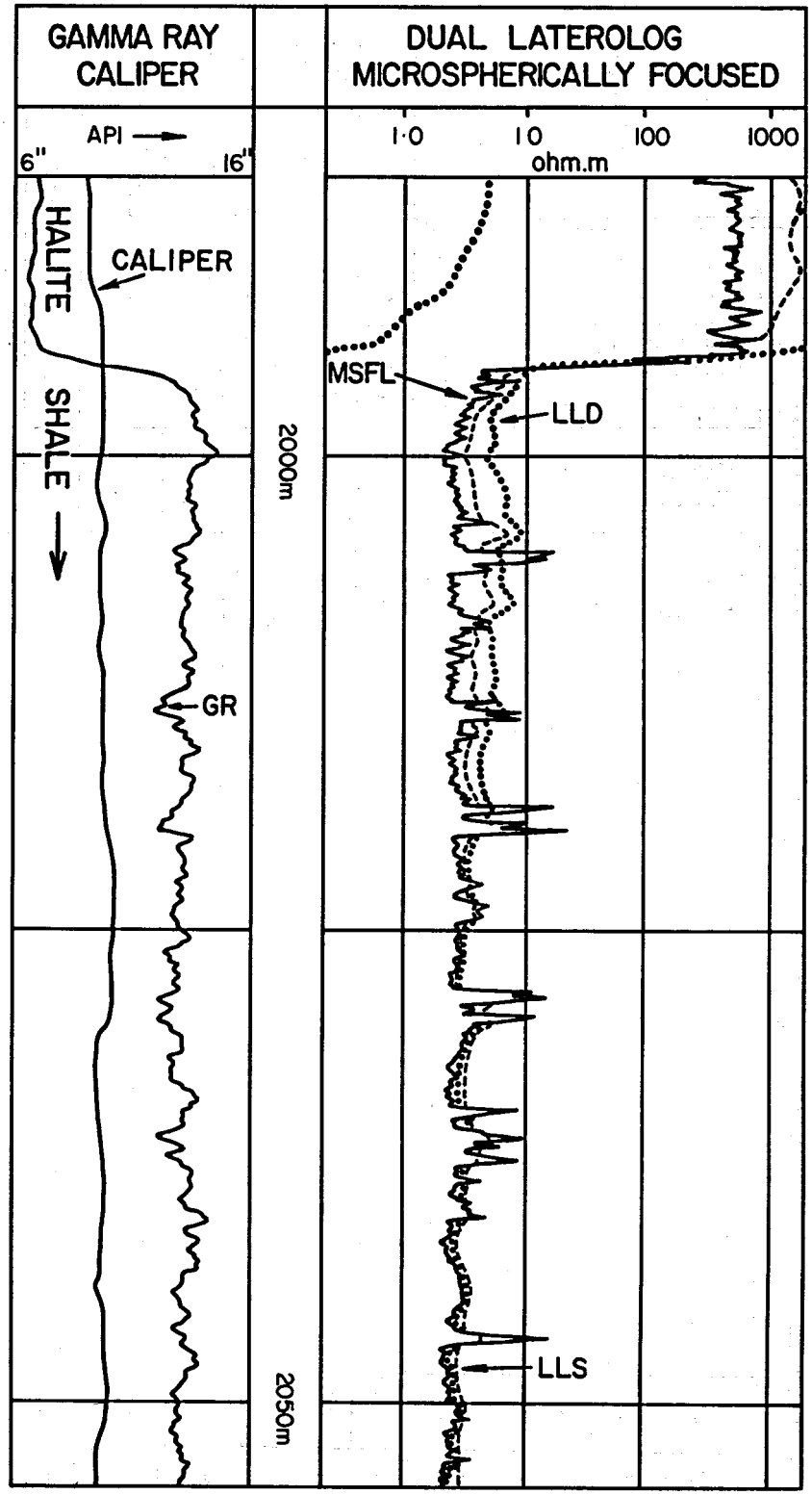

Figure 1: WELL G. The casing shoe is at 850 metres

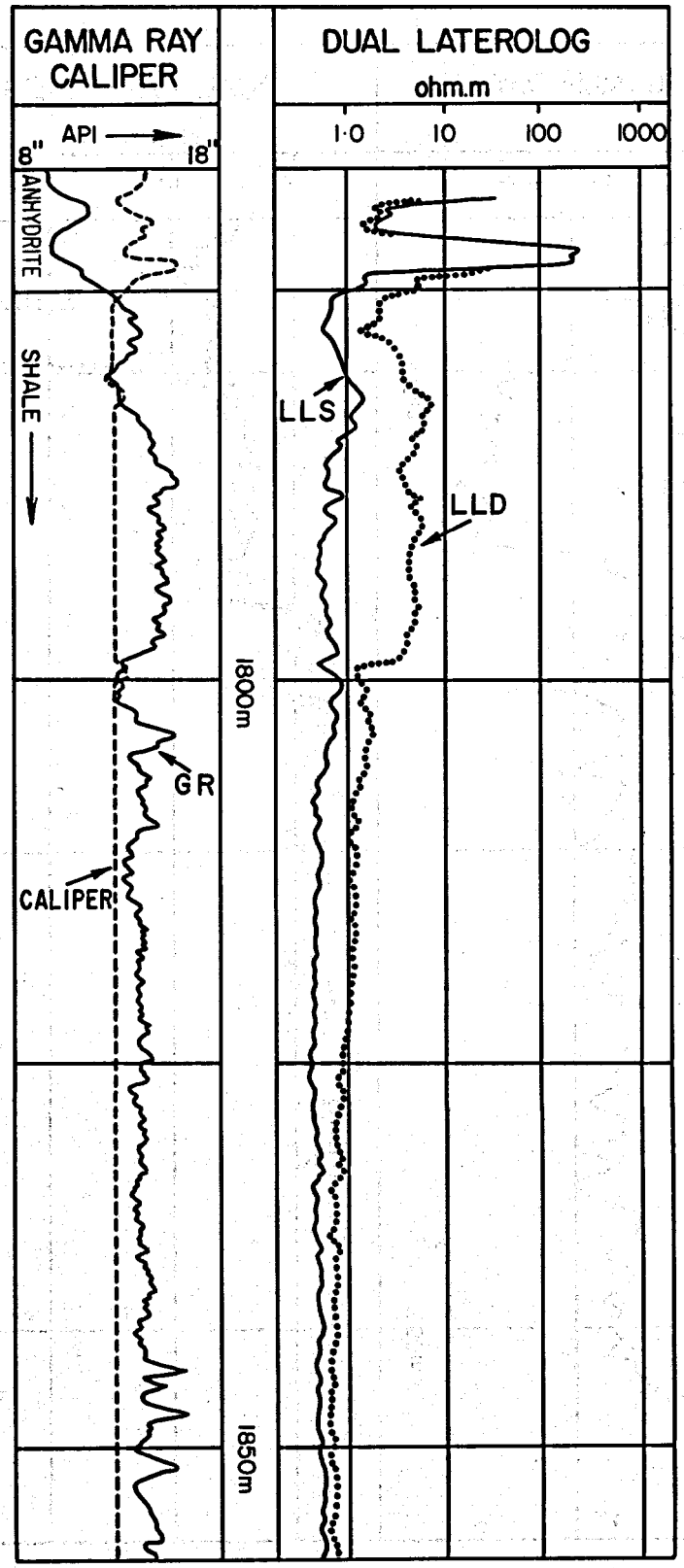

Figure 2: WELL B. The casing shoe is at 1238 metres

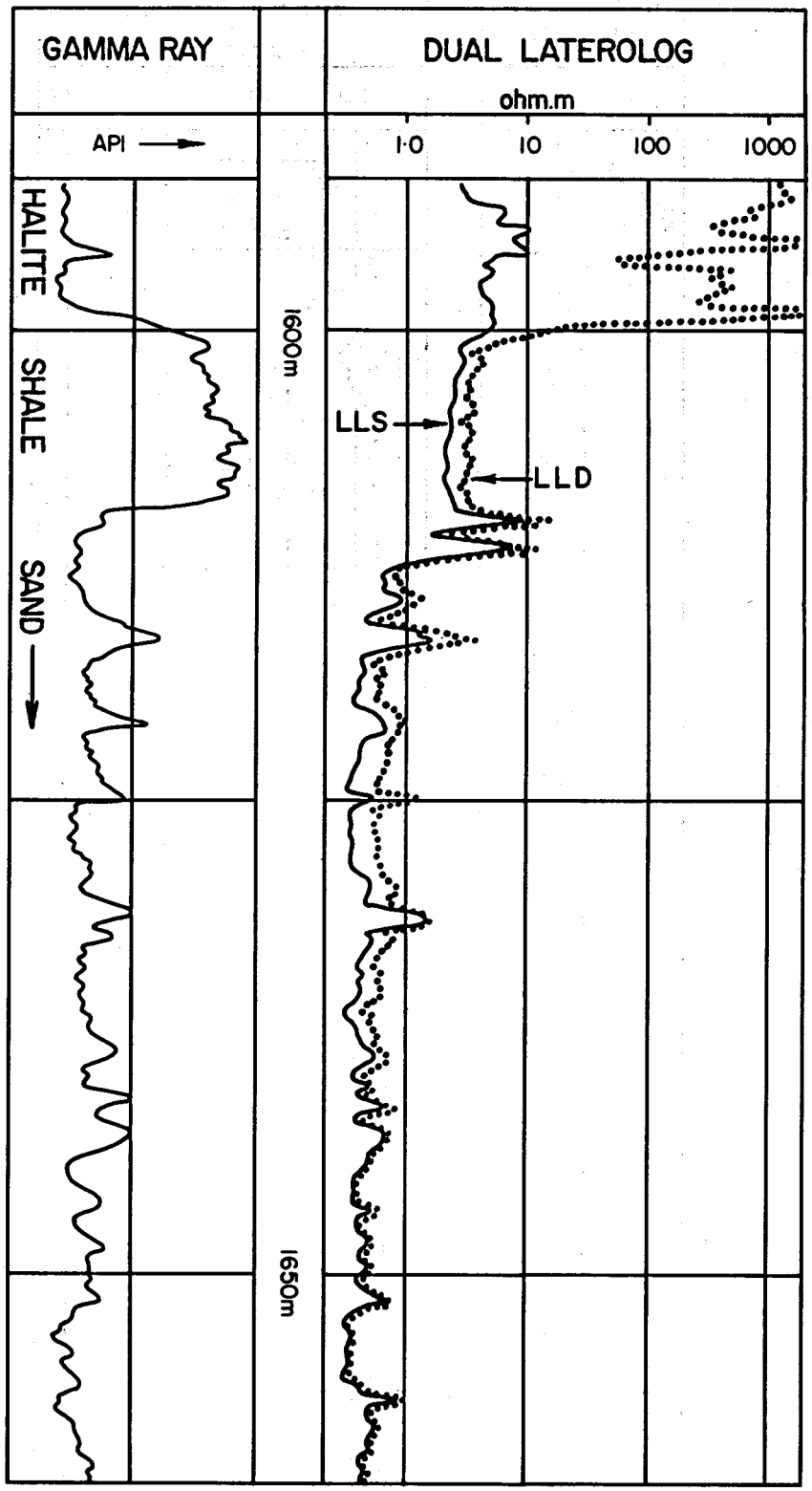

Figure 3: WELL A. The casing shoe is at 1505 metres.

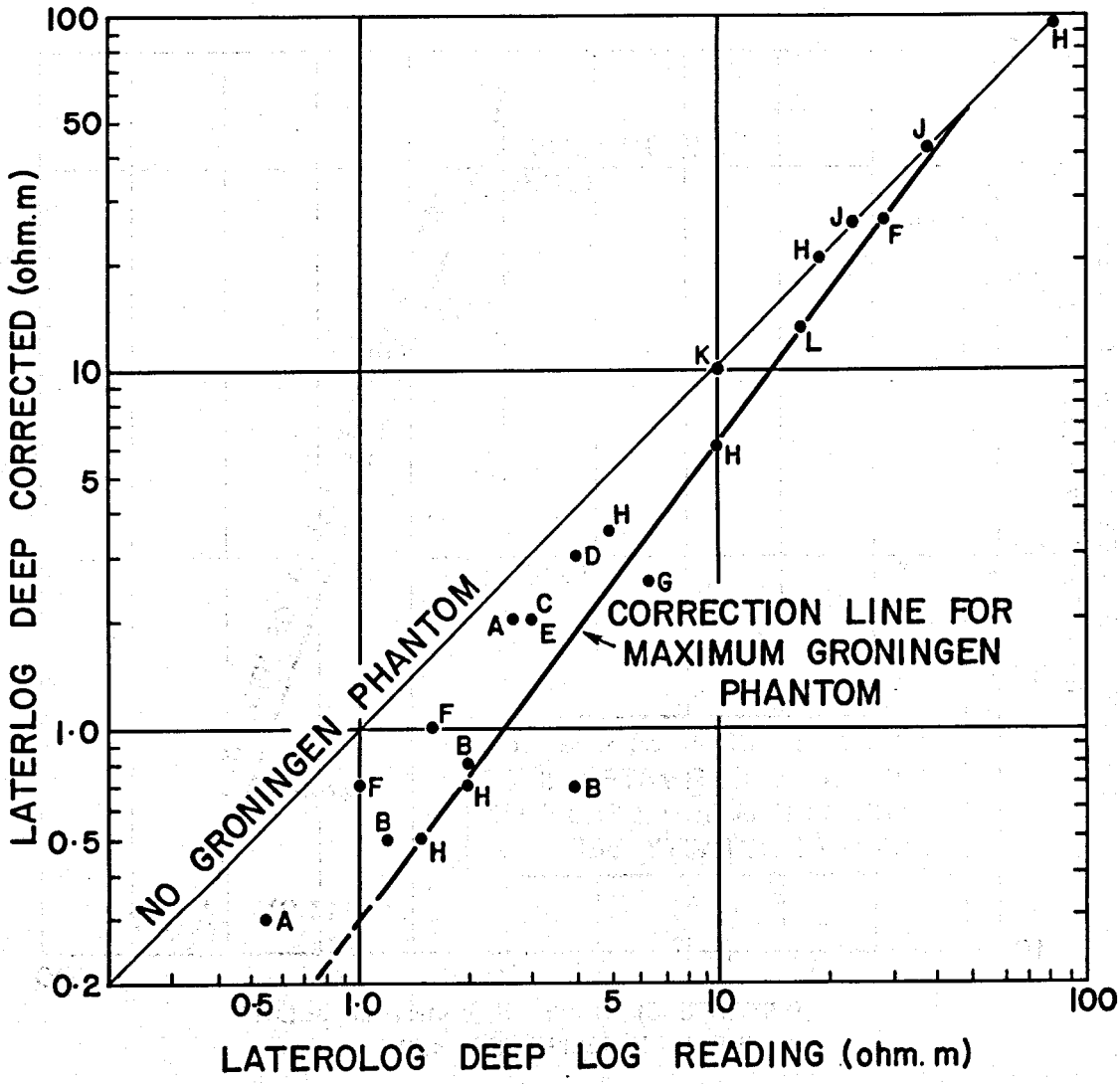

Figure 4: Deep Lateolog Resistivity Corrections when the Groningen Phantom is present

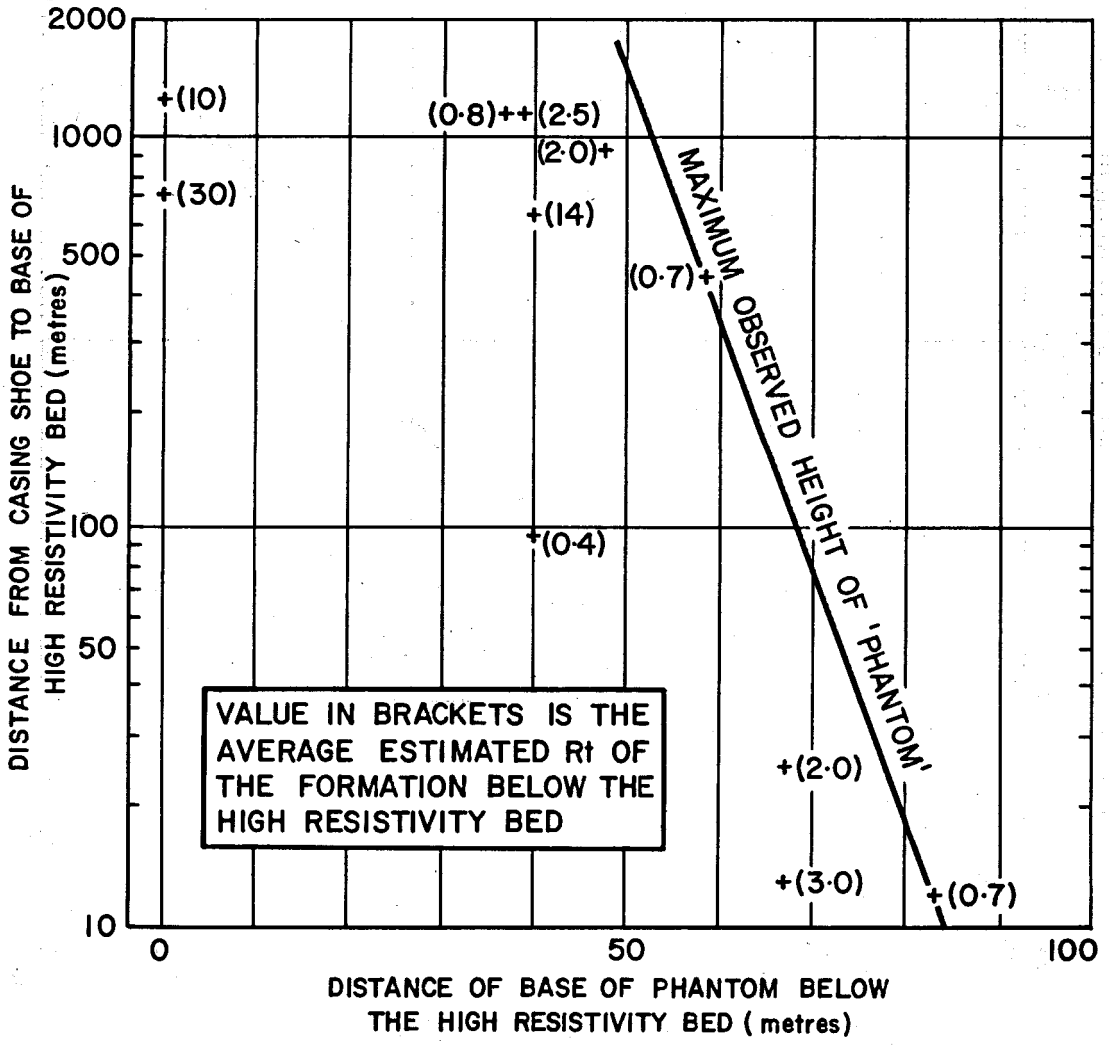

Figure 5: Distance of Casing Shoe above the base of the high resistivity bed versus the height of the Groningen Phantom.

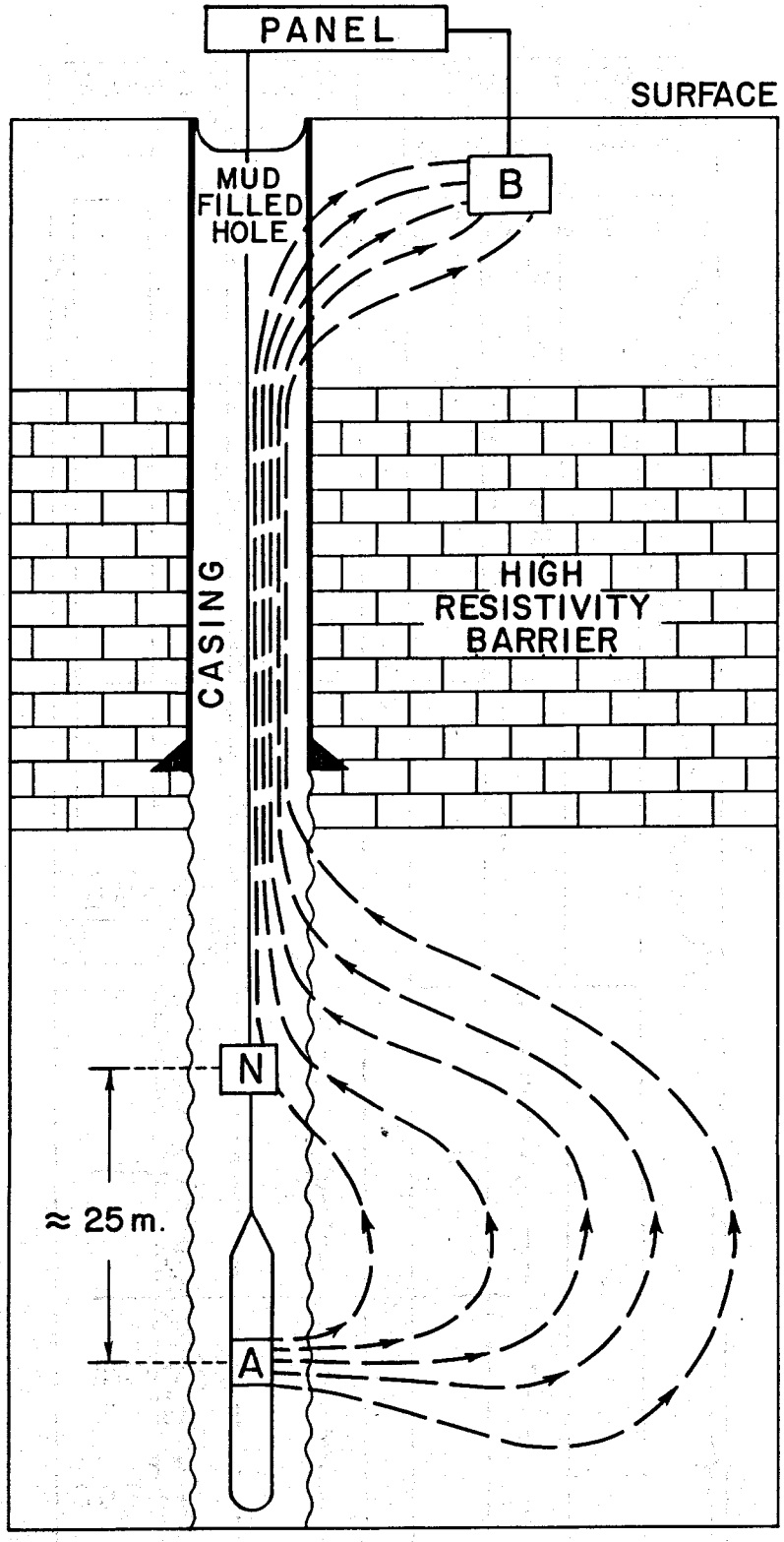

Figure 6: Schematic of the deep Laterolog measure current flow paths when the Groningen Phantom is present.
'A' is the current emitter electrode
'B' is the current return electrode
'N' is the potential reference electrode

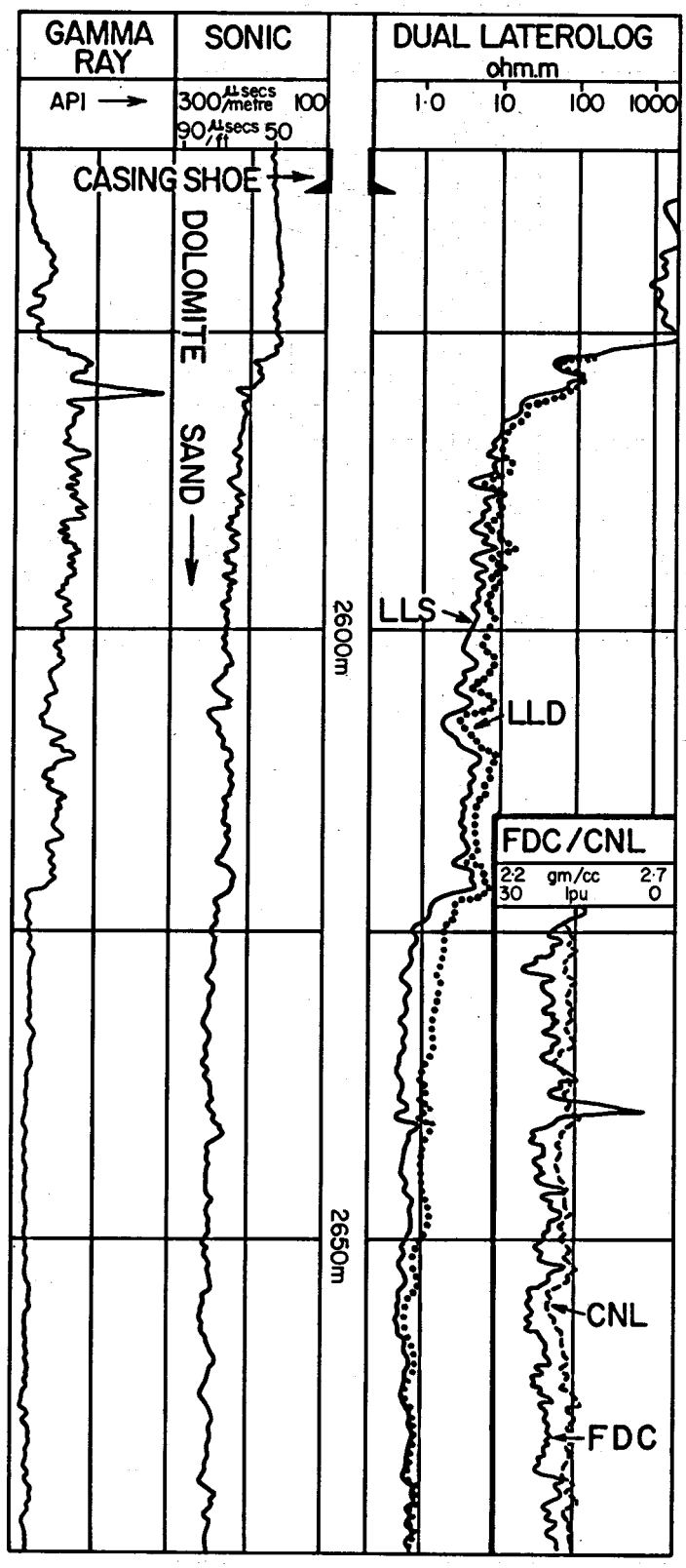

Figure 7: WELL H. The casing shoe is at 2563 metres

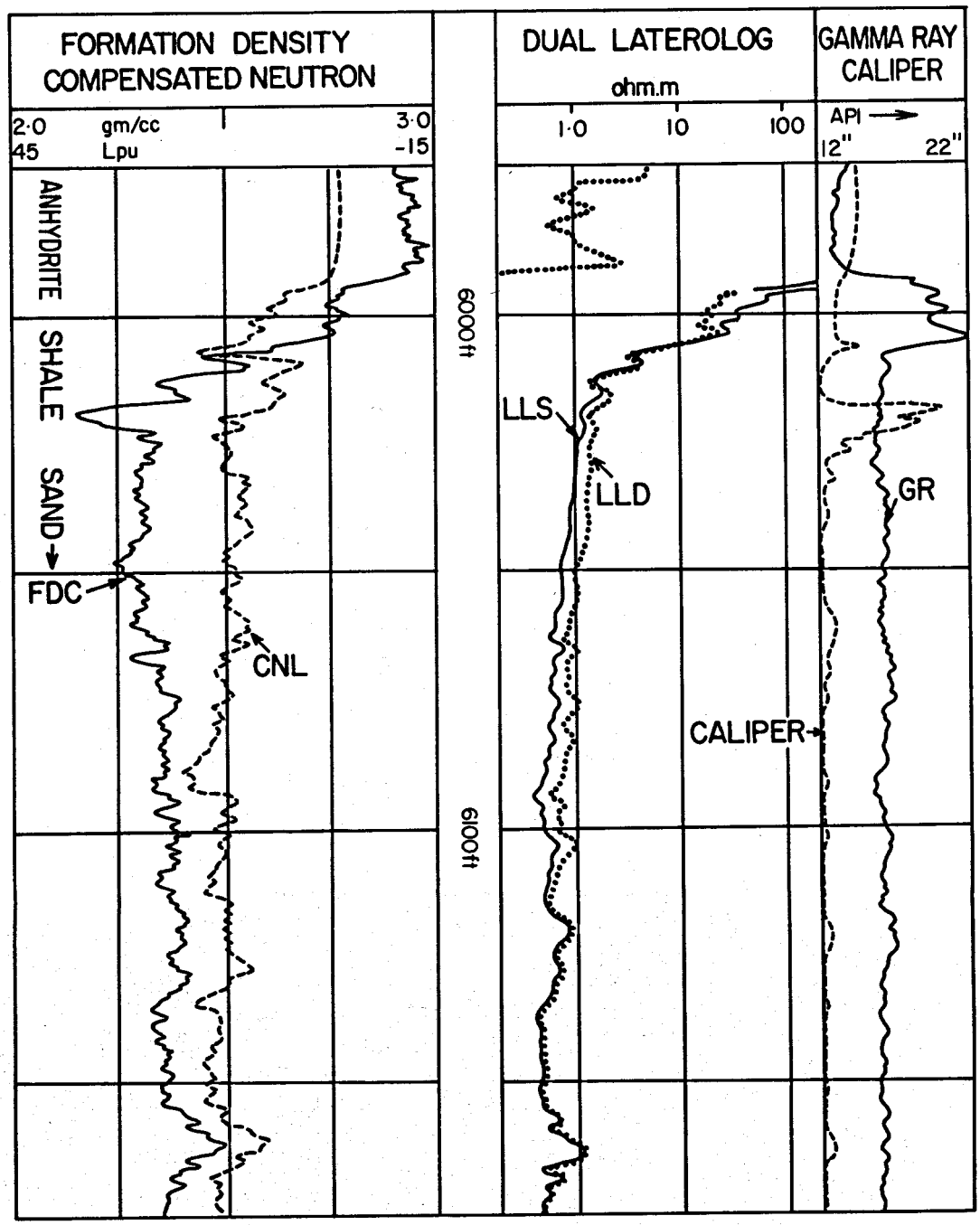

Figure 8: WELL F. The casing shoe is at 2223 feet.

THE COMPU-LOG CONCEPT AND PRACTICE

By: R. Kinkade, J. West, J. Hallenburg

ABSTRACT

The Compu-Log system is a computer based mineral logging system. The system handles and transmits all information digitally at all times. The information is recorded in raw form and processed by the computer on site. The result is a greater speeded-up logging system of vastly improved accuracy, flexibility, and versitility. Raw data and processed data are available at the location.

The Version 3 Compu-Log is the 3rd generation of a computer-centered logging system using the trade name Compu-Log by Century Geophysical Corporation.

CONCEPT

The basic concept of the Compu-Log system is to allow a digital computer in the truck to handle all logging information, record keeping, rigorous analysis, housekeeping, and the operational chores of mineral logging. With a computer based system, the routine duties of logging, as well as more sophisticated tasks, are precisely and consistantly performed under program control. Data are collected and processed digitally instead of as analog signals and quality is continually monitored. Data is automatically recorded together with correct depth and identification information. The computer keeps the operator informed of its progress and status and proceeds according to his instructions, prompting him where necessary in order to assure that he does not omit steps or perform them in the wrong order. Complete log data is permanently recorded in digital form and is available for reprocessing at any time.

HISTORY

The original concept of the Compu-Log was to use the computer to plot a log. This system was a digital adaption of an analog system using the computer primarily as a substitute for analog instruments. The prototype unit was field tested in October to December of 1975. It plotted a log in "real time" and punched a paper tape containing the logged values in half-foot increments. This unit performed well, was relatively trouble free, and thus indicated the feasibility of a commercial digital logging system.

It was immediately apparent, however, that a computer based system was capable of much more than simply drawing a log. Therefore, the system was redesigned and the new system, known as Version 2, was introduced in May, 1976.

The Version 2 Compu-Log recorded all data directly, in raw form, on magnetic tape. These data were then processed from the tape to present a log of the hole with all curves, scales and scale changes, and identification information listed. The gamma ray data were then examined for uranium mineral (grade) values above a specified cutoff and an AEC GAMLOG program modified for this environment was used to calculate and plot the mineral grade at the bottom of the log. The deviation information (logged going downhole using 50

S

foot stations) was plotted, and the vertical depths of anomalies were printed alongside cable depths on the mineral grade, plot.

The Version 2 Compu-Log used the same Century 8000 series downhole analog tools used by the analog systems. In these tools the signals are derandomized in an accumulative register to reduce the cable effect upon the dead time (or coincidence problems) and sent uphole for collection and recording by the computer.

Thus the Version 2 Compu-Log retained all the advantages the 8000 series equipment has over conventional analog systems and added the advantages and flexibility of computer processing and control. It allowed a permanent magnetic tape record of raw data for repeated or later processing, gave routine analysis on site, and eliminated many of the human errors.

This system operated well. There were initially some problems with tape drives and auxiliary power plants which were soon corrected. In general, the introduction of the V2 Compu-Log was accompanied by fewer problems than is usual in the start-up of most new systems. The V2 units are now almost phased out, but did yield about 22 unit-years of experience. The success of the V2 systems demonstrated the value of a well designed digital logging system, and immediately encouraged investigation of further improvements in data quality, and ease and consistancy of operation which could be gained through taking fuller advantage of digital technology. This resulted in the Version 3 System.

The Version 3 Compu-Log was introduced in May 1977. It retains many of the Version 2 features, but takes fuller advantage of the presence of the computer. All signals are recorded by the probe continuously while traveling uphole and are digitally encoded in the probe for transmission directly to the computer. This results in less signal distortion, greater apparent bandwidth, and higher possible logging speed as well as virtual independence from cable effects on signals.

Century now has about 75 V3 Compu-Log units in routine operation and has accumulated about 25 unit-years of experience with this system. With these systems, the time on location and in the hole has been greatly reduced and they have performed with fewer maintenance problems. The quality of information has risen rapidly while costs have remained level or dropped slightly. The amount of usable data has increased greatly. Moreover, all information and analysis are available on site as well as being permanently recorded for future reprocessing.

The Compu-Log system was initially applied to uranium logging because of Century's greater experience in that field and the large amount of information available. It now is being applied for coal logging and other minerals where less experience and literature exist. The initial techniques and formats appear to be applicable to most mineral exploration, and they can be modified by reprogramming as new and better techniques are discovered.

OPERATION

The Version 3 Compu-Log system for uranium collects data from a natural gamma detector (7/8" x 4" crystal scintillation detector), spontaneous

potential system, single point resistance system (2 3/8" x 1 3/8" electrode), 17" neutron-neutron porosity system, a solid-state hole deviation device and a temperature sensor. All data reflecting counting rates are stored in cumulative registers, and the accumulated values are read out each tenth of a second. These data together with the signals from the other sensors are encoded and transmitted to the surface by a time shared multiplexing system. The effective dynamic range of each channel is 655,350 counts per second. The digital data stream from downhole consists of 9 8-bit bytes each tenth of a second.

The Version 3 Compu-Log System for coal collects data from a natural gamma ray detector (1.125" x 4.5" crystal), an 8.5" gamma-gamma density system, a single-arm hole caliper, and a focussed resistivity device. The digital data stream for coal is similar to that for uranium but with a different length reflecting the fact that there are fewer sensors.

For all of the applications, the operation of the system while recording from the probe is similar. At the surface the computer sorts and decodes the data, compares the values with the previous values, notes the differences, performs any necessary data conversions, averages values in tenth foot increments.

The recordings on tape are averages of the tenth second readings accumulated for each tenth of a foot. The gamma ray, density, and neutron readings are in counts per second, the S. P. is in millivolts, the resitance is in ohms, the resistivity is in ohmeters, and the caliper, temperature, and 5 components of deviation are in proportional volts.

Included on the magnetic tape is a header record. It includes all of the identification and other necessary information for use of the log. Included are the actual K-factor, time and location data, tool type, and tool serial number. Any deviations from norms are called to the attention of the operator before being recorded. These include things such as an improper tool operation or type or faulty constants or missing data.

All processing and plotting are done from the magnetic tape. None is done directly from input data.

PROCESS

The logging process starts with putting the probe on the cable and bringing the system alive by loading the logging program into the computer.

The Compu-Log system does not retain its programs in memory longer than needed for 1 log. Each program is entered as it is needed. Thus, there are no storage problems and no degradation when the program is not used for several days. The downhole tool type determines the program to be used. Thus the function of the complete truck system depends only upon the programs and tool type. The function may be changed, to any extent, merely by changing tool type and/or the programs.

When the program tape has been read, the computer will request choices from two options:

1. Is this a plot from a tape or is a hole to be logged?
2. Is this a new client (stored header information will be erased) or can a portion of the previously entered header information be reused?

The computer will then check the probe to determine the type and serial number. If at this time or any time during the logging phase the wrong probe is attached or if there is inconsistent information from the probe, the computer will inform the operator. Calibrations are made automatically either before the probe is removed from the tool rack, or before the probe can be put in the hole. The calibration information is used during plotting to normalize data to primary calibrations.

A master list of options will then be displayed, along with data form the sensors (such as depth, gamma counts per second, etc.).

Many of the options such as the recording track on the tape, the starting depth (usually zero), header data, and the hole number must be entered before the logging can begin.

The probe is then lowered to the log bottom depth (usually bottom of the hole) and the computer keeps track of the depth. At the bottom, the operator informs the computer that he is at the bottom and he is then supplied information about the highest and lowest values of the S. P. for later plot scale selection. The data from the probe is displayed on the operators monitor at this time and while logging and can be printed out. The log can be aborted at this point if desired and the process restarted.

Logging speed is normally 60 feet per minute (3600 feet per hour). This is set by the sampling and averaging intervals of 1/10 second and 1/10 foot. However, in the event the information is not interesting, as, if the hole has already been logged or if there is a long uniform zone, the logging speed can be increased to as much as 180 feet per minute (10,800 feet per hour) with some sacrifice in statistical accuracy. In this case the computer will average the record data every two or three tenths of a foot, depending upon the logging speed. The present Version 3 programs plot the log from the tape after the hole is logged. Future ones may plot the log as the tool comes out of the hole with a lag of a foot or two.

As the hole is being logged, data are sent up every tenth of a second for all curves except the S. P., temperature, and deviation. The S. P. is sent every two tenths of a second. Temperature and five components of deviation are sent up sequentially, alternating with the S. P., so that complete information is received at the surface for deviation and temperature every 1.3 seconds. These data are recorded on the tape in blocks representing 5 feet of hole on tape with an identifier and a depth figure beginning each block.

Near the top of the hole the computer monitors logging speed and depth to be sure that the probe is stopped at the surface. A 15 second warning will sound as the sonde approaches the surface.

SENSORS

The increased apparent bandwidth, multiplexing, and digital handling allow for greater flexibility in number, variety, and linearity of sensors than with an analog system. The following descriptions of the 9000 Series sensors illustrate this.

GAMMA RAY

The increased transmission capability and the short deadtime of a well designed digital logging system allow a larger gamma ray detector crystal to be used. The 9000 Series Compu-Log System is capable of handling the equivalent of 1 to 655,350 counts per second per channel. Therefore, a 0.875 inch diameter by 4 inches long crystal for uranium and a 1.125" x 4.5" long crystal for coal have been incorporated. The uranium conversion factor of the detector (9055) is 5.58×10^{-6} for half foot intervals and the system deadtime is about 1 microsecond. These values, which are made possible with a digital system, have several implications:

1. For uranium grades below 0.56% the counting rate ($<$ 48,000 cps) is low enough that, because of a real 1 microsecond deadtime, less than +5% correction need be made. Thus, the counting rates are statistically reliable.

2. For most gamma ray logging, the counting rate is high enough because of the crystal size and transmission system that the statistical sample is large. The probable error in all cases in uranium logging is 0.48 x that for a 3/4" x 1" crystal (a usual analog size). This means a more reliable reading in low grade deposits and an easier curve to use in sands, shales, and other lithology determinations. In coals the probable error is 0.38 x that of a 3/4" x 1" crystal.

3. Linear uranium grades ($\pm$5%) can be read directly from the gamma ray curve up to 0.60% $_{e}U_3O_8$.

4. The equivalent-grade limit of the system is high enough (22%) that there is never any danger of saturation from too high a counting rate.

With a digital system equipped with a printer, printouts of raw data are available on site. The Version 3 system for uranium provides a finished printout which includes a mineral grade analysis for 3 cutoff grades and indicates the best interval of any predetermined thickness. For coal, an estimate of the ash content can be furnished.

NEUTRON AND DENSITY SYSTEMS

These two systems have the same wide limits that the gamma ray system has. However, these systems have not been implemented to the fullest advantage as yet. The source sizes and detector sensitivities can (and probably will) be increased in the future. The lower limit of sensitivity of all of these circuits is one count per second per smoothing interval.

A printout of raw data is available on site. Normally, the density curve is plotted as linear density and the neutron curve as counts per second (but will be presented as sandstone porosity).

SPONTANEOUS POTENTIAL

The S. P. signals are read with a high impedance input, stable amplifier which is referenced to a surface electrode. The impedance of this circuit is high enough ($>$ 1000 megohms) that any effects due to circuit current are

S

negligible. Care has been exercised to insure that bimetallism and formation shorting are not problems. This is done by insulating the probe and breaking metallic paths in the tool.

Because of the need for a surface reference for the S. P. one cable wire has been used exclusively for that circuit. This is inconvenient since with a multiplexed digital system it is the only real reason for requiring a multiconductor cable. The sensitivity and resolution of this circuit are 0.1 millivolt. A printout of data is available on site.

RESISTANCE AND RESISTIVITY

The uranium system (9050/9055) uses a single point resistance circuit. This circuit was retained because, at present, the primary use of this curve in the mineral industry is for correlation. The single point system is ideal for this. This will be converted to resistivity later through the use of the computer.

The single point circuit is a straight-forward, constant current, ohmeter circuit measuring the grounding resistance of the electrode. The response is linear with resistance. The signals are digitized and encoded downhole and used directly by the computer. The presence of the computer appears to make it feasible to correct for borehole effects and plot resistivity as long as the resistivity contrast of the formation to the mud is not too high.

The coal system demands a much more sophisticated resistivity method because of the wider range (1 to several thousand ohmeters). Therefore, this system incorporates a guard electrode resistivity system. Electrode monitoring and control are done in an analog manner. The resistivity signal is digitized and encoded downhole.

A printout of raw data is available on site.

HOLE DEVIATION

In the mineral industry hole deviation is an important measurement to determine mineral body location and because of the critical nature of mineral thickness determination. Also, poor directional control and the use of "pull-downs" instead of drill collars are common in mineral drilling.

The need for a second run in the holes, the long turn-around time, and the large chance for errors in operation and calculation ruled out the use of the conventional photographic system in the design of the Compu-Log System. The existing surface readout systems are delicate and have severe maintenance and interpretation problems. Therefore, Century elected to develop its own continuous deviation system.

The Deviometer used on the 9055 uranium system and (eventually) on the 9030 coal system reads 3 components of the earth's magnetic field and 2 components of probe position with respect to the gravitational field. The system has no delicate moving parts. The raw data from these sensors are stored on tape and later calculated in 5 foot increments. During plotting of the log the Deviometer information is processed by the computer to plot a plan view of the hole and correct the depths of the anomalies to vertical depths.

All peripheral information is also plotted. The processing and plotting of this type of raw data is made possible by the presence of a digital computer supporting routine scientific computation. A printout of data is also available.

The 5 foot recording interval for deviation data eliminates the errors inherent in long station plotting.

TEMPERATURE

Temperature readings are taken at 5 foot intervals. These are not plotted except on request. Then they are plotted with the line printer only.

GENERAL

After considering the performance improvement made possible by a digital system in the data gathering phase, the fact that the raw data from the hole is recorded and is permanently available on magnetic tape allows several further advantages:

1. There is a minimum of possibility for permanent distortion of the data before recording.

2. Display of data on the monitor screen and the ability to plot a log evidence of a valid recording of data.

3. Processing may be done at any time. It is not limited to the time while logging.

4. The raw data can be reformatted to a form which is directly readable by another computing system. This allows the user to store the log data in an information retrieval system and to reprocess the data using his own programs at his leisure. Century currently provides a reformatting service yielding a standard 9 track computer tape (Century format A Data Interchange Tape) with options allowing compatability with all standard computing systems.

5. New processing techniques may be employed as they are developed.

6. A large degree of capability is available for salvaging or correcting faulty recordings or for retrieving usable information when it is not possible to relog the hole.

7. Information storage is very compact and information is easily retrievable.

8. Experimental or routing processing may be done conveniently and accurately using complete logs of original data if desired. No hand editing, digitizing, or other laborous or error prone techniques need be employed.

S

ABOUT THE AUTHORS

KINKADE

WEST

HALLENBURG

Robert R. Kinkade received his M.S. Degree in Mathematics from Oklahoma State University in 1958 and has done additional graduate study at Oklahoma State and at the University of Kansas.

He was a member of the Mathematics faculty of the University of Tulsa from 1960 to 1969. He then worked for Amoco Production Company as a Research Scientist in Geophysical Research before joining Century Geophysical Corporation in 1976.

He is currently a Project Engineer in charge of Data Processing, which includes software development for Century's Compu-Log Systems.

Jerry B. West has worked for Radio Station KBEC in Waxahachie, Texas as Chief Engineer.

For three years he was with Collins Radio Company in Richardson, Texas, R and D facility. He worked on the development of automated test equipment for the Navy A3J Line Support.

At Danemiller-Smith, Incorporated, he was Equipment Applications Engineer. Then he founded Systems Development, Incorporated. He obtained extensive experience with the development of Gamma Ray measuring equipment and telemetry techniques of Gamma Ray detector outputs for well logging applications. He developed improved coupling techniques for reducing dead time of Geiger detectors and down hole stabilizers for sodium iodide detectors involved in spectral measurements.

He is now Vice President of Engineering with Century Geophysical Corporation.

Jim Hallenburg graduated from Northwestern University with a B.S. in Physics after having spent 3 years in the Air Force as a bomber pilot and instructor. He joined Schlumberger Well Surveying Corporation (Schlumberger Well Services) in 1947 in the Research Department. He was later transferred to the Engineering Department.

At Schlumberger, Hallenburger worked on dipmeters, S. P. problems, modeling, multiplexing, explosives, photographic, induction log, and focussed log problems. He was Project Engineer on the West Texas system, the selective S. P., the Micro Log, the Formation Density Log, the 1-11/16" Gamma Ray Neutron, the High Temperature Gamma Ray Neutron, and the Calibration Pits.

Hallenburg left Schlumberger to go to the Mohole Project and was in charge of logging operations.

At the close of the Mohole Project he was Chief Engineer of the Wire Line Division of the Western Company before he formed Data Line Logging Company in Casper Wyoming. Data Line was bought by Teton Exploration (United Nuclear) and Hallenburg stayed as Geophysical Manager until 1975. In 1975 he joined Century Geophysical Corporation as Manager of the Casper Region. In 1976 he was transferred to Tulsa in Applications Engineering where he is Manager.

S

URANIUM ORE BODY ANALYSIS USING THE DFN TECHNIQUE

By: J. West, and J. Hallenburg

ABSTRACT

The theory of the Delayed Fission Neutron (DFN) and Prompt Fission Neutron (PFN) uranium logging systems is reviewed. The use of the DFN in the field is described. The problems encountered in calibration, interpretation, and comparison with other techniques are covered. The results of the technique are accessed and illustrated and the costs are reviewed.

INTRODUCTION

The Delayed Fission Neutron DFN system is a borehole geophysical system which measures the amount of in situ uranium directly. It does not have a problem with disequilibrium as the present gamma ray techniques have.

The DFN technique now has about 18 tool-months experience in commercial use.

DFN TECHNOLOGY

The Delayed Fission Neutron (DFN) system makes use of a system originally described by Givens, Caldwell, and Mills.[1] Uranium 235 will undergo a fission reaction when it is exposed to thermal neutrons. In addition, fission can be induced in uranium 238 by bombardment by fast neutrons. These reactions result in additional neutrons and fission fragments being emitted. The fission fragments, themselves are fissile and decay with the emission of neutrons. The anomalous population of neutrons after bonbardment of uranium by neutrons can be interpreted quantitatively as indicating the presence of fissile material, such as uranium.

The DFN system has been described by W. W. Givens, et al.[2]

There are several reactions which may be examined when a fissle material, such as U235 is exposed to thermal neutrons. When the uranium fissures, neutrons and fission fragments result promptly. These prompt neutrons result in an anomalous population of neutrons. The size of this population is a function of the original neutron flux and the concentration of fissile material present. A technique makes use of this by examining the population of prompt neutrons when they have moderated to epithermal energies. This is the prompt fission neutron (PFN) system developed by Sandia Laboratories under contract to the DOE. This method has been described by Bivens et. al.[3]

The neutron-emitting fission fragments have an average half life of less than 22 seconds. They decay, emitting more neutrons to add to the neutron population. These neutrons, also, are a function of the fissile material concentration and the neutron flux density. The techniques detecting this population are the delayed fission neutron systems.

There are two delayed fission neutron systems in use at this time. One system, developed by IRT under contract to ERDA (DOE) and described by D. K. Steinman[4] uses a Californium 252 source. It measures the delayed fission neutron population by a combination of source position manipulation, timing, and spacing. The other system, developed by Mobil Research Corp. (Givens, et al)[2] and commercially operated under license by Century Geophysical Corporation uses a pulsed neutron generator. This latter is the system which we will discuss.

The Century DFN service was started, on a limited basis, in November 1976. The original interpretation technique used and the system itself were essentially the same as Mobile had evolved. The calibration and operating techniques were similar to Mobil's.

The first Century DFN probe was 2.75 inches diameter and 9 feet long. The generator assembly was contained in the midsection. The neutron detector was about 12 inches below the generator and a gamma ray detector was about 12 inches below the neutron detector.

The neutron detector is pulsed with a 5 kilovolt pulse to ionize the deuterium gas within the ion source. These deuterons are then accelerated by a 125KV potential onto the tritium target. The field gradient is about 62KV per centimeter. The deuterons impinge upon the tritium target and the resulting reaction is:

$$^{2}H_{1} + {}^{3}H_{.} \quad {}^{4}He_{2} + n$$

The timing sequence is a pulse of neutrons 8 to 10 microseconds long and containing about 5×10^{7} neutrons. This is followed by a 10 to 13 millisecond hold off to allow the prompt reactions to take place. The neutron detectors are then gated on for 37 to 480 milliseconds depending upon the device. The epithermal and thermal neutron population is measured. The original 2 per second repetition rate was later changed to 3 per second for the 3.75 inch probe and 10 per second for the 2.5 inch probe to maintain the neutron flux rate at 10^{8} per second.

Since the higher repetition rates use the same pulse duration and wait time, the higher rates result in a lower effeciency. At 10 pps the smaller DFN (2.5") probe has about 90% of the effeciency of the 3.5" probes with high output generators.

Since the neutrons used for fissioning the uranium 235 as well as the product neutrons are being moderated substantially by the hydrogen content of the formation, the DFN system is porosity and borehole sensitive. To circumvent this problem, a neutron-thermal neutron porosity log (AmBe source) (9055 tool) is used to normalize DFN ASSAY readings. That is, the uranium grade is taken as a function of both the DFN count and of the neutron-neutron system reading. The n-n log is made first in a standard log suite (GR, SP, R, N-N, Deviation) at 60 feet per minute over the entire hole. A DFN reading is then taken for 3 minutes at each of a number of preselected points.

In addition to the ASSAY reading, which is a point by point measurement, the DFN system makes a continuous log, called the SCAN mode log. Even

at 4 feet per minute logging speed the statistical sample is small, forcing the use of the SCAN mode qualitatively, only.

It has been found that, while the pulse to pulse neutron flux varies, the medium term variation (seconds to minutes) is small. The long term variation is progressive and negative. Therefore, the short term variation may usually be averaged out, but the long term variation must be taken into account.

One source of the long term variation or degradation of the generator is the inclusion of deuterium into the thin layer of the target material by bombardment.

The degradation of the neutron generator is compensated for by applying a correction factor to the DFN ASSAY count. The correction factor is determined by irradiating a teflon ring by the generator neutrons for 3 minutes The radiation resulting from the activation products (Predominately the β decay of ^{19}F) is read with a carefully calibrated gamma ray well-counter before each log.

A calibration procedure (continuous) has been suggested (Givens, et al)[2] using the activation of ^{17}O to ^{17}N to ^{16}O, with emission of decay gammas, by high energy neutrons. Although our early systems incorporated this method, we feel the natural variation of formation and borehole oxygen content is too great for a desireable calibration.

Uranium 238 and other elements in the formation are fissile besides the ^{235}U. ^{238}U will react with fast neutrons. However, since the ratio of ^{235}U to ^{238}U is usually constant at 0.7 to 99.2, this reaction aids the determination of uranium content.

Thorium 232 and oxygen 17 will also react with fast neutrons. The ^{238}Th content will cause anomalous uranium readings, since it is difficult, at this time, to seperate the uranium and thorium readings. However, the thorium content of most sedimentary deposits of uranium seem to be low.[5] Oxygen 17 readings can be used to determine the barren intercept of the evaluation calculation.

Thus, we have determined that the uranium content, P, of a formation traversed by a borehole is:

$$P = 1.08 \times 10^{-4} \left(\frac{380DC_D}{.95\,NC_N} - 380 \right) \text{ Pounds per cubic foot,}$$

Where D is the DFN count for 3 minutes, C_D is the correction factor for the DFN generator, N is the Neutron-Neutron (Century 9055) counting rate, and C_N is the normallizing factor for the 9055 neutron curve. The value of P can be converted to percent U_3O_8 by weight with the following relation:

$$\% U_3O_8 = \frac{1.602P}{d_b} ,$$

where d_b is the wet bulk density (or in situ bulk density) of the uranium bearing formation. The value of d_b may be determined from cores, a density run in a similar, barren formation, or a determination from an acoustic velosicy log or another porosity log.

The logging procedure now, is:

1. Run the (9055 system) natural gamma ray, single point resistance, S. P., neutron-neutron, deviation and temperature. (The data are all stored on tape).

2. The DFN probe is calibrated.

3. Then a recording is made in the SCAN mode.

4. The SCAN intervals are picked from the 9055 gamma ray curve.

5. Suitable intervals are then picked from the SCAN log for the ASSAY masurements.

6. The probe is lowered to the bottom of the ASSAY interval and the computer takes 3 minute ASSAY readings, moving the probe so as to obtain one-half foot between each reading without buildup effects.

7. These readings are stored on tape.

At the conclusion of the ASSAY interval the computer combines the DFN ASSAY data with the proper level 9055 neutron-neutron data, calculates the uranium mineral amount in pounds per cubic foot of formation, calculates the uranium mineral grade in percent by weight (if the bulk density value is available), prints the values as a function of depth, and plots a mineral grade bar graph at the bottom of the DFN SCAN log.

This DFN system can be run on the standard Compu-Log unit with the addition of a power supply.

REFERENCES

1. W. W. Givens, R. L. Caldwell, and W. R. Mills, "Cyclic Activation Logging" submitted to The Log Analyst, Dec. 1967.

2. W. W. Givens, W. R. Mills, C. L. Dennis, and R. L. Caldwell, "Uranium Assay Logging using a Pulsed 14 mev Neutron Source and Detection of Delayed Neutrons", Geophysics, Vol. 41, No. 3, June 1976.

3. H. M. Bivens, G. W. Smith, Dal H. Jensen, E. L. Jacobs, and L. G. Rice "Pulsed Neutron Uranium Borehole Logging with Epithermal Neutron Dieaway" Symposium on Exploration of Uranium Ore Deposits, IAEA, Vienna, Austria 76'.

4. D. K. Steinman, "252 C_f Based Logging System for In Situ Assay of Uranium Ore", IRT Corp. Technical Bulletin Intel-RT 7019-005.

5. John W. Gabelman, "Expectations from Uranium Exploration". AAPG Bulletin, Vol 60/11, pt. 1, Nov. 1967.

Note: A biographical sketch and a photo for Mr. West and Mr. Hallenburg are presented in Paper S.

U

USE OF THE SPONTANEOUS POTENTIAL CURVE IN A MINERAL MAPPING TECHNIQUE

By: James K. Hallenburg

ABSTRACT:

The spontaneous potential curve is a record of several components. The use of the diffusion-absorption component to determine formation water resistivity is well known. A technique is proposed which appears to reflect changes of the redox components. A mapping technique is proposed which may be useful in locating sedimentary mineral trends. A hypothesis is advanced which may partially explain several observed phenomena.

INTRODUCTION

Mineral exploration and, to a lesser extent, petroleum exploration depend upon knowing the state of the host formation with respect to alteration, oxidation, and general chemistry. These are determined in various ways but few of them rigorously. These three factors are important with respect to the transport, deposition, and location of minerals and hydrocarbons. Mapping of the iron redox interface, in the form of examining cuttings from hematite staining is a viable technique used to estimate the location of the mineralized trend or geochemical cell in uranium exploration (21). This method is slow, tedious, and has a long turn-around time.

Since the spontaneous potential signal is known to be composed of a redox component among other things (5, 6, 10), the information to map a redox interface appears to be contained in the S.P. curve. It appears to be extractable and explainable. A mapping method using the S.P. curve is proposed as a substitute or a verification of the hematite staining method.

REDOX INTERFACE

Several years ago the theory of roll-front deposition of minerals, principally uranium, was proposed by several people (1, 2, 3, 8). This theory has been advanced to cover deposition of minerals other than uranium (4). Related mechanisms have been recognized, such as the "Reduction Bubble" theory advanced by Shockey, and redox methods for oil exploration (5, 6, 9). The subject is treated in detail by Garrels and Christ (7). Other papers have been published on the subjects and their omission from the bibliography was because of lack of availability for researching.

Briefly, all of these theories, ideas, and techniques deal with the proposition that certain minerals can be altered by oxidation and transported by ground waters in an oxidized state. They can be deposited in a reduced state and concentrated at a redox interface. The redox state of the mineral or metal, the presence of a hydrocarbon, and the redox state of the immediate environment are directly and closely interrelated.

Better and faster methods of recognizing the state of oxidation of a horizon and its relation to the electrochemical conditions would be valuable as an exploration tool. Such a method and a hypothesis to attempt to explain

it, is presented here in the hope that someone may further evolve this and related techniques.

THE S. P. CURVE

The spontaneous potential (S. P.) curve has been recorded, used, and studied for many years in the petroleum industry. It has been very much neglected in mineral exploration because it is not well understood.

The spontaneous potential is a combination of several naturally occuring potentials in the earth measured with a voltmeter, usually with reference to a fixed electrode (10, 11, 12, 13, 20). The primary components are: the diffusion-absorption component (11), the electrofiltration component (10, 12, 13) and the redox component (5, 6, 10).

The difussion-absorption component of the S. P.curve (10, 11) is the component used in the petroleum industry almost to the exclusion of any of the others. It is the measurement made in a sand, with reference to the "shale-line" of shale potential, which is used to calculate the value of the information water resistivity, Rw and is the basis for many porosity and most water saturation determinations. Its use has been extremely important to precise in situ analysis of petroleum reservoirs.

The electrofiltration component (12, 13) of the S. P. curve is of interest mostly as an interfering signal, although some use has been made of it. In our work, minerals exploration, the electrofiltration component shows up as a changing potential due to the movement of mud filtrate into a freshly drilled formation.

For the most part, very little investigation has been done into the redox component of the S. P. curve and its possible uses (5, 6).

If we assume that the formation and borehole have come to a hydraulic and mechanical equilibrium, the electrofiltration component will have become low and stable. On this basis, we can assume that the recorded S. P. curve is composed chiefly of the diffusion-absorption component and the redox component.

The redox component, Eox will be evident regardless of whether the measurements are in sands or shales. This component should show up as a general base line shift from formation to formation (See Figure 1). It is a change of the absolute value of the S. P. Depending upon the relative concentrations, Eox may be high but usually is somewhat less than 270 millivolts, (7, 22).

The electrical mode which appears applicable to a redox situation seems to be a static situation as shown in Figure 2. We appear to be measuring the layered charges on the wall of the borehole. This would indicate that the measurement is probably very sensitive to the impedance of the measuring system.

The reduced formation has a predominantly negative charge while the oxidized formation is more positive. The borehole forms a (usually) non-reactive path for the measure electrode across the interface. The resulting charge concentrations in layers on the wall of the borehole result in an

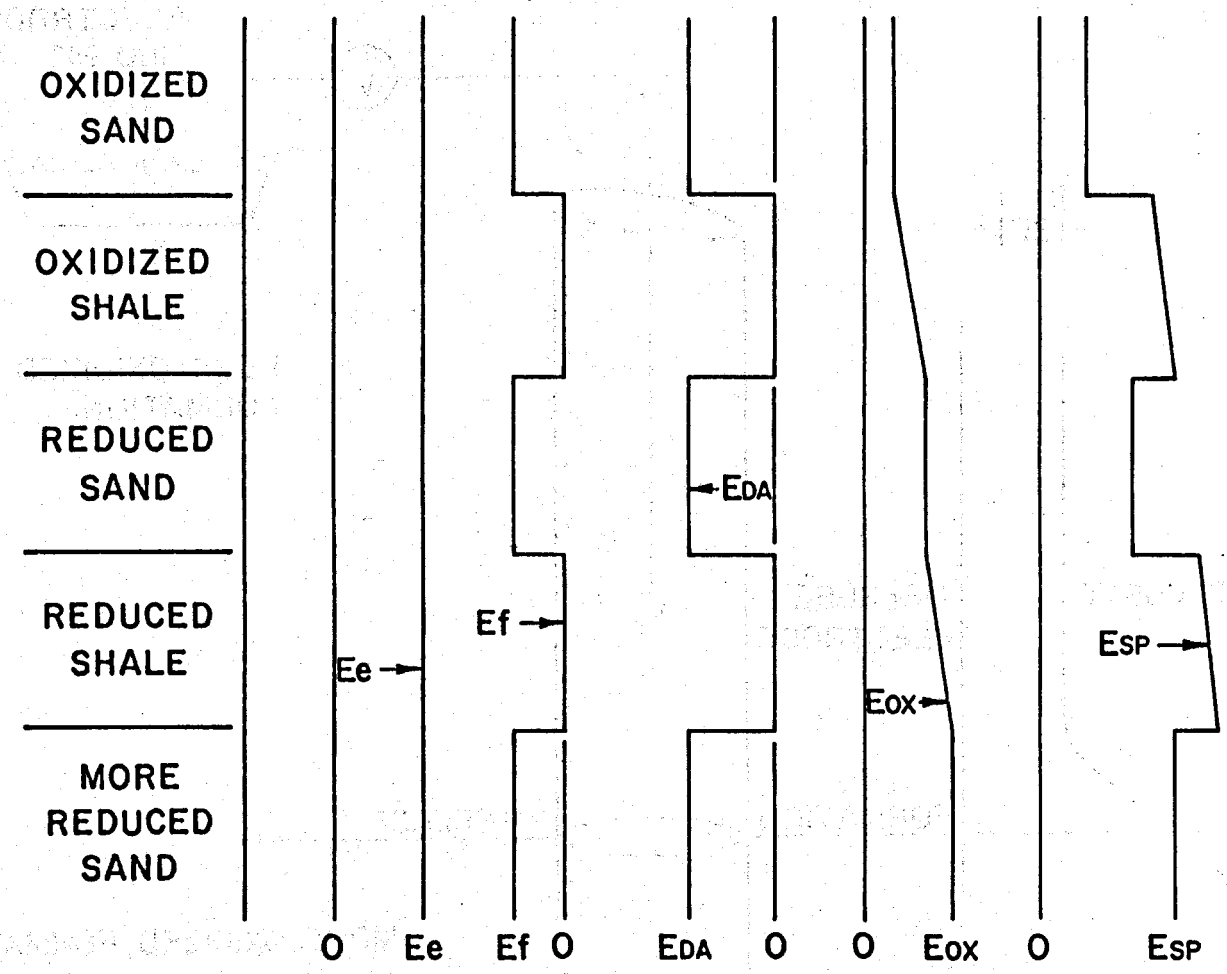

Ee = ELECTRODE POTENTIAL
Ef = ELECTROFILTRATION POTENTIAL
E_{DA} = DIFFUSION - ABSORPTION POTENTIAL
E_{OX} = REDOX POTENTIAL
E_{SP} = RESULTANT S.P. POTENTIAL

$$E_{SP} = Ee + Ef + E_{DA} + E_{OX}$$

SIMPLIFIED S.P. CURVE

FIGURE 1

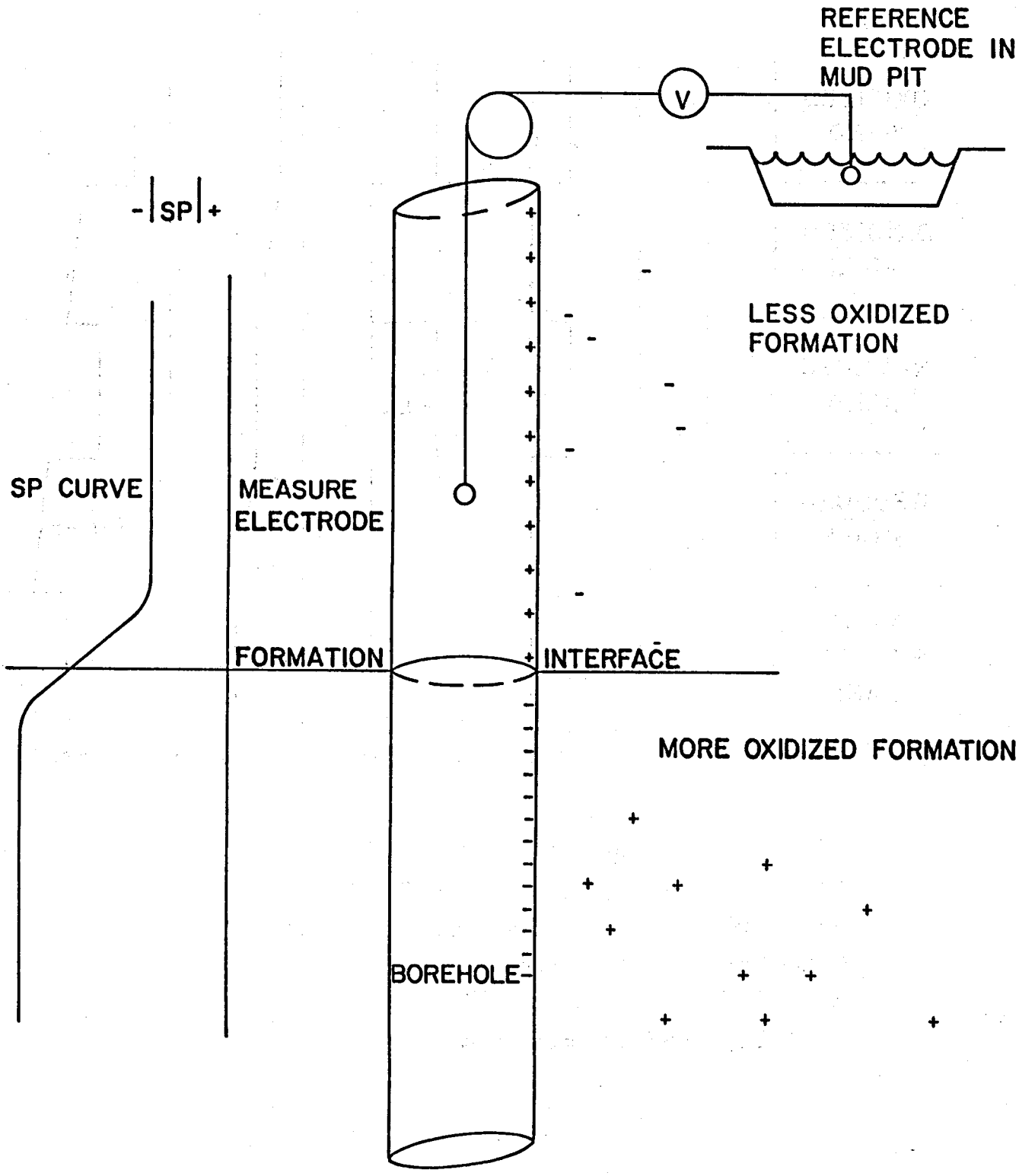
REFERENCE
ELECTRODE IN
MUD PIT
V
-|SP|+
LESS OXIDIZED
FORMATION
SP CURVE
MEASURE
ELECTRODE
FORMATION
INTERFACE
MORE OXIDIZED FORMATION
BOREHOLE

FIGURE 2

indication of the S. P. base line as indicated in Figure 2. (Note that the borehole polarity is of the opposite sense to the formation polarity.) Therefore, a base line shift in the negative direction would indicate approaching an oxidizing bed (with its more positive S. P.) while a shift to the positive direction would indicate approaching a reducing bed (and its more negative potential). This situation is indicated by the diagram, Figure 2.

The phenomena described have been pointed out on the log, Figure 3. The change of the S. P. base line, due to the redox component is hypothesized to be as is shown in Figure 3 (as the drawn-in base line). As the electrode approaches a change in redox state, the base line of the S. P. curve will change to anticipate it. If the movement, or shift is to the left, or negative the zone being approached will be more oxidized than the previous one. A movement to the right or positive indicates the adjacent bed is less oxidized than the previous one. This direction of shift is illustrated in Figure 2. The deflections (Figure 3) in the sands, as at 350' are primarily due to the change in diffusion-absorption potential from the clays (310'). Except for changes in clay content of the sand, these will stay relatively constant throughout a sand.

MAPPING

It appears that we should be able to measure and map the redox situation in an area if we use the shifts described in the previous section.

We had available many hundreds of existing logs in one area where a redox interface map (21, 23) had been made from the lithology logs. In the same area, the shift of the base line of the S. P. curves was used as an indicator of relatively greater or lesser states of oxidation of three sands. The relative positions of the base line and its shifts were compared to the base line of another formation known to be reduced (from examination of area cuttings and cores). A shift to the left was tabulated as more oxidized than the reference sand. A shift to the right of the S. P. base line was tabulated as less oxidized or more reduced than the reference sand.

Using the tabulations of S. P. shifts we made maps which were compared with the map made from the lithology logs. (Unfortunately, we cannot present the maps in sufficient detail to be effective because of confidential material which they contain):

1. The map made from the lithology log was a map of the ferric-ferrous interface. This map was used as a reference to compare the S. P. maps. The area covered was about 10 sections in the Grants mineral belt (21).

2. S. P. maps were made from the log of same boreholes used for the ferric-ferrous map (1 above). These maps treated three Westwater member sands separately.

In spite of differences there were great similarities in the comparisons. It appears that the zones between the oxidized and reduced zones on the lithology map (these were zones which had both oxidized uranium compounds and reduced iron indications in the samples). (21, 23 correspond to areas which are greatly convoluted on the S. P. maps. Also, to a great extent,

these appear to be zones where not all three sand members are in the same state.

This technique was further tested in the Black Hills area of South Dakota. Again it agreed with existing trend maps and could be used to predict trend extensions (22).

It is felt that this is a useable method to map the redox situations to help clarify poorly defined situations. It is hoped that others may aid in evolving a viable exploration technique from it.

Eh - pH DIAGRAMS

En - pH plots have been studied by several people. Garrels and Christ (7) have investigated them in detail. Briefly, they have studied the interrelations of various metal compounds and aqueous solutions of metals with respect to redox or Eh potentials and the acid-base or pH condition. Since we measure the redox potential as a component of the S. P. curve, we should be able to relate our measurements to Eh - pH diagrams.

pH

The pH of most of our solutions apparently fall within a relatively narrow range. Measurements on cuttings from water wells at Gillette, Wyoming, were about pH 6.5 to 7.5 in the surface oxidation zone (24). Below in the grey sands and shales the pH measured from 7.0 to 8.0

Investigators at the U.S.G.S. (in a conversation) mentioned temporary pH readings as low as 2.0 in pumice being leached. They further remarked that the pH increased rapidly with time to a much higher value.

Hawkes and Webb (14) state that mine waters fall in the range of pH5 to pH9 with most of the occurrences between pH6 and pH8. The notable exception to this is in the neighborhood of oxidizing sulfides. See Figures 4 and 5.

In general, unless we are very close to a geochemical cell or unless there is an excess of carbonates, the limit of the pH range is probably 6.5 to 8.0.

Eh

If we compare the ferric-ferrous interfacies (Figures 6 and 7) with uranium interfacies (Figure 8) on the Eh-pH diagrams, we find the beginning of the hematite zone is not the beginning of the oxidized (soluble?) uranium zone. This difference means that the uranium deposition may have taken place inches or miles from the iron redox interface on the reduced iron (or fresh) side. In the Wyoming basins it often appears to be inches. In the New Mexico mineral belt it often appears to be a much greater distance. Apparently, iron alteration and uranium deposition points are not the same thing. However, we must keep in mind that the distances we are really dealing with are electrical distances. We can only approximately relate these to physical distances.

There are several things which may affect the physical distances between redox interfacies. The rate of transport, concentration, and activities of reductants in situ can certainly affect the width of the transition zone.

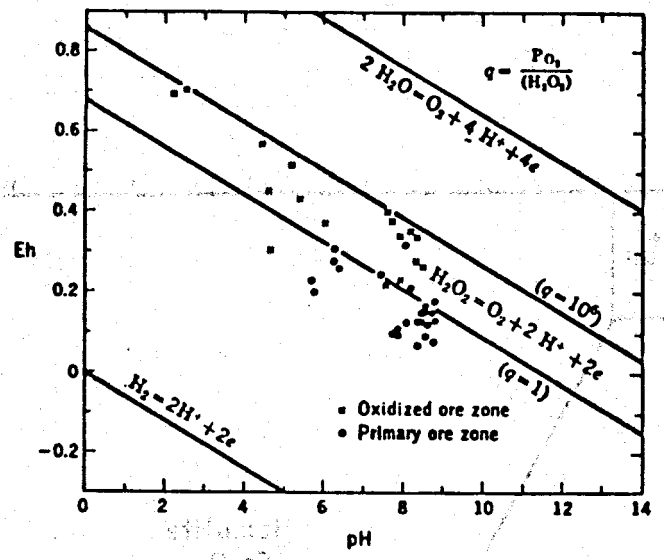

Fig. 4 – Eh and pH values of mine waters. From Sato and Mooney (1960).

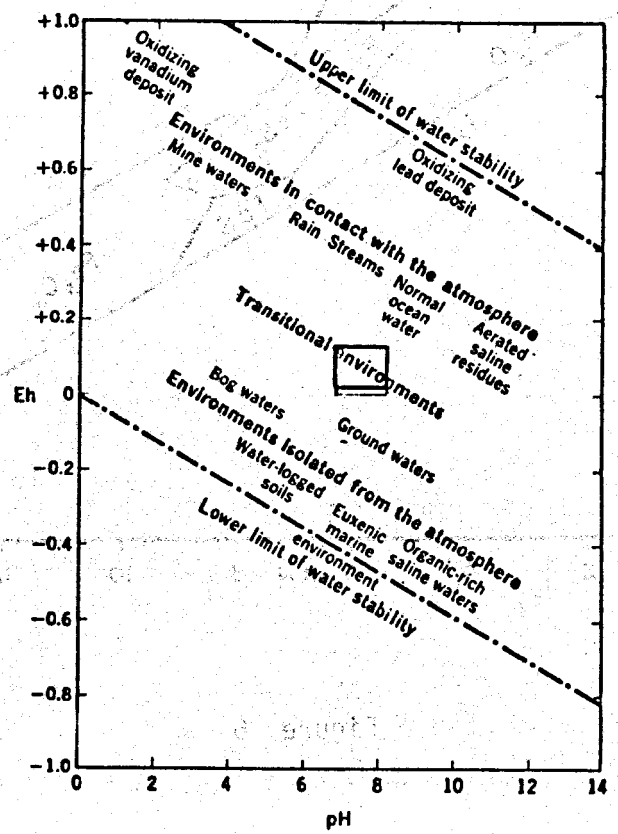

Fig. 5 – Approximate position of some natural environments as characterized by Eh and pH. From Garrels (1960).

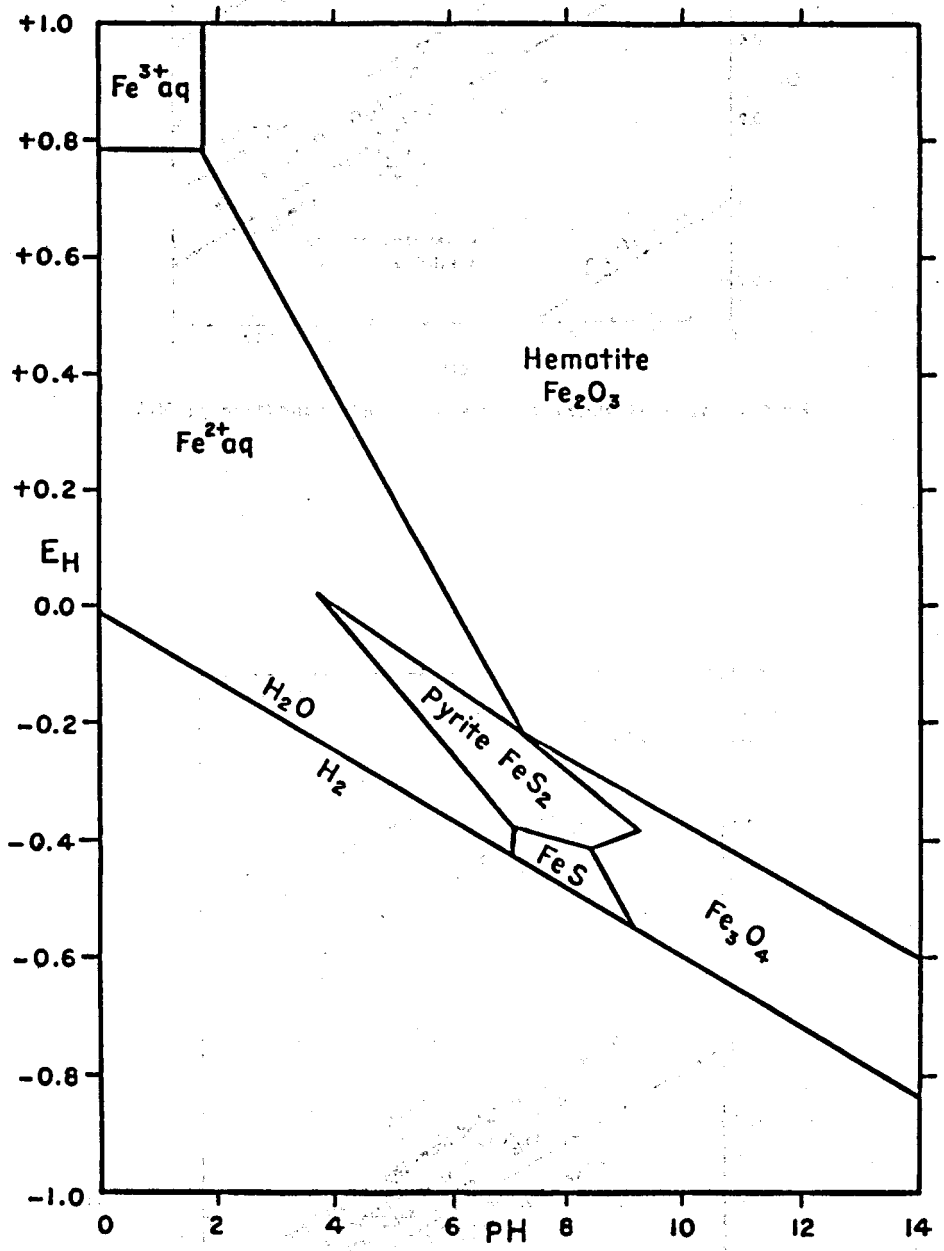
+1.0
+0.8
+0.6
+0.4
+0.2
E_H
0.0
-0.2
-0.4
-0.6
-0.8
-1.0
$Fe^{3+}aq$
$Fe^{2+}aq$
Hematite
Fe_2O_3
H_2O
H_2
Pyrite FeS_2
FeS
Fe_3O_4
0
2
4
6
pH
8
10
12
14

Figure 6

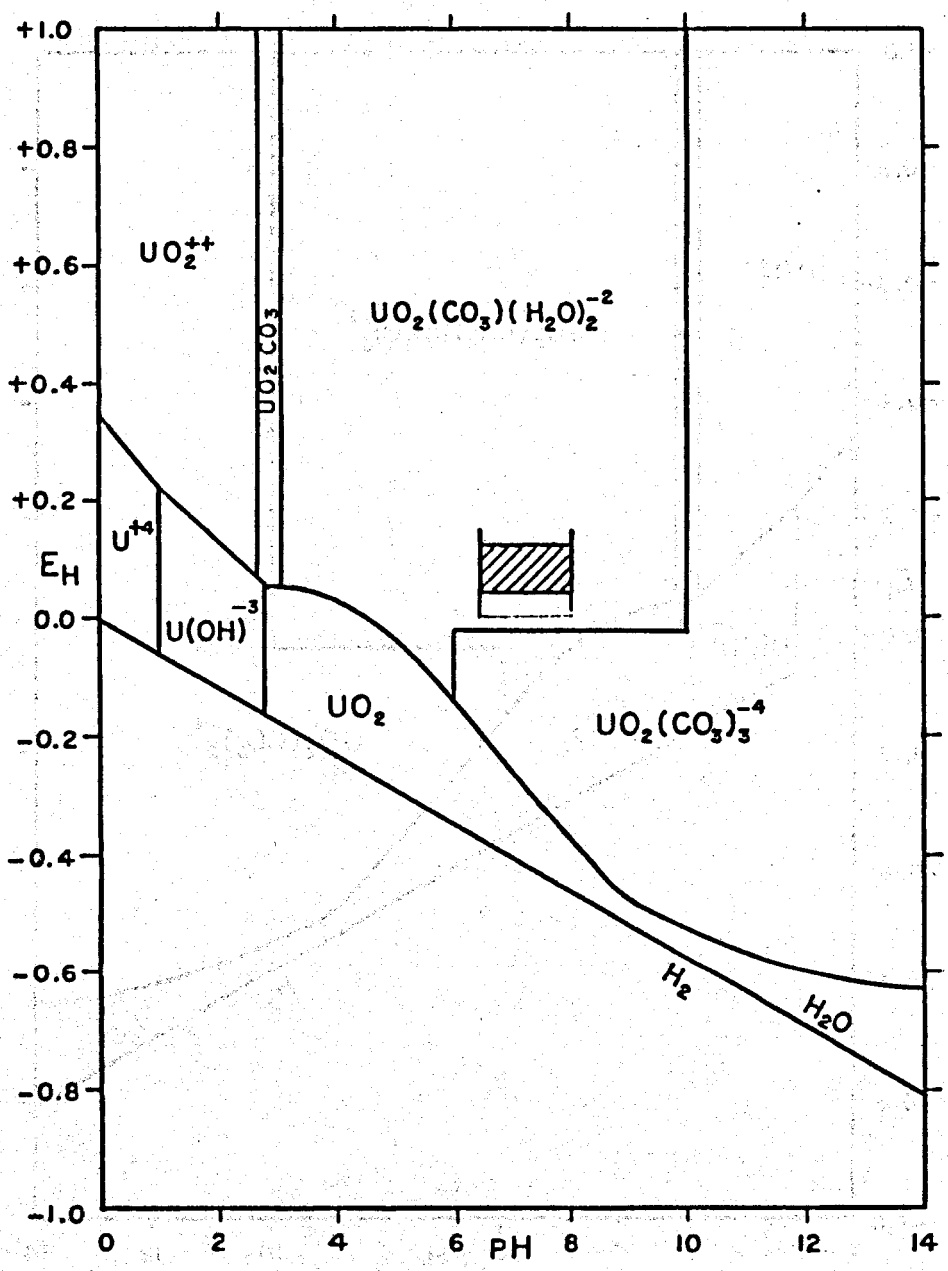
+1.0
+0.8
+0.6
+0.4
+0.2
0.0
-0.2
-0.4
-0.6
-0.8
-1.0
E_H
UO_2^{++}
UO_2CO_3
U^{+4}
$U(OH)^{-3}$
$UO_2(CO_3)(H_2O)_2^{-2}$
UO_2
$UO_2(CO_3)_3^{-4}$
H_2
H_2O
0
2
4
6
pH
8
10
12
14

Figure 7

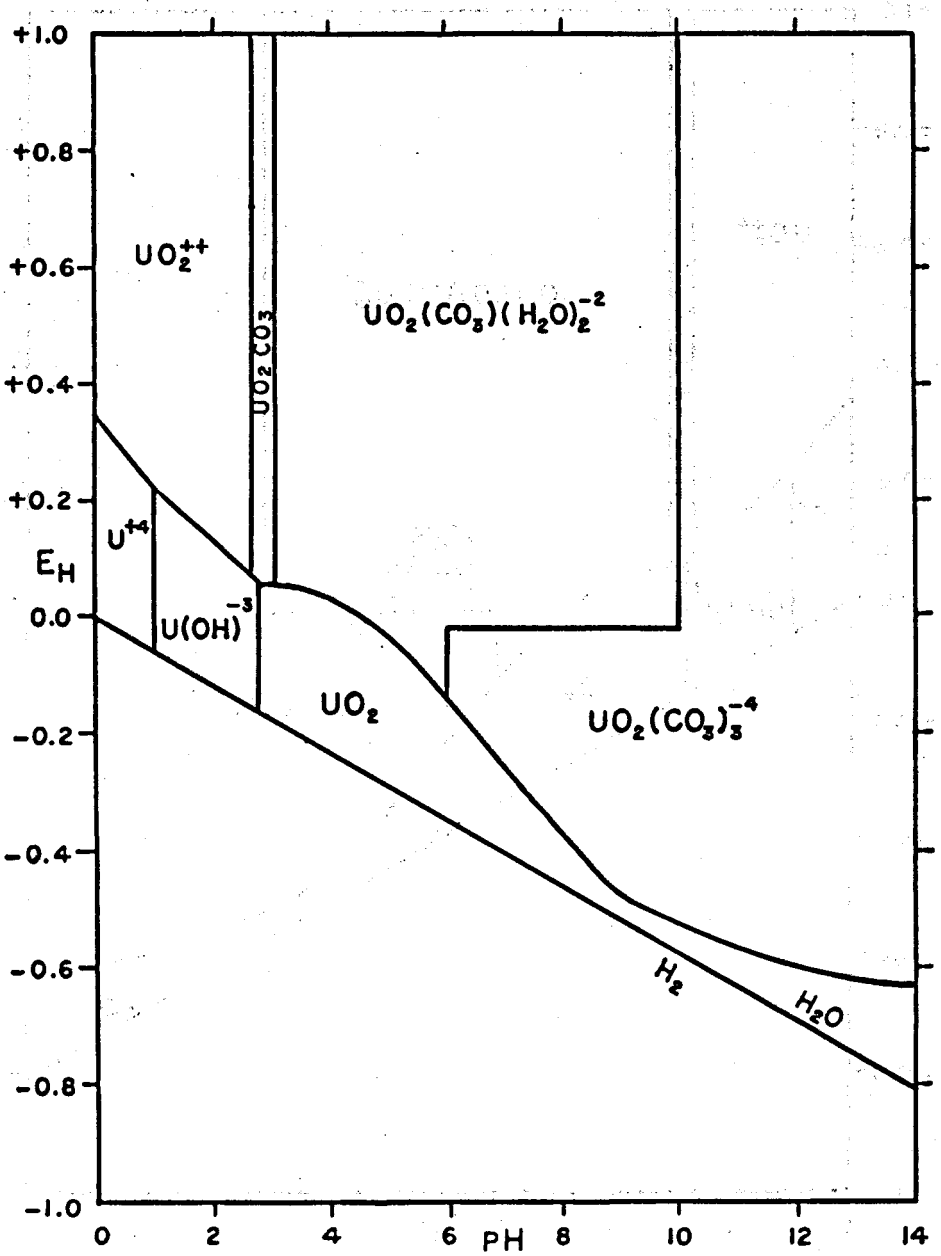
+1.0
+0.8
+0.6
+0.4
+0.2
0.0
-0.2
-0.4
-0.6
-0.8
-1.0
E_H
UO_2^{++}
UO_2CO_3
$UO_2(CO_3)(H_2O)_2^{-2}$
U^{+4}
$U(OH)^{-3}$
UO_2
$UO_2(CO_3)_3^{-4}$
H_2
H_2O
0
2
4
6
pH
8
10
12
14

Figure 8

If we compare Figure 6, an iron diagram, with Figure 8, the uranium compound diagram we can see that, in the range of pH 6.5 to pH8, oxidized uranium (soluble?) compounds can coexist with ferrous compounds which are traditional indicators of "freshness" in uranium exploration. Hematite (ferric iron) does not appear until well within (50 to 150 millivolts) the stable soluble uranium compound range.

These situations appear to be the base of the problem of comparing "altered-fresh" interfacies of lithology logs with uranium occurances. In other words, uranium deposition should occur well into the electrical "fresh" zone of a geochemical cell.

CONCLUSION

It is felt that this paper outlines a possible new exploration technique. Certainly, more work is needed in all phases of it before it can be proved. However, it appears to be a viable technique. We wish we had had the opportunity to pursue this further, in greater detail and more rigorously. It is to be hoped that someone may have that opportunity. It is also to be hoped that someone may be able to make some use out of this technique.

BIBLIOGRAPHY

1. The Conceptual Uranium Roll and Its Significance in Uranium Exploration. Haus H. Adler, Volume 59, 1964, pp. 46-53, Economic Geology.
2. Some Characteristics of Roll Type Uranium Deposits at Gas Hills, Wyoming. John W. King and S. Ralph Austin, October, 1965, A.E.C. paper.
3. Concepts and Methods of Uranium Exploration, R. Rackley, P. N. Shockey, M. P. Dahill, W.G.A. Earth Science Bulletin, Volume 1, #3, September, 68'.
4. Copper-Silver Solution Fronts at Paoli, Oklahoma, P. N. Shockey, A. R. Renfro, and R. J. Peterson, Economic Geology, Volume 69, #2, pp. 266-268, March/April, 1974.
5. New Electric Technique Can Locate Gas and Oil, Dr. S. J. Pirson, April, 1971, World Oil.
6. Environmental Logging and Mapping in the Search for Minerals, Dr. S. J. Pirson, March/April, 1970, Log Analyst, Volume XI, #2.
7. Solutions, Minerals, and Equilibria, Robert M. Garrels and Charles L. Christ, Harper and Row, 1965, L of C #65-12674.
8. Implications of Some Elements Associates with Uranium Deposits, Shirley Basin, Wyoming. U.S.G.S. Prof. paper 550C, pp. 167-173.
9. Accumulation of "Red Bed Type" Sulphide Ores - A Process of the Sabkha Depositional Environment, A. R. Renfro, Economic Geology, Volume 69, #1, pp. 33-45
10. Geophysical Well Logging, Quarterly of the Colorado School of Mines, Volume 57, #2, April, 1962.
11. The S. P. Log: Theoretical Analysis and Principles of Interpretation. H. G. Doll, Technical Publication #2463, AIME, Class G, Petroleum Technology, 1948.
12. An Investigation of the Electrokinetic Component of the Self Potential Curve, M. R. J. Wyllie, Technical Paper #2940, Petroleum Transactions, AIME, Volume 192, 1951.

13. Streaming Potential and the S. P. Log, M. Gondouin and C. Scala. Paper #864-G, Society of Petroleum Engineers of AIME.
14. Geochemistry in Mineral Exploration, H. E. Hawkes and J. S. Webb, Harper & Row, 1962.
15. Reference Electrodes, Theory and Practice, David D. J. Ives and George J. Janz, Academic Press, 1961, 1969, L of C #60-16910.
17. Geobotany and Geochemistry in Mineral Exploration, R. R. Brooks, Harper & Row, 1972, L of C #72-181541.
18. Chemistry, Principles and Properties, Michell J. Sieko and Robert A. Plane, McGraw Hill, 1966.
19. Handbook of Chemistry and Physics, 51st Edition.
20. A Resume of Spontaneous Potential Measurements, J. K. Hallenburg, 12th Annual Logging Symposium Transactions, SPWLA, 1971.
21. Conversations with R. J. Peterson of Teton Exploration Drilling Company (1970-1974).
22. Measurements made by the author in 1949 in Houston and 1974 in North Dakota. Both sets of measurements are undocumented at this time.
23. Measurement made by the author and undocumented.

Note: A biographical sketch and a photo of Mr. Hallenburg are presented in Paper S.

ESTIMATION OF FORMATION PRESSURES IN CLEAN GAS SANDS FROM THE DUAL-SPACING TDT* LOG

by

J. S. Blackburn
Schlumberger Well Services
Louisiana Inland Division, Lafayette, Louisiana

R. C. Brimage
Schlumberger Offshore Services
Gulf Coast Division, New Orleans, Louisiana

ABSTRACT

An empirical technique is described in which the data from Dual-Spacing TDT logs are being used to estimate formation pressures in cased holes in South Louisiana. It employs the near- and far-detector count rates, and porosity and saturation data, to estimate Σ_g (macroscopic thermal-neutron-capture cross section of the gas), and therefrom to obtain information about formation pressures in clean gas sands in pressure-depletion reservoirs.

Log examples will be shown which indicate that, under favorable conditions (i. e., clean sands, light, dry gas, bulk-volume fraction of formations liquids known, and proper hole conditions), it is possible to estimate the formation pressures in South Louisiana wells within about 10 to 15 percent error.

INTRODUCTION

Since its introduction, the Dual-Spacing TDT has been very useful for formation evaluation in cased holes. Used with a simultaneous Gamma Ray log it provides data for the determination of formation porosity and water saturation, for formation-fluid identification and location of fluid contacts, for correlation, and for reservoir monitoring. In addition, separations of the overlaid near- and far-detector count-rate curves recorded with appropriate scale sensitivities, along with the Σ values (macroscopic thermal-neutron-capture cross sections), have been useful for the identification of the fluid types (water, oil, or gas) in the formations.

Further observations have indicated that in low-pressure-gas zones the separations of the overlaid near- and far-detector count-

* Mark of Schlumberger.

rate curves are larger than in zones with normal pressures. This, supported by the study of many South Louisiana logs, has led to the concept that proper treatment of the data from the Dual-Spacing TDT can yield estimations of formation pressures in clean gas sands.

This paper will describe an empirical technique being used to do this in cased holes in South Louisiana. Following a brief discussion of the Dual-Spacing TDT and its typical responses, the technique for determining formation pressures will be developed. Four log examples will be presented to show how the technique works. The examples indicate that under suitable conditions it is possible to estimate the formation pressures within about 10 to 15 percent error.

THE DUAL-SPACING TDT LOG

Previous papers have discussed the details of thermal-neutron-decay-time (pulsed-neutron-capture) measurements[1-3] and techniques for interpretation of the corresponding logs.[3,4]

The Dual-Spacing TDT is a 1 11/16-inch (43-mm) diameter tool with dual detectors.[3,5] It is run with a combinable Gamma Ray tool, and the combined length is 32 ft (9.75 m). Its pressure and temperature ratings are 16,500 psi (113,800 kPa*) and 300°F (150°C).

Fig. 1 is a typical recording for South Louisiana. Track 1 (left-hand track) includes a Gamma-Ray log and a Casing-Collar log. The Gamma Ray log is used for correlation, lithology identification, and determination of shale-volume fraction. The Casing-Collar log is used for depth control for subsequent runs with other devices (e.g., perforating guns or packers). A Ratio curve is recorded in Track 2 (middle track). The Ratio curve is computed from the net count rates of the two detectors:

$$\text{Ratio} = \frac{\text{Near-detector counts (net)}}{\text{Far-detector counts (net)}}$$

Near- and far-detector count rates are recorded as a Near-Far Count-Rate Display in Track 3 (at right). The Σ curve is recorded over Tracks 2 and 3. Σ is a measurement of the macroscopic thermal-neutron-capture cross section of the formation. It is used to help predict the type of fluid in the pore space.

Fig. 1 illustrates some typical responses of the curves recorded with the Dual-Spacing TDT.

---

* 1 psi = 6.895 kPa (kilopascals).

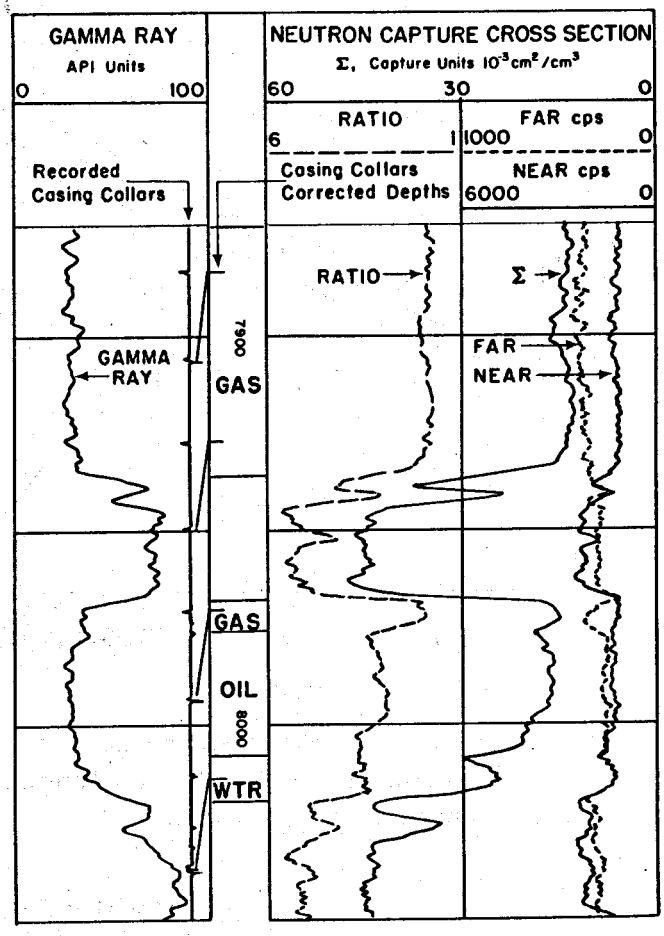

Fig. 1
South Louisiana recording of Dual-Spacing TDT illustrating typical responses in gas, oil, and water sands.

THE NEAR-FAR DISPLAY

It was the study of the Near-Far Count Rate Display that led to the determination of formation pressures from the Dual-Spacing TDT. The count rate of the Near detector (sometimes designated as N_1) is recorded on a scale of 0 to 6,000 counts per second and the count rate of the Far detector (sometimes designated as F_1) is recorded on a scale of 0 to 1,000 counts per second. In South Louisiana, the two curves recorded in this fashion generally overlay or "track" each other in clean, water-bearing sands. They usually "track" or separate slightly in oil sands and have a greater separation in gas sands. The Near-Far Display is therefore diagnostic of gas in clean sands. It was also observed that some gas sands had more pronounced separations than other gas sands on the Near-Far Display. Fig. 8, shown later, illustrates such a separation. The zone in Fig. 8 with this large separation happened to be a gas sand with known low pressure.

These observations led the authors to surmise that the separation of the Near-Far Display was a function of the amount of hydrogen in the formation. If the hydrogen content was high (as in water or oil sands) the separation was little or none, and if the hydrogen content

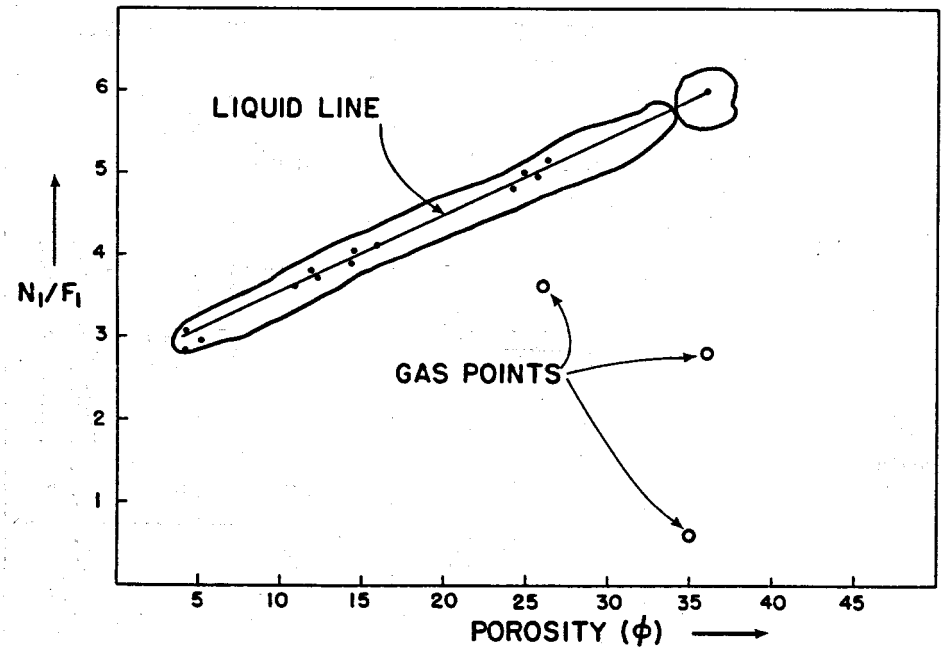

Fig. 2
Plot of Near-Far count-rate ratio versus porosity.

was low (as in low-pressure gas sands) the separation was greater. It related to the amount of the hydrogen in the formation, and hence to the pressure in a gas sand.

AN EMPIRICAL CHART

Fig. 2 shows the Near-Far ratio (N_1/F_1) plotted in ordinate versus porosity (ϕ) in abscissa. The circumscribed points are all from known water sands. They have a definite trend, and an average "Liquid Line" has been drawn through them. The single circumscribed point at the upper right is for ϕ = 35 p.u. and N_1/F_1 = 6; this is the value of N_1/F_1 for which the Near and Far curves track together on the log. Lower values of N_1/F_1 correspond to separations between the Near and Far curves, with the Far curve to the left of the Near curve. On the "Liquid Line" of Fig. 2 lower values of N_1/F_1, corresponding to larger relative separations between the Near and Far curves, are for levels with lower porosities. This is in line with the earlier supposition that the Near-Far separation is generally observed to increase as the hydrogen content of the formation decreases.

The above implies that, if N_1/F_1 values are plotted versus porosity points for water-saturated sands should fall on or very close to the Liquid Line.

It was further noted that if N_1/F_1 is plotted versus porosity in gas sands, the plotted points fall below the Liquid Line, as shown in Fig. 2. As the pressures in the gas sands decrease, the points plot further

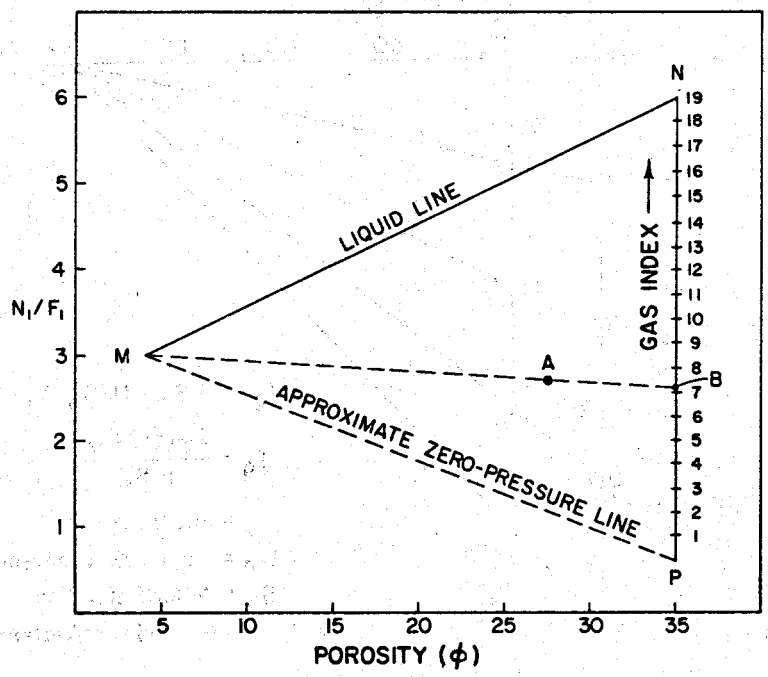

Fig. 3
Empirical chart based on Fig. 2.

from the Liquid Line. By study of some wells with extremely low pressures it was estimated that a formation having a porosity of 35 percent and filled with zero-pressure gas would have an N_1/F_1 ratio of 0.6. This corresponds to the lowest point on Fig. 2.

Fig. 3 is an empirical chart based on the discussion above. Line MN is the Liquid Line. Point M indicates the lowest porosities observed. Point P corresponds to 35-percent-porosity sand and zero-pressure gas. The scalings on Line PN will be taken in this paper to correspond to values of "Gas Index". Line MP, which closes the chart, connects points that would be at approximately zero pressure, at least for the higher porosities.

The Gas Index

Fig. 3 illustrates how an "Apparent Gas Index" is found. Point A corresponds to a gas sand with an N_1/F_1 value of 2.7 and a porosity of 27.5 p.u. The dashed line is passed through the apex (Point M) and Point A to find Point B on the Gas-Index scale, for an Apparent Gas Index of 7.1.

The Apparent Gas Index (I_{ga}) is taken to be proportional to the hydrogen index contributed by the fluids in the formation. Thus, it will be affected by both the gas and the water present. In order to determine a Gas Index (I_g) pertaining to the gas itself, a correction must be made for the contribution of the water. To do this we assume the relation,

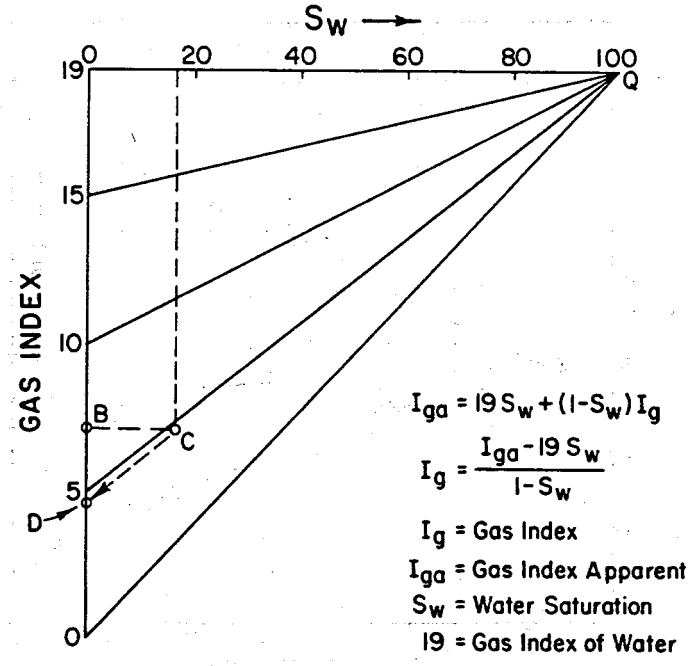

Fig. 4
Chart for adjusting Apparent Gas Index to remove the effect of formation water present.

$$I_{ga} = I_w S_w + (1-S_w) I_g$$

where I_w is the "Gas Index" of the water. Solving for I_g,

$$I_g = \frac{I_{ga} - I_w S_w}{1 - S_w}$$

Fig. 4 illustrates how this water correction is done. In the example shown we start at Point B with an "Apparent Gas Index" of 7.1. Water saturation was determined to be 17 percent, so a line is constructed horizontally from Point B to Point C corresponding to S_w = 17 percent on the scale at the top. From Point C a line is constructed along the trend of the diagonal lines (using Point Q as pivot point) to Point D to find a corrected Gas Index (I_g) of 4.5.

I_g is taken to be proportional to the amount of hydrogen in the gas. Since hydrogen is the element in gas making the principal contribution to its cross section, I_g is taken to be proportional to Σ_g also. Empirically it has been found that if we make I_w = 19 gas-index units, then $I_g \approx \Sigma_g$.

Fig. 5 combines Figs. 3 and 4. This is the complete empirical chart that is being used for the interpretation of Gas Index ($\approx \Sigma_g$). The construction lines show completely the example of Figs. 3 and 4 ($N_1/F_1 = 2.7$, $\phi = 27.5$) for S_w = 17 percent. A Gas Index ($\approx \Sigma_g$) of 4.5 is found.

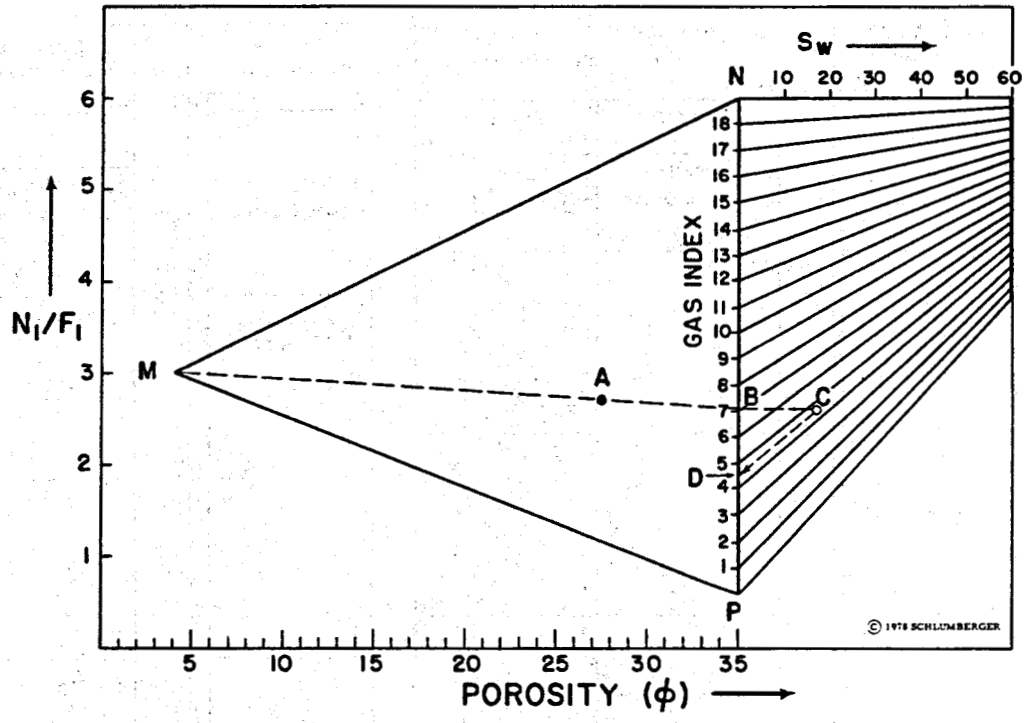

Fig. 5
The complete empirical interpretation chart.

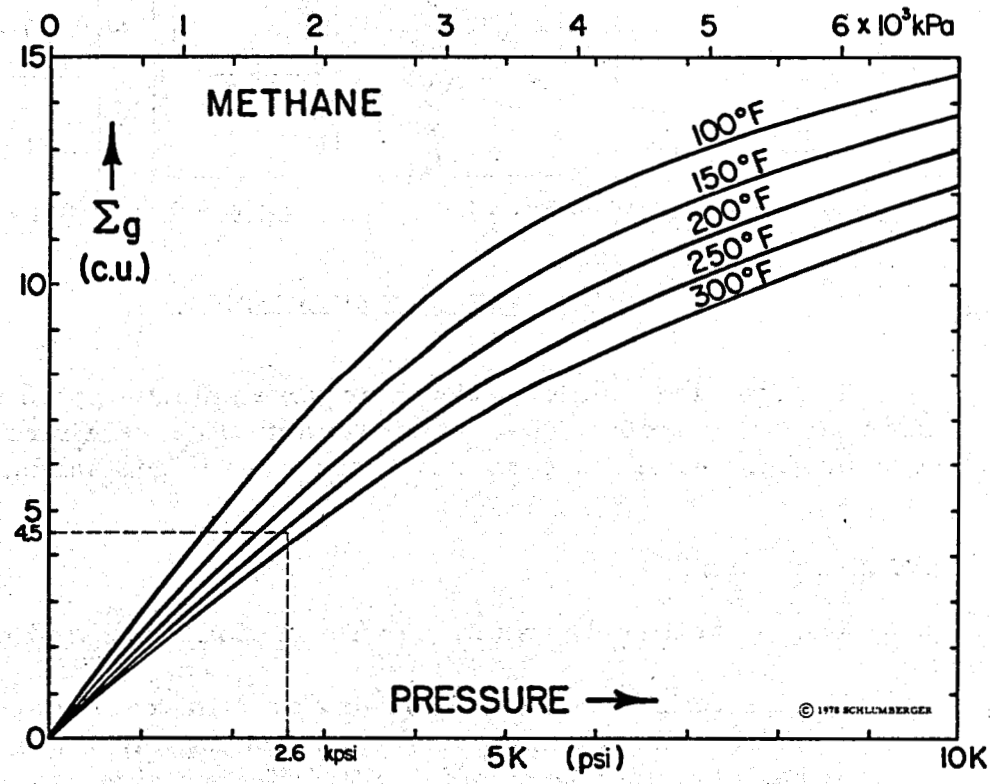

Fig. 6
Plot of Σ_g versus pressure for methane.

Once we have Σ_g, the pressure of the gas can be estimated from the chart of Fig. 6, which has been constructed on the basis of methane gas. In our example, Fig. 6 is entered with $\Sigma_g = 4.5$ to find, at a temperature of 260°F (127°C), a pressure of 2,600 psi (18,000 kPa).

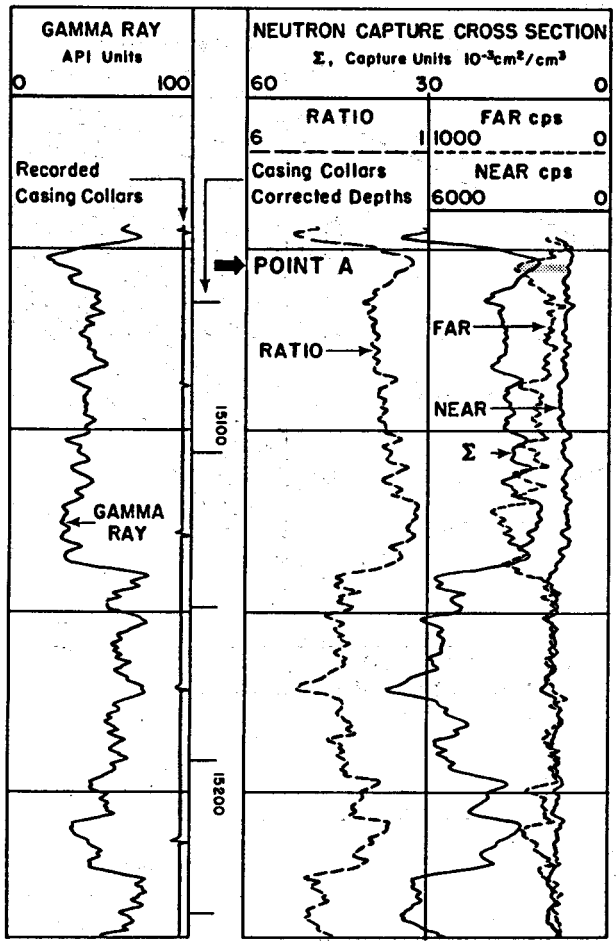

Fig. 7 - Dual-Spacing TDT for Example 1.

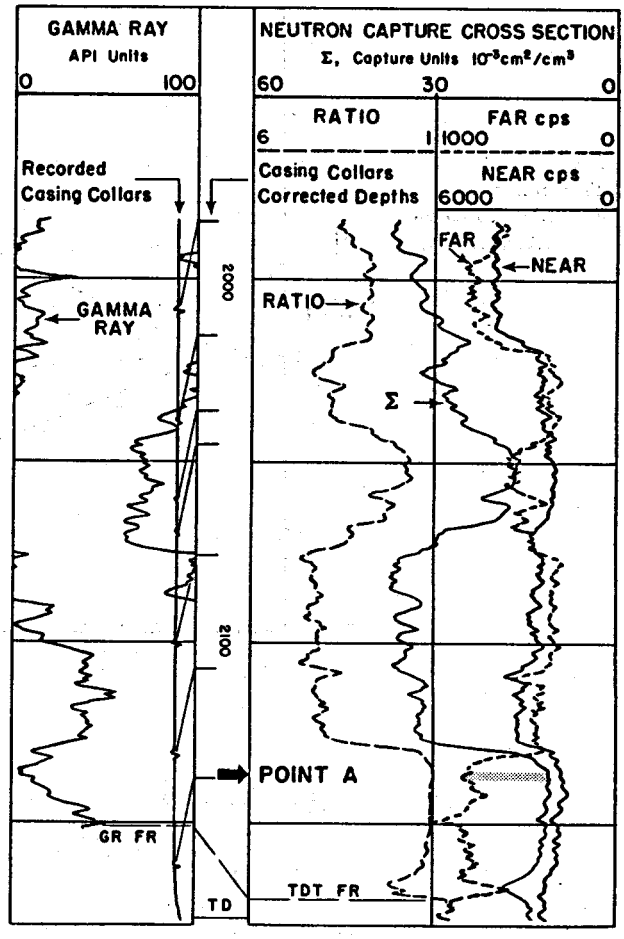

Fig. 8 - Dual-Spacing TDT for Example 2.

FIELD EXPERIENCE

The four log examples to follow were selected from a study of logs from about 50 wells. They illustrate actual cases where the technique was used to determine formation pressures in gas sands.

Well Conditions

The 50-well study was made with the following well conditions:

1) The wells had either 5 1/2-in. or 7-in. casing and were filled with salt water at the time of logging. The technique has also been successful with different-size casings and also with different fluids in the wellbore (for example fresh mud). However, some caution should be used in these instances, since it is necessary to normalize the data to the foregoing conditions of casing size and salt-water casing fluid.

2) Gas sands were selected which had less than 10 percent V_{sh} (bulk-volume fraction of shale). The presence of shale increases the N_1/F_1 ratio and tends to give a Gas Index that is too high, thus, also, too high a reservoir pressure.

3) The gas sands selected were pressure-depletion reservoirs (with no water encroachment). Because the amount of hydrogen in the formation is a function of both connate water and gas, to determine the Gas Index it is necessary to know the water saturation rather accurately. In a depletion-drive reservoir we might determine this satisfactorily from the original open-hole logs, or from the Dual-Spacing TDT itself. In cases of water encroachment, it is less easy to know the actual water saturation in the zone contributing to the TDT readings.

Log Examples

Example 1

Fig. 7 shows the Dual Spacing TDT log for Example 1. For Point A, near the top of the log:

N_1/F_1 = 2.6 as determined from the Near and Far curves of the Dual-Spacing TDT log.

ϕ = 26 p.u., determined from the open-hole Compensated-Density log.

S_w = 17 percent, from open-hole log analysis.

Formation temperature = 260° (127°C), measured with maximum-reading thermometer.

V_{sh} (volume fraction of shale) = 0, from the Gamma Ray log run with the TDT log.

The formation pressure given by the well operator was 2,300 psi (15,900 kPa).

Fig. 11 indicates the corrected Gas Index, hence Σ_g, to be 4.0. Fig. 12 indicates that a Σ_g of 4.0 at a formation temperature of 260°F (127°C) corresponds to a reservoir pressure of 2,300 psi (15,900 kPa). This coincides with the value given by the well operator.

Example 2

For Point A, near the bottom of Fig. 8:

N_1/F_1 = 2.18, determined from the Dual-Spacing TDT log.

ϕ = 35 p.u., from open-hole Compensated Density log.

S_w = 27 percent, from open-hole log analysis.

Formation temperature = 85°F (29.4°C), measured with the maximum-reading thermometer.

V_{sh} = 0, from the open-hole Gamma Ray log run with FDC* (Density).

The formation pressure given by the well operator was 200 psi (1,380 kPa).

Fig. 11 indicates the corrected gas Index, hence Σ_g, to be 0.5. Fig. 12 indicates that a Σ_g of 0.5 at a formation temperature of 85°F (29.4°C) has a reservoir pressure of 170 psi (1,170 kPa). This differs by 15 percent from the value given by the well operator.

Example 3

For Point A, near the middle of Fig. 9:

N_1/F_1 = 3.8, from the Dual-Spacing TDT log.

ϕ = 26 p.u. from the open-hole Sonic log.

S_w = 22 percent from open-hole log analysis.

Formation temperature = 260°F (127°C) from maximum-reading thermometer.

V_{sh} = 10 percent from the Gamma Ray log run with TDT log.

The formation pressure given by the well operator was 8,600 psi (59,300 kPa).

Fig. 11 indicates the corrected Gas Index, hence Σ_g, to be 10.4. Fig. 12 indicates that a Σ_g of 10.4 at a formation temperature of 260°F (127°C) has a reservoir pressure of 7,650 psi (52,700 kPa). This differs by 11 percent from the value given by the well operator.

---

* Mark of Schlumberger.

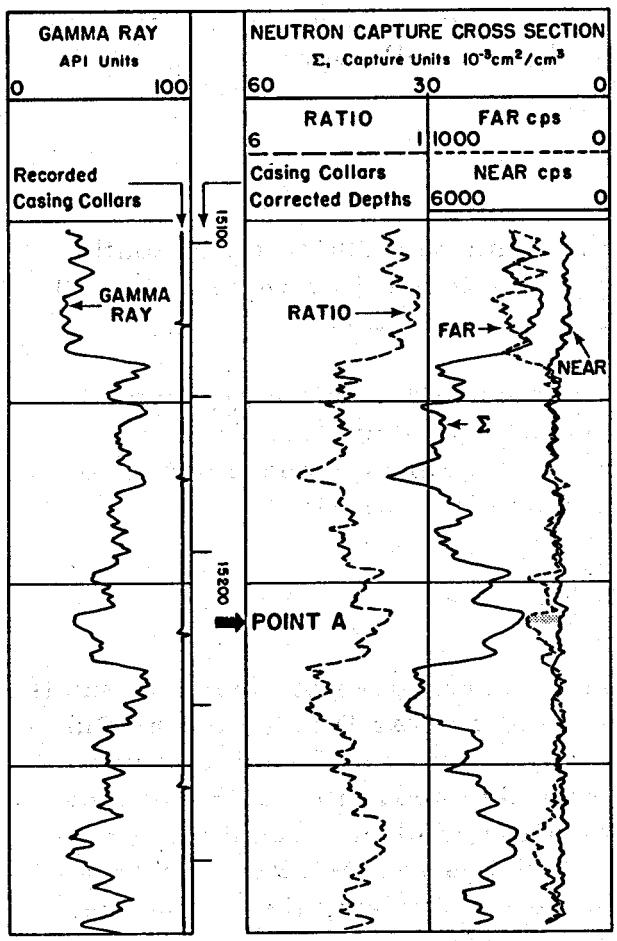

Fig. 9 - Dual-Spacing TDT for Example 3.

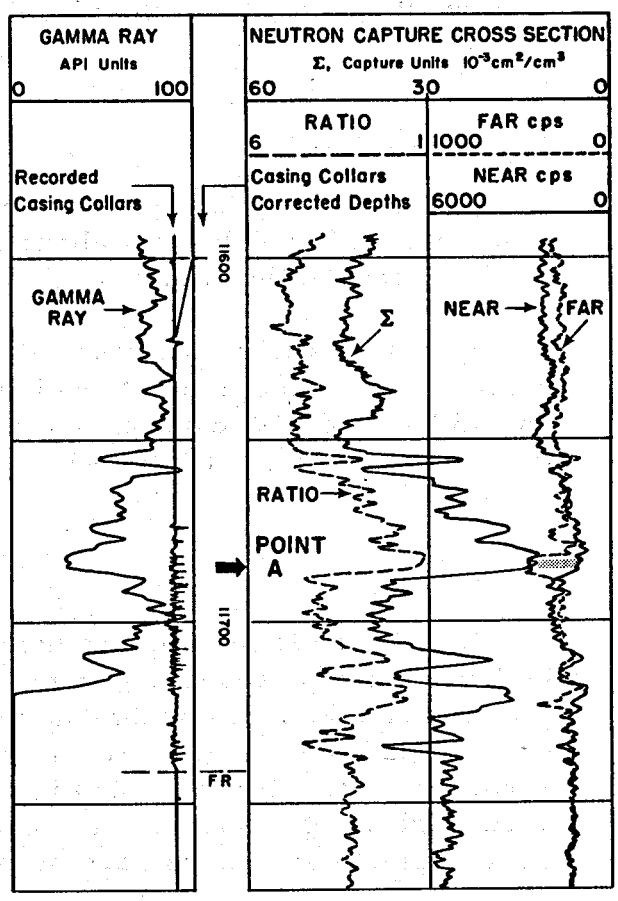

Fig. 10 - Dual-Spacing TDT for Example 4.

Example 4

For Point A in Fig. 10:

N_1/F_1 = 2.5, from the Dual-Spacing TDT log.

ϕ = 21 p.u., from the open-hole Sonic log.

S_w = 20 percent, from open-hole log analysis.

Formation temperature = 220°F (104°C), from maximum-reading thermometer.

V_{sh} = 0, from Gamma Ray log run with open-hole Sonic log.

The well operator indicated the pressure to be 1,300 psi (9,000 kPa).

Fig. 11 indicates the corrected Gas Index, hence Σ_g to be 2.0. Fig. 12 indicates that a Σ_g of 2.0 at a formation temperature of 220°F (104°C)

corresponds to a reservoir pressure of 1,050 psi (7,200 kPa). This differs by 19 percent from the value given by the well operator.

Further Remarks

The technique has been used in approximately 300 wells in South Louisiana with results that about 80 percent of the time were within 10 to 15 percent of the values given by the well operator.

Sometimes this technique may be usable to recognize pressure-depletion oil zones in solution-drive or gas-cap-drive reservoirs. It should be used with caution, however, because it is necessary to know the liquid saturation (water saturation plus oil saturation).

SUMMARY

It is possible to estimate the downhole pressures of clean gas sands in depletion-type reservoirs by using the Near-Far Display on the Dual-Spacing TDT log. The technique uses an empirical approach that under proper conditions usually gives results within about 10- to 15-percent error or less. This technique is especially useful in recognizing pressure-depleted gas sands. In several instances recompletions in pressure-depleted gas zones have been avoided by applying this technique.

ACKNOWLEDGMENT

The authors wish to thank the oil companies who graciously supplied well information and the log examples for this paper.

REFERENCES

1. Hilchie, D.W., Mills, W.R., Dennis, C.L., and Givens, W.N.: "Some Aspects of Pulsed Neutron Logging", Trans. SPWLA Ninth Annual Logging Symposium (June, 1968), Paper Q.

2. Wahl, J.S., Nelligan, W.B., Frentrop, A.H., Johnstone, C.W., and Schwartz, R.J.: "The Thermal Neutron Decay Time Log", Soc. Pet. Eng. J., Vol. 10, No. 4, (December, 1970), pp. 365-379.

3. Dewan, J.T., Johnstone, C.W., Jacobson, L.A., Wall, W.B., and Alger, R.P.: "Thermal Neutron Decay Time Logging Using Dual Detection", Trans. SPWLA Fourteenth Logging Symposium, (May, 1973), Paper P (not published in transactions).

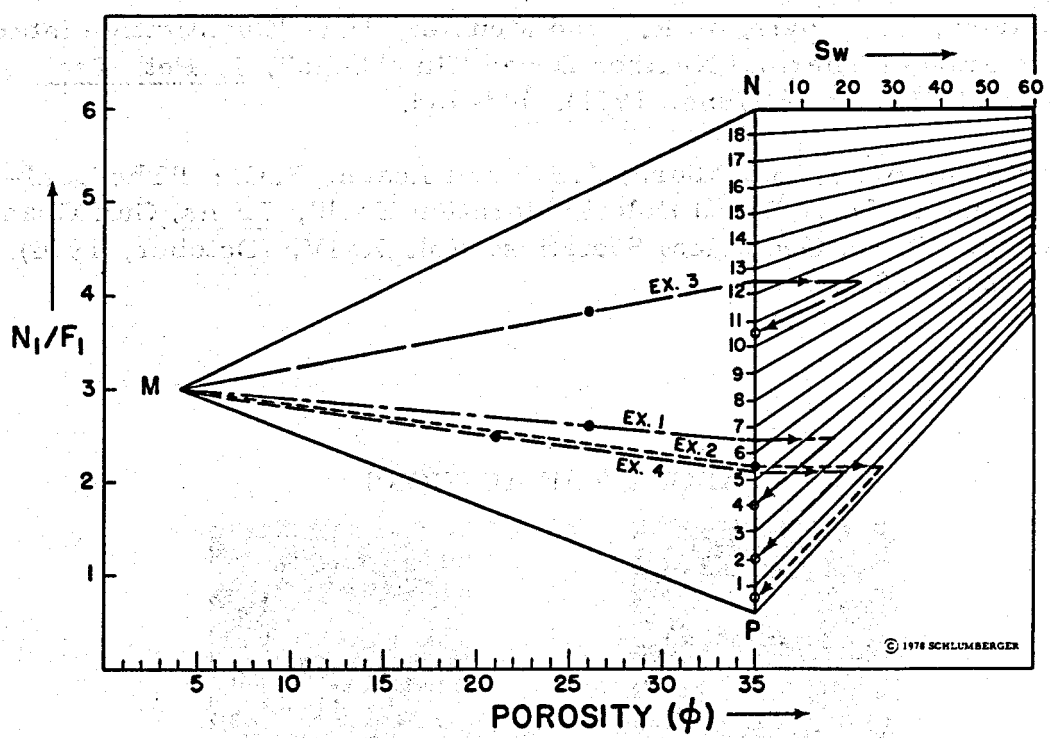

Fig. 11 - Σ_g estimations for field examples.

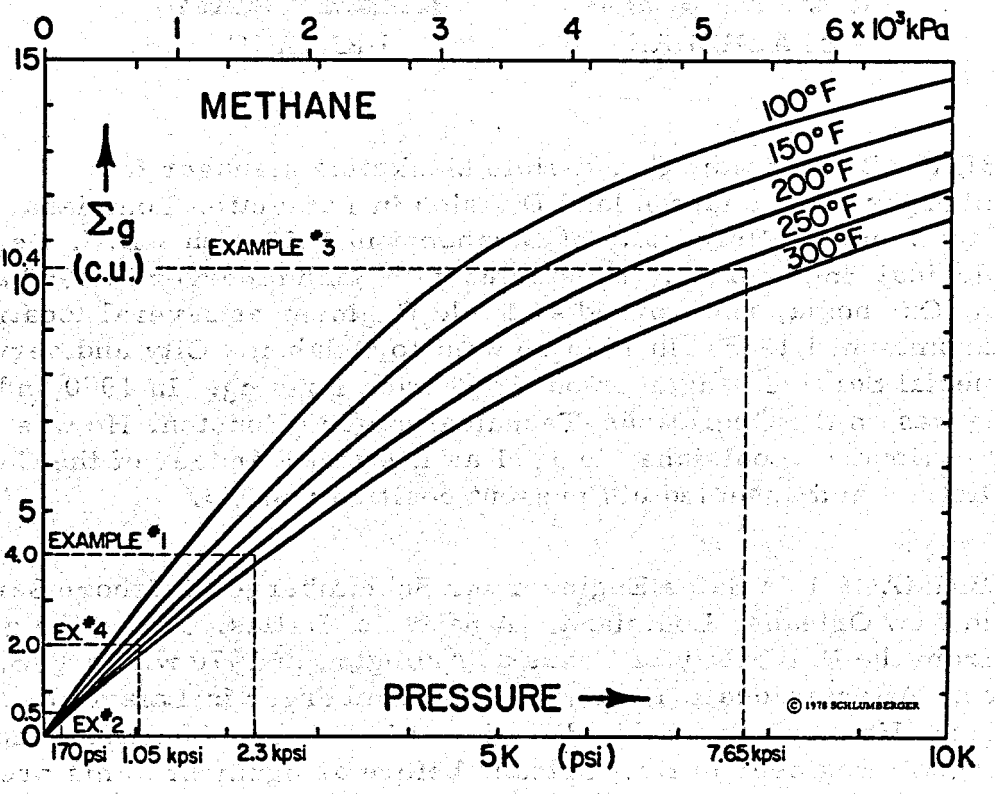

Fig. 12 - Pressure estimations for examples.

4. Clavier, C., Hoyle, W.R., and Meunier, D.: "Quantitative Interpretation of Thermal Neutron Decay Time Logs", J. Pet. Tech., Vol. XXIII, No. 6 (June, 1971), 743-763.

5. McGhee, B.F., Blackburn, J.S., and Leach, B.C.: "The Dual-Spacing TDT: A Cased Hole Exploration Tool", Trans. Gulf Coast Association of Geological Societies, Vol. XXIV, (October, 1974), pp. 235-246.

ABOUT THE AUTHORS

BLACKBURN

BRIMAGE

J.S. BLACKBURN is the Cased-Hole Marketing Manager for Schlumberger's Louisiana Inland Division in Lafayette, Louisiana. He graduated from the University of Oklahoma in 1959 with a B.S. Degree in Geological Engineering. He started with Schlumberger in 1959 at Duncan, Oklahoma, and worked as Field Engineer at several locations in Oklahoma until 1965. In 1965 he went to Oklahoma City and served as a Special Services engineer on Production Logging. In 1970 and 1971 he was on the Operations-Technical staff in Houston. He was transferred to Houma, Louisiana, in 1971 as District Manager of the Cased-Hole District and assumed his present position in 1973.

R.C. BRIMAGE is a Sales Engineer for Schlumberger Offshore Services in New Orleans, Louisiana. A native of Dallas, Texas, he graduated from the University of Texas at Arlington in 1970 with a B.S. in Physics. After graduation, he joined Schlumberger in Lafayette, Louisiana. He served as a Field Engineer in Houma, Louisiana and as a Synergetic Engineer in New Orleans before assignment to his present position.

EVALUATION OF VERY LOW-POROSITY CARBONATES (Malossa, Italy)

by

J. Suau, Schlumberger Inland Services, London, England
R. Roccabianca, AGIP, Milano, Italy
M. Cigni, AGIP, Milano, Italy
C. Boyeldieu, Schlumberger Inland Services, London, England
M. Spila, Schlumberger Italiana S.p.A., Milano, Italy

ABSTRACT

Evaluation of very-low-porosity carbonates as found in Malossa is difficult because the porosities are very often nearly the same as the resolutions of conventional logs. Special care must therefore be taken during both data-acquisition and data-processing stages in order to obtain reliable evaluations.

As discussed in this paper, random errors can be eliminated by a suitable logging procedure whereas systematic errors have to be compensated for by carefully normalizing log data with respect to a fixed geological model.

A formation-factor formula well adapted to the Malossa dolomites is proposed.

INTRODUCTION

Geological Information

The discovery of the hydrocarbon deposits of Malossa Field (Fig. 1) is a result of research and exploration activities pursued by AGIP since the fifties.[1] Structures favorable for hydrocarbon accumulations were located by seismic reflection methods. This proved to be the only appropriate prospecting method in the Po valley. The prospecting activities were performed in two phases--an analog phase and a digital phase.

The analog phase was able to define structural characteristics down to an average depth of 2,000 to 2,500 meters (6,600 to 8,200 ft), thus leading to the discovery of the natural-gas deposits in the Pliocene and

Miocene. The digital phase, dating from 1967/68 supplied information on the structural features of very deep strata. This made possible the discovery of the Malossa Field which produced from depths around 5,400 meters (17,700 ft) within the Mesozoic formation of the "Main Dolomite".

Hydrocarbon deposits have also been found at Malossa in younger sediments. Drilling is often complicated by high pressure gradients, especially when the geology is very disturbed.[2]

Production in the Malossa Field is primarily gas, typically with 1 m^3 of oil and 0.1 m^3 of LPG (liquified propane gas) per 1,000 m^3 of gas. Reservoir pressures and temperatures can be as high as 475 atmospheres (7,000 psi) and 150°C (300°F) respectively.

The Formations

The target formations in Malossa Field are almost-pure, massive limestones and dolomites, with little mixing of the two lithologies. Similarly, shales appear mostly as isolated beds. Porosity is generally very low, between 1 and 3 percent. However, streaks with porosities ranging from 5 to 10 percent may be found.

These very-low-porosity formations are of prime interest because of their considerable thicknesses and because they can be produced, probably through the interfaces with the more porous streaks, or through fractures. Quantitative interpretation of these very-low-porosity zones is thus extremely important. Porosities and average values for water saturation are obtainable with reasonable relative accuracies. Quantitatively, the presence of hydrocarbons should be clearly recognized in the more porous zones. In the very low porosities detection can be somewhat more qualitative.

LOG RESPONSES

A typical set of logs in one of these carbonate reservoirs is presented in Fig. 2. The following remarks can be made about the behavior of the logs recorded in these low-porosity formations. Formation density is consistently high; for this reason the count rate of the Formation Density logging equipment is low, and the statistical variations of the measurement are higher than usual. The borehole is generally in excellent condition. However, some rugosity of the wall or small random pad tilts may affect the Near-Detector reading. The Compensated-Neutron-Porosity tool gives an excellent measurement at very low porosities. However, the function former used in the surface equipment to

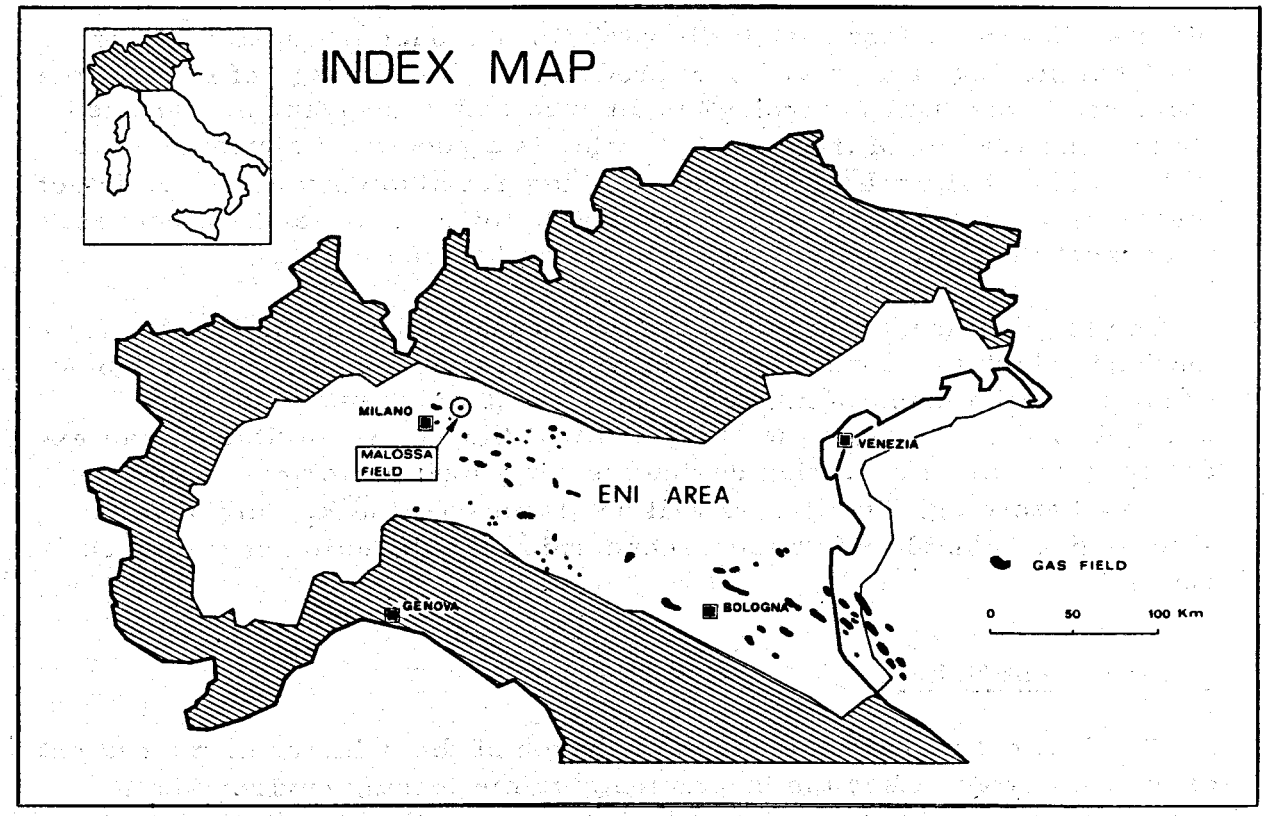

Fig. 1 - Map of north Italy showing location of Malossa Field.

compute an apparent Neutron porosity becomes less accurate, and it is necessary to use the Far- and Near-Detector count-rate values, or their ratio, directly.

The Sonic log provides an excellent measurement of interval-transit time. However, one should remember that in the presence of secondary porosity the interval transit time may be pessimistic and tend to measure only a low, minimum porosity.*

The combination of very low porosities and rather fresh formation waters results in high resistivities, even when the formations are water bearing. Furthermore, porosity variations (within the very-low-porosity range) produce the appearance of a succession of thin beds. The borehole effect on the Induction-log reading is negligible, since the borehole is normally very small and the mud brackish, so that the Induction log gives R_t measurements that would be acceptable except for shoulder

* In heterogeneous formations the Sonic log records the shortest interval transit time (t) available from paths on different sides of the borehole. This shortest value of t tends to be related to a "minimum" porosity which is usually close to the primary porosity.

effects. However, fast resistivity variations reduce the usefulness of the Induction log, and it will only produce a crude average of R_t. On the other hand, the Dual Laterolog* is an excellent measurement of resistivity. The reading of the deep Laterolog is a good first approximation of R_t. The shallow Laterolog and R_{xo} log are also very useful to detect invasion, which is diagnostic of permeable formations, and, of course, to correct the deep-resistivity readings for invasion effects.

The R_{xo} log usually provides a good measurement in the invaded formations (which are normally the more interesting zones), probably because a small amount of mud cake is present which has smoothed the borehole wall. It should also be noted that the R_{xo} sonde itself is an excellent (four-arm) centering device insuring good performance of the shallow Laterolog. Finally, as will be discussed, the R_{xo} log may be able to give valuable information concerning the detection of fractured zones.

Measurement Noise

We shall define noise as any disturbance of the primary measurement originating from either the instruments or the logging environment, in other words any effect causing a departure from the simple interpretation model generally used. We shall also distinguish between two kinds of noise that will be identified as A.C. and D.C. A.C. noise is "high frequency" (i.e., rapidly variable in comparison to the sequence of formations) while D.C. noise is of a nearly-constant nature (i.e., practically constant for a logging run). Examples of A.C. noise are statistical variations in radioactive tools and the variable part of borehole effect on pad tools or tools sensitive to their position in the hole. Examples of D.C. noise are effects of borehole diameter (when nearly constant), mud weight, pressure, temperature, uncertainty on matrix parameters, slight miscalibrations of the tools (due to pad wear on the FDC* tool, for example), electronic bias of some components, etc.

Each of the two kinds of noise is treated differently. A.C. noises are eliminated by improving individual recordings of each log independently. D.C. noises can all be treated together. Assuming we have a good geological model for some of the formations (say the very low-porosity, clean limestones) we can normalize the logs to this model. Total D.C. noise is thus cancelled without particular regard to its individual components or their origins.

The bases of the proposed method are thus the following:

---

* Mark of Schlumberger.

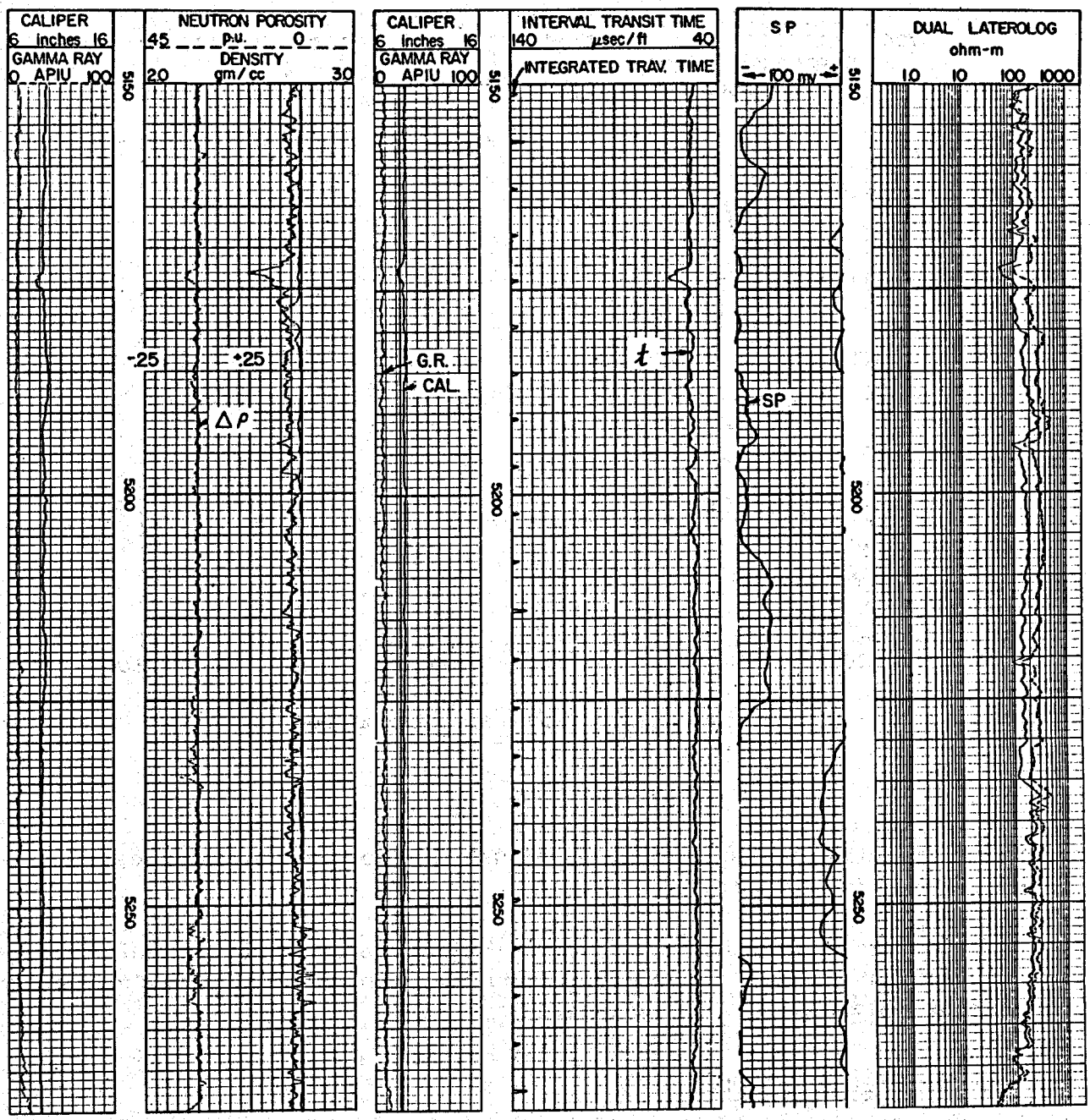

Fig. 2 - A typical set of logs from Malossa Field.

a) A.C. noise is minimized by improving the quality of the logs.

b) D.C. noise is normalized out by comparison to a fixed geological model.

In a nutshell, we postulate that the logs can provide results with relative accuracies (relative to the model to be used) much better than

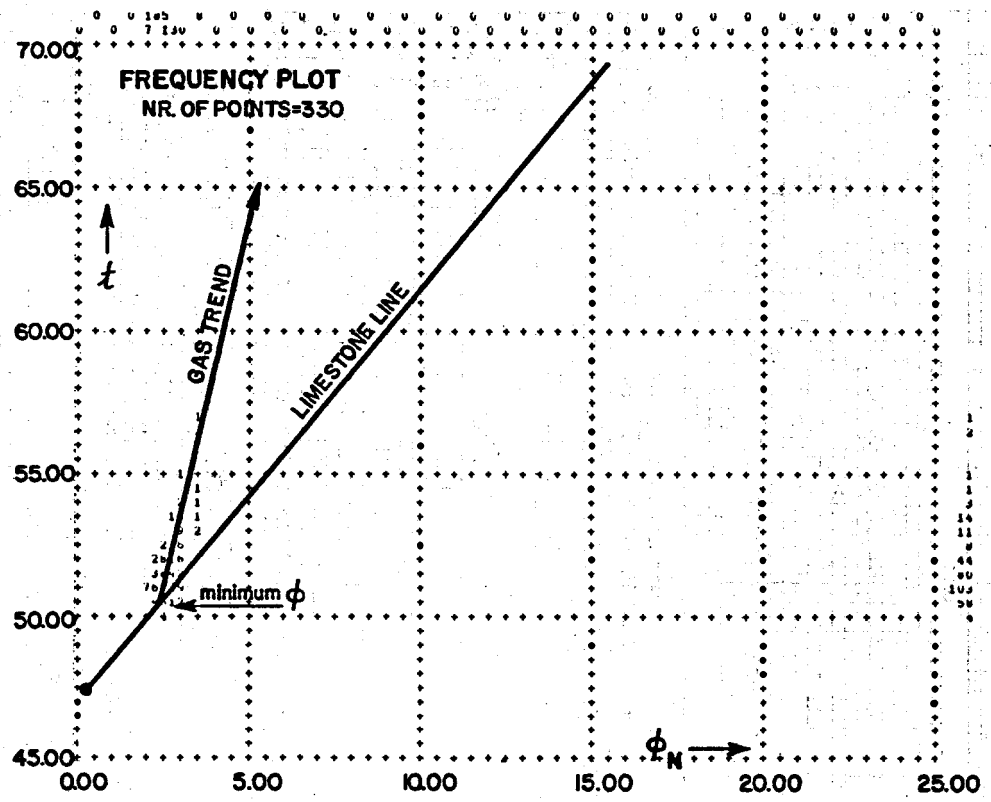

Fig. 3 - Frequency crossplot of Sonic interval transit time versus Neutron porosity.

their own absolute accuracies. Obviously the normalization process needs to be very accurate.

Before going into the details of the method we should investigate hydrocarbon effects. These are not considered to be noise, but they can have important effects on the logs.

Hydrocarbon Effects

In the Malossa area, the hydrocarbons are gas and very light oil; as a result, the hydrocarbon effects on porosity logs can be important and should be corrected carefully. This effect can be predicted from the tool responses and particularly from their depths of investigation in very low porosities.

The Sonic log, which generally has a very shallow depth of investigation, has one even more shallow in the case of gas, and its response can be expected to remain almost unaffected by the gas. The depth of investigation of the Density log is more shallow than usual because of the low porosity, and this tool should also exhibit very little gas effect

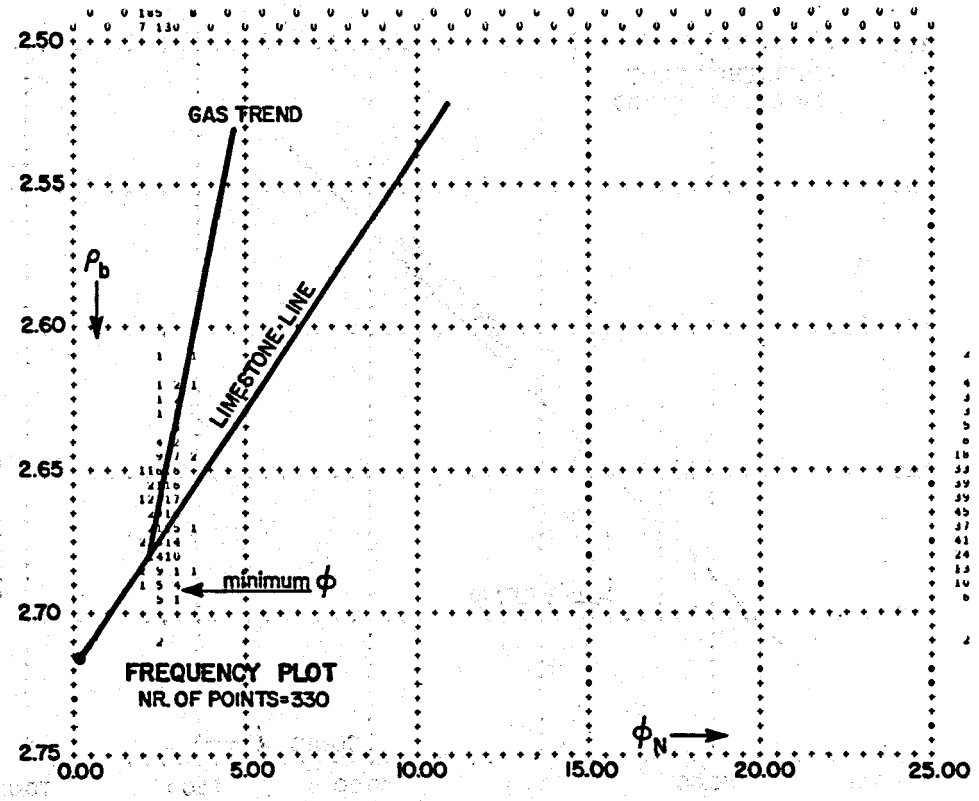

Fig. 4 - Frequency crossplot of bulk density from Density log versus Neutron porosity.

except at the higher porosities. On the other hand, the Neutron log investigates considerably deeper under these conditions and should be far more affected by gas than the other porosity logs.

Such behavior can be verified on crossplots of the three porosity logs plotted in pairs in gas-bearing zones. The minimum porosity will normally plot as a cluster of points close to the lithology line and increasing porosity will define a trend, which in water-bearing formations follows the lithology line; for example, in clean limestones the points would follow the limestone line. Gas effects on the porosity logs being crossplotted will cause the points to follow a different trend.

Figs. 3, 4, and 5 are crossplots in a gas zone in a Malossa limestone. Fig. 3 is a Sonic-Neutron crossplot; it suggests no gas effect on the Sonic log, but a large effect on the Neutron log. The apparent hydrogen index of the formation at maximum porosity seems to be about half its value in a water-filled pore space. Fig. 4 is a Density-Neutron crossplot which suggests little gas effect on the Density value, but a strong effect on the Neutron. Fig. 5, which is a Density-Sonic crossplot, is not as clear; quite a few points tend to plot along the limestone line

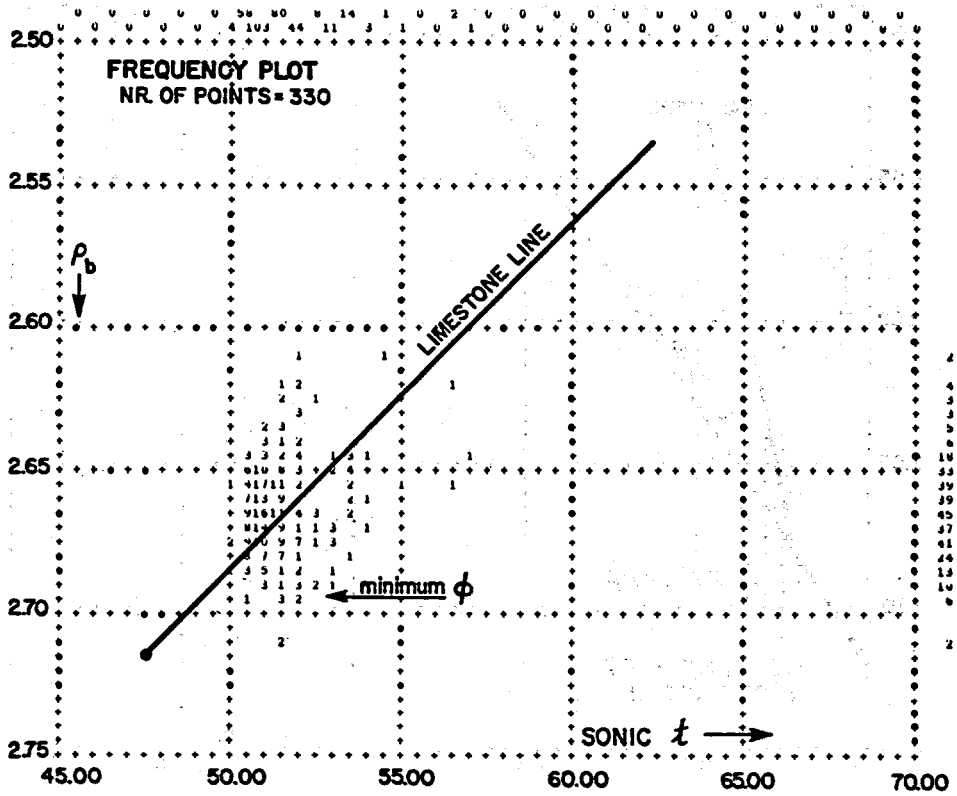

Fig. 5 - Frequency crossplot of bulk density from Density log versus Sonic interval transit time.

(indicating no gas effect). However, another trend is indicated that could be due to either gas effect on the Density log at higher porosities, or to some secondary porosity, or to a combination of the two.

LOG IMPROVEMENT TECHNIQUES

Minimization of A.C. Noise

A.C. noise includes, in particular, statistical variations in radioactivity measurements and local variations of borehole effect. Both affect mostly the Density log.

In order to reduce statistical variations, logging speed must be reduced or several independent runs must be averaged. The solution used in Malossa is to average two runs recorded at the slow speed of 900 ft/hour (275 m/h) instead of the 1,800 ft/hour (550 m/h) commonly used over the most interesting zone. The usual repeat run is also made over this particular interval and, if necessary run over all the formations of interest.

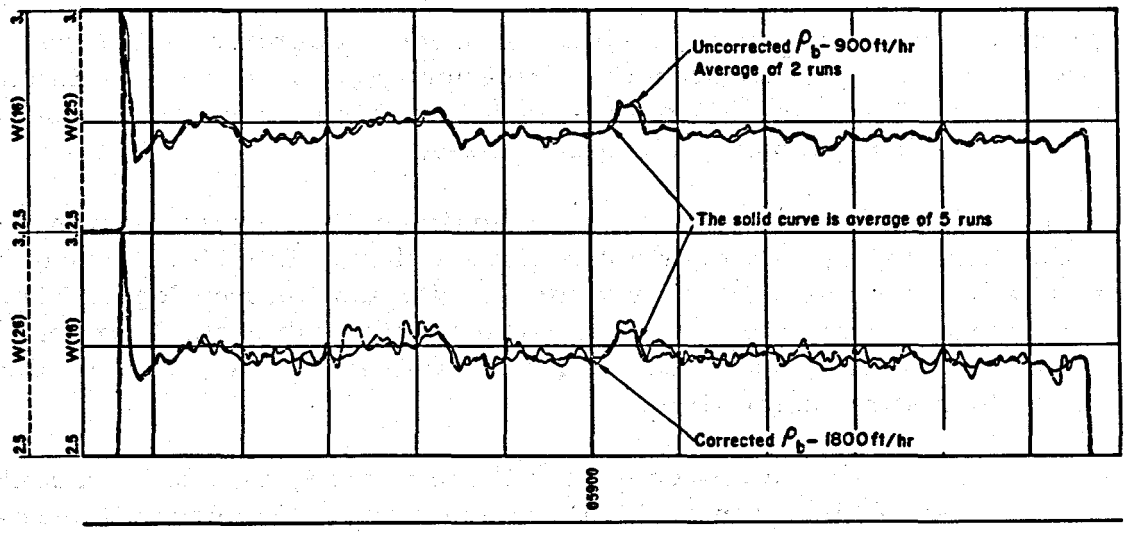

Fig. 6 - Illustration of curve improvement by averaging repeat runs and by reducing logging speed.

Local variations of pad position have been shown to affect mostly the short spacing, with little effect on the long spacing. Thus, in these types of hard formations, since the borehole is generally good and the mud cake thin, local variations in the short-spacing measurement are not related to mud-cake thickness. In this case, therefore, it is better to use the Density log uncompensated.

The combined effect of these special procedures can be appreciated on Fig. 6. Two sets of curves correspond to curves run at two different recording speeds, 900 ft/hr (275 m/h) and 1,800 ft/hr (550 m/h). In each case, the solid curve is an improved measurement made by averaging five different runs. It is obvious that, unless one is interested only in an average measurement, a standard Density run produces unacceptably high statistical variations; the upper dashed curve obtained by averaging two uncompensated Density logs recorded at low speed is nearly perfect as compared with the average of 5 runs (upper solid curve).

The need for averaging the Neutron-porosity measurement is much less stringent, but since the Neutron and Density are run in combination, this is obtained as a bonus. On the other hand, as explained above, because of the low degree of accuracy of the function former around the zero-porosity value, the Far- and Near-detector readings and their ratio are used to compute an improved Compensated Neutron porosity value.

Log Normalization

In theory, the geological model is an idealized average Malossa well.

In practice, however, the normalization process operates mainly by comparisons of log behavior in the formation types occurring statistically more often: very-low-porosity, clean limestones, and, to a lesser degree, very-low-porosity, clean dolomites.

Only the porosity logs have to be normalized. Moreover, it was found that the Sonic log usually does not require a shift. Therefore, it can be used to aid in the normalization of the Density and Neutron logs. The normalizing process (i.e., the comparison of the subject well or logging run to the geological model) can be made using either one, two, or three porosity logs at the same time.

The normalization of any one of the three porosity logs to its model is done by use of histograms of log-reading amplitudes versus the frequency of occurrence of the different amplitudes. For a given well, the histogram is made over the clean, very-low-porosity limestone or dolomite interval where water saturation can be expected to be high. To create the model, histograms are averaged over the field. Logs of individual wells are then normalized by matching their histograms with that of the model for that log. This is very easy, but since the result will be sensitive to porosity variations around the field it should not be expected to yield a relative accuracy better than 1 to 2 p.u. (porosity-percentage units). This is why normalization on the basis of a single log is never used in Malossa.

A better method is to compare the logs in pairs, by the use of crossplots. Examples of this type of normalization are given in Figs. 7, 8, and 9. Each figure presents the crossplot before and after the required shift. Since the Sonic log normally does not require any shift, the Sonic-Density and Sonic-Neutron plots will produce directly the necessary shifts for the Density and Neutron logs. This method is still somewhat sensitive to variations of lithology but should be able to provide a relative accuracy of the order of 1 p.u. Two-porosity crossplots are a kind of "quick-look" normalization.

Finally, a comparison with the model can be made using all three porosity logs at the same time. This is done by representing the apparent porosity at each particular depth as a three-dimensional vector, the components of which are the Density-, Neutron-, and Sonic-log readings. This vector is compared to the model, also represented as a vector. Various shifts are applied to the Density- and Neutron-log data, and a correlation function is computed between the model distribution and the distribution on the log. The maximum correlation found defines the optimum shifts for Neutron and Density logs. Three-porosity-log normalization is used systematically to provide final results. These lithological models have also been used with success in other very

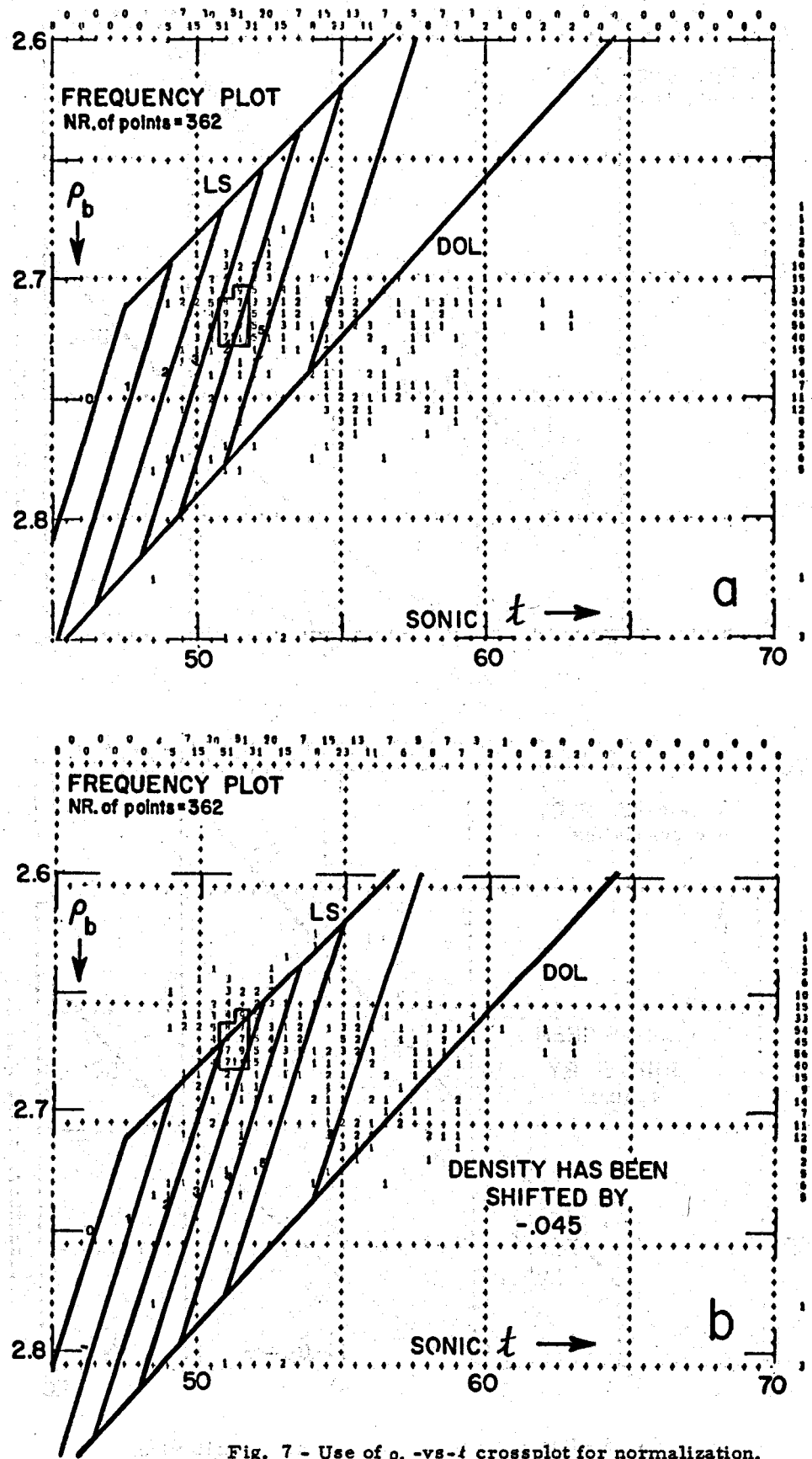

Fig. 7 - Use of ρ_b-vs-t crossplot for normalization.

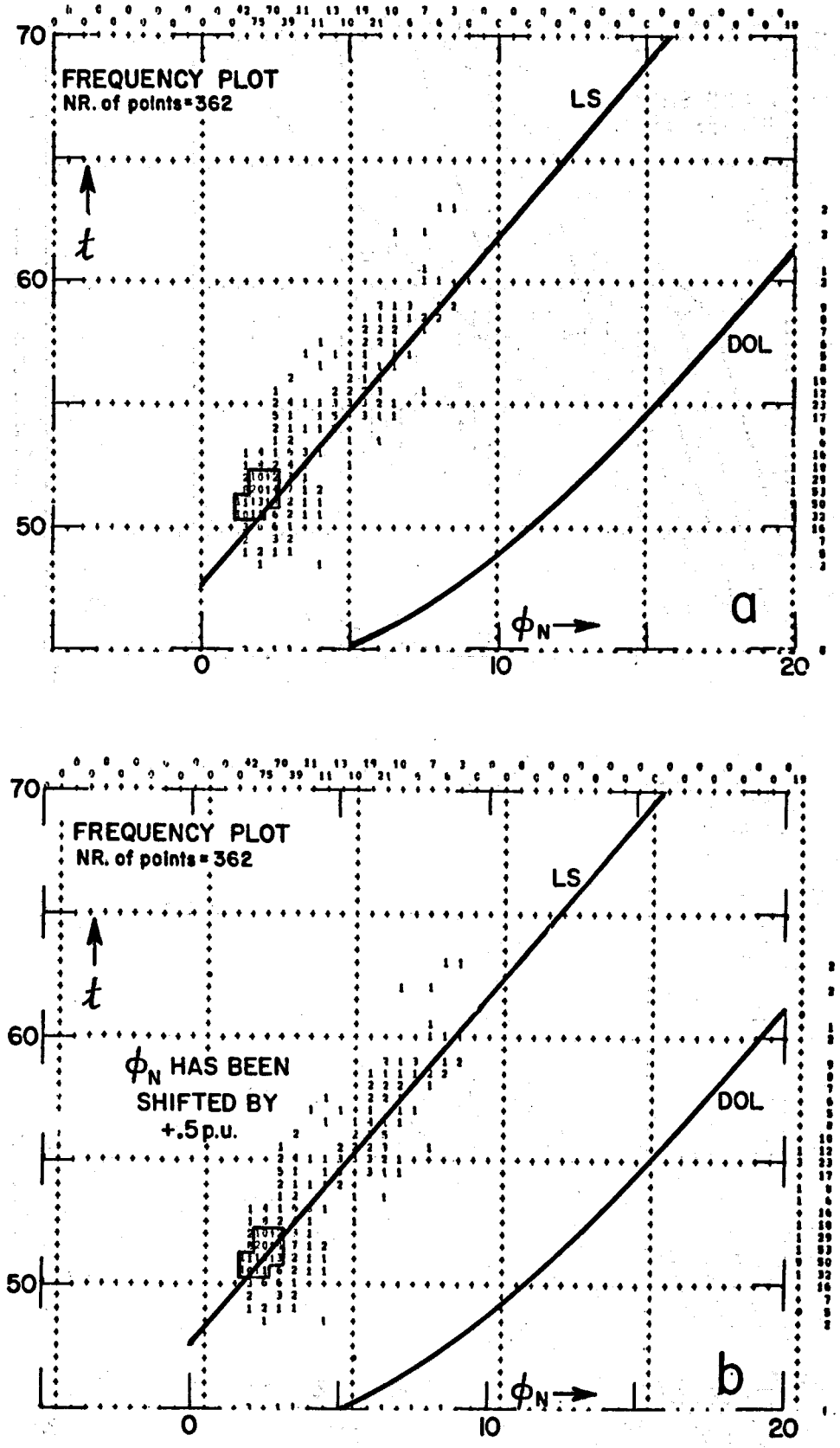

Fig. 8 - Use of t-vs-ϕ_N crossplot for normalization.

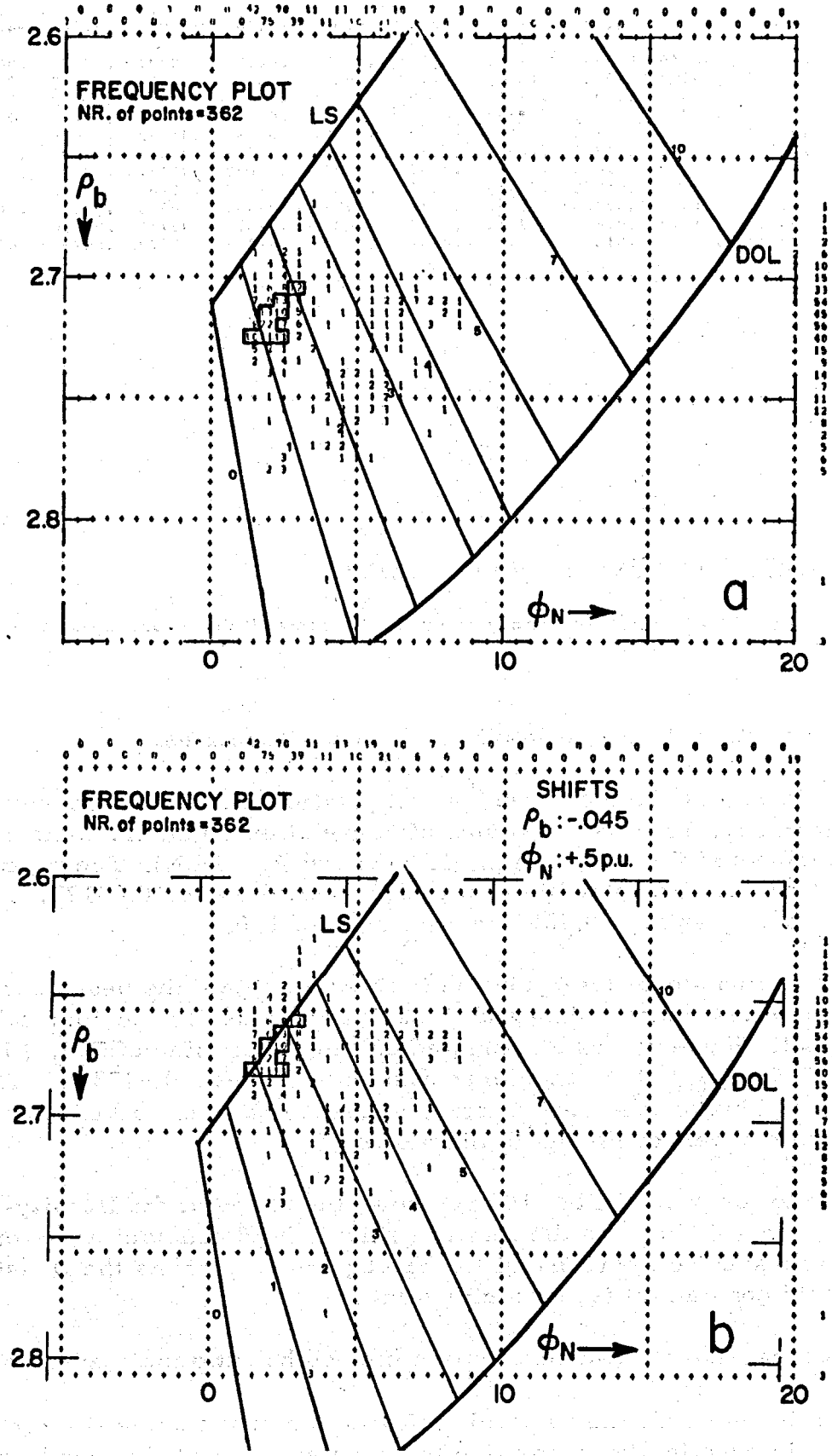

Fig. 9 - Use of ρ_b-vs-ϕ_N crossplot for normalization.

RHOB \ PHIN	5.00	4.00	3.00	2.00	1.00	0.00	-1.00	-2.00	-3.00	-4.00	-5.00
0.050	.03540	.06944	.09508	.11780	.27233	.13929	.02309	.00807	.00521	.00174	.00124
0.040	.04247	.08353	.12344	.15478	.41129	.20282	.03605	.01118	.00722	.00286	.00219
0.030	.04590	.10053	.13982	.18116	.54362	.27761	.04674	.01430	.00892	.00360	.00249
0.020	.04647	.09947	.14475	.19884	**.63172**	.34398	.06070	.01648	.01082	.00436	.00255
0.010	.04574	.08541	.13811	.19368	.62608	.39061	.06536	.01652	.01006	.00383	.00240
0.000	.03587	.06878	.11321	.16861	.53850	.39148	.06332	.01613	.00792	.00356	.00167
-0.010	.02630	.05098	.08606	.13411	.39977	.34249	.05829	.01441	.00572	.00268	.00110
-0.020	.01837	.03181	.05576	.08914	.26338	.26512	.04483	.01262	.00466	.00238	.00098
-0.030	.01159	.01953	.03406	.05792	.15344	.17590	.03455	.00945	.00348	.00171	.00073
-0.040	.00734	.01119	.02198	.03261	.08923	.10377	.02370	.00731	.00290	.00137	.00071
-0.050	.00417	.00668	.01305	.02030	.05315	.06100	.01442	.00572	.00237	.00127	.00055

SHIFTS ON RHOB 0.020 ON PHIN 1.0 CORR COEFF 0.631724

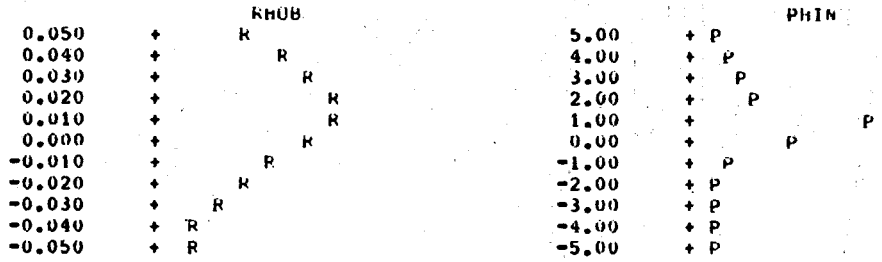

SHIFTS ON **RHOB 0.015** ON **PHIN 0.9** CORR COEFF **0.647394**

Fig. 10 - Printout illustrating normalization using all three porosity logs.

different parts of Italy and in other European countries.

Fig. 10 is an example of such a computation for a Malossa well. The printout in Fig. 10 lists the values of correlation functions computed for various shifts in the values of ρ_b (RHOB) and ϕ_N (PHIN). The maximum correlation value in the table at top is the boxed value, 0.63172, corresponding to a ρ_b shift of 0.020 and a ϕ_N shift of 1.0.

A two-dimensional interpolation is made to obtain the best shifts for the Density and Neutron data and a maximum value for the correlation coefficient. These values are printed on the bottom line of Fig. 10 as $\Delta\rho_b = 0.015$, $\Delta\phi_N = 0.9$, and correlation coefficient = 0.647394. This maximum value of the correlation coefficient is a measure of how closely the subject well conforms to the model.

In the lower part of Fig. 10 are shown the shape of the Density-shift correlograms (R plot) as the Neutron shift is held constant at its optimum value and the Neutron-shift correlogram (P plot) as the Density log is held constant at its optimum value.

This three-porosity normalization method has two main advantages:

a) by using all the available information at the same time it is practically insensitive to small variations of porosity or lithology.

b) it is completely free of subjective bias.

As a result its relative accuracy is considered to be of the order of 1/4 p.u.

THE FORMATION FACTOR-POROSITY RELATION

In very low porosity the cementation factor, m, is expected to be considerably higher than 2 and to become, in fact, a function of porosity. In Malossa, present experience suggests the following rules:

1) In pure limestones the standard Archie $F_R - \phi$ (resistivity formation factor-porosity) formula with m = 2 has been found to apply remarkably well down to the minimum porosity.

2) In the very-low-porosity dolomites the cementation exponent, m, was suspected to be higher than 2. A statistical study made in a water-bearing dolomite of one of the early Malossa wells suggested to AGIP the following formula for the Malossa dolomites:

$$m = 1.94 + 0.0062/\phi$$

In the very-low-porosity range, this is reasonably equivalent to m = 2.21.

This result is illustrated in Figs. 11a and 11b where the apparent value of the resistivity formation factor (F_R) is plotted against porosity (ϕ) on a log-log scale.

The value of F_R is obtained from the deep-investigation resistivity tool assuming S_w = 100 percent and R_w = 0.1 ohm-m.

In Fig. 11a porosity is obtained from the CORIBAND* interpretation (after the required shifts on the porosity logs to conform to the present Malossa dolomite model).

In Fig. 11b porosity is derived from the Sonic log.

The following remarks can be made:

1) The points on Figs. 11a and 11b can be divided into two separate groups. The first group includes a large majority of points which fall between the line for m = 2 and the curve corresponding to the "Shell Formula" suggesting as an average the proposed "AGIP Formula".

---

* Mark of Schlumberger.

The second group is much more scattered and falls below m = 2, as low as m = 1.6; it is believed that these correspond to fractured zones where such low values of m are to be expected.[3-5] This last interpretation is strongly supported by the comparison of Figs. 11a and 11b. The Sonic log, which largely ignores the fractures, exaggerates the effect.

2) On Fig. 11a there is a rather large scatter of points on either side of the AGIP line. This is attributed to the poorer quality of the logs (based on present standards): R_t was from an Induction log, the FDC was run too fast, and the CNL* ratio was not available in this early Malossa well. Unfortunately, it is still the only well containing a proved 100-percent water-bearing dolomite. Should we obtain another water-bearing dolomite in a new well, a much better plot should be obtained. It is worth noting that Fig. 11b where Sonic porosity is used, gives a much better grouping in the non-fractured formation.

QUICK-LOOK INTERPRETATION

The Density-Neutron-Gamma Ray log, even before normalization, will usually give a quick-look definition of the gross lithology, identifying clean limestones, dolomites, and shale beds. Next, a qualitative detection of the presence of hydrocarbon is to be made. A rather good method is to crossplot the deep Laterolog and Sonic readings in any reasonably clean and consistent zone. An example is given in Fig. 12. Since R_w is reasonably constant at about 0.1 ohm-m, the water lines can be drawn for either limestone or dolomite. The Density-Neutron quick-look will usually suggest which matrix model is applicable.

In moderately porous zones the presence of gas will often be clearly indicated (see Fig. 12). One should remember, however, that apparent saturation obtained this way may be quite pessimistic due to the partial inability of the Sonic log to respond to secondary porosity. This should not prevent qualitative detection however. In very tight zones, gas detection will be more difficult and should be considered on a statistical basis. Finally, gas detection by the Laterolog-Sonic plot should be confirmed by a more detailed study of the Density-Neutron and Sonic-Neutron crossplots in the same zones; the Neutron log should exhibit a strong gas effect.

Qualitative permeability information may be obtained from the Dual Laterolog-R_{xo} tool, the presence of an invaded zone being, of course,

---

* Mark of Schlumberger.

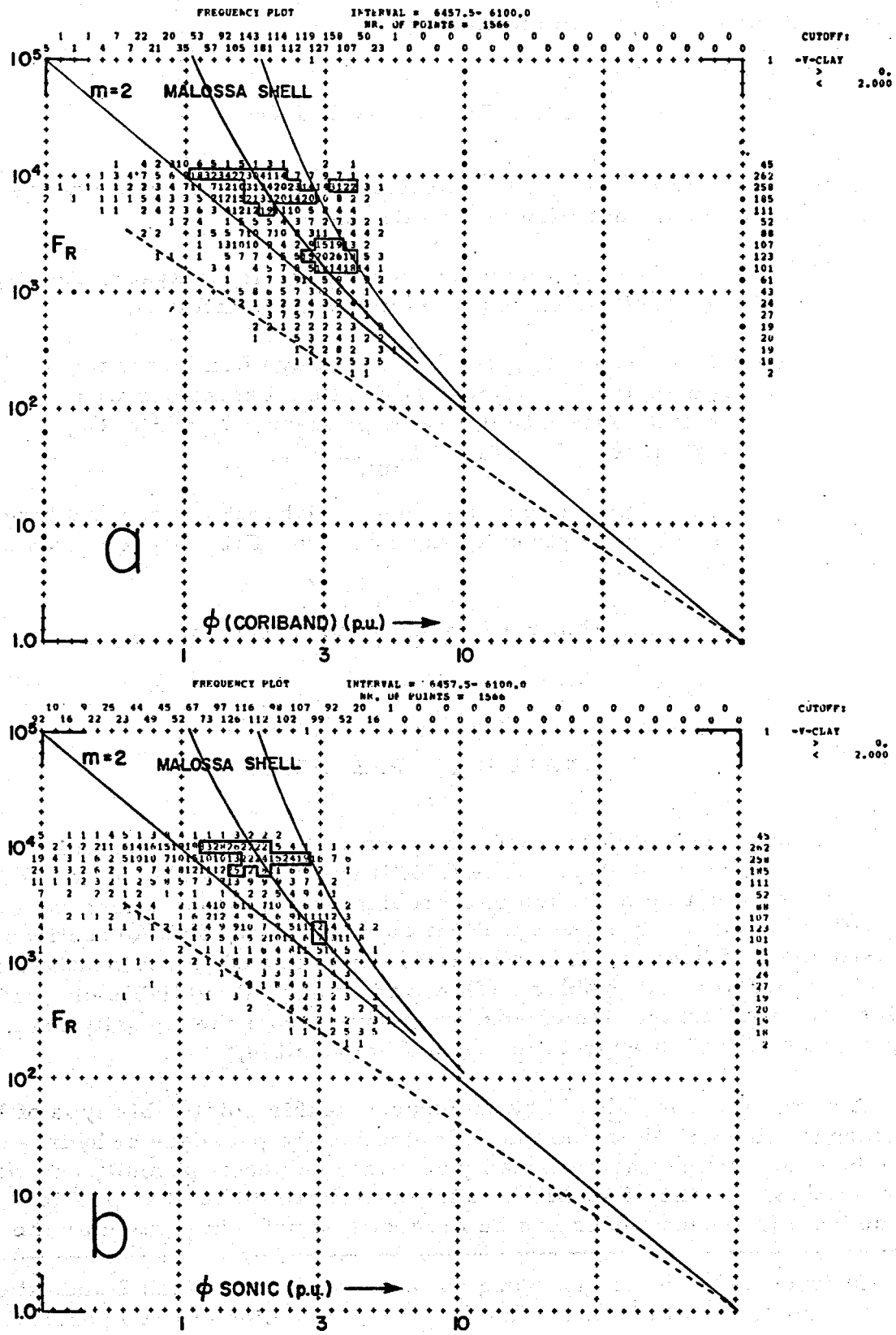

Fig. 11 - Frequency crossplot of F_R from deep-resistivity log versus a) ϕ from CORIBAND processing and b) ϕ from Sonic log.

the indicator of appreciable permeability.

FRACTURE DETECTION

Although fractures cannot be detected with absolute certainty their presence may be deduced from the following:[3-5]

1) Secondary Porosity Index: the Sonic porosity is systematically less than Density-Neutron porosity over the interval.

2) The Dual Laterolog-R_{xo} combination may often be the most powerful detector. The Deep and Shallow Laterologs will tend to be parallel, with a LLd/LLs ratio around 2, while R_{xo} reads much less and close to* $R_{mf}/\phi^{1.6}$.

3) The HDT** Dipmeter curves often show breaks in the fractured zone; this effect is strongly enhanced by a FIL**-type presentation.[6]

4) The $\Delta\rho$ curve is also very sensitive to fractures.

FINAL INTERPRETATION

Detailed interpretation should be attempted only after careful normalization of the porosity logs. The CORIBAND process should be used. There should not be too much of a problem in limestone where the Gamma-Ray log normally is an excellent clay indicator, and corrections are easily made if necessary. Dolomites, which are often radioactive, present a more difficult problem. However, using all available clay information, and particularly the crossplots derived from the porosity logs, a good quantitative interpretation should be possible.

A word of caution should be introduced at this point: this type of log interpretation will do a good job of detecting the presence of hydrocarbons and computing reasonably accurate values of porosity and water saturation. On the other hand, it is much more difficult to predict whether the hydrocarbons can be produced or not. In particular the

---

* In fractured zones m is expected to be much lower than 2 and often is around 1.6; on the other hand, S_{xo} should be close to 100 percent.[3-5]

** Mark of Schlumberger.

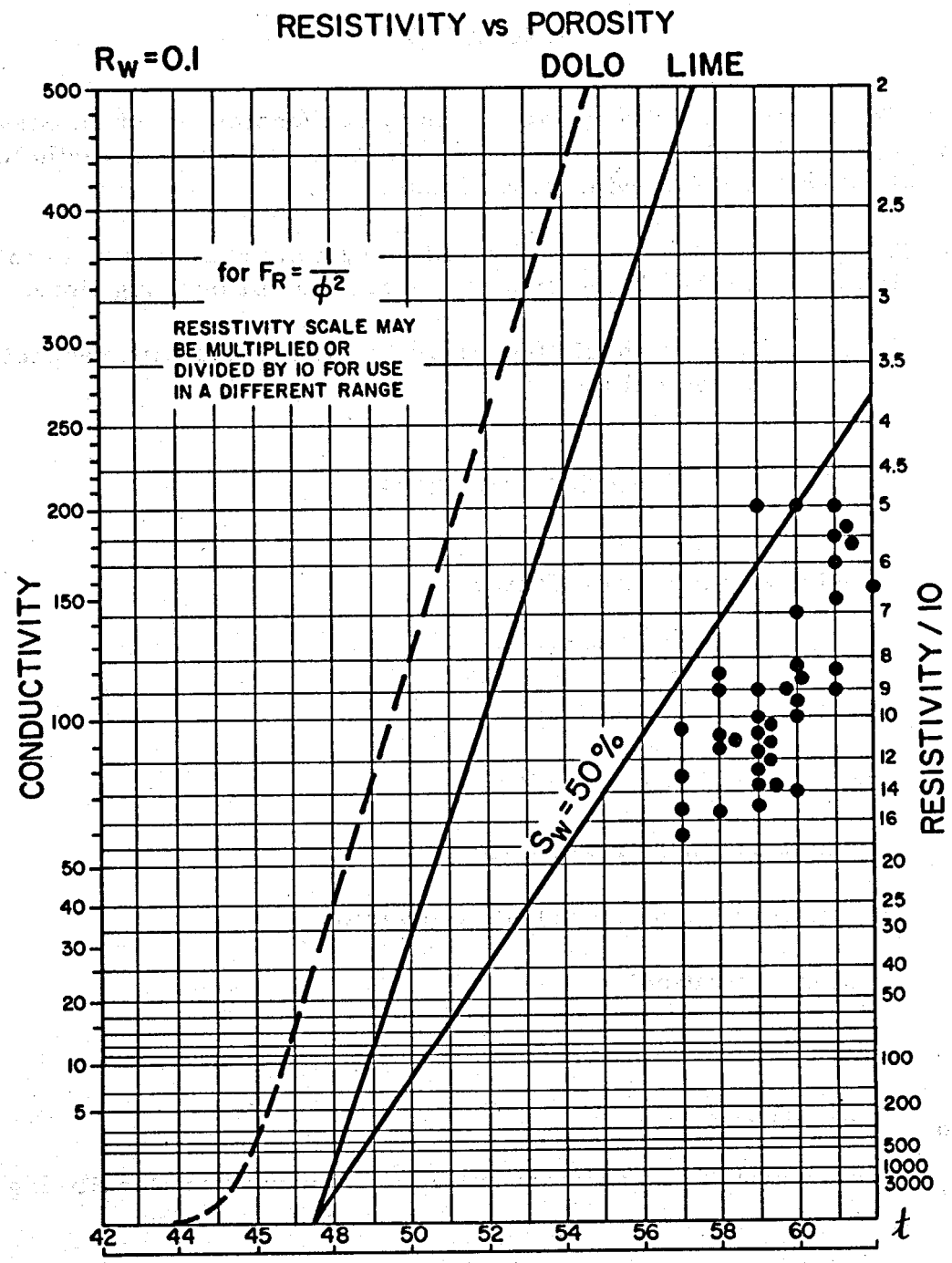

Fig. 12 - Crossplot of deep-Laterolog resistivity versus Sonic interval travel time.

effect of extensive damage in the formation is very difficult to assess. Local experience normally will fill the gap.

An example of computer-processed interpretation in a Malossa well is given in Fig. 13. The section corresponds to the logs of Fig. 2. The computed logs produced independently by AGIP and Schlumberger are presented together.

CONCLUSION

Log interpretation in very low-porosity carbonates is not an easy problem. Consistent and reasonably accurate results can nevertheless be obtained with the following provisions:

1) The quality of logging data should be optimized as has been indicated, possibly at the expense of some additional rig time.

2) The porosity logs should be carefully normalized with respect to a local geological model.

NOMENCLATURE

F_R	resistivity formation factor
m	exponent in $F_R - \phi$ relation
R_{mf}	mud-filtrate resistivity
R_t	true formation resistivity
R_w	formation-water resistivity
R_{xo}	resistivity of zone flushed by invasion
S_w	water saturation
t	Sonic interval transit time
ρ_b	bulk density
$\Delta\rho$	correction made automatically on Compensated Density log
ϕ	porosity
ϕ_D	porosity from Density log
ϕ_N	porosity from Neutron log

* The symbols used in this paper conform in the main to the SPE-SPWLA Revised Standard Letter Symbols and Computer Symbols for Well Logging and Formation Evaluation--1975, published in The Log Analyst, November-December issue, 1975, pages 45-59.

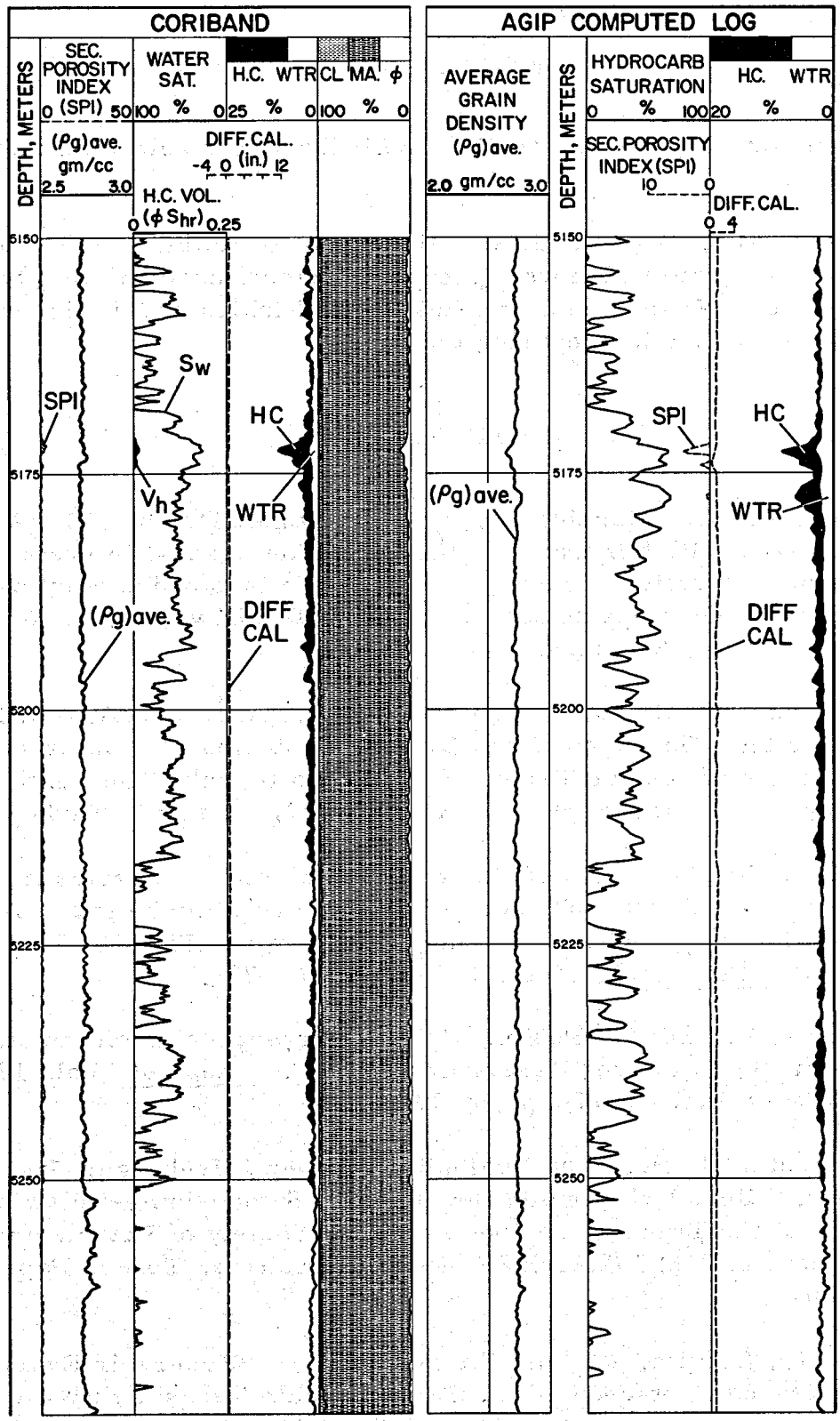

Fig. 13 - Computed logs in Malossa well produced independently by Schlumberger and AGIP.

ACKNOWLEDGMENT

The authors are very grateful to AGIP for kindly releasing the pertinent data.

Our special thanks go to J. C. Minne who wrote the porosity normalization program which we consider extremely useful in this type of interpretation. We also wish to thank E. E. Finklea and F. Segesman for their assistance in preparing the paper.

REFERENCES

1. Groppi, Dr. G., Muzzin, Dr. Ing. A., Vaghi, Dr. Ing. G. (AGIP S. p. A. --Attivitá Minerarie): "Erdolfeld Malossa--Die erste Kohlenwasserstoffgewinnung aus dem tiefen Mesozoikum unter der Po-Ebene", Gemeinschaftstagung OGEW/DGMK vom 4, bis 6 (October 1976), Salzburg.

2. Bongiorni, D., Crico, V., and Fenati, D. (AGIP S. p. A. --Attivitá Minerarie): "Geophysical and Drilling Problems Encountered in the Exploration of Deeper Structures in the Po Basin", The Tenth World Energy Conference (September 19-23, 1977), Istanbul, Turkey.

3. Aguilera, R.: "Analysis of Naturally Fractured Reservoirs from Conventional Well Logs", Society of Petroleum Engineers of AIME Rocky Mountain Regional Meeting (1975), Paper No. SPE 5342. Also in J. Pet. Tech. (July, 1976), pp, 764-772.

4. Aguilera, R. and Van Poolen, H. K.: "Current Status on the Study of Naturally Fractured Reservoirs", The Log Analyst, Vol. 18, No. 3 (May-June, 1977), pp, 3-23.

5. Neustaedter, R. H.: "Log Evaluation of Deep Ellenburger Gas Zones": "Deep Drilling and Development Symposium--Delaware Basin" of the Trans-Pecos Section of the Society of Petroleum Engineers of AIME (March 28, 1968), Monahans, Texas, Paper No. SPE 2071.

6. Beck, J., Schultz, A., and Fitzgerald, D.: "Reservoir Evaluation of Fractured Cretaceous Carbonates in South Texas", SPWLA 18th Annual Logging Symposium (June 5-8, 1977), Houston, Paper M.

ABOUT THE AUTHORS


SUAU


ROCCABIANCA

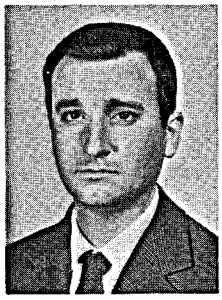
CIGNI


BOYELDIEU


SPILA

JEAN SUAU is in charge of Interpretation Development for Schlumberger Europe. He graduated from École Polytechnique in Paris in 1950, and he received his MS-EE degree from Columbia University in 1964. He joined Schlumberger in 1950, and served in the Middle East, the Far East, and South America before coming to Schlumberger-Doll Research Center in 1961. There he became Head of the Interpretation-Research Department. Returning to France in 1971, he remained in interpretation-research work at Clamart. Since 1974 he has been located in London.

RUFFO ROCCABIANCA is Chief Log Analyst in AGIP's Log Interpretation Department. He graduated from Istituto Minerario of Massa Marittima, Italy, in 1947. After about 5 years in Australia with Australian Iron and Steel of Port Kembla he returned to Italy in January, 1956, and joined AGIP, where he was assigned to the Log Interpretation Department. Since 1968 he has regularly been giving training courses on well-log interpretation to geologists and engineers of AGIP and AGIP affiliates. He has been a member of the SPWLA since 1967.

MICHELE CIGNI is Senior Log Analyst at the Interpretation and Development Section of the AGIP Subsurface Department. He graduated in 1956 from the mining high school of Massa Marittima, and was employed by AGIP Mineraria as Wellsite Geologist in the same year. In 1959 he joined the AGIP headquarters in Milano as Log Analyst. He assumed his present position in 1969.

C. BOYELDIEU is at present Marketing Manager for Schlumberger Europe. He graduated in 1951 from the Institut Industriel du Nord in Lille, took a degree in Metallurgy from the Institut Supérieur des Matériaux in Paris. He later attended the École Nationale Supérieure du Petrole where he received an Engineering degree in 1955. He then joined Schlumberger holding various positions from Field Engineer to District Manager in Algeria, Germany, Austria, and Libya. In 1962 he joined the Sales Interpretation group in Paris and was later Sales Engineer in North Europe and Libya. From 1971 until recently he was Marketing Manager for Schlumberger in South America.

MASSIMO SPILA is a Schlumberger Sales Engineer in Milano, Italy. He obtained a degree in Electrical Engineering at the University of Rome in 1956. He joined Schlumberger in November, 1956, and worked as Field Engineer and then as Center Manager in many countries. Since 1971 he has worked as Sales Engineer in Paris, Venezuela, and now in Italy.

WELL LOG INTERPRETATION OF SHALY SANDS WITH THE PROGRAMMABLE CALCULATOR

by

Kenneth D. Thompson
Schlumberger Well Services, Corpus Christi, Texas

ABSTRACT

Algorithms for the programmable calculator are described for level-by-level, open-hole, shaly-sand analysis for use with three log combinations: 1) resistivity and Sonic logs only; 2) resistivity, Formation Density, Compensated Neutron, and Gamma Ray logs only; and 3) resistivity, Sonic, Formation Density, Compensated Neutron, and Gamma Ray logs. The SP may also be used as a shaliness indicator.

An algorithm for cased-hole logs is also described, which uses the Dual-Spacing Thermal-Decay-Time log and a Gamma-Ray log. The interpretation utilizes the dual-water model of shaly sands. Level-by-level values of water saturation, porosity, and bulk-volume-shale fraction are generated from the calculator programs.

Both open-hole and cased-hole example logs are analyzed and interpreted. Results are compared with computer-processed interpretations made on the same wells. The calculator interpretations do not provide certain features of the computer products, nor are they as accurate. However, they enable the well operator to make expedient decisions on core points, formation-test points, and pipe setting.

INTRODUCTION

There has been much interest in the new programmable pocket calculators for use in log interpretation.[1] They offer the log analyst the promise of more accurate and comprehensive well evaluations completed with less time and effort than was previously possible manually or with charts.

This paper describes algorithms for the use of the programmable calculator in shaly sands for several log combinations. The algorithms are designed for calculators with 224-step program capacity. Programs can be stored on magnetic strips, eliminating the need to manually reprogram the machine each time the same calculation is repeated. The 100-step variety of calculator can handle resistivity-Sonic combinations, and can do the more complex algorithms if the computation is broken down into

separate subprograms. In the development of these programs, a Texas Instrument SR-52 was used, but a Hewlett-Packard HP-67 would have served as well.

Because the manner of use differs in detail for different calculators, we shall make no attempt to explain procedures of programming the algorithms to be described. When the reader has familiarized himself with the use of his calculator, he should be able to devise his own programs from the flow charts given.

The algorithms to be described are:

for three open-hole log combinations:

- Resistivity and Sonic logs
- Resistivity, Density, Neutron, and Gamma-Ray logs
- Resistivity, Sonic, Density, Neutron, and Gamma-Ray (and/or SP) logs

for a cased-hole log combination:

- Dual-Spacing Thermal-Decay-Time and Gamma-Ray logs

ALGORITHMS FOR OPEN-HOLE LOGS

Sonic and Resistivity Logs

Even a smaller calculator can compute Sonic porosity (ϕ_{SV}) and apparent water resistivity (R_{wa}) and water saturation (S_w) from an Induction-Sonic combination. Where necessary, determination of water resistivity (R_w) from the SP and true formation resistivity (R_t) from a Dual Induction-Laterolog** or Dual-Laterolog combination can be done by calculator in separate programs. Algorithms for these computations were presented by Bateman and Konen in Ref. 1.

---

* The symbols used in this paper conform in the main to the SPE-SPWLA Revised Standard Letter Symbols and Computer Symbols for Well Logging and Formation Evaluation--1975, published in The Log Analyst, November-December issue, 1975, pages 45-59.

** Mark of Schlumberger.

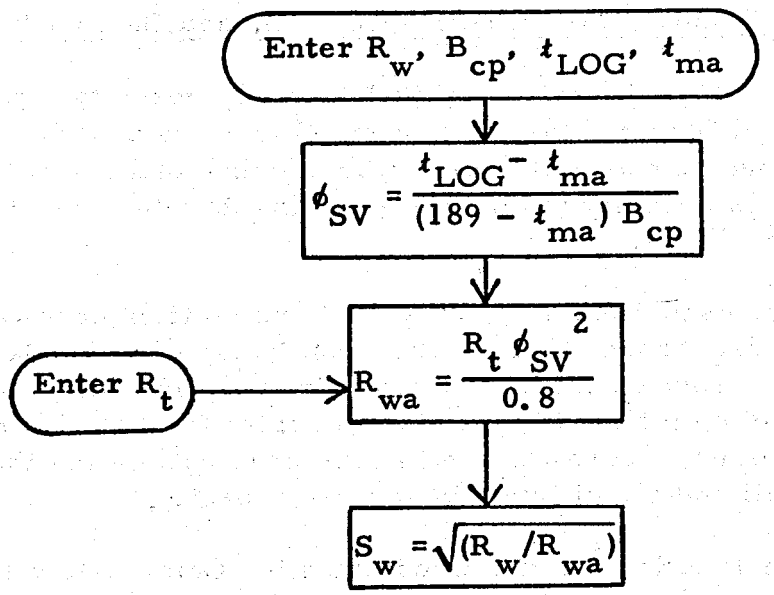

Fig. 1 - Flow chart for computation of ϕ_{SV}, R_{wa}, and S_w from Resistivity, Density, Neutron and Gamma Ray logs.

However, for a "quick-look" R_{wa} approach separate programs are often not necessary. The flow chart of Fig. 1 illustrates the technique, where

B_{cp} = correction factor for lack of compaction in relation for Sonic-log porosity

t_{LOG} = interval transit time in microseconds per foot from Sonic log

t_{ma} = interval transit time of the rock-matrix material

ϕ_{SV} = porosity from Sonic log

A value of R_w is not needed as an external input when nearby water zones exist. In this case, begin the analysis with a water zone. Calculate ϕ_{SV} from t_{LOG}, B_{cp}, and t_{ma}, enter R_t, and calculate R_{wa}; then enter the R_{wa} value in the display register and store it as R_w.

A value of B_{cp} can be chosen to normalize ϕ_{SV} so that the R_{wa} values calculated in wet sands can be made to equal the R_w values from local knowledge or experience. If B_{cp} is in error, the normalization of R_w to a known water sand with the same compaction will still produce good values of S_w.

Resistivity with Density, Compensated Neutron, and Gamma Ray Logs

Having values for true resistivity (R_t), Density porosity (ϕ_D), Neutron porosity (ϕ_N), and Gamma-Ray count rate (γ), the log analyst can use a more sophisticated approach that determines bulk-volume-shale fraction (V_{sh}) and corrects porosity (ϕ) and water saturation (S_w) for shaliness and hydrocarbon effects.

The Sonic log, used alone for porosity, is not sufficient to correct for shaliness and hydrocarbon effects. The Density log with the Gamma Ray log will provide porosity corrected for shaliness, and adding the Compensated Neutron log makes it possible to correct for light hydrocarbons as well. Good values of porosity are important in estimating the flow potential of a well and the ultimate reservoir capacity.

Shale-volume-fraction computations using the Gamma-Ray log alone are only approximate and subject to error. A later section will describe the use of the SP as another shale indicator, but the computation of shale-volume fraction is still restricted with the programmable calculator as compared to the greater versatility available to computer processing. With a computer many shale indicators can be used, and they are aided by the computer's capability to select parameter values on the basis of statistics derived from the logs over large sections of the well.[2]

The method to be described here has been applied to Gulf Coast sands ranging in age from Cretaceous to Pleistocene. No clean sands are required for the method to work. If none are available, an estimate must be made of the Gamma-Ray-log value in a clean sand. For the computation of shale-volume-fraction (V_{sh}) input data are:

γ_{sd} = Gamma-Ray-log value in clean sand,

γ_{sh} = Gamma-Ray-log value in shale,

γ_{LOG} = Gamma-Ray-log value at the level to be interpreted,

ϕ_{Dsh} = porosity from Density log in shale, and

ϕ_{Nsh} = porosity from Neutron log in shale.

ϕ_{Dsh} and ϕ_{Nsh} are picked from shale beds having the highest values of ϕ_N. These values approximate the wet-clay parameters (ϕ_{Ncl} and ϕ_{Dcl}).

From empirical studies comparing Gamma Ray log values with SARABAND* shaliness computations, the following relationships were

* Mark of Schlumberger.

established for shaly-sand sequences.*

$$G = (\gamma_{LOG} - \gamma_{sd})/(\gamma_{sh} - \gamma_{sd}) \quad (1a)$$

$$(V_{cl})_{GR} = G/[1 + (1-G)/(1.25\ (\phi_{Nsh} + \phi_{Dsh})^2)] \quad (1b)$$

where

G is a Gamma-Ray-log linear shaliness indicator

$(V_{cl})_{GR}$ is the bulk-volume fraction of clay as computed by the above empirical equation (1b) using G from Eq. 1a.

The bulk-volume fraction of clay, V_{cl}, should be increased by the bulk-volume fraction of silt, V_{sl}, to derive bulk-volume fraction of shale, V_{sh}. However, to simplify the computation, V_{sl} is assumed to be negligible, and $V_{cl} = V_{sh}$. This should not affect our porosity determination much, as ϕ_{Dsh} and ϕ_{Nsh} were chosen to approximate the clay values of ϕ_D and ϕ_N. In the following it should be understood that the subscripts "cl" and "sh" are used interchangeably.

Although the above process for evaluating V_{sh} appears involved, only one log value (γ_{LOG}) and four zone parameters (γ_{sd}, γ_{sh}, ϕ_{Nsh}, and ϕ_{Dsh}) are required for input.

With V_{sh}, ϕ_{Nsh}, and ϕ_{Dsh} known, ϕ_N and ϕ_D may be corrected for shaliness:

$$\phi_{Dcor} = \phi_D - V_{sh}\,\phi_{Dsh} \quad (2a)$$

$$\phi_{Ncor} = \phi_N - V_{sh}\,\phi_{Nsh} \quad (2b)$$

Hydrocarbon effects can be eliminated with one of the two approximations:

$$\phi = \sqrt{\frac{\phi_{Dcor}^2 + \phi_{Ncor}^2}{2}} \quad (3a)$$

or

$$\phi = 0.7\,\phi_{Dcor} + 0.3\,\phi_{Ncor} \quad (3b)$$

---

* Information from J. Dumanoir.

Eq. 3b is simpler to program and has worked well empirically, so it is used in the algorithm.

Water saturation is calculated from the total-shale relation described by Simandoux:[3]

$$\frac{\phi^2 S_w^2}{0.8\, R_w\,(1-V_{sh})} + \frac{V_{sh}\, S_w}{R_{sh}} - \frac{1}{R_t} = 0 \qquad (4)$$

Eq. 4 is solved as a quadratic equation in S_w. The only additional inputs needed are R_t, R_w, and the resistivity of shale, R_{sh}. R_{sh} is taken from zones similar to those chosen for ϕ_{Nsh} and ϕ_{Dsh}. Better results are usually obtained if R_{sh} is taken 2 to 4 times the minimum log reading in shale sections. However, as V_{sh} may be low because of some silt content not taken into account, R_{sh} can afford to be low also, for the ratio V_{sh}/R_{sh} to remain constant. Picking R_{sh} as an average shale resistivity appears to work well.

R_w can be chosen from local experience, from normalization of R_{wa} to a water-bearing sand, or from the SP. Either a chart solution, or a calculator solution as described in the literature[1], can be used for the SP.

All together, the analyst must supply the zone parameters ϕ_{Nsh}, ϕ_{Dsh}, γ_{sd}, γ_{sh}, R_w, and R_{sh}. Log values required are ϕ_D, ϕ_N, R_t, and γ_{LOG}. Thus, ten calculator entries are required. These are assignable to the ten user-definable keys on the calculator.

The flow chart for such an algorithm is as shown in Fig. 2. The program used by the author required 200 program steps.

Resistivity Log with Density, Neutron, Sonic, and Gamma Ray Logs

Addition of the Sonic log to the FDC*-CNL*-GR combination log supplies the analyst with a pore-space-fraction of dispersed shale, q, which serves as a producibility index. The following relationship approximates "q".

$$q = (\phi_{SV} - \phi)/\phi_{SV} \qquad (5)$$

---

* Mark of Schlumberger.

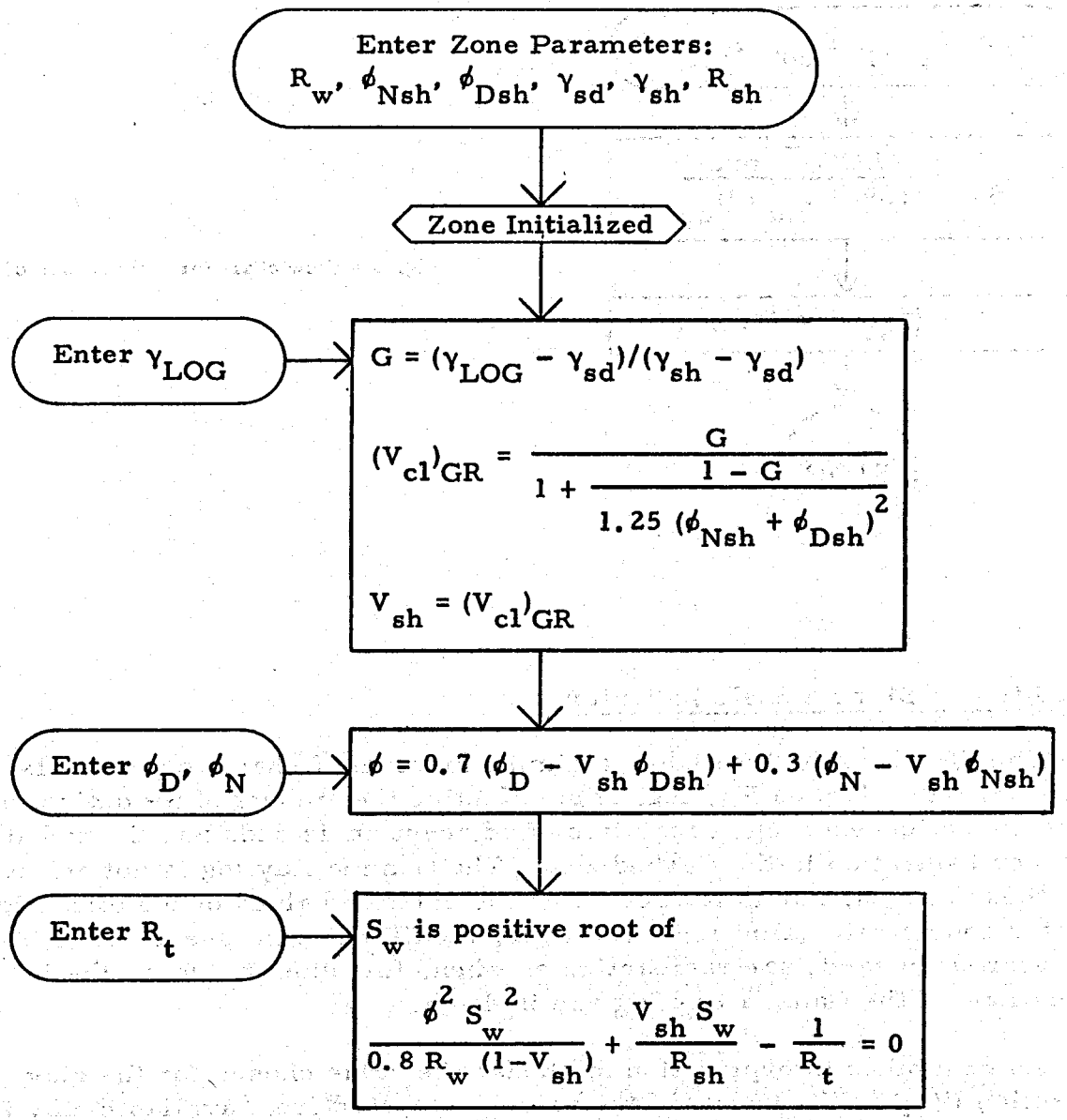

Fig. 2 - Flow chart for computation of V_{sh}, ϕ, and S_w from Resistivity, Density, Neutron, and Gamma Ray logs.

where ϕ_{SV} is porosity from the Sonic log.

Using $\phi = \phi_D$, field experience has shown that whenever the q calculated in a zone exceeds one-half of the value of q calculated in a shale interval, the zone will exhibit poor flow characteristics.

When Sonic data are available, the computation continues from Fig. 2 to that indicated in Fig. 3. Operationally, it is simpler to run the computation of Fig. 3 as a separate program after ϕ has been computed from the flow chart of Fig. 2. This enables the analyst to enter and retrieve all data by user-definable keys.

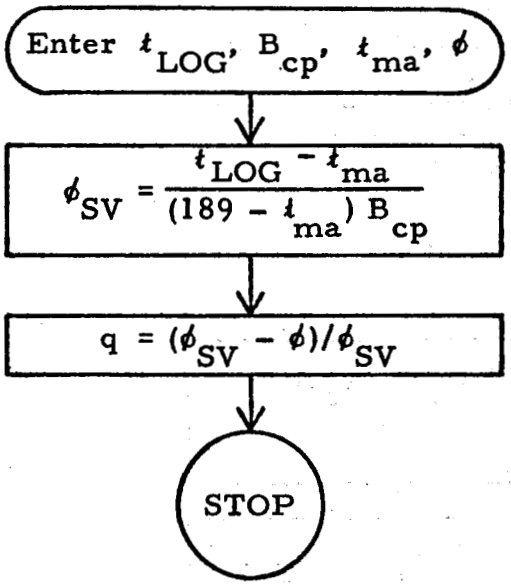

Fig. 3 - Flow chart for computation of q.

Addition of SP as a Shale Indicator

The SP cannot be treated as a simple function of shale volume as is done with the Gamma Ray log. Also affecting the amount of SP deflection are the cation-exchange capacities of adjacent shale beds and the hydrocarbon saturation in the flushed zone. The Gamma Ray log is not affected by these effects, nor is it affected by the relative values of the formation-water and filtrate salinities. However, the SP can be a useful shale indicator when sands are radioactive or when, for other reasons, the indications of the Gamma Ray log are in doubt.

As with other interpretation methods, the value chosen for the clay fraction (V_{cl}) is the lowest of the values computed from available clay indicators, in this case the lower of $(V_{cl})_{GR}$ or $(V_{cl})_{SP}$.

As verified by laboratory studies,[2,4,5] $(V_{cl})_{SP}$ is computed from a hyperbolic curve fit between X and α_{SP} given as

$$\alpha_{SP} = \frac{K(1 - X)}{X + K} \qquad (6)$$

where

K is a function of shale activity and water salinity which is determined as will be explained,

α_{SP} is the SP reduction factor due to shaliness: $\alpha_{SP} = E_{SP}/E_{SSP}$.

$X = Q_v/(Q_v)_{sh} = W_{cl} \cdot V_{cl}/(\phi S_{xo} + W_{cl} V_{cl})$,

E_{SP} is the SP-log deflection from the shale line,

E_{SSP} is the Static SP (clean sand),

Q_v is the cation-exchange capacity in the zone of ionic diffusion between connate water and invading filtrate,

$(Q_v)_{sh}$ is the cation-exchange capacity in the nearby shales,

W_{cl} is the volumetric fraction of water in the wet clay, and

S_{xo} is the flushed-zone water saturation.

As previously noted, the "shale" values chosen are essentially those of the "wet-clay" point, so $\phi_{Dsh} \approx \phi_{Dcl}$. Thus, W_{cl} is calculated as

$$W_{cl} = (\phi_{Dsh} - \phi_{Ddc})/(1 - \phi_{Ddc}) \qquad (7)$$

where ϕ_{Ddc} is the Density-log porosity at the "dry clay" point. A value of $\phi_{Ddc} = -12$ p.u. was chosen to approximate the dry-clay value. Thus, $W_{cl} = (\phi_{Dcl} + 0.12)/1.12$.

S_{xo} could be estimated as

$$S_{xo} \approx S_w^{1/5} \approx \left(\frac{0.8\, R_w}{\phi_D^{\,2}\, R_t}\right)^{1/10} \qquad (8)$$

However, because of limited program capacity, it is simpler to ignore the hydrocarbon effect and set $S_{xo} = 1$. Then,

$$(V_{cl})_{SP} = K \phi S_{xo} (1-\alpha_{SP})/[W_{cl}(1 + K) \alpha_{SP}]$$

$$\approx \frac{K}{1+K} \phi_D \left(\frac{1.12}{\phi_{Dsh} + 0.12}\right)\left(\frac{1}{\alpha_{SP}} - 1\right) \qquad (9)$$

where we have taken $\phi \approx \phi_D$ and $\phi_{Dcl} \approx \phi_{Dsh}$.

The only variable not yet accounted for is K. K is the degree of curvature of the hyperbolic fit. Very low values of K imply severe SP reduction with even small amounts of shale content. Since K is primarily a function of the cation-exchange capacity of the adjacent-shale beds, it is best determined for a local area. By using computed logs representative of an area, values of K can be determined level by level from

$$K = X\,\alpha_{SP}/(1-X-\alpha_{SP}) \qquad (10)$$

K will show a wide variation in clean sands, but in shaly zones, K should vary around a mean value. In well consolidated Gulf Coast sands, K = 0.2 works well in most cases. The fit is best when the SP deflection in apparently clean sands is considered to be only 80 to 85 percent of SSP. For K = 0.2,

$$(V_{cl})_{SP} = \frac{0.187\,\phi_D\left(\frac{E_{SSP}}{E_{SP}} - 1\right)}{(\phi_{Dsh} + 1.12)} \qquad (11)$$

As with the q computation, the computation of V_{sh} with both SP and Gamma Ray logs is more easily done in a separate program run before the ϕ and S_w computations. This avoids the necessity of direct storage into memory which is undesirable because of the limited amount of user-definable keys and program capacity available. If direct storage is used for all input data, the 224-step program capacity is barely sufficient to perform all the computations shown on Fig. 4. Fig. 4 is the complete flow chart for computation of V_{sh}, ϕ, S_w, and q from R_t, ϕ_D, ϕ_N, γ, SP, and t.

OPEN-HOLE LOG EXAMPLE

From Induction, Sonic, Density, Compensated-Neutron, Gamma-Ray, and SP data, a complete well evaluation can be made in open hole. In the example well twelve levels were computed using the programmable calculator. In addition to the six log-data values, zone parameters were selected for ϕ_{Nsh}, ϕ_{Dsh}, γ_{sh}, γ_{sd}, E_{SSP}, R_{sh}, B_{cp}, t_{ma}, R_w. The eight zone parameters and six log values were input directly into Memories 1-15 by STORE commands. The program then successively displayed values for clay-volume fraction (V_{cl}), porosity (ϕ), water saturation (S_w), and producibility index (q) for each point.

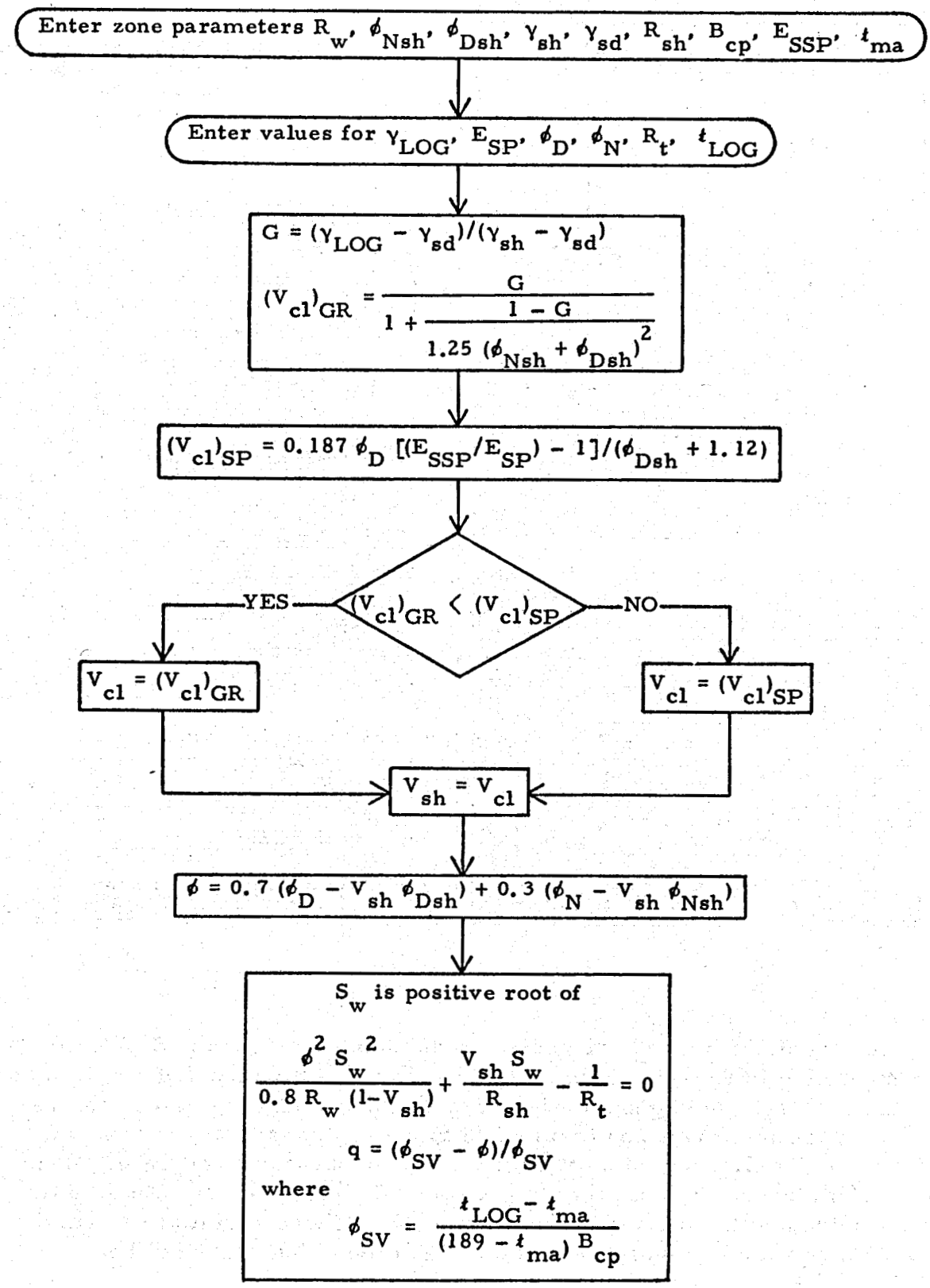

Fig. 4 - Flow chart for calculating V_{sh}, ϕ, S_w, and q from Resistivity, Density, Neutron, Sonic, Gamma Ray, and SP logs.

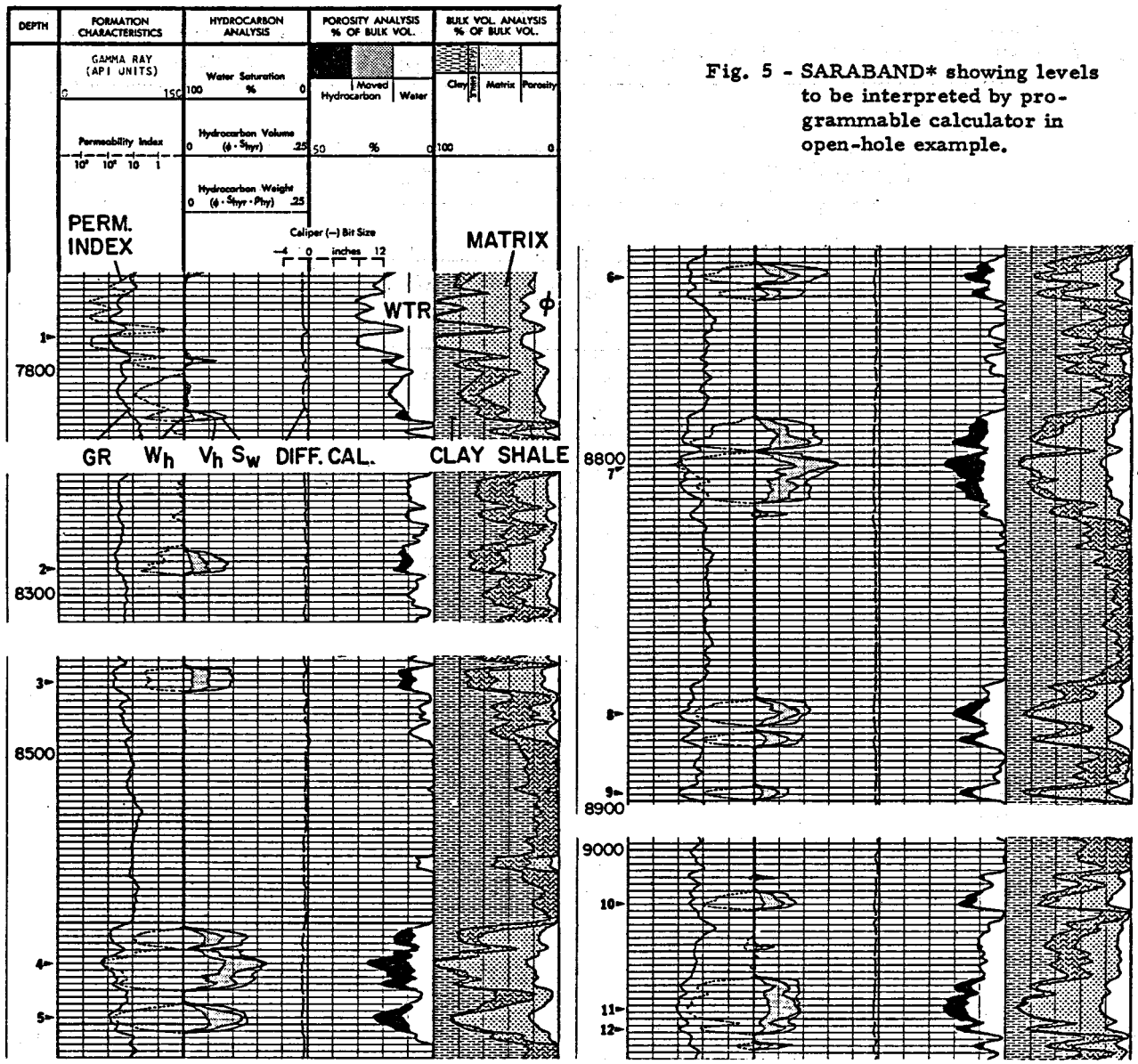

Fig. 5 - SARABAND* showing levels to be interpreted by programmable calculator in open-hole example.

The levels of interest are noted in the depth track of the SARABAND* presentation in Fig. 5. Table 1 compares SARABAND outputs with those of the calculator and describes each zone on the basis of calculator results. Wireline formation tests were taken in Zones No. 7 and No. 2. Zone No. 7 delivered 40 cu ft with some condensate and filtrate. Zone No. 2 produced 0.7 cubic feet of gas and 9,500 cubic centimeters of filtrate mixed with 7-percent formation water. These results are compatible with the log analyses made by both the calculator and the SARABAND program.

---

* Mark of Schlumberger.

Depth (ft)	Source	ϕ	S_w	V_{cl}	q	Description
7,790	SR-52	29	100	4	7	Clean, wet.
(No. 1)	SARABAND	30	100	0		
8,292	SR-52	14	72	22	38	Shaly, tight. No flow.
(No. 2)	SARABAND	15	65	30		
8,478	SR-52	15	56	18	37	Shaly, tight. No flow.
(No. 3)	SARABAND	14	60	28		
8,562	SR-52	25	32	5	13	Gas, fairly clean sand.
(No. 4)	SARABAND	26	35	0		
8,578	SR-52	24	46	11	31	Shaly, gas.
(No. 5)	SARABAND	23	49	15		
8,743	SR-52	16	45	22	45	Shaly, gas, tight. No flow.
(No. 6)	SARABAND	16	42	22		
8,800	SR-52	25	33	10	28	Gas, somewhat shaly.
(No. 7)	SARABAND	24	32	11		
8,873	SR-52	22	59	11	22	Slightly shaly, gas, possible
(No. 8)	SARABAND	21	55	14		water cut.
8,899	SR-52	17	81	10	26	Shaly, wet.
(No. 9)	SARABAND	17	72	13		
9,016	SR-52	18	71	29	39	Shaly, tight. No flow.
(No. 10)	SARABAND	18	67	27		
9,047	SR-52	26	60	12	15	Slightly shaly, gas. Possible
(No. 11)	SARABAND	24	62	10		water cut on production.
9,053	SR-52	21	70	15	19	Shaly, gas. High water cut
(No. 12)	SARABAND	19	67	18		on production.

Table 1
Open-Hole
Log-Analysis
Example

On a level-by-level basis, the two interpretation methods yield substantially the same conclusion. The calculator method is not a continuous interpretation, however. It cannot easily provide the curve shapes which may reveal saturation gradients or which may have stratigraphic significance for the geologist; nor can it integrate total porosity-footage of hydrocarbon-footage necessary for reservoir computation. Also, permeability is not computed. However, the well operator will have enough information at the wellsite to make knowledgeable decisions about the general productive capacity of the well, the advisability of setting pipe, and the need for further data by coring and testing.

ALGORITHMS FOR CASED-HOLE LOGS

In the typical case where a cased-hole log must be used for the primary formation evaluation of an old well, an electric log with Spontaneous Potential may be the only available open-hole information. A Thermal Decay Time log with a Gamma Ray curve can be run in cased hole to provide values of bulk-volume-shale fraction and porosity, and water saturation under existing conditions. Available data for the computation are Gamma Ray, SP, Ratio, and thermal-neutron-capture cross section (Σ). Also, the Near/Far Count-Rate overlay can identify gas, and thus aid in the analysis.

The technique described in this section is an application of the "Dual Water" model of shaly sands.[6] This method does not rely as heavily on accurate bulk-volume-fraction-shale determinations as the earlier-used Σ-ϕ crossplots, thus it allows greater error in shale determination without seriously affecting water-saturation calculations. This is most important when no open-hole logs are available at all. An excessive shift for shaliness on the Σ-ϕ crossplot could drive the computed S_w value to zero or even to negative values.

In the Dual-Water model the water in the formation is considered to be of two types: water bound to the clay surfaces and free water* in the pores. The bound-water conductivity is indicated as C_{wB} and the free-water conductivity as C_{wF}. The conductivity (C_{wM}) of the two waters taken as a mixture is**

$$C_{wM} = (1-S_{wB})\, C_{wF} + S_{wB}\, C_{wB} \qquad (12)$$

where S_{wB} is the fraction of total porosity (ϕ_T) occupied by the bound water. ($S_{wB} = V_B/\phi_T$.) Total porosity is the total pore space available for bound water and for free water and hydrocarbons. C_{wM} is used in a saturation relation of the form used by Waxman et al.[4, 8]

Without going into further details on the use of this method with open-hole logs (discussed in Ref. 7), we shall here adapt its use to cased-hole logs plus SP.

---

* It should be understood that free water is not all producible water since it includes the irreducible water saturation (S_{wi}).

** The notation used here and in Ref. 7 differs in many respects from that used in Ref. 6.

The first step in the interpretation is to determine S_{wB}. S_{wB} must be calculated for each level to be analyzed except shale points, where $S_{wB} = 1$. The S_{wB} value used is taken as the minimum value of S_{wB} as calculated from the SP and the Gamma Ray log.

A good estimate of S_{wB} from the Gamma Ray is the simple linear shale-indicator relationship:

$$(S_{wB})_{GR} = (\gamma_{LOG} - \gamma_{sd})/(\gamma_{sh} - \gamma_{sd}) \qquad (13)$$

The value of γ_{sd} should be chosen as a minimum reading, or less if no sand is clean. The γ_{sh} value, however, should be chosen as an average value in a representative shale. Crossplots have indicated that $(S_{wB})_{GR}$ is generally better if one inputs γ_{sh} as 60 percent of the maximum Gamma Ray excursion from the sand line.

S_{wB} cannot be determined directly from the SP, as it is also a function of hydrocarbon saturation. With certain assumptions about shale and mud properties and downhole temperatures, we can use the following relationship:

$$(S_{wB})_{SP} = S_w/(1 + B) \qquad (14a)$$

where, as found empirically,

$$B = 7.5\,(10^{E_{SP}/81} - 1)/(10^{E_{SSP}/81} - 10^{E_{SP}/81}) \qquad (14b)$$

In the interpretation illustrated here, S_w was assumed to be equal to 1; thus S_{wB} from the SP in hydrocarbon-bearing zones was overestimated. A more elaborate system would first calculate water saturation by using $S_{wB} = 1/(1 + B)$, then use an iterative process alternately recalculating $S_{wB} = [S_w/(1 + B)]$ and S_w.

The second step in processing point-by-point TDT* data is to pick total porosity (ϕ_T) from a Σ-Ratio crossplot, or from an otherwise known value of porosity. The Σ-Ratio crossplot selected must be chosen according to casing size and borehole salinity. The ϕ_T computed by this means will be a valid estimate of ϕ_T in liquid-filled formations. However, in gas-bearing zones it will be too low, and an external estimate must be used.

---

* Mark of Schlumberger.

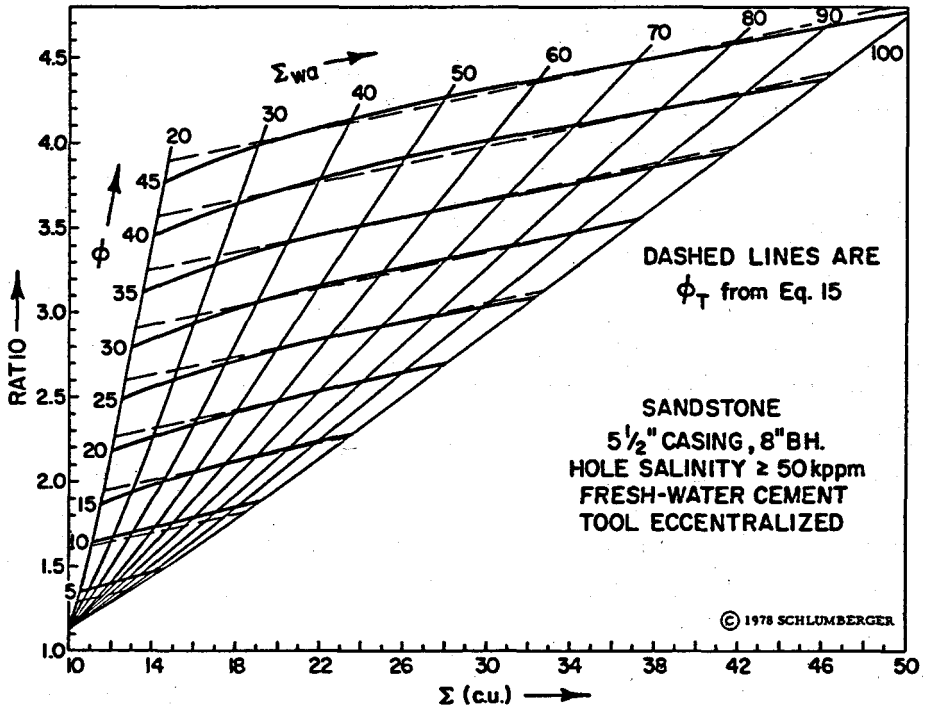

Fig. 6
Ratio-Σ chart. The dashed lines indicate the approximation of Eq. 15.

The example program uses a linear approximation

$$\phi_T = 0.161\ \underline{R} - 0.0043\ \Sigma_{LOG} - 0.114 \qquad (15)$$

where $\underline{R}$ is the reading of the Ratio curve of the TDT. Fig. 6 is for 5 1/2-inch casing with borehole salinity greater than 15 ppk NaCl. Fig. 6 compares the actual chart[9] with the linear approximation of Eq. 15.

Other linear estimators of the form

$$\phi_T = a\ \underline{R} + b\ \Sigma_{LOG} + C \qquad (15a)$$

may be used with adequate results for other casing sizes and borehole salinities.

The next step is to compute Σ_{wa} (apparent cross section of all formation fluids taken together) for different water-saturated cases and therefrom to obtain Σ_{wF} and Σ_{wB} where

Σ_{wF} is the Σ value of the free formation water

Σ_{wB} is the Σ value of the bound water

We make use of the fact that

$$\Sigma_{LOG} = \phi_T \Sigma_{wa} + (1-\phi_T)\Sigma_{ma}$$

or

$$\Sigma_{wa} = [\Sigma_{LOG} - (1-\phi_T)\Sigma_{ma}]/\phi_T \qquad (16)$$

where

Σ_{ma} is the Σ value of the rock matrix. Σ_{ma} is assumed to be 10 in the example flow charts.

A theoretical relation for Σ_{wa} is

$$\Sigma_{wa} = \Sigma_{wF}(S_{wT} - S_{wB}) + \Sigma_{wB} S_{wB} + \Sigma_h (1 - S_{wT}) \qquad (17a)$$

where

S_{wT} is the fraction of total porosity filled with water (both free and bound)

Σ_h is the Σ value of the hydrocarbon

Thus in a pure shale, where $S_{wT} = 1$ and $S_{wB} = 1$,

$$\Sigma_{wa} = \Sigma_{wB} \qquad (17b)$$

and in a shaly water sand, where $S_{wT} = 1$,

$$\Sigma_{wa} = \Sigma_{wF} (1 - S_{wB}) + \Sigma_{wB} S_{wB} \qquad (17c)$$

Thus, using Eq. 17b, Σ_{wB} can be determined from the Σ_{wa} value in shales computed by Eq. 16. Then, knowing Σ_{wB}, Eq. 17c can be used to determine Σ_F from the values of Σ_{wa} and S_{wB} in a water-saturated shaly sand.

S_{wT}, ϕ, and S_w can then be computed using the following relations:

$$S_{wT} = \frac{\Sigma_{wa} - \Sigma_h - S_{wB}(\Sigma_{wB} - \Sigma_{wF})}{(\Sigma_{wF} - \Sigma_h)} \qquad (18a)$$

$$\phi = (1 - S_{wB})\,\phi_T \qquad (18b)$$

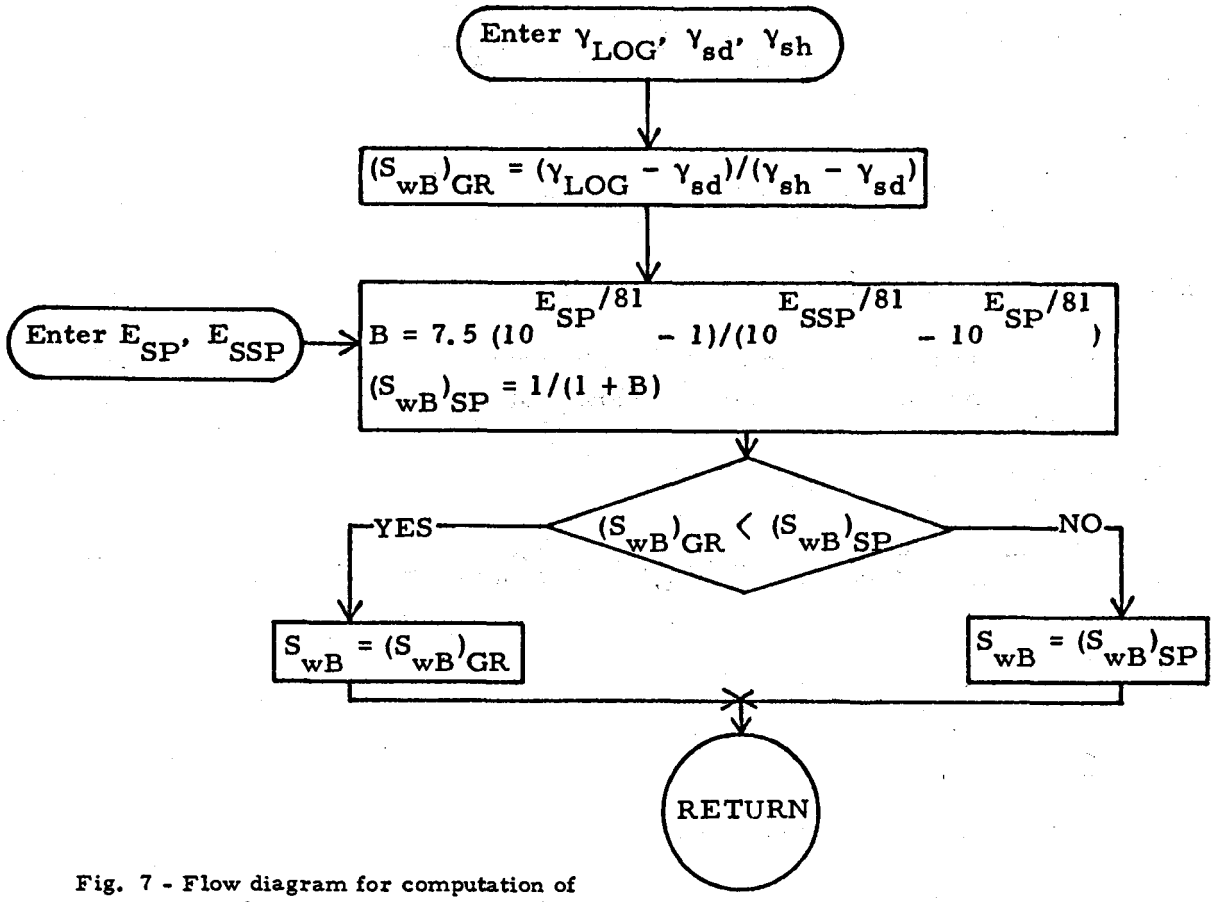

Fig. 7 - Flow diagram for computation of S_{wB} from Gamma Ray or SP log.

$$S_w = (S_{wT} - S_{wB})/(1 - S_{wB}) \qquad (18c)$$

where

ϕ = porosity available for free water (total porosity less bound water),

S_w = fraction of porosity ϕ filled with water.

The example interpretation is written as a main flow diagram and an auxiliary flow diagram. The auxiliary flow diagram (Fig. 7) calculates S_{wB} from SP and Gamma Ray logs level-by-level throughout the well. The main flow diagram (Fig. 8 with subroutine of Fig. 9) makes the interpretation of the TDT data.

The main flow diagram consists of three stages. The first stage calculates Σ_{wB} from a point that is representative of a shale zone using Eq. 17b. The second stage calculates Σ_{wF} from representative water sands within a zone using Eq. 17c. The values of Σ_{wB}, Σ_{wF}, and input value, Σ_h,

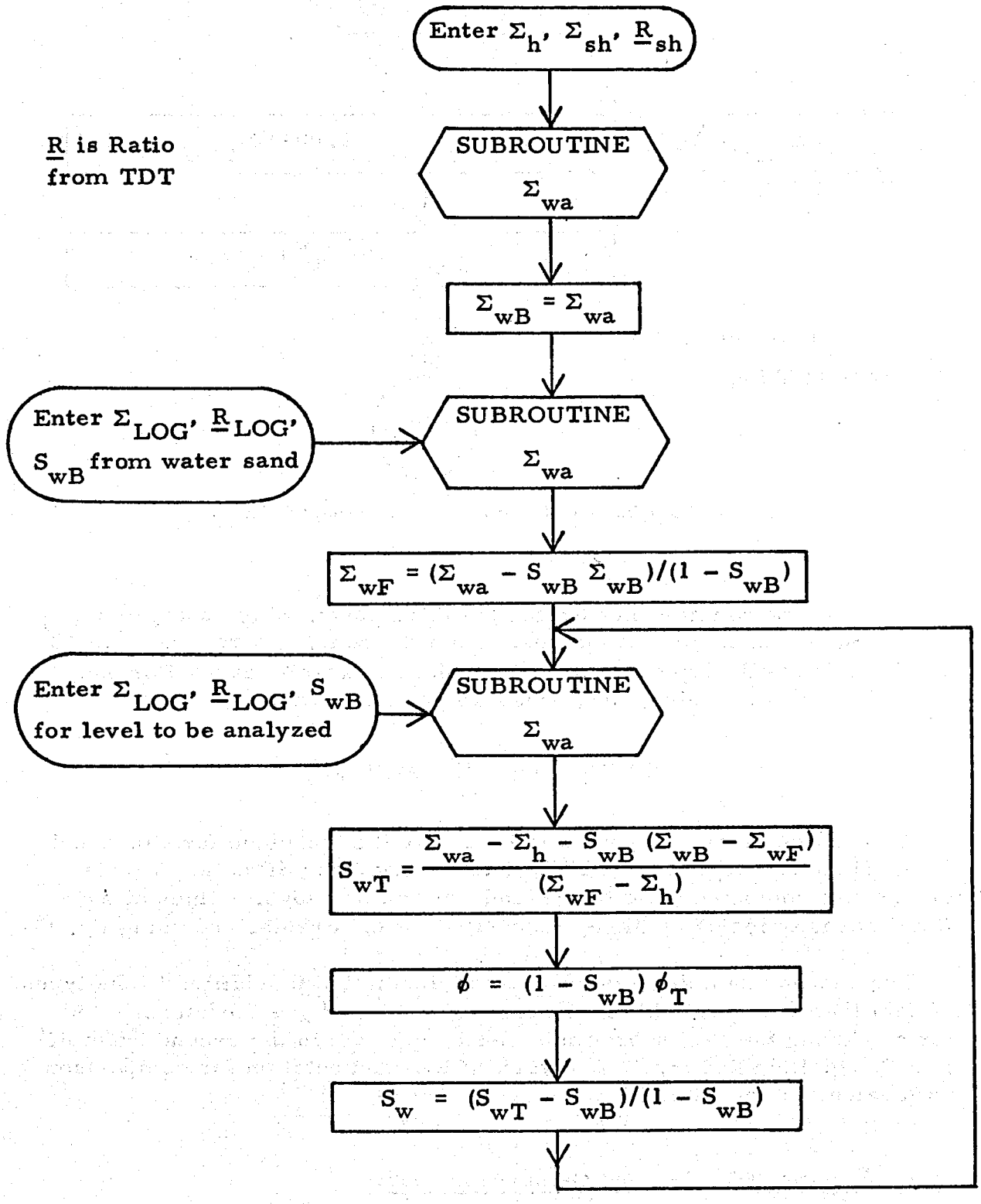

Fig. 8 - Main flow diagram for TDT interpretation.

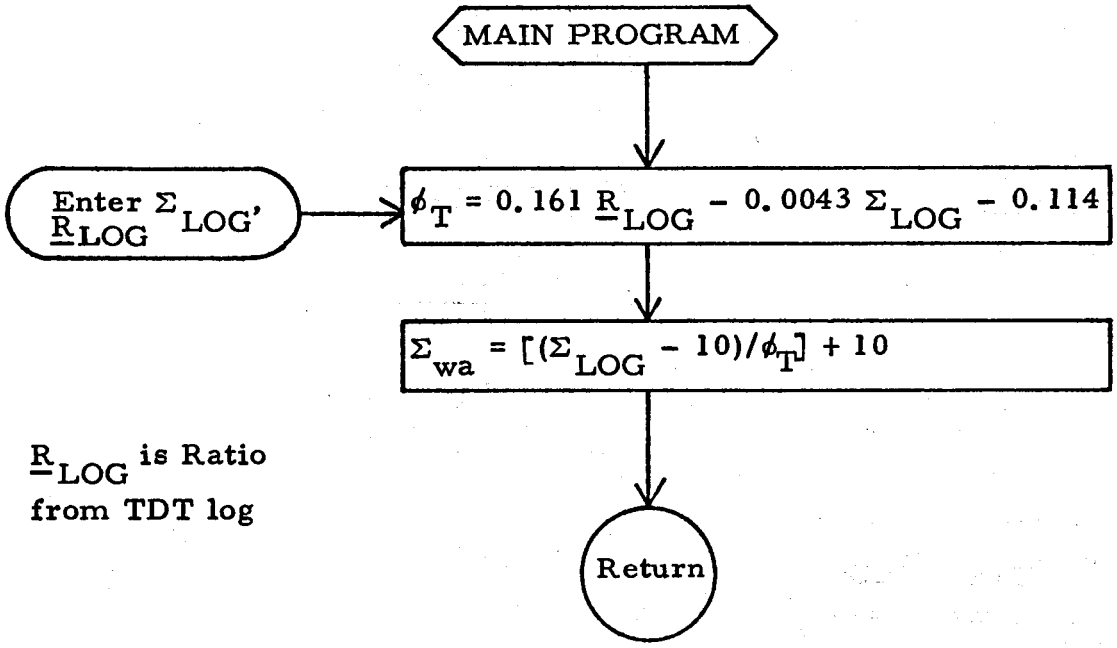

Fig. 9 Flow diagram of subroutine for computation of Σ_{wa}.

are the zone parameters needed for the third stage, which computes S_{wT}, ϕ, and S_w for each point of interest within the zone. Σ_h ranges from 18 to 20 c.u. for oil, depending upon the solution gas-oil ratio. For gas, $\Sigma_h \leq 10$ c.u., depending upon pressure and temperature.

CASED-HOLE EXAMPLES

Two examples are presented to illustrate the technique for cased-hole logs. The first utilizes only TDT, Gamma Ray, and SP data. Values of S_{wB} are computed from the SP and Gamma Ray logs. Values of ϕ_T (total porosity including shale-associated water) are derived using Eq. 15.

The second example uses open-hole information in addition to the types of data that were available in the first example. ϕ_D is then substituted for ϕ_T during the Σ_{wa} subroutine. Also available in the second example is a Cased-Hole Reservoir Analysis* (CRA) computation for comparison with calculator results.

Example with TDT, SP, and Gamma Ray Data

A Dual-Spacing Thermal Decay Time log is presented in Fig. 10 with an open-hole SP log traced on. The Gamma-Ray log was recorded in

* Mark of Schlumberger.

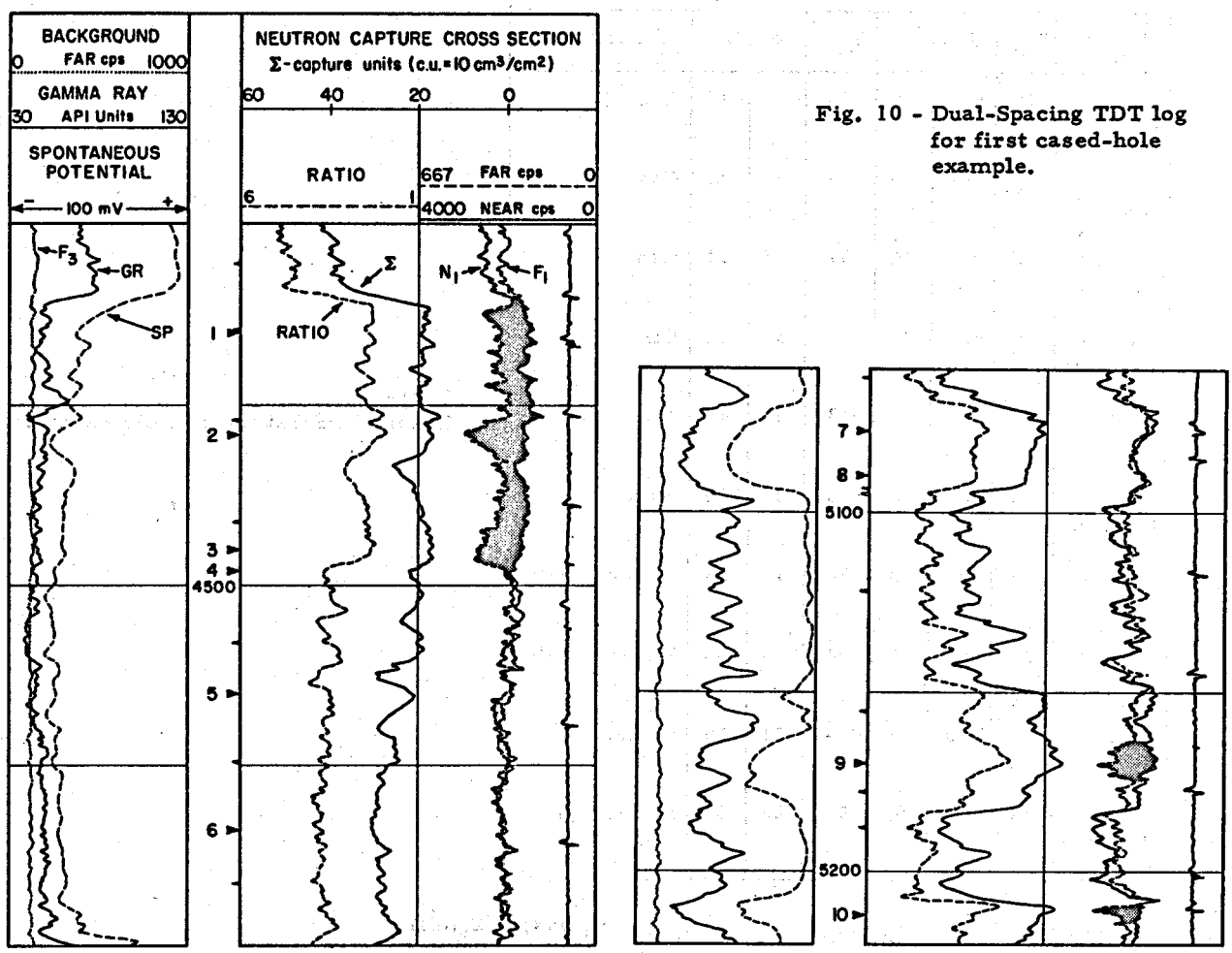

Fig. 10 - Dual-Spacing TDT log for first cased-hole example.

conjunction with the TDT log. Ten levels, as marked in the depth track, are analyzed by the programmable calculator. The initial step in the analysis is to utilize the Near/Far Count Rate overlay for gas indication. Levels 1, 2, 3, 9, and 10 show gas separations between the curves, so a Σ_h of 5 for shallow gas will be used for these levels. For all other levels, a value of $\Sigma_h = 21$ will be used, typical of oil.

The auxiliary program, for S_{wB}, is loaded on the calculator first. Zone parameters ESSP (or maximum SP deflection), γ_{sh}, and γ_{sd} are entered. Then, level-by-level, values for Gamma Ray and SP deflections from the shale baseline are entered, producing an S_{wB} value for every non-shale level.

The main program is loaded at this stage. The first calculation establishes a Σ_{wB} value from a representative shale point. In this example the shale at 5,127 feet is used. Σ and Ratio values are entered, and $\Sigma_{wB} = 78$ is generated. This value is retained in storage for all following computations until another shale point is entered.

Depth (ft)	S_{wB}	Gas	ϕ_T	S_{wT}	ϕ	S_w	Description
4,430 (No. 1)	13	yes	36	50	31	42	Gas
4,458 (No. 2)	5	yes	36	38	34	34	Gas
4,490 (No. 3)	8	yes	36	37	33	31	Gas
4,496 (No. 4)	5	no	36	47	34	44	Oil
4,530 (No. 5)	5	no	36	43	34	40	Oil
4,567 (No. 6)	6	no	36	100	34	100	Water
5,077 (No. 7)	26	no	23	88	17	84	Water, shaly
5,090 (No. 8)	29	no	26	92	19	88	Water, shaly
5,170 (No. 9)	42	yes	36	29	31	19	Shaly, gas
5,212 (No. 10)	29	yes	36	53	26	34	Shaly, gas

Table 2
Results of First Cased-Hole Example.

PARAMETERS:	E_{SSP}	γ_{sh}/γ_{sd}	Σ_{wB}	Σ_{wF}	Σ_h(gas)	Σ_h(oil)
	80	80/39	78	65	5	21

The second calculation generates Σ_{wF} from a water sand (clean or shaly). If the analyst is not certain which point to use, he may test several, picking the highest value obtained for Σ_{wF}. The program requires Σ, Ratio, and S_{wB} information from the point chosen as representative of water. This value of Σ_{wF} will be retained until another water-bearing entry is made, corresponding to a salinity or temperature change. Level 6 is selected as representative water in this example.

Points of interest are then computed. A HALT command is included in the Σ_{wa} Subroutine to provide a means of altering ϕ_T in gas zones. The ϕ_T computed by the program will generally be too low in gas-filled reservoirs, and an external estimate must be supplied by the analyst on the basis of either open-hole porosity logs or depth-porosity relationships established for the area. In this field example, 36 p.u. is known to be a valid estimate for ϕ_T at this depth. When the calculator halts after entering S_{wB}, the calculated value of ϕ_T on the display is replaced by 0.36, entered on the

keyboard. Then RUN is pressed to continue with the computation of S_{wT}. This is necessary only for gas points; otherwise, press RUN and continue.

In shaly hydrocarbon zones, unreasonably low values are found for S_w. Chart evaluations and CRA computations utilize a limit on S_{wB} to avoid this, but memory limitations prevent such a safeguard on the SR-52. When S_w was less than (S_{wT} - 0.020), the S_w value was ignored, and S_{wT} - 0.20 was used as the final saturation, S_w. When $S_w < 0.30$, S_w must be limited to (S_{wT} - 0.10).

Results are summarized in Table 2. From the computation and Near/Far Count Rate data, Levels 1, 2, 3, 9, and 10 are analyzed as gas. Levels 4 and 5 are oil-bearing, and Levels 6, 7, and 8 are wet. Also, Levels 7, 8, 9, and 10 exhibit considerable shaliness.

TDT Example with SP, Gamma Ray, and Open-Hole-Porosity Data

The second cased-hole example combines open-hole-porosity data with TDT, SP, and Gamma Ray logs. In this example ϕ_D is used for ϕ_T instead of the cased-hole ϕ_T value computed from Eq. 15. ϕ_{SV} from a Sonic log would more appropriately estimate ϕ_T, since ϕ_D excludes some of the bound-water porosity in ϕ_T. However, both ϕ_{SV} and ϕ_D differentiate between gas and low-porosity zones, whereas ϕ_T from Eq. 15 does not.

Fig. 11 is a section of the TDT log on a 2-in-per-100-ft scale with an SP curve traced on. Points analyzed by the calculator are marked in the depth track. The Near/Far Count Rate separation identifies Level 1 as gas-bearing. Also, Level 2 is known to contain some gas, even though the sand was shaly and porosity was low. Levels 3, 4, 5, 6, and 7 have no indication of gas. A Σ_h value of 4 is selected for Points 1 and 2 for low-pressure gas. $\Sigma_h = 20$ is chosen for Points 3-7, corresponding to oil.

S_{wB} values are first computed from SP and Gamma Ray logs. The shale at 6,775 feet is used for the Σ_{wB} computation. $\Sigma_{wB} = 75$ c.u. is calculated. Level 7 at 6,892 feet appears to be water-bearing, so it is used for the computation of Σ_{wF}. However, we substitute the Density porosity value, 30.5 p.u., for the ϕ_T computed by Eq. 15. A similar process is used for Levels 1 through 6 later in the computation. A value of $\Sigma_{wF} = 64$ c.u. is derived.

Table 3 tabulates the results of the computation. For comparison, values of ϕ and S_w are also included from a CRA computerized interpretation. The actual CRA presentation is shown in Fig. 12. Point 1 is gas productive. Level 2 is shaly and tight, but has some non-commercial gas. Levels 3, 4, 5, and 6 are oil productive while Level 7 is wet. The primary

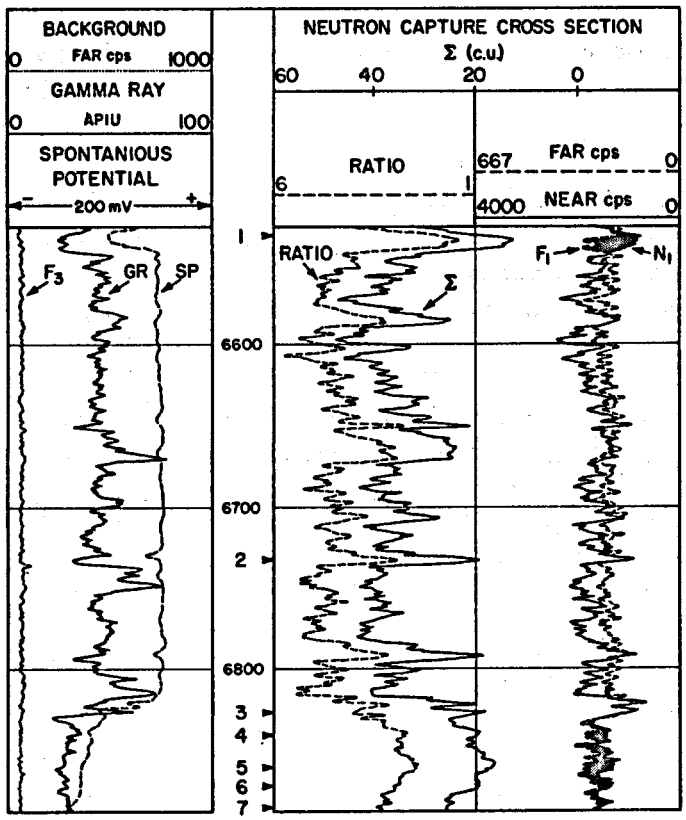

Fig. 11 - Dual-Spacing TDT log for second cased-hole example.

reason for differences in water saturation between the calculator's results and the computer's results is the assumption in the calculator version that Level 7 was completely wet. The computer saw Level 7 as having some oil saturation as compared with totally water-bearing zones below.

CONCLUSION

Field interpretation of well logs, in the absence of available wellsite computer processing can be greatly enhanced by the use of programmable calculator. More complex interpretation techniques are available with less time and better accuracy than those possible from hand calculations and chart solutions. The complexity of the technique is still limited by the memory and storage capacities of the individual calculator, and, in the text presented here, several simplifying approximations were introduced in order to stay within the calculator's capabilities.

Also, the process still requires level-by-level computation, but it releases the analyst from the mechanics of the interpretation. He can direct his attention to good depth correlations between logs and to determining whether hole conditions or other adverse circumstances are affecting the log readings. He can reflect on the significance of the program outputs in terms of the performance of the well. In general, he can make better use of the information that is available to him in the field.

ACKNOWLEDGMENT

The author wishes to thank the oil companies who released the logs used in this paper.

Table 3
Results of Second Cased-Hole Example.

Depth (ft)	Source	S_{wB}	Gas	$\phi_T = \phi_D$	S_{wT}	ϕ	S_w	Description
6,537 (No. 1)	SR-52	14	yes	28	31	24	20	Gas
	CRA					26	19	
6,734 (No. 2)	SR-52	36	yes	19	91	12	86	Water with gas, shaly
	CRA					7	75	
6,829 (No. 3)	SR-52	15	no	28	46	24	37	Oil
	CRA					27	44	
6,844 (No. 4)	SR-52	12	no	29	52	26	46	Oil
	CRA					28	41	
6,862 (No. 5)	SR-52	0	no	32	27	32	27	Oil
	CRA					32	23	
6,874 (No. 6)	SR-52	0	no	34	44	34	44	Oil
	CRA					34	40	
6,892 (No. 7)	SR-52	1	no	30.5	100	30.5	100	Water
	CRA					30.5	86	

PARAMETERS:	E_{SSP}	γ_{sh}/γ_{sd}	Σ_{wB}	Σ_{wF}	Σ_h(gas)	Σ_h(oil)
	92	40/26	75	64	4	20

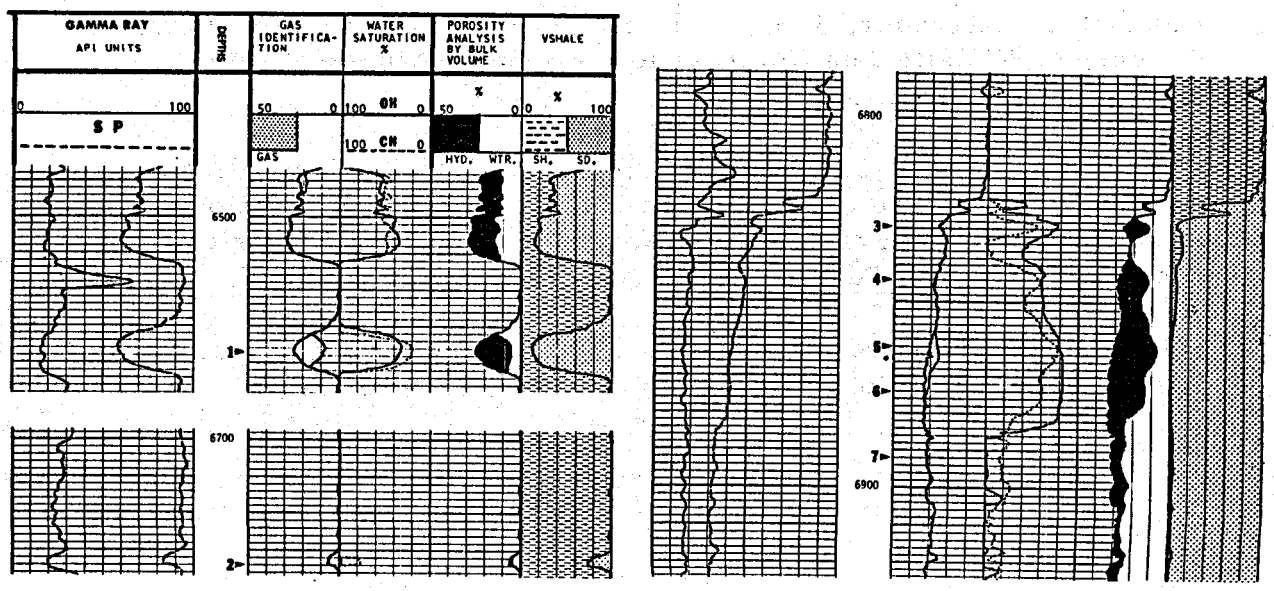

Fig. 12 - CRA presentation for second cased-hole example.

REFERENCES

1. Bateman, R.M. and Konen, C.E.: "Wellsite Log Analysis and the Programmable Calculator", SPWLA Eighteenth Logging Symposium, June 5-8, 1977.

2. Poupon, A., Clavier, C., Dumanoir, J., Gaymard, R., and Misk, A.: "Log Analysis of Sand-Shale Sequences--A Systematic Approach", J. Pet. Tech., July, 1970, pp. 867-881.

3. Simandoux, P.: "Dielectric Measurements in Porous Media and Application to Shaly Formations", Revue de l'Institut Francais du Petrole, 1963.

4. Waxman, M.H. and Smits, L.J.M.: "Electrical Conductivities in Oil-Bearing Shaly Sands", Soc. Pet. Eng. J., June, 1968, pp. 107-122.

5. Smits, L.J.M.: "SP Log Interpretation in Shaly Sands", Soc. Pet. Eng. J., June, 1968, pp. 123-136.

6. Clavier, C., Coates, G. and Dumanoir, J.: "The Theoretical and Experimental Bases for the 'Dual Water' Model for the Interpretation of Shaly Sands", 52nd Annual Fall Technical Conference and Exhibition of the Society of Petroleum Engineers of AIME, Denver, Oct. 9-12, 1977, Paper SPE 6859.

7. Best, D.L., Gardner, J.S., and Dumanoir, J.L.: "A Computer-Processed Wellsite Log Computation", SPWLA Nineteenth Annual Logging Symposium, June, 1978.

8. Waxman, M.H. and Thomas, E.C.: "Electrical Conductivities in Shaly Sands--I. The Relation Between Hydrocarbon Saturation and Resistivity Index; II. The Temperature Coefficient of Electrical Conductivity", J. Pet. Tech., February, 1974, pp. 213-225.

9. Schlumberger Limited: "Log Interpretation, Volume II--Applications", 1974, Chapter 5, "Formation Evaluations in Cased Holes".

ABOUT THE AUTHOR

KENNETH D. THOMPSON is a Sales Engineer with Schlumberger Well Services in Corpus Christi, Texas. He received a B.S. in Electrical Engineering from the University of Texas in 1968, and an M.B.A. from the University of Michigan in 1972. He worked for IBM as a Product Engineer in 1968 and joined the U.S. Navy later that year as an Electronics Duty Officer. In 1972 he was employed by Schlumberger Offshore Services in Houston as a logging engineer. In 1975 he transferred to the Houston Log Interpretation Center as a Synergetic Engineer. In 1976 he assumed his present position.

THE METHOD OF AUTOCALIBRATION AND ITS COMPUTER APPLICATIONS /SAIK SYSTEM/

by

Janusz FRYDECKI - Warsaw University, Faculty of Geology
Zdzisław DEBSKI - Municipal Information and Computer Centre of Warsaw SOETO
Stefan BASISTA - Enterprise of Geophysical Prospecting PPG

ABSTRACT

The paper presents an original method of autocalibration against the background of the current knowledge of methods identyfying the mineral composition of rocks. Autocalibration is an attempt to solve the problem of quantitative interpreting the results of well logging. On the basis of this method a system was developed of automatic complex interpretation of well log data, known as SAIK.

The autocalibration method eliminates the necessity to calibrate log data. Neither it necessitates the use of data resulting from laboratory tests of cores, although the SAIK system can make use of this kind of information. Properly adjusting the crossplot technique by analyzying the limit conditions of given plots, indispensable calibration coefficients can be obtained, which makes it possible to effect the quantitative data interpretation.

The use of autocalibration allows of interpreting the measurement data obtained in the past and disqualified at that time due to poor quality and lack of calibration. Autocalibration has the character of a filtration method that separates the information searched for from that coming out as a side effect and embraced by log data.

The paper also gives an outline of the SAIK system as an application of the autocalibration method in practice.

INTRODUCTION

The late 1960's were a period of great progress in interpretation methods and techniques of well-logging. To the fore came on the one hand problems connected with the calibration of well-log data obtained by means of various methods, first of all those of radiometry, and on the other hand questions connected with fractional, lithofacial and mineralogical analysis. The latter problem, initiated by overlay-type methods, culminated in the cross-plot interpretation technique.

New interpretation methods and new conceptual solutions have been met half-way by computer technique. In many instances it is difficult to find the correct answer to the question: what is the cause and what is the consequence - the interpretation method or the computer? The computer technique, due to its enormous potentials regarding data processing, their multiple computerization, multiple and multi-variant processing, iteration concluding, optimization and convenient storage with very simple information retrieval, etc., has created a new quality in interpretation. The computerized interpretation systems of well-log data SARABAND and CORIBAND, formed on the turn of the 1960's and developed and improved so far, especially as regards CORIBAND, are the best and, from the methodical viewpoint, the most complete interpretative solution now. However, they necessitate a logging technique with complete calibration supported by as sophisticated, complex and expensive equipment as that actually used by such firms as SCHLUMBERGER, DRESSER-ATLAS or GEARHART-OWEN only. Yet these systems do not solve the problem of making use of the data obtained from bore holes in the past years, since calibration itself and the equipment quality left much to be desired at that time.

In the same period, the system KAROTAZH-1 developed in the USSR, methodically adopted to the equipment existing in the CMEA member countries. Its application, however, was greatly limited. The shortcomings of calibration and the deficiencies of the logging technique made the authors look for conventional and traditional solutions, so practically they returned to the methods of manual interpretation used before. That is why, irrespective of its unquestionable historical significance, the system is not promising of development.

Many small firms and geophysical centres in the world have also started investigations in making use of the computer technique and computerized data processing. Many small and even more expanded programmes were created satisfying certain single methodical needs, often functioning on an interaction basis. Such semi-automatic programmes are often labelled "interpretation systems". Their formation is fully justified by economic or publicity reasons.

All in all, this is a positive phenomenon, since the development of fully computerized systems for large-scale projects necessitates considerable experience. And those pseudo- or quasi-systems can offer a lot of valuable methodical information indispensable for large-scale comprehensive systems.

Quantitative interpretation of well-log data is nothing but a kind of fractional-lithofacial analysis. The very interpretation of rocks porosity assuming that clay and monomineral matrix are absent is nothing but quantitative solving of the following rock pattern:

$$[\text{matrix} + \text{pores}]$$

On the other hand, the assessment of the rock pores' saturation is a more developed fractional analysis, following the pattern:

$$[\text{matrix} + \text{pores} \times /\text{water} + \text{bitumens}/]$$

The clay content, so familiar to analysts, adds to a more sophisticated pattern, namely:

$$[\text{matrix} + \text{clay material} + \text{pores}]$$

or

$$[\text{matrix} + \text{clay material} + \text{pores} \times /\text{water} + \text{bitumens}/]$$

The problem put in this form and interpretation understood in this way make it possible to present in detail the fundamental task of well-logging in the form of an elementary equation describing the fractional model of the rock:

$$\sum_{i=1}^{n} V_i = 1.0 \qquad /1/$$

where: V_i - relative /fractional/ volume of i-th element of the examined rock /i-th fraction/
n - number of fractions

Depending on the accepted rock model, either simplified or extended by any fractions, the task of interpretation will be to assess particular fractions and to determine their size.

The choice of the proper rock model, reflecting reality as much as possible, and the solving of the elementary equation are the basic aim of data processing in well-logging. The ways of solving may vary depending on the local factors and on the objective assessment of the available potentials. Individual geophysical centres and companies have employed various methods that extremely differ from each other sometimes.

Pure pragmatism is suggestive of a typical calibration of the logging equipment as the first solution. This is the way of main Western companies and on the basis of the model stand in Houston, where with a group of rock blocks of different lithology, porosity and saturation, unfortunately uncertain, although large-scale preventive measures have been taken, bases have been created for identifying the rocks' fractional composition and for modelling their structure. These processes of modelling and identifying are based on empirical and partly physical relations, thus forming the deterministic trend in interpretation. This deterministic approach to interpretation confines modelling to a number of fractions that can satisfy the condition:

$$n \leq N+1 \qquad /2/$$

where: n - number of fractions /as above/
N - number of employed and interpreted independent methods of well-logging /basic number of equations/

The number of equations is greater by one than the basic number due to the existence of the elementary equation /1/.

The existing dependence of the results of individual well-logging methods on fractional changes in the examined rocks makes it possible to solve a system of equations, and this system, in cases of linear variability, has a very simple matrix form. This style, based on Roper and Jones' expansion and solely making use of the so-called "porosity" methods /PN, PA, PGG/ is the basis of interpretation in Western systems.

The system is complemented by correlation crossplots, attractive in their form, since they offer a convincing illustration of fractional variability which is a familiar way for geologists thanks to its form of lithological triangles.

Believers in statistical methods represent a different style of interpretation. In this respect, the following two trends can be noted:

a. statistics is applied to find out the factors characterizing a generalized universal function, for instance a polinomial of any order, and this function combines the results of one or more well-logging methods with fractional changes in the examined rock;

b. statistics is applied similarly to characterize the determined function resulting from either the laws of physics or experiment, and as a rule this function combines a single method or rather its results with fractional changes in the examined rock.

Both trends are characterized by the tendency to embellish the obtained result by the examination and illustration of statistical distributions, and also by the evaluation of probabilities, medians, standard deviations or correlation coefficients, etc., which in many instances plays the fundamental role in this kind of interpretation and even is the objective of work. Moreover, as a rule, statistical trends are based on findings resulting from the examination of cores, from borings testing and from other geological and well-log data. Finally, the interpretation practically consists in a very simple "pictures comparison", i.e. in the comparison of the picture resulting from the model obtained for a given region, structure and formation, etc., with that resulting from investigations in the examined bore hole. This way is correct as long as the examined hole and the parameters recorded there relevantly belong to the same set as that of the obtained model. However, practically, the fundamental classical researcher's approach, i.e. making every effort to answer the basic questions in natural sciences - why and how - is unlikely as a rule.

A determinist and at the same time statistical approach to the problem of well-log data interpretation is characteristic for methods based on autocalibration. This mixed style assumes the existence of generalized, but not universal relations. Every function results from the physics of a phenomenon and is so generalized that it takes into consideration more factors than those taken into account in the basic physical relation. In this case, modelling is effected by way of successive approximations and iteration making use of successive results. The process is optimized as long as the desired result is obtained. In the course of data processing, new variables add to the model of the rock. Of course, the number of fractions is also limited, but within the limits resulting from fundamental statistical laws and common sense. The covariability of individual well-logging methods, i.e. simultaneous "responding" to the same geological phenomena, naturally in the way specific of each method, makes it possible to evaluate calibrating coefficients in the accepted functional models, and as a result to attain the assumed objective - fractional interpretation.

BASIC RELATIONSHIPS

A solution to the question of quantitative interpretation of the well-log data obtained in Poland so far is the autocalibration method /5,7/ and the SAIK system of complex automatic interpretation of well-log data constructed on its basis. The principles of autocalibration and the SAIK computer system's operation, and also examples of the results obtained by means of this system were presented during many international geophysical symposia already. The presentation embraced the first generations of the system SAIK-1 and SAIK-2 with their modifications SAIK-2opty and SAIK--2optymal, and also SAIK-3 as compared with the systems CORIBAND and KAROTAZH-1. Unlike these systems, SAIK does not necessitate data

calibration or even information from laboratory tests of drill cores, although it can make use of such information. The problem of obtaining respective calibration parameters was solved in this case by means of autocalibration.

In addition to porosity, practically the greatest effect to bear on the results of well-logging methods is that of clay material present in the rock, and also the variability of its content. For particular methods, the effect of these factors can be illustrated in the first approximation in the following way.

Acoustic logging /PA/

Taking the basic assumption that changes in the results of acoustic logging of velocity /interval time/ correspond to those of porosity and clay content, accepted was the Wyllie expanded model of mean times reflected in the formula:

$$\Delta t = \sum_{i=1}^{n} \Delta t_i V_i \qquad /3/$$

This is a linear model.

For the assumed boundary values the course of the relationship /3/ is illustrated by Fig. 1. All the recorded values are within the triangle of the vertexes Δtsz, Δtił and Δtw; its sides are straight segments reflecting the function /3/ for Kp = 0, S = 0 /porous clays/ and Ci = 0. The presence of clay in the rock makes the side / Δtsz, Δtw/, corresponding to Ci = 0, shift upwards in parallel.

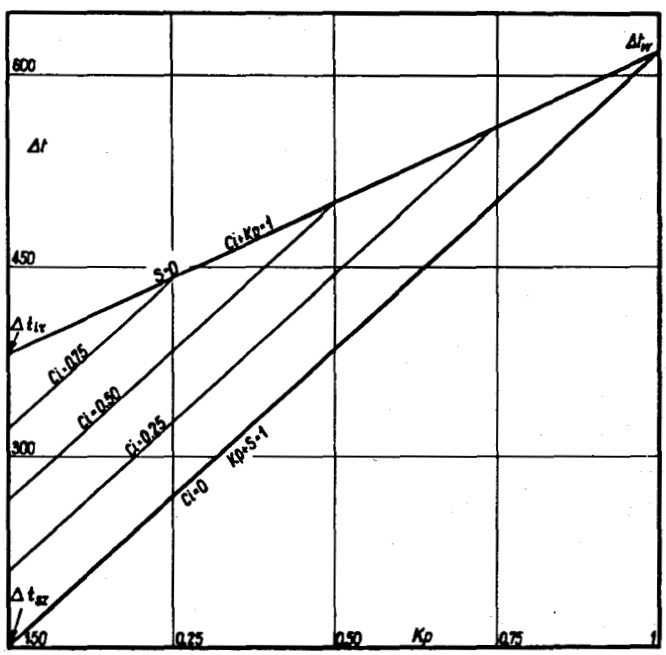

Fig. 1
Dependence $\Delta t = f(Kp, Ci)$

Neutron logging /PN, PNG, PNN/

Taking the basic assumption that changes in the results of neutron methods correspond to those in hydrogen content in the rock, and hence, through water and bitumens, to changes in porosity and clay content, the model was accepted schematically described by the formula:

$$In = In_o + N_o \log \sum_{i=1}^{n} N_i V_i \qquad /4/$$

or for monomineral case:

$$dIn = \frac{\lg w}{\lg w/Kp1} - \frac{1}{\lg w/Kp1} \cdot \lg(Kp + w \cdot Ci) \qquad /5/$$

For the assumed values the course of the relationship Ing = f /Kp, Ci/ is illustrated by Fig. 2. The illustration shows that all the results are grouped in a bent triangle; the upper limit is the curve for Ci = 0, while the bottom limit is the curve for porous clay.

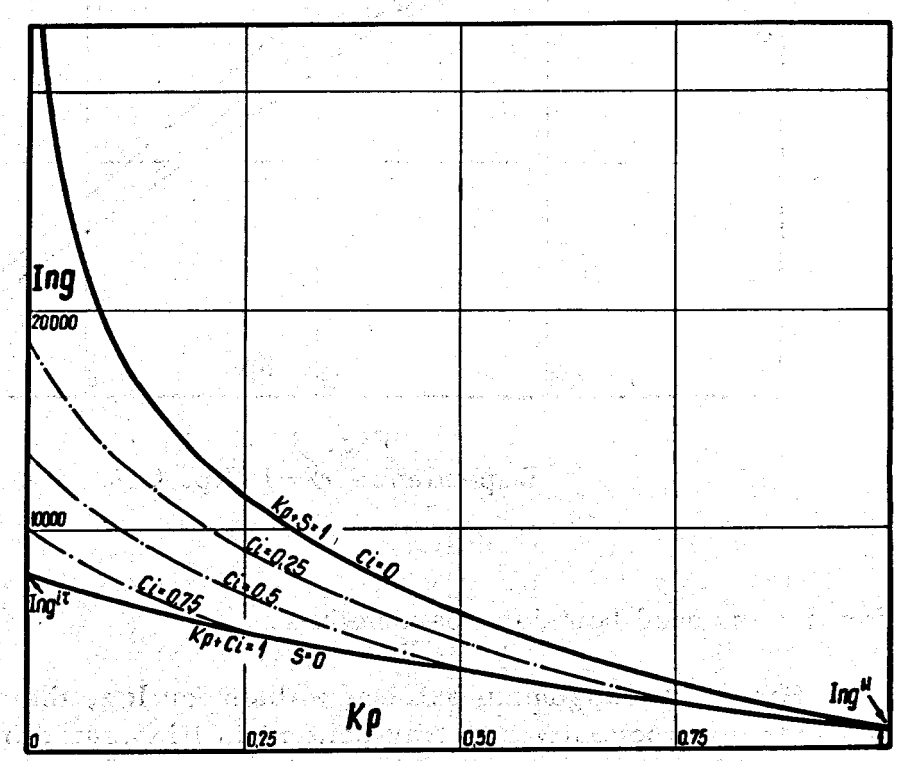

Fig. 2
Dependence
Ing = f /Kp, Ci/

Gamma-Gamma density logging /PGG/

Fig. 3 illustrates the relationships:

$$\delta_{GG} = \sum_{i=1}^{n} \delta_i V_i \qquad /6/$$

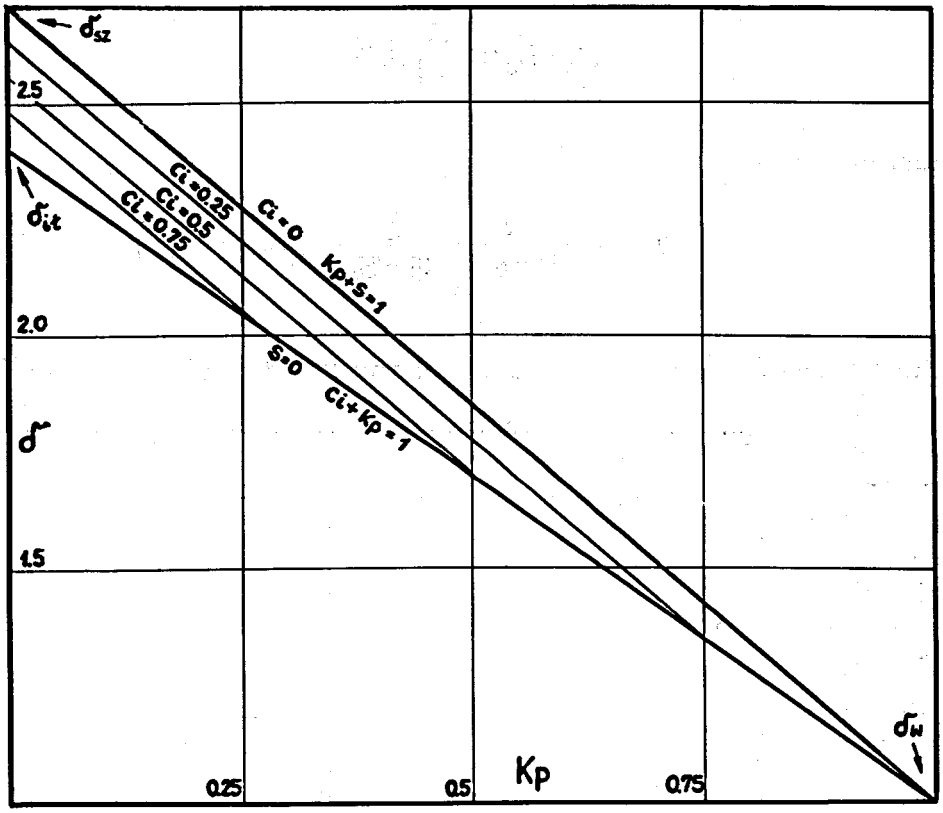

Fig. 3
Dependence $\delta = f(Kp, Ci)$

for the assumed boundary parameters.

Similarly, assuming extreme values for Igg, the dependence of direct Igg logs upon porosity and clay content is illustrated by Fig. 4. In both cases the boundary curves refer to the cases: Ci = 0 and S = 0 /porous clays/.

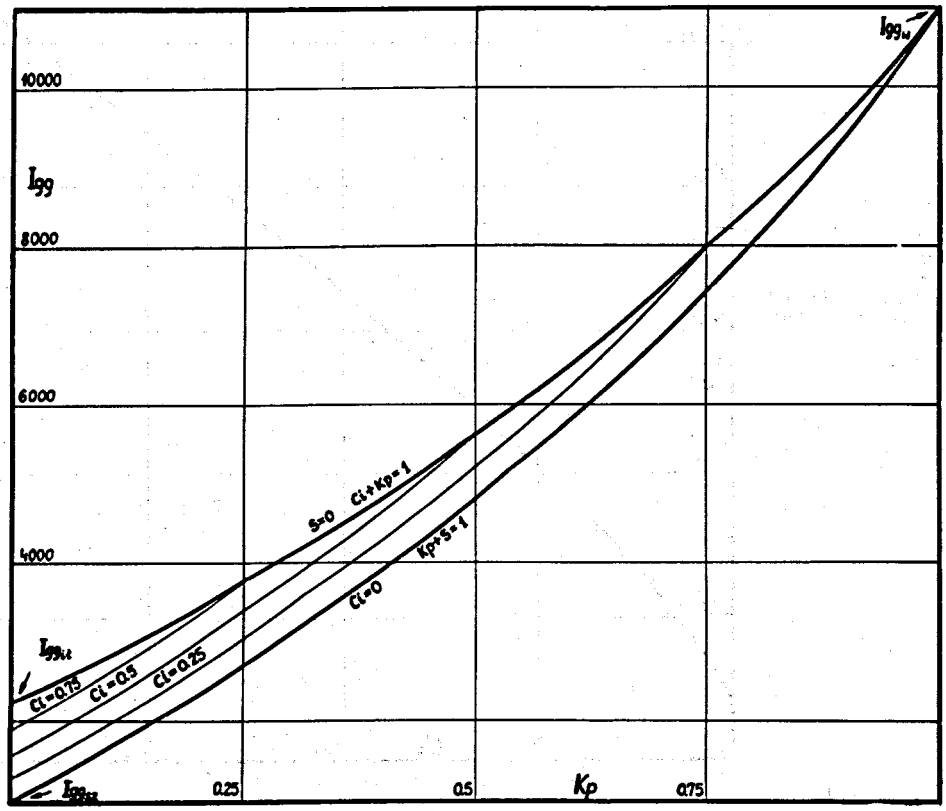

Fig. 4
Dependence Igg = f /Kp, Ci/

Logging of the intensity of natural gamma radiation /PG/

Taking the basic assumption that changes in the intensity of natural gamma radiation correspond to those in the clay content of the rock, the model was accepted following the formula:

$$Ig = Ig_0 + (Ig^1 - Ig_0) \cdot \left(\sum_{i=1}^{3} Ci_i \right)^{\alpha} \qquad /7/$$

in the most frequently used simplified form.

$$k \cdot d\,Ig = Ci^{\alpha} \qquad /8/$$

For the assumed boundary values the course of this relationship is illustrated by Fig. 5.

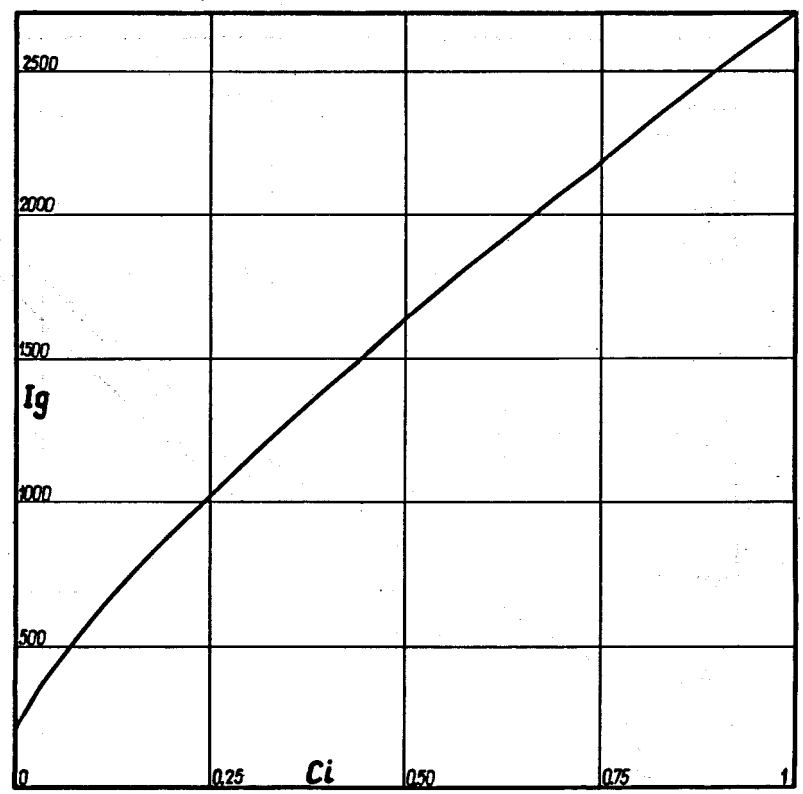

Fig. 5
Dependence Ig = f /Ci/

PO resistivity logging /or other electrometric methods determining the resistivity or electrical conductivity of rocks/

Taking the basic assumption that changes in rock conductivity are conditioned by those in porosity, in mineralization of deposit water, in saturation and clay content, and taking into consideration a great number of models used by various authors for the effect of clay content, a relatively universal formula was accepted /9/ reduced to clay content and porosity.

$$\sigma = \sum_{i=1}^{n} a_i \hat{\sigma}_i V_i^{m_i} K_{W_i}^{n_i} \qquad /9/$$

For the assumed boundary values the course of the relationship /9/ is illustrated by Fig. 6. All the recorded values are between two curves; the upper limit is the curve for porous clays, and the bottom limit is the curve for Ci = 0 /the latter curve assumes the form of straight line in the system of unilogarithmic axis/.

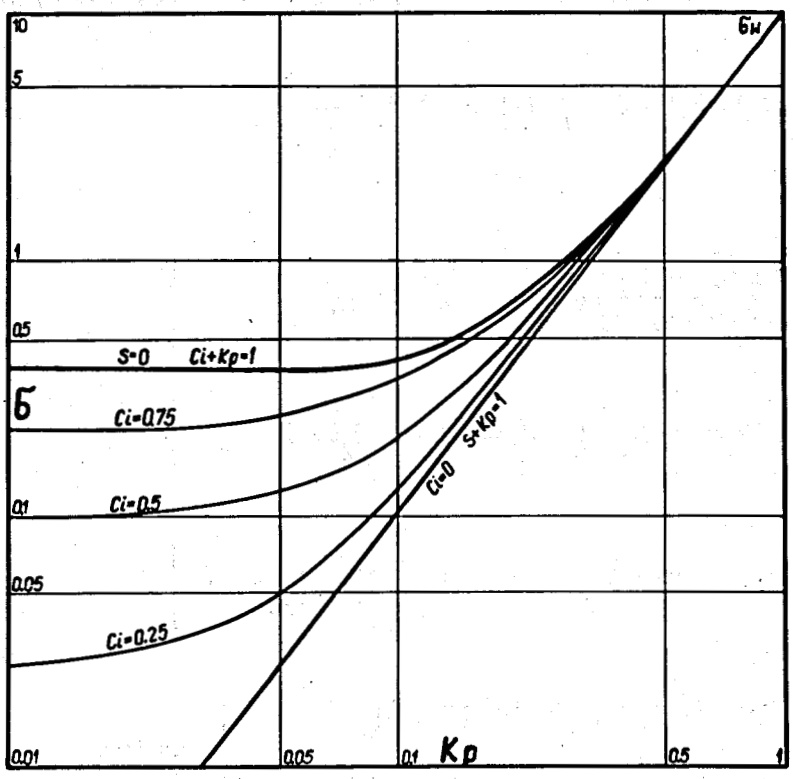

Fig. 6
Dependence $\delta = f(Kp, Ci)$

CORRELATION CROSSPLOTS OF MAIN LOGGING METHODS FOR AUTOCALIBRATION

Correlation crossplots of particular logging methods make it possible to determine calibration parameters of these methods. This method -- autocalibration - consists in making use of the functions combining the recorded geophysical parameter with reservoir parameters under specific extreme conditions. For example, extreme conditions can correspond to zero porosity, zero clay content or to the absence of matrix /porous clay/.

A correlation crossplot of neutron and gamma logs is illustrated by Figs.7 and 8. The set of results is enclosed in a bent triangle; the upper limit is the curve for Kp = 0, the bottom limit is the curve for porous clays - S = 0. The vertexes of this pseudotriangle are $/lg_{tło}$, $lng_w/$, $/lg_{il}$, $lng_{il}/$ and $/lg_{tło}$, $lng_{Kp=0}/$; the latter, due to the fact that the model was accepted of changes in neutron logs in the function of porosity according to the formula /5/, lies in the infinity of the axis lng.

Autocalibration resulting from the PN vs PG correlation crossplot can take the following course:

$$\{/1/\wedge/5/\wedge/7/\wedge/8/\wedge \sum KW = 1.0\}\wedge$$

$$\wedge \left\{ \begin{array}{l} a_1 = In_1 + \dfrac{(In_0 - In_1)\ lg\ (Ig_1 - Ig_0)}{\alpha\ lg\ W/Kp1} = a_2 = a \\ b_1 = \dfrac{In_0 - In_1}{\alpha lg\ W/Kp1}\ ;\ b_2 = \alpha \cdot b_1\ ;\ c_1 = Ig_0 = c_2 = c \\ d_2 = \dfrac{(Ig_1 - Ig_0)^{1/\alpha}}{W} = d\ ;\ c_2 = 1/W - 1 = c\ ;\ f_2 = 1/\alpha = f \end{array} \right\} \wedge$$

$$\wedge \left\{ \begin{array}{l} F_1(Ig,\ Kp=0) = a_1 - b_1\ lg(Ig - c_1) \\ F_2(Ig,\ S=0) = a_2 - b_2\ lg\left[d_2 - c_2(Ig-c)^{f_2}\right] \end{array} \right\} \Longrightarrow$$

$$\Longrightarrow \bigwedge_{Ig \neq c} \{In(Ig)\}\ \{In: [In \leq F_1(Ig, Kp=0)] \wedge [In \geq F_2(Ig,\ S=0)]\} \qquad /10/$$

Examination of the data set {In, Ig} and assessment of the values {a, b, c, d, e and f} make it possible to formulate a simple problem in the form of:

$$\bigvee_{\{a....f\}} \{/10/ \Longrightarrow In = a - b_2\ lg\ [d \cdot Kp + (Ig - c)^f]\} \qquad /11/$$

and the reverse problem:

$$\bigvee_{\{a....f\}} \{/10/ \Longrightarrow Kp = d^{-1}\left[\exp_{10} \frac{a - In}{b_2} - (Ig - c)^f\right] \wedge$$

$$\wedge\ Ci = (1 + c)\ d^{-1}(Ig - c)^f\ \} \qquad /12/$$

Therefore, a correlation crossplot of neutron logs in the function of gamma log results, assuming the boundary conditions Kp = 0 and S = 0, leads to the determination of the relationship of In and Ig with porosity /11/ and to the formulation of a reverse problem, i.e. to the determina-

tion of porosity reduced by the clay effect, and also of the clay content itself in the function In and Ig as well as Ig, respectively.

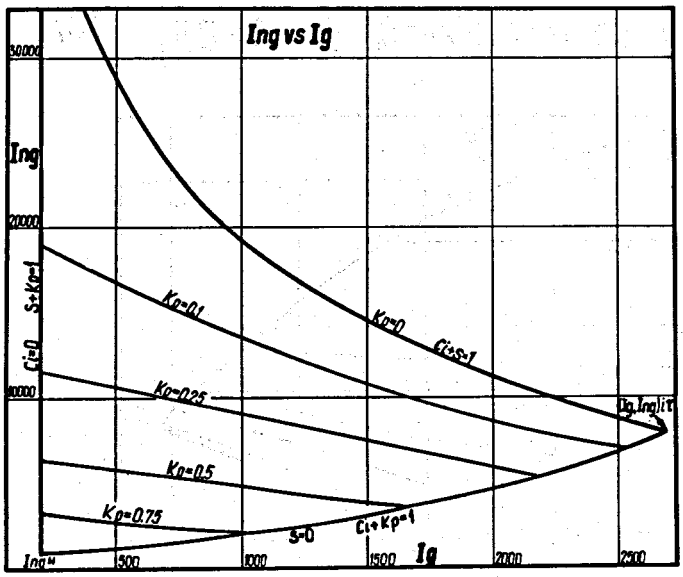

Fig. 7
Correlation crossplot Ing vs Ig
/linear scale/

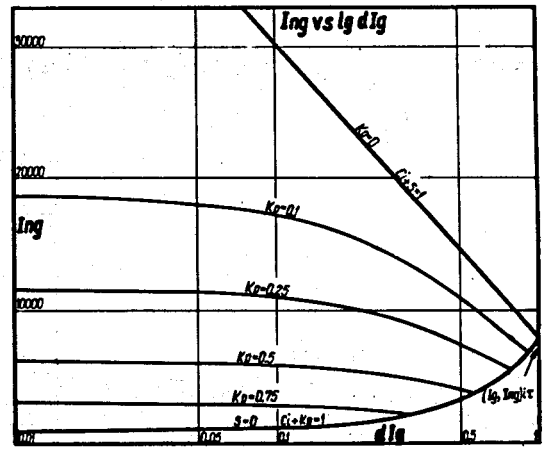

Fig. 8
Correlation crossplot
Ign vs lg dIg

Comparison between electrometric and gamma logs is presented in Fig. 9. This set of data is limited by the following two curves: the upper curve for porous clays /S = 0/ and the bottom curve for Kp = 0.

Autocalibration resulting from the correlation crossplot PO vs PG can have the following course:

$$\{/1/\wedge/7/\wedge/8/\wedge/9/\wedge \sum KW = 1.0\} \wedge$$

$$\wedge \left\{ \begin{array}{l} a_3 = \dfrac{\hat{a}\, G_i}{(Ig_1 - Ig_0)^{\beta/\alpha}} = a_4 = a \;;\; b_3 = \beta/\alpha = b_4 = b \;; \\ c_3 = Ig_0 = c_4 = c \;;\; d = \dfrac{\hat{b}\, G_W}{(Ig_1 - Ig_0)^{m/\alpha}} = d \;; \\ c_4 = (Ig_1 - Ig_0)^{1/\alpha} = c \;;\; f_4 = 1/\alpha = f \;;\; m_4 = m \end{array} \right\} \wedge$$

$$\bigwedge \left\{ \begin{array}{l} F_3\ (Ig\ ,\ Kp=0) = a_3\,(Ig - c_3)^{b_3} \\ F_4\,(Ig\ ,\ S=0) = a_4(Ig-c)^{b_4} + d_4\left[c - (Ig - c_4)^{f_4}\right]^{m_4} \end{array} \right\} \Longrightarrow$$

$$\Longrightarrow \bigwedge_{Ig \neq c} \{\sigma\,(Ig)\} = \{\sigma : [\sigma \geq F_3(Ig, Kp=0)] \wedge [\sigma \leq F_4\,(Ig\ ,\ S=0)]\} \qquad /13/$$

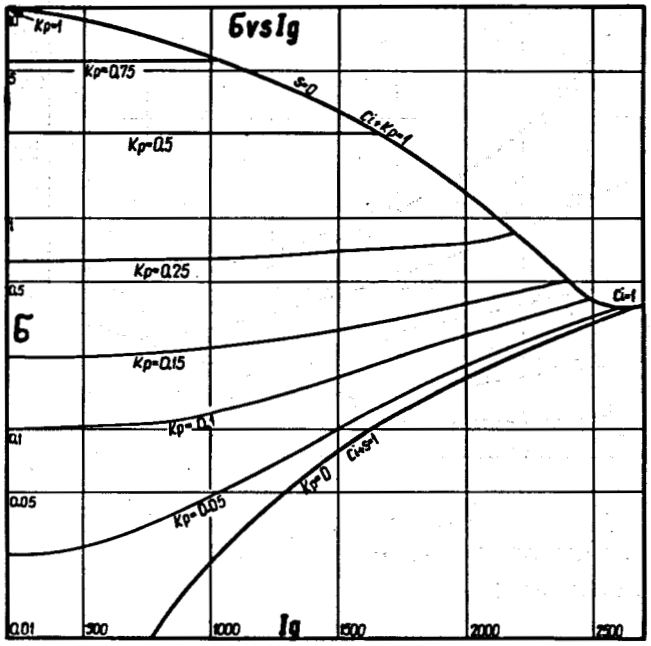

Fig. 9
Correlation crossplot σ vs Ig /linear scale for Ig; logarithmic scale for σ /

Similarly, one can formulate the following simple problem:

$$\bigvee_{\{a.....m\}} \{/13/ \Longrightarrow \sigma = a\,(Ig - c)^b + d\ c^m\ Kp^m\} \qquad /14/$$

or the reverse problem:

$$\bigvee_{\{a....m\}} \{/13/ \Longrightarrow \left(Kp = c^{-1}\ d^{-1/m}\left[\sigma - a\,(Ig - c)^b\right]^{1/m} \wedge\right.$$

$$\left. \wedge\ Ci = c^{-1}\,(Ig - c)^f)\right\} \qquad /15/$$

Therefore, it was demonstrated, as in the previous example, that a correlation crossplot of electric logs in the function of gamma logging, assuming the boundary conditions Kp=0 and S=0, leads to assessment of simple and reverse relationships, so to calibration.

The correlation crossplot Δt vs Ig in Fig. 10 represents a pseudo-triangle with the vertexes $/Ig_{tło}$, $\Delta tsz/$, $/Ig_{tło}$, $\Delta tw/$ and $/Ig_{ił}$, $\Delta tił/$. The data set $\Delta t = f/Ig/$ enclosed by this pseudotriangle is limited by the upper curve for porous clays $/S=0/$ and by the bottom curve for $Kp=0$.

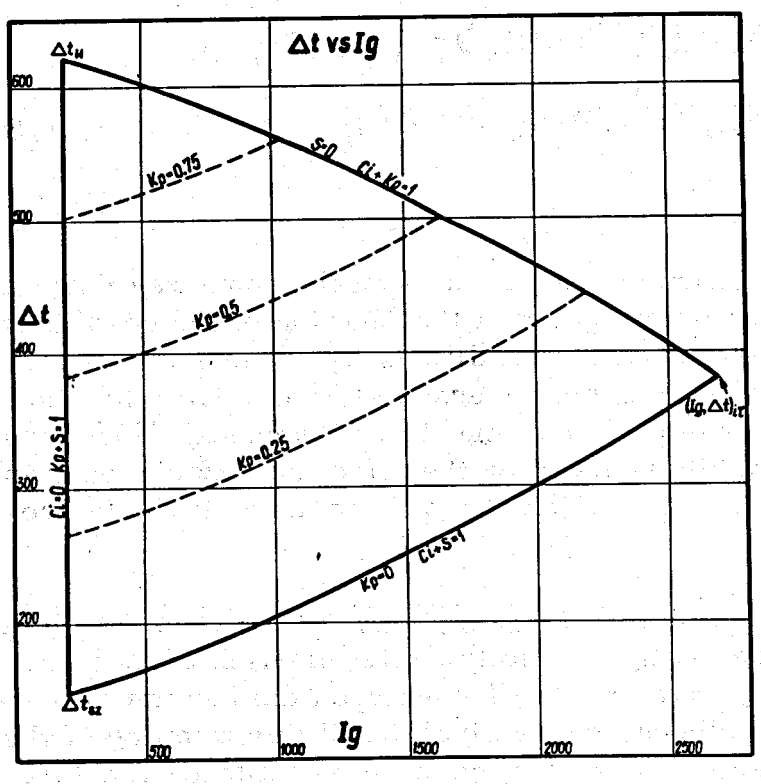

Fig. 10
Correlation crossplot
Δt vs Ig

Autocalibration resulting from the correlation crossplot PA vs PG can have the following course:

$$\{/1/\wedge/3/\wedge/7/\wedge/8/\wedge \textstyle\sum Kw = 1{,}0\} \wedge$$

$$\wedge \left\{ \begin{array}{l} a_5 = \Delta tsz;\ a_6 = \Delta tw;\ c_5 = Ig_0 = c_6 = c;\ f_5 = \frac{1}{\alpha} = f_6 = f; \\ b = \dfrac{\Delta tił - \Delta tsz}{(Ig_1 - Ig_0)^{1/\alpha}};\quad b = \dfrac{\Delta tw - \Delta tił}{(Ig_1\ Ig_0)^{1/\alpha}}; \end{array} \right\} \wedge$$

$$\wedge \left\{ \begin{array}{l} F_5(Ig,\ Kp=0) = a_5 + b_5 (Ig - c_5)^{f_5} \\ F_6(Ig,\ S=0) = a_6 - b_6 (Ig - c_6)^{f_6} \end{array} \right\} \Longrightarrow$$

$$\Longrightarrow_{Ig \neq c} \{\Delta t(Ig)\} = \{\Delta t : [\Delta t \geq F_5(Ig, Kp=0)] \wedge [\Delta t \leq F_6(Ig, S=0)]\} \quad /16/$$

hence, the simple problem:

$$\bigvee_{\{a.....f\}} \left\{ /16/ \Longrightarrow \Delta t = a_5 + b_5 (Ig - c)^f + (a_6 - a_5) Kp \right\} \qquad /17/$$

and the reverse problem:

$$\bigvee_{\{a....f\}} \left\{ /16/ \Longrightarrow \left(Kp = (a_6 - a_5)^{-1} [\Delta t - a_5 - b_5 \ (Ig - c)^f] \wedge \right. \right.$$
$$\left. \left. \wedge \ Ci = (a_6 - a_5)^{-1} (b_5 + b_6)(Ig - c)^f) \right\} \qquad /18/$$

Therefore, the third example demonstrates in the same way that a correlation crossplot of acoustic logging in the function of the results of gamma logging, assuming the boundary conditions Kp = 0 and S = 0, leads also to the determination of simple and reverse relations, i.e. to the determination of the relationship of Δt and Ig with porosity /17/ and to the determination of porosity reduced by the effect of clay content, and also of clay content itself in the function Δt and Ig as well as Ig, respectively.

The employed simple models /11/, /14/, /17/ and hence the reverse models /12/, /15/, /18/ naturally lead to the determination of those parts of clay content and porosity that exert influence upon the results of neutron, electric or acoustic methods, respectively, and this meaning of these parameters should be accepted. The determination of calibration coefficients' values /the sets {a,...,f} , {a,...,m} and {a,..., f} respectively for a given type of cross correlation/ can be effected by means of analysing the whole data set in a correlation crossplot and, through the elimination of useless data /filtration/ or their transformation, the parameters are obtained of the boundary curves for Kp = 0 or S=0, hence direct interpretation methods can be determined. It is demonstrated below that to avoid serious errors it is more advisable to make use of some coefficients only which necessitates the use of three methods in calibration at the same time.

Only three examples are discussed here, and procedure is similar for each of them, and also for any other combination. The correlation crossplot PGG vs PG is presented in Fig. 11. The data set /Igg and Ig/ is enclosed by a bent triangle with the vertexes /$Ig_{tło}$, Igg_{sz}/, /$Ig_{tło}$, Igg_{w}/ and /Ig_{il}, Igg_{il}/. The boundary curves correspond to the conditions: Ci=0 /straight line/, S=0 /porous clays - upper limit/ and Kp=0 /clay rocks - - bottom limit/.

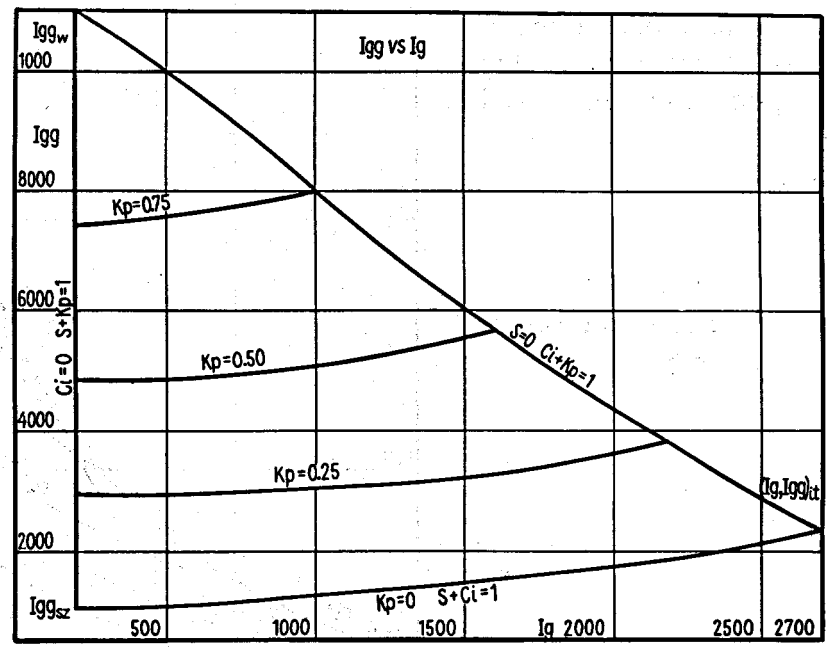

Fig. 11
Correlation cross-plot Igg vs Ig

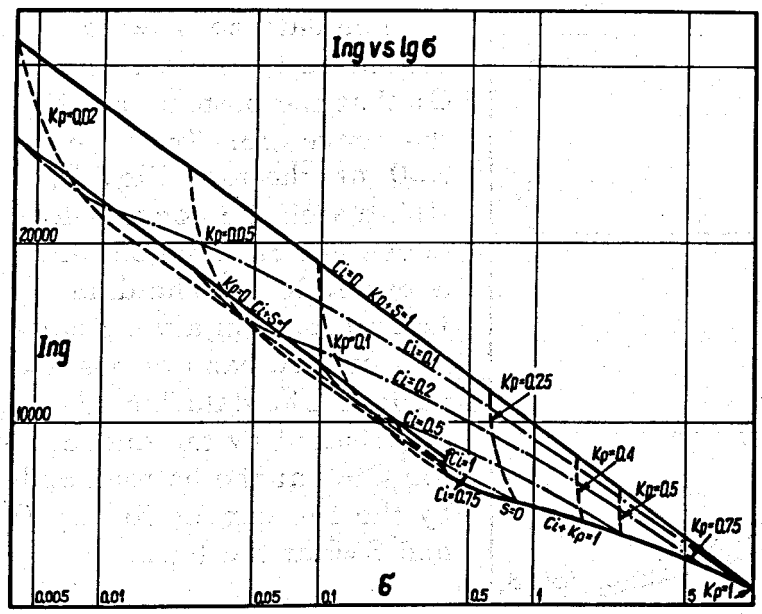

The correlation cross-plot of the results of neutron and electrometric logs is presented in. Fig. 12. The data set is within the area with the upper limit in the form of the straight line for Ci=0 and with the bottom limit in the form of approximate straight line for Kp=0 and curve for S=0 /porous clays/.

Fig. 12
Correlation crossplot Ing vs lg σ

The correlation crossplot of acoustic and electrometric logs is presented in Fig. 13.

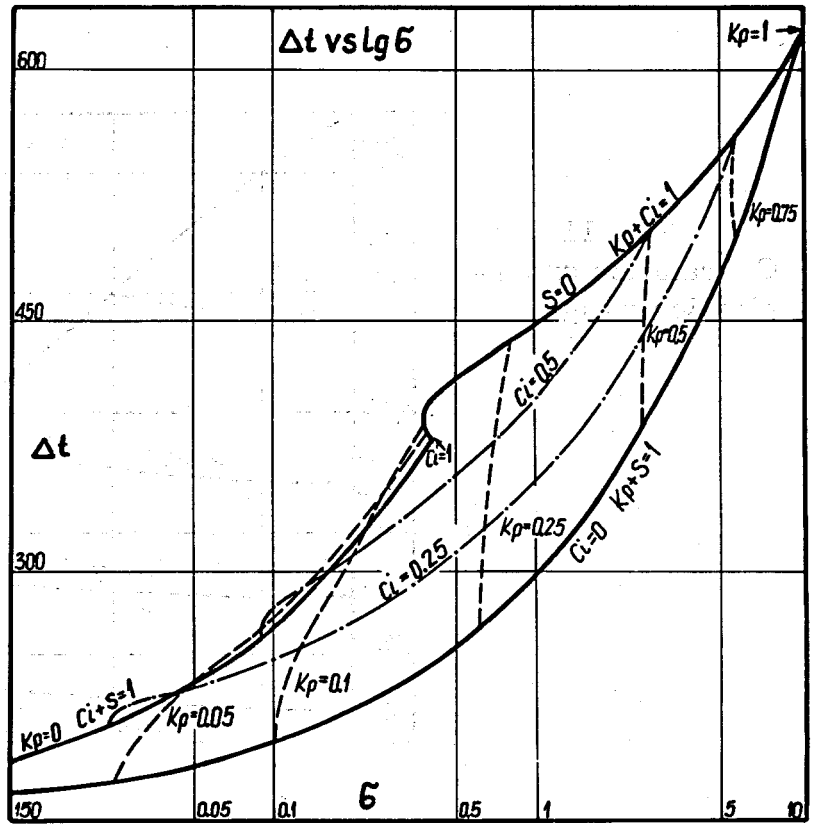

Fig. 13
Correlation crossplot Δt vs lgσ

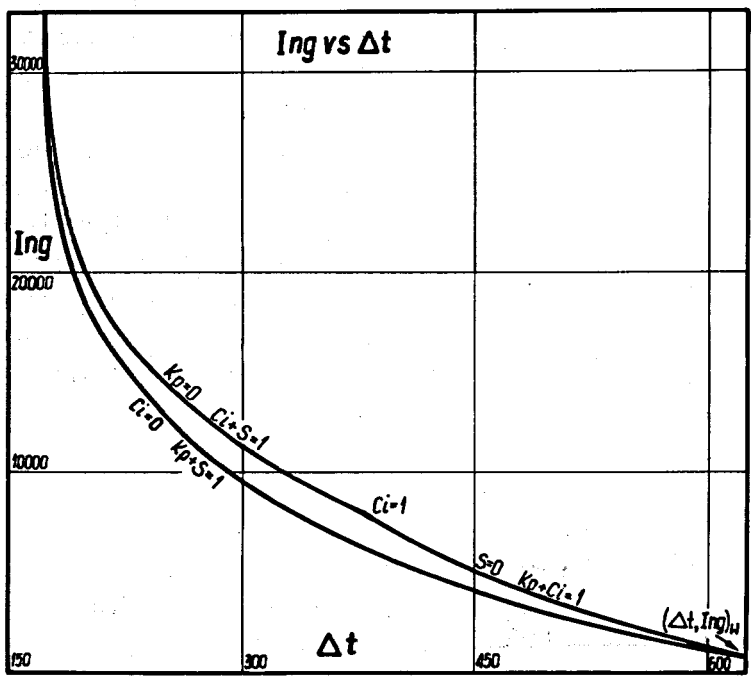

Fig. 14
Correlation crossplot Ing vs Δt

The data set Δt=f/σ/ is limited by the curve for Ci=0 at the bottom and by the curves for Kp=0 and S=0 at the top. Fig. 14 illustrates the correlation crossplot of neutron and acoustic logs. The data set is contained in a very narrow curved band of observation. The data Ing=f/Δt/ are limited by the curve for Ci=0 at the bottom, and by the two curves for Kp=0 and S=0 at the top.

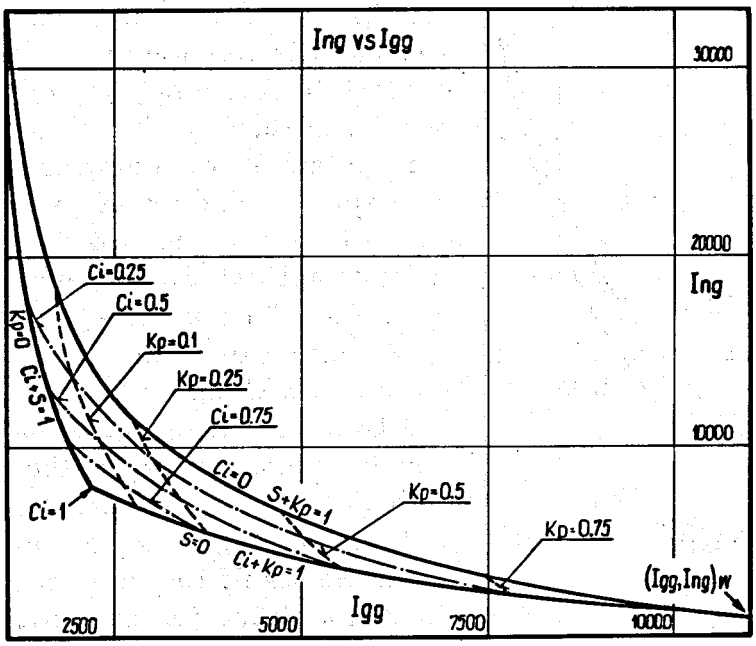

The correlation crossplot Ing vs Igg is presented in Fig. 15. As in all the previous cases, the data set is enclosed by a bent triangle with the two definite vertexes: water and clay, and with the third vertex in infinity, due to the assumed model.

Fig. 15
Correlation crossplot
Ing vs Igg

The correlation crossplot Igg vs Δt /Fig. 16/ is a typical slightly bent triangle with definite vertexes for water, clays and matrix.

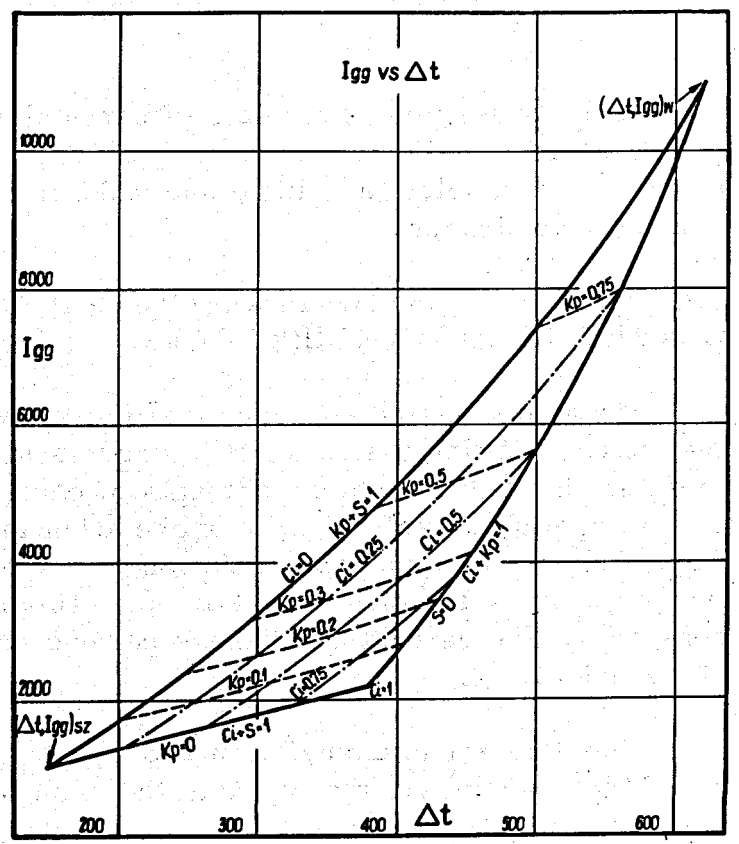

Fig. 16
Correlation crossplot
Igg vs Δt

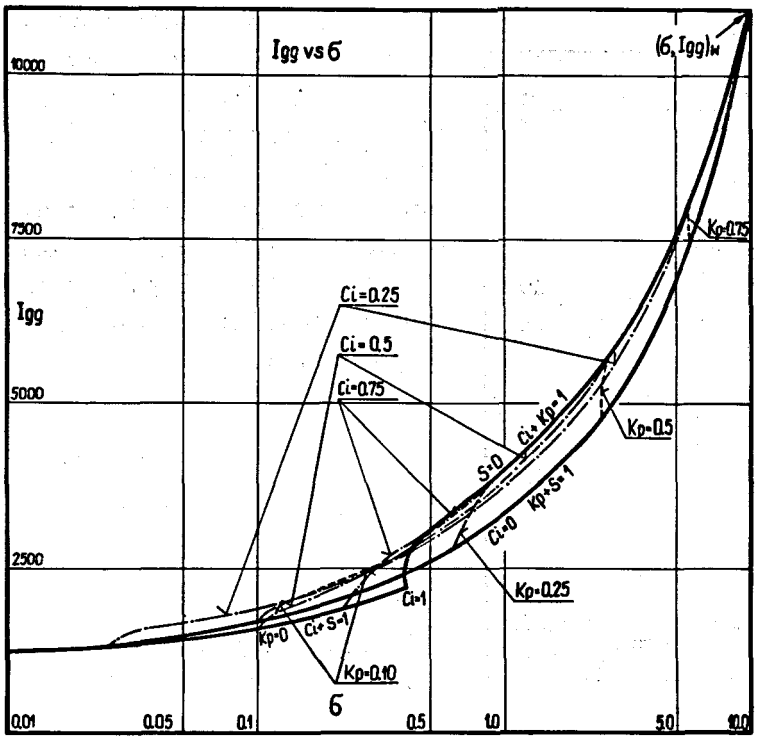

The correlation crossplot of the results of gamma-gamma density logging and resistivity logging /Igg vs6/, presented in Fig. 17, closes the review of correlation crossplots. The arrangement of data set is extremely complicated, where the effects of porosity and clay content overlap and intersect making up a curved band of difficult-to-determine parametres of the curves limiting the set. This crossplot does not recommend itself for use in the autocalibration method.

Fig. 17 Correlation crossplot Igg vs σ

In the presented crossplots of particular logging methods of little practical usefulness are the crossplots Igg vs σ and In vs Δt. The remaining crossplots are lucid and make it possible clearly to determine boundary conditions.

METHODS OF ESTIMATING THE PARAMETERS OF BOUNDARY CURVES IN AUTOCALIBRATION

It was demonstrated above that the knowledge of the parameters of the curves limiting the data set in correlation crossplots makes it possible to determine calibration coefficients of particular well-logging methods, i.e. to specify a problem in interpretation in a simple and reverse way. Depending on the kind of correlation crossplots, the parameters of the limiting curves are the basis for estimating most or all the necessary constants. The estimation of these parameters is multi-staged, by way of iteration.

The data set in correlation crossplots presents a "cloud" of points $y_i = f/x_i/$, where y_i and x_i are the cross-correlated results of the presented logging methods. This set has its extreme values: x^{min}, x^{max}, y^{min} and y^{max}. When stretching on this set a regular rectangular net-

work, limited by the extremes of the set, with the following dimensions of a single rectangular "mesh" /element/:

$$\frac{x^{max} - x^{min}}{n}, \qquad \frac{y^{max} - y^{min}}{m} \qquad /19/$$

one can obtain the superficial discretion of the set. Therefore, the network will have n columns and m lines, i.e. it will have n·m elements. Each element can have 0.1 or more observation points.

Since the linearization of well-determined curves is almost always possible using elementary algebraic transformations, it is possible to consider for example the estimation of the boundary curve's parameters such as for instance for the condition Kp=0 in the crossplot PN vs PG /Figs.7 and 8/. This is the upper limiting straight line. Therefore, for calculations one uses only the data embraced by the upper k elements of the network for a given column, starting with the first filled-in /non-zero/ element. In this way, one determines the data set nearest to the upper limit, and its dimensions do not exceed n.k elements of the network.

The further procedure confines itself to the estimation of the parameters of linear regression, using for example the smallest squares method in its orthogonal variant:

$$y - \bar{y} = \frac{r}{|r|} \frac{S_y}{S_x} (x - \bar{x}) \qquad /20/$$

where $\bar{x}$ and $\bar{y}$ are mean values, Sx and Sy are standard deviations of the sets {x} and {y}, respectively, selected by means of the above-discussed method. The straight line determined in this way additionally necessitates parallel shifting upwards by the value of the Sy line which will result in the first estimated approximation of the upper limiting straight line.

Methods to determine one of the limits is schematically presented in Fig. 18. Using methods of statistical and geometric division of the area embracing grouped data one can approximately determine the equation of the upper limiting straight line. Additional suitable shifting is necessary. The application of the so-called reduction lifter in the next steps of the iteration process, including corrections considering porosity and clay content, will make the solution more precise. The course of the iteration process is presented in Fig. 22.

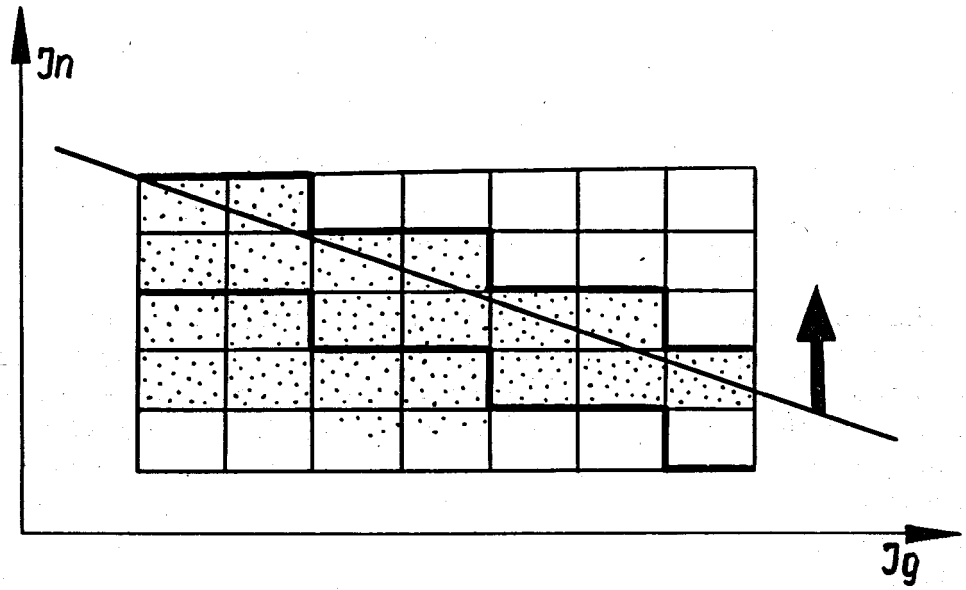

Fig. 18
Examples of geometric presentation of a data set in correlation crossplot

Using the parameters of the limiting curves /straight lines/ determined in this way, one can further estimate the set of the calibration coefficients necessary in interpretation. As a result, one can begin preliminary quantitative interpretation, i.e. estimation of porosity Kp and clay content Ci, etc., for every point, using the existing relationships.

In the case analysed above by way of example for the crossplot In vs Ig /Figs. 7 and 8/, the aim is to estimate the parameters of the boundary straight line satisfying the condition Kp=0.0. The first approximation is obtained by means of the observed values selected in the above-described way. However, it would be advisable to transform the input data set to observe the boundary condition and at the same time to eliminate the smallest possible number of data. For this purpose the "dynamic reduction filter" is used improving the input data and reducing them so that they correspond to near-zero porosity. Already knowing the values of Kp_i for the i-th point, using the relationships /5/, the input value dIn_i is calculated as if the measured effect came from clay content only, omitting porosity. The reduced value dIn_i can be put in terms of the following relationship:

$$dIn_i^{red\,Kp} = - \frac{lg\left[\left(\frac{W}{Kp1}\right)^{-dIn_i} - R\,\frac{Kp_i}{W}\right]}{lg\,\frac{W}{Kp1}} \qquad /21/$$

where: dIn_i and Kp_i - input values for dIn and the interpreted Kp for the i-th point; w and Kpl - extreme neutron values of porosity, estimated as a result of preliminary processing /as above/; $dIn_i^{red\ Kp}$ - transformed input value dIn for the i-th point reduced by a certain part of the effect coming from porosity Kp; R - reduction coefficient or rather reduction function determining what part of the effect coming from Kp should be taken into consideration in the carried out reduction. R satisfies the condition:

$$0.0 < R \leq 1.0 \qquad /22/$$

At the initial stage of processing it is not recommended to eliminate the whole effect coming from porosity Kp, since the error of the interpreted value Kp can be considerable at the preliminary estimation of calibration parameters. On the other hand, in the course of improving the quality of calculations in successive iterations it is possible systematically to increase the figure R which can be obtained by dynamic linking of R with the number of the successive approximation, e.g.:

$$R = r\ /nr\ iter/^z \qquad /23/$$

where r - reduction coefficient dependent on the expected number of iterations embracing the re-estimation of the values of the searched for parameters; z - possible index regulating the dynamics of filtration; nr iter -- number of a successive iteration.

Another exemplary formula for the reduction filter for the correlation crossplot PO vs PG, based on the relationship /9/, can have the following form:

$$\sigma_i^{red\ Kp} = \sigma_i - R \cdot a \cdot Kp_i^m \cdot \sigma w \qquad /24/$$

where σ_i and Kp_i - the input value σ and the interpreted value Kp for the i-th point; a, m - Archie coefficients, as related to the relationship /9/, estimated as a result of the first or j-th iteration; σw - set conductivity of deposit water, $\sigma_i^{red\ Kp}$ - processed input value σ for the i-th point reduced by a certain part /determined by the reducer R/ of the effect coming from porosity Kp. Similarly, one can also form formulas specifying reduction filters for other sets from other methods.

The sets of input data - $\{dIn_i^{red\ Kp}\}$ or $\{\sigma_i^{red\ Kp}\}$, etc., - reduced by means of the dynamic reduction filter are the input data in the following step, and the whole process with the eliminating network and with the estimation of regression parameters is repeated. So, the presented methods leads to processing the sets so that the initial irregular "cloud" in the correlation crossplot produces as narrow a band of data as possible representing the boundary curve /or straight line/. By way of iteration, using ever more intensive reduction, after a proper number of steps, the effect can be practically obtained of complete elimination and the found parameters of regression are those searched for.

The numbers n, m and k for the network as well as r and z for the dynamic filter should be selected experimentally, taking into account the size of the set, the distribution of parameters and the statistically indispensable smallest number of points in a single element of the network, etc., and both geological and statistical conditions. Also economic factors can have an effect to bear for example on the value of the reduction coefficient r, since assuming a limited number of iterations, for instance as regards the value L, there must be:

$$r \leq L^{-z} \qquad /25/$$

The process of estimating the parameters of boundary curves should additionally take into consideration geological and physical limitations. For example, when in a concrete correlation crossplot one of the coordinates' values exceeds a physically possible value /grave error/, the point they produce can and should be eliminated by employment of simple limitations. Similarly, when as a result of interpretation a significant saturation with bitumens is obtained for a given point in the j-th iteration, such a point, as abnormal, should not have a bearing on the estimated parameters and must be eliminated. In anticipation of the further discussion on errors and on the resulting conclusions, it is necessary to mention here that a data set should have a limited area of changes that ensures an optimum solution to the problem. This element, too, can be effected on the basis of conventional limitations imposing the condition that estimation solely embraces point complying with respective requirements, e.g. Ci greater than 0.05, etc.

Of importance to the iteration process of autocalibration are systematic control of the obtained results' correctness as well as control of their quality and of their improvement degree at successive steps. However, no possibilities exist of direct control, of referring to real patterns. If they existed, there would be no need for autocalibration. Therefore, indispensable are indirect methods controlling the estimation process of the searched for parameters and assessing their value.

Autocalibration is performed for a number of logging methods at a time, for instance for PN+PO+PG. As a result of obtaining calibration parameters, a number of geological factors are interpreted such as porosity Kp and clay content Ci, etc. Taking into consideration the above-mentioned concrete case, one can obtain for instance the sets $\{KpN_i\}$ and $\{KpR_i\}$ resulting from the estimation of rock porosity according to neutron and electric data with reduced clay content /see the relationships/. The objective is to obtain the maximum convergence of these data. Therefore, a measure of the quality of those calibration parameters can be the mean square deviation d_1 of the two sets. Another measure of quality can be the classical correlation coefficient d_2 of the two sets, since it determines the convergence of both interpretation results that should give a well-determined straight line in the crossplot KpN=f/KpR/. Significant will also be the tangent of this line's inclination angle whose deviation from the value 1.0-d_3 will be a measure of the calculations result's correctness.

When assessing interpretation quality, geological criteria should be taken into consideration. The number of cases, when the value Kp differs from the real limits - d_4, and similarly Ci - d_5, and also /Kp + Ci/ - d_6 /negative numbers or those greater than 1.0/ is also an important element of estimation. Similarly, one should note d_7 - cases of interpreted considerable saturation with bitumens that cannot be too frequent as abnormal phenomena.

All in all, the quality factor D can be defined as a function of the following kind:

$$D = (1-d_1)^{w1}\, d_2^{w2}(1-d_3)^{w3}(1-d_4)^{w4}(1-d_5)^{w5}(1-d_6)^{w6}(1-d_7)^{w7} \qquad /26/$$

where w1 - w7 are the weights of particular quality factor elements whose experimental choice should take into consideration emphasis on factors of greatest significance to a given problem to be solved.

If geophysical methods are available making it possible to investigate porosity, for instance from electrometry /KpR/, neutron logging /KpN/, acoustic logging /KpA/ and density logging /KpGG/, the final quality factor can be presented in the following way:

$$D_\Sigma = D^{wg1}(KpR, KpN)\cdot D^{wg2}(KpR, KpA)\cdot D^{wg3}(KpR, KpGG)\cdot \qquad /27/$$
$$\cdot D^{wg4}(KpN, KpA)\cdot D^{wg5}(KpN, KpGG)\cdot D^{wg6}(KpA, KpGG)$$

where wg1, wg2 ....., wg6 are the weights of individual elementary quality factors satisfying the condition:

$$\sum_{i=1}^{6} wgi = 1 \qquad /28/$$

The elementary quality factor testing the convergence of two porosities originating from two different well-logging methods satisfies the law of convertibility:

$$D(KpI, KpJ) = D(KpJ, KpI) \qquad /29/$$

The value of the quality factor is standardized up to the interval $<0.0, 1.0>$.

The greater the quality factor, the better the evalutation of both porosities.

The total quality factor calculated on the basis of porosities resulting from different well-logging methods is interpreted in the same way.

Interpretation of many bore holes by means of the SAIK system demonstrates that under favourable conditions the elementary quality factor ranges from 0.7 to 0.85. If the quality factor drops below a certain definite value, the comment is printed: attention - uncertain interpretation result or attention - uninterpretable data.

Such standardization of quality function can also be interpreted between particular bore holes.

It is assumed that an interpretation result of a greater quality factor is better.

Therefore, the quality factor D currently evaluates the correctness of procedure in successive iterations and can be additionally used in controlling the estimation process of calibration parameters in autocalibration.

OUTLINE OF THE COURSE OF BASIC OPERATIONS IN SAIK SYSTEM

The courses of individual basic operations performed in the system SAIK-2opty are presented in a schematic form below /Fig. 19/

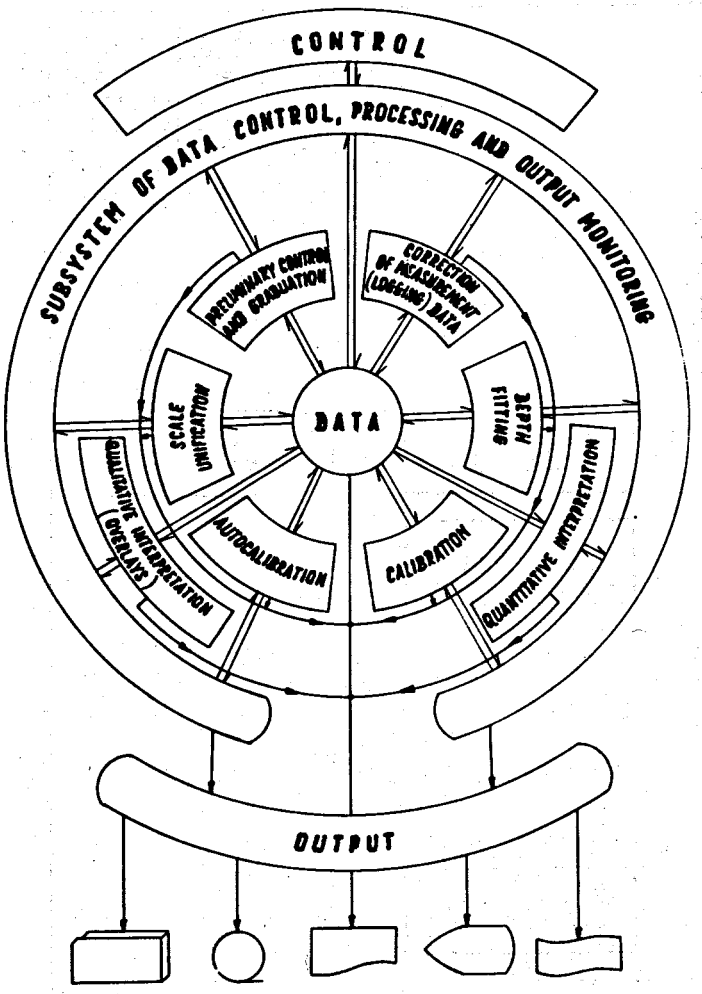

Fig. 19
Organizational scheme of SAIK system

The course of preliminary operations is illustrated schematically in Fig. 20. Successively, they are organizational operations, reading-in the control and input data, putting them in order and controlling the number of data.

Next come the modification and unification of the quanting step for the whole data set. These operations are effected by means of Tchebyshev or Lagrange's interpolation, using a polynomial of a definite order.

Then comes the unification of radiometric data, and next, when the existence is assumed of mutual depth shifts of individual profiles, depth fitting is performed.

This is followed by the correction of radiometric data to eliminate the diameter effect, and then a number of organizational operations are performed, and autocalibration comes next.

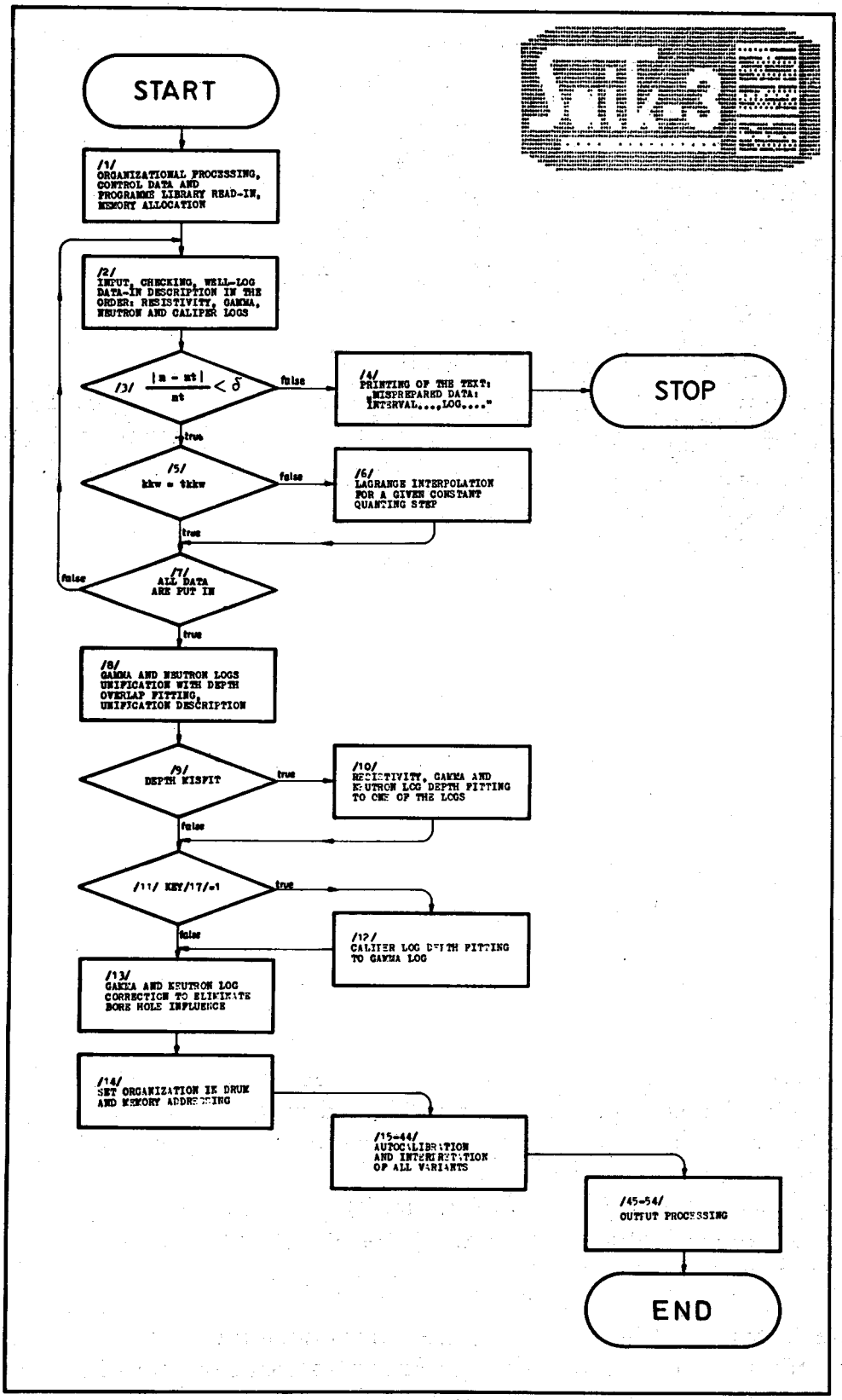

Fig. 20 Diagram of preliminary operations

$$[(PN \text{ vs } PG) \wedge Kp = 0.0] \Longrightarrow dIn = a \cdot lg\, dIg + b$$

$$[(PO \text{ vs } PG) \wedge Kp = 0.0] \Longrightarrow lg\, G = c \cdot lg\, dIg + d$$

$$[(PO \text{ vs } PN) \wedge Ci = 0.0] \Longrightarrow lg\, Pp = e \cdot dIn + f$$

$$\Downarrow$$

$$m = -\frac{ae}{c}\,;\quad \alpha = \frac{1}{c}\,;\quad K_{Ci} = \exp\left(\frac{b}{a}\right);\quad Gi = \exp\left(d - \frac{bc}{a}\right);$$

$$\frac{W}{K_{p1}} = \exp\left(-\frac{c}{a}\right);\quad W = \exp\left(\frac{cf}{ae}\right);\quad K_{p1} = \exp\left(c \cdot \frac{[f+e]}{ae}\right);$$

Fig. 21 Scheme of autocalibration PN vs PO vs PG

The autocalibration course, in accordance with the scheme presented in Fig. 21, is illustrated in Figs.22 and 23. Preliminary operations, specification of the initial consecutive numbers of the variant and limitations /of the filter/, and also determination of the starting point are followed by preliminary interpretation. The sets are determined of relative differential parameters of radiation intensity, and then, after the first autocalibration, the scales are corrected of radiometric data. Then come the remaining autocalibration operations, according to the scheme presented in Fig. 21. The so-called "system variant" is effected in that way.

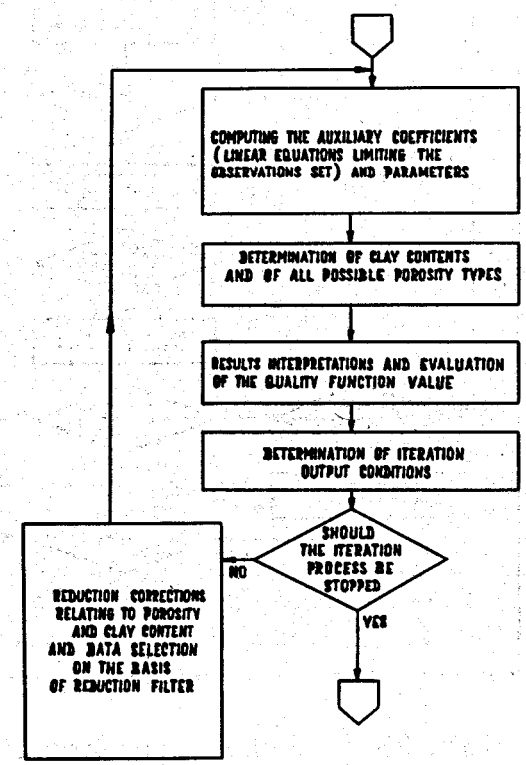

Fig. 22
Scheme of the main iteration process

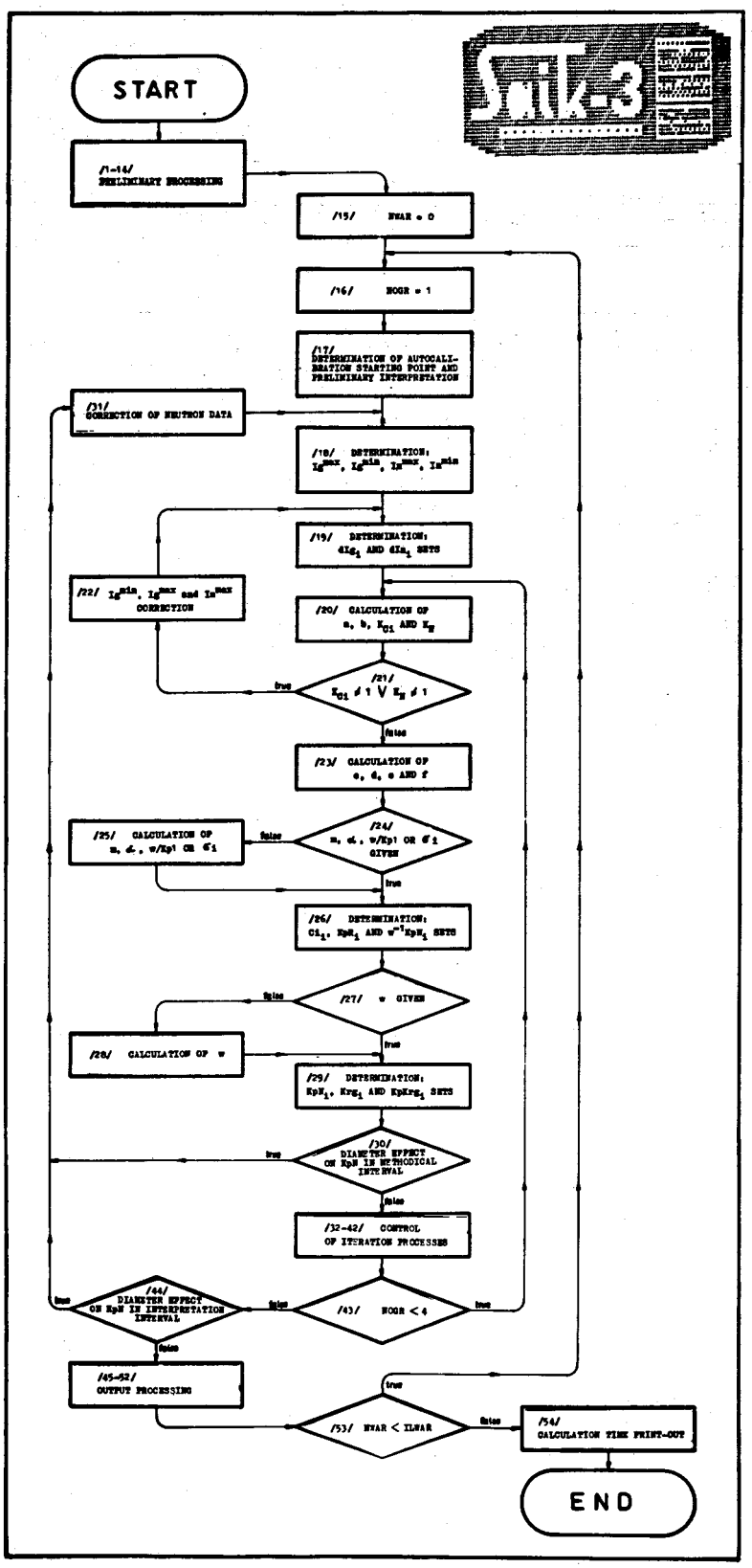

Fig. 23 Scheme of autocalibration course

If some of the calibration coefficients were known before and were included into the control data, the so-called "interpreter's variant" is effected, i.e. their values are used in the further processing.

The lacking parameters are determined on the basis of autocalibration in accordance with the scheme presented in Figs. 21 and 22.

Further on, the coefficient sets are determined of clay content Ci_i, porosity from electrometric data KpR_i, porosity from neutron data KpN_i, saturation with bitumens Krg_i, and of linear resources per depth unit $Kp\,Krg_i$. Later, it ascertained whether there is the diameter effect on the results obtained by neutron methods. If, despite the earlier correction of netron logging, such an effect is signalled, a correction is determined empirically and neutron data are re-corrected. This operation, as seen in Fig. 23, is performed by way of iteration, initially within the interval selected for determining autocalibration parameters /i.e., methodical interval/, and then within the whole interval chosen for interpretation.

Observation of porosity in logging also allows of separating the zones of the same lithology or structure of rocks or those exerting the same influence on the recorded physical phenomena.

An analysis of the value of the RL coefficient expressed by the following dependence makes possible lithological division for the whole log :

$$RL = R1|KpR-KpN| + R2|KpR-KpA| + R3|KpR-KpGG| + R4|KpN-KpA| + R5|KpN-KpGG| + R6|KpA-KpGG| \qquad /30/$$

where: R1, R2, ..., R6 are the weights satisfying the following condition:

$$\sum_{i=1}^{6} Ri = 1 \qquad /31/$$

Each component of this dependence embraces the two investigated porosities and, due to absolute value, has the same character. The coefficient of the weight Ri represents the value of this effect taking into consideration the weight of individual well loggings.

The criterion of the attachment of a definite depth point /in a log/ to the selected lithological type is the fact that the coefficient RL is comprised by the employed numerical interval. This allows of dividing the data

set into lithological sub-sets. It is assumed that in the first cycle all the depth points belong to the same lithological type. After maximizing the function of the quality factor, division is carried out into two sub-sets; in one of them the lithological criterion /RL/ does not satisfy the attachment condition. Then, the function of the quality factor is maximized and division into the further sub-sets takes place in this sub-set. In this way, as a result of successive selections, points are chosen belonging to the same lithological type.

Thus, the depth points in the log are divided into sub-sets satisfying the attachment condition except for one sub-set that does not. It is assumed that the last sub-set satisfying the attachment condition is the /final/ zone of the same lithology, whereas the remaining zones are approximate. As a result of this process, the lithological type is determined of the least certainty. This is a "purging" operation or preliminary lithological splitting. Then, by combining the sub-set not satisfying the attachment condition RL with the successive sub-set satisfying this condition, the maximization is effected of the quality factor function and lithological division is performed. The next final zone is obtained of the successive lithology. This procedure is continued as long as the predetermined number of lithological types is separated. Owing to the statistical character of this process it is necessary to check up whether sub-sets of the same type have a sufficient number of depth points.

The final effect of such lithological division is determination of the parameters indispensable to interpretation performed for every lithological type separately.

The sets of reservoir and packing rocks parameters determined in this way are put to final quantitative interpretation. The same number of lithological coefficients RL are calculated for every depth point in the log as that of the predetermined lithological types. The final criterion of attachment to a definite type is minimization of the factor RL within individual lithological types.

The results of rock porosity obtained from neutron logging have been analysed many a time already. On the basis of such an analysis, J.B. Nikolova /1971/ presented an improved variant of comprehensive methods to interpret neutron and gamma log data with view to determining the porosity coefficient.

When the porosity coefficient Kp for shale formations is determined using the neutron method, total water KpN includes water in the clay component, according to the following formula:

$$KpN = \widetilde{KpN} - Ci \cdot w \qquad /32/$$

where : w - total water /humidity coefficient/ connected with clay component; Ci - clay content.

The implementation of this method is limited by lack of direct information about the value w. It is often assumed that w in reservoir rocks is equal to the mean square value of w corresponding to the shales neighbouring the reservoir rock under investigation. As a rule, the value w ranges from 6 to 60 per cent. The assumption that w is the same for pure shale and for clay material in the neighbouring rocks can be correct for reservoir rocks with laminated shale, where clay material has the form of thin interlayers. In general cases or for formations with a structural or dispersed shale, the value w does not necessarily have to be the same. Changes in the dispersion of matrix grain, clay content and in the fractional and mineral composition of clay material should be followed by changes in total humidity in clay material. Humidity in the clay component of reservoir rock can be determined for layers with known porosity /Kp/ and clay content /Ci/, according to the formula /32/.

For carbonate rocks of Trias, Jura in the central and western parts of Northern Bulgaria, on the basis of laboratory data, J.B.Nikolova obtained values of w changing /from 20 to 88 per cent/ in the function of the apparent porosity of the matrix /$\widetilde{KpN}$/. Changes in $\widetilde{KpN}$ between 0 and 10 per cent were followed by increase in w up to 70 per cent, the further increase in $\widetilde{KpN}$ was followed by a slow growth of w up to 80 per cent on the average.

Replacing the symbol w of humidity, which is considered to be constant, by the symbol wbg which is variable humidity depending on clay content and porosity, the correlation between wbg, Ci and $\widetilde{KpN}$ is expressed by the formula /modo J.B. Nikolova, 1972/:

$$wbg = \frac{0.38\ \widetilde{KpN}}{Ci^{0.79}} \qquad /33/$$

The character of changes in wbg depends on the effect of the matrix strenght on the current condition of clay in the diagenesis process and can be explained in accordance to the scheme of the process of secular condensation of clay deposits.

In the process of autocalibration in the SAIK system, parameters and coefficients of calibration are estimated, among others for neutron and gamma radiometric methods. Estimated are also the average humidity w of clay material in the log as well as the quotient of the extreme neutron porosity

wkp = w/Kpl /J. Frydecki 1974, 1975/. These parameters can also be used on the basis of the information obtained by means of classical calibration or by the statistical processing of the data from bore cores and from well-logging using regressive analysis.

On the basis of the typical correlation of neutron method results in the function of porosity the formula /5/, the model of variable humidity in the "Bulgarian variant", analogically to that obtained by J.B. Nikolova, has the following form:

$$wbg = \frac{bbg \cdot w \cdot wkp^{-dIn}}{Ci^{abg}} \qquad /34/$$

The parameters of the Bulgarian coefficient of humidity in clay - abg and bbg are estimated by means of the method of smallest squares with Cramer's orthogonalization.

Assuming that:

$$y_i = \log /w.wkp^{-dIn_i}/ \qquad /35/$$

$$x_i = \log /Ci_i/ \qquad /36/$$

the searched for coefficients can be expressed in terms of the formulas:

$$\left.\begin{aligned} abg &= sign/r/\ \frac{Sy}{Sx} \\ bbg &= \frac{w}{10^{/\bar{y} - abg\ .\ \bar{x}/}} \end{aligned}\right\} \qquad /37/$$

where: $\bar{y}$, $\bar{x}$ - mean values of variables y_i, x_i

Sy, Sx - standard deviations of variables y_i, x_i

r - correlation coefficient.

The interpreted values of humidity in clay wbg in comparison with the interpreted values of clay content Ci and porosity Kp are presented for a series of bore holes in Poland, USSR, GDR and Hungary.

In the presented fragment of logging, using the system SAIK-2 optymal, at the Moskovskaya bore hole /fig. 24/, one can observe similar considerable variability in wbg. The results obtained there were: abg = = 1.43, bbg = 0.38, w = 0.15.

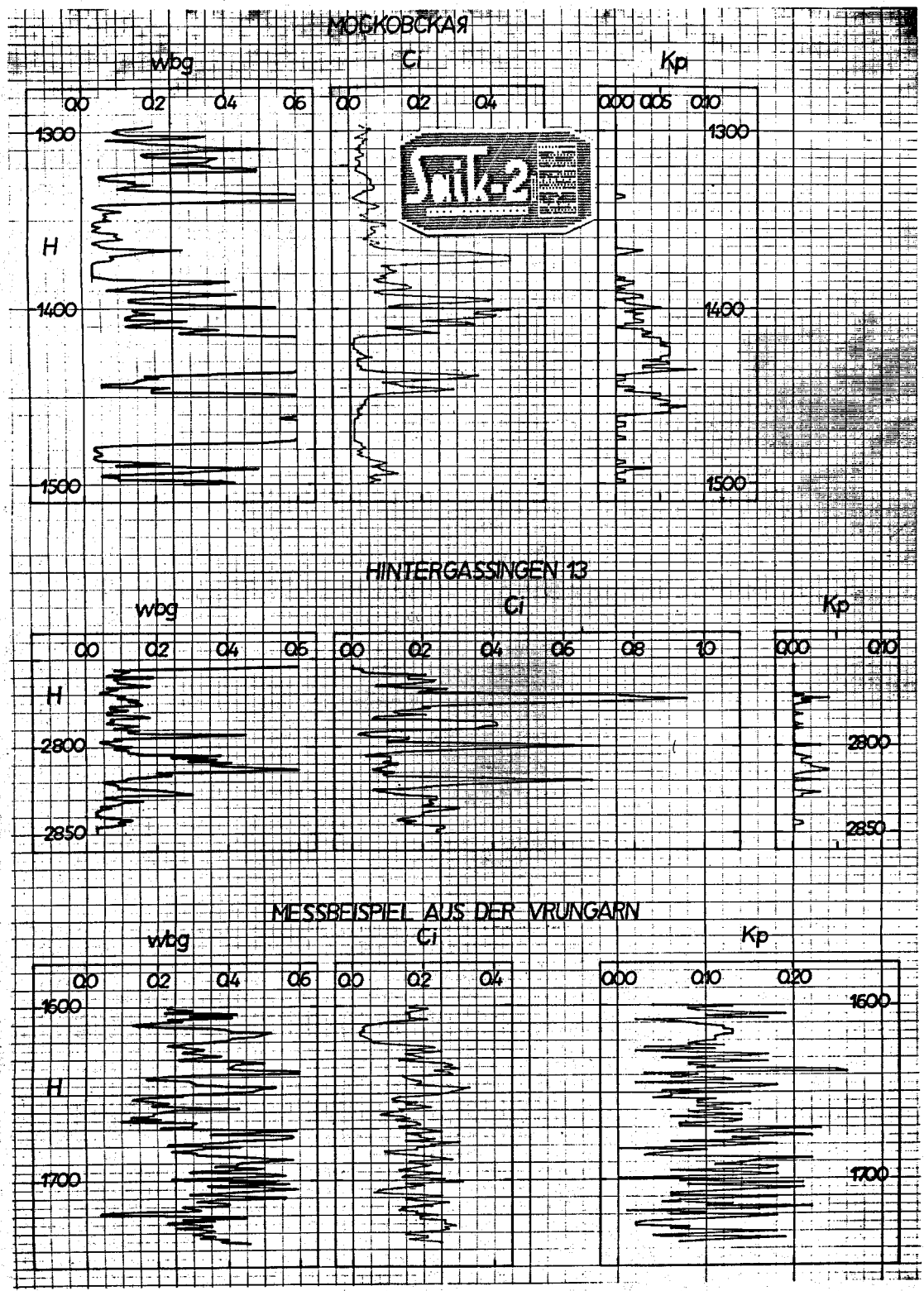

Fig. 24 Curves of changes in the humidity of clay material wbg, clay content Ci and porosity Kp as estimated on the basis of autocalibration in the system SAIK-2 optymal at the bore holes Moskovskaya /USSR/, Hintergassingen /GDR/ and Messbeispiel aus der VR Ungarn /Hungary/.

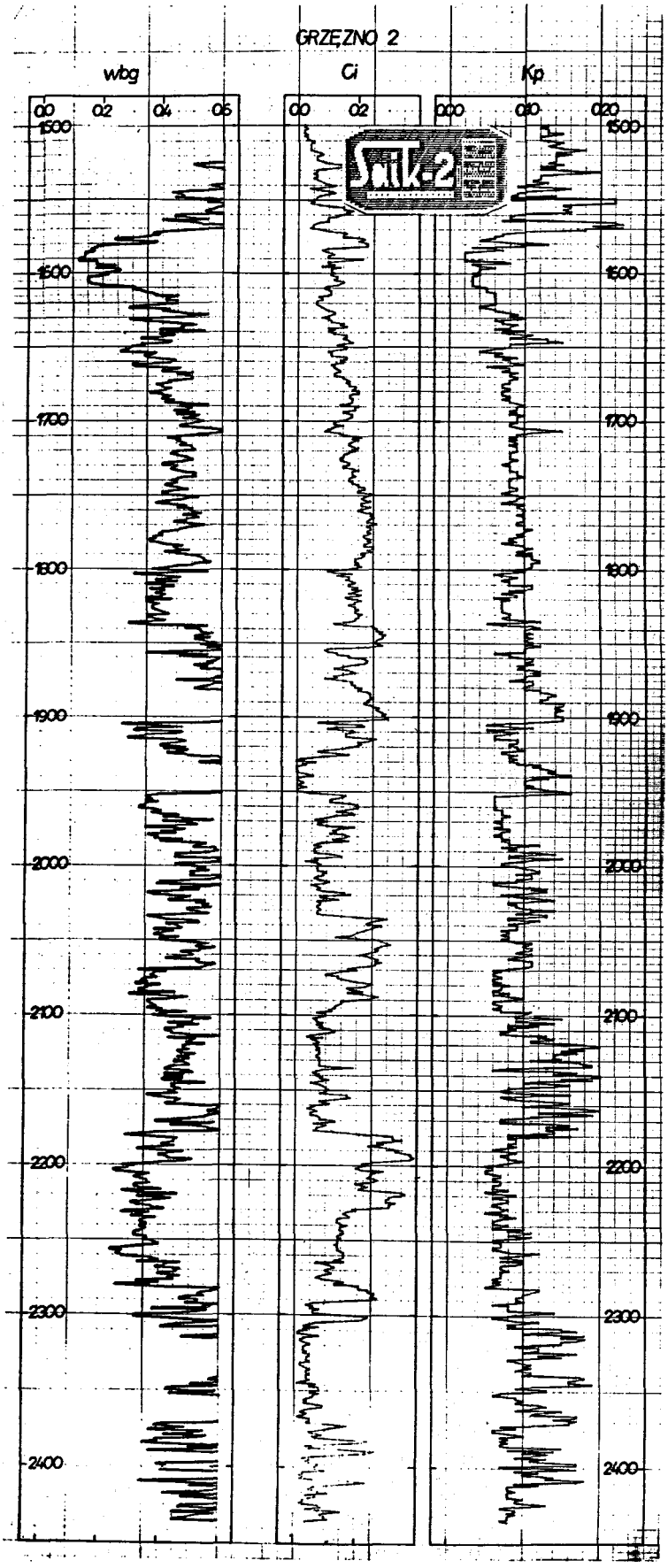

Fig. 25
Curves of changes in the humidity of clay material wbg, clay content Ci and porosity Kp as estimated on the basis of autocalibration in the system SAIK-2 optymal at the bore hole Grzęzno 2.

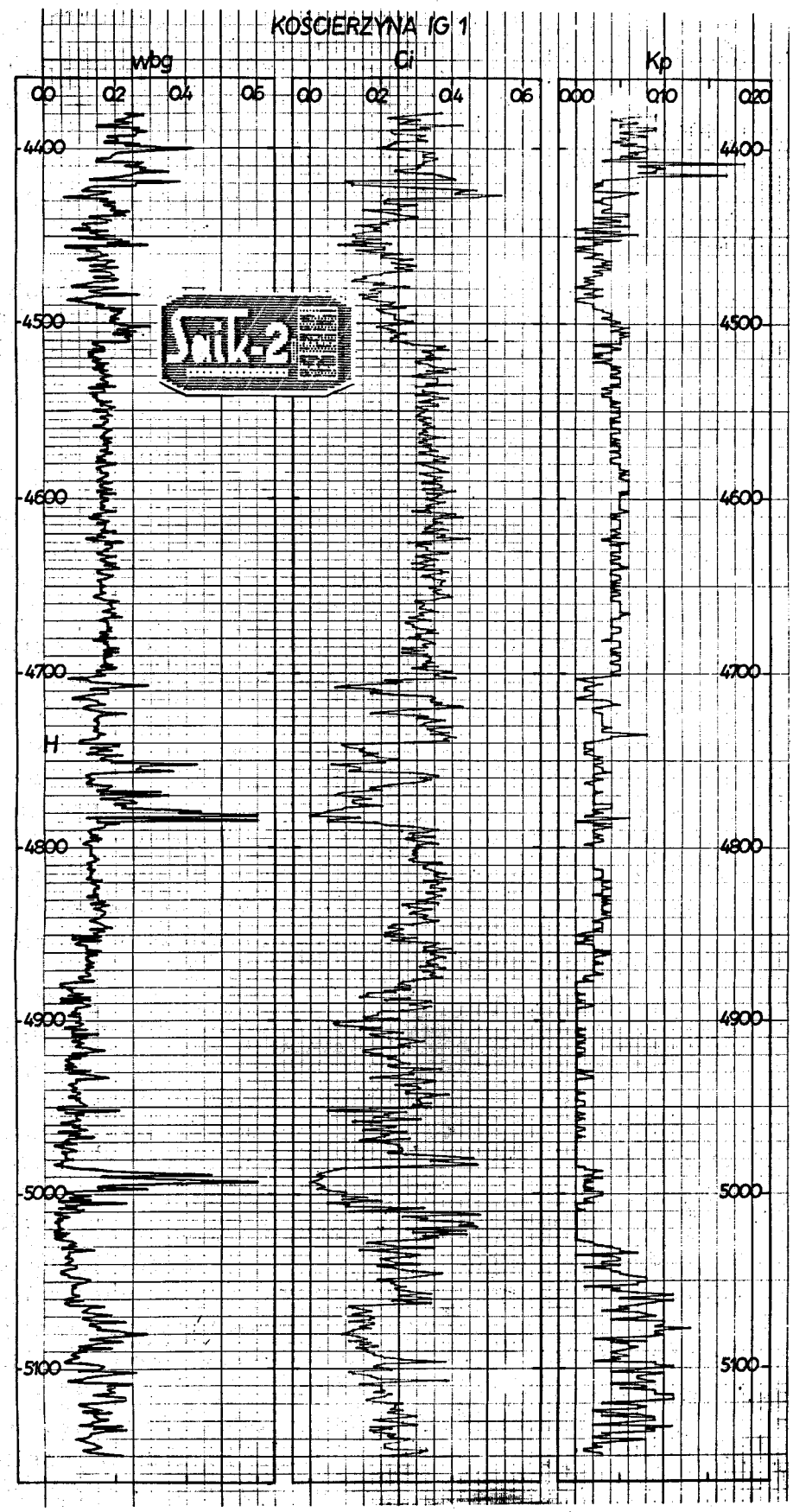

Fig. 26
Curves of changes in the humidity of clay material wbg, clay content Ci and porosity Kp as estimated on the basis of autocalibration in the system SAIK-2 optymal at the bore hole Kościerzyna IG.1.

On the other hand, step changes in wbg can be observed at the bore hole Hintergassingen 13, where the respective coefficients were: abg = 1.20, bbg = 1.00, w = 0.16 /Fig.24/. Considerable variability can be observed on the other hand at the Hungarian bore hole, where wbg ranges between 22 and 60 per cent on the average which is due to relatively great fluctuations of porosity Kp and to slight changes in clay content Ci. The results obtained there were: abg = 1.03, bbg = 0.51, w = 0.60.

At the bore hole Grzęzno 2 /Fig. 25/, one can observe a subsequent increase of wbg with depth, with fluctuations resulting from changes in clay content Ci and porosity Kp. The results obtained there were: abg = 0.59, bbg = 1.00, w = 0.38. This correlation, however, cannot be observed between wbg changes and depth at the bore hole Kościerzyna IG.1 /Fig. 26/ which is the deepest of the presented exemplary holes. In the latter, changes in wbg markedly accompany those in Ci and Kp and generally range from 10 to 30 per cent. At great depths, one can see more justifiable relatively low values in wbg. The results obtained there were: abg = 1.20, bbg = 0.52, w = 0.14.

So far, no significant effect has been noted of changes in either the depth or in the age of formation on wbg /the presented examples practically embrace a full age range - from the early Mesozoic to the late Paleozoic eras/, although the latter example /Fig. 26/ is indicative of such a possibility. On the other hand, the use in calculations of the variable model of humidity in clay in the "Bulgarian variant" wbg unmistakebly increases the effectiveness of identification of the rocks under investigation, thus improving the "quality factor" in the iteration process of optimization. At the same time, it seems that it will be advisable to use such a variable form in the process of evaluating the electric parameters of clay material, concretely of its electric conduction.

ERRORS AND GEOLOGICAL EFFECTIVENESS OF AUTOCALIBRATION

An important element of an analysis of the autocalibration method's effectiveness is discussion of the effect of "non-zero" boundary conditions on the obtained results. The method makes use of the form of a function under the boundary conditions of zero porosity, zero clay content or zero matrix volume. Deviations from this condition, therefore, can deform the calibration parameters obtained in this way and it is important to be aware of possible errors. Other errors, e.g. those resulting from poor logging, need no discussion, for they have a direct bearing on the obtained results.

Autocalibration PN and PG performed at the two basic boundary conditions $Kp^{min} = 0$ and $S^{min} = 0$ already makes it possible on the basis of these two logs /as demonstrated above/ to evaluate KpN and Ci and as a

rule gives all the indispensary calibration coefficients for these methods. The maximum error of this evaluation, calculated by means of the absolute differential method, depends on errors in the evaluation of individual coefficients, and also on the value of the assessed porosity. Relative errors in the evaluation of individual coefficients are especially dependent on the fact of obtaining and using the boundary conditions $Kp^{min} = 0$ and $S^{min} = 0$, and the estimated value of the relative error assumes the form of the following dependence:

$$\frac{\Delta KpN}{KpN} = S^{min} + \left(1 + \frac{w\,Ci}{KpN}\right) lg \left(1 + \frac{Kp^{min}}{w\,Cl}\right) \qquad /38/$$

illustrated in Fig. 27.

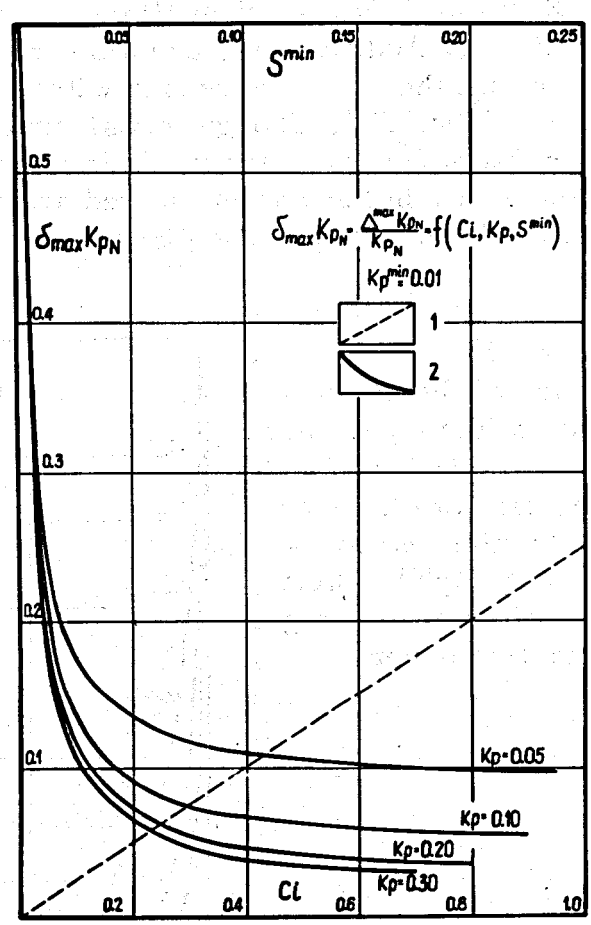

Fig. 27
Dependence of the maximum error of the evaluation of porosity from PN - KpN - on clay content and on the evaluated porosity value for $Kp^{min} = 0.01$ and for variable S^{min}.
1 - error connected with S^{min} /top scale/
2 - error connected with Kp^{min} /bottom scale/

The illustration refers to four cases of the evaluated porosity Kp = 5, 10, 20 and 30% and presents the effect of the element connected with non-zero boundary porosity and with the value of clay content in the horizons used in autocalibration /continuous curves/, and also the effect of non-zero boundary value S^{min} /dashed curve/. According to the dependence /38/, the total maximum error results from the sum of both elements. The effect of S^{min} on the maximum error is of linear character and needs no discussion except for it is an important result-blurring element.

On the other hand, an analysis of the other element leads to the conclusion that its effect is relatively inconsiderable on clay contents exceeding 5-10 per cent. Therefore, it is clear that for small Ci values, rapidly grows the possibility of false judgement, so the conclusion is drawn that observations corresponding to clay contents greater than 5-10 per cent should be used for correlation crossplots assuming the boundary condition Kp=0. This problem is clearly illustrated as regards the most important coefficient a /formulas 10-13/ of the greatest effect on the judgement of KpN depending on changes in Ci and Kp^{min} /see Fig. 28/. Cases were analysed for Kp^{min} = 0.01, 0.02 and 0.04 as well as a full interval of Ci value variations. The least advantageous case of Kp^{min}= 0.04 entails false judgements of this coefficient /which has the most significant bearing on evaluations of KpN then/ smaller than 10 per cent already for clay contents exceeding 5 per cent. Additionally, one also arrives at the intuitively apparent conclusion that the error increases with the decrease of porosity under examination /Fig. 27/. Though incosiderable, this factor cannot be eliminated. On the other hand, the remaining elements of the error can be reduced considerably in the way presented above and, if possible, by the elimination of the boundary condition S^{min} = 0 from autocalibration.

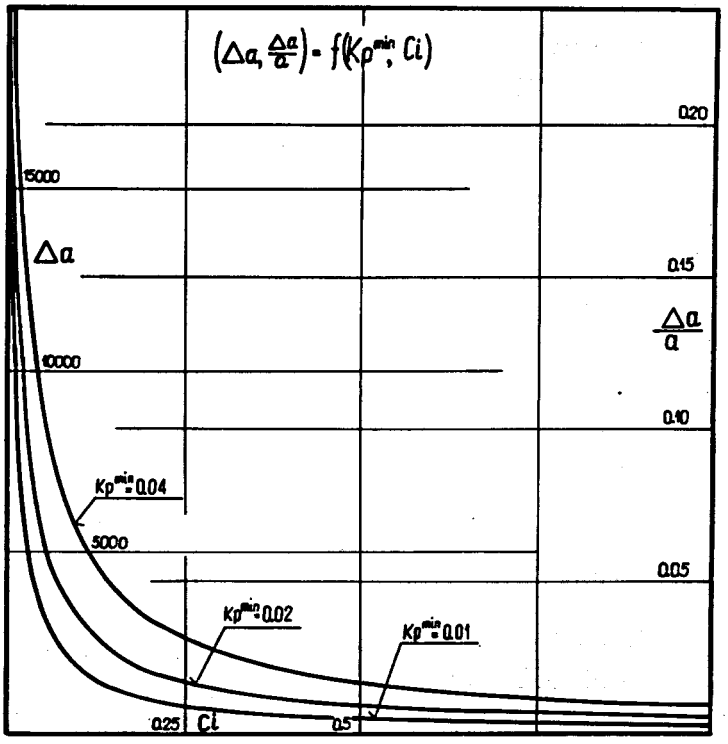

Fig. 28
Dependence of the evaluation error of the coefficient a for autocalibration In vs Ig in the function of clay content Ci and minimum boundary porosity Kp^{min}. Left axis - absolute error; right axis - relative error

The maximum relative evaluation error of clay content Ci also depends on S^{min} and just is S^{min} which, of course, needs neither illustration nor comment. In the boundary values Kp^{min} and S^{min} were known, the real porosity and clay content values could be put in terms of the

following formulas:

$$KpN = \left(1 + S^{min} + \frac{Kp^{min}}{W\,\overline{Ci}}\right) \cdot \overline{KpN} + Kp^{min} \qquad /39/$$

$$Ci = (1 - S^{min})\,\overline{Ci} \qquad /40/$$

where: $\overline{KpN}$ and $\overline{Ci}$ - porosity and clay content are evaluated according to the presented methods assuming the boundary conditions $Kp^{min} = S^{min} = 0$.

Autocalibration P0 vs PG makes it possible, as above, to estimate porosity KpR and clay content Ci. The maximum relative evaluation error of KpR estimated using the absolute differential method can be reflected by the formula:

$$\frac{\Delta KpR}{KpR} = \frac{1}{m}\left[\frac{Kp^{min}}{KpR}\right]^{m} + S^{min} \qquad /41/$$

As shown in the formula, the error depends on the value of the stimated porosity. Here, too, the element connected with the non-zero boundary value S^{min} is a separate linear component. That is why, the illustration of error variations /Fig.29/ is presented in the same way as the previous illustration by separating the two main component from one another. Similarly, the three boundary values $Kp^{min} = 0.01$, 0.02 and 0.04 were considered for a full interval of Kp variations. Figs. 29a and 29b present linear and logarithmic variants of errors, respectively. The value of the maximum error significantly depends on S^{min} and, to a far smaller extent, on Kp^{min}.. The basic conclusion drawn from this analysis is the same as before. If it is possible to eliminate the use of boundary condition $S^{min} = 0$, the error is relatively small for greater values of the estimated porosity. Unfortunately, for low-porosity formations, the relative error rapidly grows /which is apparent even intuitively/ and no possibility exists to reduce it.

When the boundary values of S^{min} and Kp^{min} are known, a possibility exists to estimate the real value of KpR in accordance with the following dependence:

$$KpR = \left[(1 - S^{min})^{m} \cdot \overline{KpR}^{m} - (Kp^{min})^{m}\right]^{1/m} \qquad /42/$$

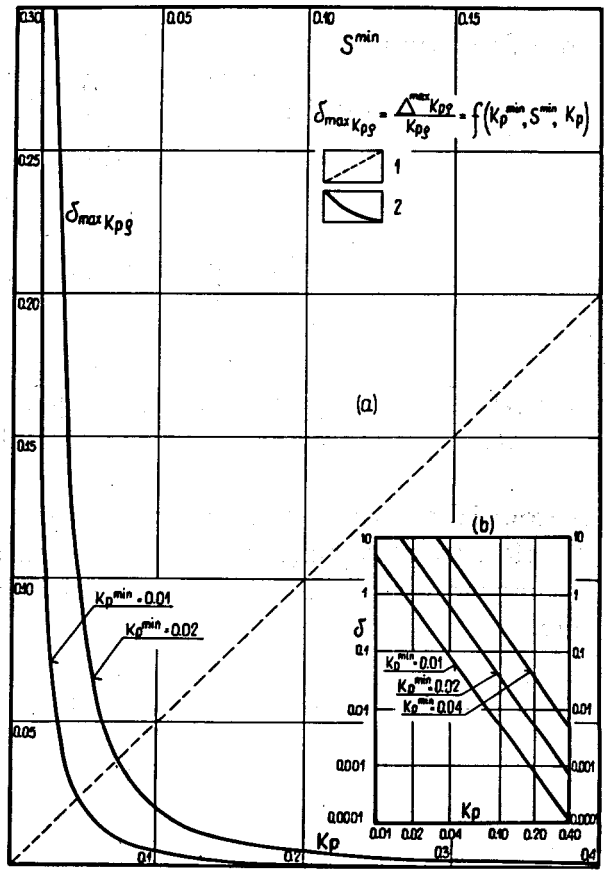

Fig. 29
Dependence of the maximum evaluation error of porosity from PO - KpR on the value of the estimated porosity and on boundary condistions Kp^{min} and S^{min}

1 - error connected with S^{min} /top scale/
2 - error connected with Kp^{min} /bottom scale/
a - dependence in linear scale
b - dependence in logarithmic scale

where symbols are the same as before.

The maximum relative error of clay content assessment is reflected in the same way as in the previous case and simply equals S^{min}.

As in the previous cases, the maximum evaluation error was considered of porosity according to PA and of clay content according to PG after autocalibration PA vs PG. Relative errors are reflected by the following relationships, respectively:

$$\frac{\Delta KpA}{KpA} = \frac{1-KpA}{KpA} \cdot KpA^{min} + S^{min} \qquad /43/$$

$$\frac{\Delta Ci}{Cl} = Kp^{min} + S^{min} \qquad /44/$$

The porosity evaluation error is illustrated in Fig. 30 in a way similar to the previous ones by separating the elements connected with Kp^{min} and S^{min} in accordance with the dependence /43/.

In this case, the error connected with Kp^{min} is also dependent on the value of the estimated porosity and decreases with its growth, whereas it

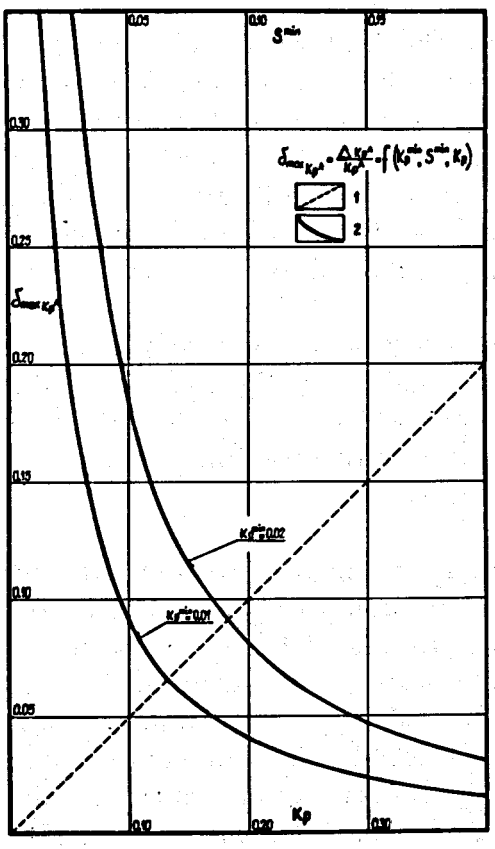

Fig. 30
Dependence of the maximum evaluation error of porosity from PA - KpA on the value of the estimated porosity and on boundary conditions Kp^{min} and S^{min}

1 - error connected with S^{min} /top scale/
2 - error connected with Kp^{min} /bottom scale/

grows linearly with the increase of Kp^{min} /two case are presented here: $Kp^{min} = 0.01$ and 0.02/. The maximum error of clay content evaluation is simply linearly connected with Kp^{min} and S^{min} and it is useless to illustrate it.

Conclusions drawn from this analysis do not substantially differ from the previous ones and actually can solely refer to the problem of S^{min} as above.

Of the same form as for PA are the relations between maximum errors for PGG - relationships, as follows:

$$\frac{\Delta KpGG}{KpGG} = \frac{1-KpGG}{KpGG} \cdot Kp^{min} + S^{min} \qquad /45/$$

$$\frac{\Delta Ci}{Ci} = Kp^{min} + S^{min} \qquad /46/$$

and that is why it is needless to illustrate or discuss them.

The general conclusion drawn from this sample analysis is suggestive of eliminating the boundary condition $S^{min} = 0$ from autocalibration and of

using it solely in emergency cases due to the lack of a third log. It is necessary, however, to realize the error made then. The remaining conclusions refer to the limitation of the information used in the autocalibration process. When making use of the boundary condition $Kp^{min} = 0$, it is advisable to use data from high clay content levels. Similarly, when using the boundary condition $Ci = 0$, it will be necessary to make use of the information concerning formations of greater porosity values.

The two basic conclusions have already been currently taken into consideration, beginning with the second generation of the system, i.e. with SAIK-2, where respective limitations were effected and the autocalibration process was solely based on the boundary conditions concerning porosity and clay content - $Kp^{min} = 0$ or $Ci^{min} = 0$.

The results of the geological interpretation of well-log data are put among others in the form of variant plots by compiling histograms of the calculated parameters. Fig. 31 shows a series of histograms for the distribution of clay content Ci in the Jurassic system /respectively: Lower Jurassic Period - J_1, Middle Jurassic Period - J_2 and Upper Jurassic Period - J_3/ and in the Lower Cretaceous Period - K_1. Individual curves mean the proportional distribution of clay content Ci in particular bore holes; the continuous thick red line is for the total distribution in all the bore holes. Some separations of the lines as well as slight local extremes are observed that can be explained by a small error of interpretation, and also and first of all by geological changes from bore hole to bore hole. All in all, very good convergence and uniformity have been obtained of particular logs which can be a basis of, for example, regional maps of the distribution of clay for these formations.

Fig. 32, too, shows histograms for clay content Ci in Jurassic and Cretaceous formations. In this case, some marked anomalies are observed and their form differs from the background and from the other curves. Deviations are observed for an M-1 bore hole within formations of the lower Jurassic J_1 and lower Cretaceous K_1 periods. The causes of these deviations are illustrated by Fig. 33, where histograms are plotted for bore hole M-1 with the basic material for interpretation, that is the curve of gamma logging. So, for the lower Jurassic formation J_1 there are practically only two extreme values of gamma radiation intensity from which only two values of clay content Ci can be interpreted, of course, since the logging of the lower Jurassic formation in this bore hole is reduced to the presented layers. In case of the lower Cretaceous formation the reduction is far greater. In bore hole M-1 only a small fragment was observed of typical Cretaceous sediments illustrated by the curve of gamma logging. Taking no account of statistical fluctuations, this is practically only one value of intensity and naturally only a single value for clay content Ci could be interpreted.

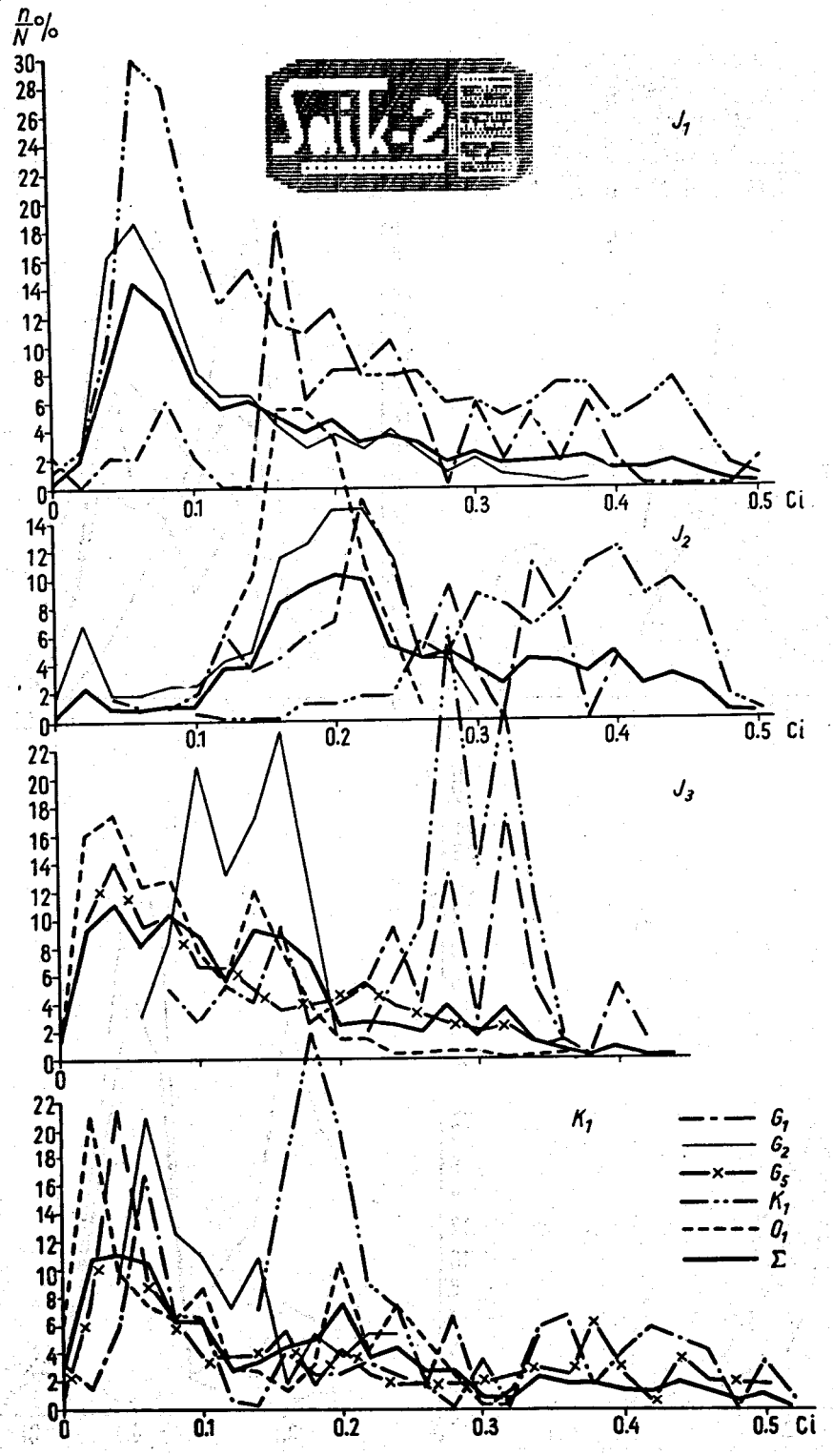

Fig. 31

Proportional histograms of the distribution of clay content Ci in region 1. J1, J2, J3 and K1 - the lower Jurassic formation, the middle Jurassic formation, the upper Jurassic formation and the lower Cretaceous formation, respectively;

G-1, G-2, G-5, K-1, 0-1 - bore holes illustrated by the presented separate variant curves;

Σ - total regional clay content Ci

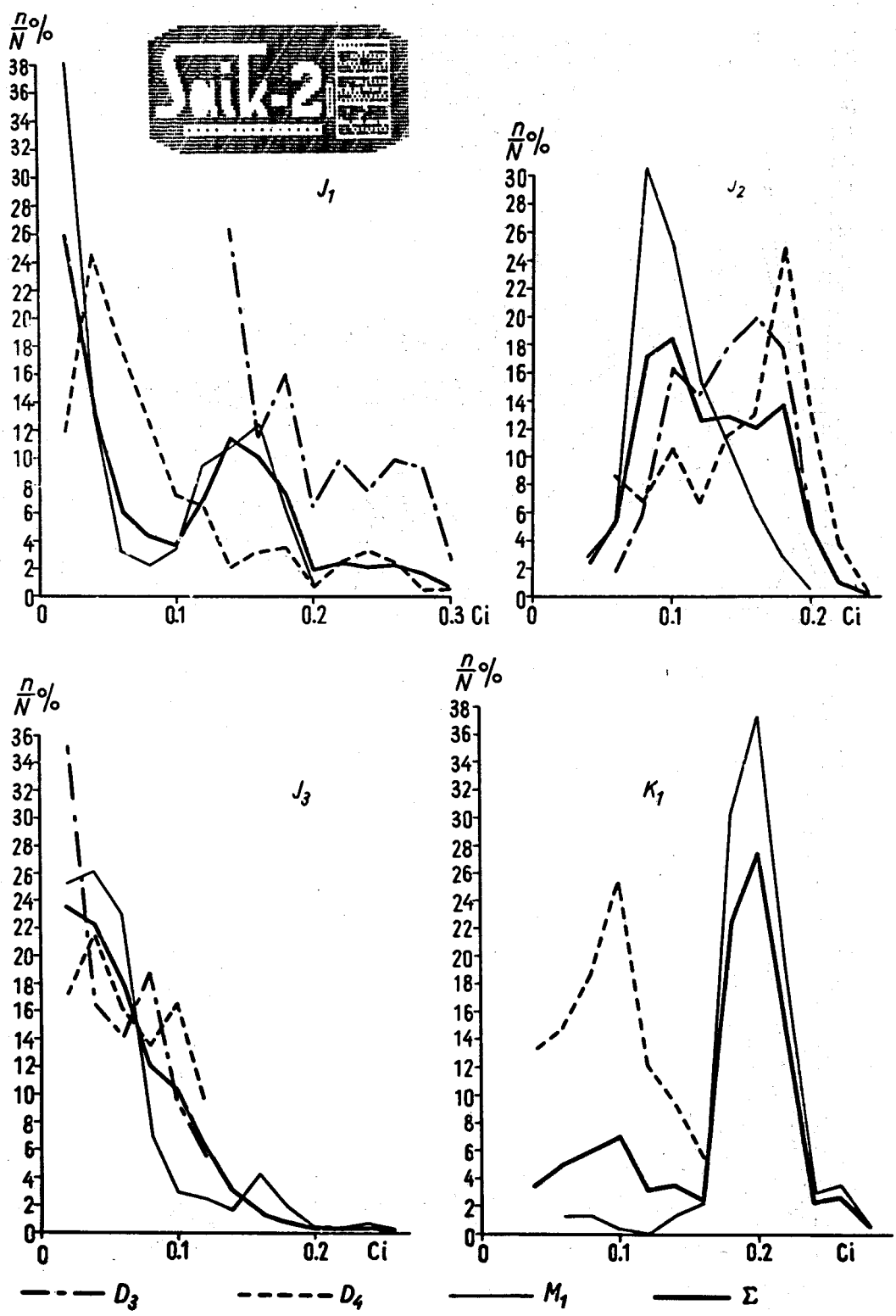

Fig. 32
Proportional histograms of the distribution of clay content in region 2.
J1, J2, J3, K1 and Σ - as in Fig. 31
D-3, D-4 and M-1 - bore holes illustrated by the presented separate variant curves

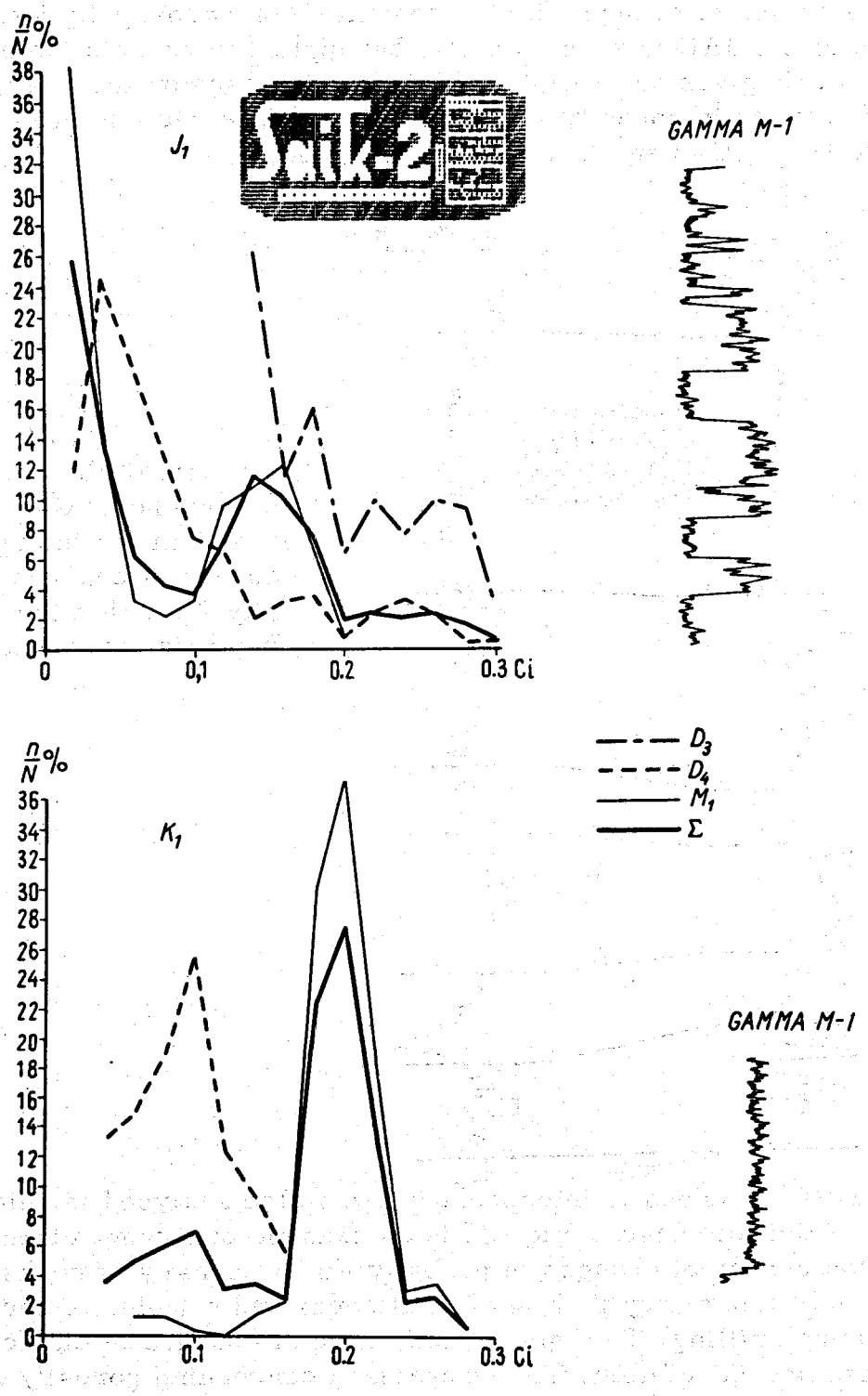

Fig. 33
Illustration of the deviation of variant curves of clay content Ci in region 2 for bore hole M-1; gamma - a fragment of the gamma log curve

The curves of changes in clay content Ci or porosity Kp interpreted by means of the SAIK system can also be applied in correlating of bore holes. Fig. 34 gives an example of correlation based on the interpreted curve of changes in porosity Kp for the middle Jurassic formations J_2. Two bore holes, G-2 and K-1 were correlated.

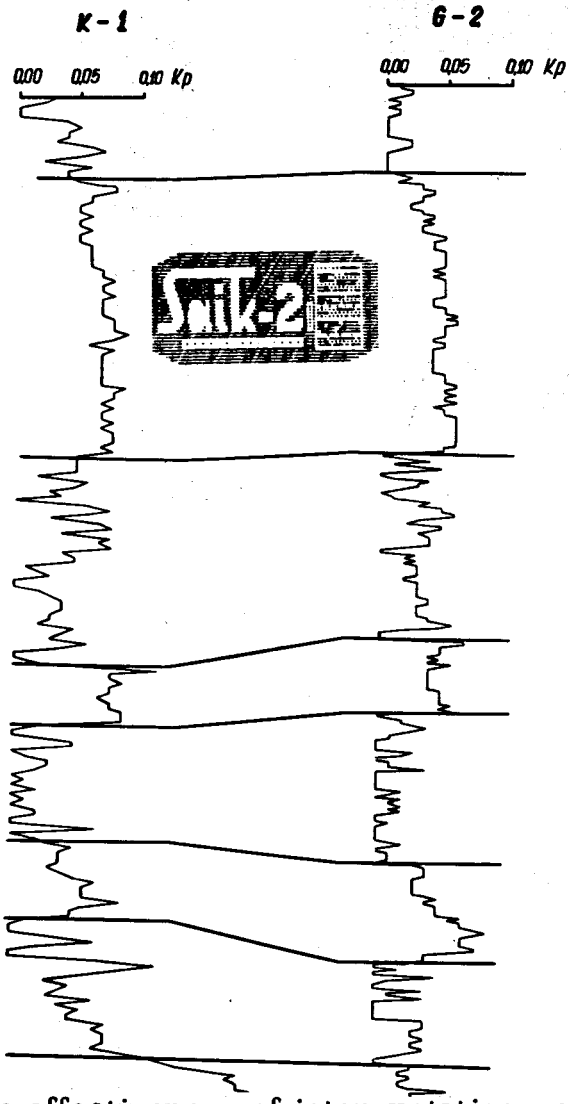

Fig. 34
Example of the correlation of bore holes G-2 and K-1 based on the interpreted curves of changes in porosity Kp within the middle Jurassic formation J_2

The effectiveness of interpretation was also analysed in relation to the early Paleozoic cases. Fig. 35 is an example of a comparison of the interpreted curves of changes in porosity Kp and density of rocks δ with the results of laboratory testing of drill cores and samples of borings collected during drilling. The interpreted curve of changes in clay content Ci is presented in addition. The comparison concerning porosity Kp shows good uniformity of the general character of changes in this parameter. A slight dispersion, greater for the results of testing the borings, gives good mutual confirmation of the results obtained in two completely different ways. On the other hand greater differences are observed in case of density δ. They occur first of all in rocks of a high clay content Ci which should be given particular attention. The cause of these differences can

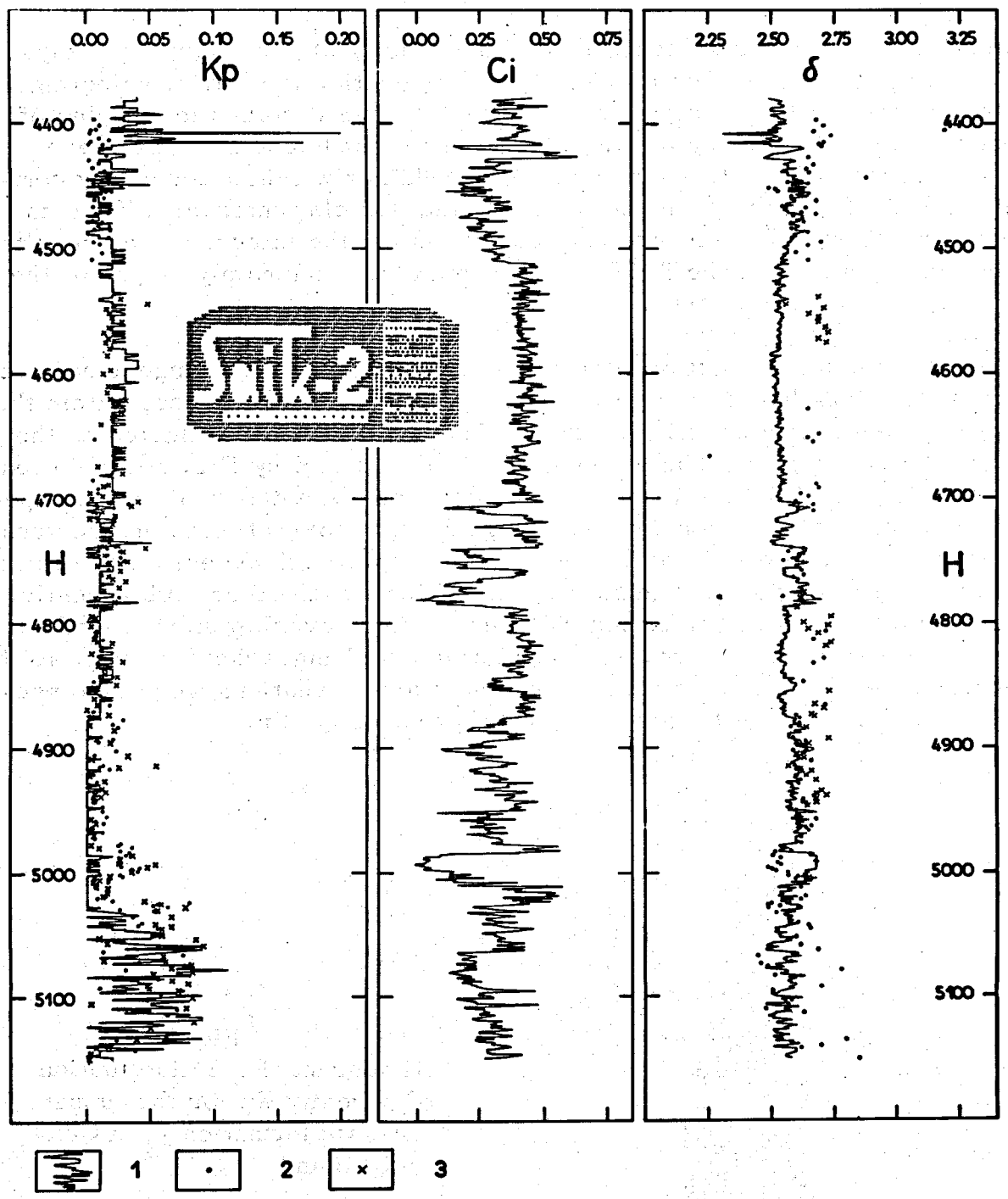

Fig. 35

Comparison of the interpretation results obtained by means of the SAIK system with those obtained through laboratory tests for the early Paleozoic period .

Kp, Ci, δ - porosity, clay content and the density of rocks, respectively;

1 - results of the SAIK system interpretation ;

2 - results of the laboratory testing of drill cores;

3 - results of the testing of borings at a field laboratory

be seen in the incorrect evaluation of the density of rock matrix or clays. However, it is necessary to take into consideration the way of selecting the samples for laboratory tests, especially when it refers to samples of borings collected during drilling. First of all sandstone samples were tested coming from small sandstone interbeddings within a large clay complex. Therefore, these are not reliable data for clay intervals. That is why, the observed differance can testify against the interpretation results obtained by means of the SAIK system, and also, and mainly, against the results of laboratory tests.

A consistent effect of interpretation operations for a large area are generalizations based on a great number of data. For instance, within the upper Jurassic formations J_3, Central Poland, data were collected on the porosity of rocks Kp. Their histogram is illustrated by Fig. 36. An attempt was made to find out the trend of depth changes - the effect of strata deposition on the value of porosity Kp - Fig. 37. Approximations were performed using power polynomials of the second, third and fourth orders. The results of approximation do not significantly differ from each other. Additionally, approximations were performed using a 50-metre overlap interval, illustrated by points in the figure. The trend of depth changes corresponded to the predictions. On the basis of the same data approximations were also permed of the surface of trends in changes of porosity Kp.

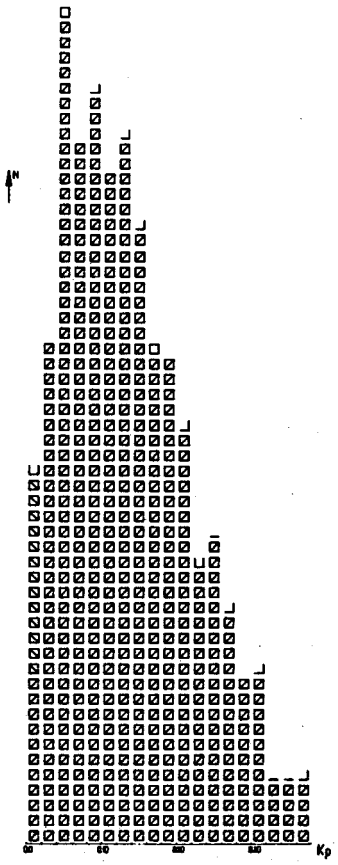

Fig. 36
Histogram of the distribution of porosity Kp for the upper Jurassic formation J_3 in Central Poland

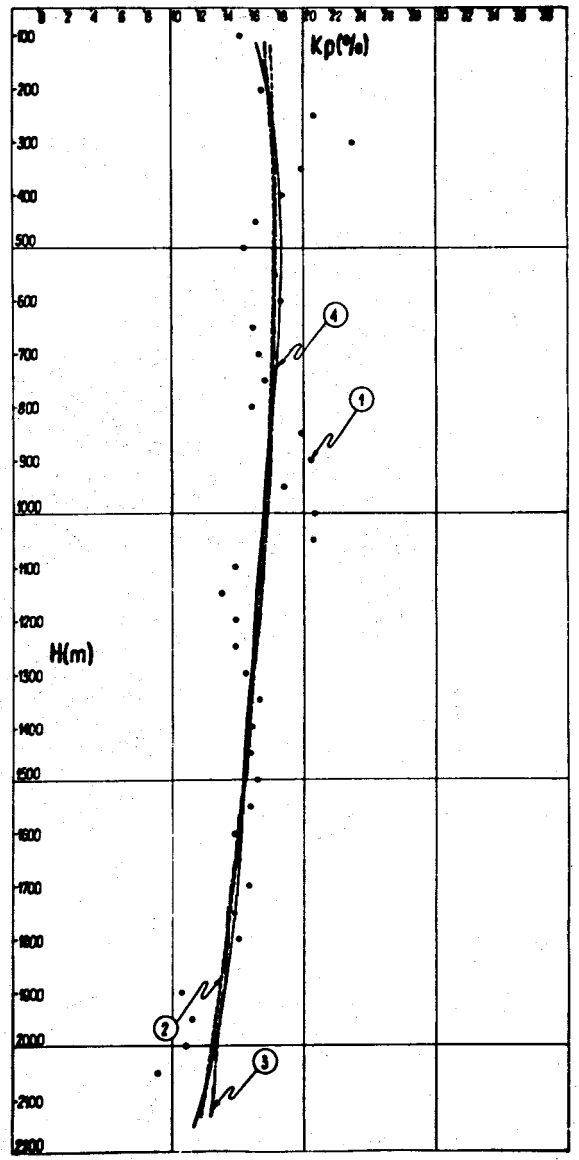

Fig. 37
Approximation of trends in depth changes in porosity Kp for the upper Jurassic formation J3 in Central Poland
H - deposition depth
1 - values averaged by intervals
2 - approximation by power polynomial of the second order
3 - approximation by power polynomial of the third order
4 - approximation by power polynomial of the fourth order

Fig. 38 illustrates approximations of the surface of trends performed using double Fourier's series for four stages of approximation. The picture of the trends in porosity Kp is compact, the anomalous spheres have similar amplitudes irrespective of approximation advancement, and the trends of changes are convergent within the reach of the method.

CONCLUSION

The SAIK system is modernized continuously as a result of:
- new possibilities of interpretation;
- implementation of mathematical equipment increasing interpretation quality;
- decreasing costs of operation.

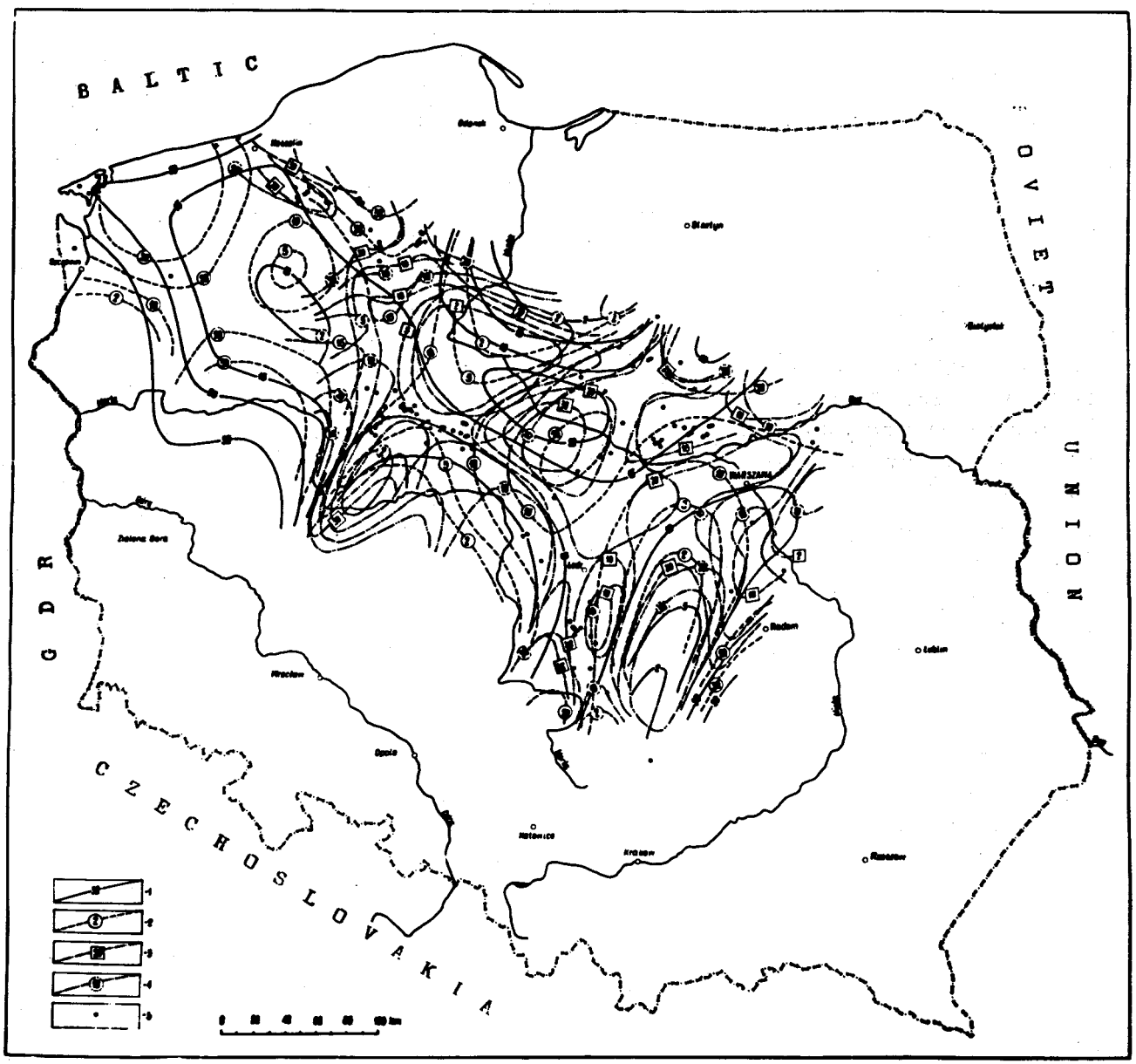

Fig. 38

Approximations of the surface of trends in changes in porosity Kp for the upper Jurassic formation J3 in Central Poland by means of double Fourier's series

1 - isolines for M=3, N=6
2 - isolines for M=3, N=8
3 - isolines for M=4, N=12
4 - isolines for M=4, N=10
5 - bore holes

M,N - so-called basic wave-lengths reflecting variability of the approximated parameter, respectively towards axis y and axis x

Large-scale investigations have been commenced in Poland in an extensive system of computerized comprehensive well-log data interpretation. The co-authors of this system are practically all interested geophysical centres. The basic concepts of the system originate from the systems SAIK--2optymal and SAIK-3 already tested and proved operative on an industrial scale. The basic quality of the new system will be its openness. This will make it possible to effect every "logical path" of processing as well as to add sub-systems of any objective and even smaller functional units. The planned fully modular structure of the system will allow of using each of the afore-discussed interpretation trends or directions.

REFERENCES

1. Burke J.A., Campbell R.L., Schmidt A.W. - The litho-porosity cross plot - a method of determining rock characteristics for computation of log data. SPWLA Tenth Annual Logging Symposium Transactions, 1969.

2. Dębski Z. Frydecki J. - Wprowadzenie do systemu SAIK. Geofizyka - biuletyn informacyjny Nr 2, Warszawa 1975.

3. Dębski Z., Frydecki J. - SAIK-2opty - zmiany i ulepszenia systemu. Ibidem, Nr 4, Warszawa 1975.

4. Frydecki J. - Scheme of statistical unification of radiometric well logging and estimation of compactness and shalyness indices. Acta Geophysica Polonica 21, p.93-111, nr 2, Warszawa 1973.

5. Frydecki J. - Scheme of the SAIK computer system of complex automatic interpretation of well logging data. Acta Geoph.Polon. 23, p. 293--299, nr 3, Warszawa 1975.

6. Frydecki J.- Metoda autokalibracji jako podstawa kompleksowej interpretacji danych geofizyki wiertniczej. Instrukcje i metody badań geologicznych IG, zeszyt 35, Wyd.Geolog., Warszawa 1978.

7. Frydecki J., Dębski Z. - Harmadik generációs SAIK számítógépes rendszer furólyuk-szelvényezési adatok komplex automatikus értelmezésére. Magyar Geofizika XVII, Evf.3., sz., p.103-110, Budapest 1976.

8. Frydecki J., Dębski Z., Basista S. - Autocalibration et ses réalisations par ordinateur /système SAIK/ comme méthode d'identification de certains paramètres géologiques de gisement. Actes du troisième Colloque annuel de diagraphies SAID /V Logging Symposium Européen SPWLA Transactions/, Paris 1977.

9. Harris M.H., McCammon R.B. - A computer-oriented generalized porosity-lithology interpretation of neutron, density and sonic logs. Journ. of Petrol.Techn. No 2, 1971.

10. Hossin M.A. /1960/ - Calcul des porosités utiles à partir des diagraphies soniques et neutron. Bull. de l'Association Française des Techniciens du Pétrole, Paris, Mars.

11. Kurtev T.J. /1967/ - Kolitchestvennaya interpretaciya rezultatov radiometritcheskich issledovaniy glistykh piestchanikov. Razvedotchnaya Geofizika, 23.

12. Nikolova J.B. /1971/ - Vrkhu izutchavaneto na kolektorskite svoystva na traskite glinesto-karbonatni sedimenti v rayona na Beli Izbor-Glavaci po sondazhnogeofizitchni danni. Bull. of the Geological Institute - Series of applied geophysics, Bulgarian Academy of Sciences, Committee of Geology, Vol. XIX-XX, p.11-22.

13. Schmidt A.W., Land G.A., Yunker J.D., Kilgore E.C. - Application of the Coriband technique to complex lithologies. The Log Analyst 13, No 1, 1972.

BIOGRAPHIES

Janusz FRYDECKI was born on June 6th, 1942. Received master's degree in physics at the Faculty of Mathematics and Physics, Warsaw University. Doctor's degree in geophysics at the Geological Institute in Warsaw.

Former teacher in physics and mathematics at Warsaw secondary schools. Former assistant and professor's assistant at the Centre of Geophysics, Geological Institute, Warsaw. Also a former senior system designer at the Municipal Information and Computer Centre of Warsaw SOETO.

At present, a professor's assistant at the Department of Geophysics, Faculty of Geology, Warsaw University, where he lectures on prospecting geophysics and well-logging . Author of training programmes in prospecting geophysics and well-logging obligatory at university geological departments. National consultant of the research project "Development and Implementation of Modern Methods and Technology of Well-Logging in Bore Holes Deeper Than 3000 m". A member of the Scientific Council to the PPG Enterprise of Geophysical Prospecting. Author of over 80 scientific and technological publications, and also of about 50 technical documentations.

Since 1965, he has been dealing with investigations in well-logging, mainly for fundamental problems as well as for geology of crude oil and gas. With his collaborators he has developed the SAIK system of computerized comprehensive interpretation of well-log data whose successive generations have been presented at many international congresses and symposia.

For investigations in autocalibration and in the SAIK system Janusz Frydecki has been awarded among others by: Rector, Warsaw University; President, Central Office for Geology; and Minister of Science, Higher Schools and Technology.

J. Frydecki is among others a member of: PTG Polish Geological Society; SITG NOT Association of Engineers and Technicians of Mining in Poland, Chief Technical Organization; Société pour l'Avancement de l'Interprétation des Diagraphies SAID; Society of Professional Well Log Analysts SPWLA.

Zdzisław DĘBSKI was born on April 5, 1941. Received master's degree in physics at the Faculty of Mathematics and Physics, Warsaw University. Worked for the PPG Enterprise of Geophysical Prospecting, initially direct at geophysical prospecting and then at the PPG Research Centre and took posts of senior geophysicist and senior specialist.

Since 1971 at the Municipal Information and Computer Centre of Warsaw SOETO as a senior specialist. Since 1966 engaged in application of computer technique in well logging. A co-author of the SAIK system. For the latter he received the Master of Technology Award and Award of the President of the Central Office of Geology. Author of 13 publications and of about 30 technical documentations presented at international symposia and congresses.

Member of SEP NOT Association of Polish Electrical Engineers of the Chief Technical Organization and of TNOiK Scientific Society of Organization and Management.

Stefan Piotr BASISTA was born on February 23, 1931. Master of Geology in geochemistry and mineralogy. Received this degree at the Department of Geology, Warsaw University and has been working with the PPG Enterprise of Geophysical Prospecting in Warsaw ever since at the following posts: engineer operator, manager of a well-logging group, head of a well-logging base, chief of the Well-Log Interpretation Laboratory and now chief, Section of Petrophysics and Modelling. Additional training in France /C.E.A., I.F.P. and B.R.G.M./. Author of over 50 technical documentations on well-log interpretation.

BASIC SYMBOLS

PA - acoustic log
PG - gamma - ray log
PN - neutron log
PNG - neutron - gamma log
PNN - neutron - neutron log
PGG - gamma - gamma log
PO - resistivity log
Ig - gamma - ray intensity
$Ig_{tło}$ - gamma radiation background intensity
$Ig_{ił}$ - gamma radiation intensity of clay
Ing - neutron capture - gamma-ray intensity
$Ing_{ił}$ - neutron capture - gamma-ray intensity of clay
Ing_w - neutron capture - gamma-ray intensity of water
$Ing_{Kp=0}$ - neutron capture - gamma-ray intensity of matrix /absence of pores/
Igg - gamma - ray dispersion intensity
$Igg_{ił}$ - gamma - ray dispersion intensity of clay
Igg_{sz} - gamma - ray dispersion intensity of matrix
Igg_w - gamma - ray dispersion intensity of water
Δt - observed interval transit time
Δt_i - interval transit time for the i-th component
Δt_w - interval transit time in the water
Δt_{sz} - interval transit time in the matrix
Kp - porosity
KpN - porosity interpreted from neutron log
KpA - porosity interpreted from acoustic log
KpR - porosity interpreted from resistivity log
KpGG - porosity interpreted from gamma-gamma log
KpI, KpJ - porosity interpreted from the i-th and j-th logs
Pp - formation factor
Kw - water saturation
Kg - gas saturation
Kr - oil saturation
w/Kpl - quotient of extreme neutron porosity values
Ci - clay content
k_{Ci}, k - proportionality constant in relation between gamma log and clay content
α - exponent of clay content

S - relative matrix volume
m - porosity exponent /comentation factor/
w - humidity of clay
n_i - saturation exponent of the i-th component
β - clay cementation factor
ρ - resistivity of the formation
σ - conductivity of the formation
σ_i - conductivity of the i-th component
$\sigma_i, \sigma_{ił}$ - clay conductivity
δ, δ_{GG} - density of the formation
D - quality factor

A COMPUTER-PROCESSED WELLSITE LOG COMPUTATION

by

D. L. Best, J. S. Gardner, and J. L. Dumanoir
Schlumberger Well Services, Houston, Texas

ABSTRACT

A new logging unit with an integrated system of surface instrumentation built around a computer allows digitally recorded logs to be merged, computed, and recorded on film at the wellsite.

The SCHLUMBERGER CYBERLOOK wellsite computer processing utilizes the recently introduced "Dual Water" interpretation model for reservoir analysis. This model considers a shaly, water-saturated formation to behave as if it contains two types of pore water: "clay water" near the surfaces of clay crystals and "far water" at a distance from the clay surfaces.

The processing is designed so that all required input parameters can be accurately selected from a first-pass merge. The computations, corrected for shale and light-hydrocarbon effects, are presented on film in a format that is easily interpreted, allowing decisions to be made at the wellsite.

Field experience has shown the processing to be very flexible, providing excellent results throughout North America in both sandstone and carbonate reservoirs.

INTRODUCTION

The computer in a CYBER SERVICE UNIT provides the capability to produce wellsite computations that are much more sophisticated than any that are possible with earlier-type logging units.[1] To take advantage of this capability, a new computer-processed interpretation program called "CYBERLOOK" processing was developed. It uses the new "Dual Water" model for the interpretation of shaly formations.[2] This model considers a shaly formation to behave as a clean formation containing two types of water: "clay water" near the surface of the clay crystals and "far water" in the remaining pore space.

The new program is intended for a wellsite computation rather than a replacement for the advanced SARABAND* and CORIBAND* programs. There is neither enough computer capacity nor time at the wellsite for that. The CYBERLOOK program is relatively easy to run, so that the field engineer is able to use it with reasonable training.

Input parameters to the computation are selected by the engineer from a merged first pass.

The CYBERLOOK log displays:

--An "F overlay"-type presentation in which the wet resistivity (reconstructed R_0) is played back with R_t.

--Continuous logs of porosity, water saturation, shale content, grain density, hole size, and bulk-volume analysis of the pore space.

CYBERLOOK processing also detects and codes the zones of good producibility and the presence of gas.

THE DUAL WATER MODEL

The concept of a shaly formation containing two waters was introduced by Clavier, Coates, and Dumanoir.[2] It will be discussed briefly here. Ref. 2 may be referred to for a more complete explanation.

Definitions

The following expressions are defined as indicated:

Total Porosity: ϕ_T, the bulk-volume fraction of the formation occupied by all fluids (hydrocarbons, far water, clay water).

Bound Water: the water associated with the shales which occupies the bulk-volume-fraction ϕ_B. In addition to the clay water in shales, there may still be some original "far water" that has not been expelled by compaction or is trapped with silt.

Free Water: the water that is not bound to shales, which occupies the bulk-volume fraction ϕ_F. It is called "free" water only to distinguish it from "bound" water, and is not meant to imply producibility (the free water includes the formation irreducible water).

---

* Mark of Schlumberger.

Total Water Saturation: S_{wT}, the portion of the total porosity occupied by bound and free water. $S_{wT} = (\phi_F + \phi_B)/\phi_T$.

Bound Water Saturation: S_{wB}, the portion of the total porosity occupied by the bound water. $S_{wB} = \phi_B/\phi_T$.

A shaly formation can be represented as follows:

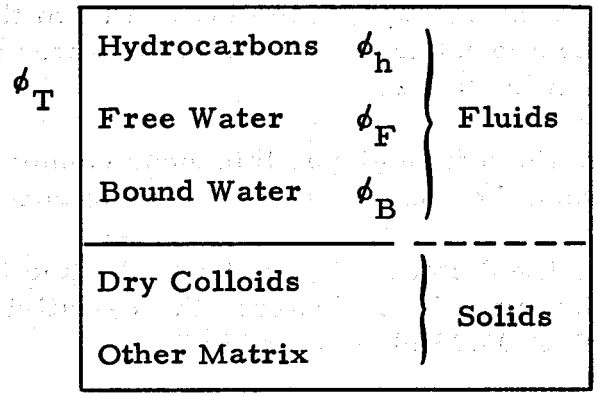

ϕ_h, ϕ_F, and ϕ_B are the bulk-volume fractions of the formation occupied by hydrocarbons, free water, and bound water respectively.

By definition,

$$\phi_T = \phi_F + \phi_B + \phi_h$$

$$S_{wT} = \frac{\phi_F + \phi_B}{\phi_T}$$

$$S_h = \frac{\phi_h}{\phi_T}$$

$$S_{wB} = \frac{\phi_B}{\phi_T}$$

$$S_{wT} - S_{wB} = \frac{\phi_F}{\phi_T} = S_{wF}$$

The "Dual Water" model is an improvement over the Waxman-Smits model[3-5] and it fits their experimental data better. The Waxman-Smits model proposed that a shaly formation behaved like a clean formation of the same porosity, tortuosity, and fluid content except that the water appears to be more conductive than its bulk salinity would indicate. The excess conductivity is due to additional cations held loosely captive in a

"diffuse" layer surrounding the clay particles to compensate for the deficiency of electrical charges in the clay crystal. Refs. 3-5 did not take into account the exclusion of salt from part of the pore volume near the clay surface. Ion distribution near a clay surface should be as shown in Fig. 1.

The thickness of the diffuse layer of Na^+ ions, X_d, is related to the salinity of the bulk water, being smaller for more saline waters.

Actually, the Na^+ ions are kept some distance from the clay surface by the hydration water around each cation and the water adsorbed on the clay surface, as shown in Fig. 2.

As a consequence, the diffuse-layer thickness cannot be less than X_H. However, $X_d = X_H$ when the connate water is saline enough.

For sodium clays, the distance X_H is about 6Å, and the Na^+ ions will be stacked in the Helmholtz plane whenever the resistivity of the brine in the pores is less than 0.425 ohm/m at 75°F.

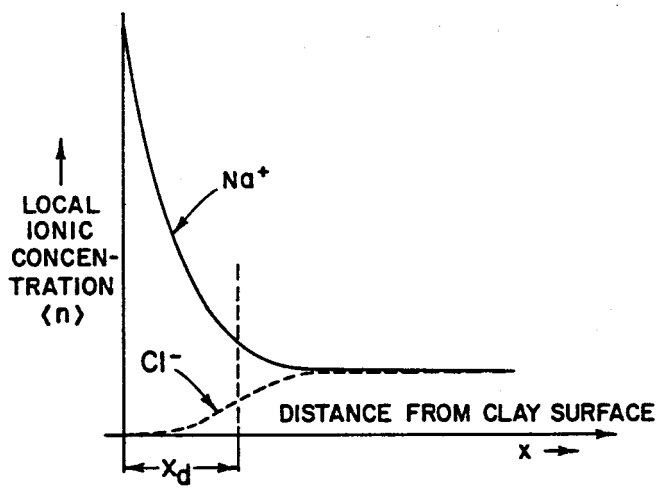

Fig. 1 (Ref. 2: Courtesy SPE)

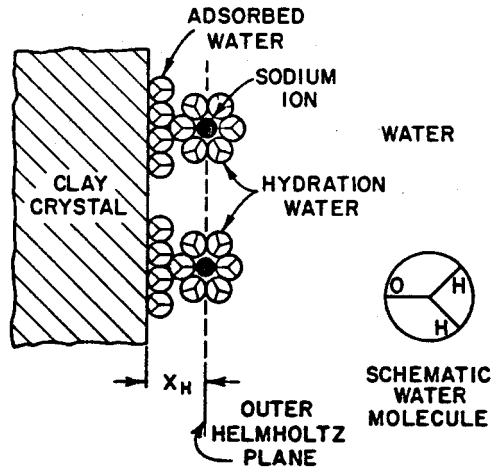

Fig. 2 (Ref. 2: Courtesy SPE)

This thin sheet of salt-free water (the "clay water") is important because clays have tremendous surface areas, as much as 6,300 acres/ft^3 (900 km^2/m^3) compared to 0.1 to 0.2 acres/ft^3 (0.014 to 0.028 km^2/m^3) for a typical clean sand, and the volume of clay water is far from negligible in comparison with the total pore volume.

Stated briefly, the "Dual Water" model says that a water-saturated formation behaves as if it contains two types of water:

1) Water near the clay (clay water), which is salt free. However, it can conduct electricity by movement of the cations necessary to balance the negative charge of the clay crystal. If the environment is saline enough, the conductivity of this water (C_{wc}) is a universal parameter for sodium clays* and depends only on temperature (C_{wc} = 6.8 mho/m at 25°C).

2) Water far from the clay (far water) which has the properties of the bulk water ($C_{wF} = C_w$).

The "Dual Water" model also shows that the "m" exponent in the Archie F - ϕ relationship is independent of shaliness and about equal to 2.

APPLICATION OF THE "DUAL WATER" MODEL IN THE CYBERLOOK PROGRAM

A. Resistivity and Saturation of a Shaly Formation

The conductivity of the free water is: C_{wF}.

The conductivity of the bound water is: C_{wB} (often, but not always, equal to C_{wc}).

The conductivity of the formation is: C_t.

The conductivity of the formation ($C_t = 1/R_t$) is given by:

$$C_t = (S_{wT} \cdot \phi_T)^2 C_{wM} \qquad (1)$$

where C_{wM} is the conductivity of the mixed water (bound and free).

The water-mix conductivity is obtained by application of

$$C_{wM} = \frac{\phi_B C_{wB} + \phi_F C_{wF}}{\phi_B + \phi_F} = \frac{S_{wB} C_{wB} + (S_{wT} - S_{wB}) C_{wF}}{S_{wT}} \qquad (2)$$

---

* It has been found that the number of Na^+ ions is directly related to the surface areas of the sodium clays whatever their type (kaolinite, illite, montmorillonite).[6]

We can solve Eqs. 1 and 2 for S_{wT}, the total water saturation

$$S_{wT} = X + \left(\frac{C_t}{C_{wF}\, \phi_T^2} + X^2 \right)^{1/2}$$

where

$$X = \frac{S_{wB}\,(C_{wF} - C_{wB})}{2C_{wF}}$$

Or, in terms of resistivities,

$$S_{wT} = Y + \left(\frac{R_{wF}}{R_t\, \phi_T^2} + Y^2 \right)^{1/2}$$

where

$$Y = \frac{S_{wB}\,(R_{wB} - R_{wF})}{2R_{wB}}$$

B. CYBERLOOK Saturation

The traditional water saturation S_w does not include bound water; thus is equal to S_{wF}.

$$S_{wF} = S_w = \frac{\phi_F}{\phi_F + \phi_h} = \frac{S_{wT} - S_{wB}}{1 - S_{wB}} \qquad (3)$$

It is obvious that $S_{wT} > S_w$ whenever bound water is present. Thus, if you are familiar with S_w, S_{wT} appears to be a pessimistic water saturation. It is also obvious that Eq. 3 for S_w will give ridiculous values of water saturation whenever S_{wB} approaches S_{wT} or 1, as it will in very shaly formations (in pure shales $S_w = 0/0$). Rather than introducing the new concept of total water saturation (S_{wT}) or cosmetically controlling S_w to prevent ridiculous answers, the CYBERLOOK concept takes a different approach.

The main objective of the CYBERLOOK program is to reconstruct the wet formation resistivity R_0. Then R_0 can be compared to R_t. The two curves are presented as in the "F overlay" technique, which allows:

first: A quality check of the computation, since R_0 and R_t should overlay in all wet formations including shales.

second: A quick-look detection of the presence of hydrocarbons ($R_t > R_0$).

A wet, shaly formation can be represented by:

Fluids	Free Water ϕ_F	ϕ_T
	Bound Water ϕ_B	
Solids	Dry Colloids	
	Other Matrix	

This shaly formation of conductivity C_0 has a total porosity, ϕ_T, containing bound water (conductivity C_{wB} and bulk-volume fraction ϕ_B) and free water (conductivity C_{wF} and bulk-volume fraction ϕ_F). We have the relationships

$$\phi_T = \phi_B + \phi_F$$

$$S_{wB} = \phi_B/\phi_T$$

In the "Dual Water" model, the formation factor is $F = 1/\phi_T^2$, so that the conductivity C_0 of this wet formation is

$$C_0 = \phi_T^2 C_{wM}$$

where C_{wM} is the conductivity of the bound water/free water mixture. C_{wM} satisfies:

$$\phi_T C_{wM} = \phi_B C_{wB} + \phi_F C_{wF}$$

or

$$C_{wM} = S_{wB} C_{wB} + (1-S_{wB}) C_{wF}$$

Then

$$C_0 = \phi_T^2 [S_{wB}C_{wB} + (1-S_{wB})C_{wF}]$$

or, in resistivity,

$$R_0 = \frac{R_{wF} \cdot R_{wB}}{\phi_T^2 [S_{wB}R_{wF} + (1-S_{wB})R_{wB}]}$$

This gives the wet formation resistivity. The CYBERLOOK saturation is defined by:

$$S_w = (R_0/R_t)^{1/2}$$

Porosity and Bulk-Volume Water

Porosity ϕ is obtained by removing the bulk-volume fraction of bound water ($\phi_T S_{wB}$) from ϕ_T. Therefore:

$$\phi = \phi_T (1-S_{wB})$$

The bulk-volume fraction of the free water is then:

$$V_{wF} = \phi S_w$$

To get these answers, four quantities must be known: R_{wF}, R_{wB}, ϕ_T, and S_{wB}. It has been found that porosity from the ϕ_N-ρ_b crossplot provides a good value of ϕ_T. S_{wB} can be obtained from traditional shale indicators. (CYBERLOOK processing uses the SP, Gamma Ray, and ϕ_N.) This leaves R_{wB} and R_{wF} to be determined.

Going back to the formula for C_0 and changing to resistivity, we have

$$R_{wM} = R_0\phi_T^2$$

An apparent fluid resistivity can be computed: $R_{wa} = R_t\phi_T^2$. It will be equal to R_{wB} when the formation is 100-percent shale, to R_{wM} when

the formation is wet, and to R_{wF} when the formation is 100-percent wet and clean.

CYBERLOOK PROGRAM DESCRIPTION

The CYBERLOOK program requires a minimum log suite which includes deep resistivity, CNL*-FDC*, and Gamma Ray or SP logs. In addition, a sonic log may be used to help the porosity computation in case of bad hole, and an R_{xo} log may be added in order to make a moved-oil-type presentation. R_t is taken to be the deep-investigation log reading, R_{ID} or R_{LLd}. If a dual induction log is available, and if desired, R_{ID} can be corrected for invasion effects.

The CYBERLOOK computation is normally made in two passes.

Pass One requires no parameter selections, only certain constants to describe borehole conditions and how the logs were recorded. In Pass One, raw data are corrected for borehole effects and computations are made to determine ϕ_{Ta}, R_{wa}, and ρ_{ga}. These are displayed along with ϕ_N, ϕ_D, R_t, Gamma Ray, and SP. From the output of Pass One, parameters are selected for Pass Two, which computes and outputs the CYBERLOOK log.

Pass Two computes the shale index from several shale indicators and converts the minimum shale index (I_{sh}) to bound-water saturation. ϕ_T is corrected for light-hydrocarbon effects. The reconstructed R_0 and S_w are computed and displayed along with ϕ, V_{wF}, and I_{sh}. Also displayed are a grain density of the whole matrix, a differential caliper, and producibility and gas-indicator flags.

The CYBERLOOK computation is checked for coherence, and, if necessary, repeated with refined parameter selections. A diagnostic playback can be made to help with particularly difficult problems.

PASS ONE

Pass One Inputs

No parameter selections are required for Pass One. However, certain constants must be specified. These are:

---

* Mark of Schlumberger.

a) Mud weight in lbs/gal

b) Bit sizes in inches

c) Pore-fluid density in gm/cc

d) Bottom-hole temperature in ^{o}F

The engineer has the means to:

a) Adjust depths

b) Straighten the SP baseline

c) Select the matrix porosity scale (limestone or sandstone) of the neutron and density logs recorded on the Pass One film.

Pass One Computations

The ϕ_N is corrected for temperature and pressure in accordance with the published chart.

The apparent total porosity, ϕ_{Ta}, is computed in accordance with the chart of Fig. 3.

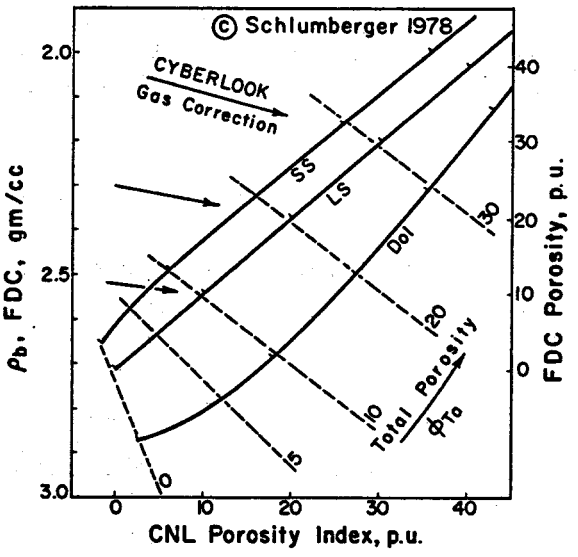

Fig. 3

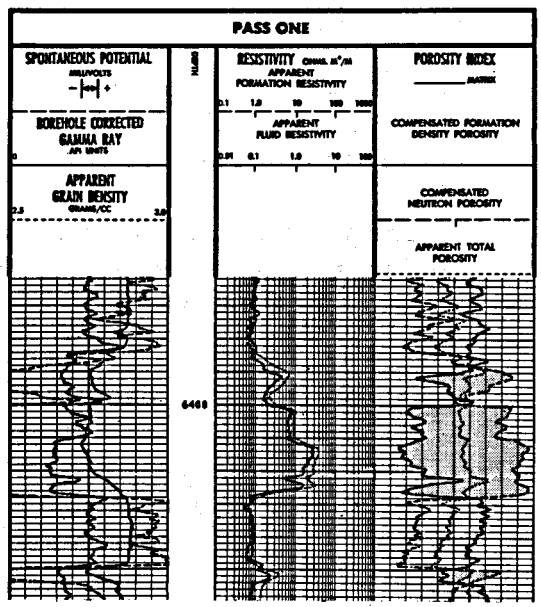

Fig. 4

Although the choice of porosity scales is optional, for display on the Pass One film, all program computations are based on ϕ_D and ϕ_N values on the Limestone scale.

The apparent grain density, ρ_{ga}, is computed from ϕ_{Ta} and ρ_b.

The apparent water resistivity, R_{wa}, is computed from R_t and ϕ_{Ta}:

$$R_{wa} = R_t \cdot \phi_{Ta}^2$$

The Gamma Ray is corrected for borehole effect, according to the published chart.

Bit size and caliper-log readings are used to compute a differential caliper.

Pass One Output

The outputs are recorded on the Pass One log (Fig. 4). The dashed curve in Track 1 is the SP. If deemed necessary, the baseline is straightened, in which case the curve will not match the recorded SP. The solid curve is the Gamma Ray and will have been borehole corrected if a caliper is available. In this case it will not match the recorded curve. The dotted curve is ρ_{ga}.

Track 2 has a four-cycle log grid, the dashed curve is R_t. The solid curve is R_{wa} computed from ϕ_{Ta} and R_t.

Track 3 has the porosity curves. The solid curve is ϕ_D, computed with a 2.65 gm/cc matrix density if the selected matrix is sand, or 2.71 if the matrix is lime. There are no "limy sand" options. The dashed curve is the ϕ_N corrected for temperature and pressure, and will probably be a little higher than the recorded ϕ_N unless the well has a low BHT. The dotted curve is crossplot porosity computed from ϕ_N and ϕ_D, and gives a good estimate of total porosity independent of the matrix. There is a gas-area coding between ϕ_D and ϕ_N whenever ϕ_N is less than ϕ_D.

Pass One Check

Pass One should be checked against the raw data to be sure the parameters have been properly input. This check should include the following:

1) Are all the logs on depth with one another?

2) Is the expected lithology confirmed by ϕ_N/ϕ_D separation and ρ_{ga}, taking into account shaliness and hydrocarbon effects?

3) Does R_{wa} in clean wet zones seem reasonable and confirm local knowledge?

4) If the SP baseline has been straightened, is it now stable?

If the answer to any of these questions is no, corrections may be required.

The Pass One computation provides a great deal of information. By itself, it is a pretty good quick-look and is usually presented along with the CYBERLOOK presentation. The ϕ_{Ta} curve gives porosity independent of lithology and not greatly affected by gas. The apparent water resistivity curve gives an R_{wa} that is independent of lithology for hydrocarbon detection. Gas detection is provided by not only the usual neutron-density crossover, but also by lower values of ρ_{ga}. Shaly-formation gas detection is possible because the SP and Gamma Ray are played back with ρ_{ga}. If time is extremely critical, Pass One can be used to advantage.

In Pass Two, the final computations are made. The output is the CYBERLOOK log.

PASS TWO

Pass Two Inputs

The CYBERLOOK computation requires all of the inputs that went into the Pass One plus some parameters that are selected from the Pass One output. Not all of these additional parameters are required on every computation. The requirements will vary depending on what shale indicators are to be used and what logs are available.

Shale-Index Parameters

Gamma Ray, SP and neutron logs can be used as shale indicators. Any one can be used alone. Any one can be rejected.

γ_{cn} - Gamma Ray in a clean zone

γ_{sh} - Gamma Ray in shales

E_{SPcn} - SP in a clean zone (preferably wet)

E_{SPsh} - SP in shales

ϕ_{Ncn} - ϕ_N in a clean zone (clean gas zone if gas is present)

ϕ_{Nsh} - ϕ_N in shales

The engineer decides which shale indicators are needed, and a "clean" and "shale" value for each indicator is then picked. These picks are usually made as the average reading in a 100-percent clean zone or a 100-percent shale. Local experience and preferences will often dictate picking a little higher or lower than the average. If no 100-percent clean or 100-percent shale zones exist, the parameter will have to be estimated or known from local experience.

Since the neutron log is often affected by gas, special care is needed in selecting its clean and shale values. It is generally not needed, but is available for emergency use in those cases where the Gamma Ray and SP are not adequate. ϕ_{Nsh} is picked from the lower neutron readings in shales. ϕ_{Ncn} is picked in a clean gas zone, or a clean zero-porosity zone--not a clean water zone. It is usually 0 to 3 p.u. in low-porosity formations, 5 to 15 p.u. in high-porosity formations.

Fluid Parameters

R_{wF} and R_{wB} are selected from the Pass One R_{wa} curve. R_{wF} is read from the R_{wa} curve in a 100-percent clean and wet zone. R_{wB} is read from the R_{wa} curve in a 100-percent shale. If there is no clean, wet zone R_{wF} will have to be estimated or taken from local experience.

Discrimination and Hydrocarbon-Correction Parameters

ϕ_{max} - maximum total porosity

ρ_g - expected clean grain density

The parameter ϕ_{max} has essentially two functions:

1) It is a discriminator to eliminate calculations in zones where the porosity reads too high. When the apparent total porosity, ϕ_{Ta}, is higher than ϕ_{max}, no water-saturation calculation is made. ϕ_{max} is selected from the Pass-One ϕ_{Ta} curve, slightly higher than ϕ_{Ta} in zones where the porosity data are good, and lower than ϕ_{Ta} in zones where the porosity data are affected by adverse hole conditions.

2) ϕ_{max} controls the curvature of the transform that is used to deduce bound-water saturation from minimum shale index.

The expected clean grain density, ρ_g, triggers the light hydrocarbon correction in CYBERLOOK processing. It is picked from the Pass One ρ_{ga} curve in a clean, wet zone or from local knowledge of lithology. ρ_g (clean matrix) is adjusted for shaliness by the program. If ρ_{ga} is lower than the adjusted ρ_g, a light-hydrocarbon correction is made.

ϕ_{SV} is obtained by the standard time-average equation. In bad hole (as indicated by the caliper) or when the apparent porosity is higher than ϕ_{max} limit, ϕ_{SV} is preferred.

A "moved-oil presentation" of the CYBERLOOK output is available for computations which have an R_{xo} measurement. The flushed-zone water saturation calculation is made in the same manner as for the uninvaded zone except that R_{mf} replaces R_{wF} and R_{xo} from MicroSFL* or Proximity* log replaces R_t.

At the engineer's option a lower limit may be imposed on R_t. R_t is often too low when taken from R_{ID} in thin resistivity beds surrounded by conductive shoulders. This problem can be compounded if an invasion correction is made on R_{ID}. To help get a more realistic value of R_t in these cases, the LL8 and R_{mf}/R_{wF} can be used to place a lower limit on R_t:

$$R_t \geq R_{LL8} \cdot \frac{R_{wF}}{R_{mf}}$$

A good LL8 and good values of R_{wF} and R_{mf} are essential. The measured R_{mf} should be checked in wet zones ($R_{mf}/R_{wF} = R_{xo}/R_t$) and by the SP.

Pass Two Computations

All of the computations covered in the Pass One computation section are repeated in the Pass Two CYBERLOOK computation.

Bound-Water Saturation

$$(I_{sh})_{GR} = \frac{\gamma_{LOG} - \gamma_{cn}}{\gamma_{sh} - \gamma_{cn}}$$

$$(I_{sh})_{SP} = \frac{E_{SP\,LOG} - E_{SPcn}}{E_{SPsh} - E_{SPcn}}$$

* Mark of Schlumberger.

$$(I_{sh})_N = \frac{\phi_{N\,LOG} - \phi_{Ncn}}{\phi_{Nsh} - \phi_{Ncn}}$$

The smallest of these three is then selected as the minimum shale index, $(I_{sh})_{min}$. The bound water saturation (S_{wB}) is computed from $(I_{sh})_{min}$ by using an experimental transform (referred to as the "S" curve) whose curvature is controlled by ϕ_{max} (Fig. 5).

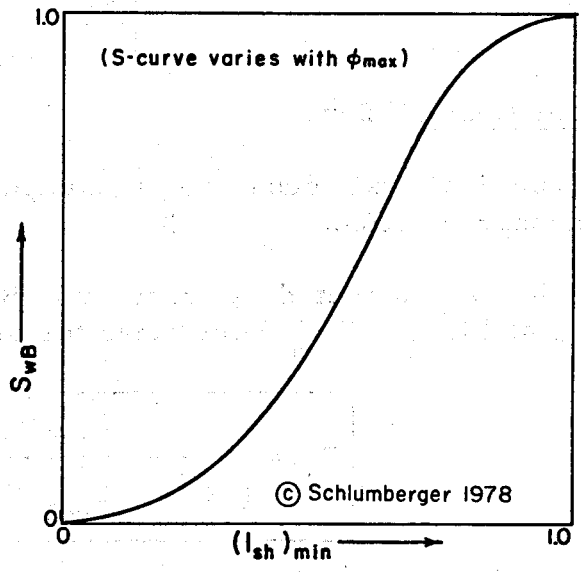

Fig. 5

The shape of the "S" curve reflects several observations:

(a) R_{wB} remains constant and S_{wB} maximum but the Gamma Ray may cover a large range of high readings (top right part of the "S").

(b) The correlation between SP reduction and clay content in slightly shaly formations (bottom-left part of the "S").

(c) A transition from clean formations to shales which exhibits a gentler slope in the more porous formations.

Light Hydrocarbon Correction - Total Porosity

The apparent total porosity (ϕ_{Ta}) is corrected for light hydrocarbon effects to reach the final total porosity (ϕ_T). This correction is triggered when ρ_{ga} is less than ρ_g. It is made by computing a correction factor, B, in two ways:

(a) Satisfying the expected grain density, ρ_g (adjusted for shaliness by the program).

(b) Satisfying the hydrocarbon volume and density effects.

The smaller of the two corrections is used to determine the final total porosity (ϕ_T) by application of

$$\phi_T = \frac{2\phi_{Ta} + B}{2 + B}$$

Other Computations

The final grain density ρ_g is computed from ρ_{ga} by correcting for hydrocarbon effect.

The reconstructed wet resistivity R_0 is computed from ϕ_T, S_{wB}, and R_{wB} and R_{wF}. S_{wB} determines the proportion of the two waters, and

$$R_0 = \frac{R_{wF} \cdot R_{wB}}{[R_{wB} + S_{wB}(R_{wF} - R_{wB})]\phi_T^2}$$

When $R_{wB} = R_{wF}$ or when $S_{wB} = 0$, this reduces to $R_0 = R_{wF}/\phi_T^2$.

The CYBERLOOK water saturation is computed from R_0 and R_t by

$$S_w = (R_0/R_t)^{1/2}$$

Porosity ϕ is computed from ϕ_T and S_{wB} by removing ϕ_B: $\phi = \phi_T(1-S_{wB})$. ϕ is limited by $\phi_{max} \cdot (1-S_{wB})$ in bad hole.

Bulk Volume Free Water V_{wF} is computed from ϕ and S_w: $V_{wF} = \phi S_w$.

Flushed Zone Water Volume V_{wxo} is computed by $V_{wxo} = (\phi \cdot S_{xo})$. S_{xo} is computed in the same manner as S_w, except that R_{mf} replaces R_{wF} and R_{xo} replaces R_t.

The Gas-Indicator Flag is computed by comparing ϕ_{Ta} with ϕ_T. It takes a larger hydrocarbon correction to raise this flag at high porosity than at low porosity.

The Producibility Flag is computed by comparing S_{wB} with ϕ_T, and, if S_{wB} is low enough, the area between the R_0 and R_t curves is shaded on the CYBERLOOK log.

CYBERLOOK OUTPUT

There are currently two CYBERLOOK presentations--the standard presentation (Fig. 6) and the presentation with moved oil when an R_{xo} log is available.

The solid curve in Track 1 is the shale index. It is the minimum shale index of the several shale indicators. The dotted curve is the grain density after correction for hydrocarbons.

Track 2 has R_t as a dashed curve and R_0 solid.

It is possible for R_0 to be less than R_t in very shaly zones and still not show hydrocarbons because S_w is boosted toward 100 percent at high shale content. If a zone is clean enough, coding will appear between the R_0 and R_t curves to indicate producibility.

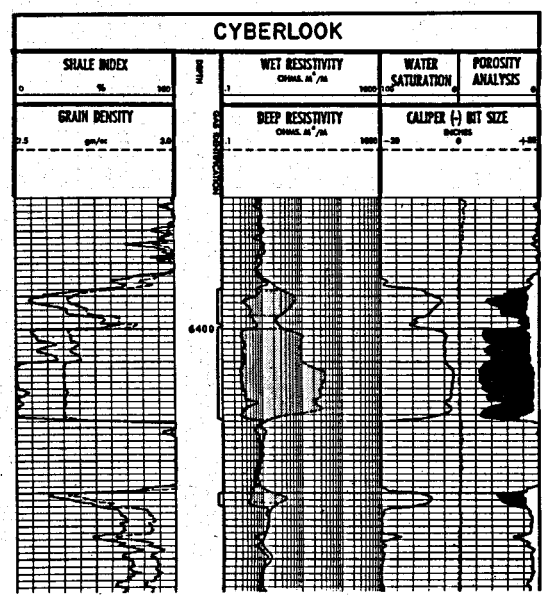

Fig. 6

The left half of Track 3 has the water saturation and the right half has the porosity and bulk volume free water. WATER coding is used from the V_w curve to the track edge and OIL coding between ϕ and V_w. If the MOP presentation is being used, moved oil will be shown by gas coding between the oil and water.

The gas flag appears in the depth track, indicating that a large enough correction to ϕ_{Ta} has been made for the hydrocarbons to be gas. A differential caliper is presented as a dotted curve with bit size in the middle of Track 3.

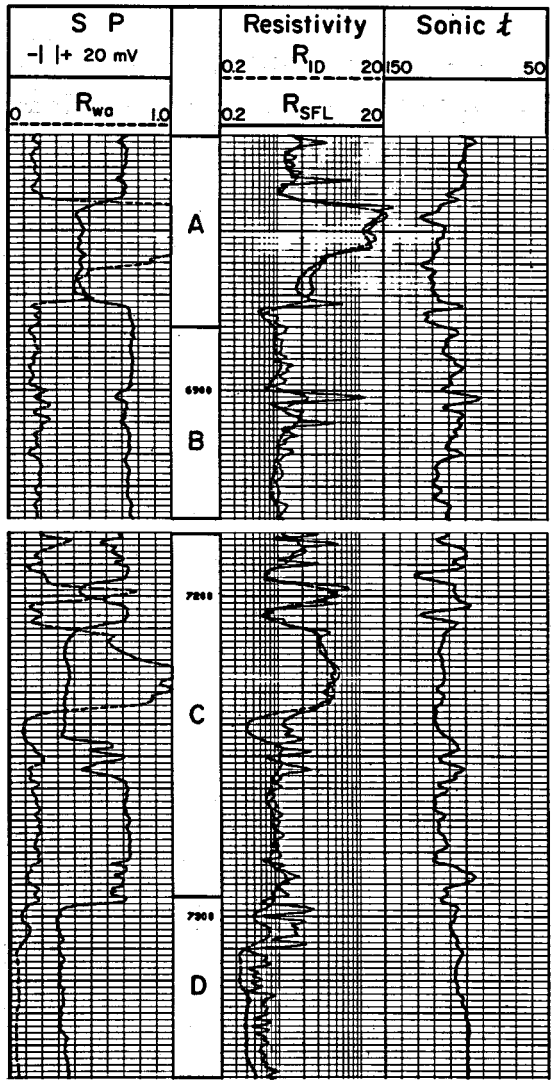

Fig. 7

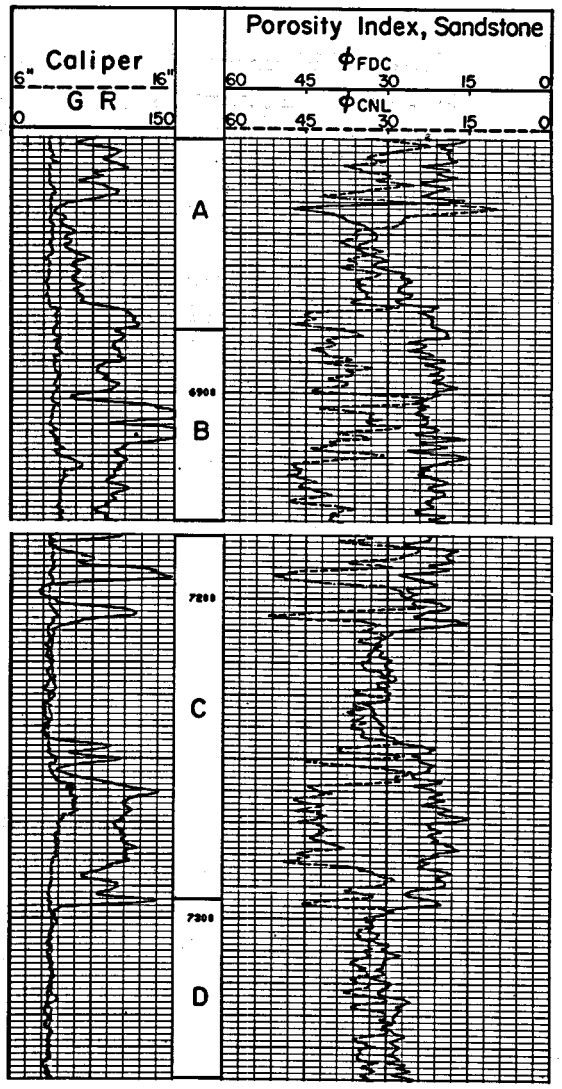

Fig. 8

EXAMPLE 1

Figs. 7 and 8 show a section of ISF*/Sonic and CNL*/FDC* logs from a well in South Texas. This interval contains a series of Frio sands and shale. The well was drilled with fresh mud.

The constants which describe the logs and borehole conditions for Pass One are:

- Neutron is recorded on "Sandstone" matrix
- Mud weight is 10.7 lb/gal
- Bottom-hole temperature is 150°F
- Pore-fluid density is 1.0 gm/cc
- Pass-One porosity matrix is sandstone

The Pass One playback is shown in Fig. 9. It has been divided into four intervals. Interval A contains a shaly, hydrocarbon-bearing sand which has a gas cap indicated by the separation of the neutron and density porosities. Interval B is mostly shale with some thin sands and can be used to select shale parameters. Interval C contains hydrocarbon-bearing sands. Interval D contains a reasonably clean water sand.

Parameters

The excellent correlation of the SP, Gamma Ray and ρ_{ga} indicates that both the SP and Gamma Ray can be used as shale indicators. ϕ_N will also be used.

The shale values for all three shale indicators are picked in Interval B. The SP reads -15 over this interval, the Gamma Ray averages 95, and ϕ_N averages 42 p.u.

The clean values cannot all be selected in one interval. The water sand in Interval D has the largest SP deflection. The sand is clean or almost clean so that the SP clean value is taken as the largest SP, -105 mV. The sands in Interval C have Gamma Ray readings that are a bit lower than the water sand in Interval D. The Gamma Ray clean value is picked from Interval C as 25.

ϕ_N gets as low as 10 p.u. in Interval A, however, ϕ_{Ncl} is taken as 3 p.u. from a large gas sand outside the section shown in this example.

---

* Mark of Schlumberger.

R_{wB} and R_{wF} are taken from the R_{wa} curve. The R_{wB} is picked at 0.1 from the average reading in Interval B. R_{wF} is picked as 0.04 from the average reading in Interval D.

The ρ_{gcl} is selected as 2.65 gm/cc for these high-porosity sands. Matrix density often comes from a knowledge of lithology and is confirmed in this example by the lower reading of ρ_{ga} in Interval D.

The caliper on the CNL-FDC log indicates several washed-out sections of hole. The washouts do not appear to have a significant effect on the porosity logs; thus the selection of ϕ_{max} is not critical for bad-hole discrimination. ϕ_{Ta} reaches 38 p.u. in the sand in Interval A, ϕ_{max} is selected slightly higher at 42 p.u. The sonic log will not be needed for porosity in bad hole.

CYBERLOOK PARAMETER SUMMARY

Shale Indicators: SP, GR, ϕ_N

E_{SPsh} =	-15 mV	ϕ_{Ncn} =	3 p.u.
E_{SPcn} =	-105 mV	R_{wF} =	0.04 ohm-m
γ_{sh} =	95 API	R_{wB} =	0.1 ohm-m
γ_{cn} =	25 API	ρ_g =	2.65 gm/cc
ϕ_{Nsh} =	42 p.u.	ϕ_{max} =	42 p.u.

CYBERLOOK OUTPUT

The CYBERLOOK presentation is shown in Fig. 10. A quality-control check of the computation is made to verify the correctness of the parameters. The shale index is very low in the cleaner parts of the sands in Intervals C and D, and high throughout most of the Interval B. The shale indicators are well calibrated.

The R_0 and R_t curves overlay as they should in all wet zones--the shale in Interval B and the wet sand in Interval D. The computation is of good quality.

Several productive zones are indicated by the CYBERLOOK. In Interval C most of the sands have good porosity, low water saturations, and producibility coding appearing between the R_0 and R_t curves. The sand in Interval A also appears to be productive, with the gas indicator raised for a few feet in the very top of the sand. The water saturation increases toward the bottom, but since the shale index is increasing at the same time, this zone might not make any water. Two thin sand stringers appear in Section B. Both are probably gas-bearing, although the gas indicator is not as strong in the top sand as in the bottom one.

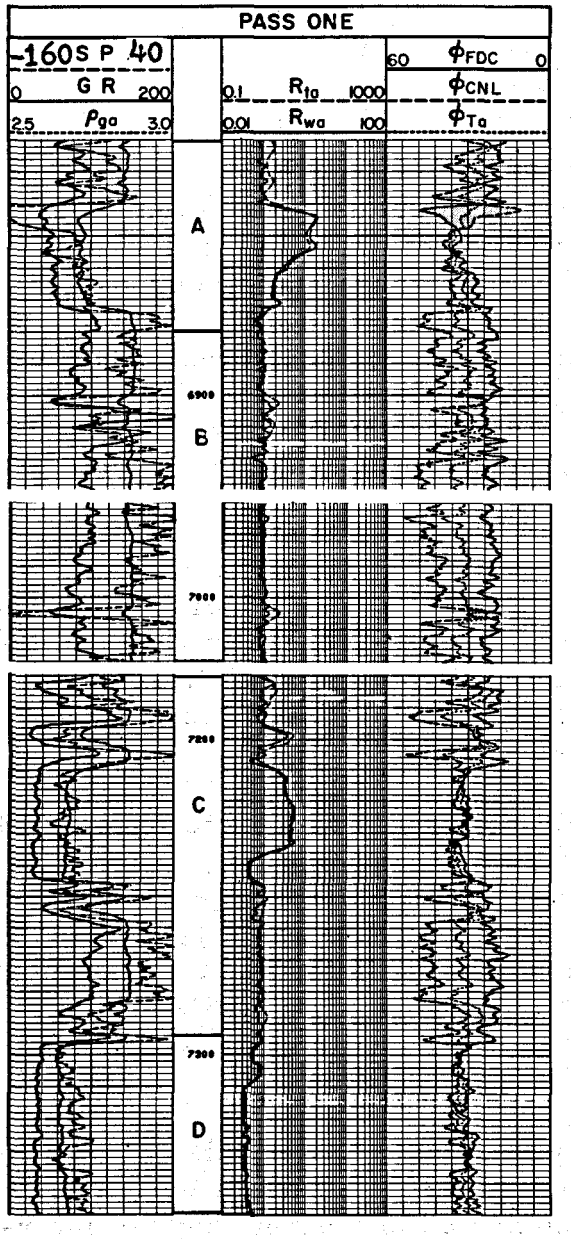

Fig. 9

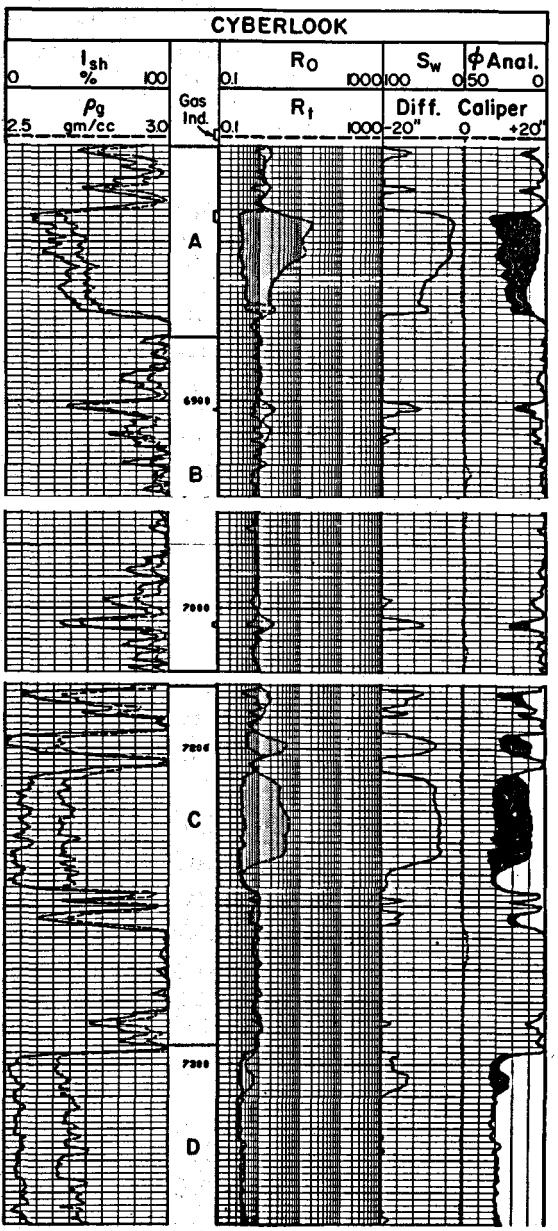

Fig. 10

EXAMPLE 2

Figs. 11 and 12 contain a section of ISF/Sonic and CNL/FDC logs from a South Louisiana well. The well was drilled with fresh mud and contains a series of Miocene sands and shale.

The constants necessary for the Pass One are:

- Neutron is recorded on "Sandstone" matrix
- Mud weight is 9.7
- Bottom-hole temperature is 158°F
- Pore fluid density is 1.0
- Pass-One porosity matrix is sandstone

Pass One is shown in Fig. 13. It has been divided into seven zones. The R_{wa} curve indicates hydrocarbons on top of water in the thickest sand of Interval A. Intervals B and E contain sands that are probably both limy and shaly. There is a broken hydrocarbon-bearing sand in Interval C. Interval D is almost all shale. The top of Interval F has a clean sand with a large ϕ_N/ϕ_D separation. The bottom has a sand with less separation between the neutron and density and is wet on the bottom. Interval G contains mainly water and is clean in places.

Parameters

Both the Gamma Ray and the SP will be used as shale indicators. The SP is pessimistic at times, but the Gamma Ray is generally good and the combination of the two should be adequate. From Interval F, E_{SPcn} is selected at -120 mV. γ_{cn} is picked at 20 from Intervals F and G. Interval D is used to pick E_{SPsh} at -15 and γ_{sh} at 95.

R_{wF} is taken from the apparent fluid resistivity which averages 0.018 ohm-m in the clean wet portions of Intervals F and G. R_{wB} is selected as 0.09 from Interval D. The ρ_{ma} is picked as 2.65 from ρ_{ga} in the clean, wet portions of Intervals F and G. There is rough or washed-out hole over much of Intervals A through E in which ϕ_{Ta} is too high. ϕ_{max} must be picked low enough to discriminate these levels while still allowing computation where the porosity readings are good. ϕ_{max} is chosen as 36 p.u.

The sonic log is needed for porosity in the bad hole of this computation. t_{ma} is picked as 55.5 to correspond with the 2.65 matrix density. t_f is taken as 189 for the fresh mud. B_{cp} computed in the wet sands of Intervals F and G is 100. B_{cp} computed in the wet sand in Interval A is 110. The caliper reading needed to trigger the sonic porosity limit is taken as 10.5 for Intervals F and G, and 10 for the remainder of the computation.

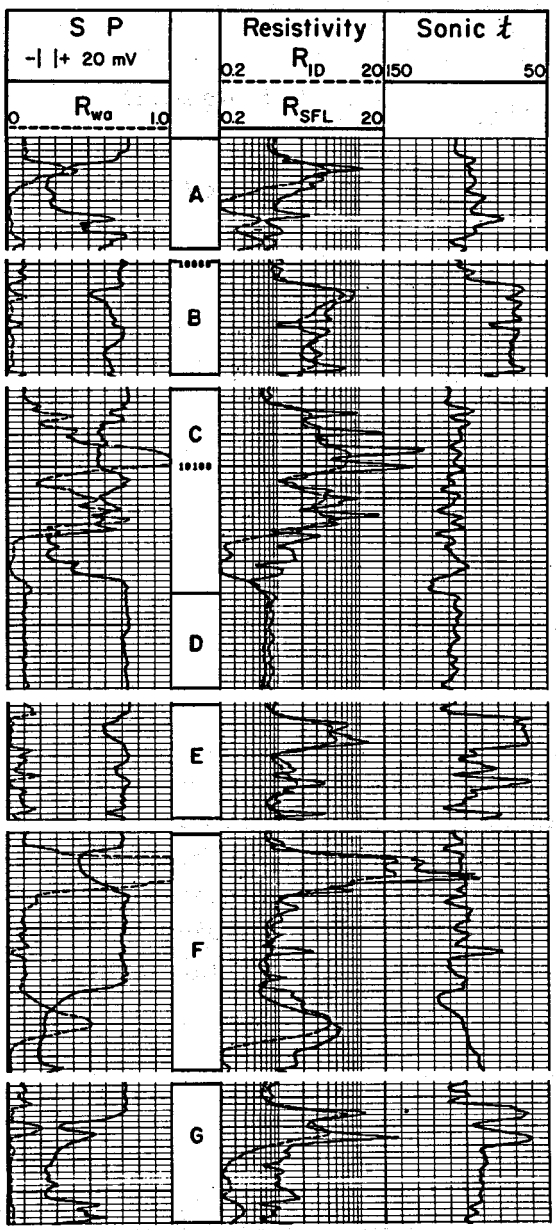

Fig. 11

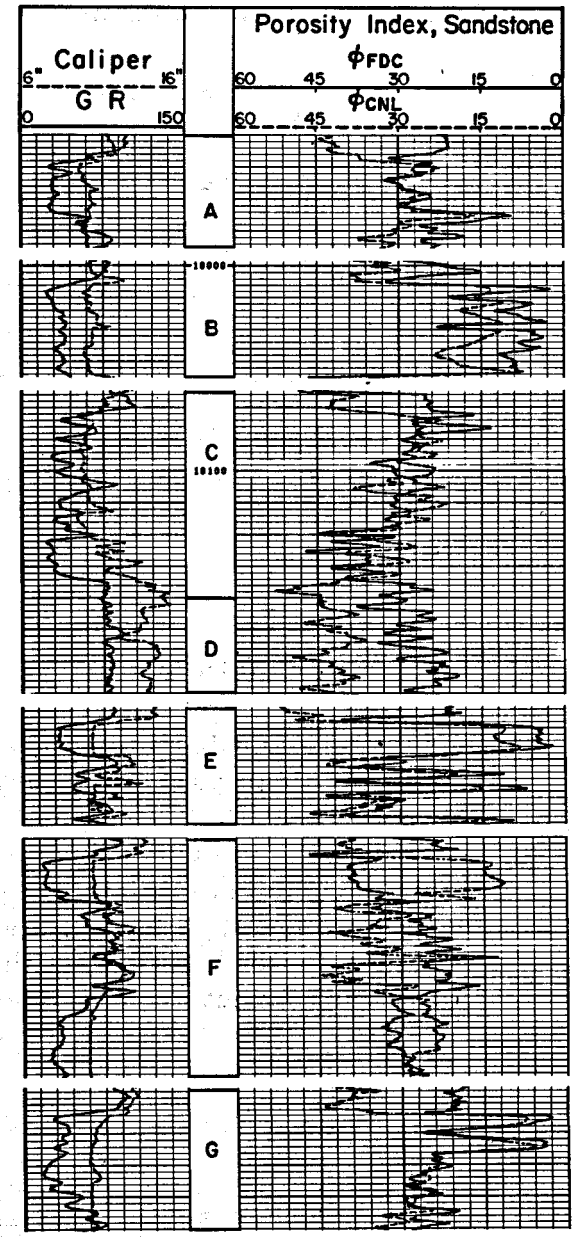

Fig. 12

CYBERLOOK PARAMETER SUMMARY

Shale Indicators: SP, GR

Interval G

E_{SPcn} = -120 mV $\quad\quad$ ϕ_{max} = 36 p.u.

E_{SPsh} = -15 mV $\quad\quad$ ρ_g = 1.65 gm/cc

Shale indicators (continued)

γ_{cn}	= 20 API	t_{ma}	= 55.5 μsec/ft
γ_{sh}	= 95 API	t_f	= 189 μsec/ft
R_{wF}	= 0.018 ohm-m	B_{cp}	= 100
R_{wB}	0.09 ohm-m	$(d_c)_{lim}$	= 10.5 in.

Changes for Interval E: $(d_c)_{lim}$ = 10 in.

B_{cp} = 110

CYBERLOOK OUTPUT

The CYBERLOOK computation is shown in Fig. 14. The shale index is low in the clean parts of Intervals F and G and near 100-percent in the shale of Interval D. The R_0 and R_t curves overlay in the wet zones of Intervals A, F, and G and in the shale. The parameters have been chosen properly and the computation is correct. The top sand in Interval F is indicated to be gas. Although there is separation between ϕ_N and ϕ_D for the bottom sand of Interval F, there has not been a large enough light-hydrocarbon correction to indicate gas.

EXAMPLE 3

Fig. 15 shows a section of DLL*/MSFL and CNL/FDC logs from a well in the Permian Basin. The sections contain the Woodford, Devonian, Silurian, and Fusselman formations.

The constants for Pass One are:

- Neutron is recorded on "Limestone" matrix
- Mud weight is 9.3 lb/gal
- Bottom hole temperature is 278°F
- Pore fluid density is 1.1 gm/cc
- Desired Pass-One porosity matrix is limestone

---

* Mark of Schlumberger.

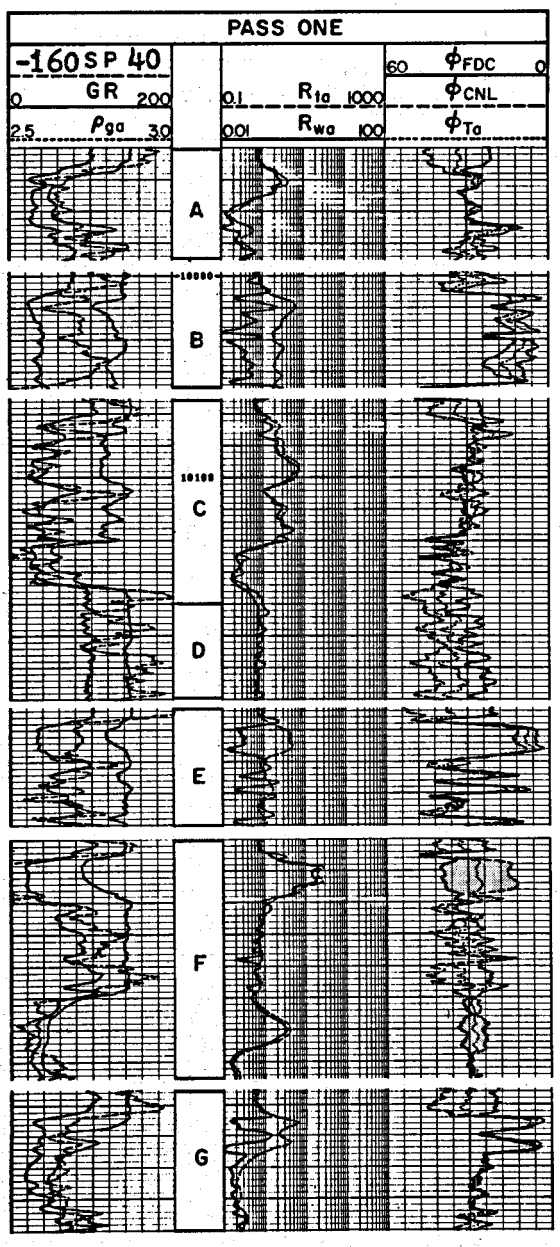

Fig. 13

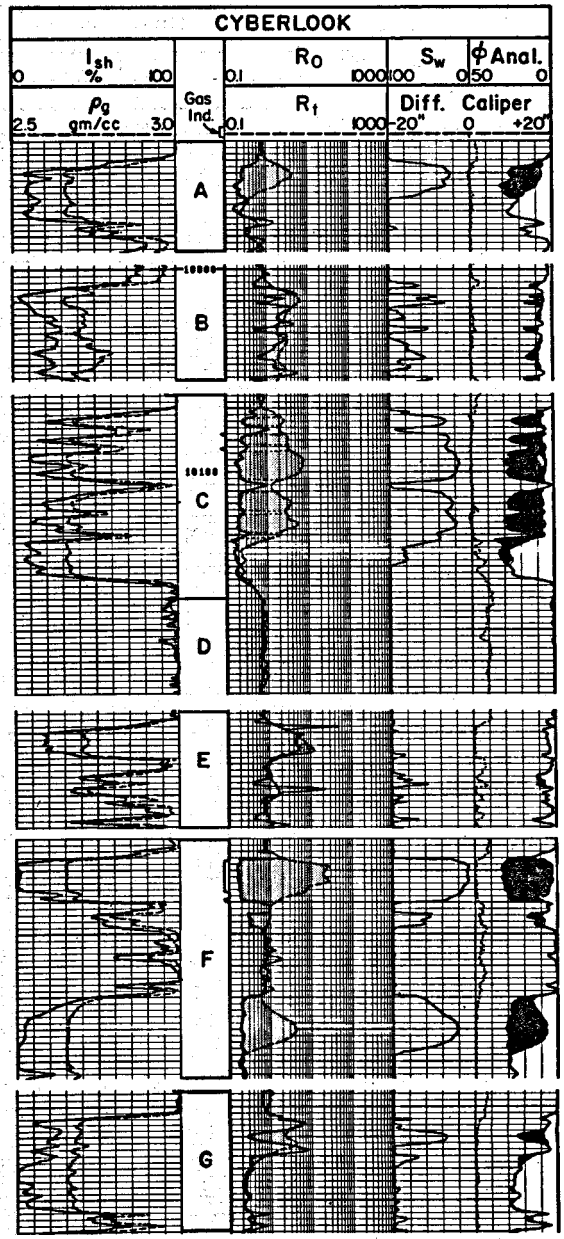

Fig. 14

Pass One is shown in Fig. 16. Four intervals are indicated on Pass One. Interval A is the radioactive, carbonaceous Woodford shale. B is a cherty Devonian lime. C is a Silurian shale with limestone. D is the Fusselman formation, and is dolomite and limy dolomite.

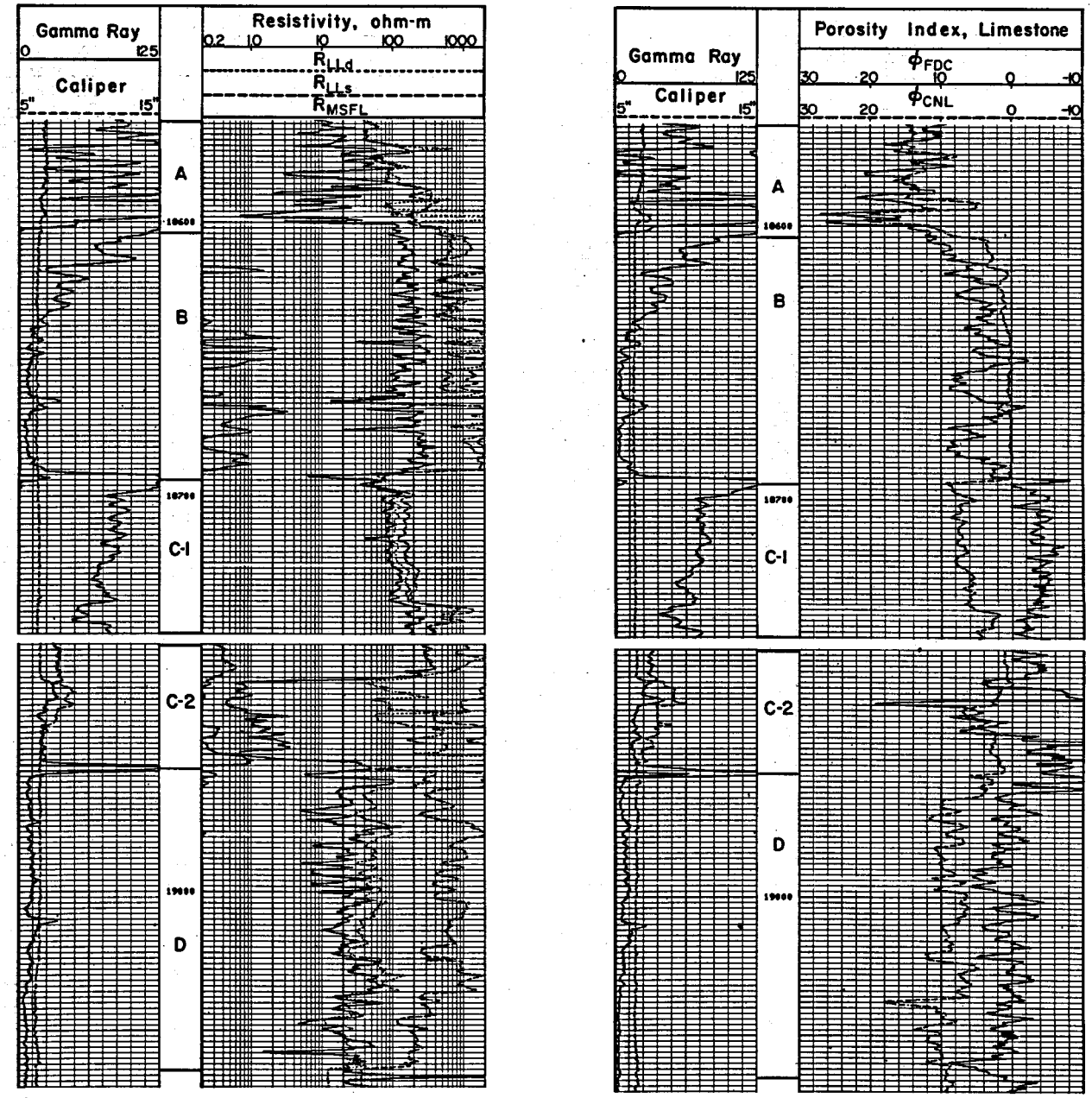

Fig. 15

Parameters

The Gamma Ray and neutron will be used as shale indicators. They are usually both good shale indicators in low-porosity carbonates. An SP was not recorded in this salt-mud well.

The clean Gamma Ray value can be found from the very low readings in both Intervals B and D: 5 API units. The clean neutron value is taken from the very low readings in Intervals B and C: zero.

The shale values are not as easy to select. The high Gamma Ray readings in Interval A must be ignored, since they are not representative of the shale in the other intervals. Interval C has Gamma Ray readings ranging from less than 60 to 100 in the shaliest levels. A value of 70 is selected. The neutron reads 10 p.u. in these same shaly levels, and this will be used for the neutron shale value.

R_{wF} is known to be 0.025 for all intervals. R_{wF} cannot be selected from Pass One since a clean, wet zone does not exist. R_{wB} is taken from R_{wa} in the top portion of Interval C. A value of 0.3 is selected. This value is not suitable for Interval A, where R_{wa} is much higher. R_{wB} will have to be changed to 10 for Interval A.

The measured value of the mud filtrate will be used. It is 0.017 ohm-m at bottom-hole temperature.

This example contains varying lithology and porosity in addition to some bad hole. This will require changes in ϕ_{max} and ρ_{ma} parameters.

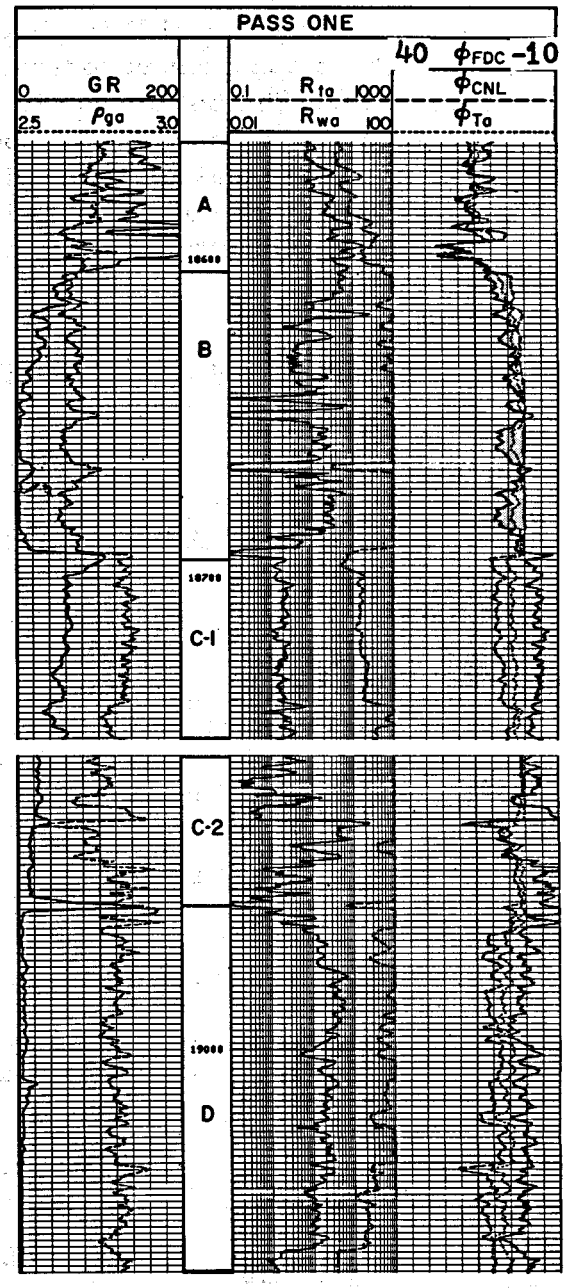

Fig. 16

Interval D is limy dolomite and a matrix density of 2.83 is selected, which corresponds to a 75-percent dolomite--25-percent limestone mixture. Interval C is indicated to be limestone by ρ_{ga} in the cleaner parts. ρ_{ma} of 2.71 is selected for this interval. Interval B is a cherty lime; ρ_{ma} of 2.68 will be used. This value will be retained for Interval A. When the majority of the log shows a gas effect on the neutron and density logs, ρ_{ma} cannot be selected from ρ_{ga} and must come from a knowledge of lithology.

ϕ_{max} for Interval D is picked as 12 p.u. which is slightly higher than the highest apparent porosity in the interval. ϕ_{max} must be changed in Interval C. The bottom portion (labeled C-2) has some washouts where the apparent porosity reads too high. ϕ_{max} is taken as 4 p.u. in Interval C-2 so that S_w calculations will not be performed with unreliable porosity data. There are no washouts in Intervals C-1 and B, so ϕ_{max} is raised to 12 p.u. and left at this value for the remainder of the computation.

CYBERLOOK PARAMETER SUMMARY

Shale Indicators: GR, ϕ_N

γ_{sh} = 70 API

γ_{cn} = 5 API

ϕ_{Nsh} = 10 p.u.

ϕ_{Ncn} = 0 p.u.

R_{wF} = 0.025 ohm-m

R_{wB} = 0.3 ohm-m

R_{mf} = 0.017 ohm-m

ρ_g = 2.83 gm/cc

ϕ_{max} = 12 p.u.

Changes for Interval C-2:

ρ_g = 2.71 gm/cc

ϕ_{max} = 4 p.u.

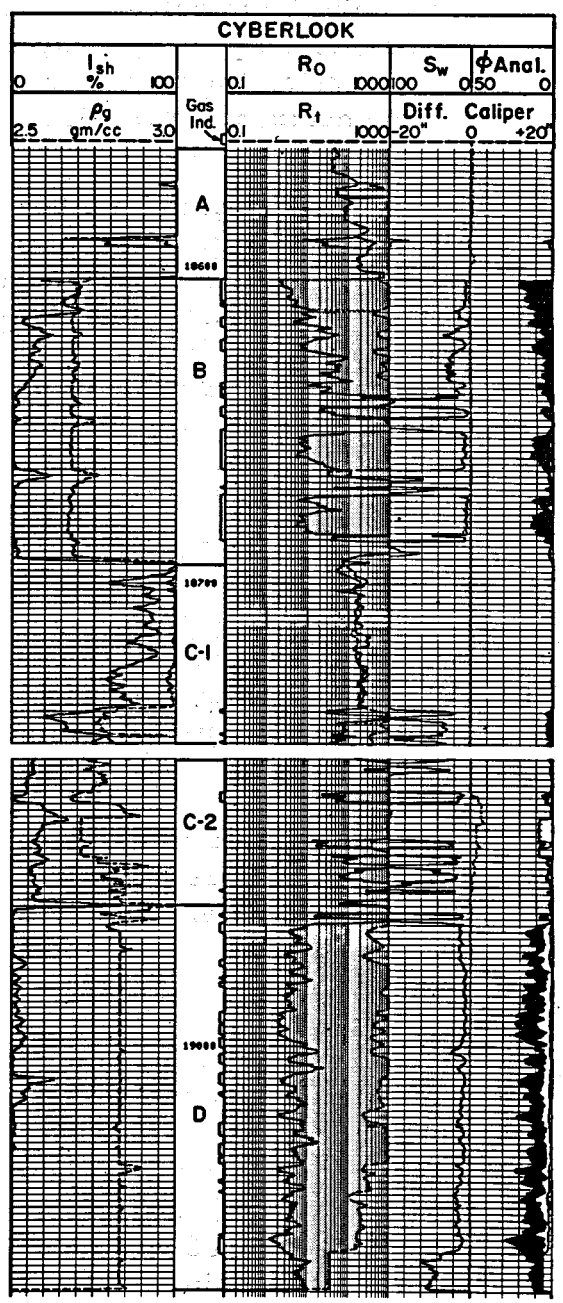

Fig. 17

Changes for Interval C-1: ϕ_{max} = 12 p.u.

Changes for Interval B: ρ_g = 2.68 gm/cc

Changes for Interval A: R_{wB} = 10.0 ohm-m

CYBERLOOK OUTPUT

The CYBERLOOK computation is shown in Fig. 17. The shale index is at or near zero for most of Intervals B and D and near 100 in the top of Interval C. The shale-indicator calibration is good. The R_{wF} cannot be checked because there is no clean wet zone, but the R_0 and R_t curves overlay in the shale, indicating a correct selection of R_{wB}. ϕ_{max} has been selected properly, since the two washed-out zones in Interval C-2 have been discriminated. Their appearance is typical of fairly clean zones which have been discriminated.

Interval D shows low S_w, ϕ, and frequent gas indications. There is also an indication of significant movable hydrocarbons. ρ_g is steady at its input value of 2.83, typical of a clean zone in which the light-hydrocarbon correction is based on a known grain density. The light-hydrocarbon correction is based on the maximum hydrocarbon effect for those levels which show a grain density of less than 2.83 gm/cc.

Interval C shows some low S_w's but has very low porosity and no indication of movable hydrocarbons. Interval B has fair porosity, low water saturation and steady gas indication. The interval shows very little movable hydrocarbons, however. Interval A is shale. A drillstem test in Interval D produced 25 MMcf/D.

SUMMARY

With the coming of Cyber Service wellsite computers, it has become possible to do continuous log processing in the field. The contemporary development of the Dual Water model in shaly sands made it practical to generate a fairly simple program which would allow systematic log analysis by computer over a wide range of well conditions.

This CYBERLOOK program has proved itself to be fast, reliable, and easy to use. Although not intended to replace the more thorough SARABAND and CORIBAND processing, CYBERLOOK logs are a valuable new basis for wellsite decision-making.

SYMBOLS

B	Light-hydrocarbon correction factor, computed in CYBERLOOK program
C_0	100-percent wet formation conductivity, mS-m
C_t	Formation conductivity
C_w	Connate-water conductivity
C_{wB}	"Bound-water" conductivity
C_{wc}	"Clay-water" conductivity
C_{wF}	"Free-Water" conductivity
C_{wM}	Conductivity of "free" and "bound" water, treated as a mixture
$(d_c)_{lim}$	Caliper limit, chosen by analyst to discriminate washout zones
E_{SP}	SP deflection from shale line, mV
$E_{SP\ LOG}$	SP from log
E_{SPcn}	SP in 100-percent clean formation
E_{SPsh}	SP in 100-percent shale
$(I_{sh})_{GR}$ $_{SP}$ $_{N}$	Shale index from Gamma Ray (or SP, or neutron)
$(I_{sh})_{min}$	Minimum I_{sh}, used for computation of S_{wB}
R_0	100-percent wet formation resistivity
R_{ID}	Deep induction resistivity, ohm-m
R_{LLd}	Deep Laterolog* resistivity
R_{LL8}	Laterolog 8 resistivity
R_{mf}	Resistivity of mud filtrate
R_t	Formation resistivity
R_w	Connate-water resistivity
R_{wa}	Apparent fluid resistivity
R_{wB}	"Bound-water" resistivity
R_{wF}	"Free-water" resistivity
R_{wM}	Resistivity of "free" and "bound" water, treated as a mixture
R_{xo}	Flushed-zone resistivity
S_w	CYBERLOOK water saturation (= S_{wF}), percent
S_{wB}	"Bound-water" saturation (fraction of ϕ_T)
S_{wF}	"Free-water" saturation (= S_w)
S_{wT}	Water saturation in fraction of ϕ_T
S_{xo}	Water saturation in flushed zone
V_w	Bulk-volume fraction of water, percent
V_{wF}	Bulk-volume fraction of "free water"
V_{wxo}	Bulk-volume fraction of water in flushed zone
γ	Gamma Ray log reading, API units
ρ_g	Grain Density (or expected grain density), gm/cc

* Mark of Schlumberger.

ρ_{ga}	Apparent ρ_g	ϕ_F	Porosity occupied by "free water"
ρ_{ma}	Matrix density	ϕ_h	Porosity occupied by hydrocarbon
ρ_f	Fluid density	ϕ_N	Porosity from the neutron log
ϕ	Porosity exclusive of that occupied by "bound water", percent	ϕ_{SV}	Porosity from the sonic log
ϕ_B	Porosity occupied by "bound water"	ϕ_T	Total porosity ($= \phi_h + \phi_B + \phi_F$)
ϕ_D	Porosity from the density log	ϕ_{Ta}	Apparent ϕ_T

ACKNOWLEDGMENT

The logs and other data used in Example 2 were from IMC Exploration Company's P. Kessler No. 2, Laurel Ridge Field, Iberville Parish, La. The authors appreciate IMC's courtesy in allowing the use of this material. Appreciation is also expressed to the oil companies which released other field data used in this paper.

REFERENCES

1. Eaton, F.M., Elliott, J.W., Hurlston, F.D., Olsen, R.S., Vanderschel, D.J., and Warren, J.P.: "The Cyber Service Unit--An Integrated Logging System", 51st Annual Fall Technical Conference and Exhibition of the Society of Petroleum Engineers of AIME, New Orleans, Oct. 3-6, 1976, Paper SPE 6158.

2. Clavier, C., Coates, G., and Dumanoir, J.: "The Theoretical and Experimental Bases for the 'Dual Water' Model for the Interpretation of Shaly Sands", 52nd Annual Fall Technical Conference and Exhibition of the Society of Petroleum Engineers of AIME, Denver, Oct. 9-12, 1977, Paper SPE 6859.

3. Waxman, M.H. and Smits, L.J.M.: "Electrical Conductivities in Oil-Bearing Shaly Sands", Soc. Pet. Eng. J. (June, 1968), 107-122. Presented as Paper SPE 1863-A at SPE 42nd Annual Fall Meeting, Houston, Oct. 1-4, 1967.

5. Waxman, M.H. and Thomas, E.C.: "Electrical Conductivities in Shaly Sands--I. The Relation Between Hydrocarbon Saturation and Resistivity Index; II. The Temperature Coefficient of Electrical Conductivity", J. Pet. Tech. (February, 1974), 213-225. Presented as Paper SPE 4094 at SPE-AIME 47th Annual Fall Meeting, San Antonio, Oct. 8-11, 1972.

6. Patchett, J.G.: "An Investigation of Shale Conductivity", Trans. SPWLA 16th Annual Logging Symposium, New Orleans (June 4-7, 1975), Paper V.

ABOUT THE AUTHORS

BEST

GARDNER

DUMANOIR

DAVID L. BEST is a Senior Interpretation Development Engineer with Schlumberger in Houston. He joined Schlumberger in 1962 after graduating from Rice University with a degree in Chemical Engineering. He has worked as a field engineer in South and West Texas and the Middle East. Since 1972 he has been involved with computer processed logs at Houston.

JOHN S. GARDNER is also a Senior Interpretation Development Engineer. He graduated from the University of Arizona with a B.S. in Electrical Engineering in 1964. He joined Schlumberger in 1964 and has had various field assignments in N. America, N. Africa, and the Far East. He is currently involved in digital computer log analysis research.

JEAN L. DUMANOIR is manager of Interpretation Development at Schlumberger's Houston Headquarters. He is a graduate of the University of Lille and Ecole Polytechnique. Jean joined Schlumberger in 1946, serving in South America and Europe in various field assignments. He held posts in Schlumberger's Ridgefield research lab, and in Schlumberger Limited offices in New York, before moving to his present position.

THE SPIDER IN THE WEB

or

THE ROLE OF THE PETROPHYSICIST IN THE WORLD'S QUEST FOR PETROLEUM

by

G. E. Dawson-Grove

Petrophysical Consultants International Ltd.
Calgary, Alberta

AA

ABSTRACT

Modern sophisticated petrophysics has a part to play in petroleum exploration, production and reservoir development, the ultimate importance of which is as yet undreamed of. In this total endeavour, the petrophysicist occupies a vital, central, potentially controlling position. He is, in fact, like a spider in his web.

The petrophysicist has an important part to play in both exploration and production. His range of interest, the range over which he can make very significant contributions, is wider than that of any other discipline involved.

This paper discusses briefly the contributions which can be made by the petrophysicist to Geophysics, Geology and Engineering, then traces his potential relationship with the economist and the politician.

However, it is Management which ultimately decides whether he does or does not fulfil his true potential.

This means two things. First, he himself has to realize just how important and potentially powerful his position is. Second, he has to sell himself.

INTRODUCTION

Modern sophisticated petrophysics has a part to play in petroleum exploration, production, and reservoir development, the ultimate importance of which is, as yet, undreamed of. In this total endeavour, the petrophysicist occupies a vital, central, potentially controlling position. He is, in fact, like a spider sitting in the middle of his web (Figure 1).

Some of you may not like the idea of being compared to a spider. Alternatively, you can liken yourselves to a general, surveying and controlling his forces on the battle field, or to a conductor

guiding and directing his orchestra, or a scientist sitting before his computer console; a really dedicated scientist might prefer to think of himself as the computer itself. However, this picture (Figure 1) serves to illustrate the point I wish to make.

Petrophysics encompasses subsurface pressure studies, fluid flow, all types of core analysis, physical chemistry and a number of other aspects of science and engineering. However, as downhole electrical logs are my specialty, I shall restrict my further remarks to consideration of the part played by them in the overall picture, in the relations between petrophysics and the other disciplines.

We in the petrophysical field have a vitally important part to play in both exploration and production. Our potential range of interest, the range over which we can make very significant contributions, is wider than that of any other discipline involved.

We have a part to play from the time a discovery is a mere gleam in the eye of the geophysicist, right through the geological studies, the drilling, completion, production and reservoir engineering phases, including secondary and tertiary recovery, until the gas or oil enters the pipeline, and the economist hangs dollar signs on it. Even then we are not finished, for beyond the economist is the politician, and then there is Management.

GEOPHYSICS

To start at the beginning: Electrical logging was born in the 1920s, when Conrad Schlumberger, who was a professor of geophysics in Paris, France, and his brother Marcel tried to develop a system for finding underground ore bodies by making electrical measurements on the surface. They went on from that to running electrical surveys, as they called them, in oilwells.

The next contribution of the geophysicist to petrophysics, in the 1950s, was the velocity survey, which ultimately gave rise to our sonic log. Since then, we adapted the geophysical gravimeter to downhole use.

More recently the geophysicist has borrowed back our resistivity log, plus the density log. There is also the Electraflex system of subsurface exploration, which has in a sense brought us back full circle.

The boundaries between petrophysics and geophysics are becoming increasingly blurred. One man who has contributed much to the integration of the two disciplines is Roy Lindseth. And now Dick Wyman has coined the word "Petrogeophysics". How about that: Petrogeophysics?

However, the point I am really stressing is the need for close co-operation between the petrophysicist and the geophysicist. Each has much to contribute to the other.

GEOLOGY

And now, what can we do for the geologist? Initially, electrical logs were used only for correlation, and measuring thicknesses. These are geological functions, albeit primitive. Then we learned to calculate porosity and saturation, and hence estimate reserves; more recently we learned to calculate also permeability and productivity. I call these basically engineering functions. However, the pendulum is swinging back towards the geological side; we can now determine lithology and mineral

composition from logs, and also rock properties such as mechanical strength and the elastic constants.

Such log-derived geological data can be of great value to the geologist. Determination of the degree of dolomitization of carbonates, and of the distribution of anhydrites, has already contributed much to the mapping of carbonate/evaporite reservoirs. Recognition of individual minerals or mineralization, of the appearance or disappearance of characteristically light, heavy or radioactive clays or other minerals, may indicate the sources of rock-building materials, directions of transport, and prevailing conditions of sedimentation. Knowledge of the mechanical strength and elasticity of hard rocks could throw much light on the study of fractured and low porosity reservoirs.

For example, a given area may be underlain by a large volume of sand, mechanically exhibiting the characteristics of good porosity, low water saturation and high permeability. However, the apparently attractive reservoir may be pervaded by diagenetic clay, kaolin, silt, dolomite/anhydrite cement, or bitumen, any of which could ruin or destroy its commercial value. AA

Or, it may be found that the shales in an important but complex petroleum productive basin, though superficially similar, may be separable into two or three recognizably and significantly different groups.

Alternatively, in a totally different geological environment, the distribution of productivity in fractured, low porosity, low permeability hard rocks may be found to be related to mineral composition, and to log-measureable (but not otherwise apparent) mechanical properties.

Log-derived information of these types plus the results of high-density dipmeter analysis, could contribute importantly to stratigraphic studies and geological mapping, i.e., to the correct interpretation of both potential and proven petroleum productive provinces.

Routine CORIBAND/SARABAND or EPILOG, LOGAN, LASERLOG, etc. types of analysis of logs are adequate for calculating the engineering parameters, such as porosity, saturation, etc., provided they are properly supervised. However, the determination of geological information, on lithology and mineralogy, or grain size, and mechanical properties, requires at present a high level of computerized custom handling of full suites of the most up-to-date electrical logs.

ENGINEERING

The tie-in between petrophysics and reservoir engineering is well-known. Historically it has been our job to calculate reservoir parameters — if anything that dates back only thirty years can be called historic.

However, the petrophysicist is contributing increasing volumes of increasingly valuable data to the drilling engineers. From his electrical logs and from mudlogs he can, among other things, predict major changes in subsurface pressures. Mudlogging has come to mean very much more than just sniffing for gas in the mud. Rich Mercer has written some important papers on this subject.

From a combination of mudlogging and drilling functions logging the drilling engineer can derive a wealth of information which helps him to do his job much more efficiently and more safely.

I wish I could think of a better term than mudlogging. It sounds so mundane. Any other terms I have heard are so ponderous. Someone should think up a good acronym. Any suggestions? I am sure the mudloggers would love to have one. Maybe they should run a competition.

Other branches of engineering to which the petrophysicist can contribute are well completion and production. The completion engineer who completes a well himself, based on his own interpretation of the logs, is asking for trouble. Many is the bed of gypsum which has been perforated for production, not to mention coals, bentonites and waterbearing conglomerates.

Under production engineering come special applications such as the study and development of low porosity gas sands and tar sands, plus fire floods, steam floods, solvent and chemical floods, and all other forms of secondary and tertiary recovery.

Only when the gas or oil enters the pipeline does the petrophysicist finally step out of the picture. Even then he may find himself dealing with the economists, and maybe even with politicians.

ECONOMICS AND POLITICS

This World is controlled by economics and politics, and it is imperative that we, as technical people, should recognize this. I am aware that in many technical societies there are strong feelings that members should not meddle in politics; in some societies, the by-laws expressly prohibit any form of political activity. But, the World is changing. We cannot afford to retire into our ivory towers, and try to shut out things that we may not like. If we do, we shall suddenly find we have no towers to retire into anymore, ivory or otherwise.

We must take a far greater interest in the economic aspects of our work, then learn to stand up and speak out, and tell people what we know, in plain language, so that they will understand, and want to hear more. Our industry has become the whipping boy of the politicians. We must learn to fight politics with politics.

If we fail to so learn, or if, having learned, we flinch, our industry will disappear, just like the dinosaur. It will be taken over by Government, and we, as individuals, shall cease to be individuals. We shall become just part of an army of hundreds of thousands of pen pushers and paper shufflers, and the Western World will inexorably run out of gas and oil.

WE IN THE PETROPHYSICAL FIELD ARE IN A UNIQUE POSITION. WE HAVE THE POTENTIAL OF KNOWING MORE ABOUT PETROLEUM EXPLORATION AND RECOVERY THAN ANY OTHER SINGLE DISCIPLINE. It is our duty to stand up, speak out, and tell people what we know.

MANAGEMENT

Before concluding, I have another important point to discuss: our potential, and position, vis-a-vis Management. It is Mangement which ultimately decides whether we do or do not fulfil our true potential.

Some of you may have heard my paper on shallow gas exploration. It was a very simple illustration of what we petrophysicists can do. We can make the difference between discovery, and no dis-

covery. However, the point I have in mind now involves a vastly different situation, where the stakes are vastly higher.

I once read an excellent paper on petrophysical problems in the Ekofisk area of the North Sea. In a technical sense, it was first class. However, the thing that really struck me was the comment, repeated in several places, that for a certain situation the minimum logging program was such and such.

In other words, to do the job properly, a full program would be necessary. To "get by", we could skimp it. I have to conclude that in this case, as in so many cases, Management favored the skimping.

Except in the case of shoe-string fly-by-night operations, we should never talk of minimum programs. To do so is the falsest of false economy. We should be thinking about maximum programs. What is the MAXIMUM contribution we can make to this operation?

AA

ONLY WHEN WE OURSELVES START THINKING ABOUT MAXIMUM PROGRAMS WILL WE BE ABLE TO SHOW MANAGEMENT WHAT WE CAN REALLY DO. ONLY THEN WILL WE BE ABLE TO MAKE OUR MAXIMUM CONTRIBUTIONS TO OUR CLIENTS, OUR COMPANIES, OUR INDUSTRY, OUR COUNTRY, AND TO THE WHOLE WORLD.

In these times of energy shortages and economic turmoil, IT IS OUR DUTY to make that maximum contribution.

To achieve the full potential of petrophysics, it must become routine to gather more, and better quality, primary data. Maximum use must then be made of all the data, and of all the high-powered expertise which is already available to work with them.

More logs should be run, at more frequent intervals. All logs should be recorded on tape, at wellsite. Complete computer processing, as is now commonplace in geophysical work, should become equally routine in the analysis of electrical logs, leading to comprehensive and co-ordinated geophysical/petrophysical study of all pertinent data on all wells, both exploratory and development, deep and shallow, "frontier" or "domestic".

It will cost money to do this, but only a fraction of what is now wasted on drilling expensive dry holes in wrong places, losing wells for "mechanical reasons", overlooking discoveries due to misinterpretation of data, and other expensive BLUNDERS. Drilling cost estimates should contain at least as much money for evaluation as is now spent on geophysical surveys, and lease acquisition.

To design a drilling program which does not provide money for full geological/petrophysical evaluation is to set up a "giant with feet of clay" (Figure 2). This comment applies to all drilling programs ranging from shallow gas development wells to the most difficult and expensive offshore/frontier wildcats. We must convince Management that such full evaluation is essential.

Eventually there will be complete integration of geophysics, petrophysics and geology, plus the rock-penetration-mechanics/subsurface-pressures aspects of drilling, and reservoir engineering. All will be devoted to one end: The most efficient and ultimately most economical way to find and recover the World's hidden stores of petroleum.

PETROPHYSICS COULD BE BOTH THE LIFE-FORCE AND THE CEMENT THAT WILL BRING AND HOLD TOGETHER THE ENTIRE FABRIC OF EXPLORATION, DEVELOPMENT AND PRODUCTION.

CONCLUSION

A more conventional representation of the position of the petrophysicist vis-a-vis the other disciplines, rather than the spider in the web, is an organization chart type of diagram (Figure 3).

This picture could be redrawn with Management being merely on the rim of the circle, along with the technical disciplines, economics and politics, and petrophysics in the centre of everything (Figure 4). However, that might be going a little too far, and some people might feel I was a little biased.

There are those who think that the job of the petrophysicist is purely supportive. They think he should be in a little box, attached to engineering or attached to geology. Those most guilty of this type of thinking are in Management, for obviously and necessarily the ideas on petrophysics of most members of Management are ten or fifteen years behind the times. This is not to criticize Management; it is a statement of fact.

There are people in Management now who may have been quite good at "log analysis" ten or fifteen years ago. Inevitably, they have been left far behind in their knowledge of what petrophysics can do, can do for them. It is up to us to teach them.

THIS MEANS TWO THINGS. FIRST, WE HAVE TO REALIZE, OURSELVES, JUST HOW IMPORTANT AND POWERFUL OUR POSITION IS. SECOND, WE HAVE TO SELL OURSELVES.

In the whole field of petroleum exploration and production, the modern, up-to-date, petrophysicist occupies a vital, central, controlling position. He is, in fact, like a spider sitting in the middle of his web (Figure 5).

ABOUT THE AUTHOR

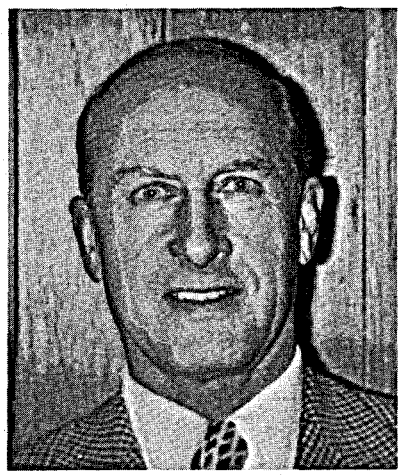

GLASCOTT E. ("D-G") DAWSON-GROVE was born in England, of Irish parents, raised in China, educated in Ireland, Hong Kong and England. He has a B.Sc. and A.R.S.M. in Petroleum Engineering (equivalent) from Imperial College, London, and an M.Sc. in Geology from the University of Cambridge. He is a Registered Professional Engineer and a Registered Professional Geologist, in Alberta.

"D-G" worked for 8 years with Shell Oil Co., U.S.A., as a Petrophysical Engineer, and for 14 years as Petrophysicist for Home Oil Co., Canada. He is now President and Chief Consultant of his own company, Petrophysical Consultants International Ltd. of Calgary.

AA

D-G is a Past President of the Canadian Well Logging Society, a past Director of the S.P.W.L.A., a Past President of the Economics Society of Alberta, a Life Fellow of the Geological Society of London, and a past District Lt. Governor of Toastmasters International for Alberta and Saskatchewan.

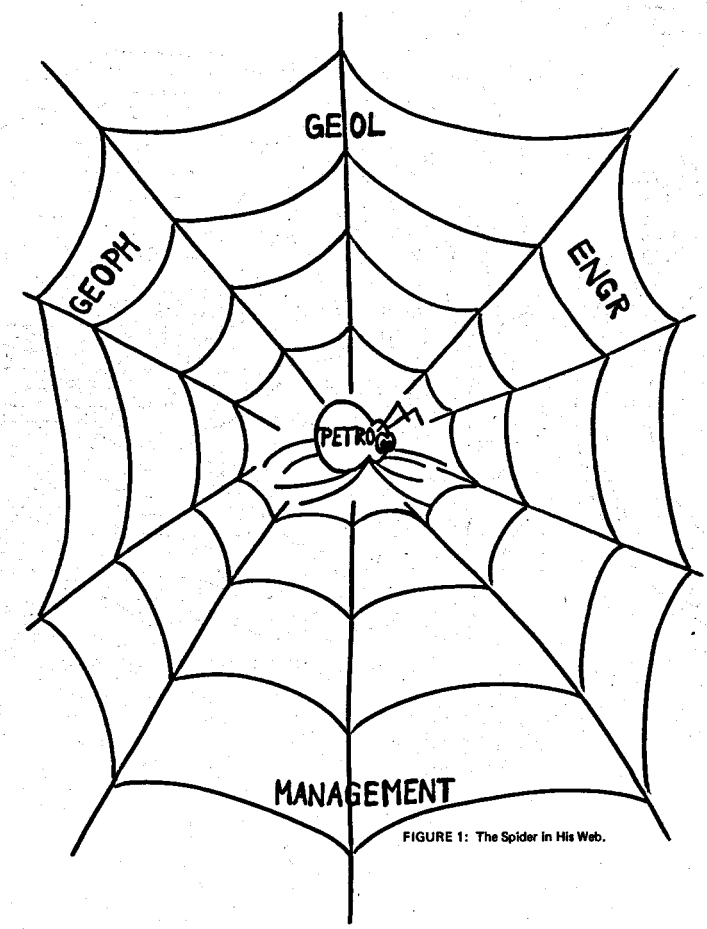

FIGURE 1: The Spider in His Web.

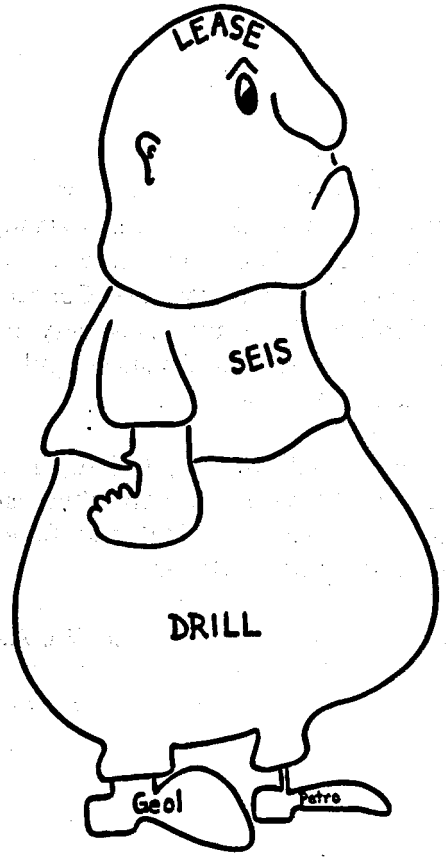

FIGURE 2: The Giant with Feet of Clay.

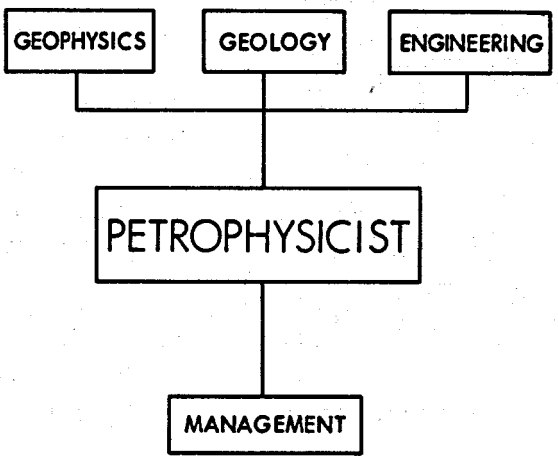

FIGURE 3: Organization Chart (conventional).

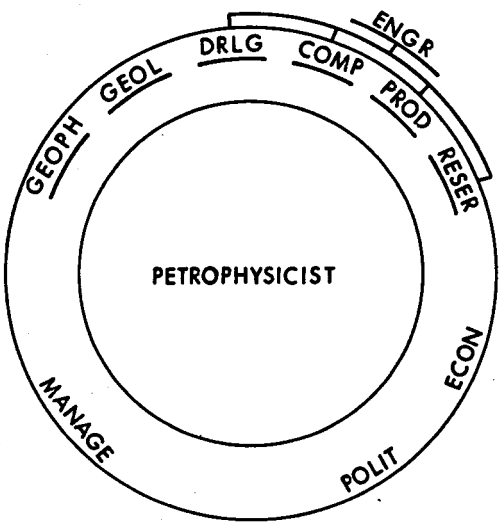

FIGURE 4: Organization Chart (alternative).

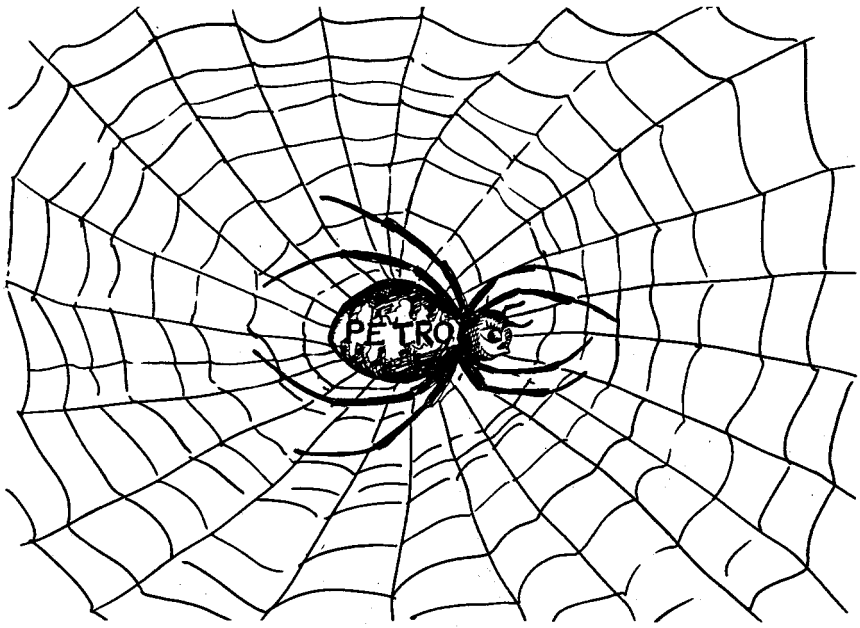

FIGURE 6: "PETRO", the all-seeing, all-hearing, all-knowing Spider.

THE PREDICTION OF WATER SATURATION AND RECOVERABLE HYDROCARBON VOLUMES IN SHALY SAND RESERVOIRS

Daniel A. Krygowski
G. R. Pickett

ABSTRACT

Four methods of well log interpretation in shaly sand reservoirs, based on empirically observed relationships, are developed. Three methods are crossplot techniques applicable to single- or multiple- well analysis. The fourth technique, based on statistical methods, requires data from existing wells in order to be applied.

The Rwa-SP crossplot method quantifies water saturation values in shaly zones by means of overlays which show the location of water-bearing trends as a function of shaliness, Rmf, and Rw. The resistivity-apparent porosity crossplot method applies correction factors to resistivity and acoustic log measurements to normalize the data to clean sand values. The resistivity-SP crossplot method is used to infer values for water saturation and porosity when no measures of porosity are available in individual wells.

The fourth method uses parameters derived from well logs to directly predict recoverable hydrocarbon volumes (in this case, primary ultimate recovery) without the knowledge of specific values of porosity and water saturation.

INTRODUCTION

Since the inception of quantitative well log analysis, one of the most persistent problems in interpretation has been the determination of water saturation in shaly, or clay-containing, sands. Beginning with the description of 'conductive solids' by Patnode and Wyllie (1950) many interpretational techniques have been proposed, but none have gained universal acceptance. Because of changing economic conditions and advances in completion technology, many of the shaly sand reservoirs formerly considered non-economic are now viewed as commercial reservoirs. With the renewed interest in shaly sands as exploration objectives, it was decided to again investigate the problems of well log interpretation in shaly sands.

The primary objective of this study was to develop empirical shaly sand interpretive techniques which could be applied with a minimum of currently available well data. The decision to approach the problem from an empirical viewpoint was made after a study of shaly sand literature. In general, those methods based on theoretical considerations tended to be cumbersome to use, either because of large numbers of required measurements, or because of specialized data. Methods based on observed (empirical) relationships could, on the other hand, be applied and modified without the necessity of rethinking underlying theory. The desire to apply the method with a minimum or currently available data was twofold; first, to minimize

the cost of data acquisition while having readily available proven technology, and second, to be able to apply these techniques to the reanalysis of previously drilled wells.

Approaches and Data

The interpretation problem was approached in two ways. The first was the modification of existing crossplot techniques to account for the effects of shaliness. The crossplots included apparent water resistivity (Rwa) -SP, resistivity - apparent porosity, and resistivity -SP methods. The second approach was the direct prediction of recoverable hydrocarbon volumes from well log data without calculation of the traditional values of porosity and water saturation. In this study, various parameters derived from uncorrected well log data were used to predict primary ultimate recovery.

The data used in this study were from two sources. Data from water-saturated shaly sand cores were from the work of Hill and Milburn (1956). They included 316 cores, each with measurements of porosity, permeability, formation factor (3 to 6 values each), electrochemical potential, and a calculated value for shaliness (b-factor). Field data were from the Mill-Gillette Field in Campbell County, Wyoming, which is oil productive from the Muddy Formation of Cretaceous age. Available data included well logs and production figures from 34 wells, and core analyses from 8 of those wells. Each well was divided into from 8 to 18 zones on the basis of well log response, and the log values for each zone were used in the interpretation techniques. Figure 1 shows a typical well in the field.

For the crossplot portion of the study, the data from the water-saturated shaly sand cores was used to determine shaliness dependent relationships which were then applied to the hydrocarbon-bearing case of the field data. By using water-saturated cores, the relationships could be studied outside the disturbing influence of hydrocarbons, and could provide a base from which hydrocarbon-induced anomalies could be recognized. For the direct prediction portion, statistical analysis of the field data provided the predictive relationships.

Core Data

The first part of the study defined two shaliness dependent relationships from the data on water-saturated shaly sand cores. The first relationship was described by Hill and Milburn (1956), and related electrochemical potential, Rw, and shaliness, "b". As shown in Figure 2, the relationship between electrochemical potential (SP) and "b" for a given value of Rw is not linear, and further, the relationship as a whole has no easy mathematical description. The second relationship was a result of the current study. From analysis of the formation factor data (Krygowski, 1977) the dependence of apparent water resistivity, Rwa (R=Ro/F), on Rw and shaliness, "b", was shown to be:

$$Rwa + 0.045 \left(\frac{Rw}{0.045}\right)^{\frac{b+0.44}{0.44}} \qquad (1)$$

This is shown graphically in Figure 3. These two relationships were then used to modify the crossplot techniques studied.

Crossplot Methods

For the Rwa-SP crossplot the two relationships discussed above were combined as follows: Figure 2 was entered with those same values of Rw and b, and a value of Rmf, and SP determined. The resulting values of Rwa and SP were plotted and generated a family of curves as in Figure 4. As in the usual Rwa-SP crossplot, the line labeled "b = 0.0" is the clean sand water-bearing line with slope of K (from SP = -K log Rmf/Rw) and intercept at SP = 0 equal to Rmf. The other lines are water-bearing lines for various degrees of shaliness. The dashed line is a line of equal Rw; that is, a set of zones which were water-bearing and of varying degrees of shaliness, but with the same Rw, would plot along that line. The water saturation of a zone is determined through the calculation of the resistivity index, I, as the ratio of the Rwa of the zone to the Rwa of the line of equal Rw at the same shaliness (same SP).

Figure 5 is an example using the data from 4 wells with the same value of Rmf from the Mill-Gillette Field. As can be seen, several zones which contained residual oil in core analysis show as anomalous with respect to the line of equal Rw (dashed line) while showing no anomalies with respect to the clean sand water-bearing line. Specifically, zones A, B, and C show water saturations of 73, 48, and 58% respectively using this technique. Other field data also showed qualitative agreement between core analyses, hydrocarbon-productive perforated intervals and this method. BB

Although the construction of families of water-bearing lines appears to be of use as a shaly sand technique, it is inconvenient in two ways. First, because the measurements were made on the water-saturated cores at 77°F, log data must be corrected to that temperature from formation temperature. Second, because of the nature of the SP relationship used, the curves change shape with changing Rmf, and a different set of curves is needed for each value of Rmf.

The second crossplot method investigated was the resistivity-apparent porosity technique described by Pickett (1966, 1973). The technique has no explicit measure of shaliness as does the Rwa-SP crossplot, and instead of a family of curves to which to compare the data, the log value itself was corrected for shaliness.

The SP log was used as the measure of shaliness of a zone. It was found that for the Rw of the formation (0.10 ohm-m @BHT) and the range of Rmf values encountered in most of the wells, the relationship between SP and shaliness, b, was of the form:

$$\frac{SP}{SP_{max}} = \alpha = e^{AB} \qquad (2)$$

where A is a function of Rmf.

Using the relationship expressed by equation 2, b can be determined, and then Rwa calculated from equation 1. The resistivity corrected for shaliness was then:

$$Rtc = Rt\ (\frac{Rw}{Rwa}). \qquad (3)$$

A correction for the acoustic log based on the work of Pickett (1960) was also investigated. A corrected acoustic traveltime was calculated using:

$$\Delta t_c = \alpha \Delta t_{SD} + (1-\alpha)\Delta t_{SH}. \qquad (4)$$

Knowing the effective pressure of the Mill-Gillette Field and the range of porosities encountered in the formation, the specific relationship was:

$$\Delta t_c = 54 - 2.4\phi - 4.0\alpha - 1.0\phi\alpha. \qquad (5)$$

where $\alpha = SP/SP_{max}$ and ϕ was determined from the density log.

Figures 6, 7 and 8 show data for 4 wells in the Mill-Gillette Field. Figure 6, using uncorrected data, shows an estimated water-bearing trend which shows Rw = 0.72 ohm-m (as compared to the measured value of 0.1 ohm-m). Zones D, E, and F are shown to have a minimum water saturation of 70%. Those zones were perforated and produced, collectively, 60 BOPD, no water. Figure 7, using corrected resistivity, Rtc, gives estimates of 0.85 ohm-m for Rw and 68% water saturation for zones D to F, a slight improvement. Figure 8, using both Δt_c and Rt_c shows an estimated Rw of 0.13 ohm-m and zones D to F with a minimum water saturation of 57%.

As with the Rwa-SP crossplots, qualitative agreement between core analysis, producrion data and log analysis was good and water saturations in zones known to be productive were lower than with conventional analysis. Unlike the Rwa-SP method, the SP relationship could be approximated, because of the limited range of Rmf values and the knowledge of Rw, to simplify the shaliness correction procedure.

Investigation of the third crossplot technique, resistivity-SP, was undertaken because of the observation that many shaly sands, including the Muddy of this study, have a limited porosity range. Although porosity induces scatter in the resistivity -SP crossplot, making it less quantitative than the previous two methods, it is still of use if measures of porosity are unavailable for all the wells of interest, especially if the scatter is controlled by a limited porosity range. If, for example, some wells of interest have no measure of porosity (as with many old wells), but the range of porosity can be inferred or estimated from data in other wells, an estimate of a probable range of water saturation can be made for at least a qualitative analysis. Figure 9 shows wells from the Mill-Gillette Field. The intercept of the clean sand line is $Rmf\phi^{-m}$ where the porosity is an average of 14.3 percent. Those zones known to be productive are shown to be anomalous, while others, above the line of equal Rw, indicate the possibility of the presence of hydrocarbons.

As stated earlier, this method is less quantitative than the two previous methods, but can give some indication of the presence of hydrocarbons and whether an area of interest bears further study.

Direct Prediction

The second approach to shaly sand interpretation was the direct prediction of recoverable hydrocarbon volumes. This approach was used in an effort to avoid the shaliness corrections necessary in the calculation of porosity and water saturation. This method used well log based parameters as the independent variables in regression equations with primary ultimate recovery as the dependent variable. Table 1 lists those well log derived parameters. In each well, a given parameter was calculated for each zone. The zones were then sorted into groups on the basis of percent of clean sand SP (see Figure 10), then the parameters summed on the basis of that sorting. To determine the optimum number of groups into which to sort the zones, a modification of the method of polynomal curve fitting described by Johnson and Leone (1964) was used. By this method, the optimum number of groups for this data was found to be three. For each well, then, an equation could be written as:

$$\text{Primary Ultimate Recovery} = C_0 + C_1\Sigma Lp_1 + C_2\Sigma Lp_2 + C_3\Sigma Lp_3$$

Where Lp_i = a well log derived parameter where "i" indicates the sorting based on SP.

Ci = constants determined by the regression equation.

and the constants determined by using the method of least squares. For the parameters using the density log, 21 of the 34 wells could be used; for those using the acoustic log, 28 of 34 wells.

The goodness of fit of each equation to the data was determined in two ways. Throughout the study, the error sum of squares was used. It is a measure of the amount of scatter in the data not accounted for by the regression equation. In the final stage a second determination of goodness of fit was also used. This was the number of values of primary ultimate recovery (of the original data) which were correctly predicted for each parameter. A "correct prediction" was arbitrarily chosen as a calculated primary ultimate recovery within a range of 15 percent of the observed value, or if the well was plugged and abandoned (observed value equaled zero), a calculated value of 10,000 barrels (10 MSTB) or less.

Table 2 is a list of the results of one of the parameters, the acoustic version of parameter 9 ($\Sigma Rwa/\Sigma h$). It is one of the prediction cases for the acoustic version of the well log parameters with 9 of 28 recoveries (32 percent), correctly predicted. The best success for the density versions of the well log parameters was 9 of 21 recoveries (43 percent).

Of the 12 parameters utilized in the study, no one parameter stood out as significantly better than the others. Attempts to improve the "goodness of fit", measured by both correct predictions and the error sums of squares, by using weighted combinations of both "porosity" tools, recalculation of primary ultimate recoveries, and elimination of certain wells, meet with little success. Neither the number of values correctly predicted nor the decrease in the error sums of squares was significant.

Although this method eliminates the need to make specific shaliness corrections, it requires a different approach than the crossplot

BB

TABLE 1: Well log parameters used in the direct prediction of recoverable hydrocarbon volumes.

Parameter	Acoustic log	Density log
1	$\Sigma Rwa = Rt\phi^m$	$\Sigma Rwa = Rt\phi^m$
2	$\Sigma Rwa \cdot h$	$\Sigma Rwa \cdot h$
3	$\Sigma Rt(\Delta t - \Delta t_m)$	$\Sigma Rt(\rho_m - \rho_b)$
4	$\Sigma Rt(\Delta t - \Delta t_m)h$	$\Sigma Rt(\rho_m - \rho_b)h$
5	$\Sigma S_h \phi h$	$\Sigma S_h \phi h$
6	$\Sigma Rt(\Delta t - \Delta t_m)^3 h$	$\Sigma Rt(\rho_m - \rho_b)^3 h$
7	Ia	Ia
8	Ia·h	Ia·h
9	$\frac{\Sigma Rwa}{\Sigma h}$	$\frac{\Sigma Rwa}{\Sigma h}$
10	$\frac{\Sigma Rwa \cdot h}{\Sigma h}$	$\frac{\Sigma Rwa \cdot h}{\Sigma h}$
11	$\frac{\Sigma Rt(\Delta t - \Delta t_m)}{\Sigma h}$	$\frac{\Sigma Rt(\rho_m - \rho_b)}{\Sigma h}$
12	$\frac{\Sigma Rt(\Delta t - \Delta t_m)h}{\Sigma h}$	$\frac{\Sigma Rt(\rho_m - \rho_b)h}{\Sigma h}$

$\phi = \frac{\Delta t - 55}{130}$ or $\frac{2.66 - \rho_b}{2.66 - 1.00}$

Ia: apparent resistivity index from resistivity-apparent porosity crossplot.

TABLE 2: Tabulation of observed and calculated values of primary ultimate recovery.

Parameter 9 (acoustic): $\Sigma Rwa/\Sigma h$

Well Number	Primary Ultimate Recovery (MSTB) Observed	Calculated	Correct Prediction
2	82.70	32.45	
3	41.70	48.93	*
5	31.20	27.46	*
6	2.81	38.24	
7	171.00	47.96	
9	36.60	118.65	
10	23.60	50.60	
11	201.00	171.07	
12	172.00	178.83	*
13	128.00	47.66	
15	8.64	32.86	
16	86.50	82.00	*
17	59.80	58.70	*
18	80.20	82.19	*
19	0	49.79	
20	0	34.80	
21	72.80	63.79	*
22	0	24.11	
23	57.50	70.74	
24	71.60	32.45	
25	124.00	32.69	
26	0	24.94	
28	0	21.58	
29	220.00	204.63	*
31	0	29.86	
33	0	27.55	
34	52.00	50.46	*
35	15.30	52.61	

BB

techniques. Not only does the method require many wells in the analysis, but it also requires those wells to have some measure of hydrocarbon potential, such as primary ultimate recovery.

DISCUSSION AND CONCLUSIONS

Four methods of well log analysis in shaly sands have been discussed. Three are applicable to the analysis of individual wells while the fourth requires a number of wells to be of use.

The Rwa-SP method quantifies shaliness without correcting log values themselves, but requires reconciliation of chart and borehole temperatures. Although the interpretive charts change shape with Rmf, each chart could be used over a range of Rmf values with little loss of accuracy, especially when the uncertainties in the log measurements are considered.

The resistivity-apparent-porosity technique differs from the Rwa-SP method in that shaliness corrections are made to the log values. Corrections can be made to one or both of the logs used in the crossplots, and if the basic relationships (from the water saturated cores) can be explicitly defined, the method can be applied using machine-assisted computation.

The resistivity -SP crossplot, although built on the most assumptions, can be of great use when little or no porosity data are available, and the assumptions are carefully made.

The fourth method, the direct prediction of hydrocarbon volumes, requires many wells with production data throughout the area of interest. Although this precludes its use in unexplored areas, it may provide the means of circumventing interpretation problems in mature producing areas.

No attempt is made to call the techniques discussed here universal. They were developed and tested using limited amounts of data and may be biased by that data. Each comes with its own set of limitations, but each is fairly easy to use, and may be applied and modified without rethinking theorectical assumptions. As with other methods which have been proposed, the validity of these methods will be measured by the success of their application.

ACKNOWLEDGMENTS

The authors acknowledge the help given by Davis Oil Company, Denver, Colorado, through release of well logs and related data from the Mill-Gillette Field, Campbell County, Wyoming.

sh

BIBLIOGRAPHY

Hill, H. J., Milburn, J. D., 1956, Effect of clay and water salinity on electrochemical behavior of reservoir rocks: Trans. AIME, v. 207, p. 65-72.

Johnson, N. C., Leone, F. C., 1964, Statistics and Experimental Design, v. 2: New York, John Wiley and Son, Inc.

Krygowski, D. A., 1977, The use of well logs to determine water saturation and recoverable hydrocarbon volumes in shaly sand reservoirs: Colorado School of Mines Thesis T-1958 (unpublished).

Patnode, W. H., Wyllie, M. R. J., 1950, The presence of conductive solids in reservoir rocks as a factor in electric log interpretation: Trans. AIME, v. 189, p. 47-52.

Pickett, G. R., 1960, the use of acoustic logs in the evaluation of sandstone reservoirs: Geophysics, v. 25, n. 1, February.

Pickett, G. R., 1966, A review of current techniques for determination of water saturation from logs: J. Pet. Tech., November.

Pickett, G. R., 1973, Pattern recognition as a means of formation evaluation: Trans. SPWLA, 14th Ann. Symp., paper A.

BB

About the Authors:

Daniel A. Krygowski

Research Geologist with the Exploration and Production Research Laboratory of Cities Service Company in Tulsa. Holds a B.A. from the State University of New York College at Geneseo, and M.S. and Ph.D. in geophysics from the Colorado School of Mines. A member of SPWLA, SEG, and SPE of AIME.

G. R. (Dick) Pickett

Professor of Geophysics, Colorado School of Mines, specializing in well logging. Current research areas include petrophysics, well log interpretation and petroleum exploration. One year (1974-75) with Petroleum Engineering Department, University of Texas at Austin. Holds B.A. and M.S. degrees from the University of Oklahoma and a D.Sc. from Colorado School of Mines in Geophysical Engineering. Active in short course teaching and consulting. Industrial experience includes eleven years with Shell Development Company and Shell Oil Company concerned with Petrophysical problems in research and operations.

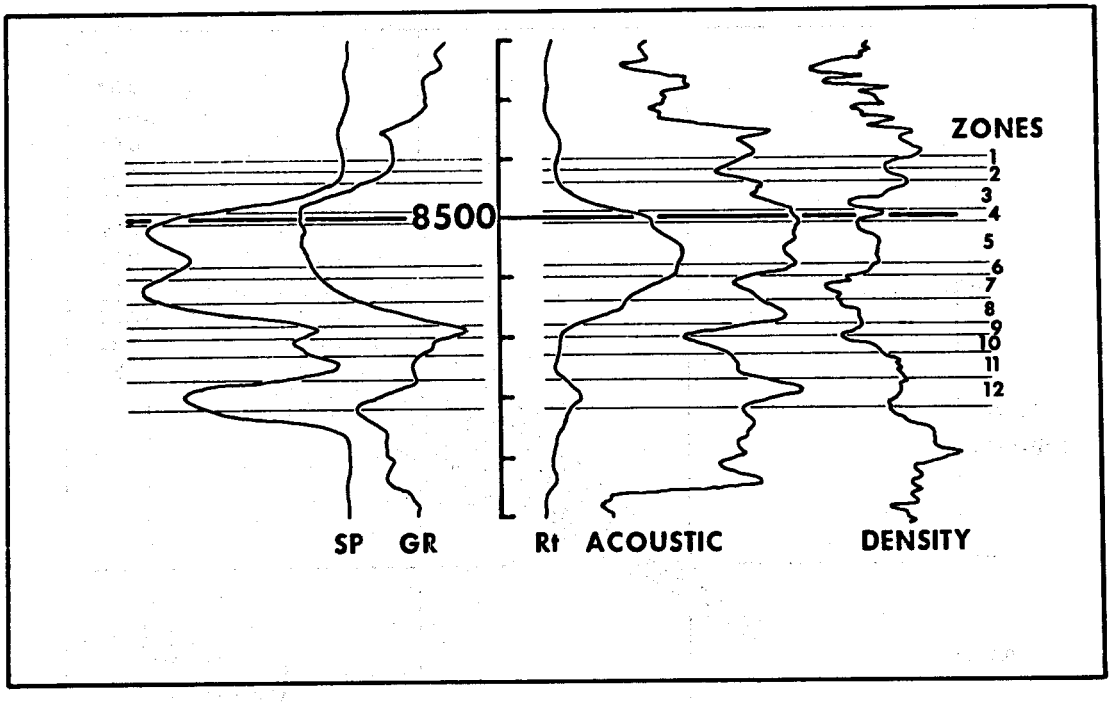

FIGURE 1: Zonation of a typical well, Mill-Gillette Field.

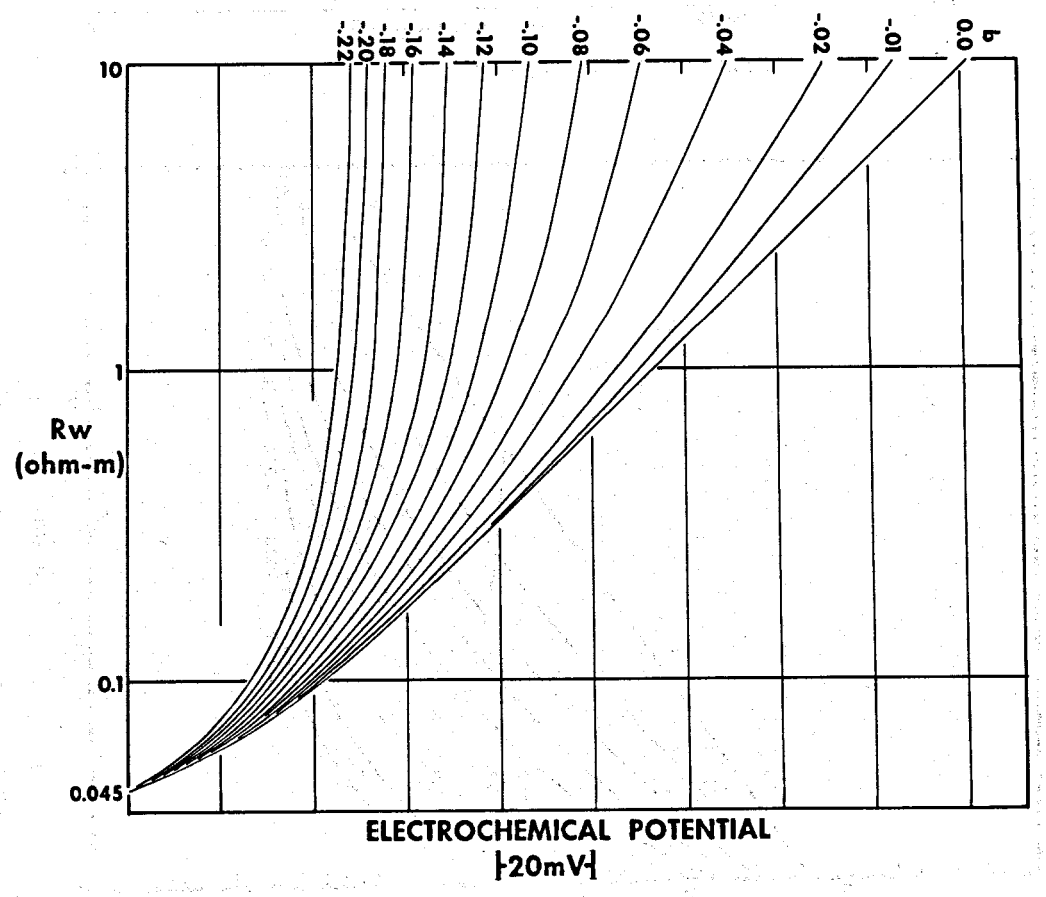

FIGURE 2: Relationship between Rw, electrochemical potential, shaliness (after Hill and Milburn, 1956).

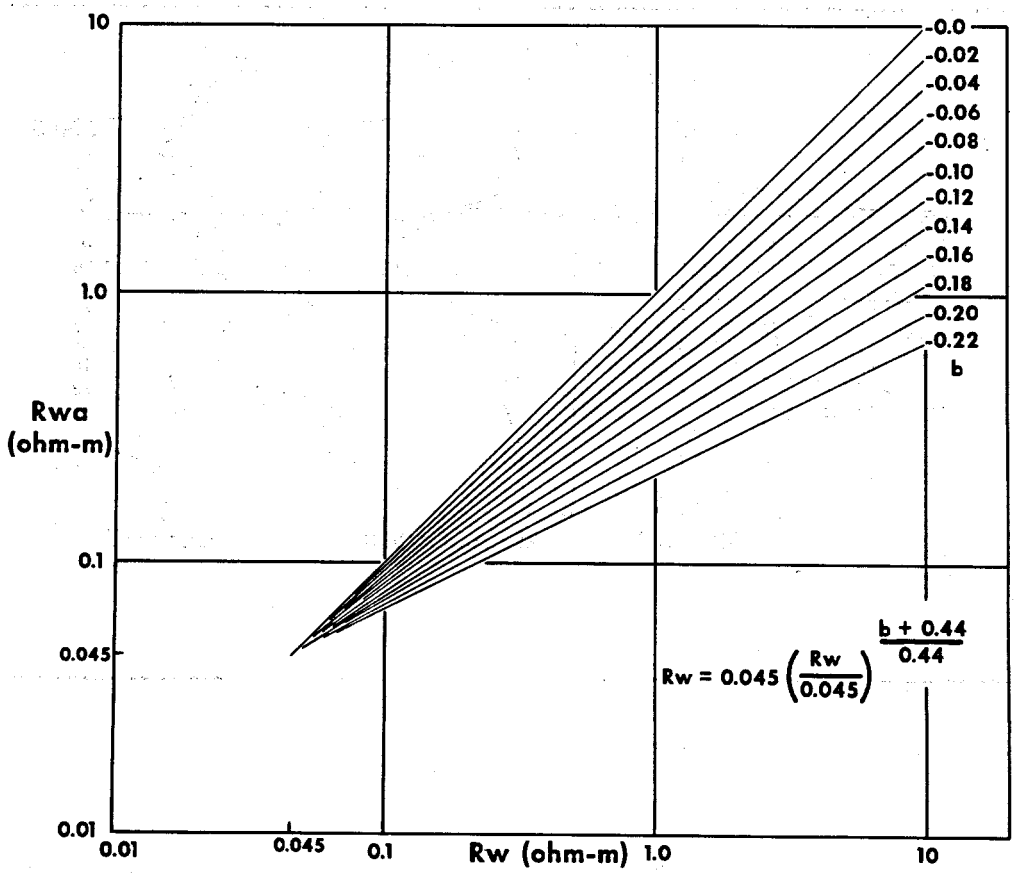

FIGURE 3: Relationship between Rw, Rwa, shaliness.

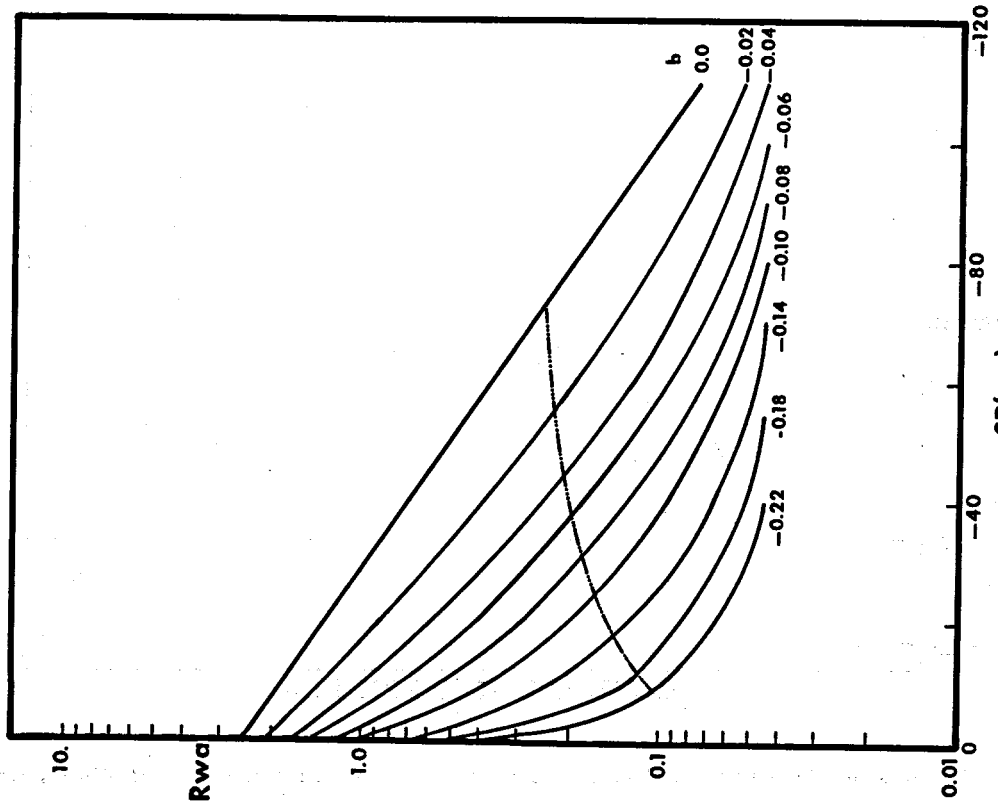

FIGURE 4: Shaliness-dependent lines of Rwa-SP crossplot.

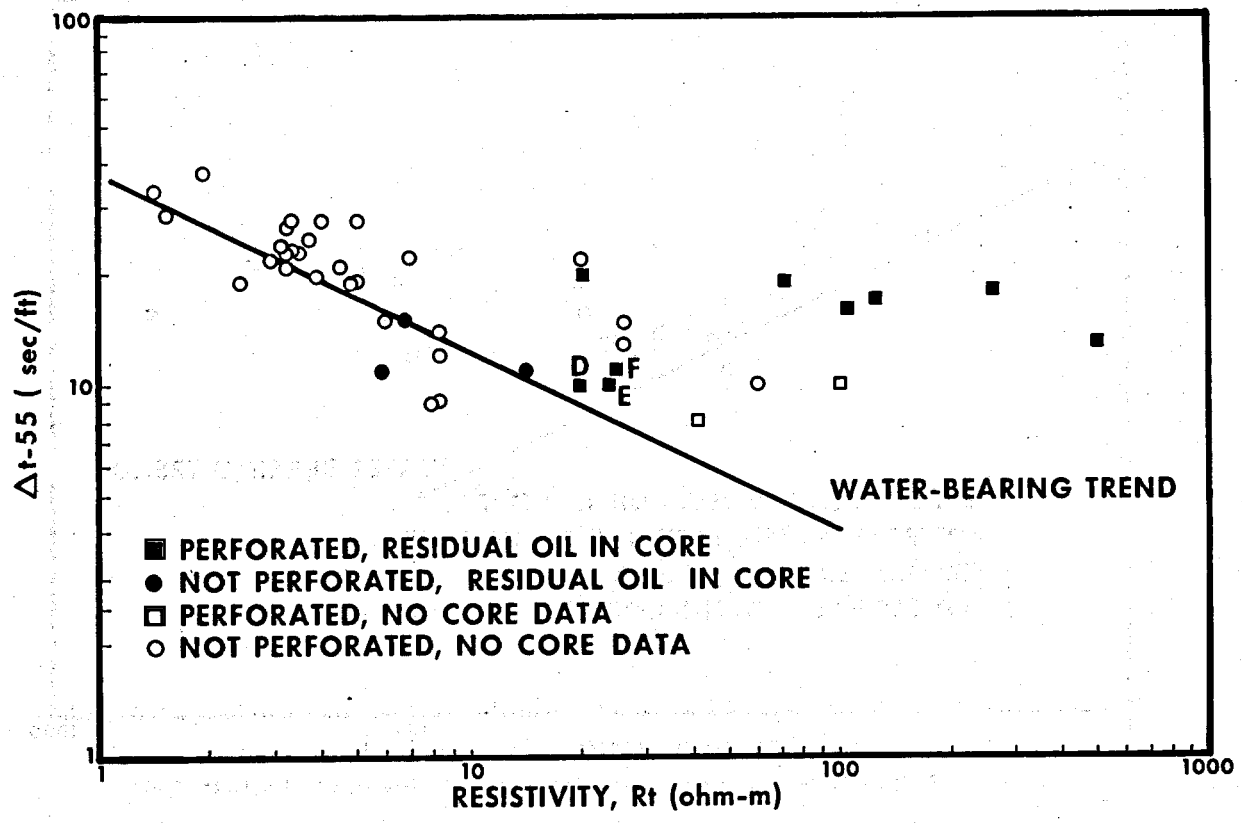

FIGURE 6: Resistivity-apparent porosity crossplot; data from Mill-Gillette Field.

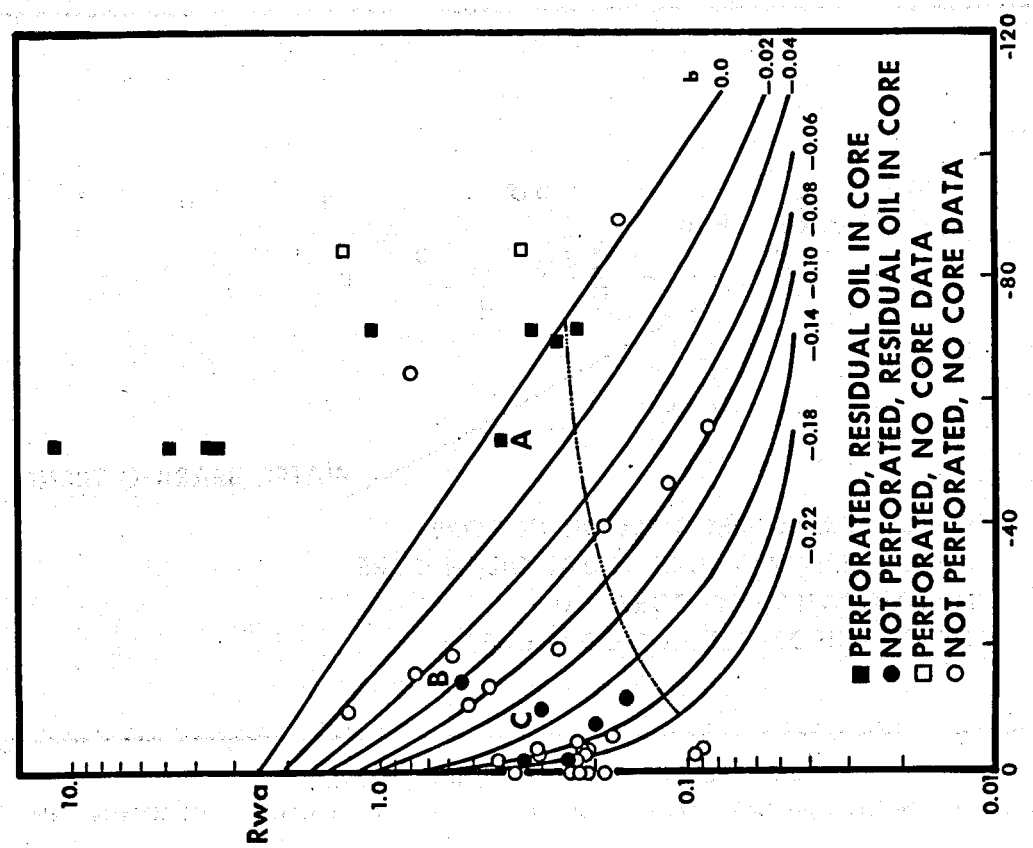

FIGURE 5: Rwa-SP crossplot; data from Mill-Gillette Field.

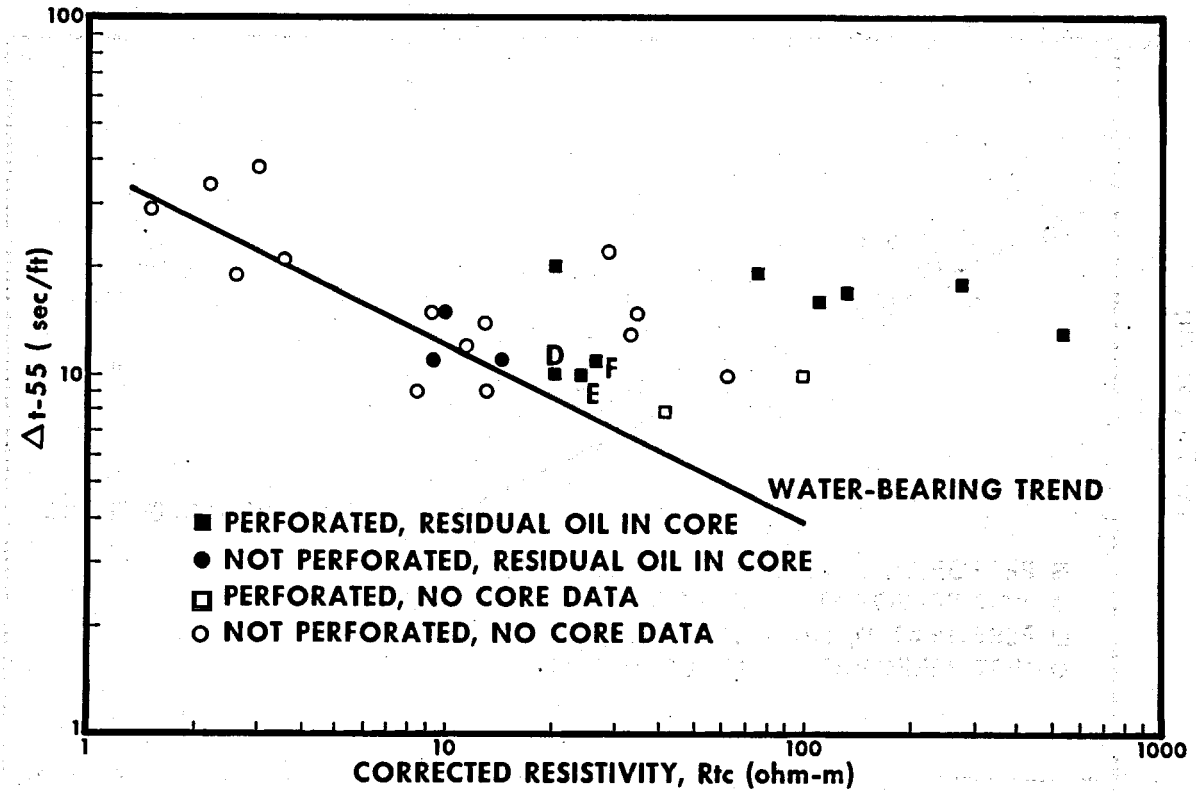

FIGURE 7: Resistivity-apparent porosity crossplot (with Rt_c); data from Mill-Gillette Field.

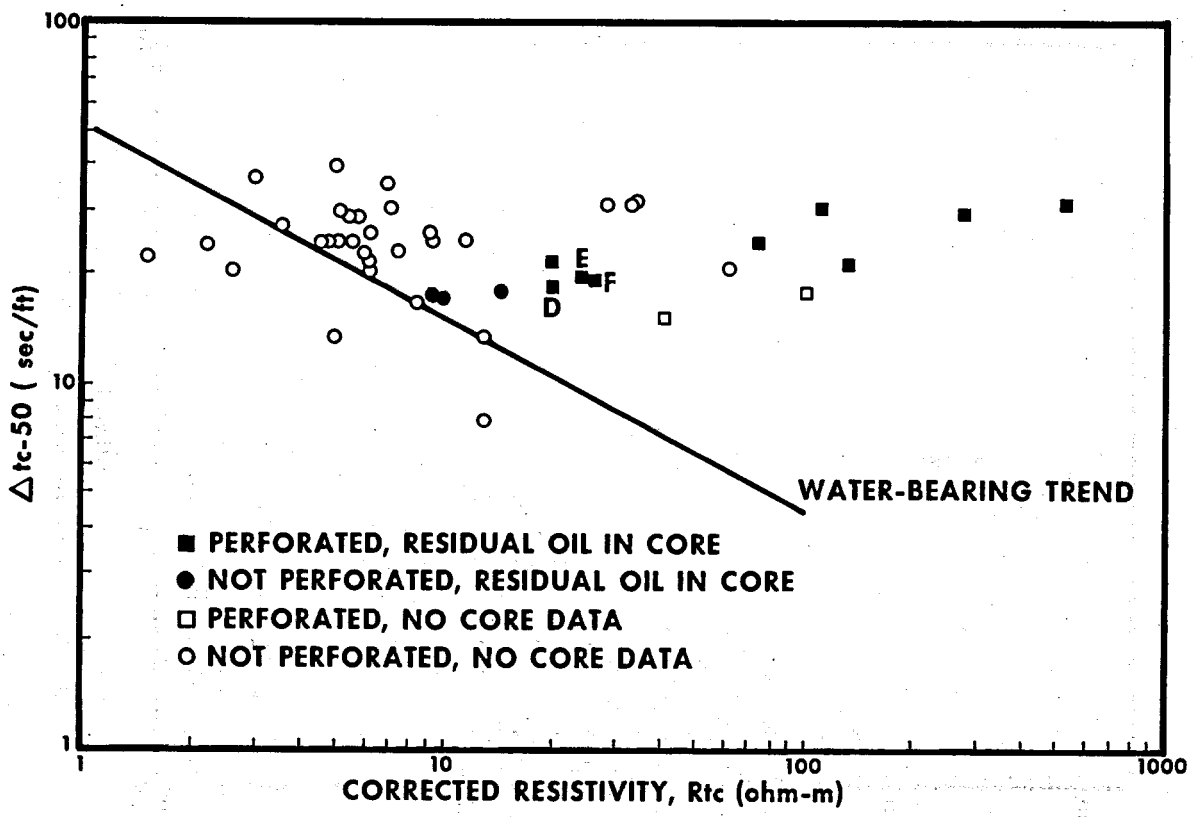

FIGURE 8: Resistivity-apparent porosity crossplot (with Rt_c and Δt_c); data from Mill-Gillette Field.

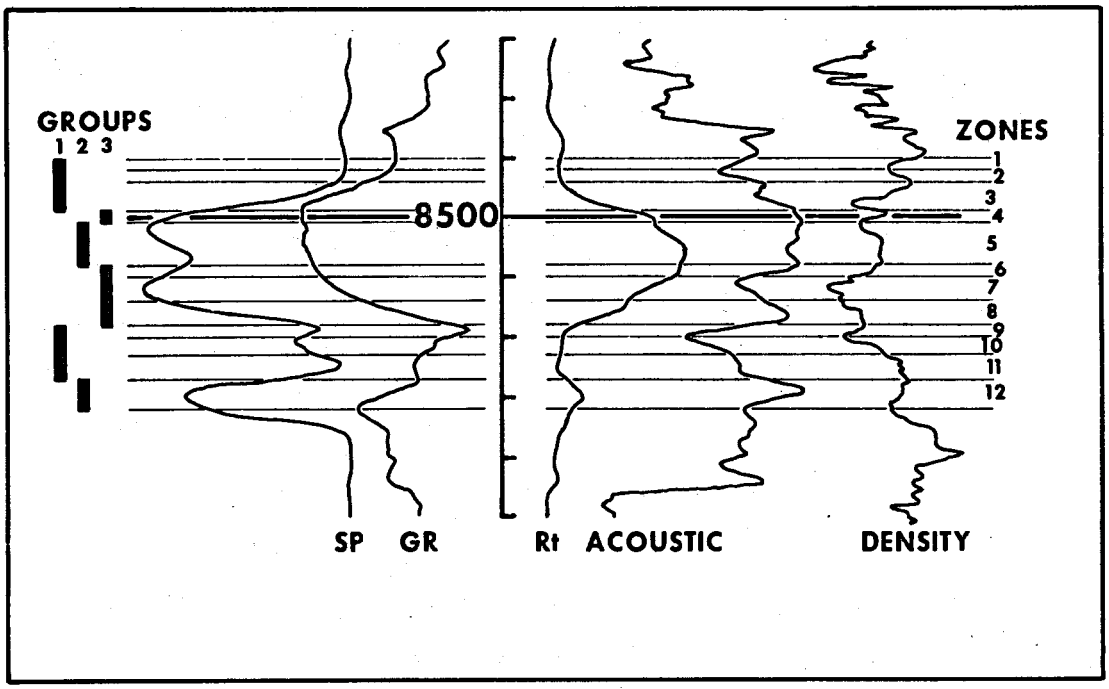

FIGURE 10: Zonation and sorting of a typical well, Mill-Gillette Field.

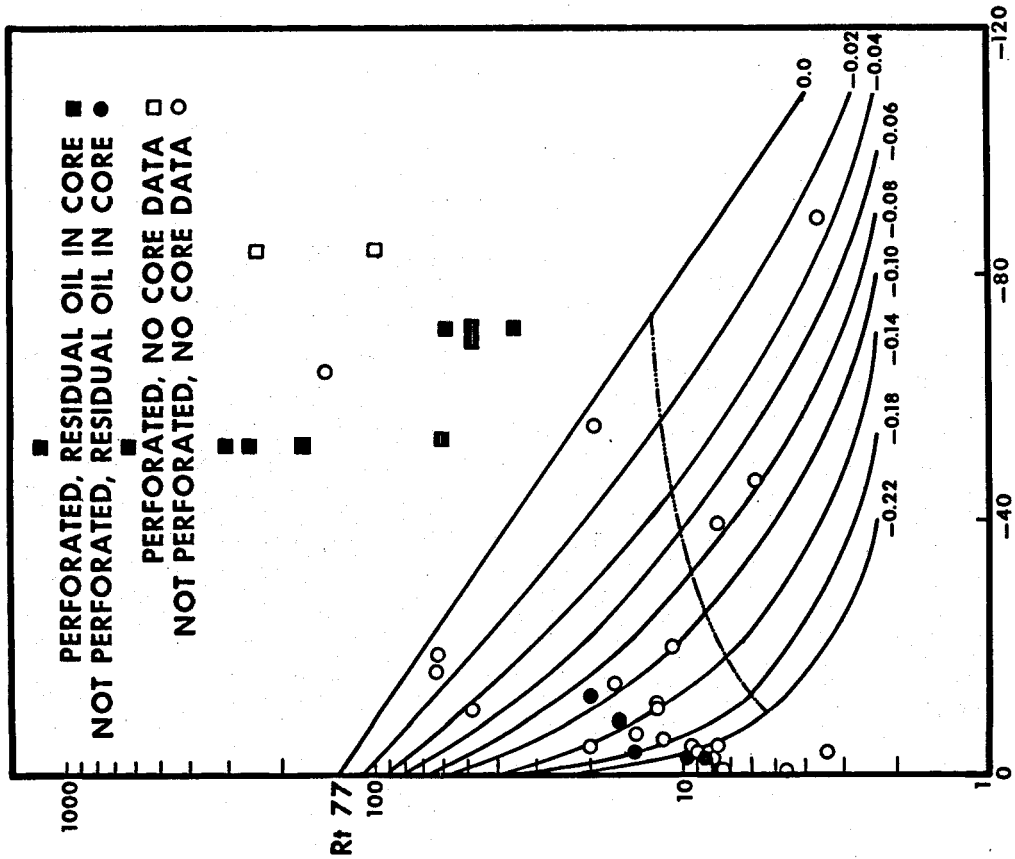

FIGURE 9: Resistivity-SP crossplot; data from Mill-Gillette Field.

BB

LOG INTERPRETATION OF SHALY FORMATIONS USING THE VELOCITY RATIO PLOT

by
Richard Leeth, WELEX, a Halliburton Company
Michael Holmes, Independent Geological Consultant

ABSTRACT

Conventional log analyses in the shaly sandstones of Western Colorado are quite difficult because of the very high shale content. Net pay and perforation intervals are often picked from neutron–density overlays after an empirical 8 to 10 porosity unit shift to obtain crossover, in addition to an arbitrary resistivity cut-off.

The Velocity Ratio Plot has been applied to three wells in the Mancos "B" formation in an attempt to more accurately delineate productive intervals. This method consists of determining the ratio of compressive to shear velocity, using the Micro–Seismogram® along with the Acoustic Velocity Log. Data presented shows that net pay determined from this method more accurately predicts initial flow rates. Long term deliverability calculations were made on the three wells, but such calculations are highly dependent on porosity and water saturation values used.

CC

INTRODUCTION

With the increasing need for oil and gas in the United States, greater concentration is necessary on the accurate definition of reservoir parameters. Part of this effort has resulted in progressively more detailed analysis of zones which would have been neglected in the past. In the Rocky Mountain area commercial production has been obtained from shaly formations that indicate a need for a more complex log analysis to correctly identify potentially productive zones. The Mancos formation of Western Colorado is such a zone where conventional shaly sand analysis is difficult because of the very high shale content. Comparison of Density and Neutron logs requires an empirical shift of 8 to 12 porosity units to obtain a Density/Neutron crossover. Frequently operators will choose completion intervals on the basis of such normalized crossover in combination with a qualitative resistivity cut-off. Fig. 1 is a typical Mancos "B" section where the Neutron log has been shifted 10 porosity units to the right because of the shale effect on the Neutron. The crossover area (Neutron porosity less than Density porosity) has been shaded on the figure.

In an effort to more accurately identify potentially productive zones in such formations, the Velocity Ratio Plot[1] has been applied to a number of wells in the area. Results to date have been encouraging.

THEORY

The Velocity Ratio Plot consists of determining the ratio of compressive to shear acoustic velocity. It has been shown that this ratio is constant for a given lithology,[2] regardless of porosity. These ratios are:

Limestone	1.9
Dolomite	1.8
Sandstone	1.6 to 1.7

Furthermore it has been shown that the compressibility of the fluid in the pore space affects the compressive velocity — a highly compressible fluid resulting in lower velocity. The shear velocity does not depend upon the compressibility in the pore spaces. Table I shows the ranges of compressibilities of formations as compared to fluid content. The compressibility of gas (and most oils with a "normal" amount of dissolved gas) as compared to water in the pore space give a low Velocity Ratio for hydrocarbon bearing zones.

TABLE I [4]

RANGE OF COMPRESSIBILITIES

Formation rock	3 to	10	x	$10^{-6}psi^{-1}$
Water	2 to	4	x	$10^{-6}psi^{-1}$
Undersaturated Oil	50 to	100	x	$10^{-6}psi^{-1}$
Gas at 1000 psi	900 —	1300	x	$10^{-6}psi^{-1}$
Gas at 5000 psi	50 —	200	x	$10^{-6}psi^{-1}$

The required data for the Velocity Ratio Plot can be obtained from the Acoustic Velocity Log in conjunction with a Micro–Seismogram®. From the Micro–Seismogram® presentation, the compressive and shear arrival times are evident. The following equation can then be used to calculate shear delta-t:

$$\Delta ts = \frac{ts - tc}{\text{Tool Spacing}} + \Delta tc$$

where:
- Δts = Shear Travel Time, micro-sec./ft.
- Δtc = Compressive Travel Time, micro-sec./ft.
- ts = Time to shear wave in micro-seconds.
- tc = Time to compressive wave in micro-seconds.

Since both waves (shear and compressive) have travelled through essentially the same amount of borehole fluid and formation, this equation gives a value corrected for borehole size. The only error would be in critical angle effects, which are negligible for normal borehole sizes.[3] Where an Acoustic Velocity Log is not run, the compressive delta-t can be generated from the Micro–Seismogram by the equation:

$$\Delta tc = tc - \frac{\frac{\Delta tf}{12}(d - d_t) - \text{Tool Delay}}{\text{Tool Spacing}}$$

where: d = borehole diameter, in.

d_t = tool diameter

Δtf = fluid travel time, micro-sec./ft.

A full wave presentation similar to the Micro–Seismogram® is recommended to generate this information as opposed to an X–Y presentation. The MSG provides the continuity of acoustic signal required, whereas an X–Y presentation gives much fewer samples per foot because of recording limitations. A typical 4' MSG response in the Mancos "B" formation is shown in Fig. 2. Positive half cycles are dark and negative half cycles are white. Compressive waves, of course, always occur first, with the shear arrivals later. As indicated, the shear wave is readily identified by a difference in slope at a time change, since there is a greater change in time for the shear arrival than for the compressive. Also the first shear arrival is frequently distorted because of phasing with the last of the compressive. Since the first compressive is indistinct and the first shear is frequently phased, measurements are taken from the second compressive and second shear. Calculations for obtaining the Velocity Ratio are shown at 3200' and 3500' on Fig. 3. The fluid wave directly down the borehole starts at approximately 800 micro-seconds, and is quite evident as essentially straight streaks from 900 on. CC

Generating a Velocity Ratio Plot in the manner described provides a lithology dependent curve that has been used to identify fluid content in formations of consistent lithology. A comparison with another lithology dependent curve could be necessary where lithology varies widely. In addition this log combination gives information regarding the presence of natural fracture systems which are essential in many areas of Western Colorado for commercial productivity.

APPLICATION

To illustrate the application of the Velocity Ratio Plot in the shaly sands of Western Colorado, three wells in the Mancos "B" formation have been studied at length —— conventional shaly sands analysis, Velocity Ratio Plots, and well test analysis. Fig. 3 shows the Velocity Ratio Plot on Well A along with the characteristically high Gamma curve. It has been found that by averaging the high values of the ratio, and multiplying that by .96, provides a satisfactory cut-off value.

Well B is shown in Fig. 4, again with the Gamma curve and the same calculation of the cut-off value.

Wells A and B were perforated in the intervals shown based on conventional shaly sand log analysis techniques. Well C, shown in Fig. 5, was perforated on the basis of low Velocity Ratios. Comparison of the Velocity Ratio Plots on the three wells clearly shows that Well C has a much higher percentage of the zone with low Velocity Ratios.

After completion, each well was tested by flowing for a few days, followed by a pressure build up test ranging from four to nine days duration. Table II summarizes the data from well tests, conventional log analysis, and Velocity Ratio Plots. Permeability—feet (k—h) values from conventional log calculations predict that Well A would have the highest production rate (deliverability) but it actually had the lowest. The log derived porosity is lower and water saturation is higher for Well C, which is also opposite to the test results. The net footage from the Velocity Ratio method is listed for each well and more accurately predicts initial production rates.

Test data were combined with conventional log analyses to determine long term deliverability predictions using a computer program. Results are shown in Fig. 6. In Well A, the Mancos "A" and "B" were commingled after separate testing. Therefore, the deliverability calculations cannot be directly compared with the other two wells. Actual well performance for the first few months of well history has agreed reasonably well with predictions. The wells are still in the process of cleaning up after fracture treatment and true well performance may not yet have been observed.

The accuracy of long range deliverability predictions depends greatly upon the values of porosity, water saturation, and net thickness which come from log analysis. Errors in these values will of course change the predicted deliverability. This is evident, as shown in Fig. 6, where the deliverability projections from Wells C and B cross. Had the net footage been taken from the Velocity Ratio method rather than from conventional log analysis, deliverability predictions could be different.

TABLE II

SUMMARY OF LOG AND WELL TEST DATA

Interval tested	Well A 2327' – 2566'	Well B 2262' – 2570'	Well C 1872' – 2088'
Avg. Flow Rate MCFPD	96	219	936
Res. Press., psig	367	370	390
kh, md ft., from well test	29	28.9	49.8
kh, md ft., from log analysis	114	95	61
SW in %, Avg. Log Analysis	37	28	42
ϕ in %, Avg. Log Analysis	8.8	8.7	5.8
Net Ft. with ratios below cut-off value	36	65	129

SUMMARY

Data presented plus other applications of the method to date in formations similar to the Mancos "B" have indicated that productive intervals can be reliably picked from the Velocity Ratio. The presence of a compressible fluid in the pore spaces results in a decreased Velocity Ratio, thus delineating production in formations in which conventional log analysis is most difficult.

Intervals to be perforated can be more accurately determined using this technique to ensure that all productive intervals are included in the completion.

Although net pay determinations are indicated to be improved, deliverability predictions in formations such as the Mancos "B" are quite difficult because of the problem of obtaining accurate porosity and water saturation in shaly formation.

REFERENCES

1. Kithas, Bill A., "Lithology, Gas Detection, and Rock Properties from Acoustic Logging Systems", Paper presented at the SPWLA 17th Annual Logging Symposium, June 9–12, 1976, Denver, Colorado.

2. Pickett, G. R., "Acoustic Character Logs and Their Applications in Formation Evaluation", Presented at the 37th Annual Fall Meeting of the Society of Petroleum Engineers of AIME in Los Angeles, California on October 7–10, 1962.

3. Gardner, G. H. F. and Harris, M. H., "Velocity and Attenuation of Elastic Waves in Sands", Presented at the 9th Annual Symposium of SPWLA in New Orleans, Louisiana, June 23–26, 1968.

4. Craft, B. C. and Hawkins, M. F., Applied Petroleum Reservoir Engineering, (Prentice–Hall, Inc., 1959), P. 149.

CC

ABOUT THE AUTHORS

Richard Leeth has been associated with WELEX, a Halliburton Company, since January, 1972. He has been stationed in Vernal, Utah; Gillette, Wyoming; Casper, Wyoming; and Denver, Colorado. At present he is log analyst for the Rocky Mountain Division in Denver.

Mr. Leeth received a BSc in Electrical Engineering from the University of Texas at Austin in 1971. He is a member of SPE of AIME and SPWLA.

Michael Holmes is an independent geologist consultant associated with H. K. van Poollen and Associates. His activities include consulting and teaching of short courses in Geology, Formation evaluation and Economics, both domestically and internationally.

Dr. Holmes has BSc and Ph. D. degrees in Geology from the University of London, and an MSc degree in Petroleum Engineering from the Colorado School of Mines. His professional experience includes geological, geophysical, and engineering positions with British Petroleum, Shell, Marathon, and Berry Wiggins.

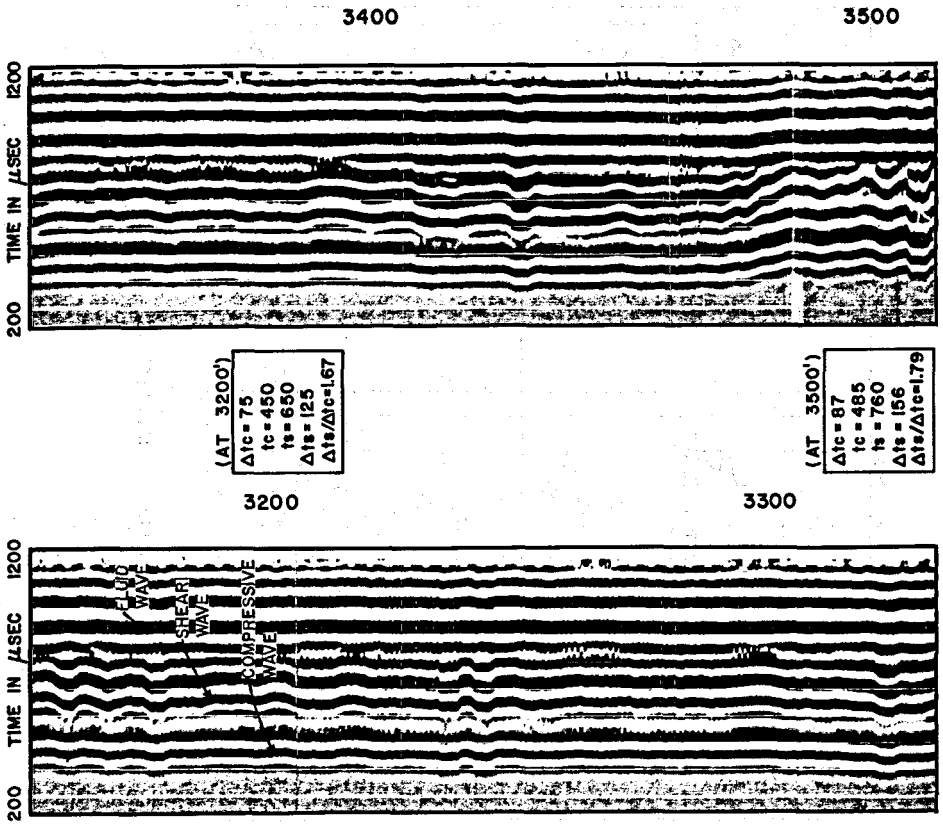

FIG. 2
MICRO-SEISMOGRAM IN MANCOS "B"

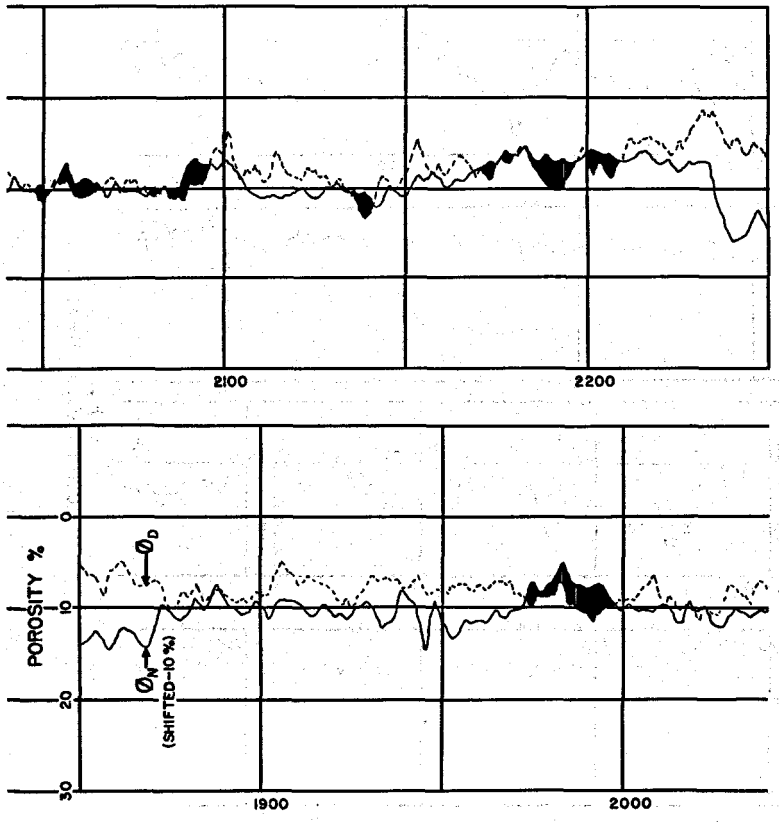

FIG. 1
NEUTRON-DENSITY OVERLAY

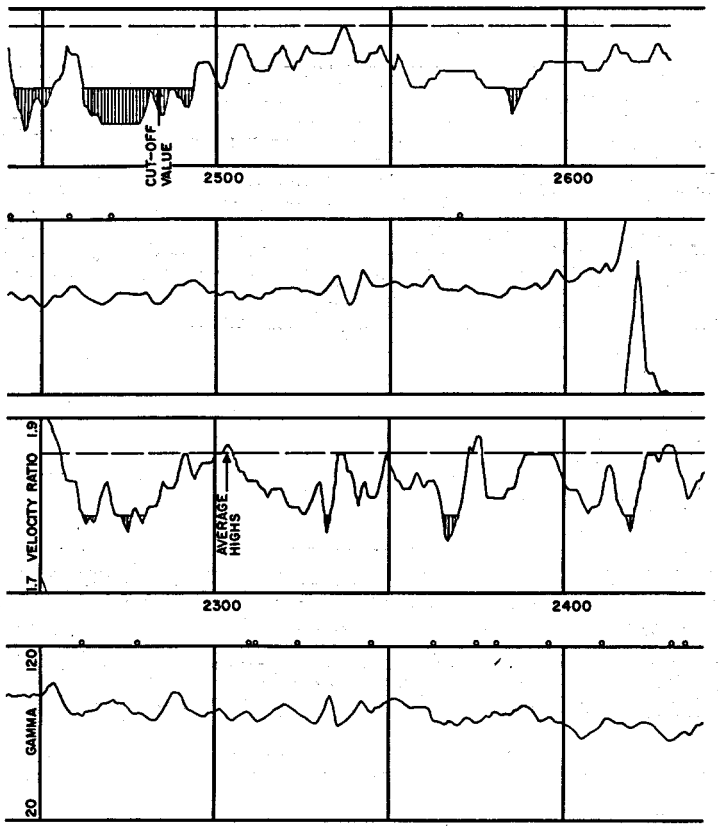

FIG. 4
VELOCITY RATIO PLOT-WELL B

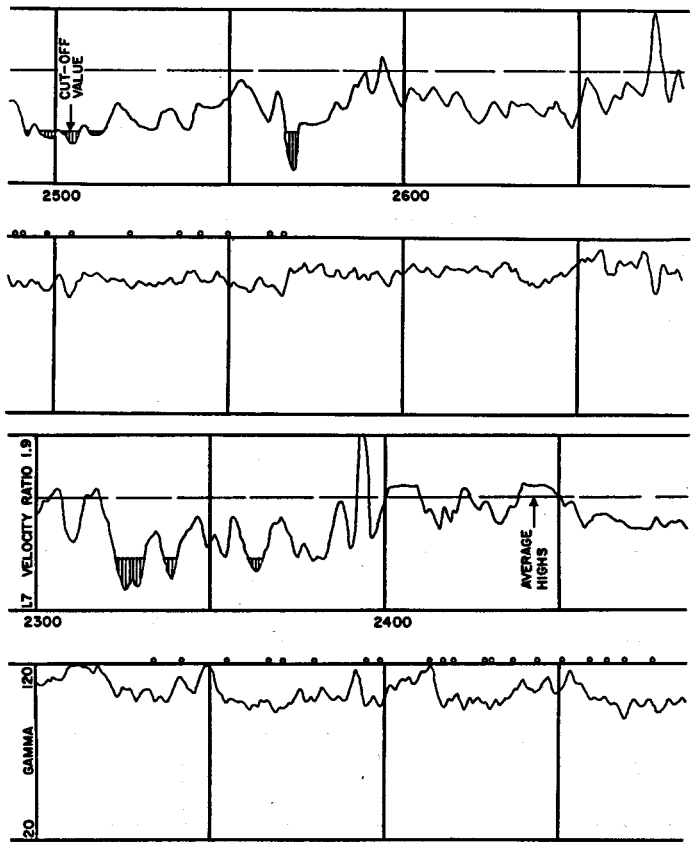

FIG. 3
VELOCITY RATIO PLOT-WELL A

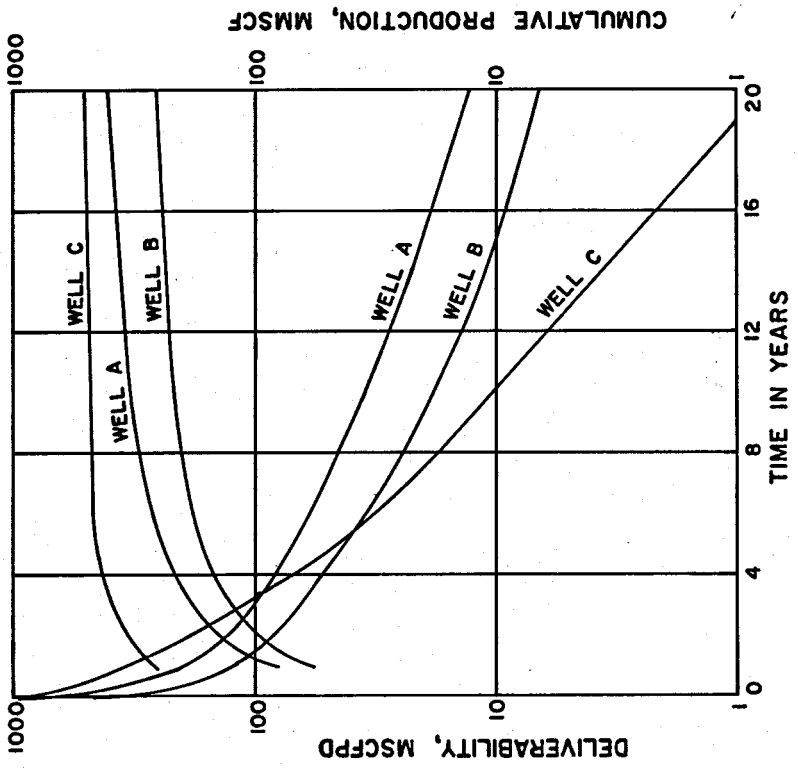

FIG. 6
WELL DELIVERABILITY PREDICTIONS

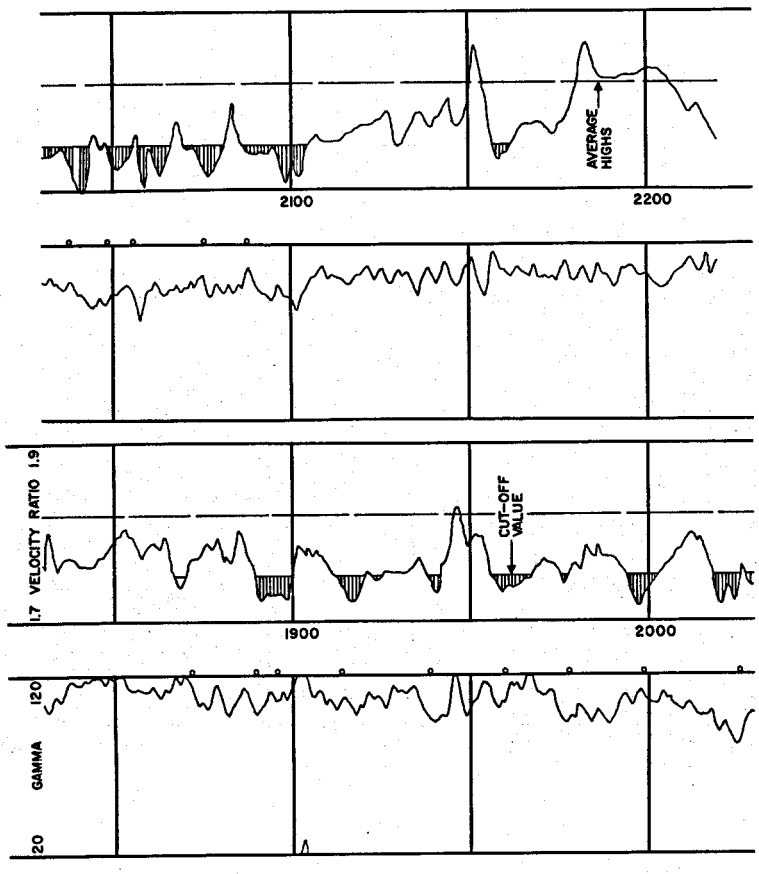

FIG. 5
VELOCITY RATIO PLOT-WELL C

PERMEABILITY DETERMINATION IN LIQUID DOMINATED GEOTHERMAL RESERVOIRS USING THE DUAL INDUCTION LATEROLOG

I. Ershaghi, E. L. Dougherty, D. Herzberg
and H. Ucok

Department of Petroleum Engineering
University of Southern California

ABSTRACT

A method has been developed to estimate the permeability profile in a geothermal well from a Dual Induction-Laterolog, a porosity log, and drilling data. The procedure is based on modeling the invasion of the drilling mud filtrate into the formation and using a history matching technique to arrive at the permeability profile. Input data to the computer model includes basic drilling mud properties, drilling hydraulics, and dimensions of the tubular goods. A permeability profile is assumed for the well and the computer program is run. The objective is to compare the invasion radius computed from the program to that derived from the logging data. The process is then repeated until a satisfactory match is obtained.

INTRODUCTION

Estimation of physical properties of reservoir rock in geothermal systems poses new challenges to existing theories and methods applicable to oil and gas reservoirs. Presence of high temperature limits the utility of existing tools and, even if the tools were available, interpretation of data opens up new frontiers in formation evaluation. Currently efforts are underway to improve the design of tools and make them resistant to the hostile environment in geothermal wellbores. Many researchers have started work on improved or new interpretation methods for estimation of rock and fluid properties from well log data. Baker et al.[1] and Sanyal and Meidav[2] summarized certain difficulties associated with formation evaluation in geothermal reservoirs.

This paper presents a new approach to estimating permeability of liquid-dominated geothermal reservoirs. The proposed technique uses a combination of drilling data together with a dual-induction laterolog. A numerical simulator of wellbore hydraulics during drilling is used to predict invasion profiles for assumed permeability profiles. Comparison of predicted invasion effects to those indicated by the dual-induction laterolog indicates whether or not the assumed permeability profile is reasonable. The method is not believed applicable to oil and gas reservoirs.

STATEMENT OF THE PROBLEM

Permeability of reservoir rock is an important parameter in reservoir assessment. Reservoir engineers need the permeability to calculate deliverabilities, to estimate interference between wells, and to complete an overall reservoir description. By and large, core analysis and measurement

of pressure transients are the most common techniques used in oil field practice to estimate reservoir rock permeability. Attempts to use well logs to estimate formation permeability have resulted in empirical correlations which may not be universally applicable. A review of the literature shows that the logging methods proposed in the past for estimating rock permeability fall into one of the following categories:

1 - methods based on Kozeny equations (electric log)

2 - methods based on acoustic logs

3 - methods based on free fluid index (NML)

4 - methods based on TDT

It is appropriate that a brief review of existing techniques be given here to acquaint the reader with the limitations that these methods may have in geothermal reservoir evaluation.

1 - Permeability from Kozeny equation

A general correlation between rock permeability, porosity and surface area may be written as shown below:

$$K = A \frac{\phi^B}{S_{wi}^C}$$

where

K = single phase permeability

ϕ = porosity

S_{wi} = connate water saturation

A, B, and C = constants

Table 1 shows some of the correlations published by different investigators[3-6]. In the above method it is assumed that the rock contains irreducible water saturation. This concept is valid only in oil and gas reservoirs where hydrocarbon is the dominant phase and water saturation is at its connate level.

Table 1

Permeability Estimates from ϕ and S_w

Correlation	Author(s)	Reference
$K = \frac{C\phi^3}{S_{wi}^2}$	Wyllie and Rose[3]	Jour. Pet. Tech., April, 1950
$K = \frac{A\phi^B}{S_{wi}^C}$	Timur[4]	The Log Analyst, 1968
$K = \frac{A}{S_{wi}^B P_c^C}$	Brown and Husseini[5]	SPWLA Trans. 1977

2 - Methods based on acoustic logs

The use of acoustic logs to estimate permeability has been suggested in the literature. Lebreton et al.[7] proposed the use of an equation of the type:

$$I_e = \alpha' \log_{10} \frac{k}{\mu} + \beta'$$

where α' and β' are approximately constant for a given borehole and $I_e = h_3/h_1$ obtained from the recorded sonic wave train. (h_1 and h_3 are peak amplitudes of two of the first arches.)

Dowling and Boyd[8] also proposed use of the sonic log to estimate formation permeability. In their approach the permeability is estimated from incremental changes in the transit time due to fluid movement caused by the sonic vibrations.

In a recent paper, Staal and Robinson[9] estimated permeability from measurement of the full acoustic wave train; their work is based on the theoretical work of Biot[10] and Rosenbaum[11]. In this technique formation permeability is related to the attenuation of the acoustic wave that corresponds in velocity to the Stonely Wave. Work in this area is in the preliminary stage.

3 - The use of nuclear magnetic log

As discussed by Seever[12], the nuclear magnetic log potentially can provide information about rock permeability.

Timur[13] demonstrated the use of the NML logs for estimation of the specific permeability of a formation from empirical correlations developed

for a given field. The major drawback of this technique is the massive amount of laboratory data required for each case to estimate the empirical coefficients.

4 - Methods based on TDT

Several authors have proposed using the Thermal Decay Time log to make a qualitative or quantitative estimate of permeability. Engelke and Hilchie[14] showed that if the mud filtrate has a higher salinity than the formation water the Neutron Lifetime log together with porosity data may be used to derive a qualitative estimate of the invasion profile and determine the permeable zones. Dowling et al.[15] proposed to alter the natural charged ion spatial distribution in the formation fluids and to measure the resulting thermal neutron decay time characteristics of the formation. Comparison to a reference rock with no alteration provides an estimate of permeability.

The problems associated with the use of the TDT in geothermal reservoirs have not been reported or discussed.

DESCRIPTION OF THE PROPOSED TECHNIQUE

During drilling and prior to running well logs, the drilling fluid percolates into the permeable sections of the wellbore (if wellbore pressure exceeds formation pressure). Mud filtrate displaces the original formation fluid near the wellbore; the mud is filtered out on the rock face and forms a mud cake. Depending upon the composition of the drilling fluid, the sealing properties of the filter cake vary. For oil and gas reservoirs it is imperative that the invasion of mud filtrate be minimized and thus a mud composition with low filter loss is desired. Bentonite, a major ingredient of oil well drilling fluid, has excellent sealing properties. Addition of certain chemicals or materials can further improve the sealing properties of the mud cake and thus minimize invasion of the formation by mud filtrate. Deep invasion in hydrocarbon saturated rocks is undesirable, because the displacement of the mobile hydrocarbon from the vicinity of the wellbore may mask the true potential of a formation. Furthermore, mud filtrate invasion often damages the native producing formation, and may greatly lower the productivity index of the well.

For a liquid dominated system the displacement of formation brine by the mud filtrate will not cause any problem with respect to fluid saturation determination. The estimation of formation water resistivity from electrical logs, however, will be sensitive to the invasion radius of mud filtrate and the problem of formation damage is still at hand.

In addition to the mud composition, the radius of invasion is dependent on rock porosity and permeability and drilling hydraulics. Ignoring the sealing properties of mud and assuming the same pressure gradient for a given rock permeability, the mud filtrate will travel farther into a formation if the porosity is low, and for the same porosity a high permeability rock will allow deeper invasion of filtrate. Since the sealing properties of the mud and the pressure gradient also play important

roles in the filtration process, the following equation may be used to depict the relationship for estimation of invasion radius:

$$r_i = f(mc, \Delta p, t, \phi, K)$$

where r_i = invasion radius

mc = mud composition

Δp = pressure differential between wellbore and formation

t = exposure time

ϕ = formation porosity

K = formation permeability

It seems theoretically possible that if one could estimate invasion radius (dual-induction laterolog) and input t, ϕ, Δp, and a measure of mc, the formation permeability may be obtained from the above equation.

ESTIMATION OF INVASION RADIUS

The use of three resistivity devices (small slam) with different geometric factor has been proposed as a means of estimating invasion radius. This is based on solving the following three simultaneous equations and obtaining the geometrical factors in addition to the correct estimation of R_t.

DD

$$\frac{1}{R_{ILD}} = \frac{G_m}{R_m} + \frac{G_i}{R_i} + \frac{G_t}{R_t} + \frac{G_s}{R_s} \quad \text{(deep induction)}$$

$$\frac{1}{R_{ILM}} = \frac{G_m}{R_m} + \frac{G_i}{R_i} + \frac{G_t}{R_t} + \frac{G_s}{R_s} \quad \text{(medium induction)}$$

$$R_{LL} = G_m R_m + G_{mc} R_{mc} + G_i R_i + G_t R_t \quad \text{(shallow focused)}$$

The above equations may be reduced to three equations containing only R_t, R_i and G_i if one assumes that the borehole and adjacent bed effects are negligible. From the geometric factors, the invasion diameter may be determined depending on the tool specifications. These multiple resistivity devices are available under different names from different service companies. (Dual-Induction Laterolog or Dual-Induction Focused Log). Usually the entire solution process is simplified by the use of charts and nomographs into which the ratios of $\frac{R_{LL}}{R_{ILd}}$ and $\frac{R_{LLM}}{R_{ILd}}$ are entered and the invasion diameter is read directly.

The Dual-Induction Laterologs give an estimate of where the mud filtrate front may be in the formations. An implicit assumption in the use of our method is the existence of sharp frontal movement and negligible dispersion and gravity segregation effects. These logs, however, do not tell us how the mud filtrate reached there.

Various parameters which may play a role in the extent of mud filtrate invasion into a given formation have been the subject of studies by many authors. The first attempt to integrate all such parameters into a simple equation mainly for computer log processing was reported by Breitenbach.[16] He indicated that for a gel-base mud the following equation may be used to estimate the invasion diameter:

$$DI = \frac{D \cdot C'}{\phi} [(0.04643 + 0.00002381\ \Delta p) \cdot API \cdot t^{1/2} + 0.00635\ (BHT - ST)\ t^{1/2} + 0.01495\ V_{mud}\ t^{1/2}]\ [1 + 0.0063\ (BHT - ST)] + D^{2\ 1/2}$$

where

API = API static filter loss, cc/30 min

BHT = temperature of the formation, °F

ST = surface temperature, °F

C' = dynamic correction factor for gel-base mud

D = borehole diameter, inches

ϕ = porosity, fraction

DI = invasion diameter, inches

Δp = pressure differential, psi

V_{mud} = annular mud velocity, ft/sec

t = time, hrs

As noted by Breitenbach this equation has limited application since it does not include the formation permeability and the initial surge loss into the formation. Furthermore, no explicit and universal technique for estimation of C' (correction for dynamic effect) is given in the above paper. In a subsequent paper Miesch and Albright[17] indicated that the C' may be assumed to be 1 for gel base mud. They also presented correlation equations for estimation of invasion diameter from driller's log parameters. The general form of the correlation may be shown as follows:

$$Log(DI) = A_0 + A_1X_1 + ... + A_{15}X_{15}$$

The coefficients were given for the deep or medium induction logs and X_1 through X_{15} represent formation and rock properties. Properties used included depth, porosity, R_w, R_m, temperature, R_{mf}, BHT, mud weight, water loss (API), hole diameter and the resistivity from an induction log. The correlations were based on 676 zones from 26 wells and the average absolute deviation for estimation of D_i was reported at 41.8 percent.

OTHER INPUT PARAMETERS

The complete history of drilling process for any segment of the borehole may be simulated by a computer program. The program requires estimate of drilling time, tripping time, and the onset of static conditions in the wellbore. In addition mud density, circulation velocity, dimensions of drill pipe, drill collar and the wellbore itself are needed. The program estimates the flow regime in different segments of the circulation path and determines the effective pressure against the formation.

The cumulative volume of filtrate invaded into permeable zones as a function of time is then computed. To do this a measure of mud cake permeability-thickness ratio is needed which may be obtained from laboratory tests on core samples. Volume of filtrate invaded is then translated into the radius of invasion using a knowledge of formation porosity.

DD

DESCRIPTION OF THE SIMULATOR

The numerical simulator used in this study consists of two computer programs. The first one (MUDPRS) is designed to model the wellbore hydraulics during drilling and estimate the complete history of mud column pressure against the drilled portion of the formation. The pressure data generated from this program is then used in the second program (MUDFIL) together with the properties of the formation and the mud cake to derive the estimated invasion profile.

Estimation of Pressure Profile

The pressure in the mud column and against any point of the formation is a function of depth, mud density, and the circulation rate. When the mud column is in static condition, a circulation rate of zero is used in the computations. For the dynamic conditions (during drilling) the circulation pressure is obtained from accounting of the pressure losses in the system.

The input data for this computer program consists of tubular dimensions and lengths, mud properties, circulation rate, drilling rate and the wellbore radius.

Estimation of the Invasion Radius

The pressure profile vs. time is obtained from the first program and by a superposition method the invasion radius is computed for different

points along the wellbore using the second computer program, (MUDFIL). The basic data include a k/h vs time table for the mud cake, mud filtrate viscosity and compressibility and the formation pressure gradient. In addition the porosity profile (from porosity logs) and an assumed permeability profile are needed.

For the assumed permeability profile the invasion radius is determined and compared with the invasion profile obtained from the dual-induction laterolog. If the two do not agree, the assumed permeability profile is adjusted and the computations repeated until a satisfactory match is obtained.

The computation of the filtrate invaded into any segment of the formation during a given time step is done by an iterative procedure. The iteration method is used because the pressure drop across the filter cake is not known.

The main equation which describes the fluid invasion into the formation may be expressed as:

$$\frac{\delta^2 P}{\delta r^2} + \frac{1}{r}\frac{\delta P}{\delta r} = \frac{1}{\eta}\frac{\delta P}{\delta t}$$

where P, r, and t are pressure, radius, and time, respectively and η is the diffusivity constant. $(\eta = \frac{k}{\mu\phi C})$. This equation may be solved for certain boundary conditions. In this study we used the Van Everdingen and Hurst[18] solution which is given in tabular form expressing the dimensionless time t_D vs dimensionless water influx Q(t). The cumulative invasion at any time is then determined from:

$$W_e = B\Sigma\Delta P \times Q(t)$$

where

$$B = 1.119 \times \phi \times C \times r_w^2 \times h$$

Δp = differential pressure at interface between filter cake and formation

The symbol Σ is used here to show the superposition effect.

The computation scheme in the (MUDFIL) program follows the iterative procedure outlined below:

1 - a value for filtrate volume, Q, is assumed for the particular time step,

2 - the expected pressure drop across the mud cake for the given Q is determined using the mud cake k/h values thereby giving the effective pressure against the formation,

3 - for the given time step the dimensionless time and the corresponding Q(t) from the Van Everdingen and Hurst solution is determined,

4 - from the Q(t) the amount of influx is determined and compared with the assumed value, Q,

5 - the process is repeated until the two influx values match within a given tolerance,

6 - by using the principle of superposition the cumulative influx is determined and translated in terms of invasion radius.

The basic wellbore parameters used in the simulator runs shown in this paper are given in Table 2. For simplicity it was assumed that the dynamic filtration prevails without any pause until the entire section is drilled through. The total static period before the commencement of the logging was ten hours.

NO MUD CAKE

In the absence of any mud cake (such as when drilling with water) the invasion radius is a function of formation permeability, porosity, and the time of exposure. Fig. 1 shows the invasion profile for a 500 ft. layer with uniform permeability (0.1 md) and porosity (0.2). The radius of invasion is largest at the top of the section, which has been exposed to a longer period of invasion. For higher formation permeabilities drilling fluid will invade farther into the formation. This fact is demonstrated in Fig. 2 for permeability varying from 0.1 md to 1000 md. The porosity of the formation also affects the radius of invasion significantly. Fig. 3 shows that for a section with uniform permeability of 10 md, changing the porosity from 0.20 to 0.1 increases the invasion radius.

The cases discussed above illustrate that in the absence of a mud cake, the invasion radius may vary from a fraction of a foot to 50 feet or higher depending on formation properties and drilling hydraulics. As long as the invasion radius does not extend beyond the depth of investigation of the deep induction tool, the method proposed in this paper may be used to estimate the formation permeability profile. The results shown above imply that for drilling with water the rock permeability must be low ($<10_{md}$) to limit the invasion radius.

WITH MUD CAKE

As is customary, the drilling fluid contains bentonite or other sealing agents to form a cake with low permeability which impedes invasion of the mud filtrate into permeable layers. Particle invasion before the mud cake is fully established will also cause a reduction in permeability in the first few inches of the formation. In this paper we assume that the effect of such permeability alteration is included in the overall permeability barrier associated with the mud cake.

The effect of the mud cake needs to be carefully evaluated in light of formation permeability and the mud composition. The two major questions are the way the mud composition, on one hand, and formation permeability on the other influence the buildup and the properties of the mud filter cake.

Effect of Mud Composition

The concentration of any clay material or other sealing agents in the mud directly affects the filter cake permeability. Since, for the purpose of this paper and the application method discussed here, we are more concerned with the permeability thickness ratio of the filter cake than with the permeability or thickness separately, we shall examine the sealing property of the mud cake in terms of k/h ratio. (Note that h is mud cake thickness.)

The rate of filtration through an already established mud cake is directly proportional to k/h. Therefore, a decreasing trend in k/h indicates reduction of filtrate throughput.

For comparative studies a static API filter press is normally used to study mud cake k/h variation versus time for different mud compositions. The method of analysis consists of plotting cumulative filtrate volume versus time. Using the slope of the plot in the Darcy equation will result in an estimation of k/h versus time.

Fig. 4 shows an API static test results for three muds with bentonite concentration of 10, 50 and 100 g/liter. As it is expected, increasing bentonite content reduces the k/h ratio significantly.

Unfortunately API static test data may not represent actual wellbore conditions. As discussed by Outmans[19], Ferguson and Klotz[20], Krueger[21] and others there are several stages of filtration in the borehole. A typical filtration schedule may be as illustrated in Fig. 5. From this plot it follows that the k/h ratio may go up or down depending on the stage of filtration. As discussed by Horner et al.[22], the only way to determine the dynamic filtration behavior of a given drilling mud is to run a dynamic test. No other test, such as the API static test is truly representative of actual downhole behavior. Studies of dynamic filtration reported by Ferguson and Klotz[20], Krueger[21], and others[23,24] show that the three main factors controlling the volume of filter loss are mud composition, pressure differential and rock permeability. Mud composition and (mainly) the matrix grain sizes determine the degree of particle invasion or pore plugging[25]. Pressure differential acts as the driving force and affects mud cake compressibility. The role of formation permeability is, however, somewhat obscure. For high permeability rocks the initial spurt loss is substantial, and there is a rapid buildup of the mud cake. Large pores of such rock also lead to particle invasion and possible internal rock permeability reduction. Subsequently the mud column acts against a low permeability filter cake and the water loss becomes negligible. For low permeability rock the initial spurt loss is low, and the transition between the formation and the mud column is a thickened mud with properties between filter cake and mud slurry. The permeability of this thickened mud is intuitively

larger than the permeability of the mud cake. Fig. 3 of the Horner et al.[22] paper shows the significance of rock permeability on cumulative dynamic filtration.

ESTIMATION OF MUD CAKE k/h RATIO

To obtain typical values for k/h ratio we tested the utility of running API static filter tests by comparing results to dynamic filtration data reported in the literature. One significant observation is that the resistance of the filtering medium affects filtration behavior. Static filtration against permeable rocks results in different filtration properties than those predicted by the API test for the same mud.

Currently we are building our own dynamic test facility for further testing of drilling muds. In the absence of dynamic filtration data, we used the data presented by Ferguson and Klotz, Bezemer and Havenar[26] and Krueger[21].

As discussed by Ferguson and Klotz[20] the major fraction of the total filtrate that invades the formation is under dynamic conditions; static filtration contributes only from 10 to 30 percent. From the data presented in Fig. 4 of Ferguson and Klotz we estimated that the k/h ratio during dynamic filtration with bentonite mud drops from an average of 0.00195 md/cm to 0.000653 md/cm. Krueger's data also show an average dynamic fluid loss rate of 0.5 ml/hr/in^2. Table 3 shows a typical k/h ratio one might expect for a high bentonite content mud and for an average rock permeability. Obviously, the concentration and particle size of the clay or other sealing materials or water loss additives will influence the k/h ratio.

The ideal test would be to conduct a dynamic-static filtration test using rock permeabilities from 1 md to 1000 md (not necessarily rock samples from the formation) and input three or more tables to the simulator and interpolate for permeabilities in between.

In the absence of reliable k/h ratio, as will be shown below, the proposed technique will result in a qualitative profile of formation permeability.

Results of Similator Runs with Mud Cake

To illustrate the simulation we assumed a permeable section 500 ft. thick with permeabilities varying from 1 md to 1000 md (as illustrated in Fig. 6) and porosities ranging from 0.05 to 0.35 (see Table 4). We ran the simulator assuming the same k/h ratio applied to all rock permeabilities. To study the effect of changing flow properties of the mud cake, we made a series of runs in which the k/h values shown in Table 3 were multiplied by a (constant) factor varying from 0.01 to 100. The invasion profiles for several factors are shown in Fig. 6. With higher permeability mud the invasion profile is very similar to the formation permeability profile. On the other hand, for lower values of mud cake permeability the invasion profile tends to smooth out and no longer resembles the formation permeability profile. In fact, when the k/h ratio is reduced by a factor of 0.01 there seems to be a trend reversal with the low permeability rocks showing

DD

deeper invasion. This confounding effect is caused by the shape of the assumed porosity profile. The low permeability zone in the middle of the section was assumed to have a low porosity with a consequent increase in invasion radius. If one assumes the same porosity (0.1) for the entire section, regardless of the magnitude of k/h ratio, the calculated invasion radius is smaller in the low permeability section as shown in Fig. 7.

The exposure time, the length of time the borehold wall is exposed to drilling fluid, also significantly affects radius of invasion. Because the mud cake properties when the filling fluid is circulating differ greatly from the properties when the fluid is not circulating, exposure time during both flow regimes (dynamic and static, respectively) must be specified to our program. Fig. 8 shows for the 500-ft. section the calculated invasion radius for two exposure times. Increasing exposure time from 10 hours (500 ft/50 ft/hr) to 25 hours (500 ft/20 ft/hr) increased invasion radius by about 30 percent.

MUD PROBLEMS IN GEOTHERMAL DRILLING

Field experience indicates that during the drilling of geothermal wells drilling fluid may undergo serious degradation. Thermal degradation of the organic compounds affects viscosity and filter loss properties. Also, the high temperatures may cause the mud to solidify and result in drilling problems. Remont et al.[27] reported on the stability and properties of some commercially available high temperature muds. Their findings indicate that most of the water base muds fail to retain their functional properties at temperatures above 350°F. In a subsequent publication Remont et al.[28] presented formulation of an improved drilling fluid suitable for geothermal application. From their data, indications are that the new formulation may retain its viscosity and water loss properties even after static aging at 500°F. In brief the new formulation calls for substitution of sepiolite for a portion of the bentonite. Furthermore, use of brown coal and sodium polyacrylate was suggested to improve filtration control characteristics. Sepiolite, a naturally occurring clay mineral, has a needle-like structure which makes it less effective than bentonite in filtration control.

As the newly formulated muds for geothermal drilling tend to be lower in solid content and somewhat higher in filtration losses, the technique presented in this paper is potentially more applicable with these newer muds.

SUMMARY AND CONCLUSIONS

We have presented a new approach for estimating formation permeability profile using a combination of several data bases which are and should be available from the drilling operation. The proposed technique consists of a wellbore simulator making use of drilling hydraulics data and mud composition hand in hand with well log data to derive a quantitative, or at least a qualitative, estimate of the permeability profile. The application of the technique requires a knowledge of dynamic filtration behavior of the drilling mud, which in our opinion should become a routine test replacing the inaccurate and rather meaningless API test.

The proposed technique is most applicable to liquid dominated geothermal reservoirs for which low solid muds are preferred and the formation contains only one fluid. Muds with medium to low sealing properties may provide invasion profiles which are related to the formation permeability distribution.

NOMENCLATURE

c = filtrate compressibility, psi^{-1}

G = geometric factor

h = mud cake thickness, cm

H = formation thickness, ft

k = filter cake permeability, md

K = formation permeability, md

P_c = capillary pressure, psi

Δp = pressure differential

Q = cumulative filter loss, cc

q = flow rate, cc/sec

$Q(t)$ = dimensionless influx (from Van Everdingen and Hurst)

R_t = resistivity of the uninvaded zone, ohm-m

R_i = resistivity of the invaded zone, ohm-m

r_i = invasion radius, ft

r_w = wellbore radius, ft

S_{w_i} = interstitial water saturation

t = time

W_e = cumulative invasion

ϕ = porosity, fraction

μ = filtrate viscosity, cp

η = diffusivity constant

ACKNOWLEDGEMENT

This study was supported by a grant from the Geothermal Division of the United States Department of Energy. Messrs. M. Azari and J. Luther assisted in the experimental work.

REFERENCES

1. Baker, L. E., Campbell, A. B., and Hughes, R. L.: "Geothermal Well Logging: An Assessment of the State of the Art," The Log Analyst (Nov.-Dec., 1975) 21-24.

2. Sanyal, S. K., and Meidav, H. T.: "Important Considerations in Geothermal Well Log Analysis," SPE 6535, paper presented at 47th Annual California Regional Meeting of SPE in Bakersfield, Calif. (April 13-15, 1977).

3. Wylie, M. R. J., and Rose, W. D.: "Some Theoretical Considerations Related to the Quantitative Evaluation of the Physical Characteristics of Reservoir Rock from Electric Log Data," Jour. Pet. Tech. (April, 1950).

4. Timur, A.: "An Investigation of Permeability, Porosity and Residual Water Saturation Relationships for Sandstone Reservoirs," The Log Analyst, vol. 9, no. 4 (July-August, 1968).

5. Brown, A., and Husseini, S.: "Permeability from Well Logs Shaybah Field, Saudi Arabia," SPWLA Transaction (1977) Part Q.

6. Barlai, Z.: "Determination of Permeability and Specific Surface Area of the Pore Channels from Well Logs in Fine Grained Sandstones," SPWLA Transaction (1976) Part C.

7. Lebreton, F., Sarya, J. P., and Moriher, P.: "Acoustic Method and Device for Determining Permeability Logs in Boreholes," U.S. Patent 3,622,969 (Nov. 23, 1971).

8. Dowling, A. J., and Boyd, J. F.: "Acoustic Permeability Log Utilizing Differential Travel Time Measurements," U. S. Patent 3,900,826 (Aug. 19, 1975).

9. Staal, J. J., and Robinson, J. D.: "Permeability Profile from Acoustic Logging," SPE 6821, paper presented at the 52nd Annual Fall Meeting of SPE in Denver, Colorado (Oct. 9-12, 1977).

10. Biot, M. A.: "Propagation of Elastic Waves in a Cylindrical Bore Containing a Fluid," Jour. of Applied Physics, vol. 23, no. 9 (Sept., 1952) p. 997.

11. Rosenbaum, J. H.: "Synthetic Microseismograms: Logging in Porous Formations," Geophysics, vol. 39 (Feb., 1974) 14.

12. Seevers, D. O.: "A Nuclear Magnetic Method for Determining the Permeability of Sandstones," SPWLA 7th Annual Symposium Transactions, pp. L1-L14, 1966.

13. Timur, A.: "Producible Porosity and Permeability of Sandstones Investigated Through Nuclear Magnetic Resonance Principles," The Log Analyst (Jan.-Feb., 1969) p. 3.

14. Engelke, C. P., and Hilchie, D. W.: "A New Qualitative Permeability Indicator," SPWLA Transaction (1971) Part M.

15. Dowling, D. J., and Boyd, J. F.: "Permeability Log Using New Lifetime Measurements," U.S. Patent 3,890,502 (June 17, 1975).

16. Breitenbach, E. A.: "A New Technique for Approximating Drilling Fluid Filtration," SPWLA Transaction (1965) Part I.

17. Miesch, E. P., and Albright, J. C.: "A Study of Invasion Diameter," SPWLA Transaction (1967) Part O.

18. Van Everdingen, A. F., and Hurst, W.: "The Application of the Laplace Transformation to Flow Problems in Reservoirs," Trans. AIME vol '86 (1949) 305.

19. Outmans, H. D.: "Mechanics of Static and Dynamic Filtration in the Borehold," Soc. Pet. Eng. Jr. (Sept., 1963) p. 236.

20. Ferguson, C. K., and Klotz, J. A.: "Filtration from Mud During Drilling," Trans. AIME (1954) 29.

21. Krueger, R. F.: "Evaluation of Drilling-Fluid Filter-Loss Additives Under Dynamic Conditions," JPT (Jan., 1963) 90.

22. Horner, V., White, M. M., Cochran, C. D., and Deily, F. H.: "Microbit Dynamic Filtration Studies," JPT (1957) 183.

23. Prokop, C. L.: "Radial Filtration of Drilling Mud," Trans. AIME (1952) 5.

24. Bezemer, C., and Havenar, I.: "Filtration Behavior of Circulating Drilling Fluids," Soc. Pet. Eng. Jr. (Dec., 1966) p. 292.

25. Krueger, R. F., and Vogel, L. C.: "Damage to Sandstone Cores by Particles from Drilling Fluids," API Drilling and Prod. Prac. (1954) 158.

26. Remont, L. J., Rehm, W. A., MacDonald, W. J., and Maurer, W. C.: Evaluation of Commercially Available Geothermal Drilling Fluids, Sandia Laboratories Report (SAND 77-7001) April, 1977.

27. _____: Improved Geothermal Drilling Fluids, Energy Research and Development Administration (IDO/1603-1) June, 1977.

DD

Table 2

Basic Data

Mud density	=	9 ppg
Drill pipe O.D.	=	5"
Drill pipe length	=	40'
Drill collar O.D.	=	7"
Collar length	=	30'
r_w	=	5.875"
Circulation rate	=	500 gpm
Formation pressure gradient	=	0.460 psi/ft
μ (filtrate)	=	0.6 cp
c	=	3×10^{-6} psi^{-1}
U (mud)	=	40 cp
Drilling rate	=	10 ft/hr (except for sensitivity studies)

Table 3

Mud Cake k/h Ratio Used For The Example Run

Time, hrs	k/h, md/cm
0.2	0.0075
0.4	0.0055
0.6	0.0041
0.8	0.0032
1.0	0.0026
1.2	0.0022
1.4	0.0020
1.6	0.0018
1.8	0.0017
2.0	0.0015
2.2	0.0012
2.4	0.0010
2.6	0.0009
2.8	0.0009
>2.8	0.0009

Table 4

Variable Porosities For The Example Run

k,md	ϕ
1	0.05
10-20	0.10
50	.17
100	.20
200	.25
300	.28
400-500	.30
1000	.35

ABOUT THE AUTHORS

ERSHAGHI

DOUGHERTY

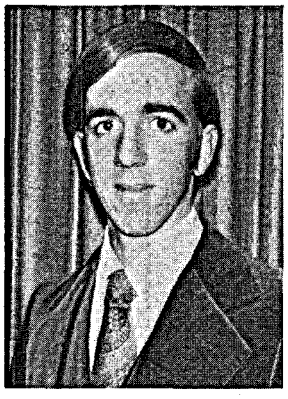

HERZBERG

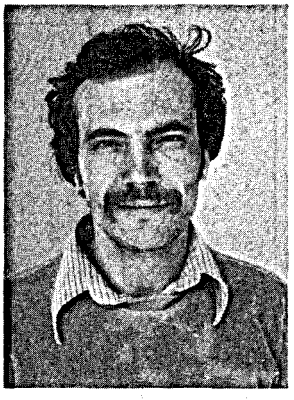

UCOK

Iraj Ershaghi is an Assistant Professor in Petroleum Engineering at University of Southern California. He holds a B.S. degree from University of Tehran and M.S. and Ph.D. from USC. All degrees are in petroleum engineering. He worked for Signal Oil and Gas Company and California State Lands Commission before joining USC. His areas of research include formation evaluation in geothermal reservoirs and enhanced recovery methods for oil and gas reservoirs. He is a member of SPWLA, SPE, CIM and AGU.

Elmer L. Dougherty is a Professor of Petroleum Engineering at University of Southern California. He holds a B.S. degree from the U. of Kansas and M.S. and Ph.D. degrees from the U. of Illinois, all in chemical engineering. Before joining USC in 1971, Dougherty worked for 18 years in industry. He received the Cedric K. Ferguson Medal in 1964. He is a member of SPWLA and SPE.

Donald E. Herzberg is a student in petroleum engineering at University of Southern California. His main areas of interest and research are numerical modeling and computer applications. He has been a research assistant on numerous projects at USC. He is a member of SPE.

Hikmet Ucok is a graduate student in petroleum engineering at USC. He is currently conducting research on improved methods of formation evaluation in geothermal reservoirs. He is a member of SPE.

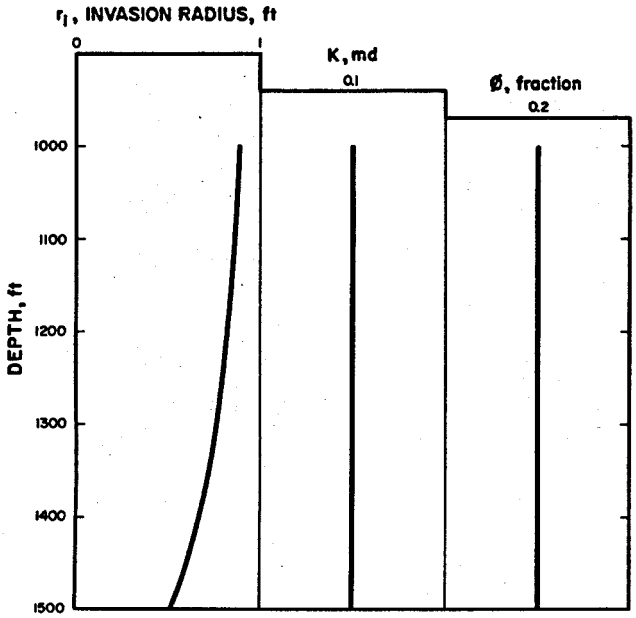

Fig. 1 Invasion Profile for a Uniform Permeability and Porosity Section (No Mud Cake).

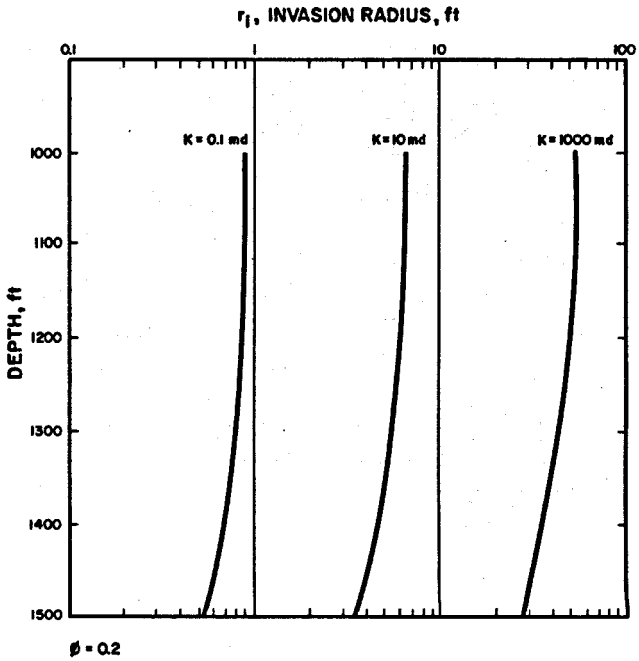

Fig. 2 Effect of Formation Permeability on Invasion Radius (No Mud Cake).

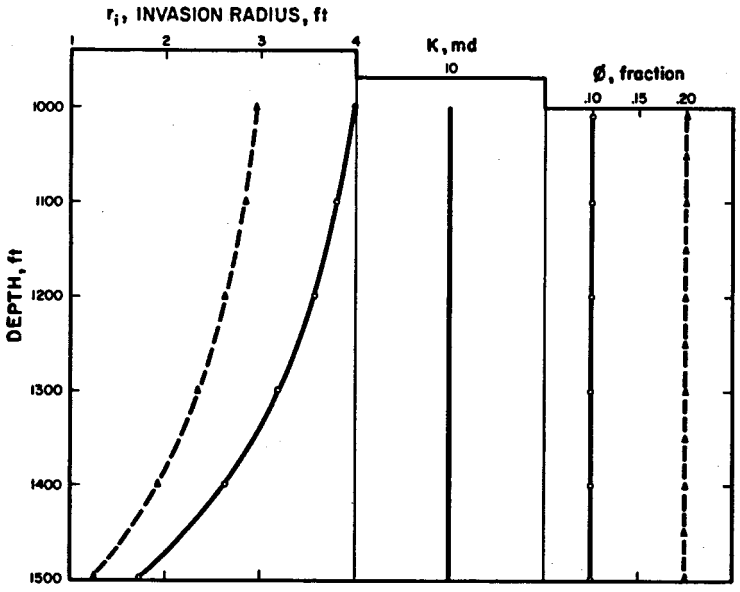

Fig. 3 Effect of Formation Porosity on Invasion Radius (No Mud Cake).

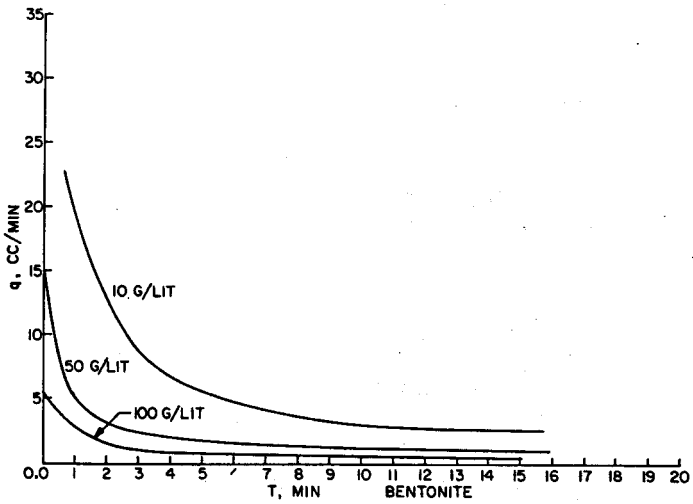

Fig. 4 Effect of Bentonite Concentration on the Filtration Rate in a Static API Test.

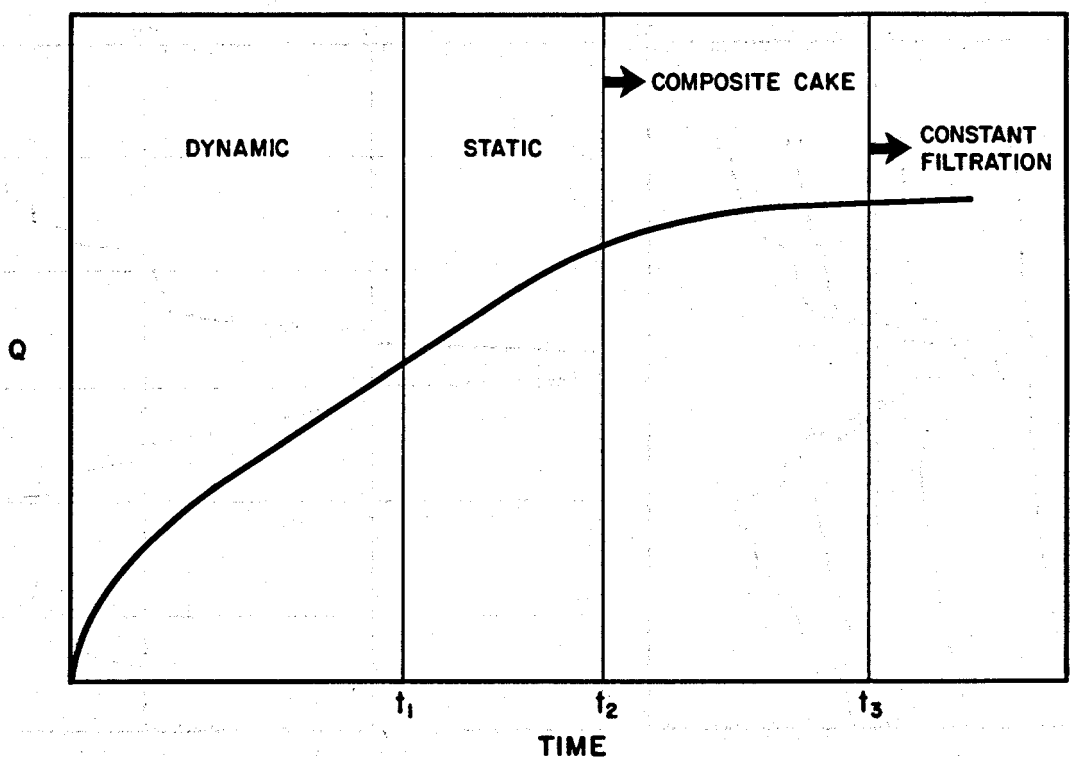

Fig. 5 Typical Mud Filtration Schedule During a Drilling Operation.

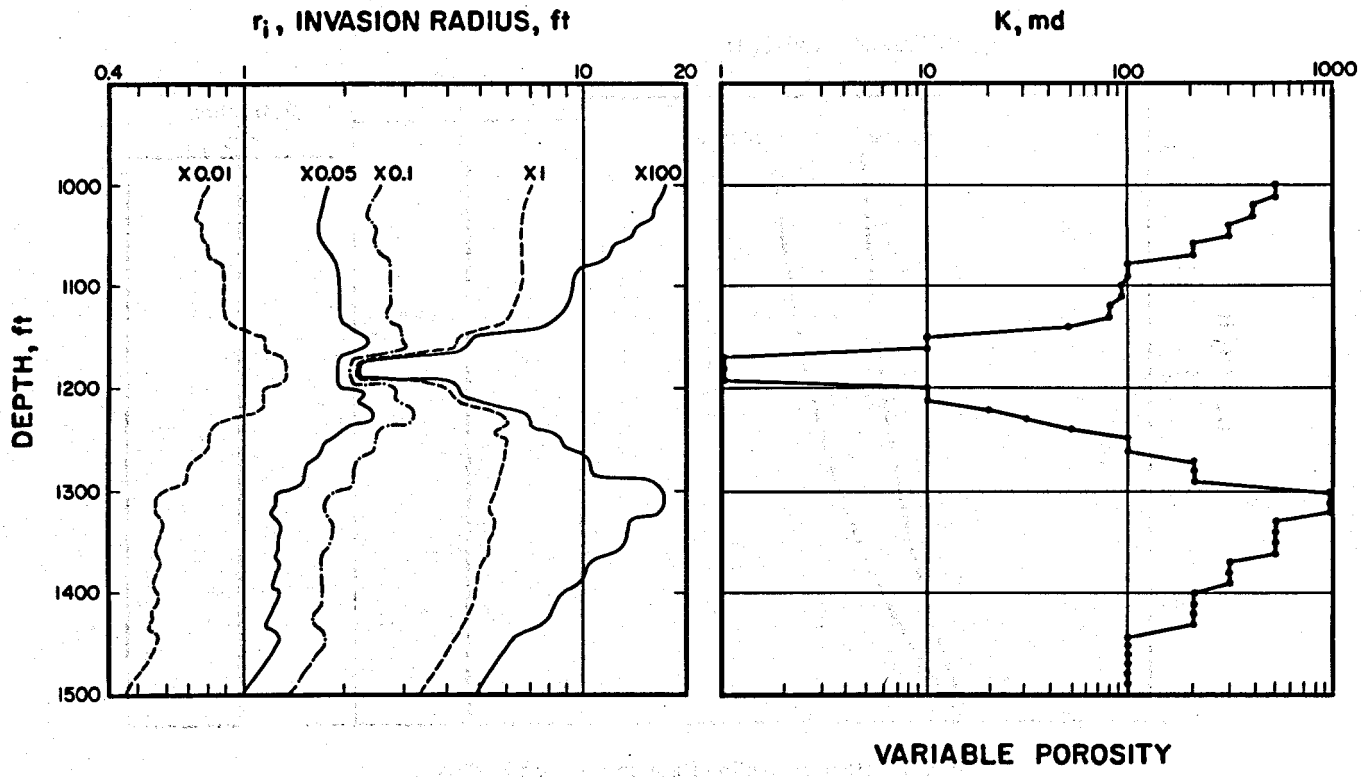

Fig. 6 Effect of Mud Cake Permeability-Thickness Ratio (k/h) on Invasion Radius (Non-Uniform Porosity).

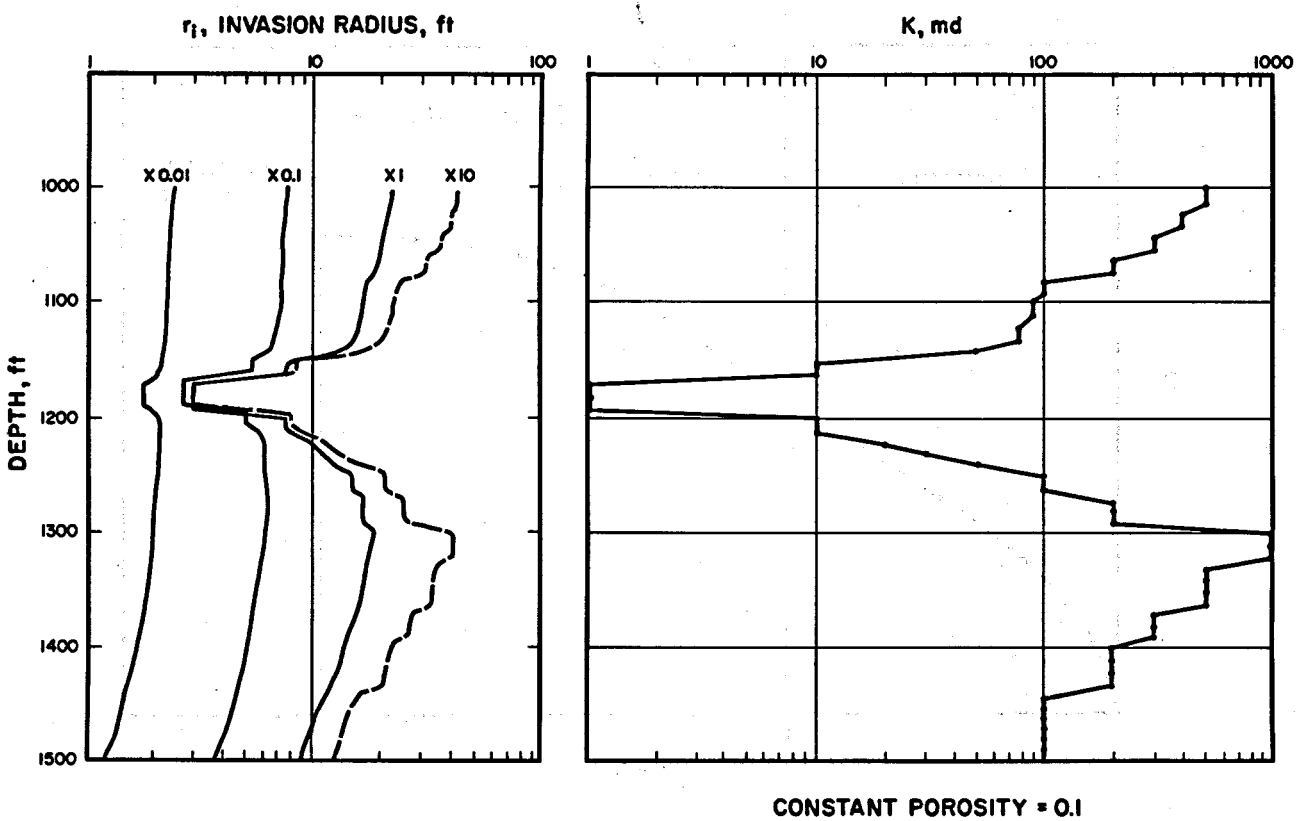

Fig. 7 Effect of Mud Cake Permeability-Thickness Ratio (k/h) on Invasion Radius (Uniform Porosity).

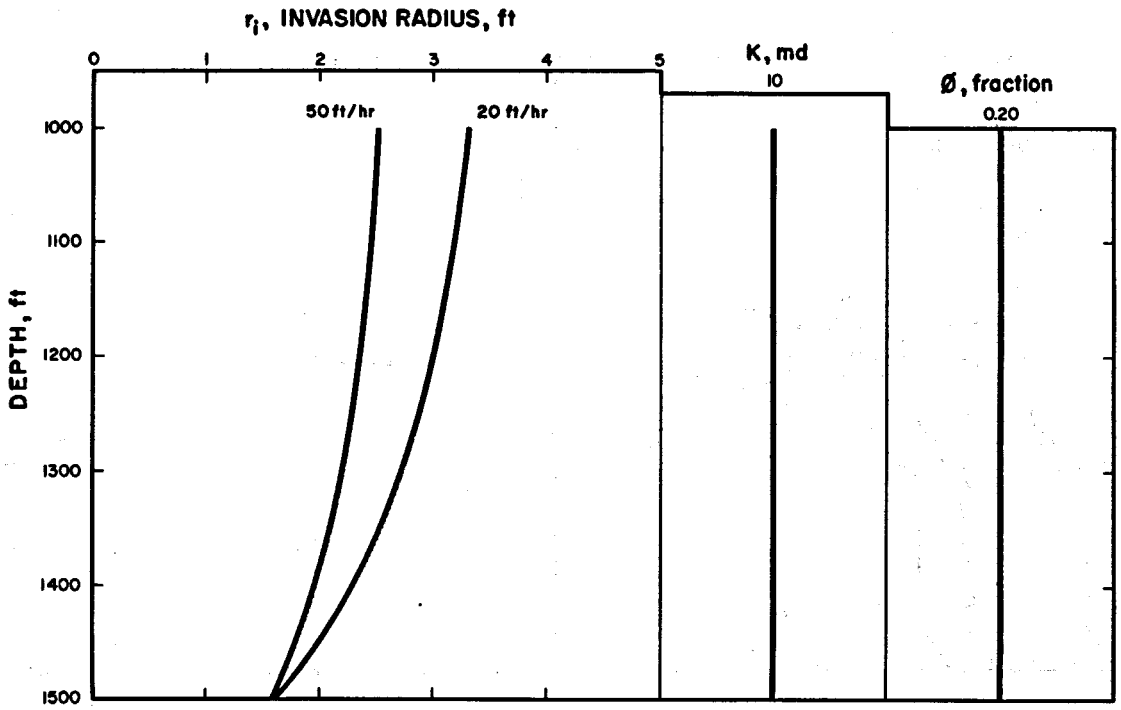

Fig. 8 Effect of Drilling Rate on Invasion Radius (Uniform Permeability and Porosity with Mud Cake).

EVALUATION OF OIL WELLS BY LOGGING METHODS IN THE USSR

V. Laptev

Temperature was the first geophysical parameter to be measured subsurface in Russia. These measurements were first carried out in Bibi-Eibath oil field (Baku) in 1906. But the broad application of geophysical well logging methods began in 1929 in Grozny where for the first time the Schlumberger resistivity logging method was introduced. Since that time the well logging geophysical service has grown up into a powerful branch of the oil industry. It provides with valuable information the most important divisions of the oil industry such as geology, drilling production.

Not only the USSR Ministry of Oil Industry, but the Ministry of Geology and Gas Ministry also have their own geophysical enterprises. In this report we shall consider the well logging state of the USSR Oil Industry.

Organization of well logging service and the volume of work

The geophysical service of the USSR Ministry of Oil Industry is the gratest in the USSR according to the volume of work to be carried. Suffice it to say that 546 million tons of oil (including gas condensate) was produced in 1977 and a production of 620-640 million tons is planned for 1980. The geophysical service is directed by the Oil Production and Field Geophysical Department of the USSR Ministry of Oil Industry. It comprises 16 geophysical unions called "trusts" situated in all the main oil producing regions of the USSR, the research office (Grozny, Tomsk), the research institute (Ufa), the geological research expedition (Moscow) and the logging equipment shops. The West Siberian oil fields are operated by the Tumen Geophysical Trust.

The main task of the geophysical service is the carrying out of well logging works and transfer of logging results to the customers, i.e. exploratory, drilling and oil producing enterprises. Transfering logging results to the customers, the geophysical service bears the responsibility for efficient solution of geological and technological problems. The research and design offices of the Oil Production and Field Department are searching and developing new, more effective logging methods as well as equipment and interpretation technique.

Types of work

The development of oil industry continiously widens the range of problems carried out by well logging. At present well logging is applied in the process of drilling, recovery or workover. The most applicable are the following types of work:

-open hole logging for determinig the lethological composition of rocks, reservoir identification, estimation

of their saturation and quatitaive determination of bed parameters for oil reserves estimation;
-evaluation while drilling of mud filtrate and drill cutting parameters to detect pay beds;
-drill pipe formation testing of open and cased holes for determining the reservoirs saturation and estimating their hydrodynamic parameters;
-monitoring the technical condition of wells for determining the deflection angle and curvature azimuth of a well, forecasting the complicated zones whilr drilling, testing the cement quality etc;
-perforation, well shooting, packers setting, reservoir stimulation to increase the recovery;
-production logging for determining the current oil saturation of reservoirs, detecting oil-water and gas-oil contacts in reservoirs and in welld, studying the inflow and absorption profiles in producing and injection wells, measuring reservoir pressure, temperature etc.

Geological and Technological Conditions of Geophysical Well Logging

The range of affected factors the geophysicians come across while logging is extremely wide. At first approach we may, however, combine oil and gas producing regions into 4 groups according to geological and technological conditions of work. Figures I and 2 show their territorial position and standart lithological-stratigraphic columns.

Group I. Includes regions located on the platform. The section is carbonaceous - terrigenous. The main productive bed complexes are represented by terrigenous reservoirs of porous type and by carbonaceous reservoirs of complex structure Sedimentary complex has a thickness of I,5-5 km The maximum temperature in wells is I00°C, well pressure is 50 MPa.
Group 2. Includes regions located on the depression. The section is carbonaceous-terrigenous and represented by thick halogen strata. The oil reservoirs are carbonaceous and consolidated terrigenous rocks with complex structure of the pore space. Sedimentary complex thickness varies from 5 to 20 km. Depths of wells are 5-7 km, temperature is about i70°C , pressure is I00 MPa. Zones of abnormal fromation pressure may occur.
Group 3. To this group belong regions located on the platform. The section is terrigenous. The oil reservoirs are represented by polymineral sands (feldspar, quartz, sulphide) of porous type various clay content. The sedimentary complex has a thickness of I,5-7 km. Depths of wells are I,5 - 4,5 km, temperature is up to I00°- I20°C, pressure is 50-60 MPa.
Group 4. To this group belong regions located on the depression. The section is terrigenous and represented by thick halogen strata. Productive complexes are represented by clay and thin-bedded sands of porous type. Sedimentary complex thickness varies from 5 to 20 km. Deep wells of about 7-8 km are typical for this group, the temperature is usually high (230°C), pressure is about I50 MPa. Zones of abnormal formation pressure may occur. The well logging service deals

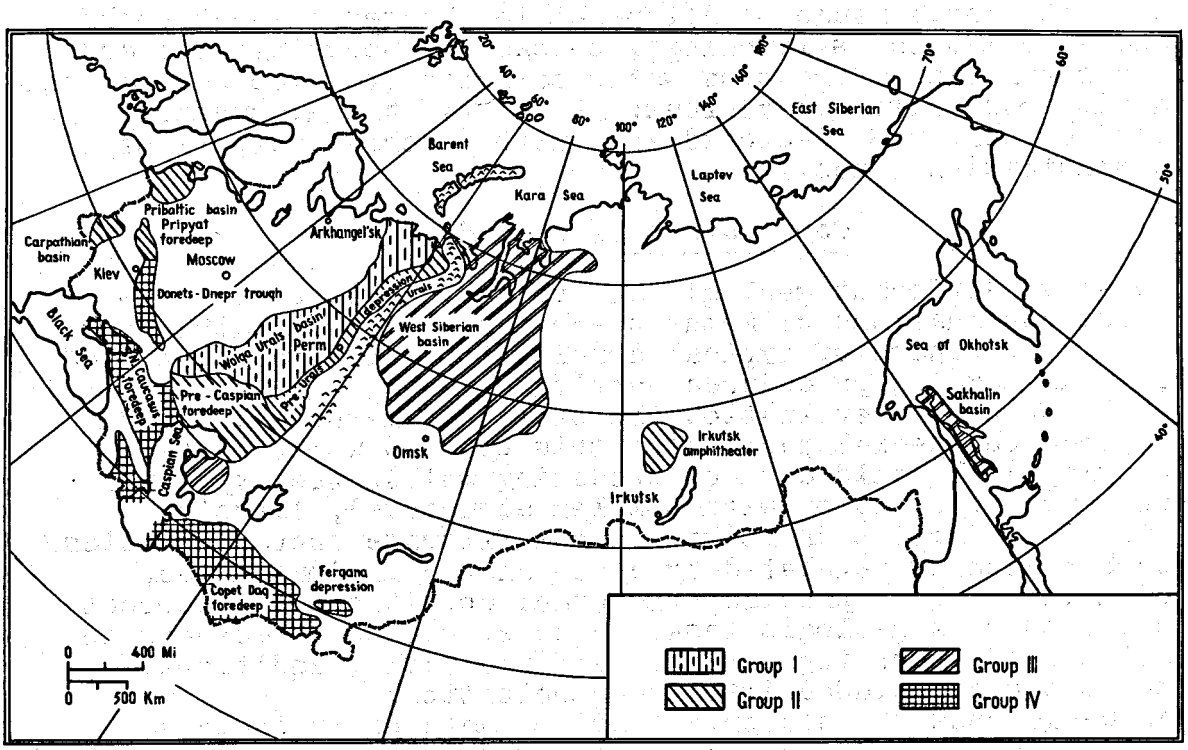

Figure I.
Geological-geophysical region division

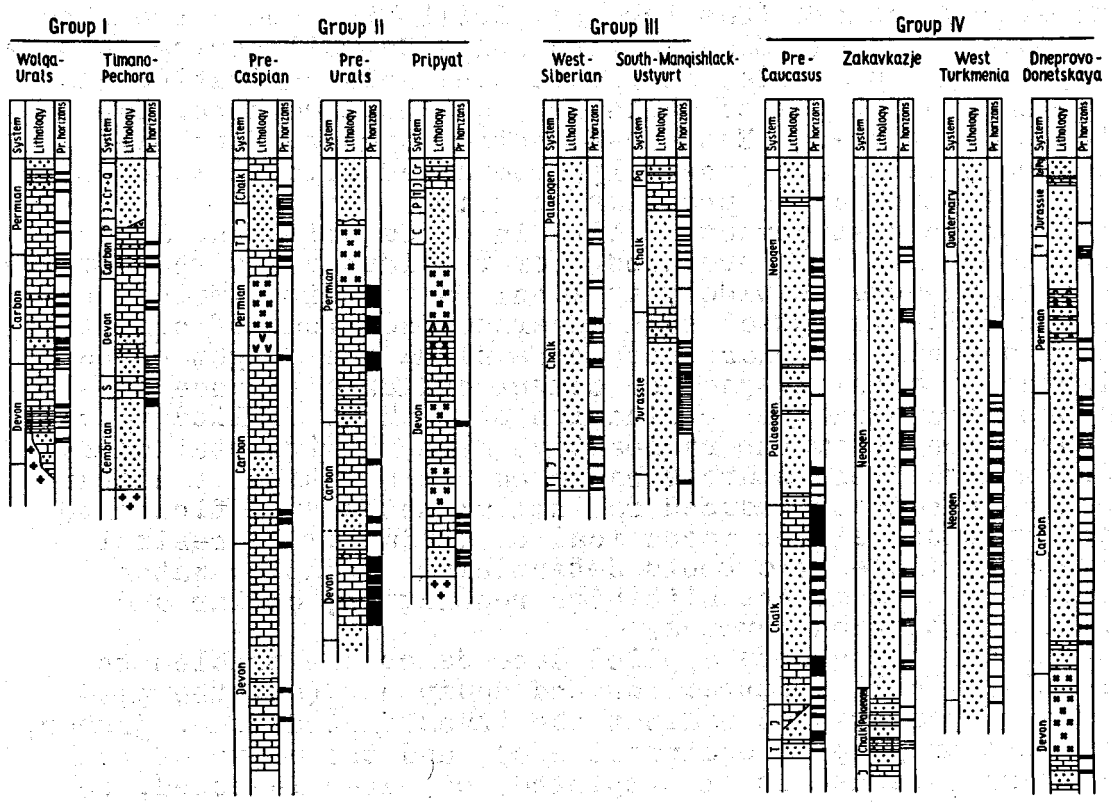

Figure 2.
Typical sections of geologic areas

with the whole range of all possible changes of such rocks characteristics as lithology, thickness, porosity, oil and gas saturation, formation water salinity etc. The surface conditions are also too various: deserts, taiga, swamps, tundra, sea, the developed area with powerful network of communication lines.

Combination of Methods

To solve different geologic and technological tasks, various combinations of methods are used. We shall give now brief references of typical combinations of methods applied in well logging procedures mentioned above.
While open hole evaluation the choice of methods applied depends on special purpose of this or that well. (prospecting well, wild cat, or producing well), the type of a reservoir (porous or with complex structure), lithological composition of rocks and mud filtrate characteristics. each region is regulated by a compulsory minimum number of methods which provide in normal conditions the correct solution of a geologic task. In case, the basic methods do not provide carrying out the required tasks, additional methods are included into the combination.
As basic ones the electric logging methods in their various modifications are normally used (i.e. Lateral Electric Sounding, SP, Induction Log, Lateral Log, Micro Laterlog, Microlog); radioactive methods (Gamma-Ray Log, Neutron-Gamma-Ray Log, Thermal-Neutron Log) acoustic methods, Caliper Logging and Dipmeter survey.
The direct methods (Gas Logging, Drill Pipe and Wire Line Formation Testing, Side Testers and side-wall coring guns) are compulsory, as a rule, in prospecting well evaluation and used in other types of wells as additional methods. The Dielectric Logging, Nuclear-Magnetic Logging, Impulse-Neutron Logging are generally used as additional methods for some complicated problems solution.
In order to test cement quality in cased holes the Acoustic and Cement Bond Log are used. For the last years the combination of both methods is widely applied. Using this combination we can reliably detect such adverse conditions of cementations as baffle coolar break offs along the height or perimeter of annular space or cement collar clearance.
In the producing the combination of methods applied is various. Among them the radioactive methods with stationary and impulse field sources based on registration of dispersed, captured and induced radiation; methods of flow rate registration (either mechanical or conductive), resistivimeters, dielectric tools determining formation water content, thermometers with high resolution, collar and interval location devices.
The number of methods applied depends on the problem to be solved, well construction and equipment (ex. the presence of perforation against the investigated zone, gusher, gas-lift or pumping equipment etc), and the drive of well recovery (whether it is completed, or water injected, or producing).

As the basic methods in the process of estimation of current oilsaturation of rocks, detection of oil-water and gas oil contacts, the Impulse Neutron Log is used as well as stationary neutron methods and thermal methods. Induction Log is used in open hole evaluations. As additional methods the broadband Acoustic Logging, the injection of radioactive tracers and drill pipe and wire line formation testing are used.
In the producing wells the investigation of inflow profiles, detection of water environment, formation pressure control is carried out by flow rate registration, Gamma - Density Log, diclectic determination of formation water content, Resistivity Log, Thermal methods, piezoelectric and Neutron methods.

Apparatus and Equipment

The surface equipment of well logging gangs is provided with the logging laboratory and the hoist both truck-mounted. Analogous registration tools are chiefly used. At present the developing of the first digital computer logging systems has begun. The hoists are equipped with one,-thress,-seven- conductor mailed cable.
To carry on geochemical investigations while drilling the mobile gas-logging stations (AGKS-4AC) are utilized supplied with chromatic tools which resolution is 10^{-4} volume percent per 6 components and tools for mud filtrate and drill cuttings luminescence analysis. They are also supplied with vacuum degassing units and analogous and digital registration.
The conventional well logging equipment for drilling wells investigation is capable to sustain the temperature of 120-150° and the pressure of 100 MPa.
Tools diameter varies from 54-140 mm, for bottom hole evaluation the psecial apparatus is manufactured capable to sustain temperature up to 200°C and pressure of 120-150MPa. Some tools are capable to operate at 240°C.
Electric logging apparatus includes the complex tools of Electric Laterlog and Laterlog (EI, ABK-T), Electric Laterlog and Induction Log tools (E3,AIK-4), Microlaterlog, Microlog and Caliper tools (E2, MBKU). We have almost finished the developing of multisonde Lateral and Induction tools. Besides that many types of another apparatus are applied.
The apparatus of radioactive methods is represented by Neutron-Log tools (DRST-3), Impulse-Neutron tools, Density Log tools (RKS-I, RGP-2). The two-sonde tools for compensated Neutron logging are being developed now, which can be combined with RKS -I and carry on simultaneous density, neutron and Gamma measurements. To test cement quality the combination of Gamma-Ray Logging with rotary Sonde and the tool determining the tube thickness (SGDT -2) is used.
Open hole acoustic logging is conducted by 3-element tools SPAK-2M and SPAK-4; to test cement quality in cased wells 2-element tools AKS-I, AKS -3 are used.
To carry special investigations the borehole acoustic tele-

viewer (KAT-I) and broadband tools AKN - I are used.
Drill pipe formation testing is conducted by one-cycle and many-cycle testers (KII and MIK).
Tools ("uralets") for many-cycle testing of open and cased holes capable to stop at any place of the wall of a borehole have been constructed, which provide testing of several objects on one trip in a well.
For sidewall rock and fluid samping the wire line formation testers supplied with distance surface monitoring (OPK) are used as well as core cut tools and samping guns (SKM,GBS).
In production logging the list of apparatus applied is very broad. In off wells investigation the tools diameter is about I00 mm, in gusher wells - about 42 mm, in pumping wells equipped with sucker rod pumps - about 28 mm. Tools are capable to sustain temperature up to 80°-I20°C, pressure - 30-60 MPa. Tools equipped with sacket rod pumps are run in into the space between casing and tubing. This technique is developed by many well logging enterprises and the volume of work is constantly increasing. In I977 such investigations were conducted in I8802 wells. Let's give brief references of these tools.
For producing well evaluation by radioactive methods the neutron generators (IGN-6) having diameter of 42 mm and the ones havine diameter of 32 mm (GNOM) are used. Also used the different tools with stationary gamma and neutron sources. The composition of recovered fluid in producing wells is determined by gamma density toold with or without packers (GGP-II,GGP-IM), registrating the volume density and natural gamma activity. Density tools equipped with packers are utilized in case of blocking of intervals by water gathered at the bottom hole. Besides radioactive methods for determining the composition of recovered fluid the induction resistivity devices (RIS-42I) and dielectric tools determining the fluid content are used. The latter are usually combined with mechanical flow rate meters (DB-28, KOBRA-36PB). Induction resistivity devices provide measurements of specific conductivity of oil-water emulsion of formation water of different salinity in the range of 0,I-300 sm m. By tools for water content investigation we determine the volume content of water in the oil.
Measuremtn of reservoir production rate is conducted by mechanical flow rate meters that can be be with packers or without them, and by thermoconductive flow rate traces. As a mechanical flow rate sensor the small rotary turbine is used; in low producing well its resolution is 0.I5 m^3 hour. In thermoconductive flow recorders the sensible element for flow rate induction is the warmed up resistor. Besides that there is a sensor for temperature measurements. The resolution of thermoconductive flow records in well with low production is 0.02 m^3 hour. The list of apparatus applied in well perforating is various too.
We'll just enumerate the most characteristic types. For cased hole perforating, jet or bullet perforators having different diameter are used. The new types of perforators are capable to operate in very deep wells where the temperature is about 250°C and pressure is I50MPa. To liquidate failures jet

torpedos are used. For bed isolation the blasting packers are applied; to increase oil recovery and well injectivity - the powder pressure generators.

Interpretation technique.

Well logging data processing is conducted by logging partics in every geophysical unit. A customer is given cross-plots, charts and well logging conclusions. Thus, during drilling wells evaluation a customer is supplied with data concerning lithologic characteristics of rocks, reservoirs identified in a column, their gas oil and water saturation. Some recommendations are given concerning testing of zones that can be of commercial interest or have unequal well logging characteristics.

After Cement Bond Log is carried out, a customer is given information of intervals having bad cement quality and of the total height of cementation. By Cement Bond Log we obtain data of actual position of casing elements (casing centralizer, packers), density of cementing, eccentricity of casing in a borehole, casing thickness.

The same results are given by gas logging, inclinometer devices, drill pipe testing and producing well evaluation.

During the process of interpretation only such techniques are applied which have been tested beforehand in concrete geological-technological conditions and have proved their efficiency. During interpretation the log analysts widely use the petrophysical relationships obtained by core samping and some other vital geologic and technological information concerning current state of field prospecting and deposit developing.

For the last years the conventional manual interpretation is being replaced by computer processed interpretation, For this purpose different systems of log interpretation have been developed determining lithology, porosity, oil saturetion of rocks, caoable to test cement quality, compute hydrodynamic strata parameters ans to interprete production logging results. As an experience the computer processed interpretation is being taken root in the Tumen Geophysical Trust (Tumenneftegeophysica) in Samotlor oil field and in Tatar Geophysical Trust (Tatarneftegeophysica) in Tatar oil fields. In both cases, besides, ordinary cross-plots a customer is given in digit and analogous form such rocks parameters as porosity, lithology and oil saturation.

The internal thickness of detailed interpretation in both cases is about 600-800 m, but however, the Tatarian section is carbonaceous, while Western Siberian - terrigenous.

Besides log interpretation the regional interpretation program systems have been developed,are being tested now. First of all they are applicable to reserves estimation. They provide determination of computed reservoir parameter, charts drawing and specifying deposit reserves.

Taking into account the advantages of computer processed interpretation over manual and the progressive development of automatic monitoring systems the application of computer machines in the field of well logging geophysics is expressed to be extensive.

Efficiency

It is quite natural that alongside with subsequent development of oil prospecting the zones of investigation become more complex.

For example, if 10-15 years ago the main productive complexes were discovered in granular terrigenous and carbonaceous reservoirs with porosity more than 10-15%, the last years, as the wells have become deeper and new regions have been investigated are characterized by consolidated carbonaceous and terrigenous productive zones with porosity less than 15% and with complex geometry of pore space (fracturous, cavernous, porous and mixed porous type).

In West Siberian and Mangishlak areas the log analysts for the first time came across the terrigenous clay reservoirs having polymineral matrix composition and abnormally low electric resistivity. For the last years the pay beds were discovered in tufa reservoirs and even in shales.

It is obvious that in such conditions the efficiency of geological problems solution by logging methods is different.

In granular reservoirs of low and medium clay content with porosity more than 10-15% and formation water salinity more than 100 gr. per litre, the efficiency of log results is 95-97%. This index is to be got by comparison of interpretation data with the results of testing in a casing.

During reserves estimation for these reservoirs such well logging parameters as effective thickness, oil saturation, oil water and oil-gas contacts position are chiefly basic parameters.

As far as the complex reservoirs are concerned to which we refer fracturous, cavernous, and clay rocks with porosity less than 10%, their evaluation presents some difficulties. The thing is that in this porosity range the resolution of a number of methods according to saturation is compatible with the level of error measurements. That is why log interpretation in these conditions can be unequal (30-35%).

To avoid missing of pay beds in such intervals with unequal geophysic responces, special direct methods are applied in accordance withgeologic service. By special methods we understand iterative well measurements by electric or radioactive methods that are conducted after the bed is drilled in; this can be done with two mud filtrates of different conductivity or different nuclear properties; before or after the well pressure is changed etc.

The application of drill pipe formation testers, core slicers, wire line formation testers and the above mentioned methods of investigation provide the substantial growth of efficiency of complex sections study. But application of such methods is very expensive and it takes too much time. That is why the problem of increase in geologic efficiency of complex reservoirs study is too urgent and works of its realization are related to search for new methods and apparatus as well as more profound petrophysical investigation of these types of reservoirs.

The next urgent efficiency problem connecting cased and uncased holes in the problem of separation of oilbearing

and waterbearing rocks at low formation water salinities. Log analysts come across this problem during interpretation of measurements obtained in wells which have been drilled in such developing areas where drilling is accompanied by intensive water injection or in areas with low initial water salinities A certain progress in this problem solution is achieved by Impulse Neutron, dielectric Nuclear Magnetic, Broadband acoustic and Direct methods utility. However, a lot of aspects of this problem are not yet solved.
Among the production logging problems the most vital is the problem of determining the current oil saturation of rocks in producing wells. It is connected with such problems of oil recovery increase as water injection (even fresh water) (gas injection, thermal influence, etc).
Here the most applicable are the nuclear methods. But thermal methods, acoustic logging are still applied in this field. During open hole investigation or cased hole with non- metallic string, the Electric Logging is advisable, especially the Induction Logging.

Future of Logging

The most important trends of improving well logging methods are the following:
I. Creating the complex equipment for open hole logging, cement bond logging and producing well evaluation. Developing the surface tools for digit registration and well logging data processing. The main purpose of these works is time shortening during well logging and log interpretation and the increase in output data quality.
2. Developing the new logging methods and direct methods improving, providing determination of bed parameters in compound reservoirs and in strata saturated with low-mineralized water.
3. Creation and improvemnt of automatic stations for geological, geophysical and technological data gathering and processing while drilling to solve geologic tasks and drill drive optimization.
4. Improving production logging methods equipment and Cement Bond Log tools for determining the current oil saturation of rocks, detecting the water flooded intervals and monitoring the producing wells drive. Developing the technique for systematic production logging in an oil field.
5. Improving compound interpretation methods (including computer process interpretation) to increase the efficiency of geologic and technologic problems solution and the accuracy of parameters determination.
6. Developing apparatus and appliances capable to operate in such adverse borehole conditions as high temperature and pressure, slant or horizontal wells and producing wells, equipped with centrifugal pumps etc.)
7. Creating and improving the technological means for metrologic apparatus monitoring and increase in apparatus reliability.

Realization of this program would rise geologic and economic efficiency of well logging methods and is of great commercial interest for our oil industry. It seems to us that some of the above mentioned problems and trends can also be of interest to log analysts of different countries and could serve as the foundation for mutual cooperation and information exchange. At present such mutually beneficial cooperation with many foreign companies is constantly and succesfully developing.

ABOUT THE AUTHOR

Laptev V.V. - engineer geophysician Graduated from Moscow Oil and Gas Institute in 1960. For 18 years he works at the problems of improving logging data interpretation. In 1967 he got his candidate degrees at the All-Union Research Institute of Nuclear Geophysics and Geochemistry (Moscow). His thesis was devoted to impalse neutron methods application.
At present he works as a deputy scientific director of the All-Union Research Institute of Oil Field Geophysics.

FORMATION EVALUATION CONCEPTS FOR GEOTHERMAL RESOURCES

By
T. W. Ehring, L. A. Lusk, J. M. Grubb, Aminoil USA
R. B. Johnson, M. R. DeVries, W. H. Fertl, Dresser Atlas Division, Dresser Industries, Inc.

ABSTRACT

The first successful well logging operation in a 500°F live geothermal steam well was carried out in the Castle Rock Springs Field in northern California on August 6, 1977.

At the present time, special high temperature equipment for geothermal wells includes the Gamma Ray/Neutron Log, Compensated Densilog®, and Caliper-Temperature Log, run on a special 5/16-inch single conductor cable.

The present paper discusses the geologic environment of geothermal steam reservoirs and presents several interpretive concepts, such as identification of lithology, determination of reservoir porosity, location of steam entry points, and estimation of steam quality.

GEOLOGIC FRAMEWORK OF THE GEYSERS AREA

The Geysers geothermal area is located 80 miles north of San Francisco in the Mayacmas Mountains along Big Sulfur Creek in the northern Coast Ranges of California as shown in Figure 1. In addition to showing the Geysers location, 15 miles south of Clear Lake, Figure 1 also illustrates the northwest trending structural grain of California geology which is prominently evidenced by the Sierra Nevadas, Great Central Valley, and the celebrated San Andreas Fault. The Northern Coastal Province of California contains a belt of branching, interlacing, and roughly parallel faults to the main San Andreas Fault. The majority of these faults are normal and demonstrate similar right lateral movement to the San Andreas. Within this geologic province, the majority of large normal faults have the downthrown side on the southwest. Movement on these faults has not occurred along one smooth plane, but on numerous arcuate segments. These major faults produce a graben-horst type geology with complex cross faulting and thrusting between the major units. The Mayacmas Mountains are a large horst, bounded on the northeast and southwest by structural as well as topographic expressions resulting from these major faults. Within this province lies the geothermal steam field.

FF

For a detailed surface geologic map of the Geysers and surrounding area, the reader is directed to the U.S. Geological Survey Open File Map 74-238 by Robert J. McLaughlin entitled "Preliminary Geologic Map of the Geysers Steam Field and Vicinity, Sonoma County, California."[1] This study represents, in the opinion of the authors, a monumental work in geologic mapping of a highly complex province and is far too detailed to be reviewed in this paper. However, a generalized geologic map, after McLaughlin, serves as Figure 2 to demonstrate the major structural units in Franciscan Rocks within the Geysers area.

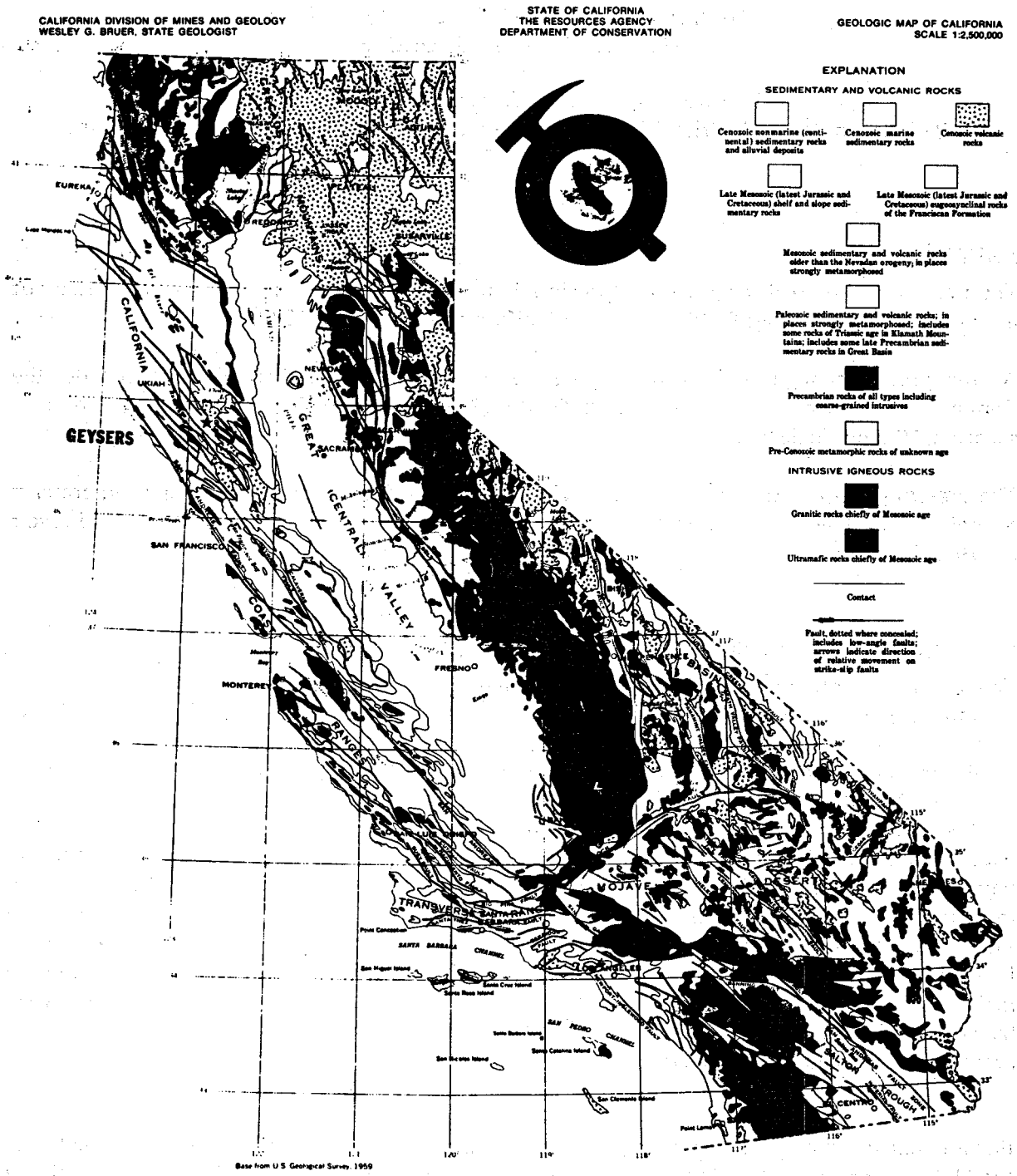

GEOLOGIC MAP OF CALIFORNIA

COMPILED BY U.S. GEOLOGICAL SURVEY
AND CALIFORNIA DIVISION OF MINES AND GEOLOGY

SCALE 1:2 500 000

0 50 100 MILES

SUBMARINE CONTOUR INTERVALS 500 AND 1000 FEET, DATUM IS SEA LEVEL

1966

FIGURE 1

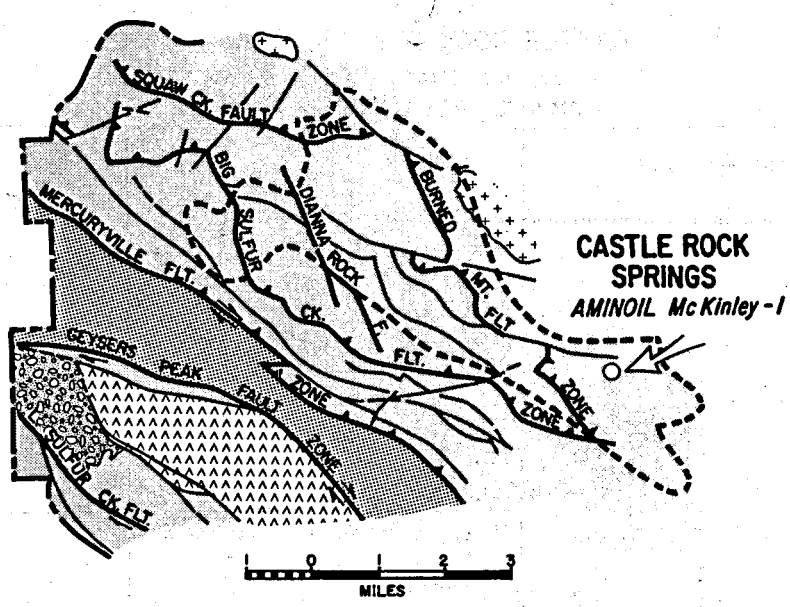

GENERALIZED GEOLOGIC MAP SHOWING MAJOR FAULTS AND STRUCTURAL UNITS IN FRANCISCAN ROCKS OF THE GEYSERS AREA

After R.J. Mc Laughlin 1974

- PROVEN LIMITS OF GEOTHERMAL FIELD
- LATE TERTIARY AND QUATERNARY VOLCANIC ROCKS
- UNNAMED LATE TERTIARY GRAVELS
- LOWER FRANCISCAN STRUCTURAL UNIT (GRAYWACKE OF LITTLE SULFUR CREEK)
- UPPER FRANCISCAN STRUCTURAL UNIT (MELANGE)
- OPHIOLITE

FIGURE 2

Superimposed on this generalized geologic map (Figure 2) is the present proven limit of the geothermal steam field. Although the field is still being explored and numerous stepout discoveries will be forthcoming, the northwest-southeast elongation is apparent. To date, the preponderance of the field lies within McLaughlin's Upper Franciscan structural unit. This structural unit is bounded on the southwest by the Mercuryville Fault and goes beneath the Squaw Creek – Burned Mountain thrust faults. Farther to the northeast and off the map lies the Collayomi Fault zone present in the Collayomi and Cobb Valleys which may provide the ultimate terminous for steam development toward the east. The rocks of the Franciscan in the Geysers area may be generally characterized as consisting of graywacke, interbedded argillite, chert, greenstone, and schist. These rocks show metamorphism and, in some areas, hydrothermal alteration. Intrusive serpentine is present in the formation with most of the serpentine in thrust fault contact with adjacent rocks. McLaughlin has broken these rock types into units for mapping and provides a detailed lithologic description. The steam field is producing from fractures within the Franciscan metagraywacke at depths of 2,000 to 10,000 feet.

The Geysers geothermal field is one of two producing vapor-dominated (dry steam) fields in the world. The other is located in Italy. This field produces more "on-line" electrical power than any dry steam or hot water geothermal area in the world, producing approximately 502 megawatts. The power is generated by turbines driven by superheated steam produced directly from the wells. The proven area outlined should double the capacity of the field when developed and, as stated above, stepout development and exploratory efforts are in a continuous process which may result in ultimate field capacity of 2,000 to 3,000 megawatts.

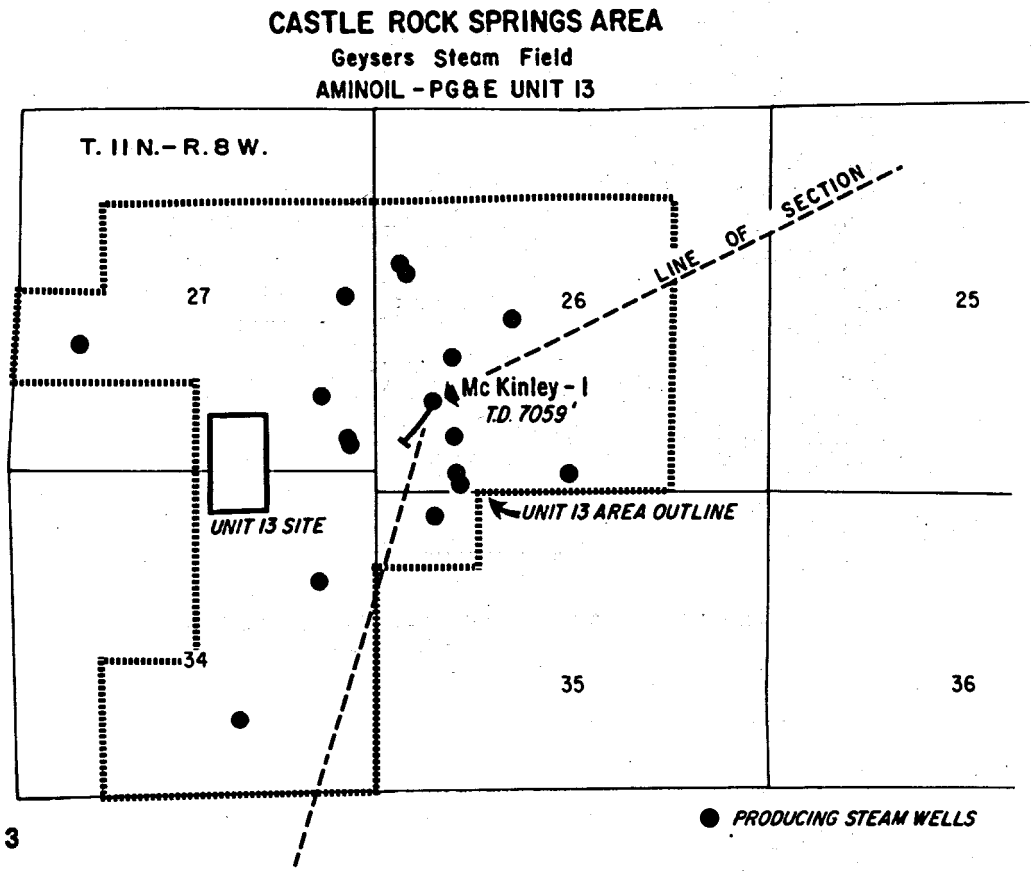

FIGURE 3

The Castle Rock Springs area is located on the southeasterly end of the Geysers geothermal field encompassing sections 26, 27, 34, and 35, Township 11 North, Range 8 West. Aminoil has dedicated an area of approximately 1,000 acres (Figure 3) to provide the steam reserves (709,560,000,000 pounds of steam) required for the 30-year life of Pacific Gas and Electric Company's Unit 13 geothermal plant. Unit 13 will be the largest single geothermal unit in the world and the first in Lake County, California. Pacific Gas and Electric Company's current construction schedule calls for the power plant to begin generating electricity on October 1, 1979. Unit 13 will be powered by Aminoil's first steam production for an electrical generating plant and, since their exploration operations in the Geysers were initiated over ten years ago, it appears to be the end of a long struggle. The plant design is for 135 megawatts, which will require approximately 2,770,000 pounds of steam per hour to operate. To provide a reasonable safety margin and allow sufficient flexibility to service individual wells, it is Aminoil's plan to develop a minimum field capacity producing rate of 3 million pounds of steam per hour. To provide this amount of steam, it will take approximately 20 wells, 16 of which have already been drilled and tested for a total current capacity of 2,245,000 pounds per hour. During 1978, Aminoil will drill an additional four wells, and at that time will have a total of 20 wells providing an average of 150,000 pounds of steam per hour per well. Individual flow rates for the wells vary from a low of 65,000 pounds of steam per hour to a high of 300,000 pounds of steam per hour. The 20 wells drilled in the 1,000-acre dedicated area will result in a well spacing pattern of 50 acres per well. Over the life of the field, replacement wells will be required to maintain the desired rate of 3,000,000 pounds of steam per hour. It is Aminoil's current forecast that one replacement will be required every three years. The steam reservoir conditions include a pressure of approximately 500 pounds per square inch and 500°F temperature. Aminoil's McKinley No. 1 well, successfully logged by Dresser Atlas and the basis of this paper, is one of the 16 wells which will supply steam to Unit 13.

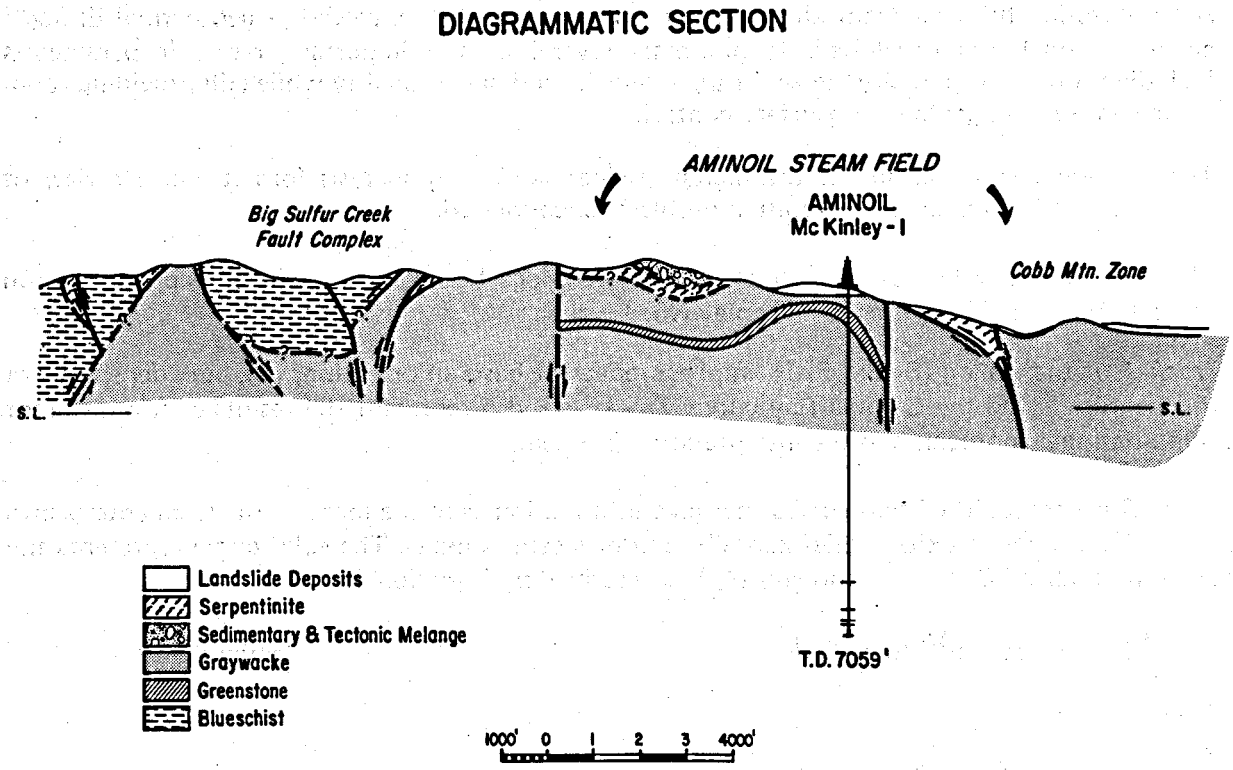

FIGURE 4

The Diagrammatic Section in Figure 4 demonstrates the complex surface geology in a northerly direction across the Castle Rock Springs area. In addition, the relationship of this surface geology with the Aminoil McKinley No. 1 producing well drilled to 7,059 feet is demonstrated. McKinley No. 1 encountered metagraywacke at 3,060 feet and continued in this lithology to the total depth. Without the use of downhole logging, subsurface geologic control such as that used for correlation in the oil industry is meager and interbedding within the Franciscan graywacke has not been consistently delineated. The general procedure for drilling in Castle Rock Springs area is to drill with mud to 3,000 feet, cement 9-5/8-inch casing at that depth, and then drill 8-3/4-inch hole with air until sufficient commercial steam is encountered. Commercial steam is something greater than 65,000 pounds per hour, depending upon steam price and drilling depth. Because of the high temperature (500°F) and the large volume (135,000 lb/hr), these steam wells heretofore have not been logged.

FF

WELL LOG ANALYSIS CONCEPTS IN GEOTHERMAL STEAM WELLS

During the latter part of 1977, McKinley No. 1 was successfully logged at 500°F over a number of producing intervals utilizing a logging suite that included the Gamma Ray Log, a Compensated Densilog®, and a Neutron-Neutron Log. As expected, the initial inspection of the logging information showed that there was indeed a difference in the philosophies of interpretation between a metamorphic and sedimentary province. For example, in metamorphic formations, there exists no classical stratigraphy. Beyond a general view of the makeup of an area, structures are mostly short range and complex. Important metamorphic features are mineral associations, chemical associations, and short range structure. Initial attempts at interpretation also brought out some fundamental differences in interpretation concepts between mineralized intervals and geothermal reservoirs. For example, mineral interpretations are frequently concerned with delineation of a particular mineral or group of minerals under essentially equilibrium conditions.

After selecting the best from all the interpretive philosophies involved, a geothermal Epilog® analysis model was developed. It pinpoints several of the important reservoir parameters including lithology, porosity, steam entry intervals, and steam quality while still providing room for expansion into geologic subsurface controls.

The following is an outline of the digital geothermal Epilog analysis format and a review of several of the formidable interpretation problems encountered.

The interpretive value of the Dresser Atlas well logs becomes immediately apparent upon inspection of the Epilog for the McKinley No. 1 well.

Track 1 of the Epilog (Figure 5) is simply a repeat of basic information, i.e., bulk density from the Densilog® and the Gamma Ray curve. *Tracks 3* and *5* represent the results of two different computational approaches to the interpretation problem.

Track 3 is composed of two curves that give information as to the location of steam entries into the wellbore, steam exits ("thief zones"), and/or steam pockets. The solid curve represents the water-normalized Densilog porosity (ϕ_d) as described by Equation 1.

$$\phi_d = (\rho_{ma} - \rho_b)/(\rho_{ma} - \rho_w) \qquad \text{(Equation 1)}$$

where:

ρ_{ma} = matrix density in gm/cc

ρ_b = bulk density as measured by the Densilog in gm/cc

ρ_w = water density at a given temperature and pressure in gm/cc

The dotted curve represents apparent porosity (ϕ_a) (Equation 2) as derived from both the Densilog and Neutron Log.[2]

$$\phi_a = (\rho_{ma} - \rho_b + \phi_n \cdot \rho_w)/\rho_{ma} \qquad \text{(Equation 2)}$$

where:

ϕ_n = the neutron porosity in per unit values.

Although it may not be immediately apparent, if the entire pore space is water-filled, then ϕ_d is equal to ϕ_a. On the other hand, if the pore space is filled with water-vapor or water and water-vapor, ϕ_d is greater than ϕ_a. This apparent contradiction can easily be seen by referring to Equation 3 and recognizing that if ρ_f is less than ρ_w, the denominator of the equation is greater, or ϕ_T is less than ϕ_d. Of course, ϕ_T equals ϕ_a in this case.

$$\phi_T = (\rho_{ma} - \rho_b)/(\rho_{ma} - \rho_f) \qquad \text{(Equation 3)}$$

where:

ϕ_T = true porosity in per unit values

ρ_f = fluid plus vapor density in gm/cc

This anomaly has been accentuated in *Track 3* of the Epilog format by darkening in the positive separation between the curves.

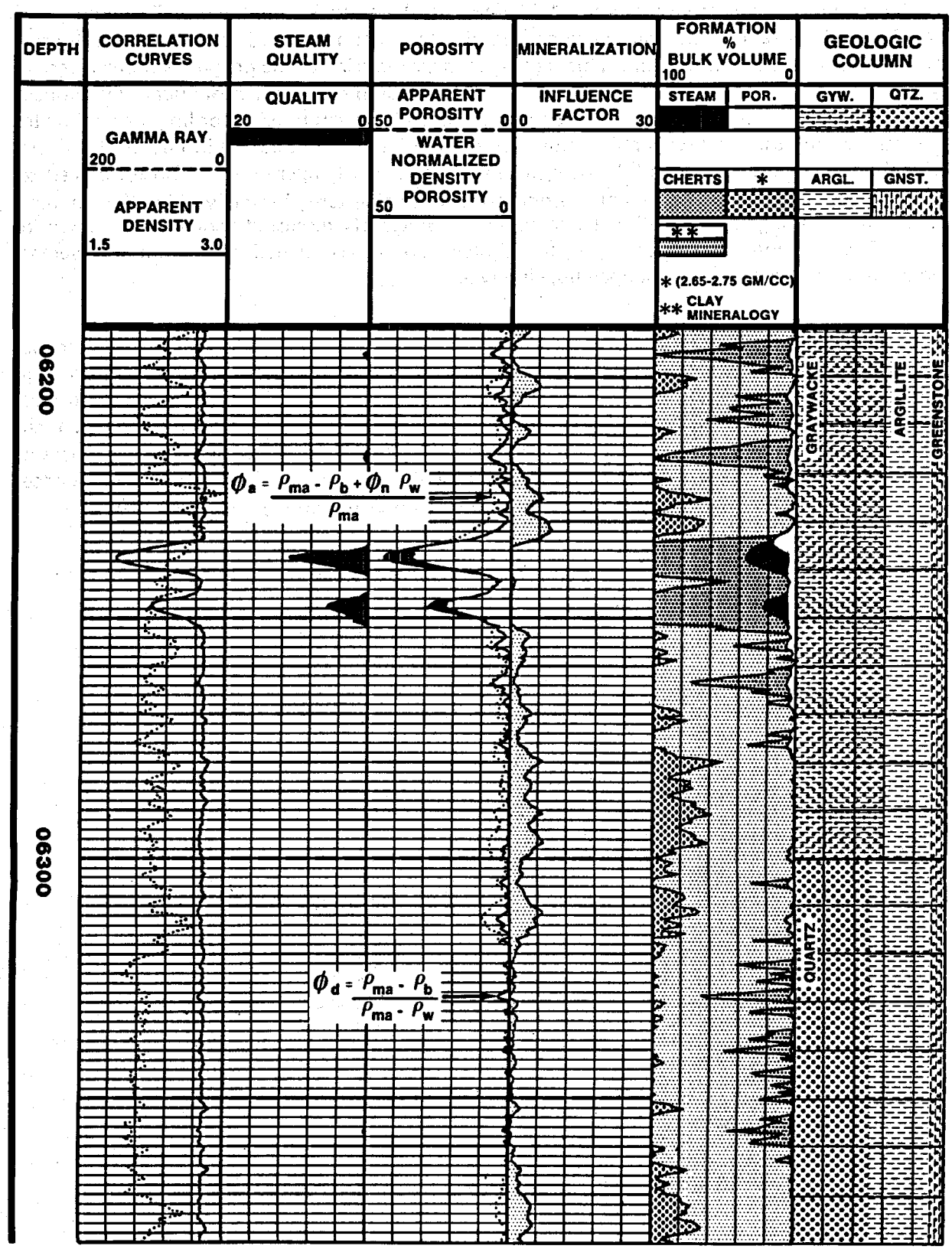
DEPTH
CORRELATION CURVES
STEAM QUALITY
POROSITY
MINERALIZATION
FORMATION % BULK VOLUME
100 0
GEOLOGIC COLUMN
QUALITY
20 0
APPARENT POROSITY
50 0
0 INFLUENCE FACTOR 30
STEAM
POR.
GYW.
QTZ.
GAMMA RAY
200 0
WATER NORMALIZED DENSITY POROSITY
50 0
CHERTS
*
ARGL.
GNST.
APPARENT DENSITY
1.5 3.0
* (2.65-2.75 GM/CC)
** CLAY MINERALOGY
06200
06300
GRAYWACKE
ARGILLITE
GREENSTONE
QUARTZ
$\phi_a = \frac{\rho_{ma} - \rho_b + \phi_n \rho_w}{\rho_{ma}}$
$\phi_d = \frac{\rho_{ma} - \rho_b}{\rho_{ma} - \rho_w}$

FIGURE 5

Since it is now possible to calculate the fluid density (ρ_f) and, therefore, the specific volume, V_ℓ, ($V_\ell = 1/\rho_f$), the steam quality can be computed directly from a standard set of steam tables for any given temperature or pressure. This is easily seen by referring to the pressure-volume diagram or water-phase diagram shown in Figure 6. The reader should recall that steam quality is defined only for the points between the saturated liquid line and the saturated vapor line. For points to the right of the saturated vapor line and to the left of the saturated liquid line or above the critical point, ρ_f and V_ℓ can still be determined, but both the temperature and pressure need to be specified. However, one does not use quality as a defining term for the working fluid in these cases. The resulting steam quality, based upon the previously discussed anomalies as shown in *Track 3* is presented in *Track 2* of the Epilog® analysis as shaded offsets for an average temperature or pressure over the open hole interval.

Although unexpected, a third possibility exists in this curve comparison: namely, ϕ_a can be greater than ϕ_d. In this case, reference to Equation 2 strongly suggests that the Neutron Log response is being strongly influenced by some matrix or fluid mineralization. Recognizing that the mineral influence mechanism is more closely related to absorption of neutrons rather than moderation of neutrons, a correlation number derived from the difference between the apparent porosity (ϕ_a) and the Densilog® porosity (ϕ_d) is presented by the influence factor. The influence factor is illustrated by the lightly shaded offsets in *Track 4* of the Epilog analysis.

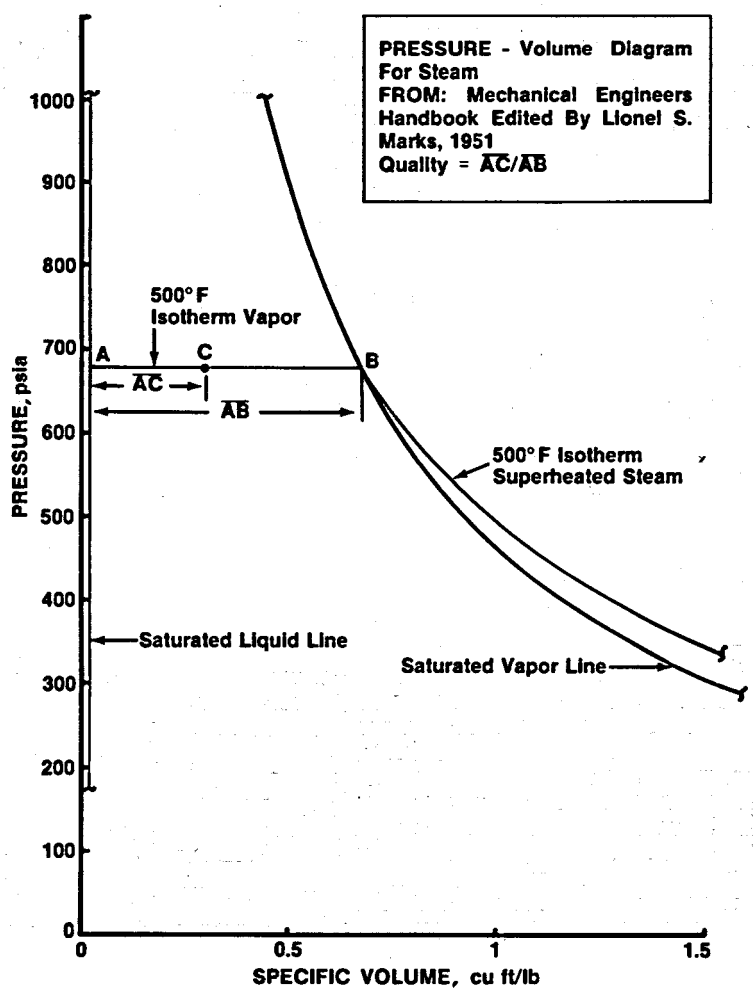

FIGURE 6

Track 5 of the Epilog® represents the standard Dresser Atlas approach to interpretation, based upon pattern recognition. Figure 7 defines the various matrix points for the Neutron Log and Densilog® responses, which form some of the more probable phase triangles. *Track 5* displays the lithologic composition and associated apparent porosity. Although this interpretive model produces formation bulk volume information more akin to stratigraphy, the presentation lends itself well to correlation with phase diagrams and other concepts used in mineral exploration, as will be outlined in the following paragraphs.

The magnitude and general shape of the steam quality curves were found to be both reasonable and consistent with known conditions and the various models used in the interpretation. The first serious question that arose was how to treat the equilibrium state of steam and water under these temperatures and pressures. Perhaps it is easier to visualize this question from a viewpoint taken from a comparison of the formation and borehole models.

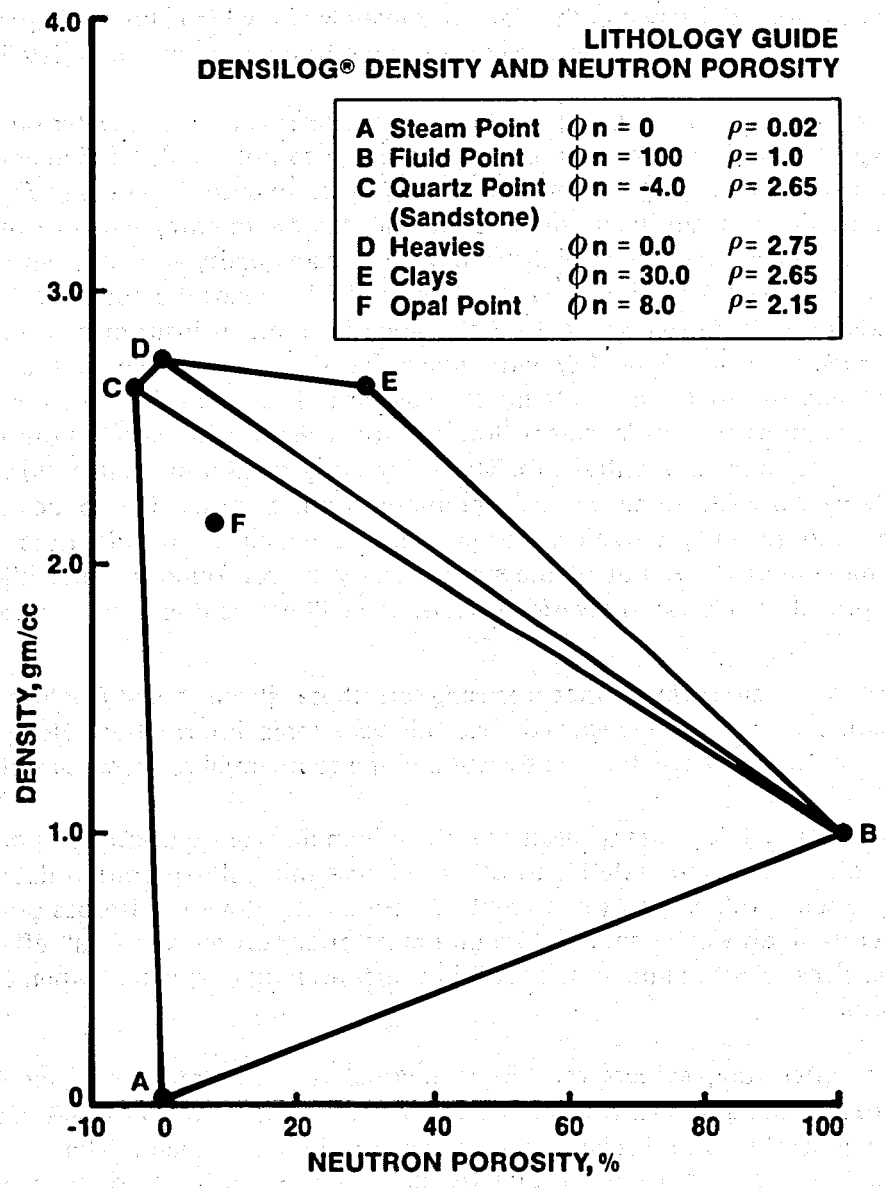

FIGURE 7

It is relatively easy to picture steam or vapor in equilibrium with a water film within the confines of the porespace. It is more difficult, however, to picture steam bubbles and water in equilibrium in the borehole. Whereas the former is a view of static equilibrium, the latter describes dynamic equilbrium or steady flow conditions. In other words, the formation might be viewed to be in a static condition, but the borehole environment must be viewed to be in a dynamic condition. An acceptable working model is to view the borehole as a long convection cell extending from the lowest subsurface steam entry point to the wellhead.

Qualitatively then, one would expect the Densilog® measurements to be not unlike those found in petroleum exploration, since counter-flow water of the convection cell everywhere wets the annulus of the borehole. This may even cause some invasion into the rock over porous intervals that are not subjected to steam flow into the borehole. Neutron measurements, however, will be adversely affected. In intervals where the convection cell is dominated by steam, the calculated porosities and the steam quality will be low. Furthermore, the lowest steam quality will be found at the deepest steam entry point in the borehole. Such conditions are consistent with observations over the logged interval in the well, McKinley No. 1, which allowed improvement on the calculated steam quality values without reconstructing the convection cell in detail.

A simple model of a steam entry interval would place the steam on top and water on the bottom with a nearly exponential decay of steam quality from top to bottom depending upon capillary pressures, the degree of fracturing, and other factors. The steam entry is shown in *Track 2* of the Epilog® (Figure 5). For a steam-filled borehole interval, the steam entry tends to fit the simple model inasmuch as there is an asymetrical distribution of steam quality vertically with a relatively rapid rise at the top of the interval followed by a less rapid fall toward the bottom of the interval. The quality increase could to some extent be explained in terms of instrument resolution. The nearly linear decrease in steam quality with increasing depth downhole in the steam-filled borehole interval suggests that the simple model may have to be modified. Such modifications would include superimposing a radial steam flow pattern which might explain both the increase and decrease of the steam quality with depth. The lower steam quality intervals following a major steam entry interval suggests some vertical communication, perhaps due to possible natural fracture systems and possible crossflow patterns too complex to be discussed at present. Likewise, this simple model does not fit the steam quality shapes found in water-filled intervals of the borehole, probably because of invasion effects, and will not be discussed at present.

Although the reader may surmise that focusing on these steam quality values is perhaps somewhat academic, it must be recognized that this very same information, along with some thermodynamic consideration, will be used to estimate the geothermal reservoir capacity.

A detailed study of the well log data suggests that the minimum average Densilog porosity tends to be somewhat on the high side relative to other in-house mineral exploration data. This does not present any serious problems to the present interpretation. However, it does point out that any detailed interpretation of the data will require close attention to even small effects like the variation of water density with temperature. This becomes even more apparent when dealing with the influence factor.

One of the most interesting aspects of this geothermal well interpretation model has been unraveling the true meaning of the influence factor. A variety of approaches have been tried for assigning the proper attributes to this correlation number or influence factor. The most successful has been to assume that the Neutron Log response is being influenced by some type of mineralization.

In general, one can qualitatively correlate the influence factor shown in *Track 4* with the clay fractions shown in *Track 5* of the Epilog® (Figure 8). Unfortunately, the Gamma Ray Log does not consistently correlate with the influence factor. These conditions suggest that the Neutron Log is not responding to either the clay mineral assemblage, as indicated by the first correlation, or to the bound water of the clays.

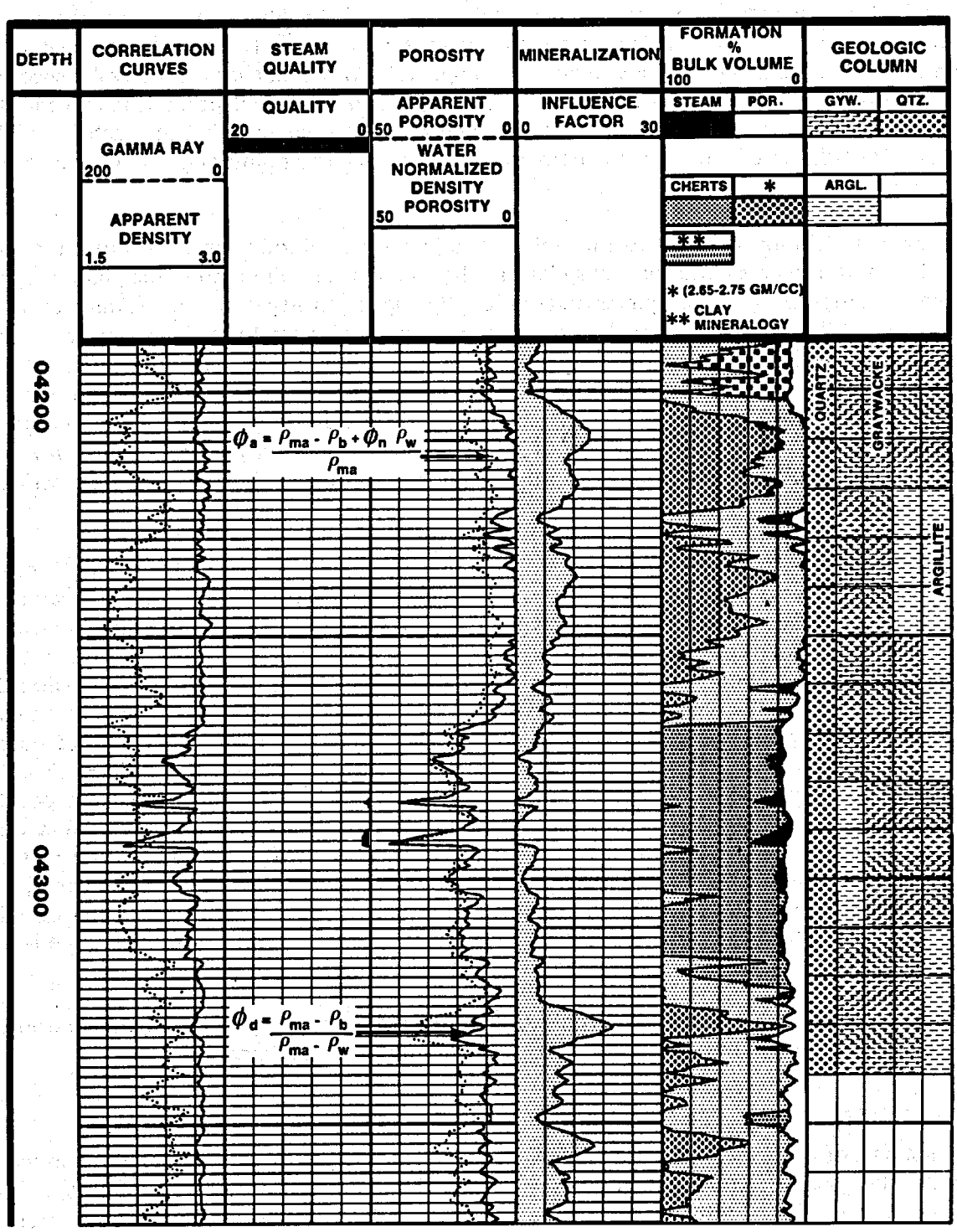

FIGURE 8

Considering for the moment that the mechanism influencing the Neutron Log more closely responds to absorption than moderation effects, two possible neutron absorbing candidates emerge from the geologic column penetrated by the McKinley No. 1 well: namely, Pyrite and Hornblende.

This correlation may not be initially obvious because of mechanical sampling difficulties in describing and constructing the geologic column of the wellbore. The data represent a microscopic evaluation of drill cuttings gathered at the wellhead. These cuttings range in size from small chips to powder. Since an air drilling operation was used over the interval logged, it is suspected that the samples have been both fractionated and offset in depth. Without accounting for fractionization or bunching of the materials, one will find a general offset in depth from 20 to 30 feet. Such displacements become more obvious at steam entry points and will, of course, vary with depth.

Further consideration of the two mineral species Pyrite and Hornblende shows that the latter would exhibit a log response that falls close to the clay matrix point used in the phase diagrams of the formation bulk volume curves. In addition, the higher density values of the minerals in the Actinolite — Tremolite series of the Hornblende are more in line with the high average densities observed in the logged section. Unfortunately, this assemblage does not completely specify the attributes needed to understand the influence factor, but it does strongly suggest that the information presented has significant chemical implications. Furthermore, it should be recognized that the delineation of such a mineral assemblage is only a short step away from mineral stability diagrams and a host of other approaches more closely related to the description of metamorphic rocks.

The presentation of the Formation Bulk Volume as shown in *Track 5* of the Epilog® may to some degree be misleading to log analysts and to geologists specializing in clastic and carbonate rock analysis. It must be re-emphasized that this track does not describe a stratigraphic section, but rather groupings of mineral assemblages and fractions thereof. Furthermore, this presentation should not be looked upon as a compositional diagram. With a little thought, one will realize that almost any point on the presentation represents 50 percent or more of silica. At present, the best analogy or descriptive name that can be applied is a phase diagram. This name, of course, aleviates the resistance to calling water or steam a mineral, but is not truly descriptive. The important point, however, is that the matrix points represent groupings of physical and possibly mineral properties which are important to the interpretation. It goes without saying that water and steam are important. Sand, of course, is a name for those physical properties favoring steam production. Heavies (2.65 to 2.75 gm/cc) is a name for those physical properties favoring flow restrictions (i.e., caprock). Clay is a name, as previously discussed, that favors the chemical properties of the medium. Names, of course, can be changed and probably will be in the future, but this should not inhibit one from proper interpretation.

It should suffice to say that we have only started to learn how to evaluate geothermal resources. We have already found, however, that the log-derived information is very useful.

CONCLUSION

The first part of this paper describes the surface geological and geophysical exploration, providing us with the general setting and subsurface regime of the area. The second part of the paper focuses on two different interpretive approaches to well log data which support both reservoir evaluation and subsurface control. Obviously, completion of the effort will not come until we are able to make models of the subsurface that are consistent with all the data available. Since this

requires not only more well log data, but also a better understanding of the instrument responses in metamorphic rocks, the final evaluation of key reservoir parameters and ideas presented here will depend upon additional research and field experiences. These data will be presented at a later date.

REFERENCES

1. McLaughlin, Robert J., Preliminary Geologic Map of the Geysers Steam Field and Vicinity, Sonoma County, California. *U.S. Geological Survey open file map 74-238* (1974).

2. Rodermund, C. G., Alger, R. P., Tittman, J., Logging Empty Holes. *The Oil and Gas Journal* (June 12, 1961).

ABOUT THE AUTHORS

Ehring

Grubb

Lusk

Johnson

Fertl

DeVries

Theodore W. Ehring (Ted) graduated in 1955 from the University of Southern California with a B.A. degree in geology. He obtained an M.A. degree in 1957 from the same university. He worked as an exploration geologist for Texaco, Inc. from 1956 until 1964 at which time he joined Aminoil (then Signal Oil & Gas) as a senior geologist. He was named district development geologist in 1967 and division development geologist for the entire western division in 1971. In 1974, he was named Manager of Development Geology for Aminoil and supervises all development geology, both domestic and international, from the Houston-based office. In this position, Mr. Ehring is vigorously involved in the geology of oil and gas, geothermal, oil shale, tar sands, and coal. He is a Registered Geologist in the State of California, No. 487, and an active member in the AAPG and the Houston Geologic Society and a member of the Science and

Technology Committee of the Houston Chamber of Commerce. He has given papers for the AAPG and written for the Journal of Petroleum Technology. In 1970, he received the Best Paper Award from the Pacific Section of the AAPG.

James M. Grubb is Division Geologist for Aminoil USA, Inc.'s Geothermal Division based in Santa Rosa, California. He joined Aminoil USA in 1974 with six years experience in mineral exploration in the Mid-Continent and Rocky Mountains. His previous assignments with Aminoil include foreign and Gulf Coast exploration.

He holds a B.S. degree in geology and business administration and an M.S. in geology from Bowling Green University.

A. Lee Lusk is currently Exploration Analyst for Aminoil USA, Houston, Texas. He received his B.B.A. degree at the University of Houston. Past experience includes two years in mud logging and core analysis and 15 years with PGAC and Dresser Industries, Inc., as logging engineer, sales engineer, district manager, and regional log analyst. In 1970, he joined Signal Oil and Gas as staff well log analyst for production and exploration, domestic and foreign. The last four years have added satellite imagery and photo geology to analysis for geothermal and oil exploration.

Ralph B. Johnson, Jr. is a Log Analyst and Research Project Engineer for Dresser Atlas. He has been previously associated with Lockheed Electronics, Mandrel Industries, Texas Instruments, and his own company.

His education consists of a B.S.E.E. degree at the University of Texas, 1957/1958, with additional graduate studies in mathematics, physics, geology, and geophysics.

Walter H. Fertl is Director of Interpretation and Field Development with Dresser Atlas in Houston, Texas. His educational background includes engineering degrees from the University of Mining at Leoben, Austria, and M.S. and Ph.D. degrees in petroleum engineering from the University of Texas. He has had 12 years of worldwide formation evaluation experience dealing with oil field operations, well logging research, and teaching. He has authored over 80 technical papers and a book, *Abnormal Formation Pressures.* He also holds 10 patents.

Fertl served for three years as an officer of the SPWLA Tulsa Chapter (including President for 1973-74). On the Board of Directors of SPWLA since 1974, he was Secretary-Treasurer from 1974 to 1975, Vice President-Publications and Editor of the *Log Analyst* from 1975 to 1977, and is currently Vice President – Technology in charge of the technical program for the Symposium in El Paso.

Marvin R. DeVries is Chief Log Analyst with Dresser Atlas in Houston, Texas. He is working on Computer Analysis and Field Development programs. His educational background is a B.S. degree in geology from West Texas State University and 10 years of formation evaluation experience, which includes positions as Logging Engineer and Log Analyst.

He is a member of SPWLA, SPE, and HGS.

A Practical Shale Compensated Chlorine Log

By J.W. Fletcher, J. Walter
NL McCullough/NL Industries, Inc., Houston, Texas

ABSTRACT

Since commercial introduction on a limited basis in June 1977, shale compensated chlorine logging (SCCL) tools in 3½ and 1 11/16 inch diameters have been run successfully on more than 20 wells along the Louisiana Gulf Coast. This modern neutron-gamma spectral survey has provided accurate, quick-look water saturation measurements through tubing and casing, which required substantially no corrections for shaliness or porosity.

In this text, SCCL instrumentation and principle of measurement are discussed along with interpretation equations and nomographs. Two selected log examples illustrate the presentation and interpretation of this new cased hole log.

INTRODUCTION

The concept of neutron-gamma spectral logging to measure water saturations behind pipe dates from the late 1950's, when several chlorine or salinity logging systems were introduced to the industry.[1-4] The utility of these early systems, however, was limited both by instrumentation and by their sensitivity to shaliness. With the advent of pulsed neutron logging in 1963, interest and investment shifted away from spectral methods toward chlorine measurement by the now well-known neutron die-away techniques.

One group to continue research in spectral logging was the Texaco Research and Technical Department at Bellaire Laboratories in Houston. Their efforts resulted in the development of apparatus and techniques known as the Texaco Shale Compensated Chlorine Logging System.[5] A key feature of the Texaco system was the development of a detector made by enclosing a sodium iodide scintillator in a high capture cross-section rare earth material which served as a thermal neutron converter. A subsequent empirical selection of counting windows was then possible which minimized not only the effect of shaliness, but also the effects of porosity, lithology and borehole fluids on the salinity measurement.

The commercial SCCL was developed from the Texaco system through important refinements in tool design, technique and presentation. The commercial casing tool is 3½ inches OD and ten feet in length. The tubing tool is 1 11/16 inches OD by twelve feet. Tools in both sizes are rated for 15,000 psi and 325°F. Readings may be taken with either tool within 1½ feet of TD.

GG

FUNDAMENTALS OF THE SPECTRAL MEASUREMENT

Figure 1 illustrates the functional blocks of the SCCL system. The tool introduces neutrons of average energy 4.5 MeV to the wellbore at the rate of 4×10^7 per second from an americium beryllium source. The neutrons are slowed by successive collisions, particularly with the hydrogen atoms of the wellbore and formation fluids.

Source neutrons slowed to thermal energy are captured by nuclei of nearby formation and wellbore elements in accordance with the distribution of each element, weighted by its thermal neutron capture cross section. Thermal neutrons in the immediate vicinity of the detector are captured by the sleeve of samarium oxide (Sm_2O_3) in which the scintillation crystal is enclosed.

The neutron captures by the constituent elements of the tool, wellbore, and the formation result statistically in emission by each element of its characteristic spectrum of neutron capture gamma rays. Four such spectra are shown in Figure 2. The statistical sample of gamma rays striking the SCCL's scintillation crystal results in transmission to the surface of an aggregate spectrum of neutron capture gamma rays representing the assorted contributing elements.

Table A: Selected microscopic neutron capture cross sections.

Element	$\sigma_{B.U}$, 10^{-24} cm^2/nucleus
Hydrogen	0.332
Boron	758.8 (n, α)
Carbon	0.0034
Oxygen	0.0002
Sodium	0.534
Aluminum	0.234
Silicon	0.160
Chlorine	33.34
Calcium	0.44
Iron	2.56
Samarium	5820.

In the behavior of the aggregate spectrum over an interval of constant well geometry, three factors predominate:

1. *Porosity*—The occurence of hydrogen in the formation pore space determines the slowing down length of the source neutrons, hence the population distribution of thermal neutrons with respect to the detector.

2. *Shaliness*—The existence in shale of the high capture cross section trace element boron presents an exception to the neutron-capture gamma-emission reaction mode. Neutron capture by boron is followed by alpha particle emission. This uncountable result complicates both neutron die-away and spectral analysis techniques.

3. *Salinity*—The concentration of the element chlorine which combines a high thermal neutron capture cross section with a preponderance of high

Figure 1. Block diagram of the SCCL system.

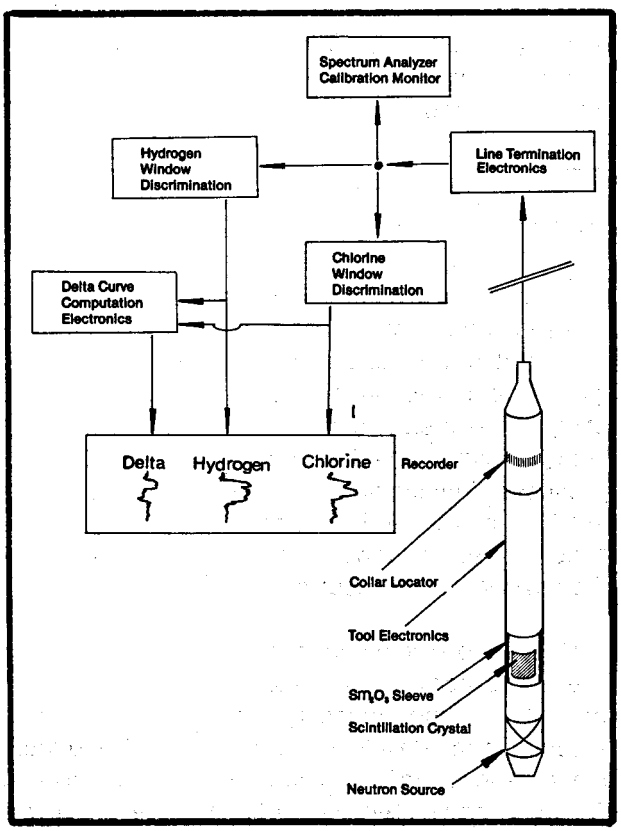

energy capture gamma emissions, may be measured by either neutron die-away or by spectral methods provided porosity and shaliness (boron) are known.

The particular advantage of the SCCL apparatus and technique is that chlorine concentration, hence water saturation, can be measured for clean or shaly formations in the 20–30% porosity range without specific knowledge of either porosity or shaliness.

Figure 2. Selected neutron capture gamma ray spectra.

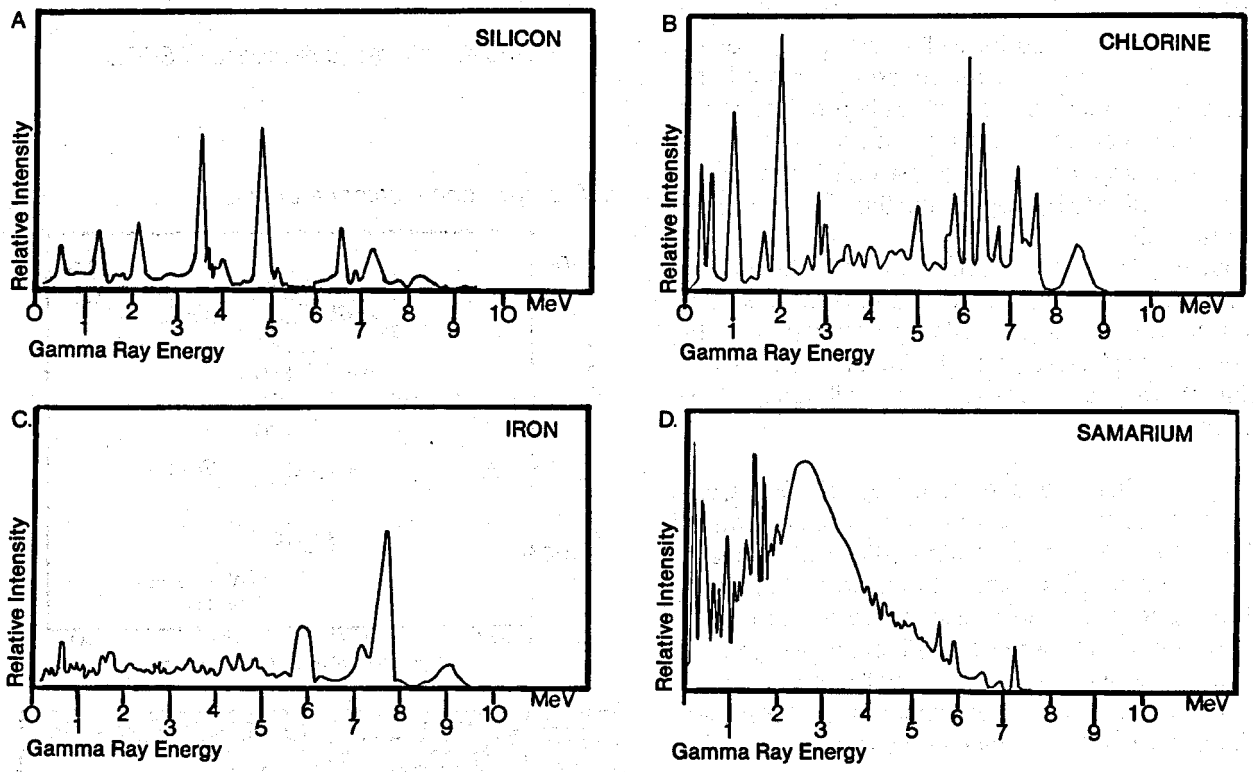

ANALYSIS OF THE AGGREGATE SPECTRUM

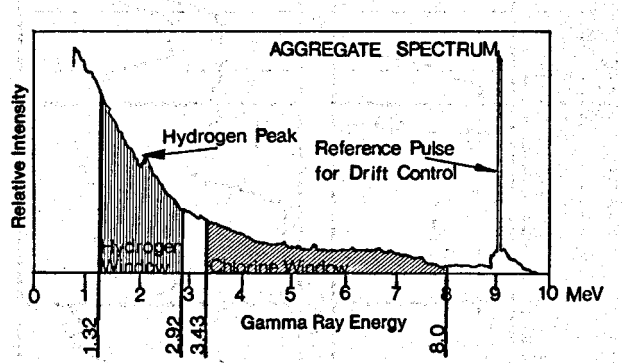

Figure 3. The aggregate gamma spectrum observed at the surface with the tool inside 7 inch casing and reacting to a 30% ϕ sand saturated with 150,000 ppm NaCl. salt water.

Figure 3 shows an aggregate gamma ray energy spectrum transmitted to the surface instrumentation in pulse height code from the SCCL tool. The portions of the spectrum compared in order to determine chlorine concentration are indicated as the hydrogen window 1.32–2.92 MeV, and the chlorine window 3.43–8.0 MeV. Selection of optimum windows was accomplished through computer-aided empirical methods which located the "best" chlorine response consistent with shale, porosity and lithology compensation, for the particular counter geometry and efficiency.

From the counting windows, the two neutron-gamma counting rate curves are recorded: (1) the *chlorine curve* from the portion of the spectrum most

affected by the high energy gamma rays from neutron capture by chlorine, and (2) the *hydrogen curve* which serves as a reference indicating the population of thermal neutrons available for capture.

Qualitatively the hydrogen curve behaves as a conventional neutron log reacting to porosity and shaliness, while the chlorine curve responds to porosity, shaliness and chlorine. When the two curves are normalized for well geometry by deflection matching through a reference water sand, the chlorine curve may be subtracted electronically from the hydrogen curve in real time to produce a Delta curve that responds only to the concentration of chlorine relative to hydrogen, and thus reflects water saturation (Sw).

Figure 4 illustrates the cross plot technique for comparison of the hydrogen and chlorine counting rates to determine Sw. Also illustrated are the schematic responses of the hydrogen, chlorine and Delta curves to a shale, water, oil, gas, shale sequence.

In the SCCL measurement, typical Gulf Coast shales appear to have chlorine concentrations relative to hydrogen averaging 60% that of nearby water sands (shales adjacent to hydrocarbon zones often appear fresher). Since water saturation decreases are recorded as deflections to the right, the Delta curve will trace the well's SP or natural gamma ray through water sands and shales, and deflect opposite to those curves in hydrocarbon zones.

The visual simplicity of the Delta curve response is illustrated in Figure 5 which compares an SCCL run June 1977 with the well's electrical log run July 1968. The well was drilled with a 9⅞ bit. The casing is 7 inch, 29 lb. Salinity of the formation water is 120,000 ppm NaCl.

The SCCL confirmed that the existing perforations from 4317 to 4354 have watered out. A gamma ray log (not shown) revealed radioactivity from deposited potassium salts indicating water had moved through the shaly stringers 4276 to 4300, accounting for their 50% Sw. The original oil-water contact shown by the electrical log at 4150 has moved to 4126 due to offset production.

The well was perforated July 1977 at 4094-4102, with initial production of 216 BOPD with 85 MCF. In February 1978, perforations were made 4064-4074 with initial production 223 BOPD with 82 MCF.

It may be noticed in Figure 5 that the productive intervals vary significantly in porosity and shaliness, but show little variation in water saturation.

Figure 4. Schematic response of SCCL.

a. The hydrogen – chlorine crossplot

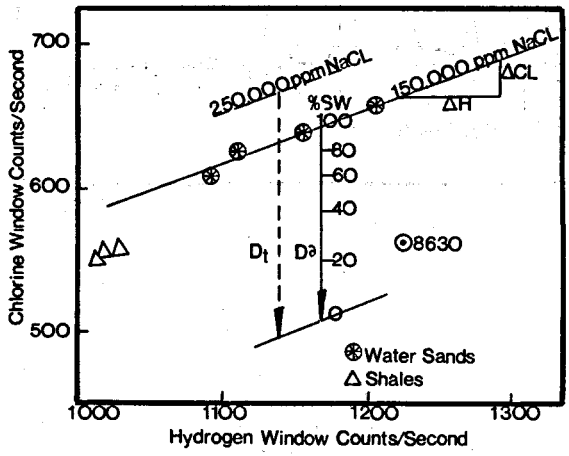

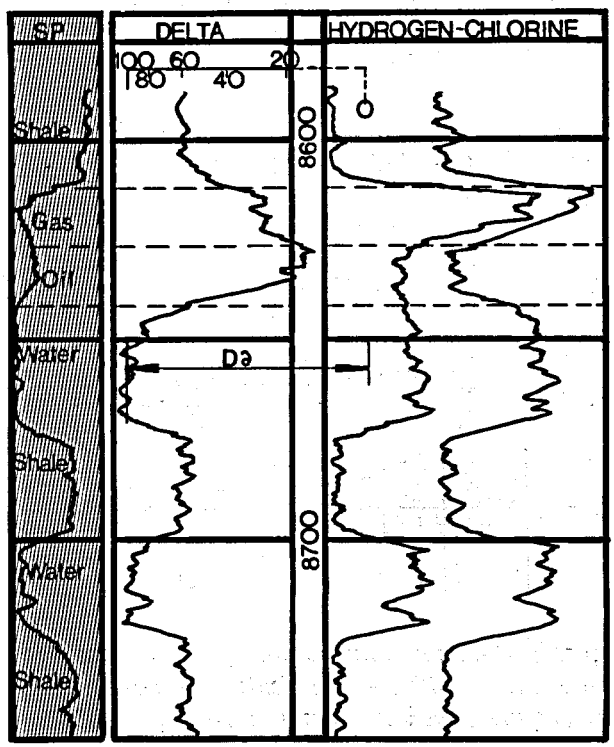

b. The hydrogen, chlorine and Delta curves.

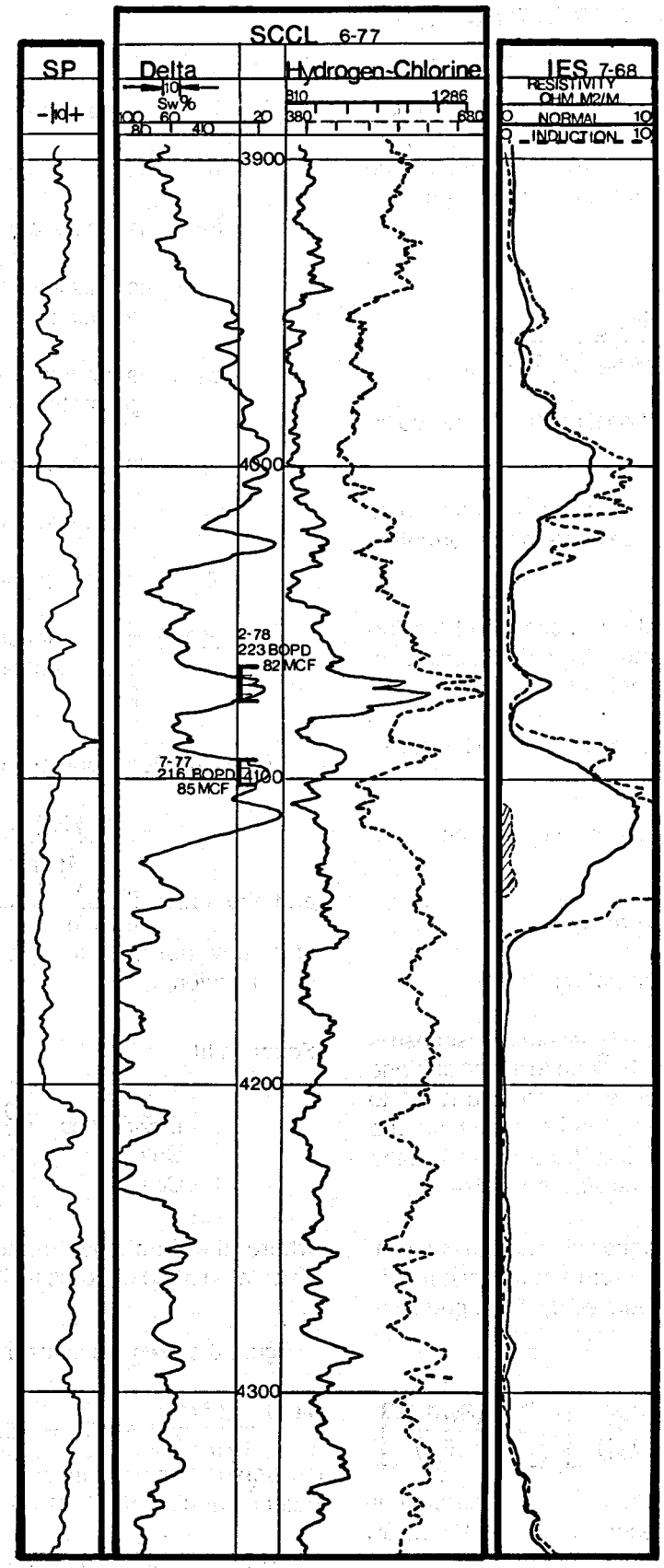

Figure 5. The SCCL in a South Louisiana oil well.

THE DELTA CURVE WATER SATURATION SCALE

The water saturation (Sw) response of the Delta curve is scaled according to the chlorine fraction of the bulk thermal neutron capture cross section of the gamma ray emitting elements in the formation.

Equation I

$$\eta = \frac{\phi Sw\Sigma_{Cl}}{\phi(Sw\Sigma_w+(1-Sw)\Sigma_{hc})+(1-\phi)\Sigma_m}$$

where η is the fractional neutron captured by chlorine,

Σ_{Cl} is the macroscopic capture cross section of chlorine in the formation water,

Σ_w is the total cross section of the formation water (Σ_{Cl} and Σ_w are functions of water salinity ∂),

Σ_{hc} is the cross section of the hydrocarbons,

Σ_m is the cross section of the clean matrix,

ϕ is matrix porosity,

Sw is water saturation.

The geometry factor in the Delta curve response is expressed as a test Delta, D_t, defined as the chlorine axis separation in counts per second from a 100% to a 0% water saturation in a 30% porosity sand at a formation water salinity of 250,000 ppm NaCl in the particular geometry— casing size, bore size.

As a function of Sw, deflection of the Delta curve in chlorine axis counts/second from a 100% water saturation reference line is predicted by the expression

Equation II

$$D(Sw) = D_t\left[\frac{\phi H(\phi)}{\phi_t H_t}\right]\left[\frac{\eta(\partial,\phi)}{\eta(\partial_t,\phi)}\right]\left[1-\frac{\eta(Sw\partial,\phi)}{\eta(\partial,\phi)}\right]$$

where D(Sw) is the Delta curve deflection in counts/second from the 100% Sw line,

ϕ is the zone's porosity,

∂ is the salinity of the formation water,

Sw is the zone's water saturation,

$H(\phi)$ is the clean zone hydrogen window counting rate at porosity ϕ,

D_t is the test Delta for the appropriate geometry,

ϕ_t is the test porosity,

H_t is the test hydrogen counts,

∂_t is the test water salinity,

$\eta(\partial,\phi)$ is the fractional capture by chlorine from Equation I at salinity ∂, porosity ϕ.

In the Gulf Coast porosity range, however,

$$\frac{\phi H(\phi)}{\phi_t H_t} \cong 1$$

and the ratios $\frac{\eta(\partial,\phi)}{\eta(\partial_t,\phi)}$ and $\frac{\eta(Sw\partial,\phi)}{\eta(\partial,\phi)}$ are substantially porosity independent permitting the simplification,

Equation III

$$D(Sw) \cong D_t \frac{\eta(\partial)-\eta(Sw\partial)}{\eta(\partial_t)}$$

Gulf Coast

where the fractional captures by chlorine are calculated at 30% porosity.

Figure 6 shows the scale factor

$\frac{\eta(\partial)-\eta(Sw\partial)}{\eta(\partial_t)}$ for ∂_t = 250,000 ppm NaCl, plotted versus water salinity for curves representing water saturation of 80, 60, 40, 20, and 0%.

Values of D_t for assorted geometries are listed in Table B. The Sw scale placed on the Delta curve is

calculated by multiplying the Sw scale factors at the appropriate formation water salinity by the D_t value for the appropriate geometry.

Notice that the scale factors for values of Sw in the range 20% to 100% remain virtually constant for salinities above 100,000 ppm NaCl. This leads to a further simplification in the interpretation of the SCCL. For formation salinities in excess of 100,000 ppm NaCl, a water saturation scale may be determined from a reference water sand without knowing the water salinity.

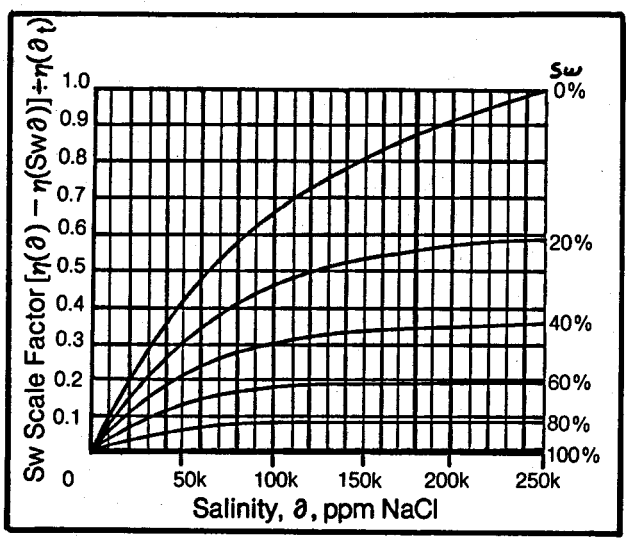

Figure 6. Delta curve scale factor versus formation water salinity.

Table B: Delta curve test response, D_t in assorted geometries. Values recorded in cemented casing, centered tubing, wellbore fluid 100,000 ppm NaCl. Formation ϕ 30%, fluid 250,000 ppm NaCl.

Geometry–inches			Test Response D_t–c/s	
Bore	Csg	Tbg	3.5 SCCL Series 1	1.6875 SCCL Series 1
6	4½		333	188
	5½		246	138
8	4½		284	166
	5½		230	125
		2⅞		90
10	4½		246	123
	5½		200	100
	7		170	100
		2⅞		63
12	4½ Dual		216	80
	7		139	88

SCCL GAS ZONE CORRECTION

To the SCCL, the reduced hydrogen index of a gas zone causes the zone to appear to have a porosity that is too low and an apparent water saturation that is too high. The required Sw correction in a gas zone is related directly to the hydrogen index of the reservoir gas, essentially a function of reservoir temperature and pressure, and gas specific gravity.

The correction chart of Figure 7 is based upon the following relationship.

Equation IV

$$Swc = \frac{H_I Swa}{1 - Swa + H_I Swa}$$

where Swc is the corrected Sw,

H_I is the hydrogen index of the reservoir gas, and

Swa is the apparent gas zone water saturation from the Delta curve.

The SCCL response to gas is illustrated in Figure 8. This offshore Louisiana well has 7 inches 35 lbs. casing. The salinity of the formation water is in excess of 150,000 ppm NaCl.

The resistive zones shown by the electrical log 13830-13769 and 13580-13490 are gas bearing and have been produced through the existing perforations indicated on the SCCL. Reservoir pressures of approximately 6000 psi have been maintained by water drive. The apparent water saturations from the Delta curve on the order of 35% for 0.65 gravity gas at 6000 psi, 210°F, correct to 20% Sw.

Figure 7. The SCCL gas zone correction.

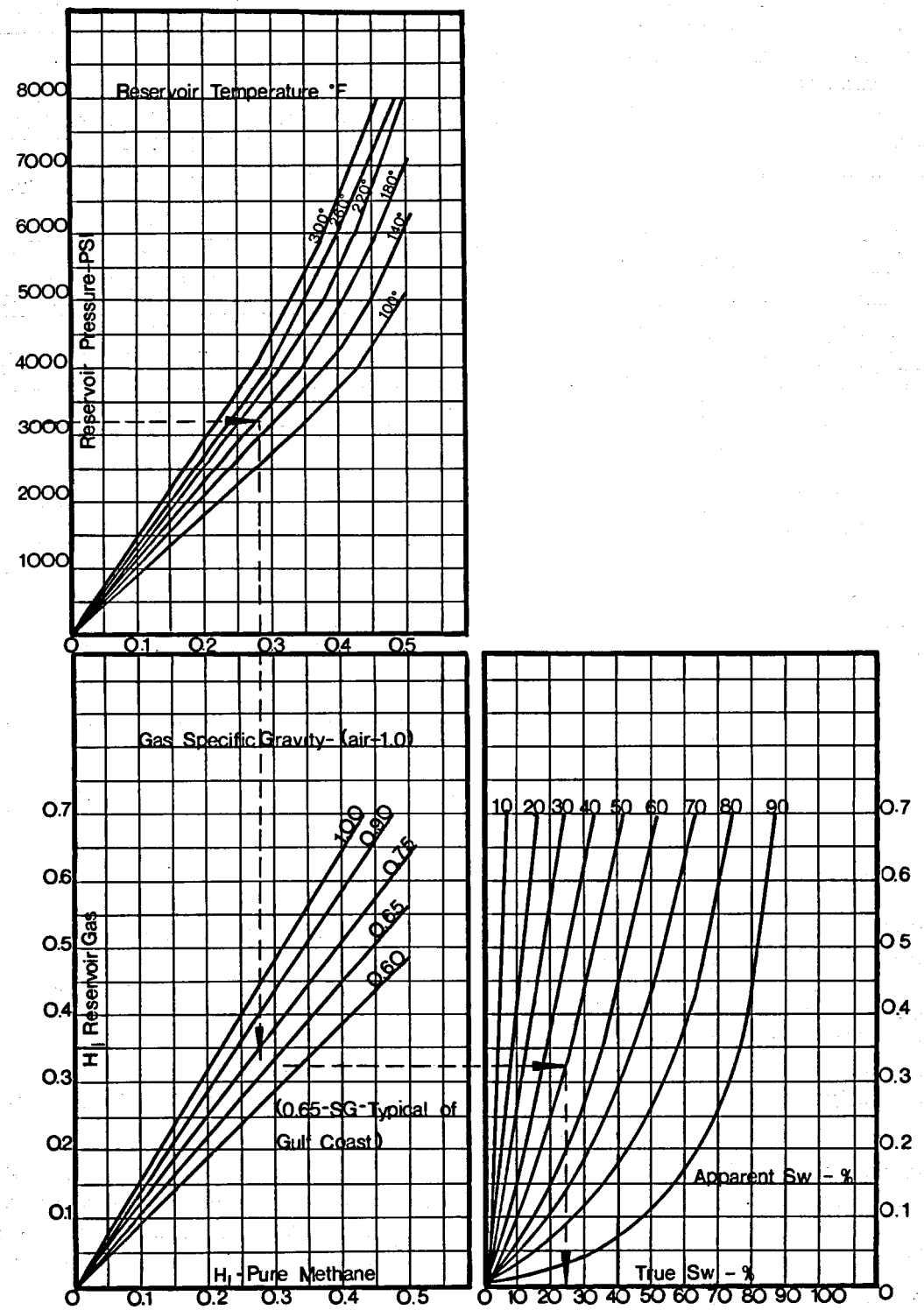

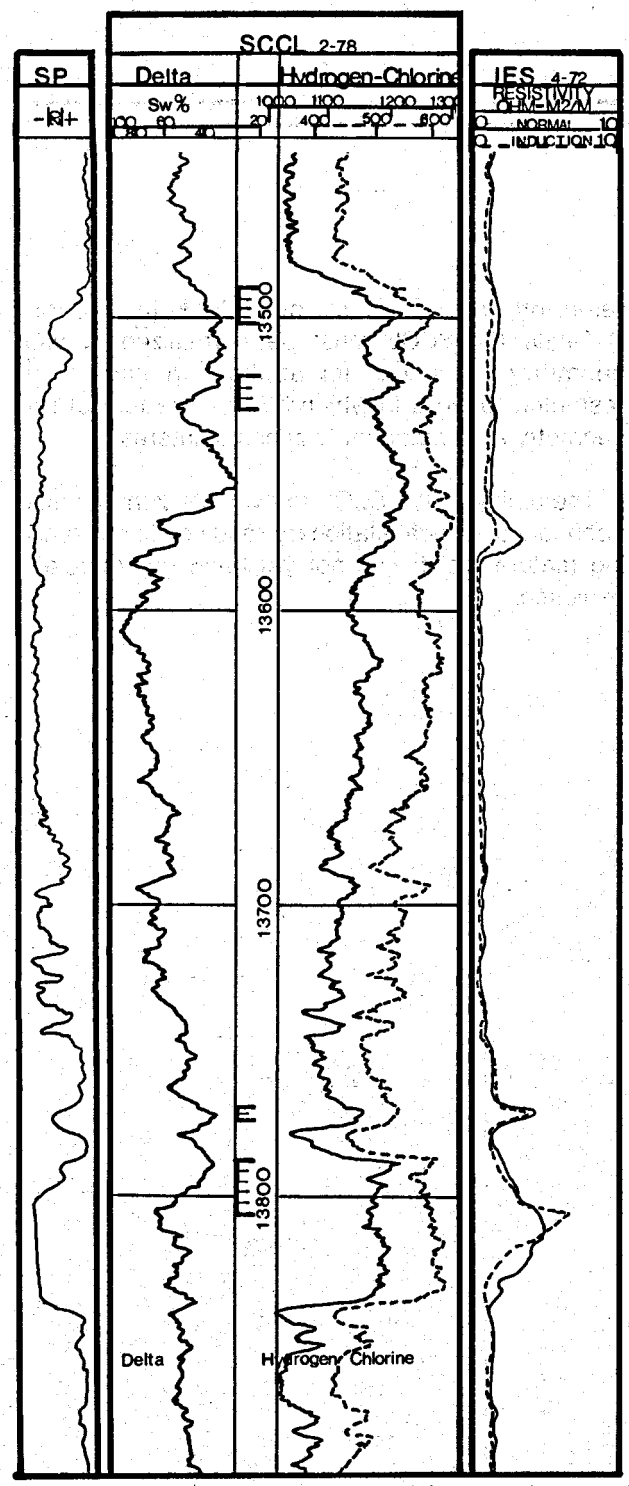

Figure 8. The SCCL response in an offshore South Louisiana gas producer.

STATISTICS, LOGGING SPEED AND TIME CONSTANT

As a concession to counting rate statistics, all nuclear well logs require a compromise to be reached relating repeatability and thin bed resolution to logging speed and time constant. Recommended SCCL logging speeds are 12 to 15 feet per minute for the casing tool, and eight fpm for the tubing tool logging casing. A logging speed of 5 fpm is recommended for logging tubing inside casing.

The time constant for the hydrogen and chlorine neutron-gamma counting rate curves is selected to equal the number of seconds required for the tool to move one foot in the well bore. The accumulated time constant applied to the Delta curve is equal to the number of seconds required for the tool to move 3 feet in the well bore.

Bed boundaries and water-oil-gas contacts are determined more precisely from the hydrogen and chlorine curves. In beds of thickness less than 6 feet, the Delta curve response should be corrected from the hydrogen and chlorine curves.

The statistical accuracy of the Delta curve response is given by:

Equation V

$$\sigma_{\%D_\partial} = 100\% \times \sqrt{\frac{V}{60S}} \times \frac{\sqrt{(Clw)} \times m\sqrt{(Hw)}}{D_\partial}$$

where $\sigma_{\%D_\partial}$ is the standard deviation in Delta as a percent of full scale deflection D_∂,

V is the logging speed in feet per minute,

S is the bed thickness over which Delta is averaged,

(Clw), (Hw) are respectively the chlorine and hydrogen counts per second in a reference water zone, and

m is the slope $\Delta Cl/\Delta H$ of the 100% Sw line (see Figure 4).

In ordinary applications a standard deviation of 5% for a 6 foot zone is acceptable. For applications requiring great statistical precision and excellent thin bed resolution, the SCCL may be used to good advantage as a stationary reading tool.

CONCLUSIONS

Modern instrumentation and such key concepts as the samarium neutron converter have revitalized the technique of cased hole reservoir evaluation by spectroscopic analysis of neutron-capture gamma rays. The Shale Compensated Chlorine Log is an attractive alternative to conventional pulsed neutron surveys in Gulf Coast lithologies since the SCCL measurement requires no correction for either porosity or shaliness. As a result, interpretation of the SCCL is uniquely straight-forward permitting quantitative reservoir evaluation by quick-look inspection. Because the SCCL must be normalized to well geometry, however, its application should be restricted to wells in which 50 or more feet of like geometry exist adjacent to zones of interest.

The ability of the SCCL to evaluate zones based upon low statistical stationary readings is a promising feature which has not yet been commercially exploited.

ACKNOWLEDGEMENTS

We wish to express our appreciation to NL McCullough for permission to publish this paper and to our research and field personnel for their invaluable contributions in the SCCL project.

REFERENCES

1. Rabson, W.R.: "Chlorine Detection by the Spectral Log", *Pet. Eng.* (March 1959) B102-B111.
2. Stroud, S.G. and Schaller, H.E.: "New Radiation Log for the Determination of Reservoir Salinity", *J. Pet. Tech.* (Feb. 1960) 37-41.
3. Waddell, C. and Wilson, J.C.: "Chlorinity and Porosity Determination in Cased and Open Holes by Nuclear Logs", SPE-AIME Paper 1456-G, Beaumont, Texas, (March 8, 1960).
4. Dewan, J.T., Stone, O.L., and Morris, R.L.: "Chlorine Logging in Cased Holes", *J. Pet. Tech.* (June 1961) 531-537.
5. McKinlay, P. F. and Tanner, H.L. "The Shale Compensated Chlorine Log," *J. Pet. Tech.* (Feb. 1975) 164-170.

ABOUT THE AUTHORS

John Fletcher is Technical Services Manager, Central Region for NL McCullough. He is a graduate of Texas Tech University, B.S. EE, 1970.

Jerry Walter is a Completion Engineer, Eastern Region for NL McCullough. He is a geology graduate of Ohio State University, 1973.

CARBON/OXYGEN LOG APPLICATIONS IN SHALY SAND FORMATIONS CONTAMINATED WITH TUFFITE MINERALS

By
E. L. Sacco
Dresser Atlas Division, Dresser Industries, Inc.
Buenos Aires, Argentina

ABSTRACT

Log evaluation of the oilfields located in the San Jorge basin (Southern Argentina) is one of the most difficult to perform. Shaly sand formations are contaminated with considerable amounts of tuffites. Salinities of formation waters are very low.

The Carbon/Oxygen system was introduced during 1976 as an attempt to solve the problem of locating overlooked pay zones behind the casing.

This paper describes the results of the first 15 wells logged and how it was necessary to develop a cross-plot technique with the Spectralog in order to solve the complex lithology problem.

INTRODUCTION

The San Jorge basin, located in southern Argentina, has been known to be oil productive since 1903. Since that time, more than 12,000 oil wells have been drilled.

This is a most difficult area to evaluate by logging. The log analysis requires the help of the core or sidewall core analysis to which too much attention is given by the geologists and engineers.

This basin (Figure 1) is of a continental type and can be defined as a thick sequence of shale, interbedded with lenticular shaly sandstones. The salinity of the formation water is low, ranging between 1,000 to 30,000 ppm. The salinity also changes erratically from one sand body to another.

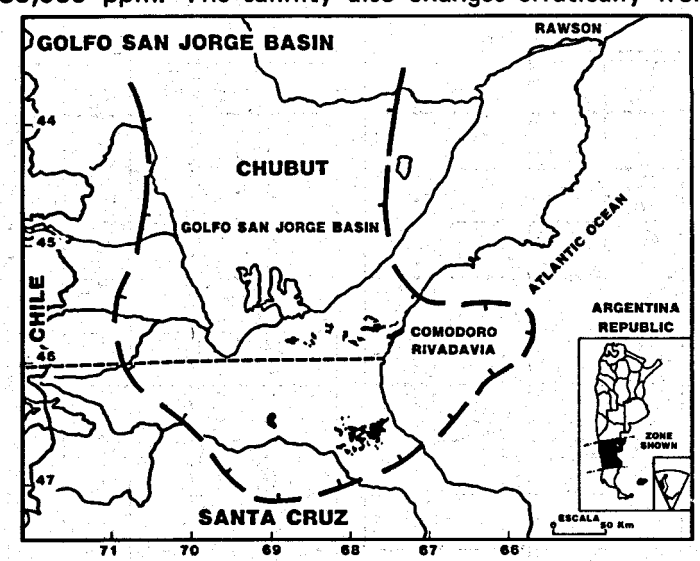

FIGURE 1

This picture is complicated by the fact that the shale and sands originated from pyroclastic rocks. As a result of volcanic action, tuff and tuffites are always present in the formations.

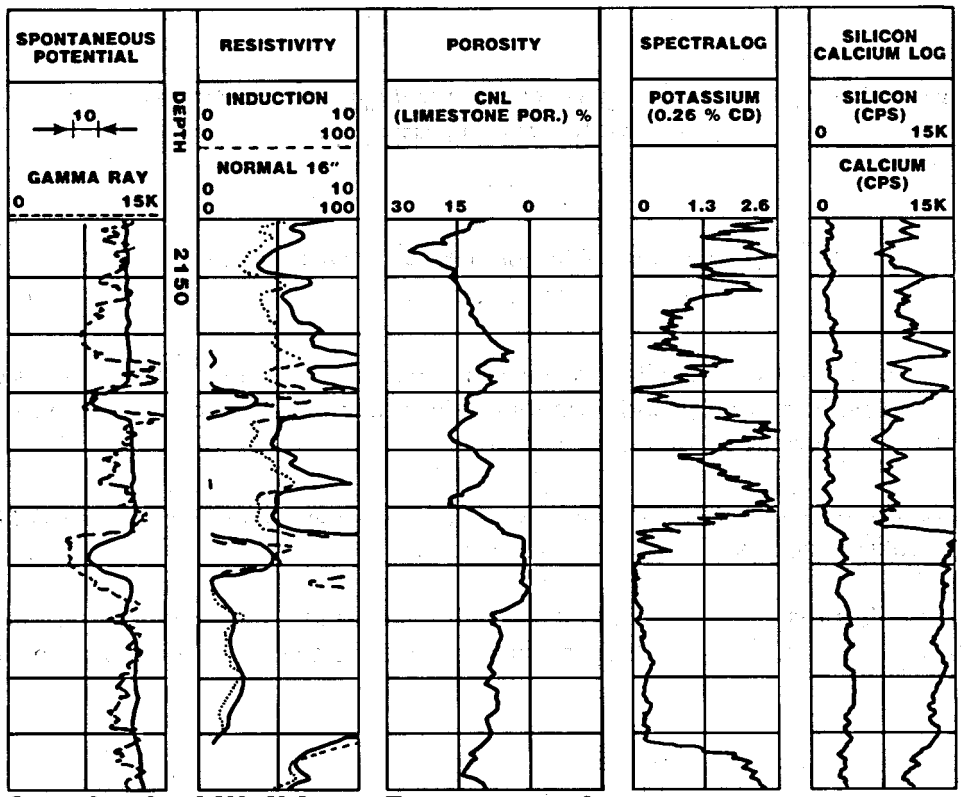

Geophysical Well Logs Representative of a Tuffite Formation (Mina Del Carmen) FIGURE 2

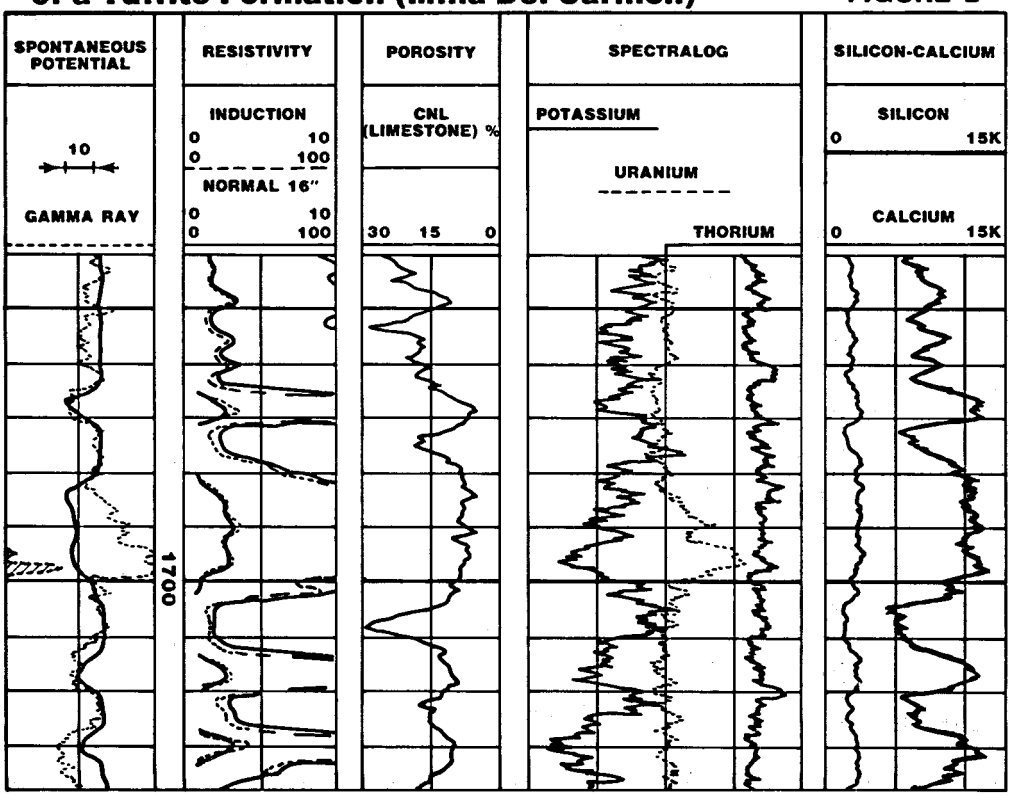

Geophysical Well Logs Representative of a Tuffaceous Shaly Sandstone Formation (Grupo Del Chubut) FIGURE 3

Teruggi and Lesta (1,5), among many others, have described the geology and lithology of this area. Figures 2 and 3 represent a composite log of a representative well of this area.

Other authors (2) have described the evaluation problem that is summarized here:

– Problems related with low salinity formation waters.

– Small salinity changes cause wide variations of water resistivity.

– Since the effect of clay on resistivity is more important at low rather than at high salinities, a good evaluation of clay content becomes essential. Unfortunately, the natural radioactivity of some sands and tuffites cause the Gamma Ray and the sand streaming potentials cause the Spontaneous Potential to become unusable as clay indicators.

– Problems related to tuffites content.

  An increase in tuffite content in a sand will increase the resistivity, decrease the permeability and increase the possibility of being water bearing.

Due to the reduced areal extension of the sand bodies, the reservoirs (lenses) are depleted rapidly. It is therefore necessary to frequently recomplete the old producing wells, trying to locate new pay zones.

As recognized before (2), it is very difficult to differentiate oil from low salinity water zones in a new well, whereas in open hole conditions, it is possible to run the most sophisticated logging tools. It is therefore understandable that it appears to be nearly impossible to locate pay zones behind the casing under these types of conditions.

The Dual Detector Neutron Lifetime Log® was tested in a first attempt to solve the problem. Success was limited because this system requires formation waters of salinities higher than 30,000 ppm, rarely found in the area.

The Carbon/Oxygen system was initially introduced in the country during 1976 in order to solve the problem. Since the beginning, results have been very encouraging.

Determining the presence of significant amounts of tuffites contaminating the shaly sandstones was the first problem that required a solution. This paper describes how the Spectralog was used to differentiate non-productive tuffites from shaly sands.

The present status of the evaluation method allows for the exact determination of pay zones as distinguished from the wet ones, independent of salinity and shaliness.

BRIEF DESCRIPTION OF THE LOGGING SYSTEMS AND MEASUREMENT OF THE CARBON/OXYGEN RATIO

The C/O measuring method is based on the detection of 4.4 million electron volt gamma rays which are emitted by carbon nuclei when bombarded by high energy neutrons. These gamma rays, which are produced by inelastic scattering of 14 million electron volt neutrons, are detected by a scintillation spectrometer in the well logging instrument. The neutrons are produced by a miniature ion accelerator which operates in a pulsed mode to produce bursts of neutrons by the nuclear reaction of high speed deuterons with a tritium target. Gamma rays from oxygen as well as those from carbon are selectively detected and measured. The ratio of carbon to oxygen has been found to be a sensitive and reliable indicator of oil saturation in reservoir sands (3).

Also, by selective timing within the instrument, gamma ray responses indicative of silicon and calcium can be recorded to aid in interpreting the C/O Log in areas of unknown lithology or in mixed lithology environments. This instrument has the capability to obtain information on the hydrocarbon content of a formation in addition to differentiating sandstone from carbonates and clean sands from limey sands.

The Carbon/Oxygen Log finds its primary application in areas where other commercial logs fail or are marginally acceptable (4).

SPECTRALOG

The Spectralog system measures the individual contributions of the primary sources of natural radiation (6).

An important improvement in the system is the ability to quantitatively define volumetric percentages of the three main radioactive elements that compose the natural ray spectrum. These elements are potassium – 40, uranium and thorium.

The Spectralog has proven to be a very useful instrument for the determination of clay content in those areas where the Gamma Ray Log shows anomalous readings. The radioactive sands in the Southern Patagonia oilfields are a good example.

CASE HISTORY

As was mentioned in the literature (7), the measurement of the C/O ratio is directly proportional to oil saturation in high porosity clean sandstones. Where this lithology becomes more complex and complicated with limestone, previous experience indicates use of the cross-plot technique of Carbon/Oxygen ratio vs. Silicon/Calcium ratio for evaluation.

These cross-plots, plus the experience of hundreds of observations accumulated by McWhirter and Thompson, comprised the method used locally during the first 10 tests of the C/O system in the San Jorge basin (8).

Results of this utilization in the area were very impressive. Regardless of the fact that the wells were old and had been worked over many times, the C/O system located more than twice the amount of oil than the conventional open hole logging system would have been capable of locating.

However, the quantitative evaluation of the C/O system was less accurate than that of the conventional method. The cross-plots of C/O vs. Si/Ca were not definitive in this complex lithology. The accuracy of our predictions suffered. While large numbers of oil zones were predicted due to high C/O value, many of these were tested wet (see Figure 4).

The Spectralog was also run during this project. During the initial evaluation, we attempted to use it only for detecting water zones with a high uranium content. A review of the Spectralogs showed a strict correspondence between the low potassium readings and the tuffite formations determined by the customer's core analysis.

Since the "Chubutiano" formations are altered pyroclastic rocks, this relation with the potassium content gave us the tool to separate the non-permeable pure tuffites from the more or less shaly ones altered and transformed in sandstones.

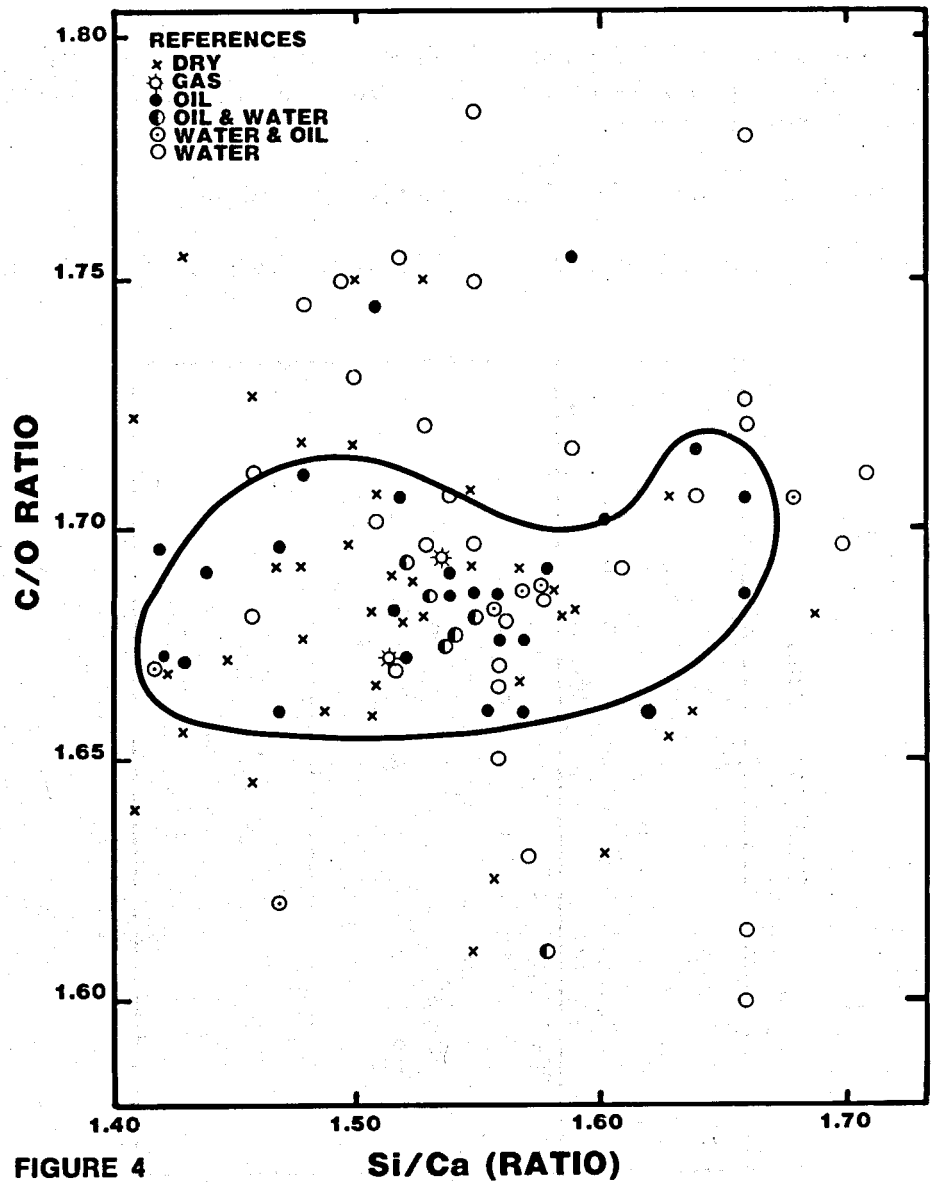

FIGURE 4

Figure 5 presents the cross-plotting of R_t versus %K for those points where sidewall cores were obtained. On the Z-axis, we have presented the lithology of such points by a symbol. In order to be clear, we are showing only those points that are classified as neat sandstones (O) or tuffites (□).

It is shown that a definite separation exists between both types of rocks. The few exceptions are explained by incorrect evaluation of the cores (points 211) and probably the only clean sandstone (point 5).

From Figure 5, we obtained the value of K = 0.6% as a limit of potassium. Points to the left of the K cutoff line fall on the tuffite zone.

We define tuffite as a compact rock, generally non-porous, composed of fine grain vitroclastic and volcanic ash. Tuffite only sporadically produces fluid, generally water, and probably from secondary porosity.

On the right side of the graph fall the points classified as sandstones. Regardless, their grains are quartz or mainly other minerals originating in the tuffite weathering. These sandstones become more shaly as the K-content increases.

In Appendix I, the mineral composition of these rocks is presented.

With this lithological or pseudo-lithological classification, we developed the following cross-plot technique.

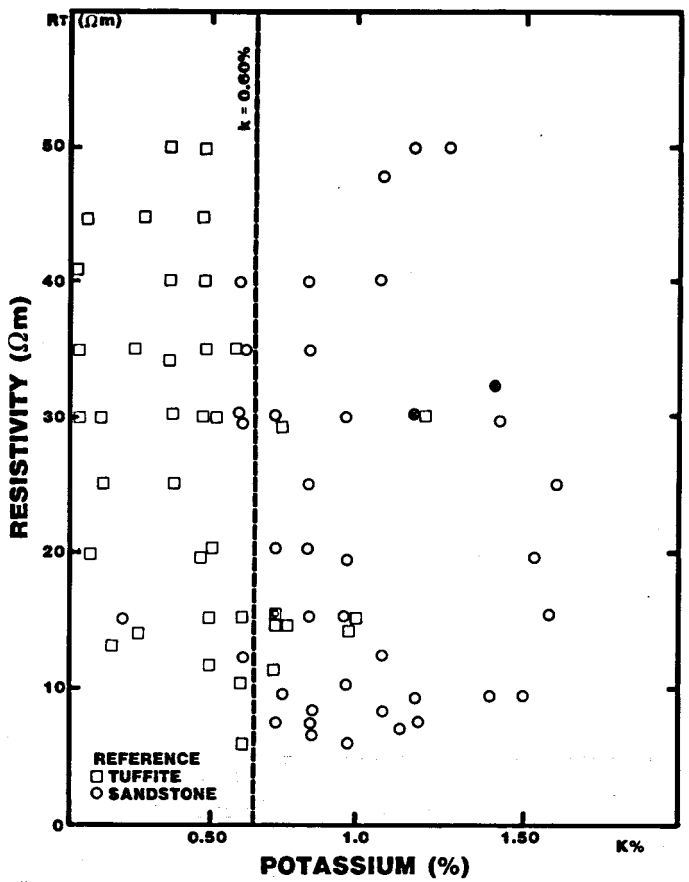

FIGURE 5

HYDROCARBON DETECTION BY THE C/O RATIO VERSUS K-CONTENT CROSS-PLOT IN SHALY SAND AREAS

The solution consists of the cross-plotting of C/O measurements versus the % potassium reading of each point tested.

We have classified the production test results with the corresponding symbol according to the customer definition:

SYMBOL:

- ✕ = Dry
- ☼ = Gas
- ● = Oil (S_W from 0% to 39%)
- ◐ = Oil and water (S_W from 40% to 69%)
- ⊙ = Water and oil (S_W from 70% to 89%)
- ○ = Water (S_W from 90% to 100%)

S_W must be understood here as the percentage of water produced in the test, and not as a water saturation of the formation.

Figure 6 includes the production test results of 13 wells that were worked over during the presentation of the C/O equipment. Each point is coded by a letter that represents the well and a number that corresponds to the zone tested. From these data, we have inferred a geometric pattern where the majority of the oil test falls. If we had used this pattern, our predictions would have been 91% accurate.

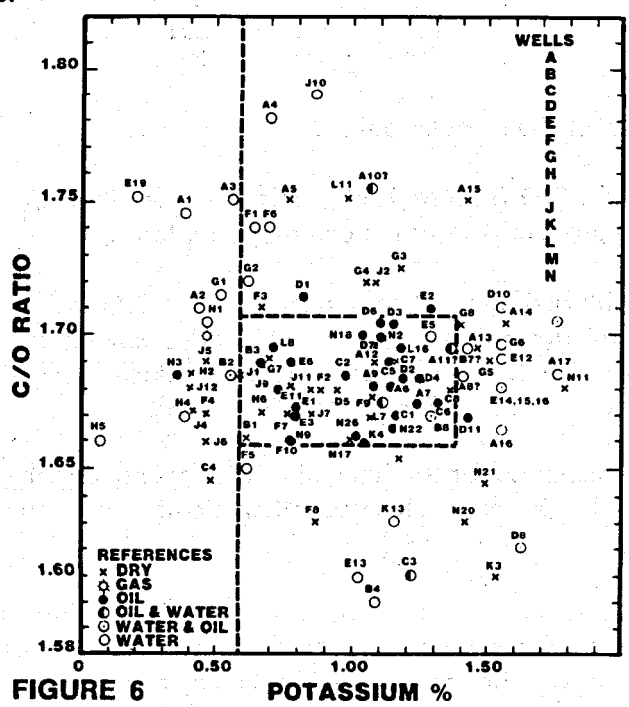

FIGURE 6

The envelope of the oil points is a rectangle whose limits have a strict justification from the geological and reservoir point of view (refer to Figure 7).

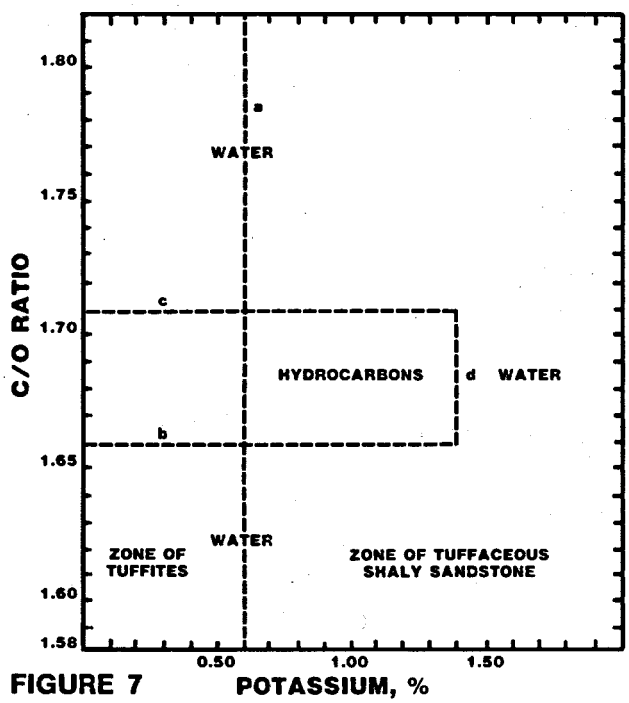

FIGURE 7

Vertical line "a" separates the formations into two types: the left zone, of tuffites, hard rocks (non-porous), and the right zone, granular rocks (generally tuffaceous shaly sandstones) with an increasing shale content to the right.

At each of these zones, we give a different treatment during the quantitative analysis. For example, for the tight zone (left), we use

$$S_w^2 = \frac{1}{\phi^{2.35}} \cdot \frac{R_w}{R_t}$$

and a shaly sand formula for the granular points.

Line "b" corresponds to a C/O ratio of 1.66 and is the lower limit of the C/O readings. Below this line, there are no oil productive zones of commercial interest.

We have tentatively established line "c" to correspond to a C/O ratio of 1.71. This value is the upper limit of the C/O relation. Above this line, oil production would be very difficult. It must be pointed out that very high C/O values will generally produce water. This fact was also noticed by McWhirter and Thompson, who performed the first 11 logs.

We are looking for an explanation for this anomaly. It is possibly due to a high calcareous cement (very rare here) or to the presence of some other element near the carbon in the inelastic spectrum.

Line "d" is the shale cutoff limit for the zone. Contents of potassium greater than 1.40% make the relative permeability to water greater than that relative to oil. In this case, the formation will produce water regardless of whether or not the C/O reading confirms a good oil saturation.

COMMENTS

1. The limits that we have suggested are susceptible to slight displacement, as the utilization of the C/O system will give more data.

2. The limits can also change for other areas. This paper covers the results of five oilfields of the Golfo San Jorge basin and its application is unique.

3. The C/O system is only applicable for hydrocarbon detection in new wells where the invasion of drilling fluid has dissipated.

CONCLUSIONS

The application of the Carbon/Oxygen Log measurements for the detection of hydrocarbon in cased holes has proven to be successful in the tuffaceous shaly sandstones with formation waters of very low salinities. The Spectralog appears to be a very useful instrument in complex lithology areas. In our case, the potassium curve must, however, be carefully calibrated.

The cross-plot of C/O versus %K provides an easy "on-site" method of evaluation. This is a must, taking into account that generally the workover job immediately follows the C/O logging operation.

The utilization of C/O Log and the Spectralog has provided 91% accuracy in the evaluation of 10 cased hole wells in the San Jorge basin. The accuracy with open hole log analysis in the same area rarely surpasses 80%.

ACKNOWLEDGEMENTS

We wish to thank the oil companies which provided us with test data, etc.

We also want to thank the people who provided their field experience in the log evaluation of this area, among them V. C. McWhirter, D. Corchuelo and C. E. Mainetti.

REFERENCES

1. Lesta, P. "Estratigrafía de la Cuenca del Golfo San Jorge," *III Jornadas Geológicas,* Buenos Aires, 1967.

2. Khatchikian, A., Lesta, P. "Log Evaluation of Tuffites and Tuffaceous Sandstones in Southern Argentina," *SPWL Fourteenth Annual Logging Symposium,* 1973.

3. Youmans, A. H. *Location of Oil by Nuclear Determination of Carbon Oxygen Ratio,* Dresser Atlas, Houston, Texas.

4. Lock, G. A., Hoyer, W. A. "Carbon Oxygen (C/O) Log: Use and Interpretation," *Journal of Petroleum Technology,* September 1974, 1044.

5. Teruggi, M. E., Rossetto, H. "Petrología del Chubutiano del Codo del Río Senguen," *Boletín Informaciones Petroleras,* April 1963.

6. Lock, G. A., Hoyer, W. A. "Natural Gamma Ray Spectral Logging," *The Log Analyst,* V. XII, M.5, October 1971.

7. Wichmann, P. A., et al. *The Carbon Oxygen Log Measurement,* Dresser Atlas, Houston, Texas.

8. McWhirter, V. C., Thompson, J. B. private communication, Dresser Atlas, Houston, Texas.

ABOUT THE AUTHOR

Eduardo L. Sacco is a Regional Sales Engineer for Dresser Atlas, Argentine Division, Buenos Aires, Argentina. He graduated in 1957 as Industrial Engineer and in 1958 as Petroleum Engineer at the Buenos Aires University.

He worked with Y.P.F. as Drilling Engineer and joined Dresser Atlas in 1962, where he was Field Engineer, District Manager and Senior Log Analyst in Chubut, Neuquén and Mendoza oilfields.

Sacco is a member of I.A.P. (Argentine Petroleum Institute), SPWLA and Society of Petroleum Engineers of AIME.

APPENDIX I

According to analysis of more than 120 samples taken from a representative outcrop of tuffite formations (5), the composition of these rocks can be a variable combination of the following minerals:

Mineral	Composition in weight	Chemical composition
Quartz	Higher than 25%	$Si\ O_2$
Plagioclases	Less than 25% (a continuous series of Feldspars, ranging from 100% Albite and 0% Anorthite to 0% Albite and 100% Anorthite)	
Albite		$Si_3\ O_8\ Na\ Al$
Anorthite		$Si_2\ O_8\ Ca\ Al_2$
Kaolinite	Less than 25%	$Si_2\ O_5\ Al_2\ (OH)_4$
Alkali Feldspar	Less than 25%	$Si_3\ O_8\ Al\ K$
Calcite	Normally absent	$CO_3\ Ca$
Dolomite	Normally absent	$(CO_3)_2\ Ca\ Mg$
Analcime	Normally absent	$Si_2\ O_6\ Na\ Al\text{-}H_2\ O)$
Montmorillonite	Less than 25%	$(Si_4\ O_{10})_3\ (Al,Mg)_8\ (OH)_{10}\text{-}12H_2\ O$
Illite and Mica	Normally absent	—

From this study, we can realize that the abundance of the elements in the tuffites is:

Major	Si, O, Al
Medium	H
Minor	K, Na, Ca, Mg, C
Rare	Fe, Li, F

The minor presence of the K element, almost only present in the Alkali Feldspar, widely justifies the very low reading of the potassium curve in front of a tuffite formation given by the Spectralog instrument.

Ten sidewall core samples taken in these oilfields are being analyzed in order to support this study. Results are not available at the time of this paper.

COAL EXPLORATION IN WEST GERMANY BY WELL LOGGING

By

K. Otto
Dresser Atlas Division, Dresser Industries, Inc.
Bremen, Germany

ABSTRACT

With the increased emphasis on the potential shortage of energy sources, large-scale, precise exploration methods are being required of the coal mining industry. New drilling methods as well as advanced well logging techniques are providing mining operators with valuable assistance.

Accurate well log analysis methods provide in-situ evaluation of coal seam parameters such as depth, thickness, impurities, dip direction and environmental lithology.

This paper briefly describes the current drilling methods and standard logging procedures and interpretation techniques being employed. A comparison of well logs and laboratory evaluation of cores is also presented.